EOS, vol. 61, no. 17, April 22, 1980, pages 195, 197, 198, 200

1980 Spring Meeting

The 1980 Spring Meeting will be he d jointly with the Canadian Geophysical Union, the Canadian Meteorological and Oceanographic Society, the Division of Aeronomy and Space Physics of the Canadian Society of Physics, and the Canadian Exploration Geophysical Society, at the Harbour Castle Hilton in Toronto, May 22–27. This is the AGU's first annual meeting outside the United States and the first to be held jointly with other societies.

Special Sessions

Frontiers in Geophysics

The Frontiers of Geophysics sessions feature four contemporary research topics of high interest to the geophysical community.

The paper by A. E. Litherland discusses radioisotope dating in which small accelerators are used, a technique that allows the dating of very small samples of material and the extension of dating techniques to other radioactive isotopes.

D. J. DePaolo's presentation addresses the study of the natural abundance of an isotope of neodymium to determine models for the earth's mantle and evolution of the continental crust. The technique has come into use only in the last few years and appears to hold promise as yet another 'window' into the earth's past. Neodymium seems to have the property of being less susceptible to temperature resetting.

A. Malahoff discusses recent (within the past few months) studies of earth structure in the region of the Galapagos Islands in which the deep submersible vehicle Alvin (named for its designer, Al Vine) was used. The relationships between rift valley structure and volcanic structure cast new light on the planet's tectonic processes.

The tectonics of Venus will be examined in J. W. Head's discussion of the data on the surface structure of the planet, which was yielded by the surface sounding radar of the Pioneer Venus orbiting spacecraft. Dramatic evidence for craterlike and large uplift structure was obtained.

Union Sessions

Geophysics of the Great Lakes

Six invited speakers will draw a picture of the geophysics of the Great Lakes, bringing into play topics that include meteorology and climatology, motion and temperature, sedimentation, and geochemistry. An historical introduction will be offered in which 25 years will be summarized every 55 seconds—thought to be an AGU record for a 15-minute presentation.

Crustal Processes of North America

Crustal activity from ancient to recent times will be explored, beginning with examination of the evolution of the lunar crust, including the 'magma ocean' and the agents that modified the early crust. The scene will then shift to earth, with discussion of the earliest rocks in the Canadian Shield. Evolution of the crust from the mantle will then be considered in papers on the various methods of age determination. Deep crustal seismic work and large-scale tectonic features will be surveyed, as will the development of the ocean basins along the continent/ocean margins, the continents and margins, and the processes of fluid migration and volcanism.

1980 AGU Spring Meeting Program Committee

General Chairman. Louis J. Lanzerotti, Bell Laboratories.

Geodesy. Clyde C. Goad, NOAA; G. LaChapelle, Department of Energy, Mines and Resources.

Geomagnetism & Paleomagnetism. Neil Opdyke, Lamont-Doherty Geological Observatory; G. W. Pearce, University of Toronto.

Hydrology. John Ritter, USGS-WRD; John A. Cherry, University of Waterloo.

Meteorology. Ronald C. Taylor, National Science Foundation; Han-Ru Cho, University of Toronto; George Pore, Atmospheric Environment Service.

Oceanography. Dana R. Kester, University of Rhode Island; Nelson Freeman, Canadian Centre for Inland Waters.

Planetology. David Strangway, University of Toronto.

Seismology. Adam M. Dziewonski, Harvard University; C. H. Chapman, University of Toronto.

Aeronomy. Thomas A. Potemra, The Johns Hopkins University; Gordon Shepherd, York University.

Cosmic Rays. J. R. Jokippi, University of Arizona.

Magnetospheric Physics. J. R. Winckler, University of Minnesota; Martin Walt, Lockheed Missiles Technology Information.

Solar and Interplanetary Space Physics. Marcia Neugebauer, Jet Propulsion Laboratory; Peter Foukal, AER, Inc.

Tectonophysics. Richard J. O'Connell, Harvard University; R. M. Stesky, University of Toronto.

Volcanology, Geochemistry, and Petrology. G. N. Hanson, State University of New York; I. H. Campbell, Erindale College.

Exploration Geophysics. Laurie Reed, Selco Mining Company.

Spring Meeting Abstracts

Union

Crustal Processes in North America

Metropolitan West
Thursday P.M.
D. W. Strangway (Univ. of Toronto), Presiding

U 1 INVITED PAPER

FORMATION OF THE EARTH

John A. Wood (Harvard-Smithsonian Center for Astrophysics, Cambridge, Mass. 02138)

It is currently understood that the solar system came together 4.6 x 10^9 yr ago from interstellar gas and dust, components of which derived from a variety of stellar nucleosynthetic processes. Between the time when this system contracted to roughly the dimensions of the present solar system and the time when the planets were formed, it is thought by most workers to have consisted of a spunout disk or nebula of formerly intersteller material, surrounding a protosun that had not yet achieved core temperatures sufficient to initiate hydrogen fusion. The dust grains which were ultimately to comprise the substance of the terrestrial planets experienced poorly understood processes, probably involving high temperatures, while still disseminated in the nebula, which had the effect of chemically fractionating them; so that the aggregate compositions of the planets, once formed, differed in some degree from one another and from the overall composition of condensible matter in the nebula. The earth appears to have incorporated a smaller share of the volatile elements, and possibly a somewhat larger share of refractory elements, than was available in the nebula at large.

The accretion of small mineral grains into large planets undoubtedly proceeded hierarchically, evolving through a series of planetesimal size-distributions with larger and larger members (ultimately the planets) at the upper end of its size range. When the growing planets were joined by the next-largest planetesimals in their zones, enough mechanical energy was converted to heat to cause large temperature increases, and the heat was buried deeply enough in major impact events to inhibit its dissipation. It is possible or even likely that the earth was melted by accretional energy, even if the process of accretion extended over 10^8 yr, as dynamical studies have indicated it would. (Geochronologic evidence from the moon is that the last sweeping-up of major planetesimals occured 4.4 x 10^9 yr ago.)

At some point in the accretion process the nebular gases and unaccreted dust particles entrained in them were dissipated, again by poorly understood mechanisms. Presumably the volatile elements that had been incompletely accreted by the planets were lost from the solar system at this time.

U 2 INVITED PAPER

CONSTRAINTS ON THE EARLY EVOLUTION OF MOON & EARTH

C.H. Simonds (Lunar Curatorial Lab., Northrop Services, Inc., Box 34416, Houston, TX 77034)

Understanding the moon's evolution at 4.55-3.9 b.y. aids in understanding the earth's early evolution despite differences in size, H_2O, CO_2 & Fe° content, oxidation state and silicate compositions. Wetherill proposes that accretion of earth and moon involves impacts of >100 km projectiles that hit the moon at 6-8 km/sec, and the earth with higher velocities, continuously reworking the outer 200 km until the planets are within 7 km of their final radius.

The lunar highlands consists of cumulate anorthosite, troctolite, norite, plus a basaltic component formed 4.5-4.2 b.y. which were reworked until the end of the major bombardment at 3.9 b.y. Calculated source magmas for the cumulates generally have 10x chondritic light REE enriched compositions. Impact played a critical role in lunar fractionation since it heated the crust and disrupted it. Superheated melt forms for impacts >7 km/sec, but that melt is insignificant in the planet's differentiation because, as has been demonstrated for the >100 m thick melt sheets at West Clearwater and Manicouagan, Que.it is a total melt, which crystallizes rapidly due to the huge quantity of cold debris with which it is mixed during crater excavation. However the crust involved in each impact is heated about 200C° which will not raise a rock's temperature from sub-solidus to super-liquidus. The cumulative effect of heating the crust in increments will be partial melting. If the magma rises to the surface as fast as it forms, it will be a partial, not total, melt and will form bodies about the size of the craters. Thus the process of impact-induced partial melting should form huge layered intrusions of basaltic composition, a process compatible with the observed lithologies.

Similar magmatic activity should have occurred on earth during the period of bombardment prior to 3.9 b.y., but more rapidly due to the additional energy from core formation and higher impact velocities causing greater localized heating.

U 3 INVITED PAPER

INFERENCES ABOUT THE EVOLUTION OF THE CONTINENTAL CRUST AND ITS SOURCES

G. J. Wasserburg (Lunatic Asylum, Div. of Geol. and Planet. Sci., Caltech, Pasadena, CA 91125)
S. B. Jacobsen

Inferences may be drawn about crustal evolution and mantle structure from the observed regularities in initial isotopic composition of Nd and Pb in crustal rocks through geologic time and the modern values of the isotopic composition of Nd, Sr and Pb in oceanic flood basalts. The continents are ancient heterogeneous bodies preserving rocks of up to ~3.8 AE while the oceanic crust is young. The young age and uniform isotopic composition of oceanic crust suggests that its isotopic character is representative of large volumes of the oceanic mantle which are convectively mixed on a short time scale. As the oceanic mantle represents the residue from which continental crust was derived the isotopic composition of the present oceanic crust should reflect with fidelity the time average characteristics of the evolution of continental crust over the history of the earth. Simple geochemical models of the growth of continental mass with time by unidirectional flow from the mantle to the crust indicates a relatively young average age of 1.8-1.5 AE for the continents. This is less than 1/2 of the age of the earth and indicates that the first 1 AE of crustal history may have been eradicated by violent early convection and implies that the dominant growth of the atmosphere took place prior to 3.6 AE. A new analysis of models of crustal growth involving crustal refluxing into the mantle have been developed which may also be represented in a simple analytical form. The results of models involving refluxing and unidirectional flow will be compared. Data on continental tholeiitic basalts of Trassic-Jurassic age from the circum Atlantic give $\epsilon_{Nd}(0.2\ AE) \approx -2$ to 0 and show distinctive continental affinities which suggest the existence of undepleted sources or a good mixing of depleted mantle and continental crust to form these magmas. A discussion will be given of the sources of these magmas emplaced in the Pangeatic landmass prior to the time of opening of the Atlantic Ocean.

U 4 INVITED PAPER

FINE STRUCTURE IN THE GEOCHEMICAL MODELING OF CRUST AND MANTLE EVOLUTION

N.M. Evensen (Department of Geology, University of Toronto, Toronto, Ontario M5S 1A1, Canada)

Evidence relating to the complementary evolution of the continental crust and of the mantle from which it was formed can be derived both from geochemical modeling based on the chemical and isotopic record as accessible at present, and from physical constraints arising from the coupling of material transport to the continents with the material transport associated with terrestrial heat loss. Available isotopic systems can provide only limited information about the timing of crustal growth when applied to averaged Earth reservoirs, so additional knowledge must be summoned from more detailed examination of the geologic record and from thermal considerations. A fundamental question is whether the rate of continental growth is basically controlled by kinetics or by a secular shift of equilibrium. The assumption of equilibrium is more predictively powerful and may be realistic for early Earth history but is certainly not fully applicable at present. In any event the geochemical evolution of "tracer" elements is not fully coupled to the growth of continental mass, and consideration of isotopes with differing chemical properties and half-lives is required to resolve the questions. To overcome the above-mentioned limitations of gross geochemical models, recourse must be made to models incorporating finer structure of the continents and mantle. The penalty is that such models embody more parameters and thus require a larger data base to constrain them. The reward is that as analytical geochemistry continues to provide such data, the predictive power of the models extends beyond whole-Earth parameters to a level of detail approaching geologic scales.

These remarks are exemplified by a model of multiple isotope evolution in a heterogenous crust and mantle.

U 5 INVITED PAPER

EXPLORING THE CONTINENTAL BASEMENT, A MAJOR FRONTIER OF MODERN EARTH SCIENCE

Jack Oliver (Dept. of Geological Sciences, Cornell University, Ithaca, New York 14853)
D. Albaugh, R. Allmendinger, C. Ando, J. Brewer, L. Brown, F. Cook, S. Kaufman, G. Long, B.Payne, S. Schilt, D. Steiner (Ithaca, N.Y. 14853)

The historical pattern of development of the science of geology, the current availability of tools for exploration, and the potential for application of new knowledge all imply that the basement rocks of the continents form a major frontier of modern geology. One of the tools, seismic reflection profiling, has now been applied to study of about a dozen sites in the United States under the COCORP project. At each site, profiles typically 50 to several hundred kilometers in length were obtained. Taken together, the results emphasize the heterogeneity and diversity of the crust from site to site and within one site. At some sites, known horizons can be traced from the surface to mid-crustal depths thereby providing a new and powerful means of identifying deep crustal structure. Examples from a number of sites surveyed by COCORP illustrate an emerging view of the crust which offers hope of a new level of understanding of this important part of the earth.

U 6 INVITED PAPER

CRUST-MANTLE INTERACTIONS

W. S. Fyfe (Department of Geology, University of Western Ontario, London, Ontario, N6A 5B7)

Evidence increases for heterogeneous sub-continental mantle. The subduction process provides a mechanism for recharging the mantle with volatile and non-refractory species on a large scale. Two principle processes contribute to crust-mantle mixing; subduction of hydrosphere species (e.g. H_2O, CO_2, S, halogens, Na, K, U) via the spilite reactions and subduction of sediments locked in surface irregularities of the descending lithosphere. This latter process may be related to spreading rate and subduction angle. Lack of meta-pelagic sediments in blue schist belts suggests massive subduction of these and implies significant reduction of the mass of continental crust as the planet cools.

U 7 INVITED PAPER

EARLY EVOLUTION OF RIFTED CONTINENTAL MARGINS

C.E. Keen (Atlantic Geoscience Centre, Geological Survey of Canada, Dartmouth, N.S., Canada)

Comprehensive studies of the deep crustal structure on the rifted margins of Eastern Canada show that the continental crust thins by amounts up to 17 km towards the ocean-continent boundary. The thinning occurs over horizontal distances of several tens to hundreds of kilometers and is perhaps the most striking and ubiquitous feature of crustal profiles across rifted margins. Such crustal thinning probably

occurred as a result of extensional forces during the early development of these margins, perhaps by brittle faulting in the upper crust and flow in the lower crust. This extension process appears to have dominated others, such as volcanism or deep crustal metamorphism, which may also have modified the continental crust during rifting. A simple model of extension in which the amount of extension is estimated from the deep crustal structure, allows the subsidence and sedimentation history, as well as the thermal evolution of the margins to be predicted. The predicted subsidence is in excellent agreement with that obtained from analysis of data in many deep exploratory wells off Eastern Canada. The predicted thermal evolution can be used to determine probable rheological models of the lithosphere which vary both with time and with position across the margins. The paleotemperatures are also useful in estimating whether the sediments, which are potential sources of hydrocarbons, will have undergone a thermal history favourable to the generation of sufficiently mature organic material.

Frontiers of Geophysics

Harbour
Thursday EVE.
L. J. Lanzerotti (Bell Labs.), Presiding

U 8

RADIOISOTOPE DETECTION AND DATING WITH ACCELERATORS

A.E. Litherland (Physics Department, University of Toronto, Canada M5S 1A7
J.C. Rucklidge (Geology Department)

The radioactive isotopes, Be-10, C-14, Al-26, Si-32, Cl-36 and I-129 have been detected at natural levels without prior isotope enrichment by using negative ions, molecular dissociation with tandem accelerators and atom counting. Positive ions and cyclotrons have also been used. Ratios of C-14/C-12 and Cl-36/Cl near 10^{-15} have been reached in measurements being carried out to develop radiocarbon (1) and Cl-36 (2) dating of milligram samples. Recent applications of the new techniques to geochronology, the detection of rare stable isotopes and their potential for the ion microprobe study of minerals will be discussed.

(1) Bennett et al, 1977, Science, 201:345-347

(2) Elmore et al, 1979, Nature, 277:22-25

U 9

EARTH STRUCTURE AND CRUSTAL EVOLUTION MODELS INFERRED FROM NEODYMIUM ISOTOPES

D. J. DePaolo (Dept. of Earth & Space Sciences, UCLA, Los Angeles, CA 90024)

Variations of the natural abundance of ^{143}Nd, the radioactive decay product of ^{147}Sm ($\tau_{\frac{1}{2}}$ = 106 Æ), suggest relatively simple models for the chemical structure of the mantle and the relationship between this structure and the evolution of the continental crust. Because Sm and Nd are cosmochemically refractory elements, the ^{143}Nd abundance in primitive, unfractionated materials in the earth can be estimated. Deviations from this abundance (ε_{Nd}) can result only from isolation of chemically fractionated materials, formed during the earth's internal differentiation, for long times. Modern oceanic basalts have positive ε_{Nd}, consistent with oceanic upper mantle being the complementary residue to the negative-ε_{Nd} continental crust. Material balance indicates that only a small portion of the positive-ε_{Nd} mantle is needed to offset the crust. Continental flood basalts (ε_{Nd}=0) suggest the existence of regions of the mantle which have retained a primitive chemistry. The observations can be explained by a layered mantle structure, with a primitive lower mantle and an upper mantle depleted of crust-components including heat-producing elements. ε_{Nd} values in Precambrian rocks are consistent with semi-continuous growth of the crust over the past ~3.8 Æ. There is no evidence of fractionated reservoirs in the earth prior to 3.8 Æ, implying either an undifferentiated early earth or rapid mixing. This contrasts with the moon, where analogous data indicate a layered mantle dating from 4.5 Æ ago. ε_{Nd} in oceanic basalts correlates with $^{87}Sr/^{86}Sr$. The correlation trend confirms the alkali-depletion in the earth and provides a baseline for studies of magma contamination by crustal materials and ocean water. ε_{Nd} of crustal rocks can be related to the time the crust was formed from the mantle and may allow better estimation of the age of the crust.

Geophysics of the Great Lakes

Metropolitan East
Monday P.M.
Ronald C. Taylor (National Science Foundation), Presiding

U 10 INVITED PAPER

THE GREAT LAKES: A BRIEF INTRODUCTION

Ronald C. Taylor (Meteorology Program, National Science Foundation, Washington D.C. 20550)

Other speakers will address a variety of scientific questions about the Lakes (in the All-Union Session) but I will attempt to provide some historical and cultural background. This might include early exploration, the antiquity of settled communities, a silly war on Lake Erie, and what Oscar Wilde thought of Niagra Falls. The latter two topics permit some scope for humor, an opportunity which will not be resisted when appropriate.

U 11 INVITED PAPER

METEOROLOGICAL AND CLIMATOLOGICAL FEATURES OF THE GREAT LAKES

Val Eichenlaub (Department of Geography Western Michigan University, Kalamazoo, Michigan 49008

As the Great Lakes heat and cool more slowly than surrounding areas, and provide water rather than land interfaces to the boundary layer, an array of meteorological and climatological modifications, collectively known as "lake effects," results. These may be classified as either "stable" (warm season) effects or "unstable" (cold season) effects. The mean seasonal progression of lake vs land surface temperatures is examined, and mean duration and intensity of "stable" and "unstable" lake effects are than surveyed with particular emphasis on lake effect snow, probably the most salient of all lake-induced climatic features.

U 12 INVITED PAPER

THE GREAT LAKES AS WIND DRIVEN OSCILLATORS

Clifford H. Mortimer (Center for Great Lakes Studies, University of Wisconsin, Milwaukee, Wisconsin 53201

Responses of large lakes and inland seas to wind impulses cover a wide range of scales in space and time. Some depend upon the presence of density stratification within the water body; some do not. Illustrations will be given, paying particular attention to those responses which exert a controlling influence on circulation, diffusion, and ecosystem dynamics.

U 13 INVITED PAPER

THE HYDROLOGY OF THE GREAT LAKES

Frank H. Quinn (Great Lakes Environmental Research Laboratory, Ann Arbor, Michigan 48104

The Laurention Great Lakes represent a unique hydrologic system encompassing the five Great Lakes, Lake St. Clair, and their connecting channels. The system drains a basin of more than 764,000 square kilometers of which approximately 246,000 square kilometers, or thirty-two percent of the area, is covered by the Great Lakes. The hydrologic regime of the system is influenced by many unique features including differential isostatic rebound from the last glaciers, a large degree of natural regulation, and the formation of a variable ice cover lasting three to four months each year with the southernmost lake having the greatest ice extent. The hydrologic variables with the greatest interest are the individual lake levels and the flows in the connecting channels. The lake levels integrate the precipitation, runoff, and evaporation components of the hydrologic cycle as well as reflect man's changes to the connecting channels and the regulation of Lakes Superior and Ontario. While the maximum hydrologic scale water level fluctuations have been within a range of six to eight feet, even relatively small changes in levels are important becuase of the multi-purpose use of the lakes for navigation, hydropower, and recreation. This presentation will examine the components of the hydrologic cycle and their impact upon the water levels and describe the transport of water through the system to the ocean. The factors influencing the formation, growth, and decay of the Great Lakes ice cover are also described with a perspective supplied by a recently developed winter severity index based upon the past 80 Great Lakes winters.

U14 INVITED PAPER

GREAT LAKES SEDIMENTATION: PAST STUDIES, PRESENT WORK AND FUTURE DIRECTIONS

David K. Rea (Oceanography Program, Dept. of Atmospheric and Oceanic Science, Univ. of Michigan, Ann Arbor, Mi. 48109)

Sediments now on the floors of the Great Lakes somehow record the hydrological and climatological history of central North America since the Wisconsin-aged glaciers began to retreat about 15,000 years ago. Since that time lake levels have been both higher and lower than at present, a history tied to glacial retreat and the ensuing isostatic rebound of depressed lake outlets. Scattered studies on the bottom sediments of the Great Lakes began in the 1920's. The pioneering work of Hough from the mid 1930's to the early 1960's lead to a general understanding of the physical stratigraphy of Lakes Huron and Michigan which like the others are characterized by a sequence of post-glacial muds overlying periglacial clays and tills. In 1961 and 1962 the D/V Submarex recovered a series of drillcores from Lake Superior which formed the basis for the first detailed stratigraphy of any of the Great Lakes. During the last decade work completed at the Canada Centre for Inland Waters has resulted in a number papers on sedimentation in Lakes Ontario, Erie and Huron, and the Illinois State Geological Survey has produced a large amount of work on Lake Michigan sediments. Present efforts at these locations and at the Universities of Wisconsin, Minnesota and Michigan are working toward a more detailed understanding of lake-floor stratigraphy and thus improved interpretation of lacustrine history. Ongoing studies of modern sedimentary processes in the Great Lakes are being coordinated by the NOAA Great Lakes Environmental Research Laboratory and by the Argonne National Laboratory. Future research on lacustrine physical sedimentation appears to be heading in two promising directions: first, filling in the details of the Late Pleistocene and Holocene paleolimnology; and second, participating in larger, cooperative efforts with chemists and biologists to approach many of todays environmental problems.

Frontiers of Geophysics

Metropolitan East and Centre
Monday EVE.
L. J. Lanzerotti (Bell Labs.), Presiding

U 15 INVITED PAPER

A SUBMERSIBLE VIEW OF ACTIVE RIFT-TRANSFORM TECTONICS ALONG THE EASTERN GALAPAGOS RIDGE

A. Malahoff
R. Embley (Both at: National Ocean Survey, NOAA, Cx4, Rockville, MD. 20852)
D. Fornari (Dept. Geol. Sci., SUNY, Albany)
W. Ryan (Lamont-Doherty Geol. Obs.)

The Galapagos Ridge terminates abruptly at 85° 23'W along a N-S striking fracture zone. Surface ship and bottom transponder controlled camera tows as well as visual observations from the DSRV ALVIN using both video and still camera were used to study this area. A detailed multi-beam surveying bathymetric net was used as a base to develop a volcanic and tectonic view of the interaction between the ridge and the fracture zone. Detailed studies of the crest and flanks of the Galapagos Ridge between 86°05'W and 85°22' were carried out during the nine dive expedition show a predominance of a tectonic over volcanic activity to the east. Activity along the crest of the ridge takes place between depths of 2500-2600 m in the form of a series of volcanic centers characterized by a median rift valley frequently filled with fresh pillow lavas and dissected by anastomatosing fissures. The median rift valley narrows eastward. The Galapagos rift terminates at 85°23'W, where the E-W lineation observed along the axis of the rift change sharply into the N-S lineations of the fracture zone. Actively faulted scarps up to 100 m in height are observed along a 500 meter wide plate boundary of the fracture zone. Extensive sulfide mineralization in the form of stacks, is present along the lateral faults of the rift valley and MnO mineralization along segments of the fracture zone, were no current volcanism was observed. The boundary between the fracture zone and the rift is very sharply defined and simple in its tectonic pattern. The observed tectonic fabric of the eastern end of the Galapagos rift serves as a model for other segments of the worlds submarine rift system with medium spreading rates of about 7 cm/yr that are offset by fracture zones.

U 16 INVITED PAPER

TECTONICS OF VENUS

James W. Head III (Brown University Providence, R. I.)

Geodesy

Altimetric and Gravimetric Results

Pier 4
Friday A.M.
E. A. Flinn (NASA Headquarters), Presiding

G 1 INVITED PAPER

RESULTS FROM THE SEASAT-I ALTIMETER/ORBIT DETERMINATION EXPERIMENT

B.D. Tapley (Dept. of Aerospace Engineering and Engineering Mechanics, The University of Texas at Austin, Austin, TX 78712)

The objectives of the SEASAT-I Altimeter/Orbit Determination Experiment Team are: (1) to assess the accuracy of the sensor measurements of h, the altitude of the spacecraft above the sea surface, $h_{1/3}$, the sea-state as measured by the average height of the highest 1/3 of the waves and σ, the sea surface back scatter coefficient or the ratio of the reflected to the incident power; (2) to determine the ability of the SEASAT-I data set to perform the task of global monitoring of wave height, global mapping of the ocean geoid, precise measurement of the sea surface topography to detect currents, tides and storm surges, to locate and map the ocean current patterns; and (3) to assess the accuracy with which the SEASAT-I satellite ephemeris can be determined and to define and develop the associated methodology to improve the ephemeris.

This presentation describes: the data set gathered during the SEASAT-I mission, an assessment of the data quality, the orbit and geophysical correction accuracies, and the plans for distributing the global altimeter data set.

G 2

TERRAIN HEIGHT ESTIMATION USING GEOS-3 ALTIMETER OVERLAND DATA

R.F. Brammer
D.W. Capp (The Analytic Sciences Corp., Six Jacob Way, Reading, MA 01867)

This paper presents results of a study being conducted to assess the accuracy with which terrain heights can be estimated using GEOS-3 altimeter data. The terrain height estimates derived from processing the GEOS-3 data have been compared to high resolution elevation data in Florida and in the Maryland-Virginia-Washington, D.C. area.

The results to be presented include a description of the terrain height estimation procedure, the optimal data smoother, and an analysis of the differences between the sets of surface and satellite-derived estimated elevations. The estimates show general agreement to within an rms of 1m - 5m.

G 3

COMPARISON OF GEOS-3 AND SEASAT ALTIMETER OVERLAND TRACKING

Ronald L. Brooks*(GeoScience Research Corp., Rt. 4 Box 129, Salisbury, MD 21801)
William B. Krabill (NASA Wallops Flight Center, Wallops Island, VA 23337)
Patricia D. Gaborski (NOAA National Ocean Survey, Rockville, MD 20852)
James Wm. Schoonmaker, Jr. (USGS Topographic Division, Reston, VA 22092)

GEOS-3 and Seasat overland altimeter measurements have been compared over areas of similar terrain in the San Joaquin Valley of California and in the Houston-Galveston area of Texas. It is observed that the Seasat altimeter height waveform processor, successfully customized for open-ocean tracking, introduces overland ranging errors as large as 5 m, due to surface specularity and changes in surface slope. The effects of specular returns on the Seasat measurements have been further evaluated over the Salar de Uyuni of southern Bolivia, the Earth's largest flat salt-covered area. The effects of surface slope changes have been examined over the Phoenix-Tucson area of Arizona. Initial attempts at retracking the Seasat overland waveforms have been successful, demonstrating the potential for achieving 10 cm overland tracking precision, compared with the observed GEOS-3 altimeter precision of about 40 cm overland.

G 4

ANALYSIS OF GEOS-3 ALTIMETRY IN HUDSON BAY

D. Delikaraoglou (Department of Surveying Engineering, University of New Brunswick, Fredericton, N.B.
D.E. Wells (Bedford Institute of Oceanography, P.O. Box 1006, Dartmouth, N.S.)
P. Vanicek (Sponsor)

In connection with the GEOS-3 satellite program, a Canadian experiment has been conducted in the Hudson Bay in order to compute tides and the sea level from altimetry data.

GEOS-3 radar altimetry data was collected from September to December 1976, during which NASA tracking was supplemented with Doppler satellite tracking from five local tracking stations. The combination of the GEOS-3 altimetry with precise orbital information derived from the Doppler data has permitted the computation of the sea surface in the Hudson Bay to submeter accuracy.

In this paper the method of computation of the sea surface will be presented, and the features of the resulting sea surface will be compared with known geoidal features.

G 5

MULTIPLE-TRACK MATCHED FILTERING FOR FEATURE EXTRACTION FROM ALTIMETER DATA

A.R. LeSchack
J.V. White
R.V. Sailor (The Analytic Sciences Corp., Six Jacob Way, Reading, MA 01867)

A previous study on the design of optimal matched filters for detection of bathymetric features from single tracks of satellite altimeter data is extended to the analysis of nearly coincident multiple subtracks, with particular application to the three-day-repeat portion of the SEASAT mission. The advantages of multitrack filtering are most apparent in the detection and localization of short-wavelength (< 100 km) features. Computed detection probabilities and false-alarm characteristics are presented, together with test results obtained from multitrack SEASAT data by the use of optimal filters matched to the predicted geoid signatures of several kinds of bathymetric features.

G 6

COMPARISON OF METHODS FOR DETECTING MESOSCALE OCEANOGRAPHIC FEATURES IN ALTIMETER DATA

Sailor, R.V.
LeSchack, A.R.
White, J.V. (The Analytic Sciences Corp., Six Jacob Way, Reading, MA 01867)

Previous studies have used GEOS-3 and SEASAT data to demonstrate that mesoscale (> 100 km) oceanographic features, such as the Gulf Stream and its associated eddy systems, can be resolved by satellite altimeters. However, these studies also showed that it is difficult to identify specific oceanographic features without the aid of surface truth data and/or a detailed reference geoid.

This paper reviews and compares several methods for extracting information about oceanographic features. The methods discussed here do not require a detailed a priori knowledge of the geoid, but use only the information customarily supplied with the altimetry, or depth information from a bathymetric data set. The following methods are discussed: 1) differencing of altimeter observations along repeat tracks; 2) bandpass or highpass filtering of the altimetry data; 3) subtraction of undulation data supplied with the altimetry (e.g. the GEM-10B undulations provided with SEASAT); 4) matched filtering of the altimetry data; 5) predicting undulations in the wavelength band of interest from a bathymetry data base and subtracting them from the altimetry data. These methods were tested with SEASAT data obtained from tracks crossing the Gulf Stream and associated eddies.

G 7

SEASAT-1 SATELLITE ALTIMETER OBSERVATIONS IN THE DETERMINATION OF A MEAN ELLIPSOID

G. B. West (Naval Surface Weapons Center, Dahlgren, Virginia 22448)

The radius and the origin of a mean ellipsoid have been determined from SEASAT-1 satellite radar altimeter observations of the ocean surface. Assuming that the altimetric geoid is the best available, adjustments are made to the ellipsoid which the DOD WGS-72 geoid heights are referenced to so that the average geoid height difference is a minimum. A least squares fitting procedure based on mean geoid heights in 5° squares is used in the determination of the ellipsoidal

parameters. The SEASAT-1 radar altimetric observations of the ocean surface were averaged to two points per second and taken from two sets of SEASAT-1 satellite tracks; one set consisted of 11 days selected from the time period day 207 to 225 and the other set contained 12 days taken from the time period day 211 to 239 with each set weighted by the number of observations in each square. In order to evaluate the consistency of results three solutions were made, one for each of the two data sets using DOD WGS-72 as the reference geoid and one for the first data set using the GEM10B as the reference ellipsoid. Solution one contained 910,074 altimetric data points and gave Δx=.1m, Δy=-.2m, and Δz=.2m as changes in the origin and a corresponding ellipsoid radius of 6378134.7m. Results from the remaining two solutions were consistent with those given here.

G 8

WHY THE EARTH'S GREATEST GEOID ANOMALY IS SO NEGATIVE

C. O. Bowin (Woods Hole Oceanographic Institution, Woods Hole, MA 02543

A technique and procedure is developed using spherical harmonic coefficients for identifying the principal harmonic contributions to individual potential field features. It is seen that the major GEM9 geoid anomalies of the earth have significantly different contributions from the various harmonics; and a degree 10 geoid is determined to be the best choice for providing a smoothed representation of the major global geoid anomalies. It is shown that the coefficients for each spherical harmonic degree have an associated maximum source depth. The higher the degree, the shallower the source depth. The Sri Lanka geoid low (-104m), the New Guinea high (+74m), the low south of New Zealand (-59m), and the central Asia low (-56m) all have large contributions from the harmonics of degree 2 and 3. The degree 3 contribution is demonstrated most likely to be the result of mass anomalies at the core-mantle interface. Only 0.2 to 3km of relief of the core-mantle boundary is required to explain the degree 3 geoid and gravity anomalies. The Sri Lanka low is the greatest geoid anomaly because it has the best spacial coincidence of peak anomalies from deep and shallow sources.

The ratio of peak gravity to geoid anomaly values provides estimates of the maximum depth to the anomalous mass. Using that depth estimate, the magnitude of either the gravity or geoid anomaly then provides an estimate of the magnitude of the anomalous mass. By subtracting the degree 3 geoid map from the degree 10 geoid a geoid map is obtained that, for the first time, demonstrates a good correlation of plate convergent zones with narrow continuous belts of positive geoid anomalies.

G 9

ADJUSTMENT OF LA COSTE AND ROMBERG GRAVIMETER OBSERVATIONS

M. M. Chin (National Geodetic Survey, National Ocean Survey, NOAA, Rockville, Maryland 20852)

(Sponsor: Charles R. Schwarz)

In this newly developed gravity adjustment system, the observation equation uses the dial reading, in milligals, as the observable quantity. Neither the gravity observation difference between the two stations nor the gravity observation itself is used. Scale factors, drift rates, intervals (tare corrections), and gravity values are the unknown parameters. Because this is a nonlinear model, the Newton-Gauss iteration procedure is used. Gross data errors are examined in the first iteration. By using the software package developed by the National Ocean Survey/NGS for processing large sparse normal equations, the size of the network that a system can handle is constrained only by hardware limitations. By partitioning the equations, very large networks can be processed in relatively small computer storage.

G 10

ANALYSIS AND SIMULATION OF MULTISENSOR SURVEYS OF THE GRAVITY FIELD

J.D. Goldstein
S.L. Baumgartner (The Analytic Sciences Corp., Six Jacob Way, Reading, MA 01867)

A technique for determining the residual errors in the estimation of gravity anomalies and deflections of the vertical from multisensor survey data has been developed. Survey alternatives include combinations of satellite radar altimetry satellite-to-satellite tracking, gravimetry, and airborne gradiometry. The method is based on Fourier analysis and yields the average power spectral density of the residuals. A brief description of the method and some examples of the results obtained are presented.

G 11

AMPLIFICATION OF LONG WAVELENGTH GRAVITY AND GEOID ANOMALIES

W. F. Haxby (Lamont-Doherty Geological Observatory of Columbia University, Palisades, New York 10964)
(Sponsor: J. R. Cochran)

The equilibrium configuration of density boundaries within a radially stratified, self-gravitating spheriod conforms to surfaces of constant gravitational potential. In the presence of a gravitational perturbation due to an inhomogeneous mass distribution, equipotential surfaces will be distorted, causing a deformation of the density boundaries. This deformation constitutes a secondary mass heterogeneity, and thus the gravity field will be modified. In the earth, where the density decreases with increasing radius, the distortion of equipotential surfaces generally results in an amplification of the anomalous field. At very short wavelengths, the amplification of gravity and geoid anomalies is very small and may be ignored in modelling studies. At wavelengths greater than 5000 km (spherical harmonic degree, L, less than about 8), however, the primary field due to the initial mass distribution is significantly modified by the amplification effect. In the case of a sphere of constant density any harmonic potential perturbation on the surface of the sphere will be amplified by the factor $(2L+1)/(2L-2)$. For the earth, the amplification factor varies with the depth and configuration of the initial mass distribution. Because the amplification factor varies with harmonic degree, the gravitational power spectrum due to a given mass distribution will be considerably modified. The amplification spectrum for surface source and dipole distributions are given as a function of the surface radius. The geoid anomalies due to buried point and dipole sources will be shown as an example.

G 12

OPTIMAL DENSIFICATION OF DEFLECTIONS OF THE VERTICAL BY MEANS OF ASTROGEODETIC AND GRAVITY ANOMALY DATA

H. Baussus von Luetzow (U.S. Army Engineer Topographic Laboratories, Fort Belvoir, VA 22060)

The method of astrogeodetic leveling, developed by Molodenskii et al, is mofified to permit optimal densification of deflections of the vertical from suitably spaced astrogeodetic and gravity anomaly data by consistent statistical collocation. In this way, error estimation is simultaneously possible. It is further shown that the modified method of deflection estimation with or without consideration of measurement errors is potentially useful in connection with performance tests of advanced inertial systems and gravity gradiometers.

G 13

LOW ORDER POLYNOMIAL APPROXIMATIONS FOR THE VERTICAL GRADIENT OF GRAVITY FOR A REFERENCE ELLIPSOID

Dr. D. Nagy, Department of Energy, Mines & Resources, Earth Physics Branch, Ottawa, Canada, K1A 0Y3
(Sponsor: L. W. Sobczak)

From the expression given by Helmert for the vertical gradient:

$$\frac{\partial g}{\partial n} = -g\left(\frac{1}{M} + \frac{1}{N}\right) - 2\omega^2,$$

low order polynomial approximations are derived which use only the four basic arithmetic operations for speedy evaluation of the vertical gradient of gravity without any loss in accuracy. The polynomial representation is necessary with most commercial data base management systems, for example, which allow only the basic arithmetic operations and provide limited core space for computations. Approximations suitable for various applications, from the well known constant of 0.3086 mGal/m to expressions yielding μGal accuracy for the highest land elevation, are easily derived using this approach. The parameters of these approximations are expressed in terms of the fundamental constants of an ellipsoidal reference surface. Numerical values calculated from some of these approximations indicate that in the context of modern gravimetry, greater attention must be given to the selection of the technique used to compute the vertical gradient.

G 14

SHOULD 5° MEAN ANOMALIES BE USED IN COMBINATION SOLUTIONS FOR THE EARTH'S GRAVITY FIELD?

Richard H. Rapp (Department of Geodetic Science, The Ohio State University, Columbus, Ohio 43210)

Higher degree potential coefficient solutions have usually been carried out using 5° mean anomalies. However the use of such large blocks can alias the coefficients found from such solutions at all degrees. Solutions for potential coefficients have been made for the study reported here using 64800 1°x 1° anomalies and 1654 5° equal area anomalies derived from these 1°x 1° anomalies. Potential coefficients were derived from each set of anomalies and compared. For degrees 2 to 12, the average percentage difference between the coefficient sets was 5%; between degrees 13 to 24, 22%, and between degrees 25 to 36, 56%. The overall undulation difference between these potential coefficient sets (degrees 2-36) was ±1.17 m. Similar results at the higher degrees were found in combination solutions with the GEM 9 potential coefficients. These studies suggest that future combination solutions should be made with 1° data instead of 5° data when the highest accuracy is desired.

G 15

THE INVERSE PROBLEM OF CONSTRUCTING A GRAVIMETRIC GEOID

V. Zlotnicki (Dept. of Earth and Planetary Sciences, Massachusetts Institute of Technology, Cambridge, MA 02139, and Dept. of Geology and Geophysics, Woods Hole Oceanographic Institution, Woods Hole, MA 02543)
B. Parsons (Dept. of Earth and Planetary Sciences, Massachusetts Institute of Technology, Cambridge, MA 02139)

Instead of computing geoidal heights from incomplete sets of gravity data through the widely used Stokes integral, the problem is analyzed as an underdetermined system of equations. Each gravity value is the result of integrating the geoid times a given kernel.

This approach defines precisely which length scales in the harmonic expansion of the geoid are well resolved by any particular data set. It is shown how to use the method on any distribution of data.

A computational procedure is given, based on a spectral expansion in the eigenfunctions of the kernel operator which span the model space. Examples are presented, first on a simplified one dimensional geometry to show the essential elements of the problem, and then on a more suitable spherical geometry.

Classical Geodesy

Pier 4
Friday P.M.
Klaus Peter Schwarz (Division of Survey Engineering), Presiding

G 16 INVITED PAPER

CLASSICAL HORIZONTAL POSITIONING

John G. Gergen (National Geodetic Survey, National Ocean Survey (NOS), NOAA, Rockville, MD 20852)

The North American Continent is covered by horizontal geodetic networks from the Northwest Territories of Canada to the southern latidues of the Central American Republics. Throughout the past 150 years, several hundred thousand points have been surveyed with various instruments and precision. The New Adjustment of the North American Datum project has as its objective the recomputation of all geodetic positions, in order to eliminate all distortions which presently exist in the network. New instruments and techniques have allowed significant progress to be made during the last decade. Doppler satellite measurements finally give positions directly without the need for auxiliary measurements. Although modern positioning techniques will be radically different from classical ones, precision surveys are still required for the monitoring of crustal motion and other engineering surveys.

G 17 INVITED PAPER

VERTICAL POSITIONING - THE STATE OF THE ART

Petr Vaníček, (Dept. Surveying Engineering, U.N.B. Fredericton, N.B.)

The paper shows the various ways heights can be defined (referred to the geoid, quasigeoid, or a reference ellipsoid) and determined (through geodetic levelling, vertical angles or 3-D positions), and what are the advantages/disadvantages of the individual definitions. The expose is then focused on levelled heights, and their transformation into dynamic, orthometric and normal heights. Next, the problems associated with heights obtained from levelling (second order refraction, crustal stability, datum uncertainty and statistical dependence) are addressed. Finally, the status of North American levelling networks is discussed and aims of the Redefinition of North American Vertical Networks are explained.

G 18

TIME EFFECTS IN THE RESETTING OF REMANENCE IN CONTACT AUREOLES.

E. McClelland Brown Department of Earth Sciences, University of Leeds, England.

The 'resetting temperature' (T_R) is the maximum blocking temperature thermally rest in a host rock heated by an igneous intrusion. This is lower than the laboratory unblocking temperature (T_{BL}) at which all the thermally reset remanence is removed in an experiment which takes place over a significantly shorter time than the natural reheating event. The host rock experiences a thermal pulse of magnitude T_R as the heat from the intrusion is distributed. The effect of this changing temperature is theoretically predicted to be equivalent to that of a square pulse of height T_R and width θ_p, the thermal pulse width. Relationships between T_R and T_{BL} have been calculated for various sizes of thermal pulse.

Experimentally determined laboratory unblocking temperature profiles from contact zones of Tertiary dykes are compared with maximum temperature (T_R) profiles obtained from heat flow calculations. These are identical at the Curie temperature of the remanence carrier as unblocking is due to randomization of atomic moments. At decreasing temperatures T_{BL} becomes increasingly larger than the calculated peak temperature as time effects increase. Experimentally determined differences between T_{BL} and T_R are compared with theoretically predicted differences and the agreement is good.

G 19

GEODETIC LEVELING AND CRUSTAL MOVEMENT IN THE U.S. PART II, NON-TECTONIC INFLUENCES

S.C. Chi, R.E. Reilinger, L.D. Brown, and G.A. Jurkowski (Dept. of Geological Sciences, Cornell University, Ithaca, N.Y. 14853)

Estimates of crustal movement provided by leveling observations may reflect tectonic deformation, near-surface non-tectonic motions, or artifacts generated by systematic measurement errors. Effective use of this technique for geodynamic purposes requires that the latter two not be misidentified as tectonic activity. Surficial movements and systematic errors have been familiar to geodesists, but the extent to which they distort or mask estimates of deep-seated movement has only recently been fully appreciated. Near-surface movements may result from sediment compaction due to fluid withdrawal (water, oil, gas), imposition of man-made loads (reservoir impoundment, building construction), variations in soil moisture and temperature causing swelling of surficial deposits, surface failure (landslides, mining activity, karst collapse), and frost heave, among other processes. Subsidence due to fluid withdrawal, well-known in the Gulf Coast, southern Arizona, and California, appears to be more pervasive and sometimes more subtle than commonly realized. Surficial movement of this type can often be identified by its close relationship with water level changes monitored in wells. Unlike fluid withdrawal and reservoir loading (relatively easy to identify), which can affect large areas ($\sim 100^2$km), other varieties of surficial instability tend to have very local effect. Systematic leveling errors, often more difficult to confirm, are suggested by unrealistically close correlations between elevation change and topography, disagreements between leveling and mareograph measurements along the coasts, and internal inconsistencies in leveling circuits. Detailed examination of movement estimates derived from NGS leveling provides numerous examples of the above and suggests practical criteria for their identification.

G 20

GEODETIC LEVELING AND CRUSTAL MOVEMENT IN THE U.S. PART III, TECTONIC DEFORMATION

R.E. Reilinger, L.D. Brown, and G.A. Jurkowski (all at: Dept. of Geological Sciences, Cornell University, Ithaca, N.Y. 14853)

Many U.S. releveling observations have been convincingly related to known tectonic phenomena. The clearest examples are coseismic and postseismic movements in the vicinity of dip-slip earthquakes (e.g., 1954 Dixie Valley, Nevada; 1964 Alaska). Such movements are often large (coseismic movements reaching a few meters) and/or closely associated with earthquake faults. Evidence for preseismic deformation is more limited due at least in part to paucity of data; examples being the 1959 Hebgen Lake, Montana and the 1971 San Fernando, California earthquakes. Detection of more subtle earth movements ($\Delta h \sim$ few cm; $\Delta V \sim$ few mm/yr) with geodetic leveling is illustrated by deformation in the Rio Grande rift which has been related to crustal magmatic activity. The validity of these movements is supported by independent geologic and geophysical observations and the internal consistency of multiple releveling data. Isostatic processes have been suggested for observed movements near Pleistocene Lake Bonneville and near the Mississippi delta. Active tilting of the Pacific northwest coast has been related to aseismic subduction. In contrast, some apparently significant elevation changes are difficult to relate to plausible driving mechanisms, particularly in the intraplate U.S. Such apparent movements commonly correlate with geologic structure and/or with geomorphic features (e.g., uplift of the Adirondacks and the Southern Appalachians), but the possibility that other than tectonic effects are the sources of the observations is not completely eliminated.

G 21

THE APPLICATION OF LAKE CHAMPLAIN WATER LEVEL STUDIES TO THE INVESTIGATION OF ADIRONDACK AND LAKE CHAMPLAIN CRUSTAL MOVEMENTS

BARNETT, Stockton, G., Department of Earth Sciences, State University of New York, Plattsburgh, New York 12901 and ISACHSEN, Yngvar W., N.Y. Geological Survey, Albany, New York 12230.

Releveled lines along the eastern flank of the Adirondack Mountains and across the central part of the dome suggest that the region is undergoing contemporary uplift (Isachsen, 1975, 1976); the line along the eastern flank suggests that the northern end of Lake Champlain is sinking at a rate of 4.0 mm/yr with respect to the southern end.

Lake Champlain, which borders the northern three-quarters of the eastern line, and has a demonstrably stable lake-level guage at each end, provides a perfect "natural level" to further refine interpretations of the region's neotectonics.

Apparent vertical movement between these guages indicated that the northern end of the lake is rising 0.7 mm/yr with respect to the southern end. This movement is opposite to that suggested by the releveling survey along the west side of the Lake.

The apparent disparity between results of the two methods may be reconciled if, recognizing that the releveling profile indicates only relative movement, one uses the lake level data to "calibrate" the releveling profile; the water level guaging profile may be superimposed on the releveling profile by drawing a line between Whitehall and Rouses Point, with an upward slope of 0.7 mm/yr to the north. The resulting profile suggests that during the 18 year interval 1955-1973 the region from Willsboro north to Rouses Point remained essentially stationary, whereas that between Whitehall and Willsboro underwent an arching of 2 mm/yr. This uparched area corresponds with the more elevated and breached part of the dome, suggesting that the present arching along the eastern Adirondacks is the continuation of more prolonged neotectonic uplift.

G 22

SPATIAL COHERENCE OF TILT FROM ONE HOUR TO ONE YEAR

G.H. Cabaniss (Air Force Geophysics Laboratory, Hanscom Air Force Base, Bedford, MA 01731)

Attempts have been made over the past ten years to improve the coherence of earth tilt measurements from instruments separated by reasonable horizontal distances. We have deployed borehole tiltmeters of four different designs in (a) three 20m uncased holes in bedrock, partially waterfilled, (b) two 5m holes cased through 4m of overburden, also partially waterfilled, (c) three 120m cased holes 100m into bedrock, and (d) three 3m cased holes in soil. Over the period range of 1-11 hours, effects associated with rainfall, pressure fluctuations, and the convective overturn of water dominate. Coherence is low and non-stationary. In the semidiurnal tidal band, the data from instruments deployed in bedrock are consistent to within several percent; those in soil are not because of both active and passive time-varying noise. Little power is present in the inter-tidal band, except at shallow depths, where it is incoherent. The diurnal tidal constants are unstable from all but the deep instruments because of thermoelastic distortions of the earth-tiltmeter system and direct temperature effects on some of the electronics. Between one day and one year the spectra are characterized by incoherent red noise, due primarily to instrument drift, with few features except those associated with the passage of frontal storms. The fortnightly tide can be extracted reliably from only the deepest instruments. All spectra except those from the latter exhibit strong, incoherent noise peaks centered at one year. In the cluster at 20m, for example, this appears to be the result of both the penetration of the annual temperature wave and seasonal groundwater circulation. Future improvements are likely to come from long-base instruments and better coupling to the earth.

G 23

THE LOS ANGELES AQUEDUCT AS A LONG BASELINE TILTMETER

P.C. Leary, P.E. Malin, R.A. Strelitz (All at: Department of Geological Sciences, University of Southern California, Los Angeles, CA 90007)

Part of the Los Angeles Aqueduct system consists of an open channel 10 feet square which carries water 110 miles from the Owens Valley to a reservoir near Palmdale. The open channel course crosses, then parallels the Garlock Fault, crosses the western Mojave, and parallels the San Andreas Fault for 10 miles.

As part of aqueduct operations, water levels

in the channel are measured to ± .01 foot daily or weekly at 26 stations. We have examined 24 months of such data and found numerous instances of systematic variations on time scales of weeks to months. Two variations correlate with other geophysical data:

i) Between October, 1978 and March, 1979, a .5 foot water level change appeared at seven stations south of the town of Mojave compared with stations to the north. Interpreted as regional tilt, simple hydraulics of open channels indicates a tilt of the western Mojave block down to the south with magnitude 20-30 microradians. This agrees in time and sense with USGS leveling data between Los Angeles and the San Andreas-Garlock fault junction.

ii) Two stations near a small fault in the Mojave block changed readings between .2 and .5 feet in the three days prior to the 6.0 Goat Mountain earthquake 125 miles to the southeast. All other stations remained unchanged.

As yet uninterpreted water level data extends back to 1969. We should be able to examine this data for evidence of the Palmdale Uplift and the 1971 San Fernando earthquake.

G 24

INVESTIGATION OF THE SIGNIFICANCE IN INCREMENTAL STRAIN VALUES NEAR PALMDALE, CALIFORNIA.

F.K. Brunner,
R. Coleman,
B. Hirsch (all at: Dept. of Geodesy, University of New South Wales, Sydney, 2033, Australia).

Repeated geodetic measurements are widely used for the determination of crustal strain rates. It has been shown previously by the authors that conventional strain analysis techniques using observation differences and an approach using the inner coordinates of a geodetic network yield identical results under certain conditions. However, the main advantages of the inner coordinate approach are that non-repeated observations can be utilised, and that different deformation models can be investigated. The computed strain should be subjected to stringent statistical tests on the basis of the observation precision and the overall deformation budget. Such a test procedure is outlined in the paper.

Field data from the SE-Palmdale network in California is the basis for a practical strain analysis, with triangulation data available for the years 1938 and 1958 and trilateration data at one year intervals from 1971 to date. Three strain models, i.e. homogeneous strain, rigid block motion and a simple surface displacement model for a fault, are used in the analysis. The strain accumulation and the strain rates are calculated and tested for significance. A continuous, although small, strain accumulation over the last forty years appears to be evident from this data set.

G 25

STRAIN ESTIMATES FROM REPEATED SURVEYS OF MICROGEODETIC NETWORKS

G.F. Margrave (Dept. of Physics, University of Alberta, Edmonton, Alberta, Canada T6G 2J1)
E. Nyland (presently at I.G.P.P., Univ. of California, La Jolla, Calif.92093)

Surveys of microgeodetic networks (apertures of a few kilometers or less) using relatively simple, inexpensive commercially available equipment are capable of measuring earth strains of 2×10^{-6} or greater. Use of such networks for strain measurements offers many practical advantages over larger networks. Trilateration alone achieves virtually the same precision as combined trilateration and triangulation with the expenditure of significantly less time and energy. Strain determinations can be made by estimating coefficients in low order polynomial expansions of the strain in the network. The technique uses the theory of generalized inverses for rectangular matrices to estimate polynomial coefficients.

This method is used to investigate the resolution of microgeodetic networks using a comprehensive suite of synthetic data. Real data from a network in Peru shows that a shear strain event of -3 microstrains occurred within this network during the period 1975-1976. A further shear strain event of +3 microstrains occurred during 1976-1978 possibly as a response to the first.

G 26

A STUDY OF THE EFFECT OF INDIVIDUAL OBSERVATIONS IN HORIZONTAL GEODETIC NETWORK

K. Thapa (Dept. of Surveying Engineering, University of New Brunswick, Box 4400, Fredericton, Canada E3B 5A3)
P. Vanicek

ABSTRACT

The concept of strain is explained and the application of strain ellipses and average differential rotations to study the compatibility of observations in a geodetic network is outlined. By examining the size of the computer plotted strain ellipses and average differential rotations one can see the consistency of the individual observations with the rest of the network.

The impacts of change in distances, azimuths and introduction of satellite determined positions on the network are given. Moreover, the effect of a piece-wise adjustment and the consequence of the selection of weights of observations are analysed. Furthermore, the influence of an extension and/or densification on an existing geodetic network is examined.

G 27

THEORETICAL AND OBSERVED SURFACE DEFORMATIONS DUE TO A DISTANT EARTHQUAKE

F. Wyatt (Institute of Geophysics and Planetary Physics, Scripps Institution of Oceanography, University of California at San Diego, La Jolla, CA 92093)

Static deformation of the earth's crust was recorded on many different instruments at Piñon Flat Observatory (PFO) due to the Imperial Valley, California earthquake of 1979. The observatory is located some 130 km from the source region at an azimuth of 8° relative to the strike of the fault.

The theoretical displacement field has been calculated by modeling the earthquake as a dislocation in an elastic homogeneous half space, with a Poisson ratio of .25 (see Press, 1965). The source region was assumed to be a rectangular area extending from the surface to a depth of 7.5 km and for 40 km along the fault. The dislocation has been approximated by 1 m of right lateral offset. These parameters were selected to produce a seismic moment of 9×10^{25} dyne-cm. The far field results of this model may be scaled in direct relation to the moment, for any fixed choice of the shear modulus (here 3×10^{11} dyne/cm^2). The table below presents the theoretical results and the data from the long baseline instruments at PFO.

STATIC DEFORMATION ($\times 10^{-8}$)

	Theory	Obs.
NS Strain (732m)	-1.82	-2.3
EW Strain (731m)	.52	
NW Strain (730m)	-1.50	-1.2
EW Tilt (50 m)	- .76	- .9

These results from long baseline instruments support the assumption that the earth's crust behaves in an elastic manner. However, the offsets recorded on 12 short baseline (1m-25m) instruments at PFO are generally an order of magnitude larger than those above. Apparently the transient seismic energy induced small local displacemnt (10^{-7}m) which resulted in large apparent strains on the short baselines.

Press, F., *J. Geophys. Res.*, 70, 2395-2412, 1965.

Space Technology
Pier 4
Saturday A.M.
James G. Marsh
(NASA/Goddard), Presiding

G 28

STATUS AND PLANS: THE FEDERAL PROGRAM FOR APPLICATION OF SPACE TECHNOLOGY TO GEODESY AND GEODYNAMICS

Edward A. Flinn (NASA Headquarters, Washington, DC 20546)

A consortium of five Federal government agencies (NASA, USGS, NGS, NSF, and DMA) has been established to coordinate the application of space technology to geodesy and geodynamics. A gravity field mapping mission (Gravsat) is being planned for 1985: user groups are studying mission requirements and benefits for geodesy and oceanography.

Laser observatories (including 8 Moblas units) are operating at 12 sites around the world, and a highly mobile truck-mounted laser station, built by the University of Texas at Austin, is being checked out prior to field deployment. Two of the three VLBI stations in the NGS Polaris network will be operating by the end of this year, and regular VLBI observations sessions have been conducted at five radio astronomy facilities in the US and Europe. A second mobile VLBI failicity is being constructed at JPL, and will be operating later this year.

Selection of sites for the mobile stations is being coordinated by an inter-agency working group, for studies of plate motion, earth rotation and polar motion, and crustal deformation in tectonic areas. Informal discussions are being held with scientific groups in Europe, Asia, South America, and the Pacific, leading to cooperative agreements for joint space observations in those areas. The initial priority will be on observations of crustal movement in the Western United States, particularly in Southern California.

G 29

PRECAMBRIAN MULTICOMPONENT NRM IN ROCKS FROM THE CANADIAN SHIELD ABITIBI SUBPROVINCE

Larry D. Schutts (Dept. of Geology, University of Toronto, Toronto, Ont. M5S 1A1)

Precambrian rocks from a well-dated, well-mapped region of the Superior Province Abitibi greenstone belt in eastern Ontario exhibit several distinct natural remanent magnetization components. Stepwise alternating field and thermal demagnetization treatments have revealed a total of four. The oldest units in the area include a thick succession of Archean basalts and the Archean gabbros which intrude them. Mean directions from six basalt sites (22 samples) and nine gabbro sites (34 samples) give similar paleopoles (24S 7E, k=18 for the basalts and 21S 2E, k=26 for the gabbros) implying the existence of a reasonably uniform characteristic remanence which post-dates initial formation and the concomitant or subsequent structural deformation. The Archean units are intruded by north trending Matachewan diabase dikes (2.6 Ga) and northeast trending Abitibi diabase dikes (2.1 Ga) which yield, respectively, paleopoles 43N 70E (14 sites, 31 samples, k=48) and 41N 232E (8 sites, 33 samples, k=51). Supposition that these two characteristic directions are primary is supported by the results of detailed gabbro-Matachewan and Matachewan-Abitibi contact tests which clearly reveal decreasing thermal effects on remanence with distance from the contact. Recent ^{40}Ar-^{39}Ar experiments by J. Hanes at the University of Toronto indicate a low level 1.8 Ga heating in the region. Fully one-quarter of the samples measured for magnetic remanence exhibit a lower coercivity-blocking temperature spectrum component which appears to correspond in age to this heating event. Directions are smeared along the younger portion of the Irving and McGlynn (1976) Track 5.

G 30

EARTH ROTATION AND TIDAL EFFECTS ON THE LAGEOS SATELLITE

D.C. Christodoulidis
E. Seifert (both at: EG&G Washington Analytical Services Center, Inc., 6801 Kenilworth Avenue, Riverdale, Md. 20840)

During the three years after its launch in May 1976, LAGEOS has been regularly tracked by a network of precise laser systems. Using these data, studies of the long term evolution of LAGEOS' inclination and longitude of the ascending node have yielded valuable information about the earth's tidal parameters and the earth's rotation. The tidal results obtained from the inclination, which is precise to 0.02 arc sec, are in agreement with the theories regarding the coupling of the liquid core to the mantle which gives a resonance amplification to the nearly diurnal tides. The node, freed from earth and ocean tidal signatures, reveals interesting structure in the rate of rotation of the earth at the millisecond level.

G 31

POLAR MOTION AND CHANGE OF LENGTH OF DAY FROM LAGEOS

M.H. Torrence
P.J. Dunn (both at: Washington Analytical Services Center, Inc., 6801 Kenilworth Avenue, Riverdale, Md. 20840)

The motion of the earth's pole and variations in the length of day have been determined from laser tracking observations of Lageos. The values of the coordinates of the pole and excess length of day are presented at 5 day intervals from May 1976 through December 1978. The solution was obtained from 32 independent orbital estimations based upon a global set of tracking stations which were derived from the full two and a half years of tracking data.

The precision of the polar motion values is 40 cm. and the excess length of day is 0.4 msec. A comparison of Lageos values with alternative techniques is presented together with the sensitivity of the results to various error sources.

G 32

MEASUREMENT OF HIGH FREQUENCY VARIATIONS IN EARTH-S ROTATION FROM DOPPLER OBSERVATIONS

R. J. Anderle (Naval Surface Weapons Center, Dahlgren, Virginia 22448)

Comparison of the computed longitude of the node of a satellite from successive independent orbit fits to Doppler observations provide a measure of variation in earth's rotation rate. Variations in UT1-UTC computed from Doppler observations of Navy Navigation Satellites for 1978 and 1979 were compared with classical observations published by Bureau Internationale de L'Heure. Doppler results with periods of six months and longer are corrupted by force field model errors in the orbit computation and variations with periods of less than a few days are corrupted by measurement errors. Variations with periods of one to five months agree with BIH data to about 1 ms.

G 33

ACCURACY ESTIMATES OF 1°x1° MEAN ANOMALY DETERMINATIONS FROM A HIGH-LOW SST MISSION

D. P. Hajela (Dept. of Civil Engineering, Virginia Polytechnic Institute and State Univ., Blacksburg, Virginia 24061)

The method of least squares collocation is used to estimate the accuracy and correlation of 1°x1° anomalies that could be determined from a high-low satellite to satellite tracking mission. The observed data is taken to be the line of sight acceleration which can be computed from the range rate data. Variables considered in this study were: a) the spherical distance from the center of the 1°x1° block within which data is selected for use; b) the accuracy of the "observed" accelerations; c) the height of the low satellites; and d) the data density or interval.

Typical results indicate that at a low satellite height of 200 km, a data noise corresponding to line of sight acceleration accuracy of 0.13 mgals, would yield a 1°x1° anomaly to an accuracy of about ± 8 mgals with an average error correlation coefficient between adjacent blocks of - 0.6. Lowering the satellite to 150 km reduces the accuracy to about ± 5 mgals but increases the correlation to about - 0.9.

This study does not consider the effects of orbit error, nor errors in the degree 12 reference field. In addition, some results could not be obtained when stable matrix inversions could not be obtained. This occured when dense data and/or low data noise was being used.

G 34

IMPROVED VENUS GRAVITY FIELD FOR ORBITER NAVIGATION

B. G. Williams (Jet Propulsion Laboratory, Pasadena, CA 91103)
R. A. Jacobson (Jet Propulsion Laboratory, Pasadena, CA 91103)

An improved Venus gravity field has been derived from the primary and extended phases of the Pioneer Venus Orbiter (PVO) mission. The coefficients for a full seventh degree and order spherical harmonic expansion of the gravitational potential have been estimated from short arcs of data (4 hours) centered at periapsis. A batch least squares process was used to combine the information from 40 data arcs distributed in longitude over two circulations of Venus by the PVO sub-periapsis point. The latitude of the sub-periapsis ranged from 14°N to 17°N. The addition of data from the second circulation by PVO has resulted in substantial improvements in the uncertainties of the lower degree and order harmonics compared to the uncertainties previously obtained from a single circulation. The equipotential surface (geoid) of the derived gravity field shows good correlation with Venusian topography.

G 35

SOME APPLICATIONS OF GPS TO GEODESY

P.D. Perreault (Stanford Telecommunications, Inc., Sunnyvale, CA 94086)
W.C. Melton (same as above)
J.J. Spilker, Jr. (same as above)

The Global Positioning System (GPS), a constellation of 18 satellites under development by the DoD has capabilities which will revolutionize Satellite Geodesy. Techniques are evolving which will allow rapid, all weather, worldwide, high precision positioning, in three dimensions, of points separated by distances greater than 30-50 km (the present limit of laser ranging devices) or by rugged terrain. With relative positional accuracies of 1-2 centimeters, these data will be used in upgrading and densification of national and global geodetic control networks and in studies of geodynamic phenomena such as polar motions, earth tides, polar ice drift, and crustal motions along a seismic fault.

This paper will discuss some applications of GPS to geodesy. In particular, we will review the capabilities, characteristics, and modes of operation of several receiver systems under consideration by various government agencies.

G 36

EVALUATION OF POLAR MOTION DATA BY LUNAR LASER RANGING

H. F. Fliegel
J. G. Williams
C. F. Yoder (all at Jet Propulsion Laboratory, Pasadena, California 91103)

The orientation of the body of the Earth with respect to its angular momentum vector is specified by three parameters: UT1 (time), and the X and Y coordinates of the pole.

Lunar laser ranging data from McDonald Observatory in Texas over 9 years has been modelled with r.m.s. residuals of 38 cm., of which 22 cm. is estimated to contain the effects inherent to the laser ranging technique.

The McDonald data alone cannot determine all three Earth rotational parameters. However, we have used them to evaluate the quality of various sources of polar motion and of data smoothing techniques. This premits one to estimate the effect of polar coordinate errors on various techniques of space geodesy employed during the 1970's.

G 37

LUNAR LASER RANGING DETERMINATIONS OF UNIVERSAL TIME

R.B. Langley (Department of Earth and Planetary Sciences, Massachusetts Institute of Technology, Cambridge, Mass. 02139)
R.J. Cappallo
C.C. Counselman III
R.W. King
I.I. Shapiro

Ranging observations of four lunar retroreflectors obtained by the McDonald Observatory between October 1970 and October 1979 have been analyzed to determine values of Universal Time (UT). The analysis was performed in three steps: 1) The MIT Planetary Ephemeris Program was used to estimate monthly tabular values of a continuous piece-wise linear model of UT simultaneously with other parameters affecting the observations. The root-mean-square of the post-fit range residuals from this analysis was 19 cm. 2) These residuals were used to estimate a range bias and a correction to UT for each day on which there were two or more observations of a single reflector spanning a period of at least 1.5 hours. The formal standard deviation of these raw estimates of UT is typically about 0.5 ms. 3) The raw estimates were smoothed by convolution with various Gaussian filters. A smoothed value of UT was determined for each day for which a raw value was computed. Values of UT at intervening epochs were determined by interpolation. A comparison of these values with smoothed BIH values in the 1979 system revealed significant differences.

G 38

TRANS- AND INTERPLATE BASELINE MEASUREMENTS USING VLBI

C. Ma (NASA/Goddard Space Flight Center, Greenbelt, Md. 20771)
for the East Coast VLBI Group

As part of NASA's Crustal Dynamics Program, 18 VLBI observing sessions were conducted at the Haystack Observatory (HO), Mass., the National Radio Astronomy Observatory (NRAO), W. Va., the Owens Valley Radio Observatory (OVRO), Ca., and the Onsala Space Observatory, Sweden between Sept. 1976 and Nov. 1979. The Mark I VLBI system was used for the first 15 sessions, the Mark III system for the last three. Meteorological and phase calibration data were used in the analysis for all sessions. Ionospheric calibration using two frequencies and timing cable calibration were used in the last two sessions. Using astrometric positions derived from all the data, the evolution of the three North American baselines was studied. The scatter in baseline length is ~3 cm for HO-OVRO, ~4 cm for NRAO-OVRO, and ~4 cm for HO-NRAO. Upper limits for yearly change in baseline length are 0.7 ± 1.4 cm for HO-OVRO, -0.7 ± 1.9 cm for NRAO-OVRO, and -1.1 ± 1.2 cm for HO-NRAO. These results, which indicate no measurable motion at the level of 2 cm per year, are consistent with the integrated local deformations over the baselines. Only an 8-month span of data to Onsala has been analyzed. The probable accuracy of the HO-Onsala baseline length is ~5 cm. Displacement Love numbers and the precession constant were also recovered.

In 1980 the Harvard Radio Astronomy Station at Fort Davis, Texas will be available and intermediate North American baselines will be measured.

G 39

RADIO INTERFEROMETRY MEASUREMENTS OF UNIVERSAL TIME, POLAR MOTION AND BASELINES FROM RECENT EXPERIMENTS WITH DEEP SPACE NETWORK ANTENNAS

J. B. Thomas
F. R. Bletzacker
E. J. Cohen
J. L. Fanselow
J. S. Scheid
L. J. Skjerve
O. J. Sovers (all at the Jet Propulsion Laboratory, Pasadena, CA. 91103)

Between November 1979 and February 1980, 12 separate radio interferometry experiments were conducted with Deep Space Network antennas, including 6 sessions on the California/Spain baseline and 6 sessions on the California/Australia baseline. Analysis of these data has yielded additional measurements of universal time and polar motion and new measurements of the baselines between antennas. The results of these measurements are presented and compared with results from previous sessions.

G 40

A VLBI SYSTEM FOR MAKING WEEKLY MEASUREMENTS OF UT1 AND POLAR MOTION WITH SOME EARLY RESULTS

T. P. YUNCK
M. G. ROTH (Both at Jet Propulsion Laboratory, Pasadena, CA 91103)
(Sponsor: Ojars Sovers)

At JPL we are in the process of bringing on line a system for making inter-continental clock comparisons and measurements of UT1 and Polar Motion on a weekly basis by means of very-long-baseline interferometry (VLBI). In this paper we describe the VLBI system and the plan of operation for the regular production phase to begin in a few months and present some experimental UT1 and PM measurements obtained in the past year. These are compared with results obtained by other methods.

G 41

A LEAST SQUARES PARAMETRIC, LONG-BASELINE INTERFEROMETRY, ADJUSTMENT

D.A. Davidson, (Department of Surveying Engineering, University of New Brunswick Fredericton, N. B.
R.B. Langley, M.I.T., Cambridge, Mass. U.S.A.
W.T. Petrachenko, York Univ. Toronto, Ont.
(Sponsor: Dr. Petr Vanicek)

Long-baseline interferometry software, and data, developed by the Canadian LBI group at York University, has been combined with a least squares parametric adjustment package. The options have been implemented to accept an input of both weighted parameters and functional parameter constraints. The results are then analysed statistically, including a chi-square goodness-of-fit test on the residuals, a rejection criteria for residual outliers, and a chi-square test on the variance factor.

The package has been developed with close regard to computer economy: a compromise having to be attained between storage space and processing time. The increased efficiency has resulted in a possibility to input a larger number of observations and, accordingly, in an improvement in accuracy. Results indicate that sub-decimetre accuracy can be achieved with the Canadian LBI System.

G 42

NUTATION BASED ON OTTAWA PZT OBSERVATIONS

P.Y. Shen (Dept. of Geophysics, Univ. of W. Ontario, London, Ontario, Canada N6A 5B7)

The method of least squares spectral analysis is applied to the latitude and time variations observed at Ottawa PZT from 1956 to 1977 in an attempt to evaluate the amplitudes of the principal, semi-annual and annual nutation terms. Motion of the BIH pole and the seasonal variations in earth's rotation were removed prior to the analysis. The results are in good agreement with other determinations using different sets of data and confirm the dynamic effects of the liquid core of the earth. Attempt is also made to identify the nearly diurnal wobble of the earth. The results are in favor, but not conclusively, of its existence.

G 43

OBSERVATIONAL EVIDENCE FOR A MASSIVE STELLAR COMPANION TO THE SUN

John P. Bagby (Space Sensors Lab.,Hughes Aircraft Co.,Culver City, Cal.90230)

At the AGU 1978 Midwest Meeting, evidence was presented for a massive stellar companion to the Sun with implications to several aspects of Geodesy. A tentative orbit (116 a.u.) and Ephemeris was presented, as well as an estimate of mass (0.02 $\odot$) for the companion. Since that time, I have studied the observational record in the literature in order to determine if evidence of the body, or satellites of it, already existed. This search has been successful. Using a sensor developed by Hughes Aircraft's Electro-Optical Lab. in the 1960's (including optical engineering performed by the author), the A. F. Geophysics Lab. eventually published in 1977, the results of a four color survey in the infra red (4.2, 11.0, 19.8, and 27.4 μ meters). Thirteen suspects were found whose characteristics suggest they could be planets of the massive stellar companion. These suspects were also found in appropriate positions in the NASA 2 μ meter Sky Survey, published in 1969. The elapsed time between the two surveys (1969 to 1971-74) has allowed the computation of the mean motion of the massive stellar companion, by averaging the vector advances of all the various planets of it. This has allowed a refinement of the orbit (e = 0.34)and mass (0.018 $\odot$).The Hughes Aircraft sensor gathered data between April 3, 1971 and September 11, 1974. Further evidence of geodesic effects by the massive companion have been analyzed and evaluated.

Geomagnetism and Paleomagnetism

Paleomagnetism of Intrusive Bodies and Their Metamorphic Aureoles

Pier 9
Thursday A.M.
H. C. Halls (Univ. of Toronto), Presiding

GP 1 INVITED PAPER

PALEOMAGNETISM OF THE NOTCH PEAK GRANITE (JURASSIC?) AND ITS CONTACT AUREOLE, UTAH

S. L. Gillett
V. C. Hover
J. J. Papike (all at: Dept. of Earth and Space Sciences, State Univ. of New York, Stony Brook, N. Y. 11794)

The Notch Peak Granite intrudes Early Paleozoic miogeoclinal rocks in the House Range, western Utah. A paleomagnetic reconnaissance of the intrusive and its contact aureole has been made as part of a detailed study to determine textural and chemical changes related to the intrusion. The Big Horse member of the Orr Formation (Upper Cambrian) has been sampled at 4 stratigraphically controlled sites, ranging from unaltered country rock 6 km from the pluton to marble ~500 m away. Two sites in skarn at the contact, and 5 sites in the granite were also sampled. The natural remanent magnetization (NRM) from the site farthest from the pluton is dominated by a present-field component, but is well-behaved upon thermal demagnetization and reveals a low-inclination, Paleozoic direction by 400°C. The 3 sites nearer the granite show more erratic magnetic behavior; generally they show a diffuse direction with steep negative inclination, present at NRM and removed above 300°C. Of these 3 inner sites, the one farthest from the pluton (2.5 km) appears unaltered in thin section, while the other 2 are extensively recrystallized. Directions from the 2 skarn sites are scattered. NRM directions from all 5 sites in the pluton are also scattered. Thermal demagnetization causes little change in direction; alternating-field (AF) demagnetization causes a very large intensity drop above 200 Oe. Stable AF directions tend to have steep negative inclinations but declinations remain rather scattered. The poorly-defined direction with steep negative inclination is grossly consistent with a Jurassic reversed position. The abrupt change of magnetic properties in the remagnetized country rock suggests that the resetting may result from chemical changes. Such changes may be very subtle, since one site showed no other evidence of recrystallization.

GP 2

EVIDENCE FOR PRIMARY, TRM COMPONENTS IN 2.7 BY THOLEIITES, KINOJEVIS GROUP, ABITIBI OROGEN

J.W. Geissman (Department of Geology, University of Toronto, Toronto, Ontario, Canada M5S 1A1)
D.W. Strangway
A.M. Tasillo
L.S. Jensen (Ontario Geological Survey, 77 Grenville, Toronto, Ontario,Canada M5S 1B3)

Alternating Fe and Mg rich tholeiitic basalts and comagmatic units of the Kinojevis Group, central Abitibi Orogen, are of potential use in further defining the Archean geomagnetic field because (1) their post-depositional structure is straightforward,(2) they overlie 2710±2 My and are overlain by 2703±2 My volcanics(Nunes and Jensen, 1980)[1], while to the west they are cut by post-deformation, Archean Matachewan dikes, and (3) they reached only a prehnite-pumpellyite facies of regional and/or ocean basin metamorphism(Jensen, 1978)[2]; primary volcanic textures are still preserved. Magnetization data from the Kinojevis units collected in flow traverses (sample/m) on either limb of a tightly-folded synclinorium are complex. Vector analysis in AF or thermal demagnetization reveals that samples often contain two or more "stable", sometimes antipodal, components of magnetization. Few in situ components are similar to those of Matachewan dikes. The magnetic mineralogy correlates with lithologic variations within flows and partial high- and low-T oxidation occurred. Components with linear decays to the origin in samples having the freshest magnetic mineralogy have an in situ direction of steep, positive inclination and southwest declination(e.g., D= 244.5°,I=64.9°,α_{95}=8.3°,k=12.3, N=23 samples, Mg tholeiite flow) on the south limb of the fold and of steep positive inclination and variable declination on the north limb. Corrected for regional structure, the directions are consistent with normal and reverse polarity Matachewan dike values, as expected from the closeness of the ages of the dikes and the Kinojevis units, and may thus be primary, TRM components.
[1]Ont. Geol. Surv. M.P. 92 [2]O.G.S. Rept. 165

GP 3

PRECAMBRIAN MULTICOMPONENT NRM IN ROCKS FROM THE CANADIAN SHIELD ABITIBI SUBPROVINCE

Larry D. Schutts (Dept. of Geology, University of Toronto, Toronto, Ont. M5S 1A1)

Precambrian rocks from a well-dated, well-mapped region of the Superior Province Abitibi greenstone belt in eastern Ontario exhibit several distinct natural remanent magnetization components. Stepwise alternating field and thermal demagnetization treatments have revealed a total of four. The oldest units in the area include a thick succession of Archean basalts and the Archean gabbros which intrude them. Mean directions from six basalt sites (22 samples) and nine gabbro sites (34 samples) give similar paleopoles (24S 7E, k=18 for the basalts and 21S 2E, k=26 for the gabbros) implying the existence of a reasonably uniform characteristic remanence which post-dates initial formation and the concomitant or subsequent structural deformation. The Archean units are intruded by north trending Matachewan diabase dikes (2.6 Ga) and northeast trending Abitibi diabase dikes (2.1 Ga) which yield, respectively, paleopoles 43N 70E (14 sites, 31 samples, k=48) and 41N 232E (8 sites, 33 samples, k=51). Supposition that these two characteristic directions are primary is supported by the results of detailed gabbro-Matachewan and Matachewan-Abitibi contact tests which clearly

reveal decreasing thermal effects on remanence with distance from the contact. Recent ^{40}Ar-^{39}Ar experiments by J. Hanes at the University of Toronto indicate a low level 1.8 Ga heating in the region. Fully one-quarter of the samples measured for magnetic remanence exhibit a lower coercivity-blocking temperature spectrum component which appears to correspond in age to this heating event. Directions are smeared along the younger portion of the Irving and McGlynn (1976) Track 5.

GP 4

PALEOMAGNETISM OF THE ARCHEAN POOHBAH LAKE ALKALINE COMPLEX, NORTHWESTERN ONTARIO

D.J. Dunlop (Geophysics Laboratory, University of Toronto, Toronto, Ont. M5S 1A7)

The 2705-Ma Poohbah Lake complex is a late synkinematic pluton emplaced during the waning phases of the Kenoran orogeny. It intrudes Archean Couchiching schists of the Quetico subprovince of the Canadian Precambrian Shield. Two units of the complex, porphyritic syenite and malignite (a nepheline-clinopyroxene-K-spar rock), as well as metasediments sampled near the intrusive contact, have a dominant reversed magnetization with mean direction D = 198° I = -27° (α_{95} = 6.8°, k = 51.3, N = 11 sites). The corresponding paleopole is 58.5°E, 52.5°N, in good agreement with the published pole (60°E, 44°N) for the 2690-Ma Matachewan dikes of the Abitibi subprovince. Normal magnetizations in the Poohbah Lake body are systematically steeper than reversed ones. They resemble, in polarity and direction, published results from the nearby 2595-Ma Shelley Lake granite (D = 4.5° I = +56; mostly normal magnetizations). The results may record apparent polar wander during slow cooling of the Poohbah Lake pluton. Alternatively the normal magnetizations may be overprints dating from a 2550-Ma thermal event (recorded by biotite K/Ar ages). Either scenario implies polarity epochs of long duration during the Precambrian.

GP 5

PALEOMAGNETISM OF NORITIC GRENVILLIAN INTRUSIVES SOUTH OF SUDBURY, ONTARIO

S. Dey, Department of Geology, University of Windsor, Windsor, Ontario, Canada N9B 3P4
D.T.A. Symons
M. Stupavsky

The Memesagemesing Lake and Caribou Lake stocks are small (~20 km^2) layered norite plutons located ~100 km southeast of Sudbury in the Grenville Province. They are strikingly similar in petrology to the Sudbury norite.

The stocks were sampled at 49 sites (10 specimens/5 cores/site). Alternating field and thermal demagnetization isolates a stable magnetization at 10 of the 24 Memesagemesing Lake sites giving a mean direction of 300°, -50° (α_{95}-10°) with a virtual geomagnetic pole at 148°E, -4°N (δ_p-8°, d_m-13°). The Caribou Lake norite stock study is only partially complete but appears to give a similar result. Alternative explanations are that the Grenville norites' remanence records: a) if the Grenville and Sudbury norites were comagmatic, metamorphism at ~1760 Ma as found in the Sudbury norite; or b) primary intrusion or remanence resetting at ~1000 Ma during the Grenville Orogeny.

GP 6

MAGNETIC PETROLOGY OF INTRUSIVE ROCKS

S. M. Cisowski
P. J. Wasilewski (both at Goddard Space Flight Center, Laboratory for Extraterrestrial Physics, Greenbelt, Maryland 20771)

Complete magnetic characterization of over 40 intrusive rocks from the Ward's North American and International collections initiates a program which strives to establish a connection between magnetic mineralogy, rock genesis, and geophysically important rock magnetic data. This presentation will focus on the correlation of opaque mineralogies, as observed in microscopic study, to magnetic properties. Magnetic parameters to be discussed include NRM and SIRM demagnetization curves, the ratio of NRM to SIRM intensity, initial susceptibility, and hystersis loop characterization. These measurements will be related to the observed textures and oxidation states of the opaque oxide grains. Emphasis will be on identifying those rock types and textures that, because of directional stability and internal consistency, provide acceptable magnetic behavior for paleomagnetic study. Also the variation of magnetic properties, such as NRM intensity, Koenigsberger ratio, and stability of remanence to A. F. demagnetization, between the various classes of intrusive rocks, will be discussed.

GP 7

RESET MAGNETIZATION IN DYKE CONTACTS AND IMPLICATIONS FOR VERTICAL MOTION IN THE SOUTHERN AND SUPERIOR PROVINCES

E.J. Schwarz (Geological Survey of Canada, Ottawa, and Ecole Polytechnique, Montreal)
K.L. Buchan (Department of Physics, Memorial University, St. John's, Newfoundland)

Oriented samples were taken along two profiles perpendicular to a 1250 Ma dyke contact near Sudbury and also along two profiles perpendicular to a 2150 Ma dyke near Matheson (Ontario). In each profile, the zone of hybrid magnetization was identified, and the maximum temperature attained in these zones was determined from the maximum blocking temperature of the reset component. Heat conduction theory yielded the contribution to this maximum temperature due to intrusion and, thus, the ambient temperature of the country rock at the time of intrusion temperatures of 280°C ± 20°C at 1250 Ma and 250°C ± 25°C at 2150 Ma were obtained. These results tend to suggest that the depth of burial of the present level of erosion was about 1 lm greater at 1250 Ma than at 2150 Ma if the Superior and Southern provinces can be regarded as one block during the last 2150 Ma.

GP 8

LIMIT OF REMANENCE OVERPRINT FROM THE GRENVILLE OROGENY IN NIPISSING AND GOWGANDA ROCKS

M. Stupavsky, Geology Department, University of Windsor, Windsor, Ontario, Canada N9B 3P4
D.T.A. Symons

Early Aphebian Nipissing diabase and Gowganda sediments were collected at 90 sites (>500 cores) along two 40 km profiles in Ontario. The profiles extend from the north end of Lake Temagami in the Southern Province across the Grenville Front to south of River Valley in the Grenville Province. Remanence overprinting from the Grenville Orogeny extends only ~1 km north of the Front into the Southern Province. After AF demagnetization the Grenville overprint is found in 3 of 6 Nipissing diabase sites which give an ~1000 Ma VGP and which also show metamorphic alteration. Similarly Gowganda clasts and matrix at 3 locations provide a uniform Grenville 1000 Ma VGP at 48°W, 38°N (δ_p=23°, δ_m=25°) before tilt correction. Beyond ~1 km north of the Front, no significant Grenville remanence survives AF demagnetization in the Nipissing diabase. It retains a stable homogenous primary remanence direction at 19 sites of 189°, 44° (α_{95}=8°) which is~antiparallel to that found elsewhere in Ontario but which gives a similar equatorial pole of 89°W, 17°S (δ_p=6°, δ_m=10°). The remanence directions of Gowganda clasts at 3 sites which are >5 km from the Front give random directions whereas the matrix sediment at 6 of the 30 sampled sites gives an ~2200 Ma VGP at 108°W, 66°N (d_p=24°, d_m=26°). In all cases tilt correction tests proved statistically insignificant.

GP 9

MULTICOMPONENT MAGNETIZATIONS IN THE GRENVILLIAN CORDOVA GABBRO, ONTARIO

J.M. Stirling (Geophysics Laboratory, University of Toronto, Toronto, Ont. M5S 1A7)
D.J. Dunlop
K. Argyle

The Cordova gabbro of southern Ontario intrudes the 1300 Ma Belmont volcanics of the Hastings Basin, an area of upper-greenschist-facies metamorphism within the generally high-grade Grenville structural province. Of 112 samples from 20 sites studied by thermal and AF demagnetization, 44 exhibit an A magnetization with mean direction D = 290° I = -58° (α_{95} = 5.7°, k = 49.3, N = 14 sites) and a paleopole at 152°E, 14°S; 41 exhibit a B magnetization, D = 302° I = +4° (α_{95} = 7.9°, k = 24.0, N = 15 sites), paleopole 170°E, 23.5°N; and 13 (from 9 sites) exhibit a C magnetization, D = 189° I = +22.5° (α_{95} = 11.2°, k = 14.6, N = 13 samples), paleopole 91.5°E, 33.5°N. A, B and C magnetizations are superimposed in many samples but thermal cleaning does not unambiguously indicate their relative ages. The A and B magnetizations resemble Grenville orogenic overprints documented in earlier studies, but the C magnetization is novel. The C could be primary: the metamorphic grade is exceptionally low and the nearby (higher-grade) Thanet gabbro preserves a pre-Grenvillian $^{40}Ar/^{39}Ar$ hornblende age of 1200 Ma. The C direction can be made concordant with 1200 Ma North American paleopoles by ~ 90° rotation about a local Eulerian pole, opening a small ocean between Grenvillia and Interior Laurentia. Closing of this ocean between 1200 and 1050 Ma would account for the Grenvillian orogeny as a collisional event. Alternatively, the C magnetization may be a Silurian overprint.

GP 10

TECTONIC AND METAMORPHIC HISTORY OF THE SUDBURY NORITE: THE EVIDENCE FROM PALEOMAGNETISM

W.A. Morris (Morris Magnetics, P.O. Box 8757, Ottawa, Canada)
(Sponsor: John Blenkinsop)

In a study of over 600 cores of Sudbury norite a number of remanence directions are found to co-exist in this single rock unit. A chronology of remanence acquisition was established by: a) comparing the degree of alteration and deformation of differing specimens, b) the areal distribution of a remanence phase, and c) the relationship of a remanence direction to a local geological structure.

Initially, (N1) the Sudbury norite occupied an open syncline (limbs dipping approximately 20°) plunging gently to the southwest. Next tectonism (F1) produced a crudely symmetrical basin, with all limbs dipping inwards between 40°-50°. Evidence from the region immediately south of the basin indicates that F1 affected only the basin, therefore F1 is probably related to a subsidence event within the basin. Completion of F1 is signified by the regional metamorphic event recorded magnetically as N2 on the south, east and west ranges. This was followed by a second deformational event (F2) which evidence suggests was a regional compressional tectonic event. As well as producing further tilting of the east and south ranges, F2 also caused the rotation about a vertical axis of the east range and possibly the eastern corner of the south range. Prior to this event (F2) in plan the Sudbury basin had the form of a broad ellipse. Acquisition of the N3 magnetization marks the completion of F2. The final deformational event (F3) recorded by the norite remanences involves the block rotation of the south range relative to the north range.

GP 11

COMPLEX MAGNETIZATION OF A DYKE AND ITS CONTACT AUREOLE

Pierre Lapointe and Peter Dankers (Earth Physics Branch, Energy, Mines and Resources, Ottawa, Ontario, Canada K1A 0Y3)

A diabase dyke and the strongly foliated Grenville gneiss in which it was intruded were sampled in detail along several parallel sections across the dyke up to 60 m in the gneiss. The well exposed very sharp contact between the 100 m wide dyke and the gneiss is characterized by a fine grained chilled margin of approximately 1 m. No effect of intrusion is visible in the gneiss. The centre of the dyke is differentiated and coarsely crystallized. Susceptibility measurements at the outcrops show a very sharp contrast between dyke and gneiss, the dyke having a much higher susceptibility value. In the dyke the susceptibility peaks in a zone between 10 m and 20 m from the

contact. NRM intensities close to the contact are approximately the same for dyke and gneiss. In the gneiss the NRM drops 1 m from the contact and in the dyke the NRM increases towards the centre. Alternating field demagnetization and thermal demagnetization reveal the same characteristic magnetizations. At least three zones parallel to the contact each having a different characteristic magnetization could be distinguished. The hardest magnetization, probably of thermo-remanent origin, was found in the centre of the dyke, whereas closer to the contact a TCRM or a thermally overprinted TRM probably dominates.

GP 12

EXTENSION OF THE MATACHEWAN AND ABITIBI DIABASE DIKE SWARMS WEST OF THE KAPUSKASING STRUCTURAL ZONE, NORTHERN ONTARIO

Richard Ernst, (Dept. of Geology, U. of Toronto)
Henry C. Halls, (Dept. of Geology, Erindale College, U. of Toronto)

On the eastern side of the Kapuskasing Structural Zone (KSZ) in Northern Ontario there is an orthogonal set of Aphebian diabase dike swarms, the Matachewan (trending N-S) and the Abitibi (trending ENE). On the western side of the KSZ is another orthogonal dike set with trends NNW (to N-S) and NE (to ENE). The purpose of this study was to paleomagnetically examine these western dikes a) to try to correlate them with the Matachewan and Abitibi swarms and b) to determine whether any relative rotation between the two orthogonal sets has occurred in association with KSZ tectonics.

This study has determined a preliminary paleomagnetic direction (calculated for a location at Timmins, Ont.) for the NNW swarm (D/I = 193°/-17°, based on 10 dikes) and for the NE swarm (D/I = 246°/57°, based on 3 dikes). Baked contact tests suggest that these paleomagnetic directions are primary.

The remanance directions of the western dike swarms are similar to the directions (averaged from previous studies) for the Matachewan (D/I = 203°/-10°) and the Abitibi (D/I = 267°/63°). Therefore, the western dikes are probably extensions of the Matachewan and Abitibi swarms. Furthermore, the paleomagnetic data are consistent with a relative rotation of about 10° between the two orthogonal dike sets, but more data are needed to confirm this interpretation.

GP 13

TIME EFFECTS IN THE RESETTING OF REMANENCE IN CONTACT AUREOLES.

E. McClelland Brown Department of Earth Sciences, University of Leeds, England.

The 'resetting temperature' (T_R) is the maximum blocking temperature thermally rest in a host rock heated by an igneous intrusion. This is lower than the laboratory unblocking temperature (T_{BL}) at which all the thermally reset remanence is removed in an experiment which takes place over a significantly shorter time than the natural reheating event. The host rock experiences a thermal pulse of magnitude T_R as the heat from the intrusion is distributed. The effect of this changing temperature is theoretically predicted to be equivalent to that of a square pulse of height T_R and width Θ_p, the thermal pulse width. Relationships between T_R and T_{BL} have been calculated for various sizes of thermal pulse.

Experimentally determined laboratory unblocking temperature profiles from contact zones of Tertiary dykes are compared with maximum temperature (T_R) profiles obtained from heat flow calculations. These are identical at the Curie temperature of the remanence carrier as unblocking is due to randomization of atomic moments. At decreasing temperatures T_{BL} becomes increasingly larger than the calculated peak temperature as time effects increase. Experimentally determined differences between T_{BL} and T_R are compared with theoretically predicted differences and the agreement is good.

Paleomagnetism: General

Pier 9
Thursday P.M.
K. P. Kodama (Lehigh Univ.), Presiding

GP 14

MAGNETIC POLARITY STRATIGRAPHY: STOCHASTIC ASSESSMENT OF DATA

Victor E. McGee, Noye M. Johnson, Dartmouth College, Hanover, N.H. 03755

The problem of compiling a local magnetic polarity column from a given set of discrete data points is essentially stochastic in nature. For the case of randomly distributed paleomagnetic sites in the time interval t, the probability C/(N-1) for discovering a polarity zone is given by

$$\frac{C}{N-1} = \frac{1}{2} - \frac{1}{8x}\left[1 - e^{-4x}\right] \quad \text{eq. 1}$$

where C is the number of polarity zones, N is the number of paleomagnetic sites $x = t/\alpha N$ and α is the mean of a Poisson distributed reversal rate curve. The standard deviation σ about the expected C value is given by

$$\sigma = \left[P(N-1)(1-P)\right]^{1/2} \quad \text{eq. 2}$$

where P = C/(N-1) from eq. 1. Published case studies of magnetic polarity stratigraphy from terrestrial, pelagic and volcanic rocks have been evaluated by means of eq. 1 and the number of polarity zones predicted from theory agrees well with the number actually found. With regard to sampling effectiveness, a uniform distribution of sample sites is more efficient for finding magnetic polarity zones than a random distribution (eq. 1). In contrast, an exponential distribution is less efficient than the random distribution.

GP 15

MAGNETOSTRATIGRAPHY OF CLASTIC SEDIMENTS IN THE FLINT-MAMMOTH CAVE SYSTEM OF KENTUCKY, USA - A NEW HIGH RESOLUTION FIELD RECORD EXTENDING BACK ONE MILLION YEARS

V. A. Schmidt (Dept. of Geology & Planetary Science, Univ. of Pittsburgh, Pittsburgh, PA 15260, USA)

The clastic sediments partially filling many passages of the Flint-Mammoth Cave System of Kentucky are excellent recorders of the earth's magnetic field at the time of their deposition. If backflooding from the local hydrologic base level is the principal means of deposition, then the age of a section should be strictly correlative to its elevation, allowing a magnetostratigraphic interpretation of the polarity record contained in the sediments. The same polarity pattern - reversed between 570 ft (174 m) and 660 ft (201 m) and normal below and above this zone - has been observed in all parts of this sprawling cave system (approx. 100 km^2 extent). Thus, the sediments in the highest passages in the cave date at least to the Jaramillo magnetochron, about 800,000 years ago. Preliminary results from nearby caves at higher elevations indicate that the total record may extend to the Olduvai magnetochron. Individual sediment sections vary up to 3 m in thickness with fine laminations indicating time windows up to a few thousand years per section. Each of the many sections available in each magnetozone appears to record detailed secular variation of the field. It is clear that this phenomenon is not restricted to this particular cave system. Suitable limestone caves throughout the world should contain high resolution records of the field covering at least the past million years.

GP 16

REVERSAL OF THE PALEOMAGNETIC FIELD IN BRUNHES-AGE LACUSTRINE SEDIMENTS IN LONG VALLEY AND MONO BASIN, CALIFORNIA

J.C. Liddicoat (Lamont-Doherty Geological Observatory, Palisades, NY 10964)
K.R. Lajoie
R.A. Bailey
A.M. Sarna-Wojcicki
P.C. Russell
M. Woodward (all at: U.S. Geological Survey, 345 Middlefield Road, Menlo Park, CA 94025)

Reversed paleomagnetic directions (D = 163°, I = -21°; VGP = 59.1°S, 274.3°E) occur in a 150-mm stratigraphic interval of laminated lacustrine silts that bracket a 20-mm bed of tephra in Long Valley, eastern California. Similar reversed directions occur in a 25-mm layer of tephra at two sites 1 km apart in laminated lacustrine silts on Paoha Island in Mono Lake, 50 km to the north. Trace-element chemistry (0.99 similarity coefficient for 11 elements; 1.00 represents a perfect match) and heavy mineral content correlate the two tephra layers and confirm the age equivalence indicated by the paleomagnetic data.

The absolute age of the reversal is not precisely known, but it is less than 700 kA -- the lacustrine deposits in Long Valley are in the caldera formed by the eruption of the Bishop Tuff about 700 kA ago, and those on Paoha Island lie stratigraphically above the Bishop Tuff. Two lines of evidence suggest the reversal occurred in late Brunhes time: 1) the reversely magnetized strata lie in the upper part of Brunhes-age deposits at each locality, and 2) on the basis of trace-element chemistry, the tephra has close affinity to rhyodacites dated at 50-150 kA by the K-Ar technique on the southwest margin of the Long Valley caldera. However, the reversal might be mid-Brunhes age because extrapolated sedimentation rates derived from ^{14}C-dated strata higher in the stratigraphic section in Mono Basin, and the depth of the Bishop Tuff lower in that section, place the age of the reversely magnetized zone at 250-300 kA.

GP 17

REFINEMENT OF THE CHRONOLOGY AND PALEOMAGNETIC RECORD AT MONO LAKE, CALIFORNIA

K.R. Lajoie (U.S. Geological Survey, 345 Middlefield Road, Menlo Park, CA 94025)
J.C. Liddicoat (Lamont-Doherty Geological Observatory, Palisades, NY 10964)
S.W. Robinson (U.S. Geological Survey, 345 Middlefield Road, Menlo Park, CA 94025)
(Sponsor: J.C. Liddicoat)

Ten new ^{14}C dates improve the temporal control between 36 kA and 13 kA for the paleomagnetic record in 7.2 m of thinly laminated late Pleistocene lacustrine silts in Mono Basin, eastern California, and revise the age of the paleomagnetic excursion reported in previous investigations. In those investigations, a linear sedimentation rate extrapolated from two ^{14}C-dated beds higher in the section tentatively placed the age of the excursion at about 25 kA. Three of the new ^{14}C dates on samples from the 0.6 m stratigraphic interval containing the excursion establish its age at 29-32 kA.

Widely spaced samples from the post-excursion portion of the stratigraphic section record swings in declination and inclination (up to 60° and 50°, respectively) and relatively high angular dispersion of the Virtual Geomagnetic Poles (VGP's). New paleomagnetic data from samples at 50-mm intervals (roughly every 150 years; α_{95} for six a.f. demagnetized specimens per measured horizon averages 3°) fill gaps in the original record and confirm, but slightly revise, the broad swings previously reported. The angular dispersion of VGP's also remains high: 19.7° (k = 16.9, n = 63). In addition, five and a half clockwise loops span the set of smoothed VGP's (5-point running mean) in the interval between 29 kA and 13 kA. The loops have an average duration of 2.9 kA, and their direction of movement is compatable with the model of westward drift of the nondipole field.

GP 18

PALEOMAGNETIC STUDY OF THE MAHOGANY OIL SHALE, UINTA BASIN, UTAH

K. G. Richardson
H. C. Noltimier (both at: Dept. Geology and Mineralogy, Ohio State Univ., Columbus, Ohio 43210

Geomagnetic polarity stratigraphy of the complete 135 foot thick Mahogany unit, Parachute Creek Member, Green River Fm, has been determined from a borehole core drilled by Chevron West in Duchesne Co., Utah. 622 subcores were taken at equal intervals and measured with a 3-axis SCT magnetometer. 70 cores were AF demagnetized at 10 mT intervals to 60 mT in initial tests. The remaining 552 cores were treated at 30, 40, 50 mT. Maximum values of the BSI occured between 30-40 mT and the polarity results are shown. Only polarity changes consistent through demagnetization and not unique to one core segment were used. The Mahogany unit polarity is mainly normal with 9 thin reversed zones. The thickest reversal lies at 7630 feet. Mauger's 1977 age for the wavy tuff above the unit is 44 my BP. Compared to the polarity history of the Middle Eocene, the unit correllates with one of three normal intervals of Late Bridgerian-Early Uintan age (44.2-44.7, 44.8-45.3, 45.4-45.9 my BP). K-Ar ages from the wavy tuff above and curly tuff below the unit are pending. Deposition rate is equal to or less than 8 mm/century implying lamination pair thickness of .08 mm or less if they are annual varves. This is consistent with the range of values quoted by Bradley in 1929 for oil shale beds of the Mahogany unit.

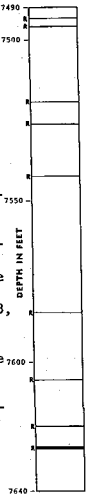

GP 19

SECULAR VARIATION IN MIOCENE LAVAS, NW-ICELAND ; SOME PRELIMINARY RESULTS

Leo Kristjansson (Science Institute, University of Iceland, Reykjavik, Iceland)
Ian McDougall (Australian National University, Canberra, A.C.T. 2600, Australia)
Norman D. Watkins† (Graduate School of Oceanography, University of Rhode Island, Kingston)
Haukur Johannesson
Kristjan Saemundsson (both at: National Energy Authority, Reykjavik, Iceland)

Assisted by senior and graduate students, the authors mapped in 1975-78 a composite stratigraphic section through the basalt lava sequence of the Northwestern peninsula of Iceland. Three oriented cores were taken from each of 1261 lavas in about 40 profiles which overlap partly in time. Pending completion of detailed K-Ar age analysis and stratigraphic correlation studies, the section is estimated to span the age interval between 13.5 and 8.8 m.y. ago.

Statistical results on the magnetic remanence of those 1118 lavas which yielded primary magnetic directions of satisfactory internal consistency ($\alpha_{95}<23.5^\circ$) include i) 53% are normally magnetized, i.e. have VGP positions north of the equator ii) 12% yield VGP latitudes below 40°N or S, and 2% yield poles within 10° of the equator iii) mean virtual dipole moments increase smoothly in strength with VGP latitude, by a factor of 4 between the equator and the geographic poles iv) there is no (< 4%) difference between overall average magnitudes of normal and reverse virtual geomagnetic dipole moments v) low-latitude (< 40°) poles do not occur preferentially in any one particular longitude interval.

These results are similar to those recently obtained by Saemundsson et al. [J.G.R., 1980] by combining data from three different paleomagnetic surveys (altogether 1201 sampled lava flows) in W- and N-Iceland.

† deceased

GP 20

LATE-GLACIAL GEOMAGNETIC EXCURSION IN LAVA FLOWS, REYKJANES PENINSULA, SW-ICELAND

Leo Kristjansson (Science Institute, University of Iceland, Reykjavik, Iceland)
Agust Gudmundsson (National Energy Authority, Reykjavik, Iceland)

The Reykjanes peninsula is the on-shore extension of the Reykjanes Ridge crest. It is mostly covered by basalt lava flows and hyaloclastite ridges of late-glacial and Holocene age, including historic flows. We have tested the magnetic polarity of a large number of lavas and dykes at over 140 localities on the peninsula, using a portable flüxgate magnetometer. Sites yielding apparently reverse directions were subsequently sampled for laboratory measurement. Three different hills were found to be largely built up of thin lava flows all having similar shallow reverse directions of primary remanence. These hills are some kilometers apart, but they may have belonged to a common fissure swarm. The mean primary remanence direction obtained from 55 stable samples is at D = 260°, I = -16°, with $\alpha_{95} = 3^\circ$. The corresponding VGP position is at 254°E, 12°S. The age of these outcrops is likely to be late Wisconsinan (< 30.000 years).

GP 21

MAGNETIC STRATIGRAPHY OF TURBIDITE-BEARING SCAGLIA LIMESTONE AT FURLO (UMBRIA-MARCHES APENNINES, ITALY)

W. Alvarez (Dept. of Geology and Geophysics, University of California, Berkeley, CA 94720)
W. Lowrie (Institut für Geophysik, ETH-Hönggerberg, 8093 Zürich, Switzerland)

Previous magnetic studies in the Apennines have dealt with pelagic limestones and marls. At Furlo, Scaglia limestone in a facies marked by calcarenite turbidites also gives good magnetic results. IRM acquisition shows that both magnetite and hematite are present. Demagnetization to 200 oe and 350°C or higher reveals a single stable direction after removal of an initial soft coercivity component. Polarity zones from the Cretaceous Long Normal Zone to the upper Maastrichtian Gubbio F+ zone (anomaly 30-31) clearly correlate to the sea-floor anomaly sequence. The foraminiferal change that marks the Cretaceous-Tertiary (C-T) boundary can be recognized despite the problem of reworking by turbidites. Some of the section is apparently missing at the C-T boundary, and identification of polarity zones near the C-T boundary is not yet certain. Zones of soft sediment slumping in the pre-Maastrichtian Upper Cretaceous bound undisturbed zones that show declinations rotated by as much 75°; these are interpreted as coherent gravity slide blocks emplaced during sedimentation.

GP 22

UPPER JURASSIC MAGNETOSTRATIGRAPHY FROM NORTHERN ITALY

J.G. Ogg (A-008, Scripps Inst. Oceanography, La Jolla, Calif. 92093)

Kimmeridgian to Berriasian pelagic limestones of the Southern Alps (N. Italy) yield a consistent magnetostratigraphy. At the eight sample sites (approx. 60 cores per site) Kimmeridgian-Lower Tithonian, red, *Saccocoma*-rich "Ammonitico Rosso" has a gradational contact to the Upper Tithonian-Early Cretaceous, white, calpionellid-rich "Maiolica". The cleaning procedure combined alternating field and thermal demagnetization. Magnetic property tests showed magnetite to be the dominant carrier of remnant magnetization. The composite magnetostratigraphy was dated by microfossils (calpionellids and *Nannoconus*) and partially corrected for differential sedimentation rates.

The "Ammonitico Rosso" has eight main polarity zones with perhaps a couple excursions or subzones. The "Maiolica" is dominated by normal polarity in the Upper Tithonian with a relatively long reversed zone beginning near the Cretaceous-Jurassic boundary (base of *Nannoconus*). The Oxfordian cherty limestones below the "Ammonitico Rosso" have mixed polarities of reduced intensity. Middle Jurassic red limestones in this region are predominantly of normal polarity, but with weak magnetization.

An attempt to match this Upper Jurassic sequence to the marine magnetic anomaly record suggests that M-17 may be the reversed polarity zone near the Cretaceous-Jurassic boundary.

A paleolatitude of $18^\circ \pm 4^\circ$N and a post-Jurassic counterclockwise rotation of $39^\circ \pm 5^\circ$ for this part of Italy is indicated.

GP 23

GROSS FEATURES OF JURASSIC GEOMAGNETIC STRATIGRAPHY FROM UMBRIAN LAND SECTIONS

J.E.T. Channell
W. Lowrie (both at: Inst. für Geophysik, ETH-Hönggerberg, CH-8093 Zürich, Switzerland)
G. Pialli (Istituto di Geologia, Universita di Perugia, Perugia, Italy)

The principal section at Valdorbia appears to represent continuous sedimentation throughout much of the Jurassic, from Upper Tithonian to Lower Toarcian. The upper 160 m. (Tithonian to Bajocian) are white/green cherty limestones and the lower 40 m. (Aalenian/Toarcian) are red and gray marly limestones. 20 m. of section in the Lower Kummeridgian/Upper Oxfordian could not be sampled due to lack of outcrop. The upper 160 m. of section is dated only at 3 stratigraphic levels: (1) base of Tithonian, (2) base of Oxfordian, (3) base of Dogger. In view of the apparent lack of hiatuses, we make a linear interpolation of stage boundaries between these fixed points. The magnetic stratigraphy of the Valdorbia section after thermal and AF treatment gives an extended quiet zone of normal polarity from Kimmeridgian to lower Dogger flanked by mixed polarity intervals.

A short second section at Gorgo a Cerbara of Tithonian age gives a stratigraphy correlatable with the upper mixed polarity zone at Valdorbia, and two pelagic limestone sections of Liassic age at Cingoli and Fonte Avellana indicate that the mixed polarity interval which appears to end in the middle Dogger at Valdorbia extends back at least as far as the Sinemurian.

GP 24

PALEOMAGNETISM OF PERMIAN SEDIMENTS FROM ALGERIA AND THE POSITION OF THE PERMIAN PALEOEQUATOR.

P. Morel
E. Irving (both at: Earth Physics Branch, Energy Mines and Resources, Ottawa, Canada K1A 0Y3
L. Daly (Laboratoire de Géomagnétisme du Parc Saint-Maur, 4 Av.de Neptune, 94100 Saint-Maur-des-Fossés, France)
A. Moussine-Pouchkine (Centre Géologique et Geophysique, U.S.T.L., Place Eugène Bataillon, 34060 Montpellier Cedex, France)

We have completed a paleomagnetic study of the Grès de Chenaux of NW Algeria (31N,3W) near Beni Abbes (97 samples, 13 sites). The localities are on the Algerian platform south of any zone of Mesozoic or Tertiary deformation. The sequence grades downward without break into fossiliferous Autunian and Stephanian shales. The age is therefore probably Permian, possibly early Permian. All samples have reversed magnetization, and a mean inclination of +11° corresponding to a paleolatitude of 5±3° S. Studies by Daly and Pozzi, and Westphal et al of red sandstone, trachyandesites and rhyodacite from the Moroccan Meseta (33N, 6W) yield mean inclination of -5° corresponding to a paleolatitude of 3±2°N. The present separation of the localities in a paleolatitudinal sense is about 4° and is consistent with the paleomagnetic results. As always, there are uncertainties in dating the rock sequences, but the results indicate that no more than several hundreds of kilometres of movement have occurred between the Moroccan Meseta and NW Algeria. They also indicate that the paleoequator for Permian time passed between these two regions. The paleoequator for North America passed through the Maritime Provinces of Canada and southwest to Arizona. Thus the placing of the paleoequator between the Moroccan Meseta and the platform of NW Algeria is inconsistent with N. Africa being situated south of eastern N. America in the Permian. These new data are consistent with a position for N. Africa immediately south of Europe at that time.

GP 25

FURTHER PALEOMAGNETIC RESULTS FROM MIDDLE PENNSYLVANIAN COALS, EASTERN AND SOUTHERN OHIO

R. C. Bartman
H. C. Noltimier (both at: Dept. Geology & Mineralogy, Ohio State Univ., Columbus, Ohio 43210

Recent paleomagnetic study of Appalachian coal from the Allegheny and Conemaugh Series further refine the stratigraphic base of the KMI. Data from time equivalent strata in Colorado and South Wales indicate four brief normal polarity intervals act as magnetostratigraphic markers in the Westphalian B-D interval or its equivalent. One normal interval (M. Kittanning) has been reported in Appalachian coal measures. Six coal seams were sampled of Alleghenian age (Clarion; L., M. and U. Kittanning; L. and U. Freeport) plus one coal and superjacent limestone of Conemaughan age (Wilgus, Cambridge ls.). All samples were measured with an SCT magnetometer and were subjected to AF and/or thermal demagnetization. Zijderveld diagrams were used to isolate primary and secondary components. The Briden Stability Index (BSI) was derived for each demagnetization interval. The results confirm at least three normal polarity intervals in the Alleghenian Series, equivalent to the Westphalian B-C interval (see figure). The remaining coals and the Cambridge ls. have reversed polarity. A study of coal of Early Conemaughan age is in progress (Westphalian C-D equivalent).

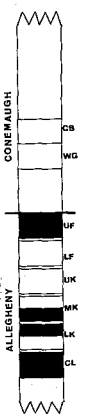

GP 26

PALEOMAGNETIC STUDY OF THE MIDDLE AND UPPER ORDOVICIAN REFERENCE STANDARD CORE CA-38, MINERVA, KENTUCKY

R. J. Stupp
H. C. Noltimier (both at: Dept. Geology & Mineralogy, Ohio State Univ., Columbus, Ohio 43210)

Core CA-38, recovered and boxed by Cominco American in 1970, represents 1200 ft continuous record of limestones and shales permitting detailed study of the complete Kope section and subjacent stratigraphic units. It is the Middle and Upper Ordovician standard for the eastern Cincinnatian region (Sweet, Harper & Zlatkin, 1974). We have examined the upper 297 ft (Upper Ordovician Maysvillian) for the geomagnetic polarity history. 613 subcores were removed at an average interval of 15 cm. 40 ft of Fairview, 240 ft of Kope and 17 ft of Point Pleasant Fms are represented. From the top 50 ft 24 pilot subcores were subjected to AF cleaning to 90 mT at 10 mT intervals. The remaining subcores were cleaned at 30, 40, 50, 60 mT. The BSI was derived for each 10 mT interval, maximum values (≥0.80) are at 40-50 or 50-60 mT. The 50 mT polarity results are shown. Only polarity reversals overlapping core segments are used. Four zones of normal polarity in the lower Kope Fm correlate reasonably well with observations of Panderodus gracilis. Intervals with inclinations near 0° are shown by hatching. The paleolatitude derived from the results lies between 10° and 12° South.

Paleomagnetism of the Phanerozoic

Pier 2 & 3
Friday A.M.
M. E. Evans (Univ. of Alberta), Presiding

GP 27

PALEOMAGNETISM OF LATE CARBONIFEROUS COAL MEASURES IN ASTURIAS

A. E. Schwartzbard (Exxon Co. New Orleans, La., 70112)
H. C. Noltimier (Dept. Geology & Mineralogy, Ohio State Univ., Columbus, Ohio 43210)
F. H. Cramer (I.I.P., Box 244, Leon, Spain)

Argand suggested rotation of Iberia in 1924. Geologic, paleomagnetic and marine magnetic studies have refined the concept to a stage of counter clockwise rotation (Jurassic-Cretaceous) followed by compression (Early Tertiary) involving intraplate displacements. We have studied the coal bearing sequences of Asturias with palynologic controls on each sample. 51 hand samples were collected from 22 localities yielding 259 oriented cores of Namurian C through Stephanian C age. The samples are limestones, shales and coal of all ranks. Most samples show multiple phases of magnetization corresponding with 3 phases of tectonic deformation recognized in the Asturian Arc from Late Carboniferous through Cenozoic Periods. Results suggest that four coal basins rotated 40°, 26°, 41°, 12° (weighted mean 25°) counter-clockwise and a normal polarity interval occurs in Westphalian D coal in the Valderrueda Basin. The diagram shows the normal polarity interval, the specimens oriented with respect to well defined shear planes striking NW, dipping NE at 70° to the bedding.

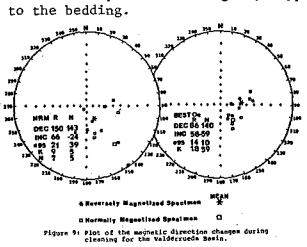

Figure 9: Plot of the magnetic direction changes during cleaning for the Valderrueda Basin.

GP 28

TECTONICS and PALEOMAGNETISM in NW SICILY

B. d'Argenio (Geological Institute, University of Naples)
R. Catalano (Geological Institute, University of Palermo)
C.B. Gregor (Dept of Geology, Wright State University, Dayton, Ohio 45435)
A.E.M. Nairn (Dept of Geology, University of South Carolina, Columbia, SC 29208)

NW Sicily is essentially a part of the Tethyan carbonate shelf that bordered northern Africa in Mesozoic times. Starting at the end of the Triassic this shelf broke into a series of tectonic units represented in Sicily by 3 platforms and 2 intervening basins. These later rode up on each other as they were transported towards Africa during the Miocene phase of the Alpine orogeny.

The basinal sequences include volcanic rocks of Late Triassic to Cretaceous age. A compilation of paleomagnetic declinations from 25 sites in these (16 sampled by the present authors and 9 by A. Schult) shows a roughly fanlike pattern stretching over about 100 km from E to W and radiating southward from the general direction of Palermo. Limestones of the Rosso Ammonitico facies (Middle to Upper Jurassic) yield directions that conform to the same general pattern.

GP 29

PALEOMAGNETISM OF THE JURASSIC TWIN CREEK LIMESTONE, WESTERN WYOMING

Chad McCabe
Bruce H. Wilkinson
Rob Van der Voo (all at: Dept. Geological Sciences, Univ. of Michigan, Ann Arbor, MI.48105).

As part of a paleomagnetic, rockmagnetic and petrographic investigation of numerous limestone units, the Twin Creek Formation was sampled from folded strata in the Wind River block and in the overthrust belt of western Wyoming. Alternating field demagnetization between 30 and 60 milliTesla reveals a characteristic direction which clusters well after structural correction. The calculated pole near 70°N, 147°E from 6 site-mean poles (a_{95} = 14°) agrees well with other Jurassic poles for North America. A fold test is not possible until further sampling is done; however, a tectonic breccia was sampled and the directions were nearly random. It is concluded that the Twin Creek Formation is suitable for paleomagnetic study, based on traditional reliability criteria such as the conglomerate test. We are currently investigating whether the magnetic carrier, preliminarily identified as magnetite, is a depositional or an authigenic phase.

GP 30

VISCOUS REMAGNETIZATION AND SUSCEPTIBILITY ANISOTROPY OF HELVETIC LIMESTONES

Roy Kligfield
J.E.T. Channell (both at: Institut für Geophysik, ETH Hönggerberg, CH 8093 Zürich, Switzerland)

The Helvetic limestones, widely distributed in the Alps, are Jurassic and Cretaceous in age, and were deposited in shallow seas on the northern margin of the Mesozoic Tethys. Fold tests demonstrate that the NRM after cleaning postdates the Miocene folding. Monitored acquisition of VRM in the laboratory indicates that the intensity of the NRM can be accounted for by the build-up of VRM during the Brunhes epoch. Alternating field demagnetization of the VRM produced in various times (T) indicates that the alternating fields required to destroy the VRM are proportional to (Log T). The acquisition and blocking temperature of the IRM suggest that haematite may be the carrier of the VRM. In thin and polished sections, haematite aggregates after pyrite are often sealed by later growth of micrite, indicating early (diagenetic) growth of haematite. Moreover, a sedimentary (compaction) magnetic susceptibility fabric is apparent after tectonic correction in the less deformed nappes, indicating that the magnetic mineral was present before compaction was complete. In more deformed nappes, the sedimentary fabric is progressively modified by deformation, as the maximum / intermediate susceptibility (elongation) planes of the magnetic grains align themselves perpendicular to the compression direction (indicated by grouping of minimum susceptibility axes).

GP 31

PALEOMAGNETISM OF JURASSIC MICRITES FROM THE JURA MOUNTAINS, SWITZERLAND

R. Johnson
Rob Van der Voo (both at: Dept.Geological Sciences, Univ. of Michigan, Ann Arbor, MI.48109).
W. Lowrie (Institut für Geophysik, ETH-Hönggerberg, CH-8093 ZURICH, Switzerland).

Weakly magnetized massive micrites (of Bajocian through Kimmeridgian age) from the Swiss Jura Mountains yield two stable paleomagnetic directions. One magnetization ('A' direction) is parallel to the present-day field prior to structural correction and fails the fold test. The other magnetization ('B' direction) is approx. Declination D=10°, Inclination I=+45°, after structural correction and passes the fold test. AF and thermal demagnetization, IRM acquisition, and optical examinations reveal the differences between the A and B type magnetizations. The A type has coercivities > 100 mT, blocking temperatures generally < 250°, and its IRM does not reach saturation in 1.3 Tesla. It is thought to reside in goethite. The B type has coercivities from 5 to 40 mT, persists in thermal demagnetization up to 400°C, and reaches saturation below 0.3 Tesla. It is concluded that the pre-folding magnetization resides in magnetite and is probably of primary (depositional) origin. The goethite may have formed by alteration of pyrite during late diagenesis after the Late Miocene-Early Pliocene folding and during subsequent erosion and karstification.

GP 32

PALAEOMAGNETISM OF UPPER CRETACEOUS LIMESTONES FROM THE MUNSTER BASIN, GERMANY

F. Heller
J.E.T. Channell (both at Institut für Geophysik, ETH Hönggerberg, CH 8093 Zürich, Switzerland.)

Three ferromagnetic minerals: magnetite, haematite and geothite have been identified in the marly limestones of the Münster basin. The blocking temperature and coercivity spectra indicate that these three minerals contribute to the NRM and IRM in varying proportions for different sampling sites. The magnetite magnetization component is considered to be primary, having the same age as the palaeontological age of the limestone. This is confirmed by two positive fold tests which indicate that the magnetite magnetization component pre-dates latest Cretaceous folding. The age of the higher coercivity magnetization components carried by goethite and haematite remains ambiguous partly because no suitable fold tests could be conducted. There is however thin-section evidence that

the goethite occurs after pyrite, and that the haematite is a subsequent dehydration product of the geothite. The haematite magnetization directions are usually significantly different from those attributed to magnetite.

The magnetite magnetization components were isolated for 191 samples from 9 sites. The mean pole position (Lat:75.8, Long:181.1, A_{95}:3.8) is one of the first Cretaceous poles from stable Europe and differs somewhat from Irving's (1977) time-averaged poles for Eurasia which rely heavily on data from Siberia and may be biased by data taken from orogenic belts (Caucasus).

GP 33

CRETACEOUS POLE POSITIONS FOR VOLCANIC AND INTERBEDDED SEDIMENTARY UNITS OF PREVIOUSLY UNDETERMINED AGE FROM NORTHWESTERN SONORA, MEXICO

K. Kluger Cohen
T. H. Anderson
V. A. Schmidt (all at: Dept. of Geology and Planetary Sciences, Univ. of Pittsburgh, Pittsburgh, PA 15260)

Volcanic and interbedded sedimentary units of undetermined age, but believed to be Cretaceous, were sampled at two localities in northwestern Sonora, Mexico for paleomagnetic purposes. One sampling site was located 45 km southwest of Caborca, Sonora and lies south of an inactive transform fault (1,2) that has been proposed to extend northwest - southeast from southern California to the Gulf of Mexico. The transform may have recorded 800 km of sinistral displacement during Mid- to Late Jurassic time. The second site was located north of the proposed transform, 30 km east of Caborca, Sonora.

Preliminary results from demagnetized samples from the site south of the transform show a pole position well in agreement with North American Cretaceous paleopoles. Demagnetized samples from the site north of the transform show a similar North American Cretaceous pole.

These preliminary results appear to establish the age of these units as Cretaceous. In addition, if the transform fault did exist in this area, gross movement along the fault ceased by the time of extrusion and deposition of these sampled units in Cretaceous times.

(1)Silver, Leon T. and Anderson, T. H., 1974 Possible left-lateral early to middle Mesozoic disruption of the southwestern North American craton margin: Geol. Soc. Amer. Abstracts with Programs, v. 6, no. 7, p. 955.
(2)Anderson, T. H. and Schmidt, V. A., 1978, Mesozoic crustal evolution of Middle America and the Caribbean: Geological Considerations: EOS v. 59, no. 4, p. 404.

GP 34

A PALEOCENE POLE POSITION FOR NORTH AMERICA

D. Jacobson
M.E. Beck, Jr. (both at Department of Geology, Western Washington University, Bellingham, WA. 98225)
J.F. Diehl (Mich. Tech. Inst., Houghton, MI. 49931)
B.C. Hearn, Jr. (U.S. Geological Survey, Reston, VA. 22092)

The Moccasin, Judith and Little Rocky Mountains are intrusive structures which partially comprise the petrographic province of Central Montana. Geological mapping shows them to be substantially undisturbed since emplacement. Extension fission track and K/Ar dating by U.S.G.S. personnel yield a Paleocene age (68-60 m.y.). Thirty-eight paleomagnetic sties consisting of 328 oriented specimens were collected; 14 sites from the Moccasins and Judiths (MJ) which are closely contiguous, and 24 from the Little Rockies (LR) some 90 km away. The mean MJ virtual geomagnetic pole (VGP) is located at 144.4° W. long., 77.8° N. lat. with a circle of 95% confidence (α95) of 7.9°. The combination of VGPs from 24 LR sites locate a pole position at 196.1° W. long., 78.9° N. lat. with an α95 of 6.8°. As the circles of confidence overlap for these two pole positions, VGPs of all sites were combined to yield a Paleocene pole position for North America at 176.2° W. long., 79.6° N. lat. with an α95 of 5.3°. This pole position enhances the apparent polar wandering path of North America for a critical period of its history.

GP 35

PALEOMAGNETIC RESULTS FROM EARLY EOCENE INTRUSIVE ROCKS, NORTH-CENTRAL MONTANA -- IMPLICATIONS FOR NORTH AMERICAN APPARENT POLAR WANDERING

J. F. Diehl
S. Beske-Diehl (both at: Dept. of Geology and Geological Engineering, Michigan Tech. Univ., Houghton, MI 49931)
M. E. Beck, Jr. (Dept. of Geology, Western Washington University, Bellingham, WA 98225)
B. C. Hearn (U.S. Geological Survey, Reston, VA 22092)

Paleomagnetic results from the Early Eocene intrusives of the Bearpaw and Highwood Mtns., north-central Montana, yield two well-defined points on the apparent polar wandering path for cratonic North America. Twenty-three sites were drilled from the central core of the Bearpaw Mtns. (54-50 m.y.b.p.), and after magnetic cleaning sixteen sites (145 samples) passed strict reliability criteria yielding a paleomagnetic pole at 80.3°N, 200.9°E (α_{95} = 6.4; kappa = 34.0). In the Highwood Mtns. (53-49 m.y.b.p.), thirty-seven sites were drilled with twenty-nine sites (225 samples) meeting reliability criteria after demagnetization. These twenty-nine sites give a paleomagnetic pole located at 81.3°N, 162.5°E (α_{95} = 7.1; kappa = 15.3). Both poles at the 95% confidence level are statistically the same and distinct from the present day rotational axis.

The above results when combined with the Eocene pole from the Absaroka Mtns., Wyoming, and the recalculated Eocene Rattlesnake Hills (Wyoming) pole yield a mean Eocene (54-43 m.y.b.p.) paleomagnetic pole at 81.9°N, 176.5°E (α_{95} = 3.4; kappa = 711.2). These data, when compared to Paleocene results from north-central Montana, the Cretaceous still-stand poles, and the well grouped Mid-Tertiary poles from the continental interior, suggest that for North America apparent polar wandering for at least the last 90 million years occurred as a succession of rapid shifts of the geomagnetic pole followed by quasi-static periods.

GP 36

WITHDRAWN

GP 37

PALAEOMAGNETIC RESULTS FROM A LATE TERTIARY-QUATERNARY VOLCANO IN NORTHERN BRITISH COLUMBIA

M.E. Evans (Institute of Earth and Planetary Physics, Department of Physics, University of Alberta, Edmonton, Alberta, Canada T6G 2J1)
T.S. Hamilton (Geology Department, University of Alberta, Edmonton, Alberta, Canada T6G 2E3)

Samples spanning a composite section of more than 1000 m have been collected from 50 separate cooling units from Level Mountain - an uppermost Tertiary to Quaternary continental shield volcano in northwestern B.C. Most sites carry a stable remanence which can be determined with high precision (Fisher's precision parameter k generally exceeds 100). These site means record a series of at least 14 magnetic polarity zones, and include several low-latitude VGP's that represent polarity transitions or geomagnetic excursions. Filtering out sites with low-latitude VGP's (N=5) and high internal scatter (N=7) leaves 38 site means, 24 of which have normal polarity and 14 of which are reversed. The average normal direction does not differ significantly from the inverted reversed direction, and the overall mean yields a paleopole at 256E, 85N (A_{95}=7°). The circle of confidence includes the spin axis but the mean itself is slightly near-sided and thus lends no support to Wilson's eccentric dipole model. Instead near-sidedness seems to be a persistent characteristic of poles obtained from western North America, suggesting that a long-term non-zonal anomaly may be present.

GP 38

0-11 MY PALEOMAGNETIC POLAR WANDER RESULTS FROM CENTRAL PACIFIC ORIENTED SEDIMENT CORES

S.R. Hammond (National Ocean Survey, NOAA, Rockville, MD 20852)
F. Theyer
E. Herrero-Bervera (Both at: Hawaii Inst. Geophysics, University of Hawaii, Honolulu, HI 96822)

Apparent polar wander results have been particularly useful in helping to determine the tectonic histories of crustal plates having extensive subaerial exposures, but there are generally fewer such results available for predominantly oceanic plates. Azimuthally oriented deep-sea cores, however, provide a means whereby apparent polar wander paths can be paleomagnetically determined in such regions. Using paleomagnetic data from four oriented, chronologically-successive sediment cores from the central equatorial Pacific, we resolved a sequence of polar positions at 1 MY intervals from 11 MYBP to the Present. While some of these positions are undoubtedly attributable in part to artificial error, (e.g., unrecognized coring induced disturbance to the sediments) most appear to have been systematically influenced by movement of the Pacific plate. Since these initial results are based on relatively few data, any rigorous comparison with other Pacific plate motion solutions is not justified; the present results, however, do appear to be consistent with earlier magnetic studies of north Pacific seamounts. Although it will be possible to confirm and extend these results into the Eocene and Miocene using existing oriented cores, the anticipated ability to recover azimuthally oriented cores with DSDP's hydraulic piston corer will allow such work to be carried out in sediment sequences well beyond the reach of conventional piston corers.

GP 39

PALEOMAGNETIC RESULTS FROM TRUK LAGOON, WESTERN PACIFIC OCEAN

Barbara H. Keating
C. E. Helsley
E. Herrero-Bervera
J. Thompson
J. Naughton (Hawaii Institute of Geophysics, University of Hawaii, 2525 Correa Road, Honolulu, Hawaii 96822)

Paleomagnetic studies were conducted on eight islands within Truk Lagoon (part of the Caroline Islands, in the western Pacific). A total of 52 extrusive and intrusive rock units were sampled. Of these, 19 produced reliable results and yielded a pole position of 336.0°E, 81.6°N.; A_{95} = 9.8. The paleolatitude is consistent with equatorial formation of the islands and subsequent northward motion of the Pacific plate. Both normal and reversed polarity was found. K-Ar age determinations from these sites yield ages of 14-19 million years.

GP 40

PALEOMAGNETISM OF LINE ISLANDS SEAMOUNTS

Wm. W. Sager, Hawaii Institute of Geophysics, Honolulu, Hawaii, 96822
B. H. Keating, Hawaii Institute of Geophysics, Honolulu, Hawaii, 96822

Nine seamounts in the Line Islands (18°N to 12°S, 170°W to 150°W) were surveyed in the fall of 1979 for paleomagnetic studies. The magnetic survey data was contoured after removal of the IGRF as well as diurnal variations. The diurnal corrections were based on magnetic observatory records from Honolulu and Papeete, Tahiti and a temporary equatorial base station on Christmas Island.

Results to date suggest that there were at least two periods of seamount formation, one of which was in the late Cretaceous. Watkins seamount, at 17°25'N, 169°20'W gives a paleomagnetic pole position of 70°N, 13°E, close to other Cretaceous Pacific seamount pole positions (as reported in Harrison et al., 1975). This pole indicates 20° of northward drift since the formation of the seamount.

Paleomagnetism of Pre Mesozoic Rocks

Pier 2 & 3
Friday P.M.
R. B. Hargraves (Princeton Univ.), Presiding

GP 41

LEAST SQUARES ANALYSIS OF MULTICOMPONENT PALEOMAGNETIC DATA: EXAMPLES FROM THE PRECAMBRIAN GUAYANA SHIELD.

T. C. Onstott (Department of Geological and Geophysical Sciences, Princeton University, Princeton, N.J. 08544)

Progressive alternating field and thermal demagnetization data on rock samples collected from the Venezuelan Guayana Shield were analyzed using several least squares methods:

1) Single component lines and two component 'remagnetization circles' were fitted to demagnetization data by a resistant stepwise procedure which employs an iteratively bisquare weighted linear least squares matrix.

2) An iterative weighted nonlinear least squares function which assumes log-normal distributions for the coercivities and blocking temperatures was used to evaluate the approximate blocking temperature and coercivity spectra while simultaneously solving for the directions of the different components.

3) An iterative cubic spline was used to smooth demagnetization data before applying regression methods 1) or 2).

The most favorable results were usually obtained by the first method when the overlaps in coercivity and blocking temperature distributions were small. When these overlaps were larger, the second method tended to give closer fits. Better results were obtained from 'noisy' data with the third method than with the first or second methods alone. Q-mode factor analysis proved quite successful in grouping the different remanent components at the site level and calculating their mean directions.

GP 42

PALEOMAGNETIC RESULTS FROM SEDIMENTS OF THE TIMISKAMING GROUP AND THE BLAKE RIVER GROUP, ABITIBI GREENSTONE BELT

A.M. Tasillo (Department of Geology, University of Toronto, Toronto, Ontario, Canada M5S 1A1)
J.W. Geissman
D.W. Strangway
L.S. Jensen (Ontario Geological Survey, 77 Grenville, Toronto, Ontario,Canada M5S 1B3)

Paleomagnetic data from cobbles in a conglomerate of the Timiskaming Group, overlying the Blake River Group(BRG)(Jensen, 1979)[1], give a positive conglomerate test. Cobbles derived from trachytic volcanics and volcanics of the BRG and Kinojevis Group display dispersed directions of magnetization. Directions from the matrix material of the conglomerate are well-grouped, with a mean in situ direction of magnetization of D=317.6°, I=68.1°, α_{95}=8.1°, k=21.4(n=15 specimens from 4 samples). Upon correcting for structure, the antipodal direction is in good agreement with those from slightly younger Matachewan dikes which cut Kinojevis and Timiskaming units farther to the west. A paleomagnetic study (93 samples, 27 sites) was done on calc-alkaline volcanics and hypabyssal intrusives of the BRG, dated at 2703±2 My(Nunes and Jensen, 1980)[2]. Both single- and multi-component magnetizations are present; there is a poor consistency of in situ directions, e.g. D=346.3°, I=78.0°, α_{95}=14.5 (N=93 samples), for vectors displaying a linear decay to the origin in vector analysis. Weak intensities of remanent magnetization (e.g., 10^{-4} to 10^{-5} Am^{-1}) in some cases prevented resolution of a linear decay of a component of magnetization. The in situ magnetization data do not agree with those from Matachewan dikes, implying that the Matachewan event did not cause pervasive overprinting. Magnetization data within individual cobbles of BRG lithologies in the Timiskaming conglomerate are as dispersed as the in situ data from the BRG itself.

[1] Ont. Geol. Survey M.P. 90, 64-69.
[2] Ont. Geol. Survey M.P. 92.

GP 43

PALEOMAGNETISM OF THE PRECAMBRIAN UNITS OF THE GUAYANA SHIELD, VENEZUELA.

R. B. Hargraves
T. C. Onstott (both at Department of Geological and Geophysical Sciences, Princeton University Princeton, N. J. 08544).

Paleomagnetic study of 300 samples (49 sites) representing five major stratigraphic units (2.1 to 1.5 Ga) give the following results:

1) two or more components of magnetization could be isolated by thermal and alternating field demagnetization.

2) the more stable components present in the metamorphic units were probably acquired during post-orogenic uplift at 2.1 to 1.8 Ga.

3) the more stable components present in the intrusive units are most likely primary TRMs acquired at 1.7 to 1.5 Ga.

4) despite the broad time span involved the corresponding site-poles are closely grouped.

5) the less stable secondary directions observed in the metamorphic and intrusive units probably represent partial remagnetization during the low-grade Nickorie metamorphic episode dated at 1.2 Ga.

The following conclusions are drawn from comparisons with African data:

1) agreement with the African Precambrian paleomagnetic data is better when South America is restored to its pre-drift position.

2) the more stable component site-poles, which after rotation straddle the equator east of Africa (20°N to 20°S and 50°E to 90°E), still remain significantly different from the African polar wander path, particularly the well-established 2060 Ma to 1880 Ma segment.

3) the rotated secondary site-poles fall close to the African polar wander path for 1.2 to 1.0 Ga. This latter correlation would suggest that Africa had become joined to South America by 1.2 Ga and would be consistent with an ensialic origin for the Rokelides Pan African belt. A preliminary Precambrian polar wander path for South America will be presented.

GP 44

PALEOMAGNETISM AND LATE PRECAMBRIAN EVOLUTION OF THE NORTH AMERICAN CORDILLERA

Michael O. McWilliams (Dept. of Geophysics, Stanford University, Stanford, CA 94305)

A synthesis of the available middle and late Proterozoic data from the Siberian platform and North America supports the suggestion of Sears and Price[1] that these two continental masses were juxtaposed in the middle Proterozoic and were rifted apart in the late Proterozoic. However, rather than placing the Siberian Platform west of the present-day United States, the data suggest that it lay to the north, west of the late Proterozoic rifted continental margin of northwestern Canada. A proposed mid-late Proterozoic APWP for Africa is very similar to the North American APWP for that interval, supporting the contention of Piper[2] that Africa lay to the west of North America in Proterozoic times. A model is developed in which Africa and the Siberian Platform comprise the 'unknown' continent which rifted away from western North America to initiate the Cordilleran geosyncline. After initial rifting, the Siberian Platform moves off to its eventual collision along the Urals, while Africa moves independently of the Siberian Platform and collides with East Gondwana along the Mozambique belt in latest Precambrian - early Paleozoic times.

GP 45

PALEOMAGNETISM OF THE CAMBRIAN UNICOI BASALTS, BLUE RIDGE, TENNESSEE AND VIRGINIA.

P.Brown
Rob Van der Voo (both at: Dept. of Geological Sciences, Univ. of Michigan, Ann Arbor, MI. 48109).

Paleomagnetic samples of amygdaloidal basalts of the Lower Cambrian Unicoi Formation of the Chilhowee Group have been collected in NE Tennessee and SW Virginia. Progressive thermal and alternating field demagnetization yielded two directions of magnetization. The direction removed last is interpreted to be primary and has a westerly declination and shallow inclination after unfolding. This direction yields a paleopole in the western Pacific near the equator which fits the North American Cambrian apparent polar wander path. The other magnetization, which is removed at intermediate temperatures or coercivities, has a southeasterly declination and an intermediate positive inclination before unfolding. This direction corresponds to Ordovician - Silurian North American paleopoles. Therefore, the magnetization is interpreted to be acquired after the (Taconic) folding.

GP 46

PALEOMAGNETISM OF THE *CREPICEPHALUS-APHELASPIS* ZONE BOUNDARY (UPPER CAMBRIAN) IN NORTH AMERICA --DIVERGENT POLES FROM ISOCHRONOUS STRATA

S.L. Gillett (Dept. of Earth & Space Sci., State Univ. of New York, Stony Brook, NY 11794)
D.R. Van Alstine (Sierra Geophysics, 150 North Santa Anita Ave., Arcadia, CA 91006)

The scatter of paleomagnetic poles from the Cambrian of North America has been variously attributed to remagnetization, tectonic rotation, rapid apparent polar wander (APW), or non-dipole behavior. Abrupt changes between successive trilobite faunal units ("biomeres" of Palmer, 1965) define several Cambrian timelines (duration perhaps 10^4y); such horizons provide precise time control to test these hypotheses. The *Crepicephalus-Aphelaspis* zone boundary (middle Dresbachian), one such horizon, has been sampled at 2 sites in Tennessee (N[samples]=29 & 48), 2 in Nevada (N=28 & 47), and 1 in Utah (N=25); the upper *Aphelaspis* zone has also been sampled in Alberta at 1 site (N=51). All sites are in thrust belts; vertical-axis rotations of 15-25° are shown by between-site declination differences in both Nevada and Tennessee. Similar rotations can be demonstrated in Alberta by declination differences in Middle Cambrian strata. In turn, paleopoles from all middle Dresbachian sites diverge from cratonic poles from Texas (Watts *et al.*, 1980) which also span this interval. These discrepancies can be explained by remagnetization or by tectonic rotations of up to 45° with respect to the craton. A divergent pole from Dresbachian strata in Arizona (Elston & Bressler, 1977) might also be rotated but probably reflects remagnetization; another pole from Missouri (Beales *et al.*, 1974) is aberrant and may also reflect remagnetization. Probably much of the scatter in Lower Paleozoic poles from North America results from vertical-axis tectonic rotations and/or remagnetization. The extent of rotations and remagnetization must be established before inferences about APW or non-dipole behavior can be made.

GP 47

PALEOMAGNETIC INVESTIGATION OF THE UPPER CAMBRIAN POTSDAM GROUP SANDSTONES, ST. LAWRENCE LOWLANDS, QUEBEC.

Maurice K.-Seguin, K.V. Rao, P. Arnal (Laboratory of paleomagnetism , Department of Geology, Laval University, Quebec, G1K 7P4).

Some 332 oriented cores were collected at 29 sites from the gently dipping sandstones of the Covey Hill (uppermost Middle Cambrian) and overlying Châteauguay (Upper Cambrian) Formations of the Potsdam Group exposed in the vicinity of Montreal. The majority of site-mean NRM directions are widely scattered with intensities 10^{-2}-10^{-3} Am^{-1} and are far displaced from present field direction reflecting the occurrence of low and high coercivity components of magnetization. The NRMs of sandstones were analyzed by means of pilot AF and thermal demagnetization tests. The more effective thermal treatment on selected samples from the Covey Hill Formation revealed the presence of antiparallel normal and reverse polarity directions at high temperature steps 600-650°C characterized by a mean magnetization around 336°, +17° with a corresponding paleopole at 48N, 143E. AF and thermal treatments on the Châteauguay sandstones gave a consistent, single and stable component of magnetization at 260°, -8° with a paleopole of 10S, 160E. Isothermal remanence acquisition experiments at room temperature indicated the presence of magnetite and hematite as the carriers of magnetization in the Covey Hill sandstones while only magnetite was found in the Châteauguay samples.

GP 48

PRELIMINARY PALEOMAGNETIC RESULTS FROM LATE EARLY ORDOVICIAN RED SHALE UNITS IN TACONIC ALLOCHTHONS, EASTERN PENNSYLVANIA

K. P. Kodama
G. G. Lash (both at Department of Geological Sciences, Lehigh University, Bethlehem, PA 18015)

Structural and stratigraphic mapping of Taconic allochthons in eastern Pennsylvania indicates a mixed terrain of tectonic blocks and slices. Geological reconstructions suggest that slices of chert, deep-water limestone, and red shale (late Early Ordovician) were emplaced into graywacke and shale (Middle Ordovician) during southeast-dipping subduction along the east coast of the North American craton. To test this hypothesis, 10 paleomagnetic sites were taken from the red shale units and the graywackes. NRM's from the graywacke sites had scattered directions and weak intensities and were not studied further. Progressive thermal demagnetization (8 steps up to 640°C) of 10 samples from four red shale sites indicate that only two sites (total of five samples) had stable final demagnetization directions based on Zijderveld plots. The mean site directions ($I = 5.1$, $D = 256.4$, $\theta_{95} = 4.5$, $n = 3$; $I = -8.7$, $D = 164.8$, $\theta_{95} = 7.2$, $n = 2$) suggest (1) small-scale tectonic rotations between blocks in accord with the structural mapping of the area (2) low paleolatitudes (within 5° of the equator) for the magnetization position of these units. Further studies are being carried out to substantiate these preliminary results; however these data suggest that North America was at least as far north as indicated by Watts and Van der Voo's (1979) Mocassin-Bays Middle Ordovician pole and not as far south as suggested by their Chapman Ridge pole.

GP 49

PALEOMAGNETISM OF FOLDED LOWER PALEOZOIC SILLS OF THE AVALON PENINSULA, NEWFOUNDLAND

J.P. Hodych (Departments of Physics and Geology, Memorial University of Newfoundland, St. John's, AlB 3X7)
R. Patzold (Geomagnetic Research Laboratory, Department of Physics, Memorial University of Newfoundland, St. John's, AlB 3X7)

Diabase sills intrude Upper Cambrian sediments at Pt. Lance, St. Mary's Bay. The sills are thought to be Upper Cambrian and must predate the probable Devonian age of folding of the sills and sediments. (K-Ar isochron dating by A. Hayatsu is in progress.) Demagnetizing the diabase uncovers a pre-folding remanence at the six sites studied (three on each limb of a large syncline). The resulting virtual paleopole will be compared with lower Paleozoic paleopoles for North America and the British Isles.

GP 50

PALEOMAGNETISM OF SOME EARLY PALEOZOIC INTRUSIVE ROCKS IN THE SOUTHERN APPALACHIAN PIEDMONT

L. Brown
C. Barton (both at: Department of Geology/ Geography, Univ. Massachusetts, Amherst, MA 01003)

Paleomagnetic samples of late Precambrian to Silurian age intrusive rocks were collected in a traverse through the North Carolina Piedmont province. Characteristically the most stable results come from samples of the eastern part of the province where data show single component magnetization directions.

Metasills in the Carolina Slate Belt give a pole position of 27°N, 103°E (alpha 95 = 6.4). These sills have early Paleozoic ages but have been metamorphosed in a later (Acadian) event. This pole is in close agreement with poles for Acadia in the Devonian. Another pluton in the Carolina Slate Belt, the West Farrington, yields a pole position that is not similar to those of the North American craton or the Acadian block.

Metamorphic bodies in the Inner Piedmont and the Blue Ridge appear to have a dominant Taconic metamorphic imprint. A metagabbro in the Bakersville area of the Blue Ridge gives a pole position similar to the mid-Ordovician pole for North America. Preliminary results from the High Shoals gneiss of the Inner Piedmont indicate a bimodal distribution of directions and a pole position that implies a younger than Taconic age.

GP 51

PALEOMAGNETISM OF SOME LATE PALEOZOIC INTRUSIVE ROCKS IN THE SOUTHERN APPALACHIAN PIEDMONT

C. Barton
L. Brown (both at: Department of Geology/ Geography, Univ. Massachusetts, Amherst, MA 01003)

The Piedmont province is generally divided into several northeast-southwest trending belts. Each belt had its distinctive history but the evolutionary history and relationship of these zones to each other and to Appalachian plate motions remains speculative. In order to provide new information about the evolution of the Piedmont region reconnaissance sampling and paleomagnetic analysis of intrusive rocks in four of the Piedmont zones was completed.

Results from an early Carboniferous (326±27 m.y.) pluton located in the Carolina Slate Belt of North Carolina indicate a pole position similar to that of the stable North American craton for the lower Carboniferous. Five sites in the Pee Dee gabbro and the Lilesville granite give a pole of 40°N, 134°E (alpha 95 = 2.8). This data puts an upper age limit of lower Carboniferous on the implacement of the Carolina Slate Belt. Another late Paleozoic pluton, the Churchland granite, located in the Charlotte Belt gives scattered directions after repeated AF demagnetization. At 40 mT a northern component is evident and work is in progress to further isolate this direction.

GP 52

PALEOMAGNETIC RESULTS FROM NORTHERN MAINE AND THEIR BEARING ON DISPLACED TERRAINS

D.J. Spariosu
D.V. Kent (both at: Lamont-Doherty Geological Observatory and Department of Geological Sciences of Columbia University, Palisades, New York 10964)

Recently reported paleomagnetic data from Lower Devonian rocks in northeastern Maine suggest this area was displaced with respect to Laurentia. Oriented samples (96) were collected at 16 sites for paleomagnetic study from the Traveler felsite to further define the tectonic history of the region.

Characteristic magnetizations of both N and R polarity were isolated by alternating field and thermal demagnetization analyses. After correction for structural tilt, the mean directions for both the N and R sites become antiparallel although the overall dispersion does not change significantly. Inverting the directions of the R sites gives a formation mean of D=25°, I=-20° (α_{95}=11°) which corresponds to a paleomagnetic pole at Lat.=29°N., Long.=82°E. (dp, dm=6°, 11°). This paleopole does not fall near other poles from the Acadian displaced terrain and is about 50° different, primarily in longitude, from the pole of the nearby Dockendorf Group which is of similar age and lithology. However, no paleomagnetic data of similar age are available from cratonic North America for comparison. Current work on later Devonian and Lower Carboniferous rocks in the same area should help resolve the significance of the Lower Devonian results.

GP 53

Paleomagnetic studies in the Avalon zone of Cape Breton Island, Nova Scotia.

K.V. RAO, and MAURICE K.- SEGUIN (Paleomagnetic Laboratory, Department of Geology, Laval University, Quebec, G1K 7P4).
E.R. DEUTSCH (Geomagnetic Research Laboratory, Memorial University of Newfoundland, St.John's Newfoundland, A1B 3X7).

As a part of a major program aimed at studying the Paleomagnetism of the Avalon zone in Cape Breton Island, 90 oriented hand samples were collected at 18 sites from radiometrically well dated granitic plutons. Published K-Ar and Rb-Sr age determinations show the existence of two generations of granites with mean values of 560 m.y. (Avalonian orogeny) and 350-410 m.y. (Acadian orogeny) respectively. Oriented sampling was concentrated on 10 sites of the younger suite in the northern highlands and 8 sites of the older suite mainly in the central part of the island. The NRM site-mean directions for both generations of granites show large scatter and are significantly different from the present field direction. Extensive pilot AF demagnetizations on more than 50 specimens from the younger suite of granites led to stable directions at given sites and yielded single characterestic remanence directions with corresponding poles as follows: 5S, 133E; 31S,77E; 59S,95E; 38½S, 168E and 25N, 92½E which are in fair agreement with contemporaneous Siluro-Devonian poles from the New Brunswick and Newfoundland Appalachians. Since the characterestic remanence directions obtained on the younger granites are always present as soft secondary components in the older granites, AF treatment was used to isolate an average high coercive force magnetization direction at 315,+10. Confidence that this residual component is primary is based on its high coercive force and on the absence of a major post-Avalonian tectonic event other than the Acadian orogeny. The stable direction corresponds to a paleopole at 33N,177E as compared with a published pole at 5N,172E for the possibly contemporaneous Cloud Mountain Basalts from Western Newfoundland. The discordance between the pole positions is compatible with the existence of an open Proto-Atlantic ocean.

GP 54

PALEOMAGNETISM OF SOME MISSISSIPPIAN SEDIMENTS OF EASTERN MISSOURI

S.A. Vincenz
S.M. Joharifard (both at: Dept. of Earth & Atmospheric Sciences, Saint Louis University, St. Louis, MO 63156)

A collection has been made from the St. Louis and Salem formations of Upper Mississippian in the St. Louis area, Eastern Missouri. Although the beds are mostly flat lying, they have been gently folded in some localities, allowing application of the fold test. The rocks sampled were limestones and sandstones with NRMs ranging in magnitude from 10^{-8} to 10^{-5} emu. cm^{-3}. Typical paleomagnetic pole positions obtained after AF cleaning were 135°, 35.6°N, dp = 1.8°, dm = 1.9° (positive pole), 114.2°, 29.1°N, dp = 17.1°, dm = 6.1° (positive pole) and 210.5°, 68.0°N, dp = 12.3°, dm = 6.1° (negative pole). The latter clearly reflects a contribution to the magnetization by the present day geomagnetic field while the former two are not unlike the Carboniferous pole positions obtained from the eastern and western parts of the American continent respectively. The data are at the moment too scarce to arrive at some definite conclusions, but extensive studies covering a wider area are being continued.

GP 55

GREAT GLEN FAULT: 2000 KM SINISTRAL DISPLACEMENT DURING THE CARBONIFEROUS

Rob Van der Voo (Dept.Geological Sciences, Univ. of Michigan, Ann Arbor, MI.48109)
Christopher R.Scotese (Dept. Geophysical Sciences Univ. of Chicago, Chicago, IL.60637)

Late Devonian paleomagnetic data from North America and Europe indicate that a 20° sinistral displacement occurred between these two continents; this movement ended before the Early Permian, for which the reconstruction of Bullard et al. (1965) appears to be valid. Since the Lewisian basement in NW Scotland and the basement of Greenland have strong geological affinities, the fault(s) responsible for the displacement is (are) likely to be further south. Published characteristic directions from Middle and Late Devonian rocks located in the Orcadian Basin of N.Scotland give a mean pole near 50°N, 150°E. When corrected for the opening of the present-day Atlantic Ocean this pole (near 50°N, 112°E) is in excellent agreement with Middle and Late Devonian poles for cratonic North America. A comparison of the Orcadian mean pole with results from rocks to the south of the Scottish Highlands (mean pole near 30°N, 154°E) reveals that paleolatitude differences of about 20° occur for contemporaneous rocks, and suggests that the Great Glen Fault accommodated the sinistral motions between Europe and North America. Previous explanations of the Orcadian results were cast in terms of implausible Late Paleozoic - Early Mesozoic remagnetizations. On the basis of Zijderveld plots, constructed from the published data, some of the previous analyses can be shown to be incorrect.

GP 56

FORMATION OF EURAMERICA IN THE PALEOZOIC

Dennis V. Kent (Lamont-Doherty Geological Observatory, Palisades, N.Y. 10964)

Comparision of Late Silurian to Late Carboniferous paleopoles from Baltica, England, Aca-

dia and Laurentia shows a pattern of APW path convergence that can be related to the progressive formation of Euramerica by collisional events and large-scale transcurrent movements between these areas. Siluro-Devonian poles from Acadia and Baltica agree on a conventional reconstruction but are distinct from contemporaneous poles from England and Laurentia. The Early Paleozoic Armorican plate of Vander Voo therefore does not include Acadia but the position of Acadia as well as of Baltic for earlier times is uncertain due to lack of reliable pre-Late Silurian paleomagnetic data. Poles from England agree with those from Acado-Baltica by the Late Devonian; the Charnoid trend of the Caledonides and perhaps the Acadian orogeny can be related to the docking of England (Armorica?) with Acadia and Baltica in the Devonian. There are some indications that the Acadian orogeny may have occurred in different locations and tectonic settings in what are now proximal areas. The Acado-Baltic-England poles come into agreement with poles from Laurentia only by the Late Carboniferous. Until this time and from at least the Late Silurian, Acado-Baltica with the addition of England in the Devonian maintained a consistent, more southerly position with respect to Laurentia. The Carboniferous sinistral transcurrent movement is apparently related to the initial stages of impingement of northward moving Africa-S. America which culminated in the Ouchita/Alleghenian/Hercynian orogeny. The final assembly of Euramerica thus coincides closely in time with the formation of Pangea.

GP 57

TOWARDS A DEFINITIVE POLAR WANDER PATH FOR NORTH AMERICA DURING THE NEOZOIC

C.G.A. Harrison (Rosenstiel School of Marine & Atmospheric Science, University of Miami, Miami, Florida 33149)
T.B. Lindh (same)

We have developed a new method for combining different paleomagnetic studies together in order to derive a polar wandering path for any continent. We shall discuss this method in reference to determining the polar wandering path for North America during the Neozoic.

Our method is different from other popular methods in that a weighting is given to each individual study which depends on the number of times we estimate it has sampled the secular variation of the Earth's field. Thus for a study in which only two lava flows are measured, a weight of not more than two will be given. Allowance is also made for the scatter of VGP's in each study. Each study is assigned an age range, and for studies in which the age of magnetization is known only poorly, the age range is made large. In order to derive a paleomagnetic pole position for a certain age range, the list of individual study poles is searched for age ranges which over lap the age range of interest. If the age range of the study is not completely encompassed by the age range of the pole, then the weighting of the study is reduced correspondingly.

We compare the result of our method with the polar wandering paths produced by Irving and by Van Alstine and de Boer. We find significant departures between our poles and the poles suggested by these authors. We shall attempt to determine whether these departures are caused by different data sets or by the different method of analysis.

Magnetic Field: Origin and Theory

Pier 9
Saturday AM.
K. Hoffman (Calif. Polytechnic. Univ.), Presiding

GP 58

A MAGNETIC DECLINATION CHART OF CANADA FOR 1980

E. Dawson
L.R. Newitt (both at: Earth Physics Branch, Division of Geomagnetism, Energy, Mines and Resources, Ottawa, Canada, K1A 0Y3)

A novel analytical approach was used to determine the complex pattern of magnetic declination (D) in Canada for 1980 from approximately 10,000 magnetic measurements in the north compound (X) and east compound (Y) of intensity. These data were obtained primarily from aeromagnetic surveys by the Earth Physics Branch (EPB), Ottawa, from years 1969 to 1976. After applying corrections for secular variation, a gridding algorithm determined over 4400 mean values of X and Y at 1 degree grid intervals over Canada. A smooth datum field was subtracted from these data and residuals ΔX and ΔY obtained. For smoothing, and to improve interpolation between grid values, a spherical harmonic expression (SHE) was fitted to the residuals to degree 180. Residuals calculated from the SHE were added to the datum values and D was determined from these reconstituted X, Y values. A D-chart was plotted using Calcomp plotter techniques. The r.m.s. fit of the input aeromagnetic data to this chart is 130 nT.

A north magnetic pole position was determined at 77.3° N and 101.8° W, just south of King Christian Island. The average pole motion since 1975 is 24 km/yr. north and 5/km/yr. west.

GP 59

MODELS OF THE MAIN GEOMAGNETIC FIELD 1957-1980

J. C. Cain (U.S. Geological Survey, Denver, CO 80225)
D. R. Schmitz (Colorado School of Mines, Golden, CO 90401)
K. Kawasaki (U.S. Geological Survey, Denver, CO 80225)
L. A. Muth (Univ. of Colorado, Boulder, CO 80302)

A new model of the main geomagnetic field was computed for the interval 1957.0-1978.5 without Magsat data (U030280) and then 1957 to 1980 including a four day sample of Magsat scalar data (U03--80). Using techniques reported at the December 1979 AGU meeting, the spherical harmonic series was computed to degree and order 24 in spatial terms and 14 in their first and second derivatives. After making corrections to most of the data to a Dst level of zero, the average external field was found to be G_1^0 (geomagnetic coordinates) = +20 nT. Due to the difference in direction between positive G and Dst, this means that at Dst = 0, the absolute Dst value is actually 20 nT.

An evaluation of the residuals for each class of data entering the pre-Magsat models showed near gaussian distribution curves, a broad distribution (cer 200 nT rms) which appeared to represent that due to local crustal anomalies, and a narrower scatter due to errors in the observations. A list of the pertinent root mean square deviation by data type for this "core" distribution is as follows (nT and nT/year):

Component	Ḣδ D	Ḟδ Ī	δH	δZ	δF	δX	δY	δZ	Total Components
Observatory	81		100	130		14	22	25	8000
Land	102	115	104	138	145				9800
Marine					81				10000
Canadian Airborne	140*		125*	134	109				11000
Project MAGNET pre-1970	138	133*			85				29000
Project MAGNET 1975-1978	(Components unuseable)				52				1000
Vanguard 3/COSMOS 49					12				4700
OGO-2,4,6					6				30000
Magsat					179 pre-Magsat model				5000
					28 Magsat model				5000

GP 60

RADIAL CURRENT FIELDS IN THE SPHERICAL HARMONIC ANALYSIS OF THE GEOMAGNETIC FIELD

K. Kawasaki (U.S. Geological Survey Denver, CO 80225)
J. C. Cain (U.S. Geological Survey, Denver, CO 80225)
D. R. Schmitz (Colorado School of Mines, Golden, CO 80401)

Measurements of the geomagnetic field by means of near-earth orbiting spacecraft contain contributions from field-aligned currents penetrating the shell of observations particularly in the auroral and polar regions. If such observations are used to create spherical harmonic coefficients of a scalar potential function, the fundamental premise on which the analysis is based, namely that the field be curl-free, is violated. This paper considers the theoretical and numerical aspects of such an analysis and concludes that radial currents penetrating the shell have little effect on the resulting coefficients so long as the analysis is based on an adequate distribution of the total horizontal vector in the shell. Also, since the fields of radial currents have no effect on the resulting scalar potential, the difference between the observed field and the field calculated from the potential will give the field of the radial currents.

GP 61

DOES SATURN'S MAGNETIC FIELD VIOLATE DYNAMO THEORY?

J.P. Todoeschuck (Department of Mining & Met. Eng., McGill University, Montreal, Quebec)
M.G. Rochester (Department of Physics, Memorial University, St. John's, Newfoundland)
D.J. Crossley (Department of Mining & Met. Eng., McGill University, Montreal, Quebec)

Recent measurements have shown that Saturn's magnetic field has a high degree of axisymmetry. This would seem to be forbidden by a fundamental theorem of magnetohydrodynamics due to Cowling. This states that an axisymmetric velocity field (expected in a rotating reference frame) cannot maintain an axisymmetric magnetic field in an incompressible fluid.

There are at least three distinct ways of circumventing this apparent conflict which will be discussed. These are (a) the existence of higher order terms in Saturn's magnetic field which have not been observed, (b) the possibility of a nearly symmetric dynamo, operating at high magnetic Reynolds number, as discussed by Braginskii and (c) a relaxation of Cowling's theorem in a compressible fluid. This last possibility has recently been investigated in some detail.

GP 62

THE DISTRIBUTION OF THE NONDIPOLE FIELD AS A FUNCTION OF THE SOURCE GEOMETRY

R. Dodson (Department of Geological Sciences, University of California, Santa Barbara, CA 93106)

The vector distribution of the nondipole field as a function of various point source geometries has been studied. Provided that the number of sources is so large that the central limit theorem applies, the distribution of most source geometries is found to be a trivariate normal distribution whose covariance matrix can be calculated from the field equations of the sources. In particular it can be shown that if the sources are identically distributed in moment and uniformly distributed on a shell (or shells) within the core, and their moments are perpendicular to the shell (or the tangential components are uniformly distributed in azimuth), then the covariance matrix is invariant with respect to geographic location and is specified by only two independent variances. This distribution is not uniform in which case only one variance is required. The paleomagnetic record indicates that the magnitude of the nondipole field vector increases sharply with increasing latitude. In terms of a source geometry, this fact can be accounted for only if the number of sources, their average moment or the variance of their moment increases with latitude. Any of these variations result in a more complicated field covariance matrix whose orthogonal axes in general do not coincide with the geographic axes.

GP 63

PALEOMAGNETIC STUDY OF A GEOMAGNETIC FIELD REVERSAL RECORDED IN THE CHUGWATER FORMATION, WYOMING.

E. Herrero-Bervera
C. E. Helsley (both at: Hawaii Institute of Geophysics, University of Hawaii, Honolulu, Hawaii 96822)

A total of 262 samples (516 specimens) were drilled at four different localities in the Red Peak member of the Chugwater Formation along a 110 km stretch between Dubois and Lander, Wyoming. The stratigraphic interval in the redbeds containing the reversal in the remanent magnetic field averages 3 m and was sampled at 3 to 20 cm spacing between samples. All samples were thermally demagnetized at 500, 620 and 660°C showing directions of magnetization of normal, reversed and transitional character as well as a decrease in the remanent intensity in the transition zone. Calculation of pole positions using short intervals above and below the

reversal individually disagree, yet the overall mean pole of the four sampled sites (49.6°N, 108.3°E) agrees well with the previous Lower Triassic poles for the Chugwater Formation published by various authors.

Results of this study suggest: (1) After the removal of secondary components by means of thermal cleaning the polarity transition exists and can be correlated between sites, (2) The dipole field which decays substantially before the polarity reversal occurs, thereby perhaps allowing the nondipole field to predominate during a portion of the transition.

GP 64

THE NON-DIPOLE FIELD DURING GEOMAGNETIC FIELD REVERSALS

I. Williams
M. Fuller (Both at: Department of Geological Sciences, University of California, Santa Barbara, CA 93106)

Virtual geomagnetic pole (VGP) paths from various records of the last reversal show a dependence on the observation site meridian. This suggests that the transition field is non-dipolar yet dominated by low order zonal harmonics (Hoffman 1977, Hoffman and Fuller 1978). Predictions from quadrupolar or octupolar transition fields have been compared with the available VGP data. However these VGP paths do not determine which of the two geometries is most important.

As an alternative approach we have used the low order zonal harmonics to model the change of inclination and intensity during a transition. The dipole energy is reduced and distributed amongst the other harmonics in a variety of "reasonable" ways.

It is interesting that neither a purely octupole nor quadrupole intermediate field fits the observed behaviour of inclination. A combination of the two fields models the data better. This analysis suggests that the decrease in intensity will not be symmetric about the change in inclination. Both the intensity change and the apparent time taken for the transition, are dependent upon the latitude of the observation site.

GP 65

ON THE DOMINANT GAUSSIAN COEFFICIENTS OF THE TRANSITION FIELD DURING THE MATUYAMA-BRUNHES REVERSAL

K. A. Hoffman, (Physics Dept., Calif. Polytechnic State Univ., San Luis Obispo 93407)

A model of the reversing geodynamo based on the assumptions (1) that reversals start in a localized region of the core and (2) that upon its onset this reversed region extends, or "floods" both north-south and east-west until the entire core is affected, has recently been shown to successfully simulate existing paleomagnetic records of the reversing field during the Matuyama-Brunhes transition (Hoffman, 1979). An analysis of the modeled field during the transition reveals that the dominant components at the time of total axial dipole decay include an axial octupole (g_3^0) and a non-axial quadrupole (g_2^1, h_2^1). Given the distribution of sites corresponding to the available records of the Matuyama-Brunhes, the existence of a significant axial quadrupole field component cannot be ruled out; however, the role of any equatorial dipole component can be neglected. The modeled minimum field intensity is found to be dependent on both site latitude and longitude. For the Matuyama-Brunhes the modeled minimum strength experienced, say, at mid-northern latitudes is about 10% of the full polarity strength, yet such values differ from site to site by more than a factor of 3.

Although not a unique solution, the findings from this analysis may be considered to be independent of the phenomenological model from which they were derived. For example, whether the above determined transitional field geometry is modeled to be produced by configurational changes of the reversing geodynamo or alternatively, to be of a stationary (non-reversing) origin has little effect on the calculated VGP path localities for a given site. These two possible situations, in principle, should be distinguishable given sufficient transition data corresponding to back-to-back (R→N and N→R) reversals.

GP 66

STOCHASTIC MODELS FOR THE POLARITY BIAS OF GEOMAGNETIC REVERSALS

Allan Cox Dept. of Geophysics, Stanford University, Stanford, CA 94305)

The main statistical features of the geomagnetic reversal process are simulated quite well by a variety of deterministic and stochastic models. However bias in the lengths of polarity intervals such as that at the end of the Mesozoic (normal polarity bias) and that at the end of the Paleozoic (reversed polarity bias) has not as yet been modeled either deterministically or stochastically. Two classes of stochastic models are presented to account for polarity bias. In the first, instabilities in the dynamo process which accompany reversals are assumed to occur at a higher rate during one polarity than during the other. In the second, the rate at which instabilities occur remains constant but a different fraction of instabilities are infertile in the two polarity states. The most likely cause of changes in reversal frequency and changes in polarity bias is mass transfer in the lower mantle capable of producing undulations and temperature variations at the core mantle interface, the latter providing the boundary conditions for the dynamo. Symmetry considerations require the presence of odd zonal harmonics in these boundary conditions during times of polarity bias. Moreover because changes in polarity bias occur with a much longer characteristic time than do changes in reversal frequency, the lower mantle processes responsible for changes in bias may well have longer time and length scales than do the processes responsible for changes in frequency. An interesting speculation is that changes in reversal frequency may reflect shifts in the location of individual lower mantle convective cells whereas changes in polarity bias may reflect changes in the entire pattern of mantle convection such as might, for example, be associated with a regrouping of the continents.

GP 67

GEOMAGNETIC SECULAR VARIATION IN SOUTHERN ITALY AND ITS APPLICATION TO ARCHEOLOGICAL DATING

G.S. Hoye (Institute of Earth and Planetary Physics, Department of Physics, University of Alberta, Edmonton, Alberta, Canada T6G 2J1)
M.E. Evans

The lavas from nine eruptions of Mount Vesuvius have been sampled at 20 sites, the dates of the eruptions (1631-1944 A.D.) covering the complete range of historically recorded lava flows. In addition, the mud flow resulting from the Plinian eruption of 79 A.D. was sampled at Herculaneum. Eleven archeological baked features (kiln, hearth, or oven) of well-determined archeological date covering the interval from the eighth century B.C. to the fourth century A.D. were also sampled.

Site mean magnetic directions from the lavas are precise (typically α_{95} is $\lesssim 2°$ for N=5) and yield an elliptical secular variation curve for the last few centuries which is in agreement with observed data for Rome after allowing for dipole variation in inclination. The (detrital?) remanence of the 79 A.D. deposit is stable and is not aligned with the present field direction.

An archeomagnetic date (lying in the second half of the first century A.D.) for a kiln situated in a *villa rustica* at San Giovanni di Ruoti has been derived using data from this study and this date is consistent with the circumstantial archeological evidence relating to the kiln.

GP 68

MAGNETIZATION IN THE LOWER CRUST

Peter Wasilewski (NASA/Goddard Space Flight Center, Laboratory for Extraterrestrial Physics, Greenbelt, Maryland 20771)
Elaine Padovani (Dept. of Earth & Planetary Science, MIT, Cambridge, MA 02139)

Deep crustal and mantle xenoliths from numerous sources along the Rio Grande rift and the Colorado plateau, granulites from high grade metamorphic terrain in North America, India, Brazil, and Africa, and a profile across the Ivrea zone have been studied in order to evaluate the distribution of magnetization in the deep crust. These preliminary studies provide additional confirmation of our idea that the Moho is a magnetic boundary. There is no evidence of exotic magnetic mineralogy or metal in any of the rocks studied. Naturally reduced basaltic rocks containing a range of titanomagnetite from $Fe_{2.4}Ti_{0.6}O_4$ to Fe_2TiO_4 with increasing dominance of ilmenite and finally metallic iron are used to model what might be expected magnetically with increasing degrees of reduction in the lower crust. The fO_2-T conditions at depth will determine the Curie point of the oxide minerals and the geothermal gradient will determine the depth at which this mineralogy is non-magnetic. Several preliminary models of continental crust magnetization are presented based on the magnetic measurements, since no single model is likely to hold for the entire continental crust. The magnetic properties of deep crustal rocks may reside entirely along the present geomagnetic field. The magnetization contrast is made up of three terms: $\chi_o H$-the induced component dependent an amount, composition and grain size of the magnetic mineralogy, M_v-the viscous magnetization which is enhanced with depth because of increasing temperature at depth and $\chi_H \cdot H$ - presently not well defined contributions due to pressure and the effect of susceptibility enhancement within 100°-150°C of the Curie point.

GP 69

AEROMAGNETIC INTERPRETATION OF THE ARCHEAN VOLCANICS IN THE KIRKLAND-LARDER LAKE AREA OF ONTARIO

Stephen Letros, (Department of Physics and Geology, University of Toronto, Toronto, Ontario M5S 1A1, Canada)
D.W. Strangway (Toronto)
(Sponsor: D.W. Strangway)

High resolution total field aeromagnetic data for the 2.7 billion year old volcanic sequences north of Kirkland Lake are being operated on by geophysical filtering techniques. This is done to enhance the data in order to derive geological information. Magnetic properties such as susceptibilities, NRM directions and intensities and known geological information are being used as a control over the interpretation. Data enhancement techniques have focused on three approaches; first vertical derivation, downward continuation and apparent susceptibility mapping. The latter technique which reduces anomaly overlap and allows for an accurate location of formation boundaries was the most useful for interpretative purposes.

Five major rock types were found in this area, these being magnesium and iron-rich tholeiitic flows, calc-alkaline volcanics and various mafic and felsic intrusives. The iron-rich tholeiites are in general extremely magnetic and the calc-alkalines only weakly magnetic. The paleomagnetic results suggest that the remanent magnetization of the iron-rich tholeiites and the ultramafic intrusives are the main source of the anomalies while negative susceptibility contrasts due to the magnesium-rich tholeiites are observed. Thus detailed geologic mapping of the thick stratigraphic sequences is possible.

GP 70

AN ALTERNATIVE EXPLANATION FOR INTERMEDIATE WAVELENGTH MAGNETIC ANOMALIES

L. Shure (Institute of Geophysics and Planetary Physics, Scripps Institution of Oceanography, University of California, San Diego, La Jolla CA 92093)
R. L. Parker (Institute of Geophysics and Planetary Physics, Scripps Institution of Oceanography, University of California, San Diego, La Jolla, CA 92093)
L. M. Dorman (Geological Research Division, Scripps Institution of Oceanography, University of California, San Diego, La Jolla, CA 92093)

Harrison and others have examined very long magnetic-field profiles and have calculated their one-dimensional power spectra. In these they expected to see, but did not find, a minimum in power at intermediate wavelengths, between 65 km and 1500 km (from sea-floor

spreading signal-to-core-signal). They have invoked mantle sources or high-intensity, long-wavelength magnetization as possible explanations.

An alternative, more plausible explanation is that one-dimensional spectra of two-dimensional fields contain contributions from wavenumbers in the perpendicular (i.e. non-sampled) direction, and that unless the sea-floor spreading anomalies are perfectly lineated at right angles to the profiles, the low wavenumber energy can be attributed to this effect. We give a numerical demonstration.

Magnetic Properties

Pier 9

Saturday P.M.

S. Cisowski (NASA) and *D. J. Dunlop* (Univ. of Toronto), Presiding

GP 71

POSSIBLE REMAGNETIZATION ASSOCIATED WITH NATIVE COPPER DEPOSITS, MICHIGAN

H.C. Halls (Dept. Geology, Erindale College, Univ. of Toronto)
H.C. Palmer (Dept. of Geophysics, Univ. of Western Ontario, London)

Thermal and AF demagnetization results are presented from paleomagnetic sites distrubuted along a 50 km strike length in the Copper Harbor Formation, Keweenaw Peninsula, Michigan, where almost 1500 metres of pebble/boulder conglomerate are interbedded with a few thin lava flows.

Three previously measured sites, using pebbles in the conglomerate (Palmer et al. 1977, EOS, 58) have now been supplemented by 8 more from the lava flows. Both studies reveal partial CRM overprinting of pre-folding age which increases along strike in a westerly direction. This westward change is expressed in the conglomerate by a greater clustering of pebble directions to westerly declinations, and in the volcanics by a change from single to multi-component behaviour.

A primary component exists in 7 volcanic sites and has a direction (299/40) about 10° from that found in the underlying Portage Lake Volcanics (PLV). The four most westerly sites yield two overprints, both of which are more resistant than the primary to either demagnetization procedure. One is relatively well determined (287/+20) whereas the other (287/+8°) is less constrained. Both directions (obtained after unfolding) are similar to the pretilting overprint found in the Copper Harbor conglomerate (279/+15).

In the underlying PLV there is also a westerly increase in hydrothermal/burial alteration, as given by secondary minerals including native copper (Stoiber and Davidson, 1959). The possibility that the magnetic overprinting seen in the Copper Harbor Formation is related to this mineralisation will be explored.

GP 72

PALAEOMAGNETISM OF A SULFIDE ORE

K.C. Claesson (Dept. of Geology, Univ. of Toronto, Toronto, Ont. M5S 1A1, Can.)
F.W. Beales
(Sponsor: G.W. Pearce)

The object of the study is the feasability of using palaeomagnetic techniques to date the magnetisation of Mississippi Valley type sulfide ores. The samples come from Nanisivik, Baffin Island, where ore (predominantly pyrite, but also sphalerite and galena) is found in dolomite of Helikian age.

Usually, the initial intensity of magnetisation is 10^{-3} amp/m, although intensities as low as 10^{-5} amp/m can be measured as the cryogenic magnetometer accepts samples 200-300cc in volume. The demagnetisation is problematic: alternating field treatment either introduces an ARM or is ineffective, probably due to the screening effect of conductive pyrite. The same mineral oxidises at 350-400°C to highly susceptible maghemite (?), always adding a large TRM, and heating the specimen packed in graphite only delays this reaction for about 100°C. Furthermore, removal of the oxidised surface shows that internal new phases, too, are likely to pick up spurious magnetic components. The results fall into two, oppositely directed, groups, suggesting a Lower Palaeozoic age of magnetisation.

GP 73

MAGNETIC PROPERTIES OF DRILLED SUBMARINE INTRUSIVE ROCKS

M. Prévot (Laboratoire de Géomagnetisme du CNRS, 94100 St. Maur-de Fossés, France)
D.J. Dunlop (Geophysics Laboratory, University of Toronto, Toronto, Ont. M5S 1A7)

We report paleomagnetic and rock magnetic properties of 50 submarine intrusive rocks drilled in DSDP Legs 30, 37 and 45: 15 doleritic gabbros (Leg 30); 10 cumulate gabbros and 16 serpentinized cumulate gabbros and peridotites (Leg 37); and 9 serpentinized lherzolites (Leg 45). The collection provides a reasonably representative vertical section through the oceanic crust. The principal magnetic mineral revealed by microscope, electron microprobe and thermomagnetic analysis is nearly pure magnetite (Tc = 515-575°C). In the doleritic gabbros, it is an abundant, coarse-grained deuteric oxidation product of titanomagnetite; in the cumulate gabbros, it is scarce and invisible, presumably occurring as inclusions in silicates; and in the other rocks, it is a sometimes abundant, fine- to coarse-grained by-product of serpentinization of olivine. NRM tends to be directionally stable during AF demagnetization or, in the case of the rather viscous doleritic gabbros, to have an underlying stable component. NRM's of the doleritic gabbros range from 1 to 7 x 10^{-3} emu cm^{-3}. If our samples are typical of layer 2B and the top of layer 3, these layers cannot be disregarded as magnetic anomaly sources. The cumulate gabbros have weak NRM's (10^{-5}-10^{-3} emu cm^{-3}). The serpentinized rocks have NRM's of 10^{-4}-10^{-2} emu cm^{-3}. The peridotites in particular are intensely magnetized (10^{-3}-10^{-2} emu cm^{-3}) and represent a potent magnetic source if serpentinization extends to great depths.

GP 74

PALEOINTENSITY AND MAGNETIC PROPERTY MEASUREMENTS OF TYPE LOCALITY SAMPLES FROM THE KOMATI FM., SWAZILAND

C.J. Hale (Dept. of Geology and Geophysics Laboratory, University of Toronto, Ont. M5S 1A7)
D.J. Dunlop (Geophysics Laboratory, University of Toronto, Toronto, Ontario M5S 1A7)

The Komati Formation is of particular paleomagnetic interest because of its great age and low degree of metamorphism. Five independent but unoriented samples from the type locality have been subjected to AF and thermal demagnetization, hysteresis, and thermomagnetic measurements as well as paleointensity measurement using the modified Thellier double heating method. The NRM is strong in all samples measured, having an average intensity of 6.2 x 10^{-3} emu cm^{-3} but the stability is variable with median demagnetizing fields ranging from 100 to 350 Oe. and initial directional swings occurred in three out of five samples. In all samples though, an appreciable fraction of the remanence has a coercivity higher than 500 Oe. Thermal work showed that the majority of magnetic carriers have blocking temperatures within 50 degrees of the Curie temperature (θc = 583°C.) and thermomagnetic curves were nearly reversible with only a few per cent decrease in saturation magnetization upon heating to 650 C. All heatings were carried out in a vacuum of less than 50 millitorr. The paleointensity measurements yielded sublinear curves and fitted slopes indicated paleointensities from 0.16 to 0.5 G. with an average value of 0.26±0.12 (1σ). Direct comparison with the present field intensity is not possible since the Komati samples are unoriented and no correction may be made for paleolatitude but it appears that a geomagnetic field roughly comparable to the present one in intensity was active as early as 3.4 Ga.

GP 75

ARCHEOMAGNETISM OF A 19TH-CENTURY POTTERY KILN NEAR JORDAN, ONTARIO

M.B. Zinn (Dept. of Physics, Erindale College, University of Toronto, Mississauga, Ont. L5L 1C6)
D.J. Dunlop (Geophysics Laboratory, University of Toronto, Toronto, Ont. M5S 1A7)

The Jordan pottery kiln near St. Catharines, Ontario was last fired about 1840. Bricks from the kiln floor have NRM's (Natural remanent magnetizations) in the range 0.2-3.7 x 10^{-2} emu cm^{-3} which are stable against AF demagnetization to 1000 Oe and thermal demagnetization to 520 or 540°C. The average NRM direction (D = 359.4° = +71.3°, α_{95} = 2.2°, k = 310, N = 15 samples) agrees well in declination with the 1845 geomagnetic field recorded at the Toronto observatory (D = 358.6°) while differing significantly from the present field at the site (D = 351.5°). However, there is an "inclination error": the NRM inclination of 71.3° is significantly shallower than either the 1845 inclination (75°) or the present field inclination (72.8°). Twenty-seven specimens of the 31 tested yielded reliable paleofield intensities by the modified Thellier double-heating method. The average paleofield intensity is 1.166±0.092 times the present field intensity. Part of the inclination error could result from systematic tilting of bricks in the kiln floor but the greater part of the error results from self-demagnetization of the kiln floor. NRM's ≥ 10^{-2} emu cm^{-3} produce an internal demagnetizing field ≳0.05 Oe opposing the vertical external field but generate no horizontal field. The result is to deflect the net internal field, and with it the NRM vector, into the plane of the kiln floor. The internal field recorded by the NRM is also weaker than the true paleofield. The 1845 field intensity at Jordan could be as much as 1.43 times the present field intensity if self-demagnetization accounts for the entire inclination error.

GP 76

RELATIONSHIP BETWEEN MEDIAN DESTRUCTIVE FIELD AND REMANENT COERCIVITY FOR DISPERSED NATURAL HEMATITE, MAGNETITE AND TITANO-MAGNETITE

Peter Dankers (Earth Physics Branch, Energy, Mines and Resources, Ottawa, Ontario, Canada. K1A 0Y3)
(Sponsor: J.L. Roy)

Remanent acquisition curves, remanent hysteresis curves and alternating field demagnetization curves were determined for a number of artificial rock specimens containing well defined grain-size fractions between 5 μm and 250 μm of natural magnetite, titanomagnetite and hematite. From these curves, the remanent acquisition coercive force H'_{cr}, the remanent coercive force H_{cr} and the median destructive field of IRM $H_{\frac{1}{2}I}$ were determined. Theoretically these parameters should be the same for an assembly of non-interacting, homogeneously distributed, randomly oriented single-domain grains. For a given hematite specimen H'_{cr}, H_{cr} and $H_{\frac{1}{2}I}$ have about the same value in spite of the strong grain-size dependence of these parameters. For each specimen of magnetite and titanomagnetite the value of H'_{cr} is larger than H_{cr} which again is larger than $H_{\frac{1}{2}I}$. However, the ratios H'_{cr}/H_{cr} and $H_{\frac{1}{2}I}/H_{cr}$ appear to be constant. An interesting relationship which appears to hold for dispersed magnetite, titanomagnetite or hematite grains between 5 μm and 250 μm, independently of grain-size, quantity and packing density of the magnetic material is:

$$H'_{cr} + H_{\frac{1}{2}I} \simeq 2H_{cr}$$

GP 77

MAGNETIC DOMAIN OBSERVATIONS OF NUCLEATION PROCESSES IN NATURALLY-OCCURRING TITANOMAGNETITES

S. L. Halgedahl
M. Fuller (Both at: Department of Geological Sciences, University of California, Santa Barbara, CA 93106)

Magnetic domain patterns have been observed with the Bitter technique in titanomagnetite

(x = 0.6) particles occurring in oceanic basalt (DSDP Leg 49). Fine particles of 15 μm or less carrying isothermal saturation remanence (I_SRM) are often observed to contain no domain walls. Application of a reverse field, however, results in nucleation of at least one wall. Thus, although these fine particles may remain as single domains in I_SRM, they reverse their magnetization by nucleation and subsequent motion of domain walls. These observations suggest that spontaneous nucleation of walls subsequent to saturation becomes more difficult as the particle size approaches the single domain limit. Nucleation processes may therefore play a critical role in controlling the remanence and stability properties of fine particles. A simple model in which nucleation is considered predicts the approximate 1/d-dependence of J_r/J_S and H_C observed experimentally in the PSD range.

GP 78

EFFECT OF POROSITY ON THE STRESS DEMAGNETIZATION OF SOME IGNEOUS ROCKS

Y. Hamano (Department of Geological Sciences, University of California, Santa Barbara, CA 93106)

Ten rock samples were stepwise demagnetized by uniaxial compression up to 300 bars. Rock types used in this study are welded tuff, dacite, andesite and basalt, and these rocks are collected in Japan. In order to investigate the effect of rock structure on the stress sensitivity, rocks with various porosities (ranges from 6% to 48%) were selected. Intensity of the NRM in these rocks ranges from 2×10^{-5} to 1×10^{-2} emu/cm^3 and that of the median destructive field (MDF) is from 35 to 860 oe. Measurements of both hysteresis properties and the Curie temperature indicate that magnetic minerals in these rocks are mainly Ti-poor titanomagnetites with multi-domain grain sizes.

The observed stress sensitivity in these rocks ranges from 0.5% to 40% at 100 bars. Comparison of the stress demagnetization curve and the AF demagnetization curve in each rock sample suggests that the magnetically softer components are demagnetized at the lower stress. However, the equivalent stress, which is defined as a ratio of the stress to the magnetic field which causes the same amount of the demagnetization, is not constant for the different rocks, and varies from 3 to 30 bar/oe. The variation of the equivalent stress is closely correlated with that of porosity. This result indicates that the stress sensitivity, besides for being function of magnetic hardness, is also largely dependent upon porosity of the rocks.

GP 79

MIMETIC SHAPE ANISOTROPY IN OOLITIC LIMESTONES

W. Lowrie (Institut für Geophysik, ETH-Hönggerberg, CH-8093 Zürich, Switzerland)
R. Kligfield (Geologisches Institut, ETH-Zentrum, CH-8092 Zürich, Switzerland)

Deformed Jurassic oolitic limestones from the sedimentary cover of the Aar Massif (Swiss Alps) contain abundant magnetite and hematite. Magnetic mineralogy was investigated by AF and thermal demagnetization, IRM acquisition, low temperature studies, and thin and polished section examination. Chamosite (an iron chlorite) occurs in concentric bands within undeformed oolites; after deformation it assumes the ellipsoidal shapes of the deformed oolites. During metamorphism as well as laboratory heating, chamosite decomposes at 400°C to produce hematite and magnetite. Newly crystallized magnetites have euhedral individual grain shapes but their overall distribution is controlled by the elliptical bands of chamosite. The resultant stringing together of magnetites gives rise to a mimetic shape anisotropy directly related to the shape of the deformed oolite. Hematite layers occur around the shapes of some of the oolites. Preferred orientation of the hematite basal planes around the oolite shapes probably contributes to the magnetic anisotropy. The low-field magnetic susceptibility anisotropy measured on Digico and cryogenic magnetometers has been correlated with the finite strains determined from the oolites. The results demonstrate that it is possible in these rocks to perform quantitative strain analysis with the magnetic susceptibility anisotropy data.

GP 80

SOME SIMPLE MODELS OF NON-INTERACTING AND INTERACTING PARTICLE MAGNETIZATION PROCESSES

R.J. Luce
V.A. Schmidt
F. Keffer (all at: University of Pittsburgh, Pittsburgh, PA 15260)

The traditional hyperbolic tangent, describing uniaxial, single-domain particles lying up or down along an applied field, fails to match experimental magnetization data not only because of its too-rapid saturation but because it yields magnetization values which are generally too high when an observed particle size is included in the tanh argument.

Consideration of particles lying at every possible angle with respect to the applied field helps correct both the high-value and saturation problems. Inclusion of inter-particle interactions, indicated by the observed clumping of particles, can also help lower the theoretical curve.

Examples of uniaxial, single-domain ensembles of 1, 2, 4, 8, and many-particle groups, over all angles, both interacting and non-interacting, are discussed. Single-domain magnetite, with its eight easy directions, is also considered.

GP 81

DISCRETE SINGLE AND PSEUDO-SINGLE DOMAIN MAGNETITES DOCUMENTED WITH SCANNING TRANSMISSION ELECTRON MICROSCOPY

N.G.Newberry (Department of Geological Sciences, U of Michigan, Ann Arbor, MI)
J. W. Geissman (Department of Geology, U of Toronto, Toronto, Ontario M5S 1A1)
D.R. Peacor (Department of Geological Sciences, U of Michigan, Ann Arbor, MI)

Single-domain (SD) and pseudo-single domain (PSD) magnetites are empirically and theoretically known to carry a stable remanence, but their presence in natural rocks has only been indirectly implied by several workers. We have, using a Scanning Transmission Electron Microscope confirmed the existence of natural single-domain sized ($< .05\mu$) grains, and determined the distribution of various-sized magnetites in rock samples. The magnetite grains were characterized by first scanning ion-thinned samples at low (5000X) magnification for small iron-bearing areas, using micro-micro electron diffraction techniques to verify that they in fact have the magnetite structure, and obtaining high resolution chemical analysis of the grains with an energy-dispersive detector. The principal lithology examined is a vitrophyre of an Oligocene ash-flow tuff exposed near Yerington, Western Nevada, whose rock magnetic properties (H_C>25 mT, H_{CR}>40 mT, MDF >mT, J_S/J_R>.25, T_C= 555°C) and blocking temperatures (580° C) suggested the presence of SD and PSD sized magnetite grains. The SD and PSD magnetites occur as scattered grains or clusters of grains within a groundmass glass. The overall magnetic behavior of these rocks derives from an integration over the properties of the small SD and PSD grains and those of the larger ($\simeq 200\mu$) grains of magnetite also present which are subdivided on a fine scale by ilmenite.

GP 82

DETERMINATION OF FINITE STRAINS FROM MAGNETIC SUSCEPTIBILITY MEASUREMENTS ON PERMIAN ROCKS FROM THE MARITIME ALPS (S. FRANCE)

W.H. Owens (Dept. Geol. Sci., Univ. Birmingham, England)
R. Kligfield (Geologisches Institut, ETH, CH-8092 Zürich, Switzerland)
W. Lowrie (Inst. für Geophysik, ETH, CH-8093 Zürich, Switzerland)

Abundant deformed reduction spots found in the Permian red shales and slates of the Maritime Alps of S. France serve as finite strain indicators. Structural studies (Graham, 1979) demonstrate that although deformation varies locally in both intensity and style, the entire region can be characterized by an overall deformation path. Magnetic susceptibility anisotropy measurements were made on these rocks with a cryogenic and a Digico magnetometer. The sedimentary magnetic fabric of undeformed regions is modified during deformation to yield characteristic magnetic susceptibility anisotropy patterns at each of 7 sites corresponding to key localities on the deformation path. The magnetic equivalent of the deformation path demonstrates that a sedimentary magnetic fabric is modified by strain, changing progressively from oblate to prolate, then back to oblate as deformation increases. An empirical correlation between natural strain and the magnetic susceptibility anisotropy has been determined for different lithologies. This agrees with the reorientation during strain of an initially uniform distribution of oblate particles (hematites), calculated according to March theory. Use of this method provides a rapid means of strain determination from magnetic susceptibility measurements, which is especially valuable where the reduction spots are missing.

GP 83

STRAIN TO MAGNETIC ANISOTROPY CORRELATION, A DISCUSSION OF A POSSIBLE UNIVERSAL RELATIONSHIP

J.S. Rathore (Department of Geophysics and Planetary Physics, School of Phyiscs, University of Newcastle upon Tyne, England)

(Sponsor: Professor S.K. Runcorn, F.R.S.)

The need for and the foundations of an empirical correlation between the strain anisotropy and the magnetic susceptibility anisotropy are discussed. The concept of a universal correlation with respect to an established strain response model is presented, as indeed is an empirical relationship which is found to hold in two separate lithologies in the British Caledonian slates. The relationship is of the type

$$\left(\frac{\chi_i}{\chi_j}\right) = \left(\frac{\ell_i}{\ell_j}\right)^a$$

where i = 123; j = 123, $i \neq j$, χ_i and χ_j are two of the three principal magnetic susceptibility axes and ℓ_i and ℓ_j are the corresponding principal strain ellipsoid axes. The existence of such a relationship is of importance since it presents the possibility of predicting strain axial ratios from the readily measurable susceptibility ellipsoids, and hence determining the tectonic fabrics of weakly strained rocks and rocks with no strain markers. Other aspects of the anisotropy technique will be discussed to demonstrate how the magnetic fabric can be of assistance in the determination of the rock fabric.

GP 84

BLOCKING TEMPERATURE OF MAGNETITES

N.Sugiura(EPS,Erindale College,Mississauga,Ontario,L5L 1C6,Canada)

The relationship between T_B(blocking temperature) and applied magnetic field was examined in order to check the validity of the theories of thermoremanent magnetization. The relationship has been tested by a rather indirect technique in which remanences were measured at room temperature in zero field. In the present study, remanences in a field at high temperature were directly measured. The temperature dependence of the remanence was compared with the calculated blocking temperature spectrum. In the case of single domain magnetites,using the coercive force spectrum determined from alternating field demagnetization of saturation remanence, the agreement between the theoretical and the experimental T_B spectrum was satisfactory. In the case of multi-domain magnetites ($d \simeq 40\mu$), if appropriate adjustable parameters(activation volume and coercive force spectrum) are chosen , a fairly good agreement between the theoretical and the experimental T_B spectrum is obtained. There are, however, curious behaviors of the remanence which can not be explained by the theories of thermoremanence of two domain grains. 1. The anomalous peak of remanent magnetization near the Curie temperature, as has been observed by Bol'shkov et al. 2. Decrease of pTRM during cooling in zero field, as was reported by Parry. We need to refine the multi-domain theories to explain these anomalous behaviors.

GP 85

MINERALOGIC AND MAGNETIC INVESTIGATION OF BASALTIC ROCKS FROM DSDP LEG 61

M. B. Steiner (Dept. of Geology, University of Wyoming, Laramie, Wyoming 82071)

The opaque phases of these intrusive and extrusive ocean theoliites have been studied by means of the electron microprobe, thermomagnetic analysis and reflected light microscopy. The properties of these largely intrusive rocks may be analogous to those of the intrusives in the deeper layers of the oceanic crust. Curie temperatures range from 155°C to 450°C. A peculiarity of this suite of samples is their almost invariable tendency to decrease in J_S and T_c after being heated to 700°C in vacuum, strongly suggesting a resorption of titanium into the spinel lattice. Microprobe analyses on 17 samples show that the titanomagnetites display a large range of x-values ($Fe_{3-x}Ti_xO_4$), between 0.51 and 0.73. Microscopic observation allows a general characterization of the low-temperature oxidation stage of the samples, which, in these mid-Cretaceous rocks, ranges from nearly unoxidized (no cracking) to medium oxidation (pronounced cracking of grains, some staining, loss of sulfides). No correlation of x-value with oxidation stage appears to exist. Likewise, no systematic difference in Fe/Ti ratio exists between grain centers and grain edges. No greater heterogeneity of within-sample Fe/Ti values exists for more or less oxidized samples. However, a striking (positive) correlation exists between the titanomagnetite x-value and the whole-rock TiO_2 wgt % of a sample. This correlation negates the use of Curie temperatures alone as an indicator of oxidation stage in this suite of samples. The correlation of Ti/Fe ratio in the titanomagnetites with the Ti content of the host basalt also calls into question the limits of the widespread assumption that x in oceanic titanomagnetites is invariably about 0.65.

GP 86

MAGNETIC MATERIAL IN THE HEAD OF A DOLPHIN

J. Zoeger (Los Angeles Harbour College, Wilmington, CA 90744)
J. Dunn
M. Fuller (Both at: Department of Geological Sciences, University of California, Santa Barbara, CA 93106)

The natural remanent magnetization of parts of the head of a common dolphin (Delphinus delphis) have been examined using a horizontal access cryogenic magnetometer. The head, which had been preserved in formaldehyde, was first cut to give transverse sections a few cms thick. These were then again cut to give samples which were elongate along their dorsal ventral axis and could be conveniently placed in the magnetometer.

All 25 samples exhibited some NRM. However, in one particular region the NRM was much stronger and a thin piece of tissue about 1 mm^2 in area was isolated, which had a moment of 10^{-5} gauss cm^3. The magnetic material is intimately associated with the dura mater to the left of the mid-sagittal line near the occipital-frontal suture. The magnetization is oriented laterally with the north magnetic pole to the animal's right.

Saturation isothermal remanent magnetization (IRM_S) was only about a factor of 20 larger than the NRM, so that the NRM is relatively strong and comparable with the remanence which might be acquired as chemical remanence (CRM) in the geomagnetic field. IRM_S was magnetically very soft having a median demagnetizing field of less than 5 oe. Neither the NRM nor the IRM_S was particularly viscous.

The discovery of strong NRM in tissue between the brain and skull in the dolphin is similar to the result obtained by Walcott et al (1979), in the pigeon. It suggests that experiments should be done to see if dolphins respond to geomagnetic field cues as a navigational aid.

GP 87

A BIOMAGNETIC CONSTRAINT ON PALEOINTENSITY

J.L. Kirschvink (Department of Geological & Geophysical Sciences, Princeton University, Princeton, N.J. 08544)
Howard D. Wildman (Department of Biology)

Numerous experiments on a variety of animals have indicated that several species are able to reliably sense the direction of, as well as minute fluctuations in, the intensity of the geomagnetic field. In honey bees and homing pigeons, this ability appears to be associated with several hundred million crystals of organic magnetite which are somehow connected to the nervous system. Because these sensory organelles must have evolved slowly over long periods of geologic time, their function and construction should allow them to work under most, if not all, conditions naturally experienced by the species. Such an adaptation would imply that some information about the geomagnetic field not readily available to geophysicists may be contained in the range of field intensity to which they respond.

A variety of experiments have shown that magnetic field detection in the honey bee steadily improves as the intensity of the background field is increased up to about 4.5 Gauss. Between 4.5 and 5 Gauss, however, all magnetic field detection is abruptly lost. If the background intensity ever reached this strength, bees from such a colony might loose their backup navigational and circadian rhythm senses, thereby reducing the representation of their genes in the next generation. The observed 5 Gauss breakdown suggests that the ancestors of the current bee population never experienced magnetic fields of that strength or greater. Elucidation of the proximate cause of the sensory loss awaits clarification of its mechanism. Other species should be tested behaviorally to determine whether or not there is consistency across taxonomic groups.

Magnetic Deep Sounding

Pier 9
Monday A.M.
D. I. Gough (Univ. of Alberta), Presiding

GP 88 INVITED PAPER

A MAGNETOMETER ARRAY STUDY IN SOUTHERN AFRICA

D.I. Gough (Institute of Earth and Planetary Physics, University of Alberta, Edmonton, Alberta T6G 2J1)
J.H. de Beer (National Physical Research Laboratory, C.S.I.R., Box 395, Pretoria 0001, South Africa)

A large magnetometer array recorded time-varying vector magnetic fields due to substorms and similar disturbances in 1977, over the tip of Africa south of 30°S. A conductive structure in the lower crust or upper mantle, under the Cape Folded Belt and southern Karroo Basin, has been discovered and its limits well defined. Anomaly maps will be shown, with a preliminary map of this Southern Cape Conductive Belt. Provisionally it is regarded as a result of accumulation of conductive oceanic crustal rocks in a Proterozoic subduction zone or marginal sea. Induction vectors based on transfer functions show strong effects related to non-random distribution of polarizations in the incident fields. Such effects are important in the interpretation of induction studies with small sets of instruments. The induction vectors will be discussed in relation to the more reliable anomaly maps of amplitudes and phases of Fourier transforms of the time-varying fields.

GP 89

MAGNETOTELLURIC SOUNDING AND MAGNETIC VARIATION PROFILING IN THE IMPERIAL VALLEY OF SOUTHERN CALIFORNIA

Luis J. Alvarez
John F. Hermance (both at: Dept. of Geological Sciences, Brown University, Providence, RI 02912)

Long period ($T \leq 10{,}000$ sec.) magnetotelluric measurements performed at three sites in the Imperial Valley of Southern California are interpreted in the light of the previous magnetic variation profiles described by Schmucker (1964, 1970) and White (1973). The magnetic variation studies of Schmucker essentially suggest a flat-lying highly conducting zone having little relief at a depth of approximately 160 km beneath much of the southwestern Basin and Range province of Arizona and Southern California. White suggested the presence of a narrow upwarp of this deep conductor to depth of 100 km or so beneath the Imperial Valley. We have used the few magnetotelluric sites we occupied in conjuction with the published magnetic variation data to construct a two-dimensional model of the Imperial Valley which has the following features: 1) the basin sediments have a profound effect on the electromagnetic response; 2) the deep crust (10-20 km) appears to be relatively conducting; 3) the upper mantle (20 km < d < 150 km) appears to be significantly more conducting (~0.02 S/m) than the magnetic variation whereas at depths greater than 100 km, the interpretation studies indicated, does not require the presence of a "super-conducting" region.

GP 90

AN ANALOGUE MODEL STUDY OF GEOMAGNETIC VARIATION ALONG THE EAST COAST OF NORTH AMERICA

J.A.Wright (Department of Physics, Memorial University of Newfoundland,St.John's,A1B 3X7)
J.P.Greenhouse (Department of Earth Sciences, University of Waterloo,Waterloo,Ont.,N2L 3G1)
H.W.Dosso (Department of Physics,University of Victoria,Victoria, B.C.V8W 2Y2)
W.Nienaber (Department of Physics, University of Vibtoria,Victoria, B.C.V8W 2Y2)
R.C.Bailey (Department of Physics, University of Toronto,Toronto,Ontario M5S 1A7)

A scaled laboratory system has been employed to model the behaviour of geomagnetic variations over the eastern coastal region of North America. The model has been constructed to take account of the finite resistivity of the landmass, the bathymetry of the surrounding oceans and the sediments of the contiguous shelves. Maps of the normalised magnetic field for two orthogonal polarisations of a uniform source (roughly parallel and perpendicular to the USA/Nova Scotia coasts) show a coast effect qualitatively as expected. Four frequencies were used covering field variations with periods of 20 to 120 min.. The broad features of the variation pattern are similar for all periods and the discussion is concentrated on the data for one hour period.

Although the strike of the Appalachians, the coastline and the edge of the condinental shelf is similar over the length of the east coast, the model results show significant differences along strike in the anomalous variations near the coast. The variation along strike is shown to be primarily because of the deflection of currents in the ocean by bays and headlands. A comparison of the model derived and actually observed transfer functions allows a separation of the coast effect from the effects of crustal structure and leads to a better understanding of the tectonics of the region.

GP 91

COMBINED MAGNETIC VARIATION GRADIOMETRY MEASUREMENTS AND MAGNETOTELLURIC MEASUREMENTS IN ICELAND

W. M. Slocum
L. J. Alvarez
J. F. Hermance (all at: Dept. of Geological Sciences, Brown University, Providence, RI 02912)

In magnetotelluric surveys one is often faced with interpreting data which, while satisfying a tensor impedance relation, must be resolved into principal resistive values parallel and perpendicular to the strike of elongated electrical heterogeneities at the surface. The objective of such an analysis is to evaluate the principal resistivity calculated using the component of the electric field polarized parallel to the strike of a surficial electrical discontinuity. Madden, Swift, and Wright have persuasively argued that for 2-D surficial structures at long periods, the parallel principal resistivity is the more representative of the average deep structure in a region. Unfortunately, in many cases the choice of the parallel strike direction is not unambiguous, and one would prefer an objective criterion on which to base this determination.

We describe a method, which follows the suggestions of Price, Schmucker, Kuckes, and Connerney, in which measurements of the magnetic field components and their horizontal gradients alone can be used to obtain an apparent conductivity of the earth. This method therefore leads to an estimate of the apparent conductivity at a particular period which is independent of the value determined from a magnetotelluric ex-

periment in the same region. We illustrate the application of combined magnetotelluric and magnetic variation gradiometry measurements in Iceland toward the resolution of an ambiguity in selecting parallel resistivity estimates at several sites in the Icelandic neovolcanic zone.

GP 92

REGIONAL RESISTIVITY STRUCTURE AT THE ROOSEVELT HOT SPRINGS, UTAH, KGRA FROM MAGNETOTELLURICS: THEORETICAL 3-D MODEL STUDIES

Philip E. Wannamaker (Dept. of Geology & Geophysics, Univ. of Utah, Salt Lake City, Utah, 84112)
Gerald W. Hohmann (Univ. of Utah)

Ninety-three MT soundings at the Roosevelt Hot Springs (RHS) show a complicated geoelectric makeup dominated by major Basin-Range structural trends. Many important effects of these trends have been simulated using conductive prisms in a conducting earth by a 3-D integral equation numerical algorithm. Regional distortions of the electric field, due to current-gathering in the Milford Valley sediments nearby to the west, invalidate 1-D and 2-D transverse electric (TE) interpretation schemes. Letting x be the northerly strike direction of regional features, principal resistivity ρ_{xy} and impedance phase ϕ_{xy} for the 3-D prismatic valley model depart significantly from the 2-D TE apparent resistivity and phase below about 0.3 Hz. In spite of this finite strike extent of the valley sediments however, principal quantities ρ_{yx} and ϕ_{yx} over much of the prism may be modeled successfully for all frequencies with a 2-D transverse magnetic (TM) algorithm. When small-scale geologic noise is present, rotation of data axes for all soundings to a uniform direction, compatible with major geologic trends or MT strike estimators not distorted to arbitrarily low frequencies by the geologic noise, generally gives best results.

GP 93

ELECTROMAGNETIC INDUCTION STUDY OF THE SWABIAN ALP, IN PARTICULAR URACH VOLCANIC AREA

M.L. Richards (Institut für Geophysik 3400 Göttingen, Postfach 876, W.Ger.)
U. Schmucker (same adress)
E. Steveling (same adress)

Surveys in 1978/79 established a profile of stations to measure electromagnetic variations along the length of the Swabian Alb, with most effort concentrated in the volcanic area of Urach. This area has a geothermal anomaly, and the associated induction anomaly has been studied by Berktold & Kemmerle, revealing a strong regional polarisation in electric field normal to strike of the Alb. Our interest is to extend the frequency range to lower frequencies in order to look for possible deeper structure. Anomalous horizontal magnetic variations near the volcanic structure are mainly in the EW component, and stronger with increasing frequency. Anomalous vertical component is another diagnostic of the volcanic remnant. Magnetotelluric soundings show a resistive crust. The impedance tensor is mildy anisotropic.

GP 94

EVIDENCE FOR A LOCALIZED DEEP CONDUCTOR UNDER THE MICHIGAN BASIN

R. C. Bailey (Department of Physics, University of Toronto, Toronto M5S 1A7)
(Sponsor: G. D. Garland)

Geomagnetic variation measurements in southern Ontario reveal the possible existence of a zone of anomalously high electrical conductivity in the crust or upper mantle lying to the west of Lake Huron. This is most clearly seen in the long period (T = 1 hour) induction vectors, which are small and point west from all sites north of Lat. 45°. Vectors at shorter periods are larger and point southwest, presumably also showing the effects of the well-described Appalachian conductor. It is possible that the conductor west of Lake Huron is associated with the Michigan Basin.

GP 95

EXACT NON-LINEAR INVERSION OF THE ELECTROMAGNETIC INDUCTION PROBLEM

David Garbasz (Institute of Geophysics and Planetary Physics, Scripps Institution of Oceanography, University of California, San Diego, La Jolla, CA 92093)
R. L. Parker (Institute of Geophysics and Planetary Physics, Scripps Institution of Oceanography, University of California, San Diego, La Jolla, CA 92093)

A new mathematical treatment of the one-dimensional electromagnetic induction problem shows that useful inroads can be made into the two problems, that of existence of solutions and that of their construction.

Existence

This problem has been completely settled, mainly because it can be reduced to a linear problem with convex constraints.

Construction

Given the "data," the response function of a finite number of frequencies, we give *exact* non-iterative ways of construction models fitting the data.

Since in this case the solutions are not normally unique we define special classes of functions (such as slab models, δ function models) and choose the unique optimal model in each class by demanding that it minimize some misfit criterion.

Applying these methods to the data set of Larsen we show a simple procedure for generating special models whose misfits are very close to that of the best filling model.

GP 96

MANTLE CONDUCTIVITY : AN INVERSION USING BAILEY'S METHOD

J. Achache (IPGP and DST, Univ. of Paris 6 and 7, Place Jussieu, 75230 Paris Cedex 05, France)
J.L. Le Mouël
V. Courtillot

We have implemented an algorithm based on Bailey's solution of the inverse problem of electromagnetic induction in the Earth. The algorithm has been successfully tested to provide reliable estimates of conductivity down to a depth of 2000 km, when synthetic data in the period range from 4 days to 11 years are used. The study was motivated by recent determinations of very long period data (Ducruix et al, 1980) and also benefited from recent redeterminations of high frequency data (Anderssen et al, 1979). Smooth data sets, which are required for the inversion, have been constructed from these various sources. The range of inverted models is less that one order of magnitude. Due to a lack of high frequency data, the conductivity of the upper 600 km of the mantle may be overestimated (order $10^{-1}\Omega^{-1}m^{-1}$). The algorithm performs well in the middle mantle, where conductivity rises steadily from 1 to 50 $\Omega^{-1}m^{-1}$. The lack of very low frequency data and limitations of the algorithm prevent one from obtaining meaningful estimates in the lower mantle. However, study of the propagation of the 1970 secular variation acceleration (Courtillot et al, 1978 ; Achache et al, 1980) provides an estimate of the mean conductivity of the whole mantle ; thus a complete mantle profile can be constructed. It is found that deep mantle conductivity probably does not exceed a few hundred $\Omega^{-1}m^{-1}$.

GP 97

GEOMAGNETIC DEPTH SOUNDING: THE PROBLEM OF SPLITTING EXTERNAL AND INTERNAL ORIGIN GEOMAGNETIC FIELDS

G. P. Gregori (Istituto di Fisica dell'Atmosfera/CNR, 00144 Rome, Italy)
L. J. Lanzerotti (Bell Telephone Laboratories, Murray Hill, New Jersey 07974)

The time-varying geomagnetic field recorded at any given site on the earth's surface is the sum of the external origin field, displaying essentially large-scale (i.e., ionospheric/magnetospheric) characteristics, and of the "internal-origin" field (displaying strictly local scale features). For this reason, the splitting of external and internal origin fields should be performed on a local scale, not global as in the classical methods due to Gauss [1838] and Vestine [1941]. We derive a procedure that indicates that at each ground-based measurement site, for a given frequency, there is a direction along which the magnetic field is of purely external origin. The derivation thus suggests that for this unique direction (which is a function of frequency) the influence of the underground conductivity structures is absent and a component of the external origin field is obtained.

GP 98

OPTIMIZING THE ANALYSIS OF REGIONALIZED GLOBAL INDUCTION PARAMETERS

P. S. Nolen
J. F. Hermance (Both at: Dept. of Geological Sciences, Brown University, Providence, RI 02912)
(Sponsor: J. F. Hermance)

The recent thrust of research at Brown University has been to address the question of lateral variations of electrical properties in the upper mantle from a depth of 50 km to the transition zone (400-600 km). A basic question is whether the transition zone is a smooth feature or is characterized by lateral variations. To effectively investigate the transition zone using natural phenomena, a frequency band must be used which has hitherto been underutilized. Regional studies have by-and-large been restricted to periods of less than $1 \cdot hr - 10^4$ sec, whereas classical global studies have been concerned with Sq variations, diurnal variations and longer period phenomena. Global studies have favoured hourly averages whereas regional studies have favoured digitizing intervals as short as 10-100 sec. The purpose of this paper is to address the question of the optimal data-processing technique for the intermediate frequency domain (1-24 hours). We have compared the analysis of specific classes of phenomena, e.g. the Sq variation as well as the storm time variation, for various sampling intervals and averaging techniques. We have found that significant degradation of the estimated parameters occurs at periods less than 24 hours when analysis is restricted to hourly averages. At present, the most effective analysis appears to be a very close sampling of digitized data (60-100 samples/hour) with filtering and decimation of the data prior to calculation of the Fourier Transforms. Moreover, we place a great deal of emphasis on constant-Q band averaging of cross-power spectra rather than averaging over fixed numbers of harmonic coefficients. Multi-station estimates appear to be less biased than single-station estimates.

GP 99

CONTINUOUS UPPER MANTLE CONDUCTIVITY MODELS AND THEIR APPLICATION TO SATELLITE DATA

E. M. Didwall (Earth & Planetary Sciences, The Johns Hopkins University, Baltimore, MD 21218)

A numerical method is presented which utilizes an electrical conductivity profile continuous with depth. This approach differs from previous conductivity models which employ homogeneous spherical shells of constant conductivity. The procedure solves for the potential of the poloidal part of the induced magnetic field within the earth by assuming a dipole (first spherical harmonic) external harmonicly varying magnetic field. This assumption reduces the field equations to ordinary differential equations which are then solved using

a Runge-Kutta algorithm. Upon solving the field equations, the frequency response function for a given conductivity profile is calculated. Using various models for crustal and upper mantle conductivity, the frequency response function for frequencies of 0.2 to 2 cycles/day is calculated. The effects of a "world ocean" of fixed conductivity of $3^S/m$ are also examined. These results are then compared to estimates of the frequency response function as obtained from analysis of satellite magnetic field data. These response functions are, in general, lower than those obtained from land observatories, with magnitudes from 0.2 to 0.34, and phases from approximately zero to 12°. For the simplest model, a conducsphere, for frequencies below 1 cycle/day, the satellite data indicates a conductivity between $0.01^S/m$ and $0.03^S/m$ while land data (Banks, 1972) indicates a conductivity near $1^S/m$.

Hydrology

Water Quality and Sediment Transport

Wellington
Thursday A.M.
E. A. McBean (Univ. of Waterloo), Presiding

H 1

EXTRACTION AND UTILIZATION OF UNPROCESSED LANDFILL GENERATED METHANE GAS

Anthony J. Crutcher
Frank A. Rovers
(both at: Conestoga-Rovers & Associates
651 Colby Drive, Waterloo, Ontario, Canada)
(Sponsor: Edward McBean)

A research study conducted by Conestoga-Rovers & Associates under contract with Environment Canada has indicated that it is technically feasible and economically viable to extract and utilize landfill gas in an unprocessed state. The study was conducted at a privately owned landfill at St. Thomas, Ontario. The gas extraction and utilization system included a three foot diameter gas extraction well, gas monitoring probes installed radially from the well, a continuously operating gas pump, waste gas outlet and an onsite greenhouse heated by a modified forced air gas furnace. The system operated continuously for a five month period in the winter of 1979. Tomato plants were planted in February 1979 and successfully grown in the greenhouse which was heated with the landfill generated methane gas. The first crop of tomatoes were picked in May 1979. The major conclusions of the study are: the recovery of landfill gas is both feasible and economical; it is feasible to use landfill gas in an unprocessed state for local space heating or process heating; and, landfill generated methane gas is a reliable fuel, given the limitations of its production.

H 2

GEOCHEMISTRY OF SELECTED LAKES IN NEW YORK STATE WITH SIMPLE MORPHOMETRY

Martin Wahlen (Division of Laboratories and Research, New York State Department of Health, Albany, NY 12201) and
Roger C. Thompson
(Sponsor: Yngvar Isachsen)

Three lakes remote from populated regions in New York State with minimal watershed areas have been investigated geochemically. Rocks and soils from the drainage area, and lake sediment cores and lake waters were analyzed for a number of major and trace element concentrations. Sediment cores were dated radiometrically (^{210}Pb, ^{137}Cs) and the sedimentation rates ranged from 0.011 to 0.013 g $cm^{-2}yr^{-1}$. ^{210}Pb-fluxes to the sediments were 0.7 - 1.2 dpm $cm^{-2}yr^{-1}$. For the ensemble of sediment core samples for each lake sectioned with a depth resolution of 1.2 cm, the concentrations of K, Ca, Ti, Mn, Fe, Rb, Sr and Zr were all log normally distributed, the average values being very close to the average values obtained in watershed soil samples. Unaltered soil material therefore accounted for the observed fluxes into the sediments. For Pb, Zn, and Cu bimodal distributions were observed with lower average values in deeper (older) sections and higher average values in more recent depositions, which are attributed to cultural pollution. For Pb the average soil concentrations were found to equal the higher, for Zn and Cu to equal the lower average sediment values, indicating effective retention on soil for Pb and higher mobility for Zn and Cu. Estimates were obtained for atmospheric and land derived contributions of Pb, Zn and Cu to the sediment inventory.

Comparison of the data sets between the acidic (pH≈4) and a nonacidic lake (pH≈7), both under similar acid precipitation, shows that more rock erosion material and clay are present in the watershed soils and consequently transported to the sediments of the nonacidic lake. This is reflected in the enhanced concentrations and fluxes of Si, Ti, Fe, Rb and Zr.

H 3

FACTORS AFFECTING CHEMISTRY OF ACID MINE DRAINAGE FROM UNDERGROUND PITTSBURGH COAL MINES

Cleason P. Smith (Geraghty and Miller, Inc., 703 Giddings Avenue, Annapolis, Maryland 21401)
Henry W. Rauch (419 White Hall, W.V.U., Morgantown, West Virginia 26506)

The chemistry of acid mine drainage from 24 drift mines in the Pittsburgh coal seam was studied in Monongalia County of northern West Virginia. These effluents exhibited the following median values for major chemical parameters: pH - 2.85; sulfate - 1100 mg/l; total hardness - 528 mg/l as $CaCO_3$; aluminum - 39 mg/l; and total iron - 254 mg/l. Assuming that pyrite dissolution is the source of sulfuric acid and iron, an average of 71 percent of the original dissolved iron still remains dissolved or suspended in drainage within the mines. Most of this iron appears to be in a dissolved state.

The pH of mine drainage ranged from 2.5 to 3.0; the acid character of these effluents probably results mainly from oxidation and dissolution of pyrite. The consistency of pH values is also attributed to other factors. The oxidation and precipitation of iron would tend to counteract pH rises resulting from ground-water dilution, carbonate dissolution, and clay mineral dissolution.

The drainage chemistry of Pittsburgh coal drift mines is related to the age of these mines, in that concentrations of sulfate, total iron, aluminum, and total hardness decrease with increasing mine age. For example, sulfate decreases about 100-150 mg/l per year over at least a 20 year span. These trends probably result from: (1) slower rates of chemical weathering of pyrite in coal and gob materials over time, associated with build ups of inert residual rinds on exposed rock surfaces; and (2) decreased amounts of fine-grained coal and rock fragments in older mines.

H 4

STATISTICAL TECHNIQUES OF STREAM EVENTS WITH APPLICATION TO HYDROGRAPH CONTROLLED RELEASE OF WASTEWATERS

Victor L. Zitta
Department of Civil Engineering
Mississippi State University
Mississippi State, MS 39762

Donald O. Hill
Department of Civil Engineering
Mississippi State University
Mississippi State, MS 39762

Discharge of wastewater during stream events has become a popular method to meet instream water quality standards in small streams while minimizing or eliminating energy costs associated with advanced waste treatment. This method, called hydrograph controlled release, is based upon the stochastic nature of stream events where an event is defined as a maximum in the discharge time series irrespective of magnitude or time of occurrence. The time span between events determines storage requirements for the wastewater. This paper sets forth a methodology applicable to the hydrologic design of wastewater discharge into receiving streams utilizing their natural stochastic rise and fall. The log-normal distribution function was deemed adequate by the Kolmogorov-Smirnov test to describe the histograms of maximum annual spans between stream events of specified magnitude. Based upon this distribution, the time of storage during low flow periods can be specified with a given cumulative probability or return period. Size of the storage system is a linear function of the volumetric inflow rate for the probability selected.

H 5

SELECTION OF OPTIMAL DIFFUSE AGRICULTURAL POLLUTANT CONTROLS

J.R. Cousins (Dept. of Civil Engineering, University of Waterloo, Waterloo, Ontario, N2L 3G1)
E.A. McBean

Because of the difficulty and cost of controlling diffuse agricultural sources of nutrients, an efficient scheme to select abatement strategies is required. A general linear programming model is developed to select from a large number of remedial measures including buffer strips, crop rotation, no-till cultivation, slow-release fertilizers, strip cropping, etc. Particular attention is given to the nonlinear and either/or characteristics of the efficiency of nutrient abatement and costs for the remedial measures. A case study application of the model to Canagagigue Creek, a tributary of the Grand River in the Lake Erie basin is included. Typical problems solved include 1300 constraints and 2250 variables. The results of multiple objective studies reflecting attention to whom the costs accrue, and the resulting overall diseconomies are developed.

H 6

COMPARISON OF DEPTH AND POINT INTEGRATED SUSPENDED SEDIMENT SAMPLES

W. G. Dorough (Chief, Water Quality and Sediment Section, U.S. Army Corps of Engineers, Omaha District, Omaha, Nebraska 68102)
W. J. Mellema (Chief, Hydraulic and Hydrology Section, U.S. Army Corps of Engineers, Missouri River Division, Omaha, Nebraska 68101)

Depth and point integrated suspended sediment sampling data collected from the Missouri River at Omaha, Nebraska is analyzed to permit a rational basis for adjusting the routinely collected depth integrated (DI) samples to more accurately reflect the amount of bed-size materials in suspension. This paper will present the results of the analysis; discuss reasons accounting for the differences in the two types of data; show graphically how the differences (by grain size fractions) vary with grain size; and provide corrective factors for adjusting the DI-samples, using the point integrated (PI) samples as the base from which to make the adjustments. The analysis is derived from 90 sampling dates over 23 years of sampling record. Each sampling date consists of ten sampling verticals in the channel cross-section with five being duplicate DI-PI sampling locations and five being DI-sampling locations without PI-samples. Each DI-PI sampling location consists of a single DI-sample, accompanied with point velocity and concentration measurements taken at four to six elevations in the vertical.

H 7

SUSPENDED SEDIMENT PRODUCTION FROM A FORESTED WATERSHED IN SOUTHEAST ALASKA

J. D. Stednick, U.S.D.A. Forest Service, Tongass National Forest, P. O. Box 1980, Sitka, AK 99835

Suspended sediment production from an undisturbed forested watershed was monitored for three years. The watershed of 34.2 square kilometers had an average 2,300 mm of annual runoff, distributed in a biomodal pattern.

Suspended sediment samples were obtained with automatic pumping water samplers, hand-held depth-integrated samplers and surface grab samples. Optical turbidity, measured as NTUs, was poorly correlated to gravimetric analysis. Grab and automatic pumping water samplers recovered comparable suspended sediment concentrations. However, grab samples collected an average of 64 percent of the suspended sediment sampled by the depth integrated sampler.

Suspended sediment pulses occurred during fall runoff events. Suspended sediment production appeared to be a function of the ratio of the change in discharge per change in time and not the magnitude of discharge. Hysteresis loops between suspended sediment production and discharge were common, but not universal for fall storms.

Suspended sediment associated with spring runoff events was uncommon. Since suspended sediment production appears to be correlated to the change in discharge over the change in time ratio and the in-stream availability of sediment, discharge cannot be used as an independent predictor of suspended sediment production for watersheds in Southeast Alaska.

H 8

CHANNEL MORPHOLOGY AND SEDIMENT CHARACTERISTICS: A COMPARATIVE STUDY OF SEMIARID AND HUMID REGIONS

Sherman N. Shewmaker Author (Dept. of Geography, Indiana University, Bloomington, IN 47405)
Lawrence J. Onesti Author (Dept. of Geography, Indiana University, Bloomington, IN 47405)

A comparative study of channel morphology and channel perimeter sediment characteristics was conducted for a set of rivers, thirty-one of which are located in the Midwest, and thirty-eight in the Great Plains. Examining drainage basins of equivalent size (518 - 67,340 km^2), the mean annual flood discharge was four times greater in the Midwest than in the Great Plains; correspondingly, both average channel width and channel depth were at least twice as great in the Midwest, however, channel width/depth ratios were greater in the Great Plains. Average percent silt and clay in the channel bank is similar for both regions, but Midwestern streams average fourteen percent more silt and clay in the channel bed. Channel shape and sediment characteristics suggest that a larger percentage of the total load for Great Plains streams is transported as bedload with the converse true for Midwestern streams.

Regression analysis suggests that discharge explains a greater amount of variation in channel morphology in both regions; however, this relationship is much stronger in the Midwest. Percent silt and clay in the channel perimeter explains a small, but in most cases significant, amount of variation in channel morphology, and this relationship is strongest in the Great Plains.

H 9

SATELLITE DETECTION OF SEICHES IN GREAT SALT LAKE, UTAH

Craig P. Berg (NOAA/National Environmental Satellite Service, Washington, D.C. 20233)
Michael Matson (NOAA, National Environmental Satellite Service, Washington, D.C. 20233)
(Sponsor: Donald R. Wiesnet)

On June 15, 1977, an unusual brightness anomaly was detected in the north arm of Great Salt Lake, Utah, on NOAA-5 Very High Resolution Radiometer (VHRR) visible band imagery and on Landsat-2 multispectral visual band imagery. Retrospective inspection of NOAA-3, 4, and 5 satellite imagery from 1974-77 revealed twelve previous cases of the anomaly, whereas post-monitoring documented nine other cases through May 1978. Comparison of lake levels in the north arm with meteorological parameters leads to the conclusion that the anomalous brightness is associated with wind-induced seiches in the north arm. Apparently the wind induces a lower water depth, turbulence, and mixing throughout the water column in the western third of the north arm, thus increasing the brightness of the surface waters chiefly from sediment resuspension.

H 10

PROCEDURES FOR A NATIONAL INVENTORY OF IRRIGATION WATER USE

T. D. Steele
F. J. Heimes (U.S. Geological Survey, Lakewood, Colo. 80225)
A. L. Higer (U.S. Geological Survey, Miami, Fla. 33155)

Withdrawal of surface and ground water for irrigated agriculture currently constitutes about 80 percent of the fresh water consumed in the United States. Approximately 92 percent of the irrigation water is withdrawn in 14 western States and Florida. Total water use for irrigation in the United States has increased from an estimated 110 billion cubic meters in 1950 to 197 billion cubic meters in 1975. This increase in irrigation withdrawals is decreasing ground-water storage in several western States. There also is increasing competition for both surface- and ground-water resources because of population growth and energy development in the western States.

Accurate estimates of national water use are required to project future demands and to provide a base for long-term planning. Procedures for conducting a national inventory of irrigation water use need to include: (1) Determining objectives, scope, total costs, and personnel requirements; (2) collating and analyzing existing data; (3) determining data to be used or collected, including water source, type of irrigation, and crop needs and consumptive use; (4) developing data acquisition (retrieval, on-site, or remote sensing) methods, and data-analysis techniques; and (5) presenting data in a form usable to water-managers and land-use planners. Such inventory procedures could help identify water-use problem areas and aid in designing water-management proposals for various regions of the United States.

Surface Water
Wellington
Thursday P.M.
Hugh Whitely (University of Guelph), Presiding

H 11

CHANGES IN THE DISCHARGE OF SELECTED RIVERS IN BRITISH COLUMBIA DURING THE PERIOD OF INSTRUMENTAL RECORDS

Gary Barrett (Department of Geography, University of British Columbia, Vancouver, B.C., V6T 1W5)
(Sponsor: Olav Slaymaker)

The average discharge of many rivers in British Columbia appears to have undergone a "step-increase" of about 20 percent in the mid-1940s. The magnitude of the change is geographically variable. In most cases the records suggest that discharge has been stationary since the increase. An analysis of selected records for the other components of the water balance - storage, evapotranspiration, and precipitation - indicates that an abrupt increase in precipitation in the mid-1940s, particularly in the winter months, was responsible for the increase in runoff. There is evidence for similar, but smaller changes apparently associated with summer precipitation regional fluctuations during the early 1930s and around 1950. The ultimate cause of the precipitation changes is uncertain, but is presumably linked with changes in characteristic synoptic patterns deriving from the westerly circulation.

H 12

SOLAR-GEOPHYSICAL CHRONOLOGY OF PRECIPITATION & RUNOFF OF THE GREAT LAKES-ST.LAWRENCE RIVER, 1826 - 1979

R. S. Goodridge, Hydraulic Engr., ex-Federal Power Comm., 7103 44th Street, Chevy Chase, Md. 20015

Solar radiations, in mid-latitude North America affect precipitation, and the residual, runoff, which lags 20-25 years. The long-term averages for graphic presentation, are based upon the postulate: The sun is a heat engine driving the global circulation through it's working fluids, the atmosphere and the oceans. Streiff, Chicago, cited hydraulic engineering as dealing with cumulative values, as small secular differences, sustained over long periods, become great and important effects. The longer runoff records began near 1860, as the Great Lakes-St. Lawrence at Ogdensburg, N.Y., 1861-1955, USGS & Corps of Engineers; 1956-1979, USGS, monthly reports, WRR. A back-sight to 1826-1860, pre-runoff precipitation, and to 1700-, Swiss sunspot numbers, Rz, converted to Zurich areas indices, Ia, after Poulakis-Tritakis, Athens, Greece, modified to allow Ia to reach zero with Rz, by graph, yields indices in percent of the Ia, 1835-1935 average, which cumulated forms the central MINOR flanked by MAJORS. See Fig.1. Scales of precipitation and runoff are fitted to amplitude of MINOR. Note rise of St. Lawrence to 201 in 1979. This rise is 53% of the linear of Ia, through Dec. 1979. An inference is that St. Lawrence flow may continue to rise to 1994, after which a recession may persist to about 2040, based on trends of the past 280 years. Possible extension from paleo-magnetic data of sediment borings from the Great Lakes, as those of Prof, Lund, from Kylen Lake, 35 miles NE of Duluth, to Seneca Lake, Geneva, N.Y., may add to that presented. The Toronto Region has much to offer to an up-date of hydrologic studies, in progress, for the Thames basin, west of London; the Rhine, above Basel; and the Indus River, at Attock.

H 13

FORECASTING MONTHLY RIVERFLOW SERIES

D.J. Noakes (Dept. of Systems Design, Univ. of Waterloo, Waterloo, Ontario, Canada, N2L 3G1)
K.W. Hipel (Dept. of Systems Design, Univ. of Waterloo, Waterloo, Ontario, Canada, N2L 3G1)
A.I. McLeod (Statistics and Actuarial Science Group, The Univ. of Western Ontario, London, Ontario, Canada, N6A 5B9)

An important consideration to hydrologists is the selection of an appropriate stochastic model to be used in the design and operation of water resource systems. The basic idea behind model selection is to choose a model from a set of models under consideration, such that the selected model best describes the data according to some criterion. Of particular interest in hydrologic applications is the performance of the model in producing one step ahead minimum mean squared error (MMSE) forecasts.

Monthly riverflow data is used to test the forecasting ability of three stochastic models. Seasonal autoregressive integrated moving average (SARIMA), monthly autoregressive (MONAR), and deseasonalized autoregressive moving average (ARMA) models are fit to a number of truncated monthly riverflow time series and one step ahead forecasts are generated and compared to the remainder of the time series. The results from sensitive statistical tests show that both the SARIMA and MONAR models often forecast better than the deseasonalized ARMA models. However, both the SARIMA and MONAR models appear to forecast equally well for the series which were examined.

H 14

FLOOD VOLUME FREQUENCY ANALYSIS FOR SMALL BASINS IN PENNSYLVANIA

Robert T. Zulick (Corning Urban Renewal Agency, Corning, NY 14830) and Larry M. Younkin (Department of Civil Engineering, Bucknell University, Lewisburg, PA 17837)

A study of annual flood volumes was undertaken as a first step in the development of a method of synthesizing design hydrographs for drainage structures which would utilize storage rather than to simply pass steady peak flow. The data were obtained from systematic stream station records for six small watersheds in Pennsylvania. The areas of the basins ranged from 8 to 98 sq.km. and the average period of record for the stations was 30 years.

Criteria for the identification of the annual maximum flow volume were established. Discharge cutoff limits equal to six times the mean annual flow for each station were used to define the beginning and end of an event. Frequency analyses were performed on the six sets of volume data using the extreme value and log-Pearson Type III distributions. A variability factor was used to test which method "best fit"

the data sets. These results were inconclusive although the log-Pearson Type III analysis is recommended. It was also found that about two-thirds of the maximum volume events were associated with the maximum peak events for the year.

H 15

A GENERALIZED MARKOV MIXTURE MODEL FOR DROUGHT SIMULATION

Richard M. Vogel (Dufresne- Henry, Inc. Precision Park, North Springfield, Ve. 05150)
Soronadi Nnaji (Civil Engineering Dept., Clemson University, Clemson, SC 29631

A variety of stochastic models have been developed to model droughts. Most of these models have been developed for generating Normal annual series. The few, exemplified by the Modified Thomas-Fiering model (MTFM), that have been developed to simulate within year flows have not satisfactorily preserved the statistics of observed droughts.

In this paper we describe a new model, the Generalized Markov Mixture model (GMMM), which is an extension, in several directions, of Jackson's Normal Markov Mixture model for annual flows. The GMMM incorporates seasonality. It allows for a skewed distribution and linear dependency in streamflow.

Model validation tests show that this model preserves the basic statistics of flow upon which it is based. It reproduces the distribution of observed drought lengths at the 95% confidence level and the distribution of drought magnitudes at the 90% level. With the above results the GMMM was superior to the MTFM though inferior to the Stanford Watershed Model (SWM). The GMMM however, preserved the most critical statistics (i.e. the maximum negative run-sum and run-length) better than the SWM.

An application of the GMMM in a reservoir sizing problem is demonstrated.

H 16

PARAMETER ESTIMATION OF ARMA MODELS

K. Adamowski (University of Ottawa, Department of Civil Engineering, Ottawa, Canada, K1N 9B4)

Linear models of time series involving autoregressive-moving average (ARMA) representation play an important role in many areas of engineering. In model development procedure, the identification stage is usually based on human observation of autocorrelation patterns, and as such is not very rigorous. This paper examines a consistent and sequential method for estimating the orders and parameters of ARMA processes, and it is based on sequential least squares estimates of pure autoregressive models.

H 17

MODELLING DISPERSION IN NATURAL FLOWS

Tom Beer (Centre for Resource and Environmental Studies, Australian National University, Canberra ACT Australia.

The dispersion behaviour of streams is generally modelled by the Fickian diffusion equation which requires the velocity U and dispersion coefficient D as known inputs. An alternative approach is to use lumped parameter models that divide the streams into a number of reaches and express the dispersion within each reach in terms of a first order differential or finite difference equation.

This paper compares the results of the two modelling strategies when they are applied to dye tracing experiments conducted on two rivers in Australia - one, a concrete lined channel near Canberra, and the other a flooded irregular creek in the Northern Territory.

Provided that the data is of a suitable form (i.e. equally spaced in time) then the lumped parameter formulation provides a better approximation to the observations than do the diffusion equation based approaches.

H 18

APPLICATION OF A FINITE ELEMENT STORM HYDROGRAPH MODEL

Dinshaw N. Contractor
Timothy C. Banta (Both at: Civil Engineering Department, Virginia Polytechnic Institute, Blacksburg, Va. 24061)

A finite element storm hydrograph watershed model is applied to several watersheds in an ungaged context. The model consists of two parts; the generation of precipitation excess, and routing of the rainfall excess to the outlet of the watershed. Soil maps and land use maps are superimposed to define homogeneous hydrologic response units (HRU). Precipitation excess, from each HRU, is determined by the Holtan equation. The routing segment employs finite element theory to solve the one-dimensional, unsteady partial differential equations of continuity and momentum with the kinematic wave approximation. The application of the finite element model to small watersheds in Virginia has met with very good results. This is the first time the model has been applied to larger basins, and to watersheds outside the State of Virginia. Six watersheds selected by the Work Group on Floodflow Frequency, Ungaged Watershed Hydrology Committee, Water Resources Council are analyzed by this model. The same input data specified by the Work Group was used. Results are compared with the 2-,10-,100-year flows obtained by frequency analysis of annual peak flows at each site. The peak flows obtained by the application of various other models are also compared with the results from the finite element model.

H 19

SOME EXPERIMENTS WITH NONPARAMETRIC MARKOV MODELLING

A. I. McLeod (Department of Mathematics, The University of Western Ontario, London, Ontario N6A 5B9)
K. W. Hipel (Department of Systems Design, University of Waterloo, Waterloo, Ontario N2L 3G1)

A class of Nonparametric Markov models which provide a very general model for nonlinear stationary time series has recently been introduced by Yakowitz. Some further developments including the use of residuals for model checking and the use of the Akaiki Information Criterion for model selection are discussed. Some experiments comparing the Nonparametric Markov model and the ARMA model for forecasting on annual geophysical time series and synthetic time series are reported.

H 20

BAYESIAN APPROACH TO HYDROLOGIC MODEL CHOICE

R. G. Quimpo (Dept. of Civil Engineering, University of Pittsburgh, Pittsburgh, Pennsylvania 15261)

Ali-Bux Brohi

Sampling variations in hydrologic data often make it difficult to discern statistical patterns which are used to discriminate among time series models for the process. This paper examines the use of Bayesian theory in choosing between two competing models of hydrologic time series.

Using synthetic data from a known generating process and assuming equal prior probabilties for two candidate models, the procedure is found to consistently yield much higher posterior probabilities for the true model. Through pair-wise analysis, the technique may be employed to choose from among several candidates. Although the procedure appears insensitive to the prior, a non-diffuse assumption is easily incorporated in the technique. The effect of data length on the discriminatory power is also examined. The procedure is tested on historic data and results are compared with other suggested techniques for model selection and validation.

H 21

A BAYESIAN APPROACH TO STORAGE YIELD ANALYSIS

M. González Sanabria
J.B. Valdés
I. Rodríguez-Iturbe

(all at: Graduate Program in Water Resources, Universidad Simón Bolívar, Caracas, Venezuela).

Reservoir capacity and storage yield estimates are highly dependent on the coefficient of variation and serial correlation parameters of streamflow series. Data generation techniques have been widely used in the determination of reservoir capacities and yields. In this type of methodologies, historical parameters of hydrological series are preserved as the best estimates of population parameters. The influence of the Bayesian approach where the parameters of the generating models are considered as random variables, is analyzed regarding reservoir capacities and yields for several Venezuelan basins, and the importance of the parameter uncertainty regarding storage-yield characteristics is explicitly evaluated for those basins. The correlation structure at the annual level is also examined by means of comparing storage yield characteristics obtained through desagregation procedures against those found through monthly synthetic generation with no explicit ties with the annual series.

H 22

MODELLING IRRIGATION WATER DEMAND

D.R. Maidment (Water and Soil Division, Ministry of Works and Development, Christchurch, New Zealand)
P.D. Hutchinson

An Irrigation Demand Assessment model (IDA) has been developed to simulate the pattern of water demand from large irrigation areas. IDA computes a time profile of irrigation demands by means of a daily soil moisture balance using measured rainfall and evaporation data, taking into account the areas of different crop and soil types, and the efficiency of the irrigation method being used. IDA has been validated against historical data supplemented by detailed field surveys and is used to estimate the demands of proposed large scale irrigation projects in the Canterbury region of New Zealand. By comparing these demand profiles with river flow data the frequency and magnitude of supply shortages is estimated.

General Groundwater

Pier 7 & 8
Friday A.M.
G. E. Grisak (National Hydrology Institute), Presiding

H 23

STATISTICAL ANALYSIS AS A TOOL IN EVALUATING THE EFFECT OF DROUGHT ON SHALLOW GROUND-WATER LEVELS

A. Zaporozec (Wisconsin Geological and Natural History Survey, Madison, WI 53706)

In arid areas, droughts and resulting water deficiencies are chronic. In humid areas, drought conditions are also quite common and cause serious problems in agriculture and water supplies. Even though the drought periods are not predictable, their effects are, and can be anticipated. Statistical analysis of long-term ground-water level measurements is a valuable tool in evaluating and mitigating the effects of drought on water levels.

Statistical analysis of water-level measurements on shallow wells in a glaciated area of northern Wisconsin indicated that it is possible to develop a method for determining the required depth of wells which would ensure water supplies in the periods of drought. Based on the premise that the water levels in a given area with

similar hydrogeologic conditions exhibit a normal probability distribution, a relationship was established between record minimum and mean water levels. By plotting results from a number of wells, a type curve was developed from which the expected minimum levels can be predicted within selected confidence limits.

The analysis of ground-water levels and evaluation of their long-term trends have - besides their value for better understanding of a hydrogeologic regime, its periodicity and genetic relations - a great value for ground-water management and disaster-prevention planning. Depth to water calculated from the developed curve can be used for constructing a map of "drought-proof" well depths. This map would indicate the areas where the required depth is greater than the saturated thickness of an aquifer, and where the problems of inadequate water supplies are likely to develop during droughts.

H 24

COMPARISONS OF STOCHASTIC MODELS OF SUBSURFACE FLOW

Allan Gutjahr (Dept. of Math, New Mexico Institute of Mining and Technology, Socorro, N.M. 87801)
Lynn Gelhar

Stochastic solutions of the differential equation describing one-dimensional flow through a porous medium are presented. The hydraulic conductivity is modeled as a spatially variable stationary random process. Analytical approximations using first-order analysis, covariance differential equations and variogram analysis, all yield consistent results. The effects of conditioning and boundary conditions (finite domain models) are discussed.

A comparison of the one-dimensional analytical solutions and Monte Carlo results for a flow system of finite length are presented. The solution based on linearization in the logarithm of conductivity is very robust and agrees well with Monte Carlo results even for large variances for the conductivity.

Conditions for the output to be stationary are explored and it is shown that while the one-dimensional system imposes stringent conditions in order for the results to be stationary, the more realistic three-dimensional physical model yields stationary solutions under very general conditions.

H 25

A STUDY OF THE GROUNDWATER INVERSE PROBLEM USING SENSITIVITY ANALYSIS AND ONE-DIMENSIONAL MODELS

C.D. McElwee (Kansas Geological Survey, University of Kansas, Lawrence, KS 66044)

Sensitivity coefficients indicate hydraulic head changes at a certain point due to a change in an aquifer parameter at any point. They can be calculated by the same techniques used for the head. A squared error functional is minimized obtaining the "best" estimate of the aquifer parameters at each node of the model. In areas which are not very sensitive to transmissivity or storativity, the initial estimates for the aquifer parameters are changed very little. In the direct inverse problem this insensitivity can lead to instability. Areas of low or high sensitivity can be delineated very easily by looking at the sensitivity coefficients. Hypothetical one-dimensional models are used to test the effectiveness of this inverse procedure. The results of this study are rather general and should be applicable to any inverse procedure. In early time periods when the drawdown is small, the model (and consequently the inverse procedure) is fairly insensitive to the transmissivity and storativity. At middle time periods, when the drawdown is substantial and hydraulic heads are changing fairly rapidly with time, the greatest sensitivity and best inverse solution results. As the steady state is approached (if one exists), the inverse solution for storativity becomes unstable since the steady state solution does not depend on storativity. However, the inverse procedure for transmissivity continues to work well as the steady state is approached. The effect of error in the data input to the inverse procedure has also been investigated. The maximum error in the aquifer parameters correlates well with the maximum error in the input hydraulic heads. The inverse procedure is well behaved and gives good values for the aquifer parameters as long as it is used where the model is sensitive and as long as the input head error is reasonable.

H 26

ANALYTICAL DESCRIPTION OF GROUND-WATER SEEPAGE ACROSS A LAKE FLOOR

H.J. Bokuniewicz (Marine Sciences Research Center, State University of New York, Stony Brook, NY 11794)

Recent measurements have shown the importance of ground-water seepage across the floors of lakes and lagoons. The subaqueous discharge is not only a source of water but also supplies dissolved chemicals across the sediment-water interface. To help define this process, an analytical solution to the steady-state Richards equation was studied in two-dimensions. This solution was used to derive an expression for the vertical flow of ground water across the floor of a large, shallow lake. The lake is assumed to rest on an aquifer of uniform thickness, l. The aquifer is homogeneous but not necessarily isotropic (its vertical and horizontal hydraulic conductivities are K_h and K_v respectively); it is unconfined and it overlies an impermeable surface. The distance from the lake shore to the ground-water divide is s and the hydraulic gradient, i, is assumed to be a constant over this distance. When $\pi s k/4l > 3$, the discharge, $q = K_v i \ln(\coth \pi x k/4l)/k\pi$ where $k^2 = K_v/K_h$ and x is the distance offshore. The width of the zone of subaqueous discharge is effectively $4l/k$. The hypothetical lake must be wide compared to this distance. The solution fails at the shore (and also at the ground-water divide) because the boundary condition is not differentiable there. As a result, the solution cannot be applied when $x < 0.06\ l/k$. The behavior here can be studied analytically for more special cases. (Supported by The New York Sea Grant Institute and the Long Island Planning Board.)

H 27

TEMPERATURE DISTRIBUTION AROUND AN INJECTION WELL AND EVALUATION OF AQUIFER THERMAL PROPERTIES

Chia Shyun Chen (Agricultural Engineering Department, Texas A&M Unviersity, College Station, TX 77843
Donald L. Reddell (Agricultural Engineering Department, Texas A&M University, College Station, TX 77843

Analytical models of hot water injection into groundwater aquifers are developed in this paper. All available analytical models of this problem assume that the caprock overlying the aquifer is of infinite thickness. However, many groundwater aquifers have caprock thickness of only a few meters. A mathematical model is developed to examine the influence of a caprock with finite thickness on the thermal response of an aquifer. In this model, the horizontal heat conduction and heat convection in the aquifer, plus the vertical heat conduction in the caprock, are considered. A steady state and two asymptotic unsteady state solutions for the water temperature distribution surrounding an injection well are obtained. One of the unsteady state solutions is for a short-time period and the other is for a long time period.

A graphical technique is developed for determining four pertinent aquifer thermal properties: (1) the horizontal thermal conductivity of the aquifer, (2) the thermal capacity of the aquifer, (3) the vertical thermal conductivity of the caprock, and (4) the thermal capacity of the caprock. Dimensionless type curves are constructed from the steady state solution. Using field data, a set of data curves are constructed using long-term observation (approaching steady state) from several observation wells. The data curves are then matched with the dimensionless type curves, and values of the four aquifer thermal properties evaluated.

H 28

FEASIBILITY OF ^{36}CL-DATING OF VERY OLD GROUND WATER

H.W. Bentley and S.N. Davis (Dept. of Hydrology and Water Resources, University of Arizona, Tucson, AZ 85721)

After a brief historical review, theory is presented which indicates ^{36}Cl concentration in groundwater is a function of time, climate, latitude, historical cosmic ray flux, and, to a small degree, sub surface neutron flux due to U and Th in the rock. Determination of ^{36}Cl/stabl chloride ratio should minimize climate effects. Pre-bomb chloride samples were collected in Arizona, Texas, and Spain, chemically processed, and counted by tandem Van de Graaff accelerator. Results show substantial agreement with theoretical predictions. ^{36}Cl content of ground-water profile of Carrizo Sand, a confined aquifer in S.E. Texas, gives water ages consistent with those indicated by hydraulic parameters if chloride variation (thought to be due to ion filtration and to historic glacial period effects) is taken into account. Oldest Carrizo water is 200,000 years old by ^{36}Cl method. Age of water from Triassic rocks from Savannah River area, South Carolina, is determined to be about 500,000 years old, which compares to 800,000 years old by helium accumulation techniques.

Work completed under NRC contract 04-78-272

H 29

STABLE ISOTOPE RELATIONS IN WATER OF THE CAMBRIAN-ORDOVICIAN AQUIFER OF NORTHERN ILLINOIS

E. C. Perry, Jr. (Department of Geology, Northern Illinois University, DeKalb, IL 60115)
R. H. Gilkeson (Illinois State Geological Survey, Urbana, IL 61801) and T. J. Grundl (Department of Geology, Northern Illinois University, DeKalb, IL 60115)

Oxygen and deuterium isotope ratios in water samples from the Cambrian-Ordovician aquifer of northern Illinois lie near the meteoric water line $\delta D = 8\delta^{18}O + 10$. For these samples $\delta^{18}O$ ranges from $-7^o/oo$ to $-12^o/oo$ and δD ranges from about $-45^o/oo$ to about $-89^o/oo$. Samples most depleted in ^{18}O and D appear to have been stored since the Pleistocene. Water with a $\delta^{18}O$ of $-7^o/oo$ approximates the isotopic composition of local meteoric water.

For a number of samples varying widely in salinity, $\delta^{34}S$ and $\delta^{18}O$ of sulfate vary linearly according to the equation $\delta^{34}S = 1.22\delta^{18}O + 0.6$ suggesting mixing of sulfate of $\delta^{34}S = +20\ ^o/oo$ (marine) with sulfate derived from oxidation of pyrite ($\delta^{34}S = 2^o/oo$) in the aquifer recharge system. Other sulfates do not fit this mixing line; the most anomalous has a $\delta^{34}S$ of $+40.3\ ^o/oo$ and a $\delta^{18}O$ of $+2.5^o/oo$. These anomalous samples have Cl/SO_4 ratios much higher than 0.4 as well as negative Eh values. We think they represent waters in which bacteria are actively reducing sulfate. A practical consequence of this process is that barium ion concentration (controlled by $BaSO_4$ solubility) locally rises to concentrations exceeding EPA drinking water standards.

H 30

EVALUATION OF ARTIFICIAL RECHARGE AND DISCHARGE VIA REMOTE SENSING

L. S. Leonhart (Rockwell Hanford Operations, P. O. Box 800, Richland, Washington 99352)

LANDSAT data have assisted in evaluating artificial recharge and discharge effects of irrigated agriculture across a 105,000-square kilometer area within the Columbia Plateau. These studies were performed in conjunction with the siting of a radioactive waste terminal-storage facility within the federally-operated Hanford Site in south-central Washington.

The methodology involved an interactive machine/operator classification of digital LANDSAT data assisted and verified by high-altitude (U-2) photographs. The completed classification was combined with a USGS data base containing digital coordinates of irrigation wells in Washington. This facilitated the segregation between lands receiving imported surface water and those being irrigated with pumped ground water (hence, constituting artificial recharge and discharge, respectively).

The results obtained revealed that over 8,600 square kilometers (or about 8 percent) of the land within the study area have been dedicated to irrigated agriculture. Approximately 1,500 irrigation wells are known to operate within this area. By assuming areally-adjusted averages for the rate of application, percentage of applied water that deep percolates, and the area of land irrigated by a single well, it is possible to estimate the quantity, distribution, and net effect of the surface/subsurface exchange of water that results from such agricultural paractices.

H 31

HYDROLOGIC ELECTRIC ANALOG MODELING IN THE SHENANDOAH VALLEY

John E. Sander (Department of Geology and Geography, James Madison Univ., Harrisonburg, Virginia 22807)

The valley of the Shenandoah River, lying within the states of Virginia and West Virginia, is an area of significant agricultural importance and recent accelerated population growth. The increased utilization of groundwater resources in this region has helped to motivate construction of a two dimensional resistance-capacitance analog model for the entire Shenandoah River watershed. This project represents an initial attempt at integrating, through model simulation, the large amount of hydrologic data that has been collected in the region for many years.

The Shenandoah Valley is composed primarily of limestone overlain by clay soil, and implicit in model design is the assumption that Darcy's law applies to groundwater flow in fractured carbonates when such flow is averaged over a wide area. Initial construction has been completed in the southern part of the Shenandoah Valley for the watershed of the Middle River. Comparison of modeled river flow patterns with field data suggests an average value of transmissivity for the carbonates appreciably higher than the regional average of 500 ft^2/day suggested by Trainer and Watkins (1975) in U.S.G.S. Water-Supply Paper 2035.

H 32

PRELIMINARY INTERPRETATION OF WELL TIDES AT CHALK RIVER (ONTARIO)

Don R. Bower, Earth Physics Branch, Energy, Mines & Resources, 1 Observatory Crescent, Ottawa, Canada, K1A 0Y3.

The level of water in seven boreholes located in crystalline rock at Chalk River (Ontario) has been monitored in order to determine the response due to the solid earth tide and to variations in atmospheric pressure with the ultimate aim of revealing hydrological parameters relevant to waste disposal studies.

Observed M_2 and O_1 tidal effects were compared to predictions based on three hydrological models. Model 1 consisted of a uniformly-porous, confined half space. Model 2 consisted of one or more horizontal plane fractures in an otherwise impermeable half space. Model 3 was similar to model 2 except the fractures were vertical and of given strike. The effect of flow friction was accounted for in the three models on the basis of linear diffusion.

It was found that the observations from six boreholes were reasonably consistent with both models 1 and 2 but clearly inconsistent with model 3. For these boreholes estimates of specific storage and porosity were obtained. In addition, two of these boreholes showed friction effects and estimates of hydraulic conductivity were possible. One of these latter boreholes exhibited a remarkable 360% change in storage coefficient which appeared to correlate with seasonal changes in well level. Observations in the seventh borehole were inconsistent with models 1 and 2 but were consistent with model 3. For this borehole a strike azimuth was defined within narrow limits.

H 33

COMPARISON OF LABORATORY AND FIELD MEASUREMENTS OF HYDRAULIC CONDUCTIVITY FOR COAL-BEARING STRATA

J. P. Schubert (Land Reclamation Program, Argonne National Laboratory, Argonne, IL 60439)

Laboratory tests using an air-type permeameter indicate that the intergranular hydraulic conductivity of sandstones, siltstones, and shales from central Pennsylvania is normally less than 2.5×10^{-9} m/s; the mean for sandstones and conglomerate was 5.1×10^{-10} m/s (n = 40) and the mean for shales, siltstones, and claystones was 6.6×10^{-10} m/s (n = 24). The K_h/K_v ratios of sandstones and laminated siltstones were between 2.0 and 3.0. Hydraulic conductivities calculated from recovery tests of pumped boreholes (n = 13) ranged from 1.11×10^{-8} to 2.19×10^{-7} m/s. Boreholes that penetrated greater percentages of sandstone generally exhibited higher values of hydraulic conductivity.

Previous investigators have shown that fractures greatly influence the storage and flow of groundwater in coal-bearing strata. However, the seepage of water from the base of sandstones in coal mine highwalls indicates that the primary hydraulic conductivity of sandstone can also play an important role. Determining the relative importance of fracture vs. primary hydraulic conductivities from well tests is a critical necessity when assessing potential interactions of groundwater flow systems with surface mining, underground mining, or in-situ gasification of coal.

H 34

SOME NEW FORMULAE FOR COMPUTATION OF FRACTURE PERMEABILITIES FROM EXPERIMENTAL DATA

D. K. Babu (Dept. of Civil Engineering, Princeton University, Princeton, N.J. 08544)

Estimation of aperture width plays a crucial role in the experimental determination of individual fracture permeability. The fracture itself is often identified in theory with the narrow opening between two smooth-walled parallel plates. It is shown that a parallel plate model with smooth walls leads to an underestimation of the permeability of the fracture. New analytical expressions are derived for computing the aperture width as well as the hydraulic conductivity from measurements of discharge rates, pressure differentials and specimen sizes. The new expressions are seen to result in a substantial increase over the existing values of fracture permeabilities. Estimates based upon the new formulae may be in closer agreement with the higher permeability values that are generally associated with field data.

H 35

EFFECT OF SAMPLE SIZE ON THE STRESS PERMEABILITY RELATIONSHIP OF NATURAL FRACTURES

K.G. Raven and J.E. Gale, Department of Earth Sciences, University of Waterloo, Waterloo, Ontario, Canada N2L 3G1.

Recent studies have shown that the effective normal stress-fracture permeability relationship may be a function of the magnitude of the fracture surface area. The effect of sample size on the permeability of natural fractures has been studied using five granite cores (10.0, 15.0, 19.3, 24.5 and 29.4 cm in diameter) containing natural fractures oriented normal to the core axis. Each fractured sample, taken from the same fracture plane, was subjected to three loading-unloading cycles with maximum axial stresses of 30MPa. In each loading-unloading cycle the steady state flowrate through the fracture plane from a central borehole was measured for specified levels of normal stress.

Both fracture deformation and flowrate exhibited a non-linear variation with changes in normal stress. Fracture deformation and flowrate hysteresis (between loading and unloading cycles)were observed for all samples. The magnitude of this hysteresis decreased with successive loading cycles. Maximum and minimum flowrates for each cycle were also observed to decrease with successive loading cycles. Calculated minimum fracture permeability at maximum normal stress varied from 1.67 $\times 10^{-2}$cm/sec for the smallest sample to 3.23 $\times 10^{-3}$cm/sec for the largest sample. This apparent decrease in the fracture permeability with increase in sample size will be discussed in terms of initial fracture seating, definition, roughness and possible variance of such fracture characteristics within a single fracture plane.

H 36

STEADY-STATE VERSUS TRANSIENT PRESSURE PULSE PERMEABILITY TESTS - LABORATORY AND FIELD RESULTS

C.F. Forster and J.E. Gale, Department of Earth Sciences, University of Waterloo, Waterloo, Ontario, Canada N2L 3G1
(Sponsor: John Cherry)

The transient pressure pulse test has been proposed as a single-well test to assess fractured rock permeabilities in the range of 10^{-8} to 10^{-12} cm/sec. To evaluate the technique the results of transient tests were compared to steady-state tests performed under controlled laboratory and field conditions. Standard field packers were used to isolate a 3 m interval in a simulated borehole (a 76 mm diameter steel tube). The isolated interval was connected to a hydrostatic pressure cell containing cylindrical rock samples (5 cm in diameter and 10 cm in length). Transient and steady-state tests were performed on samples of Berea Sandstone (steady-state K_p = 0.6 to 2.3 $\times 10^{-4}$ cm/sec) and fractured Stripa granite (steady-state K_f = 1.9 $\times 10^{-3}$ cm/sec at maximum confining pressure of 13.8 MPa). Calculated transient conductivities were one to two orders of magnitude less than the corresponding steady state values. Also, packer compliance caused variations of up to 50% in transient test conductivities and temperature variations of $\pm$ .01°C significantly affected the shape of the pressure-time decay curve.

A field experiment was performed on an array of five, 30 m long, boreholes collared 330 meters underground in a fractured granitic mass. Twenty-three borehole cavities were isolated and shut-in pressures monitored. Steady-state tests in 2 m intervals gave conductivities that ranged from less than 4×10^{-11} cm/sec to 2×10^{-7} cm/sec. Results of transient tests performed in the same intervals show that there was no direct correlation between steady-state conductivity and pressure pulse decay time.

Role of Laboratory Methods in Hydrologic Investigations

Pier 7 & 8
Friday P.M.
Leonard F. Konikow (USGS) *A. Ivan Johnson* (Woodward-Clyde), Presiding

H 37 INVITED PAPER

VALIDITY OF CUBIC LAW FOR FLUID FLOW IN A DEFORMABLE FRACTURE

P. A. Witherspoon Earth Sciences Division, Lawrence Berkeley Laboratory, Berkeley, Ca. 94720
J. S. Y. Wang, Lawrence Berkeley Lab.
K. Iwai, Nakano-Corp. Niigatashi, Japan
J. E. Gale, Univ. Waterloo, Waterloo, Canada

The validity of the cubic law for laminar flow through open fractures consisting of parallel planar plates has been established by others with apertures ranging down to a minimum of 0.2 μm. The law in simplified form is $Q/\Delta h = C(2b)^3$, with Q the flow rate, Δh the difference in hydraulic head, C a constant depending on the flow geometry and fluid properties, and 2b the fracture aperture. The validity of this law for flow in a closed fracture with surfaces in contact and aperture decreasing under stress has been investigated at room temperature using homogeneous samples of granite, basalt, and marble. Tension fractures were artificially induced. The laboratory setup used radial or straight flow geometries, and apertures from 250μm down to 4μm, the minimum size attainable under a normal stress of 20 MPa.

The cubic law was found to be valid with fracture surfaces held open or being closed under stress, independent of rock type. Permeability was uniquely defined by fracture aperture and was independent of the stress history. The effects of deviations from the ideal parallel plate concept only cause an apparent reduction in flow and

may be incorporated into the cubic law by replacing C by C/f, f varying from 1.04 to 1.65.

The model of a fracture being closed under normal stress is visualized as controlled by the strength of the asperities in contact, which are able to withstand significant stresses, while maintaining space for fluid flow with decreasing aperture. The magnitude of the aperture controls flow (dependent on $(2b)^3$). Slight changes in aperture dominate any other change in the geometry of the flow field. There is no noticeable shift in results in passing from open to closed fracture.

H 38 INVITED PAPER

COMPARISON OF LABORATORY, IN SITU, AND ROCK MASS MEASUREMENTS OF THE HYDRAULIC CONDUCTIVITY OF METAMORPHIC ROCK AT THE SAVANNAH RIVER PLANT NEAR AIKEN, SOUTH CAROLINA*

I. Wendell Marine
E. I. du Pont de Nemours & Co. (Inc.)
Savannah River Laboratory, Aiken, SC 29801

In situ testing of exploratory wells in metamorphic rock indicates that two types of fracturing occur in the rock mass: that consisting of small openings that permit only extremely slow movement of water, and that consisting of openings of sufficient size to permit transmission of water at a significantly faster rate. Laboratory methods are unsuitable for measuring hydraulic conductivity in the hydraulically transmissive fractures; however, for the virtually impermeable rock, values comparable to the in situ tests can be obtained. The hydraulic conductivity of the rock mass over a large region can be calculated by dividing the inferred travel distance by the age of the water as determined by the helium content of the water. This hydraulic conductivity value falls between the values measured for the two types of fractures, but is closer to the measured value for the virtually impermeable rock. This relationship is attributed to the control of the regional flow rate by the virtually impermeable rock where the discrete fractures do not form a continuous open connection through the entire rock mass. Thus, laboratory methods of measuring permeability in metamorphic rock are of value if they are properly applied.

* Work done under USDOE Contract No. DE-AC09-76SR00001.

H 39 INVITED PAPER

Role of Laboratory - Scale Measurements in Mass Transport Modeling

Leslie Smith (Dept. of Geology and Geophysics, University of Utah, Salt Lake City, Utah)
Franklin Schwartz (Dept. of Geology, Univ. of Alberta, Edmonton, Alberta)

The adequacy of the dispersion-convection equation in describing transport at the scale of a laboratory column is well documented. Conventional modeling of mass transport in groundwater systems invariably involves a simple scaling-up of the porous medium dispersivity from the very small values observed in column experiments to the much larger values calculated from field trials. There is increasing evidence to suggest that this approach is inadequate because of problems in defining a unique dispersivity value for an expanding plume. An alternate modeling technique has been proposed which accounts for macroscopic dispersion not as a large-scale diffusional process but as mixing caused by spatial heterogeneities in hydraulic conductivity. The basic data requirement for this transport model is the macroscale structure of the spatial variability in hydraulic conductivity. Hydraulic conductivity is assumed to be a random variable with a mean, standard deviation and a spatial autocorrelation between neighbouring points. This structure can be estimated from a set of point values of hydraulic conductivity, obtained either from measurements on cores in the lab or from falling head tests in piezometers. The effects of small scale heterogeneities can be incorporated through a term dependent on the lab-scale dispersivity.

H 40

SIMULATION OF THE TRANSPORT OF ION-EXCHANGING SOLUTES USING LABORATORY-DETERMINED CHEMICAL PARAMETER VALUES

Albert J. Valocchi (Department of Civil Engineering, Stanford University, Stanford, Cal. 94305)
Robert L. Street

The use of numerical simulation models as predictive tools in the analysis of solute transport problems requires the determination of geologic, hydraulic, and geochemical parameter values. This paper deals with the use of laboratory-determined selectivity (distribution) coefficients in the simulation of the transport of ion-exchanging solutes governed by local chemical equilibrium. The transport model has been applied to a pilot field operation involving the injection of advanced-treated municipal wastewater into an alluvial aquifer in the Palo Alto, Ca., baylands region.

Basic hydrogeologic parameters, such as porosity, bulk density, and aquifer thickness, were determined via analysis of observation well logs and core samples. Data on the breakthrough of a conservative tracer at the various observation points was utilized to determine an approximate velocity field and dispersivity values. The chemical parameters, selectivity coefficients and cation exchange capacity, were determined using standard batch laboratory experiments on aquifer core material. Using these parameter values, the simulation model was run to predict the breakthrough of major cations at the observation wells. The predicted results agree very closely with the actual field data. This agreement suggests that, for this particular case, laboratory-determined chemical parameters can be successfully used in field-scale transport simulations.

H 41 INVITED PAPER

COMPARISON OF REGIONAL, IN SITU, AND LABORATORY HYDRAULIC CONDUCTIVITIES OF THE CRETACEOUS PIERRE SHALE

C. E. Neuzil (U.S. Geological Survey, Reston, VA 22092)
J. D. Bredehoeft (U.S. Geological Survey, Reston, VA 22092)

A recent study of the hydrology of the Cretaceous Pierre Shale utilized three techniques for measuring the hydraulic conductivity of "tight" materials. Regional hydraulic conductivity was obtained from a hydrodynamic model analysis of the aquifer-aquitard system which includes the Pierre Shale. Local conductivities were obtained in situ in a borehole using specially designed slug tests. Laboratory values were obtained from consolidation tests on core samples.

The laboratory tests and in situ tests yielded comparable values; the regional hydraulic conductivity was two to three orders of magnitude larger. This suggests that the lower values represent intergranular hydraulic conductivity of the intact shale and the regional values represent secondary permeability due to fractures. Calculations based on fracture flow theory demonstrate that small fractures can account for the observed differences.

H 42

Using Field Measured and Laboratory Measured Hydraulic Parameters to Predict Infiltration and Drainage.

T. L. Jones (Rockwell Hanford Operations, Richland, WA 99352), J. B. Sisson, A. H. Lu, and W. A. Jordan

Sponsor: A. G. Law

Field and laboratry tests were conducted to estimate soil hydraulic conductivity and desorption parameters. Significant differences were found between field and laboratory desorption curves while certain laboratory procedures produced estimates of hydraulic conductivity comparable to the field values. Differences in the desorption curves may be due to hysteresis. The field and laboratory estimates were used in a numerical model to predict infiltration and drainage and the results were compared to field data. One laboratory procedure estimated the saturated conductivity higher than others. Using this estimate, the model overpredicted the advance of the wetting front. Using field estimated hydraulic conductivity and desorption cruves resulted in predictions which agreed better with field data. These results indicate that certain laboratory procedures may provide useful hydraulic conductivity data but differences between field and laboratory measured desorption curves may be more significant than previously thought.

H 43

MODELLING OF POTASSIUM MIGRATION FROM THE CFB BORDEN LANDFILL

J.F. Sykes (Dept. of Civil Engineering, University of Waterloo, Waterloo, Ontario N2L 3G1)
(Sponsor: L. Konikow)

In laboratory experiments, the migration of potassium chloride through unsaturated sand columns was analyzed. Batch studies were undertaken to develop independent estimates of the parameters of adsorption. Based on these parameters, the use of equilibrium or kinetic sorption models alone in conjunction with the convection-dispersion equation did not adequately describe the experimental results for potassium breakthrough. However, excellent predictions were obtained using a combined equilibrium-kinetic Freundlich sorption model with parameters being determined from both column tracer breakthrough data and the equilibrium and kinetic batch experiments. Estimates of the fraction of active sorption sites in the column were obtained through model calibration.

To simulate the migration of potassium from the Canadian Forces Base (CFB) Borden landfill, the saturated conditions and lower field as compared to column velocities are such that adsorption can be assumed to be governed essentially by equilibrium. To further simplify the model and numerical computations, the Freundlich isotherm is linearized such that it gives the correct adsorbed concentration for the potassium leachate concentration and is environmentally conservative for all lower concentrations. It is felt that this approach is warranted in light of the uncertainty in many of the field parameters and processes (for example potassium leaching and the historical development of the landfill). Comparisons between the measured potassium plume and predicted results as determined using both finite difference and finite element models are favourable and substantiate the methodology.

H 44

POROSITY PERMEABILITY RELATIONSHIPS IN STRATIFIED GLACIAL DEPOSITS

W.E. Kelly (Dept. of Civil & Environmental Engineering, University of Rhode Island, Kingston, R.I. 02881)

Relations between formation factor or electrical resistivity and aquifer permeability have been reported for a range of geologic materials. For stratified glacial deposits in southern Rhode Island the controlling factor appears to be a tendency for low permeability sediments to deposit at high porosities and therefore low formation factors; this explains the observed inverse relationship between formation factor and permeability but needs to be documented. A series of in-place density measurements have been made and samples collected for laboratory grain size and permeability determination. Preliminary analysis indicates that in-place porosities decrease as the median grain size and sorting coefficient increase, while permeability increases as median grain size increases and the sorting coefficient decreases. When regression equations using the median grain size and the sorting coefficient are combined, the inverse relationship between in-situ porosity and permeability is demonstrated. The relationship exhibits considerable scatter but a clear trend is evident. Relations using other grain size and distribution parameters are being tested.

in the nitrate, bromide, dissolved oxygen and bicarbonate concentrations. The observed decrease in the bromide concentration was used to correct the nitrate data for the effects of physical dilution of the injected groundwater slug.

Data collected using the above procedure provided convincing evidence that denitrification can proceed at substantial rates in groundwaters. The results also showed the experimental procedure to be an effective means of investigating denitrification rates and the geochemical factors affecting the denitrification process.

Modeling of Groundwater Pollutants

Pier 7 & 8
Saturday P.M.
Ardhesh K. Tyagi (Univ. of Kansas), Presiding

H 52

MODELING OF CONTAMINANT MIGRATION IN HETEROGENEOUS MEDIA

Franklin Schwartz (Dept. of Geology, Univ. of Alberta, Edmonton, Alberta)
Leslie Smith (Dept. of Geology & Geophysics, University of Utah, Salt Lake City, Utah)

A stochastic approach to macroscopic dispersion can be used to model contaminant migration in heterogeneous media. Transport of a contaminant is simulated using a hybrid deterministic-probabilistic technique. Results indicate that transport is influenced in a complex way by geologic layering, within layer heterogeneities in hydraulic conductivity and porosity, by porous medium-fluid interactions, location of the input zone and the release rate of contaminants from primary containment. Those parameters capable of changing both the magnitude and direction of advective transport are of primary importance in influencing predictive ability. The arrangement of units with different mean hydraulic conductivities, the standard deviation and spatial continuity in hydraulic conductivity, and hydraulic anisotropy can be identified in this respect. Other parameters such as porosity, and processes such as cation exchange act only to change the magnitude of the velocity. For this reason, spatial variations in these parameters are of secondary importance in contributing to uncertainty. Depending upon the relative time scales of the release function and the transport process, lack of information about timing and concentrations added at the source may cause greater uncertainty than the heterogeneity. In certain geologic systems, patterns of contaminant migration can be predicted with more certainty. Features such as layering and hydraulic anisotropism can constrain the flow of contaminants to specific directions, thus limiting the size of the region through which contaminants are likely to spread.

H 53

MATHEMATICAL MODELING OF CHEMICAL TRANSPORT IN SOIL COLUMNS

K. L. Kipp (U.S. Geological Survey, Lakewood, CO 80225

Three one-dimensional models of mass transport were used to characterize the movement of selected chemical species (chloride, lithium, and phenol) in saturated and unsaturated laboratory and field soil columns. The chemical-soil interaction mechanisms for the models were; no sorption, linear equilibrium sorption, and linear kinetically-controlled sorption.

Parameters calculated from the column elution curves were the velocity, and the kinetic sorption, and dispersion coefficients. These parameters were calculated by minimizing the sum of the squares of differences between measured and computed concentrations. This minimization used a combination of nonlinear regression techniques that included steepest descent, Newton-Raphson, and Marquardt methods with improvement of the gradient matrix. Beale's measure (a test of non-linearity) was used to determine if calculations of confidence regions and intervals, using linear techniques, were appropriate. Sensitivity tests with synthetic data identified the factors that contributed to the uncertainty of the parameters. Statistical evaluations that included plots of residual errors, calculation of their variance, white noise tests and covariance tabulation were used to evaluate the accuracy of the calculated parameters.

Significant cross correlations between the dispersive and sorptive parameters were often observed. In many cases it was possible to distinguish the sorption model that gave a best fit to the data. However, loss of information due to tail truncation and measurement error can make it impossible to identify the most realistic sorption model. Application of these solute transport models to unsaturated columns was successful only for nearly homogeneous soil profiles.

H 54

A MODEL OF TWO PHASE MASS AND HEAT TRANSPORT IN POROUS MEDIA

Bryan J. Travis (Geosciences Division, Los Alamos Scientific Laboratory, Los Alamos, NM 87545)
Alvin H. Davis (same address)

A versatile multidimensional model of three component, multi-phase mass and heat transport in porous media is presented. Differences from other porous flow models are noted. The model is not limited to Darcy flow. Time dependent conservation equations are solved for each mass species and for energy transport in the fluid and in the matrix. Table look-ups are used to provide accurate calculations of internal energies, densities, viscosities, etc. The model compares well with analytic similarity solutions and with three laboratory experiments. The first experiment is the injection of steam into cold dry sand, the second is the injection of hot, dry nitrogen into cold, wet samples of tuff. The third experiment is the two-phase convection experiment of Sondergeld and Turcotte.

H 55

SOLUTE TRANSPORT DURING INFILTRATION INTO REACTIVE SOILS

K.B. Laryea*
M.J.L. Robin
D.E. Elrick (all at Dept. of Land Resource Science, University of Guelph, Guelph, Ontario, Canada, N1G 2W1)

In non-reactive and unstructured soils the dispersion of solutes during infiltration can be described by diffusion about a moving plane and by assuming the complete displacement of the initial soil water solution by the displacing soil water solution. Flow in soils is generally such that the dispersion coefficient can be taken as velocity independent. It follows that similarity in $xt^{-\frac{1}{2}}$ occurs for the water content and solute content profiles. The analysis is extended to the movement of K^+, an ion that reacts with the soil particle surfaces. Non-linear adsorption of K^+ is taken into account by solving the dispersion equation using simulation techniques (CSMP and GASP IV).

H 56

IMPROVED ACCURACY OF FINITE ELEMENT SIMULATION OF GROUNDWATER CONTAMINANT TRANSPORT USING A HIGHER ORDER TIME APPROXIMATION

Sirous Haji-Djafari, (D'Appolonia Consulting Engineers, Inc., Pittsburgh, PA 15235)
David C. Wiggert, (Civil Engineering Department, Michigan State University, East Lansing, MI 48824)

The finite element formulation of groundwater flow and mass transport equations results in a system of first order linear differential equations. These equations are normally numerically integrated using a finite difference method for the time derivative. In this study, using the finite element method, a procedure for obtaining finite difference relations was presented. Utilizing this technique, the recurrence formulas for the first, second, and third order time approximations for the first order differential equation were derived. In these recurrence formulas, the time scale, Θ , can be varied from an explicit time difference scheme, where Θ is equal to zero, to an implicit scheme, where Θ is equal to one.

To test this technique, the first and second order time approximations with various Θ values were used in the solution of convective-dispersion equations for simulation of groundwater contaminant transport. A more accurate result was obtained in this simulation using a second order time approximation than using a first order approximation. In addition, better accuracy was achieved using Θ greater than 1/2, with Θ = 2/3 providing the least error.

Thus, it was concluded that better accuracy is possible if the higher order time approximation with Θ greater than 1/2 is used in the finite element simulation of groundwater contaminant transport.

H 57

MATRIX DIFFUSION IN SOLUTE TRANSPORT THROUGH DISCRETE FRACTURESIN POROUS ROCK

E.A. Sudicky (Department of Earth Sciences, University of Waterloo, Waterloo, Ontario N2L 3G1)
E.O. Frind (Department of Earth Sciences, University of Waterloo, Waterloo, Ontario N2L 3G1)
D.H. Tang (Intera Environmental Consultants, Houston, Texas 77079)

A new analytical solution is developed to describe reactive and nonreactive solute transport through discrete fractures located in a porous matrix. The problem is formulated by coupling two one-dimensional differential equations, onerepresenting advective-dispersive transport along a fracture, the other representing diffusive transport in the unfractured matrix. Processes included in the model are advection and dispersion in the fracture, diffusion into the matrix, solute adsorption and radioactive decay. Adsorption of reactive species onto the face of the fracture is considered separately from that occurring in the matrix because of the possibility of different chemical properties. The closed-form analytical solution provides a computationally efficient means of illustrating the effects, on solute transport, of the processes considered. Potential applications of the model include the simulation of contaminant migration from an underground waste repository, where the major escape path may be along a dominant fracture. Matrix diffusion can, in this case, play an important role in limiting the extent of contamination along this route.

AGU Symposium on Urban Hydrometeorology & Canadian Hydrology Symposium 80 Hydrology of Developed Areas

Metropolitan East
Monday A.M.
Jean Rousselle (Ecole Polytechnique) and *J. W. Deller* (Purdue University), Presiding

H 58 INVITED PAPER

MONITORING AND FORECASTING CONVECTIVE RAINFALL OVER CHICAGO

John L. Vogel (Illinois State Water Survey, Urbana, Illinois, 61801)

H 45

FIELD AND LABORATORY CALCULATIONS OF HYDRAULIC CONDUCTIVITY OF A CLAY-RICH TILL, WEST VALLEY, NY

Prudic, D. E. (U.S. Geological Survey, Albany, N.Y. 12201)
(Sponsor: Leonard Konikow)

Hydraulic conductivity of a clay-rich till was evaluated through field and laboratory studies as part of a study of the movement of radioisotopes at a nuclear-waste landfill near West Valley, NY. In general, horizontal hydraulic conductivity values from core samples as determined in the laboratory agreed with values calculated from slug tests in which water was suddenly removed from piezometers finished in the unweathered till.

Slug tests were analyzed by two methods. One method assumed horizontal flow to the screen, the other assumed spherical, isotropic flow. Average horizontal hydraulic conductivity values from slug tests of 10 piezometers were $5x10^{-8}$ centimeters per second (cm/s) by the first method and $2x10^{-8}$ cm/s by the second method.

Laboratory tests of core samples were designed to determine the extent to which anisotropy and increased pressures with depth may affect hydraulic conductivity. Nine core samples were analyzed for horizontal and vertical hydraulic conductivities; horizontal values averaged $4.0x10^{-8}$ cm/s; vertical values were only twice as high, suggesting little anisotropy in the till. Consolidation tests were done on four core samples to determine changes in hydraulic conductivity with pressure. Vertical hydraulic conductivity values decreased by about 40 percent at a pressure increase from zero to the 7 kilograms per square centimeter that would prevail at a depth of 30 meters. This decrease suggests that the hydraulic conductivity of the till may decrease with depth as overburden pressures increase.

Laboratory measurements on cores could not evaluate the effects of scattered fractures observed in the upper 5 meters of till. Preliminary digital-model results as well as slug tests from shallow piezometers suggest that the till is at least 10 times more permeable in the upper 5 meters, where fractures are prevalent.

Tracers in Groundwater

Pier 7 & 8
Saturday A.M.
Warren Wood (Texas Tech. Univ.), Presiding

H 46 INVITED PAPER

EVALUATION OF F2 BACTERIOPHAGE FOR TRACING MOVEMENT OF VIRUSES IN GROUNDWATER

D-S. Wang (Baylor College of Medicine, Houston, Texas 77030)
C.P. Gerba (Baylor College of Medicine, Houston, Texas 77030)

Land disposal of wastewater poses a potential for contaminating groundwater with pathogenic viruses. Since little is known about the movement of human enteric viruses in groundwater, it is necessary to develop methods for tracing their movement in groundwater. For this purpose, it is desirable to use a tracer that closely resembles human disease causing enteric viruses but that represents no health hazard or pollution problem to the environment. A potential usefulness of f2 bacteriophage as a tracer of human enteric viruses in groundwater is evaluated.

The f2 phage is a small tailless RNA virus which resembles very much enteric viruses in both size and morphology. It has been used previously as a model for viral movement through soils. Reviews of the literature indicate that f2 phage adsorbs poorly to soils, clays, and sewage solids and penetrates into groundwater together with the percolating effluent during land application of wastewater at a rapid infiltration site. Preliminary soil column studies in this laboratory also indicated that adsorption of f2 phage by soils was much less than those of animal viruses. Additionally, f2 was found to survive much longer than poliovirus in wastewater.

In view of its high mobility and viability in the environment, together with its non-pathogenic property, f2 phage is considered to be a suitable tracer for viral movement in groundwater.

H 47 INVITED PAPER

INVESTIGATION OF GROUNDWATER FLOW BY MEANS OF TRACERS IN QUATERNARY GRAVELS OF BAVARIA

BEHRENS, H., Institut für Radiohydrometrie der Gesellschaft für Strahlen- und Umweltforschung mbH, München, D-8042 Neuherberg (Germany)
SEILER, K.-P. (D-8042 Neuherberg)
RAUERT, W. (D-8042 Neuherberg)
(Sponsor: John B. Robertson)

Fluorescent dye tracers and in some cases in addition radioactive tracers were applied to investigate groundwater flow on distances up to some 1000 meters.

In a glacially overdeepened valley tracer injections were performed into homogeneous as well as into inhomogeneous buildup gravels with groundwater flow parallel to bedding; furthermore seepage perpendicular to bedding in the unsaturated zone was studied with tracers. Groundwater flow without groundwater discharge was compared with the flow during a one-year pumping test. Results on groundwater flow velocities, longitudinal and to some extend transverse dispersion were obtained; these parameters are affected by the position of the injection to the pumping well and by orientation of groundwater flow to bedding.

Tracer experiments in other areas indicated, that tracer passage in single observation points is affected by unsteady state conditions in the flow field as well as by hydrodynamic dispersion. Furthermore inhomogeneities of the aquifer may have a large influence on transverse dispersion.

Although the used tracers generally showed conservative behaviour in the cited experiments, under the influence of seepage water from a waste dump Eosin was destroyed.

H 48 INVITED PAPER

BOMB TRITIUM AS A TRACER OF YOUNG WATER IN UNCONFINED SANDY AQUIFERS

B.C.E. Egboka, J.A. Cherry, R.N. Farvolden (Dept. of Earth Sciences, University of Waterloo, Waterloo, Ontario N2L 3G1, Canada).

Since the beginning of the era of atmospheric tests of nuclear devices in 1952, rain and snow have contained concentrations of ^3H that have been well above pre-1952 levels, and, as a consequence, ^3H can serve as an identifier or tracer of post-1952 water in groundwater flow systems. In this study patterns of ^3H occurrence were delineated in three unconfined sandy aquifers with shallow depths to water table. Depth versus ^3H profiles were obtained using detailed piezometer nests and multilevel samplers. In two of the three areas, the upper part of the aquifer has abundant ^3H, whereas the lower zones have no detectable ^3H. Functions for ^3H input to the groundwater systems were developed from records of local precipitation, long-term ^3H in precipitation data from Ottawa, Canada, and short-term local ^3H records. In all three study areas, the maximum ^3H concentrations were a small fraction of the maximum values for precipitation recorded in the 1960's. The large decline in maximum concentrations and the general patterns of ^3H occurrence were attributed to differential rates of seasonal recharge, local irregularities in the flow patterns, radioactive decay, molecular diffusion, and mechanical dispersion. In areas from which the most detailed field data were obtained, simulations of the ^3H patterns were used to obtain estimates of dispersivity.

H 49 INVITED PAPER

TRANSPORT OF TECHNETIUM, IODINE, RUTHENIUM, AND ZIRCONIUM IN THE UNSATURATED ZONE

M.Albertsen
G.Matthess (Geologisch-Palaeontologisches Institut, Kiel University, Kiel Germany F.R.)

The transport of technetium, iodine, ruthenium and zirconium in 3 typical sandy soils was investigated with laboratory experiments, which simulated fall-out events, using soil columns (1 m length, 0.30 m diameter). Evaluation of the breakthrough curves in the percolate and of the depth distribution of the radionuclides in the soil columns after 6 months yielded the average transport velocity, which could be compared with the average water velocity measured by tritium tagging. Three qualitative mobility relations were observed:

Ranker : Tc > Ru > I > Zr
Podsol : Tc > Ru > I > Zr
Brown forest soil: Tc ≈ Ru > I > Zr

Relations exist between some physicochemical soil properties and the retardation of radionuclides due to adsorption (eg. retardation of iodine and technetium by organic substances).

The average retardation factors of the radionuclides and the hydrodynamic soil parameters are used in a model which gives a quantitative assessment of the hazard of groundwater contamination by a fall-out event in areas covered with comparable soils.

H 50

GEOCHEMISTRY OF BROMIDE AND IODIDE IN NATURAL WATERS: IMPLICATIONS FOR TRACER STUDIES

D.O. Whittemore
M.H. Savage (both at: Kansas Geological Survey, University of Kansas, Lawrence, KS 66044
G.L. Feder (U.S. Geological Survey, Denver, CO 80225

Recent studies have shown that Br, and in many cases, I ions are reliable tracers for natural waters. An understanding of the geochemistry of Br and I in surface and ground waters can aid in determining suitable study sites and in interpreting the results of tracer investigations. Ratios of both Br/Cl and I/Cl range widely in natural waters and generally decrease with increasing Cl concentration. Weight ratios of Br/Cl and I/Cl usually range from $10^{-1.3}$ to $10^{-3.2}$ and $10^{-2.3}$ to $10^{-5.0}$, respectively, for fresh waters (Cl = 0.1-1000 mg/l), and from $10^{-2.6}$ to $10^{-4.0}$ and $10^{-4.4}$ to $10^{-5.8}$, respectively, for saline waters derived from mixing with halite solution brines. Oil-field brines have much higher Br/Cl and I/Cl than halite solution brines and much higher I/Cl than seawater; consequently, pollution by oil-field brines can be traced even in the presence of other saline waters.

Ratios of Br/Cl and I/Cl may thus prove more useful than absolute concentrations of Br and I in tracer studies where changes in chemistry of the waters occur in the system to which these tracers are applied, such as in the mixing of different waters. Adding Br and I to natural flow systems may enhance the ability to trace ground water flow. For example, enhanced tracing of the movement of many saline waters by Br and I additions is possible due to the low concentrations of Br and I, despite high levels of Cl. Simultaneous addition of Br and I to well above natural levels may show not only the movement of water by dissolved Br, but also a qualitative measure of the adsorptive capacity of the medium for certain anionic species as indicated by the greater adsorption of I than of Br.

H 51

AN APPLICATION OF TRACERS TO STUDIES OF DENITRIFICATION IN GROUNDWATER

M.R. Trudell (Alberta Research Council, Edmonton, Alberta)
R.W. Gillham and J.A. Cherry (Department of Earth Sciences, University of Waterloo, Waterloo, Ontario N2L 3G1)
(Sponsor: Emil Frind)

In situ investigations of geochemical reactions are commonly frustrated by an inability to separate the effects of physical and chemical processes on the observed trends in concentration. In this study, an experimental procedure using a non-reactive tracer was developed for studying the process of denitrification in hydrogeologic environments.

A specially designed well point was used to withdraw a volume of groundwater from a geologic zone in which denitrification was believed to be an ongoing process. After the addition of nitrate and the non-reactive tracer (bromide), the volume of groundwater was reinjected through the same well point. Water samples collected periodically from the injected groundwater zone were used to show changes with time

A radar-rainfall system to monitor and forecast quantitative amounts of rainfall from convective storms over Chicago in real time was tested during the summer of 1979. Such a system can give urban hydrologists present and future patterns of rainfall, providing the data necessary to make decisions about the deployment and storage of storm water in sophisticated water management systems.

The radar-rainfall system is composed of a 10-cm digital radar coupled with a mini-computer and 22 telemetered raingages which are used to adjust radar-indicated rainfall as it approaches the urban region. Objective analysis methods accumulated the rainfall at 3.2 kilometer intervals over 42,000 square kilometers. Individual radar echoes were tracked using an interactive graphic display technique, and data obtained from this analysis were used to make objective forecasts for three regions over Chicago for the next 30-, 60-, and 120-minutes.

The radar-rainfall system was located 65 kilometers southwest of the center of Chicago. Results from the test indicate that the system was capable of monitoring and forecasting quantitative rainfall amounts. Also, the results point to the need for skilled operators to interpret and monitor the objective analysis and forecast schemes.

H 59

NEW DATA COLLECTION EQUIPMENT FOR MINING DEVELOPMENTS

J. WHITING
K. BINDLE (SASK. Research Council, Saskatoon, Canada)

The Saskatchewan Research Council (SRC) has developed three battery operated systems to enable mining companies to supply water and air quality data for scrutiny to regulatory agencies.

A field Water Quality Monitor capable of up to 10 sensor inputs has been tested. The present system uses the following sensors: temperature, water depth, conductivity, pH, dissolved oxygen. The field tested monitor has the capability of operating for a period of three months on a 12 volt battery pack.

A Hydrometeorological Satellite Sending Unit has been built which is capable of monitoring water flow (rate and depth), temperature (water and air), precipitation (snow and rainfall), wind (speed and direction). Alpha and radon radiation sensors and monitoring by integration, mean and standard deviation are presently being researched.

The hydrometeorological unit is presently configured to a transmitter which conditions the data and sends to a GOES Satellite. The system is presently in use on the MacFarlane River in Saskatchewan. The data is retrieved every day with graphical output every month.

A Water and Effluent Sampler capable of taking samples in containers varying from 10 mℓ to 5 litres has been developed and used at SRC. These samplers can be supplied with refrigeration and heating to enable the system to be operated in the extremes of the climate of Canada. Typical sampling periods range from 72 seconds to 14 days with individual or integrated samples.

The use of chemically inert materials in the construction of the sampler prevents foreign contamination or corrosion problems associated with refinery plants.

H 60

URBAN STORMWATER CONTROL PACKAGE FOR AUTOMATED REAL-TIME SYSTEMS

Dennis M. Morrow (Dept. of Envrn.Quality, Land Quality Div., Dist. IV, Sheridan, WY 82801)
John W. Labadie (Dept. of Civil Engineering, Colo. State Univ., Ft. Collins, CO 80523)
(Sponsor: Jacques Delleur)

A stormwater control package (SWCP) has been synthesized to facilitate the development and implementation of fully automatic computer control for combined sewer flow management. The SWCP is a methodology for integrated application of computer models for inflow forecasting, sewer routing, and operational storage control in a simulated real-time environment.

The forecasting model used in the SWCP is of the autoregressive transfer function type. Model parameters are updated in real-time by a sequential regression algorithm which processes available data from the storm event in progress. Options available include lead time variation, weighting the storm in progress vs. historical data, and model order. The control policy model used in the package is built around a blend of optimization and fully dynamic unsteady flow routing. The multidimensional nonlinear control problem is decomposed by a heuristic dynamic programming algorithm which uses orthogonal polynomials to represent the temporal system state. Options in the control policy include reactive and adaptive or anticipatory operating strategies. The adaptive strategies use forecasted inflows and forecast error statistics.

The SWCP is applied to the Marina Branch of the North Shore Outfalls Consolidation Project, City of San Francisco, which is currently under construction. Some computational experience is presented on the advantages of utilizing anticipatory control over reactive or set-point control.

H 61

RAINFALL FREQUENCY ANALYSIS FOR URBAN DESIGN

W.E. Watt. Dept. of Civil Engineering, Queen's University, Kingston, Ontario K7L 3N6
M.J. Nozdryn-Plotnicki

An investigation was carried out into the appropriateness of the probability distribution and fitting technique adopted by the Atmospheric Environment Service (AES) for rainfall frequency analysis.

The Extreme Value Type 1 (EV1) distribution was assessed for three long term Canadian stations: Victoria, St. Thomas and Quebec. The EV1 distribution appears to provide a reasonable fit for durations varying from 5 minutes to 6 hours, but is not clearly superior to another two-parameter distribution, the lognormal.

The fitting technique adopted by AES, known as modified moments or regression, was also assessed by comparing it with three other fitting techniques: moments, maximum likelihood and adjusted maximum likelihood as suggested by Kimball. This comparison was carried out using Monte Carlo simulation techniques over the parameter space deemed to be representative of short duration rainfall data for Canada. It was found that, in terms of estimating quantiles such as x_{10} and x_{100}, the modified moments technique was the poorest with regard to both bias and efficiency. In general, the maximum likelihood estimates were the most efficient and were relatively unbiased.

H 62

TIME DISTRIBUTION OF SHORT DURATION STORM RAINFALL IN CANADA

HOGG, W.D. (Hydrometeorology Division, Atmospheric Environment Service, 4905 Dufferin Street, Downsview, Ontario, M3H 5T4

The paper examines the time distribution of actual one and twelve hour rain events at 35 locations across Canada. The rainfall events are selected according to predetermined intensity criteria. Mass curves with various probabilities are presented for specific locations and for regional groupings. Antecedent rainfall for the five days prior to the event, is also discussed.

H 63

EXTREME VALUE ESTIMATES OF SNOWMELT

LOUIE, P.Y.T.
HOGG, W.D.
(Hydrometeorology Division, Atmospheric Environment Service, 4905 Dufferin Street, Downsview, Ontario, M3H 5T4

Some urban design problems require extreme value estimates of rainfall over several days duration. In the Canadian climate, snowmelt events lasting several days may also provide significant volumes of water which must be considered in these design problems. This paper presents extreme value estimates for snowmelt events of one to ten days duration for several Canadian locations. The snowmelt values are based on point estimates derived from simple models using standard climatological data.

H 64

KINEMATIC DESIGN STORMS FOR URBAN HYDROLOGY

William James (Civil Engineering Department, McMaster University, Hamilton, Ontario, Canada, L8S 4L7)
John J. Drake (Geography Department, McMaster University, Hamilton, Ontario, Canada L8S 4L7)

The paper explores the use of a numerical storm model as a pre-processor for a detailed urban runoff model. The proposed storm model generates hyetographs for each subcatchment, thus simulating the spatial and temporal growth and decay of a system of storm cells as they track across the urban catchment system.

Traditionally, design storms are developed from statistical analysis of rainfall records; the methodology was designed for use with flood predictions based on the rational formula. This synthetic temporal distribution is typically applied uniformly across the catchment. The resultant rain distributions are unlike observed rain storms.

Large cells of uniform rainfall intensity are rare even in prolonged frontal events. Rain cells tend to be elliptical, aligned subparallel to the front and moving sub-parallel to it. Rainfall is typically most intense near the leading edge of the cell. Convective cells tend to be circular with a circular rainfall intensity pattern. Statistics of the size and distribution of rain cells can be obtained most readily from weather radar studies.

AGU Symposium on Urban Hydrometeorology & Canadian Hydrology Symposium 80 Hydrology of Developed Areas

Harbour B
Tuesday A.M.
William Pugsley (Atmosphere Environment Service), and *Harry Wenzel* (Univ. of Illinois), Presiding

H 65 INVITED PAPER

REAL TIME ESTIMATION OF MEAN AND COVARIANCE STRUCTURE OF RAINFALL

Edward R. Johnson (Department of Civil Engineering, Georgia Institute of Technology, Atlanta, Georgia 30332)
Rafael L. Bras (Department of Civil Engineering, Massachusetts Institute of Technology, Cambridge, Massachusetts 02139)

Short-term rainfall prediction in time and space requires parameter estimation in real time. Several methods for estimating the non-stationary mean, the non-stationary variance, the residual covariance, and the storm velocity of a rainfall event using raingage data alone are discussed. Performance of suggested techniques are illustrated with examples. Alternate methods which may be more appropriate when radar data is available are proposed.

H 66

HYDRAULIC LABORATORY AND FIELD INVESTIGATIONS FOR INLET CONTROLS

R. Townsend, (Dept. of Civil Engineering, University of Ottawa, Ottawa, Ontario K1N 9B4)
P. Wisner, D. Moss, (Dept. of Civil Engineering University of Ottawa, Ontario, Ontario K1N 9B4)

The first part of this paper presents various appreciations of inlet controls for separated and combined sewers. The second part presents a series of tests conducted in the hydraulic laboratory of the University of Ottawa on an experimental facility representing at the scale 1/1 a street section an inlet. Hydraulic performance and observations on clogging led to practical recommendations for a large development in the Township of Vaughan, Ont. Field observations were also conducted and are briefly discussed.

H 67 INVITED PAPER

INVESTIGATION OF SOIL CONSERVATION SERVICE URBAN HYDROLOGY TECHNIQUES

Duke G. Altman (Espey, Huston & Assoc., Inc., P.O. Box 519, Austin, TX 78767)
Dr. W. H. Espey, Jr., (Espey, Huston & Assoc., Inc., P.O. Box 519, Austin, TX 78767).
Arlen D. Feldman (U.S. Army Corps of Engineers, HEC, 609 2D Street, Davis, CA 95616).
(Sponsor: Leo R. Beard)

The ability of certain SCS hydrologic techniques in predicting the effects of urbanization on flood peak discharges and frequency relationships for sets of urban and undeveloped watersheds in the Austin and Dallas, Texas regions was studied. Comparisons are made between calculated versus optimized runoff curve numbers and lag times as well as synthetic (HEC-1 and design storms) and annual series frequency curves for the four watersheds. The SCS techniques are reviewed in consideration of the findings. The general nature of the SCS techniques make their use very attractive as a universal method, especially in areas with little or no rainfall/runoff data. This paper presents some of the positive aspects as well as limitations of the techniques.

In general, the SCS methods produced low estimates of peak discharge, especially in urban areas. Reasons for the low peak discharge estimates are presented. The capability of SCS hydrologic techniques in predicting the effects of urbanization on flood discharges is evaluated.

H 68

URBANIZATION IMPACTS ON PENNSYLVANIA FLOOD PEAKS

David F. Kibler (Department of Civil Engineering, The Pennsylvania State University, University Park, PA. 16802)
Robert P. Craig (U.S. Army Engineers School, Fort Belvoir, VA.)
Gert Aron (Department of Civil Engineering, The Pennsylvania State University, University Park, PA. 16802)

The impact of man-made change on the hydrology of developing watersheds is frequently measured in terms of the ratio: flood peak after development to flood peak before development over a range of return periods. However, the analysis of urbanization effects on flood frequency presents a vexing problem because of a general lack of flood data in urban areas and also because of non-stationarity in the development process. Clearly, the flood peak ratio depends on the impervious fraction and percent of basin sewered and these factors have been taken into account in recent urban flood peak models. In general, these models are developed either by: (1) split-sample analysis of available annual flood data; or (2) by computer simulation using mathematical watershed models capable of representing man-made changes. The present paper discusses the results of work in-progress to characterize the impact of urbanization on small developing watersheds in Pennsylvania.

H 69

APPLICATION OF HYDROLOGICAL MODELS FOR FORECASTING RISING WATERS

GIGNAC, Claude
ROUSSELLE, Jean (respondent)
EL-JABI, Nassir
(Ecole Polytechnique de Montreal
C.P. 6079, Succursale A, Montreal (Quebec)
H3C 3A7)

Within the framework of a study of a system to announce rising waters, short-term hydrological forecasting is an essential and important stage. This communication presents two hydrological models which have been applied to respond to this objective. It concerns the model used by l'Hydro-Quebec for calculating natural deposits and the WRB (Water Resources Branch) model of Environment Canada. These two models are easy to use and are able to furnish results that are as satisfying as those from certain more complex models. The authors have tried to verify the accuracy of these models in reproducing the actual traits of the output. They were calibrated and verified on the basin of the Eton River, an area of 642 km^2, which is situated in southern Quebec. A few hydrograms are presented and the results show that these models can simulate the outputs in an acceptable manner at the time of forecasting short-term water risings.

H 70

TECHNICO-ECONOMIC SYSTEMATIZATION OF FLOOD PLAINS

EL-JABI, Nassir
ROUSSELLE, Jean (respondent)
Gignac, Claude
(Ecole Polytechnique de Montreal
C.P. 6079, Succursale A, Montreal (Quebec)
H3C 3A7)

The planning of water resources as well as the management of the banks imply that studies that are technical as well as economic and social be undertaken.

In the present study the interest will lie in the administration and the rational planning of flood plains where they will be considered an integral system formed of hydrological, hydrometrical, physical, and economic components.

The approach used is that of digital simulation, which consists of considering the process of rising water as well as its impact on flood plains as a complex system which permits estimation of the hydrological characteristics (height of submersion, period of return) for each economic unity of the different sectors of activities (residential, agricultural, industrial, commercial) in the flood plains. This consideration permits establishing functions of "flood-damage" transfer which can be regionalized in time and in space.

H 71 INVITED PAPER

INFLUENCE OF DEVELOPMENT ON THE HYDROLOGICAL CYCLE

Neil S. Grigg
(Assistant Secretary for Natural Resources, NC Department of Natural Resources & Community Development, and Director, UNC Water Resources Research Institute, on leave).

The hydrological cycle is a marvelous engine for collecting, transporting and cleaning water. Development has always followed the availability of water. Modern urban, industrial and agricultural developments have adverse effects on the water cycle, however, and solving the resulting problems constitutes the most serious problem in water management today. Urban impacts on the water cycle are perhaps the most severe. Others include: agriculture, mining, silviculture and construction. The final result of these activities is an environmental impact, sometimes acceptable, sometimes destructive. but not always anticipated. The span of concern for hydrology must include the influence of man on the water cycle. Using the results of hydrological studies of the last twenty years current awareness of the impacts of development is assessed. Included are research results, findings from nonpoint pollution studies, modeling predictions and meteorological implications. A linkage between urban stormwater management and water management in general is established through the common environmental preservation objective. Methods for prediction are reviewed and research needs are discussed. Needs of policy-makers at the three levels of government are compared to the supply of technology made available through hydrological research. Suggestions are made for researchers to relate their work closer to the practical technology needs of government and business.

H 72

URBANIZATION EFFECTS ON STREAMFLOW ON THE SPEEDVALE WATERSHED, GUELPH

H.R. Whiteley, (School of Engineering, Univ. of Guelph, Guelph, Ontario. N1G 2W1)
W.T. Dickinson, R.W. Irwin (School of Engrg., Univ. of Guelph); M.H. Quast (Env. Canada).

Outflow rates from the 2 Km^2 Speedvale watershed on the northwest corner of Guelph changed significantly when the land use on the watershed changed from rural to urban. Data from eight years prior to urbanization and four years after construction of commercial/industrial buildings have been analyzed.

The frequency of flow peaks, especially in the months May through October, have increased dramatically following urbanization. Time to peak has decreased from about 6 hours to less than one hour. The proportion of input appearing as stormflow has increased markedly. During extended dry periods outflow rates have increased since outflow is now perennial while periods of zero streamflow were common prior to urbanization.

H 73

OVERCONTROL OF URBAN RUNOFF: DISCUSSION OF SEVERAL CASE STUDIES

P. Wisner. (Dept. of Civil Engineering, University of Ottawa, Ottawa, Ontario K1N 9B4)

The first part of the paper presents a critical review of the "zero runoff increase" policy used by various regulatory agencies in Canada and the U.S. Requirements for flexibility are illustrated by examples taken from recent projects.

The second part introduces the principle of "overcontrol". Reduction of postdevelopment flows to less than predevelopment flows maybe achieved in order to reduce existing flooding in the major drainage system of downstream areas.

The third part presents examples of application of this principle in several canadian projects and discusses the economics and other implementation aspects.

AGU Symposium on Urban Hydrometeorology & Canadian Hydrology Symposium 80 Hydrology of Developed Areas
Harbour B
Tuesday P.M.
J. W. Delleur (Purdue Univ.), and *Raymond Perrier* (Ministry of Environment), Presiding

H 74

DETECTING HYDROLOGIC CHANGES - A CASE STUDY

W.T. Dickinson (School of Engineering, University of Guelph, Guelph, Ontario, N1G 2W1)
T.C. Sharma.

In response to current interest and concern regarding the possibility and extent of changes in the water balance in developed areas, a strategy has been developed for detecting hydrologic change(s). This strategy has been implemented in a case study of the Grand River Watershed in southern Ontario.

The variables selected for consideration include annual precipitation, winter precipitation, annual runoff, and annual peak mean daily discharge. The methodology involves a rational division of the data set into two or more time sequences, and the determination and comparison of corresponding statistical parameters reflecting mean, variance, autocovariance, skewness, and extremal properties.

Analysis of data for the Grand River has revealed no hydrologic changes in the selected precipitation variables i.e. the sequences can be considered to be stationary random processes with constant means and variances. However, the mean annual runoff volume has increased approximately 18 percent over the period of record, and probability of flooding at Galt has more than doubled since 1942. Suggested causes of these changes are offerred but not confirmed.

H 75

EVALUATION OF URBAN DEVELOPMENT IMPACT ON STORM RUNOFF BY DIGITAL COMPUTER

Y.S. Fok (Dept. of Civil Engineering, University of Hawaii, Honolulu, Hawaii 96822)

E.T. Murabayashi (Water Resources Research Center, Univ. of Hawaii, Honolulu, Hi. 96822)

The impact of urban development on storm runoff has been evaluated by means of a modified ILLUDAS model. Using storm runoff data obtained from an experimental urban watershed model was calibrated for hydrograph simulation. Different land cover such as paved impervious land, supplemented paved land and grass land of an urban area was programmed as subroutines. The impact of these urban land covers on storm runoff was evaluated by changing those impervious land covers back into pervious covers to facilitate the pre-urbanization condition for a subsequent storm hydrograph simulation. Therefore, the before and after effect of urban development on storm hydrograph can be compared by modifying the land covers. With six storm events recorded, the evaluation shows the peak flow can be increased 3.77 times after urbanization. This magnitude of increased runoff is comparable to the 4.96 times reduction in infiltration rate found in the same experiment.

H 76

ESTIMATING RUNOFF POLLUTION FROM LARGE URBAN AREAS

Shaw L. Yu (Dept. of Civil Engineering, University of Virginia, Charlottesville, VA 22901)
William Whipple, Jr., and James Di Louie (Rutgers University, New Brunswick, NJ 08903)

Presented in this paper are results of several studies that examined the extent of runoff pollution from large urban areas, illustrated by the Delaware Estuary. Pollutants including BOD, NH_3-N, NO_3-N, PO_4-P, and suspended solids were measured during storm events for a number of watersheds in Trenton, N.J. and Philadelphia, Pa. Quantitative analyses were made on the basis of storm event loading determinations, related statistically to storm characteristics such as storm intensity and duration, and antecedent conditions, and to land use patterns. Considerable data were obtained and were compared with results obtained previously and extended to the urban areas adjacent to the Delaware Estuary. Comparisons were also made with estimates made by others for the National Commission on Water Quality, and for Section 208 Studies of the Delaware Estuary Region. Although urban runoff loads from cities adjoining the estuary are of considerable significance, they are far exceeded by loadings which presumably originate from combined sewers, industrial effluents, and areas upstream in tributary watersheds. For water quality management of large areas, neither a delivery ratio nor a source sampling approach is adequate, because all of the various sources of major pollution loadings are not evaluated by either. In this paper a sampling strategy to provide sufficient data for a more complete analysis is outlined.

Meteorology

Remote Sensing and Radiation

Bay
Thursday A.M.
J. Drummond (Univ. of Toronto), Presiding

M 1

MILLSTONE HILL RADAR OBSERVATIONS OF WINDS AND TURBULENCE

B.J. Watkins
R.H. Wand (all at: Northeast Radio Observatory Corporation, Haystack Observatory, Westford, Massachusetts 01886)

The Millstone Hill 440 MHz radar (Westford, Ma) has been upgraded for studies of atmospheric turbulence and winds. Scattering from turbulence has been observed from altitudes 1-24 km.

The antenna is a 150 foot diameter steerable dish, and we describe some initial results of experiments with the antenna pointed at low elevation angles (~15 degrees) gathering data from the upper troposphere and lower stratosphere (7-15 kms).

The objective of these experiments has been to investigate the occurrence of waves in both the radial wind component and the refractivity turbulence structure constant (C_N^2). Fluctuations and waves in both quantities are frequently observed. On one occasion, waves in C_N^2 (period 20 minutes) with up to an order of magnitude variation were observed at a height of 10 km. They were restricted to a height interval of about 1 km located at and below a level of velocity shear, and begun at the time of shear formation.

M 2

A PHYSICAL MODEL TO ESTIMATE DAILY INSOLATION FROM VISIBLE SATELLITE MEASUREMENTS

G. Diak (Space Science and Engineering Center, 1225 W. Dayton Street, Madison, WI 53706)
C. Gautier, S. Massé

We present a model designed to estimate the incident solar radiation at the surface from GOES Satellite brightness measurements in clear and cloudy conditions. In this simple physical model, water vapor absorption and Rayleigh Scattering are introduced by means of their climatological effects on shortwave radiation in Southern Canada, but the main emphasis is on cloud effects. Cloud albedo and absorption are derived from brightness measurements on the assumption that they both are linearly related to the brightness. This simple treatment however, applied to individual picture elements represents quite accurately the bulk effect of clouds, as illustrated by our results. Comparisons with daily insolation measurements from three pyranometers located in Toronto, Montreal and Ottawa in Spring and Summer 1978 showed that the satellite estimates were, on the average, within 9% of the ground measurements for a large variety of cloud conditions. The hourly variations measured on the ground. This study has shown that a simple model is sufficient for the determination of the incident solar radiation when the high spatial and temporal coverage of a geostationary satellite is used.

M 3

DAILY INSOLATION CLIMATOLOGY OF CANADA FROM GOES MEASUREMENTS

S. Massé (Space Science and Engineering Center, 1225 W. Dayton Street, Madison, WI 53706)
C. Gautier, G. Diak, M. Valin

A physical model will be presented to estimate the incident solar radiation at the surface (insolation) from GOES Satellite brightness measurements in clear and cloudy conditions. This model uses full resolution, hourly visible images. Hourly and daily insolation have been estimated for Toronto, Ottawa and Montreal and compared with ground pyranometer measurements. The satellite estimates and the ground pyranometer measurements compare favorably - the estimates falling within less than 10% of the pyranometer measurements.

This model is now being applied to hourly GOES data for an equivalent of four months' worth of data (120 days) spread over four seasons. The GOES data set has been randomly selected on grounds of data quality (recording and navigation). The results of this application will be presented as weekly, monthly and seasonal insolation maps for Southern Ontario and Quebec.

M 4

MONITORING URBAN HEAT ISLANDS USING SATELLITE DATA

Michael Matson (NOAA/National Environmental Satellite Service, Washington, D.C. 20233)
(Sponsor: Donald R. Wiesnet)

High-resolution satellite thermal infrared sensors now provide a capability whereby the urban heat island phenomenon can be routinely monitored and quantified. Variation of urban heat islands diurnally, seasonally and during different meteorological conditions can also be ascertained using the satellite data. Examples of satellite thermal information for several North American metropolitan areas are presented using the 1 km resolution NOAA-5 and NOAA-6 data, the 8 km GOES data, and the 0.5 km HCMM data. Such thermal information may prove useful to modellers and meteorologists concerned with urban boundary layer climates.

M 5

SUMMER PRECIPITATION FREQUENCY OF THE NORTH CENTRAL U.S. FROM SATELLITE MICROWAVE OBSERVATIONS

Philip A. Durkee (Department of Atmospheric Science, Colorado State University, Fort Collins, Colorado 80523)
Thomas H. Vonder Haar (Department of Atmospheric Science, Colorado State University, Fort Collins, Colorado 80523)

The Nimbus-6 electrically scanning microwave radiometer (ESMR-6) is used to observe raining areas over the north central U.S. from June 11 through August 31 of 1976. A technique is developed whereby the frequency distribution of microwave brightness temperatures over the area is analyzed to determine a threshold temperature below which precipitation is assumed. Local noon and midnight observations are examined yielding information about the diurnal characteristics of summer precipitation in this area. Finally, precipitation frequency analyses from the ESMR-6 observations are compared to hourly raingage observations.

M 6

A RADAR TO SATELLITE DATA TRANSFER FUNCTION FOR INFERRING PRECIPITATION RATES OVER THE EASTERN PACIFIC

John Spagnol (Pacific Weather Centre, A.E.S. Vancouver, Canada)

One of the most difficult analyses the operational forecaster at the Pacific Weather Centre has to perform is the delineation of the precipitation areas over the Pacific. A detailed quantitative assessment of precipitation intensities has virtually been impossible using the conventional data set.

The recent installation of the SCEPTRE radar at Abbotsford has helped, but only marginally. The range of the radar extends

to about 100 km west of Vancouver Island. This range gives only two or three hours warning before the precipitation area moves overland. At present, the operational forecaster requires this information two days upstream from the British Columbia regions.

The GOES satellite data set effectively covers the Pacific two or more days upstream from the B.C. coast. Ingraham (1979) developed a method of nowcasting precipitation rates from satellite imagery. A similar approach can be used to develop a simple transfer function from the radar to the satellite data. Using this function and the satellite data set, the radar precipitation data may be extrapolated outward into the Pacific.

This paper describes the transfer function and the possible operational system that could be developed at the Pacific Weather Centre.

M 7

HIGH SPECTRAL RESOLUTION CALCULATIONS OF INFRARED CLOUD REFLECTIVITY AND TRANSMISSION

Alan C. Stanton, Lawrence S. Bernstein, and David C. Robertson
(Aerodyne Research, Inc., Bedford, MA 01730)
(Sponsor: Fritz Bien)

The reflected and transmitted flux from atmospheric water and ice clouds in near-infrared molecular absorption bands is studied using a Monte Carlo radiative transfer model. In many clouds the molecular absorption optical depth near line center dominates scattering and absorption by particles, and the reflected and transmitted flux thus exhibit high-resolution spectral structure ($\Delta\omega \sim .01$ cm^{-1}). Accurate monochromatic calculations of the type reported here are required to characterize cloud signals for high resolution atmospheric studies. These calculations also provide a useful check on approximate methods which are used in radiation budget models to describe molecular absorption in clouds.

M 8

REMOTE SENSING OF CLOUD PARAMETERS - RESULTS FROM JUNE 1979 OBSERVATIONS

Robert J. Curran (all at: Laboratory for Atmospheric Sciences, Goddard Space Flight Center, Greenbelt, MD 20771)
Michael D. King
Man-Li C. Wu

A program is being developed to observe cloud physical and radiation properties in an effort to aid in understanding the effects of clouds on the earth's climate. As part of this program the authors, are developing remote sensing techniques to be applied to remote observations of clouds made from a high altitude aircraft. The instruments involved in making the remote observations include a seven channel multi-spectral radiometer and an airborne lidar. The radiometer has channels in the near infrared and thermal infrared, chosen to provide observations necessary for inferring several cloud physical parameters.

The instrumentation described was flown on the NASA WB-57 in May and June 1979, as part of the Severe Environmental Storms and Mesoscale Experiment in the midwestern U.S. Analysis of the data acquired from these flights has been focused on verifying cloud altimetry utilizing the O_2 A-band at 0.76 μm and cloud thermodynamic phase. The altitude verification is made using lidar determination of cloud top height as compared to the results obtained from passive radiometry. Remote sensing of cloud thermodynamic phase has used observations made at 1.61 μm. The theoretical development of the 1.61 μm reflectances have been reported earlier. Recent observations at 2.12 μm are presently being used to augment the interpretation of the 1.61 μm determinations.

M 9

SIMULATION DE L'ENERGIE SOLAIRE AU SOL

Gaston Paulin, Service de la Météorologie, ministère de l'Environnement, 194, avenue Saint-Sacrement, Québec, P.Q., Canada, G1N 4J5.

Le régime journalier du rayonnement solaire global au sol a été reconstitué aux six stations du réseau radiométrique de base canadien situées au Québec à l'aide d'un modèle numérique simulant le transfert de l'énergie solaire à travers l'atmosphère. Les données d'humidité atmosphérique, de trouble atmosphérique et d'albédo au sol ont été interpolées dans le temps et l'espace à partir de la climatologie mensuelle connue de ces champs. La nébulosité a été tirée des séquences horaires des durées d'ensoleillement observées à ces mêmes stations et échelonnées sur une même période de 974 jours. On a estimé les limites de précision du modèle en déterminant l'erreur quadratique moyenne entre la valeur calculée et mesurée pour 1, 2, 3, ... et 20 jours consécutifs. On a ainsi trouvé que l'erreur quadratique moyenne diminue rapidement pour les regroupements de 1 à 10 jours et se stabilise pour les périodes plus longues. L'amplitude de l'erreur quadratique moyenne varie saisonnièrement et latitudinalement étant en général plus faible en été et au sud. La variabilité des valeurs journalières simulées n'est que légèrement supérieure à celle des données journalières mesurées. Il est démontré finalement que l'utilisation journalière des résultats du modèle est préférable à l'utilisation de la climatologie du régime solaire.

M 10

INSTRUMENTAL DETERMINATION AND MODEL ESTIMATION OF LONGWAVE IRRADIANCE AT THE GROUND

William J. Blackburn (Department of Geography, McMaster University, Hamilton, Ontario, Canada)
John A. Davies (Department of Geography, McMaster University, Hamilton, Ontario, Canada)

Incoming longwave irradiance is commonly determined by direct measurement with an Eppley pyrgeometer or as a residual from pyrradiometer measurements of incoming total (solar and longwave irradiance and pyranometer measurements of solar irradiance. Two models of the Eppley pyrgeometer have been manufactured. The first used a KRS-5 dome which heats by absorption of solar radiation thus becoming an unwanted source of longwave radiation for the thermopile. For this reason, uncertainties in measured irradiance have meant that the data base against which models could be tested was limited. A modified version of the Eppley pyrgeometer designed to eliminate the solar heating problem is fitted with a silicon dome. In this study, all three instrumental determinations were used. Data suggest, although we cannot unreservedly confirm, that the most reasonable measurements of longwave irradiance were obtained using the silicon-domed pyrgeometer. Measurements made at Hamilton, Ontario under cloudless or near cloudless skies have also been compared with model estimates.

M 11

COLOR CHANGES RELATED TO SOIL EROSION IN SOUTHWEST KANSAS AS DETECTED BY LAMDSAT

P. Jacobberger (McDonnell Center for the Space Sciences, Department of Earth and Planetary Sciences, Washington University, St. Louis, MO 63130)

Over 8 million acres of crop and range land in Kansas and surrounding states were damaged by wind erosion during the winter of 1975-76. In the vicinity of Liberal, Kansas, visible soil removal amounted to 3-6 cm; this is equivalent to a topsoil loss of 167-333 tons/acre /yr. Three Landsat scenes, centered over the Liberal area and acquired 13Mar76, 01Apr76, and 06May76 were digitally ratioed and contrast-enhanced to accentuate color and albedo differences. Striking color and albedo differences do exist among the three frames. Boundaries between major soil units (chestnut soils, reddish prairie soils, etc.) can be readily discerned. Analysis of image data for a test area (chosen for its visible qualitative color and albedo changes) reveals a marked reddening of the surface from 13Mar to 01Apr. Similar analysis of a control area shows little change over the same time frame. The two areas are similar in size and are underlain by the same soil type. The reddening of the test area is consistent with wind stripping to reveal subsoil layers; this hypothesis is also consistent with Soil Conservation Service records which show several dust storms occurring in the area between 01Mar76 and 25Mar76, and no rain until 15Apr76. According to these same records, over 25,000 acres of land in a single county were in fact wind-damaged during March 1976.

Atmospheric Chemistry

Queen's Quay
Friday P.M.
Julio V. Iribarne (Univ. of Toronto) and *T. E. Graedel* (Bell Labs), Presiding

M 12

GRAPHICAL TECHNIQUES FOR THE PRESENTATION OF RESULTS FROM ATMOSPHERIC CHEMICAL MODELS

T.E. Graedel (Bell Laboratories, Murray Hill, NJ 07974)

The results of atmospheric chemical model computations are voluminous and complex. The model developer must, in practice, be as ingenious in analyzing and presenting the results as he is in the model formulation if maximum information is to be extracted and communicated. Graphical presentations of results are often significant aids in these processes. Using calculations of nitric acid and ozone concentrations in an urban region as functions of time and two spatial dimensions, a variety of graphical displays have been devised and evaluated. These displays include plots of concentration and rate variation with time, superposition of concentration gradients, model validation by graphical comparison with robust estimates of data, and plots of concentration and kinetic rate parameters as functions of both space and time. The results suggest that three-dimensional plots of source and sink rates as well as of concentrations in parameter-distance-time space are of particular utility.

M 13

THE SEASONAL VARIABILITY OF THE VERTICAL DISTRIBUTION OF ATMOSPHERIC AMMONIA

J. M. Hoell (Langley Research Center, Hampton, Va. 23665) C. N. Harward (Old Dominion Univ., Norfolk, Va. 23508) W. A. McClenny (Environmental Protection Agency, Research Triangle Park, N. C. 27711)
(Sponsor: Joel S. Levine)

Remote measurements of the vertical distribution of ammonia have been obtained at Langley Research Center, Hampton, Va. over a 1-year time period beginning in the latter part of March 1979. These vertical profiles were inferred from high resolution solar transmittance data on the 927.32323 cm^{-1} ammonia absorption feature obtained using an infrared heterodyne radiometer (IHR). Ground level in situ measurements, initiated in June 1979, have also been obtained periodically in order to collaborate and supplement the profile data. The in situ data were obtained using a technique to preconcentrate ammonia via selective adsorption on teflon beads with subsequent thermal desorption into an opto-acoustic cell for quantitative analysis.

Results from the remote measurements indicate enhanced tropospheric levels of ammonia during the spring time period which decrease to relatively stable levels during the summer months with a further decrease during the winter months. Spring profiles exhibited ground level values around 10 ppb decreasing to about 1 ppb at 10 Km. The summer profiles exhibited ground level concentration of approximately 1 ppb decreasing to the sub-ppb levels at 10 Km. The in situ measurements also indicated summer ground level ammonia concentrations in the 1 to 2 ppb range. From the in situ data, ground level winter concentrations were found to be in the .1 to .5 ppb range. These low levels coupled to the decrease in ammonia with altitude were below the sensitivity of the IHR. The enhance spring levels are thought to be results from the volatilization of ammonium nitrate fertilizer applied to agricultural fields in early spring.

M 14

THE AMMONIA BUDGET OF THE ATMOSPHERE/BIOSPHERE SYSTEM

Joel S. Levine (NASA Langley Research Center, Hampton, Va. 23665)
Tommy R. Augustsson (Old Dominion University, Norfolk, Va. 23508)
James M. Hoell (NASA Langley Research Center, Hampton, Va. 23665)

A one dimensional tropospheric photochemical model has been used to study the processes, i.e., homogeneous and heterogeneous loss and vertical transport, that control the vertical distribution of tropospheric ammonia, as measured by the Infrared Heterodyne Radiometer (IHR). The homogeneous loss of NH_3 was found to be controlled by its reaction with OH (the loss of NH_3 due to photodissociation ($\lambda \leq 230$ nm) important in the stratosphere is negligible in the troposphere). The characteristic time for homogeneous loss due to OH varies from about 40 days at the surface to about 180 days at 10 km. The best fit characteristic time for heterogeneous loss is in excess of 10 days, and the characteristic vertical transport time is about 35 days.

Seasonal IHR and in situ NH_3 measurement suggest that the application of ammonium nitrate agricultural fertilizer may represent the largest anthropogenic perturbation to atmospheric composition yet detected--increasing surface NH_3 levels more than an order of magnitude, at least on a regional scale. Ammonium nitrate fertilizer appears to be a significant source of exchangeable NH_4^+ in the biosphere, along with the bacterial decomposition of the dead biomass, and to a lesser degree, the precipitation and dry deposition of atmospheric NH_3. Measurements also suggest that the volatilization of ammonium nitrate fertilizer is very rapid--less than a month after the application of the fertilizer.

M 15

THE SULFUR BUDGET OF THE TROPOSPHERE

Tommy R. Augustsson (Old Dominion University, Norfolk, VA 23508)
Joel S. Levine (NASA Langley Research Center, Hampton, VA 23665)
Surendra N. Tiwari (Old Dominion University, Norfolk, VA 23508)

Several anthropogenic activities appear to be major and ever-increasing sources of sulfur to the global troposphere. Yet, of all global tropospheric species budgets, the sulfur budget is perhaps the least understood and least studied. The vertical distribution of the sulfur species has been investigated using a one-dimensional tropospheric model, that includes the photochemistry and chemistry of the oxygen, nitrogen, carbon, and hydrogen species. The sensitivity of calculated profiles of tropospheric SO_2, COS, H_2S, CS_2, as well as the short-lived intermediate species to various poorly known and uncertain model input parameters will be discussed. Some of the poorly known model input parameters include the reaction path and reaction rate of several key sulfur species reactions, as well as the roles of heterogeneous loss and dry deposition in controlling the sulfur species budget. The sensitivity of calculated sulfur species to perturbations in other tropospheric species, such as OH, will be discussed. Calculated sulfur species profiles will be compared with the very limited set of measurements of tropospheric sulfur species.

M 16

A COMPUTED SULPHUR BUDGET FOR EASTERN CANADA

M.P. Olson (Atmospheric Environment Service, Toronto, Canada)
E.C. Voldner, K.K. Oikawa

The Atmospheric Environment Service Long-Range Transport of Air Pollutants trajectory and concentration models have been used to compute the concentration, deposition and transboundary fluxes of sulphur in the Eastern Canadian region for the year 1978.

Back trajectories have been computed from selected points in the region and concentrations determined at the points by using a North American SO_2 annual emissions inventory and parameterizing the physical and chemical processes. Sulphur budgets were computed from the transboundary fluxes and sulphur depositions.

The preliminary results indicate that 15% of the U.S. sulphur emissions enter E. Canada primarily across the lower Great Lakes. About 60% of the transboundary sulphur is deposited in E. Canada and accounts for one-half of the deposition in the region. Emissions within the region contribute the other half of the total Eastern Canadian sulphur deposition.

M 17

MEASUREMENTS OF ATMOSPHERIC CS_2 AND THEIR IMPACT ON THE RELATIVE IMPORTANCE OF CS_2 IN THE GLOBAL SULFUR CYCLE

P. J. Maroulis
A. R. Bandy (Chemistry Department, Drexel University, Philadelphia, Pa. 19104)

Our recent ground level measurements of tropospheric CS_2 made at Philadelphia, Pa. and Wallops Island, Va. indicate that the CS_2 concentration from background areas is approximately 30 pptv and that CS_2 levels in anthropogenically influenced regions are five to ten times higher. Using 30 pptv as the background level of CS_2 and published rate data for the reaction of OH with CS_2, OCS and SO_2 we estimate that CS_2 can account for a maximum of 20 percent of atmospheric OCS and a maximum of 33 percent of background SO_2.

M 18

THE PHOTOCHEMICAL BUDGET OF TROPOSPHERIC OZONE

W.L. Chameides, A. Tann, P. Walker (Dept. of Physics, Univ. of Florida, Gainesville, Florida 32611)

The importance of photochemistry in the tropospheric ozone budget and whether photochemistry supplies a net source or sink of tropospheric ozone are presently questions of intense scientific debate. In this work we present results obtained from a time-dependent photochemical box model and a global two-dimensional diagnostic model which have been used to study ozone photochemistry. The results indicate that, given the low NO_x abundances recently observed, photochemical destruction dominates over production of ozone over most of the earth's surface, although both processes appear to be globally significant when compared to the stratospheric source.

M 19

A STRATOSPHERIC SOURCE FOR REACTIVE NITROGEN IN THE UNPOLLUTED TROPOSPHERE

H. Levy II
Geophysical Fluid Dynamics Laboratory/NOAA
Post Office Box 308
Princeton, NJ 08540
J. D. Mahlman
W. J. Moxim
(Sponsor: Syukuro Manabe)

Recent measurements of very low NO and HNO_3 mixing ratios in the atmospheric boundary layer over the tropical Pacific suggest that downward transport of reactive nitrogen (NO_y) from the stratosphere, though a small source when compared to combustion, may be important in the unpolluted troposphere. A GFDL 3-D generalized tracer field has been scaled so that its downward flux into the troposphere is balanced by the calculated stratospheric production of NO_y. While the model results show stratospheric NO_y to be a significant source for the remote troposphere, they do not rule out contributions from either the long-range transport of combustion NO_y or the insitu production by lightning. The model NO_y climatology in the unpolluted troposphere shows a strong interhemispheric asymmetry due to greater downward NO_y flux in the northern hemisphere and a steep drop off to a minimum in the tropics resulting from a combination of model features (tropical rainbelt, ITCZ, and Indian monsoon) which have been well documented in the real atmosphere.

M 20

REASSESSING THE IMPORTANCE OF WETLANDS AS A GLOBAL SOURCE OF TROPOSPHERIC METHANE

Robert C. Harriss (NASA Langley Research Center, Hampton, Va. 23665)
Daniel I. Sebacher (NASA Langley Research Center, Hampton, Va. 23665)
(Sponsor: Joel S. Levine)

A continuous sampling Gas-Filter Correlation (GFC) system has been developed for measuring methane emissions from soil and water surfaces to the atmosphere. The system has high sensivity (0.01 ppm) and fast response (1 sec.), enabling rapid in situ quantification of emissions using both closed and open chamber techniques. Natural methane emissions have been studied in several habitats and over a wide range of environmental conditions in the Great Dismal Swamp, Virginia. Primary factors contributing to variations in methane emission rates were soil temperature and episodic soil disturbance.

Our results suggest that a reassessment of the importance of wetlands as a global source of tropospheric methane is necessary. Previous estimates of annual methane emission rates for natural waterlogged organic soils may be 1-3 orders of magnitude too high.

M 21

CONTINUOUS MONITORING OF ULTRA-TRACE CONSTITUENTS IN AIR NEAR GROUND LEVEL USING APCI MASS SPECTROMETRY

J.A. Buckley, N.M. Reid, D.A. Lane (SCIEX INC., 55 Glencameron Road, Thornhill, Ontario, Canada)
J.B. French (University of Toronto, Institute for Aerospace Studies, Toronto, Ontario, Canada)

Methodology and results are given for continuous monitoring of trace constituents in urban or rural air using a mobile atmospheric pressure chemical ionization mass spectrometer system. Traces common to urban air are shown in both positive and negative ion spectra, e.g. NH_3, SO_x, NO_x, alcohols, aromatic aldehydes, ketones, aromatic esters, phenols, substituted benzenes, halides such as Cl, HCl, HF, carboxylic acids. Comparisons of urban air from widely separated geographic sites are given. Detectability limits for specific compounds lie in the range .001 to 1000 ppb. Selective ionization by CI reagent gas addition is used, for example, to separate H_2SO_4 and SO_2 in the mass spectrum.

The methodology is applicable to continuous monitoring of diurnal, seasonal or geographic variations, assessment of polluted atmospheres, or to laboratory studies of atmospheric ion chemistry.

M 22

ION-INDUCED GAS-TO-PARTICLE REACTIONS

C.M. Banic (University of Toronto, Toronto, Ont. M5S 1A7)
G.L. Diamond
J.V.Iribarne

The influence of ions on homogeneous heteromolecular nucleation has been studied in several systems.

1. Nucleation of NH_4Cl from NH_3 + HCl occurs according to theory in the absence of ions or radicals. H_2O does not enter the embryo formation reaction, but acts as a catalyst. Introduction of ions or radicals to the reactants increases nucleation rates and reduces the thresholds.

In these cases the shape of the nucleation curves indicates a changed reaction mechanism. Negative ions are the most efficient at producing particles, and the particles so formed are charged.

2. Nucleation from SO_2 + H_2O occurs only in the presence of ions. Positive ions are slightly more efficient than negative; radicals do not have an effect. Nucleation rates increase with SO_2 concentration to a plateau and increase

strongly with H_2O concentration. The nucleation curves do not change with O_2 concentrations varying from a few ppm to 20%, indicating that oxygen does not enter the nucleation reaction. The mechanism of oxidation to H_2SO_4 is not yet understood. Ions are efficient even when introduced as stable "terminal ions" such as $SO_4^-(H_2O)_n$. The particles are uncharged and appear to acquire a stable equilibrium size.

3. Nucleation curves from $SO_2 + NH_3 + H_2O$ have also been determined for positive and negative ions and varying humidities.

Comparison of results 1. and 2. points to two entirely different types of ion action.

Ion clusters appearing with varying ageing times (10 microseconds and higher) in these systems are being studied by mass spectroscopy.

M 23

TIME TREND ANALYSIS OF TOTAL OZONE MEASUREMENTS

D. S. St. John (Petrochemicals Dept. E. I. du Pont de Nemours & Co., Wilmington, DE 19898)

(Sponsor: Adair C. Barlow)

Time trend analysis of monthly average total ozone measurements through 1978 show no depletion consistent with that hypothesized as due to chlorofluoromethanes (CFM's). The methodology and quality of the data are such that a depletion half as large as the 1.6% calculated by current chemical models would almost surely have been detected.

The 14 Dobson stations with records from 1958 through 1978 show (+0.06 ± 0.9)% (2σ). Nineteen other stations with shorter records show (-0.44 ± 1.7)%. The larger uncertainty shows that random fluctuations are more easily misinterpreted as trends in shorter data sets. These 2σ limits include all uncertainties uncorrelated from station-to-station.

The insensitivity of the results to details of the statistical method and the ability to detect a small trend had one been present are illustrated.

Either the calculated ozone depletion from CFM's is in error, or actual depletion has been cancelled by some other effect of similar magnitude but opposite sign.

M 24

THE TUNGUSKA METEOR FALL: EFFECTS ON OZONE AND ATMOSPHERIC OPACITY

R. C. Whitten
O. B. Toon
C. Park (All at NASA Ames Research Center, Moffett Field, CA 94035)
R. P. Turco (R & D Associates, Marina del Rey, CA 90291)

In June 1908, a huge meteor plunged Earthward over Siberia and exploded high in the troposphere. We estimate that the Tunguska meteor fall generated as much as 6×10^{35} NO molecules between 10 and 60 km, and may have released 5×10^{34} H_2O molecules. The stratospheric NO_x injection caused by the Tunguska meteor was at least ten times larger than that attributed to the 1961-62 U.S.-U.S.S.R. nuclear test series. Thus, the Tunguska event represents the largest impulsive NO_x perturbation of the stratosphere ever recorded by man.

We have utilized our one-dimensional atmospheric photochemical model to calculate the time-dependent O_3 and NO_2 variations likely to have accompanied the Tunguska fall. We compare predicted NO_2 opacity variations with atmospheric opacity changes measured in 1908. Other unusual atmospheric phenomena, such as the intense nightglow which persisted over Europe for several weeks following the event, are discussed in view of the massive photochemical disturbance. We also consider the possible weather consequences of large meteor events that might be inferred from the Tunguska fall.

M 25

STRATOSPHERIC HYDROXYL RADICAL CONCENTRATIONS: NEW LIMITATIONS SUGGESTED BY OBSERVATIONS OF STRATOSPHERIC SULFUR GASES AND SULFATE AEROSOLS

R. P. Turco (R & D Associates, Marina del Rey, CA 90291)
R. C. Whitten
O. B. Toon
E. C. Y. Inn (All at NASA Ames Research Center, Moffett Field, CA 94035)
P. Hamill (Systems and Applied Sciences Corp., Hampton, VA 23666)

We have analyzed recent measurements of stratospheric SO_2 and OCS abundances and deduced new limits for OH concentrations below 30 km. In our study, we utilized a detailed sulfate aerosol model to calculate the sensitivity of gaseous and particulate sulfur distributions to OH abundances, 'eddy' diffusion coefficients and several other key model parameters. We conclude that current model predictions of OH concentrations are overestimated by a factor of 3 or more below 30 km. We show that simulated HNO_3/NO_2 concentration ratios and ClO mixing ratios can be brought into reasonable agreement with observations when lower OH concentrations are adopted. Some recent indirect tropospheric OH measurements also suggest smaller OH abundances in the lower atmosphere. Lower OH may be partly explained by pressure, temperature and humidity sensitive HO_x reaction rate coefficients, which lead to more efficient recombination of HO_x radicals in the stratosphere. Recent laboratory kinetics studies by W.B. DeMore, B.A. Thrush and others support this hypothesis.

We have recomputed the ozone perturbations caused by SSTs, N_2O and CFMs with reduced OH concentrations. Considering a fleet of 500 advanced SSTs, we find a 3% ozone column decrease with lower OH, compared to a 3% increase predicted with a 'recommended' photochemical dataset. For a doubling of N_2O we calculate an 8% ozone reduction where previously we calculated a zero net change. For CFMs, the steady-state ozone depletion corresponding to 1975 fluorocarbon release rates is 11%, down from 16% predicted earlier.

M 26

STRATOSPHERIC MEASUREMENT OF HCl AND HF

H.L. BUIJS, (Bomem Inc., 910 Place Dufour, Vanier, P.Q. G1M 3B1, Canada)
D.J.W. KENDALL, G.L. VAIL and J.-N. BERUBE

A high-resolution interferometric spectrophotometer carried aloft during a recent balloon flight from Alamagordo, New Mexico has observed the solar infrared absorption spectrum in the wavelength regions where the fundamental vibration-rotation bands of HCl and HF are located (approximately 3000 cm^{-1} and 4000 cm^{-1} respectively). Reduction of the spectral data has permitted volume mixing ratio profiles of both species to be determined from 17.5 to 38 km. The results will be compared with other recent determinations.

M 27

REACTIVITY OF STRATOSPHERIC AEROSOLS IN LABORATORY ENVIRONMENTS

D. M. Hayes (LFE Corporation, Environmental Analysis Laboratories, Richmond, CA 94804)
Kenneth G. Snetsinger
Guy V. Ferry
Verne R. Oberbeck
Neil H. Farlow (All of NASA Ames Research Center, Moffett Field, CA 94035)

For the past 20 years investigators have identified crystals of $(NH_4)_2SO_4$ and $(NH_4)_2S_2O_8$ in stratospheric aerosols analyzed in the laboratory. A few researchers have suggested that if the aerosol is sulfuric acid, the droplets might be reacting with traces of ammonia in room air to form the sulfate crystals. Others, however, have discounted this as a minor effect. After extensive testing using a protective atmosphere of purified argon, we have discovered that sulfuric acid aerosols are extremely reactive to traces of ammonia in our environment.

Therefore, to determine if stratospheric aerosols might similarly react, we built a new airborne sampler and associated laboratory equipment that protects the particles with purified argon immediately after collection until final analysis. Using these elaborate procedures, we find that aerosols we collect from the stratosphere do not contain sulfate crystals. When we expose these samples for an hour or so in the laboratory air, however, the fluid droplets convert to $(NH_4)_2SO_4$ and $(NH_4)_2S_2O_8$. These findings cast doubt on the previous detection of crystalline sulfate in any unprotected sulfuric acid samples. We are continuing to collect stratospheric particles processed with argon to determine if the absence of sulfate crystals is typical for all seasons and locations.

M 28

THE METEORITIC COMPONENT OF STRATOSPHERIC AEROSOLS

P. Hamill (Systems and Applied Sciences Corp., Hampton, VA 23666)
R. P. Turco, (R & D Associates, Marina del Rey, CA 90291)
O. B. Toon
R. C. Whitten (both at NASA Ames Research Center, Moffett Field, CA 94035)

Meteoric dust and vapors contribute to the composition of stratospheric aerosols. Using a one-dimensional photochemical/microphysical model of atmospheric gases and particles up to 110 km, we have made detailed calculations of the composition of stratospheric aerosol particles in the size range from 0.001 μm to 3.0 μm. Meteoric 'smoke' particles dominate the aerosols smaller than 0.1 μm above 20 km, while micrometeorites are the predominant natural particles larger than 1 μm above the tropopause. Meteoric metals react with, and neutralize, sulfuric acid vapor, altering the H_2SO_4 height distribution. We discuss the effects of meteoric materials on aerosol properties and on H_2SO_4 concentrations. We present estimates of the particulate surface area, and the surface characteristics, available for heterogeneous reactions in the stratosphere. We compare model predictions with a variety of observational data.

Analysis and Weather Forecasting

Pier 2 & 3
Saturday A.M.
G. A. McPherson (Atmospheric Environment Service), Presiding

M 29

THE EDDY KINETIC ENERGY SPECTRUM IMPLICIT IN A STATISTICAL MODEL FOR GEOPOTENTIAL. IMPLICATIONS FOR WEATHER FORECASTING.

H.J. Thiebaux, Department of Mathematics, Dalhousie University, Halifax, N.S. B3H 4H8

Statistical models for the geopotential field which have been used to derive spatial lag-correlation functions (LCFs) for objective analysis have implications for the eddy kinetic energy spectrum which influence the distribution of energy in analysed fields. This paper establishes correspondences between the parameterization of LCFs and spectral properties of the geostrophic wind field, for spatially coherent statistical representations. The results are considered in light of recent studies indicating that general circulation models of the atmosphere suffer from systematic loss of kinetic energy which is most pronounced during the initialization process and the early stages of a forecast cycle. The similarity of the isobaric KE spectrum derived from a two-dimensional second-order autoregressive model for the height field to spectral estimates in current literature, as well as the close fit of the corresponding LCF to observed correlations, suggest that use of this statistical representation in the

objective analysis of data assimilation could retain important features of atmospheric energy distributions in initializations.

M 30

APPLICATION OF SEASAT WIND DATA FOR OPERATIONAL WEATHER FORECASTING

Appleby, W.A. (AES, Downsview, Ont., M3H 5T4)
Chu, L.
Haering, P.
Overland, J.
Peteherych, S.
Spagnol, J.
Woiceshyn, P.

(Sponsor: Clive Jarvis, CMOS)

An experiment was conducted to test the impact of Seasat scatterometer data on a surface pressure analysis. Six Seasat passes off the west coast of Canada and the U.S.A. - Sept. 1978 - were chosen for the experiment. Surface pressure analyses using Seasat wind data were compared with surface pressure analyses produced, using conventional data, at the time of the Seasat overpass. In both cases the analysis was done manually.

The addition of Seasat wind data resulted in significant changes in the surface analysis. Placement of important meteorological features such as lows, highs, troughs, ridges and fronts was improved. It allowed for the more accurate determination of pressure gradients which also permitted a finer resolution analysis (i.e., 2 m bar contours instead of 4 m bar). Colls were easily identified and often small scale eddies and circulations were revealed.

Even where there was little change in the surface analysis by the input of SASS data, the degree of certainty in the final analysis was increased. There appeared to be no time penalty in performing the analysis with Seasat wind data.

M 31

EXPERIMENTS IN REGIONAL OBJECTIVE ANALYSIS FOR OPERATIONAL USE

A. Maarouf and L. J. Wilson
Atmospheric Environment Service, Downsview, Ont.
(Sponsor: E.C. Jarvis)

An objective analysis technique using second-degree orthogonal polynomials in two or three dimensions is described. The principal advantages of the technique are its capability of operating without an initial guess field and the feasibility of implementing it on existing minicomputers in regional weather offices. Tests of the method indicated that the second-degree polynomial representation yielded acceptable objective analyses. A few analyses of derived meteorological parameters are presented to demonstrate the utility of the method for diagnosis of atmospheric conditions, especially those prior to severe storm occurrences.

M 32

RECENT WORK ON A REGIONAL GRID-POINT P.E. MODEL

David Davies (Atmospheric Environment Service, 2121 Trans-Canada, Dorval, Quebec H9P 1J3)

The time-dependent boundary conditions have been completely revised to eliminate boundary noise and pillow effects. In the new procedure, time-dependent values of height, normal wind component, vorticity, surface pressure and dew point depression are provided along the boundaries by the operational spectral model. Outflow is allowed for thickness, vorticity, dew point depression and surface pressure, but not for the normal wind component. Many of the previously existing problems arose from doing extrapolations of the wind fields outside the grid to evaluate the cross-boundary components of the horizontal advection terms in the momentum equation. The extrapolations are avoided in the new procedure by specifying a divergence value for use in the evaluation of these advection terms only. This specified divergence value is currently taken to be zero, but it may be preferable to add the divergence to the list of time-dependent quantities passed from the driving model.

A 5-level version of the model with the new boundary procedures has been integrated quasi-operationally to 24 hours with a 127 km grid over North America for about a year, and gives forecasts which are generally equal in quality to the spectral model at low levels in the centre of the grid. The 5-level grid-point model usually out-performs the spectral model on small low centres with a simple structure, but will give poorer forecasts when the wrong branching evolution is predicted in branch-point situations which arise in association with complex flow structures.

Some 10-level integrations have been carried out, and these give forecasts which are much better than their 5-level counterparts at high levels, but only slightly better at low levels.

M 33

R. Gabison, Author (MSRB, Atmospheric Environment Service, 4905 Dufferin St., Downsview, Ontario, Canada.)

B. DeLorenzis, Author, (MSRB, Atmospheric Environment Service, 4905 Dufferin St., Downsview, Ontario, Canada).

A MESOSCALE NUMERICAL MODEL FOR THE PREDICTION OF LAKE-INDUCED SNOW-SQUALLS AND APPLICABLE TO THE HP 1000 MINICOMPUTER

by R. Gabison
MSRB, Atmospheric Environment Service, Canada
B. DeLorenzis
MSRB, Atmospheric Environment Service, Canada

Abstract

In this nested-grid mesoscale model, hourly predicted values of temperature, moisture and heights obtained from a larger-scale NWP model (127 km) are first interpolated to the mesoscale mesh of 31.75 kms and subsequently modified hourly by thermal and moisture advection by heat and moisture flux-divergence and by topographical effects.

Hourly snowfall rates from the mesoscale model are summed over the 24 hour period and compared with those observed at synoptic stations in the Ontario snow-belt where the model has been extensively tested.

Effects of lake freeze-up on the predicted snowfall are shown to be compatible with those observed climatologically.

The model requires only 44000 octals (18 K) of memory storage and 8 - 12 minutes execution time for a 24 hour prediction on the HP 1000 Minicomputer in use at Canadian Regional Weather Offices.

M 34

THE USE OF MULTILINEAR REGRESSION TECHNIQUES TO OBTAIN AN OBJECTIVE SURFACE WIND FORECAST

K. H. JONES (PRAIRIE WEATHER CENTRE, WINNIPEG, MAN., R3C 3V4)

Surface and upper air data for Winnipeg from 1973 to 1977 were used in a step-wise multiple linear regression technique to develop equations for predicting surface wind. The equations are of the general form:

$$\hat{Y} = a_0 + a_1X_1 + a_2X_2 + \ldots + a_kX_k$$

The dependent variables used were the two wind components U and V and the wind speed S. A second estimate of wind was also obtained from the two components. The independent variables consisted of around 50 various upper air data at 12Z and 00Z.

Equations were developed for 12Z, 18Z, 00Z and 06Z for each season of the year. Most equations contained 6 variables with the number of independent variables ranging from 4 to 8. The spectral model was used for input of the independent data (perfect prog technique) when the model was tested operationally. The regression equations have been running operationally since Oct. 79. Good results have been obtained from the verification of 6 months of independent data from Sept/79 to Feb/80.

M 35

VISIBILITY ESTIMATES FOR THE OPEN OCEAN SUMMER SEASON USING MODEL OUTPUT STATISTICS

P. G. Yavorsky (Dept. of Meteorology, Naval Postgraduate School, Monterey, CA 93940)
W. T. Aldinger, Jr. (Naval Western Oceanogr. Center, Box 113, Pearl Harbor, HI 96860)
R. J. Renard and
W. van der Bijl (Dept. of Meteorology, Naval Postgraduate School, Monterey, CA 93940)
(Sponsor: Olivera Haney)

Continuing experiments using a model output statistics scheme to specify horizontal visibility over the open ocean by a stepwise multiple linear regression program is described. The visibility predictand is defined variously as a function of the ten synoptically-reported visibility codes, in both probability and categorical modes. The predictors are mostly continuous analysis and prognosis numerical parameters, available twice daily (0000 and 1200 GMT) from Fleet Numerical Oceanography Center, Monterey, CA. The dependent data for the diagnostic runs are represented by over 9000 0000 GMT surface ship synoptic observations from the North Pacific Ocean (30-60N) June 1976 and 1977. June 1979 data from the same area are used for the independent check of the diagnostic equations, as well as providing data for developing 24- and 48-hr prognostic estimates. Parameters contributing significantly to the explained variance of the predictand are sensible and evaporative heat fluxes, relative humidity, sea-level pressure and meridional wind speed. Categorical estimates of visibility are verified on both the dependent and independent data sets by percent correct and Heidke Skill scores. Other facets of the problem will be discussed as time allows.

M 36

FORECASTING CLOUD AMOUNTS USING MULTILINEAR REGRESSION TECHNIQUES

G. D. MACHNEE (PRAIRIE WEATHER CENTRE, WINNIPEG, MAN., R3C 3V4)

Using surface and upper air data for Winnipeg from 1973 to 1977 linear regression equations of the general form:

Using 6 hour averages of cloud amount as the dependent variable and up to 50 various independent variables consisting of surface and upper air data considered, equations were written for 1200Z and 0000Z for all months of the year. The correlations vary for different months of the year. Winter months were found to have lower correlation coefficients than summer months. Two sets of equations were written, one to use numerical forecasts from LFM and the other set to use Spectral Model forecasts. Persistence was also considered. Verification was done using LFM forecasts and will also be done using Spectral forecasts.

M 37

FORECASTING CLOUDINESS USING MULTIPLE DISCRIMINANT ANALYSIS

R. D. HOLDHAM (PRAIRIE WEATHER CENTRE, WINNIPEG, MAN., R3C 3V4)

A statistical approach was applied to the problem of forecasting mean cloudiness in four six hour periods of the day. Data for three winter months was grouped into cloudy (greater than 5/10ths) and not cloudy (less than 6/10ths) through these periods, and Multiple Discriminant Analysis was used to generate the joint probabilities that the independent variables were associated with one group or the other. Selecting variables was done on a partly subjective, partly objective basis. Results are incomplete as yet but the procedure has been tested on forecast values of the predictors and on an independent set of data.

M 38

AN OPERATIONAL EVALUATION OF PROBABILITY OF PRECIPITATION AMOUNT FORECASTS GENERATED FROM STATISTICAL AND ANALOGUE TECHNIQUES

T. Agnew, Forecast Research Division, Atmospheric Environment Service, Downsview, Ontario, Canada, M3H 5T4
J. Alexander, Ontario Weather Centre, Atmospheric Environment Service, Toronto International Airport, Ontario, Canada

An extensive evaluation of probability of precipitation amount forecasts is currently being carried out at the Ontario Weather Office in Toronto, Canada. Three different techniques to produce these probabilities are compared. These techniques are Regression Estimate of Event Probabilities (REEP), Multiple Discriminant Analyses (MDA) and an Analogue technique. A wide variety of scores are generated to determine the differences in the techniques and to try to evaluate which is most suitable in an operational decision making environment.

The techniques are applied in a perfect prog manner so that quality of the produce is sensitive to errors in the forecast fields. The statistical techniques are developed from a 10 year dependent sample of observations, analysis and derived fields. The predictand is precipitation amount in four categories over a 12 hour period. The analogue technique uses a 24 year database of NCAR analysis at 1000 and 500 mb. For each forecast period, the 20 best correlations to the current progs are determined. The frequency of precipitation amount for those 20 cases at a particular station determines the probability for each category.

The product is used in the office as guidance material by the forecasters as well as for specialized forestry and agriculture forecasts. Preliminary results indicate that REEP and MDA are superior to Analogue. In general, MDA is sharper than REEP in the probabilities that it generates. Although this tends to produce a larger error if the forecast model is in error, the probabilities are better for decision making.

M 39

VERIFICATION OF CEILING AND VISIBILITY

FORECASTS – AN ALTERNATIVE TO THE

RANKED PROBABILITY SCORE APPROACH

P. Dubreuil (Atmospheric Environment Service St-Laurent, Quebec, Canada. H4M 2N8)

An aviation terminal forecast verification scheme is proposed that considers the terms variable (VRBL) and occasional (OCNL) in the forecasts as their definition suggests: an occurrence for a portion of the total forecast period, rather than as a probability of occurrence at any time, as assumed by the ranked probability score (RPS) approach. The term RISK, also according to its definition, is considered as a probability of occurrence of less than 50% without specifying a precise percentage.

The method can assess the accuracy and the precision of a forecast independently, with scores that have a straightforward interpretation. A useful feedback to operational forecasters is possible because the meaning of the forecast is not modified in any way, and because the scores can be easily interpreted without any external reference, such as climatology or persistence.

Finally, a method is proposed to compensate for the great variations in the climatological frequencies of the different ceiling-visibility classes chosen to represent user needs. Without this compensation, mean scores are biased towards the most frequently observed class, which happens to be the easiest to forecast but the less significant to the user.

Thunderstorms, Lightning & Cloud Physics

Pier 2 & 3
Saturday P.M.
W. F. Hitschfeld (McGill Univ.), Presiding

M 40

FURTHER STUDIES OF THUNDERSTORM FORMATION AREAS IN ALBERTA

F.E. ROBITAILLE, ASD, ALBERTA RESEARCH COUNCIL

Observational studies of the low-level flow associated with convective clouds southwest of Rocky Mountain House, started in 1978, were continued in 1979. These studies were conducted as part of the Alberta Hail Project and included measurements by the University of Wyoming Queen Air aircraft and a network of pilot balloon and rawinsonde stations.

Analysis of 1978 data are presented to suggest that towering cumulus clouds were rooted in the lowest 100 m of the atmosphere.

Two days of observation in July 1979 are discussed. The characteristics of 20 July, a day with cumulonimbus activity in the study area, are compared with those of 25 July, a day with weak connection in the study area.

M 41

THE DYNAMIC EFFECT OF CONVECTION IN THE TROPICAL ATMOSPHERE

Mary Ann Jenkins (Dept. of Physics, University of Toronto, Toronto, Ontario, Canada)
Han-Ru Cho

A formulation to represent the effects of cumulus clouds on the large scale vorticity equation in terms of the properties of the cumulus cloud ensemble is proposed. The processes of cumulus convection which modify the large-scale vorticity field are vertical advection of mean vorticity, twisting of vorticity, and the divergence of horizontal eddy vorticity flux created by cumulus clouds. All three processes are included in a representation formulation to complete the theory of cloud parameterization.

Upper air and surface data from the GARP Atlantic Tropical Experiment (GATE) are used to examine the interaction between the synoptic scale motion and the convective scale activity. Heat, moisture and potential vorticity budgets observed during Phase III of GATE are presented. The diagnosed ensemble mean cloud properties are also presented. Vorticity budgets are discussed and apparent vorticity sources predicted from theory are compared with observations. The agreement between the theoretically predicted apparent vorticity sources and the observed cloud effects for the analyzed periods is good and these results appear to confirm the validity of this representation theory.

M 42

THE EFFECT OF THE C.N. TOWER ON LOCAL LIGHTNING CLIMATOLOGY

W. Janischewskyj, (University of Toronto, Toronto, Ontario, M5S 1A4)
Jen-Shih Chang (McMaster University, Hamilton, Ontario, L8S 4M1)
H. Linck, (Georgetown, Ontario, L7G 3R9)
T.R. McComb, (National Research Council of Canada, Ottawa, Ontario, K1A 0R8)

Rising to a height of 553 m above ground level (AGL) the C.N. Communications Tower in Toronto is the highest free-standing structure in the world and offers a unique opportunity to evaluate the effect of tall structures on local lightning climatology. Lightning flashes to the tower, and to open country in S.W. Ontario, have been videotaped and cumulative probability distributions for the temporal characteristics of flashes from each group are presented. These distributions show that in the flashes to the tower there are more long duration flashes, more flashes with five or more strokes, and more short inter-stroke intervals than in flashes to open country. Electric field measurements have been made using a radio-active probe mounted on the roof of the sky pod of the tower at a height of 365 m AGL. The correlation between the measured field profile and thunderstorm activity is being investigated. A network of lightning flash counters has been set up in the Toronto area and measurements are being made of the ground flash density in the area surrounding the Tower. A short film (2 min.) of lightning flashes to the C.N. Tower will be shown.

M 43

THE RELATIONSHIP BETWEEN LIGHTNING FREQUENCY IN SOUTHERN ONTARIO AND SOLAR SECTOR BOUNDARY CROSSING

Jen Shih Chang (Dept. Engineering Physics, McMaster University, Hamilton, Canada L8S 4M1)
R. Blais (Hydro Quebec Research Institute J0L 2P0)
C. L. Crozier (Atmospheric Environment Service, Toronto, Canada M3H 5T4)
W. Janischewskj
H. Link
G. Stamoulis (Department of Electrical Engineering, University of Toronto, Toronto, Ontario)
G. G. Shepherd(CRESS, York University, Toronto, Canada M3J 1P3)

The frequency of lightning flashes in southern Ontario, as a function of time with respect to solar magnetic sector boundary corssings is presented for 1978-79. The daily number of lightning flashes was measured with an Ontario Hydro type lightning flash counter, a Hydro-Quebec goniometric lightning flash detector, and a Q-Tech lightning flash counter at the Woodbridge AES site (N43°47.6',W79°33.7') near Toronto. For the 1978 summer the lightning frequency is lower by a factor of 2-3 during a positive sector (magnetic field directed away from the sun) as compared with a negative sector. For the 1979 summer the lower lightning frequency during the whole observing period makes this effect less evident, but for both summers there is a depression in lightning frequency for 1-3 days on the positive side of the boundary crossing. Thus although observations were made for only 7.5 months, the data strongly indicate a sector boundary influence on local lightning flash frequency.

M 44

A MODEL TO PREDICT ELECTROMAGNETIC FIELDS FROM LIGHTNING RETURN STROKES

R. L. Gardner (Department of Physics and Cooperative Institute for Research in Environmental Sciences, University of Colorado, Boulder, CO 80309)

When measured waveforms from transients due to lightning return stroke electromagnetic fields are presented in the literature the data are frequently normalized to a particular distance. The assumption used in the literature (e. g., Y. T. Lin, PhD Thesis, Univ. of Florida, 1978) is that the remaining variation in the waveforms is due to variations in the lightning return stroke current. It is shown in this paper that this assumption does not adequately separate propagation and source effects. This incomplete separation is because a wave propagating over the earth is more severely attenuated with distance than a wave propagating over a perfectly conducting plane as calculated by, for example, LeVine and Meneghini (J. Geophys. Res., 83, 2377, 1978). The additional attenuation for frequencies below about 100 Hz is due to waveguide effects of the earth-ionospheric waveguide. Additional attenuation above about 10 kHz is caused by imperfectly conducting earth effects.

A theoretical model is presented here that, for frequencies above 1kHz treats the earth as a homogeneous half-space (J. R. Wait, Electromagnetic Waves in Stratified Media, Pergamon, 1970) and the anisotropic ionosphere using a single bounce treatment (J. R. Wait, Proc. I. R. E., 50, 1623, 1962). Below 1kHz the model calculates the fields using waveguide techniques (Wait, 1970). An attenuation function is presented which can be used to remove the added propagation path attenuation (in addition to 1/r) from data so that effects of the source variations may be studied more easily. The attenuation function is shown to vary somewhat with source model details. Therefore, a different attenuation function may required for a vertical stroke than for a cloud-to-cloud discharge. The results for the model predictions are shown to agree with the data of Uman, et. al. (Radio Science, 11, 985, 1976).

M 45

HAILPAD WIND MEASUREMENTS AND HAILFALL SAMPLING ERRORS

G.S. Strong (Alberta Hail Project, Red Deer, Alberta)
E.P. Lozowski (Department of Geography, University of Alberta, Edmonton, Alberta)

Two distinct but related problems are discussed in connection with using hailpads to

measure fine scale variations in hailfall. A simple semi-objective method of measuring mean wind speed during hailfall using only a hailpad is described. Subsequent data shows the existence of *windcores*, a fine scale horizontal pattern of wind speeds with variability on a scale of hundreds of meters, similar and related to that of the hailfall.

While attempting to obtain better estimates of hailpad sampling errors, extremely fine patterns of hailfall on a scale of a few meters were initially analyzed; these have been tentatively called *hailspots*. Monte Carlo experiments failed to disprove the existence of hailspots solely on the basis of stochastic sampling errors.

M 46

EFFECT OF ROTATION ON THE ICING OF CYLINDERS AND ITS IMPLICATIONS FOR HAILSTONE GROWTH

G. B. Lesins (Dept. of Physics, University of Toronto, Toronto, Ontario)
P. I. Joe
R. List

Rotating cylinders were iced in a closed circuit wind tunnel over a temperature range of $-2^{\circ}C$ to $-18^{\circ}C$, a liquid water content range of 2 gm^{-3} to 30 gm^{-3} and at an air velocity of 18 ms^{-1}. The net collection efficiency, ice fraction and total mass growth rate were measured for rotational frequencies of 0.5 Hz to 35 Hz. These measurements showed a significant and complex variation of the growth parameters as a function of the rotation. It is believed that hailstones growing in a thunderstorm have similar rotation speeds and hence rotation effects may significantly alter the growth rate.

M 47

THE PRODUCTION OF RAIN SIZED DROPS BY THE ICE ACCRETION PROCESS

P.I. Joe (Dept. of Physics, University of Toronto, Toronto, Ontario)
G. B. Lesins
R. List

Icing experiments were performed to investigate the loss of collected water from a slowly rotating cylinder (0.5 Hz). The losses resulted in the production of rain sized drops. The spectrum of the shed drops were measured as a function of temperature ($-5^{\circ}C$ to $-18^{\circ}C$) and liquid water content (9 gm^{-3} to 40 gm^{-3}) and showed a peak at about 1 mm. The experiments demonstrates one more link between the growth of hail and the production of rain.

M 48

AEROSOL CONCENTRATIONS AND RELATED ICE NUCLEATION ACTIVITY: TENT STUDIES

R.C. Schnell (Both at Atmospheric Physics & S.W. Miller Chemistry Laboratory, NOAA, R-31, Boulder, CO 80303)

Samples of surface soils, decayed plant litters, kaolin, and ice nucleation active bacteria were puff aerosolized into a 2.75-m^3 mylar tent and then analyzed for particle size distribution and ice nucleation activity over periods ranging up to 12 hours. The aerosol size distributions were measured with overlapping Particle Measuring Systems FSSP and ASSAP probes over a particle diameter range from 0.09 μm to 45 μm. Ice nucleus concentrations were determined by using a combined membrane filter-drop freezing technique. Analysis shows that appreciable amounts of aerosolized material were suspended in the tent up to 5 hours after aerosolization. The largest masses of soil and vegetation aerosols were observed in the 0.1 μm to 0.8 μm particle diameter range with the greatest mass of the bacteria aerosols in the 0.8 μm to 1.2 μm diameter range. Aerosols were observed to be active at about the same initial freezing nucleus temperature (varying from $-2.5^{\circ}C$ to $-12^{\circ}C$) as were the bulk samples of the same material tested with the drop freezing technique. Ice nucleation activity at temperatures warmer than $-10^{\circ}C$ to $-12^{\circ}C$ could be measured for periods of up to 4-5 hours after aerosolization for most soil and vegetation aerosols. Scanning electron microscope studies indicated that longer suspended particles consisted mainly of fibrous or spongy organic material or were bacteria.

M 49

EFFECTS ON AIR QUALITY AND CLOUD MICROPHYSICS OF A COAL-FIRED POWER PLANT

R.F. Pueschel (All with Air Resources Laboratories, NOAA, Boulder, CO 80303)
E.W. Barrett
D.L. Wellman
J.A. McGuire

An instrumented aircraft was used to measure in situ atmospheric composition, and aerosol and cloud drop size distributions inside broken stratocumulus clouds in the vicinity of the Homer City, PA coal-fired power plant. On the average, increases in the concentration of NO by a factor of 50, of NO_2 by five, SO_2 by 80, condensation nuclei by 20, and of the light scattering coefficient by two, and a decrease of ozone by four were observed in the clouds downwind of the power plant. The power plant operation also affects the aerosol and cloud drop size spectra, represented by generalized gamma distributions. The fine particle modal radius is decreased from 0.05 to 0.02 μm, and their number concentration per cm^3 is increased from 2,000 to over ten million. The haze particle modal radius at 0.6 μm and their concentration of 200/cm^3 are little influenced by the power plant operation. Important for evaluating the inadvertent weather modification potential of coal-fired power plant operations are the findings of an increase downwind of the Homer City plant of the mean cloud drop modal radius from 3.0 to 4.0 μm and of the mean liquid water content from 0.01 to 0.02 grams per cubic meter, which are statistically significant at the 5 and 10 percent confidence levels, respectively.

M 50

WATER QUALITY AND ICE NUCLEUS STUDIES

S.W. Miller (Both of NOAA/APCL, R-31,
R.C. Schnell Boulder, CO 80303)

Clean water that would consistently supercool below $-20^{\circ}C$ (0.01-cm^3 drops tested with the Vali drop-freezing technique) was needed for an ongoing program measuring daily atmospheric ice nucleus concentrations at Boulder, Colorado (Schnell, 1979). Earlier laboratory research had shown that tap water distilled and deionized in a commercial apparatus produced inconsistent and unreliable first freezing events varying from $-6^{\circ}C$ to $-18^{\circ}C$, and that some of this variability could be traced to the season of the year. During the winter, distilled tap water produced appreciably fewer freezing nuclei per unit volume than did spring and summer tap water from the same source. By constructing a simple pure glass still and completely cleaning the unit once per week, it was possible to consistently produce water with initial freezing nucleus activity colder than $-20^{\circ}C$. Filtering this water through Nuclepore and Millipore filters invariably added freezing nuclei to the water, some with initial freezing points as warm as $-15^{\circ}C$. Increased ice nucleus activity in the clean distilled water was traced directly to initial cleanliness of the distilling apparatus and storage containers, non-airtight storage of the samples, and/or contamination of the water during preparation of the ice nucleation tests. Since water transfers and nucleation tests were conducted in a positive pressure clean air hood, the need for careful handling of the components for ice nucleation tests and for consistent control checks became evident.

Schnell, R.C. A new technique for measuring atmospheric ice nuclei active temperatures from $-20^{\circ}C$ to approaching $0^{\circ}C$, with results. Preprints, Seventh Conference on Inadvertent and Planned Weather Modification, Oct 8-12, Banff, Alberta. AMS. Boston, Mass.

M 51

TRACKING CLOUD SEEDING MATERIALS

A.G. Eddy, Amos Eddy, Inc.
318 Royal Oak Drive, Norman, OK 73069
E.R. Reinelt, University of Alberta,
Edmonton T6G 2H4

The conflicting results of numerous cloud-seeding programs continue to provide ample scope for controversy. This is especially true of operational cloud-seeding evaluations based on simplistic statistical analyses which fail to take into account the natural variability of precipitation. Alternative testing procedures are clearly required to sort out the issues.

This paper examines the relationship of the trajectories of cloud-seeding materials (released operationally on seeded days) to the rainfall collected in gauges located downstream. It is a follow-up study of an exhaustive statistical analysis by Eddy et al. (1979) of rainfall data for North Dakota. Two hypotheses are to be tested:

(1) Seeding has produced a significant increase in the growing season rainfall.
(2) Seeding has resulted in a significant change in the nature of the rainfall by increasing the number of days with light rainfall.

It is shown how these hypotheses can be approached on the basis of some 100 sets of trajectories examined for the 1977 growing season.

M 52

A NEW APPROACH TO MODELING FOG OPTICAL PROPERTIES

Louis D. Duncan (US Army Atmospheric Sciences Laboratory, White Sands Missile Range, NM. 88002)
Richard D. H. Low (Same)

With the advent of satellite and aviation meteorology, there is often a need to know the spectral transmission of fogs/clouds in the visible and the IR windows. Fog drop-size data collected recently with an optical particle device invariably exhibit a bimodal (or sometimes multi-modal) distribution in contrast to the drop-size spectra of a single mode observed in the past with a mechanical particle impactor. Visibility being a routinely observed quantity, it is proposed that it be used as the basic parameter to derive drop-size distributions from which extinction coefficients (and hence transmission) in the IR windows can be readily computed.

In a preliminary investigation, models have been fitted to the fog data collected at Meppen, FRG, during February and March, 1978. These models are formulated as the sum of two gamma distributions, while preserving the basic characteristics of the observed spectra, in particular, their bimodal appearance. The models accept visibility as an input and then generate a distribution consistent with this input.

The model requires six parameters to determine a drop-size distribution. It is shown that constants can be assigned to two of these parameters. Algorithms, based on curve fitting, are developed for computing the other parameters as a function of visibility. Tables and graphs are presented to demonstrate the models' capability to reproduce the features of the observed drop-size spectra, and then comparisons are made of liquid water content and IR extinction derived from measured and model drop-size distributions.

Boundary Layer & General Meteorology

Pier 5
Monday A.M.
Gordon McBean (Atmospheric Environment Service), Presiding

M 53

SUPERROTATION IN PLANETARY ATMOSPHERES: A PIROUETTE

H. G. Mayr
B. J. Conrath
I. Harris (all at: NASA/Goddard Space Flight Center, Greenbelt, MD 20771)

In earlier attempts to understand superrotation, the perception of angular momemtum conservation has been a problem. The reason for this is, we contend, that the atmospheric moment of inertia has tacitly (but incorrectly) been assumed to be invariant. On a planet with its rotation axis perpendicular to the orbital plane, the equatorial region is heated preferentially. The compressible viscous atmosphere expands and large scale motions in the form of Hadley cells are set up that effectively transport mass from the equator toward the poles, closer to the rotation axis. As a result, the atmosphere's moment of inertia decreases and its rotation rate must increase (superrotation) to conserve angular momentum. On Uranius where the rotation axis is in the orbital plane, one should observe four seasons with alternating super- and sub-rotation as the planet revolves around the Sun. In support of this interpretation, mechanical analogies are discussed, one being the spin-up in the pirouette. Moreover, dimensional analysis and results from a self consistent spectral model are presented to describe thermo-dynamic processes (including the moving flame effect) which lead to super (or sub) rotation in viscous atmospheres.

M 54

THE GENERATION OF MESOSCALE SURFACE WIND PATTERNS ON EARTH AND MARS

R. L. Rankin (Arizona State University, Tempe, AZ 85281)
A. R. Peterfreund
G. C. Eckerman

Mesoscale surface winds are important to aeolian processes on Earth and Mars. In the absence of significant synoptic scale weather phenomena these surface winds exhibit regular diurnal patterns which depend on spatial and temporal variations in temperature and temperature derivatives as well as local topography.

Due to the transfer of heat between the ground and adjacent air, a temperature gradient is formed in a direction normal to the inclined surface. The differences in the horizontal components of these gradients generate an upslope wind when the surface is being heated and a downslope wind when the surface is being cooled. A model based on these concepts has been developed and is used to compare a region of the Snake River Plain (SRP) in Idaho with the Viking Lander I site. The two-dimensional model predicts the average hourly horizontal velocity of these winds at a height of 10 m, assuming temperature and topographic variations as the governing parameters.

Data was collected on the SRP during August of 1978 and was used to validate the model on Earth. For Mars, the Viking Lander data provides a means of validating the model in the martian environment. Preliminary computer runs have generated surface wind fields that show good correlation with the SRP data. In addition the overall flow patterns correspond well with the observed diurnal variations. Validation of the model using Mars data is yet to be carried out.

M 55

FINITE AMPLITUDE KELVIN-HELMHOLTZ BILLOWS

G. Klaassen (Dept. of Physics, University of Toronto, Toronto, Ontario, Canada M5S 1A7)
W.R. Peltier (Dept. of Physics, University of Toronto, Toronto, Ontario, Canada M5S 1A7)

The evolution of finite amplitude KH waves in a stratified shear flow is a strong function both of the dissipation (as represented by Reynolds and Prandtl numbers) and of the initial conditions from which the initial inviscid instability commences. We will describe a sequence of time dependent numerical simulations of wave growth from states with rather high initial Reynolds number such as are appropriate in oceanographic and meteorological applications. When the Prandtl number is sufficiently high the behaviour of the billow in the long time limit corresponds to a nearly sinusoidal limit cycle. If the initial conditions contain an infinitesmal perturbation at a wavelength corresponding to the first spatial subharmonic of the fastest growing mode of linear theory then vortex pairing occurs in the late stages of evolution. Both of these phenomena may be understood in terms of a weakly non-linear theory.

M 56

STOCHASTIC SIMULATION OF THE DIFFUSION EQUATION BY TURBULENT LAYERS IN STRATIFIED FLUIDS

Edmond M. Dewan (Aeronomy Division, Air Force Geophysics Laboratory, Hanscom AFB, MA 01731)

The numerical simulation of the diffusion equation involves an averaging of the dependent variable at neighboring points of the discrete lattice. For example, a typical algorithm for

$$\frac{\partial \Psi}{\partial t} = K \frac{\partial^2 \Psi}{\partial Z^2}$$

is given by $\Psi(Z, t + \Delta t) = \frac{1}{6}[\Psi(Z - \Delta Z, t) + 4\Psi(Z,t) + \Psi(Z + \Delta Z, t)]$ where $K\Delta t/(\Delta Z)^2 = \frac{1}{6}$.

It will be shown that this algorithm could in principle be simulated by means of a certain sequence of patterns of thin, horizontal, turbulent mixing layers which are arranged in a certain way with respect to the vertical coordinate, Z. Total mixing within the layers is assumed. In a more realistic stratified fluid, the turbulent layers would form in a random way. Nevertheless, it will be demonstrated that they can simulate the above process in a stochastic manner. Slides (or digital computer moving pictures - if available) will be shown to demonstrate this effect for several examples.

Stratified turbulence (with total layer mixing) therefore leads to a new type of diffusion coefficient, K, where

$$K = \frac{\alpha L^2}{\Delta t}$$

Here L^2 is average square layer thickness, Δt a characteristic time within which all of Z would be covered by overlapping layers, and α is a constant of order unity.

Stratospheric and oceanic temperature profiles show possible evidence of total mixing within turbulent layers. This would imply that the above form for K may be preferable to the usual estimate $K = \bar{\epsilon}/3N^2$ where $\bar{\epsilon}$ is the average eddy eddy dissipation rate and N is the buoyancy frequency.

M 57

COMPARISON OF ALTERNATIVE PARAMETER SELECTION METHODOLOGIES FOR THE GAUSSIAN PLUME ATMOSPHERIC TRANSPORT MODEL

D. E. Fields, S. J. Cotter, and C. W. Miller
Health and Safety Research Division
Oak Ridge National Laboratory
Oak Ridge, Tennessee 37830

We have used the DWNWND Gaussian plume computer code to simulate normalized 22.5° sector average dispersant concentrations at downwind distances from 400 to 7000 meters distant from a 51 meter high release point. Model results were compared to sector average values obtained in fluorescein release experiments performed at Hanford, Washington between 1967 and 1973. Dispersion parameterizations used were Pasquill-Gifford (PG) and Brookhaven (B), and dispersion parameters σ_y and σ_z were for atmospheric stability classes determined from either temperature gradient ($\Delta T/\Delta z$) or wind direction standard deviation (σ_θ) measurements. Comparisons between experimental and simulated values were made as dispersion parameterization, stability class determination method, deposition velocity v_d, and gravitional fall velocity v_g were varied. Agreement was expressed as the correlation coefficient r. Values of r ranged from significant at the p = 0.01 level to insignificant at even the p = 0.05 level. Best results were found with v_g = 0 m/sec, v_d = 0.018 m/sec, and a PG dispersion parameterization based on a σ_θ stability determination, yielding r = 0.43 (significant at the p = 0.01 level). When 400 meter data comparisons were omitted, the best correlation between observed and predicted values was a significant correlation at the 0.01 level, r = 0.51, for a B parameterization based on $\Delta T/\Delta z$ and v_g = 0, v_d = 0.018 m/sec. Our analyses suggest that one may not unreservedly choose either a B or PG parameterization for all cases.

M 58

WIND SHEAR EFFECT ON LATERAL SPREAD DURING THE PLUME - DOMINATED PHASE OF DISPERSION

E.D. Leavitt (Intera Environmental Consultants Calgary, Alberta)
D.S. Davison

The interaction between vertical mixing and a velocity shear gives rise to enhanced lateral dispersion. Assuming homogeneous turbulence and a linearly varying lateral velocity, Smith (1965) predicted that the lateral dispersion due to the wind shear varies as $X^{3/2}$ where X is the downwind distance from the source. For typical values of atmospheric turbulence the shear contribution is small (e.g., Pasquill, 1974). However, this conclusion is contradicted by Slawson et al (1979) using data collected in a study sponsored by Syncrude in Northern Alberta. They detected significant shear effects on lateral dispersion at distances between 2 km and 10 km from a buoyant source. This conclusion is explained if allowance is made for the enhancement of vertical turbulence over ambient levels during the initial stages of the growth of a buoyant plume. Smith's approach is modified and used to develop an expression which relates the effect of the wind shear to source strength. Comparison is made with Slawson's data and with other plume data collected during the Alberta Oil Sands Environmental Research Program.

M 59

THE RELATIVE IMPORTANCE OF WIND SPEED, STABILITY, AND GROUND ROUGHNESS IN THE CALCULATION OF DOWNWIND CONCENTRATIONS OF FREEWAY EMISSIONS

S. Machiraju (AeroVironment, Inc., Pasadena, CA)
D. M. Wilbur (Same)

Though it is well known that both meteorological and terrain factors play a role in the dispersion of gaseous pollutants from freeways, the exact nature of the dependence is not obvious. This is partly due to the fact that the three major variables influencing dispersion--namely, wind speed, stability condition, and ground roughness--are inter-dependent, and moreover, that both the mutual and individual relationships to dispersion are non-linear ones. To obtain a more quantitative understanding of this interdependence, a parametric variation of wind speed, stability, and ground roughness was performed for fixed emissions using a freeway model that has been well validated. The wind direction was also fixed to be blowing across the freeway. From the results of this parametric variation we can conclude that: (1) At a given location the concentration increases as the stability passes from an unstable to a stable condition; (2) For all stability conditions, the concentration decreases with increasing wind speed (after an initial critical value is reached); (3) For a given stability condition and wind speed, the concentration decreases with increasing ground roughness at downwind locations and increases with increasing ground roughness at upwind locations.

This qualitative behavior is as expected. Looking at the quantitative aspects, we can further conclude that: (1) For a given wind speed, the largest change in concentration occurs as we pass from more stable to less stable conditions, with this transition region varying as a function of wind speed; (2) For a given stability condition, the changes in concentration due to changes in wind speed are of comparable magnitude to the changes due to varying stability; (3) For a given stability condition, an order of magnitude increase in ground roughness can result in a 50-100% reduction in the concentration; and finally, (4) The primary influence is from stability condition and wind speed, with ground roughness playing a secondary role.

M 60

THE DYNAMIC EFFECTS OF LOW LEVEL JETS AND RELATED WIND SHEARS ON THE RATE OF SPREAD OF FOREST FIRES

Douglas Chan (Dept. of Physics, University of Toronto, Toronto, Ontario, Canada)
Han-Ru Cho

A model is proposed to explain the high correlations of blow up forest fires in the presence of low level jets and related vertical wind shears. Blow up forest fires are forest fires burning and spreading at rates much faster than the burning conditions would indicate. And low level jets are characterized by horizontal wind profiles which are decreasing with height. The model is based on the dynamic interactions of vorticity and the fire. The result is the tilting of vortex tubes by air motion induced by the fire. And calculations can be done using the vorticity equation.

Preliminary calculations based on a typical negative wind shear showed an initial increase in the horizontal wind velocity in the direction of fire propagation. The increase is confined to the center axis of the fire. Therefore this model can account for an increased rate of fire spread and the typical long and narrow ('cigar-like') profile of burning as observed in blow up fires.

The main conclusion that can be drawn is that the tilting of the vorticity field by air motion induced by the fire is one major factor in the explanation of blow up forest fires.

M 61

OBSERVATION OF WIND SHEAR USING A DOPPLER ACOUSTIC SOUNDER DURING SOUTHERN ALBERTA CHINOOKS

T. Mathews, Department of Physics, The University of Calgary, Calgary, AB, Canada T2N 1N4
S.A. Leelananda, R.H. Hicks and P.J. Irwin, Department of Physics, The University of Calgary, Calgary, AB, Canada T2N 1N4

An acoustic sounder designed to measure horizontal wind profile has been built and operated during the winter of 1979-80. The sounder consists of a central array of transducers directed vertically upwards and two inclined receivers placed 100 m from the central transmitter, along perpendicular baselines. 100 ms burst of 1600 Hz pure tone is transmitted by the central transducers and backscattered signals are received by the remote receivers. Doppler shift in the frequency of received signals is used to determine the horizontal wind in the height range of 70-400 m. The sounder is located 20 km west of Calgary in the lee of the Rocky Mountains, an ideal location to study Southern Alberta Chinooks.

During the past winter, many Chinooks were observed and we have obtained wind profiles during several of these. During the early phase, strong winds of 30-40 m/s were observed at higher levels while surface winds were low. Later these strong winds descended to the ground level. Wind shears of 30-40 m/s per 100 m seems to be typical during Chinooks.

M 62

A NEW TROPOPAUSE DEFINITION FROM SIMULTANEOUS OZONE-TEMPERATURE PROFILES

J. M. Roe
W. H. Jasperson (both at: Control Data Corporation, Minneapolis, Minn. 55440)

Historically, the tropopause has been defined arbitrarily in terms of particular features present in a temperature profile. This paper suggests a new definition which is consistent with the assumption that the tropopause is a boundary between the ozone rich air of the stratosphere and the ozone poor air of the troposphere.

In this study, several hundred simultaneous temperature and ozone profiles from the middle 1960's and the latter 1970's were examined in order to arrive at a tropopause definition based on temperature and yet consistent with the ozone evidence. These data span a wide range of latitudes and seasons. Agreement between the traditional temperature derived World Meteorological Organization (WMO) defined tropopause and a tropopause defined subjectively on the basis of ozone gradients was found to be only 68%. However, a modification of the WMO tropopause definition, which relaxed the thickness criterion and allowed the temperature gradient criterion to vary with different soundings, produced a 95% agreement.

M 63

THE HIGH VARIATION OF THE D/H OF PRECIPITATION FROM WINTER STORMS OVER THE NORTHEASTERN UNITED STATES: A NEW METEOROLOGICAL AND CLIMATIC TOOL?

Lawrence, J. R. (Lamont-Doherty Geological Observatory of Columbia University, Palisades, New York, 10964).
White, J. W. C. (L-DGO, Palisades, NY 10964)
Smiley, D. (Mohonk Trust, New Paltz, N.Y. 12561)

The hydrogen isotopic composition of individual storms passing over the northeastern United States is highly variable particularly during the winter months. Subdivision of the isotopic data into three categories was possible on the basis of the tracks and types of storms. The study period was July, 1977, to July, 1978. Category 1 represented large low pressure storms that originated in the southern or central U. S. and moved northeastward west of the Appalachians toward the St. Lawrence Valley. Category 2 represented large low pressure storms that originated in the Gulf of Mexico or near Cape Hatteras and moved northeastward along the eastern seaboard. Category 3 consisted of weak summer storms commonly occurring as a result of a weak eastward moving coldfront. In two instances hybrid storms occurred. The δD values of the three categories were: (1) $-55\pm32^{o}/_{oo}$ (2) $-94\pm11^{o}/_{oo}$ and (3) $-47\pm16^{o}/_{oo}$. The percent of the total annual precipitation in each was: (1) 54% (2) 19% and (3) 27%. The cause of the differences in δD values of the three categories are unknown, although it seems essential that a Raleigh distillation effect must have been important. Incomplete data for the period July 1978 to July 1979 yield similar isotopic patterns although the number of hybrid storms was greater.

M 64

ORGANIC COMPOUNDS IN RAIN AND SNOW

P.A. Meyers (School of Public and Environmental Affairs, Indiana University, Bloomington, IN 47405), R.A. Hites

As part of a general study of the fluxes of organic materials to lakes and their sediments, we have determined seasonal changes in organic contents of precipitation. Rain and snow samples were collected at a location in southern Indiana during fall, winter, and spring. Their dichloromethane extracts have been analyzed by capillary GC and GC-MS. A variety of natural and anthropogenic compounds was found, including n-alkanes, branched alkanes, polycyclic aromatic hydrocarbons, and several types of oxygenated and halogenated compounds. Most of the precipitation samples contained a relatively small number of dominant compounds, although the relative contributions changed with season. In general, rain held more of higher molecular weight compounds such as n-alkanes than did snow. Concentrations of materials in rain decreased during the fall, remained low during the winter, and increased in the spring. This pattern reflects the availability of biologically produced materials. Snow contained higher concentrations than were present in rain, suggesting that snow crystal formation more effectively scavenges organic matter from the atmosphere than does rain drop condensation.

M 65

NEAR REAL-TIME WATER BUDGETS ON A NATIONAL SCALE

P.Y.T. Louie (Atmospheric Environment Service), W.I. Pugsley (Atmospheric Environment Service)

In an effort to monitor and quickly assess variations of climatic parameters in time and space with respect to hydrological activities, a simple water budget technique based on the Thornthwaite model has been implemented in a near real-time mode. Daily water budgets are computed for approximately 345 synoptic stations across Canada and the northern U.S. using their basic meteorological observations. These water budget components are accumulated and averaged over seven day periods and, using an objective analyses scheme, are available in map form about two days after the end of each period. The limitations and applications of the model outputs are discussed.

M 66

MEDICAL BIOMETEOROLOGY: YESTERDAY TO-DAY AND TOMORROW

Simon M. Kevan (Department of Geography John Abbott College, Ste Anne de Bellevue, Que. H9X 3L9)

A brief overview of the past, present and future status of medical biometeorology is given. It is pointed out that North America has had a long and rich tradition of medical biometeorological research, but, that in recent years interest in the more general aspects and practical applications of this research has declined. The European, especially the central European, academic communities have been playing a much more active role in conducting research concerning weather and health issues. Comments are made on their findings and methodology, as well as on their experiences with medical meteorological forecasting. Attention is focused on the types of difficulties which would be encountered by North American research workers if they were to initiate a medical biometeorological programme of a similar nature.

M 67

CLIMATIC HISTORY OF TENDER FRUIT GROWING AREAS IN ONTARIO

W.D. Wyllie (Ontario Region, Atmospheric Environment Service, Toronto, Ontario)
D.M. Brown (Agrometeorology, Land Resource Science, University of Guelph, Guelph, Ontario, N1G 2W1)

Features of extreme winter temperatures that are damaging to tender fruit buds, trees and vines are provided for the past 55 years in the tender fruit growing areas. Specific examples of climatic conditions that led to severe damage to peach trees are discussed. Temperature conditions in the first 30 years are compared with those in the last 25 years. It is apparent that the relative frequency of occurrence of below zero ^{o}F ($-18^{o}C$) winter temperatures is about the same in both periods, although colder temperatures -5 to $-10^{o}F$ (-20.5 to $-23.3^{o}C$) appear to be more frequent in this region in the last 25 years.

The effect of preconditioning of trees and vines, due to mild autumn and early winter conditions, on the likelihood of damage by extremes in winter are assessed based on the accumulation of degree-days $>5^{o}C$ after October 15th. Mid-winter mild spells are also assessed for their subsequent effect.

M 68

METEOROLOGICAL FACTORS CONTRIBUTING TO SUNFLOWER HEAD MOTH INFLUXES IN SASKATCHEWAN

D.J. Bauer (Atmospheric Environment Service) Saskatoon, Sask.
A.P. Arthur (Agriculture Canada) Saskatoon, Sask.

The sunflower moth Homeosoma electellum (Hulst.) is not indigenous to the Canadian Prairies. Moths arriving in Sask. are thought to have migrated from Texas where they winter. Introduction of sunflowers as a cash crop in Sask. has led to a concern about sunflower moth infestations and an interest in predicting the arrival of these moths. Forecasts of meteorological conditions favorable to migration could be used to alert farmers of possible infestations and allow them to take early control measures.

Using data on the arrival of sunflower moths in Sask. during the 1975 and 1976 seasons reverse trajectories to northern Texas were determined. Surface to 700 mb wind fields as well as temperature and stability parameters were examined to establish a set of parameters favorable to such migrations.

Based on the criteria determined by analysing the 1975 and 1976 migrations forecasts of probable infestations were made during 1977, 1978 and 1979. Canadian Meteorological Centre surface, 850 mb, 700 mb and 500 mb prognostic charts were used to identify suitable situations.

Although there is a need for further investigation into the migration activities of the sunflower moth results from the past three years suggest that reliable forecasts of their arrival in Sask. can be made two to three days in advance.

Large-Scale Dynamics and Climate

Pier 2 & 3
Tuesday A.M.
A. Robert (Canadian Meteorological Centre), Presiding

M 69

EDDY HEAT FLUXES AND STABILITY OF PLANETARY WAVES

Lin, Charles A., Canadian Climate Centre, 4905 Dufferin St., Downsview, Ontario, M3H 5T4
Sponsor: CMOS

The stability of baroclinic Rossby waves in a zonal shear flow is examined, using a linear, quasi-geostrophic, two-level, adiabatic and frictionless mid-latitude β-plane model. The perturbations consist of truncated zonal Fourier harmonics. The two important zonal scales are the basic wave scale and the radius of deformation. The ratio of these scales, together with two non-dimensional parameters which describe the barotropic and baroclinic basic wave amplitudes, constitute the three parameters in the parameter study of the stability problem. Parameter space is partitioned according to the dominant energy source for instability.

For the case of interest to the atmosphere, the basic state consists of a wavenumber one Rossby wave in a zonal flow with vertical shear close to the minimum critical shear of the two-level model. The most unstable mode grows at the baroclinic time scale and is almost stationary relative to the basic wave. Maximum perturbation amplitude is at wavenumber three, intermediate between the response scales of the two destabalizing mechanisms: vertical shears of the zonal flow and basic wave. The perturbation meridional scale is close to the radius of deformation; maximum development occurs at a position where the basic wave shear is a maximum. Applications to planetary scale waves that transport heat are considered.

M 70

GLOBAL ENERGY AND ENSTROPHY FLUXES AND SPECTRA

Lambert, Steven J., Canadian Climate Centre, 4905 Dufferin St., Downsview, Ontario, M3H 5T4.
Sponsor: CMOS

Using the two dimensional spectral index, n, the degree of the associated Legendre polynomial expansion, energy and enstrophy spectra are computed for January ,1979. The calculations are done globally on ten pressure levels using the FGGE level III-a data produced by the American National Meteorological Center.

The fluxes of energy and enstrophy, obtained by integrating the non-linear interactions among the n scales, are examined in light of the criteria for the existence of an inertial subrange.

M 71

THE STRATOSPHERIC MEAN ZONAL FLOW IN WINTER

R. S. Quiroz (National Meteorological Center NOAA, Washington, D. C. 20233)

With the aid of radiation measurements from Vertical Temperature Profile Radiometers on NOAA satellites, the mean zonal geostrophic flow is determined at heights from the mid-troposphere to the lower mesosphere. The data are presented in the form of latitude-height cross-sections for individual months of four recent winters (1975-76 to 1978-79); and as time-height sections at 65°N, each over several weeks, for specific stratospheric warming events during the four winters. A strikingly coherent behavior from troposphere to mesosphere is noted during the warming events, with both leads and lags in the vertical propagation of zonal wind minima and maxima. By contrast, the mean zonal wind field in a winter of only weak warming activity (1975-76) was relatively undisturbed. Relationships among the strengths of the tropospheric, mid-stratospheric polar night, and lower-mesospheric jets are discussed. Meridional shifts of the mesospheric jet between 25 and 60°N are evidently related to the character of stratospheric warming activity in each winter. These results call for special care in deriving climatological "atmospheres."

M 72

THE INTERANNUAL VARIABILITY OF SURFACE PRESSURE, TEMPERATURE AND PRECIPITATION MAY 1963 TO APRIL 1973

M.J. Stefanick (Geophysical Fluid Dynamics Program, Princeton University, Princeton, New Jersey 08544)

The geographical and temporal variations of any meteorological field can be described as a sum of standing waves in many different ways. This standing wave decomposition can be made in such a way that its components are the least sensitive to atmospheric noise (natural variability) as is possible. This noise insensitive decomposition is applied to the sequence of 120 mean monthly fields (all points north of 30^{o}S) of surface pressure, temperature and precipitation which have been assembled by A. Oort (in prep.). The first noise insensitive component for the surface pressure is shown to be, from its spatial pattern, the Southern Oscillation. The first two components of the surface temperature are shown to be related to El Nino, both from their spatial patterns and from time series events in 1965 and 1972, and to the Southern Oscillation time series. The first two components for the precipitation are evidently due to station errors, but the third component shows strong similarities to the time series for surface pressure.

M 73

RELATIONS BETWEEN CLIMATIC FLUCTUATIONS AND VOLCANIC ERUPTIONS ASSESSED THROUGH LIKLIHOOD CONSIDERATIONS

Harvey A. Singer (Dept. of Geological Sciences, State University of New York at Binghamton, Binghamton, N.Y. 13901)

It has been proposed that stratospheric-level veils of fine dust from great, explosive volcanic eruptions initiated a new climatic regime which favored Pleistocene glaciation. Recent data shows that many cooling episodes began significantly prior to the coinciding major eruptions. Further, it is questioned whether such magnitude eruptions occur with the frequency needed to cool the atmosphere. Two simple hypotheses are thus confronted: (1) eruptions precede and cause climatic cooling, or (2) eruptions follow and are triggered by the cooling. Since the data is limited to the consequences of the two hypotheses the most that can be done is to weigh each according to the adequacy with which, in probability terms, they describe those consequences, either of which can do so. Rather than standard testing techniques, liklihood theory is used to determine the relative abilities of the hypotheses to account for the data. Each occurrence of an eruption and a cooling period together is classified into one of two association types on the basis of prior onset of either event. The statistical model used is a binomial distribution of types, in which it is assumed that eruptions sufficiently separated in time and space from each other are independent events. Three time scales are studied. The conclusions are biased on the scales of 10^2 and 10^4 years due to the nature of the climatic variations and eruptions. On a scale of 10^3 years, the order of time required by the Pleistocene glaciers to fully develope or melt, the method of maximum liklihood yielded a best supported value for the binomial parameter of ½ of obtaining either association type, indicating that either hypothesis (1) or (2) is equally likely to account for a connection between eruptions and cooling episodes.

M 74

PREDICTED IMPACT ON LOCAL FOG AND CLOUD CONDITIONS BY GENERATING OPEN WATER AT THE COAST OF JAMES BAY

E. Vowinckel (Department of Meteorology McGill University, Montreal, Que. H3A 2K6)
Svenn Orvig (Department of Meteorology McGill University, Montreal, Que. H3A 2K6)

It is anticipated that if rivers in the Rupert Bay area are dammed for hydroelectric power production, areas of ice free water will be generated off the river mouths. The possibility of a change in local climate is examined, specifically the effects of increased condensation of water vapor.

Wind directions between S and NW will carry air to the shore over such open water for 77 per cent of the time in winter, and the air mass modification has been calculated for each day of the period January - March for the four years 1972 - 1976. An energy budget program was used, which permits evaluation of all surface energy exchange terms and determines the change in vertical structure of the air mass along its trajectory.

The results show the expected changes in occurrences of condensation. When a 10 km trajectory over open water is compared with passage over solid ice, a net increase of condensation took place in all atmospheric layers examined (up to 500 m). Out of 436 cases, the number of occurrences of condensation in the lowest layer (0 - 10 m) increased from 17 downwind from ice to 26 downwind from open water. Thus, the cases with condensation increased from 3.9% to 6% of the total. In the higher layers the net change was greater, and it can be concluded that the bulk of the additional water vapor will be condensed in the form of St or Sc clouds. This is due to the simultaneous input of moisture and heat over the open water.

M 75

TWO JANUARY SIMULATIONS USING THE FIVE- AND TEN- LEVEL VERSIONS OF THE AES/CCC GENERAL CIRCULATION MODEL

Boer, G.J., N.A. McFarlane, J.D. Henderson, R. Laprise, Canadian Climate Centre, 4905 Dufferin Street, Downsview, Ont. M3H 5T4
Sponsor: CMOS

Two January simulations using the AES/CCC spectral general circulation model are presented. One of the simulations was made using a five-level version of the model while the other was made using a ten-level version having the same number of computational degrees of freedom and hence half the horizontal resolution.

A comparison of the results of these simulations with climatology and with each other gives some information on the utility of general circulation models of modest resolution and on the trade-off between horizontal and vertical resolution in models of this type.

M 76

A SPECTRAL GENERAL CIRCULATION MODEL WITH MINTZ-ARAKAWA PHYSICS

Sargent, Neil, Canadian Climate Centre, 4905 Dufferin St., Downsview, Ontario, M3H 5T4
Sponsor: CMOS

For studies in longer range climate simulation a fast, cheap General Circulation Model with moderately sophisticated physics would be useful. To this end a two-level spectral GCM with semi-implicit time stepping and Mintz-Arakawa physics is being developed at the Canadian Climate Centre. The spectral dynamics are handled by the transform method and necessitate a Phillips σ coordinate but dispense with stabilizing diffusion and short time steps. The Mintz-Arakawa physics must be modified slightly to accommodate these differences.

The model is currently being tested on January conditions. Zonally averaged mean and transient eddy quantities and the meridional

flow are well reproduced. Standing waves and mean sea level pressure patterns are still not completely satisfactory. Work continues on this model which runs at ~ 400:1.

M 77

A SEASONAL ENERGY BALANCE MODEL WITH ICE-ALBEDO AND BIOGEOPHYSICAL FEEDBACKS.

Tzvi Gal-Chen (National Center for Atmospheric Research, Boulder, CO 80307)
Amir Shabbar (Prairie Weather Center Atmospheric Environment Service, Winnipeg, Manitoba R3C-3V4, Canada)

The zonally averaged mean annual energy balance model of Gal-Chen and Schneider (1976, Tellus 28, 108-121) is extended to allow seasonal simulations. The zonal seasonally effective thermal inertia is allowed to vary on a seasonal time scale to account for some of the effects of the seasonal variation of the oceanic mixed layer. Separation is made between atmospheric albedo and surface albedo. The combined planetary albedo is calculated using theory of two-stream approximate solution to multiple scattering. The atmospheric albedo is held fixed and the surface albedo is allowed to change according to changes in surface temperature and the position of the tree line. The position of the tree line is a function of the insolation and surface temperature in July. A distinction is made between the albedo of a snow covered tundra (poleward of the tree line) and a snow covered forest. Thus both ice-feedback and bio-feedback are included. The infrared emission to space and the dynamical parameterizations are essentially the same as in Gal-Chen and Schneider (1976). When biofeedback is omitted it is found that the annual model and the seasonal model respond similarly to changes in solar constant. When biofeedback is included and allowed to interact with ice-feedback the seasonal model is more sensitive than the annual model. Implications of this latter finding for the astronomical theory of ice ages are discussed.

M 78

COMPARATIVE ASSESSMENT OF SUBSURFACE ENERGY STORAGE PARAMETERIZATION SIN SEASONAL CLIMATE SIMULATIONS

K. E. Taylor (Dept. of Physics, Univ. of Florida, Gainesville, FL 32611)
(Sponsor: W. L. Chameides)

A brief review of seasonal energy budget data highlights those characteristics that are of primary importance for accurate seasonal cycle simulations in climate models. The summary includes estimates of the magnitudes and phases and also of spatially averaged energy fluxes at the surface, at the top of the atmosphere, and across the equator. When appropriate, the hemisphere is separated into a marine sector and a continental sector to provide a more precise description of the energy budget. Several previously used paramterizations and one new parameterization for subsurface energy storage are then evaluated in light of these observations. The phase lags and seasonal amplitudes of the surface temperature and the total energy stored beneath the surface are the main focus because of their major importance to the simulations, especially the possibility of ice cap growth and decay. The parameterizations for subsurface energy storage are compared and assessed in terms of (1) their ability to simulate the natural system, (2) their physical basis, (3) the methods used to determine the model parameters, especially with regard to tunability and sensitivity, and (4) their relative complexity and potential for future applications in models of higher resolution.

M 79

ORIGIN OF ICE AGES

Peter Fong (Physics Department, Emory University, Atlanta, Georgia 30322)

The dynamics of the growth and waste of the cryosphere, which is coupled with the dynamics of the hydrosphere and the atmosphere, is worked out in a simplified model. The mathematical system is represented by a set of simultaneous differential-integral equations which are deterministic and may be solved numerically. The dynamical history of the last Pleistocene glaciation, that is, the rate and extent of the last glacier advance, may be accounted for by a global heat deficit of 0.13% of the insolation lasting throughout the glacial period. This perturbation triggers a chain reaction of glacier advance by ice-albedo positive feedback which is later stabilized because of the geometry of the icecap and the infrared negative feedback. The coupling with the hydrosphere leads to a lowering of the ocean surface temerature of 2.1°C, a prediction in good agreement with the observed lowering of 2.3°C. Note that the eccentricity changes of the earth's orbit leads to a change of the insolation from -0.17% to +0.014%, which is of the right order of magnitude to initiate Pleistocene glaciation according to our model. Previous climate models are not sufficient (by a factor of 10) for the eccentricity changes to do so.

The mathematical study of the process of glacier retreat brings out a hysteresis effect of the climate cycle. The retentivity may explain the observed fact that the interglacials of the Pleistocene are progressively colder whereas the glacial periods are progressively milder.

The theory of glacier retreat can be readily applied to investigate the climate effect of the CO_2 increase due to the use of fossil fuels. The result is that the principal effect would be the melting of the icecaps rather than the increase of the temperature as generally conceived. The Eastern Antarctic ice sheet, according to recent studies, might have partially wasted in the last interglacial and thus is also vulnerable. The CO_2 effect could be more serious than we thought.

Oceanography

Remote Sensing: The Noss System and Ocean Applications

Pier 7 & 8
Thursday A.M.
Peter Cornillon (Univ. of Rhode Island), Presiding

O 1 INVITED PAPER

THE NOSS COLORIMETER

George A. Maul (National Oceanic and Atmospheric Administration, Atlantic Oceanographic and Meteorological Laboratories, 15 Rickenbacker Causeway, Miami, Florida 33149)

The National Oceanic Satellite System proposes to include a visible/infrared multispectral scanner called the NOSS colorimeter. Details of the number of channels, their central wavelengths and bandwidths will be finalized in the summer of 1980. In consideration of the IUCRM panel recommendations, the nine colorimeter channels will probably be: 430-450 nm, 510-530 nm, 550-570 nm, 630-650 nm, 675-695 nm, 740-760 nm, 830-850 nm, 870-890 nm and 10.5-12.5 μm. Instrument design will be very similar to the Coastal Zone Color Scanner which is on NUMBUS-7, except that three additional channels are included, and the resolution from the proposed sun-synchronous 700 km altitude orbit will be about 800 m. The NOSS colorimeter is designed to optimize the quantitative detection of chlorophyll and sediments but will only provide qualitative sea surface temperature measurements.

NOAA D-G, operational meteorological spacecraft, are planned to meet the need for quantitative sea surface temperature measurements. These spacecraft will have an Advanced Very High Resolution Radiometer with five channels as follows: 550-680 nm, 720-1100 nm, 3.55-3.93 μm, 10.3-11.3 μm, 11.5-12.5 μm. Two thermal infrared channels in the 10-13 μm water vapor window are designed to correct the measurements for absorption and re-emission by the atmosphere. The 850 km altitude orbit of the AVHRR will provide daily global coverage at 4 km resolution and local area (direct acquisition) coverage at 1 km resolution. Orbital configurations between NOSS and NOAA-n have not been decided, but coincident quantitative chlorophyll, sediment and temperature information is not anticipated.

O 2 INVITED PAPER

THE NOSS SCATTEROMETER: A MICROWAVE MEASUREMENT OF OCEAN WIND VECTOR

W. Linwood Jones and William L. Grantham, (NASA Langley Research Center, Hampton, Virginia 23665)
Victor E. Delnore (Kentron Corp., Hampton, Virginia 23665)

During the mid 1980's, the joint NASA/NOAA/DOD National Oceanic Satellite System (NOSS) will be launched to provide limited operational oceanographic measurements. This paper presents an overview of the microwave scatterometer on NOSS and will address the following topics:

1. Brief discussion of parameters observed.
2. NOSS Scatterometer heritage.
3. Hardware Description
4. Post-launch validation plans.

O 3 INVITED PAPER

SATELLITE ALTIMETRY APPLICATIONS TO OCEANOGRAPHY

James G. Marsh
Robert E. Cheney (Geodynamics Branch, Goddard Space Flight Center, Greenbelt, MD 20771)

Satellite-borne radar altimeters have provided the first direct observations of sea surface topography and demonstrated the potential of satellite altimetry in the study of ocean circulation. The most recent altimeter flown on Seasat in 1978 attained a precision of 5-8 cm., a four-fold improvement over the previous GEOS-3 instrument. In order to adequately analyze the altimeter data for dynamic ocean processes, precision orbit and geoid data are required. Recent orbit computations based upon laser and Unified S-Band tracking data and using state-of-the-art models of the earth's gravity field, atmospheric drag, and solar radiation pressure have yielded height errors on the order of one meter for these spacecraft. This height error tends to be long wavelength with the dominant period equal to the period of the orbit. Over distances of a few thousand kilometers, orbit error appears as a tilt and bias in the sea surface topography. Using a combination of the altimeter data and precision orbital information, mean sea surfaces have been computed. The resolution of the surfaces ranges from 0.25° in the N.W. Atlantic to 1° in some of the southern ocean areas, and the accuracy in most areas is approximately 30 to 40 cm. Because these mean surfaces closely approximate the actual geoid, they can be used to detect transient ocean features in regions where high resolution gravimetric information is not available.

O 4

ON DETERMINATION OF THE OPTICAL PROPERTIES OF SEA WATER FROM LANDSAT DATA

Sasithorn Aranuvachapun (Department of Oceanography, University of British Columbia, 6270 University Boulevard, Vancouver, B.C., Canada. V6T 1W5)
(Sponsor: Natural Sciences and Engineering Research Council of Canada)

LANDSAT radiance data are used to estimate the diffuse reflectance $L_d(\lambda)$ due to the optical properties of sea water in the surface layer. The radiance $L_w(\lambda)$ is then used to calculate upwelling, downwelling irradiances and the scattering function of the sea water. The calculation assumes that the upwelling irradiance is attributed to back scattering, reflection and attenuation of both the sea water and the small suspended particles at very low concentration. Similarly, the downwelling irradiance results from forward scattering transmittance and extinction processes. The model is also extended to approximate scattering, attenuation coefficients and penetration depth.

0 5

ATMOSPHERIC CORRECTIONS TO SATELLITE-MEASURED BRIGHTNESS TEMPERATURES USING DUAL-WINDOW RADIOMETER DATA

E.P. McClain (National Environmental Satellite Service, NOAA, Washington, D.C. 20233)
C.C. Walton (National Environmental Satellite Service, NOAA, Washington, D.C. 20233)

Thermal-infrared measurements in two atmospheric windows (3.55-3.93μm and 10.5-11.5μm) from the Advanced Very High Resolution Radiometer (AVHRR) on NOAA-6, NOAA's polar orbiting environmental operational satellite, have been used to obtain geophysical verification of a proposed method for making atmospheric corrections to the satellite-measured brightness temperatures for sea surface temperature estimates.

Atmospheric corrections were simulated by calculating the 3.8 and 11μm brightness temperatures from atmospheric transmittance models using a geographically and seasonally diverse sample of atmospheric temperature and water vapor profiles from radiosonde observations. An excellent linear relationship was found between the brightness temperature difference, $T_{3.8}-T_{11}$, and the atmospheric correction ($T_{sfc}-T_{3.8}$ or $T_{sfc}-T_{11}$). Atmospheric corrections and brightness temperature differences obtained from a global sample of AVHRR dual-window measurements and independent sea surface temperature observations were found to be similarly related, the two independent sets of regression lines having virtually identical slopes and intercepts.

0 6

INTERANNUAL VARIABILITY OF THE SOMALI CURRENT SYSTEM DURING THE SUMMER MONSOON

Otis B. Brown (Rosenstiel School of Marine and Atmospheric Science, Miami, FL 33149)
Robert H. Evans

Spin-up and mature phases of the Somali Current system have been monitored during the summer monsoons of 1975-1979 utilizing ship and satellite derived sea surface temperature (SST) maps. The most striking feature of the interannual variability is the presence of a strong crescent-shaped frontal feature at ∿5°N latitude during 1976 and 1979, but not in other years. In situ current measurements show this front to be associated with southern separation of the Somali Current. In all years the strong front feature at ∿10°N latitude traditionally associated with Somali Current separation and the "Great Whirl" is observed. Mean frontal location maps by year are presented with a brief discussion of weekly to monthly temporal variability.

0 7

THE SPACE-TIME STRUCTURE OF THE SHELF/SLOPE WATER BOUNDARY

Peter C. Smith, Bedford Institute of Oceanography Dartmouth, Nova Scotia, Canada, B2Y 4A2

Sea surface temperature data, obtained from satellite infrared imagery (VHRR) and ships of opportunity and embodied in weekly maps ("Experimental Ocean Frontal Analysis" or EOFA charts) are used to define the space-time structure of the shelf/slope water boundary (SSB) off Nova Scotia. Frontal positions are digitized on a 10X10 km grid and analyzed according to methods described by Halliwell and Mooers, (JGR,84,p.7707).

In the region from 60° to 65°W, the surface expression of the SSB lies 120± 70km off the shelf break. The western end of this region is a preferred site for the formation of warm-core anticyclonic eddies by the Gulf Stream, which produce fluctuations in the SSB position. The space-time autocorrelation indicates temporal and spatial scales (4 wk,130km) and westward propagation at 0.04ms^{-1}, consistent with the disturbances caused by the eddy field. Empirical or thogonal function analysis reveals that 78% of the SSB variance is contained in the first four modes.

Low-frequency currents, temperature and salinity from a two-year mooring program at the shelf break south of Halifax (42-43°N,63-64°W) are discussed in light of the SSB data. The formation of a Gulf Stream eddy produces 140km wave like disturbances in the SSB and distinct 20d oscillations in the alongshore current component at the shelf break. Accompanying the event is a large-scale onshore displacement of the SSB, which is detected in the amplitude of the dominant empirical mode. On a seasonal basis, this mode is correlated with the alongshore current variance in the 10-30d spectral band

0 8

SEA SURFACE TEMPERATURE FIELDS FROM SEASAT SMMR MEASUREMENTS

C. Gautier (Space Science and Engineering Center 1225 W. Dayton Street, Madison, WI 53706)
S. Massé

Fields of SMMR brightness temperatures at various frequencies are statistically studied so as to derive information about their content. This statistical analysis is applied, in particular, to sea surface temperature (SST) retrievals with special emphasis on regions of strong SST gradients (Gulf Stream). Regions of strong SST gradients are often covered with cloud bands oriented perpendicular to the gradient, making the SST retrievals more difficult. However, our statistical analysis shows that the brightness temperature fields contain the information which we need if we are to differentiate the cloud and water vapor gradients from SST gradients. Results illustrating this statement will be shown.

Comparisons will also be shown between SST obtained from SMMR data using different algorithms, IR data for the same area, and ship measurements, when available. These comparisons will be discussed from a perspective of the performances of the various algorithms.

0 9

ON THE RELATIONSHIP BETWEEN NORMALIZED RADAR BACKSCATTERING CROSS SECTION AT MICROWAVE FREQUENCIES AND THE WINDS AND WIND STRESS OVER THE OCEAN.

W. J. Pierson Inst. Marine and Atmos. Sci. City College, N.Y., N.Y. 10031

The power law relationship between the NRCS and (1) the wind speed at 19.5 m, (2) the total wind stress and (3) that part of the wind stress that supports high frequency waves is investigated. Scatter plots of the 19.5 m wind are shown to have distinctive biasses as a function of the meteorologically determined wind if either (2) or (3) above should have been used instead of the wind speed in the power law relationship. It is found that (3) is probably the correct relationship and that the 19.5 m wind can be more accurately predicted from the SASS measurements by removing the bias observed in the scatter plots.

0 10

THE SEASAT-A SATELLITE SCATTEROMETER OCEANIC WIND MEASUREMENT

W. Linwood Jones,
E. M. Bracalente
L. C. Schroeder, (NASA Langley Research Center, Hampton, Virginia 23665)
Jon L. Sweet,
John L. Mitchell, (Kentron Corp., Hampton, Virginia 23665)

Ocean surface wind fields measured by the SeaSat-A Satellite Scatterometer are presented. Also comparison diagrams are shown which illustrate the accuracy of scatterometer inferred winds compared to in situ measurements.

0 11

EXAMINATION OF GEOID MODELS FOR ALTIMETRIC DETECTION OF MESOSCALE OCEAN FEATURES

Robert E. Cheney
James G. Marsh (Geodynamics Branch, Goddard Space Flight Center, Greenbelt, MD 20771)

Determination of ocean circulation from satellite altimetry involves removal of the gravitational signal using geoid models. We have examined several geoid models with regard to the study of mesoscale ocean circulation in different regions of the world. The models include gravimetric geoids of varying resolution and altimetric geoids (mean sea surfaces) for selected regions using both the GEOS-3 and Seasat data sets. Seasat altimeter profiles were used as the input data in each case. In the western North Atlantic, where all models can be compared, the best results are obtained using the detailed gravimetric geoid model. Features such as the Gulf Stream and rings formed by the Stream can be clearly detected. The apparent dynamic height accuracies attained in this area permit quantitative analyses of phenomena such as variability of the Gulf Stream transport. In other areas such as the Southern Ocean and western North Pacific, where no detailed gravimetric geoids exist, altimetrically-derived surfaces may provide an effective means of detecting transient rings and eddies.

0 12

GULF STREAM VARIABILITY DERIVED FROM SEASAT ALTIMETRY DATA

H. Michael Byrne
Patricia E. Pullen (both at: National Oceanic and Atmospheric Administration/Pacific Marine Environmental Laboratory, Seattle, Washington 98105)

Seasat Altimetry data in the North Atlantic region was investigated for the repeat orbit period, September 11 to October 9, 1978. Analysis of sequential passes along the same ground track was used to determine the magnitude and direction of movement of the Gulf Stream for each three day period. Changes in the horizontal position of the current along the altimeter track were found on the order of 20km between repeated orbits. In the region south and west of Bermuda centered at 25°N, sequential pass analysis indicated variations in surface topography with scales of approximately 325-350 km.

A comparison was made between altimetry data for rev 1310 and coincident infrared data taken from the NOAA-5 polar orbiting satellite. The position of the northern boundary of the Gulf Stream determined by the surface temperature gradients in the infrared data agreed well with the position determined using the altimetry data.

0 13 INVITED PAPER

NATIONAL OCEANIC SATELLITE SYSTEM (NOSS)

V. E. Noble, DoD Associate NOSS Project Scientist, Code 4006, Naval Research Laboratory, Washington, D. C. 20375

Previous experiments (SKYLAB, GEOS, SEASAT, NIMBUS-7) have demonstrated the feasibility of making oceanographic measurements from satellites. Requirements for measurements of oceanographic parameters are similar for both military and civilian operational applications. NOSS is being planned as a limited operational demonstration to serve common goals. The baseline sensors (Large Aperture Multifrequency Microwave Radiometer, Radar Altimeter, Scatterometer, and modified Coastal Zone Color Scanner) are evolutionary improvements of previous instruments. 25% of the system capability (sensor, data system) is being reserved for research applications. An essential feature of NOSS is data delivery through TDRSS to a Primary Processing Facility (PPF) for near-real-time derivation of earth-located oceanic parameters, with "best-pipe" relay to the primary user facilities: DOD/FNOC/SPC, DOC/NOAA/NESS. Operational, Developmental, and Research users (government agencies, commerce/industry, and academic/institutional) will obtain data products from the primary user facilities. System definition studies will be executed in CY 1980. A five-year demonstration period is planned (1986-91). NOSS is a tri-agency (DOC/NOAA, DOD, NASA) program.

Pre-Pleistocene Climates

Metropolitan Centre
Thursday A.M.
Wolfgang Berger (Scripps Institute of Oceanography), and *John C. Crowell* (Univ. of California), Presiding

O 14 INVITED PAPER

VALUE OF PALEOCLIMATE TO CLIMATE PREDICTION

John Imbrie (Dept. of Geological Sci., Brown Univ., Providence, RI 02912)

O 15 INVITED PAPER

PALEOCLIMATIC MODELING

W.L. Gates (Climatic Research Institute, Oregon State University, Corvallis, OR 97331)

The problem of reconstructing pre-Pleistocene climates with the aid of models is primarily dependent upon the ability to assemble the geographical and geophysical data required as boundary conditions. For that part of the Cenozoic era during which the distribution of continents, oceans and mountains are similar to the present, it is possible to use atmospheric models to simulate the global climate in response to a specified distribution of ocean surface temperature and ice sheet topography. For most of the Mesozoic and all of the Paleozoic eras, the use of both atmospheric and oceanic models is required to determine the climate as a function of the estimated continental and oceanic paleography. From such integrations extending over a few years' time, wind-driven surface ocean currents and temperature of surface waters can be estimated; temperature simulation of the deeper ocean (and hence the surface temperature in long-term equilibrium) requires integration over several centuries. The geography of the major ice sheets and the character of the land surface, however, are specified beforehand. In a comprehensive climate model these features would be simulated along with the atmosphere and ocean and interactive components of the total climate system.

By assembling a series of quasi-equilibrium climates at selected times in the past, the evolution of global climate may be inferred. The massive calculations for such a program of paleoclimate systhesis, however, has prompted the search for simplfied models which directly address the time-dependent interactions of the atmosphere-ocean-ice-biomass climate system over long periods of time. The major difficulty of such models is the satisfactory representation of the climate's nonlinearity, and their generally low resolution has restricted their use in studies of modern climate. When properly calibrated, however, simplified climate models should prove useful with the relatively coarse paleoclilmatic data, and serve at least to sketch out the broader features of geological climate.

O 16 INVITED PAPER

ANALYSIS OF TRANSIENT EVENTS IN OCEAN HISTORY

W. H. Berger (Scripps Instituion of Oceanography, Univ. of Calif., San Diego, La Jolla, CA 92093)

The deep-sea record shows long-term trends, low frequency fluctuations (which are sometimes referred to as cycles), and step--like transitions from one climatic state to another. A prime example is the recent deglaciation event. These steps are natural experiments which yield clues to the behavior of the "exogenic system" whose output is the record. Event analysis considers to what degree a step is forced from without, and to what degree it represents instability within. Events which are part of a trend are prime candidates for discovering positive feedback mechanisms.

One class of events may be associated with the collapse of transient reservoirs of accumulated solar energy. Several of the major events (Cretaceous termination, Eocene termination, mid-Miocene event, Messinian event, 3 million-year event) may belong in this class.

O 17 INVITED PAPER

SOLAR, ASTRONOMICAL, AND ATMOSPHERIC EFFECTS ON CLIMATE

James B. Pollack (NASA-Ames Research Center, Moffett Field, CA 94035)

O 18 INVITED PAPER

VARIABILITY OF GLOBAL CLIMATE DURING THE CENOZOIC AS INDICATED BY OXYGEN ISOTOPIC ANALYSIS OF DEEP-SEA SEDIMENTS

T.C. Moore, Jr., N.G. Pisias(Univ. of RI, Kingston, RI 02881), and CENOP Participants

Late Pleistocene climatic change is characterized by large fluctuations in the northern hemisphere ice sheets. fractionation of O-isotopes by processes that produce ice sheets result in large amplitude variations in the isotopic composition of calcareous fossils. Studies of late Pleistocene sediments indicate that the variations in climate are characterized by psuedo-periodic fluctuations, with the dominant 100,000 yr. cycle. Superimposed on this cycle are periodic components associated with orbital variations of the earth. Studies of the early Pleistocene isotopic data shows that the total variability of the signal has decreased, and that the dominant 100,000 yr. cycle found in the late Pleistocene is absent.

Of importance to the Cenozoic studies to climate is the question, how has the variability of climate changed with time and how has its frequncy components changed? Have variations in earth's orbits always played a role in forcing climate change and how has the response to this forcing evolved?

Although detailed analysis of deep sea sediments are not yet available to allow studies of the frequency domain character of Cenozoic climate and oceanographic change, enough isotopic data from benthic fossils are available to give a picture of variability in deep ocean conditions. A compilation of isotopic analyses indicates that 3 periods during the Cenozoic are marked by large variations: the Middle Eocene, Middle Miocene, and Pleistocene. Starting in the Middle Miocene the degree of variability in the deep Atlantic is greater than that of the Pacific. The degree of difference in variability between the two oceans appears to be greatest at intermediate depths.

O 19 INVITED PAPER

PHANEROZOIC HISTORY: TWO GREENHOUSE CYCLES

Alfred G. Fischer (Dept. of Geological and Geophysical Sci., Princeton, U.,Princeton, NJ 08540)

O 20 INVITED PAPER

SEASONALITY AND THE STRUCTURE OF THE BIOSPHERE

J.W. Valentine (Department of Geological Sci. University of California, Santa Barbara, CA 93106)

Seasonality is an important biological parameter. High seasonality in density-independent environmental parameters requires broad adaptive responses. Even more significant is seasonality in density-dependent resource supplies, which plays a basic role in constraining the adaptive strategies of organisms. This is particularly true where primary productivity is highly seasonal, for species must then develop strategies to cope with a boom-and-bust economy in trophic resources. Unpredictability in environmental fluctuations can add to the seasonal effects but even perfectly predictable seasonality creates an evolutionary response in life histories as shown by Boyce.

In the sea today, latitudinal gradients in species richness parallel the gradients in seasonality of solar radiation. This species gradient is modified, and further trends are created, by trends in seasonality of nutrient supply that are chiefly related to effects of continentality. Similar effects are found on land but the modifying trends have other immediate causes. These trends and gradients are believed to result from variation in life history strategies based on responses primarily to patterns of seasonality of trophic resources. Similar species patterns are known from the fossil record; they have great potential for the interpretation of past patterns of seasonality.

O 21 INVITED PAPER

STABLE ISOTOPES IN CLIMATIC RECONSTRUCTION

Samuel M. Savin (Dept. of Geol. Sci., Case Western Reserve Univ., Cleveland, OH 44106)

Variations in the relative abundances of oxygen, hydrogen, and carbon isotopes can provide information on past climates. The best known of the isotope paleoclimatic methods is based on the temperature-dependent O- isotopic fractionation between Ca, CO_3 and water. Analyses of deep sea formaniferal carbonates have yielded a detailed record of glacial-interglacial fluctuations during Pleistocene time. Isotopic studies of tertiary and late cretaceous formanifera have clarified the main features of marine climate in high and low latitudes during the past 100 m.y. Major Antarctic glaciation developed rapidly ca. 15 mybp (middle Miocene), associated with a decoupling of high and low latitude temperatures. Only relatively modest cooling occurred during Tertiary-Cretaceous boundary times. The general temperature trend during the past 100 m.y. has been downward, but it has been neither smooth nor monitonic.

The number of well preserved carbonate samples suitable for precise isotopic temperature analysis rapidly diminishes with increasing age. It is unlikely that isotopic methods will yield information about pre-Cretaceous climates in the detail achieved for younger times. However, climatic information of far lower accuracy and precision can still be extremely useful. O- and H- isotopic studies of cherts have provided climatic information and will continue to do so in the future. Cherts are most likely to provide useful temperature limits for early pre-Cambrian times.

Other isotopic systems have shown promise for yielding climatic information of varying quality. These include: O- isotopes in marine opal; O- and H- isotopes in groundwaters; O- and H- isotopes in paleosols; O- isotopes in subglacially precipitated calcites; C-isotopes in marine organic matter; and O- and H- isotopes in terrestrial matter.

O 22 INVITED PAPER

CLIMATIC ACME EVENTS ON SEA AND LAND

Bilal U. Haq (Woods Hole Oceangraphic Inst., Woods Hole, MA 02543)

Major climatic fluctuations in the geologic past have left retrievable records in the sediments from which the paleoclimate can be reconstructed. One such record is the widespread latitudinal domination of certain floral and faunal elements during times of peak climatic change. Climatic acme events are characterized by major latitudinal shifts of assemblages during the climatic fluctuations. These temporal migrationary patterns have become a reliable tool for paleoclimatic interpretations.

Recognition of acme events involves delineation of cycles of latitudinal migration of assemblages in stratigraphic sequences over wide geographic areas. In the Cenozoic, for example, planktonic foraminifera and calcareous nannoplankton show numerous major shifts through latitudes in the Atlantic Ocean. Amongst the more pronounced are the shift of low latitude assemblages into high latitude in late Paleocene - early Eocene, and the restriction of low latitude assemblages to a narrow equatorial zone and dominance of cosmopolitan taxa elsewhere, in the late Eocene - early Oligocene. These and other changes in the paleobiogeography have been successfully used to reconstruct the Cenozoic paleoclimate of the Atlantic.

More practically, acme events can be used to refine the biostratigraphic framework of higher latitudes where marker species are often absent, providing more precise correlations between low and high latitudes. Assuming that times of maximum environmental change

are contemporaneous over wide geographic areas, the migrationary maxima can be considered to define synchronous horizons. The precision with which these horizons approximate synchronous surfaces depends on our ability to unambiguously identify maximum latitudinal migrations and on the complexity of the cycles and the method used to delineate them.

O 23 INVITED PAPER

OCEAN GATEWAYS IN CLIMATE CHANGES

W. A. Berggren (Dept. of Geology and Geophysics, Woods Hole Oceanographic Inst., Woods Hole, MA 02543, and Dept. of Geology, Brown University, Providence, RI 02912)

The ocean represents one of the most important components of the global climatic system. With a specific heat per unit mass of four times that of air, water (i.e. the ocean) has a thermal capacity over 100 times that of the atmosphere. At the present time the energy imbalance from incoming solar radiation between the summer and winter hemispheres and from low to high latitudes. There is little variation at present in temperature and energy transport with the ocean acting as an effective buffer for such energy changes.

The question may be asked: has the ocean played the same role in the meridional transport of energy over the past 200 my. The answer is unequivocally no. Present continent-ocean geometry is the result of a long (200 my) history of changing spatial configurations. The role of gateways (and barriers) is fundamental for recreating the scenario of past circulation histories (and their concomitant effect on paleoclimate). We are at but an early stage in understanding this history but we can outline a tentative scenario. In general terms Mesozoic circulation is latitudinal, Cenozoic circulation longitudinal (meridional). The role of gateways (and barriers) in climatic change is believed to have been rather minor during the Mesozoic; in the Cenozoic the role of gateways has become more pronounced and has probably played a fundamental role in the enhanced climatic deterioration which has taken place over the past 50 my.

Pre-Pleistocene Climates

Metropolitan Centre
Thursday P.M.
Wolfgang Berger (Scripps Institute of Oceanography), and *John C. Crowell* (Univ. of California), Presiding

O 24 INVITED PAPER

THE ARCTIC OCEAN AND POST-JURASSIC PALEOCLIMATOLOGY

David L. Clark (Department of Geology and Geophysics, University of Wisconsin, Madison, 53706)
(Sponsor: Thomas M. Usselman)

An ice-covered Arctic Ocean, such as that of the present, affects world climates differently than would an ice-free Arctic Ocean. Yearly net heat loss in the modern Arctic is an important factor in driving atmospheric circulation. Also, changes in extent of Arctic ice-cover correlate with shifts in major storm tracks and lower latitude precipitation distribution. Conversely, an ice-free Arctic Ocean would severely change the earth's heat balance and alter lower latitude weather patterns. It follows that the role played by the Arctic Ocean in paleoclimatology can be judged by the history of its ice-cover.

Conditions of the pre-Cretaceous Arctic Ocean are unknown but during the late Cretaceous and Early Cenozoic there was no ice-cover. Periods of high primary productivity and intensified upwelling prevailed and a deep-sea Pacific connection existed. An open Arctic contributed to a limited world thermal gradient. The ice-cover formed first during the Middle Cenozoic resulting in an increased thermal gradient and altered atmospheric circulation. For a minimum of 5 m. y. the Arctic Ocean ice-cover and its role in world climates have been relatively stable.

O 25 INVITED PAPER

ANCIENT SOILS AND ANCIENT CLIMATES

Franklyn B. Van Houten (Dept. of Geological and Geophysical Sci. Princeton U. Princeton, NJ 08544)

Global distribution of recent laterites throughout the intertropical climate belt of easterly winds (25N-25S latitudes) suggests that most of the ancient ones, toether with commonly associated oolitic iron deposits, reflect a warm-humid (seasonally variable) climate. Because widespread lateritization requires prolonged weathering with little erosion ancient laterites were favored by locations and by episodes of relative stability.

Plotted on continental drift reconstructions, most paleolaterites lie 1) within the ancient intertropical humid climate zone, 2) on stable cratonic blocks, especially in their interiors or along trailing "east-coast" maritime margins, and 3) in a late or post-orogenic framework. During late Devonian-carboniferous and later Permian-early Triassic dispersal of Asiatic continental fragments and during the opening of Tethys and the Atlantic basin (early to mid Jurassic, early Cretaceous, late Cretaceous, and Eocene) laterites and sedimentary iron deposits developed as far north as 60-70. In Eocene time laterites were also widespread on northward-drifting Australia as far south as 45.

Calcrete and calcareous red soils that reflect warm, seasonally dry climate, can develop in spans of several thousand years. Most of the paleocalcretes were preserved in intermittently aggrading nonmarine sequences flanking orographic belts that plot within 40N and S latitudes on continental drift reconstructions.

Development of early Paleozoic to late Precambrian (600-2300 M.Y.) laterite, calcrete, and sedimentary iron formations implies that vascular land plants were not necessary for producing aluminous and ferruginous regoliths, and that an oxidizing humid to semiarid climatic regime prevailed. The few known paleosols older than 2300 M.Y. (2200 M.Y. in South Africa) are not laterites, but they provide no substantial evidence for an oxygen-deficient atmosphere.

O 26 INVITED PAPER

CLIMATIC SIGNIFICANCE OF LAKE AND EVAPORITE DEPOSITS

Hans P. Eugster (Johns Hopkins University, Baltimore, MD 21218)

Lake deposits are sensitive indicators of paleoclimatic changes. Particularly useful are glacial and saline lakes. The latter are not related to latitude and form when evaporation exceeds inflow, recording a complex balance between climate, hydrology and tectonics. Changes in depositional conditions are indicated by lithologies, sedimentary structures, and mineralogy and often result in transgressive-regressive cycles. Local differences may override general climatic conditions. This is illustrated by a reinterpretation of the Eocene Green River climate. A climate exemplified by Holocene SE California is preferred to that of the Gulf Coast States (Bradley, 1963).

Climatic interpretation of marine evaporites depends on their special hydrologic requirements. Three stages are distinguished, with each stage dominated in turn by Ca-sulfates, halite and K-Mg salts. The bulk of marine evaporites belong to stage 1. A sabkha setting is a good depositional model. Sea water can be concentrated up to 10 fold. Thick halite deposits may accululate in a deep, stratified basin such as that suggested by Harvie et al. (1980) with evaporation up to 20 fold. For the last stage we prefer the playa model of Valyashko (1972) which requires relative humidities of less than 60-45%. Final products are hygroscopic and it is not easy to reconcile the requirements for extreme aridity with a marine setting (Kinsman, 1976; Hardie, 1979).

O 27 INVITED PAPER

NON STEADY-STATE OCEAN CHEMISTRY: CARBON CYCLING AND CHANGES IN GLOBAL CLIMATE

Michael A. Arthur (U.S. Geological Survey, Denver, Co. 80228)

The cycling of biogeochemical elements through the ocean has apparently not been in a steady state over the last 120 m.y. Substantial chemical changes in sea water and in the rate and direction of cycling of carbon, for example, are evidenced by significant changes in the rates of accumulation of carbonates and organic carbon in the ocean basins, by times of deposition of peculiarly wide spread marine chemical facies such as phosphorites, and by changes in the carbon isotopic composition of pelagic calcareous microfossils. There seems to be a direct association of changes in global climate with the ocean chemical changes.

Eustatic sea level changes may be the first-order control on ocean chemistry and climate, but other "events" appear to trigger rapid changes in ocean chemistry which, in turn, lead to climate change. These are essentially instantaneous (1-3 m.y.) events, superimposed on longer periods of ocean chemical trends and climate changes as related to paleopositions of continents, eustatic sea level, and possibly rates of tectonic uplift and volcanism. Two examples are the relatively sudden isolation of the northern South Atlantic in Late Aptian time and of the remanent Tethys ocean in Late Miocene (Messinian) time. The rapid deposition of evaporites in these low latitude basins probably lead to pronounced depletions of certain chemical elements (e.g., Na, Cl, Ca, S, C, and nutrients) in the remainder of the world oceans. The Aptian episode led to climatic warming because of an atmospheric Co_2 excess resulting from the transfer of major amounts of calcium carbonate and sulfate to evaporite facies, while the Messinian events apparently caused further global cooling in an already glacial world, perhaps because the resultant less saline ocean enhanced the production of sea ice at high latitudes.

O 28 INVITED PAPER

TERTIARY MARINE AND NONMARINE CLIMATIC TRENDS

Wolfe, J.A., (U.S. Geological Survey, MS 95, 345 Middlefield Road, Menlo Park, CA 94025).
Poore, R. Z.

Planktic microfossil migration patterns and 18O analyses from the Paleocene and Eocene of the Atlantic Basin indicate pronounced cooling events and the end of the early Paleocene, near the early-middle Eocene boundary, at the beginning of the late Eocene, and probably at the end of the Eocene. These cooling events were separated by warm intervals that are less well-dated. Biostratigraphic correlations by means of planktic organisms to the Mississippi embayment sequence indicate an isochronous series of temperature fluctuations as evidenced by changes in the physiognomy of land plant assemblages. Cooling trends during the Paleocene and Eocene are apparently isochronous with regressions in the Mississippi embayment sequence. Physiognomic analyses also indicate a prounced drying trend during the Paleocene and Eocene.

Warm intervals in the Eocene were characterized by major poleward expansion of tropical planktic assemblages and tropical forests, low mean annual range of temperature (high equability), and a low altitudinal temperature gradient in extra-tropical regions.

Temperature fluctuations during the Neogene were of much lesser magnitude than those during the Paleocene and Eocene; Neogene warm intervals were only moderately warmer than present. Latitudinal temperature gradients increased during the Neogene; by the end of the middle Miocene, oceanic circulation patterns closely resembled those of the present. Although continental climates were less equable during the Neogene than during the Eocene, mean annual range of temperature has significantly decreased during the Neogene.

O 29 INVITED PAPER

THE TERMINAL CRETACEOUS EXTINCTION EVENT

Thierstein, Hans R. (Scripps Inst. of Oceanography, Univ. of Calif., San Diego, La Jolla, CA 92093)

Paleontological and geochemical evdience indicates that terminal Cretaceous extinctions were triggered by an unannounced, sudden catastrophe with possibly major climatic consequences. High resolution stratigraphy in continuous marine sedimentary sections, along with recent refinements in biostratigraphic, paleomagnetic and radiometric dating techniques, suggest that the event occurred in a

time-span of less than a few thousand years. The evolutionary consequences of the catastrophe appear to have been more severe among the holopelagic plankton and the large vertebrates, although exact correlation of the event between marine and terrestrial extinctions is controversial. Quantitative evolutionary and biogeographic studies on oceanic phytoplankton remains indicate that pelagic environments were stable over the last few million years of Cretaceous time. Stable isotopic changes in planktonic carbonate shells suggest a drastic salinity drop or temperature increase of oceanic surface waters, and a major shift in the global distribution and pathways of carbon at extinction time, followed by a period of evolutionary and environmental instability. This evidence and the survival and the blooms of salinity-tolerant neritic phytoplankton taxa immediately after extinction time support the Arctic injection model. Injection of cool, low-salinity waters onto the surface of the world ocean would result from the reconnection with the world ocean of a temporarily isolated Arctic basin. Anomalously high iridium concentrations measured in boundary clays straddling the extinction event in several sections, however, may be interpreted as evidence for a large meteorite impact, resulting in the temporary shielding of sunlight by dust. This, in turn, would have strongly affected photosynthesis in plants--the base of the terrestrial and marine food chains.

O 30 INVITED PAPER

THE JURASSIC CLIMATE

A. Hallam (University of Birmingham, Birmingham, England)

Initially, climatic criteria in the Jurassic stratigraphic record are discussed. There is no convincing evidence of tillites, and evaporites and coals are considered to be more reliable than laterites and limestones. The wide distribution of reef corals, ferns, non marine reptiles and lungfish, and the large latitudinal range of many marine invertebrate genera, together with the absence of tillites, point strongly to the existence of an equable climate. Oxygen isotope data from belemnites are considered to be untrustworthy.

Climatic changes in space and time are then discussed. There is evidence of a western arid and two eastern humid belts in the supercontinents of Laurasia and Gondwana, with a slight increase in aridity through the period. No significant change of global temperatures through time is discernible, except perhaps a slight tendency towards warming, as inferred from plant distributions in Eurasia. The Fischer and Arthur model of cyclic alternations of polytaxic and oligotaxic episodes is thought not to apply to the Jurassic.

O 31 INVITED PAPER

GLOBAL TECTONICS AND PALEOCLIMATES

Warren Hamilton, (U.S. Geological Survey, Denver, Colorado, 80225)

Paleontologic, lithologic, and paleomagnetic indicators show that climatic zones have been expanded poleward, relative to present zones, during most of geologic time, and compressed equatorward during subordinate cold periods, and that equatorial climates have varied little. Each landmass received a complex paleoclimatic record as it moved through waxing and waning zones.

Little is yet known, however, about circulation of ancient ocean and atmosphere, because distributions of land and sea are poorly constrained. Rifting and collision have operated throughout at least post-Archean time, so uncertainties in positions of landmasses multiply with age. There are major problems even for Cretaceous configurations. Great changes in oceanic circulation and world climate accompanied such minor Cenozoic events as the raising of the central American connection; similar events are yet invisible in most of the pre-Cenozoic record. Valiant published reconstructions are valid at best only for subassemblies of unknown relationship to other subassemblies. Migrations of components of collision aggregates must have been complex, and continents must have undergone great internal deformations, but few details are known. Progress requires integration of paleolatitudinal evidence for plate motions with paleobiogeographic, stratigraphic, petrologic, and tectonic evidence for plate connections and interactions.

O 32 INVITED PAPER

CONTINENTAL GLACIATION THROUGH GEOLOGICAL TIME

John C. Crowell (Dept. of Geological Sciences, University of California, Santa Barbara, CA)

The record of continental glaciation, contained primarily in strata revealing a glacial imprint, provides clues to times of climatic refrigeration on Earth extending back as far as 2.5 b.y. The oldest established ice age (Huronian) occurred in now southern Canada, primarily between 2.2 and 2.4 b.y. ago, and was suceeded by at least 1250 m.y. without widespread glaciation. Beginning about 950 m.y. ago, several ice ages ensued: three apparent culminations in the late Proterozoic, one near the Ordivician-Silurian transition, a possible ice age in mid-Devonian times, and a strong ice age lasting about 90 m.y. in the late Paleozoic. From mid-Permian time (about 240 m.y. ago) until Early Miocene (about 25 m.y. ago) no continental ice sheets have been documented. We are now living in the Late Cenozoic Ice Age, but within and interglacial stage.

Data available indicate that the causes of these climatic extremes are rooted in terrestrial changes and not in changes in the heat flux from the sun. The main cause of climatic changes on Earth is crustal mobility, involving the movement and rearrangement and freeboard of continents. Change in world-average sea level, perhaps resulting from world-average changes in the rate of seafloor spreading is important. When continents are sited in polar regions, they influence the arrangement of ocean and air currents. Complex feedbacks in turn, including albedo changes, bring about climate change.

O 33 INVITED PAPER

PALEOZOIC DATA FOR THE CLIMATOLOGIST'S CONSIDERATION

A. Boucot (Dept. of Geology, OR St.U.,-Corvallis, OR 97331) J. Gray (Dept. of Biology, U. of OR, Eugene, OR 97403)
(Sponsor: Thomas M. Usselman)

Global biogeography based chiefly on shallow-marine benthos, (affords insights into changing oceanic circulation patterns) and carbonate-noncarbonate rock distribution indicating regions of warm and cool climate, respectively. Secondary data are the distribution of marine evaporites, suggesting arid regions and redbeds indicative of warm regions. Paleosols (including kaolinitic clays, bauxites, manganese deposits, calcretes) help identify warm areas, and some forms of seasonality. Oceanic regressions and transgressions onto continents indicate the percent of surface covered by water through time. Coal distribution (Late Devonian through Permian) indicates high humidity regions. Glacial deposits demonstrate two intervals of highest climatic gradient (latest Ordovician, Pennsylvanian-Early Permian). Biogeographic and benthic animal community information show intervals of moderate to low global climatic gradient. Growth morphology, growth habits, and anatomy of plant organs can support climatic inferences related to humidity and seasonality from Devonian onwards. The apparent advent of higher land plants in later Ordovician times suggests something about soil formation, O_2 and CO_2 levels. Location of mountain belt roots provide data about mountain caused peturbations. Paleowind data is available for some late Paleozoic locations. Sedimentary phosphorites provide data concerning potential upwelling regions adjacent to continents.

Although the paleogeography is fairly well known for the continents their relative positions are speculative. Inadequacy of data for each time interval is partially compensated for an internally consistent synthesis for the entire Paleozoic.

Ocean Dynamics of the Outer Grand Banks

Harbour B
Thursday P.M.
Paul E. LaViolette (NORDA) and *James L. Mueller* (NASA-Goddard), Presiding

O 34 INVITED PAPER

THE NORTH ATLANTIC CURRENT CANNOT BE A BRANCH OF THE GULF STREAM

L. V. Worthington (Woods Hole Oceanographic Institution, Woods Hole, Mass. 02543)

It is usually thought that the North Atlantic Current east of the Grand Banks is a branch of the Gulf Stream. I demonstrate that the flux of oxygen in the pycnocline of the North Atlantic Current exceeds that in the Gulf Stream pycnocline by 13.64×10^6 & s^{-1}. The only source that can enrich the Gulf Stream is the high-oxygen "Mixed Water"; however, the amount of oxygen in this water cannot sustain this oxygen drain for more than 30 days.

If the North Atlantic Current is part of a single, ocean-wide gyre, its waters must return to low latitudes across the central and eastern North Atlantic; I show that this requires an incremental salt flux of 25×10^9 g s^{-1}, more than twelve times the excess salt flux from the Mediterranean Sea into the North Atlantic.

O 35 INVITED PAPER

THE COLD WATER TROUGH AT THE TAIL OF THE BANKS

R.A. Clarke (Atlantic Oceanographic Laboratory, Bedford Institute of Oceanography, Dartmouth, Nova Scotia, B2Y 4A2)
R. Reiniger (Atlantic Oceanographic Laboratory)
(Sponsor: S.D. Smith)

A long, narrow body of cold fresh water is commonly found stretching to the south-east from the Tail of the Grand Banks of Newfoundland along or near the axis of the south-east Newfoundland Ridge. The feature is bounded on the south by the joined Gulf Stream/Slope water currents and on the north by their continuation, the North Atlantic Current. An extensive set of XBT observations plus profiling CTD profiles (Batfish) were obtained in late May, 1972. These data are analysed to illustrate the sharp frontal structure and possible interleaving associated with this structure. We finally offer some hypothesis concerning the importance of the feature in modifying the water found in the North Atlantic Current.

O 36 INVITED PAPER

VARIATIONS IN THE FRONTAL STRUCTURE OF THE SOUTHEASTERN GRAND BANKS

P.E. La Violette, NORDA, NSTL Station,MS 39529

An examination of ship, aircraft, and satellite data taken as part of the Grand Banks Experiment during 1978 and 1979 shows persistent cyclic patterns present in the meanders, extrusions, and eddies which compose the thermal front between the cold, southward moving Labrador current water and the warmer, northward moving Atlantic waters. Moreover, these cyclic patterns were found to overlay specific bathymetric features of the Grand Banks such as: The Southeast Newfoundland Ridge, the Newfoundland Sea Mounts, and the Flemish Cap. Oceanographic surveys using aircraft precision radiation thermometers and ship and aircraft expendable bathythermographs show that the strong horizontal thermal gradients present in the surface waters extend deeper than 1000 meters. The present study particularly concentrates on the cycle of the frontal pattern overlaying the Southeast Newfoundland Ridge. The satellite infrared imagery show that although this pattern expands in a cyclic fashion, it does not seem to have a definite period. The expansion is usually in the form of long extrusions of cold water which possibly blocks and deflects the eastward movement of the Gulf Stream. The extreme persistence of these three cyclic patterns, their association with thermal structure as deep as 1000 meters, and their close alignment with bathymetric features deeper than 4000 meters, indicate they are not minor features caused by local wind stress on the surface layer, but are related to the circulation of the entire water column.

O 37

SUBPOLAR CIRCULATION IN THE NORTH ATLANTIC OCEAN

M. S. McCartney (Woods Hole Oceanographic Institution, Woods Hole, MA 02543)
L. D. Talley (Woods Hole Oceanographic Institution, Woods Hole, MA 02543)
(Sponsor: Ray Schmitt)

An upper water circulation scheme for the northern North Atlantic Ocean to the north and east of the Grand Banks is described. The scheme includes two basic gyres, an anticyclonic gyre between the Banks and Europe, south of about 52°N, and a cyclonic gyre north of 52°N between the coast of Labrador and Scotland. The anticyclonic gyre is bounded in the west by the North Atlantic Current. This turns east near 52°N and forms the boundary between the anticyclonic and cyclonic gyres. Part of the transport of this current turns southward to form the anticyclonic gyre, and a main tracer for this movement is a family of Mode Water pycnostads similar to the 18° water south of the Gulf Stream, but with temperatures of 15° to 10°C. The remaining Current transport turns north around the Rockall Bank/Channel, where a 9°C pycnostad is the main indicator. A bifurcation occurs at the Channel head, where part enters the Norwegian Sea (Worthington estimates 8 x $10^6 m^3 s$) and part turns west. The westward branch flows south of the Greenland-Iceland-Scotland sill system, with the main axis of flow being above the 1000 to 2000 meter isopaths, and extends all the way to the Labrador Sea. The main tracer for this movement is a family of Mode Water pycnostads with temperatures of 9° to 3.5°C. The transport system closes with a southward flow of Labrador Sea water - the 3.5°C Mode Water. We estimate that the warm water to cold water turnover represented by this system is about 18 Sverdrups, 8 of which enter the Norwegian Sea, and 10 of which participate in the 15° to 3.5°C Mode Water conversion.

O 38

DISTRIBUTION AND CIRCULATION OF LABRADOR SEA WATER

L. D. Talley (Woods Hole Oceanographic Institution, Woods Hole, MA 02543)
M. S. McCartney (Woods Hole Oceanographic Institution, Woods Hole, MA 02543)
C. H. Pilskaln (Harvard University, Cambridge, MA 02138)
(Sponsor: Ray Schmitt)

The cyclonic circulation of surface Mode Waters in the northern North Atlantic ends in the Labrador Sea where additional cooling and freshening creates an even denser water mass, the Labrador Sea Water (LSW). The LSW then spreads at intermediate depths and is found throughout the northern North Atlantic north of 40°N, the western North Atlantic north of 34°N and along the western boundary to 20°N.

The distribution and characteristics of LSW are mapped using a minimum in potential vorticity, $f/\rho\ \partial\rho/\partial z$ (with small relative vorticity) as the primary water mass tracer. Along the core, potential vorticity, salinity and density increase away from the Labrador Sea, suggesting the importance of mixing.

A tentative mid-depth circulation scheme based on LSW characteristics and inferences from dynamic topography shows preferential spreading from the Labrador Sea along the North Atlantic and Labrador Currents, and recirculation back into the Labrador Sea in the northern currents completing the large cyclonic gyre. An eastward extension of the Gulf Stream turning southwest near 45°N, 20°W is also inferred.

The time dependence of LSW formation is seen in Ocean Weather Station Bravo data from 1964-1973 which shows a low salinity cap over the Labrador Sea from 1968 to 1971, inhibiting LSW formation. Large heat flux into the atmosphere in 1971-72 removed the fresh cap, allowing LSW formation the following year.

O 39

DIRECT MEASUREMENTS IN THE LABRADOR CURRENT

D. G. Mountain (Coast Guard Oceanographic Unit, Washington, D.C. 20590)

Direct current measurements were made at four locations in the Labrador Current along the eastern edge of the Grand Banks from August 1978 to June 1979. At 43°52'N and at 45°45'N one mooring was located near the center of the current and another 18 km to the east on the edge of the current. Each mooring had two vector averaging current meters at about 160m and 450m depth.

During the fall and winter the Labrador Current flowed southward parallel to the isobaths. During the spring the southward velocity at all of the current meters steadily decreased over a month long period until the Labrador Current reversed direction and flowed northward over intervals of up to 15 days duration.

The variations of the current are characterized at subinertial frequencies by spectra that are red. They exhibit high vertical coherence, but low horizontal coherence which precludes the making of transport estimates. The current variations are not significantly coherent (80% level) with the local wind stress or atmospheric pressure variations. However, the reversal of the Labrador Current in the spring was likely related to observed large scale atmospheric pressure changes.

O 40

SEA STATE VARIABILITY ACROSS THE GRAND BANKS FRONTAL REGIME

C. R. McClain (NASA/Goddard Space Flight Center, Greenbelt, MD 20771)
P. E. LaViolette (NORDA, NSTL Station, MS 39529)
W. D. Hart (Science Systems and Applications, Inc., Lanham, MD 20801)

During May, 1979, airborne laser profilometer surveys of the sea surface were conducted over the Tail of the Grand Banks. Additional measurements taken simultaneously were ART (airborne radiation temperature), AXBT (airborne expendable bathythermographs) and lagrangran drift estimates of the current velocities across the feature. The profilometer data consisted of two star patterns each centered on the thermal boundaries defining the two fronts being studied. Large variations in significant wave height and sea surface skewness are detected and correlate strongly with the front's location. Attempts to derive ocean wave power spectra from the star-pattern tracks are made in order to investigate the current's interaction with the wave field components.

O 41

SPACEBORNE RADAR MEASUREMENTS OVER THE OUTER GRAND BANKS

L.S. Fedor (Wave Propagation Laboratory, NOAA, Boulder, CO 80303)
G. S. Brown (Applied Science Associates, Apex, N.C.)
Paul E. LaViolette (Naval Ocean Research and Development Activity, NSTL Station, MS)

This paper presents preliminary analyses of SEASAT radar altimeter measurements obtained over the Grand Banks area. The purpose of this study is to determine the impact of complex frontal and bathymetric structure on spaceborne radar altimeter measurements. The study is unique in that it examines variations in sea surface height, waveheight, and backscattered power as recorded by the altimeter. Furthermore, these measurement variations are correlated, where possible, with thermal signature data obtained from spaceborne visible and infrared imagery. While previous investigations have studied the effects of thermal boundaries upon sea surface height measurements, this represents the first effort to determine the impact upon waveheight and backscattered power measurements. With the three independent altimeter measurements, it is felt that variations in these measurements can be related to specific geophysical effects. The study was significantly aided by the frozen orbit of SEASAT wherein a groundtrack was repeated every three days.

O 42

COMBINED ACTIVE-PASSIVE MICROWAVE MEASUREMENTS OF THE SEA SURFACE IN THE GRAND BANKS FRONTAL REGION

V.E. Delnore, Kentron International, Inc., Hampton, VA 23665
R.F. Harrington,
W.L. Jones, and
C.T. Swift, NASA Langley Research Center, Hampton, VA 23665

As part of an effort to develop all-weather-day/night techniques to remotely sense oceanographic parameters important in air-sea interaction, a NASA research aircraft equipped with a radar scatterometer and a stepped-frequency microwave radiometer overflew the Grand Banks oceanic front region. The flight was made to coincide with ship observations and with environmental satellite passes.

A discussion of the scatterometer and radiometer measurements is presented, with emphasis on the techniques and advantages of a combined active-passive airborne survey. The oceanic front is clearly discernible in the measurements.

The scatterometer responds to the radar scattering coefficient of the sea surface, from which near-surface wind velocities are inferred. The radiometer measures the microwave brightness temperature at various frequencies, from which sea surface temperature can be calculated. The data sets are independent; however, analysis of the two are coupled through the second order dependence of the brightness temperature on wind speed.

O 43

OBSERVATIONS OF TOPOGRAPHIC ROSSBY WAVES IN THE LABRADOR CURRENT

A.A. Allen (Northeast Fisheries Center, NMFS, Woods Hole, Mass. 02543)
(Sponsor: W. R. Wright)

A current meter array was placed on the lower continental slope off Hopedale, Labrador, during March 1976 by the Bedford Institute, N.S. The array, combined with 27 CTD stations, provided information on the spatial and temporal variability at the offshore edge of the Labrador Current and estimates of volume transport. The current regime contained the southward flowing surface (30-50 cm/s) and bottom (20-40 cm/s) boundary currents - the Labrador Current and the Denmark Strait Overflow. Offshore at the 3000 m isobath a rather unexpected persistent northward flow (10-30 cm/s) was found. Moreover, large amplitude ($\pm$ 23 cm/s), low-frequency (8-10 days) fluctuations dominated the mean currents, producing periods of strong steady flow, interspersed with periods of weak, highly variable flow which often contained complete reversals. An offshore phase speed of 16-19 cm/s of the major fluctuations was apparently due to weakly bottom-trapped topographic Rossby waves at 8-10 d periods. The enhancement of the surface fluctuations which lagged the bottom fluctuations by 22-34 hr was due to a positive interaction of the 8-10 d topographic Rossby waves with the baroclinic surface currents. Additional evidence of this positive interaction was found in the 5 successive CTD sections along the mooring line. The observed baroclinic surface velocity field varied in phase with the 8-10 d topographic Rossby waves. The presence of large short-term fluctuations in the current will tend to mask any longer-period (seasonal, year-to-year) variations in the flow of the Labrador Current. Therefore, the use of a single annual hydrographic section for establishing flow must be used with caution.

O 44

NUTRIENT DISTRIBUTIONS IN THE LABRADOR CURRENT

J.R.N. Lazier
A.R. Coote (both at: Bedford Institute of Oceanography, Box 1006, Dartmouth, N.S., Canada, B2Y 4A2)

The values of nitrate, silicate and phosphate in the water over the Labrador continental shelf are higher, at the same densities, than in the waters upstream in the Baffin Island Current, due to mixing with nutrient-rich drainage and intermediate waters in Hudson Strait and Ungava Bay. These higher values remain relatively constant from Cape Chidley to the Strait of Belle Isle. This is partially due to the strong jet-like part of the Labrador Current, centered over the continental slope, that restricts exchange between the waters of the shelf and the deep sea. High nutrient and low oxygen values were found in one of the deep isolated depressions of the marginal trough, indicating local enrichment and recent renewal.

Lake and Ocean Sediments

Bay

Thursday P.M.

R. L. Thomas (Canada Centre for Inland Waters), Presiding

0 45

CONTOURITES IN LAKE SUPERIOR

JOHNSON, Thomas C. (Department of Geology and Geophysics, University of Minnesota, Minneapolis, MN 55455)
CARLSON, Thomas W. (Department of Geology and Geophysics, University of Minnesota, Minneapolis, MN 55455)
EVANS, James E. (Department of Geology and Geophysics, University of Minnesota, Minneapolis, MN 55455)
(Sponsor: Clem Chase)

Contourites are accumulating in an area 15 km wide and 65 km long at the base of the slope off the Keweenaw Peninsula in Lake Superior. Seismic reflection profiles (3.5 kHz) from this area are not typical of those found elsewhere in the lake. The profiles show distinct wavy reflectors in a scoured trough at a depth of 200 m at the base of the slope, hyperbolic echoes adjacent to the trough, and overlapping echoes farther lakeward. These acoustic features are identical to those found in marine environments where contourites are deposited. Box cores from the lakeward margin of this area contain irregular, thin sand layers with sharp upper and lower contacts, interbedded with sandy clays. The sandy clays are trough cross laminated in some horizons, and plain laminated in others. During periods of strong, steady winds, particularly in spring or fall when the water column is isothermal, we suspect that the Keweenaw current accelerates and extends to the lake floor 200 m below, where it winnows the sediment in some areas, and redeposits eroded material in nearby waves and mounds. This is the first report of contourites in a lacustrine environment.

0 46

NEAR-BOTTOM SUSPENDED SEDIMENT GRAIN-SIZE DISTRIBUTIONS IN LAKE MICHIGAN

N. Hawley (Department of Atmospheric and Oceanic Sciences, University of Michigan, Ann Arbor, MI 48109)

Examination of the grain-size distributions of suspended sediments collected from 1,3,5, and 10 m above the bottom of Lake Michigan reveals significant differences from the size variations with depth predicted using a non-cohesive sediment model (the Rouse equation). Most samples show an enrichment in the larger sizes near the bottom, suggesting that aggregation occurs. Other samples, however, show an enrichment of the smaller sizes, indicating rupture of the larger particles. In order to investigate the deposition and transport of these particles, a one-dimensional numerical model which incorporates both particle aggregation and rupture has been constructed. Sediment properties, including shear strength, fall velocity, and density, have been calculated as a function of size from the available literature. The results of this model suggest that particle aggregation and rupture are processes which significantly affect the size distribution of suspended particles near the bottom. Results to date indicate that the efficiency of inter-particle collisions in forming larger particles is considerably less than 100%, and that particle rupture occurs at shears lower than those previously reported. The effects of varying particle characteristics are examined and the implications for deposition are discussed.

0 47

GEOCHEMICAL PROCESSES INFLUENCING SUSPENDED PARTICULATE AND BOTTOM SEDIMENT COMPOSITION IN LAKE MICHIGAN

James E. Mackin
Robert M. Owen (both at: Dept. Atmos. & Oceanic Sci., U. of Michigan, Ann Arbor, MI. 48109)

Water and surface sediment samples were collected at six stations along a transect across the southern basin of Lake Michigan to determine the influence of physical and geochemical processes upon the composition of both settling particulate matter and bottom sediments. Filtered particulate matter and bottom sediments were extracted in an acid-reducing agent and concentrations of Ca, Cr, Fe, Mg, and Mn were determined by atomic absorption spectrophotometry (AAS). Transparency, total suspended matter, and particle grain-size profiles in the water column suggest formation of aggregates in surface waters and release of associated fine-grained mineral matter at mid-depth. The accelerated sinking of fine particles by this mechanism produces enriched concentrations of primarily Fe, Mg, and Mn in near-bottom particulates. Profiles of the ratio of Ca/Mg indicate formation of a high Mg-calcite on settling carbonate minerals. Mean concentrations of Fe, Mn, and Mg were enriched and Cr depleted in bottom sediments relative to suspended particulate matter by nearly an order of magnitude. These data strongly suggest that the composition of bottom sediments primarily reflects post-depositional processes. Furthermore, enhanced heavy metal concentrations in surface sediments are probably poor indicators of the accumulation of anthropogenic inputs to aquatic systems.

0 48

USE OF STEROLS AS INDICATORS OF SOURCE INPUT CHANGES IN GREAT LAKES SEDIMENT

M.J. Leenheer (Department of Atmospheric and Oceanic Science, The University of Michigan, Ann Arbor, Michigan 48109)
P.A. Meyers (Department of Atmospheric and Oceanic Science, The University of Michigan, Ann Arbor, Michigan 48109)

Sterol distributionsin subaqueous sediments provide information about changes in organic matter sources and about postdepositional alteration processes which have occurred in sediments. We have determined the amounts and types of sterols present in two sediment cores and in selected samples representing potential sources of the sterols found in sediments. The sediment cores record the most recent 500 years of Lake Huron and 1000 years of Lake Michigan Holocene deposition. Potential source input samples include freshwater plankton samples and soil samples obtained from an eroding shoreline bluff. Sterols were examined in two sample extracts: 1) unbound sterols obtained by solvent extraction and 2) bound sterols released by alkaline hydrolysis of the sample. The unbound fractions contain significantly more sterols than the bound extracts. Sterol distributions in plankton samples are generally dominated by C_{27} sterols while those of the soil samples contain higher proportions of C_{29} sterols. In the sediment the concentrations of individual sterols decrease with depth except for those of bound stanols, indicating a general degradation except where preserved by reduction and incorporation into humic matter. Relative proportions of sterols indicative of aquatic source input and those indicative of terrigenous input change with sediment depth. These variations may reflect selective degradation of different types of sterols or they may record changes in organic matter sources to the Great Lakes.

0 50

MULTICHANNEL RESULTS — CAPE BASIN

James A. Austin, Jr. (University of Texas Marine Science Institute, 700 The Strand, Galveston, TX 77550)
Elazar Uchupi (Dept. of Geology and Geophysics, Woods Hole Oceanographic Institution, Woods Hole, MA 02543)

Prominent acoustic horizons are identified beneath the passive continental margin off southwest Africa using 3400 km of 12- and 24-fold multichannel seismic data collected by UTMSI during an IPOD site survey program in the Angola and Cape basins. One of these horizons, "AII" (Emery et al, 1975), has been previously observed on single-channel profiles and correlated with the geology sampled by DSDP hole 361. "AII" appears to mark the boundary between late Early Cretaceous carbonaceous sandy mudstones/sandstones and Upper Cretaceous shales.

On the multichannel profiles, "AII" resembles a topset horizon overlying a sequence of gently seaward-dipping foreset deposits which thin basinward and bury inferred oceanic basement in the Cape Basin. Both the seismic and available stratigraphic information suggest that the pre-"AII" section is a deltaic and/or submarine fan complex, and it may mark the first major episode of "drift" sedimentation following the Early Cretaceous separation of Africa and South America.

The gas potential of the pre-"AII" sequence is good because of its high terrestrial organic carbon content and updip terminations against "AII." However, optimum drilling targets appear to be in deep water beneath the continental slope.

0 51

GEOLOGIC OBSERVATIONS IN THE HELLENIC TRENCHES FROM THE SUBMERSIBLE "CYANA"

HEAT-CYANA Scientific Team (X. LePichon, J. Angelier, J. Boulin, D. Bureau, J.P. Cadet, A. Chapel, J. Dercourt, G. Glacon, H. Got, D.E. Karig, N. Lyberis, J. Mascle, L.E. Ricou, F. Thiebault).

Fifteen dives in the submersible "Cyana" were made within three areas of the Hellenic trench system, both along the WNW trending Ionian section, where northeasterly subduction is dominant, and along the NE-trending Strabo trench, which is a left-lateral strike slip feature. The 10 dives made in area 2, south of Crete, provide the most data concerning recent tectonism. Although preceeding reflection profiles displayed a typical ridge-basin pattern on the inner (N) slope, very little evidence of active tectonism was observed there. Rather, northward vergent thrusting on the outer (S) slope appears to accommodate most plate shortening. This deformation is most intense as the base of the outer slope, dying out within several km to the south. Surficial calcareous crusts serve as passive strain markers to delineate this deformation. Only post-Messinian calcareous pelagics and, probably, sections of Messinian strata were observed to be involved in deformation and accretion on the lower slopes. Large cavernous cliffs and circular uplifts were attributed to Messinian evaporitic units. Recent sedimentation on both slope and in the trench axis is dominated by rapidly deposited pelagic calcareous mud. Downslope movement of surficial sediment is very common, occurring as thin slides, but there is very little evidence for gravitational transport of the older accreted sediments. The morphological pattern of joints and faults is compatible with subduction of the Mediterranean floor toward the northeast, but it is complicated by Messinian diapirism and apparently by deformation within the thick pre-Messinian strata.

0 52

MORE EVIDENCE FROM THE DEEP SEA ON THE DEPTH OF GLACIAL EROSION IN NORTH AMERICA

M. Bell (Dept. of Earth and Environmental Sciences, Wesleyan University, Middletown, Conn. 06547)
E.P. Laine (Graduate School of Oceanography, University of Rhode Island, Narragansett, Rhode Island 02881)
(Sponsor: Margaret Leinen)

Interpretation of seismic reflection profiles from the Sigsbee Abyssal Plain, the Northern Gulf of Mexico, and the Mississippi Fan has led to a minimum estimate of the volume of glacial age sediment (<3.0 my) derived from the Mississippi River. Corrections have been made for the contributions of other rivers debouching into the Gulf of Mexico, biogenic calcium carbonate, and fluvially eroded sediments. This estimate of the volume of glacially eroded sediment in the Gulf of Mexico is combined with similar estimates for the western North Atlantic Ocean, and Laurentian Cone, the Arctic Ocean, and the Beaufort Sea. The result indicates between 100 and 150 meters of solid rock has been stripped from North America by continental glaciation.

0 53

CARIBBEAN FRACTURE ZONES: CLUES TO CARIBBEAN TECTONIC EVOLUTION

W. D. MacDonald (Dept. of Geological Sciences, State University of New York, Binghamton, N.Y. 13901)

At least two families of fracture zones are found in the Caribbean. The Cayman system, bordering the Cayman trough, may be no older than Late Tertiary. Its pole has been re-estimated by a least-squares method at 19.4S 074.6W. Changes in curvature along the Cayman fracture zones indicate a migration of the pole of relative rotation in late Tertiary time. The present Cayman pole lies about 30° from published CARB/NOAM instantaneous poles, for which several explanations are feasible. An older family of fracture zones, the Hess system, is identified by fracture zones concentric about the best-fit pole of the Hess escarpment; that pole is 53.6N 117.7W. The Hess system is probably late Cretaceous and trends ENE across the Colombian and Venezuelan basins. This tectonic fabric suggests an ENE-WSW spreading direction for these basins, in conflict with published spreading interpretations in both basins based on magnetic anomalies. Explanations are suggested for these apparent conflicts, and suggestions are made for future oceanographic geophysical research.

0 54

INITIAL RESULTS OF A SEABEAM SWATH MAPPING SURVEY OFF NORTHERN CALIFORNIA AND OREGON

R. Embley (All at: National Ocean Survey, NOAA, Rockville, MD 20852)
A. Malahoff
S. Hammond

A multibeam swath mapping sonar system, SEABEAM, has now been installed aboard the NOAA Ship SURVEYOR. From February to April 1980, a cruise will have been undertaken off the coasts of Oregon and California to both test and calibrate the SEABEAM system and to conduct a multi-faceted geological and geophysical survey of the Southern Gorda ridge, Mendocino fracture zone, and Gorda basin. In addition, several reconnaissance lines will be run over the Blanco fracture zone, Blanco gap, and the Cascadia basin in preparation for a continuing study of the tectonics of the northwest Pacific by the National Ocean Survey in cooperation with scientists from several academic research institutions. Initial results from several overlapping swaths across the California continental slope between 37° and 38°N show that SEABEAM is capable of reliable mapping of seafloor features having wavelengths of about 5 m in as much as State 5 seas. Navigational control is provided by digital Raydist and Loran-C supplemented by satellite positions. Preliminary interpretation of seismic reflection profiles and the real-time SEABEAM contour maps indicate that the continental slope off central California appears to be marked by numerous sediment slides tens of kilometers long and up to 300 meters in width.

Ocean Climate Scale Variability

Metropolitan Centre Friday A.M.

James Baker (Univ. of Washington), and *George Needler* (Bedford Institute), Presiding

0 55 INVITED PAPER

ACOUSTICS AND ALTIMETRY FOR GLOBAL OCEAN MEASUREMENT

C. Wunsch (Department of Earth & Planet. Sci., Massachusetts Institute of Technology, Cambridge, Mass. 02139)

Measurement of the ocean for understanding its dynamics and for determining the climatological consequences requires observations of a global fluid such that the smallest energetic spatial scales are resolved. One must observe spatial scales as small as the baroclinic Rossby radius of deformation for long periods. The situation is closely analogous to that faced in observing the atmosphere, but by comparison, the oceanic data base is woefully inadequate. Preliminary experiments of the past two years suggest a potential solution. Studies of the Seasat altimeter data set show that this form of instrument is capable of determining with useful accuracy both time-independent and time-dependent geostrophic surface flows. Present uncertainties in the mean general circulation are translatable into surface slope uncertainties exceeding 25cm over spatial scales of 300 km and longer. These are accessible with realizable improvements in the marine geoid. Temporal variability of the circulation is measureable at the less-than-10cm-value over all scales. Preliminary experiments with acoustic tomography have shown that three-dimensional density field fluctuations are measureable with useful accuracy over long distances. Thus tomography is a system with attractive economics for large-scale determination of baroclinic fluctuations in the ocean on spatial scales exceeding about 50 km. With the navigational accuracy of the Global Positioning System (GPS) tomography could be done from ships as well as from moorings covering very large areas of ocean in a few days. Combined altimetry/tomography could provide a global scale system in which the mass field was determined acoustically and the geostrophic reference velocity was determined from the altimetry providing a system comparable to the present global weather net.

0 56 INVITED PAPER

MONITORING CLIMATE SCALE VARIABILITY IN THE OCEANS FROM SPACE

Robert Stewart (Scripps Inst. Oceanography, La Jolla,CA, 92093)

The primary oceanographic variables of interest to climatology, e.g. heat fluxes, transport, and storage, cannot be observed from space. Instead, other related variables are observed, e.g. surface temperature, wind speed, currents; and even these observations are subject to relatively large, systematic errors.

This leads to two distinctly different measurement strategies: i)make accurate measurements and thoroughly understand their errors, or ii)accept inaccurate observations and directly correlate these with climate, e.g. use upwelling radiance(associated with surface temperature) in correlations with other climate variables.

In either case, the long-term monitoring of these variables requires very accurate calibrations of the instruments, and thorough documentation of their performance and the analysis of their data.

The secondary oceanic variables now measured from space include: i)sea-surface temperature, ii)wind speed, iii)surface currents, iv)ice boundaries, and v)the positions of thermal features. None have been observed for long times, and the most important, sea-surface temperature, has large, systematic errors.

0 57 INVITED PAPER

OCEANOGRAPHIC INSTRUMENTATION FOR THE CLIMATE PROBLEM

Richard I. Scarlet (EG&G, Environmental Consultants, Waltham, MA 02154

In-situ ocean measurements on a global scale are limited by the cost and logistics of present oceanographic instrumentation. These limitations result from the cost of ship time to deploy and maintain instruments, limited data storage capacity of instruments, minimal data transmission capability of present instruments, and the requirement for highly trained crews to deploy and operate the instruments.

Instrumentation developments presently in progress promise to alleviate many of these problems. The developments include: air deployable moorings, telemetering moorings, greatly increased storage capacity and survivability of in-situ instruments, and new generations of instruments suitable for routine use on ships of opportunity. These developments are reviewed and the implications of these technologies to the global climate measuring problem are discussed.

0 58 INVITED PAPER

PHYSICAL PROCESSES INVOLVED IN THE HEAT BUDGET OF THE UPPER OCEAN

J.C. McWilliams (National Center for Atmospheric Research, Boulder, Colorado 80307)

A broad survey is made of our present knowledge of the component processes in the heat budget of the upper layers of the ocean (i.e., latent sensible and radiative heat fluxes through the noviface, lateral advective transports, sensible heat fluxes through the pycnocline, and changes in local heat storage) on time scales from seasonal to decadal and space scales from 1000 km to global. Magnitudes of these quantities are estimated on a regional basis. Some suggestions are made for future experiments on these processes in order to complement ocean climate monitoring.

0 59

A PILOT MONITORING SYSTEM FOR EL NIÑO

James J. O'Brien (Department of Oceanography, Florida State University, Tallahassee, FL 32306)

It is suggested that the interannual variations of the zonal winds between 145°W and 175°E and within 5° of the equator are responsible for triggering El Niño. According to Wrytki (1975), El Niño is preceeded by strong southeast trades which accumulate water in the western Pacific. This precursor may be monitored from the existing sea level network or in the late 1980's by the proposed NASA satellite, TOPEX. If the southeast trades then weaken in the central Pacific, an internal downwelling Kelvin wave will be excited (Hurlburt, Kindle & O'Brien, 1976) which will strengthen poleward currents along the coast of South America. These will advect poleward water of equatorial origin.

In Goldenberg & O'Brien (1980), we show that the central Pacific region, mentioned above, exhibits a maximum amount of interannual energy (periods longer than 20 months) in the zonal wind stress. Kindle (1979) has calculated a complete El Niño simulation based on the weakening of winds in this central Pacific region. Busalacchi & O'Brien (1980) have shown that the seasonal wind field can simulate the seasonal variability of the tropical Pacific surface currents.

If the proposed NASA satellite, NOSS, can measure surface winds, then the scientific community can monitor the zonal winds in this small equatorial region on a weekly or monthly time scale and search for events which could trigger El Niño. If rapid data analysis is available, a 2-3 month forecast of possible El Niño events could be predicted.

0 60

SYNOPTIC ESTIMATES OF AIR-SEA FLUXES

R.F. Marsden (Department of Oceanography, University of British Columbia, Vancouver, B.C. V6T 1W5)
S. Pond

Synoptically averaged wind, temperature and humidity data were used to examine the effect on the calculation of bulk surface momentum, latent heat and sensible heat fluxes. The data consisted of 10 to 21 years of three-hourly sea surface meteorological observations from 9 weatherships on the North Atlantic Ocean and 2 weatherships on the North Pacific Ocean. By grouping according to wind speed category and applying a multivariate regression, a series of characteristic curves were found quantifying the ratio of the averaged and directly determined flux values. Significant corrections (>25%) were found for averaging lengths greater than 1/2 day and moderate winds. Residual errors were reduced from maximum values of 40 to 50% of the 3H variance with no correction applied to less than 10% of the 3H variance with the application of corrections. The temperate latitude corrections could be geographically averaged with little loss in accuracy. An empirical formula was found which adequately predicted the corrections and facilitated application of the technique.

O 61 INVITED PAPER

A RELATION BETWEEN THE T/S CURVE AND GLOBAL HEAT AND ATMOSPHERIC WATER TRANSPORTS

H.M. Stommel (Woods Hole Oceanographic Institution, Woods Hole, MA 02543)
G.T. Csanady (Woods Hole Oceanographic Institution, Woods Hole, MA 02543)

From historical data on the distribution of temperature and salinity on vertical sections across the oceans over complete latitude circles it is possible to test the compatibility of certain meteorologically determined meridional fluxes in the ocean of sensible heat and fresh water, as functions of latitude. It is also possible to check the proportion of this flux that each ocean basin carries separately.

The information from both these sources leads to estimates of the magnitudes and distribution of the meridional oceanic mass flux over the salinity-temperature plane, and yields some indication of the probable physical processes operating (e.g. isopycnal mixing vs. large-scale advective currents).

O 62 INVITED PAPER

OCEAN MODELS AND POLEWARD HEAT TRANSPORT

K. Bryan (GFDL/NOAA, Princeton, NJ 08540)
P. Delecluse (GFD Program, Princeton University, Princeton, NJ 08540)

Estimates of poleward heat transport by ocean currents vary considerably in magnitude, but agreement exists that ocean heat transport is of the same order as atmospheric transport, and in the Northern Hemisphere it is a maximum in low latitudes. Numerical experiments show that the poleward flow of surface waters in the Ekman layer compensated by a return flow in the main thermocline is a viable mechanism for accounting for a large fraction of the poleward heat transport at low latitudes. At middle and higher latitudes the situation is more complex. Transient eddies and the large standing horizontal gyres may be important. Ekman transport in the region of the atmospheric westerlies actually inhibits poleward heat transport by forcing warm surface waters toward the equator. The "roaring forties" of the Southern Hemisphere are particularly effective in this respect. At very high latitudes the models suggest that direct thermohaline circulations are increasingly important.

The following explanation is offered to explain the observed fact that the heat transport by the Northern Hemisphere oceans is strongest at low latitudes. At low latitudes wind and thermohaline effects cooperate to transport heat poleward, while at higher latitudes these two effects tend to oppose each other.

O 63

ESTIMATION OF HEAT FLUX IN THE NORTH ATLANTIC BY INVERSE METHODS

Dean H. Roemmich (Woods Hole Oceanographic Institution, Woods Hole MA 02543)

Meridional heat flux in the North Atlantic is calculated from hydrographic data using geostrophic velocities and observed temperatures at 24°N, 36°N, and 48°N. Reference level velocities are obtained by the inverse method (Wunsch, 1978, Roemmich, 1978), with mass and salt conserved in 14 layers separated by isopycnal surfaces. The indeterminacy of the inverse problem may be expressed as a dependence of the solution on the initial reference level, or equivalently, as an inability to resolve small scales in the data. In the heat flux calculation, the best resolution is found at 24°N and the worst at 48°N. Inclusion of ageostrophic contributions leads to estimates of the total heat flux of 120×10^{15} watts at 24°N and 80×10^{15} watts at 36°N. At 48°N, the heat flux appears to be small. Uncertainties in the estimates are discussed.

O 64

UPPER OCEAN MODELS FOR CLIMATE STUDIES

J. R. Miller (Department of Meteorology & Physical Oceanography, Cook College, Rutgers University, New Brunswick, N.J. 08903)

Energy balance climate models have been used to conduct sensitivity experiments such as determining the effect of atmospheric CO_2 increases. The approach to equilibrium can vary significantly depending on how the coupling with the upper ocean is parameterized. The purpose of this study is to compare previous parameterizations with hydrographic data along a meridional section in the central Pacific and to suggest a hierarchy of simple models that could be used to improve these parameterizations. The thickness of the upper oceanic layer that is allowed to interact with the atmosphere is a crucial parameter. This thickness can be specified in terms of deepest mixed-layer depth or by analysis of the spectral signature when a sufficiently long time series is available. Climatological two-layer and three-layer models, with time-varying upper layers but fixed total depths, are developed based on the observational data. A two-layer empirical model in which the upper layer depth is a function of sea-surface temperature can be easily modified to account for changes in climatic regimes. Finally a mixed-layer model is developed to reproduce the observed features as functions of surface heat fluxes and wind stress. These simple models should be of use to climate modelers who seek more realistic parameterizations of the coupled ocean-atmosphere system.

O 65

HEAT BUDGET OF TROPICAL OCEAN AND ATMOSPHERE

Stefan Hastenrath (Meteorology Department, University of Wisconsin, Madison, WI 53706)

Heat budget estimates for the global tropics are derived from recent calculations of the oceanic heat budget and satellite measurements of net radiation at the top of the atmosphere. Oceanic meridional heat transport in the Pacific is directed from the tropics into either hemisphere; in the Atlantic it is northward from high southern latitudes all the way to the arctic; and it is directed southward in the Indian Ocean. Oceanic heat gain in the Pacific offsets deficits in the higher southern latitudes of the Atlantic and Indian Ocean sectors, as well as in the Atlantic as a whole. Meridional heat transport for all oceans combined is largest around 30°N and 25°S, where it accounts for 53 and 35% of the total poleward transport. Atmospheric transport is largest and effects the bulk of the total transport in midlatitudes.

Appreciably different estimates of net radiation at the top of the atmosphere, and of oceanic and atmospheric heat export must be regarded as compatible within the broad error limits indicated at present for all three terms.

O 66

OCEAN HEAT TRANSPORT AT 25°N IN THE ATLANTIC

Mindy M. Hall (Woods Hole Oceanographic Institution, Woods Hole, Mass. 02543)
Harry L. Bryden (Woods Hole Oceanographic Institution, Woods Hole, Mass. 02543)

We recently estimated ocean heat transport in the Atlantic across 25°N to be 1.1×10^{15}W northward. Error analysis indicates that the eddy contribution, defined as that due to deviations in temperature and meridional velocities from their zonally-averaged values, causes the largest uncertainty in our estimate of heat transport. While the net eddy contribution is only $.02 \times 10^{15}$W, its uncertainty is $\pm .25 \times 10^{15}$W. Direct current and temperature measurements across 28°N also indicate that the net eddy contribution is small in this region. The meridional circulation implied by our procedure is similar to that proposed by Worthington but with substantially greater southward flow in the cold (< 4°C) deep water.

Our estimate and other direct estimates of ocean heat transport in the Atlantic agree reasonably well with indirect estimates derived from Bunker's charts of air-sea exchange. While it is difficult to compare these values with those obtained from satellite radiation measurements and atmospheric transport estimates because of the lack of knowledge of ocean heat transport in the Pacific, the satellite-derived estimates appear to be too large by a factor of almost 2. To make the comparison properly, a deep hydrographic section across the Pacific and a good estimate of Kuroshio transport at 25°N is needed to complement our direct estimate in the Atlantic.

O 67

THE COLOR OF THE OCEANS AS A STABILIZING FACTOR FOR THE EARTH AGAINST RUN-AWAY TEMPERATURE EXTREMES

Michael D. Papagiannis, Dept. of Astronomy Boston University, Boston, MA 02215

Changes in the Earth's albedo, such as those produced by the expansion or retreat of ice coverage, tend to reinforce themselves and thus lead either to a run-away glaciation or to a run-away greenhouse effect, in either case, with disastrous consequences for life on Earth. Changes of the cloud coverage with temperature, or changes of the sea-level and hence of the exposed land area with glaciation could change the albedo in the opposite direction and thus reverse these trends. An important contribution could also come from changes in the color of the oceans with temperature, a global effect which we are currently investigating. Since the oceans cover more than 70% of our planet, a mere 10% change in their albedo due to a small variation in their color, would change the average temperature of the Earth by about 4°K, which is more than the estimated decrease in the average temperature of the Earth during an ice age. Thus, if the oceans would turn darker when it gets colder and lighter when it gets warmer, they would provide an excellent safety mechanism against major temperature changes. Supporting such an effect of temperature on the color of the oceans is the observation that warmer seas tend to have lighter colors (Caribbean, Mediterranean, etc.), while colder seas tend to have darker colors (Northern Atlantic, Black Sea, etc.). Long-term temperature changes have a distinct effect on the kinds of microorganisms and phytoplankton that live in the seas, which in turn represent a significant factor in determining the color of the seas. It is thus possible that life on Earth is making a substantial contribution toward its own survival by stabilizing our planet against run-away temperature extremes.

Lagranian and Eulerian Studies of Ocean Currents

Harbour B
Friday A.M.
Philip Richardson (Woods Hole Oceanographic Institution), Presiding

O 68 INVITED PAPER

SOFAR FLOATS IN THE POLYMODE LOCAL DYNAMICS EXPERIMENT

James F. Price (Woods Hole Oceanographic Institution, Woods Hole, MA 02543)
H. Thomas Rossby (University of Rhode Island, Kingston, RI 02881)

SOFAR floats deployed during the POLYMODE Local Dynamics Experiment produced a unique set of coherent, deep ocean Lagrangian measurements. Approximately 18 floats were set at 700 m and at 1300 m depths, with nearest neighbors at 30 km distance.

While the arrays remained intact, the data may be used to estimate the potential vorticity balance. The most striking motion at 1300 m depth was an oscillatory flow over gentle, large scale topography. Potential vorticity balance was achieved by the beta effect and topographically induced stretching acting in phase to change the relative vorticity. The time and

space scales of this motion match the corresponding barotropic, planetary/topographic plane wave dispersion relation.

The rate of breakup of the arrays is a measure of horizontal diffusivity. Two-particle relative dispersion statistics at both levels are consistent with the predictions from two-dimensional turbulence theory; for neighbor separation, $D \leq 100$ km, relative dispersion increases approximately as D^2. The magnitude of the relative dispersion scales approximately with the velocity variance.

O 69 INVITED PAPER

"SATELLITE TRACKED DRIFTING BUOY OBSERVATIONS OF THE NORTH PACIFIC SUBTROPICAL GYRE"

G. J. McNally (Scripps Institution of Oceanography University of California, San Diego 92093)
W. C. Patzert (Scripps Institution of Oceanography University of California, San Diego, 92093)
(Sponsor: William Patzert)

From June 1976 through February 1979, satellite tracked drifting buoys have been deployed throughout the North Pacific as part of various NORPAX investigations. Drifters have been deployed off the southern tip of the Japanese Island of Honshu in the Kuroshio, the mid-latitude eastern North Pacific, off the California Coast and in the Tropical Pacific parts of Hawaii. The sum of all the drifter trajectories provide a unique picture of the large-scale flow around the North Pacific Subtropical Gyre. Examinations of the details of these trajectories reveal mesoscale energetics whose characteristic time and space scales differ around the gyre.

O 70

GULF STREAM PATH MEASURED WITH FREE-DRIFTING BUOYS

P. L. Richardson (Woods Hole Oceanographic Institution, Woods Hole, MA 02543)

Recently 35 free-drifting buoys measured near surface currents in the Gulf Stream system. Buoy trajectories show that the Stream is at times strongly influenced by the New England Seamounts. This influence is manifested as 1) a quasi-permanent, 100 km, southeastward deflection of the Stream and the frequent occurrence of a ring-meander over the seamounts, 2) large amplitude meanders beginning at the seamounts and extending eastward, 3) strong mesoscale eddies over and near the seamounts. Small 20 km diameter eddies appear to be generated by individual seamounts; larger 150 km eddies are the result of the integrated effect of the seamounts on the Stream. A chart of the mean temperature field at a depth of 450 m agrees with several of the patterns seen in the buoy trajectories. West of the seamounts the mean path of the Gulf Stream is due eastward. Over the seamounts the path turns sharply northeastward and the isotherms in the Stream abruptly diverge.

O 71

EVIDENCE OF STEADY, ANTICYCLONIC DRIFT AROUND SABLE ISLAND, NOVA SCOTIA

J.A. Pompa, ORI, Inc., Silver Spring, MD 20910

During September and October 1977, a Lagrangian current measurement program was conducted in the waters of the Scotian Shelf around Sable Island. The program consisted of remote tracking of free-floating drifters from three sites on the island using radio-direction finding (RDF) techniques and the release of 990 expendable plastic surface and bottom drifters. Results of the tracking indicated not only a strong correlation with the wind, but also showed a pronounced easterly drift in the waters north of the island concurrent with a steady westerly drift south of the island. This is indicative of a steady current moving in an anticyclonic sense around the entire island. Analysis of tidally averaged drifts indicated a speed of 16 cm/sec at the surface and 10 cm/sec at 20 meters depth. These results were further supported by returns of the expendable drifters, which showed a definite pattern of recovery based on tidal stage at time of release. This is further evidence of a type of island circulation, predicted theoretically by Longuet-Higgins (1969), and observed around Bermuda (Stommel, 1954), the Hawaiian islands (Patzert and Wyrtki, 1974) and elsewhere. The circulation process is important to the understanding of sediment movement around the island, particularly the migration of sand waves, as well as the potential drift of spilled oil from petroleum production facilities in the area.

O 72

DISPERSION IN THE GULF STREAM

D.F. Paskausky
N.C. Edwards, Jr.
D.F. Cundy (U.S. Coast Guard Research and Development Center, Groton, CT 06340)

Five satellite-tracked, drifting buoys (undrogued with temp. sensors) were released on a line crossing the Gulf Stream core east of Florida at 28.1N; 1) 79.9W; 2) 79.8W; 3) 79.7W; 4) 79.6W; 5) 79.5W on 30 Jan 1979. Dispersion was rapid: maximum separation between any buoy pair was 96 km after 3 days; 354 km after 19 days; 925 km after 29 days; 1640 km after 53 days. Buoy 5), easternmost buoy, moved along the cold side (15-22C) to 39N, 48.5W in 90 days, crossed the stream and spent 40 days in a cold core ring (~18C) before migrating eastward in Sargasso Sea water (22-23C). Buoy 4) meandered downstream to 36.5N, 67.5W in 60 days when it was recovered and taken to Bermuda. Buoys 3) and 2) broke out of the stream to the east after 11 days and made one anti-cyclonic revolution in cold water (~20C). Buoy 3) then drifted east and stalled in Sargasso Sea water (~24C) near 29N, 72W for 4 months. Buoy 2) continued east for 2 months with 4 cyclonic revolutions (dias. 190, 95, 50, 25 km). It then migrated southwest ~195 km and performed 3 more cyclonic turns before rejoining the stream 2 months later. Buoy 1), westernmost buoy, broke out of the stream to the east on day 3 and wandered in the Sargasso Sea (centered on 29N, 77.5W) for 2 months. It then rejoined the stream and moved eastward on the cold side, breaking out for 10 days into cold shelf water (12C) near 42N, 58W.

Geostrophic winds over the region were variable. Drift trajectories indicate that Gulf Stream dynamics and associated phenomena such as rings are the primary forcing factor rather than wind.

O 73

LAGRANGIAN MEASUREMENTS OF SURFACE CURRENTS SOUTH OF NOVA SCOTIA

R. W. Trites, Marine Ecology Laboratory, Bedford Institute of Oceanography, Dartmouth, Nova Scotia B2Y 4A2.

As part of a more comprehensive oceanographic study of the southwestern Scotian Shelf area, nine satellite tracked buoys and more than seven thousand drift cards and bottles were released between April 1979 and January 1980. Of particular interest are the events which lead to offshore excursions of the buoys. Discussion is focussed on a comparison between the buoy motions and the Gulf Stream meanders and eddies as identified by the U.S. Naval Oceanographic Office Experimental Ocean Frontal Analysis maps.

O 74

MEAN BAROCLINIC FLOW IN AN OPEN BAY

K. Drinkwater, Marine Ecology Laboratory, Bedford Institute of Oceanography, Dartmouth, Nova Scotia B2Y 4A2.

(Sponsor: Edward Horne)

Current meter arrays moored in St. Georges Bay, Nova Scotia during the summer of 1974 and 1975 revealed highly baroclinic flow. A clockwise gyre with velocities of order $0.1 ms^{-1}$ dominated the mean circulation in the upper layers of the Bay while a net mean bottom outflow of $<0.02 ms^{-1}$ was observed at the mouth. Heat budget considerations show a greater increase in heat content in the Bay than that expected by surface heat flux. The rate of increase is consistent with an advective heat flux calculated from the observed mean currents. The lower layer outflow is thought to be a bottom frictional response to upper layer flow parallel to the mouth of the Bay.

O 75

VERY LOW FREQUENCY CURRENT FLUCTUATIONS NEAR THE NORTHEAST GULF OF ALASKA SHELF BREAK

Gary Lagerloef
James Schumacher (both at NOAA Pacific Marine Environmental Laboratory, 3711 15th. NE, Seattle, WA 98105
Robin Muench (SAI/Northwest, 13400 B Northrup Way #36, Bellevue, WA 98005)

Current observations were obtained nearly continuously from 20, 50, 100 and 175 m near the northeast Gulf of Alaska shelf break over a three-year period. Mean flow was alongshore to the northwest throughout the observation period, with higher speeds during winter. Very low frequency oscillations (<0.1 cpd) were prominent current features and were vertically coupled to depths greater than 100 m. There was a long-term, interannual trend toward increasing kinetic energy with time in this very low frequency band. No clear correlation was present between local winds and low frequency fluctuations except on the seasonal time scale. Instead, these fluctuations must be related to larger scale, non-local processes such as meso-scale ocean eddies.

O 76

CURRENT OBSERVATIONS DURING THE PASSAGE OF HURRICANE FREDERICK

L. K. Shay
J. J. Tamul (both at: U.S. Naval Oceanographic Office, NSTL Station, MS 39522

Six subsurface current meter arrays deployed within 75 miles of the Alabama coastline in the Gulf of Mexico during July-October, 1979 show the dynamic response to the passage of Hurricane Frederick on September 12, 1979. Each array contained from three to four Aanderaa RCM-5 current meters measuring speed, direction, and temperature at a 10 min. sampling interval in water depths of 100m to 520m.

The most significant feature in all records is the presence of an atmospherically induced inertial current of approximately a 24 hour period which persisted for nearly two weeks following the passage of Frederick. The response of the near shore array was markedly less energetic than the deeper arrays as indicated by the kinetic energy spectra and also showed a modification in the current response due to the close proximity of the coastline. In general, the speed range over the entire water column for all meters was between 75-80cm/sec, while the deepest array recorded the highest current speeds of 135-140cm/sec near the surface. The temperature records for all current meters indicated a temperature increase of from 1°C in the deepest array to about 4°C in the shallowest array at the onset of the storm, followed by a large temperature drop with a gradual warming of the water column in a two week period.

O 77

THE FLOW THROUGH THE STRAIT OF BELLE ISLE

PETRIE, B. (Bedford Institute of Oceanography P.O. Box 1006, Dartmouth, N.S., B2Y 4A2)

GARRETT, C and TOULANY, B. (Dalhousie University Halifax, N.S., B3M 4J1)

In 1963, several tide gauges and current meters were deployed for 50 days in the Strait of Belle Isle, which connects the Gulf of St. Lawrence to the Atlantic Ocean. We present a dynamical interpretation of the flow variability demonstrating in particular that the surface transport through the Strait is in geostrophic balance with the sea level difference across the Strait. This permits the use of 8 years of sea level data, from permanent gauges on opposite sides of the Strait, for a study of flow variability on a variety of time scales. For periods between a few days and a few months the fluctuations are highly coherent with large scale meteorological forcing, although the strength of coupling of wind to water and a friction coefficient for flow through the Strait vary significantly with season. At longer periods the dominant forcing mechanism is not clear, but the data do suggest winter inflow through the Strait of about 0.5Sv and substantial interannual variability.

0 78

CIRCULATION STUDIES SOUTH OF THE GULF STREAM AT 50°W

R.M. Hendry (Atlantic Oceanographic Laboratory, Bedford Institute of Oceanography, Dartmouth, Nova Scotia, Canada, B2Y 4A2)

One year of moored velocity data has been recovered from 4000 m depth in 5420 m of water at several sites near 38°N, about 150 km south of the mean axis of the Gulf Stream at 50°W. The data show a mean flow with an eastward component of 3-6 cm-s^{-1}, which is similar to recent observations at 55°W. This suggests large zonal scales for the deep mean motion south of the Stream. Eddy kinetic energy at 4000 m has decreased by a factor of 2-3 at 50°W compared to 55°W, although there is still appreciable low frequency variability in the regional circulation.

0 79

BOUNDING THE NORTH ATLANTIC CIRCULATION

Karl K. Stenn

John R. Booker (both at: Geophysics Program, Univ. of Wash., Seattle, WA 98195)

This work estimates barotropic currents for a portion of the North Atlantic. We use geostrophic baroclinic currents which have been calculated from measured density gradients. We further assume conservation of mass to find the barotropic currents. Since there is not a unique answer, we then use a technique developed by Backus (1970) and Parker (1977). With it, it is possible to use knowledge of the magnitude of the currents to place numerical bounds on parameters which are functions of the currents. Results are then compared with those of other workers.

0 80

THE FRACTION OF VERTICAL ISOTHERM DEFLECTIONS ASSOCIATED WITH EDDIES: AN ESTIMATE FROM MULTISHIP XBT SURVEYS

W.J. Emery (Department of Oceanography, University of British Columbia, Vancouver, B.C., Canada. V6T 1W5)
C.C. Ebbesmeyer (Evans-Hamilton, Inc., Seattle, Washington 98115)
J.P. Dugan (Naval Research Laboratory, Washington, D.C. 20375)

Six multiship XBT surveys in the area between 29° and 42°N in the North Pacific and North Atlantic Oceans were examined with respect to the following questions: What fraction of significant vertical isotherm deflections may be associated with horizontally closed eddies, and which of these eddies have identifiable thermal expressions at the sea surface? From all six surveys 45 significant deflection features, with amplitudes exceeding one standard deviation, were selected from isotherm deflections in the central vertical temperature sections. Approximately half of these deflections could be identified as parts of horizontally closed eddies (mean diameters ~150 km). In turn, approximately a third of the eddies were associated with a significant anomaly (≥0.5°C) of sea surface temperature. Examples of both isolated and close-packed eddies were observed. Most of the eddies identified in the western North Atlantic were in the region of increased eddy kinetic and potential energies associated with the Gulf Stream. In this area the number of eddies per unit area equalled approximately 0.14 eddies per 10^4 km^2 (~1 square degree).

0 81

THE NSF OCEANOGRAPHY SECTION: WHAT IT IS AND HOW IT OPERATES

Robert E. Wall (NSF, Washington, D.C. 20550)

The Oceanography Section and its four Program Offices manage a research project support program to help develop and maintain high quality basic research in the ocean sciences. It is important that scientists be aware of the substance of the Section and the rationale, constraints, and groundrules under which it operates. To this end, the project support program of the section will be characterized by the processes it goes through to get and spend money and by a dissection of the four Programs themselves, the proposals they receive, and the grants they make. The information presented will bear on such questions as:

What is the scientific substance in each of the four Program areas?
How is it determined?
What are the funding levels and trends?
How are these funding levels determined and on what time frame?
What is the character of the 740 proposals considered for support in FY1979?
How does the peer review system as used by the Oceanography Section operate?
How are interdisciplinary, multidisciplinary, or collaborative research proposals handled?
What is the character of the 360 grants awarded in FY1979?
What part of the Section's FY1979 funding went to the various institutions? to scientist's salaries? to support graduate students? to purchase equipment? and to cover indirect costs?

Paleo-Oceanography

Harbour A
Friday A.M.
Margaret Leinen (Univ. of Rhode Island), Presiding

0 82

GRAIN SIZE AND ACCUMULATION RATE OF THE EOLIAN COMPONENT OF SOME NORTH PACIFIC SEDIMENTS

David K. Rea
Thomas R. Janecek (both at: Dept. Atmos. & Oceanic Sci., U. of Michigan, Ann Arbor, Mi. 48109)

The inorganic, non-authigenic fraction of deep-sea sediments recovered far from continents should be dominated by wind-blown dust. We have isolated this component in samples from DSDP Sites 310 and 466 on Hess Rise, 463 on the Mid-Pacific Mountains, and from the large diameter piston core (GPC-3) recovered 1000 km north of Hawaii. Changes in the mass accumulation rate (MAR) and grain size (ϕ_{50}) of the eolian component should record changes in continental climate, volcanism, wind intensity, and distance to source. GPC-3 contains the most continuous Cenozoic record and has already been analysed for quartz and Al accumulation, commonly accepted eolian indicators. Eolian MAR's in this core vary from a low of 0.008 g cm^{-2}10^{-3}y^{-1} 44 to 35 mya to a maximum of 0.23 g cm^{-2}10^{-3}y^{-1} about 1 mya. A large increase occurs about 3.5 mya, with lesser jumps about 15 and 25 mya. These particles range in size from 8.9 Ø to 8.0 Ø, covarying with the eolian, quartz and Al accumulation rates. Sections from the north central Pacific contain only an upper Miocene to Recent record and show about a five-fold increase in eolian MAR's since the late Miocene, with maxima at 4 to 6 and 0 to 2 mya. Higher values occur beneath the westerlies than under the tradewinds. Grain size of these materials ranges from 8.8 Ø to 7.8 Ø and also covaries with MAR. Together, all these sites show a 5 to 7-fold increase in eolian MAR and a doubling of the mass of the average wind-borne particle since the late Miocene. Published mineralogy of these samples suggests that the general increase in all eolian indicators since the Pliocene reflects the onset of northern hemisphere glaciation and the Quaternary increase in Pacific-area volcanism. The secondary peak in the central Pacific sites (310, 463, 466) apparently reflects increased early Pliocene volcanism (Kennett, et al.,1977).

0 83

CHEMICAL STRATIGRAPHY AND PALEOENVIRONMENT OF CENOZOIC NORTH PACIFIC SEDIMENTS

M. Leinen, Graduate School of Oceanography, University of Rhode Island, Kingston, RI, 02881
G. R. Heath and C. Muratli, School of Oceanography, Oregon State University, Corvallis, OR, 97331

Cenozoic sediments recovered in cores from the central North Pacific are lithologically very homogeneous, fine-grained red clays. In spite of this litholigic uniformity, geochemical and mineralogical studies show that pronounced changes in pelagic sedimentation have taken place in the North Pacific over the Cenozoic. These changes have imparted strong geochemical signals to the sediment which can be correlated over distances of thousands of kilometers. Magnetic reversal stratigraphy, ichthyolith stratigraphy, ash layers and natural remnant magnetization peaks serve to establish the validity of the correlation between geochemical records.

The chemistry and mineralogy of central North Pacific cores show several paleoceanographic and paleochemical features: 1) a decrease in the importance of detrital sedimentation between the latest Cretaceous and the Cenozoic; 2) enhanced accumulation of hydrothermal phases between 40 and 50 Ma; 3) enhanced accumulation of authigenic phases associated with diagenetically altered ash layers deposited between 25 and 35 Ma from explosive vulcanism in western North America; and 4) differences in the chemistry and mineralogy of detrital phases transported to the North Pacific by the northeast trade winds and the Northern Hemisphere westerlies.

0 84

DETAILED ^{230}TH AND ^{231}PA CHRONOLOGY IN 13 CENTRAL PACIFIC BOX CORES

Augusto Mangini (Dept. of Geology & Geophysics, Yale University, New Haven, CT 06520) (Sponsor: K.K. Turekian)

^{230}Th and ^{231}Pa profiles were measured on box cores of siliceous and calcareous ooze sediment from small areas between Clarion and Clipperton Fracture Zones. The cores were recovered during a W. German program (RV Valdivia cruises 05, 08) to study geophysics, geology and geochemistry of the North Central Pacific Mn-nodule province. ^{230}Th and ^{231}Pa yield average sedimentation rates of 2.4 and 4 mm/ky during the Late Quaternary for the siliceous and calcareous ooze, respectively. Due to bottom transport the thickness of the Quaternary layer varies from more than 10m to a few cm in cores taken within a short distance of one another. In 5 siliceous ooze cores only 5-18 cm sediment with excess activities (<400,000y) unconformably overlies old Tertiary material. The age of the last major change from an erosional to a depositional regime may be dated at around 68,000y B.P. This age also marks a change in the accumulation rate in 2 cores accumulating for more than 300,000 years. Preferential scavenging of ^{230}Th in comparison to ^{231}Pa in the water column is shown by ^{230}Th/^{231}Pa activity ratios around 30 in the uppermost 4-10 cm sections. The ^{230}Th/^{231}Pa activity ratio of the sedimenting particles was modeled to be 20-22 instead of the theoretical value of 10.8 expected from production in the water column.

0 85

VARIATIONS OF GEOCHEMICAL ENVIRONMENTS IN PELAGIC SEDIMENTS OVER THE LAST 3 MILLION YEARS

Paul C. Henshaw, Jr. (Chevron Oil Field Research Co., P. O. Box 446, La Habra, CA 90631)

Thirteen cores from various pelagic regions of the Pacific Ocean have been analyzed for 21 trace elements and mineralogy to determine variations, both in space and through time, in geochemical environments of deposition. By selecting nine trace elements (Ce, Cr, Ba, Cs, Sc, Fe, Co, Eu, and La) the influence of the major sources--continental, biogenic, hydrothermal, and hydrogenous--can be estimated. For the

North Pacific cores, two major groups are seen: fossiliferous cores with and without manganese nodules, which display a two-component, continental-biogenic system; and nonfossiliferous, micronodule-containing cores which display a significant hydrogeneous component. The Southern Equatorial Pacific cores studied were dominated by a hydrothermal source factor. Analyses of clays and magnetic minerals increased the definition of each geochemical group.

O 86

EVIDENCE FOR AN OCEANIC WARMING AT THE ONSET OF THE LAST GLACIAL MAXIMUM (25-20,000 YBP)

Crowley, T. J. (Dept. Physics, Univ. Missouri St. Louis, St. Louis, MO 63121)
(Sponsor: Philip B. James)

Some recent results indicate that sea-surface temperatures (SST) remained at interglacial levels in the subarctic North Atlantic during initiation of ice-sheet growth. Faunally-derived SST-estimates from North Atlantic and some North Pacific low- and mid-latitude sites also indicate an inverse response between SST and ice volume growth at 25-20,000 YBP, the time of rapid ice advance towards the last glacial maximum. Although in many of the North Atlantic sites the SST-increases were only 1-2 °C, within the standard error of estimate for single samples, the consistent response over a large region suggests that the pattern is real. Where SST-increases are larger or accompanied by marked faunal shifts, they can be related to changes in the local oceanic circulation: for example, decreased upwelling in the eastern equatorial Pacific, or increased advection of warm North Atlantic Current waters.

O 87

GLACIAL MELTWATER INFLOW INTO THE GULF OF MEXICO DURING THE ILLINOIAN GLACIAL AND SANGAMONIAN INTERGLACIAL

W. Fred Falls (Dept. of Geology, Univ. of South Carolina, Columbia, S.C. 29208)
Douglas F. Williams

Oxygen isotopic analyses of planktonic foraminifera (Globigerinoides ruber and Globorotalia truncatulinoides from three piston cores in the southwest Gulf of Mexico record glacial meltwater run-off in the surface waters of this marginal basin. Two distinct, negative oxygen isotopic anomalies occur at approximately 125,000 and 140,000 years before present (YBP). Cores TR126-23, TR126-24 and TR126-29 were analysed at 1000 to 1500 year intervals across the W/X biostratigraphic boundary (which approximates the 5/6 isotope stage boundary). The 125,000 YBP anomaly corresponds with maximum rapid deglaciation of the North American ice sheet of Illinoian age. Upon correcting the shallow-dwelling G. ruber data for the -1.85°/oo change due to ice volume, an additional -0.5 to -1.2°/oo meltwater effect is observed. Analyses of deep-dwelling G. truncatulinoides in core TR126-29 record a total isotopic change of -1.55°/oo. The 140,000 YBP anomaly occurs just prior to the point of maximum glaciation and correlates with a sizable volcanic ash layer in TR126-23 and TR126-24. The G. ruber data records as much as a -1°/oo anomaly and the G. truncatulinoides data records only a -0.4°/oo anomaly. The carbon isotope data shows a positive correlation with the oxygen isotope data at the 125,000 YBP anomaly and the same correlation at the 140,000 YBP anomaly except in TR126-29.

O 88

A CONTINUOUS RECORD OF LATE NEOGENE CARBONATE CYCLICITY: HPC SITE 502, WESTERN CARIBBEAN

W. L. Prell (Dept. of Geol. Sci., Brown University, Providence RI 02912)
J. V. Gardner (U. S. Geol. Survey, Menlo Park CA 94025) and
Scientific Staff of DSDP Leg 68

We used the DSDP hydraulic piston corer to recover an almost continuous, undisturbed composite record (230 m) from Holocene through late Miocene (~8 my). Site 502 consists of four holes located on a small topographic high in the western Caribbean about 220 km north of Panama. The sediment grades from foram-nanno marl of Quaternary and late Pliocene age to nanno marl and calcareous clay in the late Miocene. Total carbonate content is cyclic and correlates well with established $\delta^{18}O$ and carbonate cycles of the Brunhes epoch. Although they vary in amplitude, carbonate cycles are continuous through the Pliocene and into the late Miocene.

On the basis of shipboard paleomagnetics and carbonate analyses, we calculated a preliminary spectrum on a carbonate time series from the mid-Pliocene (2.92 to 3.80 my). The spectrum shows a concentration of variance near periodicities of 250K and 43K yr, the latter being coherent with the variation of planetary obliquity. A carbonate spectrum in piston core V12-122 (0 to 460K yr) shows concentrations of variance at 100K yr and 42K yr. These preliminary results suggest that: (1) periodicities related to obliquity are impressed on the sediments to at least 4 my, and (2) the climate system is nonstationary at the 100K yr periodicity.

O 89

CALCIUM CARBONATE DISSOLUTION IN THE SOUTHERN OCEAN DURING THE LAST 0.69 MILLION YEARS

David Gribble (Dept. of Geology, Univ. of South Carolina, Columiba, S.C. 29208)
Douglas F. Williams and Bruce H. Corliss

During the last 0.69 million years, the carbonate dissolution pattern in the Southern Ocean appears to be in-phase with that in the Atlantic (i.e., enhanced dissolution occurs during glacial periods). A major complicating factor in this region is the migration of the Polar Front which controls the regional production of calcium carbonate. Calcareous ooze predominates north of the Polar Front, while to the south (50-60°S), siliceous ooze is the major sediment type. Three Eltanin piston cores from water depths of 3200 to 3942 m and beneath the subantarctic water mass were used in an attempt to separate the productivity and dissolution effects. The shallowest core (E49-18, 3200m) is well above the present $CaCO_3$ compensation depth (CCD) at 4500m and was used to determine the timing of Polar Front migrations. The cores were correlated with oxygen isotope and paleomagnetic stratigraphy. The total $CaCO_3$ content decreases, and foraminiferal fragmentation, benthic/planktonic ratios and radiolarian/foraminiferal ratios increase as the degree of dissolution increases. In the two deep cores (E45-79 and E45-74), the oxygen isotope data become difficult to interpret after isotope stage 13. The glacial/interglacial isotopic difference decreases from 1.2°/oo between stages 1 and 2 to 0.6°/oo between stages 11 and 12. In the shallower core, the isotopic difference remains fairly constant (1.6°/oo between stages 5 and 6 and 1.5°/oo between stages 11 and 12). $CaCO_3$ content decreases in all cores during glacial periods and indicates that dissolution and productivity of calcium carbonate in the Southern Ocean are in-phase with dissolution in the Atlantic Ocean during the Late Quaternary.

O 90

SEDIMENTARY HIATUSES ALONG THE SOUTHERN CONTINENTAL RISE OF AUSTRALIA

Douglas F. Williams (Dept. of Geology, Univ. of South Carolina, Columbia, S.C. 29208)
Michael Ledbetter

To better understand the consequences of Antarctic Bottom Water (AABW) flow on sedimentation along the southern continental rise of Australia, paleomagnetic, biostratigraphic and lithologic studies were performed on over 40 piston cores from cruises 53 and 55 of the USNS Eltanin. The cores are located along the entire margin from the Naturaliste Plateau to the South Tasman Rise. Subtropical foraminiferal zonations were used to correlate the magnetic polarity records to the geomagnetic polarity time scale. Widespread hiatuses during the Cenozoic were discovered in cores between water depths of 2000 and 3000 fathoms along the margin. Six of the cores have late Brunhes sediments at the core tops separated by late Gauss-early Matuyama sediments. Three cores from the flank of the Naturaliste Plateau have Late Miocene to Middle Miocene sections with little or no Plio-Pleistocene sediments. Lithological changes in the cores and preservational trends in the foraminiferal faunas also make it possible to determine temporal changes in the depth of the carbonate compensation depth (CCD) along the margin. The foraminiferal faunas from the Miocene sediments show evidence of moderately severe dissolution at water depths 1200 meters shallower than the present level of the CCD. Regional patterns in carbonate sediments and red clay/manganese micronodules, combined with the age distribution of the cores, suggest that the long-term history of AABW flow along the southern continental rise of Australia can be correlated to erosional events observed in deep basins surrounding Antarctica.

O 91

LATE QUATERNARY PALEOCLIMATIC AND PALEOGLACIAL HISTORY OF THE PACIFIC SUB-ANTARCTIC AND ANTARCTIC REGION.

M. Trinchitella (Exxon Co. USA, Houston, Texas, 77001).
M. G. Dinkelman

Sedimentological and micropaleontological analyses on closely spaced samples from twelve piston cores collected from the Bellinghausen-Amundsen Basin revealed four glacial and three interglacial events during the last 194,000 years. Oxygen isotope stages (OIS) 2 and 6 record glacial maxima of near equal severity. The warmest interglacial event occurs during OIS 5e and a less intense warming occurs in OIS 3.

Regional sedimentation rates were found to be higher during interglacials and lower during glacial events. These differences are related to both direct and indirect regional effects due to changes in the intensity of the Antarctic Circumpolar Current. The utility of the Cycladophora davisiana stratigraphy is extended 7° to 8° south of the Polar Front Zone. C. davisiana abundance intervals "b_2" and "h" correlate to glacial maxima and are most reliable for regional correlations. A stratigraphy based on the abundance changes of the diatom Eucampia balaustium is documented and developed for the last 194,000 years. Eight abundance intervals ('a' to 'f') were recognized and calibrated to the oxygen isotope stratigraphy in deep-sea core E45-74 from the southern Indian Ocean. Peak abundances of E. balaustium occur during increased glaciation and are easily recognizable for correlation throughout the study area.

O 92

DEEP-SEA VOLCANIC ASH AS A PALEOWIND INDICATOR

T. C. Huang (Graduate School of Oceanography, University of Rhode Island, Kingston, R.I. 02881)

Deep-sea air-fall ash distribution in sediment cores provides information on the direction and speed of the tropospheric and lower stratospheric prevailing wind during the time of eruption. Spatial variations in ash thickness, concentration or accumulation rate and in selected ash size ranges produced by single eruptions in several volcanic regions have been used to delineate the direction and extent of ash cloud axis and the width of lateral ash dispersion. From these, together with the modeling of downwind ash distribution and eruptive cloud height, the paleowind speed and direction can be derived.

In the Azores, four highly explosive eruptions occurred at about 125×10^3 and 33×10^3 years ago. The ash distributions reveal that the east-north-eastward prevailing winds have an average speed (33 km/hr) of about half of the present N. Atlantic wind speeds. In New Zealand, an average eastward wind speed of about 40 km/hr has been estimated based on the ash distributions produced by the explosive eruptions during the past 690×10^3 years. In the northern Lesser Antilles, a change in the

ambient wind directions between the two periods (23×10^3 to 11×10^3 years and 11×10^3 years to the present) has been detected based on the ash distributions in a series of N-S traverse cores. In the area north of 17°N latitude the ash accumulation rates in the cores east and west of the islands remain about the same during the two periods. At about 17°N latitude, a marked difference in the rates between the two sides has occurred during the two periods. The change in wind direction may have been associated with a latitudinal shift of the meteorological boundary during the climatic change.

O 93

BENTHIC BIOTURBATION OF THE DEEP-SEA RECORD: SIGNAL DISTORTION, IMPULSE RESPONSE FUNCTIONS AND SIGNAL RESTORATION

W.H. Hutson, (School of Oceanography, Oregon State University, Corvallis, Oregon 97331)

Benthic organisms disturb adjacent sedimentary layers, thus distorting the true deep-sea record. For example, bioturbation disperses an instantaneously deposited tracer, such as a thin ash or microtektite deposit. The resulting vertical distribution, or "impulse response function" (IRF), is an accurate description of the mixing process. Furthermore, the IRF may be used numerically as a weighted moving average to simulate the process of bioturbation. For example, numerical experiments indicate the following relationship exists between the IRF and amplitude attenuation:

$$A' = A \cdot [Hmax/\Sigma H], \quad (1)$$

where A and A' are the original and attenuated amplitudes, and Hmax and ΣH are the maximum and sum of IRF values.

The above relationship may be used to reconstruct the deep-sea record in the following manner: (a) A measured signal is first converted into a series of "impulses" above or below a baseline (as defined by adjacent points); (b) The following equation is used to approximate the original amplitudes, Â:

$$\hat{A} = A' \cdot [\Sigma H/Hmax] \quad (2)$$

(c) These estimated amplitudes may then be converted into a reconstructed signal by adding the appropriate baseline values.

Numerical experiments demonstrate this approach and illustrate that its effectiveness is a function of both (a) the length and shape of the IRF distribution relative to sample spacing, and (b) the sharpness of transitions within the signal itself.

O 94

BENTHIC MIXING INTENSITY IN THE 9300 B.P. SUBPOLAR NORTH ATLANTIC

Glenn A. Jones (Lamont-Doherty Geological Observatory of Columbia University, Palisades, NY 10964)

A new non-dimensional convolution mixing model that allows both the use of any mixing filter, and the quantification of the integrated mixing intensity has been tested on ash zone 1 (9300 B.P.) in nineteen cores from the subpolar North Atlantic. A best fit of the mixing model to the observed dispersed ash in each core is made, then the amount of integrated mixing necessary for the best fit is calculated. In all cases the model accurately fits the observed data.

Geographically, plots of integrated mixing produce consistent patterns. The lowest mixing values (five cores) occur in a narrow band between 45°-50°N and 25°-40°W (lack of core coverage prevents the extent of the E-W trend from being clearly defined). Two paleo-oceanographic interpretations can explain the observed integrated mixing distribution: (1) If both large volumes of Laurentide meltwater (Kennett and Shackleton, 1975) and increased sea ice from the Labrador Sea were vented to the subpolar North Atlantic subsequent to 11,800 yrs B.P. to significantly lower sea-surface salinity in the 5° band, vertical oceanic mixing could have been inhibited, with a resultant decrease in both surface water productivity and benthic activity. (2) The present subpolar North Atlantic contains a region of low surface productivity centered around 53°N and 27°W. During 9300 B.P. this feature could have been shifted to the south as the 9300 B.P. subarctic convergence was displaced southward relative to the modern position by almost 5°.

O 95

PALEOCEANOGRAPHIC INFORMATION FROM THE TEST SHAPE OF GLOBOROTALIA TRUNCATULINOIDES: RESULTS OF FOURIER SHAPE ANALYSIS

Nancy Healy-Williams (Dept. of Geology, Univ. of South Carolina, Columbia, S.C. 29208)
Douglas F. Williams

Fourier series shape analysis of the test of Globorotalia truncatulinoides has resulted in an effective differentiation of phenotypic and ecophenotypic variation. Amplitudes of the 2nd harmonic (indicative of elongation) are strongly correlated with coiling direction while the 3rd harmonic (triangularity) is highly correlated with average surface water temperature and latitude but varies as a function of coiling direction (100% to 5% sinistral). This effect is believed to be phenotypic rather than ecophenotypic. The G. truncatulinoides were obtained from 16 trigger core tops and 4 piston core tops from the southern Indian Ocean. The coiling direction of the assemblages ranged from 100% sinstral to 5% sinstral. Samples were chosen for good preservation and were within the cool subtropical and subantarctic water masses (from 19°S to 47°S). Closed form Fourier series analysis is a mathematical expression of cosines used to describe any shape outline to a specified degree of exactness. Fourier series not only provides an exact characterization of shape but also separates the components of the whole form enabling us to see how each is affecting the total shape. The 2nd and 3rd harmonics were chosen because the harmonic amplitude spectra indicates that these contain the most information from the 20 harmonics generated during the analysis. The results of this study point to the unique potential of Fourier shape analysis in biometric and paleoceanographic studies of foraminifera.

O 96

OXYGEN ISOTOPIC EXCHANGEABILITY OF BIOGENIC SILICA

LABEYRIE L.D. (C.F.R., CNRS, 91190 Gif/Yvette, France)
JUILLET A.M. (C.F.R., CNRS, 91190 Gif/Yvette, France)
(Sponsor : Claude Lalou)

Paleoclimatic studies using biogenic opal $^{18}O/^{16}O$ ratio measurements have been hampered by a lack of reproducibility. Opal isotopic ratios as those of other hydrated minerals, are strongly affected by the dehydration treatments preceeding oxygen extraction; dehydration involves hydroxyles combination which introduces extraneous oxygen in the structure. We have utilized a method recently developped, which promotes oxygen isotopic equilibration during the hydroxyle combination to study oxygen exchangeability of biogenic silica at different temperatures. This method insures a ±0.09‰ (1σ) reproducibility. Estimation of the amount of exchangeable oxygen is done by exchange of the silica with waters differing largely in isotopic composition. For a 6 hour exchange at 150°C, this amount decreases from 15-20% in diatom valves silica from phytoplankton or modern sediment to 5-6% in samples a few thousand years old. This decrease is due to the higher solubility of the organic and water-rich outer silica layer. The amount of exchangeable oxygen in older samples (a few million years old) is lowered to 1-2%, possibly due to partial recrystallization. Exchangeability of diatom silica increases significantly by heating over 250°C (50% of exchangeable oxygen at 300°C, 60% at 500°C in 6 hours), during the silica reorganisation which occurs at these temperatures.

O 97

U IN FORAMINIFERA TESTS

Margaret Delaney (Dept. of Earth & Planetary Sciences, M.I.T., Cambridge, MA 02139)

Uranium concentrations in foraminiferal calcite reported in the literature range from values as high as 1.20 ppm to a lower value of 0.025 ppm. Uranium and thorium isotope activities were measured by isotope dilution alpha spectrometry in four late Pleistocene and Holocene foraminiferal carbonate samples from 2 piston cores taken on the north flank of the Rio Grande Rise (30°S, 35°W; 2158 m. and 2330 m. water depth). Tests were separated with a 150 μ sieve and ultrasonically cleaned.

Samples were then subjected to reductive cleaning with a dithionite-citrate-hydroxylamine hydrochloride solution to clean the surfaces of any iron-manganese oxide coatings and any adsorbed nuclides. Results from several larger sieved samples were consistent with those from a smaller hand-picked sample. There is 0.027 ± 0.008 ppm U in the calcite lattice (1.14×10^{-8} moles U/moles Ca), in agreement with the lowest literature value, 0.025 ppm (Ku, 1965). The observed distribution coefficient is therefore 0.008; the experimentally determined range is 0.2-0.04 for inorganically precipitated calcite (Kitano and Oomori, 1971). The $^{230}Th/^{234}U$ activity ratios range from 5.5 to 26, indicating that the cleaning method does not effectively remove ^{230}Th from the surfaces. The upper limit for the thorium concentration in foraminiferal calcite is 0.023 ppm (9.96×10^{-6} moles ^{232}Th/mole Ca). Dating by ^{230}Th ingrowth measurements is not feasible because of the low concentration of uranium in foraminiferal tests and the difficulty of removing ^{230}Th from their surfaces.

O 98

ANOMALOUS IRIDIUM AT THE CRETACEOUS-TERTIARY BOUNDARY: THE IMPACT HYPOTHESIS

L.W. Alvarez (Lawrence Berkeley Laboratory, University of California, Berkeley, CA 94720)
W. Alvarez (Dept. of Geology and Geophysics, University of California, Berkeley, CA 94720)
F. Asaro, H.V. Michel (Lawrence Berkeley Laboratory, University of California, Berkeley, CA 94720)

Anomalous concentrations of Iridium occur at the Cretaceous-Tertiary (C-T) boundary in three areas of Western Europe and are interpreted as evidence for an influx of extraterrestrial material related to the biotic extinctions. Iridium increases above the background level by 27x in Italy and by 160x in Denmark. Jan Smit (Univ. of Amsterdam) has found a ≥ 100x increase in southern Spain. The Ir source is probably not a supernova. We suggest that impact of a ca. 10-km Apollo object would deposit the observed iridium and would cause the extinctions by injecting dust expelled from a ca. 150 km diameter crater into the stratosphere, where it would strongly attentuate the sunlight for several years, thus suppressing photosynthesis and bringing about the collapse of food chains. Iridium measurements are now being made on C-T boundary material from New Zealand, the South Atlantic, and Montana, and on Permian-Triassic boundary material from China.

Measurements In the Gulf Stream

Harbour B
Friday P.M.
Philip Richardson (Woods Hole Oceanographic Institution), Presiding

O 99

VARIABILITY IN THE NORTHWALL OF THE GULF STREAM

D.N. Connors (Code 3635, Naval Underwater Systems Center, Newport, RI 02840)
M.P. Fecher (Code 3635, Naval Underwater Systems Center, New London, CT 06320)

The Northwall of the Gulf Stream has been investigated using a data set consisting of eight XBT/XSV transects obtained from Oct-Nov/1979 between 65° and 66°40' W Long. In six of these a station spacing of about 1.2 km permits a relatively high resolution of the thermal structure. Continuous measurements of temperature were also obtained for the sea surface and either 20 m or 180 m; data are also available from satellites and VNX-8 overflights.

During a period of rapidly changing winds the

upper ocean displayed; strong horizontal temperature gradients, interleving, or a relatively well mixed layer. The mean slope of the Northwall ranged from 4 to 18 m/km. On several of the transects the 15°/200 m criteria for defining the northern edge of the stream encompassed a distance of 20 km or more. In one instance the 15° isotherm showed a wave like variation with an amplitude of 15-20 m about the 200 m depth. On a second transect stations 600 m apart, within and near a sea surface slick, showed a difference of 55 m in the depth of the 15° isotherm about the 200 m level.

O 100

MAPPING OCEAN CURRENTS BY MEANS OF OVER-THE-HORIZON HF RADAR

D.B. Trizna (Naval Research Laboratory, Washington, D.C. 20375)

Results are reported for preliminary experiments in mapping the Gulf Stream by means of currents measured by an HF radar. Operating in the over-the-horizon mode of propagation via stable E-layer paths, components of current vectors radial to the radar are mapped on a range-azimuth grid roughly 6 km on a side, using a large aperture receive array 1100 m in extent. Radial currents of the order of a meter per second were observed and appear to be associated with sharp bends in the Gulf Stream.

O 101

PARTICLE ACCELERATION AND ANOMALOUS ION DRAG IN A LABORATORY PLASMA UNDERGOING MAGNETIC FIELD LINE RECONNECTION

W. Gekelman
R. L. Stenzel, N. Wild (All at: Dept. of Physics, Univ. of California, Los Angeles, CA 90024)

The spatial and temporal history of the anomalous ion drag term $mn\nu^*v$, in the neutral sheet of a laboratory plasma undergoing magnetic field reconnection has been measured. Extensive measurements of the plasma pressure nkT_e, magnetic forces $\vec{J}x\vec{B}$, and ion velocity flow fields $\vec{v}$ have been performed in a highly reproducible repetitive plasma with the aid of digital data acquisition and mass storage. The pressure is found to peak at the contact points of the separatrix, near the edge of the neutral sheet. It exhibits large transverse gradients creating space charge fields and Hall currents. The magnetic force density $\vec{f} = \vec{J}x\vec{B} - \nabla(nkT_e)$ arises from axial currents driven by an induced electric field and transverse Hall currents. The ion flow field is directly measured using differential particle collectors. The acceleration due to $\vec{f}$ is directly compared with $mn\ dv/dt$. It is found that an anomalous ion drag limits the acceleration. Only after several Alfvén times does the fluid develop the classical flow pattern with jetting from the edges of the neutral sheet.

O 102

COASTAL-TRAPPED AND FRONTAL-TRAPPED WAVES IN A BAROCLINIC WESTERN BOUNDARY CURRENT

John M. Bane, Jr. (Marine Sciences Program and Department of Physics, Univ. of N. Carolina, Chapel Hill, NC 27514)

Four types of stable, sub-inertial Rossby-like waves have been found to propagate alongshore in a model baroclinic boundary current similar to the Gulf Stream as it flows along the continental margin of the southeastern United States. The two-layer model incorporates a general bottom topography with continental shelf and slope, and a thermal-wind mean current confined to the upper layer. The four wave components are: the familiar continental shelf wave, quasi-geostrophic edge wave, and complementary mode edge wave, plus a new frontal-trapped wave, which has wave amplitude maxima within the cyclonic side of the Stream. The dispersion diagram for a particular topography/density/current setting may be interpreted as a composite of the four components' dispersion curve families. As in other, similar problems a mode-coupling resonance between two components allows the characteristics of the two to be interchanged. The cases studied show the phase speeds of the various components to be affected by the location of the surface density front, the width of the continental shelf, and whether the inshore boundary is a vertical wall or a sloping beach. In general, the continental shelf waves (the quasi-geostrophic edgewaves) are faster (slower) for a shelf with a coastal wall than for one with a sloping beach. The complementary mode edgewaves and the frontal-trapped waves are fastest with the surface front farthest from shore.

O 103

ON THE VARIATIONS OF LOW-FREQUENCY MOTIONS ALONG 70°W

W. Brechner Owens (Woods Hole Oceanographic Institution, Woods Hole, MA 02543)
Harry L. Bryden
James R. Luyten

An analysis of a nine-mooring array centered at 31°N, 70°W, which was part of the POLYMODE Local Dynamics Experiment, indicates a marked change in eddy structure and trebling of kinetic energy from that seen in the MODE Experiment at 28°N. The ratio of shallow to deep kinetic energies is frequency independent in contrast to the MODE results in which the lowest frequencies were much more baroclinic. This tendency along 70°W can be reconciled with other data sets along 55°W and 60°W only if one compares similar locations with respect to the Gulf Stream-Recirculation system. Array representations of the velocities in the upper thermocline indicate that this increase is associated with a much richer mix of spatial scales than was seen in MODE.

O 104

SEASAT SCATTEROMETER MEASUREMENT OF THE GULF STREAM

Peteherych, S. (AES, Downsview, Ont., M3H 5T4)

(Sponsor: Clive Jarvis, CMOS)

Microwave radar backscatter from the ocean has been shown to be due to Bragg scattering from centimeter-length capillary ocean waves with the strength of the radar backscatter being proportional to the capillary wave amplitude. A variety of mechanisms can alter the wave amplitude. Internal waves, organic films, surface wind, currents and bottom topography are a few examples.

For the Gulf Stream, sunglint features and features in aircraft radar imagery are associated with the frontal processes present in the area.

Observations suggest that these features are often due to roughness variations which in turn are due to variations in the stability of the atmospheric boundary layer caused by the large water temperature difference between the Gulf Stream and adjacent areas.

Seasat scatterometer data reveals variations in radar backscatter which are related to Gulf Stream frontal features. Examples are presented for differing meteorological conditions and the implications for ocean current monitoring are discussed.

O 105

THE USE OF SATELLITE RADAR IMAGES TO STUDY MAJOR OCEAN CURRENTS

H.J. Schultz
R.A. Shuchman (Both at: Environmental Research Institute of Michigan, Ann Arbor, MI 48107)
G.A. Meadows (Department of Atmospheric and Oceanic Science, The University of Michigan, Ann Arbor, MI 48109)

SEASAT SAR (synthetic aperture radar) and altimetry data were compared with in-situ observations and bathymetric data to investigate satellite remote sensing techniques for studying major ocean surface currents. SAR images of the Gulf Stream region show linear surface features representing regions of increased radar backscatter. Since microwave scattering theory predicts an enhancement of radar cross section for regions of increased surface roughness, areas of strong current shear along the Gulf Stream boundary should be discernible on the imagery. The location of the Gulf Stream boundary as determined from the SAR images shows close agreement with the position calculated from the altimetry data and in-situ observations. Application of this technique permits large scale observations of ocean surface features which are impractical by conventional means. In addition, SAR techniques offer significant advantages over other remote sensors by retaining small scale as well as synoptic sea surface information.

O 106

THE ROLE OF RINGS IN THE CIRCULATION OF THE NORTHWESTERN ATLANTIC

Donald B. Olson (Rosenstiel School of Marine and Atmospheric Science, Miami, FL. 33149)

The significance of Gulf Stream rings to the circulation of the region northwest of Bermuda is considered. First the energetics of cyclonic rings are reassessed and earlier estimates of ring available potential energy (APE) shown to be in error. Based on the new ring APE calculations and similar estimates for the subtropical gyre the contribution of rings to the gyre is discussed. The dependence of the results on the ring population and different strategies for obtaining the "mean" gyre APE are explored. The results are also contrasted with recent modelling efforts. The discussion of ring energetics is followed by one on the role of rings in the potential vorticity, heat, and salt balances. While there are large errors involved with estimates of these three budgets it is possible to provide a first order description of them given some simple assumptions. Finally comments are made on means for improving the quality of these types of estimates.

O 107

SATELLITE AND HYDROGRAPHIC OBSERVATIONS OF GULF STREAM RING PERTURBATIONS

Thomas W. Spence (Department of Oceanography, Texas A&M Univ., College Station, TX 77843)
Richard Legeckis (National Environmental Satellite Service, Washington, D.C. 20233)

Thermal infrared data from the NOAA polar orbiting satellite and hydrographic observations from surface ships have been used to describe wave-like perturbations around the circumference of a Gulf Stream cyclonic eddy in April 1977. After rectification, satellite images show an elliptical feature near 36.5°N, 69.5°W. During mid-April, the orientation of the major axes rotated counterclockwise at $\omega = 5 \times 10^{-6}\ s^{-1}$, about 15% of the maximum surface gradient velocity. Estimates of ω are obtained from the temperature field observed by XBT and from the drifter track obtained by Richardson (*J. Phys. Oce.*, 10, 90-104, 1980). The perturbation is described as a stable mode of azimuthal wave number two propagating in the direction of the mean flow.

O 108

AXBT MEASUREMENTS OF A GULF STREAM RING ABOVE MUIR SEAMOUNT

R.H. Feden
J.M. Bergin (both at: Acoustics Division, Naval Research Lab, Wash., D.C. 20375)

Airborne expendable bathythermograph (AXBT) measurements were made of a gulf stream ring on 14 and 16 May 1979. The ring was centered above Muir seamount which rises to within about 1km of the surface. At the 300m depth level the ring has dimensions of about 200km x 130km based on the 17°C isotherm. The lowest temperature recorded at the 300m depth level was 11.1°C which gives a temperature contrast of about 7°C between ring center and exterior Sargasso Sea conditions. The most significant aspect of the measurements involves a complex azimuthal structure which seems to imply a four-lobed structure to the ring. This structure may equivalently be viewed as implying a wavelike structure to the ring. The vertical amplitude of the wave is approximately 100-150m based on the topography of the 17°C surface. A strong surface signature appears to be associated with the deeper thermal structure. There is evidence of a cool band of surface water in an annular region located above the deeper

wavelike structure. An interpretation of the cool band is that the 18°C thermostad has been raised to the surface by the wave and has partially mixed with the warmer surface water.

O 109

GULF STREAM RING STRUCTURE AND EVOLUTION OVER A SHORT TIME INTERVAL

J.M. Bergin (Acoustics Division, Naval Research Lab, Wash., D.C. 20375)

An extensive program of measurements of a gulf stream ring was conducted in June 1979 approximately 200km north of Bermuda. The primary aim of the oceanographic measurements was to determine the large scale ring structure and its evolution over the period of observation. A preliminary discussion of the measurements carried out by one of three participating ships shall be given. Measurements were made by expendable bathythermograph probes and a rapidly sampled sea chest thermistor. During a seven day period two pinwheel patterns were made of the ring. The isotherm pattern at 300m indicates that the ring has an egg-shape as opposed to a circular shape with dimensions of about 200km x 130km. A change of about 600m in the vertical occurs for the depth of the 10°C isotherm as one goes from the exterior Sargasso conditions to the center of the ring. A comparison of the two estimates of the ring structure at 300m seems to imply that the ring structure is rotating about the vertical with a rate of about 10°/day. The importance of the measurements is that they imply gulf stream rings may have a substructure possibly due to the mixed barotropic-baroclinic instability mechanism theoretically studied by Hart and others.

O 110

DEEP VELOCITY OBSERVATIONS BENEATH A GULF STREAM MEANDER OFF ONSLOW BAY

E.R. Levine (Code 3635, Naval Underwater Systems Center, Newport, RI 02840)
J. Bergin (Code 5110, Naval Research Laboratory, Washington, D.C. 20375)

Velocity and temperature measurements were obtained form an Aanderra current meter moored 52m above the bottom (540m depth) at 33°32.0'N, 76°15.1'W from August 17-21, 1977. During this period, 18 traverses of a 100km XBT-CTD section were made between 33°43.5'N, 76°47.2'W and 32°39.0'N, 75°12.0'W, which crossed the current meter mooring and were oriented approximately perpendicular to the Gulf Stream.

Results from the hydrographic survey show that the Gulf Stream axis as defined by the 15° isotherm at 200m shifted offshore approximately 25km and returned in four days. A comparison of vertical sections at maximum and minimum seaward displacements show changes in the depth of the 15° isotherm of 100-150m. Results from the moored current meter indicate that the near bottom flow was to the northeast along the bathymetry when the Gulf Stream was inshore; however when the Stream was offshore the ~ 40cm/sec deep flow was to the north or northwest, moving opposite to the direction of upper ocean flow indicated by isotherms.

Thus, during the growth of the meander, a compensating onshore flux was observed at depth. Assuming a two-layer ocean bounded by the 15° surface, the observed deep currents and changes in vertical structure are consistent with an intrusion of deep cold water with a vertical extent of several tens of meters over the duration of the onshore flow.

O 111

WINTERTIME GULF STREAM MEANDERS IN ONSLOW BAY, NORTH CAROLINA

David A. Brooks (Dept. of Oceanography, Texas A&M University, College Station, TX 77843)

The intensity and nature of cyclonic Gulf Stream meanders in Onslow Bay are dependent on the details of the quasi-permanent offshore Stream deflection that occurs ≈ 150 km upstream off Charleston, SC. At times of extreme offshore deflection of the Gulf Stream surface thermal front, fluctuations in the subsurface temperature and flow fields have small amplitudes and several-day periods in Onslow Bay. At times of less extreme deflection, however, large wavelike meanders of the type described by Webster (1961) with a prominent time scale of about 1 week form in the lee of the deflection and propagate downstream at ≈ 35 km d^{-1}. Satellite images suggest that the meanders grow temporally but not spatially. The mid-depth, shelf-break, subtidal flow variance increases by about a factor of 5 during the intense meander activity, which was present in Onslow Bay about 60% of the time from January to May 1979. The meandering currents were in-phase and coherent vertically, incoherent with the local winds, and marginally coherent with coastal sea level fluctuations. Satellite images and vorticity considerations suggest that the large meanders form when the Stream is relatively nearshore and interacts with the shelf-slope topography. Whether or not they form may be a sensitive function of flow parameters upstream of the deflection.

O 112

ROTARY SPECTRA OF GULF STREAM MEANDERS OVER THE CONTINENTAL SLOPE OFF ONSLOW BAY, NORTH CAROLINA

Mark E. Luther
John M. Bane (both at: Curriculum in Marine Sciences, University of North Carolina, Chapel Hill, NC 27514)
David A. Brooks (Texas A&M University, College Station, TX 77843)

A rotary spectral analysis of current data from the inshore edge of the Gulf Stream off North Carolina shows a strong cyclonic rotational component of the current hodograph in the frequency range of 0.1 to 0.3 cycle/day. The current records from four moorings in an L-shaped array cover the period January to May 1979. The rotary spectra for all the current records show a large portion of the rotating variance to be in the positive frequency band of 0.11 to 0.14 cycle/day, corresponding to cyclonic rotation of the current vector at periods of 7 to 9 days, with the peak at 8.2 days. A complex vector demodulation of the time series is performed in this band. Estimates of downstream phase speed of 39 to 45 km/day, and wavelengths on the order of 300 km, confirm earlier estimates obtained from a one-sided spectral analysis of the data. These values are consistent with observations from an airborn XBT survey and from satellite infrared imagery of the area.

Waves and Air-Sea Interaction

Metropolitan Center
Friday P.M.
M. Donelan (Canada Centre for Inland Waters), Presiding

O 113

A NEW WIND-WAVE-CURRENT RESEARCH FACILITY AT THE UNIVERSITY OF DELAWARE

R. J. Lai and Jin Wu
(College of Marine Studies, University of Delaware, Newark, Delaware 19711)

A Wind-Wave-Current Research Facility has been constructed to study air-sea interaction and environmental fluid dynamics. This facility consists of two closed, controlled flow loops within the same tank; one loop is water and the other is air. The width and height of the tank are 1 m and 1.3 m respectively and the length is 42 m. The tank can be tilted to generate a uniform current and is equipped with a heat exchanger to heat and cool the water. The direction of wind in the tunnel can be reversed and the wind system also has separate heat exchangers to control temperature and humidity of the air flow. The range of bulk Richardson number (Ri_g) can be set to ± 0.05 and the wind velocity can reach 20 m/s with wind tunnel of 60 cm height. A mechanical wavemaker is also available and can be mounted to either end of the tank.

Preliminary data of this facility will be presented which include profiles of wind velocity, humidity, temperature, and current.

O 114

AN OPTICAL SCANNER FOR MEASURING SLOPE AND CURVATURE STATISTICS OF OCEAN WAVES

S. P. Haimbach, Y-H. L. Hsu and Jin Wu
(College of Marine Studies, Univeristy of Delaware, Newark, Delaware 19711)

The sea surface features shorter waves riding on longer waves. Recently, there is a great deal of interest in determining statistic patterns of fine structures of the sea surface under various wind conditions. The ripples composing these structures not only are directly involved in both wave generation by the wind and wave-energy dissipation by viscosity, but also reflect and scatter acoustic, light and other electromagnatic waves impinging on the sea surface.

An optical scanner, utilizing the light reflection principle, has been designed and tested. The instrument scans the sea surface at a high speed and the data can be analyzed to determine slope and curvature distributions in any direction with respect to the direction of the wind. Some preliminary results along with description of scanner operation and procedures of data analysis are also presented.

O 115

C_{10}

Jin Wu (College of Marine Studies, University of Delaware, Newark, Delaware 19711)

A scaling law of wind-stress coefficients is presented to illustrate explicitly that the coefficient increases with wind velocity and decreases with fetch; physical reasonings of both trends are discussed. Besides being shown previously to be related to a criterion determining airflow separation from waves, the Charnock relation is further associated with the critical roughness Reynolds number identifying regimes of the atmospheric surface layer. Intrinsic errors and limitations of the Charnock relation, which provides an overall correlation between stress coefficient and wind velocity, are illustrated. A probable nondimensional expression, a refinement of the Charnock relation, is proposed between the roughness length and the wind-friction velocity involving not only gravity but also surface tension and viscosity. Previous compilation of wind-stress data obtained with eddy-correlation and wind-profile methods is found to be consistent with recent results obtained with similar techniques. A single, linear-law empirical formula for estimating oceanic wind-stress coefficients at all wind velocities is suggested, and appears to provide a better representation than the power-law formula proposed earlier. Finally, recent results on relating roughness length to sea-surface irregularities, and on relating stress coefficient to roughness Reynolds number and to dominant-wave characteristics are discussed.

O 116

AN EXTENDED MILES' THEORY FOR WAVE GENERATION BY WIND

D. S. Riley (Dept. of Mathematics, The University, Southampton, U. K.)
W. H. Hui (Dept. of Applied Mathematics, University of Waterloo, Waterloo, Ontario, Canada)
M. A. Donelan (Hydraulics Research Division, National Water Research Institute, Canada Centre for Inland Waters, Burlington, Ontario, Canada)

Miles' inviscid theory of surface wave generation by wind is (a) modified by replacing the logarithmic shear flow with a mean turbulent velocity profile over a flat plate which applies down to the plate surface, and (b) extended to include the effects of air flow turbulence

by considering the wave modified mean flow as representative of the mean of the actual turbulent air flow over water waves and using this in a mixing-length model.

Modification (a) increases the magnitude of the in-phase (with wave height) component of the perturbation pressure but has only a small effect on the out-ofphase component. In contrast, the air flow turbulence is shown to increase the out-of-phase component of pressure by a small but significant amount, whilst leaving the in-phase component almost unchanged. It also gives rise to a damping of waves travelling against the wind. When the modifications (a) and (b) are combined, the present extended Miles' theory is compared with the recent field experiments of Snyder, Dobson, Elliottand Long.

0 117

ESTIMATES OF KINETIC ENERGY, SHEAR, AND REYNOLDS STRESSES FROM OBSERVATIONS OF WIND WAVE MOTION NEAR THE SEA SURFACE

David Shonting (Naval Underwater Systems Center, Newport, RI 02840)
Robin Robertson (Dept. of Ocean Engineering, University of RI, Kingston, RI 02882)

Analysis is made of Eulerian velocities associated with wind waves measured with miniature ducted impeller meters in the upper 10 m from a pier platform in Narragansett Bay. The fast response sensors are shown to spectrally resolve the particle motions of the wind generated waves. The velocities displayed an exponential decrease in variance ("eddy" kinetic energy) with depth. Running variances of vertical velocities with depth displayed flow of energy from the surface clearly related to changing wind stress and propagating downward at 0.5 cm/s. Running mean horizontal velocities display a vertical shear varying with wind speed. Beneath the velocity effects of surface waves an ambient turbulence level appears independent of depth and ranged from 5-20 erg/cm^3.

Running values of estimated Reynold stress beneath the sea surface indicate that "bursting" plays an important role in the momentum flux and that long term temporal (or spatial) "averaged values" of oceanic wind stress vectors may be misleading. Evaluation of the equation of the eddy kinetic energy balance provides order of magnitude estimates for the eddy energy dissipation and pressure work terms.

0 118

SIMULTANEOUS MEASUREMENTS OF BUBBLES AND SPRAY PRODUCED BY BREAKING WAVES

Y.-H. L. Hsu and Jin Wu
(College of Marine Studies, University of Delaware, Newark, Delaware 19711)

Sea spray can be produced by several mechanisms; among them the bursting of air bubbles entrained by breaking waves has been considered by many as the principal mechanism. This, however, has not been verified experimentally.

Simultaneous measurements of water droplets in the air and air bubbles in water are performed in a laboratory wind-wave tank. The results include temporal size distributions of droplets and bubbles and the correlation of these results with those of wave breaking.

0 119

EVAPORATION COEFFICIENT OF THE SEA SURFACE FROM EDDY FLUX MEASUREMENTS

S.D. Smith (Atlantic Oceanograhic Laboratory, Bedford Institute of Oceanography, Dartmouth, Nova Scotia, Canada, B2Y 4A2)
R.J. Anderson (Atlantic Oceanographic Laboratory)

Eddy correlation measurements of water vapor, heat and momentum fluxes have been made at a fixed tower near the water's edge on a low, sand island. The quantity of evaporation data collected is nearly equal to the total of similar data in the literature, and extends the range of conditions to include stable stratification and downward vapor flux. The evaporation coefficient

$$C_E = \langle \rho_v u_3 \rangle / [U_{10}(\rho_s - \langle \rho_v \rangle)]$$

has a value of 1.3×10^{-3} in neutral conditions. The coefficient is found to vary with stability in accordance with accepted empirical profile laws and to increase significantly with increasing wind speed at this shoal location.

Our values of the Bowen ratio of sensible to latent heat flux are found to vary widely with meteorological conditions and do not conform to empirical functions of temperature only as proposed by several authors.

0 120

COMPARISON OF WIND WAVE SPECTRA DETERMINED FROM SYNTHETIC APERTURE RADAR IMAGERY AND FROM A TOWER IN LAKE MICHIGAN

David J. Schwab
Paul C. Liu (both at: NOAA, Great Lakes Environmental Research Laboratory, Ann Arbor, MI. 48104)
Robert A. Schuchman (Environmental Research Institute of Michigan, Ann Arbor, MI. 48107)

Directional wave spectra calculated from digitized synthetic aperture radar (SAR) images of waves on Lake Michigan are compared to a wave directional spectrum determined from measurements taken at a solar-powered research tower and to a one-dimensional spectrum determined from a Waverider buoy. The SAR system was operated by ERIM on a track across Lake Michigan on Oct. 6, 1977. The tower and Waverider buoy were deployed by GLERL offshore of Muskegon, Mi. from July to Oct., 1977. Peak energy frequencies determined from the spectra are within one frequency band and wave direction with 20°, but the SAR image intensity spectrum does not have the same shape as a wave height spectrum. Wave refraction is observed in the SAR spectra and wave directions are within 10° of classical wave refraction calculations.

0 121

PHASE VELOCITY OF GRAVITY WAVES FOR LOW AND MODERATE WIND CONDITIONS

B. L. Gotwols, G. B. Irani, B. D. Morgan (all at: The Johns Hopkins University Applied Physics Lab., Laurel, MD 20810)

During a six-day interval, images of sea surface gravity waves were obtained with a charge coupled device television camera mounted on the Stage I tower. The area analyzed was a rectangle with approximate dimensions 7 x 26 m.

Two 17-second image sequences have been analyzed: one representing low wind conditions (<1 m/s) and decaying seas, the other moderate wind conditions (~9 m/s) and building seas. Each sequence consists of 256 images, for an effective sample rate of 15 frames/s. Each image has been digitally processed to remove perspective distortion, and then a three dimensional power spectrum was calculated. In this ω-$\vec{K}$ space, wave dispersion causes the spectral density to be distributed about a well-defined locus, from which the wave phase velocity may be calculated. In both data sets the computed phase velocity agrees with linear theory to within ~10%.

A new technique for calculating (two dimensional) wave-number directional spectra from optical images has also been developed. Integration of the three dimensional spectrum over ω from zero to the temporal Nyquist frequency yields a directional spectrum which does not possess the 180° ambiguity in wave propagation direction usually present in optically determined directional spectra.

0 122

EQUILIBRIUM RANGE SLOPE FOR SHALLOW WATER GRAVITY WAVE SPECTRA

C.E. Knowles (Department of Marine Science and Engineering, North Carolina State University, Raleigh, N.C. 27650)

According to Phillip's hypothesis, the equilibrium range in the frequency spectrum of wind-generated surface waves has a -5 slope and is given by:

$$S(\omega) = \beta g^2 \omega^{-5} \qquad (1)$$

Kitaigordski, et al(1975)have suggested a possible dependence of this spectrum for finite depth seas on the water depth, h, and on dimensional grounds obtained a new universal power law

$$S(\omega) = \beta/2gh\omega^{-3} \qquad (2)$$

As the authors point out, the equilibrium range in (2) is determined by spectral components for which the long-wave approximation is valid, but show results that suggest the range of applicability is much greater than that. Empirical data obtained for a shallow sea with a horizontal-bottom, fit a -3 slope quite well. Recently, Thornton (1977) derived a expression similar to (2) for the velocity spectrum in the equilibrium range and demonstrated the -3 slope from near shore measurements. The empirical data described above was from an ocean environment in 4 and 1.5m of water, respectively.

The results discussed in this paper are from a wave recording site in a relatively large enclosed estuary, for depths of about 1.3m and winds from about 315°T with speeds of 8m/sec. In all cases (even those with multiple peaks in the range) a -3 slope fit the data much better than a -5 slope, even though the condition of horizontal bottom relief probably was not satisfied.

In addition, the non-dimensional spectral peak frequency, ν, when plotted against non-dimensional fetch, $\tilde{x}$, had the same -.33 power slope as the JONSWAP relation

$$\nu = 3.5\tilde{x}^{-.33} \qquad (3)$$

but had a constant of 4.2, as long as the fetch used was the effective fetch with a cosine distribution about the wind axis. Agreement was very poor for a simple fetch.

0 123

AN OPERATIONAL SEA STATE MODEL FOR FORECAST SUPPORT OF OFFSHORE DRILLING

T. B. Low, Meteorological & Environmental Planning Ltd., Downsview, Ontario M3J 2C4
R. Goodman, Esso Resources Canada Ltd., Calgary, Alberta, T2G 2B3
T. E. Keliher, Nordco Ltd., St. John's, Nfld. A1B 3T2

Offshore drilling in petroleum exploration is highly affected by meteorological and oceanographic conditions. Accurate forecasting of the surface wind field and the resultant sea state are necessary to carry out the drilling operations in a safe and cost effective manner. Such exploratory drilling was performed in the Davis Strait at 63.0° N latitude and 59.0° W longitude during the summer months of 1979.

In order to provide supporting forecasts of the ocean wave parameters, the Wilson-Trajer numerical wave-ray model was implemented for the drill site and run during the drilling period. Waves were generated at 300 km intervals over a radial grid according to Wilson's (1955) parameterization of the Sverdrup and Munk (1947) wind wave relationships for deep water. These waves were propagated towards the drill site and attenuated according to the Bretschneider (1970) decay curves. The model was run with 12 hr. time steps and provided forecasts at each time step for 48 hours. The input wind field consisted of geostrophic winds over 25 grid points, and the surface wind and fetch at the target point. Forecasted sea parameters were the sea and swell wave heights and periods and the 12 hr. maximum swell component. These parameters could be combined into a significant wave height forecast. Verification by visual observations and buoy data showed the model to be an effective tool for sea state predictions in this area.

Southern Ocean Studies I

Harbour B
Saturday A.M.
Worth D. Nowlin (Texas A&M), Presiding

0 124 INVITED PAPER

POLEWARD HEAT FLUX BY MEAN GEOSTROPHIC MOTIONS IN THE SOUTHERN OCEAN

Roland A. de Szoeke
Murray D. Levine (both at School of Oceanography, Oregon State University, Corvallis, OR 97331

A method has been devised for calculating net oceanic poleward heat flux by mean geostrophic motions using historical hydrographic data. The method depends on integrating along a path of constant vertically-averaged potential temperature, and does not depend on assuming a "level of no motion." The method was applied to the circumpolar Southern Ocean between 50°-60°S. The errors in the calculation were carefully estimated by statistical methods. "Worst-case" and "best-case" error estimators were devised, differing in assumptions about vertical correlations of errors. The heat flux estimate was an insignificant -3 X 10^{13} W (polewards), since the worst-case and best-case standard deviations were 3 X 10^{14} W, and 7 X 10^{13} W, respectively. For comparison, Gordon (1975) has estimated the heat lost by the ocean to the atmosphere between the Polar Front and Antarctica to be 3.8 X 10^{14} W; estimates of atmospheric poleward heat flux are of similar order.

Our estimate, with its standard error, precludes a heat flux by mean geostrophic motions of such magnitude. To account for Gordon's figure another mode of oceanic heat transport must contribute, possibly eddy heat flux as suggested by Bryden (1979), or intense topographically trapped bottom currents.

O 125 INVITED PAPER

OBSERVATIONS OF EDDIES AND THEIR EFFECT IN THE ANTARCTIC CIRCUMPOLAR REGION

Harry L. Bryden (Woods Hole Oceanographic Institution, Woods Hole MA 02543)

Eddies have been observed in all regions of the Southern Ocean. These eddies have horizontal scales of 30 to 120 km, are vertically coherent from the sea surface to the bottom, and have kinetic energy at least as large as that of the time-averaged Antarctic Circumpolar Current. These eddies also are observed to transport heat poleward, perhaps enough to balance the heat lost to the atmosphere by waters south of the polar front, and the entire water column contrubutes to this poleward heat flux. Such eddy heat transport suggests reconsideration of the classical model of meridional circulation in which Antarctic Intermediate Water and Antarctic Bottom Water flow equatorward and North Atlantic Deep Water flows poleward. It is possible that the meridional temperature and salinity distributions, which led to this classical circulation model, are maintained by eddy fluxes of heat and salt with no net circulation. Because baroclinic instability theory predicts poleward eddy heat transport which is observed and because it is difficult to maintain zonally-averaged meridional circulation in the circumpolar region where no net zonal pressure gradient can exist, it is sensible to replace the classical conveyor belt mechanism of meridional heat transport with the mechanism of eddy heat transport with no net mass transport.

O 126

AUSTRALASIAN SOUTHERN OCEAN FRONTAL STRUCTURE - SUMMER 76/77

R.J. Edwards (CSIRO/Oceanography, Cronulla, N.S.W., Australia)
W.J. Emery (Department of Oceanography, University of British Columbia, Vancouver, B.C., Canada. V6T 1W5)

Fourteen north-south expendable bathythermograph temperature sections are used to define the positions of the Subtropical convergence, the Subantarctic Front and the Polar Front in the Australasian sector of the Southern Ocean. The data were collected by supply vessels transiting to the Antarctic mainland in the austral summer of 1976/77. Frontal features are identified on the basis of both temperature structure and observations of surface salinity. The Polar Front is found to be more convoluted than the other fronts leading to wide and narrow sections of the Antarctic Polar Frontal Zone between it and the Subantarctic Front. Southwest of Australia the Subantarctic Front shifts north to join the Subtropical Convergence and the Antarctic Polar Frontal Zone is at its widest. After a southward shift of all three fronts, south of eastern Australia, they separate to give almost equal separations of about 700 km between fronts southeast of New Zealand. The homogenous Subantarctic Mode Water between the Subantarctic Front and the Subtropical Convergence is found to be progressively warmer towards the west.

O 127

INTRUSIONS AT THE POLAR FRONT

E.P.W. Horne
J. Toole
T.M. Joyce (all at: Woods Hole Oceanographic Institution, Woods Hole, Mass. 02543)

CTD data taken across the polar front south of New Zealand will be presented. The data contains a lot of interleaving with layers on the order of 10-100 m thick and extending over distances of up to 9 km in the cross-frontal direction. The polar front will be shown to be coincident with the maximum temperature variance over the intrusion wavelength. A new method for lag correcting CTD data down to scales of 1 m will be briefly discussed and the importance of doing this correction properly when mixing ratios are calculated is stressed. The layers will be shown to cross density surfaces as they intrude with density changes consistent with those predicted by applying laboratory formulae for double diffusive fluxes at the layer interfaces. The heat, salt and density fluxes across the front will be estimated by applying the model of Joyce (1977) to the data and their importance to the overall thermohaline balance in the southern ocean discussed.

O 128

THE NATURE OF THE POLEWARD HEAT FLUX DUE TO LOW-FREQUENCY CURRENT FLUCTUATIONS IN DRAKE PASSAGE

F. Sciremammano, Jr. (Coastal Plains, Inc., Atlantic City, NJ 08401)

Values of poleward heat flux and its variability are presented for nineteen long-term current meter records obtained in Drake Passage during 1975, 1976 and 1977. Most of the records (10) are in the center of the passage near the historical location of the Polar Front where the flux is found to average 1.7 W cm^{-2} with a range of .9-2.8 W cm^{-2} and a standard deviation of .7 W cm^{-2}. A large spatial variability is present in the measured heat flux. During one six month period, heat flux values differing by factors of 2.7 and 2.1 occured in current meters operating concurrently and separated by 40 km and 13 km, respectively. There is no obvious depth dependence in the measured heat flux.

The heat flux process is shown to be dominated by events with time scales of 5-60 days and longer which occur on the order of 3 to 10 times per year at any location. In general, three or fewer events contribute most of the flux for the year.

A comparision of measured scales, vertical phase structure and propagation speeds agree very well with those calculated from linear baroclinic instability theory applied to the eastward current jets observed in Drake Passage. The mechanisms giving rise to the destablizing vertical shear and those responible for the eventual equibration of the fluctuations are not yet clearly identified, but may be specific to Drake Passage.

These findings suggest that caution should be exercised in the extrapolation of mean heat flux values obtained from point measurements in the Southern Ocean.

O 129

MERIDIONAL FLUX OF SILICA IN THE DRAKE PASSAGE

J.C. Jennings, Jr. (School of Oceanography Oregon State University, Corvallis, Or 97331)
(Sponsor: Louis I. Gordon)

A linear regression of dissolved silicate (SiO_2) on temperature (T) for Drake Passage ISOS stations in the polar frontal zone allows cross-frontal fluxes of silicate to be estimated from low-frequency heat flux calculations based on current meter records. Between 1000 m. and 3000 m., a consistent $\Delta SiO_2/\Delta T$ is found with a mean value of 31.6 $\mu g\text{-}atom \cdot l^{-1} \cdot {}^{\circ}C^{-1}$. Comparison with the heat flux data results in an estimated equatorward flux of dissolved silicon of 3-7 x 10^6 $g.s^{-1}$ in the Drake Passage. Because the cross-frontal slope of the dissolved silicate isopleths is less than that of the isopycnals, diffusion along isopycnals in this region will result in a poleward flux of dissolved silicon which is of the same order as the cross isopycnal low-frequency flux. The combination of these two processes may help to explain the silicate enrichment of Antarctic waters without requiring large vertical diffusion coefficients or generalized upwelling.

O 130

SPECULATIONS ON THE IMPACT OF ZOOPLANKTON EXCRETION ON THE NH_4^+ CYCLING IN THE SOUTHERN OCEAN

D.C. Biggs (Dept of Oceanography, Texas A&M University, College Station, TX 77843

Ammonium (NH_4^+) is a preferred nitrogen source for phytoplankton growth and the principal nitrogenous waste excreted by zooplankton and micronekton. Zooplankton excretion apparently provides a significant percentage of the total daily nitrogen requirements of phytoplankton in tropical and subtropical oligotrophic open-ocean regions, and in some coastal and upwelling regions as well, but little is known of its relative importance for phytoplankton production in the Southern Ocean. In austral summers 1978 and 1979, NH_4^+ was present at average concentrations of 0.2 ug-at $liter^{-1}$ and 1.0 ug-at $liter^{-1}$ in the euphotic zones of the Ross Sea and Scotia Sea, respectively, and was excreted by resident zooplankton at rates of 0.9 ug-at NH_4^+ g^{-1} wet wt h^{-1} (or greater). Using these data in conjunction with estimates, made by other Southern Ocean researchers, of 0.7 g wet wt m^{-3} for epipelagic zooplankton biomass and a daily phytoplankton nitrogenous requirement of 90 ug-at N m^{-3}, I suggest that NH_4^+ excretion by epipelagic zooplankton is adequate to supply about 16% of the daily nitrogen requirement of southern ocean primary production or daily regenerate 2% - 8% of the total amount of NH_4^+ present in Antarctic surface waters. Since zooplankton densities within patches (i.e., krill swarms) may be several orders of magnitude greater than the regional mean biomass, biogenic regeneration of NH_4^+ may spatially and temporally be adequate to supply 100% of the nitrogen requirement for primary production and to rapidly turn over NH_4^+ in the photic zone.

O 131

USE OF THE ANTHROPOGENIC CO_2 SIGNAL AS A TRACER IN THE SOUTHERN OCEAN

C-T Arthur Chen, (School of Oceanography Oregon State University, Corvallis, OR 97331)

Publication of the excellent GEOSECS alkalinity and total CO_2 data has made it possible to calculate the anthropogenic CO_2 increase in the oceans, directly, instead of resorting to the indirect study of the transient tracers, namely, tritium and C-14. Because of the relative abundance of CO_2 data as compared to the limited number of measurements for transient tracers, detailed vertical profiles showing the"excess CO_2" penetration can be studied at far more stations than previously possible. These profiles can be used to analyze the structures of water columns and movement of water masses. They can also supplement the transient tracers data in providing dating information for waters less than 130 years old.

Preliminary results in the Southern Ocean regarding the variations in the depth of anthropogenic CO_2 penetration across the Polar Front, and the Drake Passage using GEOSECS, IGY and the Phoenix Expedition data will be presented.

O 132

FURTHER CONSIDERATION OF THE SEASONALITY OF ANTARCTIC SEA ICE

Arnold L. Gordon (Lamont-Doherty Geological Observatory, Palisades, New York 10964)

Each spring-summer period, within the 60°-70°S belt of the

Southern Ocean, the winter accumulation of sea ice disappears within 100 days. Estimates of the amount of heat needed to accomplish this task are in excess by a factor of two over what may be expected to be provided by the atmosphere. The remainder must come from the large reservior of heat lying below the Southern Ocean pycnocline.

The annual ocean heat loss in the 60°-70°S belt is calculated to be about 27 Kcal/cm^2.yr. Upward motion of the pycnocline induced by Ekman divergence would supply about 11 Kcal/cm^2.yr. It is suggested that the remaining 16 Kcal/cm^2.yr. is derived from diffusive cross-pycnocline flux, requiring an effective K_z/ℓ of 2.0 cm^2/sec. While this value seems large, it is noted that the Southern Ocean pycnocline separating cold-fresh surface from warm-salty deep water is relatively weak. The weakly stable pycnocline is a consequence of the (P-E) + R value, which is only large enough to marginally counter the buoyancy removal of the upwelling deep water due to atmospheric cooling. Slight annual variations of (P-E) + R would have strong effects on the pycnocline stability, cross-pycnocline heat flux and hence seasonally of the Southern Ocean sea ice.

O 133

SEA ICE, WINTERTIME CONVECTION AND THE TEMPERATURE MINIMUM LAYER IN THE SOUTHERN OCEAN

John M. Toole (Woods Hole Oceanographic Institution, Woods Hole, MA 02543)
(Sponsor: R. Schmitt)

The air-sea interactions of the near surface waters of the Southern Ocean are investigated with a three-dimensional, time-dependent, numerical model. The surface waters in this region in summer are characterized by a relatively warm surface mixed layer with low salinity. Below this layer, a cold temperature extremium is usually observed which is believed to be the remnant of a deep surface mixed layer produced in winter.

Wintertime convection of the surface mixed layer is shown to be strongly influenced by the presence of sea ice. The ice acts to insulate the ocean which could inhibit convection though the heat flux through leads in the ice and the brine ejected during ice formation can continue to drive convection. The sea ice in turn is sensitive to the structure in the underlying water. Heat which is transported to the sea ice by vertical convection or lateral advection is seen to inhibit ice growth.

The numerical model computes the annual sea ice field oscillation in the Southern Ocean and its effects on the near surface waters. The observed characteristics of the surface mixed layer and the temperature minimum layer are reproduced well by this model. The predicted annual heat flux from the Southern Ocean to the atmosphere is not large but this results is strongly dependent on the lead area in the sea ice field.

O 134

FINESTRUCTURE IN THE CIRCUMPOLAR DEEP WATER

Daniel T. Georgi (Woods Hole Oceanographic Institution, Woods Hole, MA 02543)

The Circumpolar Deep Water (CDW) potential temperature/salinity (θ/S) relationship changes markedly between the Drake Passage and the Southwestern Indian Ocean. After the CDW has traversed the South Atlantic, the mean θ/S relationship has rotated towards higher salinities for θ greater than 1°C and towards lower salinities for θ less than 1°C. Lateral mixing with the warmer and saltier North Atlantic Deep Waters (NADW) and the colder and fresher Weddell Deep Waters is responsible for this change. The thermohaline finestructure, temperature and salinity inversions, observed on continuous salinity-temperature-depth soundings in much of the South Atlantic presumably is the signature of this lateral mixing.

Deep water finestructure is particularly evident in the southwestern Argentine Basin: 1°C temperature inversions with 100 to 250 m vertical scales. This finestructure occurs primarily between 1500 and 2500 m, the depth of the NADW/CDW confluence. The intensity of the finestructure is quantified by calculating the temperature-gradient variance in the 32 to 256 m vertical wavelength band.

The southwest Argentine Basin finestructure intensities are compared to those calculated with data from the Drake Passage, Scotia Sea, the central and eastern Atlantic and the southwest Indian Ocean. Only the finestructure in the 36.9 to 37.08 potential-density (relative to 2000 db) range was considered. The largest variance levels occur in the Argentine Basin, the smallest in the Drake Passage, while those in the Southwest Indian Ocean were intermediate. Variance levels in the Scotia Sea were similarly low to those in the Drake Passage except for a few isolated stations which reveal the influence of NADW.

The temperature-gradient variance data from the Argentine Basin is then used to estimate the lateral heat and salt flux in the NADW/CDW confluence. The calculated lateral heat flux is of order 1 x 10^{-4} °C m s^{-1} and the lateral diffusivity of order 100 m^2 s^{-1}.

O 135

CIRCUMPOLAR PROPERTIES OF ANTARCTIC INTERMEDIATE AND SUBANTARCTIC MODE WATERS

Alberto Piola (Woods Hole Oceanographic Institution, Woods Hole, MA 02543)
(Sponsor: Daniel T. Georgi)

Antarctic Intermediate Waters (AAIW) and Subantarctic Mode Water (SAMW) are studied by examining their density and salinity modal characteristics around Antarctica. The study is focussed on two zones: 35°S to 40°S and 40°S to 45°S. Each zone is subdivided into 15 regions. For each region, a density and a salinity histogram are plotted with class intervals of .05 Kgm/m^3 and .02 ‰ respectively.

Changes are gradual across each of the three oceans and are presumed to represent changes of AAIW and SAMN properties. Large salinity and density changes (.15 ‰ and .5 Kgm/m^3) occur between the Southeast Atlantic and Southwest Indian Oceans. Further analysis of the transition region indicate that these changes are not due to variations of AAIW properties but represent two different and distinct water masses.

Similarly, discontinuities are observed in the Southern Tasman Sea which can be explained by AAIW circulation involving two different types: the fresher AAIW (34.35 ‰) entering from the south and the saltier (34.45 ‰) entering from the northeast.

Ocean heat content seasonal variation and ocean-atmosphere heat fluxes are estimated by comparing summer and winter oceanographic data in the Scotia Sea. The results agree with those arrived at by the analysis of long term meteorological observations.

Southern Ocean Studies II

Harbour B
Saturday P.M.
Worth Nowlin (Texas A&M), Presiding

O 136 INVITED PAPER

SVERDRUP RELATION IN THE SOUTHERN OCEAN

D. James Baker, Jr. (Department of Oceanography University of Washington, Seattle, WA 98195)

New data on wind and hydrography, and direct current measurements in the Drake Passage as part of the International Southern Ocean Studies (ISOS) allow a crude but quantitative test of the hypothesis that the Antarctic Circumpolar Current (ACC) is governed by the Sverdrup relation. The dynamic topography of Gordon, Molinelli, and Baker shows a southward flow in the Southeast Indian Ocean, in agreement with southward Sverdrup flow calculated from the wind stress data in that region. The wind stress curl is substantially weaker in both the South Atlantic and South Pacific Oceans. The magnitude of the southward geostrophic flow is in agreement with the magnitude of the flow through the Drake Passage (estimated from the ISOS measurements), most of which turns northwards after leaving the passage. Thus the main driving region for the ACC may be in the Indian Ocean.

O 137

ATMOSPHERIC STOCHASTIC FORCING OF THE SOUTHERN OCEAN

Yves J. F. Desaubies (Woods Hole Oceanographic Institution, Woods Hole, MA 02543)
(Sponsor: Raymond Schmitt)

The forcing of an idealized model of the Southern Ocean is considered. The ocean is taken to be bounded to the south by a latitude circle, unbounded to the north, the bottom to be flat. A decomposition of the ocean motion in vertical, zonal and meridional is effected and those modes are regarded as having random phases, i.e. uncorrelated Fourier components. The atmospheric pressure and wind stress fields are likewise decomposed. The response for the bottom pressure is estimated by summation over the barotropic and baroclinic modes. The response to the zeroth order zonal mode (the zonally averaged) wind field is of particular interest and is dominated by the wind stress (rather than the pressure) for all frequencies of interest. The frequency power spectrum is estimated. Comparisons with data by Wearn and Baker are made.

O 138 INVITED PAPER

THE GENERAL CIRCULATION OF SOUTHERN HEMISPHERE OCEANS: EDDY-RESOLVING NUMERICAL EXPERIMENTS

W.R. Holland (National Center for Atmospheric Research, Boulder, Colorado)

Studies of closed, mid-latitude ocean basins as well as open (channel) geometry oceans using eddy-resolving models have begun to explore the role of eddies in the general circulation. For the most part these two types of geometry have been treated separately whereas in actual southern hemisphere oceans the termination of continental barriers (at their southern ends) may lead to active interaction between the Circumpolar Current and mid-latitude gyre circulations.

These circumstances are explored in a preliminary set of numerical experiments in multiply-connected basins geometrically similar to oceans of the southern hemisphere. Initial results show that eddy dynamics play a central role in determining the large-scale mean flow. The nature of the western boundary currents (analogues of the East Australian, Agulhas, and Falkland Currents) and of the Circumpolar Current is strongly dependent upon the geometry of the boundary and the structure of the wind forcing. Important factors include the latitude at which the boundary terminates and the relative amplitudes of mid- and high-latitude wind stresses. Other geometrical complications (such as the New Zealand land barrier) are also important.

O 139

GEOSTROPHIC TURBULENCE IN WIND-DRIVEN, β-PLANE CHANNEL

James C. McWilliams (National Center for Atmospheric Research, Boulder, Colorado 80307)

An equilibrium turbulent numerical solution is obtained for a model ocean which is adiabatic, hydrostatic, baroclinic, and quasigeostrophic and is driven by a steady, inhomogeneous, zonal surface wind stress. This is perhaps the simplest analog for the Antarctic Circumpolar Current involving explicit calculations of the large-scale turbulence. The interior diffusive processes are weak (i.e., the Reynolds number is large), but there is a quadratic drag force at the bottom. The mean circulation is balanced by lateral and vertical turbulent fluxes of heat, momentum, and potential vorticity; the turbulence is maintained by baroclinic conversions of mean potential energy (i.e., "baroclinic instability.") Wavenumber spectra for the turbulence are smooth functions of wavenumber and exhibit an extensive "inertial range" where the kinetic energy spectrum varies as k^{-3}, as in isotropic, homogeneous, 2D turbulence (which this solution is not). The turbulent energy balance in this inertial range is between non-linear transfer T from other wavenumbers and local dissipation by bottom drag; this result is in contrast to the vanishing T is classical, inviscid inertial range theory. A brief discussion is presented on the relation between this idealized calculation and theoretical interpretations of Circumpolar Current phenomena.

Ocean Modelling
Pier 4
Saturday P.M.
N. G. Freeman (Canada Centre for Inland Waters), Presiding

0 140

THE RELATION BETWEEN WIND OVER THE SOUTHERN OCEAN AND THE ANTARCTIC CIRCUMPOLAR CURRENT

R. B. Wearn, Jr. (Applied Physics Laboratory, University of Washington, Seattle, WA 98195)
D. J. Baker, Jr. (Department of Oceanography, University of Washington, Seattle, WA 98195)

Wind stress over the Southern Ocean is calculated from the southern hemisphere grid point atmospheric pressure data to determine the spatial distribution and time variability of the stress. The data is compared with geostrophic velocity at 500 m determined from bottom pressure gauges across the Antarctic Circumpolar Current at Drake Passage. Over time scales longer than about 30 days, the integrated wind stress over the Southern Ocean is highly correlated with velocity averaged across the passage, with wind leading velocity by about 9 days. These results are consistent with the rate at which momentum is put into the Southern Ocean by the wind.

0 141

BAROCLINIC INSTABILITY IN DRAKE PASSAGE

Daniel G. Wright (Woods Hole Oceanographic Institution, Woods Hole, MA 02543)

Eddy-like motions with periods of 10 to 20 days and horizontal length scales (eddy diameters) of 50 to 100 km have been observed in Drake Passage. A linearized baroclinic instability model is applied to this area and a comparison with observational results is made. Horizontal length scales, periods and the vertical structure of the perturbations are consistent with the conjecture that the observed motions tap the potential energy of the mean state by the process of baroclinic instability. Further, some indication of the nature of the development of these waves as they propagate through the Passage is obtained.

0 142

ROLE OF BATHYMETRY IN THE ANTARCTIC CIRCUMPOLAR CURRENT

Greg Holloway (Dept. of Oceanography, University of Washington, Seattle, WA 98195)

(Sponsor: D. James Baker, Jr.)

A classical question concerning the Antarctic Circumpolar Current (ACC) is how to balance the wind input of zonal momentum or, equivalently, to balance the wind driven meridional Ekman transport. A very feasible mechanism can be found in the interaction of a mean zonal flow with underlying topographic features if there is a correlation $\overline{vh}$ where v is meridional velocity at the bottom, h is the bottom elevation and overbar denotes zonal average. Can we predict $\overline{vh}$ from dynamics? Previous analytical studies have been restricted unrealistically, e.g., to steady solutions, simple topographic shapes, uniform upstream flows, small perturbation amplitudes. Here we pose the problem statistically dynamically: given a zonal wind stress, given the variance spectrum of actual Southern Ocean bathymetry and assuming equivalent barotropic dynamics, we seek the wavenumber spectra of velocity covariance and of velocity topography correlation. Preliminary solutions are obtained by a renormalized perturbation method.

0 143

KINETIC ENERGY LEVELS AT DRAKE PASSAGE FROM LONG TERM OBSERVATIONS, 1975-1978

W. D. Nowlin, Jr. (Department of Oceanography, Texas A&M University, College Station, TX 77843)
R. D. Pillsbury (School of Oceanography, Oregon State University, Corvallis, OR 97331)
Joseph Bottero (School of Oceanography, Oregon State University, Corvallis, OR 97331)

Kinetic energy levels in the deep water across Drake Passage and through the water column in the central passage are described. The 31 current records examined span the years 1975 through 1978. The energy spectra from these nearly year long records show no significant year-to-year variation but pronounced spatial variability. The kinetic energy of the mean motion (K_M) at depths greater than 2000 m increases southward from northern to central passage locations. Examination of fluctuation kinetic energy (K_F) by period bands shows that the energy level for periods between 2 hr and 2 day is rather uniform across the passage. However, large values of K_F in the northern passage result primarily from more meso-scale activity between 2- and 50-day periods, although there is also some increase in K_F at that location for periods greater than 50 days. Cumulative plots of K_M and K_F versus time show that kinetic energy densities approach long term values for specific records after intervals of the order of 4 months.

Fluctuation kinetic energy values in the Antarctic Circumpolar Current (ACC) at Drake Passage are compared with reported values from the North Atlantic. Values south of Cape Horn are comparable to those in the Gulf Stream. At other Drake Passage locations, K_F values are an order of magnitude greater than those in the interior of the North Atlantic subtropical gyre. Near the Polar Front in the ACC there is evidence for near surface as well as near bottom increases in kinetic energy of the fluctuations relative to the mean motion.

0 144

ICE SHELF WATER IN THE WEDDELL SEA

Arne Foldvik (University of Bergen Bergen, Norway)
Theodore D. Foster (University of California, Santa Cruz, CA 95064)
Jason H. Middleton (University of New South Wales, Kensington, Australia)

Ice Shelf Water is characterized by temperatures below the freezing point at one atmosphere pressure. Ice Shelf Water forms when sea water flows beneath the antarctic ice shelves and is cooled to the in situ freezing point. In the Weddell Sea Ice Shelf Water flows out from under the Filchner Ice Shelf around the Filchner Depression in a clockwise manner and spills over the sill into the oceanic basin of the Weddell Sea. Hydrographic work and moored current meter measurements at the sill made during the Norwegian Antarctic Expeditions 1977 and 1979 have shown that approximately 0.8×10^6 $m^3 s^{-1}$ of water with temperatures below the atmospheric freezing point flow over the sill.

0 145

MIXING PROCESSES NEAR THE SHELF BREAK IN THE SOUTHERN WEDDELL SEA

Theodore D. Foster (University of California, Santa Cruz, CA 95064)
Arne Foldvik (University of Bergen, Bergen, Norway)
Jason H. Middleton (University of New South Wales, Kensington, Australia)

The joint work by the Polarsirkel and the Glacier during the International Weddell Sea Oceanographic Expedition in 1977-80 has resulted in several closely-spaced hydrographic sections and long-term current meter records in the sehfl break region of the southern Weddell Sea. The hydrographic sections showed that the tongue of Warm Deep Water, which intrudes onto the shelf, breaks up into an irregular pattern, perhaps even into discrete blobs. The current meter records showed there were no significant correlations between the currents at the different moorings except at the tidal frequencies indicating that the horizontal scales of the mixing processes are probably smaller than the spacing between moorings, a minimum of 37 km for the current meters retrieved in 1979.

0 146

THE RESPONSE OF NARRAGANSETT BAY TO METEOROLOGICAL FORCING

R.B. Gordon
M.L. Spaulding
F.M. White (all at: Department of Ocean Engineering, University of Rhode Island, Kingston, RI 02881)

Previous measurement programs of currents and sea level in Narragansett Bay have indicated that wind plays an important role in driving the circulation, especially at subtidal frequencies (i.e. periods greater than the diurnal tides). The spatial extent of these measurements has, however, been insufficient to determine the general response of the Bay. In the summer and fall of 1977, the National Ocean Survey, NOAA conducted a survey during which sea level and current measurements where made throughout Narragansett Bay. Results of analysis indicate that at periods of ten days and longer, the sea level oscillations in the Bay are due to a shelf wide response. At periods of five days, the response is related to the sea level variations in southern New England Bight (Long Island Sound to Buzzards Bay). At two day periods, the response is directly related to the winds over the Bay.

High coherence between adjusted sea level and wind stress measured at Green Airport in Warwick, Rhode Island suggest the suitability of modeling the sea level response stochastically. In addition, volume flux has been calculated based on these sea level records in order to estimate the relative importance of the subtidal oscillations in flushing the Bay.

A three-dimensional deterministic model of the response to meteorological forcing has been applied to the Bay and compared with the measurements.

0 147

OBSERVATION AND MODELLING OF FRONTAL UPWELLING

C.L. Tang (Bedford Institute of Oceanography, Dartmouth, N.S., Canada B2Y 4A2)

A density front in the northwestern Gulf of St. Lawrence has been observed during two CTD surveys in 1978 and 1979. This front is formed as a result of fresh water discharge from the St. Lawrence Estuary. Evidence of upwelling in the frontal zone can be seen in the vertical temperature distribution, and from the satellite data in which a band of cold surface water coincides with the frontal zone. A two-layer model for a stationary front is constructed to explain the upwelling. Friction plays a key role in driving a cross-front circulation. The interfacial Ekman transport beneath the frontal layer draws the water upward from below the frontal zone in a shear layer of thickness $E^{\frac{1}{2}}$, where E is the Ekman number. An outer Stewardson layer of thickness $E^{\frac{1}{4}}$ feeds the $E^{\frac{1}{2}}$ layer, and at the same time serves as a return channel for the upwelled water. On the side of the heavier water, there is no significant vertical motion near the surface outside the $E^{\frac{1}{2}}$ layer. The water there participates passively in the circulation and acts mainly to satisfy the continuity and the boundary conditions. The seasonal variation of the upwelling, the effect of stratification in the lower layer, and surface convergence in the frontal zone are discussed. The eddy and diffusion coefficients are calculated from the width of the upwelling zone in the northwestern Gulf of St. Lawrence.

O 148

ATMOSPHERICALLY FORCED EDDIES IN THE NORTH-EAST PACIFIC

A.J. Willmott (Departments of Mathematics and Oceanography, Univ. of British Columbia, Vancouver, B.C. V6T 1Y4
L.A. Mysak

In the Northeast Pacific eddies are observed in the thermal anomalies. In particular, a pronounced eddy is frequently observed a few hundred kilometres west of Sitka, Alaska, latitude 57°N. This paper investigates a possible mechanism for the production of such eddies. The Northeast Pacific ocean is approximated by a quarter-plane region, and a continuously stratified, inviscid, linear model is used to study the reflections of wind-driven perturbations by the two boundaries. In the model the perturbations take the form of planetary waves, and by choosing a forcing function which is sinusoidal in time the problem reduces to solving the forced Helmholtz equation in a quarter-plane region. From the solution to this equation, the perturbation density field is derived. In general, it consists of a large number of eddies which result from the superposition of multiply reflected planetary waves. It is also found that tilting the quarter-plane from the north-south direction dramatically increases the size of the eddies in the perturbation density field. The perturbation velocity field is also computed from the solution to the Helmholtz equation, and it is found that the flow field does not in general consist of closed streamlines.

O 149

A TWO-DIMENSIONAL, BRANCHING MODEL STUDY OF THE POTOMAC RIVER CIRCULATION

D-P Wang (Energy and Environmental Systems Division, Argonne National Laboratory, Argonne, IL 60439)

A semi-implicit, two-dimensional (in a vertical plane), branching model is developed for circulation in the partially mixed estuary. The time integration of the semi-implicit scheme is not sensitive to the horizontal grid size, and consequently, the model is very efficient in the application to multiple branches.

The model is exercised under realistic external forcings for the coupled Chesapeake Bay proper - Potomac River system. The results show good agreement with the observations over the 40 day simulation. Extension of the model to salt intrusion and water quality study is suggested.

O 150

FINITE-ELEMENT APPROACHES FOR A CHESAPEAKE BAY CIRCULATION MODEL

R. Walton (Water Resources Engineers/CDM, Springfield, VA 22151), D.R. Lynch (Assist. Prof., Resource Policy Center, Thayer Sch. of Eng., Dartmouth College, Hanover, NH 03755)

As part of EPA's Chesapeake Bay Program, a 3-D circulation model is being developed. The size of the Bay dictates that a numerical model give special consideration to the spatial variability of the forcing functions, and the economy and accuracy of the solution technique.

The class of methods chosen was the 2-D finite-element approach using linear triangles, because of its geometric flexibility and rigorus mathematical description. The selected model will be used as the kernel for the 3-D circulation model by describing the Bay as a series of layers linked vertically through continuity.

The two models chosen for further considerations use the same basic differential equations to describe fluid motion, but differ in the approximation techniques. CAFE-1 uses an implicit formulation and requires matrix inversion. It is, however, a tried and proven model. WAVETL is more recent model using an explicit, lumped-mass approach. It diagonalizes the mass matrix, reducing storage and removing the need for matrix inversion. It also models a wave equation instead of the continuity equation, to introduce natural damping of high frequency noise, and thus eliminates dependence on artificial viscous terms.

The models were compared for a 41 node problem in the upper part of the Chesapeake Bay to compare the models accuracy, stability and relative economy. This paper describes the comparison and model selection.

O 151

SOME PRELIMINARY EXPERIMENTS WITH AN ISOPYCNIC COORDINATE OCEAN CIRCULATION MODEL

Douglas B. Boudra (Rosenstiel School of Marine and Atmospheric Science, Miami, FL 33149)
Rainer Bleck (Rosenstiel School of Marine and Atmospheric Science, Miami, FL 33149)

Sponsor: Donald B. Olson

A density coordinate ocean model is being developed to study ocean circulation and heat transport from the scales of baroclinic eddies to basin wide gyres. The first application was to coastal upwelling fronts, but current simulations emphasize description of the large scale circulation while resolving mesoscale eddies.

At present, two ocean configurations are being utilized to establish requirements for model stability and to study the model energetics. The first has four layers, a 50 km grid spacing on a 33 X 26 matrix with a north-south orientation, and is forced with a latitudinally varying double gyre wind stress pattern. The second is an idealized section of the western N. Atlantic including the Gulf Stream region. It has five layers, a 37.5 km grid point spacing on a region 2600 km by 3000 km, and is forced with a climatological February wind stress pattern. At this stage, bathymetry, diabatic forcing, and salinity are neglected.

The stability requirements for the pure density coordinate model appear to be too stringent to allow adequate simulation of both mesoscale and gyre-scale circulation simultaneously. A recently developed hybrid vertical coordinate model, which allows motion through a coordinate interface when layer thickness decreases below a critical value and in the opposite direction when dynamic constraints permit, has produced encouraging results. Simulations from both basin configurations and both model formulations are illustrated.

O 152

NUMERICAL MODELING OF TSUNAMI FLOODING

C.H. Lewis, III (Department of Geology and Geophysics, University of Hawaii, Honolulu Hawaii, 96822. Currently at NOAA;AOML, Virginia Key, Florida.)

W.M. Adams (Dept. of Geology and Geophysics, University of Hawaii, Honolulu, HI,96822. Currently on sabbatical leave at NOAA;AOML, Virginia Key, Florida, under Inter-government Personnel Act.)

One and 2-D Finite Difference programs have been developed for modeling tsunami flooding. Fully centered differences are used: some high-frequency noise occurs but it is stable and is not due to the nonlinear terms, hence no averaging is necessary. A graphics capability of creating movies showing the results at every time step has been found necessary to assure arrival at a believable and correct conclusion. Comparison of results with analytical results, while appropriate, does not assure that a program is satisfactory; misuse is not only possible but probable. Most applications documented in the scientific literature allow aliasing in the horizontal interfaces, the vertical interfaces, or both. Smoothing of the moving boundary-the shoreline- is necessary to avoid the introduction of spurious high spatial frequencies.

A movie will be shown to emphasize this need for seeing all computer results-- not just the final results.

O 153

A LABORATORY STUDY OF THE SHELF AND SLOPE CIRCULATION DRIVEN BY SURFACE COOLING AND OFFSHORE HEATING

Takashige Sugimoto (Geophysical Institute, Tohoku University, Sendai, 980, Japan; present address, Woods Hole Oceanographic Institution)
J. A. Whitehead, Jr. (Woods Hole Oceanographic Institution, Woods Hole, MA 02543)

The dynamics of shelf circulation and the shelf break exchange processes between shelf and offshore water are studied by use of a rotating hydraulic model. The model basin consists of a square shelf (50 cm x 50 cm x 5 cm deep) connected by a narrow (10 cm wide) slope to a deeper basin (30 cm x 50 cm x 15 cm deep). The enclosed fluid is cooled through the top lid and heated through the offshore sidewall.

The observed phenomena are primarily controlled by the nondimensional parameter Rd/L (ratio of the Rossby radius of deformation to the horizontal scale of the shelf), but also by the Ekman number. For large values of Rd/L, a vertical circulation occurs with sinking motion limited to a narrow zone adjacent to the inner "coast". For moderate values of Rd/L, a single horizontal circulation of basin scale develops. This gyre is cyclonic in the upper layer and anticyclonic in the lower layer. Sinking is observed in the gyre also, where small but very strong cyclonic whirls, similar to "chimneys" in the polar ocean, are produced intermittently. These whirls penetrate to the bottom and transport cooled surface water into the lower layer. For small values of Rd/L, the single gyre breaks up into several smaller eddies, the number of which increases with decreasing Rd/L. The model dynamics and the role of the outflowing jet occurring over the shelf break and slope will also be discussed.

O 154

THREE DIMENSIONAL GEODETIC INVERSION METHOD FOR OBTAINING STRESS IN THE LITHOSPHERE

K. Ikeda (Department of Earth and Planetary Sciences, Massachusetts Institute of Technology, Cambridge, MA 02139)

Three dimensional geodetic inversion method to obtain incremental stress in the earth are presented with a preliminary result on the application to the data from Palmdale, California. Geodetic inverse problem is formulated as an elliptic operator equation with Cauchy's boundary condition applied to a body that is cut out of the earth under the surface on which displacements are known. Three dimensional finite element scheme provides a discretized form of the operator. Data obtained from geodimeter and levelling survey, together with a stress free condition on the free surface provide boundary conditions. The inversion scheme is tested using artificial data generated by Mindlin's buried point force solution with the result showing satisfactory accuracy of the inversion scheme. The incremental stress obtained during the period 1959 to 1972 shows the dominance of horizontal tensional stress in the direction of N48°W with magnitude 2.1 bar at the depth of 3.75 km. During the period 1974 to 1977 the maximum principal incremental stress turns to be horizontal compression in the direction of N40°W with magnitude 2.2 bar at the depth of 3.75 km while minimum principal stress is near vertical. The compressional stress increases with depth to 4.2 bar at the depth of 6.5 km and 7.0 bar at the depth of 8.75 km without changing directions so much. The sense and direction of the principal incremental stress during the period 1974 to 1977 and its magnitude are consistent with the fault plane solutions obtained for swarm activities and geomagnetic change observed in this area during this period. The obtained incremental stress also explains the increase of seismicity by an order of magnitude in this area during the period 1974 to 1977.

O 155

MODELLING EFFLUENT FIELDS DISCHARGED FROM SUBMERGED OCEAN OUTFALLS

D. P. Krauel (Royal Roads Military College, Victoria, B. C., V0S 1B0)

A model is developed to predict the concentration distributions and their probabilities in the effluent field discharged from a submerged ocean outfall. Three phases in the

dispersion process are modelled: initial dilution, turbulent diffusion, and decay. Readily obtainable environmental parameters such as wind speed and direction frequency distributions, water current speed and direction frequency distributions, and the density stratification frequency distribution are employed to predict "worst case" concentrations and their probabilities at selected locations. The model is applied to a coastal embayment near Victoria in which a sewer outfall already exists and a second outfall is proposed. A monitoring program of the existing outfall has collected limited data on the spatial and temporal coliform distributions. These data are used to determine the standard deviation of the lognormal frequency distribution for coliform counts at a fixed shoreline location near the existing outfall. The standard deviation of the coliform frequency distribution is dependent upon the standard deviation of the frequency distributions for the environmental parameters causing the dispersion of the effluent. Therefore it is assumed that the standard deviation is constant for all locations within the immediate area which experience similar environmental forcing. The determined standard deviation and the predicted "worst case" coliform counts at various shoreline locations are combined to predict the frequency distribution of coliform counts for comparison with legislated environmental standards.

O 156

THERMALLY INDUCED AIR AND WATER CIRCULATIONS ASSOCIATED WITH ESTUARINE WATERS

Kuldip P. Chopra (Physics Department, Old Dominion University, Norfolk, VA. 23508)

It is common to find a few degrees difference in surface air temperatures over estuarine water and the adjoining land masses. This thermal contrast, further enhanced by evaporation and flow of water, may produce local air circulations, the estuarine water mass acting as a reversed heated island. Following an analogy with the land and sea breeze theory, it can be shown that the average wind speed V induced by a temperature gradient ∇T is given by

$$V^2 = \frac{R \nabla T}{2(1+h/L)K} \ln (p_0/p_1)$$

where L and h are horizontal and vertical extents of the solenoid (assumed rectangular), p_0/p_1 is the ratio of air pressure at ground and upper levels of the solenoid, R is the gas constant, and K is a dimensional constant which depends on eddy viscosity in the surface layer. It is estimated that these induced breezes may develop speeds as high as 12 knots. Wind-driven surface currents combined with upwelling of water caused by evaporation, may produce cross-sectional circulations in water. These induced air and water circulations have a bearing on local mixing and quality of our environment.

Coastal and Lake Dynamics

Metropolitan West
Monday A.M.
C. R. Murthy (Canada Centre For Inland Waters), Presiding

O 157 INVITED PAPER

KINEMATIC FEATURES OF LARGE SHALLOW LAKES ILLUSTRATED IN TIME LAPSE PHOTOGRAPHS

Bernard C. Kenney (National Water Research Institute Branch, Freshwater Institute, 501 University Cr., Winnipeg, Manitoba R3T 2N6)

Observations are presented from several hypereutrophic lakes in western Canada. These lakes have a characteristic length $O(50$ km) and a characteristic depth $O(4$ m). During the open water season there is a propensity towards the production of surface foam which is associated with intense blooms of blue-green algae. The observations are documented in the form of time lapse photographs of natural foam, algal cells and artificial Lagrangian tracers using both aerial and high oblique terrestrial photography from the top of a 20 m tower.

The boundaries of the algal blooms often consisted of sharp frontal zones. Single streak lines produced by downwelling at the frontal zones and various kinematic features of streak arrays (windrows) are discussed. Results are also presented on strongly non-linear advective disturbances and on features of the near surface shear.

O 158

OBJECTIVE ANALYSIS OF CURRENTS IN A HOMOGENEOUS LAKE

Desiraju B. Rao
David J. Schwab (both at: NOAA, Great Lakes Environmental Research Laboratory, Ann Arbor, MI. 48104)

The large-scale mean currents in lakes having the dimensions of the Great Lakes are characterized by nearly non-divergent character. Hence, most of the kinetic energy of the mean currents is contained in the rotational component of the flow field which can be determined from the transport streamfunction. The horizontal velocity vector ($\vec{V}$) and the vertical component of vorticity (ζ) are given by $\vec{V} = \vec{k} \times h^{-1} \nabla \psi$ and $\zeta = \nabla \cdot h^{-1} \nabla \psi$. ∇ is the horizontal gradient operator. h is the equilibrium depth of the lake and is a function of the horizontal coordinates (x,y). If, in principle, one is given the vorticity field $\zeta(x,y)$, the self-adjoint inhomogeneous equation $\nabla \cdot h^{-1} \nabla \psi = \zeta(x,y)$ can be uniquely solved for ψ which is subject to the condition $h^{-1} \psi = 0$ on the boundaries and the current vector can be obtained from $\vec{V} = \vec{k} \times h^{-1} \nabla \psi$. In practice, however, one does not have the ζ field. Hence, the transport streamfunction is expanded in terms of the eigenvectors of the self-adjoint problem $\nabla \cdot h^{-1} \nabla \psi_\alpha = \mu_\alpha \psi_\alpha$ with $h^{-1} \psi_\alpha = 0$ on the boundary. The eigenvalues μ_α and the associated eigenfunctions ψ_α for a particular lake can be determined numerically. The expansion coefficients for the spectral functions are determined by minimizing in a least square sense the difference between the calculated $\vec{V}$ field and available current meter data. Since ψ_α's are known over the entire domain of the basin, we can now reconstruct the field of currents at all grid points in the basin. This method has been applied to analyze data gathered in Lake Ontario during the winter months of 1972-73 as part of the International Field Year on the Great Lakes.

O 159

DOES ENTRAINMENT LEAD TO SEPARATION ?

P.H. LeBlond (Department of Oceanography, University of British Columbia, Vancouver, B.C. V6T 1W5)

Under conditions of weak entrainment, the flow in a well stratified deep estuary is idealized as that of a two-layer fluid and may be described within the framework of rotational hydraulics. The depth of the upper layer and the reduced gravity to which it is subject become functions of downstream distance, as entrainment dilutes the fresh water and adds to the upper layer volume flux.

The role of entrainment effects on possible separations and critical transitions is examined and the results compared to observations from the St.Lawrence estuary.

O 160

EXCHANGE FLOW BETWEEN TWO STRATIFIED BASINS

B. Eid, W. James (Civil Engineering, McMaster University, Hamilton, Ont., Canada L8S 4L7)
F. Boyce (NWRI, CCIW, Burlington, Ont. L7R 4A6)

To estimate production and respiration cycles in interconnected lake basins, it is necessary to account for all fluxes of the active materials across the basin's boundaries. This is particularly complex when two dissimilar basins exchange water through a connecting channel, the interchange is wind induced, and the flow is influenced by stratification and bottom topography.

In this study a two-layer system is modeled; the dynamics of the flow is simulated by assigning average velocity and density to each layer. The hydrodynamic equations of two-layer densimetric flows are derived for arbitrary geometry and different boundary conditions. The effect of surface, interfacial and bottom shear stresses on transitional flows, which may be subcritical throughout the channel or involve critical (or control) sections, is studied.

The model is applied to the exchange flow between the central and eastern basins of Lake Erie at Pennsylvania Ridge.

O 161

APPROXIMATE STUDY OF FREQUENCY OF WIND-INDUCED CURRENTS IN A PROPOSED RESERVOIR

JEI-HSUAN HUANG
Ebasco Services Incorporated
Two World Trade Center
N.Y.C., N.Y. 10048

A procedure is introduced where joint frequency of wind-induced current speed and direction in a reservoir can be numerically investigated and graphically illustrated for the entire reservoir. The steady-state vertically-integrated two-dimensional free surface flow equations are used as the basic model. The bottom stress is linearized with an averaged friction speed. The joint frequency of speed and direction of over-water winds is discretized for wind direction only. The procedure is suitable for small to medium-sized reservoir where the Coriolis effect is generally negligible in the wind-induced current patterns.

O 162

A MOMENTUM BALANCE FOR THE SURF ZONE AND NEARSHORE REGION

G.A. Meadows
A.T. Jessup
A.J. Plueddemann (All at: Department of Atmospheric and Oceanic Science, The University of Michigan, Ann Arbor, MI 48109)

Recent simultaneous collection of longshore current velocity data and incident wave conditions from multi-instrumented surf zone arrays have enabled detailed momentum balances to be calculated for the nearshore region. Recent implementation of this analytical procedure has resulted in the recognition that momentum sources to the nearshore region, other than the incident wave field, may be responsible for a significant portion of the surf zone flow field (Meadows, 1979).

Theoretical calculations based upon the radiation stress formulation of Longuett-Higgens (1970), of the distribution of longshore current velocity across the active surf zone are compared with In-Situ field observations. Continuous fifteen minute time series of water level elevation and longshore current velocity were obtained at eight monitoring stations distributed across the nearshore region. In addition, incident wave horizontal particle velocity, breaking wave angle and wind speed and direction were also measured at selected locations across the surf zone. These data were used to ascertain the relative contributions of; the longshore component of nearshore wind stress, the shoreward flux of wave momentum and the momentum associated with the ambient nearshore circulation of the region, on surf zone water motions. The results of this analysis indicate that only under very specific incident wave and beach conditions, is the longshore momentum flux associated with the incident wave field the only significant term of the nearshore momentum balance.

0 163

SUBTIDAL SEA LEVEL VARIATIONS IN LAKE PONTCHARTRAIN

Wen-Ssn Chuang (Coastal Studies Institute, Louisiana State University, Baton Rouge, La. 70803)
Erick M. Swenson (Center for Wetland Resources, Louisiana State University, Baton Rouge, La. 70803)

Lake Pontchartrain has a major tidal pass connecting it to Mississippi Sound and then to the Gulf of Mexico. The subtidal variability in this system and its relation to wind forcing are examined from surface elevation data measured by the Waterways Experiment Station (U.S. Army Corps of Engineers) from mid-August to November 1978. The coherence of sea level in the Lake and Pass relative to that of the Sound was high at all time scales; amplitude was similar, and the time lag was 7 hours in the Lake. Despite the fact that winds during this season were mostly from the north, sea-level fluctuations were coherent only with east-west wind. The north-south wind, on the other hand, can set up a surface slope across the Lake, which accounts for less than 3 percent of the total sea-level variation.

As the east-west (alongshore) wind is the most effective driving force for shelf circulation, results of this study indicate that large atmospherically induced exchange probably exists between the Lake and the coastal ocean through the narrow tidal pass.

0 164

EMPIRICAL EIGENFUNCTION ANALYSIS OF DAILY NEARSHORE PROFILES, EASTERN SHORE OF LAKE MICHIGAN

T.A. Test, G.E. Birchfield (Department of Geological Sciences, Northwestern University, Evanston, Ill. 60201)

Nearshore profiles measured daily at nine adjacent locations near Holland, Michigan during June-July 1970 show a different pattern of topographic variation than that described for Pacific Coast beaches. Empirical eigenfunction analysis of the profiles for thirty consecutive days reveals two almost equally dominant modes of variation which are temporally associated with the passage of frontal systems over the lake. Longshore transport processes appear to be as important as onshore-offshore transport in determining the short-term, small-scale variations observed in the study area.

Empirical eigenfunction analysis is confirmed as an effective descriptive tool for the study of short time-scale nearshore topographic variation. More than 95% of the variation in a typical profile can be described with as few as four to five eigenfunctions. The functions cannot be expected to have a direct correspondence to traditional descriptive terminology.

0 165

F. A. Godshall and R. G. Williams

Center for Environmental Assessment Services, Environmental Data and Information Service, National Oceanic & Atmospheric Administration, Washington, D.C. 20235

Classification of Acadian Shelf Waters

As part of a comprehensive analysis of the climatology and oceanography of the area, Cape Sable to Montauk Point out to the 2000 m isobath, temperature and salinity structures (profiles) within the first 200 m of depth have been classified for each month. The quasi-objective classification, based on approximately 12,000 hydrographic casts, was performed by means of the Jalickee - Hamilton technique of asymptotic singular decomposition. The temperature/salinity data were first decomposed into three characteristic profiles (eigenfunctions in depth), and associated cast-dependent coefficients (eigenfunctions in time). The first eigenfunctions appear to be related to profile normals; the second eigenfunction to the seasonal variation in the depth distribution of temperature (or salinity); and the third eigenfunction to the magnitude of the vertical gradient.

In order to classify the water structures, the eigenfunctions were transformed into three groups corresponding; respectively, to a coastal water, a shelf/slope water, and a slope water structure. Maps of classified stations delineated the geographic areas of the water structure classes and temperature/salinity scatter plots from each class give the water mass characteristics.

0 166

ON THE DYNAMICS OF EQUATORIAL OUTFLOWS WITH RELEVANCE TO THE AMAZON'S BASIN

Doron Nof (University of Miami, CIMAS-RSMAS 4600 Rickenbacker Causeway, Miami, Florida 33149)

A simplified model is considered in order to describe the dynamics of outflows of rivers or sea straits located at or near the equator. The model is steady, inviscid and nondiffusive but the motions are not constrained to be quasi-geostrophic. The geometry of the oceanic basin into which the outflow debouches is approximated by a wedge and the vertical structure of the flow is represented by two layers of different densities. Approximate solutions to the potential vorticity equation and the Bernoulli integral are obtained analytically.

It is found that, due to the β effect, an equatorial outflow is deflected toward or away from the coasts depending on the basin geometry and the direction of its axis. The deflection is accompanied by separation and "blocking" which results in coastal or equatorial trapping. When the angle between the coastlines forming the basin is larger than 120° and the basin's axis of symmetry is directed toward the northeast, as is the case of the Amazon's basin, the outflow is deflected away from the coasts and separates from both walls. Consequently, the outflow penetrates into the ocean interior as an isolated current.

A possible application of this theory to the processes responsible for the formation of isolated lenses containing Amazonian water, such as those observed off the South American Coast, is discussed. It is shown that these isolated lenses may be related to the profound seasonal variability of the Amazon's discharge and the subsequent variability of the separation points. Such a variability can lead to a seasonal formation of isolated segments containing Amazonian water which undergo geostrophic adjustment, close upon themselves, and form isolated lenses.

Trace Metal and Radioisotope Marine Geochemistry

Harbour C
Monday A.M.
Michael Bewers (Bedford Institute), Presiding

0 167

FLUXES OF THORIUM ISOTOPES AND PROTACTINIUM FROM A SEDIMENT TRAP EXPERIMENT IN THE DEEP PACIFIC

R. F. Anderson (Woods Hole Oceanographic Institution/Massachusetts Institute of Technology Joint Program in Oceanography, Woods Hole, MA 02543)
M. P. Bacon
P. G. Brewer (both at: Woods Hole Oceanographic Institution, Woods Hole, MA 02543)

Fluxes of thorium isotopes and protactinium have been measured at five depths at a sediment trap site southeast of Hawaii (15°21'N, 151° 28'W; 5792 m water depth). Th-228 results indicate that the trapped material at all depths consists primarily of large, rapidly settling particles originating at or near the sea surface which settle through the 5000 m water column in approximately one year. Settling particles scavenge Th-230 and Pa-231 during their descent through the water column, resulting in increasing specific activities of both nuclides with depth.

Activity ratios of unsupported Th-230/Pa-231 in sediment trap samples are greater than 10.8, the ratio of their production by uranium decay. The ratio is lowest near the surface (18 at 978 m), increases to a maximum of 35 at 4280 m, and decreases to 25-30 in the sediments. Several lines of evidence indicate that the high Th/Pa ratios in sediment trap samples are not caused by incorporation of old resuspended sediments. Rather, in open-ocean, low-particle-flux environments, thorium is more effectively scavenged than protactinium from seawater by the sinking particles. Ratios of the measured fluxes of unsupported Th-230 and Pa-231 to their rates of production in the overlying seawater are less than 20% above 1000 m, increase to a maximum of 73% for Th-230 and 26% for Pa-231 at 2778 m, and decrease slightly nearer the bottom. The flux of particles is capable of removing only a portion of the Pa-231, and probably Th-230 as well, produced at this site by uranium decay. The remaining Th and Pa are transported horizontally to more reactive scavenging environments where they are then stripped from seawater.

0 168

SURFACE CHEMICAL PROPERTIES OF NATURAL MARINE PARTICULATES

L. Balistrieri
J.W. Murray (both at: Department of Oceanography, University of Washington, Seattle WA 98195)
P.G. Brewer (Department of Chemistry, Woods Hole Oceanographic Institution, Woods Hole, MA 02543
(Sponsor: Bruce Taft)

We have combined field observations of trace metal scavenging with theoretical surface chemistry models to determine the adsorption properties of sinking particulate matter in the deep sea. The model equations yield equilibrium constants which describe metal interactions with deep ocean particulates. These equilibrium constants are then compared with the equilibrium constants which define trace metal interactions with the surface of model metal oxides (e.g., SiO_2, $YAlO_3$, $\alpha FeOOH$ and am. $Fe_2O_3 \cdot H_2O$) and model organic compounds (acetate, lactic acid, salicylic acid and seawater humic acids). The comparisons indicate that trace metal-particulate matter interactions in the sea highly resemble interactions between trace metals and organic compounds. This suggests that the adsorption properties of natural marine particulates are controlled by organic coatings.

0 169

SURFACE CHEMICAL PROPERTIES OF BIOGENIC SILICA. I. HYDROXIDE ADSORPTION IN 0.700M NaCl at 25.0°C

D. B. Kent
M. Kastner (both at Scripps Institution of Oceanography, La Jolla, CA 92093)

Adsorption onto biogenic silica surfaces is a potentially important process in the removal and transport of metal ions in sea water. The flux of silica from shallow to deep waters and its accumulation rate in the sediment are quantitatively important; and the specific surface areas (SSA) of biogenic silica particles are large relative to biogenic carbonate particles.

Diatom species were cultured, the organic matter was oxidatively removed, and SSA were measured by the BET method. The amount of hydroxide adsorbed (surface excess hydroxide, Γ_{OH^-}) as a function of pH was determined by alkalimetric titrations in 0.700M NaCl at 25.0°C. The titration data were corrected for hydroxide consumed by the bulk solution and by dissolved silica.

An overall similarity in the patterns of the Γ_{OH^-} versus pH isotherms was obtained for two diatom species, with SSA of 72 and 176 m^2/g and for the synthetic silica BDH, with a SSA of 81 m^2/g. Adsorption of hydroxide begins at about pH 4.0, rises slowly until around neutral pH, above which it rises extensively as a function of pH. The adsorption of hydroxide by the silica surface is interpreted as the reaction of surface silanol groups (referred to as "sites") with hydroxide to produce a deprotonated charged siloxy group $\equiv SiO\text{-}H + OH^- = \equiv SiO^- + H_2O$. The observed differences in the amounts of hydroxide adsorbed by the two diatom species and by BDH silica indicate that the site density for hydroxide adsorption by the pennate diatom Navicula pelliculosa is approximately three times that of BDH silica. The centric diatom Skeletonema costatum has an intermediate site density. These results indicate that biogenic silica particles have a large capacity for adsorption of metal ions from sea water.

O 170

TRACE METALS IN THE NORTHWEST ATLANTIC OCEAN

P.A. Yeats (Bedford Institute of Oceanography, Dartmouth, Nova Scotia, Canada)
J.A. Campbell (Department of Oceanography, University of Liverpool, Liverpool, U.K.)
(Sponsor: J.M. Bewers)

Vertical distributions of Al, Cr, Mn, Fe, Ni, Cu, Zn and Cd have been measured for a station at 53°N and 41°W in the North Atlantic Ocean. Total Al, Mn and Fe show mid-depth concentration minima with sharp concentration increases within 200 m of the sea surface and the sediments. Dissolved Mn and Fe do not show concentration increases in the bottom nepheloid layer. Total Cr, Ni, Cu, Zn and Cd show a variety of profiles indicative of several different mechanisms controlling the various distributions. Surface depletion is observed for Cr and Ni whereas Cu shows surface enrichment. Zinc shows evidence of both very near surface enrichment and depletion at slightly greater depth. Near 3200 m a concentration maximum is seen for Cr, Ni and Cu. Possible mechanisms for these observations will be discussed.

O 171

PARTICLE MIXING RATES AND FLUXES OF DISSOLVED SILICA FROM DEEP-SEA SEDIMENTS BASED ON ^{32}Si MEASUREMENTS

D. J. DeMaster (Dept. Marine Science and Engr., North Carolina State Univ., Raleigh, NC 27650)

^{32}Si profiles from a south Atlantic Antarctic sediment and an equatorial Pacific sediment yield particle mixing rates of 200 and 50 cm^2/ky, respectively. The Antarctic ^{32}Si mixing rate is in good agreement with the ^{210}Pb mixing rate from the same sediment, whereas the Pacific ^{32}Si mixing rate is 5 times smaller than the ^{210}Pb mixing rate from the same sediment. The discrepancy in the Pacific sediment mixing rates may result from differential mixing of robust radiolarian tests containing ^{32}Si activity and fine-grained clay material containing the majority of the excess ^{210}Pb activity.

The inventories of ^{32}Si in the Antarctic and Pacific sediments are 2.6×10^{-3} and 0.58×10^{-3} dpm/cm^2, respectively. The observed inventories of ^{32}Si are 2 to 4 times greater than predicted from the product of the ^{32}Si specific activity of surface plankton, the biogenic silica accumulation rate, and the ^{32}Si mean life. The high ^{32}Si inventories result from the interaction of particle mixing, sedimentation, and dissolution. In an unmixed sediment column the siliceous tests with the highest ^{32}Si activity are at the sediment-water interface where the most intense dissolution occurs. In a mixed sediment column some of the high ^{32}Si siliceous tests are mixed downward, being replaced by older ^{32}Si-poor tests. The reduced ^{32}Si activity near the interface decreases the dissolved flux of ^{32}Si out of the sediment column which increases the sedimentary inventory of ^{32}Si. The flux of dissolved silica out of deep-sea sediments can be calculated from the inventory of ^{32}Si. Based on mass balance calculations and ^{32}Si inventories, the dissolved fluxes of silica out of the Antarctic and Pacific sediments are 3×10^{-4} and 2×10^{-5} g $SiO_2/cm^2/y$, respectively. These silica fluxes are compatible with the solid phase biogenic silica profiles and are 5 to 10 times lower than the fluxes predicted from modeling pore water silica profiles.

O 172

CD, ZN, CU, AND BA IN FORAMINIFERA TESTS (CORE V22-174)

Edward A. Boyle (Dept. of Earth & Planetary Sciences, M.I.T., Cambridge, MA 02139)

The trace element content of 3 species of planktonic foraminifera from the upper 100 cm (< 30,000 yrs. bp) of LDGO core V22-174 (10°S, 13°W, 2630 m) has been determined. Ultrasonic and reductive cleaning combined with a mild CO_2 dissolution are used to separate the lattice-bound trace metals from ferromanganese and aluminosilicate contaminants. The procedure reduces contaminant levels by three orders of magnitude. Most samples have contaminant mole ratios less than 5×10^{-6} for Fe/Ca, 3×10^{-5} for Mn/Ca, and 10^{-5} for Al/Ca.

Cd and Zn show no correlation with residual contaminant levels. Cd and Zn contents increase with decreasing calcification temperatures, as expected from the water column distribution of these elements. Downcore Cd/Ca ranges are: G. conglobatus, $2\text{-}23 \times 10^{-9}$; G. Tumida, $22\text{-}32 \times 10^{-9}$; G. truncatulinoides, $22\text{-}40 \times 10^{-9}$. Zn/Ca ranges are: conglobatus, $2\text{-}30 \times 10^{-6}$; tumida, $15\text{-}35 \times 10^{-6}$; truncatulinoides, $20\text{-}70 \times 10^{-6}$. The variance of the Cd and Zn concentrations over time is consistent with the expected degree of upper water column trace metal variability. Cd and Zn do not show a simple glacial-interglacial signal, however.

For Ba and Cu, less reproducible values are observed on separately-processed samples and there is no discernible down-core signal. It is likely that residual contamination affects the observed values. The observed ranges are $1\text{-}30 \times 10^{-6}$ for Ba/Ca and $0.2\text{-}1.0 \times 10^{-6}$ for Cu/Ca. The lattice-bound fraction is probably near or below the observed lower-bound.

Foraminifera may be significant carriers in the oceanic cycling of Zn, but are definitely not important for the transport and removal of Cu, Ba, and Cd.

Since the Cd distribution in the oceans is identical to that of phosphate and Zn strongly resembles silicate, the variations in these trace elements in foraminifera may be useful in the reconstruction of past nutrient patterns in the ocean. Nutrient distributions are controlled in part by the deep and intermediate circulation of the ocean, so the trace metal variations also can be used to constrain past ocean circulation patterns.

O 173

GEOCHEMISTRY OF PARTICULATE MATTER IN THE SANTA BARBARA BASIN, CALIFORNIA

A. M. Shiller (Scripps Institution of Oceanography, La Jolla, CA 92093)
N. B. Price (Grant Institute of Geology, Edinburgh, United Kingdom)

The Santa Barbara Basin off southern California is a shallow (600 m) near-shore basin. The waters below sill depth (475 m) are generally low in oxygen and show evidence of nitrate reduction. During the spring of 1978 a particulate profile was obtained from this basin. Elemental composition of these particulates was determined by thin-film XRF and compared to the composition of basin sediments and sediment-trap material. Particulate matter from the surface waters showed enrichment in elements associated with planktonic material; the composition of the fine fraction of sediment-trap material agrees well with the composition of mid-water particulates; differences are noted between sediment and particulate composition. Additionally, a near-bottom turbid layer was found to be greatly enriched in iron. Although water from this turbid layer was characteristic of basin waters, the underlying water showed evidence of input from sill depth. Previous workers have recorded the transport of red-brown oxidized material to the basin during flooding of the nearby Santa Clara River. Analysis of river particulates, local soils, and basin sediments suggests that this input of iron-rich material to the basin is a common phenomenon. Much of this iron is probably remobilized in the sediments.

O 174

WITHDRAWN

O 175

DISSOLVED AND PARTICULATE CHROMIUM IN THE COLUMBIA RIVER AND ESTUARY

R.E. Cranston (Atlantic Geoscience Centre, Geological Survey of Canada, Bedford Institute of Oceanography, Box 1006, Dartmouth, N.S., Canada, B2Y 4A2)
J.W. Murray (Dept. of Oceanography, Univ. of Washington, Seattle, WA 98195)
(Sponsor: A.C. Grant)

Columbia River and Estuary water samples were analysed to determine dissolved Cr species and particulate Cr concentrations. Flocculation and spike experiments were done to understand the processes controlling the distribution of Cr. Dissolved Cr chemistry is of interest because there are two markedly different species found in most water samples ($Cr(OH)_2^+$ and CrO_4^{2-}). River water contained an average of 3.2 nM dissolved Cr (98% as CrO_4^{2-}) and 1.8 nM particulate Cr, while estuary samples contained an average of 2.4 nM dissolved Cr (88% as CrO_4^{2-}) and 2.8 nM particulate Cr. Dilution plots suggest that CrO_4^{2-} is conservative in the estuary, while flocculation processes increase the Cr(particulate) and $Cr(OH)_2^+$ concentrations. Up to 28% of the dissolved Cr in river water could be removed by adsorption onto or flocculation with freshly formed particles. Over 70% of Cr(III) spikes were removed by adsorption onto particles and container walls within one hour of their addition. CrO_4^{2-} spikes behaved conservatively.

O 176

THE DISTRIBUTION OF MANGANESE IN THE CASCADIA BASIN

C.J. Jones
J.W. Murray (both at: Department of Oceanography, University of Washington, Seattle WA 98195)
(Sponsor: Bruce Taft)

The marine geochemistry of manganese is discussed on the basis of six vertical profiles of dissolved and acid soluble Mn in the Cascadia Basin. The manganese distributions are controlled by "external" inputs, biological cycling, and in-situ scavenging. There is a maximum concentration at the surface resulting from desorption from atmospheric particulates rather than upwelling or diffusion of Mn from reducing nearshore sediments. The Columbia River was not an important source of manganese at the time of sampling. Concentrations decrease through the photic zone because of uptake by marine organisms. Dissolved manganese reaches a mid-depth maximum corresponding to the oxygen minimum. Two possible explanations are the regeneration of Mn via oxidation of organic matter or advection of reduced Mn away from anoxic slope sediments. Bottom water values of dissolved manganese are very high (0.212-2.18 ppb) at stations on the slope and shelf. Migration of manganese out of pore waters probably causes these elevated levels. At the two offshore stations, a maximum in both dissolved and acid soluble Mn is observed at 2100-2500 m. This is the depth of the Juan de Fuca Ridge, suggesting that the maximum reflects a hydrothermal input. Concentrations again decrease toward the bottom.

O 177

COPPER IN SURFACE WATERS OF THE BERING SEA

David T. Heggie, (Inst. Marine Science U. of Alaska, Fairbanks, AK. 99701)
Present Address (Graduate School of Oceanography, U. of Rhode Island, Narragansett, RI 02882)

Concentrations of copper were measured in the surface waters (<100m) of the Bering Sea during the summer of 1977. Measurements were made by differential pulsed anodic stripping voltammetry on filtered (0.4μm), acidified (pH = 2.5) seawater samples with a precision of 10%. Seawater samples were collected from the central Bering Sea south of St. Lawrence Is, extending across the continental shelf break. Two water masses were defined in the area: continental 'shelf' water with salinities between 29.5‰ and 32.2‰ and temperatures between 12°C and -2°C; and continental 'slope' water with salinities between 32.0‰ and 33.2‰ and temperatures between 11°C and 0°C. The water masses comprise a frontal system delineated by the 100m isobath. Copper concentrations show marked differences across this front. Copper concentrations in 'slope' water varied between 0.1 and $0.6 \mu g \ell^{-1}$, (mean $0.29 \pm 0.13 \mu g \ell^{-1}$ (4.5n. mole ℓ^{-1}) and in contrast copper in continental 'shelf' water was more variable $0.2 - 1.2 \mu g \ell^{-1}$ with a significantly higher mean concentration $0.50 \pm 0.27 \mu g \ell^{-1}$ (7.8n. mole ℓ^{-1}). All continental shelf stations at depths less than about 100m showed copper gradients directed into the sediments, indicative of a flux of copper from the sediments to the overlying water. Estimates of the riverine and atmospheric copper input to the area indicate they

are insufficient to support the copper concentrations in continental shelf waters. It is hypothesized that surface sediment remobilization and sediment seawater exchanges are principally responsible for the elevated copper concentrations in continental 'shelf' waters.

Particle Size and Flux Measurements in Marine and Fresh Water System

Harbour C
Monday P.M.
Prithviraj Mukherji (Univ. of Rhode Island), Presiding

O 178 INVITED PAPER

THE ROLE OF PARTICLE SIZE DISTRIBUTIONS IN DETERMINING ACOUSTICAL BACKSCATTERED ESTIMATES OF VERTICAL OCEANIC PARTICLE DISTRIBUTIONS.

John Proni, (NOAA/AOML Miami, Fla. 33149)
Raj Mukherji, (U.R.I. School of Oceanography, Kingston, R.I. 02881)
Dana Kester, (U.R.I. School of Oceanography, Kingston, R.I. 02881)

Acoustical techniques have now shown to be of use in guiding oceanic chemical sampling and in determining horizontal dispersion patterns of particulate matter dumped in the ocean. However, in order to establish the limits of accuracy of acoustical estimates of the particulate concentration field the relationship between particle size distribution and acoustical backscattered intensity must be determined. The relationship is examined using data from a recently (July 1979) conducted dredge material dump experiment in the N.Y. Bight. One approach in which the acoustical backscattered intensity is regarded as the 6th moment of the distribution and the total suspended mass is regarded as the 3rd moment of the distribution is presented and is compared with data from the New York Bight.

O 179 INVITED PAPER

BREAKAGE OF FLOCS IN SUSPENDED MATERIAL SIZE MEASURING

Ronald J. Gibbs, (College of Marine Studies, University of Delaware, Lewes, DE 19958)
Lohit Konwar and Luis A. Cifuentes.

In the marine environment, clay material as well as other inorganic and organic materials are destabilized because of the effect of high concentrations of dissolved salts. These destabilized particles can then form flocs. In order to understand the hydrodynamic processes of transport and deposition of the suspended material, information on the size & character of the flocs must be obtained.

These flocs are easily broken during sampling and analysis. Simulating taking of samples using a pipette, tests were conducted of breakage of flocs upon passing through orifices that ranged in size from 125 to 3486μm in diameter with very low sucking pressure. Tests conducted on a variety of flocs showed breakage by all but the largest orifices. Breakage varied with the strength of the flocs.

The effect of Coulter-counter analysis on floc breakage was tested on a variety of samples. Many, but not all, flocs are broken up when passing through the orifice of the Coulter counter. Care must be used in interpreting these size distributions. All stages of sampling and analysis must be investigated as sources of breaking flocs if an accurate measurement of the size distribution existing in the environment being sampled is to be obtained.

O 180 INVITED PAPER

LARGE VOLUME IN SITU FILTRATION STUDIES OF PARTICLE SIZE DISTRIBUTIONS AND VERTICAL MASS FLUX.

James K.B. Bishop (Lamont-Doherty Geological Observatory, Palisades, NY, 10964)

Over the past several years the Large Volume in-situ Filtration System (LVFS) has been deployed in the upper 1500 m of tropical oceans. Approxiamtely 20 m^3 of seawater is filtered through a filter series consisting of 53 um Nitex mesh and a pair of 1 um glass fiber filters to trap particulate matter for size distribution and chemical analysis.

The particle size distributions have been compared to power-law distributions of the form:

$$N_d = a\, d^{-m}$$

where N_d is the cumulative number of particles greater than size, d, and m and a are the slope and intercept of the $\log[N_d]$ vs $\log[d]$ plot. A fit of the larger sized particles to this distribution is used to predict the abundances of material larger than the size limit sampled.

The measured and extrapolated size distributions of fecal pellets and fecal matter as well as of Foraminifera and diatoms are combined with semi-empirical settling models based on Stokes' Law to yield estimates of the vertical mass flux of these particulate matter phases.

The interpretation of flux profiles is dependent on:

1) Relative scales of temporal and spatial variability of particle production and distribution.

2) Changes in the size distribution of the material during its filtration.

3) The validity of the power law extrapolations.

4) The applicability of settling models to oceanic particulate matter.

Recent profiles from the Panama Basin will be used to illustrate these points.

O 181

INTERMEDIATE NEPHELOID LAYERS OBSERVED OFF OREGON AND WASHINGTON

H. Pak (School of Oceanography, Oregon State University, Corvallis, Or. 97331)

Two distinct kinds of particle maxima (nepheloid layers) were observed off Oregon in November 1971 and off Washington in October 1978 by an in situ light transmissometer: one in the thermocline in the euphotic zone and the other at intermediate depth well below the thermocline. The thermocline nepheloid layer is associated with well-defined maxima of dissolved oxygen, chlorophyll-a, and phaeophytin, and these associations suggest that the nepheloid layer is primarily composed of phytoplankton undergoing active photosynthesis. The intermediate nepheloid layer is found in connection with the bottom waters near the shelf break and shares some of the characteristic properties of the bottom water: high concentration of suspended particles, low concentrations of dissolved oxygen, chlorophyll-a, and phaeophytin. The particle size distributions in the intermediate nepheloid layer are different from those in the clear water above the nepheloid layer but similar to those in the bottom nepheloid layer. Two hypotheses for the generation of intermediate nepheloid layers, settling and horizontal advection, are examined, and the data support the latter hypothesis.

O 182

ACOUSTIC DETECTION OF PARTICLES IN A FLUID

Marshall H. Orr (Department of Ocean Engineering, Woods Hole Oceanographic Institution, Woods Hole, Mass. 02543)
Elizabeth J. Howard

Multifrequency towed acoustic backscattering systems (20-500 kHz) are being used in oceanographic research to detect near surface (0-150m) particle distributions caused by both natural and manmade processes. The results to date have been mostly qualitative, with little information concerning particle size distribution or concentration being derived from the acoustic work. Laboratory tank experiments have recently been conducted at an operating frequency of 1.6 MHz to determine the sensitivity of acoustic systems of particles of known concentration and size distribution. The experimental results, as well as numerical projections concerning the sensitivity of acoustic systems to particle concentration and sizes as a function of acoustic frequency will be discussed. The numerical projections and towed acoustic data in both industrial chemical waste disposal areas and areas containing natural particle distributions indicate that particles of large size (> 200μ) may not be uncommon even though standard sampling and sizing techniques do not detect them.

O 183

FLOCCULATION KINETICS OF NATURAL CLAY SEDIMENTS

Joan E. Lathrop
Ronald J. Gibbs (both at: College of Marine Studies, Univ. of Delaware, Lewes, Delaware, 19958)

The importance of mineralogy, particle size, and ionic strength on the flocculation of natural sediments was studied by means of flocculation rate experiments on a Delaware Bay mud sample, size segregated into fractions of .5-1, 1-2, and 2-4 um. Concurrent studies were performed with American Petroleum Institute (API) standards of montmorillonite, kaolinite, and illite similarly size-fractionated to provide a basis for comparison with the literature and to predict the effect of mineralogy on the stability values (which are inversely proportional to the flocculation rates) of the sample from Delaware Bay. The experiments were performed in artificial seawater of various salinities. A tank-type reaction mixer was used to stir the clay suspensions at a constant rate. Particle number concentrations were determined at specific time intervals by microscopic counting. A modified form of the Smoluchowski rate equation for fluid motion flocculation was used to describe the coagulation process and determine the stability values for the clay suspensions. The velocity gradient and floc volume fraction were held constant. Stability values of montmorillonite were lower than those for kaolinite and illite which were statistically indistinguishable at less than 5‰. At 17.5‰ all API standards were destabilized equally. As predicted by theory, both the effect of initial particle size on the flocculation rate was insignificant, and the stability value decreased with increasing salinity. An important conclusion is that the stability values and thus the flocculation rates for the natural sample are significantly different from those of the API standards. This could be attributed to differences in their physical nature, and the presence of organic coatings, metallic coatings, and/or organic particles.

O 184

SEDIMENT ACCUMULATION RATES OBTAINED FROM WATER COLUMN PARTICLE SIZE DISTRIBUTIONS USING COAGULATION THEORY

James R. Hunt (Environmental Engineering Science, California Institute of Technology, Pasadena, CA 91125)
(Sponsor: Norman H. Brooks)

Coagulation and sedimentation mechanisms have been used previously to predict size distributions which account both for observed oceanic size distributions and for an increase in total suspended volume at oceanic thermoclines. Coagulation by Brownian, shear, and differential sedimentation were considered, each dominant in a separate particle size interval. The steady state particle size distribution predicted for shear coagulation was

$$n(d_p) = A_{sh}(E/G)^{\frac{1}{2}}\, d_p^{-4}$$

where A_{sh} is a dimensionless constant, E is the particle flux through the size distribution, a consequence of the steady state assumption, and G is the fluid shear rate. Laboratory experiments using clay particles in artificial seawater have verified the Brownian and shear predictions. The purpose of this paper is to review the theoretical derivation and experimental verification of the predictions and then to apply the results to obtain an estimate of the particle volume removed to the sediments by particle coagulation. Vertical profiles of particle size distributions obtained by Lerman, Carder and Betzer (1977), which agree with the shear predicted size distribution, are used to obtain a sediment accumulation rate. This calculation requires estimates of A_{sh} and the vertical variation in fluid shear rate.

O 185

PARTICLE SIZE AND COMPOSITION OF DEEP-SEA SUSPENDED MATTER IN THE NORTH ATLANTIC

M.J. Richardson
C.D. Hollister (both at: Woods Hole Oceanographic Institution, Woods Hole, MA 02543)

An examination of the horizontal and vertical variability of size and composition of suspended particulate matter at two sites (southeast of New York and south of Iceland) in the deep North Atlantic demonstrates the profound influence of resuspension of sediments on the near-bottom nepheloid layer material.

Particle size distributions were measured at sea with a Coulter Counter. Size distributions differed between near bottom nepheloid layer samples and the above clear water samples. The latter samples have a uniform distribution approaching equal volumes in logarithmically increasing size grades from 1-20 μm, the range of particle sizes measured. Nepheloid layer samples have single-mode (∿6μm) distributions.

Compositional studies were carried out by counting particles in photographs taken with a scanning electron microscope. Particles smaller than coccoliths were not included in the counts. General compositional differences noted are a decrease in the percentage of coccoliths and an increase in the percentage of clays and mineral matter from clear water to nepheloid layer waters. These results suggest resuspension of the more refractory materials into the nepheloid layer.

O 186

DIURNAL PATTERNS IN PARTICLE FLUXES AND COMPOSITION IN THE EUPHOTIC ZONE OF THE CARIBBEAN SEA

P. R. Betzer (Marine Science Department, University of South Florida, St. Petersburg, Florida 33701)
D. W. Eggimann, K. J. Karcich, D. J. Walter, P. B. Ortner, D.L. Johnson, D. W. Atwood, and G. R. Harvey
(Sponsor: Kent A. Fanning)

Free-floating sediment traps were deployed at two locations in the upper 100 meters of the open eastern Caribbean Sea. Flux measurements were made at 20 and at 100 meters over a full day (24 hours), during daylight hours, and during the evening. The movements of the deep scattering layer into and out of the upper 100 meters were monitored during each deployment with a 20 KHz acoustic system. Particle fluxes recorded during the night averaged over five times those recorded during the day. Scanning electron micrograph and energy dispersive x-ray analysis of the trapped material revealed a distinct compositional difference for materials collected during these two periods. The diurnal contrast in aggregate composition suggests that the processes which are primary controls over the large particle fluxes are different during those two periods of the day.

O 187

THEORETICAL AND EXPERIMENTAL LIGHT-SCATTERING FUNCTIONS FOR LAKE MICHIGAN DIATOMS

E.B. Hurwitz
G.A. Meadows (Both at: Department of Atmospheric and Oceanic Science, The University of Michigan, Ann Arbor, MI 48109)

To date, the use of light-scattering techniques to study the geochemical nature and hydraulic parameters of suspended materials has come mainly from marine studies. Relatively little information has been reported concerning characteristic optical information such as size distribution, concentration, shape parameter, and index of refraction, of suspended particulates in fresh water basins.

Theoretical light-scattering functions for spherical particles were calculated using Mie Scattering theory for orientations angles from 0° to 180°. This analysis was performed for a distribution of particle sizes and indices of refraction which are characteristic of the Great Lakes.

Several species of centric diatoms, were cultured including Cyclotella meneghiania and Stephanodiscus binderanus using a W.C. medium. The invitro light-scattering functions of these diatoms were measured for a known concentration/ml. and size distribution. These measurements were obtained using a helium-neon laser, polar nephelometer designed by the Department of Atmospheric and Oceanic Science, The University of Michigan. This instrument is capable of determining the light-scattering function based upon scattered light intensity measured at 37 specific angles between 0° and 180° in 5° increments. These scattering functions were then analyzed and compared with theoretical Mie scattering functions. A similar procedure was carried out using diatoms directly from Lake Michigan sample water. Results from these analyses indicate that with proper calibration from representative samples of known optical properties, the general characteristics of naturally occurring diatom communities can be determined through nephelometry.

O 188

IN SITU ANALYSES FOR SIZE, SHAPE, SETTLING ORIENTATION AND SETTLING SPEED OF OCEAN PARTICLES BY HOLOGRAPHIC PHOTOMICROGRAPHY

Kendall L. Carder (Marine Science Department, University of South Florida, St. Petersburg, Florida 33701)

An "in situ" holographic recording system is described that provides data on the size, shape, speed and orientation of particles settling in a sediment trap. The primary advantage of holography is that diffraction patterns from all of the particles (not just those in one plane) in the coherent light beam can be recorded and reconstructed into particle images. The system employs low power, off-the-shelf components. Image reconstruction is assisted by means of a computer-controlled digital video processor.

Particles in the size range 2 to 3000 μm can be recorded and reconstructed, and settling or swimming speeds from .5 to 10^{-5} cm/sec can be determined. The advantages and limitations of the system are discussed along with examples of data acquired by this technique.

Tidal Hydrodynamics of Semi-Enclosed Basins and Coastal Regions

Metropolitan West
Monday P.M.
Bruce Parker (NOAA), Presiding

O 189 INVITED PAPER

RECTIFICATION OF TIDAL CURRENTS OVER SLOPING BOTTOM TOPOGRAPHY WITH APPLICATION TO GEORGES BANK

J.W. Loder (Dept. of Oceanography, Dalhousie University, Halifax, N.S., Canada B3H 4J1)
C.J.R. Garrett

Significant contributions to the mean circulation of tidally-energetic shallow seas can arise from the nonlinear interaction of tidal currents. We discuss the rectification of tidal currents over sloping bottom topography by extending the work of Huthnance (1973). Neglect of mean current-tidal current interaction and truncation of the Taylor series for Stokes velocity are only possible if the tidal excursion is much less than the topographic length scale. This is not usually true. We show how the mean flow and the Stokes velocity may be determined for arbitrary ratio of these length scales (assuming uniformity along isobaths). The results have implications for the resolution required in numerical models, and are used to examine the role of tidal rectification in driving the observed clockwise gyre around Georges Bank. The rectification of M_2 tidal currents on the Bank's sloping sides is predicted to make an important year-round contribution to the observed gyre, but with the mean Lagrangian velocity only approximately two-thirds of the mean Eulerian. Extension to the vertical structure of the associated cross-isobath flow is discussed.

O 190 INVITED PAPER

TIDES AT PORT MANSFIELD, LAGUNA MADRE, TEXAS

Bernard D. Zetler (Scripps Institution of Oceanography, University of California, San Diego, La Jolla, CA 92093)

The tides at Port Mansfield are so small (mean diurnal range of about 2 cm), they are nearly lost in a noise (meteorological) continuum. Nevertheless, a precise tidal analysis is necessary to provide the data for a determination of the elevation of mean high water, the boundary between private and state ownership in an oil-producing area with a very flat terrain. Although response tidal analysis has been shown to be somewhat superior to classical harmonic analysis in various previous tests, no advantage is found in these circumstances of extremely low signal-to-noise ratio.

O 191 INVITED PAPER

EFFECTS OF FRICTION ON SHELF TIDES: SOME RESULTS FROM ANALYTIC MODELS

H.O. Mofjeld (NOAA Pacific Marine Environmental Laboratory, 3711 15th Ave. NE, Seattle, WA 98105)

Analytic models assuming constant depth H show that the horizontal distribution of tides on continental shelves is relatively insensitive to the type of friction used. For Kelvin waves, the distributions are generally similar with quadratic friction (linearized at the frequency of interest) or with vertical eddy viscosity A. An exception is the regime near the inertial frequency f where quadratic friction causes the cophase lines to slant backward while small viscosity causes forward-slanting; away from f and/or with larger viscosity, the cophase lines also slant backward with viscosity. The shortening of the wavelength is similar for either type of friction and occurs for Kelvin, Sverdrup (propagating) or Poincaré (standing) waves. The offshore decay scale of Kelvin waves is increased by friction at very low frequencies. There is an angular frequency $(Af/2)^{\frac{1}{2}}/H$ below which waves actually satisfy diffusion, rather than wave, dynamics because friction is more important than acceleration in the force balance. This frequency is well-below the principal tidal bands for the open shelf; but in shallow embayments and rivers, the tides can be diffusive. The studies with viscosity show that the vertical structure of tidal currents is a strong function of frequency and of the local, horizontal distribution of tidal height. Well-below f there are quasi-steady, bottom Ekman layers, near f a complicated elliptical structure and well-above f colinear bottom Stokes layers with a smaller vertical scale than the Ekman height.

O 192

ON THE COMPUTATION OF BAROTROPIC TIDES IN DEEP INLETS

Bruno M. Jamart
Donald F. Winter (both at: Department of Oceanography, University of Washington, Seattle, WA 98195)

Tidal motion in semi-enclosed basins is essentially periodic. Hence, the solution of the shallow water wave equations in Fourier space (or in terms of harmonic constituents) can be an efficient alternative to the conventional time-stepping procedures. We describe a numerical method based on that premise which combines variational calculus, an iterative scheme, and the finite element method to determine the spatial variations of the Fourier coefficients of water height and depth-averaged horizontal velocities.

A simple version of the procedure has been applied to Knight Inlet, a long, deep, narrow,

steep-sided fjord in British Columbia. The extraction of tidal energy through internal mechanisms associated with the flow over the sill is represented by a body force linear in the local depth-mean velocity and inversely proportional to the time-mean depth. Computed results for the barotropic tidal flow agree fairly well with observations. When the Coriolis term is retained, specification of the surface elevation across the open boundary is inappropriate, and a different boundary condition is proposed (specification of flow direction along the mouth of the estuary, and of tidal height at one point thereon). It is suggested that Poincaré waves generated at the sill and decaying away from it might be responsible for the significant cross-channel motions observed in the vicinity of the sill.

O 193

TIDAL CURRENTS OFF A MULTI-INLET COASTLINE

J. O. Blanton (Skidaway Institute of Oceanography, P. O. Box 13687, Savannah, Ga. 31406)

Vertical profiles of currents were measured for four tidal cycles every 2 hrs at two locations off the Georgia coast. Nine km separated the two sites. Site A was located at 13 m depth in relatively flat topography. Site B was located at 12 m depth in a rugged area of low ridges and troughs.

Tidal currents at both locations traced ellipses whose vectors rotated clockwise. Orientation of the ellipses as well as the ratio of minor to major axes (S) differed between the two locations. The orientation shifted clockwise with increasing depth and seemed to be affected by the proximity of large tidal inlets 15 km away. Ellipses at Site A (flat topography) had relatively low values of S while those at Site B (ridge/trough topography) had significantly higher values, and tidal motion was nearly circular at some depths.

It seems likely that the undulating topography at Site B was responsible for the uniformly higher S values. The length scale of the topographic features at Site B is comparable to a tidal excursion. This condition is dynamically favorable for the generation of residual tidal currents (Zimmerman, 1978) and the higher S values are thought to be Eulerian expressions of the residual currents.

Tidal currents on shallow shelves have many characteristics found in estuaries and embayments. Frictional effects extend to the surface. Close to a multi-inlet coastline, tidal currents appear to be affected by the tidal flow of the inlets as well as by the scale of local topographic features.

O 194

TIDE-INDUCED HORIZONTAL MIXING IN THE UPPER REACHES OF THE BAY OF FUNDY.

Peter E. Holloway (Department of Oceanography, Dalhousie University, Halifax, N. S. Canada, B3H 4J1).
(Sponsor: Chris Garrett)

A one-dimensional advection-diffusion equation is used in analysis of the salinity distribution in the upper reaches of the Bay of Fundy, where measurements show the water to be vertically well-mixed. Best agreement between data and theory is obtained for numerical solutions to the equation where variations along the estuary in cross-sectional area and advective velocity (induced by fresh water input from rivers) are considered, and where the longitudinal dispersion coefficient equals 150 $\bar{u}_* \bar{h}$. The bar denotes a cross-sectional average, u_* is the r.m.s. friction velocity from the bottom stress averaged over a tidal period and obtained from a numerical model of the tidal regime (Greenberg, 1979), and h is the water depth.

The model is used to predict changes in the salinity distribution that would result from the construction of a tidal power barrage across part of Minas Basin.

O 195

TIDAL MIXING, SUMMER STRATIFICATION AND FRONTS IN GREATER COOK STRAIT, NEW ZEALAND

M.J. Bowman
S. Chiswell (both at: Marine Sciences Research Center, SUNY at Stony Brook Stony Brook, NY 11794)

Closely spaced mid-summer hydrographic data gathered in the shelf seas of central New Zealand (10,000 n miles^2) Jan. 9-Feb. 5, 1980 are used to compare water column bulk stratification, potential energy deficit and frontal features with modeling predictions of the "h/u^3" stratification index.

Bulk stratification and potential energy deficit distributions correlate strongly with h/u^3 predictions (which vary by a factor of 3000 over the study region) in almost all areas.

Frontal boundaries located near critical values of h/u^3 (~25) did not necessarily possess surface manifestations, presumably due to active wind stirring. Cross frontal temperature gradients also appeared to depend strongly on the spatial gradient of h/u^3.

O 196

TIDE AND TIDAL CURRENT DYNAMICS ON THE INNER LOUISIANA SHELF

M. W. Szabados (NOAA/National Ocean Survey, Rockville, MD 20852)
L. E. Hickman, Jr., MD 20852

(Sponsor: Henry R. Frey)

The National Ocean Survey (NOS) deployed current meters, meteorological stations, wave gages, and water level gages along the western coast of Louisiana from June 1978 through May 1979. Tide and tidal current data were investigated using harmonic and spectral techniques.

The principal harmonic constituents of the tidal currents were displayed graphically as tidal current ellipses. Ellipses of the semi-diurnal harmonic constituent, M_2, indicate that the tidal current and tidal forces were in phase. Results from the cross spectral analysis between currents and water level measurements also indicate that the semi-diurnal tidal current and tidal sea surface fluctuations were primarily in phase. This phase relationship suggests the presence of barotropic tidal currents.

The data also exhibit a baroclinic tidal current response to the tidal forcing. This is suggested by the tidal current ellipses of the diurnal harmonic constituents, K_1 and O_1. Investigation of the major axes of the ellipses showed that the amplitude and phase angle are incoherent in the diurnal frequency band. Temporal and spatial variability of the density field are also reported.

O 197

TIDES AND TIDAL DISSIPATION OF THE EASTERN BERING SEA SHELF

Carl A. Pearson (National Ocean Survey, NOAA)
Harold O. Mofjeld (both at NOAA Pacific Marine Environmental Laboratory, 3711 15th Ave. NE, Seattle, WA 98105)

Pressure gage and current meter data acquired on the eastern Bering Sea Shelf from 1975 through 1979 have been analyzed for tidal constituents and have been used, along with historical data, to construct cotidal charts and tidal current ellipse diagrams. Although S_2 is anomalously small in the Bering Sea, the tides are predominately semidiurnal throughout most of the shelf region. In Norton Sound, however, the diurnal tides predominate. The tide wave enters the Bering Sea through the central and western Aleutian Island passes and progresses as a free wave to the shelf region. Largest tidal amplitudes are found over the southeastern shelf region, especially along the Alaska Peninsula and interior Bristol Bay. The semidiurnal tide propagates as a Kelvin wave along the Alaska Peninsula but appears to be converted on reflection in interior Bristol Bay to a Sverdrup wave. A large standing Sverdrup (Poincaré) wave resulting from cooscillation in Kuskokwim Bay is evident on the outer shelf. The semidiurnal tides are small in Norton Sound where an amphidrome is located. The diurnal tides, which can have only Kelvin wave dynamics, cooscillate between the deep basin and the shelf area. Diurnal amphidromes are found between Nunivak Island and the Pribilofs, and west of Norton Sound. Tides are small in the Bering Strait. Tidal currents were found to be significantly reduced during winter ice cover in the Northern Bering Sea.

Tidal energy dissipation in the eastern Bering Sea is estimated by the energy flux method at $2\text{-}3 \times 10^4$ megawatts, or about 1% of the global total. This is far smaller than many earlier estimates, but in agreement with recent model results. Most of this dissipation is accounted for by the M_2 tide and is concentrated in Bristol Bay.

O 198

TIDAL CURRENTS IN APALACHICOLA BAY, FLORIDA

L. Vansant (Dept. of Oceanography, Florida State University, Tallahassee, Florida, 32306)
Y. Hsueh

A numerical model of the tidal currents is developed for Apalachicola Bay, a well-mixed estuary located on the Gulf of Mexico on the North Florida coast. Open ocean tides at the east and west ends of the bay force co-oscillations of the bay water which are modelled on the basis of traditional shallow water dynamics, i.e., the vertically integrated and linearized momentum and continuity equations for the flow of a homogeneous fluid damped by a quadratic bottom friction.

Model results indicate:

(1) The inviscid resonance period of the bay is approximately 3 hours.
(2) The total energy of the system approaches the equilibrium value in about one day following the imposition of tides at the open boundaries.
(3) Water exchange between the bay and the open ocean occurs predominantly through the relatively narrow and deep west opening.
(4) The maximum tidal range occurs in East Bay, a shallow arm of the estuary.
(5) The residual current is strongest along the barrier island to the south, where water depths are greatest.

O 199

TIDAL HYDRODYNAMICS OF APALACHICOLA BAY, FLORIDA

Donald Steven Graham (Department of Civil Engineering, the University of Florida, Gainesville, Florida, 32611)

The hydrodynamics and water quality of Apalachicola Bay , a major estuary on the north Florida Panhandle, are being studied for the purposes of developing management techniques for this type of water body and to improve knowledge about this new National Estuarine Sanctuary. Apalachicola Bay is not a geomorphologically "classic" estuary, but rather is semi-enclosed by two barrier islands and is connected to the Gulf of Mexico by four passes. Differences in the tidal phase and amplitude at the passes result in a circulation which is characterized by a large net nontidal flow to the west. Wind is an important dynamic agent in this estuary also.

The project is using the MIT CAFE-1 DISPER-1 2-dimensional finite-element model system which is found to be quite accurate. Both field work and specially-processed LANDSAT images are being used to calibrate the models. To be most effective,field measurements need to be taken in such a manner as to be compatible with model requirements. By using preliminary model runs with reasonable default parameter values and remotely-sensed data to plan the field measurement program, much greater efficiency may be had.

0 200

THE ATTENUATION OF TIDAL WAVES IN A LONG NARROW SEMI-ENCLOSED BASIN

PARKER, Bruce B., (National Ocean Survey, NOAA, Rockville, Maryland 20852)

The amplitude of a tidal wave as it enters and propagates up a semi-enclosed basin, reflects at the head, and propagates back down (and is superimposed on the incident wave) can be attenuated by: (1) the frictional resistance to flow of the bottom and sides of the basin, (2) wave scattering caused by cross-sectional irregularities, (3) local loss at the head of the basin due to imperfect (partial) reflection, and (4) localized loss at locations of numerous islands and/or side channels (where portions of the wave split off, enter these channels, and either do not return or return out of phase with the main wave).

Using cotidal and corange charts determined from extensive tidal data from the Strait of Juan de Fuca-Strait of Georgia, a one-dimensional analytical model is used to show the relative importance of each of the above-noted mechanisms in this waterway. The M_2 tidal wave undergoes a 17% amplitude reduction in the area of the San Juan Islands and undergoes an imperfect reflection at the northern end of the Strait of Georgia (because of the small channels connecting it to the Pacific Ocean), reducing the amplitude of the reflected wave by 18%. The continuous attenuation of the M_2 wave is represented by an exponential damping coefficient of 0.75 per M_2 wavelength (i.e., a 53% reduction in amplitude per M_2 wavelength); this includes the effect of both frictional losses and wave scattering. The K_1 tidal wave is similarly affected by the San Juan Islands and the imperfect reflection at the northern end of the Strait of Georgia. However, the continuous attenuation is much less, being represented by an exponential damping coefficient of only 0.1 per K_1 wavelength (i.e., a 10% reduction in amplitude per K_1 wavelength). The greater attenuation of the M_2 wave is mainly a result of the greater effect of wave scattering on the M_2 wave than on the K_1 wave, and the greater frictional loss because of larger M_2 than K_1 current amplitudes.

Mixed Layer and Upper Ocean Studies

Harbour B
Monday P.M.
Terry Joyce (Woods Hole Oceanographic Institute), Presiding

0 201

THE UNSTABLE TURBULENT MIXED LAYER AS A SOURCE OF DOWNWARD PROPAGATING NEAR-INERTIAL MOTION

John Kroll (Department of Mathematical Sciences, Old Dominion University, Norfolk, VA 23508)

It has been observed in the ocean that near-inertial period motion propagates downward from the surface and can be of considerable magnitude in the deep ocean. But the linearized boundary layer equations of motion predict that the inertial motion generated in the mixed layer by the wind is at exactly the local inertial frequency which will not propagate downward. The linear stability of large-scale perturbations of the turbulent slab model of the mixed layer above a continuously stratified inviscid bottomless ocean is being analyzed. The model is crude especially since a lateral eddy coefficient is used to close the system, but preliminary results are interesting. A critical point for instability with a frequency slightly greater than the local inertial frequency is found for uniform flow (no oscillations) in the mixed layer. This implies that the Ekman transport is a possible source of inertial energy in the deeper ocean.

0 202

A MIXED LAYER EXPERIMENT ON THE SCOTIAN SHELF

N.S. Oakey (Atlantic Oceanographic Laboratory, Bedford Institute of Oceanography, Dartmouth, Nova Scotia, Canada, B2Y 4A2)
J.A. Elliott (Atlantic Oceanographic Laboratory)

During September-October, 1976 an experiment to study the mixed layer was set up on the Scotian Shelf near Emerald Basin south of Halifax. The ten day experiment at a fixed site included an extensive time series of velocity microstructure profiles to depths of 100 m using the tethered free fall instrument OCTUPROBE. From these, we have obtained estimates of dissipation levels. Dissipation in the mixed layer was strongly correlated with the wind speed and represents ~0.5% of the energy flux at 10 m. In this experiment there was a weak, but permanent, density gradient in the surface layer defined principally by salinity and as well there was a strong shear of the horizontal current extending into the surface layer. A possible mechanism for generating the velocity microstructure may be through shear instability rather than direct mechanical mixing from the surface.

0 203

THE RELATIONSHIP BETWEEN DOWNWARD IRRADIANCE AND UPPER OCEAN STRUCTURE

J. J. Simpson (Scripps Institution of Oceanography, La Jolla, CA 92093)
T. D. Dickey (Institute for Marine and Coastal Studies and Dept. of Geological Sciences, University of Southern California, Los Angeles, CA 90007)

The relationship between downward irradiance and upper ocean structure has been studied using a numerical model. Two general classes of irradiance parameterizations were utilized. The first (Case I) employed a single attenuation length while the second (Case II) involved two attenuation lengths. The latter formulation provided for enhanced absorbance in the upper few meters. Wind speeds of 0, 1, 2, 3, 4, 5, 10 and 20 m sec^{-1} were used for the simulations. A one-dimensional second moment turbulent closure model was selected for the study so that heat could be treated differentially with depth. The Case II results indicated warmer surface temperatures, shallower mixed layers, and more intense thermoclines than Case I for wind speeds less than 10 m sec^{-1}. Results converged for higher wind speeds. There was considerably greater sensitivity to wind speed for Case II when compared with Case I. Mean horizontal velocity as well as thermal structure was sensitive to the empirical formulation of downward irradiance. The results of this study provide strong indications that downward irradiance and its proper parameterization are important in determining upper ocean structure.

0 204

SEASONAL VARIABILITY OF THE OCEANIC THERMOCLINE

M. A. Cane (Meteorology Department, M.I.T., Cambridge, MA 02139)
E. S. Sarachik (Center for Earth and Planetary Physics, Harvard University, Cambridge, MA 02138)
(Sponsor: Peter Müller)

A linear baroclinic model of thermocline response to periodic winds on an equatorial β-plane is described. In terms of a parameter $\phi = \omega L/c$, where ω is frequency of forcing, L the basin size, and c the Kelvin wave speed, it is shown that for small ϕ (Atlantic) the thermocline depth response tends to be in phase with the wind while for ϕ near unity (Pacific) only the eastern part of the basin responds in phase. An interesting quasi-resonant behavior at $\phi = n\pi/4$ is illustrated.

0 205

HORIZONTAL ADVECTION OF TEMPERATURE IN THE SEASONAL THERMOCLINE DURING JASIN 1978

T. M. Joyce (Woods Hole Oceanographic Institution, Woods Hole, MA 02543)
R. H. Käse and W. Zenk (Institut für Meereskunde, Kiel, West Germany)
(Sponsor: M. G. Briscoe)

The temporal changes in the low-frequency thermal structure during a two week period in August-September 1978, are discussed from moored data collected during the JASIN experiment. While some changes in the thermal structure appear to be related to local winds, the dominant low-frequency variability in the seasonal thermocline can be explained as horizontal advection of a spatially varying temperature field, and associated thermal wind, by geostrophic currents with no vertical motion or mixing required. This advection of temperature may be important not only for the 1-D heat budgets but also for the tracing of fronts as they are advected through the JASIN area.

0 206

DYNAMICS OF DOUBLE-DIFFUSIVE INTRUSIONS

Eric S. Posmentier (Southampton College of L.I.U., Southampton N.Y. 11968)
Charles B. Hibbard (Lamont-Doherty Geological Obs., Palisades N.Y. 10964)

The growth rate of double-diffusive intrusions has been evaluated using Stern's (1967) model, which assumes vertical T/S gradients in the salt fingering domain and compensating horizontal T/S gradients.

For a given vertical scale, various cross-gradient and along-gradient tilts correspond to a variety of modes including different growth mechanisms, growing or damped vertically-propagating intrusions, and decaying perturbations. The relative importance of the processes causing momentum, salinity, and temperature changes is discussed for each mode.

A quartic equation is obtained for the tilt at which the growth rate is maximum; however, near-maximimum growth rates occur at widely differing along-gradient tilts.

When the salinity perturbation reaches an amplitude of 1%, the effective coefficients of horizontal diffusion can exceed 10^6 and 10^7 cm^2/s for salt and heat, respectively. Three derivatives of S,T, and density (Eulerian, Lagrangian, and synoptic along-core) are found to have different signs and phases, confounding attempts to confirm double diffusion by fine-scale observations. T-S diagrams in intrusion-affected regions can assume a variety of shapes.

0 207

SCATTERING FROM VOLUME VARIABILITY

L. Goodman (Code 480, Office of Naval Research Arlington, VA 22217)
K. Kemp (Code 3633, Naval Underwater Systems Center, Newport, Rhode Island 02840)

Acoustic scattering cross sections for medium fluctuations have been derived from the fundamental wave equation. The effect of a finite scattering volume has been analyzed. Fluid velocity fluctuations can be shown to produce no backscatter at scattering angle $\theta = 180^0$, independent of the statistical form of the velocity field. Scattering from sound speed fluctuations for the atmospheric and oceanic cases is compared. Using a cylindrically symmetric form about the vertical direction for temperature fluctuations, explicit expressions for the scattering cross sections are obtained. These results depend strongly on the parameter α, the ratio of the vertical length scale of the temperature variability to the horizontal length scale. For a typical echo sounder operating at 20 kHz, scattering strengths based on observed values of temperature microstructure are of order -120 dB if isotropy is assumed ($\alpha = 1$). For the layered case, where the horizontal scale of the variability is larger than the horizontal dimension of the scattering volume, scattering strengths are of order -70 dB. These results can be extended to other frequencies provided the medium variability spectrum is known.

0 208

SEASONAL SEA LEVEL ALONG THE EASTERN U.S.

John P. Blaha (PMEL/NOAA, Seattle, WA 98105)

Comparisons among three monthly series - tide gage heights, longshore surface wind stress, and surface wind stress curl - suggest a systematic seasonal influence of the Gulf Stream surface current on coastal sea level from Key West to Sandy Hook. Tidal heights from 1955-1975 are adjusted to uniform atmospheric pressure and for the effect of seasonal heating in steric heights. Adjacent land stations which report resultant monthly winds are compared to sea level during 1965-1975. From surface stresses obtained from the FNWC atmospheric pressure analysis, wind stress curl is computed over several latitude bands and compared to sea level during 1955-1975.

Seasonal sea level shows much likeness to curl. The strong semiannual trend is associated with latitudes 20-26°N. Sea level anomalies to the seasonal trend appear to be the effect of a quasi-steady response to longshore winds. The longshore slope of seasonal sea level is $\pm 1.5 \times 10^{-7}$ between Atlantic City and Sandy Hook and generally between $\pm .7 \times 10^{-7}$ and $\pm 1.5 \times 10^{-7}$. Although curl has a strong semiannual constituent from 17 to 26°N, sea level at Key West and Miami do not.

0 209

ON THE MEAN SEA LEVEL SLOPE IN THE FLORIDA STRAIT

Frank Chew (NOAA/AOML, Miami, FL 33149)
Emery I. Balazs (NOA/NOAA, Rockville, MD 20852)

The 1979 releveling of geodetic benchmarks along the Florida Keys allows a fresh determination of the slope of the mean sea level (MSL) between Key West and Miami. In this study, the result of the releveling is used to find the MSL slope for the 18 month period of December, 1970, to May 1972, when tidal data at three intermediate locations are also available. Averaged over this period, the MSL along the left (facing downstream) edge of the Florida Current shows a pronounced minimum in a region between Key West and Miami. Approximately, the slope down from Key West to the minimum is 11 cm/150 km, and the slope up from the minimum to Miami is 3 cm/115 km. This minimum feature has not been previously reported.

Observationally, the mean slope pattern is supported, in part, by the moored current data of Lee and Mayer, and, in part, by the surface current data of Richardson, Schmitz, Niiler, and Brooks. Dynamically, the mean slope pattern is indicative of the non-linear, or inertial nature, of the Florida Current. For the pattern can be interpreted as an expression of the banking mechanism in a fast, meandering flow, with the downward slope primarily a reflection of a downstream increase in centripetal acceleration, and the upward slope, an increase in centrifugal force.

0 210

SHALLOW WATER INTERNAL WAVE SPECTRA

A.S. Bennett (Atlantic Oceanographic Laboratory Bedford Institute of Oceanography, Dartmouth, Nova Scotia, Canada, B2Y 4A2)

Internal waves have been observed with a Batfish variable depth towed body on the Scotian Shelf. Spatial spectra of vertical displacement are presented and compared with the Garrett and Munk deep sea spectra. The relationship of large amplitude wave packets to these spectra is discussed.

0 211

ON THE VERTICAL EXCHANGE WITHIN THE PHILIPPINE SEA

Joseph L. Reid (Scripps Institution of Oceanography, La Jolla, CA 92093)
Arnold W. Mantyla (Scripps Institution of Oceanography, La Jolla, CA 92093)

The Philippine Sea is separated from the Pacific Ocean by the ridges extending southward from Japan to New Guinea. Over most of this distance the ridges extend shallower than 2000 m and at only one place is there a passage as deep as 4500 m. Additional ridges inside the Philippine Sea, with a sill depth of about 3900 m, separate the Sea into western and eastern basins.

Thus the major source of the deep and abyssal waters within the Sea is the passage near Guam, and the abyssal characteristics receive no other lateral supply. Any deviation from the source characteristics must result from processes within the Philippine Sea.

The differences in the relations of the characteristics inside the Sea from those at the sill are consonant with a simple vertical exchange within the Sea, without involving lateral processes. In particular the oxygen-temperature and oxygen-density relations indicate that the exchange has been effective through the depth-range from about 2000 m to the bottom.

Marine Geochemistry

Metropolitan East
Tuesday A.M.
Robert H. Byrne (Univ. of South Florida), Presiding

0 212

LEAD COMPLEXATION IN SEAWATER

Robert H. Byrne (Department of Marine Science, University of South Florida, St. Petersburg, Florida 33701)
(Sponsor: Kent A. Fanning)

Ultraviolet absorbance spectra of lead have been obtained in natural seawater. Lead absorbance spectra in the wavelength range between 215 and 300 nanometers are highly pH dependent. Variability of the observed spectra is related principally to the variation in $CO_3^=$ concentration with pH. Pb^{++}, $PbCl^+$ and $PbCl_2^0$ species which are dominant at low pH have a composite absorbance maximum near 240 nanometers. The $PbCO_3^0$ species has an absorbance maximum at 225 nanometers and is found to be the dominant inorganic form of lead within the normal pH range of seawater. Deconvolution of the absorbance data obtained in natural seawater directly provides formation constants appropriate to seawater speciation calculations. Speciation schemes constructed using data directly obtained in the medium of interest do not require knowledge of activity coefficient behavior as a function of ionic strength or medium. The information obtained in this study of natural seawater enriched (6 micromolar) in lead provides an evaluation of the various lead speciation models constructed using formation constants obtained either at low ionic strength or in simple seawater analogs.

0 213

TRACE METAL PROFILES IN PORE FLUIDS FROM HEMIPELAGIC AND RED CLAY SEDIMENTARY PROVINCES

J.J. SAWLAN
J.W. Murray (both at: Department of Oceanography, University of Washington, Seattle WA 98195)
(Sponsor: Bruce Taft)

Concentrations of trace metals were measured in pore fluids from "end member" sedimentary provinces in the East Tropical Pacific Ocean. Oxidizing red clay environments display low levels of Mn and Fe. Nickel concentrations are similar to bottom water values ($\sim$10 nM kg^{-1}) throughout these profiles. In the surface sediment pore fluids, copper is considerably enriched relative to bottom water. At lower levels in red clay profiles copper concentrations decrease to 15-25 nM kg^{-1}.

In hemipelagic sediment pore fluids, Mn and Fe gradients are conspicuous. Nickel profiles in these sediments reflect the manganese data. Above the depth of manganese reduction, nickel concentrations parallel bottom water values as in red clay profiles. Within the zone of manganese reduction, nickel concentrations increase to values more than 40 times greater than bottom water. Copper concentrations in the top 2 centimeters of these hemipelagic profiles, again display enrichment relative to bottom water. At the level of manganese reduction, there is a concomitant increase in Cu.

Two processes are suggested to be responsible for the observed pore fluid trace metal profiles. First, reduction and dissolution of manganese and iron results from direct involvement in organic matter oxidation. Nickel and copper appear to be released into solution by the reduction of these host carrier oxides. Second, some metals (notably Cu) may be released into the pore fluid directly from decomposing organic matter.

0 214

ND AND SR ISOTOPES IN FERROMANGANESE DEPOSITS AND TERRIGENOUS CLAY

Goldstein, Steven L. (Lamont-Doherty Geological Observatory, Palisades, N. Y. 10964)
O'Nions, R. K. (Department of Mineralogy and Petrology, University of Cambridge, U. K.)

$^{87}/^{86}Sr$ and $^{143}/^{144}Nd$ can be used to determine sources of Sr and Nd in sediments and seawater. Work at Lamont and Cal Tech has shown that Fe-Mn deposits from different oceans exhibit distinctive ranges of $^{143}/^{144}Nd$. All exhibit $^{87}/^{86}Sr$ close to seawater (.7091).

$^{143}/^{144}Nd$ has been measured on clay taken from cores in which Mn nodules lie close to the core top. All clay samples measured thus far show $^{143}/^{144}Nd$ within the ranges exhibited by Fe-Mn deposits from the same ocean. A Mn nodule located at 400 cm in Indian Ocean core V20 186, and clay above and below 400 cm, have been analyzed for $^{87}/^{86}Sr$ and $^{143}/^{144}Nd$. Nodule and clay contain an acetic acid leachable component with $^{87}/^{86}Sr$ close to seawater. Post-leaching $^{87}/^{86}$ Sr values for the nodule are less than .7111, whereas sediment values range from .7263-.7298, clearly indicating different Sr provenances. In marked contrast, both nodule and clay exhibit $^{143}/^{144}Nd$ close to .51200, indicating that provenance of the REE in the clay and nodule may be the same.

The $^{143}/^{144}Nd$ in Fe-Mn deposits and terrigenous clays, lower in the Atlantic than the Pacific, may reflect erosion of older continent into the Atlantic and younger continent into the Pacific. Dissolved $^{143}/^{144}Nd$ in seawater may be controlled by ion exchange with terrigenous clay. A hydrothermal Mn crust from the Galapagos spreading center exhibits $^{143}/^{144}Nd$=.512473±30, undistinguishable from Pacific Mn-nodules (Goldstein and O'Nions 1979) and Pacific seawater (Piepgras, et al. 1979). If the Galapagos case is representative, an insignificant amount of Nd is exchanged during circulation of seawater through MORB ($^{143}/^{144}Nd$>.5130), and direct mantle input of REE into the oceans is negligible.

0 215

COMPARATIVE MINERALOGY, MICROCHEMISTRY AND DIAGENETIC FEATURES INSIDE MANGANESE NODULES FROM MANOP SITES H AND S

Virginia Mee Burns (Department of Earth and Planetary Sciences, Massachusetts Institute of Technology, Cambridge, Mass. 02139)
Roger G. Burns
Marjorie Styrt

Scanning electron microscope (SEM), electron microprobe (EMP), and x-ray diffraction (XRD) measurements of manganese nodules collected from hemipelagic sediments in the Guatemala basin (Site H; 6°33'N, 92°46'W; 3470m) and siliceous ooze sediments southeast of Hawaii (Site S; 11°07'N, 140°05'W; 4722m) reveal different chemical, mineralogical, and textural features which correlate with compositions of underlying sediments and pore waters at each site. Manganese concentrations are significantly higher, and Fe, Al, Si contents considerably lower, in the micron-wide growth bands inside the Site H nodules than in the Site S nodules. The Mn-rich bands in Site H nodules are enriched in Na and Ca, have lower Mg contents, and are drastically depleted in Ni and Cu (in particular) compared to the Ni-Cu-Mg-rich manganese nodules from Site S. Such analytical data correlate with the identification by XRD of coexisting Mn^{2+}-bearing birnessite and todorokite in nodules from the more reducing hemipelagic sediments at Site H compared with δ-MnO_2 and Ni^{2+}-Cu^{2+}-Mg^{2+}-bearing todorokite in nodules from the more oxidizing environment at Site S. Observations by SEM reveal biogenic debris in

all nodules to be pseudomorphously replaced by Mn oxides, the process being more extensive in Site H nodules. In the Site S nodules, the meshwork todorokite crystallites frequently are associated with authigenic phillipsite and barite. The latter phases have not been identified in the Site H nodules, in which the birnessite-todorokite assemblages have a platey-bladed habit.

0 216

CURRENT PHOSPHORITE FORMATION IN MEXICAN CONTINENTAL SHELF SEDIMENTS

R. Jahnke (Department of Oceanography, University of washington, Seattle WA 98195)

Pore water and sediments obtained from the Pacific continental shelf off Mexico in October, 1979 were analized for dissolved phosphate, calcium, alkalinity, hydrogen ion, and total solid phosphorus. These analyses produced strong evidence that phosphorites are currently forming in these sediments.

Interstitial water phosphate concentrations decrease with depth in the sediment resulting from either increasing rates of input at the sediment surface or consumption within the sediment. At two of the stations, the profiles are linear to a depth of 40 cm. Diffusion calculations show that the gradients cannot be formed seasonally suggesting consumption at depth. Profiles from the other stations exhibit zones of large curvature implying consumption at these horizons. All pore waters are highly supersaturated with respect to solubility values reported for marine apatites.

There is a large subsurface maximum in total solid phosphorus at the station displaying the largest curvature in the pore water profile. This maximum coincides with the zone of greatest curvature and is consistant with the hypothesis that dissolved phosphate is being consumed in this region. X-ray diffraction analysis of the sediments from this zone resulted in six peaks corresponding to "d" spacings reported for other marine apatites. The relative intensities of these peaks approximately agree with previously measured values. Assuming steady state, the rate of growth of apatite in this zone is .17 mg apatite/cm^3/yr.

0 217

CALCITE DISSOLUTION: AN IN SITU STUDY IN THE PANAMA BASIN

Robert Thunell (Dept. of Geology, Univ. of South Carolina, Columbia, S.C. 02908)
Susumu Honjo and Robin Keir (Woods Hole Oceanographic Institution, Woods Hole, Mass.)

An in situ study has been carried out to determine the relationship between calcite dissolution and water-column carbonate chemistry in the Panama Basin. Fourteen pre-weighed samples of planktonic foraminifera were attached to a deep-sea mooring line at six different levels (665m, 1268m, 2265m, 2869m, 3769m and 3791m) and deployed for 123 days. After recovery, percentage weight loss and number of broken foraminiferal tests were determined. In addition, carbonate saturation, expressed as $1-\Omega$, was calculated from measurements made at a hydrographic station close to the mooring site. Both weight loss and percentage of broken foraminiferal tests show that very little dissolution is occurring above 2869m. Below this depth dissolution increases rapidly, suggesting that the "hydrographic lysocline" may be at approximately 3000m in this region. These findings are consistent with a study of Panama Basin surface sediments which show that the "sedimentary lysocline" is also close to 3000m. A comparison of the dissolution trends observed in both the in situ and surface sediment studies with the water-column carbonate chemistry indicate that the level of increased dissolution is not associated with the transition from saturation to undersaturation with respect to calcite.

0 218

RADIOACTIVE & STABLE ISOTOPE STUDIES OF NAUTILUS POMPILIUS: RATE AND ENVIRONMENT OF GROWTH

J.K. Cochran (All at Dept. of Geology & Geophysics, Yale Univ., New Haven, CT 06520)
D.M. Rye
N.H. Landman

The growth rate and environment of growth of Nautilus pompilius are being studied using the ^{238}U decay series nuclides ^{226}Ra, ^{210}Pb and ^{210}Po and stable isotopes of C and O. To date one juvenile specimen recovered live in the Philippine Islands has been studied. Radiochemical analyses of the body chamber and the 9 most recently formed septa show that ^{210}Pb ($t_{1/2}$ = 22.3y) is incorporated into the shell in excess of its grandparent ^{226}Ra ($t_{1/2}$ = 1622y) and granddaughter ^{210}Po ($t_{1/2}$ = 138d) relative to the concentrations in ambient sea water. The $^{210}Po/^{210}Pb$ activity ratio (corrected to the time of capture of the Nautilus) increases systematically from 0 in the most recently formed septum (septum 26) to 1.0 by septum 19. Assuming that an individual septum is formed rapidly compared with the length of time between septa, the pattern of ingrowth of ^{210}Po to radioactive equilibrium with ^{210}Pb yields a period of 60 to 90 days between formation of septa. $\delta^{18}O$ values for the first 7 septa (septa 1-7) range from -1.4 to -1.0‰. There is a pronounced break in $\delta^{18}O$ between the 7th and 8th septa, with values for septa 8-26 varying from 0.5 to 1.2‰. The break in the $\delta^{18}O$ pattern coincides with a decrease in septal spacing and may correspond to the end of the embryonic stage. $\delta^{13}C$ values for septa 1-10 vary from -1.4 to -.6‰. A break in $\delta^{13}C$ values occurs between septa 10 and 11, with $\delta^{13}C$ for septa 11-26 ranging from 0.0 to 1.5‰. There is a positive correlation between $\delta^{13}C$ and $\delta^{18}O$ for septa 11-26. This may relate to a varying rate of individual septal deposition with more recently formed septa deposited closer to isotopic equilibrium with sea water. Alternatively a weak correlation between ^{210}Pb activity and $\delta^{13}C$ implies that the $\delta^{18}O$ and $\delta^{13}C$ variations may be related to depth in the water column or proximity to shore.

0 219

SEDIMENTARY PROCESSES IN THE INNER NEW YORK BIGHT: EVIDENCE FROM Pb-210 AND Pu-239,240

L.K. Benninger (Dept. of Geology, Univ. of North Carolina, Chapel Hill, NC 27514)
S. Krishnaswami (Physical Research Laboratory, Ahmedabad 380009, India)

Seven sediment box cores 20-50 cm in length from the inner New York Bight were analyzed for water content, loss on ignition (LOI) and excess Pb-210; three were also analyzed for Pu-239,240. Excepting some depth horizons in a core from a dredge-spoil dumpsite, every sample analyzed contained excess Pb-210. Variations in the concentration of excess Pb-210 with depth in the sediment at all stations correlated strongly with LOI, which apparently traces that fraction of the sediment which is active in removing reactive elements from the water column. In the cores analyzed for Pu-239,240, every sample contained finite Pu, and Pu concentrations showed strong correlation with excess Pb-210.

The radionuclide distributions may be viewed as products of sediment accumulation or of mixing. The most reasonable accumulation model yields very rapid rates of sediment accumulation: 0.5-3.2 g/cm^2/yr. At the other extreme the relationships between excess Pb-210 and LOI are compatible with mixing of a Pb-210 carrier phase (traced by LOI) into the pre-existing substrate with little or no actual accumulation. Bulk sediment properties suggest a compromise: episodes of sediment migration during which fines carrying reactive elements are mixed into the mobile substrate. Thus real local sediment accumulation might be largely fed by sediment redistribution.

Measured inventories of excess Pb-210 and Pu at these stations are minimum estimates but are still greatly in excess of those supportable by direct atmospheric deposition: lateral supply is required. Incorporation of sedimentary fines into the sand substrate could make this environment an important repository of reactive elements.

0 220

ADVECTIVE VERTICAL PROCESSES IN THE UPWARD TRANSPORT OF PARTICULATE MATERIALS AND DISSOLVED METALS FROM MINE TAILINGS DISCHARGED INTO TWO DIFFERENT FJORD SYSTEMS.

M. Waldichuk, (Fisheries and Oceans Canada, West Vancouver, B.C., Canada V7V 1N6)

Tailings are discharged from a copper-molybdenum mine (40,000 tons day^{-1}) into Rupert Inlet at the northwest end of Vancouver Island, and from a zinc-lead mine(1,500 tons day^{-1}) into Agfardlikavsâ fjord on the central west coast of Greenland. Various residual metals, e.g. copper, zinc, cadmium, lead and molybdenum, are present in the tailings from both mines. Strong tidal currents through Quatsino Narrows cause intensive turbulence and upwelling with resuspension of the mine tailings at the entrance to Rupert Inlet. The intensity of resuspension of the tailings is related to tidal range, freshwater runoff, and the density of inflowing seawater. Release of metals from these tailings into the seawater appears to be minimal, and uptake by marine organisms has not been significant.

On the other hand, metals have leached markedly from the tailings in Agfardlikavsâ fjord. Lead concentration, for example, has increased to about 1 mg L^{-1} in the bottom water, or about three orders of magnitude above the natural background. Metals in the bottom water are distributed through the water column with winter turnover, caused by the increased density of surface water resulting from freezing. The upward flux of dissolved metals through turnover of the water column is further enhanced by the winter intrusion of dense seawater over the entrance sill of Agfardlikavsâ fjord. As a result of spreading of dissolved metals into the surface waters of both Agfardlikavsâ and the seaward fjord Qaumarujuk, there has been a significant uptake of metals by the marine invertebrates and eelgrass in this area.

0 221

EVAPORATION COEFFICIENT OF THE SEA SURFACE FROM EDDY FLUX MEASUREMENTS

S.D. Smith (Atlantic Oceanograhic Laboratory, Bedford Institute of Oceanography, Dartmouth, Nova Scotia, Canada, B2Y 4A2)
R.J. Anderson (Atlantic Oceanographic Laboratory)

Eddy correlation measurements of water vapor, heat and momentum fluxes have been made at a fixed tower near the water's edge on a low, sand island. The quantity of evaporation data collected is nearly equal to the total of similar data in the literature, and extends the range of conditions to include stable stratification and downward vapor flux. The evaporation coefficient

$$C_E = \langle \rho_v u_3 \rangle / [U_{10}(\rho_s - \langle \rho_v \rangle)]$$

has a value of 1.3×10^{-3} in neutral conditions. The coefficient is found to vary with stability in accordance with accepted empirical profile laws and to increase significantly with increasing wind speed at this shoal location.

Our values of the Bowen ratio of sensible to latent heat flux are found to vary widely with meteorological conditions and do not conform to empirical functions of temperature only as proposed by several authors.

0 222

FOSSIL FUEL CO_2 BUILDUP IN BAFFIN BAY

E.P. Jones (Bedford Institute of Oceanography, P.O. Box 1006, Dartmouth, Nova Scotia, Canada B2Y 4A2)
E.M. Levy (Bedford Institute of Oceanography, P.O. Box 1006, Dartmouth, Nova Scotia, Canada)

We report changes in the total inorganic carbon in the water of Baffin Bay which we interpret to reflect increases in atmospheric carbon dioxide due to fossil fuel combustion. The changes are revealed from differences at different depths in the alkalinity and total inorganic carbon values which are corrected for calcium carbonate dissolution and decay of organic matter and are comparable to the changes reported for GEOSECS Atlantic stations[1,2] and Pacific stations[3]. From helium-tritium data, the oldest water in Baffin Bay is Baffin Bay Bottom Water, believed to be a few hundred years old. This water is thus old enough to be not influenced by the post-industrial atmospheric CO_2 concentration build up. Although the precise origin of this water is uncertain, it is most likely formed primarily from Atlantic Water possibly coming from the Arctic Ocean as does the overlying Deep Water. The intermediate layer above the Deep Water is also from the Atlantic Ocean, having entered Baffin Bay through Davis Strait. The upper layer (about 200 m) is primarily Atlantic water also, but influenced by runoff. Thus, because the water at most depths is

ultimately of Atlantic origin, we believe our observations at different depths further document in the ocean the well established increases in atmospheric CO_2 concentrations due to fossil fuel combustion.

0 223

OCCURRENCE OF CARBON MONOXIDE IN RECENT SEDIMENTS OF LAKE ERIE AND SOME NEARBY POLLUTED HARBORS

D.D. Adams, N.J. Fendinger and D.M. Parrish (Department of Chemistry, Wright State University, Dayton, Ohio 45431)

Carbon monoxide was measured in the interstitial water of diver-collected cores from Lake Erie's central basin, Cleveland Harbor and Hamilton Harbour (Lake Ontario) during the spring and summer of 1979. Sediments were processed immediately on board ship within a helium gas filled glove box and stored at 4 °C in special jars containing degassed salt solution. Equilibrated head space gases (Ar, N_2, CO_2, CH_4 and CO) were analyzed by dual detector (TCD and FID) gas chromatography. Concentrations of CO with depth in the sediments (from 2 to 93 cm) ranged from 1 nmole (0.022 ml) to 49 nmole (1.1 ml) per liter of interstitial water for 55 sediment samples. Two cores from Hamilton Harbour had values from 2 to 21 nmoles per liter and a Cleveland Harbor core provided similar concentrations (5-15 nmoles/l). At one station in Lake Erie's central basin, average CO values in the surface 30 cm were depleted by about half (from 5.7 to 2.6 nmoles/l) between July and August, probably due to methane production. Carbon monoxide escaping from the sediments as bubbles, for a nearby station in July, measured 38 ppm. The major gases collected above the sediment surface were methane and nitrogen. Present studies in our laboratory indicate that CO is produced in sediments stored in the dark at 4 °C, suggesting that such bacterial processes occur during winter conditions when methane production is minimal.

Arctic Geophysics and Oceanography: Lorex and Fram I

Metropolitan West
Tuesday A.M.
J. R. Weber (Energy, Mines and Resources), Presiding

0 224 INVITED PAPER

LOREX 79. INTRODUCTION

J. R. Weber (Earth Physics Branch, Energy, Mines & Resources, Ottawa, Canada K1A 0Y3)

In the spring of 1979 the Earth Physics Branch in cooperation with the Polar Continental Shelf Project coordinated a multidisciplinary geophysical and oceanographic polar expedition to investigate the nature and origin of the Lomonosov Ridge (LOREX 79). While a main camp and two satellite camps were transported by the Transpolar Current across the ridge from the Amerasia Basin to the Eurasia Basin over a 2-month period, the following studies were conducted by 38 government and university scientists and technicians: astro and satellite navigation; bathymetry; gravity; shallow, intermediate and deep seismic; heat flow; magnetovariational and magnetotelluric measurements; aeromagnetics; coring and dredging; seafloor photography; CTD, sound velocity and current measurements to 2000 m; bottom current measurements; chemical analysis of the water column; acoustic studies between LOREX and FRAM 1. Preliminary results from sediment cores and dredged rock samples indicate that in Cretaceous time the Lomonosov Ridge was part of the Barents continental shelf. It is theorized that it was rafted to its present position by the seafloor spreading process. The results of some of the investigations suggest that the ridge is composed of continental rock, others seem to indicate that the bulk of the rocks are oceanic thus implying that another tectonic process may have taken place prior to the onset of the spreading process. Concurrently with LOREX the U.S. - sponsored multidisciplinary project FRAM 1 was operating north of the N.E. coast of Greenland. The purpose of this session is to snythesize all aspects of the various studies as they apply to Arctic Ocean structures and their origins as well as to the dynamics of the water-masses of both the North Polar region and the Eastern Arctic Basin.

0 225

SURFICIAL GEOLOGY AND GEOMORPHOLOGY OF THE LOMONOSOV RIDGE

S.M. Blasco (Geological Survey of Canada, Bedford Institute of Oceanography, Dartmouth, Nova Scotia B2Y 4A2)
C.F.M. Lewis (Nova Scotia B2Y 4A2)
B.D. Bornhold (British Columbia V8L 4B2)

High resolution reflection seismic and bathymetric profiling, sediment sampling and seabed photography were conducted from ice station LOREX in April and May of 1979, as the ice floe drifted over the Lomonosov Ridge close to the north geographic pole. A continuous 3KHz, bathymetric-subbottom profile reveals a ridge relief of 2,800 m, the crest rising to within 1,400 m of sea surface. Assymetric in shape, the Amerasian flank has slopes as steep as 12°, but the Eurasian flank slopes do not exceed 7° along the drift path. The continuous shallow seismic reflection profiles indicate the ridge consists of en echelon fault blocks that give the crest an irregular morphology. Less than 75 m of stratified, unconsolidated sediment, primarily associated with the fault-block tops, appears to have been deposited on the ridge crest prior to faulting. Seabed photographs show these sediments to be undergoing erosion by current scour. The presence of neritic dinoflagellate *Luxidinium propalulum* in reworked seabed material taken from the top of a core recovered from the ridge crest indicates that these sediments may be mid-Cretaceous in age. This suggests that faulting (and separation from the Barents Continental Shelf?) was possibly initiated no earlier than mid-Cretaceous. More than 1,100 m of stratified, unconsolidated sediments infill the Makaron and Fram basins directly adjacent to the ridge. These flat-lying sediments unconformably abut against the ridge flanks.

0 226

STRUCTURES OF THE ARCTIC OCEAN

J.A. MAIR (EARTH PHYSICS BRANCH, EMR OTTAWA, ONTARIO, K1A 0Y3)

The Fram, Makarov and Canada Basins of the Arctic Ocean have distinctly different crustal structures suggesting that they were formed at various times by different spreading mechanisms. The Canada Basin, characterized by a 2 to 4 km thick sedimentary layer and a distinct oceanic layer 3B of 7.7 km/s, has the thickest crust and is probably the oldest of the three basins. It may have formed by back-arc spreading during the early Cretaceous. The crust of the Makarov Basin has a thin sedimentary layer of less than 1 km and is only 8 to 9 km in total thickness. The crust of the Fram Basin has a similarly thin sedimentary layer but is 3 to 4 km thicker overall than the Makarov Basin. These latter measurements were taken in an area very near the North Pole, separated by a thin section of the Lomonosov Ridge. The Ridge, in this area, appears to be composed of mainly oceanic rocks, however, a thin veneer of continental crust overlying this root material may be present. The Makarov Basin may be the result of back-arc spreading during early Tertiary, with the Alpha-Ridge as the, now foundered, island-arc. The Fram Basin probably began to open, contemporaneously with Baffin Day, about 70 my ago, by spreading of the Nansen-Gakkel Ridge. The Lomonosov Ridge emerges from this scenario as a very long-lived feature in spite of its great length and slim profile, firstly as a strike-slip shear zone, 150-120 my ago, secondly as a part of the European continental shelf from which the Alpha Ridge migrated 60-40 my ago and finally as a fragment of the European shelf, rifted from it by the opening of the Nansen-Gakkel Ridge.

0 227 INVITED PAPER

MONITORING OF MICROEARTHQUAKE ACTIVITY ON THE NANSEN RIDGE FROM ICE STATION FRAM-I IN THE ARCTIC OCEAN.

Y. Kristoffersen Norw. Polar Res. Inst. Oslo, Norway
E. Husebye NORSAR, Kjeller Norway

An array of sonobuoys was operated for 6 weeks on adjacent ice floes as the ice station FRAM-I drifted southward from the Pole Abyssal Plain onto the western flank of the Nansen Ridge. The array geometry was cheked by a transponder navigation system.
A significant microearthquake activity with 1-2 events pr. hour was recorded as the array came within about 30 km. of the active spreading center. Most of the recorded events are located on a portion of the Nansen Ridge where very few teleseismic events have been observed over the past two decades. The locus of the microearthquake activity correspond with the eastern side of the axial rift as determined by spot depth measurements and the axial magnetic anomaly from the NARL aeromagnetic survey.

0 228

INTERMEDIATE REFLECTION PROFILES

A. Overton, (Geological Survey of Canada, Ottawa, Canada K1A 0E8)
J.R. Weber, (C.G.U.) (Sponsor)

Seismic reflection profiling of the sedimentary column and basement structures was conducted along the drift path of ice station Lorex during April and May, 1979. This work was part of a multidisciplinary program to gain knowledge of the nature and origin of the little studied Lomonosov Ridge, the major submarine ridge which divides the Arctic Ocean basin. The drift path extended from the Makarov basin, across the Lomonosov Ridge, and into the Fram basin in the vicinity of the North Geographic Pole. More than 200 high quality seismic reflection records and digitally recorded magnetic tapes were taken at regular time intervals along the drift path. A cross shaped array was used with explosive sources at the centre so that reflections can be analysed in terms of dip angle, depth, and position. Estimates of seismic velocities may also be obtained for selected reflections which originate from both sedimentary layers and basement features. No reflections are observed from within the ridge. Digital processing of the magnetic tapes may extract depths to the Mohorovicic Discontinuity in detail along the drift path.

0 229

CRUSTAL REFRACTION AND SEISMIC REFLECTION RESULTS FROM FRAM 1

H.R. Jackson (Bedford Institute of Oceanography, Atlantic Geoscience Centre, Box 1006, Dartmouth, Nova Scotia, Canada B2Y 4A2)
I. Reid (Dalhousie University, Halifax, Nova Scotia, Canada)

Nine refraction lines in split configuration were located at distances up to 110 km from the Mid-Arctic Ridge. On lines parallel to the ridge shallow and slow mantle velocities were measured. A crustal thickness of only 3 km is defined. On lines perpendicular to the ridge higher mantle velocities suggest anisotropy. Shear wave conversions of compressional mantle arrivals occur at the sediment basement interface. The reflection line that crosses the refraction lines where the ocean bottom seismometer was launched shows outcropping basement when P-S conversions are not recorded. From sediment thicknesses measured on the reflection record and P to S delay times on the horizontal geophone, P to S ratios of 4.6 were calculated for oceanic sediments up to 1.5 seconds thick. Sedimentation rates of 10 cm/1000 years were estimated using magnetic anomaly identification. The proximity to the Greenland shelf may explain the high sedimentation rates.

O 230 INVITED PAPER

LOREX GRAVITY: IMPLICATIONS FOR LOMONOSOV RIDGE COMPOSITION AND COMPENSATION

J. F. Sweeney
J. R. Weber
D. W. Halliday (all at: Earth Physics Branch, Dept. of Energy, Mines and Resources, Ottawa, Canada K1A 0Y3)

In the vicinity of the North Pole the Lomonosov Ridge is characterized by a linear free-air gravity high that ranges between 60 and 85 mGal. Flanking lows of up to -50 mGal are centered along the base of the ridge in the Fram and Makarov basins respectively. The gravity minimum in the former basin is generally 10 to 15 mGal less negative than that in the latter, and suggests that isostatic compensation for ridge topography is more pronounced toward the Makarov Basin. Gravity model calculations indicate an average density not greater than about 2.45 g/cm^3 for material comprising the ridge. The combination of the average rock density with seismic P-wave velocity (≥ 4.7 km/s) determined for the ridge is not typical of oceanic type rocks. This and the near absence of low - density unconsolidated sediment on the ridge suggests that in the area studied, the Lomonosov Ridge may be composed largely of low-porosity rocks of sedimentary origin.

O 231

BATHYMETRY AND TECTONIC STRUCTURE OF THE LOMONOSOV RIDGE BASED ON GRAVITY AND PLUMB-LINE DEFLECTION OBSERVATIONS

J. R. Weber, J. F. Sweeney and D. W. Halliday (Earth Physics Branch, Energy, Mines and Resources, Ottawa, Canada K1A 0Y3)

Some 320 individual depth soundings and gravity measurements and some 750 line kilometres of echo soundings and gravity recordings from the LOREX 79 and from the 1967 and 1969 Dominion Observatory North Pole Expedition have been analyzed. From the depth soundings a 100 m contour map of the Lomonosov Ridge has been compiled. The map extends from the Marvin Seamounts in the Makarov Basin (basin depth 3940 m) across the ridge (minimum depth 951 m) into the North Polar region (depth 4250 m) of the Fram Basin and covers an area of about 40,000 km^2. The survey shows that the ridge crest is located between 15 and 25 km further south than had been previously assumed. Based on three gravity observations established across the Lomonosov Ridge and on one plumbline deflection determination made near the North Pole in 1969 a 2-dimensional model for the Lomonosov Ridge was postulated consisting of a structure of continental rocks, 130 km wide and 27 km deep, imbedded in an oceanic crust. On LOREX five additional plumbline deflection measurements were carried out across the ridge ranging in magnitude from 5 to 16 arc seconds and pointing towards or away from the ridge axis depending on the distance from it. Both, these plumbline deflection measurements and the detailed LOREX gravity data, fit the 1969 model remarkably well. The model has been refined to take into account LOREX data on bathymetry and on seismically determined sedimentary and crustal thickness, but basically our interpretation has not changed, namely, that the Lomonosov Ridge is a structure of continental origin.

O 232

MAGNETOVARIATIONAL AND MAGNETOTELLURIC STUDIES OVER THE LOMONOSOV RIDGE AND THE MAKAROV AND FRAM BASINS OF THE ARCTIC OCEAN: OPERATION LOREX

P.A. Camfield
R.D. Kurtz
M.J. Drury
E.R. Niblett (all at: Earth Physics Branch, Energy, Mines and Resources Canada, Ottawa, Canada K1A 0Y3)

Magnetovariational and magnetotelluric fields were digitally recorded over the period range 30-86000s at three ice stations which drifted across the Lomonosov Ridge near the north pole in April and May 1979. Geomagnetic variations from polar cap source currents provided continuous moderate-level sounding signals with energy well distributed with period. Such signals are ideally suited to the statistical nature of power-spectral processing methods. Vertical-field response arrows from transfer functions in the period bands 5, 10, 30 and 60 min generally point away from the Ridge axis, showing the flow of electric currents in the sea to be parallel to the Ridge in the adjacent deep Basins rather than in the (resistive) Ridge itself. Preliminary magnetotelluric analysis in the range 150-5000s yields steeply-rising parallel log ρ_a - log T curves, with apparent resistivities over the Ridge greater by factors of 3-5 than the resistivities over the Basins. Two-layer interpretations suggest the presence of up to a kilometer of highly-conductive sediments in the Basins. On the Ridge, such sediments are apparently absent, in accord with the results from marine geology.

O 233

AEROMAGNETIC RECONNAISSANCE: LOREX PROJECT

Peter Hood (Geological Survey of Canada, Ottawa)
Margaret Bower

An aeromagnetic reconnaissance of the Lomonosov Ridge has been carried out as a contribution to the LOREX project. The Convair 580 aircraft of the National Aeronautical Establishment was utilized to fly a series of lines along approximately 500 km of the Lomonosov Ridge and orthogonally to it at a height of 300 m. The aircraft was equipped with ASQ-501 cesium magnetometers in wingtip pods and a GSC self-orienting cesium magnetometer was mounted high in the tail section of the aircraft.

Although the correlation between the anomalies on the flight lines is not conclusive, a zone of anomalies in excess of 1000 gammas appears to strike parallel to the ridge crest. The calculated magnetizations of the causative bodies producing the anomalies correspond to those normally associated with basic rocks such as oceanic basalt. On the southern flank of the Lomonosov Ridge, a series of U-shaped anomalies are reminiscent of those due to a graben-like feature such as have been observed in the Melville Bay area of NW Greenland and elsewhere. Thus the aeromagnetic results appear to indicate that the Lomonosov Ridge is composed of igneous rather than sedimentary rocks or at least has had a considerable amount of associated igneous activity during its recent geological past. If the Lomonosov Ridge is indeed composed of basaltic rocks, it appears likely because of its parallelism with the Nansen Ridge over a distance of 1600 km that its formation is the result of a sea-floor spreading process and it is possibly a dormant spreading ridge.

O 234

TECTONIC IMPLICATIONS FROM THE WEST-ARCTIC OCEAN BASIN AEROMAGNETIC SURVEYS

P.T. Taylor (Geophysics Branch, NASA Goddard Space Flight Center, Greenbelt, MD 20771)
P.R. Vogt
L.C. Kovacs (both at: NRL, Washington, DC 20375)
G.L. Johnson (Arctic Program, ONR, Arlington, VA 22217)

Over 42,000 line-kilometers of low level (152m) aeromagnetic data were recorded by the U.S. Navy during three field seasons; these data cover a swath from the north slope of Alaska to the north geographic pole. Flight lines were spaced between 10 to 20 km. The east-west oriented aeromagnetic profiles across the Canada Basin-Beaufort Sea suggest that Alaska was moving away from the Queen Elizabeth Islands of the Canadian Arctic from 153 mybp (anomaly M-25 time) to 141 mybp (M-19), at an opening rate of 4.6 cm/yr. An extinct spreading center is defined by a positive free-air gravity anomaly, with the relic spreading axis generally paralleling the 150^{o}W meridian. We are unable to recognize a coherent pattern of lineated anomalies over the Alpha Ridge; therefore, its origin remains uncertain. A series of sea-floor spreading anomalies have been mapped in the Fletcher (Makarov) Basin. Spreading began in the Upper Cretaceous (anomaly 34; 80 mybp) and continued until mid-Eocene (anomaly 19; 47 mybp); total opening rate was about 1.5 cm/yr. During the opening of the Fletcher Basin, rifting began in Baffin Bay and the Norwegian and Labrador Seas and Eurasian Basin. Our results suggest a tectonic coupling between these areas with the Nares Strait functioning as a triple junction.

O 235

HEAT FLOW MEASUREMENTS IN THE VICINITY OF THE NORTH POLE.

Alan Judge (Earth Physics Branch; Energy, Mines and Resources Canada, Ottawa, Canada K1A 0Y3)

Vic Allen

During Lorex-79 a total of 42 gradiometer penetrations of sea-bottom sediments were completed; 22 in the Makarov Basin, 10 on the Lomonosov Ridge and 10 in the Fram Basin. A new light-weight digital recording Bullard-style thermal gradiometer with 7 thermistor sensors spaced at 40 cm intervals commonly gave sediment penetrations of 3 m using 45 kilos of lead weight in water depths to 4200 m. Using a needle probe over 300 conductivity measurements were completed on 21 cores. Bottom water temperatures and water temperature profiles were collected both over the ridge and the two adjacent basins. Temperature gradients in the sediments varied from 59 to 69 mKm^{-1} in the Makarov Basin, 40 to 60 on the Ridge flanks and crest and from 75 to 90 in the Fram Basin. Preliminary heat flows over the ridge and Basin, similar to the very few previous results reported from the region, provide some important constraints for the origin and nature of the Lomonosov Ridge.

O 236

UTILIZATION OF PASSIVE MICROWAVE FOR ICE DYNAMICS STUDIES IN THE BEAUFORT SEA AREA

V. Neralla, Atmospheric Environment Service 4905 Dufferin Street, Downsview, Ont. M3H 5T4
R.O. Ramseier, Atmospheric Environment Service 4905 Dufferin Street, Downsview, Ont. M3H 5T4

A simple procedure to calculate the concentration of sea ice over a given area is discussed. The model consists of a momentum equation, continuity equation for concentration and a constitutive law. The momentum equation incorporates air to ice stress, water to ice stress, Coriolis force and internal ice resistance. Since our interest is in the short-range, small scale prediction, as a first step, we have neglected sources and sinks terms in the continuity equation for concentration. A constitutive law based on a linear viscous rheology with both shear and bulk viscosities is used in the model. These viscosities have been treated as functions of concentration.

Electrically Scanning Microwave Radiometer (ESMR) and Scanning Multichannel Microwave Radiometer (SMMR) data have been used for testing the model. The surface winds are obtained from an available regional model. This study demonstrates the use of ESMR and SMMR data for sea ice dynamics studies. Applications of this data for real time sea ice forecasting activities have also been discussed.

O 237

A NUMERICAL INVESTIGATION OF A VARIABLE THICKNESS SEA ICE MODEL

W.D. Hibler, III (USA Cold Regions Research and Engineering Laboratory, Hanover, NH 03755)

A numerical investigation of a variable thickness model of the Arctic ice cover is carried out. The model consists of an ice thickness distribution (similar to that developed by Thorndike et al. 1975) coupled to a viscous plastic constitutive law. Open water creation due to shear and redistribution of ice due to deformation are included. The numerical scheme is formulated in a fixed Eulerian grid with advection terms explicitly included. In the thickness distribution code an arbitrary number of irregularly spaced thickness levels are allowed.

To examine the behavior of this model a multi-level seasonal simulation over several annual cycles is carried out for the Arctic basin. In this experiment a redistribution function consistent with observed and hypothesized physics of the ridging process is used. For ice growth and decay a time independent thermodynamic model together with a fixed depth mixed layer is used. Input fields consist of climatological forcing for the heat budget computations together with

time varying observed winds over a one year period. The results are analyzed to determine the agreement with observed thickness and drift characteristics and to determine the relative contributions of dynamics and thermodynamics. Of particular interest is the nature of the marginal sea ice zone in summer and the nature of ridging off the Canadian Archipelago.

0 238

MODELLING THE AIR-ICE-OCEAN INTERACTION: THE EQUILIBRIUM SOLUTION

H. S. Gaskill, (Dept. of Mathematics and Statistics, Memorial University of Newfoundland, St. John's, Nfld, AlB 3X7)
R. J. Lopez, (Dept. of Mathematics and Statistics, Memorial University, St. John's, Nfld., AlB 3X7)
Gordon Swaters, (C-CORE, Memorial University of Newfoundland, St. John's Nfld., Alb 3X7)

We consider the problem of momentum transfer from a moving air mass to an ice cover to an underlying ocean. Several descriptions of the air column are employed involving driving forces based on geostrophic and ten meter winds. Linear and quadratic stress laws are employed to describe the air-ice and ice-ocean driving mechanisms. Several descriptions of the water column are used to study the effects of currents on the equilibrium ice velocity. Sensitivity studies for the various models will be discussed.

Arctic Geophysics and Oceanography: Lorex and Fram I

Metropolitan West
Tuesday P.M.
J. R. Weber (Energy, Mines & Resources), Presiding

0 239

RESULTS OF A LEAD DRIVEN CONVECTIVE MODEL FOR ARCTIC MIXED LAYER CIRCULATION

T. L. Kozo (Polar Science Center, University of Washington, Seattle, Washington 98105)

A numerical, nonlinear, time-dependent two-dimensional convective model has been formulated using typical measured ambient conditions as initial input to uncover the dominant physical factors and simulate experimentally obtained circulation characteristics under a refreezing lead.

For temperatures found in the Arctic Ocean mixed layer during cooling of surface waters in a lead, convection is primarily salinity-controlled since brine is continuously expelled from newly forming ice.

The model output for a specified surface salinity injection function (0 geostrophic current) results in horizontal current velocities of .05 m/sec, eddy diffusivities of .01 m^2/sec, density fluxes of 4 x 10^{-5} $kg/m^2 \cdot sec$ and a subsequent increase in the depth of the mixed layer. The circulation cells are symmetric with respect to the lead boundaries.

Imposition of a constant geostrophic current shows a resultant circulation cell asymmetry associated with increased salt advection in a forced convective regime.

0 240

THE INADEQUACY OF THE DYNAMIC METHOD IN THE ARCTIC OCEAN

P. Greisman (U.S. Coast Guard R & D Center, Avery Point, Groton, CT 06340)

The dynamic method by which deep sea currents are computed utilizes the horizontal density gradient to determine the vertical current shear which is then integrated in the vertical. Even if the flow meets all the restrictions imposed by the geostrophic approximations, the dynamic method may still fail due to an additional constraint imposed by baroclinic instability of the flow. Such instabilities occur when the vertical current shear exceeds a critical value specified by the product of the square of the internal Rossby radius of deformation and the horizontal gradient of the planetary vorticity

$$\Delta U_{max} = \left(\frac{gH}{f^2}\frac{\Delta\rho}{\rho}\right)\left(\beta + \frac{f}{H}\frac{\partial H}{\partial z}\right)$$

The maximum sustainable steady state shear is limited by this criterion. In the Arctic the topographic component nearly always dominates and the values for ΔU_{max} range from 70 cm/sec over the continental slopes to less than 1 cm/sec over the abyssal plain. The relatively weak stratifications found in most regions of the Arctic Ocean is the main cause of this limitation.

This criterion may explain why direct measurements in diverse locations in the Arctic usually reveal considerably stronger currents than dynamic computations indicate. In regions of weak stratification, therefore, direct current measurements are absolutely essential to determine the important depth-independent (barotropic) component of flow.

0 241

ANOMALOUS BEHAVIOR OF THE PACIFIC T-MAX IN THE BEAUFORT SEA AS OBSERVED DURING THE 1975-76 AIDJEX EXPERIMENT

T.O.Manley (Lamont-Doherty Geological Observatory of Columbia University, Palisades, N. Y. 10964)

During the 1975-76 Arctic Ice Dynamics Joint Experiment (AIDJEX), a total of 1391 continuous STD profiles to 750 m were taken at four drifting manned camps in the Beaufort Sea, over a year long period.

One of the more pronounced features observed in the upper 100 m of the water column was the characteristic temperature-maximum between 50 and 100 m. Observed temperature deviations were warmer by 0.35°C in the central part of the Beaufort Sea as compared with the large scale mean calculated by Coachman and Aagaard. The horizontal scale of this feature is on the order of 10000 km^2. The AIDJEX data provides a 3-dimensional view of this core layer from the center of the Beaufort Sea to the eastern part of the Alaskan slope, some 2000 km^2. From the center of the Beaufort Sea to the Alaskan shelf, the core cools by 0.47°C and deepens by 30 m.

The reason for the large difference in heat content of this layer maybe due to an anomalously large area of open water in the Chukchi Sea, extending as far as 75N during the summer of 1974. This represents an increase of almost twice the normal ice free zone observed in, the years 1975 and 1976. The lag between this event and the observed T-max anomaly is less than 9 months.

0 242

OCEANOGRAPHIC MEASUREMENTS AT THE FRAM I ICE STATION

K.L.Hunkins, Lamont-Doherty Geological Observatory of Columbia University, Palisades, N.Y. 10964
T.O.Manley, same address as above

The first extensive series of continuous high-resolution profiles of temperature and salinity in the Fram Basin were taken daily to a depth of 700 m northeast of Greenland from FRAM I as it drifted along a track 150 km in length between Mar. 29 and May 6, 1979. These profiles are compared and contrasted with an extensive set of profiles taken from the AIDJEX Big Bear camp in the Canada Basin during April 1975. A cold low salinity surface layer appears in both data sets which is relatively constant in salinity (30.5‰) and depth (50 m) in the Canada Basin. During the FRAM I drift the mixed layer varied from 50 m to zero in depth and from 31.5 to 32.5‰ in salinity as a frontal zone about 10 km wide was crossed. The Pacific Water of the Canada Basin with its temperature maximum is replaced by a temperature minimum at 75 m or a steady increase in temperature with depth at FRAM I. Vigorous baroclinic eddies are found in the 50-300 m depth range in the Canada Basin but none were observed from FRAM I. The Atlantic Water core has the same temperature at both locations (~ 0.4°C) but is 500 m deep in the Canada Basin compared with 400 m in the Fram Basin. However, the Fram Basin Atlantic Water is marked by abundant fine structure with depth scales of ~ 10 m while in the Canada Basin, the Atlantic temperature maximum has a smooth parabaloidal shape. These observations suggest a greater vertical heat exchange in the Fram Basin.

0 243

PHYSICAL OCEANOGRAPHY IN THE CENTRAL ARCTIC

E.R. Pounder (Marine Sciences Centre, McGill University, Montreal, Que. H3A 2T8)

As part of LOREX 79, ice station ICEMAN was established April 4, 1979 at 88°41'N, 175°43'E and operated to May 28, 1979 (89°52.3'N, 48°26'W). During the first few days of the drift ICEMAN passed over the Lomonosov Ridge, recording a minimum depth of 956 m. Oceanographic measurements were made daily for 40 days. Each day a profile of current, conductivity, temperature and depth was made to a maximum depth of 1400 m using an RCM-4 Aanderaa current meter. CTD readings were continuous but the meter had to be stopped to give correct current readings so that current profiles were only sampled, if frequently. Each run took about 8 hours. In addition, another Aanderaa meter was moored at 5 m and sampled currents every 10 minutes throughout the experiment and an Inter-Ocean current meter moored at 40 m was used for frequent time-series readings. Current directions are uncertain to about ± 20°. Direction was sensed with a compass, the directing field is small and the magnetic variation near the pole is uncertain and rapidly changing. Some good calibrations on variation were obtained from sun shots but there was a long period of overcast in the middle of the experiment.

Currents were generally small, often below the effective threshold of 3 cm s^{-1}. On the average they were directed toward the Ridge from the Atlantic side. On the assumption (very uncertain) of temporal and spatial invariance of currents, an estimate is made of the volume transport across the Ridge in the vicinity of the North Pole.

0 244

OCEANIC HEAT FLUX AT FRAM I INFERRED FROM ICE GROWTH AND TEMPERATURE GRADIENTS

Miles G. McPhee (USACRREL, Hanover, N.H. 03755)
Norbert Untersteiner (Univ. of Washington, Seattle, WA 08195)

While the fate of heat advected into the Arctic Basin by inflowing Atlantic Water is not well understood, it is thought to have an important impact both on the total climatic energy budget of the region and, more particularly, on the thickness characteristics of sea ice. Indications are that the basin-wide, average upward heat flux is of order 1 to several Wm^{-2}, but little is known of either its spatial or temporal variability. It was speculated that the oceanic heat flux at Fram I might be more intense than the basin-wide average because of its proximity to the Atlantic inflow through Fram Strait; thus a simple experiment was performed in which temperature profiles and ice growth were measured in young ice using in situ thickness gauges and thermocouple strings. Over the experiment the ice grew about 40 cm from an initial thickness of 50 cm. Given the thermal conductivity and heat of fusion in ice of known salinity, the imbalance of upward conduction and heat released by freezing provides an estimate of heat flux from below. Consideration of our measurements, and the errors associated with them, implies that the absolute value of oceanic heat flux was less than 2 Wm^{-2} during Fram I (i.e., from 5 Apr 1979 to 9 May 1979 in the vicinity of 84°30'N, 8°W). This was consistent with measurements of salinity and temperature in the upper ocean which showed the water to be near its freezing point well into the steep pycnocline.

0 245 INVITED PAPER

MOORED CURRENT MEASUREMENTS OVER THE LOMONOSOV RIDGE

Knut Aagaard (Dept. of Oceanography, Univ. of Wash. 98195)

During the LOREX two current meters were moored near the crest of the Lomonosov Ridge in water 1440 m deep and two on the lower Eurasian flank in 3565 m of water. In each case one instrument stood 25 m above the bottom and the other 200 m. The two instruments on the crest and the upper one on the flank recorded satisfactorily, while tape-reading problems at present prevent reporting on the fourth instrument.

Speeds in the abyss were extremely low, reaching a maximum of 3.8 cm sec^{-1}, with a vector mean velocity of 0.4 cm sec^{-1} toward northeast, i.e., approximately along the isobaths. Currents over the crest were considerably higher, reaching 12.2 cm sec^{-1} in the case of the near-bottom instrument, and were in fact strongest near the bottom. The flow over the crest was characterized by a series of pulses of variable strength and time scale, but with a component directed toward the Canadian Basin. These pulses probably represent overflow across the ridge of deep water from the Eurasian Basin destined to sink adiabatically and fill the Canadian Basin abyss.

0 246

ACOUSTIC WAVE PROPAGATION

H.W.Kutschale (Lamont-Doherty Geological Observatory of Columbia University, Palisades, N. Y. 10964)
B.Allen and C.Monjo (same address)

The FRAM I-LOREX acoustic experiment was highly successful, providing high-quality acoustic data in a portion of the Arctic Ocean previously inaccessible to scientists from the U. S. The experiments involved long-range propagation from explosive sources over a 750 km portion of the Eurasian Basin, as well as measurements of ambient noise. Recording at both sites was done continuously for several weeks over the band 1 to 150 Hz to monitor seismic activity originating on the Nansen Ridge. Numerous earthquakes were recorded from hydrophones and geophones. About two dozen shots and several earthquakes were analyzed on a sound spectrograph to separate the normal modes of propagation of the explosive signals and to characterize the spectral character of P and S waves from earthquakes. P and S waves from earthquakes recorded at Iceman, 300 to 1000 km from the Nansen Ridge, may provide a sensitive tool for measuring crustal and upper mantle structure. The main thrust of data analysis has been to provide input for the TRISTEN acoustic experiment at FRAM II. Excellent agreement was obtained between measured SOFAR signals and signals computed from the FFP and PE pulse computer codes. The present measurements, combined with measurements obtained over a twenty-year interval in the Amerasian Basin, indicate that pulse compression will be achieved in most areas of the Arctic channel by transmitting time reversed waveforms corresponding to the first normal mode.

0 247

ARCTIC OCEAN HYDROGRAPHIC FEATURES AND TRACE ELEMENT DISTRIBUTIONS AT LOREX SATELLITE CAMP 1

R. M. Moore (Dept. of Oceanography, Dalhousie University, Halifax, N.S., B3H 4J1)
(Sponsor: A. J. Bowen)

The hydrography at LOREX Satellite Camp 1 in the central Arctic Ocean, occupied during April and May 1979, is presented. Nutrient data suggest the existence of a deep water flow from the Canadian Basin into the Eurasian Basin over the Lomonosov Ridge.

Profiles of trace metals are shown and their relationship with the stratification and biological activity of the Arctic Ocean described.

0 248

CARBONATE CHEMISTRY IN THE CENTRAL ARCTIC OCEAN

Malcolm G. Lowings
Department of Oceanography
Dalhousie University
Halifax, Nova Scotia B3H 4J1
Canada

(sponsor: A. J. Bowen)

We report the results of pH and alkalinity measurements made during the Lomonosov Ridge Experiment (LOREX) in April and May of 1979. These studies were undertaken from Satellite Camp One as a part of the overall chemical oceanographic programme at this location.

Further evidence for a strongly advective feature at a depth of 90 to 100 m in the Polar Mixed Layer (PML) is presented. The presence of an advecting layer is reflected by the consistently different values of pH and alkalinity encountered at these depths during the drift of the satellite camp across the Lomonosov Ridge. On 3 separate occasions, markedly lower values of pH were observed in an approximately 40 m thick layer of water, centered at the indicated depths. Correlates in other data from the site and sources for the advective feature are also discussed.

Calculated values of the partial pressure of carbon dioxide (pCO_2) are presented. This information is used to describe the saturation states of water masses in the central Arctic Ocean. Initial calculations suggest that the PML is saturated with respect to atmospheric concentrations of carbon dioxide.

0 249

FRAM TRITIUM

H. Göte Östlund (Rosenstiel School of Marine and Atmospheric Science, Univ. of Miami, Miami FL 33149)

The atmospheric testing of thermonuclear devices in the early 60s introduced a label of tritium in the form of HTO into precipitation and all surface waters. This tag is a characteristic, but not unique, tritium value for the runoff which makes an addition to each yearly "crop" of Arctic waters formed since 1954. The temperature-salinity relationship in any arctic water mass can thus be used to deduct the year of formation, by mixing, of a water mass.

Data on the 'Arctic Water', down to 200 m at the 1979 FRAM I station indicate a time of formation of AD 1964 ± 1. For the underlying Atlantic water, we have not yet been able to pinpoint a time, but three different age parcels of that water passed the station during its occupancy. The ice at the station has most likely frozen from the waters that still underlaid it at time of occupancy.

0 250

LOREX SATELLITE NAVIGATION

D. Wells (Bedford Institute of Oceanography, Dartmouth, N.S. B2Y 4A2)
J. Popelar (Earth Physics Branch, Ottawa K1A OE4)

Drift of the three LOREX ice camps was computed using Transit satellite navigation data. Drifts of from below 0.03 m/s to over 0.3 m/s were encountered. First single pass 2D fixes and their covariance matrices S were computed. To overcome the problem of poor cross-track coordinates (due to high satellite elevations characteristic of high latitude use of Transit), these fixes were combined and smoothed in three different ways.
a) a Kalman filter using S to represent the relative along and cross track fix accuracies;
b) a cubic spline using the trace of S to represent the accuracy of each fix; and
c) treating each fix as a single line of position ignoring the cross-track coordinate entirely.
In addition standard multipass, multistation 3D fix software, modified to incorporate a linear station drift between passes, was used. Using the cubic spline, smoothed velocity standard deviations were below 0.015 m/s about 50% of the time, and below 0.03 m/s about 80% of the time. The effect of ice velocity on the 2D fixes was reduced by iterating the processing once, using smoothed ice velocities in recomputing the 2D fixes. Most of the processing was performed on a minicomputer at the LOREX main camp.

0 251

LOREX ASTRO NAVIGATION AND DEFLECTION OF THE VERTICAL MEASUREMENTS

G. W. Johnson (Department of Civil and Mineral Engineering, University of Minnesota, Minneapolis, MN 55455)
R. L. Lillestrand
(Sponsor: J. R. Weber, CGU)

Astronomic observations and Transit satellite data have been used to determine several deflections of the vertical along the drift paths of the LOREX stations. Results indicate deflections up to 15 arc seconds and a change of magnitude and direction as the Lomonosov Ridge is approached.

A Wild T-4 and an observing program of 7 to 9 preselected navigational stars were used to determine a series of astronomic position fixes. Accuracies of ± 1 to ± 2 arc seconds both in latitude and longitude were obtained. Transit satellite data were used for defining geodetic positions along the drift paths. To obtain maximum accuracy these data were used as lines of positions (LOP's) rather than as point fixes.

Individual deflections of the vertical were obtained by correlating the astro position fixes with Transit LOP's for the time span (usually several hours) encompassed by the fixes. The path of the sea ice drift was not precisely known between fix times, and it was necessary to choose segments for which the path could reasonably be defined.

Sufficient astro and Transit data were available from the experiment to compute five deflections of the vertical. Depending on the position of the stations relative to the ridge, these values ranged from 5 to 15 arc seconds with their experimental error estimated at ± 2 to ± 3 arc seconds.

Pacific Equatorial and Shelf Dynamics

Metropolitan East
Tuesday P.M.
S. J. Prinsenberg (Canada Centre for Inland Waters), Presiding

0 252

THE ORIGIN OF THE PACIFIC EQUATORIAL 13°C WATER

Mizuki Tsuchiya (Scripps Institution of Oceanography, La Jolla, CA. 92093

Maps have been prepared to show the ocean-wide distributions of depth, acceleration potential, salinity, oxygen, phosphate, silica, and nitrate for the isanosteric surface of 160 cl t^{-1} which nearly coincides with the core of the equatorial 13°C water in the eastern Pacific. The maps indicate that the characteristics of the 13°C water can be acquired in the surface layers of the Tasman Sea and transferred to the subthermocline layers of the eastern equatorial Pacific via the anticyclonic subtropical gyre, the equatorial undercurrent, and the subsurface south equatorial countercurrent.

0 253

A PACIFIC EQUATORIAL TEMPERATURE SECTION FROM 172°E TO 110°W DURING WINTER-SPRING 1979

David Halpern (Pacific Marine Environmental Labor-atory, 3711 15th Ave. N.E., Seattle, WA 98105)

A composite zonal-depth temperature section was made along the equator between 172°E to 110°W, a distance of nearly 8.6×10^3 km, by combining temperature profiles recorded at about 1-degree interval on 28 February 1979 between 172°E and 158°W with profiles recorded at 1/4-degree interval from 23 April to 2 May 1979 between 153°W and 110°W. Coincident with the zonal temperature section, which combined with salinity data produced dynamic height anomalies, were moored current measurements in the upper ocean at three equator-sites (166°E, 152°W and 110°W).

The thickness of the mixed layer decreased from about 100 m near 180° to 10 m near 110°W. The

depth of the thermocline was about 125 m near 180° and approximately 50 m to the east of 120°W. At 166°E the Cromwell Current velocity core depth was found near the bottom of the thermocline and at 152°W and 110°W it occurred within the central region of the thermocline.

The surface dynamic height anomaly relative to 270 db tilted upward toward the west between 172°E and 120°W, with maximum inclination occurring from 153°W to 133°W. West of 120°W the force of the westward wind-stress and the eastward pressure force were about the same magnitude. East of 120°W the zonal gradient of the 0/270 db steric sea level was indistinguishable from a horizontal surface. East of 132°W the directions of the 270/400 db pressure force of the zonal wind field were both westward, indicating that the influence of the prevailing westward wind-stress was confined to the region above the thermocline.

0 254

SEA LEVEL VARIATIONS IN THE EASTERN EQUATORIAL PACIFIC

S.P. Hayes (Pacific Marine Environmental Laboratory/NOAA, 3711 15th Ave. NE, Seattle, WA 98105)
Pedro Ripa (Centro de Investagación Científica y Esenanza Superior de Ensenada, Ensenada, BCN, Mexico)

An array of three bottom pressure and temperature guages was deployed on the Galápagos Islands in late June 1979 and recovered and redeployed in November 1979. Instruments were located at latitudes of 1°20'N, 0°, and 1°S along longitude 91°40'W in mean water depth of 20m.

Low pass filtered pressure time series showed excursions of ∿20 mb during the five month deployment record length. The time series were too short to determine the frequency of the dominant low frequency fluctuations. However, these fluctuations were coherent over the array. Superimposed on the large low frequency pressure variability were small amplitude high frequency, nontidal oscillations over a spectrum of frequencies. Temperature fluctuations also showed dominant low frequency variability; however, the fluctuations were more poorly correlated between stations than the pressure fluctuations.

Pressure and temperature time series were decomposed into empirical orthogonal functions in an attempt to isolate symmetric and antisymmetric equatorial trapped modes. Vertical structure eigenfunctions were calculated from CTD hydrographic data collected near the equator at 110°W.

Influence of the island land mass on the eastward propagating waves and the equatorial undercurrent was investigated in the framework of a linear theoretical model.

0 255

DEEP JETS AS EQUATORIAL WAVES IN THE WESTERN PACIFIC OCEAN

C.C. Eriksen (Department of Earth and Planetary Sciences, Mass. Institute of Technology, Cambridge, MA 02139)

Vertical profiles of current and density made within 5° latitude of the equator along 168°E and 179°E (the vicinity of the Gilbert Islands) reveal multiple deep current reversals which are confined to the equator. These current jets have amplitudes of roughly 5 to 20 cm/sec, vertical scales of order hundreds of meters, and time scales longer than the 1 mo. measurement cruise.

WKBJ stretching and scaling, and subsequent spectral analysis of these profiles indicates that: 1) meridional trapping varies roughly as the square root of the vertical scale; 2) both east and north currents are coherent over meridional separations of 0°45' within roughly 1°30' of the equator; and 3) zonal current lags vertical displacement by $\pi/4$ in depth within 0°45' of the equator. Zonal coherence scales are smaller than the smallest separation of 3°30' along the equator. Kinetic energy decreases near the island chain.

A simple sum of linear free equatorial Rossby, Kelvin, and mixed Rossby-gravity waves can account for the observed equatorial intensification. Rossby modes with periods of at least 1 year must be included; the jets are confined too broadly to be explained by Kelvin or mixed Rossby-gravity modes alone. Coherences are consistent with downward flux of Kelvin wave energy. Spectra also suggest more energy in long than short Rossby waves.

0 256

OBSERVATIONS OF AN UPWELLING EVENT OFF THE WEST COAST OF BRITISH COLUMBIA

Howard J. Freeland
Institute of Ocean Sciences
Sidney, B. C., V8L 4B2, Canada.

An extensive co-operative program to study the near-shore circulation of the Pacific North West was initiated in 1979. The project is called the Coastal Ocean Dynamics Experiment, or CODE.

During the summer of 1979 a water mass of low temperature, high density and very low oxygen concentration appeared on the continental shelf of Vancouver Island and remained through the months of July and August. The event is an upwelling event in a general sense, in that the water is raised up from below the shelf break before inundating the shelf, but is not a classical locally-driven upwelling event.

The author will describe observations of the event and will discuss the possible origins of the water mass.

0 257

CURRENTS ALONG THE WEST COAST OF VANCOUVER ISLAND

W.R. Crawford
R.E. Thomson
W.S. Huggett (all at: Institute of Ocean Sciences P.O. Box 6000, Sidney, B.C. V8L 4B2)

Sea level gauges and current meter arrays have been moored on the continental shelf and slope of Vancouver Island since May 1979. During the summer of 1979, two meteorological buoys were placed in one of these arrays, located off Estevan Point. There are five separate moorings in this array beginning 15 km from Estevan Pt., and ending 100 km from shore at the outer edge of the continental slope.

The low passed (half power at 40 hr) alongshore currents, measured at the two moorings on the shelf, are coherent with the local alongshore wind component and with adjusted sea levels at shore. The average current at 20 m depth from mid-May to mid-August is southeastward at 10 cm/sec, and decreases in magnitude with depth. The fluctuating components decrease in magnitude from peaks of 40 cm/sec near shore to 15 cm/sec on the mid-slope and 10 cm/sec at the outer slope.

Adjusted sea levels are similar along the entire island, but currents measured beyond the shelf break correlate poorly with these sea levels. However, alongshore currents on the continental slope are found to be coherent over distances of 150 km alongshore.

0 258

THE EFFECT OF A MODERATELY BROAD SUBMARINE CANYON ON FLOW ALONG THE CONTINENTAL SLOPE

Barbara M. Hickey (Department of Oceanography, University of Washington, Seattle, WA 98195)

The effect of a moderately broad submarine canyon (half-width ∿ 20 km) on low-frequency flow along the continental slope is examined and compared with available models. Subsurface taut-wire moorings were deployed for a four-month period in the head of Quinault Canyon off the Washington coast, at similar depths about 30 km south of the canyon axis and on the adjacent continental shelf. The primary result is that north-south fluctuations over and within the canyon are coherent with those over the region of smooth topography. However, the amplitude of the fluctuations is a factor of two smaller over and within the canyon than in the region of smooth topography, except near the bottom. These quasi-barotropic fluctuations are coherent with fluctuations over the shelf and represent the response to driving by local wind stress. Fluctuations at depths above the lip of the canyon follow the isobaths. This is consistent with the steady flow result for a canyon whose width is larger than the internal radius of deformation as in this case (Allen, 1976). Fluctuations below the canyon lip have significant cross-isobath components. Lastly, the California Undercurrent (a baroclinic non-local feature whose signature is mean poleward flow over the upper slope) is able to follow the curving isobaths into the submarine canyon.

0 259

RESONANT INTERACTIONS BETWEEN SHELF WAVES, WITH APPLICATIONS TO THE OREGON SHELF

William W. Hsieh (Dept. of Oceanography, University of British Columbia, Vancouver, B.C. V6T 1W5)
Lawrence A. Mysak

Neglecting stratification, friction and atmospheric forcing, we show that the nonlinear long wave equations allow resonant interactions to occur between three continental shelf waves. Equations governing the amplitude and the energy of individual waves in a resonant triad are derived. The nonlinearity allows energy to be transferred between the waves, but with the total energy conserved. While the shelf waves typically have periods of several days, the energy transfer has a time scale of a few weeks. We also find evidence of resonant shelf wave interactions on the Oregon shelf in the spectral analysis of Cutchin and Smith (1973), where the three observed peaks at 0.22, 0.40 and 0.65 cpd agree well with the resonant frequencies deduced from our theory. The good agreement between theory and observation suggests that non-linear energy transfer may play a much more significant role in shelf wave dynamics than was previously realized.

0 260

SHELF-FJORD EXCHANGE ON THE WEST COAST OF VANCOUVER ISLAND

D. J. Stucchi (Institute of Ocean Sciences, Patricia Bay, Sidney, B. C.)
W. H. Bell

Recent current meter observations from both the inner and outer basins of Alberni Inlet show major periods of deep water exchange during the early summer months. Strong density currents on the sill slope are observed in both basins during these inflow periods. The periods of exchange are coincident with the increasing density of the adjacent continental shelf water. An unusual feature of the exchange is the reduction in the dissolved oxygen content of the deep water due to the low dissolved oxygen (<2 ml/l) of the intruding shelf water. Synoptic data provide evidence of major shelf-fjord exchanges occurring above sill depth (100 m).

0 261

SEA-SURFACE TEMPERATURE VARIABILITY OF THE CALIFORNIA CURRENT SYSTEM

K. C. Vierra (College of Marine Studies, University of Delaware, Lewes, DE 19958)
C. N. K. Mooers (Dept. of Oceanography, Naval Postgraduate School, Monterey, CA 93940)

To describe the oceanic variability off the U.S. West Coast (to 130W), the NMFS's biweekly sea-surface temperature charts were digitized on a one degree grid for seven years, 1972 through 1978. Of course, the overall mean sea-surface temperature field is indicative of the net advective effects of the California Current and coastal upwelling. The overall standard deviation and the range of the monthly means are small near the strongest upwelling center, Cape Mendocino. Mode 1 of an empirical orthogonal function (EOF) analysis accounts for 88.2% of the variance and depicts a strong seasonal cycle offshore, while nearshore the seasonal variation is reduced due to the influence of coastal upwelling. Mode 2 accounts for 5.0% of the variance and depicts a meridional variation hinged around Cape Mendocino. There is good agreement between biweekly averages of daily coastal station temperatures and nearshore values from the NMFS charts. The

EOF analysis of the anamalous (departure from seven-year biweekly means) sea-surface temperatures indicates an interannual cycle which is related to the atmospheric circulation. With Bakun's upwelling indices and coastal wind data, sea-surface temperature variations are demonstrated to be associated with atmospheric forcing. Hence, patterns of sea-surface temperature variations are related to some degree to recognizable processes, suggesting some intrinsic predictability to the California Current System.

0 262

INTERLEAVING STRUCTURE IN THE SHELF-SLOPE WATER FRONT OF THE NEW YORK BIGHT

R.W. Houghton (Lamont-Doherty Geological Observatory, Palisades, New York 10964)

During spring and summer of 1979 a series of 3 cruises studied the fine structure (3-30m) interleaving at the shelf-slope water front in The New York Bight south of Nantucket. The objective of this study is to relate this hydrographic structure and mixing processes in the frontal zone with the distribution and growth and decay of the phytoplankton population. A closely spaced (2-3km) array of CTD stations repeated for several tidal cycles was used to resolve the temporal and spacial variability of the fine structure. The longshore scale of the intrusive features was often less than 10km and at times comparible to the cross-shelf scale (4-6km). A mean long-shore drift of approximately 0.05 ms^{-1} was often interupted by irregular tidal motions such that cross-shelf motions become predominate. Calving of the cold pool was observed and this contributed to the cross-shelf structure of the phytoplankton distribution. Intrusions of warm salty slope water were observed both above and below the outer edge of the cold pool.

Planetology

Venus Ionosphere, Thermosphere and Composition

Harbour A
Monday A.M.
Richard Hodges (Univ. of Texas), Presiding

P 1

SUPRATHERMAL ELECTRON FLUXES OBSERVED IN THE VENUS NIGHTSIDE IONOSPHERE

K. Spenner
V. F. Novak (both at: Fraunhofer Institut Für Physikalische Messtechnik, Freiburg, West Germany)
W. C. Knudsen
K. L. Miller (both at: Space Sciences Laboratory, Lockheed Palo Alto Research Laboratory, Palo Alto, CA 94304)
P. F. Michelson (Department of Physics, Stanford University, Stanford, CA 94305)
R. C. Whitten (NASA Ames Research Center, Moffet Field, CA 94035)

The suprathermal electron distribution between 10 and 40 eV measured by the Pioneer Venus retarding potential analyzer in the nightside ionosphere is presented. The observed fluxes are low compared with the dayside fluxes. The spectrum gives no indication that the nightside ionosphere is mainly produced by particle precipitation. Strong variations in the particle fluxes have not been found which could account for the strongly variable nightside plasma density. The observations support the idea presented by Knudsen et al. that the nightside ionosphere is mainly maintained by plasma transport from the dayside.

P 2

PIONEER VENUS OBSERVATIONS OF IONOSPHERIC COMPOSITION AND DYNAMICS

H. C. Brinton
H. A. Taylor, Jr.
S. J. Bauer
R. E. Hartle
R. E. Daniell (all at: NASA/Goddard Space Flight Center, Laboratory for Planetary Atmospheres, Greenbelt, MD 20771)
P. A. Cloutier (Rice University, Houston, TX 77001)

Extensive in-situ measurements of the composition and dynamics of the Venus ionosphere were obtained from the Bennett ion mass spectrometer on the Pioneer Venus orbiter between December 1978 and August 1979, while periapsis traversed a complete diurnal cycle. During quiet periods, an abundant ionosphere was observed both dayside and nightside, dominated by O^+ above $\sim$200 km (except for a predawn region where H^+ exceeded O^+) and by O_2^+ down to typical periapsis heights of $\sim$160 km. At an altitude of 200 km the most prominent ions observed were O^+, O_2^+, CO_2^+, C^+, N^+, CO^+ (N_2^+), NO^+, H^+, and He^+, with trace amounts of O^{++}, O_{18}^+ and H_2^+. Important features of the diurnal variation at this altitude include (1) sharp decreases in the concentrations of most ions at the terminators, and (2) asymmetric nightside bulges in the distributions of H^+ and He^+, with peaks in the predawn sector. Results on ionospheric dynamics include observations of three related plasma regimes, including (1) the bowshock-ionosheath region, (2) the thermal ionosphere, and (3) a superthermal ion layer interfacing with the ionosphere at the ionopause and extending outward to variable heights above the planet. Observed orbit-to-orbit variations in the bowshock-ionosheath and the ionosphere-superthermal plasma layer indicate close coupling among these plasma regimes.

P 3

A PIONEER VENUS VIEW OF THE IONOPAUSE FORMATION PROCESS

L. H. Brace
R. F. Theis (both at NASA/Goddard Space Flight Center, Laboratory for Planetary Atmospheres, Greenbelt, MD 20771)
C. T. Russell (University of California, Los Angeles, CA 90024)
J. A. Wolfe (NASA/Ames Research Center, Moffett Field, CA 94035

Pioneer Venus measurements of ionospheric electron densities and temperatures, solar wind fluxes and magnetic field intensities are employed to investigate the processes by which the solar wind interacts with the ionosphere of Venus to form the ionopause. These data are consistent with a model in which the upstream solar wind pressure is conveyed to the ionosphere by means of the compressed interplanetary magnetic field which is in static pressure equilibrium with the ionospheric plasma at the ionopause. The observed orbit to orbit variability of the ionopause height is produced by changes in solar wind pressure which, when the pressure is increased, impulsively removes plasma in the form of detached plasma clouds. The ionopause then reforms at a lower altitude where a new pressure balance is established. These orbit to orbit variations are superposed on a global ionopause configuration in which the ionopause altitude increases from about 300 kilometers at the subsolar point to about 1000 kilometers at the terminator, an effect that arises from an associated decline in magnetic field pressure toward the terminator.

P 4

O^{++} IN THE VENUSIAN IONOSPHERE

J. L. Fox (Aeronomy Laboratory, Dept. of Electrical Engineering and Dept. of Chemistry, University of Illinois, Urbana, IL 61801)
G. A. Victor (Harvard-Smithsonian Center for Astrophysics, Cambridge, MA 02138)

Altitude profiles of the O^{++} densities in the Venusian ionosphere are computed, using a neutral model based on measurements made by the Pioneer Venus Orbiter mass spectrometer for daytime conditions. Double photoionization of atomic oxygen is the most important source of O^{++}. O^{++} ions are lost by charge transfer to O, N_2 and probably to CO_2 and CO. The calculated profiles agree well with the ion densities measured by the PVO ion mass spectrometer. Dissociative charge transfer of O^{++} to N_2 is found to be an important source of N^+ at high altitudes. The effect of O^{++} on the ion chemistry is discussed.

P 5

DYNAMICAL RESPONSE OF THE DAYSIDE IONOSPHERE OF VENUS TO THE SOLAR WIND

R. E. Hartle
H. A. Taylor, Jr.
S. J. Bauer
L. H. Brace
R. E. Daniell, Jr., (all at NASA/Goddard Space Flight Center, Laboratory for Planetary Atmospheres, Greenbelt, MD 20771)

Ion composition and electron temperature measurements made respectively by the Orbiter Ion Mass Spectrometer (OIMS) and the Orbiter Electron Temperature Probe (OETP) on the Pioneer-Venus orbiter are used to infer the dominant processes involved in the dynamic response of the Venus ionosphere to the solar wind. The analysis is confined to the topside ionosphere in the vicinity of the subsolar point where the strong solar wind interaction makes it possible to easily identify forces imposed upon the ionosphere by the solar wind. Height profiles of the ion composition and electron temperature in the main body of the topside ionosphere, lying between the ionopause and chemical equilibrium regions, reveal that the ionosphere is frequently in a compressed state. This region of the ionosphere is interpreted in terms of a stationary equilibrium where the compression is due to the $\vec{j}x\vec{B}$ force induced by the solar wind. Under compression, this bulk force pushes downward on the ionosphere and is balanced by the net force resulting from the sum of the upward pressure gradient force and the downward force of gravity. In the ionopause region, the compressive $\vec{j}x\vec{B}$ force is even stronger; the opposing pressure gradient force implies the presence of horizontal ion drifts that erode the top of the ionosphere.

P 6

THERMAL PLASMA PRESSURE IN THE IONOSPHERE OF VENUS

K. L. Miller
W. C. Knudsen (both at: Space Sciences Laboratory, Lockheed Palo Alto Research Laboratory, Palo Alto, CA 94304)
K. Spenner
V. F. Novak (both at: Fraunhofer Institut für Physikalische Messtechnik, Freiburg, West Germany)

The ionospheric thermal plasma pressure on Venus has been derived as a function of altitude and solar zenith angle from median values of electron and ion temperatures and concentration observed by the Pioneer Venus retarding potential analyzer. The pressure as a function of altitude reaches a maximum near 175 km throughout the dayside. On the nightside the altitude of the peak rises to near 250 km at the anti-solar point. Near the sub-solar point the peak thermal plasma pressure is approximately 5 x 10^{-8} dyne cm^{-2}. The thermal plasma pressure is typically balanced at the ionopause by the pressure of an external magnetic field. We anticipate that when the external magnetic-field pressure exceeds the peak thermal plasma pressure, the balance requires an increased magnetic field within the ionosphere. The peak thermal plasma pressure at the sub-solar point corresponds to a magnetic field of 110 γ. The thermal plasma pressure is observed to decrease from the subsolar point to approximately 150 deg solar zenith angle, with the largest gradient near the terminator. The pressure gradient is in a direction to cause flow of ionization in an anti-sunward direction and thus contribute to the maintenance of the nightside ionosphere. However, pressure gradients are found to be insufficient to generate the high ion velocities observed by the RPA.

P 7

CHARACTERISTICS OF THE STEADY MAGNETIC FIELD OBSERVED IN THE VENUS DAYSIDE IONOSPHERE

J.A. Slavin
J.G. Luhmann
R.C. Elphic
C.T. Russell (all at: Institute of Geophysics and Planetary Physics, University of California, Los Angeles, CA 90024)
J.D. Mihalov
J.H. Wolfe (both at: NASA Ames Research Center, Moffett Field, CA 94035)

Analyses of the "DC" component of the magnetic field observed near periapsis (150-180 km altitude) by the Pioneer Venus Orbiter magnetometer suggest that the strength of the dayside ionospheric field is related to solar wind dynamic pressure (ρv^2). Practically no steady magnetic field is found when ρv^2 is less than about 3×10^{-8} dynes cm^{-2}. When the pressure exceeds the aforementioned value, the magnitude of the steady field is proportional to the dynamic pressure. Maximum values of the DC field of $\sim 100\gamma$ are seen when ρv^2 is $\sim 8 \times 10^{-8}$ dynes cm^{-2}. Ionopause field strengths are similarly correlated with the value of ρv^2, while ionopause altitudes are inversely correlated with this quantity. On occasion, the direction of the steady field appears to be related to the direction of the field at the ionopause, further emphasizing the intimate connection between the solar wind and the Venus ionosphere.

P 8

SUPRATHERMAL ELECTRON ENERGY DISTRIBUTION WITHIN THE DAYSIDE VENUS IONOSPHERE

W. C. Knudsen
K. L. Miller (both at: Space Sciences Laboratory, Lockheed Palo Alto Research Laboratory, Palo Alto, CA 94304)
K. Spenner
V. F. Novak (both at: Fraunhofer Institut Für Physikalische Messtechnik, Freiburg, West Germany)
P. F. Michelson (Department of Physics, Stanford University, Stanford, CA 94305)
R. C. Whitten (NASA Ames Research Center, Moffet Field, CA 94035)

The suprathermal electron energy distribution has been derived for the dayside ionosphere from data returned by the Pioneer-Venus orbiter retarding potential analyzer. The shape and magnitude of the spectrum are consistent with solar EUV being the only significant production source within the ionosphere. The magnitude of the spectrum and its variation with altitude suggest that significant vertical transport is occurring with electrons being lost upward through the ionopause. The heat input to the thermal electron gas from the measured suprathermal electron flux fails by a factor of 5 or more to supply the heat needed to maintain the observed thermal electron temperature profile when the field-free (parallel to the magnetic field) electron conductivity is assumed.

P 9

PIONEER VENUS ORBITER MAGNETOMETER OBSERVATIONS: STRUCTURE AND CHARACTERISTICS OF THE VENUS IONOPAUSE

R.C. Elphic
C.T. Russell
J.G. Luhmann (all at: Institute of Geophysics and Planetary Physics, University of California, Los Angeles, CA 90024)
L.H. Brace (Laboratory for Planetary Atmospheres NASA/Goddard Space Flight Center, Greenbelt, MD 20771)

The dayside Venus ionopause is usually observed as the interface between the low β (ratio of plasma thermal to magnetic pressure) magnetosheath, and the high β ionosphere. The currents which flow on the ionopause are generally such as to exclude the highly compressed solar wind magnetic field from the Venus ionosphere. Inferred characteristic total thicknesses of the dayside ionopause current sheet are of order 50 ± 25 km, several thermal ion gyroradii. Typical current densities at the ionopause are of order 10^{-8} amps/m^2, roughly an order of magnitude larger than current densities at the terrestrial magnetopause.

Multiple ionopause crossings suggest the presence of waves on the boundary, with peak-to-peak amplitudes of 60-200 km, and periods (in the moving spacecraft frame) of 50-120 sec. Generally, the ionopause appears to have the structure of a tangential discontinuity, with the magnetosheath field lines draped across the dayside ionosphere. However, magnetic signatures sometimes suggest highly turbulent conditions at the boundary.

P 10

STUDY OF NIGHTSIDE VENUSIAN ELECTRON TEMPERATURES

W. R. Hoegy
L. H. Brace
R. F. Theis (all at NASA/Goddard Space Flight Center, Laboratory for Planetary Atmospheres, Greenbelt, MD 20771)

Electron temperatures in the nightside Venus Ionosphere are studied by comparing two dimensional solutions of the heat conduction equation with an empirical model of the electron temperature based on Pioneer Venus measurements. The theoretical and empirical models are confined to a narrow latitude band at low latitudes. The energy calculation includes solar EUV heating at the terminator, electron cooling to ions and neutrals, and heat conduction within the ionospheric plasma. Heating at the ionopause by the shocked solar wind is included through an upper boundary condition. Several simple, uniform magnetic field models are found to be inconsistent with the empirical temperature structure. An optimum magnetic field for the equatorial region is derived by solving for the heat flux directions which force energy conservation while constrained by the observed temperatures within the range of 80^o to 180^o SZA and 160 km to 700 km. The resulting heat flux vectors suggest a magnetic field that connects the lower nightside ionosphere (less than 300 km) to the dayside ionosphere and connects the upper ionosphere (greater than 300 km) to the ionosheath. Thus, the lower ionosphere is heated through conduction of heat from the dayside and the upper ionosphere is heated by the solar wind in the ionosheath, with heat flowing downward and from the nightside to the dayside. The suggested magnetic field appears to be consistent with the magnetic field directions observed by the Pioneer Venus magnetometer.

P 11

THE ONSET AND DEVELOPMENT OF KELVIN-HELMHOLTZ INSTABILITY AT THE VENUS IONOPAUSE

R. S. Wolff
B. E. Goldstein
C. M. Yeates (all at: Jet Propulsion Laboratory, California Institute of Technology, Pasadena, CA 91103)

We investigate the Kelvin-Helmholtz instability at the Venus ionopause resulting from the flow of the (shocked) solar wind tangential to the ionopause for the case where the interplanetary magnetic field is oriented normal to the direction of flow. It is found that gravity stabilizes the long wavelength perturbations and the finite thickness of the boundary layer stabilizes short wavelength modes. The magnetic viscosity due to finite Larmor radius effects either destabilizes the boundary or stabilizes it according to whether the solar wind electric field points away from or towards the ionosphere. For solar wind and ionosphere plasma parameters consistent with Pioneer Venus observations we find that the instabilities with the greatest growth rates (shortest growth times) have wavelengths of 50-150 km and growth times of 0.5 to several seconds. In addition, we show how distortion of the ionopause by Kelvin-Helmholtz instability can lead to the formation of magnetic "flux ropes" inside the ionosphere as well as ionospheric "bubbles" embedded in the solar wind.

P 12

COMPOSITION OF THE VENUS LOWER ATMOSPHERE FROM THE PIONEER VENUS MASS SPECTROMETER

R. R. Hodges, Jr. (The University of Texas at Dallas, P. O. Box 688, Richardson, Tx 75080)
J. H. Hoffman (The University of Texas at Dallas P.O. Box 688, Richardson, Tx 75080)

Data from the Pioneer Venus Sounder Probe Neutral Mass Spectrometer confirm that the major constituents of the lower atmosphere of Venus are CO_2 and N_2, with the latter having a mass abundance of about 3%. The data allow the order of up to 1000 ppm of water vapor, and 500 ppm of SO_2 and COS below the clouds, but lower bounds for the abundances of these compounds cannot be established because they appeared in large amounts as lingering products of the reaction of cloud droplets deposited on the gas inlet leak to the mass spectrometer. The presence of several minor constituents on Venus is more certain. Of particular significance is the discovery that there is a hundred-fold excess of nonradiogenic argon and neon on Venus over terrestrial abundances in addition to a small deficit of radiogenic ^{40}Ar. The isotopic ratios of carbon, oxygen, and nonradiogenic argon are similar to these on earth. Other minor constituents detected on Venus include helium and ethane, and there is strong but presently inconclusive, evidence of H_2S. Through laboratory simulation it has been shown that the measured pattern of volatile release during the evaporation of cloud materials blocking the inlet leak correspond to the volatiles produced when a leak is coated with an 85% concentration solution of H_2SO_4 and immersed in a Venus atmosphere simulator.

P 13

VENUS THERMOSPHERE: DIURNAL VARIATION OF THE NEUTRAL GAS COMPOSITION AND KINETIC TEMPERATURE

H. B. Niemann
W. T. Kasprzak
A. E. Hedin
N. W. Spencer (all at NASA/Goddard Space Flight Center, Laboratory for Planetary Atmospheres, Greenbelt, MD 20771)

In situ measurements are being made of the neutral gas composition in the thermosphere of Venus with the Pioneer Venus Orbiter Neutral Mass Spectrometer (ONMS). Number densities of the major constituents CO_2, CO, N_2, O, N, and He are obtained once per earth day at approximately 140 km to 250 km altitude near 18° north latitude for two diurnal cycles. Atomic oxygen is the major constituent above 155 km on the dayside, and also on the nightside up to 180 km where helium becomes the major constituent. Average day and night densities of CO_2, CO, N_2, O, and N remain nearly constant but the magnitude changes abruptly at the terminator from high dayside values to low nightside values. Helium varies in the opposite way and a bulge is observed on the nightside near the morning terminator. Turbulence on the nightside is indicated by large orbit to orbit variations in the observed densities. Results obtained during the first and second diurnal cycles are in agreement to about 20%. Changes are noted however in detail on the shape of the helium bulge and the orbit to orbit variation. Kinetic temperatures inferred from scale heights are 295 K at local noon and 110 K at local midnight. Similar to the density variations, the average temperature values remain relatively constant during day and night but change abruptly at the terminator.

P 14

EDDY MIXING IN THE VENUS THERMOSPHERE

U. von Zahn
K. H. Fricke (both at: Physikalisches Institut, Universität Bonn, 5300 Bonn 1, W.-Germany)
D. Krankowsky (Max-Planck-Institut für Kernphysik, 6900 Heidelberg, W.-Germany)

The composition of the dayside Venus thermosphere, as measured by the neutral gas mass spectrometer on board the Multiprobe Bus of the Pioneer Venus Mission, can be well described by assuming a vertical eddy coefficient $K = 2 \times 10^{13} \cdot n^{-1/2}$ $cm^2 s^{-1}$, where n is the total number density in cm^{-3}. Comparisons will be made with pre-Pioneer Venus and with other Pioneer Venus determinations of K in the Venus atmosphere, as well as with measurements of K in the homopause regions of Earth and Mars. The consequences of the assumed K dependence on number density and of those K profiles used in pre-Pioneer Venus model calculations will be discussed with respect to the Venus exospheric H abundance, the thermospheric O abundance, and the tropospheric He abundance. Implications of the assumed strength of vertical mixing on the energy balance of the Venus upper atmosphere will be commented upon.

P 15

RESPONSE OF VENUS' THERMOSPHERE TO CHANGES IN SOLAR FLUX

M.A. LeCompte (Laboratory for Atmospheric and Space Physics and Department of Astro-Geophysics, University of Colorado, Boulder, CO 80309)
(Sponsor: A.I.F. Stewart)

The Pioneer Venus Orbiter Ultraviolet Spectrometer has measured limb intensity profiles at 2890 A (the CO_2^+ UV doublet) and 2160 A (the (0,1) Cameron band of CO), obtaining the topside scale height and the zenith column emission rate adjusted to the subsolar point. The latter quantity is closely related to the solar ionizing flux, and correlates well with the solar 10.7-cm flux when adjusted for the differing solar longitudes of Venus and Earth. No large variations in the topside scale height are seen, suggesting that Venus is similar to Mars in that T_∞ is not sensitive to the solar EUV flux, but is unlike Mars in that there are no other sources of significant shortterm variations in T_∞. The airglow intensities will also be compared with ionospheric electron densities.

P 16

EMPIRICAL MODEL OF THE NEUTRAL TEMPERATURE AND COMPOSITION OF THE VENUS THERMOSPHERE

A. E. Hedin
W. T. Kasprzak
H. B. Niemann (all at NASA/Goddard Space Flight Center, Laboratory for Planetary Atmospheres, Greenbelt, MD 20771)
A. Seiff (NASA/Ames Research Center, Moffett Field, CA 94035)

Direct measurements of neutral CO_2, O, CO, N_2, He, and N densities from the Pioneer Venus Orbiter Neutral Mass Spectrometer (ONMS) are described in terms of a spherical harmonic representation (latitude and local time coordinates) of exospheric temperature and 150 km densities using Bates temperature profiles. Terms up to the fifth harmonic are required to fit the rapid density variations at the terminator, unlike the earth's thermosphere where three harmonics are sufficient. A global average temperature of 200°K is derived with a final harmonic variation of 54%, which is three times larger than the variation in the earth's thermosphere. The temperatures are basically determined from the altitude variations of oxygen and are accurate to no more than ± 10%. The altitude profiles are extended downward to 100 km using empirical formula to provide a transition through the turbopause region.

Planetary Tectonics

Metropolitan Centre
Monday A.M.
W. Quaide (NASA Headquarters), Presiding

P 17 INVITED PAPER

THE VENUS CRUST FROM PIONEER RADAR

Harold Masursky, Branch of Astrogeologic Studies (U.S. Geological Survey, Flagstaff, AZ 86001)

Altimetry and image data, obtained by Pioneer Venus and Earth-based radars, have provided a first look at the global hypsometry, regional morphology, surface roughness characteristics of Venus from which a preliminary interpretation of planetary crustal history can be made. The distinctly unimodal distribution of relief (20% "lowlands", 70% "upland plains", and 10% "highlands") may indicate that most of the planet's ancient crustal material is preserved in the upland plains province where Venera 8 landed and reported a "granitic" composition. Circular features that may be impact craters are common on this terrain unit. The highlands, Ishtar Terra and Aphrodite Terra, stand 11 and 8 km above mean planetary radius (6051.4 km). From analysis of the gravity and altimetry data, they may represent continental regions whose mass is about 80% compensated due to crustal thickening beneath these features by 1) underplating of silicic rocks by mantle convection, 2) local differentiation associated with mantle plumes that balance the composition and thickness of the crust, or 3) continental growth by plate tectonic processes or alternatively lateral crust and mantle variations. There is no global array of mid-basin ridges, indicative of global plate tectonism nor subduction troughs marginal to the continents. Complex ridge and trough regions that lie east of the two terrae, the radiating ridges near Beta and the marginal mountains of Ishtar may be the result of local crustal motions.

The lowlands may be due to filling of depressions (where the crust is thinner) like the basins and lowlands on the Moon, Mars and the Earth. Veneras 9 and 10 landed east of Beta and reported basaltic composition for these rocks.

P 18 INVITED PAPER

TERRESTRIAL CRATERING STUDIES: APPLICATION TO HISTORIES OF PLANETARY EVOLUTION

M. R. Dence (Earth Physics Branch, Energy, Mines and Resources, Ottawa, Canada, K1A 0Y3)
R. A. F. Grieve (Earth Physics Branch, Energy, Mines and Resources)

The accessibility and geological control afforded by terrestrial impact craters, of which ~80 with $1 < D > 140$ km are currently recognized, provide information not available from other planetary bodies on cratering processes and their influence on crustal evolution. Structural studies of craters in different media indicate the great complexity of mass motions during the later stages of cavity formation and ejecta deposition. Central peak formation is seen as a function of the weakening of target materials during initial shock-induced movements, the strength of the target rocks under those conditions and the extent to which the structure attains equilibrium. Multiple rings result from successive vertical oscillations converging towards this equilibrium position. A modified proportional growth model is favoured for estimating the depth of the primary excavation. These conclusions indicate that, although volumetrically rare, some ejecta from multi-ring basins derived from original depths of ~60 km, and may be present in returned lunar highland samples. The failure of shock waves to reset isotopic systems in > 90% of material excavated casts doubts on models which ascribe the 3.9 ± 0.1 by peak in lunar highland ages to the formation of specific large basins. A Phanerozoic terrestrial cratering rate of $0.35 \pm 0.13 \times 10^{-14}$ km^{-2} yr^{-1} for D > 20 km, when combined with lunar data, indicates the asteroidal flux in the inner solar system has been constant within a factor of 2 over the last ~3.0 b.y. The combined cratering rate curve can be used as a time scale to assign an approximate age to the development of major tectonic features on other planets.

P 19 INVITED PAPER

PLATE TECTONICS AND MANTLE CONVECTION

E.R. Kanasewich (Department of Physics, University of Alberta, Edmonton, Alberta, Canada T6G 2J1)

Paleomagnetic observations, oceanic magnetic lineations and the present continental margins are used in a computer algorithm to reconstruct maps for seven periods throughout the Phanerozoic Era. Geologic evidence is used to reconstruct major plate boundaries. The results suggest the presence of a slowly evolving mantle-wide convection system which is symmetric about the earth's spin axis. The dominant pattern during the early Paleozoic and Cenozoic Eras may be described in terms of spherical harmonics of the third order. The earth's present gravity and non dipole magnetic field is examined for evidence of this pattern. Of particular use are special map projections such as the Eckart and azimuthal-equidistant ones with the major oceanic plate determining the orientation of a pseudo-equator.

P 20

DO DEEP MOONQUAKES REPRESENT SHEAR FRACTURES?

Junji Koyama (Galveston Geophysics Laboratory, Marine Science Institute, The University of Texas, Galveston, Texas 77550 and Geophysical Institute, Tohoku University, Sendai 980, Japan)
Yosio Nakamura (Galveston Geophysics Laboratory, Marine Science Institute, The University of Texas, Galveston, Texas 77550)

S-wave particle motions of deep moonquake signals observed at the Apollo lunar seismic stations have been analyzed to test a hypothesis that deep moonquakes represent shear fractures. Observations of S-wave polarization angles at three stations are just enough to determine the orientation of a double-couple force system, representing a shear fracture, at each moonquake focus. Focal mechanism solutions thus obtained for category A_1 moonquakes are in agreement with our earlier results based on relative amplitudes of P and S waves. The nearly horizontal fault plane we found by these analyses also coincides with the plane of the computed maximum tidal shear stress in the A_1 focal region. The polarization angles of S-waves vary with the tidal phase of the moon. This variation is also consistent with that of amplitude ratios of P- and S-wave envelopes. These analyses suggest that deep moonquakes represent shear fractures controlled not by tectonic stresses but by tidally induced shear stresses in the lunar interior.

P 21 INVITED PAPER

MARTIAN SURFACE TECTONIC FEATURES AND THE STATE OF STRESS IN THE INTERIOR

R. S. Saunders (JPL, Caltech, Pasadena, CA 91102)
R. J. Phillips (Lunar & Planetary Institute, Houston, TX 77058)

Tectonic features on Mars have been mapped globally using Viking and Mariner 9 pictures. These features include graben and other fractures and faults, which are generally taken to represent extension, and wrinkle ridges, which are taken to represent compression.

Gravity and topography information are used to model stress conditions in the martian interior. The two types of models that are used to examine stress trajectories that might result in structural deformation at the surface are a flexural model and a two-element isostatic model (Sleep and Phillips, GRL, 1979). Since these two models yield different stress patterns we use the photogeologic mapping of structures to test the competing models. The flexural model is more consistent with the observed structural patterns.

We would conclude that most of the structural features associated with Tharsis are a result of loading, not expansion or doming, thus extensional tectonics is not a strong constraint on the thermal history and the real problem is to understand the origin of the Tharsis load. The model yields both extensional and compressional features. We speculate that the oldest fractures may be associated with uplift or doming but that the majority of fracturing and all ridges result from relaxation of the Tharsis load.

P 22 INVITED PAPER

FRACTIONAL MELTING, DENSITY DISTRIBUTION AND MANTLE CONVECTION BENEATH THE THARSIS PLATEAU, MARS

A. A. Finnerty
R. J. Phillips (both at: Jet Propulsion Lab, Caltech, Pasadena, CA 91103)

The existence of a large volcanic pile in the Tharsis region of Mars, over thick lithosphere where there is no evidence of plate tectonics, raises the possibility that extreme igneous fractionation during partial melting of a single source region in the martian mantle may have taken place. Regardless of the model mantle composition, the liquid formed by partial melting will be enriched in Fe over the residual crystals. Because of extraction of Fe, the residuum will be less dense than the parent rock. For example, 10% to 20% partial melting of garnet lherzolite yields a residuum that is 0.05 to 0.10 gm cm^{-3} less dense than the parent for terrestrial compositions (Jordan, 1979). The density contrast is increased for larger degrees of partial melting and for more Fe-rich parent compositions.

If gravity and topography data for Tharsis are fit to an isostatic model, a mantle density con-

trast of more than 0.1 gm cm^{-3} is required if mean lithospheric thickness is less than 450 km (Sleep and Phillips, 1979). These authors note that temperature contrasts alone are not sufficient to cause this density contrast, and suggest that it is caused by chemical differences.

The density calculations of Jordan (1979) support this hypothesis. We further suggest that if the low-density region in the mantle beneath Tharsis exists and is due to fractional melting, large-scale convection in the upper mantle beneath Tharsis cannot have taken place since the cessation of volcanism, otherwise the density contrast would have been annihilated by mixing. If older volcanic flows have not been covered by younger flows or by wind-borne dust, high spatial resolution spectral scanning may reveal variations of Fe/Mg and Ti/Mg in Tharsis, supporting our hypothesis.

Venus, Comets, Jupiter and Saturn

Harbour A
Monday P.M.
J. Pollack (Ames Research Center), Presiding

P 23

THE NIGHT AIRGLOW OF VENUS: CONSTRAINTS ON THERMOSPHERIC CIRCULATION

S.W. Bougher (Laboratory for Atmospheric and Space Physics and Department of Astro-Geophysics, University of Colorado, Boulder, CO 80309)
(Sponsor: A.I.F. Stewart)

The transport of atoms of N and O from the dayside to the nightside thermosphere produces a chemiluminscent night airglow consisting of the γ and δ bands of nitric oxide. The zenith intensity of this glow depends only on the vertical flux of N atoms, and the altitude of the emitting layer depends on the vertical flux of O atoms and on the strength of vertical eddy mixing. The morphology of the airglow, as shown in images obtained by the Pioneer Venus Orbiter Ultraviolet Spectrometer, therefore reflects both the high altitude supply of atoms from the dayside and their transport through the lower thermosphere. Present results indicate downward fluxes of 10^{10} N atoms and 10^{12} O atoms $cm^{-2}sec^{-1}$, averaged over the dark hemisphere, and large values of K comparable to those found in the dayside. Analyses of the location and size of bright nightglow patches will be presented. Inferences drawn from the nightglow measurements will be compared with independent sources of information on nightside conditions, including mass spectrometer measurements of N and O, IR brightness temperatures near 100 km, and Venera measurements of the near-UV nightglow.

P 24

THE CONFIGURATION OF THE VENUS BOW SHOCK

R. F. Theis
L. H. Brace
K. H. Schatten (all at: NASA/Goddard Space Flight Center, Laboratory for Planetary Atmospheres, Greenbelt, MD 20771)

Over 400 bow shock crossings measured from December 1978 to December 1979 by the Orbiter Electron Temperature Probe (OETP) on Pioneer Venus have been used to form a simple empirical model of the bow shock. The formula which is referred to as an "Archimedian Hyperboloid" is as follows:

$$\rho = C_1/(\pi-\psi-C_2) - C_1\psi/(\pi-C_2)^2,$$

where ρ = distance from planetary center in Venus radii (R_V), ψ = solar zenith angle in radians (corrected by a 5^o abberation), C_1 = 4.22 ± .05, and C_2=0.26 ± .01. The constants C_1 and C_2 are determined by a least squares fit where the perpendicular distance to the surface is minimized. This functional form leads to an average standoff distance of 0.46 ± .03 R_V from the planet's surface, and an asymptotic cone angle of 14.8^o ± 0.7^o. Using an average ionopause altitude of .06 R_V and assuming this to be the effective obstacle to the solar wind flow, the nose of the Venus shock extends 0.4 R_V above this level. Since this value is consistent with the other terrestrial planets, this suggests that there is very little solar wind absorption by the atmosphere on the average. The Archimedian Hyperboloid fit was chosen, as opposed to the more usual ellipsoidal form, because of the theoretical need for an asymptotic cone angle consistent with shock theory. This form is consistent with the Spreiter and Stahara (1980) single fluid MHD model of the bow shock around a non-magnetic planet. This form may be fitted to a typical calculated bow shock with a deviation of ~.03 R_V.

P 25

BOW SHOCK ACCELERATED PROTONS AND THE MAGNETIC FLUX ROPES OF VENUS

S. A. Curtis
W. R. Hoegy (both at NASA/Goddard Space Flight Center, Laboratory for Planetary Atmospheres, Greenbelt, MD 20771)

A mechanism for the generation of the Venus flux ropes is developed using the free energy of the MHD collisionless shock at Venus and the intermittent penetration of the interplanetary field lines into the Venus ionosphere. The penetrating field lines provide a linkage between the shock associated current system and the ionosphere. Specifically, the field lines act as a conduit by which the high energy component of the post-shock protons can enter into the ionosphere. The post-shock proton distribution function is assumed similar to that of the earth; a bimodal distribution with the high energy component aligned in the magnetic field direction. This is believed to be the characteristic form of distribution for a quasi-perpendicular shock geometry (Greenstadt and Fredericks, 1979). The helical structure of the flux ropes can then be generated by a combination of the magnetic field of the field-aligned high energy proton current and associated plasma waves moving along the penetrating interplanetary magnetic field which composes the axial component of the flux rope. Specific plasma instabilities that contribute to the helical structure are discussed and comparisons with published magnetic flux rope observations (Russell and Elphic, 1979) are made.

P 26

MAGNETIC FIELDS RELATED TO ION-NEUTRAL COUPLING IN THE ATMOSPHERES OF UNMAGNETIZED PLANETS

J.G. Luhmann
R.C. Elphic (both at: Institute of Geophysics and Planetary Physics, University of California, Los Angeles, CA 90024)

The magnetic fields produced by the terrestrial ionosphere current systems that are driven by neutral atmosphere motions have been analyzed in great detail. Analogous effects can occur in the atmospheres of unmagnetized planets if even a small "external" field is applied, for example, by solar-wind field penetration. The magnitudes of the atmospheric dynamo fields at Venus are estimated and compared with the fields observed by the Pioneer Venus Orbiter magnetometer.

P 27

COMPOSITION OF THE ULTRAVIOLET COMA OF COMET BRADFIELD (1979ℓ)

P. D. Feldman and H. A. Weaver (Physics Dept., The Johns Hopkins Univ., Baltimore, Md. 21218)
M. C. Festou (Space Physics Res. Lab., Univ. of Michigan, Ann Arbor, Mi. 28190)

Observations of the ultraviolet spectrum of Comet Bradfield (1979ℓ) were made in January and February 1980 with the International Ultraviolet Explorer. The heliocentric distance of the comet varied from 0.71 a.u. to 1.36 a.u. The evaporation of water from the cometary nucleus could be studied in detail as all three dissociation products, H, OH and O, were observed simultaneously and the dust/gas ratio of the comet was extremely low. Preliminary analysis of the data with the aid of a Haser model indicates that the water production rate decreases with heliocentric distance considerably faster than r^{-2}. The spatial imaging capability of IUE gave resolution of ~1000 km when the comet was 0.2 a.u. from the Earth, and was used to identify CS as a parent molecule evaporated from the nucleus. The production rate of CS relative to water is $\approx 5 \times 10^{-4}$ at 0.71 a.u. C(^{1}D) atoms, identified by the CIλ1931 line, appear to be produced by reactions in the coma, probably dissociative recombination of CO^+ even though the CO^+ abundance is rather low.

P 28

HYDROGEN PRODUCTION RATES FROM GROUND-BASED FABRY-PEROT OBSERVATIONS OF COMET KOHOUTEK

F. Scherb (Dept. of Physics, University of Wisconsin, Madison, Wis. 53706)
F. L. Roesler (Dept. of Physics, University of Wisconsin, Madison, Wis. 53706)

The only ground-based observations of a cometary hydrogen corona that have been obtained up to the present were carried out during the apparition of Comet Kohoutek (1973f). Hydrogen Balmer α (Hα) emission from the gas cloud surrounding the comet was detected using a Fabry-Perot spectrometer at Kitt Peak National Observatory. We have re-examined these observations using (1) new solar full-disk Lyman β emission line profiles obtained recently, (2) a new calibration of the absolute sensitivity of the Fabry-Perot spectrometer, and (3) corrections for atmospheric extinction instead of the geocoronal Hα comparison method used previously to obtain absolute comet Hα intensities. The new values for cometary hydrogen production rates are in good agreement with results obtained from Lyman α observations of Comet Kohoutek.

P 29

A CRYOGENIC TECHNIQUE FOR COLLECTING A SAMPLE ON A COMETARY RENDEZVOUS MISSION

T.E. Economou (E. Fermi Institute, University of Chicago, Chicago, IL 60637), A.L. Turkevich, R.J. Szara, E. Franzgrote

An important scientific objective on a cometary mission is to obtain a complete chemical analysis of the comet. It is proposed to do this by collecting on board the spacecraft an unfractionated sample of the coma material (both dust & volatiles). This can be achieved by exposing a large area (~0.2 m^2) of a thin film of solid xenon at ~65°K to the cometary flux. A cold surface should be an efficient trap for volatiles. Laboratory studies have shown that properly prepared xenon film can collect dust particles of velocities expected in a cometary coma (30-200 m/sec) with an efficiency comparable to that of oil film. Typical mission profiles for a Tempel-2 rendezvous suggest that a one day collection period would provide samples of many mg.

After collection, the xenon on board the spacecraft would be heated in a closed system to vaporize volatile components (H_2O,CO_2,etc.), and then the entrained particles concentrated by deposition on a small area impactor plate. This sample then would be available to on-board instruments such as an Alpha Particle Instrument with α, p and x-ray modes that could identify and determine more than 99% of the atoms. The volatiles could either be condensed and analysed by pressure-temperature relations or analysed chromatographically. The volatile sample would be large enough to determine important isotopic ratios such as D/H, $^{13}C/^{12}C$, $^{18}O/^{16}O$, as well as minor constituents with a mass spectrometer.

Such a collection scheme thus would "put a comet back together" while at the same time minimizing the hazards to sensitive surfaces on the spacecraft.

P 30

THE PRODUCTION OF TYPE 1 TAIL RAYS

David B. Beard (University of Kansas, Lawrence, Kansas 66045)

Of the three competing ionization processes in cometary atmospheres only one, ionization by fast electron impact, can generate the observed physical properties of Type 1 comet tails. Photoionization by solar ultraviolet radiation is a relatively negligible contribution because of low photoionization cross-

sections for the amount of incident ultraviolet radiation. Charge transfer from solar wind protons is a major cause of cushioning the solar wind in the comet atmosphere but cannot produce tail rays because charge transfer, in common with photoionization, cannot produce the observed high concentration of cometary ions nor provide them with their large kinetic energies. Fast electrons will produce a high density of cometary ions and will energize them to kinetic energies of many tens of electron volts required by the observed growth rate of the waves. The fast electrons required will occur at observed discontinuity surfaces in the solar wind and the random occurrence of the discontinuties explain why the production of Type 1 tail rays is sporadic in nature. The discontinuities can result in a fast shock structure in the cometary atmosphere which produces the energetic electrons. Electron ionization is very efficient due to the high mobility of the electrons and the tail rays are of smaller diameter, as observed, than is possible by any competing process.

P 31

STUDY OF THE JOVIAN UPPER ATMOSPHERE BY A VOYAGER 2 ULTRAVIOLET STELLAR OCCULTATION EXPERIMENT

M. C. Festou, S. K. Atreya, and T. M. Donahue (Atmospheric & Oceanic Science, University of Michigan, Ann Arbor, MI 48109)
D. E. Shemansky, B. R. Sandel, A. L. Broadfoot (Space Sciences Institute, University of Southern California, Tucson, AZ 85713)

On July 9, 1979, the B7 star α-Leo was occulted by Jupiter as viewed from the Voyager 2 spacecraft at a distance of 1.51×10^6 km from Jupiter. The ultraviolet spectrometer on Voyager followed the star during occultation and recorded its spectrum in the range 51.3nm - 169nm with a resolution of 0.9nm. Data were obtained during ingress and egress. Absorption profiles for molecular hydrogen were obtained over an altitude range of 500 km and extinction by various hydrocarbon species over an altitude interval of 50 km. These data permit a determination of the altitude of the homopause and the temperature distribution above the homopause.

P 32

CONFIGURATION OF THE CURRENT SHEET IN JUPITER'S MAGNETIC TAIL

K. W. Behannon
L. F. Burlaga
R. P. Lepping
N. F. Ness (all at: NASA/Goddard Space Flight Center, Laboratory for Extraterrestrial Physics, Greenbelt, Maryland 20771)

Magnetic field observations by Voyager 1 and 2 of the current sheet in the Jovian magnetotail are consistent with a disk-like structure near the planet connecting smoothly to an extended sheet in the distant tail. Well-defined sheet crossings were observed approximately every 5 or 10 hours by Voyager 2 outbound over a Jovicentric radial distance range of ~20 R_J to ~175 R_J. In the majority of cases, multiple crossings consisting of 3 or 5 traversals were observed. Minimum variance analyis (MVA) of Voyager 2 crossings produced a total of 51 cases (out of 54) with eigenvalues sufficiently well-separated so that reliable estimates of sheet normal components could be obtained. In 18 of the crossing cases (35%), the sheet was consistent with being a rotational discontinuity. In the remaining 33 cases (65%), the sheet was consistent with being either a rotational discontinuity with a small normal component (relative normal $B_z/\langle|\underline{B}|\rangle < 0.3$) or tangential discontinuity. An average relative normal component of 0.27 was found for all 51 crossings. The normal vectors were found to have a broad distribution in latitude angle, θ_N, probably due in part to torsional or flapping motions of the sheet. The most probable orientation for the normals tended to be more nearly perpendicular than parallel to the solar magnetospheric equatorial plane, as expected. The longitudinal angles, ϕ_N, of the normal vectors were found to be tightly constrained to the cross-tail direction, suggesting little deviation of the down-tail axis of the sheet from the planet-sun line. Comparisons of the Jovian tail current sheet with the dayside sheet and with the earth's magnetotail sheet will also be presented.

P 33

JUPITER'S 10-HOUR MODULATED MAGNETOSHEATH

R. P. Lepping
L. F. Burlaga
L. W. Klein (all at Goddard Space Flight Center, Laboratory for Extraterrestrial Physics, Greenbelt, Maryland 20771)

Large scale magnetic field directional oscillations have been discovered in Voyager 1 and 2 and Pioneer 10 magnetic field data for the periods when the spacecraft were outbound through the magnetosheath of Jupiter. These large scale structures occur with a quasi-period of about 10 hours (or 5 hours occasionally) which is Jupiter's rotational period. The direction changes (mostly north south and of a few minutes to two hours in length) delineating these structures are closely restricted to a plane parallel to Jupiter's local magnetopause, according to a minimum variance analysis of the field for all three spacecraft. Similar directional changes occurred in the inbound magnetosheath for the Voyager spacecraft according to the analysis, but the occurrence was much less frequent. Also the north-south components of the field and plasma velocity are strongly anticorrelated for Voyagers 1 and 2 while they are in the outbound magnetosheath; other components show weak correlations (J. Belcher and H. Bridge, private communication). Some magnetopause and bow shock crossings on Voyager 2 outbound are phase locked with some of these structures. These features may be accounted for in terms of field line draping around the magnetopause of the convected IMF and solar wind, where the modulation is controlled by the motion and shape of the magnetopause, which directly depends on the rotation of the magnetosphere.

P 34

EFFECT OF PARTICLE BOMBARDMENT ON OUTER GALILEAN SATELLITE SURFACES

E. M. Sieveka and R. E. Johnson (Dept. Nuclear Engineering and Engineering Physics, University of Virginia, Charlottesville, Va. 22901)

The ionic and neutral particle environment near the outer Galilean satellites is modeled in order to predict the effects of sputtering and magnetic entrainment on the removal and transport of particles from the satellite surfaces. Over geologic time sputtering due to bombardment by particles trapped in the Jovian magnetosphere may have removed or redistributed large amounts of material from the Galilean satellite surfaces. If neutral, these sputtered particles will follow ballistic trajectories with the possibility of escape for energies over a few eV. If the particle is an ion or is ionized in flight it will become trapped by the corotational magnetic field of Jupiter. It may then return to the surface with an energy related to the relative velocity of satellite and field, or it may be swept free of the parent satellite and become part of the magnetospheric plasma. Of primary interest in this study is the effect of particles returning to the surface on the long term redistribution of satellite surface material.

P 35

IUE OBSERVATIONS OF H Ly α EMISSION FROM SATURN

J. T. Clarke and H. W. Moos (Physics Dept., The Johns Hopkins Univ., Baltimore, Md. 21218)
A. L. Lane (Jet Propulsion Laboratory, Pasadena, Ca. 91103)
(Sponsor: Paul D. Feldman)

A north-south spatial profile of the H Ly α emission from Saturn was obtained on 19 January 1980 using the IUE short wavelength spectrograph. The overall emission brightness was on the order of 1 kR, and a pronounced north-south asymmetry in the emission was observed. Possible interpretations of this asymmetry in regard to the observing geometry will be discussed. Further observations are scheduled for the time of ring-plane crossing on 12 March 1980.

P 36

ENERGETICS OF THE SATURN IONOSPHERE

J. H. Waite, Jr.
S. K. Atreya
T. E. Cravens
A. F. Nagy (all at: Space Physics Research Laboratory, Department of Atmospheric and Oceanic Science, University of Michigan, Ann Arbor, Michigan 48109)

The ion and electron energy equations have been solved for the Saturn ionosphere and coupled to the existing ion composition model reported on earlier by Waite, Atreya and Nagy (1979). The photoelectron heating rate has been carefully determined by means of a two stream calculation in an atmosphere consisting of H_2, He and H. The important electron cooling processes due to vibrational and rotational excitation of H_2 have been re-examined for the Saturn ionosphere for high neutral temperatures. Implications for the Saturn ionospheric structure will be discussed and the possibility of heat sources other than photoelectrons will be considered.

P 37

DOUBLY DIFFERENTIAL CROSS SECTIONS OF SECONDARY ELECTRONS EJECTED FROM H_2 BY ELECTRON IMPACT (25 - 250 eV)

T. W. Shyn
W. E. Sharp (both at: Space Physics Research Laboratory, University of Michigan, Ann Arbor, Michigan 48109)

Hydrogen molecules are a major constituent of the atmosphere of Jupiter and Saturn. Extensive laboratory measurements of doubly differential cross sections of secondary electrons ejected from H_2 by a crossed-beam method is reported. The incident energies used were 25, 40, 60, 100, 150 and 250 eV. The energy and angular range of secondary electrons measured were from one-half of the difference between the incident energy and ionization potential down to 1.0 eV and from 12° to 156°, respectively. Absolute singly differential cross sections and total ionization cross sections have been obtained. Disagreement of the present results with previous measurements by other workers is found, particularly, below 15 eV. Significantly more low energy electrons (up to a factor of 2) are produced than previously thought. The total ionization cross section deduced from these data agree very well with the accepted cross section found from other methods above 40 eV.

P 38

A MODEL OF THE TITAN CLOUDS

O. B. Toon
J. B. Pollack (both at NASA Ames Research Center, Moffett Field, CA 94035)
R. P. Turco (R & D Associates, Marina del Rey, CA 90291)

We have constructed a simple model of the physical processes controlling Titan's clouds. We find that clouds which qualitatively match the present observational constraints can be constructed for a wide variety of model atmospheres including those with low atmospheric pressures (25 mbars) and high atmospheric pressures. We find: high temperatures (160°K) are required through most of the upper several optical depths of cloud; the aerosol mass production level is well above the unit aerosol optical depth level so that the aerosols do not directly affect the photochemistry producing them; the aerosol mass production rate is probably greater than 3.5×10^{-14} gm cm^{-2} sec^{-1}; the particles are probably aspherical but equidimensional; and the eddy diffusion coefficients cannot be as large as 5×10^6 cm^2 sec^{-1} except in the top optical depth of the cloud. We also find: increases in mass input cause a decrease in the mean particle size as required to explain the observed correlation between the solar cycle and Titan's albedo; the sticking coefficient need not be extremely low as has been proposed, but it could be low due to photoelectric charging of the particles; and, the lifetime of particles near the unit optical depth level is a few months as needed to explain the observed temporal variability. Although Titan's aerosols are optically thick in the vertical direction, they are so extended that the horizontal visibility is larger than that found anywhere at the Earth's surface.

Planetary Tectonics
Metropolitan Centre
Monday P.M.
D. Matson (JPL), Presiding

P 39

SEARCH FOR MARTIAN HOT SPOTS

Gregg Vane
Terry Z. Martin (both at: Jet Propulsion Laboratory, Caltech, Pasadena, CA 91103)
(Sponsor: David E. Thompson)

Results will be presented of a thorough search of the Viking orbiter infrared thermal mapper (IRTM) data set for the presence of hot spots on the surface of Mars. The data set consists of surface thermal emission observations in the regions 6.1-8.3um, 8.3-9.8um, 9.8-12.5um, and 17.7-24um. These observations,converted to brightness temperatures, have been subjected to a computer test designed to look for spikes of 10^{0}K or greater, relative to the immediately adjacent data points. IRTM data resolution varies from about 150 km at apoapsis to about 1.5 km at periapsis; sufficient data have been taken since 1976 to cover a considerable fraction of the planet's surface at high resolution. An estimate of the completeness of the search will also be presented.

P 40

ANALYSIS OF PAST IO INFRARED MEASUREMENTS: IMPLICATIONS OF INTERIOR HEAT FLOW

D.L. Matson
G.A. Ransford
T.V. Johnson (all of JPL, Caltech, Pasadena, CA 91103)

We have reexamined the existing ground-based measurements of Io's thermal emission at infrared wavelengths of 8.4 μm, 10.6 μm and 21 μm. We find present in these data the signature of "hot spots", presumably similar to those seen by Voyager. It is possible to extract from these data the total amount of power radiated. Since the "hot spots" are believed to be a result of deep seated activity in Io, and because the remainder of Io's surface is an extraordinarily poor thermal conductor, the power radiated by the "hot spots' is essentially the total heat flow. Our analysis yields a heat flow of $(2 \pm 1) \times 10^{3}$ mW m^{-2} (also erg cm^{-2} sec^{-}) which in the usual heat flow units is (48 ± 24 μcal cm^{-2} sec^{-1}. This value is tremendously large compared to the Earth (1.5 μcal cm^{-2} sec^{-1}) and the Moon (0.5 μcal cm^{-2} sec^{-1}), but is characteristic of active geothermal areas on the Earth. A heat flow value this large rules out a lunar-type model (i.e. a rigid sphere) for the interior of Io.

P 41

TECTONICS ON EUROPA AND GANYMEDE

M.C. Malin (Department of Geology, Arizona State University, Tempe, Arizona 85281)

Voyager spacecraft television observations of Europa and Ganymede show landforms that suggest tectonic processes. On Ganymede, these processes include modification of impact craters and formation of high albedo grooved and ridged terrain. Evidence from crater studies suggests that viscous relaxation plays an important role in producing the observed size-frequency relationships. Size-dependent relaxation is clearly seen in examples where "small" (< 10km diameter) secondary craters are well preserved around "large" (> 150km diameter) primary craters that have undergone significant modification. A few crater-like forms show large domical interior structures--a ring moat and dome morphology suggestive of diapirism. Grooved and ridged terrain develops at the expense of older, darker, more heavily cratered terrain. Little global organization or control is observed; in some areas a concentric pattern of troughs has provided guidance to groove and ridge development. Evidence of the sense of movement (extension, compression, normal) is poor. Alternatives include extension with subsequent intrusion, extension with subsequent effusion, extension with subsequent foundering, in situ foundering, and intrusion controlled rifting with transform faulting. Europa shows a global pattern of "dark" markings. These may be either trough walls and floors showing subtle photometric "shadowing", or trough walls and floors displaying slightly lower albedo. Much narrower linear and accurate ridge forms show local, cuspate variations in plainmetric form. Both compression and extension are apprently at work on Europa.

P 42

FAULT OFFSETS AND PROPOSED PLATE MOTIONS FOR EUROPA

Paul M. Schenk
Carl K. Seyfert (both at: SUNY College at Buffalo, Buffalo, NY 14222)

Voyager II photography has revealed the existence of strike-slip faulting on Europa. The faulting is revealed by the measurable displacement of two earlier fractures across the fault trace, at approx. 168° W, 25° S. A set of sub-parellel 'grooves' are also offset, at approx. 170° W, 23° S. The amount of the fracture offsets and the maximum width of the dark, wedge-shaped feature from which the fault eminates are both 25±3 KM. Here the ice crust has been rifted apart and fault motion has occured along the fragment contacts. This fault opens into a second, dilating fracture that is twice offset by features analogous to transform faults, at 174° W, 22° S, and 176° W, 20° S. Analysis of the motions along the transform faults produced a 'spreading pole' at 175° W, 45° S for the rifting motions.

The above features result from the rotation about the spreading pole of a large ice plate southward from the main crustal shell. A peculiar bright lineament marking the southern boundary of the plate may be the compressional component of this rotation. The lack of rifting nearby and its strike radial to the spreading pole support this suggestion.

We propose that this local rifting, plate rotation and apparent compression defines a Europa-style plate tectonic environment. The localized nature of the rifting suggests that a small but powerful energy source, perhaps a tidally driven, irregular volcanic plume(s), is generating a rising convection pattern beneath the fractured crust. The scalloped ridges seen near the terminator are nearly concentric about the proposed plume location and may be additional compression features.

P 43 INVITED PAPER

MULTIRINGED BASINS: A MANIFESTATION OF THIN LITHOSPHERE TECTONICS

H.J. Melosh (Dept. of Earth and Space Sciences, SUNY Stony Brook, Stony Brook, NY 11794)
W.B. McKinnon (Div. Geol. and Planetary Sci., Caltech, Pasadena, CA 91125)
P. Winkelstein (Dept. of Earth and Space Sciences, SUNY Stony Brook, Stony Brook, NY 11794)

Large impact basins are characterized by one or more concentric mountainous rings. Although some rings form relatively symmetric annular swells, such as the inner rings of Compton, others are asymmetric, with steep inward-facing scarps and gentle outer slopes. It seems plausible that these asymmetric rings are due to normal faulting. The sense of motion on these faults is such as to move crustal rocks radially inward toward the site of the impact crater (which is consequently partly filled), coupled with a rotation such that the basinward side of the scarp is downthrown.

We show that this pattern is a direct consequence of the collapse of a crater when the excavation depth is commensurate with the lithosphere of the planet. Traction on the base of this lithosphere, caused by flow of deeper lying asthenospheric material toward the crater cavity results in radial extensional stress and concentric normal faults--the multiple rings.

The number and spacing of the rings is a function of the crater diameter and lithosphere thickness. When the lithosphere thickness is comparable to the crater diameter, the asthenosphere flow pattern is strongly influenced by the rigid upper layer and only one or a few rings form. When the lithosphere is very thin and weak it cannot influence the flow pattern and is passively fragmented by the inward movement of asthenospheric material. Such a thin lithosphere may account for the large number of rings around the large basins on Callisto. A thicker lithosphere results in more "normal" multiple rings, such as that surrounding the young basin on Ganymede. Multiple rings cannot form around a crater if the lithosphere is too thick.

P 44 INVITED PAPER

WHOLE MANTLE CONVECTION, RADIOGENIC HEATING, AND THE FLATTENING OF THE SEA FLOOR

W.R. Peltier (Dept. of Physics, University of Toronto, Toronto, Ontario, Canada M5S 1A7)
G.T. Jarvis (Dept. of Physics, University of Toronto, Toronto, Ontario, Canada M5S 1A7)

If the oceanic lithosphere is the thermal boundary layer of the large scale convective circulation in the Earth's mantle then its' observed properties are highly diagnostic of the manner in which the convective circulation is driven. In particular, the observed variations of heat flow and bathymetry as functions of ocean floor age place strong constraints on the extent to which the convective circulation could be driven by radiogenic heating from within. Such models fit the observations best when whole mantle convection is assumed. The implications of these results to the problem of the Earth's thermal history will also be discussed.

Planetary Surface and Interior Processes
Queen's Quay
Tuesday A.M.
Norman Evensen (Univ. of Toronto), Presiding

P 45

VIKING LANDER OBSERVATIONS OF RECENT CHANGES IN THE MARTIAN SURFACE

S. D. Wall (Jet Propulsion Laboratory, Pasadena, CA 91103)
K. L. Jones (Planetary Rsearch Inc., Pasadena, CA 91106)
(Sponsor: David Thompson)

The Viking landers have observed the surface of Mars for almost two Martian years since their landings in 1976. Besides their extensive visual, chemical and meteorological characterization of the areas, they have recorded notable changes in the surface. The most catastrophic change occurred at the lander 1 site where two landslide slumps of fine-grained material were seen, one quite recently. The nearer slump to the lander revealed a parallel surface about 1 cm deep, implying that lateral structure exists in the dust dunes. More significantly, the lack of similar features predating the landing implies that surface redistribution is sufficient to cover such events. A second change, seen at both sites is a general increase in albedo and redness of the surface.

At the lander 2 site a white condensate was observed to appear and disappear during both winters over a 250-sol period. The ground became white as temperatures reach CO, saturation point, but the condensate persisted long after temperatures rose to minima of 175 K, suggesting the involvement of small amounts of H_2O. Multispectral and photometric data were acquired and will be compared with temperatures and pressures. Color changes as the condensate disappeared suggest that dust may have been deposited simultaneously.

This abstract presents one phase of research at the California Institute of Technology, Jet Propulsion Laboratory, sponsored by the Mars Data Analysis Program under NASA contract NAS7-100.

P 46

SAPPING PROCESSES IN MARTIAN AND TERRESTRIAL VALLEYS

J.E. Laity (Jet Propulsion Laboratory, Caltech, Pasadena, CA 91103)
(Sponsor: David E. Thompson)

Sapping has been proposed as an important mechanism for valley extension on Mars and in some terrestrial valley systems which exhibit

similar network pattern and morphology. Sapping is a process by which valleys extend headward or slopes retreat owing to the collapse of valley walls following the undermining of basal support. Field work is in progress to investigate operative sapping processes for canyon formation on the Colorado Plateau. Tributary valley systems there are morphologically analogous to martian valley systems based on a similarity of network patterns, amphitheater terminations of first order tributaries, large scale, and evident structural control. Sapping appears at least as important as the local intermittant fluvial erosion in extending and modifying these valleys.

Seepage and sapping along canyon walls operates largely as a mass movement phenomenon, similar to scarp retreat, but may exploit zones of structural weakness such as joints. Large-scale regional joint sets increase the permeability of the sandstones and serve as pipes for laterally flowing groundwater. Water emerges at a seepage point in the cliff face, often at an alcove, and the canyon migrates headward along the joint line as sapping undermines the steep cliff faces and causes collapse of massive sandstone slabs. Canyon cutting along regional joint systems stimulates exfoliation joint development which helps maintain the steepness of the canyon wall. The exploitation of drainage basin area by canyon networks according to orientation and other structural and lithologic controls will be discussed as well as available data to constrain the process on Mars.

P 47

LONGITUDINAL GROOVING IN MARTIAN OUTFLOW CHANNELS

D.E. Thompson (Jet Propulsion Laboratory, Caltech, Pasadena, CA 91103)

Linear fluid instability analysis has been developed to test the growth or decay of longitudinal helicoidal perturbations imposed at the base of fluids of exponentially stratified viscosities. It is assumed that growth of such perturbations can lead to secondary flow patterns at the fluid base in the form of large roller vortices which have the potential of eroding and forming the longitudinal grooving and fluting patterns observed in channel bottoms of major outflow channels on Mars. By assuming an arbitrary but exponentially stratified viscosity profile in the fluid, the propensity for growth of the vortex pattern can be linked to specific types of fluids, and thus particular fluids can be classified according to their ability to erode or carve the observed features under Martian conditions. The particular problem solved identifies the type of fluid necessary to carve the fluting pattern in a region of converging flow in Tiu Vallis, Mars.

Results indicate that in Tiu Vallis, the grooves could be formed most reasonably by vortex motion in a mudflow or debris-laden slurry. The source of the debris flow would be the chaotic collapse terrain just upstream of the observed features. Characteristic velocities of anywhere between 1 cm s^{-1} to 100 m s^{-1} would correspond to Reynolds numbers in the growth range of the vortex perturbations identified on the resulting stability diagram. Similar vortex motion is found to develop in pure water, lava, or even ice, but the actual Reynolds numbers necessary to allow growth of the flow pattern are unreasonable in these fluids according to hydraulic constraints and channel characteristics observed in Tiu Vallis.

P 48

BISTATIC RADAR STUDIES OF MARS

Richard A. Simpson (Center for Radar Astronomy Stanford University, Stanford, CA 94305)
G. Leonard Tyler

Radiowaves (at 0.13 m wavelength) were transmitted from the Viking Orbiters, scattered from the surface of Mars, and received on earth during the 1977-78 opposition. These provide information on the dielectric constant and roughness of the planet's surface at scales of tens of centimeters to about one hundred meters. The oblique geometry for this experiment permitted forward scattering studies of Mars' surface at latitudes well removed from the ±25° band to which earth-based observations are limited. The results show the remainder of Mars' surface to be varied, but apparently within the bounds established for the equatorial region from the earth-based orbservations. The north polar cap, for example, has variable roughness, but a typical value for rms surface tilt lies within the 1-4° range. This suggests that whatever processes form and shape the cap, the structure which remains is similar to that of the smooth rock and soil plains found elsewhere on the planet.

P 49

LACK OF MINERALOGIC CONTROL ON SOLAR WIND IMPLANTED ELEMENTS (SWE) IN LUNAR SOILS

Abhijit Basu (Dept. of Geology, Indiana Univ., Bloomington, IN 47405)

Experiments have shown that SWE retentivity of minerals vary considerably (≤ X100). Therefore, soils with different mineralogic compositions (Mc) can have different concentrations of SWE despite similar irradiation. If so, the use of SWE in determining exposure ages, etc. of lunar soils, meteorites and parent body regoliths should be corrected for Mc of the target. However, because monomineralic rocks are rare and because impacts tend to homogenize regoliths, the effects of differential SWE retention in reality may be less than expected. The total concentration of SWE in any soil is composed of a volume- and a surface-correlated component (Ct=Cv+Cs).Cv is due to preirradiation and cycling, and is nearly independent of in situ irradiation. Cs is, therefore, most sensitive to Mc.

Linear regressions were performed on the size-concentration data of 22 lunar soils for ^{4}He, ^{20}Ne, ^{36}Ar, ^{84}Kr and ^{132}Xe to obtain Cv by the ordinate-intercept method; Cv was accepted only if r > 0.90. Ct being known, Cs was obtained from Cs=Ct-Cv. Mc of these soils (90-150μm fraction) were recalculated on an agglutinate + soil breccia free basis to avoid effects of recycling. Multiple regression analyses and F-tests show that there is no statistically valid correlation between Mc and either Cs or Ct of any of the SWE. This suggests that either (a) the ordinate-intercept method fails even to approximate Cv, or (b) the differentially retained SWE is not only in Cs but is substantially in Cv due to diffusion of SWE into the interior of minerals, or (c) impact homogenization of planetary regolith obscures the effects of differential retention. Available size-concentration data do not appear to support the first two possibilities. Therefore, the current practice of using SWE abundance for estimating exposure ages etc. with complete disregard to the mineralogic compositions of targets is quite valid.

P 50

VERY LARGE TERRESTRIAL CRATER FORMATION RESULTING FROM THE IMPACT OF AN APOLLO ASTEROID*

Jon B. Bryan, Donald E. Burton, and Lloyd A. Lettis Jr.,
(Earth Sciences Division, Lawrence Livermore National
Laboratory, P O Box 808, Livermore, CA 94550)

Recently Alvarez et al. hypothesized that solar obscuration resulting from the impact of an asteroid was responsible for the Cretaceous-Tertiary extinction about 65 million years (my) ago.[1] They estimated that this Apollo object was about 10±3 km in diameter and produced a 175 km diameter crater. Such a crater would be larger than the largest recognized terrestrial craters,[2] at Sudbury, Ontario, Canada (age: 1840±150 my) and Vredefort, South Africa (age: 1970±100 my), each 140 km in diameter.

We are applying the computational approach used in modeling the formation of the Barringer Crater to this large impact.[3] Impact conditions include a mass of 2.1×10^{15} kg and a velocity of 25 km/s, corresponding to a kinetic energy of 6.6×10^{23} J (about 160 teratons). The amount of material injected into the stratosphere by such an impact is of particular interest in the Alvarez hypothesis, and will be modeled, as well as crater formation.

P 51

STAIRCASE ARGON SPECTRA FROM TERRESTRIAL MELT ROCKS

R.J. Bottomley (Walla Walla College Marine Station, Anacortes, WA 98221)
D. York (Dept. of Physics, Univ. of Toronto Toronto, Canada M5S 1A7)

Ideal melt rock from a terrestrial impact crater should be totally reset by the impact, and when dated by 40Ar-39Ar techniques should yield a plateau. Results will be presented from several craters of unknown age in which the spectra do not define plateaux. Samples of melt rock from Strangways crater in Australia and Saaksjarvi crater in Finland show a monotonic increase in age with increasing release temperature. This appears to be the melt rock equivalent of the partial thermal overprinting expected on theoretical grounds in rocks of normal lithology in which only the low temperature sites are completely reset. Although this phenomenon complicates the straightforward application of argon dating to some melt rocks, a maximum age for the cratering event can often be obtained from the datum.

P 52

CONSTRAINTS ON THE COMPOSITION OF MARS

Kenneth A. Goettel, Dept. of Earth and Planetary Sciences and McDonnell Center for the Space Sciences, Washington University, St. Louis, MO 63130

Models for the density distribution within Mars were computed by numerical integration of the equations of hydrostatic equilibrium, using values of 3.933 g/cm^3 for the mean density and 0.365 for the moment of inertia factor of Mars. Cores of composition Ni, Fe, Fe_3O_4, and FeS were considered: corresponding core radii range from 1315 to 1890 km, with core masses ranging from 13 to 26% of the mass of Mars. Calculated central pressures range from 365 to 445 kb. Calculated, zero-pressure densities, corresponding to the range of core compositions considered, range from 3.47 to 3.41 g/cm^3. For a given core composition, the uncertainty in the calculated mantle density is estimated to be about 0.05 g/cm^3.

These revised estimates of the density of the mantle of Mars differ significantly from earlier estimates, and thus necessitate re-examination of models for the composition of the mantle of Mars and models for the bulk composition of Mars. These density results are consistent with Mars being composed of the solar proportions of major, rock-forming elements (Mg, Si, Fe, S, Ca, Al, Na). With this bulk composition, about 30% of the total Fe in Mars is present as FeO in mantle silicates, with the remainder present as Fe metal or FeS in the core. The mantle of Mars appears to be enriched in FeO relative to the terrestrial mantle, but the degree of enrichment is less than previously estimated. Work in progress includes assessment of the implications of these results with respect to the mineralogy and petrology of the Martian mantle and evaluation of other composition models which are consistent with these density results.

P 53

SEISMIC ENERGY RELEASE OF THE MOON

Neal R. Goins (Mobil Research and Development Corp., P.O. Box 900, Dallas, TX 75221)
Anton M. Dainty (Division of Geophysical Sciences, Georgia Institute of Technology, Atlanta, GA 30332)
M. Nafi Toksöz (Department of Earth and Planetary Sciences, M.I.T., Cambridge, MA 02139)

Previous estimates of the seismic energy released by lunar events have not properly accounted for instrument bandwidth, variations in corner frequency, and the effects of the strong near-surface scattering layer. Equations that include the effects of these factors have been developed and applied to the seismograms and displacement amplitude spectra from both near-surface and deep moonquake events. The results are values for M_o (seismic moment), E_S (seismic energy release), E_{yr} (seismic energy released annually by each event class), $\Delta\sigma$ (stress drop), and m_b (equivalent Richter magnitude). Several different approaches are used in deriving the necessary equations including a strong scattering formalism, and the various results are in close agreement. The calculated values indicate that overall lunar energy release is totally dominated by the shallow events ($E_{yr} \sim 2 \times 10^{17}$ ergs/yr for shallow events vs. $E_{yr} \sim 8 \times 10^{13}$ ergs/yr for deep events). In addition, the deep event energy release is easily accounted for by tidal energy dissipation, and the deep event stress drops (largest values ∿ 0.8 bars) are comparable to the calculated tidal stresses. The overall seismic energy release of the moon is about 9 orders of magnitude less than that observed terrestrially. In contrast, the heat flow energy of the two planets is within two orders of magnitude, illustrating that the seismic

characteristics of a planet are controlled more by tectonic state and style than by relative magnitude of driving forces.

P 54

DISTRIBUTION OF K AND Cs BETWEEN IMMISCIBLE LIQUIDS IN THE SYSTEM Fe-S-Si-O TO 45 KB WITH PLANETARY APPLICATION

Wuu-Liang Huang (Lunar & Planetary Institute, Houston, Texas 77058)
(Sponsor: Richard J. Williams)

The melting relations and distribution of K and Cs in portion of the system has been determined at high pressures. In contrast with the phase relations at 1 atm, ferrosilite is stable as a primary phase at high pressures, because of the incongruent melting of ferrosilite to quartz plus liquid, and the boundary between the one- and two- liquid fields on the join $Fe_{1-x}O$-FeS-SiO_2 shifts away from silica with increasing pressures. If the effect of pressure on the composition of immiscible liquids can be extrapolated to the pressure at the mantle -core, a dense, immiscible Fe-S-O liquid sinking through a silicate mantle should not carry appreciable amounts of silicon with it. The significance of K to the thermal history of the outer core has been widely recognized. In the present study, K has been found to have limited solubility in metal sulfide liquids at pressures up to 45 kb. The speculation (Carmichael & Budowinski,1979) that K may dissolve significantly in metal-metal sulfide liquids after undergoing first order isomorphic transition has been tested by determining the distribution of Cs between sulfide and silicate liquids as an analogy to K. At 45 kb, 1400°C and 27 kb, 1300°C only limited amount of Cs has been detected in quench sulfide liquids even at pressures beyond the isomorphic transition of Cs. If Cs is a good analogy to K and the high pressure element distribution are quenchable, then these results suggested that the isomorphic transition in K may not increase its solubility in metal sulfides.

Seismology

Earthquakes; Seismology

Metropolitan East
Thursday A.M.
C. Rebollar (Univ. of Alberta), and *S. S. Alexander* (Pennsylvania State Univ.), Presiding

S 1

ALBERTA ROCKY MOUNTAIN EARTHQUAKE SWARM: PRELIMINARY RESULTS

C. Rebollar and E.R. Kanasewich (Dept. of Physics, University of Alberta, Edmonton, Canada T6G 2J1)
E. Nyland (presently at I.G.P.P., University of California, La Jolla, California 92093)

Since January 1976 the Edmonton 6 component (3 short period and 3 long period) digital station has been registering a swarm of small earthquakes that seem to originate about 190 km SW of Edmonton. Because of lack of coverage by nearby stations it is not possible to obtain extremely precise locations. However, teleseismic epicenter locations lie roughly within 52.26±.38°N and 115.22±.13°W. Magnitude of the events is usually less than 4.5 Ml. From a flat layer model for Southern Alberta travel time curves were made for different source depths. Very clearly differences of S-P, S-Sn and P-Pn indicate source depths of 28±4 km. Spectral analysis is currently underway to determine source parameters.

S 2

SEISMICITY OF THE OROZCO FRACTURE ZONE: OVERVIEW OF THE PASSIVE PHASE OF ROSE

Project ROSE scientists*

We present locations calculated for approximately 50 earthquakes which occurred along the Orozco Fracture Zone during the period of ROSE II (Rivera Ocean Seismic Experiment - Leg II). Locations were calculated using the HYPOINVERSE program developed by the USGS. Arrival times recorded by 26 ocean bottom seismometers belonging to eight institutions were used to locate the events. Although most events were not well recorded at all stations, 17 locations were calculated using at least 10 readings. All locations are considered accurate to within, at worst, a few kilometers.

The zone of tectonic activity defined by the seismicity is confined to what one would expect to be the active portion of the transform and confirms and further defines the complex tectonic pattern suggested in a preliminary study which used a subset of the current dataset (Tréhu et al., 1979). The majority of the events define a narrow line of activity parallel to the current spreading direction and situated along a topographic trough. Another zone of diffuse activity marks an offset in the transform and indicates a complicated tectonic regime. Most of the events are shallow and appear to be crustal.

*Project ROSE scientists are from the following institutions: University of California at Santa Barbara, University of Hawaii, Instituto Oceanografico (Manzanillo), Lamont-Doherty Geological Observatory, Massachusetts Institute of Technology, Naval Ocean Research Development Agency, Oregon State University, Scripps Institution of Oceanography, University of Texas at Galveston, University of Washington, Woods Hole Oceanographic Institution.

S 3

SEISMIC RUPTURE PATTERNS IN OAXACA, MEXICO

F. Tajima and K. McNally (both at Seismological Laboratory, 252-21, California Institute of Technology, Pasadena, California 91125)

The seismic activity and patterns of large earthquake occurrence have been investigated for the region of the Oaxaca, Mexico earthquake (M_S = 7.8, 20 Nov. 1978), and adjoining areas for the period 1964 to 1973. The JHD method was employed to relocate the hypocenters of earthquakes using the Oaxaca mainshock as the calibration event. The relocated hypocenters show reduced scatter with greater concentration along the coast of Mexico near the Middle America trench. We have also found that the standard single event locations cause aftershock areas to be enlarged by about 30%. Large earthquakes which occurred in Oaxaca in 1965 and 1968 have been relocated by about 45 km at N15°E and 60 km at S50°W respectively, to the original epicentral determinations. These improved locations allow better definition of seismic gaps and slip calculations. It appears that two sections of the fault in Oaxaca may remain unbroken by the recent earthquakes in 1965, 1968, and 1978. Furthermore, the seismic slip in these events is less than half that calculated for each of the major sequences in Oaxaca at the turn of the century in 1899/1903 and again in 1928/1931. The relocations also indicate that faulting in this area is bilateral as opposed to updip unilateral propagation typical of subduction zones elsewhere.

S 4

THE SEISMICITY OF THE GULF OF MEXICO

Cliff Frohlich
David B. Dumas (University of Texas Marine Science Institute, Galveston, Texas 77550)

The Gulf of Mexico is not truly aseismic, as precisely four earthquakes have been located within the central portion of the Gulf in the past 20 years. All the events are quite small, with magnitude of 5.0 or less. However, for the event of 24 July 1978 (080613.2, 26.50N, 88.78W M_b=4.9), it has been possible to determine both its focal depth (15 km) and its focal mechanism (see figure below).

The focal depth has been determined from the presence of a water surface reflected phase (pwP) which arrived 10 to 11 sec after P and was clearly recorded on short period vertical seismographs at more than 15 stations. The polarity of this phase is opposite from the polarity of the initial P phase on all available high quality records. A depth of 15 km places this event just above the Moho as determined from refraction studies in this region.

Clear first motions could be determined from about a fifth of the available short period records, and only these were used to determine the focal mechanism. Although only one of the focal planes is well-determined, all possible mechanisms have a strong thrusting component.

Multichannel reflection lines in this region show only flat-lying sediments, with almost no indication of any faulting or tectonic activity. There is some evidence that the Gulf events occur along zones of weakness associated with Mesozoic rifting.

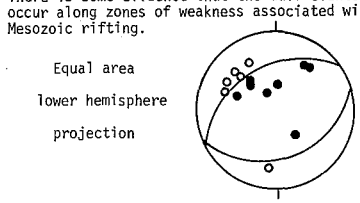

S 5

A MICROEARTHQUAKE STUDY OF THE PLATE BOUNDARY, NORTH ISLAND, NEW ZEALAND

M. Reyners (Lamont-Doherty Geological Observatory of Columbia University, Palisades, New York 10964)
(Sponsor: Paul G. Richards)

The seismicity, structure and tectonics of the Indian/Pacific plate boundary in the North Island of New Zealand have been studied by means of a 210 km-long microearthquake traverse oriented in the direction of a dip of the subducted Pacific plate. The geometry of the top of the Pacific plate is inferred from a band of concentrated microearthquake activity approximately 10 km thick which is identified with the crust of the plate. The Pacific plate has two knee-like bends, one where the top of the plate is about 25 km deep, the other below the volcanic front, where the plate is about 70 km deep. Fault plane solutions indicate that seaward of the shallower bend the Pacific plate is being loaded by the Indian plate, whereas landward of this bend the Pacific plate is sinking under its own weight.

A lack of microearthquakes in the Indian plate below the trenchward half of the traverse is related to the Indian and Pacific plates being currently unlocked. Below the other half of the traverse microearthquakes in the Indian plate are concentrated in the 25-42 km depth range, shallower activity being largely confined to the vicinity of the volcanic front. Fault plane solutions suggest the 25-42 km-deep activity results from stresses set up by locking and unlocking of the plates, while the shallower activity results from local stresses related to volcanic phenomena.

S 6

SPACE-TIME DISTRIBUTION OF SHALLOW AND INTERMEDIATE EARTQUAKES IN THE NEW HEBRIDES ISLAND ARC

J-M. Marthelot
B.L. Isacks (both at: Dept. of Geological Sciences, Cornell University, Ithaca, NY 14853)

An analysis of the space-time distribution of PDE locations along the New Hebrides island arc since 1961 reveals two well defined zones with an anomalous rate of activity several times higher than average for the depth range considered. The first zone, at depths less than 70 km, coincides with the interruption of the trench north of Efate and with a gap of intermediate seismicity. Its rate of earthquake occurrence has been remarkably uniform for the last 18 years, in contrast to other parts of the arc where temporal changes are related to major sequences of thrust events. As this zone is a gap for major earthquakes, the anomalous activity may be related to creep at the plate boundary; another

possibility is that this boundary is locked in the precursory stage of a major thrust sequence. However a precursor time of 18 years would imply an earthquake with a magnitude larger than that observed in the past in the New Hebrides.

The second zone, at depths between 70 and 200 km beneath Santo, corresponds to the down-dip extrapolation of the d'Entrecasteaux fracture zone. It shows a clear increase of activity which starts 1 year after the major shallow thrust sequence of August 1965 in South Santo and lasts almost to the time of the adjacent major thrust sequence of December 1973- January 1974 in North Santo. A large intermediate earthquake with an unusual mechanism indicative of transverse faulting in the slab occurred in this zone during the period of high activity. The two adjacent thrust sequences and the intermediate depth activity may thus be closely related, possibly through diffusion of a stress pulse away from the August 1965 sequence.

S 7

AFTERSHOCKS OF THE PETATLAN, MEXICO, EARTHQUAKE OF 14 MARCH 1979 (M_S = 7.6)

F.R. Zúñiga
C.M. Valdés (both at Instituto de Ingeniería, UNAM, México 20, D.F., México)
R.P. Meyer (Geophysical & Polar Research Center, University of Wisconsin, Madison, WI 53706)
J. Havskov
S.K. Singh (both at Instituto de Ingeniería, UNAM, México 20, D.F., México)

About 300 events covering a period of 30 days, recorded on 10 digital, 5 analog tape, and 4 smoked-paper seismographs have been analyzed to determine the aftershock sequence of the Petatlan earthquake. Aftershock areas for the first 54 hours, first 5 days, and first 30 days are: 1400 km^2 (44 x 32 km), 2200 km^2 (55 x 40 km), and 3850 km^2 (70 x 55 km), respectively. The area grows landward with time, with its major axis parallel to the coastline. The PDE epicenters for major aftershocks are displaced by 25-80 km, all lying east of the epicenter determined from the field array. The b-value is about 1.6. Projected on a line N 20° E (parallel to the trench) the hypocenters define a dip of about 30°.

S 8

AFTERSHOCK SURVEY OF THE 1978 BERMUDA RISE EARTHQUAKE

S.P. Nishenko (Lamont-Doherty Geological Observatory of Columbia Univ. and Dept. of Geol. Sci., Palisades, New York 10964)
G.M. Purdy
J.I. Ewing (both at: Woods Hole Oceanographic Institution, Woods Hole, Massachusetts 02543)

The Bermuda rise earthquake of March 24, 1978 (O.T. 0042 36.30; m_b 6.1) occurred 380 km southwest of Bermuda in seafloor of Mesozoic age (near anomaly M4, ~118 mybp). The teleseismic location and focal mechanism studies indicate that the event occurred along a northwest trending fracture zone, near the M11-M4 spreading discontinuity associated with the opening of the south Atlantic.

We conducted an aftershock survey for this event during June 19-28, 1978 using a tripartite array of ocean bottom hydrophones. Over 150 events, $0 \leq m_b < 2$, were recorded during the ten day period. Larger events detected by the array locate in a tight cluster at a depth of 10 to 12 km in the vicinity of the teleseismic main shock location.

S 9

LOCATIONS AND MECHANISMS FOR AFTERSHOCKS OF THE JANUARY, 1980, LIVERMORE, CALIFORNIA, EARTHQUAKE SEQUENCE*

Joseph M. Mills, Jr., Frederick E. Followill, Robert F. Rohrer (University of California, Lawrence Livermore Laboratory, Livermore, CA 94550)

The principal shocks and aftershocks of the January, 1980, Livermore, California, earthquake sequence appear to be clustered into at least three epicentral regions. Permanent and portable three-component digital seismic stations provided horizontal and vertical ground motion data for P- and S-wave forms. The focal mechanisms of this sequence indicate predominantely strike-slip motion. Relocation of these events indicates activity on more than one fault during the first few weeks following the principal earthquakes.

S 10

A REINTERPRETATION OF THE MEIZOSEISMAL AREA OF THE 1886 CHARLESTON EARTHQUAKE

David C. Amick (Ebasco Services Inc., 2211 W. Meadowview Rd., Greensboro, North Carolina 27407)

(Sponsor: Umesh Chandra)

Initial investigations following the Charleston earthquakes of August 31, 1886, indicated two areas of MM intensity X damage. Based upon this data, Dutton postulated two "Epicentrums" for the Charleston earthquakes. This idea has been rejected by various authors who suggest a northeast-southwest trending basement fault connecting Dutton's two "epicentrums". Epicenter trends, focal mechanisms and isoseismic investigations for recent Charleston events indicate reverse faulting along northwest striking planes. Therefore, an apparent discrepancy exists between historical and recent data.

On December 15, 1977, at 0715 (UCT), a magnitude 2.0 earthquake occurred in the Charleston-Summerville region. This event was followed twelve hours later by a magnitude 2.7 earthquake that was felt locally with a maximum intensity of V. Five hours after this felt event, four Sprengnether MEQ-800 portable seismographs were deployed in the epicentral area to supplement the stations of the South Carolina Seismographic Network and Charleston-Summerville "Mini-network". During the next four days, this expanded network recorded additional events. A total of six events (M_L 1.7 - 2.7) were recorded. These six earthquakes originated from two distinct source areas. The events of December 15 and 20, 1977, lie along the northwest epicenter trend defined by other instrumentally located Charleston-Summerville events. Focal mechanisms for these events indicate reverse faulting along a northwest striking plane. Isoseismal data for the felt event also exhibits a northwest-southeast trend. The events of December 16 and 18, 1977, originated 25 kilometers to the southwest and the preliminary hypocenters preclude the possible association of these events with the fault plane defined by the Summerville events. The two source areas are located very near Dutton's "epicentrums" of the 1886 Charleston earthquake. This tends to support Dutton's original contention that two epicenters exist for the Charleston events.

S 11

SEISMICITY, EARTHQUAKE MECHANISMS AND TECTONICS OF IRAN

Umesh Chandra (Ebasco Services Inc., Boone Building, 2211 West Meadowview, Greensboro, North Carolina 27407)

Regional epicenter maps and focal mechanism solutions of earthquakes were used to investigate the tectonics of Iran. In general, the seismic activity in Iran follows closely the trends of three major mountain belts, Caucasus-Kopet Dagh, Elburz and Zagros ranges. Also a northwest trend across the Central Iranian Plateau, with no known structural relationship is observed. There is some suggestion of possible trends transverse to the Zagros trend. The most notable of these is a NNE trend (about 50 km wide and 250 km long) whose southern end lies in the strait of Hormuz. Significant earthquake activity occurs in the northern part of the Lut Block and along its eastern boundary.

Focal mechanism solutions show thrust faulting along the general trend of the Elburz ranges. Thrusting motion is also noted along northwest faults in the region of convergence of Elburz and Kopet Dagh ranges. A predominance of northwest thrust faulting is also noted throughout the entire stretch of the Zagros Folded Belt. The seismic activity west of 49°E, occurs mainly along the northwest striking, right lateral Main Recent Fault rather than on the nearby Main Zagros Thrust. The arching up of geological formations along a NNE axis, NNE alignment of epicenters and focal mechanism solutions near Bandar Abbas and north of it, suggest that the colliding edge of the Arabian plate in the region north of Oman Peninsula is in the form of a projected promontory. The focal mechanism solutions confirm a trench-arc subduction zone along the Makran continental margin.

S 12

RAMPART SEISMIC ZONE OF CENTRAL ALASKA

P. Yi-Fa Huang (Dept of Earth and Planet. Sciences) M. I. T., Cambridge, Mass. 02139
N. N. Biswas (Geophysical Institute) University of Alaska, Fairbanks, Alaska 99701

The characteristics of the Rampart seismic zone located in central Alaska is being investigated from the aftershock sequence of Rampart earthquake (M_L = 6.8) of 1968. The magnitude of the aftershocks ranged from 1.6. to 4.89 which yielded a b-value of 0.96±0.09 and outlined a NNE-SSW oriented aftershock zone of about 200 km long and 10 km wide. The zone is marked by crustal and subcrustal hypocentral distribution along a plane dipping steeply ($\sim$ 84°) towards west.

Fault plane solutions for the aftershock sequence show an initial strike-slip motion followed by normal faulting. The trend of the after shock zone does not follow either any mapped trace of faults through the area or any lithologic interface of significance. Further, as the Rampart seismic zone lies outside the area of lithospehric plate subduction in interior Alaka, it is interpreted to represent the formation of a relatively new intraplate fracture caused by regional northwest compression.

S 13

VERTICAL CRUSTAL MOVEMENTS IN THE VICINITY OF THE 1931 VALENTINE, TEXAS, EARTHQUAKE

James F. Ni (Department of Geological Sciences, Cornell University, Ithaca, N.Y. 14853)
Robert E. Reilinger, and Larry D. Brown

Deformation possibly related to an earthquake in Texas has been revealed from analysis of precise leveling data collected by the National Geodetic Survey. Relative elevation changes deduced from first-order leveling surveys conducted between 1910 and 1957 show that at least two areas in western Texas near the epicenter of the 1931 Valentine earthquake (M = 6.4) subsided relative to their surroundings. Observed subsidence east of Van Horn, Texas, is attributed primarily to the combined effects of groundwater withdrawal and topography-related survey errors. In contrast, relative subsidence near Valentine, Texas, of 11.2 ± 1.0 cm extending over a distance of about 20 km does not appear to be due to either near-surface effects or leveling errors and thus may represent tectonic deformation. The spatial pattern of the observed subsidence near Valentine is generally consistent with that expected for normal faulting along an approximately NW-SE-striking, west-dipping, buried fault, although no such fault has been identified at the surface. This orientation and sense of movement is consistent with regional E-W extension and with the first P motions reported for the Valentine earthquake. If the observed subsidence was caused by the 1931 earthquake, the leveling data suggest that the epicenter for this event lies considerably closer to Valentine than originally reported.

S 14

HINGE FAULTING AND ITS CORRELATION WITH SURFACE GEOLOGY IN NORTHERN COSTA RICA

H. B. Liaw
T. Matumoto (all at: Marine Science Institute, University of Texas, Galveston, TX 77550)

A composite focal plane solution of nine well-recorded microearthquakes has been determined beneath Nicoya Peninsula, Northern Costa Rica. These earthquakes, presumably occuring along the Benioff zone of the Cocos plate underthrusting the Caribbean plate, were recorded by the Arenal seismic network. This network is installed and operated under a cooperative program between the Instituto Costarricense de Electricidad and the University of Texas since 1974. One of the focal planes striking N67°E (dips 85°SE), agrees with the trend N70°E delineated by the epicenter distribution. We interpret this focal plane as the fault plane of a hinge fault. This hinge faulting and the aftershock pattern of the 1978 shock (M=5.7) suggests the Cocos plate is breaking beneath the Nicoya Peninsula. The surface expressions of the overriding Caribbean plate show close relationships with this breakage. On the Nicoya Peninsula, there is a suggestion of a series of parallel faults striking east-northeasterly. Inland in Northern Costa Rica, a structural discontinuity separates the Quaternary volcanic range in the north from the Tertiary

volcanic range in the south. Along the strike of the hinge fault, the projection of it passes through the discontinuity. Further north, the projected line meets the Hess Escarpment of the western Caribbean. Another structural discontinuity is observed 50 km SE of the aforementioned discontinuity. Together with the higher-than-normal seismic activity and the great shocks of M=7.3 in 1939, this second discontinuity indicates another hinge faulting near the southern end of the Nicoya Peninsula.

The study may suggest that the deep seated fault of the overriding lithosphere created by the offset of the subducting plate can propogate upward to the surface and thus modify the surface physiography; or that the inhomogeneity of the overriding plate can control the faulting of the subducting plate.

S 15

RELATION OF EARTHQUAKE FOCAL MECHANISMS TO TECTONIC STRUCTURAL FEATURES OBSERVED ON SATELLITE IMAGERY

S. S. Alexander, B. Lee and C. Petrus (Geosciences Department, Geophysics Program, The Pennsylvania State University, University Park, PA 16802)

Well-constrained focal mechanisms for earthquakes whose hypocenters are accurately established have been correlated with satellite images, especially LANDSAT, both for active seismic areas such as Southern California and for less active areas such as the eastern U.S. Commonly there are spatially more sharply defined structural features, distinctive lineaments and intersections of them for example, in association with recent seismic activity, even when no surface faulting is observed. We suggest that with the combined interpretation of seismic and image data we can better characterize the neo-tectonic history of an area and possible identify localities where future activity will be concentrated.

In addition, the equivalent earthquake focal mechanism for the "tectonic release" generated by the largest French underground nuclear explosion detonated in the Hoggar granite in Algeria is consistent with strike-slip movement on a set of northeast trending linear features observed on LANDSAT imagery, rather than with the major N-S trending faults near the test site. The inferred maximum compressive stress in this intra-plate area of Africa is horizontal and oriented approximately in a N80E direction.

Crustal Structure

Pier 7 & 8
Thursday P.M.
R. A. Young (Phillips Petroleum Co.), and *D. M. Jurely* (Princeton Univ.), Presiding

S 16

REGIONAL PROPAGATION IN THE USSR

I. Samowitz (Sierra Geophysics, Inc., Arcadia, CA 91006)

Regional phases play an important role in discrimination. By thoroughly investigating the literature, the USSR has been regionalized into 10 tectonic provinces. Types of data used for the regionalization include crustal structure, seismicity, Moho properties, wave velocities, attenuation, regional phase propagation, gravity, and upper mantle structure. Pn velocities varied from 7.6-7.8 km in the Baikal Rift Zone (a region similar to the Basin and Range Province) to 8.1-8.5 km/s in Kazakh. Depth to Moho varied significantly, typical values in the Pacific Transitional zone ranged from 8-42 km while in Russian Central Asia typical values ranged between 50-70 km.

Using simple sources, we have synthesized seismic waveforms that propagate within these tectonic regions in order to determine the character of the waveforms at regional distances, primarily focusing on short period Pn, PL, and Lg. The depth of the source has also been varied to compare the effect of the hypocentral depth. Regional WWSSN recordings from explosions in Kazakh have been used to check the accuracy of the synthetic seismogram calculations.

S 17

SEISMIC WAVE PROPAGATION IN SOUTHEASTERN CHINA

J.J. Pulli (Dept. of Earth and Planetary Sciences, Massachusetts Institute of Technology, Cambridge, MA 02139) (Sponsor: K. Aki)

As the first step in the study of the seimicity of eastern China, we have been investigating the transmission properties of the crust and upper mantle in this area. The WWSSN stations CHG, SEO, and ANP which border the area of interest provide convenient observation points for wavepaths crossing eastern China and have been used exclusively in this study.

Preliminary results indicate that seismic velocities are anomalously low in the area. For example, we measured a Pn velocity of 7.67 lm/sec, much lower than the 8.1 km/sec Pn velocity found in the eastern U.S.. Group velocities of Rayleigh waves are also low, for instance, 2.9 km/sec at 20 sec and 3.3 km/sec at 30 sec. We have also found an azimuthal variation of group velocities for Rayleigh waves arriving at CHG. Lg velocities are also low, and measurements of Lg attenuation has yielded a value of anelastic attenuation of 0.007 km^{-1}. This compares with a value of 0.001 km^{-1} in the eastern U.S..

We are presently combining our results from the various seismic phases studied to form a model of the crustal structure in terms of the tectonic setting of the area.

S 18

CRUSTAL STRUCTURE BENEATH TURKEY

Nezihi Canitez
M. Nafi Toksöz (both at: Dept. of Earth and Planetary Sciences, M.I.T., Cambridge, MA 02139)

Travel times and station residuals of P-waves and phase and group velocities of surface waves are used to study the crustal structure and lateral heterogeneities. Average station residuals of teleseismic P-waves are all negative (early) in western and positive (late) in eastern stations. Local travel times give a P_n velocity of 7.9 km/sec in eastern and northern Turkey and 8.1 km/sec in western Turkey. The group velocities of Rayleigh waves are higher in central and eastern Anatolia than those in western Turkey and the Aegean region. In addition, there is a 120 mgal gravity anomaly across the North Anatolian Fault Zone.

These data suggest there are (a) strong lateral variations in the crust/upper mantle structure between the Aegean region (west) and central and eastern Anatolia and (b) a strong structural discontinuity across the North Anatolian Fault Zone.

S 19

CRUSTAL STRUCTURE OF THE NORTHEASTERN UNITED STATES: CONTRASTS BETWEEN THE GRENVILLE AND APPALACHIAN PROVINCES

Steven R. Taylor
M. Nafi Toksöz (both at: Dept. of Earth and Planetary Sciences, M.I.T., Cambridge, MA 02139)

Average crustal models for the northeastern United States are computed by combining P and S wave travel times from regional earthquakes with surface wave dispersion data. The Precambrian Grenville Province in New York State has a relatively homogeneous crust with nearly constant P and S wave velocities of about 6.6 and 3.7 km/s, respectively, and an average crustal thickness of 37 km. The Paleozoic New England Appalachians have a slightly thicker (approximately 40 km) crust with two well-defined layers. The upper crust in the Appalachians shows relatively low P and S velocities of about 6.1 and 3.6 km/s, respectively, to about 15 km where an abrupt increase to 7.0 and 4.1 km/s occurs. Both regions show similar P_n velocities of approximately 8.1 km/s. A time term analysis using P_n data shows that a relatively thick or low velocity crust parallels northeast-trending geologic structures and Bouguer gravity lows in central New England.

The Grenville Province is mainly remobilized older basement of Superior or Hudsonian age. In contrast, the synclinoria in the New England Appalachians contain deep water continental rise or back arc basin metasediments which were probably deposited on oceanic crust. Much of the suture zone between the two belts is well marked by a belt of serpentinites, a linear gravity high and a rapid change in crustal velocities. The observed differences in structure between the two orogenic belts may reflect contrasts in their tectonic evolution.

S 20

SEISMIC CRUSTAL STRUCTURE NORTHWEST OF THUNDER BAY, ONTARIO

Roger A. Young (Phillips Petroleum Company, Bartlesville, OK 74004)
Gordon F. West (University of Toronto, Toronto, ONT M5S 1A7)

A crustal-scale seismic experiment on the Precambrian Shield northwest of Thunder Bay, Ontario, defines the velocity structure down through the uppermost mantle. Fan surveys--with ranges of 125 km and 200 km-- show both a regional increase in average velocity which correlates with the English River gravity high and also travel-time delays which correlate with mapped geologic features of more local extent. Deep seismic sounding--employing large open pit mine blasts recorded at ranges from 75 to 350 km--shows clearcut P_g, P_n, and P_{SM} first arrivals with apparent velocities of 6.34, 7.7, and 8.3 km s^{-1}, respectively. Travel-time modeling shows that a widespread sub-Mohorovicic (SM) boundary exists at about 50 km depth. Synthetic seismogram modeling of P_MP amplitude and waveform characteristics requires a lamellar crust-mantle transition zone of appreciable thickness, perhaps a few kilometers. A fundamental velocity of 6.0 km s^{-1} characterizes the upper and mid-crust beneath both gneissic and metavolcanic-plutonic terrain requiring a predominant lithology more felsic than basalt. In contrast, gneissic terrain exhibits a two-layer crust with a high velocity lower crust; but metavolcanic-plutonic terrain shows no Conrad discontinuity and a low velocity lower crust.

S 21

SEISMIC REFRACTION STUDIES OF LAKE SUPERIOR CRUSTAL STRUCTURE

J.H. Luetgert
R.P. Meyer (both at Geophysical & Polar Research Center, Univ. of Wisconsin, Madison, WI 53706)

A series of seismic refraction lines shot in Lake Superior has been analyzed using simple travel-time inversion techniques extended by laterally inhomogeneous ray tracing. The lines were shot by a single ship firing airguns and explosives, with radio-controlled buoys as receivers.

The upper 12 km of crust have been modeled, showing the velocity distribution down to and including the Upper Refractor, an anomalously shallow, high-velocity (6.4-6.9 km/sec) suite of refractors underlying the Lake Superior Basin.

Three profiles spanning the western end of the lake confirm the essentially synclinal structure of the crust suggested by the geology of the lake margins and by previous seismic measurements.

Travel-time offsets observed on many of the profiles provide more precise definition of crustal faulting inferred from extrapolation of known faults on land and from gravity and aeromagnetic surveys. There is evidence for extension of the Isle Royale fault to the west, for

extension of the Keweenaw fault to the east, and for the existence of the postulated Thiel fault roughly between the tip of the Keweenaw Peninsula and the Slate Islands.

S 22

STRUCTURE OF THE J-ANOMALY RIDGE, SOHM ABYSSAL PLAIN, AND NOVA SCOTIAN SLOPE AND RISE

W. J. Ludwig (Lamont-Doherty Geological Observatory, Palisades, NY 10964)
B. E. Tucholke (Woods Hole Oceanographic Institution, Woods Hole, MA 02543)

The J-Anomaly is a high-amplitude magnetic anomaly formed between anomalies M0 and M1. It trends northeastward from the eastern end of the New England Seamounts to the Newfoundland Ridge south of the Grand Banks. Single-channel and multichannel seismic reflection profiles show that anomalies M0 to M2 (including the J-Anomaly) are associated with the crest of a basement ridge now buried by turbidites of the Sohm Abyssal Plain. The ridge slopes gently to the east, and sharply to the west with several 0.5-1.5 km scarps. Velocity structure beneath the ridge crest is similar to that farther east beneath the flank of the Mid-Atlantic Ridge, but the ridge has an anomalously smooth upper surface and distinct sub-basement layering. The thickness of sediments beneath the Sohm Abyssal Plain increases westward from 0.7km over the J-Anomaly Ridge to about 3.8 km in the central part of the plain.

Beneath the upper continental rise off Nova Scotia at a sea-floor depth of 4000 m, sediment thickness increases to 8 km and reflection geometry changes abruptly from flat-lying and layered to acoustically chaotic (the "sedimentary ridge province"); this province is 75 km wide and 1000 km long and hitherto has been attributed to piercement and deformation of strata by salt diapirism. Detached diapirs are observed in profiles made parallel to the lower slope, but they do not constitute the entire structure of the ridge, nor do they form a 'salt front' near the 4000 m isobath. The overall structural character of the province suggests compressional deformation and uplift of rise sediments, possibly caused by a short-lived episode of underthrusting north of the New England Seamounts. Most diapirism may have occurred after these compressional forces were relaxed.

S 23

CRUSTAL STRUCTURE OF THE DEEP GULF OF MEXICO FROM O.B.S. REFRACTION AND MULTICHANNEL REFLECTION DATA

A.K. Ibrahim
J. Carye
G. Latham (all at Univ. of Texas, Marine Science Institute, Geophysics Lab., Galveston, Texas 77550)

Twelve reversed 110 km long refraction profiles located in the deep Gulf of Mexico provide a new set of data for interpreting the deep structure and origin of the Gulf of Mexico. The data were collected using ocean bottom seismographs. Explosives ranging in size from 1 lb to 120 lbs were used as the source of energy.

The data show up to 4 layers of sedimentary rocks with total thickness of between 5 and 8 km and having layer velocities ranging between 1.8 km/sec to 4.7 km/sec. Underlying the sedimentary section beneath most of the deep Gulf is an intermediate layer with velocities between 5.1 km/sec to 5.7 km/sec. Beneath the intermediate layer is a crustal layer 5-6 km thick with velocities 6.3-7.0 km/sec, overlying mantle with velocities 7.8 and 8.2 km/sec.

These data confirm the previously held idea suggested by earlier refraction data that most of the deep Gulf basin is underlain by an oceanic crustal layer.

S 24

THE CRYSTAL STRUCTURE OF THE REYKJANES RIDGE AT 59°30'N

A.W.H. Bunch (Department of Geodesy and Geophysics, University of Cambridge, Cambridge CB3 OEZ, England)
B.L.N. Kennett (Department of Applied Mathematics and Theoretical Physics, University of Cambridge, Silver Street, Cambridge CB3 9EW, England)

In order to examine the development of the oceanic crust in the neighbourhood of a slowly spreading ridge, a seismic refraction experiment was carried out at 59°30'N on the crest of the Reykjanes Ridge. Three 120km long overlapped split profiles were shot parallel to the trend of the ridge, on the eastern flank, using up to five recording sonobueys. The profiles were at distances of 0, 30 and 90km from the ridge axis, corresponding to approximate crustal ages of 0, 3 and 9 Myr. Data from the main profiles were supplemented by using a large chamber air gun during the recovery of the buoys.

There is no indication of a significant magma chamber at the ridge crest, although a slight P velocity inversion in Layer 3 suggests a zone of elevated temperature. Away from the crest there was a slight positive velocity gradient in Layer 3. Layer 2 was most effectively modelled by a region of varying velocity gradients, which thinned with age and the transition to Layer 3 is marked by a sharp change in velocity gradient. The transition to mantle velocities is also best modelled by a high velocity gradient rather than an interface.

Although some lateral variation in properties is apparent along the profiles, the lateral velocity gradients were sufficiently weak to allow an effective analysis in terms of laterally uniform models.

S 25

SEISMIC REFRACTION AND CONTINUOUS REFLECTION PROFILES OVER THE NELSON FRONT

Z. Hajnal (Dept. of Geological Sciences, University of Saskatchewan, Saskatoon, Sask., S7N OWO)
G.L. Cumming, E.R. Kanasewich (Dept. of Physics, University of Alberta, Edmonton, Alta., T6G 2J1)
A.G. Green, J.A. Mair (Div. of Seismology, E.M.R., Ottawa, Ont., K1A 0Y3), D.H. Hall (Dept. of Earth Sciences, University of Manitoba, Winnipeg, Man., R3T 2N2), R.F. Mereu (Dept. of Geophysics, University of Western Ontario, London, Ontario, N6A 5B7)*

* Participating members of the CO-CRUST Consortium for Crustal REconnaissance Using Seismic Techniques)

The Nelson Front represents the geologically and geophysically recognizable contact zone between the Churchill and Superior geologic provinces in the Canadian Shield. In the southern part of the zone, four refraction profiles indicate that the crustal thickness varies from 41 km in the Superior province to 48 km in the Churchill province. Nearly vertical reflection profiles reveal a multilayered crust and exhibit patterns indicative of deep-seated crustal faults, providing evidence that the entire crust is disturbed in the boundary zone. Geophysical results show that the front is at least 250 km wide, significantly wider than is estimated from surface geology.

S 26

SEIMSIC IMAGING OF THE ELBERTON GRANITE, USING COCORP SOUTH APPALACHIAN DATA

Donna M. Jurdy
Robert A. Phinney (both at Department of Geological and Geophysical Sciences, Princeton University, Princeton, New Jersey 08544)

The COCORP seismic reflection lines pass through the Blue Ridge and Inner Piedmont provinces to the Kings Mts. slate belt and on to the coastal plain. We have reprocessed a portion of the COCORP profile which passes across the Inner Piedmont of Georgia. In this area the Elberton Granite appears at the surface as intrusive into the metasediments and in seismic section it appears transparent. A sequence of layered reflections, thought to be equivalent to the Valley and Ridge sediments beneath the crystalline thrust sheet, is difficult to establish. Our reprocessing involves filtering and beamforming operations to investigate this supposed extension of the thrust and to study the flanking reflections at 2 to 4 seconds, which give the appearance of a diapir.

S 27

VELOCITY-DEPTH INVERSION FROM THE TAU-P PLANE FOR LARGE APERTURE COMMON MIDPOINT SEISMIC DATA FROM THE CARIBBEAN

(All at: Lamont-Doherty Geological Obs. Palisades, N.Y. 10964)
P. Buhl
P.L.Stoffa
J.B. Diebold

Six expanding spread two-ship seismic experiments were performed in the Venezuela Basin of the Caribbean. They provided multichannel common midpoint data with offsets as large as 70 km, and a maximum seismogram spacing of 100 meters. Twenty-four traces per shot were obtained with explosive sources.

Each of the six X - T data sets were transformed to the parameters of $\tau - p$ (intercept time - ray parameter) by stacking each group of 24 traces along linear trajectories, performing time shifts based on trajectory slopes and group offsets, and adding the resulting $\tau(p)$ traces. Aliasing was largely eliminated by coherency thresholding.

The critically refracted and postcritically reflected arrivals used in the inversions were detected in the $\tau - p$ plane by virtue of their high amplitudes. The shapes of the envelopes of the $\tau(p)$ traces were used to establish confidence bounds in $\tau - p$. The selected $\tau - p$ points were used to obtain V(Z) functions by recursively solving the formula for intercept times in horizontally layered media. This is an extension of the standard slope-intercept method. The resulting V(Z) functions are presented in terms of two-way traveltime for comparison to near vertical reflection profiles. The $\tau - p$ confidence bounds are mapped into V(Z) by finding successive worst-case inversions for each velocity sampled. The results are quite well constrained, due to the large number of $\tau - p$ points used.

The deepest arrivals sampled in each profile are interpreted as wide angle reflections from the Moho. The inversion method can be shown to be as good as, or superior to, the Herglotz integral method in the presence of discontinuous velocity functions and for discrete $\tau - p$ data.

S 28

INVERSION OF REFRACTION DATA BY WAVE-FIELD MIGRATION

R. W. Clayton (Dept. of Geophysics, Stanford University, Stanford, CA 94305)
G. A. McMechan (Pacific Geoscience Center, Earth Physics Branch, Dept. of Energy, Mines and Resources, Box 6000, Sidney, B.C. V8L 4B2, Canada)

The process of wave equation migration is adapted for refraction data in order to produce velocity-depth models directly from the recorded data. The procedure consists of two linear transformations: a slant stack of the data produces a wave field in the p-τ plane which is then migrated using $\tau=0$ as the imaging condition. The result is that the data wave field is linearly transformed from the time-distance domain into the slowness-depth domain, where the velocity profile can be picked directly. No traveltime picking is involved, and all the data are present throughout the inversion.

The method is iterative because it is necessary to specify a velocity function for the migration. The solution produced by a given iteration is used as the migration velocity function for the next step. Convergence is determined when the migrated wave field images the same velocity-depth function as was input to the migration.

The method obviates the problems associated with determining the envelope of solutions that are consistent with the observations, since the time resolution in the data becomes transformed into a depth resolution in the slowness-depth domain.

The method is illustrated with several synthetic examples, and with a refraction line recorded in the Imperial Valley, California.

S 29

AXIMUTHAL VARIATION OF P-WAVE RESIDUALS FOR STATIONS IN NORTHERN CALIFORNIA

G. W. Simila (Department of Geological Sciences, California State University, Northridge, Northridge, CA 91330)

Teleseismic P-wave residuals from seventy events have been analyzed for a seven station array (dimension 220 x 400 km) in central and northern California. Relative residuals with

respect to Berkeley (BRK) show a pronounced azimuthal dependence on wave approach. Stations in northern California show mainly negative residuals from west to east. The northern Coast Range station exhibits an average positive residual of +0.5 sec. The southern Klamath Mtns. station shows large negative values (-1.6 sec) for azimuths 0-130°. The southern Cascade Range station displays an average negative value (-0.7 sec). Four stations from north to south along the Sierra Nevada foothill region are characterized by negative residual values of -0.2 - -0.6 sec. A simple ray tracing technique was utilized to model the corresponding velocity increases in the upper mantle. In addition, several crustal velocity models in these regions have been determined from dispersion analysis of Rayleigh wave group velocities.

Earthquakes; Premonitory Phenomena

Metropolitan East
Thursday P.M.
W. R. McCann (Lamont-Doherty) and *P. Talwani* (Univ. of South Carolina), Presiding

S 30

BIOLOGICAL PREMONITORS OF EARTHQUAKES: A VALIDATION STUDY

W.H. Kautz(SRI International, Menlo Park, CA 94025)
L.S. Otis(SRI International, Menlo Park, CA 94025)

The purpose of the research reported herein is to test the validity of the long held notion, supported primarily by anecdotal reports and by recent reports from the People's Republic of China, that anomalous animal behavior precedes at least some earthquakes, presumably in response to one or more as yet unidentified precursors. In this project, currently in its third year, a network of more than one thousand volunteer observers of animals has been established in selected seismic areas in California. A carefully worked out reporting protocol, employing a telephone "hot line," daily and weekly routine reports from observers, and a novel statistical method for the analysis of reports vis-a-vis earthquakes have been developed. For the year since the network reached its present extent (about 2/15/79), none of the five California main shocks with $M \geq 5$ occurred well within the network, although the epicenters of two of them fell on its fringes. Results from these two events are inconclusive, though suggestive and encouraging. A statistical simulation of the present network, based on earthquakes of prior decades, indicates a high probability of capture of at least one magnitude 5+ event by the observer network within the next year. It is concluded that members of the community may participate constructively in data collection for certain kinds of earthquake research, suggesting that this potential resource be tapped for other geophysics research programs.

S 31

A REFORMULATION OF THE EARTHQUAKE PREDICTION PROBLEM

Allan G. Lindh (U.S. Geological Survey, Menlo Park, California 94025)

An Earthquake Prediction (EQP) has come to imply a statement of when and where an earthquake will occur, how large it will be, and some measure of the uncertainty of the prediction. This definition does not correspond to the nature of the problem, or to the observed data, and has created unreasonable expectations. The discrepency between what we observe and what is needed for a responsible EQP is so large that none are attempted, even though most would agree that some changes do reflect an increased probability of a large earthquake. I believe we have in effect painted ourselves into a corner.

Another approach would be to acknowledge the statistical nature of EQP, and approach it via probability density functions in space and time, or earthquake probability density maps (EQPDM). Construction of an EQPDM would start from a seismic hazard map, based on geologic identification of active faults. This 2-dimensional risk function would then be multiplied in appropriate areas by temporal risk factors based on i) Plate Tectonic considerations, ii) Geodetic strain and seismicity patterns, iii) Changes in geodetic strain and seismicity rates, iv) Short- term changes in tilt, water level, etc. The size of the multiplying factor would reflect the confidence that a change had occurred and that it might be related to a future earthquake. Each temporal perturbation would also have an associated decay constant, so that for instance, short term changes would only lead to short term increases in risk. One strength of this approach is that it is quantitatively testable. Another is that it eliminates the artificial distinction between EQ hazard assessment and EQ prediction. Its weakness is that it involves a large number of subjective judgements concerning the significance of the observations. This subjectivity cannot be avoided however, and this approach forces the judgements to be quantified and tested.

S 32

EVIDENCE FOR A POSSIBLE SEISMIC GAP NEAR UNALASKA ISLAND IN THE EASTERN ALEUTIANS, ALASKA

L. House
L.R. Sykes (both at: Lamont-Doherty Geological Observatory and Dept. of Geol. Sci., Columbia University, Palisades, New York 10964)
J.N. Davies
K.H. Jacob (both at: Lamont-Doherty Geological Observatory of Columbia University, Palisades, New York 10964)

The aftershock zone of the Aleutian Islands earthquake of 1957 (magnitude, Mw = 9.1) stretched along the North American-Pacific plate boundary from 180°W to 163°W. The eastern 200 km of this aftershock zone, located southeast of Unalaska Island, experienced only six moderate size ($m_b = 6$) or larger aftershocks, all located along the northern (arcward) edge. Within this 200 km long segment the rest of the width of the plate interface (the main thrust zone) lacked known aftershock activity and has experienced only two earthquakes ($m_b = 5$) of magnitude 5 and larger since 1957. In the three years before the 1957 main shock, two clusters of seismicity occurred within the future aftershock zone: one at the western end, near 180°W, the other at 168°W. Arrival times of the 1957 tsunami at tide gauges along western North and South America indicate a source area whose eastern end was located at about 167°W rather than at the eastern end of the aftershock zone, 200 km further east (163°W).

These observations strongly suggest that this 200 km long segment near Unalaska Island either did not rupture during the 1957 earthquake or at least did not break in the same manner as the rest of the 1957 aftershock zone. We cannot rule out the possibility that this segment slips aseismically. Since almost all other segments of the convergent margin in Alaska undergo episodic seismic deformation we infer that this 200 km long Unalaska portion does also. If it were to rupture during a single earthquake, this possible gap is large enough to produce an earthquake of magnitude 8 or larger.

S 33

SEISMIC POTENTIAL AND SEISMIC REGIMES OF THE SOUTHWEST PACIFIC

W.R. McCann (Lamont-Doherty Geological Observatory and Dept. of Geol. Sci., Columbia Univ., Palisades, New York 10964)

During this century wide variations occurred in the distribution of large earthquakes of shallow focus along the convergent plate boundaries of the Southwest Pacific. These variations appear to be, for the most part, spatially related to the rapid changes of tectonic regimes along the strike of these seismic zones and thus may represent long-term features of the seismicity.

The Tonga-Kermadec arcs appear to accomodate at least some plate motion aseismically. Clear changes along strike in the seismic nature of this subduction zone may reflect changes in the amount of aseismic motion between the plates and thus reduce our ability to confidently estimate the seismic potential of this region. The southern half of the New Hebrides arc may produce several large shocks in the next few decades. In particular the segment between 18° and 20°S has experienced few moderate events in the last 25 years and thus appears to be the most likely site for future shocks. A large segment of the coast of New Guinea appears to be a likely site for one or more large shocks in the next few decades. Much of the plate boundary near the Solomon Islands has ruptured during large shocks in the last 10 years and thus will probably remain relatively quiescent for a few decades. The frequency of large shallow earthquakes is remarkably low in the central Solomons. In this region a spreading center in the Woodlark basin is interacting with the island arc. Thus, the aseismic character of this part of the Solomons arc for large and moderate size earthquakes may be a permanent feature as it may stem from the tectonic setting of the region.

S 34

TRANSVERSE STRUCTURAL FEATURES, DISPLACED TERRANES AND THEIR RELATION TO RUPTURE ZONES OF GREAT EARTHQUAKES ALONG THE ALASKA-ALEUTIAN PLATE BOUNDARY

J.N. Davies
G. Bond (both at: Lamont-Doherty Geol. Observ. of Columbia Univ., Palisades, NY 10964)

Many workers have observed that the ends of aftershock zones of great-thrust-type earthquakes coincide with structural features transverse to the Aleutian Arc. Features transverse to the Aleutian arc have been associated with the trends of Shirshov and Bowers' Ridges and the edge of the Bering Shelf. Other transverse features have been postulated to cross the arc at both the western and eastern ends of Kodiak Island and through Prince William Sound. We propose that many of these transverse features represent structural boundaries between displaced terranes that have arrived at their present positions as a result of plate motions. We further propose that more subtle transverse features exist in the eastern Aleutian Islands-western Alaska Peninsula region. Here, these features represent extensional faulting of pre-Pliocene terranes that are continuous from the Alaska Peninsula through the Pribilof Islands region of the Bering Shelf. We suggest that most of these transverse features delimit adjacent portions of the overthrusting plate that are relatively mechanically independent. Thus, strain energy resulting from the underthrusting of the Pacific plate beneath these portions of the North American (Alaska-Aleutian) plate can be stored and released independently from one region to the next. Historically these independent regions, either singly or in various combinations, appear to correspond to the rupture zones of great thrust-type earthquakes along the Alaska-Aleutian plate boundary.

S 35

LOCAL SEISMIC ACTIVITY PRECEDING THE PETATLAN, MEXICO EARTHQUAKE OF 14 MARCH 1979

Hsu, Vindell
J.F. Gettrust
C.E. Helsley
E. Herrero
T. Jordan (all at: Hawaii Institute of Geophysics, Univ. of Hawaii, Hono., HI 96822)

Local seismic activity preceding the Petatlan Mexico earthquake of March 14, 1979 (Ms=7.6) was monitored by a network of portable seismic recording stations that had been deployed by the Hawaii Institute of Geophysics. Seventeen events large enough in magnitude to be recorded by a majority of the stations in the network occurred during the 35 hours preceding the main shock. Epicenter locations of these events tended to converge towards the epicentral position of the large event during this period of time; the frequency of occurrence of foreshocks increased during the 10 hours prior to the main shock.

Lineation of foreshock epicenters indicates the existence of faults trending N23°E; these faults are probably related to compression between the Cocos and North American plates.

S 36

INDUCED EARTHQUAKES CAUSED BY PRECEDING EARTHQUAKES

K. Yamashina (Earthq. Res. Inst., Univ. Tokyo, Tokyo, Japan 113)

After large earthquakes, minor events frequently occur close to but isolated from the focal region of the main shock. They are

called here "induced earthquakes". In the present paper, examples of induced earthquakes are collected and their mechanical correlation is discussed.

Typical cases are (1) extension of the faulting, (2) activity in the conjugate direction of the principal faulting, (3) inland shallow activity associated with large thrust earthquakes along trenches, (4) secondary faulting adjacent to the principal faulting, etc.

Mechanically many of these induced earthquakes occurred in a region where differential strain (and stress) or, in other words, shear strain (and stress) on their nodal planes was probably enhanced by preceding events. It suggests that strain and stress changes (especially the components above) caused by preceding earthquakes play a certain role in the subsequent seismic activity. The present effect might be helpful for planning temporal observations after large earthquakes and/or for studying mechanical conditions of earthquakes occurrence.

S 37

CLUSTERING OF STRONG EARTHQUAKES IN THE SAN FRANCISCO BAY REGION

by W. L. Ellsworth, A. G. Lindh, and W. H. Prescott (U.S. Geological Survey, Menlo Park, California 94025)

In historic time strong earthquakes ($M \geq 5\frac{1}{2}$) in the San Francisco Bay Area (Lat 37° to 38°N) exhibit temporal clustering in excess of the Poisson expectation (P = 0.1). Pairs of earthquakes which may be related include 1836 (M 6½) and 1838 (M 7), 1856 (M 6) and 1858 (M 6), 1865 (M 6) and 1868 (M 6½), 1903 (M 5½) and 1906 (M 8), 1911 (M 6½) and 1914 (M 5½), 1955 (M 5½, 5½) and 1957 (M 5½), and August 1979 (M 5½) and January 1980 (M 5½). In no case are these events related as aftershocks or swarms, and they commonly involve widely separated faults. If the apparent clustering is not an artifact of the short historic period (1855 to 1980), then the existence of a regional-scale physical process may be inferred. A mechanism which could account for the observed seismicity pattern is eventful shear strain episodes at lower and intermediate lithospheric depths in the North American-Pacific plate interface zone. Observable manifestations of such episoles might include secular changes in geodetically measured strain or regional variations in microearthquake occurrence rates or patterns.

A preliminary examination of microseismicity and geodetic strain rates discloses no changes, as of mid-1979, in obvious association with the 1979-1980 earthquake pair. Thus, the most recent pairing could be a coincidence, or the hypothesized deep strain event could either have occurred since mid-1979, or have been of smaller amplitude than 0.2 μstrain. As a corollary to the hypothesized effect of aseismic slip at depth, great earthquakes also produce first order perturbations to the stress state in the surrounding region. The longest inter-event time in the historic record follows the 1906 earthquake (1914-1955). Its long duration is plausibly related to the strain drop of the 1906 event.

S 38

THE HAICHENG FORESHOCK SEQUENCE

Lucile Jones (Dept. of Earth and Planetary Sciences, Massachusetts Institute of Technology, Cambridge, Ma 02139)
Wang Biquan (Institute of Geophysics, State Seismology Bureau, Beijing, People's Republic of China)
Xu Shaoxie (Institute of Geophysics, State Seismology Bureau, Beijing, People's Republic of China)

We have examined the locations and radiation patterns of the foreshocks to the 4 February 1978 Haicheng earthquake using four stations. The foreshocks were located relative to a master event. They occurred very close together, no more than 6 km apart. Nevertheless there appear to have been two clusters of foreshock activity. The majority of events seem to have occurred in a cluster to the east of the master event along a NNE-SSW trend. There also appears to be a second cluster of foreshocks located to the northwest of the first. Thus it seems possible that the majority of foreshocks did not occur on the rupture plane of the mainshock which trends WNW, but on another plane nearly perpendicular to the mainshock plane. This inference is supported by differences among the radiation pattern of the foreshocks.

We also examined the radiation patterns of the foreshocks, primarily through the amplitude ratiogs of P and S waves (Ap/As) recorded at each station. While the rations were relatively constant at the more distant (Δ =100-200 km) stations, two very different waveforms were recorded throughout the sequence at Yingkou (Δ =20 km). Calculations of the amplitude ratios for the (very different) fault plane solutions of the mainshock and of some of the largest foreshocks showed that two different waveforms should be recorded at Yingkou.

S 39

SEISMICITY CHANGES PRECEEDING CENTRAL ASIAN EARTHQUAKES

D.W. Simpson (both at: Lamont-Doherty Geological Observatory of Columbia University, Palisades, New York 10964)
M.J. Kristy (Also with Dept. of Geol. Sci., Columbia University)

The Gissar-Kokshal fault zone south of the Tien Shan Mountains in Central Asia is one of the most active areas of intraplate seismicity in the world. Since 1949, four earthquakes greater than magnitude 6.5 have occurred along the section of this fault north of the Pamir Mountains, almost completely filling a seismic gap which had existed for at least 80 years. The two most recent of these earthquakes, the 1974 Markansu (M_S = 7.4) and 1978 Zaalai (M_S = 6.7) events, were each preceeded by a short period of increased activity in the future epicentral area some years prior to the main shock. The size of the maximum earthquake within the active period and its time before the main shock increase with the magnitude of the main shock. The maximum earthquake within the active period occurs at the same location as the future large shock. A segment adjacent to the 1978 earthquake, occupying the only unbroken portion of the former gap, has recently shown a similar burst of activity, suggesting that it may be the site of the next large earthquake of this sequence.

Large premonitory earthquakes are also observed near the sites of seven other earthquakes with magnitudes 7.0 to 8.3 in the Tien Shan since 1880. The premonitory time interval and magnitude of the premonitory earthquake increase with the size of the main shock in a manner similar to that observed for the Pamir zone section of the Gissar-Kokshal.

S 40

A CHANGE IN THE FOCAL MECHANISM OF SMALL EARTHQUAKES PRIOR TO AN M_S 6.7 EARTHQUAKE IN THE CENTRAL ALEUTIANS

Selena Billington (CIRES, University of Colorado, Boulder, CO 80309)
E. R. Engdahl (U. S. Geological Survey, Box 25046, DFC, Denver, CO 80225)

A method has been developed to objectively composite, by computer, P-wave first motions from events occurring within a small source region. The method has been applied to earthquakes in the vicinity of an m_b 5.7 (M_S 6.7) shallow-focus earthquake that occurred on November 4, 1977 in the central Aleutians. The data are clear first motions (an average of six per earthquake) routinely recorded at stations of the Adak network for about 350 shallow-focus earthquakes which have m_b greater than about 2.7 and which occurred from August 1974 through June 1978. Although the coverage of the focal sphere for these earthquakes by the Adak network is not complete enough to permit the determination of absolute focal mechanism solutions, the method does distinguish between moderately different mechanisms. The most common mechanism is a thrust mechanism for which the strike of the nodal planes is roughly northeast; this mechanism is consistent with telesesimically determined mechanisms of larger thrust earthquakes in the central Aleutians. However, in the immediate vicinity of the hypocenter of the main shock and starting about 11 months before the main shock, the mechanisms of small events changed. The "precursory" mechanisms are thrust mechanisms for which the strikes of the nodal planes are rotated clockwise with respect to the typical mechanism by several tens of degrees. This change in mechanism coincides approximately in space and time with a increase in the rate of occurrence of small-magnitude earthquakes before the main shock; it is the second example of a precursory change in focal mechanism of small earthquakes before moderate earthquakes in the Adak region.

S 41

PRESEISMIC AND COSEISMIC STRESS ANOMALY ACCOMPANYING LYTLE CREEK, CALIFORNIA, EARTHQUAKE OF OCTOBER 19, 1979

B. R. Clark (Leighton and Associates, Inc., 17975 Sky Park Circle, Irvine, California 92714)

Anomalous readings from vibrating wire Stressmeters at San Antonio Dam on the Cucamonga fault, 60km east of Los Angeles, were recorded during the period September 27, 1979 through January 3, 1980 on three independent sensors installed 19m below the ground surface. On October 19, a minor earthquake (M =4.1) occurred at Lytle Creek, 15km northeast of the San Antonio Dam site. The Lytle Creek earthquake is suspected of being the source of the anomaly. However, two other earthquakes of interest also occurred during this period (Calexico, M =6.6, d=225km; Malibu, M =4.2, d=100km). The Lytle Creek earthquake was a right-lateral, strike-slip event on a small fault parallel to the northwest-trending San Jacinto fault. Readings taken on November 3 showed large changes on all three sensors, although the magnitude and sign of the changes were different on each, reflecting their different azimuthal orientations. At its maximum, the anomaly consisted of 2.4 bars compression in the N12°E direction and 1.2 bars decompression in the N78°W direction. By January 3, 1980, the sensor readings had all returned to their original long-term trend levels.

The anomaly detected at San Antonio Dam is a part of a record of approximately 2.5 years of consistently increasing stress levels (approximately 3 bars/year) in a north-south orientation. The minimum principal change (E-W) is also compressive. The long-term changes at San Antonio Dam are the largest of any of the four Stressmeter sites and are consistent in orientation with a stress pattern expected to induce thrust movement along the frontal faults at the southern edge of the San Gabriel Mountains, in a densely populated urban area.

S 42

THE AUGUST 25, 1979 LAKE JOCASSEE EARTHQUAKE AND ITS IMPLICATIONS ON RESERVOIR INDUCED EARTHQUAKES

Pradeep Talwani
D. Stevenson (both at: Geology Dept., Univ. of South Carolina, Columbia, S. C. 29208).

A magnitude 3.7 $m_{b(Lg)}$ (BLA) earthquake occurred at 09.31 p.m. (EST) on August 25, 1979 at Lake Jocassee. The occurrence of this event was a surprise in that, a) it was the largest event recorded at Lake Jocassee and occurred nearly four years after the start of the reservoir induced seismicity and b) it occurred when the seismicity level had dropped considerably. This event was deeper than earlier activity ($\sim$ 2-3km) and associated with normal faulting, whereas earlier activity at Lake Jocassee was associated with strike slip faulting.

Hydrofracture and overcoring stress measurements in the top 300m indicate very large horizontal stresses and stress gradients--both greater than the lithostatic gradient. However the observation of normal faulting at about 2 km depth indicates that at those depths the vertical stress is the largest principal stress. This implies that the large horizontal stresses are concentrated to small depths ($\sim$ 1 km?). This might explain the common occurrence of induced microearthquakes in the Piedmont and place a limit on the size of the reservoir induced earthquakes.

Seismic Source: Estimation of Stress Drop

Metropolitan East
Friday A.M.
A. T. Linde (Carnegie Institution of Washington), and *D. B. Larson* (Lawrence Livermore Laboratory), Presiding

S 43

A TECHNIQUE FOR HIGH RELATIVE ACCURACY IN THE DETERMINATION OF EARTHQUAKE STRESS DROPS

A. T. Linde (Dept. of Terrestrial Magnetism, Carnegie Institution of Washington, Washington, D.C. 20015)
R. Stefansson (Icelandic Meteorological Office, Reykjavik, Iceland)
I. S. Sacks (Dept. of Terrestrial Magnetism)

Estimates of stress drops have been made in numerous studies of far field radiation. The method most often employed is to use the seismic moment (from long period amplitude) and a corner frequency. Typically the results for stress drops show a large scatter. For complex source functions, however, corner frequency estimates do not necessarily give reliable measures of the source dimensions. Thus the large variations in stress drops may not be real.

We have been able to remove much of the scatter by using a variation of this technique. We estimate the moment in the standard manner but, rather than use corner frequencies, we calculate total radiated energy. The ratio of energy to moment then gives a measure of stress drop.

Records from the Carnegie broadband seismograph at Akureyri, Iceland have been used to apply this technique to several suites of earthquakes in northern Iceland. Estimates of radiated energy (for earthquakes in the magnitude range 3.5 - 4.5) were obtained by integrating over a frequency range (from a few tenths to several hertz) such that the integral converged. The method is sufficiently stable that, for small spatial groups of earthquakes, we are able to detect systematic temporal changes as small as a factor of 3 in the stress drops.

S 44

EFFECTIVE STRESS DROPS OF MODERATE EARTHQUAKES IN THE EASTERN ALEUTIANS

J. Mori (Dept. Geol. Sci. and Lamont-Doherty Geological Observatory of Columbia University, Palisades, NY 10964)

Estimates of the effective stress drop are calculated for 11 earthquakes of limited magnitude range (m_b = 5.1-6.1) but diverse tectonic settings in the eastern Aleutians. Effective stress drop represents the difference between initial stress and dynamic frictional stress. Digitization of the P arrivals from short period WWSSN records are deconvolved for instrument response and band passed filtered to obtain velocity and displacement seismograms. The effective stress is then proportional to the initial slope of the velocity plot.

Although a large scatter exists in the results, the following trends in the stress measurements can be recognized: intermediate depth earthquakes (100-150 km) have effective stress drop of 50-100 bars; normal-faulting events close to the trench have effective stress drops of 100-300 bars; shallow (10-40 km) earthquakes along the main thrust zone have varying stress drops of 50-500 bars, with the two high stress drop earthquakes located in areas which are relatively inactive seismically.

S 45

FOCAL MECHANISMS OF EARTHQUAKES NEAR THE NORTHEASTERN BOUNDARY OF THE CARIBBEAN PLATE

A.L. Kafka (Lamont-Doherty Geological Observatory of Columbia University, Palisades, New York 10964)

The tectonic processes and present day motion along the northern and northeastern boundaries of the Caribbean plate are not clearly understood. Although the northern boundary appears to be characterized by transform fault motion in the Cayman trough region, the region to the east of the Cayman trough between Hispaniola and the Lesser Antilles has many characteristics of a subduction zone. Within this northeastern region thrust faulting earthquakes, a deep trench, and negative gravity anomalies are found. Thus, this northeastern region does not conform to any simple concepts of plate boundary tectonic processes.

In this study focal mechanisms have been determined for four earthquakes in the northeastern region of the Caribbean plate. These results, combined with focal mechanism results of other investigators, suggest that the northeastern Caribbean can be divided into four distinct regions based on both geographical location and style of faulting. In the northern Lesser Antilles, thrust faulting earthquakes appear to have slip vectors which trend southwest, whereas for an easterly motion of the Caribbean plate we would expect slip vectors to be trending westward. Also, there is a region of dense seismicity slightly to the east of the Lesser Antilles for which we observe strike-slip faulting. In the region between Puerto Rico and the northern Lesser Antilles various types of earthquake focal mechanisms are observed, and the tectonic processes are complex. The Hispaniola region is characterized by two distinct types of thrust faulting earthquakes. Within this region some events have east striking fault planes, whereas others have north striking fault planes. These results are discussed in terms of the present day tectonic processes of the Caribbean plate.

S 46

STRESS DROPS OF SMALL EARTHQUAKES IN THE NORTHEASTERN CARIBBEAN

Arthur Frankel (Lamont-Doherty Geological Observatory and Department of Geological Sciences of Columbia University, Palisades, New York 10964)

The seismic moments and stress drops of 23 earthquakes ($1.2 \leq M \leq 2.4$) that occurred during an earthquake swarm in the Virgin Islands were determined from the analysis of their P-waveforms. The data consist of digitally-recorded seismograms collected by a short-period seismic network operating in the northeastern Caribbean. The events of the swarm are particularly useful for comparing the relative stress drops of small earthquakes, because of their similar source to receiver paths and focal mechanisms.

The digital seismograms were deconvolved to remove instrument response and yielded simple velocity waveforms and unipolar displacement pulses. The fault radius of each event was estimated from the rise time of the displacement pulse and the seismic moment was calculated from the area under the displacement pulse. The static stress drop was determined from these parameters. Estimates of the dynamic stress drops were obtained from the slope of the initial portion of the ground velocity waveform.

The stress drops calculated for these earthquakes varied from about 1 to 10 bars. The data clearly illustrate that both the static and dynamic stress drops of these earthquakes generally increased with the size (moment) of the events. The fault radii for these shocks increased with seismic moment, but only by a factor of 1.5 for a 10-fold increase in seismic moment. These observations imply that, for these small earthquakes, the final fault radius is a function of the stress drop that occurs during the rupture process.

S 47

SCALING MODEL OF EARTHQUAKE SOURCE SPECTRA FOR INTRAPLATE EARTHQUAKES IN JAPAN FROM 1926 TO 1977

Junji Koyama
Masayuki Takemura
Ziro Suzuki (all at: Geophysical Institute, Faculty of Science, Tohoku University, Sendai 980, Japan)

Source spectra of 163 major earthquakes in the lands of Japan and under the Japan sea are investigated. The magnitudes of those earthquakes are from 4.3 to 7.5, which are determined by Japan Meteorological Agency (JMA). M_{JMA} is determined from maximum amplitudes of seismic waves with period of about 4 sec, therefore M_s-M_{JMA} and M_{JMA}-m_b relations provide us with another information on the scaling of earthquake source-spectra being independent of the Gutenberg-Richter's relation between M_s and m_b. A scaling model of earthquake source-spectra, which is constrained by the relations among M_s, M_{JMA}, and m_b, is derived.

Further analysis is made to justify the present scaling model by introducing two new parameters; a characteristic period T_c and seismic-moment factor M_e. The former is defined as an average value of apparent periods of maximum amplitudes at many stations, and the latter is an average of products of maximum trace amplitude and its apparent period multiplied by epicentral distance. T_c is shown to relate somehow to the period of corner frequency and M_e the seismic-moment density at the period of T_c. M_e is well described to be proportional to the cube of T_c. This results may indicate the constant stress drop on the fault plane for earthquakes with M_s larger than 2.0. The present scaling model also satisfies the relation between seismic-moment densities at the period T_c and static seismic- moment independently determined, therefore, it is concluded that the source spectra with M_s larger than 2.0 are well described approximately by the present model.

S 48

FIRST ANALYSIS OF THE STATISTICAL DISTRIBUTION OF STRESS DROPS

M. Caputo, (Istituto di Fisica, Univ. di Roma, Italy)

The statistical analysis of seven sets of stress drops measured in seven different Earthquake's sequences or aftershock's series of scattered Earthquakes in Italy, Japan and California reveals that the density distribution function of stress drop p is nearly proportional to p^{-c_2} ($1 < c_2 < 2$). This may imply that a large amount of creep takes place in the process of accumulation of large stress drops or that there is a particular distribution of the direction of the faults with respect to that of the major tectonic force acting in the region.

S 49

BODY-WAVE SPECTRAL ANALYSIS OF AFTERSHOCKS OF THE MT. DIABLO-GREENVILLE EARTHQUAKE SEQUENCE, JANUARY 1980*

Keith K. Nakanishi
Howard J. Patton, (both at: Earth Sciences Division, Lawrence Livermore Laboratory, University of California, Livermore, CA 94550)

We have carried out a spectral analysis on P- and S-waves of selected aftershocks of the Mt. Diablo-Greenville earthquake sequence to measure corner frequencies, low frequency amplitude levels, and high frequency rolloffs. These events were recorded on our three-component short-period digital seismic network operating in the Livermore Valley within 40 km of the epicenters. The USGS local magnitudes of these events are between 1.2 and 2.7. Preliminary results are that (1) S-wave corner frequencies are higher than P-wave corner frequencies, (2) seismic moments, M_o, and local magnitudes, M_L, are related by the formula, $\log M_o = 1.2\ M_L + 16.8$, and (3) high frequency rolloff of S-wave spectra varies from -4.5 to -2.2 and appears to be correlated to epicentral distance. These results are discussed with respect to the regional dependence of moment-magnitude relationships and models of earthquake faulting.

S 50

EARTHQUAKE SLIP HISTORIES DERIVED FROM NEAR-FIELD STRAINGRAMS RECORDED ON SACKS-EVERTSON BOREHOLE STRAINMETERS

J. A. Snoke (Dept. of Geological Sciences, VPI&SU, Blacksburg, VA 24061)
A. T. Linde
I. S. Sacks (both at: Dept. of Terrestrial Mgnetism, Carnegie Inst. of Washington, Washington, D. C. 20015)
S. Suyehiro (Seismological Division, Japan Meteorological Agency, Tokyo, Japan)

Data from about 30 well-located, nearby earthquakes in the magnitude range 2-4.3 were recorded on a tripartite net of Sacks-Evertson borehole strainmeters installed in the Matsushiro region (Honshu, Japan). These strainmeters have a high sensitivity (better than 10^{-11} in strain), a large dynamic range and a frequency response of zero to a few hertz. Hence, information about both the static strain step and the dynamic rupture process can be obtained from these records: Such information provides constraints on the slip history for these earthquake.

We have modeled the Matsushiro-region events using synthetics. The program used for this study gives the response of a dilatometer installed at the free surface of a uniform elastic half space to a double-couple point source (with a variable time history) located within the half space. Analysis to date shows that some events have rise times of at most a few tenths of a second but rupture durations of several seconds. This result is consistent with the conclusion drawn by Hartzell & Brune (BSSA, 69 (1979), 1161-1173) that for even some relatively small earthquakes, the rupture process cannot be characterized by a single velocity of rupture propagation.

S 51

SOURCE PARAMETERS OF THE AFTERSHOCK SERIES OF THE PETATLAN, MEXICO, EARTHQUAKE OF 14 MARCH 1979 (M_S = 7.6)

J. Havskov
S.K. Singh
C.M. Valdés
F.R. Zúñiga (all at: Instituto de Ingeniería, UNAM, México 20, D.F., México)
R.P. Meyer (Geophysical & Polar Research Center, University of Wisconsin, Madison WI 53706)

About 50 selected events in the first 30 days of the aftershock series ($2.0 \leq M \leq 5.0$) locally recorded on 5 analog tape and up to 10 digital event recorders are being analyzed. The spectra of these events is providing insight into stress drops, corner frequencies, and the relation between seismic moment and magnitude.

S 52

A NEGATIVE SEARCH FOR AN ULTRA-LOW FREQUENCY COMPONENT TO THE MAY 29, 1976 YINAN EARTHQUAKES

Lisa M. Stewart (Dept. of Geology & Geophysics, Box 2161, Yale University, New Haven, Conn. 06520)
Emile A. Okal

Following Nagamune's[1977] claim of a giant but very slow component to the source of the 1976 Yinan [Yunnan] earthquakes, we have conducted a systematic study of the ultra-low frequency ($\nu \geq 1.25$ mHz) content of a number of tiltmeter, strainmeter and IDA records of the events.

In the time domain, only two records suggest the presence of a slow component in the seismic source, requiring a moment amplitude as large as 5×10^{29} dynes-cm. Such a large moment is incompatible both with the extent of the aftershock zone and results in the Fourier domain, where no systematic correlation is found between the observed energy spectrum and the Earth's normal modes. Furthermore, the fast decay of the low-frequency energy with time is inconsistent with known values of the Earth's attenuation, even when allowing for splitting.

We must therefore conclude that the apparent signal present in a few records is due to noise -- probably instrumental instability -- rather than to an ultra-low frequency seismic source.

S 53

SOURCE DIMENSION VERSUS RUPTURE PROPAGATION: A POTENTIAL DISCRIMINANT

Robert L. Sax (ENSCO, Inc., Alexandria, VA, 22314)
Rudolf Unger, (Universidad Nacional de Tucumán, Tucumán, Argentina)

Measurements derived from the instantaneous phase and frequency of Eurasian earthquake and presumed nuclear explosion signals were averaged over a number of world-wide stations. The results suggest a linear relationship between the instantaneous frequency and the amount of early multiple signals or pulse complexity. For a given pulse complexity, the frequency of the presumed explosion signals is higher than the frequency of the earthquake signals. The frequency is inversely related to source dimension. In a time frame of several seconds, the presence of early multiple signals may indicate complex rupture propagation. The relationship thus may reflect that in rupture propagating earthquakes the energy is released stochastically in relatively small parts. Ruptures of tectonic energy release forced by explosions then would appear to be smaller than earthquake ruptures. These relationships need to be verified with a larger, world-wide data base.

S 54

A LARGE NORMAL FAULT EARTHQUAKE IN THE OVERRIDING WEDGE OF THE ANTILLES SUBDUCTION ZONE: THE ANTIGUA EARTHQUAKE OF OCTOBER 8, 1974

J. W. Dewey (U.S. Geological Survey, MS 967, Box 25046, DFC, Denver, CO 80225)
W. R. McCann
A. J. Murphy (both at Lamont-Doherty Geological Observatory, Columbia University, Palisades, NY 10964)
S. T. Harding (U.S. Geological Survey, MS 966, Box 25046, DFC, Denver, CO 80225

A large earthquake (M_S = 7.1 - 7.6) occurred in the overriding wedge of the Caribbean plate on October 8, 1974. Hypocenters of locally recorded aftershocks suggest that the main shock rupture extended from a depth of 40 kilometers, immediately above the inferred thrust interface between the Caribbean and American plates, to shallow crustal depths of about 10 km. The focal-mechanism solution and aftershock hypocenter locations imply that the earthquake occurred on a southeast-dipping normal fault that strikes north-northeast to northeast, transverse to the regional strike of the northern Lesser Antilles arc. The location and focal mechanism of the 1974 shock are similar to those of small earthquakes occurring in the Adak Canyon region of the Central Aleutians and studied by LaForge and Engdahl (1979). Both the northern Lesser Antilles and the Central Aleutians are zones of oblique plate convergence, and normal faulting transverse to the island arc in the overriding wedge may be a consequence of this oblique convergence.

The position of the earthquake above the Benioff Zone and the normal fault focal mechanism of the 1974 earthquake indicate that the shock has not released a significant amount of the elastic strain thought to have been accumulating along the thrust boundary of this segment of the Lesser Antilles arc since the great earthquake of 1843.

LaForge, R. and E. R. Engdahl, Bull. Seism. Soc. Am., 69, 1515, 1979.

S 55

STUDIES OF SEISMIC SOURCE DECOUPLING USING SCALE MODEL EXPERIMENTS*

D. B. Larson (Lawrence Livermore Laboratory, Livermore, California 94550)
(Sponsor: Gordon D. Anderson)

Experimental free-field measurements made in a variety of scale-model experiments in Na Cl, are being analyzed to provide a better understanding of the processes involved in cavity decoupling. The available data are being transformed to reduced velocity potential in the frequency domain for convenience in making comparison. The results from small-scale experiments using LX04 explosive as the energy source are compared with results from the Cowboy series of field tests using pelletized TNT and with the Salmon and Sterling experiments using nuclear explosives. These experimental results are also compared with simple elastic theory and show significant deviations from the predictions of that theory.

Seismic Source: Systematic Inversion for Source Mechanism

Metropolitan East
Friday P.M.
R. G. North (MIT), and *L. Ruff* (California Institute of Technology), Presiding

S 56

ESTIMATION OF THE SEISMIC MOMENT TENSOR FROM TELESEISMIC BODY WAVE DATA WITH APPLICATIONS TO INTRAPLATE AND MANTLE EARTHQUAKES

T. J. Fitch (Applied Seismology Group, MIT Lincoln Laboratory, 42 Carleton Street, Cambridge, MA 02142)
D. W. McCowan (Marine Science Institute, University of Texas, 700 The Strand, Galveston, TX 77550)
M. W. Shields (Applied Seismology Group, MIT Lincoln Laboratory, 42 Carleton Street, Cambridge, MA 02142)

Amplitude data from direct and near source reflected phases, are inverted to obtain point-source moment tensors. The L1 norm is used as an optimum solution criterion thereby allowing first motions to be included in the data set. Long period P waves from an intraplate earthquake located between the Caribbean arc and the mid-Atlantic ridge at a depth of 25 km reveal a source with a moment time function in the far field that has rise and fall times of 2 ± 1 sec. By implication, the duration of faulting was short by comparison with shallow earthquakes of similar size at active plate margins. Approximately 89% of the total moment of 0.8×10^{25} dyne-cm pertains to a change in deviatoric stress, which is represented almost totally by a double couple. A 20% increase in the double couple component was achieved by a systematic steepening by 5 to 8° of take-off angles for ray paths to teleseismic distances. Amplitudes and first motion polarities from a deep earthquake beneath the Bonin arch yield a moment tensor that is 72% double couple and 19% compensated linear vector dipole. A similar steepening of the ray paths in this case consistent with a 7% reduction in the compressional velocity at the source depth results in a double couple component of more than 90%. Lateral heterogeneity in the source region precludes a simple interpretation of this apparent velocity reduction.

S 57

$P_{n\ell}$ WAVEFORMS IN SOURCE PARAMETER STUDIES

Terry C. Wallace (Seismological Laboratory, 252-21, California Institute of Technology, Pasadena, California 91125)
Don V. Helmberger, George P. Mellman, (All at Seismological Laboratory, California Inst. of Technology)

A technique has been developed for the inversion of the beginning portion of the vertical and radial seismograms containing P_n and P_L, the $P_{n\ell}$ phase, to determine source parameters. The method is designed for smaller events in which sufficient WWSSN teleseismic waveform data is not available. An error function of the form below is

$$e = 1 - \frac{\int f\, g}{\left(\int f^2\right)^{1/2}\left(\int g^2\right)^{1/2}}$$

calculated, where f is a long period seismogram, g is a synthetic, and the integral is a zero lag cross-correlation. An objective function, which is the sum of the squares of the error functions is minimized in terms of the three fault parameters. Although the system is non-linear, a simple iterative

technique is used to converge on the correct fault parameters. The method utilizes the fact that the synthetic is constructed with the three fundamental faults; the cross-correlations between the data and the three fundamental faults only has to be calculated once. This makes recalculating the error functions and partials for each iteration very fast, and the procedure is efficient. It is also possible to incorporate absolute amplitude information in the inversion depending upon the circumstances. Results from the application of this technique, using the Green's functions generated in an earlier paper, Helmberger and Engen (1980), to some west coast earthquakes are presented.

S 58

SURFACE-WAVE MOMENT TENSORS FOR EXPLOSIVE SOURCES

R. G. North (Applied Seismology Group, MIT Lincoln Laboratory, 42 Carleton Street, Cambridge, MA 02142)
T. J. Fitch (Applied Seismology Group, MIT Lincoln Laboratory, 42 Carleton Street, Cambridge, MA 02142)

A few presumed explosions in Eastern Kazakh exhibit large differences in surface wave radiation from those for the "average" explosion source in this region. These differences, as observed at 15-50 sec periods on digital SRO/ASRO seismograms, include enhanced Love wave generation and substantial azimuthal asymmetry and phase reversals of the Rayleigh waves. The short-period P-waves show little variation. We have attempted to quantify these differences in terms of the seismic moment tensor. The results do show moment tensor differences, particularly enhanced Mxy, but they are extremely difficult to interpret due to resolution problems which are fundamentally unavoidable for very shallow sources and furthermore aggravated by the clear undesirability of constraining $\Sigma M_{ii}=0$ for explosive sources.

S 59

USE OF IDA NETWORK FOR FAST DETERMINATION OF EARTHQUAKE SOURCE PARAMETERS

H. Kanamori (Seismological Laboratory, 252-21 California Institute of Technology, Pasadena, California 91125)

A method is developed to invert IDA (International Deployment of Accelerograph) data in terms of a seismic moment tensor (linear) and/or a dislocation (fault) source (nonlinear). Amplitude and phase spectra of multiple Rayleigh waves constitute the basic data. Although the formulation is valid only for a point source, the effect of the source finiteness is included, to the first order of approximation, by using the phase difference between the odd and even order Rayleigh waves. In order to minimize the effect of the regional variation of phase velocities, Rayleigh waves in a period range from 200 to 300 sec are used for inversion. The method works best for events with M_s between 6.5 and 7.5. In addition to its use for routine determinations of earthquake source parameters, the method is particularly useful for the analysis of slow earthquakes. The results obtained for a slow earthquake in the Bouvet Island region (December 18, 1978) will be reported. Since the method is very fast, it may also be incorporated in the on-line Tsunami warning system.

S 60

SIMULTANEOUS DETERMINATION OF SEISMIC MOMENT TENSOR AND HYPOCENTRAL PARAMETERS.

Teh-An Chou
Adam M. Dziewonski(Dept. of Geological Sci., Harvard University, Ma. 02138)

We have developed an efficient and stable method for routine determination of seismic source parameters. After an initial estimate of the moment tensor is obtained using the approach of Dziewonski(1978), an iteration procedure allows for simultaneous refinement of the elements of moment tensor, origin time, depth and epicentral coordinates of an earthquake. Appropriate differential kernels are synthesized by superposition of all overtones of normal modes with periods longer than 45 sec.(Buland, 1976). Filtered digital recordings from SRO and ASRO stations represent the input, the part of the records used in the analysis spans the time from the arrival of the P-wave until arrival of the surface waves, these are not included in the analysis because they are strongly affected by the lateral heterogeneity.

We have studied several earthquakes of M_b from 5.5 to 7.0 spanning range of depth from 10 to 600 km. Relocation resulted in changes of epicentral position with respect to PDE coordinates by as much as 130 km and over 30 km in depth, in extreme cases. Generally, the method is very stable(particularly the directions of the principal axes) and convergence is rapid. The following table gives the moments and directions of the principal axes of the moment tensor for a few of the analyzed earthquakes.

Date	Scale Fact.	T-axis Val	T-axis Dip/Az	N-axis Val	N-axis Dip/Az	P-axis Val	P-axis Dip/Az
03/07/78	10^{25}	4.0	52/58	0.0	9/160	-4.0	36/256
03/15/78	10^{25}	4.6	12/65	1.4	59/177	-6.0	27/328
10/01/78	10^{24}	5.4	74/76	0.0	0/167	-5.4	15/257
04/24/79	10^{25}	2.5	26/163	0.5	3/71	-3.0	64/336
09/06/78	10^{26}	1.9	67/143	0.0	22/320	-1.9	1/50

S 61

INVERSION FOR FAULT DISLOCATION USING TELESEISMIC BODY WAVES

Ivan H. Henson (Shell Oil Co., P.O. Box 831, Houston, TX 77001)
Charles A. Langston (Geosciences Department, Penn State University, Univ. Park, PA 16802)

Teleseismic P and S wave form data from the February 9, 1971, San Fernando earthquake was modeled using a linear inverse technique to obtain the distribution of dislocation on finite fault models. Fault geometry and rupture velocity were perturbed around a previously published two-fault segment model for the San Fernando earthquake. Fault planes were decomposed into discrete patches and the weights of each patch were found by a linear time-domain least-squares inverse technique. Results from the best fitting teleseismic models are in qualitative agreement with previous static and dynamic near-field studies; A gradual decrease in slip downdip, with an increase at the bottom of fault, is found. However, there are still significant differences in detail. In particular, the teleseismic moment is only 0.8×10^{26} dyne-cm, a factor of two smaller than the near field results. The inclusion of variable dislocation did not significantly improve the teleseismic body wave source model for the San Fernando data. It does, however, represent an additional tool for constraining and testing various hypotheses concerning the seismic source and may be used for seismic data any type.

S 62

PATH EFFECTS IN CONTINENTAL AREAS ON LONG PERIOD RAYLEIGH WAVES AND THE MOMENT TENSOR INVERSION METHOD

B.A. Romanowicz (Massachusetts Institute of Technology, Cambridge, MA 02139 and IPG, 4 Place Jussieu, 75230, Paris, France)

The moment tensor inversion method for long period Rayleigh waves seems to be successful for the determination of depth and mechanism of moderate size earthquakes (mb: 5.0 to 6.0) if the propagation effects can be accurately corrected for. This has been demonstrated for mid-ocean ridge events (Tréhu et al., 1979). For events located in the middle of complicated continental areas, a more involved iterative method has to be used (Patton, 1978).

We are here investigating the influence of path effects on the moment tensor inversion for events located in Central Asia, taking as a reference the average phase velocities determined by Patton. We have studied several earthquakes situated 1000 to 2000 km away from Patton's reference point, for which well constrained fault plane solutions are available. It appears that, although the phase velocities have to be known accurately, the critical factor in the success of the moment tensor inversion is rather the matching of observed and theoretical amplitudes. Thus, an accurate depth and mechanism determination can be achieved for pure strike slip events, for which the depth signature in the amplitude spectrum appears as a strong minimum, in most cases at periods greater than 20 sec, and in all azimuths. For events with a larger dip slip component, the success of the inversion is strongly limited by the available period range (~20 to 90 sec), the azimuthal distribution of stations and the difficulty to model multipathing and focussing effects on amplitude. Based on these results, the most promising approach is to determine the path effects using pure strike slip events and then apply the moment tensor inversion to a more general class of seismic sources.

S 63

SHORT PERIOD WAVEFORM INVERSION FOR SOURCE TIME FUNCTIONS

Larry Ruff, Seismological Laboratory, Caltech, Pasadena, CA 91125
George Mellman, Sierra Geophysics, 150 N. Santa Anita, Arcadia, CA 91006

The waveforms of underground nuclear tests recorded at WWSSN short period stations are quite coherent, maintaining similar peak to peak amplitude ratios despite a large variation in the absolute amplitudes. These waveforms have been successfully modeled with synthetic seismograms, primarily dependent upon the source time function and attenuation. Our objective is to devise a formal inversion procedure for the determination of the source function. As a purely time domain method is preferable, the waveforms are characterized by their most obvious features: the relative peak amplitudes and peak times. The source time function is represented in a two parameter functional form plus the pP-P time delay. In general, inverting for source functions is a non-linear process. Thus, the theoretical properties of this inversion scheme have been investigated with the main results, (i) with modest damping, there is a consistently stable approach to the near-vicinity of the answer, (ii) errors in the attenuation (t*) affect the result in a smooth predictable manner, (iii) surprisingly, the pP-P time is well resolved in all cases. The procedure works well theoretically, however, investigations with actual data have demonstrated the sensitivity of model results to data errors. Therefore, the major restriction on the accuracy of this method is the quality of the data. For the events tested thus far some have yielded good results; an excellent agreement between the synthetic seismogram and the data, and the source parameters are well resolved. In other cases in which the source parameters are not well resolved, the mismatch between synthetic and data is generally in the latter part of the waveform, particularly in the last downswing.

S 64

SOURCE PARAMETER INVERSION OF A RESERVOIR-INDUCED EARTHQUAKE: LAKE KARIBA, AFRICA, 23 SEPTEMBER 1963

Gregory B. Pavlin (Dept. of Geosciences, Penn State University, University Park, PA 16802)
Charles A. Langston

Source parameters of the largest induced earthquake associated with the impoundment of Lake Kariba (09:01:56.8 GMT, 23 September 1963) were determined utilizing a moment tensor formalism of the generalized inverse technique. Inversions for both purely deviatoric and dislocation point source parameters were accomplished with long and short period body wave data from the World-Wide Standard Seismic Network. The source of the earthquake was inferred to be a normal fault with the parameters: $m_b = 6.3$; $M_S = 6.1$; strike = 193±8°; dip = 53±2°; rake = 270±4°; depth = 8±0.5 km; skewed-triangular source time function of 2.5±0.5 sec; moment = 5.0×10^{24} dyne-cm; radial fault plane dimension of 6.±1.0 km; and a stress drop range of 8 to 20 bars. The hypocenter was relocated to 16.7°S - 28.6°E using P and S arrivals from four African stations(WWSSN). This location coincides with the region of known foreshocks and aftershocks. The location also coincides with an intersection of some major mid-Zambezi Valley faults, trending N50°E, with lineaments mapped from LandSat multispectral imagery, trending N20°W to N40°W. Photo-interpretation resulted in the mapping of over 400 lineaments which principally transect the previously known faults of this rift valley. The lineaments may be linked with the Precambrian Katangan Metamorphism(800 Myrs), and in some areas, may be related to Jurassic dolerite dykes. A more complicated tectonic history of the region is inferred. Besides having a potentially significant role in the seismicity of the region,

these lineaments, and their intersections with known faults, may well have an impact upon future mineral exploration in the region.

S 65

SURFACE DEFORMATION AND AFTERSLIP ASSOCIATED WITH THE LIVERMORE VALLEY, CALIFORNIA, EARTHQUAKES OF 24 AND 26 JANUARY, 1980

D.P. Schwartz
K.J. Coppersmith
A.P. Ridley (all at: Woodward-Clyde Consultants, Three Embarcadero, Suite 700, San Francisco, CA 94111)

Coseismic surface rupture was observed along the Greenville fault following earthquakes on 24 Jan. (M5.5) and 26 Jan. (M5.2, USGS; M5.8, U.C. Berkeley). Well-defined first event deformation occurred 8 km southeast of the instrumental epicenter along a 6.5-km-long zone containing two, and possibly five, surface traces. Rupture was continuous in the northern 1.4 km of this zone where approximately 3 cm of right slip was measured across two fault traces in Tertiary sandstone terrane; the southern 5.1 km contained discontinuous en echelon cracks, plus cracks of problematic origin in asphalt pavement, developed mainly in Quaternary alluvium. Second event deformation was concentrated in the southern portion of the zone; existing individual cracks lengthened and widened, numerous new cracks appeared in pavement, and the northern rupture extended .5 km to the south.

Monitoring of ground cracks through 27 Feb. indicates afterslip on fault traces in both bedrock and alluvium. Right slip on a prominent fault trace in alluvium was perceptable on 30 Jan., increased to 2 mm (5 Feb.), 4 mm (10 Feb.), and 7 mm (27 Feb.). Monitoring is continuing.

Ground cracks observed on the conjugate Las Positas fault prior to the second event have increased in number and length through 27 Feb., suggesting concurrent slip during the first event and continuing strain release along this fault.

S 66

RECENT LARGE EARTHQUAKES ALONG THE MIDDLE AMERICA TRENCH AND THEIR IMPLICATIONS FOR THE SUBDUCTION PROCESS

Eric P. Chael
Gordon S. Stewart (both at Seismological Laboratory, 252-21, California Institute of Technology, Pasadena, California 91125)
Krishna Singh (Instituto de Geofisica, Ciudad Universitaria, U.N.A.M. 20, D.F. Mexico)
Karen McNally (Seismological Laboratory, California Institute of Technology, Pasadena, California 91125)

Several large shallow earthquakes (M_s > 7.0) have occurred along the Middle America Trench since the installation of the WWSSN network. Included are the 1965, 1968, and 1978 Oaxaca events, the 1970 and 1973 events, and the 1979 Petatlan event. These earthquakes have been studied in an attempt to identify similarities and differences between them that may lead to a better understanding of fracture and subduction processes. The events have seismic moments ranging from 3.2×10^{27} dyne-cm for the 1978 Oaxaca event to less than half of this for the 1968 event. All events are of predominantly thrust type, consistent with subduction to the northeast of the Cocos plate. Body waves of the 1965, 1968, 1978 and 1979 events along the trench indicate rather simple faulting processes. These events all had focal depths of 15 - 20 km and stress drops on the order of 10 bars. Similarities which Ohtake, Matumoto, and Latham (1977) identified in the precursory seismicity of events along the Middle American Trench thus appear to continue through the mainshock and aftershock sequences. The 1970 and 1973 events, the eastern- and westernmost, respectively, of the events studied here, show greater complexity in their body waves, perhaps representing the transition to regions with more complicated tectonics.

S 67

EVIDENCE FOR ANOMALOUSLY DEEP SLIP PRIOR TO A MAJOR OCEANIC TRANSFORM EARTHQUAKE

James L. Muller
Wai-Ying Chung
Sean C. Solomon (Dept. of Earth & Planetary Sciences, M.I.T., Cambridge, MA 02139)

It is generally held, on the basis of reliable depth determinations and moment vs. slip relationships, that the earthquake generation zone on most oceanic transform faults is confined to shallow depths (upper 5-10 km). We present evidence that some slip at substantially greater depth (40-50 km) is associated with an earthquake on the Gibbs transform fault in the north Atlantic. The M_S = 6.9 earthquake of 16 October 1974 was preceded by a foreshock 8.5 minutes earlier and by a 'precursor' event several seconds before the main shock (Kanamori and Stewart, 1976). Relative locations of these events show the first two to be 45 to 50 km deeper than the main event. A moment tensor inversion of the Rayleigh waves from the foreshock shows possible solutions at 10 km and at 45 km depth. The solution obtained at 10 km depth, however, shows left-lateral fault motion with a substantial dip-slip component, while the solution at 45 km depth shows right-lateral fault motion compatible with the transform geometry and the mechanism of the main event and is therefore preferred. This latter solution yields a double couple scalar moment of 1.0×10^{24} dyne-cm. Synthetic P-wave seismograms constructed for the precursor show that both 10 and 45 km depth are compatible with the observed waveforms. The fault plane solutions obtained from the foreshock moment tensor inversion, the precursor P-wave amplitudes and a comparison of the short period P waveforms for the foreshock and precursor all show right-lateral motion on a fault with azimuth slightly greater than the 95° strike of the transform. This solution is also compatible with P-wave first motions reported by Kanamori and Stewart (1976) for the main shock.

S 68

SOURCE PARAMETERS OF THE OCT. 15, 1979 IMPERIAL VALLEY EARTHQUAKE FROM NEARFIELD OBSERVATIONS

Ralph J. Archuleta (USGS, M/S 77, 345 Middlefield Road, Menlo Park, CA 94025)
Robert V. Sharp (USGS)

On Oct. 15, 1979 the Imperial fault slipped right-laterally at the time of the Imperial Valley earthquake (Ms=6.9). The epicenter was 6.5 km south of the U.S.-Mexico border, but visible surface slip on the Imperial fault begins 3.9 km north of the border and extends northward for 30 km. As of Nov. 7, 1979, right lateral surface slip averaged 34 cm; a maximum slip of 80 cm occurred 9 km north of the border. Using an average shear modulus of 2.0×10^{11} dynes/cm^2, density of 2.7 gms/cm^3 and a depth of 8 km, we determined a moment Mo=1.6×10^{25} dyne-cm for the 30 km segment. If we include the 10 kms between the epicenter and the observed slip, Mo=2.2×10^{25} dyne-cm. From the average slip we estimate a static stress drop of 54 bars--a lower limit.

Twenty-five accelerometers operated by the USGS were located within 22 km of the surface trace. Two of the stations--El Centro 6 and 7- are on opposite sides of the fault but within .8 km of the fault. Using the difference in the parallel component of particle velocity (26 cm/sec) after the rupture front, we derive an effective stress drop of 25 bars. Using the absolute time on the accelerograms, the location of the epicenter and the character of the particle velocity for stations 6 and 7, we estimate a rupture velocity of 2.25 km/sec, .86 the average shear wave speed in the upper 10 km of the crust. Based on directivity of a unilateral rupture, this velocity predicts a ratio of peak SH particle velocity of station 6 to Bonds Corner station of 2.54; the observed ratio is 2.47.

S 69

BROAD-BAND TIME DOMAIN MODELLING OF EARTHQUAKES FROM FRIULI, ITALY

Cipar, John (Seismological Laboratory, California Institute of Technology, Pasadena, California 91125)

Short and long-period teleseismic body waves and surface waves from two earthquakes of the Friuli, Italy sequence are interpreted in terms of source properties. Both events occurred on September 15, 1976: at 03h 15m (M_s = 6.0) and at 09h 21m (M_s = 5.9). All the data for the earthquake at 09h 21m can be adequately explained by a single model. Time domain modelling of SP records suggests a model consisting of two point sources, separated by 1.3 sec. (1st source: depth (h) = 7.5 km, duration (t_c) = 1.65 sec, seismic moment (M_o) = 0.17×10^{25} dyne-cm; 2nd source: h = 6 km, t_c = 2.3 sec, M_o = 0.55×10^{25} dyne-cm). The focal mechanism for both sources is: strike = 56°, dip = 67°S, rake = 70°. LP body waves agree in moment and waveform with this model. The moment estimated from surface waves is somewhat larger: $1\text{-}1.5 \times 10^{25}$ dyne-cm. SP records for the 03h 15m shock can be fit quite well by a model with two sources separated by 2.1 seconds. (1st source: h = 3.8 km, t_c = 1.75 sec, M_o = 0.24×10^{25} dyne-cm; 2nd source: h=4.2 km, t_c = 1.5 sec, M_o = 0.12×10^{25} dyne-cm). The focal mechanism for both sources is: strike= 230°, dip = 60°N, and slip = 133°. The total M_o is 0.36×10^{25} dyne-cm from SP body waves, while surface waves yield a moment of $1\text{-}1.5 \times 10^{25}$ dyne-cm. Although the LP body waves of the 03h 15m shock are obscured by noise, they do not appear to agree with the SP model quoted above in that they seem to require a source of longer duration and larger M_o. These observations suggest differences in source spectra between the two earthquakes. For the 09h 21m earthquake, the spectrum appears to be essentially flat from the SP body wave to surface wave band. On the other hand, the spectrum of the 03h 15m shock has more energy in the surface wave band relative to the SP body wave band.

Attenuation: Measurements and Interpretation

Pier 5
Saturday A.M.
E. R. Kanasewich (Univ. of Alberta) and *M. L. Smith* (Univ. of Colorado), Presiding

S 70

IN-SITU MEASUREMENT OF ABSORPTION AND DISPERSION IN SEDIMENTARY ROCKS

E.R. Kanasewich (Department of Physics, University of Alberta, Edmonton, Alberta, Canada T6G 2J1)
D.C. Ganley (Union Oil Company of Canada, P.O. Box 999, Calgary, Alberta, Canada T2P 2K6)

The spectral ratio method for measuring absorption and also dispersion from seismic data has been examined. Corrections for frequency dependent losses due to reflections and transmissions have been shown to be an important step in the method. Synthetic examples have been used to illustrate the method and the method has been applied to one real data case from a sedimentary basin in the Beaufort Sea. Measured Q values were 43±2 for a depth interval from 549 to 1193 meters and 67±6 for a depth interval of 945 to 1311 meters. Dispersion was also measured in the data and is consistent with Futterman's model.

S 71

LATERAL VARIATION OF SURFACE-WAVE ANELASTIC ATTENUATION ACROSS THE ATLANTIC OCEAN

J.A. Canas (Department of Earth & Atmos. Sci., Saint Louis University, St. Louis, MO 63156)
B.J. Mitchell

Fundamental-mode Rayleigh waves generated by several earthquakes situated along great-circle paths between pairs of seismograph stations on the American and European coastal regions and on Atlantic islands have been analyzed to obtain anelastic attenuation coefficients, group and phase velocities, azimuthal anisotropy coefficients, and specific quality factors. Inversion of the dispersion and attenuation data yield shear velocity models and shear wave internal friction models for several regions of different age in the Atlantic Ocean.

The results obtained in this study are that (1) the anelastic attenuation coefficients and internal friction are related to the age of the

Atlantic Ocean floor, older regions being characterized by higher Q values, (2) a low-Q zone is well developed in the upper mantle of all regions less than 65 m. y. in age, but is poorly developed in older regions, (3) comparison of the results of this study with earlier results for the Pacific Ocean indicate that the anelastic attenuation coefficients and the Q_β^{-1} values for the ridge region of the Atlantic Ocean are much smaller than for the East Pacific Rise. For regions of similar age in both oceans, the attenuation coefficients and Q_β^{-1} values are smaller for the Atlantic than for the Pacific. Inversion of the attenuation data suggest that the low-velocity, low-Q zone under the Atlantic Ocean floor is more poorly developed there than beneath the Pacific. Since plates separate more slowly in the Atlantic than in the Pacific this comparison suggests that the velocity of plate motion is slower when attenuation coefficients and internal friction values are smaller. The Rayleigh wave velocities and shear wave models support the results of earlier workers who found little influence of the Mid-Atlantic ridge on the Rayleigh velocities.

S 72

ELASTIC AND ANELASTIC EARTH STRUCTURE FROM LINEARIZED INVERSION OF WAVEFORM DATA

A.M. Dziewonski (Dept. of Geological Sciences, Harvard University, Cambridge, MA 02138)

If the differences between a starting model and the real Earth are small, it is possible to interpret the discrepancy between the observed and predicted waveforms in terms of perturbations in the Earth's structure. Let F_n represent the spectrum of the nth orbit wavegroup, for example R_3, and F_{n+2} the spectrum of a wavegroup that travelled one additional circumference. The objective is to determine $F_2 = \exp[-2\pi i a k(\omega)]$ such that $F_n \cdot F_2 = F_{n+2}$; where $k(\omega)$ is the complex wavenumber, a functional of the elastic and anelastic parameters of the Earth's structure. Given F_2^0 computed for the starting model, we linearize the problem and request that

$$\omega_1 \int^{\omega_2} | (F_{n+2} - F_n \cdot F_2^0) - F_n \cdot \delta F_2^0 |^2 \, d\omega = \min.$$

The perturbation in the j-th iteration: $\delta F_2^{(j)} = -2\pi i a \delta k^{(j)}(\omega) \cdot F^{(j-1)}$ is expressed in terms of changes in the Earth's structure:

$$\delta k^{(j)}(\omega) = \int_0^1 \underline{G}(r,\omega) \cdot \delta \underline{m}^{(j)}(r) dr$$

where $\underline{G}$ are the differential kernels and $\underline{m}$ represents the set of elastic and anelastic parameters. The inverse is heavily damped as the total perturbation in $k(\omega)$ can be quite large; F_2 is recomputed after each iteration.

Tests of the algorithm on synthetic data with and without noise indicate that it is convergent and that it yields satisfactory results even when the traditional methods of measuring attenuation and dispersion fail. The reason is that by tying the perturbation in F_2 to the Earth's structure we apply a powerful filter that rejects incoherent noise. The method is particularly well suited to routine processing of digital data and its application should result in greatly improved estimates of attenuation and dispersion of mantle waves in a broader frequency band.

S 73

A NEW APPROACH TO MEASUREMENTS OF DISPERSION AND ATTENUATION OF MANTLE WAVES

J.M. Steim and A.M. Dziewonski (Dept. of Geological Sci, Harvard Univ, Cambridge, MA 02138)

The perturbation technique described by Dziewonski (this issue) can be applied to the analysis of arbitrary length records of earthquakes rather than, as it is traditionally done, to individual pairs of wavegroups. If the transfer function corresponding to a single traverse of a mantle wave around the globe is $f_2(t)$, then convolution of a seismogram s(t) with f_2 shifts all the wavegroups by one complete orbit. This is illustrated in the diagram:

s(t)	R_2	R_3	R_4	R_5	R_6	R_7		
$s(t)*f_2(t)$			R_4	R_5	R_6	R_7	R_8	R_9
difference	R_2	R_3	0	0	0	0	$-R_8$	$-R_9$
		t_1				t_2		

Thus, if $f_2(t)$ is the transfer function for the real Earth, the difference trace should be null from t_1 to t_2. A conservative estimate of t_1 is the circumferential group travel time at the minimum group velocity (approx. 3 hours for mantle Rayleigh waves, for example); t_2 is simply the time at which the record terminates. Given $f_2(t)$ for a starting Earth model, we linearize the problem and impose the least squares condition

$$\int_{t_2}^{t_1} \{[s(t) - s(t)*f_2^0(t)] - s(t)*\delta f_2(t)\}^2 dt = \min.$$

Transformation of the equation above to the frequency domain reduces the problem to that described by Dziewonski with the advantage that the need for isolation of individual wavegroups is eliminated.

In the search for regional differences in attenuation and dispersion, we apply this method to analyze recordings from the IDA and SRO networks; the details will be presented at the meeting.

S 74

DETERMINATION OF Q FOR LOW ORDER SPLIT NORMAL MODES - INVERSION IN THE FREQUENCY DOMAIN

Michael G. Schnapp (CIRES, Univ. of Colo./NOAA, Boulder, COLO. 80309)
(Sponsor: Charles B. Archambeau)

Inversion of spectra derived from high quality, very-long period records of large earthquakes for the Q of low order normal modes has been conducted in an effort to add to the sparse reliable estimations of Q that have been made in previous investigations. The problems in determining Q of low order normal modes arising as a result of the frequency splitting of these modes have been dealt with by incorporating an inversion process that performs a least squares fitting of the actual complex amplitude spectrum with that of an ideal damped split-mode oscillator. Tests of the inversion technique consisting of superimposing noise derived from real seismograms on the synthesized time series of damped split-mode oscillators indicate that the values obtained from the inversion accurately reflect the actual Q. These test results, together with the exceptional fits of both the complex amplitude spectra and the time series envelope functions when the inversion technique is applied to real data from large earthquakes, suggest that the values of Q so obtained are reliable (for the 1960 Chilean earthquake, Q's determined for the 0S2, 0S3, and 0S4 modes are 436, 155, and 152, respectively).

In addition to finding Q, the inversion method, also, yields estimations of the complex excitation amplitudes of the singlet modes of oscillation within the multiplet of modes for each normal mode inverted. These amplitudes can then be used to investigate source properties.

S 75

ANALYSIS OF SPLIT NORMAL MODES FOR THE 1977 INDONESIAN EARTHQUAKE

Seth Stein, Jeffrey A. Nunn (Department of Geological Sciences, Northwestern University, Evanston, IL 60201

The longest period spheriodal modes, ${}_0S_2$-${}_0S_5$, are well recorded on IDA gravity meter records of the August 19, 1977 (Ms 7 3/4) Indonesian earthquake. We model these modes, which are split into singlets by rotation and ellipticity, using time domain synthetics. These synthetics explicitly include the effects of source and station location and fault geometry.

In addition to matching the time domain singlet interference patterns, we also use this data to measure the attenuation of these longest period modes. Due to the difficulties in measuring Q^{-1} for these split modes, and the fact that previous measurements were made on the older Chilean and Alaskan earthquake data, the uncertainty in previous values is rather large. It is desirable to reduce this uncertainty in view of the special significance of these modes for lower mantle attenuation structure. We measure Q^{-1} using both time domain and frequency domain fits to the computed synthetics.

S 76

SIMULTANEOUS ESTIMATION OF TERRESTRIAL EIGENVIBRATIONS

Roger A. Hansen (Seismographic Station, University of California, Berkeley, Calif. 94720)

Recently, time domain methods have been shown to be advantageous in determining the quality of observations of terrestrial eigenvibrations. Complex demodulation has successfully been used in estimating amplitude, period, decay constant Q, and phase for various spheroidal and torsional modes. Non-linear regression in the frequency domain yields formal uncertainties in each estimate. A crucial problem arises in isolating neighboring modes of nearly the same frequency and comparable amplitude. Complex demodulation displays can be used to identify such interferences as beating. In such cases, the assumption of stationarity is violated in the regression analysis yielding biased results. Improved resolution has now been made by formulating the regression scheme to estimate simultaneously small sets of neighboring spectral peaks so that stationarity is not violated. Computed values can be shown to be best estimates in a statistical sense. An analysis of variance yields the covariance matrix of the solution. This provides estimates of the correlations between spectral parameters. The procedure has been applied to seismograms recorded following the August 1977 Indonesian Eq. (M_S=8.0 BRK). The time series used were recorded by a network of broadband (to 100sec) displacement seismometers located in Northern California, and by seven gravimeters of the world wide IDA network. A representative example of the simultaneous estimation of two adjacent modes is for the neighboring modes of ${}_0S_{11}$ and ${}_2S_7$ recorded at the Halifax station of the IDA network. These modes were previously unresolvable by complex demodulation of the above data. The Fourier amplitude spectrum shows a single broadened peak with period 535.53 ± .175 and Q of 572 ± 214 when fit with one mode. A more satisfactory result is obtained when fitting two modes. The estimates of period are 537.98 ± .152 sec and 535.11 ± .143 sec, and for Q are 234 ± 31 and 216 ± 25, respectively.

S 77

VARIATIONS OF ANELASTIC ATTENUATION IN THE MANTLE UNDER THE UNITED STATES - A SYNTHESIS

Z. A. Der
T. W. McElfresh, A. O'Donnell and B. W. Barker (all at: Teledyne Geotech, 314 Montgomery St., Alexandria, Virginia.)

Studies of teleseismic P and S wave amplitudes and spectra in the short and long period bands show that large lateral variations exist in the attenuative properties of the upper mantle under the United States. The existence of high frequency energy in the short period teleseismic P and S waves observed (4 Hz for P and 2 Hz for S from deep events) in the north central, shield areas of the U.S. can only be explained by a high Q upper mantle. Such high frequency energy is much reduced or undetectable in most of the southwestern U.S. Besides these major contrasts, details in regional variations of upper mantle Q are presented. The regional variations in Q also show a good correlation in details with a large number of related geophysical variables. All observations can be explained with freuqency and regionally dependent Q_α and Q_β with most of the anelastic losses occurring in shear deformation.

S 78

MANTLE Q_S FROM BODY WAVES - DIFFICULTIES IN DETERMINING FREQUENCY DEPENDENCE

I. S. Sacks (Dept. of Terrestrial Magnetism, Carnegie Institution of Washington, Washington, D.C. 20015)

There have been a number of studies of Q_S for the earth's mantle covering a period range from hundreds of seconds (free earth oscillation decay) to less than a second. These results have been compared to determine a frequency dependance for Q. There are, however, difficulties, particularly at the shorter periods. Because Q_S is low (~200-300), periods of 1 s. or less are heavily attenuated relative to the longer periods. Linearity of the seismograph (particularly of the recording medium) limits the detectability of short period components. Non-linearity results in an overestimation of the short period energy.

By analysing data from magnetic tape recording seismographs (magnification peaking at 6 Hz), we obtained reliable ScS data up to about 1.5 Hz. From the spectral ratio of ScS/ScP, we determine the Q_S for the mantle without having to assume the source spectrum. Over a frequency range of 0.3 to 1.5 Hz, the

Q_μ (~250) is not significantly different from the values determined from multiple ScS observations in the 10 - 60 millihertz range or from the free oscillation results.

It is concluded that these data do not require a frequency dependent Q.

S 79

ANELASTICITY NEAR THE INNER CORE BOUNDARY

V.F. Cormier (Dept. of Geological Sciences, Harvard University, Cambridge, MA 02138)

Short period seismograms are synthesized for PKP phases in anelastic earth models having real velocity profiles given by the PEM models. The synthetics were constructed using a synthetic technique valid at grazing incidence, a source time function appropriate for deep focus earthquakes, and an instrument response for a short period WWSSN seismograph. The synthetics illustrate that at a velocity increase the T-Δ cusps inferred from amplitude data are affected considerably more by anelasticity on the upper side of a discontinuity rather than by the anelastion the lower side of the boundary. A comparison of the frequency content of the observed and synthetic PKP phases requires either one of two types of Q distributions to exist near the inner core boundary (ICB): (1) a thin low Q zone just below the ICB, or (2) a thin low Q zone on both sides of the ICB with Q^{-1} 1.5 times larger below the ICB than Q^{-1} above the ICB. In both classes of models the thinness of a low Q zone trades off with the intensity of attenuation, e.g., a Q of 200 in the upper 200 km of the inner core fits the observed spectral ratios and time domain amplitudes as well as a Q of 130 in the upper 100 km of the inner core. Class (1) models fit both amplitude and spectral ratio data well and are consistent with the P velocity, S velocity and density jumps of the PEM models at the ICB. Class (2) models, however, require a larger impedance contrast at the ICB than that given by the PEMs. In order that class (2) models fit both low (0.08 Hz) and high (1.0 Hz) frequency body wave data, they must be associated with dispersive elastic moduli at the ICB such that the P velocity jump is larger and/or the S velocity jump smaller at the ICB at 1 Hz than at 0.08 Hz. A comparison of low frequency (0.08Hz) and high frequency (1.0Hz) body wave data suggests that the ICB is sharp and its position is frequency independent. Body wave data in the 0.08-2.0 Hz band cannot resolve any frequency dependence of the anelasticity of the inner core.

S 80

THE FREQUENCY DEPENDENCE OF Q_μ IN THE MANTLE

Gordon N. Shudofsky
F. A. Dahlen (Both at: Department of Geological and Geophysical Sciences, Princeton University, Princeton, N. J. 08544)

Recent analyses of the period and Q of the Chandler wobble have indicated that the shear attenuation of the mantle may exhibit a weak frequency dependence between the middle of the normal mode band and 14 months. If this dependence is of the form $Q_\mu \sim \omega^\alpha$, an α between 0.05 and 0.2 in the lower mantle, where the Chandler strain is concentrated, is most consistent with the data. Recently acquired high-quality Q observations of selected normal modes recorded by the IDA network, together with the recent long- and short-period Q_{ScS} observations of Sipkin and Jordan, have made it possible to search for a frequency dependence of this magnitude within the seismic band itself. In this paper, we shall investigate whether the Chandler wobble results are consistent with this latter set of data, and whether and to what extent Q_μ in the upper mantle may be similarly frequency dependent.

S 81

ANELASTICITY AND THE CHANDLER WOBBLE

Martin L. Smith (Cooperative Institute for Research in Environmental Sciences, Univ. of Colorado/NOAA, Boulder, Colorado 80309)
F. A. Dahlen (Department of Geological and Geophysical Sciences, Princeton University, Princeton, New Jersey 08540)

We have extended the calculation of the theoretical Chandler eigenfrequency to account for the nonhydrostatic portion of the Earth's equatorial bulge and for the effects of mantle anelasticity upon the period and Q of the wobble. The latter calculation uses small parameter perturbation theory for rotating continua and is rigorously correct. We find that if the wobble is wholly dissipated by mantle shear dissipation, and if Q_μ is the uniform Q of mantle shear at 14 months and Q_0 is the Q of the Chandler wobble, then

$$Q_0 = 1.8 Q_\mu$$

for model 1066A. If we adopt the Q model B of Sipkin and Jordan (1980) and assume that Q varies with frequency as ω^α between 30 seconds and 14 months, then the theoretical Chandler period and Q fall within the 68 per cent confidence intervals of Wilson and Haubrich (1976) if

$$0.002 \leq \alpha \leq 0.09 ,$$

while the Q model QM1U of Sailor and Dziewonski (1978) leads to

$$0.11 \leq \alpha \leq 0.19 .$$

In all cases the limits arise from exceeding the uncertainty in observed period.

S 82

NONLINEAR DISSIPATION MECHANISMS - EVIDENCE FROM EARTH TIDES

Duncan Carr Agnew (Cooperative Institute for Research in Environmental Sciences, Univ. of Colorado/NOAA, Boulder, Colorado 80309)

To explain the apparent frequency independence of Q in rocks, several investigators have proposed that the dissipation mechanism is nonlinear, perhaps involving friction. A consequence of such a nonlinearity is that for a sinusoidal applied stress the strain will contain higher harmonics of the driving frequency. For the kinds of hysteresis loop usually proposed only odd harmonics are produced. The semidiurnal earth tide stresses the Earth sinusoidally, with peak strains of 10^{-8}. I have looked for harmonics of this tide in a 5-year record of tidal strains from one of the laser strainmeters at the Pinon Flat Observatory in southern California. The third harmonic (M_6 tide) has an amplitude of 1.2×10^{-12}, not significantly above the noise. This measured amplitude means that the harmonic must be 80 dB below the fundamental (M_2). For seismic values of Q, most nonlinear models of dissipation predict a larger third harmonic and so would seem to be ruled out by this observation.

S 83

SEISMIC Q OF THE UPPER MANTLE OF THE MOON

Yosio Nakamura (Galveston Geophysics Laboratory, Marine Science Institute, The University of Texas, Galveston, Texas 77550)
Junji Koyama (Galveston Geophysics Laboratory, Marine Science Institute, The University of Texas, Galveston, Texas 77550 and Geophysical Institute, Tohoku University, Sendai 980, Japan)

The seismic Q of the lunar interior has been known to be unusually high ever since the first observation of lunar seismic signals, with the reported values ranging from 1600 to 4800. We have recently determined frequency dependence of both P- and S-wave Q's in the upper mantle of the moon in a frequency range of roughly 2 to 8 Hz. The method involved computations of the derivatives of power spectral densities with respect to frequency and their regressions with respect to travel times. The Q determined for P waves is about 4000, and is nearly independent of frequency; while S-wave Q increases from 6000 at 3 Hz to 30,000 at 7 Hz. Standard errors of Q^{-1}, as estimated from the variances of the above regression slopes, are roughly $\pm 1.0 \times 10^{-4}$ for Q_P^{-1} and $\pm 0.4 \times 10^{-4}$ for Q_S^{-1}. The determined Q_S is approximately proportional to the square of frequency, but $Q_S \propto f$ is also within the error bounds. The extremely high Q for shear waves suggests that certain dissipation mechanisms due to compressional heat loss may be a dominant factor.

S 84

COMPRESSIONAL WAVE VELOCITY AND ATTENUATION IN BASALT MELT

C.S. Rai (Hawaii Institute of Geophysics, University of Hawaii, Honolulu, Hawaii 96822
M.H. Manghnani, K.W. Katahara

Using a continuous-wave interferometric method, measurements of ultrasonic V_P and Q_P^{-1} have been made in an alkalic olivine basalt to 1400°C. This method provides an alternative to the pulse transmission technique employed in previous studies. The method is potentially capable of also measuring V_S and Q_S^{-1} below solidus temperatures.

Preliminary data on the temperature and frequency dependence of V_P and Q_P^{-1} are presented. Q_P values for the basalt melt at 1300°C are in the range 10-40 at MHz frequencies. Implications of these results are discussed in view of recent field measurements of seismic velocity and attenuation in geothermally active areas.

Earth's Structure and Lateral Heterogeneities

Pier 5
Saturday P.M.
C. A. Langston (Pennsylvania State University) and *R. F. Mereu* (Univ. of Western Ontario), Presiding

S 85

UPPER MANTLE STRUCTURE NEAR THE EAST PACIFIC RISE AT LATITUDES 15°N and 12°N FROM SEISMIC REFRACTION DATA COLLECTED DURING THE ROSE PROJECT

G. M. Purdy (Woods Hole Oceanographic Institution, Woods Hole, MA 02543

J. I. Ewing (Woods Hole Oceanographic Institution, Woods Hole, MA 02543

Comparisons are made of the propagation characteristics of the upper mantle near the East Pacific Rise in two areas approximately centered at latitude 15°N and 12°N. The data are refraction seismograms recorded by ocean bottom hydrophones from explosive sources varying in size from 200 lbs to 1 ton in the range window 30 to 100 km. Consistent patterns in the amplitude distributions of the low frequency (~ 5Hz) energy are recognized and modelled to allow comparisons to be made between the two areas. At 15°N a striking relationship is recognized between the azimuth of the ray path, the relative amplitudes of the phases in the first 2 seconds of the record, and the known direction of sea-floor spreading.

S 86

ANISOTROPY IN THE UPPER MANTLE STRUCTURE OF EURASIA

Liao, A.H. (Institute of Geophysics and Planetary Physics, University of California, Los Angeles)
Knopoff, L.

Fundamental mode Rayleigh and Love wave phase velocities are used to study the anisotropy and the upper mantle structures in different tectonic provinces within the Eurasian continent. The periods range from 30 sec to 250 sec. The phase-travel time data have been obtained for many long paths that traverse the continent between the earthquakes and WWSSN stations around its perimeter. Several linear and nonlinear inversions based on various parameteri-

zations of the upper mantle of the regions and various combinations of data sets were performed. Regionalization is performed taking into account broad scale geological information.

The results show that the upper mantle structures of Eurasia can be grouped into shield-type and non-shield-type. The shield areas include the Siberian shield as well as the Tibetan plateau, both having high velocity material extending to great depth; if a low-velocity channel is present, it has at most a small contrast to the lid that overlies it. The rest of the continent has a thin, high-velocity lid, overlying a low velocity channel of marked velocity contrast.

The results of the inversions for both Love and Rayleigh wave data indicate that the shear-wave velocity is 4.34 ± 0.02 km/sec in the channel. For the lid, the velocities determined from the two data sets differ, being 4.56 ± 0.01 km/sec from the Rayleigh wave data set and 4.77 ± 0.02 km/sec from the Love data set. The apparent anisotropy in the lid and its absence in the channel is the reverse of the results for the Pacific Ocean basin.

S 87

REGIONALIZED CRUST-MANTLE STRUCTURE OF CHINA FROM PATH-SEGMENT INVERSION OF OBSERVED SURFACE WAVE DISPERSION

Y. T. Yeh (Institute of Earth Sciences, Academia Sinica, Taiwan, Republic of China)
S. S. Alexander (Geosciences Department, The Pennsylvania State University, University Park, Pennsylvania 16802)

A newly developed path-segment inversion method is used to infer the crust-mantle structures in mainland China and surrounding areas from observed surface wave dispersion. Based on other available information, mainland China is subdivided into 4 crustal blocks: (1) Chinghai-Tibet, (2) South-China, (3) North-China, and (4) Northwest-China. Group velocity dispersion of both Rayleigh and Love waves were measured for a number of paths by a multiple bandpass filtering technique. The resulting mixed-path dispersion curves were grouped into 4 sets, based on the composite propagation paths, and each set was inverted by the path-segment method. The inverted regional structure is significantly different for each crustal block and the differences extend to a depth of at least 100 km. These observed differences place additional constraints on any viable reconstruction of the tectonic history of this region. Some of these implications are discussed as they relate to previously proposed plate-tectonic interpretations for mainland China.

S 88

A NOTE ON SPECTRAL NULLS IN RAYLEIGH WAVES

Charles A. Langston (Department of Geosciences, The Pennsylvania State University, University Park, PA 16802)

The occurrence of depth-dependent spectral nulls in Rayleigh waves from some double point sources is a well known phenomenon and has been used in many surface wave studies to determine source depth. In mode theory these nulls occur because of a zero in particular eigenfunctions. An alternative and physical way of viewing the formation of Rayleigh waves from deviatoric sources is to decompose the Rayleigh wave into parts associated with the S and P waves. Depth dependent nulls result from the destructive interference of these two different Rayleigh waves. A particularly simple example is given of these effects by investigating Lamb's problem for an impulsive and symmetric moment tensor point source. These simple observations may have some use in interpreting the results of large code calculations of exotic seismic sources and provides some insight into surface wave propagation in layered media.

S 89

MULTIMODE ANALYSIS OF L_g USING THE SCARLET ARRAY

Michel J. Cara
J. Bernard Minster
Ronan J. Le Bras (all at: Seismological Laboratory, California Institute of Technology, Pasadena, California 91125)

In laterally homogeneous crust-upper mantle structures, the short period L_g phase can be explained in terms of normal mode superposition. Overtones of either Love or Rayleigh type exhibit very close group velocity curves near 3.2-3.5 km/s, generating the impulsive wavepacket L_g; phase velocity curves, on the other hand, are well distinct at periods greater than 2 s for a wide range of realistic crustal models. This suggests the use of wavenumber analysis techniques to isolate different overtones from seismograms observed on arrays of stations.

We show on a synthetic example that a 500 km long linear array of 12 stations allows us to isolate the different modes at periods of a few seconds, by using the UC diagram technique which Cara (1978) successfully applied to the S_a phase at longer periods.

The SCARLET array provides a good opportunity to apply such a technique to observed L_g. Preliminary results show that strong peaks observed on UC diagrams can generally be interpreted as higher Rayleigh modes (particularly for the second and third higher modes). Weaker peaks, and in some cases other strong peaks, cannot be explained in terms of coherent cylindrical propagation of a few higher modes across the array of stations, even after taking into account spatial aliasing.

We suggest that observed short period (2-5 sec) L_g in Southern California result from the superposition of a simple multimode signal and coupled noise due to lateral refractions, lateral reflexions and mode conversions. Even in cases where the L_g wave train is complicated, we have succeeded in retrieving spatially averaged phase velocity dispersion curves for the first few higher Rayleigh modes excited by mid-crustal sources.

S 90

RELATIVE ARRAY DIAGRAM SCANNING OF CRUST AND UPPER MANTLE, SOUTHERN CALIFORNIA

Marianne C. Walck
J. Bernard Minster (both at: Seismological Laboratory, California Institute of Technology, Pasadena, California 91125)

We have systematically partitioned the SCARLET array into a set of 160 overlapping circular subarrays of 100 km aperture, and an additional 40 subarrays with specialized geometries. The P arrivals from 148 recent teleseisms are utilized to generate relative array diagrams, which represent the differences in $dT/d\Delta$ and azimuth estimates from individual subarrays and the entire 150 station network for each event. Because this technique eliminates effects of structure in the lower mantle and source regions, it is ideally suited for study of the upper mantle and crust beneath the array. From this data set emerges a rather complex, laterally varying and depth dependent image of Southern California crust and upper mantle structure. The structural information, however, which is spatially averaged through subarray analysis is not uniform over the entire network. In regions with strong shallow lateral variations, such as Imperial Valley, the Los Angeles and Santa Barbara basins, and the central Transverse Ranges, the influence of near surface structure dominates and deeper features are not easily discernable. Alternatively, subarrays in regions with more transparent shallow structure, such as the Mojave Desert, yield information about deeper lateral inhomogeneities over areas far exceeding the aperture of the subarray.

S 91

STRUCTURE BENEATH EASTERN WASHINGTON FROM THE INVERSION OF SEISMIC AND GRAVITY DATA

W. L. Rodi (Systems, Science and Software, P. O. Box 1620, La Jolla, California 92038)
J. M. Savino (Systems, Science and Software, P. O. Box 1620, La Jolla, California 92038)
J. F. Masso (Systems, Science and Software, P. O. Box 1620, La Jolla, California 92038)
T. H. Jordan (Scripps Institute of Oceanography, University of California, San Diego, La Jolla, California 92093)

We have applied a joint inversion algorithm to teleseismic P-wave delays and Bouguer gravity data from eastern Washington to infer the three-dimensional velocity and density structure of the crust and upper mantle beneath a portion of the central Columbia Plateau (45.5° to 48°N latitude and 118.5° to 120.5°W longitude).

Our joint inversion procedure solved for the velocity and density perturbations in a six-layer three-dimensional grid of blocks extending from the surface to 300 km depth. The perturbations in the two parameters were assumed to be functionally related by a depth-dependent coefficient. Our final model gives excellent agreement with both the gravity and teleseismic data.

The most significant features of the model occur in the southern portion of the region. Here we find a high velocity and density zone in the crust, which may be an expression of crustal thinning in this area. Complementing this is a low velocity anomaly in the mantle between depths of roughly 50 and 200 km. The anomalous zone is at least 100 km wide and has velocities 0.2 km/s lower than the surrounding mantle. This may be associated with a thermal disturbance related to the development of the Columbia Plateau basalts.

We are presently inverting P-wave arrival time data for events in eastern Washington recorded at regional and near-regional distances simultaneously with Bouguer gravity data. The simultaneous modeling of these two data sets should provide a more detailed three-dimensional model of the crustal structure in the central Columbia Plateau region.

S 92

A STUDY OF UPPER MANTLE STRUCTURE UNDER WESTERN RUSSIA

I. N. Gupta (Teledyne Geotech, 314 Montgomery St., Alexandria, Virginia 22314)
A. C. Chang and B. W. Barker

Short-period, vertical component data from WWNSS stations are used to obtain time-distance plots of P waves for epicentral distance, Δ, in the range of 5° to 40° for underground nuclear explosions and for shallow earthquakes in Western Russia. The observed data are compared with theoretical time-distance curves based on various postulated compressional velocity distributions for the upper mantle beneath Western Russia. Both explosion and earthquake data provide good agreement, up to a depth of about 700 km, with King and Calcagnile's (1976) model which does not postulate a low-velocity layer in the uppermost mantle. For greater depths, Massé and Alexander's (1974) velocity model provides a better fit.

Magnitude and arrival-time residual data, as reported in the ISC bulletins, for underground nuclear explosions in Western Russia (including Novaya Zemlya) for the years 1971 to 1976 have also been analyzed. A computer program which takes averages within a variable-width sliding window, after weighting with a cosine taper and rejecting highly abnormal observed values, is used to study normalized amplitudes and residuals versus Δ. Explosion sites are divided into three groups: Semipalatinsk, Novaya Zemlya, and all other West Russia sites. Both amplitude and residual plots show significant differences amongst the three site regions. The largest departure from the Gutenberg and Richter's (1956) or Veith and Clawson's (1972) curves, reflected in all amplitude-distance curves, occurs for Δ about 20°. Furthermore, the Semipalatinsk data show an anomalous maximum in the amplitude values in the range $\Delta = 32°$ to 35°. These results appear to suggest that significant lateral variations, extending to depths of 800 km or more, exist in the upper mantle structure beneath Western Russia.

S 93

SEISMIC WAVE PROPAGATION THROUGH A CRUST WITH RANDOM LATERAL AND VERTICAL INHOMOGENEITIES

R.F. Mereu (Dept. of Geophysics, University of Western Ontario, London, Ontario N6A 5B7, Canada
S. Ojo U.W.O. London, N6A 5B7

The structures of the earth's crust often derived from long range refraction observations differ significantly from the more complex structures obtained from the high resolution deep seismic reflection methods. In this paper a random media method of modelling the crust is presented which explains the reason for the discrepency. The starting model is a single layered crust with a vertical velocity gradient. A two dimensional set of small smoothed random velocity deviations is then superimposed on the vertical gradient model. The maximum deviation of velocity from a mean at a given depth and a correlation distance derived from a smoothing filter are two parameters used

to vary the amplitude and size of the velocity anomalies. The resulting models show short reflectors at various depths in agreement with deep seismic reflection experimental observations. On the other hand, numerical experiments using ray tracing techniques showed that the effect of the lateral and vertical velocity anomalies is to scatter the energy and break up the continuous travel-time curve from the vertical gradient model into segments of different slope similar to those observed in many long range refraction experiments. Many of the numerical experiments produced a Pg segment and a p* segment with an apparent Conrad discontinuity at a depth of 10 to 20km, the apparent depth being a function of the correlation distance used in deriving the random model.

S 94

EVIDENCE FOR DIFFERENCES IN OCEANIC AND CONTINENTAL UPPER MANTLE STRUCTURE FROM ARRAY SIGNAL COHERENCE MEASUREMENTS

S.B. Ojo (Dept. of Geophysics, University of Western Ontario, London, Ontario N6A 5B7, Canada.

R.F. Mereu U.W.O. London N6A 5B7

A method was developed to extract useful information about the scattering characteristics of different p wave travel paths from the ratio of the incoherent energy to total incident energy of the signal recorded at an array station. The method is based on the assumption that when a ray passes through a homogeneous earth, the energy that arrives at an array station will be relatively coherent. When the ray path however encounters both lateral and vertical inhomogeneities, much of the energy is scattered and arrives at the array as incoherent energy. This incoherent energy was measured using both beam forming and n-th root beam forming methods. An analysis of the results obtained from applying the method to array records from the Gauribidanur seismic array (GBA) in southern India indicated that much less scattering of seismic energy occurs in the upper mantle under oceans to the south of the array compared to the continental upper mantle to the north of the array. These differences can be correlated with the tectonic history of the region.

S 95

UPPER MANTLE HETEROGENEITIES BENEATH CENTRAL EUROPE

Eystein S. Husebye (NTNF/NORSAR, 2007 Kjeller, Norway)
Jan Hovland (NTNF/NORSAR, 2007 Kjeller, Norway)
David Gubbins (Dept. of Geodesy & Geophysics, Cambridge, United Kingdom)

An inversion of ISC travel time data from selected earthquakes in the distance range 30°-90° to'53 stations in Central Europe has been used to model velocity down to 600 km depth. The model explains 0.1 to 0.2 s of the residuals leaving 0.5 s unexplained as noise. The uppermost 100 km of the mantle and crust contains inhomogeneities that correlate remarkably well with the geology. This may be due to deep-seated thermal anomalies or, in some areas, to delays introduced by passage of the rays through sedimentary cover. The deeper anomalies are smaller and unrelated to those in the lithosphere, which suggests that the asthenosphere is decoupled from the rigid lithosphere. The structure at 600 km depth is again quite inhomogeneous and can be explained by undulations of the 650 km discontinuity. The models show some suggestion of a high velocity slab trending from E to W beneath the Alps.

S 96

THEORETICAL pP TRAVEL TIMES AND RAY PATHS FOR DESCENDING SLAB MODELS

Donald S. Michniuk (Seismographic Station, University of California, Berkeley, Calif. 94720)

The aim of this work is to examine the effect of subducting slabs on the time and amplitude of the reflected phases pP, sP, and sS. These phases, crucial for computation of focal depths and mapping slab geometries, have been generally treated only for radially symmetric Earth models. Comparisons of times for realistic models are made against the Jeffreys-Bullen travel time diagrams.

The main results come from a three-dimensional ray tracing program specially developed for subduction geometries in realistic Earth models.

Ray paths are found to be very sensitive to variations in slab structure, depending on take-off angle and source location and different percentage velocity contrasts between slab and lithosphere.

The ray calculations have located significant shadow zones with surface regions of defocusing and focusing. For example, for the model CAL6, a 7% velocity increase in a slab 120km thick dipping at 45° exhibits at normal ray emergence a shadow with low amplitudes over several degrees distance near $\Delta = 77°$. At this distance, the travel time differs with the JB tables for pP by 8 seconds. Travel-time tables as a function of azimuth about the focus for various depths are compared and the minimum Δ for the existence of the pP phase at various azimuths is determined. These theoretical results are also compared with a number of pP observations, e.g., the 1940 and 1977 Romanian earthquakes.

S 97

SEARCH FOR VELOCITY ANOMALIES IN THE NEW HEBRIDES ISLAND ARC FROM RESIDUALS OBSERVED WITH COMBINED LAND-OBS STATIONS OF A TEMPORARY NETWORK

E. Coudert
B.L. Isacks ; R. Cardwell (all at:Geol. Sciences, Cornell University, Ithaca, NY 14853)
A. Chen ; G. Latham (Marine Science Institute, University of Texas, Galveston, Texas 77550)
J. Dubois ; R. Louat (Office de la Recherche Scientifique et Technique Outre-Mer, 75008 Paris, France)

In the summer of 1977, a network of land and ocean bottom seismograph (OBS) stations operated in the southern New Hebrides island arc. The stations covered a large cross-section of the arc from the Loyalty islands, 100 km west of the trench, to the back arc trough 200 km east of the trench. The well-located intermediate depth earthquakes determine a well defined Benioff zone with a 70° apparent dip and 20 km thickness. These results are in agreement with other studies from worldwide data. Moreover, comparison of locations of four events obtained independently with the local and with the worldwide network does not show any large bias. The pattern of P wave time residuals at local stations for events well located by the local network shows several features. No significant residuals are observed at the stations on the island arc. However, the residuals at an OBS located near the trench suggest a high velocity anomaly associated with the slab and a low velocity anomaly along the path between the shallow events located near the plate boundary thrust zone and the OBS station. The high velocity anomaly restricted between 70 and 200 km depth also explains the difference between the hypocenters determined with and without the two stations located west of the trench. The apparent contradiction between a high velocity slab and the lack of large bias in our determinations with a horizontally layered model can be partly explained by the width of the local network and the steepness of the New Hebrides Benioff zone. New results from a combined land-OBS network operating near Efate Island in 1978 will also be presented.

S 98

RESULTS OF SEISMIC RAY TRACING USING A TWO-DIMENSIONAL MODEL OF THE CENTRAL ALEUTIAN SUBDUCTION ZONE

E. R. Engdahl (U.S. Geological Survey, Box 25046, DFC, Denver, CO 80225)
Selena Billington (CIRES, University of Colorado, Boulder, CO 80309)
Cliff Frohlich (Marine Science Institute, University of Texas, Galveston, TX 77550)

A two-dimensional ray-tracing scheme, used successfully by Engdahl and W. Lee in 1976 to locate earthquakes in California, is used to locate shallow earthquakes along the thrust zone south of Adak in the central Aleutians. The two-dimensional velocity model for the upper 50 km of the region was derived from published geophysical studies that include reflection and refraction profiles, thermal and gravity modelling, and the results of microearthquake monitoring by the Adak local seismograph network. The data consist of P- and S-arrival times both at stations in the Adak network and at a network of eight OBS (Ocean Bottom Seismometer) stations deployed about 50 km offshore of Adak to record seismic activity during a six-week period in 1978.

Although large uncertainties exist in the velocity model, it serves as a first-order approximation to account for the large differences in structure beneath land and OBS stations and to provide insight about structural effects on seismic waves passing through the region. Lateral variations in velocity are shown to distort azimuths and focal angles of seismic rays used in focal mechanism determinations and to cause systematic mislocation of shallow earthquakes when Adak network data alone are used. Results of this study will be used to precisely calibrate the region for more accurate location of earthquakes by the land-based net.

Mathematical Methods: Wave Propagation

Queen's Quay
Monday A.M.
J. H. Woodhouse (Harvard Univ.) and *R. C. Y. Chin* (Lawrence Livermore Lab.), Presiding

S 99

MODELING OF TELESEISMIC BODY WAVES FROM SUBMARINE EARTHQUAKES IN A VERTICALLY HETEROGENEOUS CRUST

Glenn C. Kroeger
Robert J. Geller (Dept. of Geophysics Stanford University, Stanford, Ca. 94305)

We can accurately model the effects of sediment and water layers on the teleseismic body waves from submarine earthquakes using a first motion generalized ray technique to generate synthetic seismograms. This method allows us to separate the effects of near-source structure from source mechanism and time history in the forward modeling process. Using an algorithm which generates all of the generalized rays in a layered stack we can quickly model complicated suboceanic structures to obtain better source depth determinations and constraining the water depth over the hypocenter. The latter aids in the precise location of the epicenter in marine regions of rapidly varying water depth such as aseismic highs and trenches. We use these techniques to study a 1975 Tsunami event near the Kurile trench and a 1965 event in the South China Sea. Both the short and long period WWSSN records are modeled using estimates of the local crustal structure.

S 100

AN ALTERNATIVE TECHNIQUE FOR RAY TRACING IN INHOMOGENEOUS MEDIA

J.S. McClain (Geological Research Div., Scripps Inst. of Oceanography, U.C. San Diego, La Jolla, CA 92093)

Ray tracing in inhomogeneous media where velocity varies in two or three dimensions is an expensive procedure. This is especially true if one wishes to fix the end points of the propagating rays. Methods for solving such problems require the solution of a system of non-linear differential equations, a highly unstable process. Here, we use the formalism of dynamic programming as an alternative approach which avoids the instability of other methods. In its simplest form, dynamic programming is a very efficient technique for examining all possible

ray paths through a structure. Thus, stability is gained while, perhaps, computing speed is lost. However, efficiency of the process increases with the number of rays required. The location of receivers and/or sources within the model is arbitrary, making the technique ideal for tracing seismic rays from earthquakes or acoustic rays in air and water.

S 101

THEORETICAL SEISMOGRAMS FOR EARTHQUAKE SOURCES AT LOCAL TO REGIONAL DISTANCES

B.L.N. Kennett (Department of Applied Mathematics and Theoretical Physics, University of Cambridge, Silver Street, Cambridge CB3 9EW, England)

It is now practicable to complete the entire response of a stratified elastic half space to excitation by a buried point source, for moderate offsets from the source.

Using a moment tensor representation for the source, both earthquakes and explosions may be modelled. Numerical problems in these calculations may be avoided by working directly in terms of the reflection and transmission properties of the stratification. For piecewise continuous media, reflection and transmission matrices are calculated recursively.

With this approach three component theoretical seismograms including P, S and surface Rayleigh and Love waves may be calculated.

S 102

SEISMIC WAVE PROPAGATION IN REALISTIC EARTH MODELS

M.R. Illingworth and B.L.N. Kennett (Department of Applied Mathematics and Theoretical Physics, University of Cambridge, Silver Street, Cambridge CB3 9EW, England

A reasonable approximation to the seismic velocity distribution in the Earth's mantle is to take a model composed of 'layers' with smoothly varying properties separated by discontinuities in velocity or velocity gradient.

The wave functions within these layers are constructed from Airy functions and an expansion in terms of parameter gradients representing multiple internal reflections. We are then able to construct the reflection properties of each layer sandwiched between two uniform half spaces with continuity properties at the limits of the layer. The effects of interfaces are introduced by using the reflection matrix between uniform half spaces with the properties at the interface.

The overall reflection properties of the stratification are then obtained by a recursive procedure incrementing layer by layer. For weak velocity gradients this leads to an effective computational procedure.

S 103

SEISMIC MODELING IN THE DOMAIN OF INTERCEPT TIME AND RAY PARAMETER

P.L. Stoffa
F. Wenzel (both at: Lamont-Doherty Geological Observatory, Palisades, N.Y. 10964)

In recent years seismic modeling has been based primarily on two methods: generalized ray theory and the reflectivity method. Variations within these methods are based on the domains of computation and the approximations applied. One common feature of both approaches is the straightforward translation of a mathematical solution to the wave equation into a computational algorithm that develops the seismic response for a given earth structure in the observation plane of seismic experiments, source-receiver offset and traveltime (X-T). We investigate an alternative approach where we develop and compare models in the domain of vertical delay, or intercept time and horizontal ray parameter (τ-p). This is accomplished by a modified version of the reflectivity method followed by a Fourier transform over frequency. In these models, the τ-p seismic response for compressional and shear waves is readily interpreted for all primary and multiple arrivals. Velocity-depth functions derived from Wide Aperture Common Midpoint Data transformed to the domain of intercept time and ray parameter are quickly refined by comparison to the synthetic τ-p data. The τ-p response can also be used to compute broadband synthetic X-T seismograms by an appropriate integration through the τ-p plane. A fast method of computing seismograms is suggested based on a weighted integration designed to automatically evaluate the points of stationary phase.

S 104

MATRIX METHODS IN SYNTHETIC SEISMOGRAMS

R. C. Y. Chin (Lawrence Livermore National Laboratory, Livermore, CA. 94550)
G. W. Hedstrom and L. Thigpen (LLNL)

The Haskell-Thomson formalism and Kennett's recursive algorithm in computing synthetic seismograms can be unified by considering the formulation of the inherent linear algebraic problem. In the Haskell-Thomson formalism, the linear system is cast in a block bi-diagonal form. In this form it is well known that numerical error propagation is severe. We rearrange the equations and variables to obtain a block tri-diagonal linear system. We decompose the coefficient matrix using a discrete invariant imbedding algorithm to obtain Kennett's recursive method involving the generalized reflection coefficients. Equivalently, the block tri-diagonal coefficient matrix may be decomposed into upper and lower block bi-diagonal matrices. Here, the upper and lower bi-diagonal matrices do not have immediate physical interpretation. The block tri-diagonal structure is also obtained in finite-element or finite-difference solutions of the transformed governing equations of elastodynamics. Richard's full-wave theory can also be cast in this form.

This work was performed under the auspices of the U.S. Department of Energy by the Lawrence Livermore National Laboratory under contract No. W-7405-ENG-48.

S 105

A GENERAL SOLUTION FOR COUPLED ELASTIC-GRAVITATIONAL DEFORMATION IN A LAYERED HALF SPACE BY POINT SOURCES

J. B. Rundle (Division 5541, Sandia Laboratories,† Albuquerque, NM 87185)

A solution for explicitly coupled, quasi-static elastic-gravitational problems in layered media is given. The perturbation equations are solved to give the general homogeneous solution for deformation in a uniform, infinite medium. It is easily shown that the eight solution vectors from the coupled equations reduce to those for the uncoupled equations in the limit of vanishing coupling constants. Due to the similarity of the equations, the solution also has application to certain problems in thermoelasticity and poroelasticity.

The solutions for various internal point sources in a layered half space are constructed out of the infinite medium solution by well-known techniques. The half space is divided into a series of horizontal layers and a matrix method is used to propagate the solution from one layer to the next. The point source is represented by a discontinuity in several of the various propagated quantities across a horizontal plane. Expressions are given for the direct calculation of surface displacements, and the behavior of the resulting displacement kernels is examined.

S 106

COMPRESSIBILITY, CORE DYNAMICS AND THE SUBSEISMIC WAVE EQUATION

M. G. Rochester (Memorial University of Nfld., St. John's, Newfoundland A1B 3X7)
D. E. Smylie (York University, Downsview, Ontario M3J 1P3)

Motions of large radial length scale in the Earth's liquid core are strongly affected by compressibility and self-gravitation, and such flows cannot be regarded as solenoidal. At 'subseismic' frequencies we can neglect density changes due to variations in flow pressure while retaining those due to transport through the pre-existing hydrostatic pressure field. We here examine some of the consequences of the subseismic approximation.

Models of the geomagnetic dynamo must take into account that for large scale flows the Proudman-Taylor theorem is violated throughout the interior of the liquid core, not just near its boundaries.

The subseismic approximation also permits the free oscillation problem in the rotating compressible stratified self-gravitating liquid core to reduce to the solution of a new single second-order scalar partial differential equation which we name the subseismic wave equation (SSWE). Internal gravity wave- and inertial wave-like solution regimes are displayed on a frequency-latitude plot. A novel separation of variables in spherical polar coordinates, for the special case of a uniformly stratified core, yields an ordinary differential equation for latitude dependence which has seven regular singularities. A new scheme for calculating values of the separation constant ensuring solutions regular everywhere in a spherical shell yields the free oscillation frequencies for the stably stratified case.

S 107

VARIATIONAL SOLUTION OF EARTH'S LONG PERIOD OSCILLATIONS

W. Moon
Dept. of Earth Sciences, The University of Manitoba, Winnipeg, Canada R3T 2N2
M. G. Rochester
Dept. of Physics, Memorial University of Newfoundland, St. John's, Canada A1B 3X7

The eigen-periods of Earth's long period oscillations are computed using the variational method for simplified rotating, slightly ellipsoidal Earth models of 1066B and B156 (stably stratified outer core). The numerical convergence is bad when the truncated solution chain is limited to two terms. However, after the solution chain (toroidal) is extended to six; $T^m_e + S^m_{e+1} + T^m_{e+2} + S^m_{e+3} + T^m_{e+4} + S^m_{e+5}$, the periods of wobble modes, core modes and lower order seismic modes are obtained. As the coupling chain is increased, the size of the final energy matrices is also increased accordingly and consequently, the Earth models used are greatly simplified using an interpolation scheme to accommodate the problem in the current computer capacity. The eigen-spectrum for Earth model B156 shows that the eigen-periods for the core mode range are bunched around 6.00 hr and near 12.00 hr period.

S 108

THE NUMERICAL SEARCH FOR FREE OSCILLATIONS OF THE EARTH'S LIQUID CORE

D.J. Crossley (Department of Mining & Met. Eng., McGill University, Montreal, Quebec)

The difficult theoretical problem of finding the spectrum of internal wave motions in the core of the Earth has been simplified by a parametric description of the fluid adopted recently. This assumes that the core fluid can be represented as incompressible and non self-gravitating as long as the Brunt-Vaisala frequency N has the same value as in a more physically reasonable (i.e. compressible and self-gravitating) model.

Solutions of this simplified model for all values of N ($\tilde{\Omega}$) have now been obtained with adequate convergence, using a truncated system of equations, in all cases except near λ ($=\omega/2\Omega$) $=1$. That the solutions are fairly accurate has been verified by numerical comparisons of the eigenvalues of two subsets of models (a) a neutrally buoyant fluid (inertial wave solutions) and (b) a fluid with a free surface (gravity and Rossby waves in the oceans).

S 109

ELECTROHYDRODYNAMIC INSTABILITY IN A SPHERICAL SHELL OF DIELECTRIC FIELD

W. Markiewicz and K. D. Aldridge, (Department of Physics, York University, Toronto, Ontario).

This paper is concerned with the electrohydrodynamic stability of a dielectric fluid contained in a spherical shell. A dielectric fluid, contained in a rigid spherical shell, is subjected to a simultaneous radial temperature gradient and radial 60 hertz electric field.

Linearized perturbation theory and the assumption of exchange of stabilities lead to an eighth order differential equation in perturbation temperature. This equation is characterized by two dimensionless parameters. The electrical Rayleigh number, analogous to the classical Rayleigh number with gravity replaced by its electrical counterpart, appears in this formulation. A second parameter, α, dependent on the size of the spherical shell and the temperature gradient, does not appear in classical stability problems.

The solution to the above mentioned equation satisfying appropriate boundary conditions yields a critical value of the electrical Rayleigh number and corresponding critical wave number at which convective motion begins. The dependence of each critical number is presented as a function of the parameter α. In the limit of zero shell thickness both the critical Rayleigh number and critical wave number agree with results for the same limiting case in the infinite plane and cylindrical shell problems.

From a geophysical standpoint the problem of electrohydrodynamic stability in a spherical shell of dielectric is of particular interest. The electric field is a central force field which can be used to model the gravity field of the Earth's fluid core in a laboratory experiment. Both theory and experiment can be extended to include rotation.

S 110

THE EFFECT OF LATERALLY HETEROGENEOUS ATTENUATION ON THE FREE OSCILLATIONS OF THE EARTH

F. A. Dahlen (Department of Geological and Geophysical Sciences, Princeton University, Princeton, N. J. 08544)

First-order degenerate normal mode perturbation theory is developed for an Earth model having lateral variations in attenuation Q_κ and Q_μ, as well as in density ρ and elasticity κ and μ. In the Earth, the fractional lateral variations in μ are of the same order as a typical average value of Q^{-1}, about 10^{-3} to 10^{-2}. If the fractional lateral variations in Q_μ are of order one, they can play as important a role as those in μ in determining the zeroth-order eigenfunctions and the first-order split eigenfrequencies of the Earth's free oscillations. The effect of laterally heterogeneous Q_κ and Q_μ on the shape of an unresolved multiplet spectrum has also been investigated, in the geometrical optics asymptotic limit. Singlet cancellation leads in that limit to the appearance of a single resonant peak, with an apparent Q^{-1} which depends only on the average of Q_κ^{-1} and Q_μ^{-1} underlying the source-receiver great-circle path.

S 111

TIME DOMAIN CALCULATIONS OF MODAL ENVELOPES FOR SLIGHTLY ASPHERICAL EARTH MODELS

J. H. Woodhouse (Dept. of Geological Sciences, Harvard University, Cambridge, MA 02138)

A method has been developed for calculating the effects of lateral heterogeneity and attenuation on the low frequency response of an earth model. The effect on a multiplet, or on a set of coupled multiplets, of splitting, quasi-degenerate coupling and attenuation is characterized by an "excitation envelope" with respect to a particular SNREI reference model. The excitation envelope is a complex vector, varying on a time scale much longer than the periods of normal modes, and can be obtained as a solution of the differential equation

$$\dot{\underline{a}}(t) = iH\underline{a}(t) \qquad (1)$$

where H is the splitting matrix for the multiplet or the appropriate partitioned splitting matrix for a set of coupled multiplets. The solutions $\underline{a}(t)$ are subject to initial conditions at the origin time, given by the usual results for the excitation of normal modes in the reference model. An advantage of the approach is that (1) may be solved for $\underline{a}(t)$ by finite difference and propagator matrix methods, without having to decompose the complex, non-Hermitian matrix H. The phases of the elements of $\underline{a}$ are related to the frequency shifts of the singlets and the amplitudes have a clear physical interpretation in terms of energy transfer or "scattering" between singlets.

Filtered accelerometer records from the IDA network are examined in order to assess the constraints which may be placed upon H for a number of low frequency multiplets.

S 112

VARIATIONAL CALCULATION OF THE TOROIDAL MODES OF A LATERALLY HETEROGENEOUS EARTH MODEL

Sandra L. Plumlee
Robert J. Geller (both at: Dept. of Geophysics, Stanford University, Stanford, CA 94305)

The current technique for calculating the normal modes of a laterally heterogeneous earth model is to use first-order degenerate perturbation theory to find the eigenfrequencies and eigenfunctions of the split singlets. However, based on one dimensional analogs to a laterally heterogeneous earth model, first-order perturbation theory may not yield answers with sufficient accuracy. Potential difficulties arise because a linear combination of only the singlets comprising the original degenerate multiplet may not be an adequate representation of the true eigenfunction of the laterally heterogeneous model. This problem can be alleviated by using a variational approach in which the trial functions include the eigenfunctions of adjacent multiplets of the original laterally homogeneous model.

We present as examples variational calculations of the low-order toroidal modes of some simple laterally heterogeneous systems in which the trial functions include several adjacent toroidal multiplets. In each case, the matrices of coupling coefficients for the trial functions are found using the Wigner-Eckart theorem and associated selection rules to simplify the integrals. The resulting eigenvalue problem is solved by inverse iteration to obtain eigenfrequencies and eigenfunctions of the laterally heterogeneous model. These calculations illustrate the differences between the perturbation methods and the more accurate variational results.

Mathematical Methods Algorithms, Inversions, Earthquakes

Queen's Quay
Monday P.M.
D. E. Smylie (York Univ.) and *C. H. Chapman* (Univ. of Toronto), Presiding

S 113

AN AUTOMATIC SEISMIC SIGNAL DETECTION ALGORITHM BASED ON THE WALSH TRANSFORM

Tom T. Goforth (Geophysical Laboratory, Southern Methodist University. Dallas, Texas 75275)
Eugene Herrin (Dept. of Geological Sciences, Southern Methodist University, Dallas, Texas 75275)

An automatic seismic signal detection algorithm based on the Walsh transform has been developed. Walsh functions form an orthogonal set of rectangular waveforms, and since the amplitude of each function is either +1 or -1, the Walsh transform can be accomplished in a computer with a series of shifts and fixed point additions. The savings in computation time relative to other orthogonal transformations makes it possible to compute the Walsh transform and to perform bandpass, Wiener, and/or adaptive filtering with a microprocessor for real-time signal detection.

S 114

AN APPLICATION OF AN ARMAc MODEL

F.W. Zwiers, (Dept. of Mathematics, Dalhousie University, Halifax, N.S. B3H 4H8

The class of Auto-Regressive Moving-Average convolution (ARMAc) models on the unit circle is a natural extension of the class of multivariate Box-Jenkins models. Formally, they may be defined as follows: Let $\{\epsilon_t(\theta)\}_{t=-\infty}^{\infty}$ be a sequence of independent and identically distributed random functions defined on the unit circle. Let p and q be non-negative integers, and let $\alpha_i(\theta)$, $i=1,\ldots,p$ and $\beta_j(\theta)$, $j=1,\ldots,q$ be fixed (i.e. non-random) functions defined on the unit circle. Then the sequence of random functions $\{X_t(\theta)\}_{t=-\infty}^{\infty}$ is said to be an ARMAc(p,q) process if it satisfies

$$X_t(\theta) + \sum_{i=1}^{p} (\alpha_i * X_{t-2})(\theta) = \epsilon_t(\theta) + \sum_{j=1}^{q} (\beta_j * \epsilon_{t-j})(\theta)$$

with probability one for all t where $*$ denotes convolution on the unit circle.

In this paper a brief review is made of previous attempts to predict the future state of a climate variable months or seasons ahead using Box-Jenkins type models. A few results pertaining to ARMAc models is suggested as being suitable for sea-surface temperature (SST) prediction. An experiment with this model is described and its outcome is compared with some previous SST prediction experiments.

S 115

TWO METHODS TO IMPROVE LOCATION ESTIMATES - PRELIMINARY RESULTS

A. C. Chang (Teledyne Geotech, 314 Montgomery Alexandria, Virginia 22314)
R. H. Shumway, R. R. Blandford and B. W. Barker

Preliminary test results of two new location methods show both methods are quite effective in reducing location errors.

The first method assumed that a great part of travel time residuals are caused by the differences between the actual structures at the source and station from the standard structure used in the program. To correct for both regions, tables of the differences between the halfway travel times from source to bottoming layer using Herrin model, and various regional models, were computed. In application, the total travel time correction for each source-to-station path is the sum of the down-ray correction of the source region and the up-ray correction of the receiver region. Resulting location errors are much smaller (about half) than the errors using the ordinary location method.

The second method considers the possibility that stations in close proximity may be measuring essentially the same travel time residual, leading to a consistent stochastic bias. The assumption that the bias is stochastic can be modelled in terms of a correlation matrix for the residuals which varies according to the separation between two stations. The method will adjust the weighting of travel time residuals in accordance with their overall intercorrelation matrix so that a large cluster of stations will not exert an inordinate effect on the estimated lo-

cation. Behavior of correlation coefficients estimated with 186 station residuals of LONGSHOT, showed 0.7 for 0-5 degree distance range, 0.3 in the 5-10 degree range and 0 for distance greater than 10. Furthermore, 186 stations were broken into 9 groupings. The correlation matrix was then smoothed by modifying it to ensure a positive definite matrix. The resulting LONGSHOT location error with the correlation matrix is reduced to 2.2 km and the confidence intervals include the true location.

S 116

TOTAL INVERSION: A General Method to Solve Direct or Inverse Problems.

Albert TARANTOLA and Bernard VALETTE

Institut de Physique du Globe (L.E.G.S.P.)
4, place Jussieu - 75230 Paris Cedex 05

The main characteristics of the method are: 1°) the theoretical relationships between data and parameters are assumed to be of the most general form: not necessarily linear, not necessarily explicit; 2°) we consider a general space containing data, model parameters and, in general, all necessary but non exactly known quantities; we assume that all *a priori* information about the problem (result of measurements, or *a priori* information about unknowns) can be made explicit by giving a vector of means and a matrix of covariances; and 3°) we obtain then a simple and powerful algorithm to solve the non-linear case, the solution for the linear case being explicit.

With the proposed approach there is no difference between direct and inverse problems.

As particular cases of the method we find a wide class of general methods already studied.

S 117

SOME EXAMPLES OF COMPUTER ASSISTED ALBEGRAIC MANIPULATIONS OF INTEREST IN SOLID EARTH GEOPHYSICS

Edo Nyland (Department of Physics, University of Alberta, Edmonton, Canada T6G 2J1)
Loren Shure (Institute of Geophysics and Planetary Physics, A-025, Scripps Institution of Oceanography, University of California at San Diego, La Jolla, California 92093)

Models of geodynamic processes, if they are at all realistic, often involve tedious, expensive and error prone algebra. Many of these routine manipulations can be automated, albeit at the expense of some loss of elegance. One of several computer languages for this purpose is REDUCE. It has been used to derive half-space Green's functions for the elastostatic problem, inner product matrix elements of a geomagnetic inverse problem, and a study of constraints on a stochastic model for induced earthquakes. The capacity of the language to generate FORTRAN code from its results can be exploited once numerical evaluation becomes justified.

S 118

INVERSION OF SEISMIC REFRACTION DATA

C.H. Chapman (Department of Physics, University of Toronto, Toronto, Ontario M5S 1A7, Canada)
J.A. Orcutt (Geological Research Division, Scripps Institution of Oceanography, University of California, San Diego, La Jolla, California 92093, USA)

In recent years, the interpretation of oceanic seismic refraction data has been improved considerably using synthetic seismograms. A better fit between the theoretical seismograms, usually calculated by the reflectivity method, and the data is obtained by trial-and-error modifications to the model. This process is very expensive and time consuming. For many purposes the approximate WKBJ seismograms are adequate for the modelling and because of their simplicity, it is feasible to replace the trial-and-error technique by an automatic scheme. The inversion is posed as a least-squares problem using the usual Euclidean norm of the difference between the synthetic and data time series as the error criterion. In the high-frequency limit, i.e. geometrical ray theory, the problem is very non-linear but for the low frequency part of the signal the system is pseudo-linear. As the Fourier transform is a linear operator, the linear system is equivalent in the time or frequency domain. The frequency domain is preferred as the singular value decomposition approximately separates the system into frequency bands, and using the damped, least-squares technique, the high frequency, non-linear data can be supressed. The technique is illustrated using the Fanfare data collected by Scripps Institution of Oceanography. Spudich and Orcutt have recently interpreted these data by trial-and-error. The damped, least-squares method converges rapidly to a model close to theirs, establishing that even for very band-limited data the technique works, and that their interpretation was very accomplished.

S 119

A RAY PARAMETER-INTERCEPT TIME SPECTRAL RATIO METHOD FOR SEISMIC REFLECTIVITY ANALYSIS

Thomas M. Brocher
Robert A. Phinney (both at: Department of Geological and Geophysical Sciences, Guyot Hall, Princeton University, Princeton, N. J. 08544)

A new method is proposed for seismic reflectivity determination of multichannel seismic reflection data. The method consists of the spectral ratio of a deeper sub-critically reflected target to that of a shallow (upper 1.5 km) post-critically reflected reference amplitude. The novelty of the proposed method is that both target and reference amplitudes are estimated in the ray parameter-intercept time (p-tau) domain, obtained by slant stacking Common Midpoint (CMP) gathers. As the reference amplitude is totally reflected, an advantage of this method over conventional spectral ratio techniques is that reflectivity determination does not require an impedance model of the reference reflector . The estimation of target and reference reflection at different ray parameters requires only a scalar correction to the observed reflectivity. The technique functions well even for reflectors having low S/N ratios, little or no lateral continuity, poor near-surface velocity control and steep dips. The method is illustrated on seismic reflection data gathered by the Consortium for Continental Reflection Profiling (COCORP) in the Rio Grande rift near Socorro, New Mexico. The estimates of the reflectivity of a proposed magma body reflector by the proposed method are compared to those from conventional spectral ratio techniques.

S 120

RELATIVISTIC SEISMOLOGY AND OPTIMAL PARAMETERIZATION OF SEISMIC TRAVEL TIMES

LeRoy M. Dorman (Geological Research Division, Scripps Inst. of Oceanography, U.C. San Diego, La Jolla, CA 92093)
Randall S. Jacobson (Marine Physical Laboratory, Scripps Inst. of Oceanography, U.C. San Diego, La Jolla, CA 92093)

Linear inversion of ray theoretical travel times (T) and distances (X) as functions of horizontal slowness p can be achieved with higher resolution when the usual $\tau(p) = T(p) - pX(p)$ parameterization is supplemented by T(p) and/or X(p) data. This occurs since the partial derivatives of the parameterized data with respect to the model parameters are sharper, hence more "resolvent." When parameterized X(p), T(p) data are (relativistically) rotated in the X, T/p plane so that the data covariance matrix is diagonal, the coordinate normal to the travel time curve is, except for a scaling factor, τ. The orthogonal coordinate (along the travel time curve) is $\zeta(p) = T(p) + pX(p)$. Thus tau and zeta form a coordinate system in which the observations are statistically independent. We note that in some respects, $\zeta(p)$ resembles $\tau(-p)$.

The parameterization operation $(X,T) \rightarrow (X,T,p)$ requires recourse to inverse theory since a trade-off exists. In this case, the data space (X,T) is a subspace of the solution space (X,T,p) so there exists a unique scaling factor which related "spread" and "error" in Backus-Gilbert terminology. A critical factor is the reciprocal of the second derivative (curvature) of the travel time curve, which is used to map uncertainty in p into uncertainty in ζ.

S 121

NEW CONSTRAINTS FOR INVERSION OF TRAVEL TIMES

John Orcutt (*Geological Research Division, Scripps Institution of Oceanography, University of California, San Diego, La Jolla, CA 92093)

Allen Olson (Institute of Geophysics and Planetary Physics, Scripps Institution of Oceanography, University of California, San Diego, La Jolla, CA 92093)

J. McClain (*)

A linear relationship exists between $\tau(p)$, delay time as a function of ray parameter, and $Z(p)$, depth as a function of slowness in a vertically stratified medium in which velocity increases with depth. Linear programming can be used to find a maximum and minimum depth to a given velocity, and in so doing, define an envelope containing all allowable velocity models. These envelopes are notoriously wide and certainly do not make use of all the kinematic data available. Data in the form of $X(p)$ bounds, distance to a given ray parameter, may also be used to reduce the velocity envelope.

We introduce three new constraints which are valuable in the inversion of profile data. The first of these involves a "crossover" constraint. Generally, when a triplication in the travel times is clear, the range interval at which the two forward branches cross is easily determined by examination. This data can be input as a constraint in the travel time problem and can substantially reduce the bound width in the vicinity of the sharp gradient. A second constraint of considerable use involves forcing the extremal solutions to predict ranges which extend to or beyond maximum or minimum ranges observed in the secondary branches of a triplicated travel time curve. Finally, precritically reflected waves can be used to place bounds on the depth to a possible reflector. The application of these constraints to various data sets is illustrated.

S 122

SUBCRITICAL RUPTURE IN THE EARTH, I: PHYSICS AND OBSERVATIONS

C. H. Scholz (also at: Dept. Geol. Sci., Columbia University)
S. Das (both at: Lamont-Doherty Geological Observatory of Columbia U., Palisades, NY 10964)

It is usually thought that a rupture propagates spontaneously when the stress intensity factor reaches a critical values, K_c, but for oxides and silicates in an aqueous environment a crack will grow subcritically, at a rupture velocity $\dot{x}$ much lower than sonic and which depends on K when $K_o < K < K_c$, as in the figure.

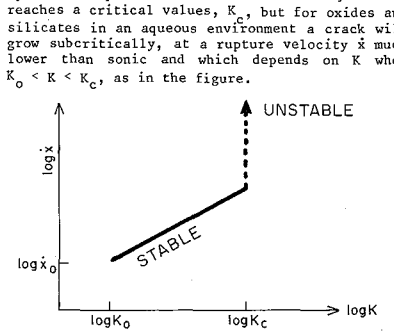

An earthquake is a dynamic stress relaxation that, on a heterogeneous fault, will load isolated regions on and around the fault plane. Subcritical crack growth will lead to delayed failure (static fatigue) of these regions, - viz., aftershocks. The rupture zone may subcritically extend along its periphery, producing an expansion of the aftershock zone and afterslip. If the subcritical rupture extension breaks through a strong barrier (high K_c) and enters a weaker region, the rupture will again become unstable, resulting in a time-delayed multiple event (e.g., doublet). All of these phenomena have been observed in the earth. This phenomenon also predicts that subcritical crack growth should precede earthquakes.

S 123

SUBCRITICAL RUPTURE IN THE EARTH, II: THEORETICAL CALCULATIONS

S. Das (both at: Lamont-Doherty Geological Obser vatory of Columbia University, Palisades, NY 10964)
C. H. Scholz (also at: Dept. Geol. Sci., Columbia University)

We theoretically model subcritical crack growth to explain time-dependent rupture processes in the earth. The stress-intensity factor K for a two-dimensional crack propagating in any mode or for a circular crack in a uniform shear stress field is given by

$$K = C\,\Delta\tau\,\sqrt{x} \qquad (1)$$

where C is a geometrical factor depending on the crack shape, $\Delta\tau$ is the appropriate component of static stress drop, and x is an appropriate linear dimension of the crack. The relation obtained between K and the crack propagation velocity $\dot{x}$ is shown in the previous abstract and can be written in the form

$$K \propto (\dot{x})^{p} \qquad (2)$$

where p is called the "stress corrosion index". From (1) and (2) we can get a very simple differential equation which can be solved to obtain the critical crack size required for unstable propagation ($\dot{x}$ comparable to sonic velocities) and the time required to reach this critical size. The physical parameters in the problem are the static stress drop $\Delta\tau$; the initial crack size; the initial crack velocity $\dot{x}_o$ and the corresponding K_o, called K_o; and the slope p of the (log K - log $\dot{x}$) curve. It is found that depending on the values of these parameters, delay times of the order of seconds to years are found. When the time delay between two events is small, they may be considered as "doublets." When it is large, they are simply two adjacent earthquakes. Among other cases, we shall model the 1854 Ansei I and II pairs, the 1944 Tonankai- 1946 Nankaido (1946) pairs and slow earthquakes.

S 124

RELATIONSHIPS OF TSUNAMI GENERATION AND AN EARTHQUAKE SOURCE

S.N. Ward (Geological Research Div., Scripps Inst. of Oceanography, U.C. San Diego, La Jolla, CA 92093)

This paper presents a theory of tsunami generation and propagation on a spherically symmetric, self-gravitating, elastic Earth in terms of normal modes. We predict the character of newborn tsunamis at regional far field distances from a simply parameterized moment tensor point source. Tsunami eigenfunctions are shown to penetrate the Earth from tens of kilometers at 2000 second period to tens of meters at 20 second period. This behavior explains why the longest tsunami periods are the only ones influenced by crust and mantle structure and why they are preferentially excited by submarine earthquakes. We find that large tsunamis need sizable parent earthquakes because over 96% of their energy is concentrated in the ocean. This makes the entire solid Earth virtually a node for tsunami generation. The excitation of tsunami modes is strongly dependent upon the moment, mechanism and depth of faulting. Calculated tsunami energy, E_T, can vary by a factor of 100 for sources of equal moment within 30 kilometers of the sea floor. Maximum E_T for dip slip and strike slip faulting with moment $M_o = 10^{20}$ nt-m is 1.5×10^{13} and 1.1×10^{12} joules. With mechanism and depth fixed, E_T is proportional to M_o. The ratio of tsunami to radiated seismic energy is less than 1% for all but the largest events. We believe that this theory coupled with a seismic source recovery technique could be a realistic basis for the forecasting of potentially dangerous tsunamis in real time.

S 125

AFTERSHOCKS AS A DATA BASE

R.A. Strelitz (Department of Geological Sciences, University of Southern California, University Park, Los Angeles, CA 90007)

Most theoretical models of the faulting process place aftershocks on the fault plane of the main event. For 'simple' strike slip events especially, aftershock locations cluster on the fault plane, especially if the epicenters are determined jointly or with empirical models (master event), corroborating the theory. By forcing the events to lie preferentially on the fault plane via an augmented norm with a penalty function, one can test the hypothesis that the aftershocks represent unreleased stress on the fault plane. If this is so, other experiments can be performed, including determination of improved station corrections, both for travel times and amplitudes. Finally, these station corrections can be examined for temporal trends indicating the more gradual unloading of the stresses, in a test of for "premonitory" phenomena.

This report will deal with the first stage of such a study - the construction of suitable models and the testing of the accuracies. If time permits, preliminary results from one of several recent large California events will be presented.

S 126

STOCHASTIC SYNTHESIS OF EARTHQUAKE CATALOGS

L. Knopoff
Y. Y. Kagan(both at: IGPP, UCLA, Los Angeles, CA 90024)

A model of earthquake occurrence is proposed that is based on results of statistical studies of earthquake catalogs. We assume that each earthquake generates additional shocks with a probability that depends on time as $t^{-(1+\theta)}$. This assumption together with one regarding the independence of branching events on adjacent branches of the event 'tree', is sufficient to permit the generation of complete catalogs of earthquakes that have the same time-magnitude statistical properties as real earthquake catalogs. If θ is about 0.5, the process generates sequences that have statistical properties similar to those for shallow earthquakes: many well-known relations are reproduced including the magnitude-frequency law, Omori's law of the rate of aftershock and foreshock occurrence, the duration of a recorded seismic event vs its magnitude, the self-similarity, or lack of scale, of rate of earthquake occurrence in different magnitude ranges, etc. A value of θ closer to 0.8 or 0.9 seems to simulate the statistical properties of the occurrence of intermediate and deep shocks. A formula for seismic risk prediction is proposed, and the implications of the model for risk evaluation are outlined. The possibilities of the determination of long-term risk from real or synthetic catalogs that have the property of self-similarity are dim.

S 127

A STUDY OF STOCHASTIC GEOMETRY OF EARTHQUAKE FAULTING.

Y. Y. Kagan
L. Knopoff(both at: IGPP, UCLA, Los Angeles, CA 90024)

The two-, three- and four-point correlation functions (moments) of the spatial distribution of shallow earthquake hypocenters have been studied for the worldwide (NOAA) and Central California (USGS) catalogs. After the non-uniformity of the depth distribution of hypocenters is taken into account, the results indicate the lack of any preferred scale of distance or configuration size in these correlation functions. Let D, S and V be the length of a segment, the surface area of a triangle and the volume of a tetrahedron formed by lines connecting 2, 3 and 4 hypocenters respectively. The probability of finding a linear, triangular or tetrahedral correlation in an earthquake catalog is approximately proportional to 1/D, 1/S and 1/V in order of decreasing degree of certainty. There is a good evidence that in the three-point case this probability is independent of the form of the triangle once the surface is fixed. A similar effect for the four-point function is also indicated though less convincingly. The results for the two- and three-point functions are consistent with the usual model that an earthquake fault is an isolated plane. The results for the four-point case rule out this model.

Seismic Risk

Harbour A
Tuesday A.M.
R. J. Geller (Stanford Univ.) and *M. J. Berry* (Energy, Mines and Resources), Presiding

S 128

APPLICATION OF THE NORMAL MODE METHOD TO MODELING STRONG GROUND MOTION

Robert J. Geller (Dept. of Geophysics, Stanford University,Stanford, Ca. 94305)
Martin W. McCann, Jr.
Haresh C. Shah (both from The John A. Blume Earthquake Engineering Center, Stanford University, Stanford Ca. 94305)

We apply normal mode methods to model strong ground motion acceleration, velocity, and displacement. We extend the use of the model to include the directivity effect and a ramp dislocation time function. The applicability of the model is demonstrated for two events in the Imperial Valley which have been previously studied by other authors, (Heaton and Helmberger, 1977), (Swanger and Boore, 1978).

Results for the 1968 Borrego Mountain earthquake and the 1976 Brawley earthquake are presented. Our findings show that reasonably good frequency resolution can be obtained out to 5-6 hertz if about 20 overtone branches are included in the synthetics. In developing synthetics of displacement, the overall character of the time signal can be quite well matched. For velocity and acceleration the time domain signals are not as well modelled as was expected, but the overall energy distribution as indicated by the Fourier amplitude spectrum is in good agreement. Having demonstrated the ability of the normal mode synthetics to match observed strong motion data, we then apply these synthetics to the prediction of strong motion of future earthquakes.

S 129 INVITED PAPER

DEVELOPMENT OF NEW SEISMIC RISK MAPS FOR CANADA.

P.W. Basham (Earth Physics Branch, Energy, Mines & Resources Canada, Ottawa, Canada, K1A 0Y3).

Research is currently being directed toward new seismic risk maps for Canada and, in due course, these maps will be assessed for purposes of making changes to the seismic zoning map and the seismic design provisions specified in the National Building Code.

The seismicity of Canada and adjacent regions has been delineated by a seismicity model composed of about 30 zones of earthquake occurrence, each having a magnitude recurrence relation derived from estimates of historical and recent earthquake rates. New attenuation relations for peak acceleration, peak velocity and other strong ground motion parameters for western and eastern regions have been derived from regression analysis of California strong motion and western and eastern Canadian intensity data. Seismic risk maps displaying these parameters at a variety of risk levels provide more information for seismic design than previously available.

Seismic risk assessment for sites of critical structures, such as nuclear power plants, makes use of the regional seismicity

model as a base for detailed investigations of seismotectonics and site-specific geologic and seismic studies to provide a combined probabilistic/deterministic derivation of design basis seismic ground motion to be used in seismic design.

S 130

ON THE SEISMIC INPUT FOR EARTHQUAKE HAZARD ANALYSIS

D. H. Chung
D. L. Bernreuter (Both at Lawrence Livermore Laboratory, Engineering Geosciences Group, University of California, Livermore, CA 94550)

If the seismicity and attenuation equations are known, the earthquake hazard can be estimated. In highly seismic areas, it is possible to identify the major tectonic sources of future seismic activity local to the site in question and then compute the future earthquake hazard. In regions of low seismicity, no major fixed sources can be identified and it is necessary to group together all the past seismic events in large seismotectonic provinces surrounding the site and then estimate the hazard based on the average past regional seismicity. Ground motion models are typically developed by correlating the magnitude of a seismic event and distance, using attenuation laws derived by fitting theoretically based equations to data from strong ground motion recording instruments. The probabilistic assessment of the seismic hazard is difficult because of the significant uncertainties associated with the source seismicity and ground motion models. In this paper, we provide an overview of the most widely used approaches to deal with these uncertainties and evaluate the seismic hazard at a site. In particular, we discuss the use of Bayes' theorem as a means of providing a rational procedure for combination of various information to arrive at the most reliable estimate of probability of future earthquake occurrence. We also discuss some useful ways of specifying the seismic hazard at a site and the advantages and deficiencies of various ways of specifying the seismic hazard at a site for the purpose of structural analysis.

S 131

DEVELOPMENT OF THE SEISMIC INPUT FOR USE IN THE SEISMIC SAFETY MARGINS RESEARCH PROGRAM*

D. L. Bernreuter
D. H. Chung (Both at Lawrence Livermore Laboratory, Engineering Geosciences Group, University of California, Livermore, CA 94550)

To evaluate the conservatism in present reactor seismic design techniques, a probabilistic based systems model is being constructed at the Lawrence Livermore Laboratory for the U.S. Nuclear Regulatory Commission. The systems model requires as input a probabilistic definition of the seismic hazard for a site located in the eastern part of the United States. The development of the seismic hazard is difficult task because: the seismic history of the eastern U.S. is very short; little strong ground motion data exist for the eastern U.S.; and, the attenuation of seismic energy is much lower in the eastern U.S. than in most seismic regions of the world.

These problems were solved by incorporating expert opinion with Bayesian statistics. We discuss how expert opinion was obtained by use of questionnaires and expert panel meetings. We outline some of the extensive studies that are being undertaken to provide added insight and to supplement expert opinion; e.g., one study employs a plausible rupture model coupled with an accurate wave propagation code to compute the relative effect that such parameters as Q, stress drop, fault dimension, fault type and depth of the earthquake have on the observed ground motion and its spectral content.

*This work was supported by the U.S. Nuclear Regulatory Commission under Interagency Agreement DOE-40-550-75 with the U.S. Department of Energy.

S 132

THE EVALUATION OF SEISMIC RISK IN NORTHERN CANADA AND APPLICATIONS TO PIPELINE RESPONSE

G. Atkinson, A.G. Davenport, M. Novak
Faculty of Engineering Science
The University of Western Ontario
London, Ontario, Canada N6A 5B9

The estimation of seismic risk in the Arctic is a matter of growing importance in evaluating the safety of northern pipeline projects sensitive to seismic ground shaking. Such estimates are statistically difficult to obtain due to the lack of a good instrumental or historical data base.

The statistical selection of design acceleration levels may be made using either the procedures proposed by Milne and Davenport (1969) or those described by Cornell (1968). The choice between the two is largely a matter of convenience. The Milne and Davenport approach appears to offer advantages in northern Canada since it avoids the seismological problem of defining tectonic zones.

A lognormal distribution of predicted acceleration is used to account for uncertainties in the model assumptions. The width of the distribution describes the degree of uncertainty and can be adjusted regionally to reflect the quality and extent of seismic information.

Seismically induced hazards to pipelines include overstressing due to travelling waves, liquefaction in silt-laden soils, and landslides. Pipeline design requires consideration of several problems not normally encountered in building design. Among those discussed are:

a) the evaluation of risk for a line segment rather than a point site
b) the relative importance of Rayleigh and shear waves according to their path length and angle of incidence
c) possible amplification of earthquake motions in transition zones from firm to soft ground

S 133

A PROBABILISTIC MODEL FOR GROUND MOTION SPECTRA BASED ON RMS ACCELERATION

Martin W. McCann, Jr.
Haresh C. Shah (both from The John A. Blume Earthquake Engineering Center, Stanford University Stanford, Ca. 94305)
Robert J. Geller (Dept. of Geophysics, Stanford University Stanford Ca. 94305)

We present a Bayesian probability model as a means to supplement current techniques with the information which can be generated by a theoretical model. We model the earthquake as a stochastic process and use a Monte Carlo simulation to vary the details of the rupture process and to generate multiple realizations of accelerations. The likelihood function obtained from the simulation gives new but also uncertain information on the RMS acceleration. Bayes theorem then is used to combine the estimates from the simulation with RMS acceleration data from empirical studies of recorded strong motion to obtain a posterior, or updated, probability distribution of RMS acceleration at the site. The updated information on the RMS is then used to scale the spectral shape information, also obtained from the Monte Carlo simulation.

We present results for the Imperial Valley earth structure from our probabilistic model. These results indicate the importance of including information on the earth structure, as well as dynamic characteristics of the rupture process, in predicting future ground motion.

S 134

LOW-LEVEL MONITORING IN THE SW YUKON AS A BASIS FOR SEISMIC RISK EVALUATION

R.B. Horner (Earth Physics Branch, Dept. Energy, Mines and Resources, Ottawa, Canada, K1A 0Y3)
C.A. Crosby

A low-level monitoring program initiated in the SW Yukon in 1978 in response to the proposal to build a natural gas pipeline along the Alaska Highway has deliniated the observed seismicity down to about magnitude 2 into two distinct, well separated zones that correlate with two major fault systems: the Fairweather-Yakutat along the coast of southeast Alaska and the Denali that runs through Alaska, the SW Yukon, northern B.C. and Chatham Strait to connect with the Fairweather off the coast of SE Alaska. A significant feature emerging from the pattern of low-level seismicity is a connection between the two systems, not along Chatham Strait but further west through Glacier Bay. The seismicity does not appear to be continuous along the Denali in the SW Yukon.

A microearthquake survey was conducted for a 6 week period in the Fall of 1979 along a 40 km stretch of the Denali near the south end of Kluane Lake. The earthquakes are randomly scattered through a broad fracture zone, about 15 km wide, bounded by the Shakwak fault on the northeast. The focal depths are predominately upper crustal. A composite P-model solution indicated left-lateral strike-slip motion on a plane striking east-west and dipping steeply to the north or right-lateral strike-slip motion on a near vertical north-south striking plane; neither of these planes align with the NW striking fracture zone.

The regional seismicity model being developed, with detailed investigations of the seismotectonics, will provide the basis for improved seismic risk estimates along the pipeline corridor.

S 135

SCALING FOR SUSTAINED STRONG GROUND MOTION IN WESTERN AND CENTRAL UNITED STATES

R.B. Herrmann (Dept. of Earth & Atmospheric Sciences, Saint Louis University, P.O. Box 8099, St. Louis, MO 63156)
O.W. Nuttli (Dept. of Earth & Atmospheric Sciences, Saint Louis University, P.O. Box 8099, St. Louis, MO 63156)

The falloff of sustained maximum ground acceleration and velocity in the western and central United States were examined to examine the compatability of the strong-motion data bases for the two regions. To do this, amplitudes and durations of sustained levels (level of the third largest peak) of ground acceleration and velocity were measured and 1 Hz bodywave magnitudes were determined for all earthquakes studied.

The conclusions are: 1) Smaller magnitude earthquakes cause motion richer in high frequency which attenuates more rapidly than that due to larger earthquakes. 2) For the same wave frequency, western attenuation is greater than central U.S. 3) When a standardized magnitude (m_b) is used, the difference between western and central U.S. data lies solely in spatial attenuation. 4) The acceleration and velocity satisfy the relations

$$\log_{10} a = A + 0.5\, m_b - G_a(r, m_b)$$
$$\log_{10} v = B + 1.0\, m_b - G_v(r, m_b)$$

where G_a and G_v describe geometric spreading and absorption and r is distance from the earthquake. 5) Peak acceleration and velocity are approximately 1.4 and 1.75 times the respective sustained values. 6) The acceleration values found are comparible with relations proposed by Schnabel and Seed and Boore et al. after M_L values are converted to m_b values.

S 136

ON THE RELATIONSHIP OF SEISMIC RISK AND ENGINEERING DESIGN

A. G. Davenport, Faculty of Engineering Science, The University of Western Ontario, London, Ontario Canada N6A 5B9

In recent years there has been a steady trend towards the description of seismic risk in statistical terms. The National Building Code of Canada was amongst the first codes to take this step and in 1975 adopted an "assigned horizontal design ground acceleration" related to statistical predictions made by Milne and Davenport of the 1/100 probability of annual exceedance.

On the face of it, adoption of this approach allows for a systematic and internally consistent approach to zoning. Nevertheless, it still poses the difficulty of defining the appropriate level of risk. This paper discusses this question.

It is pointed out that other sources of uncertainty, aside from the peak ground acceleration level specified, also exist in the prediction of risk. These include the spectral amplification, the ductility, the foundation effect, and the structural capacity. These other uncertainties also contribute to the

failure risk. The algebra for collectively dealing with these uncertainties is described.

Using a balanced risk concept, in which the expected failure costs are balanced against increased costs of strengthening the structure, the optimum design acceleration and return period for a given site is determined. The sensitivity of the total cost to variations in this design acceleration is also examined and shown to be slight. This indicates there is some latitude in the rational description of the earthquake level.

The paper attempts to reconcile these views with current practices and point to aspects where improvements might be made.

S 137

SEISMIC ATTENUATION DATA APPLIED TO A CANADIAN CONTEXT.

H.S. Hasegawa, P.W. Basham and M.J. Berry (Earth Physics Branch, Energy, Mines & Resources Canada, K1A OY3).

The generation of seismic attenuation relations for application throughout Canada is based upon a number of considerations. The lack of a sufficiently large data base of strong ground motion records of Canadian earthquakes necessitates the use of appropriate records from similar tectonic environments where there is an adequate data base. For the west, records from primarily California earthquakes are appropriate. For the east, where an appropriate analogue is not available, appropriate attenuation relations are derived using the fact that both intensities and higher mode surface waves attenuate less rapidly than in the west.

Regression analyses are performed on a carefully selected data base using Kanai's empirical relation for the following types of ground motion: peak and sustained levels of acceleration, velocity and displacement; Fourier amplitude spectra; pseudo-velocity response spectra at both low and high levels of damping, and intensity. It is found that within the resolution of the data, the rate of attenuation with distance for each of these is the same.

S 138

PROBLEMS OF AN EXPANDING FIELD OF APPLICATIONS IN SEISMIC RISK

Neville C. Donovan (Dames & Moore, 500 Sansome Street, San Francisco, CA 94111)
(Sponsor: D.H. Chung)

The basic procedures used in seismic risk evaluation have been available for more than 10 years. As the applications have developed and more researchers have entered the field refinements in the modelling and the use of assumed parameters have been suggested and published. Some examples of these charges are the incorporation of probable fault rupture dimensions and seismicity relationships with a memory. Most of these suggested refinements, when used with seismicity and motion attention relationships that were not developed in consideration of the special conditions produced an increase in the annual probability of occurrence. This continuous increase must be questioned and requires a re-examination of the total consistency of the assumptions and their applications.

Recent earthquakes have greatly increased the strong motion data in the near (less than 20 kilometers) field region. These data show that the assumptions of a linear relationship between ground motion level and event size are open to serious question. In addition it has become apparent that the characterization of near field motion must be considered separately. Data are shown illustrating the problems outlined and suggestions are given which could result in more stable and consistent application of seismic risk analysis procedures rather than continuing the escalation of the recent past.

S 139

ROBUSTNESS OF CANADIAN SEISMIC RISK ESTIMATES

Dieter H. Weichert (Pacific Geoscience Centre, Earth Physics Branch, Box 6000, Sidney, B.C. V8L 4B2, Canada

The current Canadian seismic zoning map is based on Milne and Davenport's application of Gumbel's unlimited extreme value asymptote. This method is sometimes very misleading: for instance, for a certain lifeline construction it gives a design value of 0.26 g, while a more judicious estimate is 0.13 g. Research in the Earth Physics Branch is currently concerned with the application to Canada of the Cornell method of seismic risk estimation, with the purpose of recommending changes in the next version of the seismic zoning map. The effect of the relatively large number of judgements incorporated in the required seismicity models must be carefully evaluated; however it appears that this method will lead to stable risk estimates in most areas of Canada. A formal convolution of all sources of uncertainty does not appear feasible or even worth while. Isolation of the dominant effects for type locations is more instructive. In general, near the risk level used in the Canadian National Building Code (0.01 per annum, or 50-50 chance in 69 years), groundmotion estimates are relatively robust towards reasonable parameters changes. For lower risk levels and/or higher seismicity, uncertainties in the maximum magnitudes and the associated groundmotion become dominant. Placement of seismic zone boundaries and association of events, especially pre-instrumental, with seismic zones remains critical, and variability of the attenuation relation can still account for a factor of two in any groundmotion estimate.

Wave Propagation: Observations and Instrumentation

Pier 9
Tuesday A.M.
E. A. Okal (Yale Univ.), and *W. A. Prothero* (Univ. of California), Presiding

S 140

SOURCE, PATH, AND STATION EFFECTS ON Lg PROPAGATION IN NORTH AMERICA

D. H. Von Seggern (Dept. of Geosciences, Penn State University, University Park, PA 16802)
S. S. Alexander (Univ. Park, PA 16802)

A statistical study was made on two Lg data sets for North America: 1) LRSM measurements for nearly 100 Nevada Test Site (NTS) shots, and 2) WWSSN and Canadian recordings of 17 eastern North American earthquakes. Decay rates of r^{-2} are acceptable for both data sets, with a tendency to a lesser rate over paths in the Canadian shield, where a mean crustal Q of roughly 2000 is indicated. For the NTS data, the Lg source terms correlate well with previously published source terms for long-period surface waves. No dependence of Lg excitation level on degree of tectonic strain release at NTS could be established, and transverse Lg does not correlate with the Love-wave radiation patterns of shots with high strain release. For the eastern North American earthquakes, source terms from the Lg analysis form a linear relation of slope one with published seismic moments determined from long-period surface waves. A dependence of Lg excitation on earthquake source depth or source mechanism was not evident. Lg seismograms for short-period transverse components were synthesized in an attempt to match the gross behavior of the Lg data; the absolute level of observed Lg excitation and its decay rate were well simulated by these synthetics. The synthetic Lg seismograms show a significant source depth dependence for models with a sedimentary layer whose velocity is significantly lower than that of the basement layer.

S 141

SEISMIC DISCRIMINATION AT NEAR-REGIONAL DISTANCES USING ONLY PN

William A. Peppin (Seismological Laboratory, Mackay School of Mines, University of Nevada, Reno, Nevada 89557)

Two small NTS explosions (12 May 1976; 02 November 1978) present 3-component, wideband data at the Lawrence Livermore Laboratory stations Mina, Kanab, Landers, and Elko. The Pn phase (first 2 seconds of the record) is analyzed on the theory that its propagation can be fairly well understood in the Basin and Range. Using the Priestley-Brune model, Pn waveforms are computed using exact Cagniard-deHoop theory. The seismograms are then inverted for the components of the seismic moment tensor (Stump, 1979). Excellent fits of all input seismograms are obtained, and the solutions show the following values for the components (11, 12, 13, 22, 23, and 33) of the moment tensor: (16, 7.1, 1.6, 14, .88, 8.2) and (64, 25, 3.3, 43, 1.9, 32), clearly showing dominantly diagonal terms. An outstanding problem of the method is the sensitivity of the inferred motions at the source to the structure assumed. In fact, the Priestley-Brune model, based on surface waves at periods in excess of 5 seconds, is inadequate for Pn (dominant frequencies 2-4 Hz).

S 142

PROPERTIES OF HIGH-FREQUENCY P_n-WAVE CODA AT TELESEISMIC DISTANCES

W.H. Menke (Lamont-Doherty Geological Observatory and Dept. of Geol. Sci., Columbia University, Palisades, New York 10964)

High frequency P_n waves from shallow to intermediate depth Caribbean earthquakes observed on short period instruments of the New York State Array are examined. In particular, the phase and amplitude coherence of the coda over wavelength-scale distances is found to decrease rapidly from near coherence at onset to incoherence 5-10 cycles into the coda. This decrease in coherence reflects a change in the frequency content of the P_n coda. The onset of P_n contains mostly lower frequency energy (1-2 hz) while higher frequencies (2-5 hz) dominate after about 4 sec. Spectral content of the P_n and direct P phases is determined, as is their variation with source depth. These data are compared with recent theoretical models of P_n propagation, in which the P_n wave is described as a sum of crust-mantle whispering gallery rays.

S 143

HIGH-FREQUENCY RAYLEIGH WAVES CHANNELED THROUGH OCEANIC SEDIMENTS FOLLOWING SHALLOW EARTHQUAKES IN THE SOUTH-CENTRAL PACFIC OCEAN BASIN

Emile A. Okal, Dept. of Geology & Geophysics, Box 2161, Yale University, New Haven, Conn. 06520

Jacques Talandier, Laboratoire de Géophysique, Commissariat à l'Energie Atomique, Boîte Postale 640, Papeete, Tahiti, French Polynesia.

Shallow seismic events East of Gambier Islands (21°S; 127°W) routinely recorded at the seismic station RKT (Rikitéa, Gambier Islands) at a distance of 7°, are characterized by a wavetrain of substantial amplitude (0.5 μm from an m_b=5.5 event), whose energy is concentrated around 0.7 Hz, and dispersed over as long as 20 minutes. The wavefront, travelling at a group velocity of 3.8 km/s identifies a Rayleigh wave, and the minimum velocity in the cauda, of about 800 m/s, suggests propagation in the sedimentary layer. This is substantiated by similar observations for two other paths in the area, remarkably free of islands and seamounts; on the contrary, this wavetrain is absent from records of comparatively sized events involving paths crossing substantial bathymetric features in the same general area. We will discuss conditions of observation and characteristics of these high-frequency Rayleigh waves, and model their dispersion and excitation.

S 144

SPECTRAL STRUCTURE OF HIGH FREQUENCY P AND S WAVES OBSERVED BY OBS IN THE MARIANA BASIN

T. Ouchi (Marine Science Inst., Univ. of Texas, Galveston, Texas 77550)
S. Nagumo (Earthq. Res. Inst., Univ. of Tokyo, Tokyo, Japan)

We have applied autoregressive models to investigate the spectral content of high frequency (1 - 30 Hz) P and S waves observed

by ocean bottom seismographs (OBS) in the Mariana basin. These data were collected in two separate experiments in July, 1973 and January, 1976. In both experiments, OBS's were placed in the central part of the Mariana basin. S-P times of the earthquakes analyzed ranged from 10 to 120 seconds. Analysis shows that autoregressive models of 10 - 30th order are more suitable for studying these data than conventional methods. For events with S-P times greater than 50 seconds, both the predominant frequency and the wave energy of observed P and S phases are confined to a narrow range, 6 - 10 Hz for P waves and 5.5 - 9 Hz for S waves. In addition, high frequency phases are also characterized by their long duration. Apparently some intrinsic property of the oceanic crust or upper mantle allows the efficient transmission of high frequency (5 - 10 Hz) seismic waves. A plausible model of oceanic upper mantle is presented which is consistent with the observed transmission of high frequency seismic waves.

S 145

HIGH FREQUENCY NORMAL MODE SEISMOGRAM SYNTHESIS - THE Pg PHASE AT NEAR-REGIONAL DISTANCES

Danny J. Harvey (CIRES, Univ. of Colo./NOAA, Boulder, COLO. 80309)

A normal mode superposition approach is used to synthesize complete seismic codas for flat layered earth models at the near-regional distance range and for P-SV phases. Short period synthetic seismograms (8 Hz bandwidth) have been computed using this method for a Basin and Range crustal model which is representative of the Southwestern U. S. These synthetics compare well with observed seismograms of underground nuclear bomb tests from the Nevada test site and in particular the strong Pg phase along with the trailing coda match between the synthetic and observed records. Some researchers have suggested that the observed Pg coda is due to lateral inhomogeneities in the crust but these results indicate that a flat layered model can account for the observed coda.

S 146

CODA OF LOCAL EARTHQUAKES

L. Martel
R. Gaulon (both at Institut de Physique du Globe, L.A. 195, Tour 24, 4 place Jussieu, 75230 Paris Cedex 05).

Several local earthquakes during the seismo-volcanic crisis in Guadeloupe Islands (1976) have been recorded by a network of 18 stations around the volcano, each site having a 3 components short period seismometer. Digital records are obtained and passed by filters centered at 2, 5, 10, 20 and 30Hz. Instantaneous amplitudes and phases are computed. The study by the coda shows that the rate of amplitude variations is identical for the 3 components in agreement with the back-scattering theory of Aki and Chouet for randomly distributed heterogeneities in the Earth. These results are confirmed by observations in the western Pyrenean region in France.

Attenuation measurements show frequency and site dependence. An attempt is made to interpret these observations by regional variations in the mechanism of scattering.

We discuss the possibility of using coda waves as a tool to investigate stress variations in a volcanic area.

S 147

ACOUSTIC PROPERTIES OF ALASKAN SHELVES IN RELATION TO THE REGIONAL GEOLOGY

Robert E. Houtz (Lamont-Doherty Geological Observatory of Columbia University, Palisades, New York 10964

More than 100 airgun-sonobuoy records obtained by the U.S. Geological Survey have been reduced to yield 600 layer solutions. An isopach map, seafloor sound velocity map, eight regional velocity functions, and high-resolution velocity inversions were computed.

Seafloor sound velocities reveal a dependence on age: Quaternary 1.6 km/s, Neogene 1.8 km/s, Cretaceous 2.5 km/s, and Triassic and older 3.5 to 4.5 km/s. Low seafloor velocities in the otherwise Cretaceous seafloor of the Colville foredeep, represent thin Tertiary sediments that onlap Barrow arch from the north. Anticlinal cores of 'mid-shelf arches' (Grantz and Eittreim) are revealed as 200 m/s increases in the Neogene of the western Beaufort shelf.

Velocity functions in this work are based exclusively on refraction solutions. Since the sound velocity in terrigenous shelf sediments is almost entirely dependent on overburden, refrac-velocities from the sediments are not affected by the dip of bedding planes.

The value of K in the least-squares determination of $V=V_0+Kt$ (t is one-way vertical travel-time) decreases towards the east from 1.74 km/s^2 just east of Point Barrow to 1.53 km/s^2 near the Mackenzie river. This decrease corresponds with an eastward increase in the Tertiary of the Brookian sequence (Quaternary to Jurassic). The value of K in the North Chukchi (also Brookian) is 2.1 km/s^2, which suggests that the Tertiary here is much thinner than on the Beaufort shelf.

High-resolution velocity inversions provide near-surface velocity gradients, which are compared with those predicted from the velocity functions. On the Beaufort shelf there is good agreement, but in the Coleville foredeep, a near-surface change of velocity gradient is not detected by the statistically derived velocity functions.

S 148

STUDY OF A SUBSURFACE FRACTURE ZONE BY VERTICAL SEISMIC PROFILING

R.R. Stewart
M.N. Toksöz (both at: Dept. of Earth and Planetary Sciences, M.I.T., Cambridge, MA 02139)
R. Turpening (M.I.T., Lincoln Laboratory Applied Seismology Group, 42 Carleton St., Cambridge, MA 02142)

A vertical seismic profiling (VSP) technique has been used to observe the shallow ground structure of the Michigan basin and an explosively fractured zone embedded therein. Both P and SH waves were used. The P waves were generated by a vertical weight drop. The SH waves were produced by a mortar source and a slanted weight drop. The down-hole receiver was a standard wall-locking three-component seismometer. Measurements were made at 8.3 m intervals up the well.

The experiment was divided into two parts: a "before" survey run on the virgin 770 m of rock, then an identical "after" survey run across an explosively fractured volume of Antrim oil shale, centered at a 400 m depth. From the before VSP survey a shallow velocity structure of the basin was calculated. Attenuation (Q) values have also been computed for selected depths. Comparison of the after observations to the before elucidated the fracture volume and elastic parameters. Travel time delays, amplitude attenuation, converted and scattered waves from the fracture zone provided consistent information on the depth (400 m), shape (ellipsoid) and size (10m x 20m x 30m) of the fractured volume.

S 149

SHORT PERIOD (0.5-7 Hz) TELESEISMIC (30°-90°) P FROM EXPLOSIONS AND EARTHQUAKES ON WAKE ISLAND HYDROPHONES

George H. Sutton
Daniel A. Walker
Charles S. McCreery (all at: Hawaii Institute of Geophysics, University of Hawaii, Honolulu, HI 96822)

Analog tape recordings from three phones of the recently reactivated Wake Island hydrophone array have been scanned for events between 30° and 90° epicentral distance. During a six month period signals from at least 75 earthquakes and 12 explosions were recorded within that range. Spectral analysis of some of those signals has revealed frequencies as high as 5-7 Hz for explosions and deep earthquakes at distances up to 83°. Lower frequencies are observed for shallow events.

S 150

TIMING AND POSITIONING OF SEISMOGRAPH ARRAYS FROM OMEGA NAVIGATION

J.F. Schneider
R.P. Meyer
L.A. Powell (all at Geophysical & Polar Research Center, Univ. of Wisconsin, Madison, WI 53706)

Tests verify our prediction that accurate timing to ±.01 sec and relative positioning to ±200 m at seismographs separated by <30 km can be achieved using the worldwide Omega navigation system VLF broadcasts. Omega is especially useful in remote parts of the world where maps are inaccurate or incomplete, or where other time sources are difficult to receive. The Omega receiving system developed at Wisconsin is very well suited to portable seismograph arrays, due to inherent low power consumption and low cost, along with the accuracy gained by long signal averaging at stationary seismographs.

Omega VLF signals are transmitted sequentially by eight stations in a pattern, tied to universal time, which repeats every 10 sec. Time corrections to an instrument's internal clock are made from the recorded Omega pattern. Position information is obtained from averaged phase differences between two or more pairs of received signals; these yield intersecting sets of hyperbolic lines of position. Absolute position can not be determined accurately, since signal perturbations cause varying and unpredictable phase instabilities which accrue over propagation paths. Relative position accuracy is achieved by comparing phase differences from receivers whose locations are poorly known with simultaneous data recorded at a known location nearby (<30 km). Thus, in this differential mode, errors accrued over long propagation paths are reduced to small relative errors.

S 151

A MICROPROCESSOR CONTROLLED OCEAN BOTTOM SEISMOMETER CAPSULE

W. A. Prothero (Department of Geological Sciences, University of California, Santa Barbara, California 93106)

A new free fall ocean bottom seismometer capsule has been designed which is more versatile, lower cost, and easier to deploy than previous versions. The pressure case consists of two .9 m long, 15.24 cm inside diameter aluminum tubes connected through common endcap. Positive buoyancy is provided by two 43.2 cm diameter glass spheres. Release is accomplished with dual explosive bolts which are bolted directly onto the endcap of the pressure housing. The electronics consist of 3 component seismometers, gain ranging amplifiers and filters, multiplexer, 12 bit analog to digital converter, microprocessor controller, digital cassette tape deck, and acoustic transponder and command system. The acoustic command system allows the number of events triggered, tape usage, and battery status to be monitored from the surface. In addition, the capsule clock can be corrected to several ms accuracy while the package is on the bottom. The gain ranging amplifiers result in 134 db of on scale range. Triggering is accomplished by short-term/long-term average, duration, and slope reversal criteria. The batteries will power the electronics for 1.5 months. A one-year version with long period response is being tested for long-term teleseismic monitoring. Checkout is largely computer automated and can be accomplished without opening the pressure case, considerably reducing the effort required to deploy the capsule. The microprocessor controller enables the system to be adapted to a wide variety of sophisticated oceanographic data sampling and recording experiments. The mechanical design is consistent with deployments of 1 year or longer. Its total estimated parts cost is $14,000 U.S. The electronics system is being mounted in a suitcase for a land version costing approximately $8,000 U.S.

S 152

EVIDENCE THAT BIOLOGICAL ACTIVITY AFFECTS OCEAN BOTTOM SEISMOGRAPH RECORDINGS

Ruth E. Buskirk
Cliff Frohlich
Gary V. Latham
Jeff Lawton (University of Texas Marine Science Institute, Galveston, Texas 77550)

Brief and impulsive signals of uncertain origin appear regularly on records from Ocean Bottom Seismographs of several institutions. These signals have been recorded on nearly all deployments of the Texas OBS, including sites at depths below 7000 m. At some sites, they account for over 90% of the events recorded.

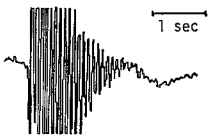

They are of short duration (usually 0.5-3.0 sec) and have a characteristic frequency (usually in the range of 5-10 Hz) that differs from site to site.

We present evidence suggesting that the signals are of biological origin, perhaps caused by animals touching the OBS unit. (1) The distribution of these signals on shallow units shows a 24-hour periodicity, while at sites below 1000 m (where there is no visible light) there is no diurnal pattern. (2) The frequency of occurrence of the signals is similar to the vertical distribution of biomass in the oceans, i.e., they appear most frequently on the shallowest OBS units. (3) Biological material has been found attached to several OBS units upon recovery.

Although they are apparently not of seismic origin, further study of these signals may be useful for three reasons: (1) Their occurrence provides a means of studying deep-sea biological activity. (2) They are a major source of noise for triggered OBS systems. (3) Their character may provide information about sediments near OBS sites.

S 153

WAKE ISLAND HYDROPHONE SEISMIC ARRAY

Charles S. McCreery
Daniel A. Walker
George H. Sutton (all at: Hawaii Inst. of Geophysics, Univ. of Hawaii, Honolulu, HI 96822)

The reactivated hydrophone array near Wake Island, a six element array of deep water bottom mounted hydrophones as well as several pairs of SOFAR depth hydrophones, is proving to be an important tool in several areas of seismological research. It's location is on the ocean side of the downgoing portion of the western Pacific Plate, having within 20-60° epicentral distance a major portion of the earth's seismicity, mostly along pure oceanic paths. During six months of recording from three phones on analog magnetic tape, body wave phases from over 130 events, worldwide, have been recorded along with numerous T-phases. Background noise on the deep phones, based on estimates of hydrophone response, indicate a -18dB/octave slope in pressure between the microseism maximum near 0.25 Hz and 10 Hz after which a slight increase in level is detected to approximately 30 Hz. Estimates of magnification of the deep phones based on signal/1 mm noise of recorded events varies from 4×10^4 to 5×10^5 at frequencies of 1-2 Hz. The range of frequencies observed is from 0.12-22 Hz (with still higher frequencies observed in T-phases). Ongoing research using this data includes: (1) high-frequency, teleseismic Pn and Sn generation and propagation (frequencies to 20 and 22 Hz for Pn and Sn respectively at greater than 30°); and (2) estimation of deep mantle Q using P at 30-90° from explosions and earthquakes (up to 7 Hz). Future topics include (1) lithospheric structure beneath the hydrophones using frequency and angle dependence of multiple surface/bottom reflections of teleseismic phases and (2) array processing for signal detection and propagation characteristics.

Seismic Risk; Panel Discussion

Harbour A
Tuesday P.M.
P. W. Basham (Energy, Mines and Resources), Presiding

S 154

INTERPRETATION OF SEISMIC HAZARD

Daniele Veneziano (Department of Civil Engineering, Massachusetts Institute of Technology, Cambridge, Massachusetts 02139)
Dae H. Chung (Engineering Geosciences Group, Lawrence Livermore Laboratory, University of California, Livermore, California 94550)

It is commonplace among seismologists and earthquake engineers that the occurrence of strong ground motions and the generation and propagation of seismic waves are deterministic phenomena. Whereas there is no conflict between such a deterministic model of the world and the fact that causal laws and states of nature are not precisely known, the problem arises how to interpret results from probabilistic analysis of future seismicity. The classical answer to this problem goes as follows: in a deterministic world, uncertainty is synonymous of ignorance; therefore, the probability of natural events must be a measure of knowledge or strength of belief. The shortcomings of this argument are also well-known: degrees of belief (1) do not necessarily satisfy the axioms of probability theory, (2) vary from individual to individual, and (3) are difficult to quantify. Due to (1) above, the mathematical theory of probability would not be strictly applicable to seismic hazard analysis; difficulty (2) makes it questionable whether important seismic design decisions should be based on degrees of belief, and (3) indicates that practical implementation is not without problems. The degrees-of-belief interpretation is not the only one possible. Take, for example, the times of earthquake occurrences. It is generally found that strong motions take place without significant regularity or clustering in time, in a way that might be described by a Poisson model. Although the Poisson model (as any other random point process) gives a wrong description of the deterministic physical mechanism, there are at least two ways in which such a process may be correct. We will discuss these two issues in greater detail.

S 155

THE DEVELOPMENT OF EMPIRICAL STRONG MOTION ATTENUATION RELATIONS FOR THE EASTERN UNITED STATES

L.H. Wight (TERA Corporation, 2150 Shattuck Ave., Berkeley, CA 94704)
K.W. Campbell (TERA Corporation, 2150 Shattuck Ave., Berkeley, CA 94704)
A.E. Bornstein (TERA Corporation, 2150 Shattuck Ave., Berkeley, CA 94704)

Because of the extremely limited strong motion data available in the Eastern United States, attenuation relations for ground motion, which are empirically derived, must be based on data from regions where such data are abundant, such as the Western United States. Historically, it is well documented that Modified Mercalli (MM) intensity attenuation is less severe in the East than in the West, a fact that must be considered when utilizing Western strong motion data.

The method proposed here and the one most commonly used is to combine a relationship between a ground motion parameter and site intensity derived with Western data with an intensity attenuation relation for the East. A key element in this development is choosing the form of the relationship used to correlate MM intensity and ground motion parameters. The relationship used should depend on the various hypotheses used to explain the differences in attenuation between the East and West inferred from the intensity data.

For instance, let the ground motion parameter be designated Y. Then, four possible hypotheses on the form of the relation between Y and site intensity (I_S) are (1) $Y = f(I_S)$, (2) $Y = f(I_S, R)$, (3) $Y = f(I_S, M)$, and (4) $Y = f(I_S, M, R)$, where R is distance and M is magnitude. The hypothesis preferred is (3) which assumes that for a given magnitude and site intensity, ground motion is the same in the East as in the West. Resulting ground motion attenuation relations are found to be quite sensitive to the hypothesis used in the development.

S 156

A PROBABILISTIC MODEL FOR EVALUATING THE HAZARD ASSOCIATED WITH GROUND RUPTURE ON A FAULT

K.W. Campbell (TERA Corporation, 2150 Shattuck Ave., Berkeley, CA 94704
L.H. Wight (TERA Corporation, 2150 Shattuck Ave., Berkeley, CA 94704)

Ground rupture hazard is defined as the probability that the maximum surface displacement (D) at a point on a fault (the site) will exceed a given amount (d) over some specified length of time (t). For an earthquake of given magnitude (M_j) and distance (x_i), this probability is comprised of a joint probability of three events. The first is the probability that surface rupture occurs, which will be designated "event E_s". The second is the probability that surface rupture extends at least as far as the point of interest (designated "event E_e"). The last is the probability that the displacement exceeds the specified value (designated "event E_d").

Mathematically, this joint probability may be expressed as

$$P(D>d \mid M_j, x_i) = P(E_d \cap E_e \cap E_s)$$

which, when simplified by means of conditional probability theory, becomes

$$P(D>d \mid M_j, x_i) = P(E_d \mid E_e \cap E_s) \cdot P(E_e \mid E_s) \cdot P(E_s)$$

The above probabilities are evaluated from empirical models relating faulting parameters to earthquake magnitude. The total hazard is evaluated by combining the above ground rupture hazard model for various values of d with an earthquake occurrence model for the fault, resulting in a probability distribution of surface displacement at the site for the time period of concern. The hazard may be alternatively expressed in terms of return period and annual probability of exceedence. The model is applied to two faults located in Southwestern Nevada as a test of the procedure.

S 157

DAMAGE RATIOS AND INSURANCE RISKS FOR SEISMIC REGIONS

Haresh C.Shah
Martin W.McCann,Jr.(both from the John A.Blume Earthquake Engineering Center,Stanford University,Stanford Ca.94305)
Franz Sauter (Consulting Engineer, San Jose, Costa Rica)

Developing a rational method to estimate insurance risk for seismic regions of the world has been a major task for researchers for many years. In 1978 December, the United Nations through UNESCO had convened a special meeting of experts in Mexico to discuss this problem and suggest possible methods of estimating damage potential for various types of buildings as well as to help develop a method for estimating earthquake insurance rate structure.This paper will present a methodology to develop such a rate structure.

Expected values of global losses for various classes of structures can be determined by the method presented in this paper. Convolution of all types of building construction together with the seismic hazard would provide the global loss estimate for a given region.

This methodology has bearing on two aspects of earthquake risk. One being the need to develop a standard to determine insurance premiums, and another is the problem of real estate investment risk analysis. Each being a seperate problem, but requiring some means of predicting future damage.

S 158

RISK ANALYSIS FOR PORE PRESSURE BUILDUP DURING EARTHQUAKE LOADING

Jean-Lou Chameau
G.Wayne Clough
Edward Kavazanjian
Haresh C. Shah (all from the John A. Blume earthquake engineering Center,Stanford University, Stanford Ca.94305)

The generation of pore pressure in granular soils due to earthquake loading is evaluated; uncertainties in soil parameters and in earthquake parameters are incorporated in the method. Available studies and data on the distribution of site parameters such as PGA and RMS for a given input parameter like magnitude are used. A complete description of the consequences of pore pressure buildup is obtained, including not only the consequences of zero effective stress state but also the consequences of any pore pressure ratio for each consequence the associated probability of occurence is computed. The proposed method asseses the hazard in terms of soil related parameters such as pore pressure and shear strain.

Studies are under way to evaluate risk in terms of structural damage and economic loss from the knowledge of the hazard at a site. The proposed technique will differentiate between those cases where ground deformations prior to liquefaction can cause damage, those situations where liquefaction can cause damage, and those situations where liquefaction, per se, may not cause damage.

Solar-Planetary Relationships: Aeronomy

U.S.-Canadian Observations Related to the 1979 Solar Eclipse I

Pier 4
Thursday A.M.
A. G. McNamara (National Research Council), Presiding

SA 1 INVITED PAPER

THE 1979 SOLAR ECLIPSE : CIRCUMSTANCES AND A SUMMARY OF CANADIAN OBSERVATIONS

A.G. McNamara (Herzberg Institute of Astrophysics, National Research Council, Ottawa, Canada, K1A 0R6)

The total solar eclipse of 26 Feb. 1979 was the last to occur in North America in this century. The eclipse path contacted land in the States of Washington and Oregon and swept eastward crossing the North Dakota/Saskatchewan border, and turning northward through lightly populated areas of Northern Ontario. Rocket launch facilities were established near Red Lake, Ontario, for a joint USA/Canadian rocket program. Eclipse maximum at ground level occurred at 16:54 UT with a duration of 172 seconds.

The eclipse atmospheric effects were complicated by a major auroral disturbance which commenced several days earlier, and which was still in progress and marked by strong magnetic activity and particle precipitation during eclipse day.

The primary function of the Canadian rocket was to carry a vacuum μ.v spectrograph for study of the solar chromosphere and corona. Also carried were two atmospheric experiments one, a photometer to measure the 1.2μ oxygen emission, and the other a multiple Langmuir probe experiment to measure ionization densities.

The NASA Lear jet was used by a Canadian investigator to observe the solar infrared emission.

SA 2 INVITED PAPER

THE 1979 SOLAR ECLIPSE: A SUMMARY OF THE UNITED STATES OBSERVATIONS AND EXPERIMENT OBJECTIVES

W.W. Berning (Physical Science Lab., New Mexico State Univ.,Las Cruces, NM 88003)

During the 1979 total solar eclipse, ground and aircraft observations were carriod out along the path of totality; near Red Lake, Ontario, sounding rocket measurements to 185 km were made.

In some respects, the 1979 observations were extensions of earlier eclipse studies but with improved instrumentation and greater concentration of rocket measurements about totality. In the rocket studies, the mesosphere and lower thermosphere were of particular interest. Among others, measurements were made of ion composition, electron density, neutral species density, ion conductivity and radiation. Over a period of several days, U.S. experimenters launched 19 small and 13 large sounding rockets.

For the sounding rocket measurements, a major objective was the testing of atmospheric models through their response to the eclipse disturbance. Earlier eclipse measurments provided near-totality electron density distributions not explained by then-existing or current models. In 1979 an abundance of data were obtained; however, particle precipitation was dominant in control of the ion chemistry and electron density in the D-region and in other aspects of the atmospheric response as well. Direct comparison with earlier eclipse experiments is difficult but the Red Lake measurements provide a good data base for testing atmospheric models. Because of their quantity and quality, the ion composition data are of particular interest.

SA 3

FALLING SPHERE DENSITY RESULTS DURING TOTAL SOLAR ECLIPSE, RED LAKE, 1979

A.C. Faire (Air Force Geophysics Laboratory, Hanscom AFB, MA 01731
Irving Michael

Preliminary atmospheric density and temperature results are reported that were derived from data acquired by an AFGL 18 cm diameter HI-BALL falling sphere during the Canadian/USA Eclipse Expedition of 1979. The sphere payload (B-2), instrumented with an omnidirectional accelerometer, was launched onboard a Nike Iroquois (NIRO) rocket vehicle (AF No. A07.712-2) from Red Lake, Ontario, Canada on 26 February 1979. Liftoff time was between third and fourth contact at 1748 GMT, approximately 54 minutes after totality at 1654 hours GMT. Excellent density/temperature results were obtained in the altitude range 40 to 102 kilometers, the region of greatest interest for eclipse-related measurements. The in situ temperature results are particularly significant, since they are essential to accurate analysis of rocketborne ion-chemistry data acquired in the D- and E-regions during the eclipse. A comparison will be made of density/temperature results obtained in the 40 to 100 km altitude range from the 18 cm sphere and other similar measurements made immediately before and after totality.

SA 4

METEOROLOGICAL BEHAVIOR RESULTING FROM THE FEBRUARY 26, 1979 SOLAR ECLIPSE

F.J.Schmidlin (Directorate of Applied Science, NASA Wallops Flight Center, Wallops Island, Va. 23337)
R. O. Olsen (Atmospheric Sciences Laboratory, White Sands Missile Range, New Mexico 88002)

Temperature and wind behavior observed during the February 1979 solar eclipse shows significant change immediately following and up to one hour after totality. Stratospheric and mesospheric data obtained from Red Lake, Ontario, Ft. Churchill, Manitoba, and other sites indicate quite clearly a cooling trend between 50-60 kilometers with the maximum temperature decrease of approximately 10°C evident near 56 kilometers. This temperature perturbation was accompanied by a large amplification of 20-30 mps of the meridional wind near 58 kilometers. These results are in agreement with those obtained at Wallops Island during the March 1970 solar eclipse. Although the stratosphere was under the large-scale influence of a stratospheric warming this was not sufficient to mask the short-term perturbations caused by radiative changes as a result of the solar eclipse.

SA 5

IONIZATION SOURCES 20-25 MINUTES BEFORE TOTALITY DURING THE 26 FEBRUARY 1979 SOLAR ECLIPSE

L.C. Howlett (Space Measurements Laboratory, UMC 41, Utah State University, Logan, Utah 84322)
K.D. Baker
L.L. Jensen

Measurement of D- and E-region ionization sources at Red Lake, Ontario, Canada indicates that during the 26 February 1979 solar eclipse an energetic particle precipitation event was in progress and largely controlled the ionization. Measurement of energetic particles, solar x-rays, Lyman-alpha and cosmic rays was made from a sounding rocket flown with approximately 60% of the solar disk obscured (≈ 25 minutes before totality). Altitude profiles of very low resolution differential energy spectra were obtained by pulse height analysis of scintillations into five approximately logarithmically related energy bins between 7 kev and 1 Mev. Vehicle spin allowed the measurement over a range of pitch angles. The lower energy channels show increasing spin (pitch angle) modulation at decreasing altitudes. At altitudes above 100 km the low energy data appears nearly isotropic over the upper hemisphere. A prominent feature observed in the measurement is microbursts of very high energy particles which occur randomly throughout the flight. The measurement of these bursts which were observed as low as 55 km on descent is not inconsistent with their being ≈ 300 kev, monoenergetic, and field-aligned. The peak power density carried by observed microbursts was >0.3 erg/cm^{2}sec sr (instrument saturation).

SA 6

LOWER IONOSPHERE PRODUCED BY SOLAR ECLIPSE-ELECTRON PRECIPITATION EVENT

R.D. Harris (Space Measurements Laboratory, UMC 41, Utah State University, Logan, Utah 84322)
L.C. Howlett
K.D. Baker

The energetic particle precipitation event in progress during the 26 February 1979 solar eclipse largely controlled the ionization of the E region. Low resolution differential energy spectra for this electron flux were limited to rocketborne measurements of scintillations distributed into five energy bins between 7 kev and 1 Mev. At these energies the measurements are of primary electrons somewhat degraded in energy. Electron densities between 80-160 km were recorded simultaneously on the same rocket with an RF probe. An auroral code used to calculate ionization rates, ion and neutral species densities, excited state production rates and vibrational populations was employed to model this event. This code was modified to utilize the calculations of Berger et al., 1974 to estimate the degraded primary flux, which was then compared with the differential flux and the measured electron profiles. Important auroral emissions were then calculated. A comparison with a 5577Å profile is presented.

Electron density profiles corresponding to the high energy pulsations in the electron spectra observed during the flight are also presented.

SA 7

ELECTRON DENSITY AND ENERGETIC PARTICLES OBSERVED DURING THE ECLIPSE OF 26 FEBRUARY 1979

L. G. Smith
M. K. McInerney (both at: Aeronomy Laboratory, Dept. of Electrical Engineering, Univ. of Illinois, Urbana, IL 61801)
H. D. Voss (Lockheed Palo Alto Research Laboratory, 3251 Hanover Street, Palo Alto, California 94304)

Electron density profiles and energetic particle fluxes have been determined from two rockets launched, respectively, at the beginning and end of totality during the solar eclipse of 26 February 1979. These, and one other rocket at the same time of day on 24 February 1979, were launched from a temporary site near Red Lake, Ontario.

The electron density profile from 24 February 1979 shows the electron density to be normal (at 1×10^5 cm^{-3}) above 110 km, to rocket apogee (130.5 km). Below 110 km the electron density is enhanced, by an order of magnitude in the *D* region, compared with data from Wallops Island at the same solar zenith angle (63°). The enhancement is qualitatively explained by the large flux of field-aligned energetic particles (mainly electrons) observed on the same rocket.

During totality, on 26 February 1979, the electron density above 110 km to rocket apogee (132.6 and 132.3 km) is reduced by the expected factor of about three. Below 110 km however the electron density is much greater than observed during previous eclipses. Again this is attributed to the additional ionization due to field-aligned energetic particles. The particle flux measured on the 26th was an order of magnitude less than that on the 24th but showed much greater variability, particularly at the higher energies (100 keV).

SA 8

ELECTRON DENSITY AND TEMPERATURE IRREGULARITIES MEASURED DURING SOLAR ECLIPSE '79

D. N. Walker
E. P. Szuszczewicz
J. C. Holmes (All three at: Naval Research Laboratory, Washington, DC 20375

Certain irregular features of the electron density and temperature profiles obtained by the pulsed plasma probe aboard the NASA Taurus Orion 33.004 Sounding Rocket during the Feb. '79 Solar Eclipse have been studied with an eye toward correlation with energetic particle precipitation measurements. In particular, evidence of a sporadic negative vehicle potential shift, electron density perturbations, and regions of increased electron temperature have been examined using data reduced from a two-probe system. In addition, measurements of mean-ion mass fluctuation spectra based on results obtained from the two probes (which are separately biased to electron saturation and ion saturation) are presented. These results are compared with electron density fluctuations during times of interest.

SA 9

W. A. Flood, (Army Research Office, Box 12211, Research Triangle Park, NC 27709)
R. Olsen (Atmospheric Sciences Laboratory, WSMR, New Mexico 88002)
D. Mott (Physical Sciences Laboratory, N.M.S.U., Las Cruces, NM 88003)

The U.S. Army Atmospheric Sciences Laboratory fielded a 2.66 MHz partial reflection experiment in the path of totality during the Feb 26, 1979 total solar eclipse. This ground-based experiment, set up and operated by personnel from the Physical Science Laboratory of New Mexico State University, was complemented by an extensive series of rocket-borne measurements of input ionization sources and resulting chemical species and electron and ion densities.

The electron density profiles deduced from the partial reflection data taken during the eclipse period are unusual in that very high electron densities were found at lower D region altitudes and D region ionization was dominated by particle precipitation. The partial reflection-derived electron densities and the many in-situ, rocket-borne probe measurements offer a unique opportunity to:

1) Intercompare ground-based and rocket-borne probe measurements of electron density.
2) Determine the response of the D region to a particle ionization source.

The results of the partial reflection experiment will be discussed in detail.

SA 10

D-REGION ION PAIR PRODUCTION RATE MODEL FOR THE 1979 TOTAL SOLAR ECLIPSE

R.D. Sears (Lockheed Palo Alto Research Laboratory, Palo Alto, CA 94304)
L.G. Smith (University of Illinois, Urbana, Il. 61801)
L. C. Howlett (Utah State University, Logan, Ut. 84322)

A model has been developed for the altitude profile of the ion production rate in the D-region during the total solar eclipse of 26 February 1979. The model is based upon rocket-borne measurements of solar Lyman alpha, solar x-ray flux in the 1-8Å spectral region, bremsstrahlung flux in the 1-10 kev energy region, electron flux due to auroral precipitation, and the cosmic ray flux. Solar x-rays and Lyman alpha appear to be the most important source of ion production in the upper D- and lower E-region, above about 90 km. In the lower D-region precipitating electrons appear to dominate throughout the entire eclipse period. Measured particle fluxes during the eclipse indicate that an energetic pulsating aurora may have been taking place. The total energy flux for precipitating electrons in the energy interval 7 kev to 1 Mev ranges from about 1 erg $cm^{-2}s^{-1}$ to about 0.1 erg $cm^{-2}s^{-1}$ at totality.

U.S.-Canadian Observations Related to the 1979 Solar Eclipse-II

Pier 4
Thursday P.M.
W. W. Berning (New Mexico State Univ.), Presiding

SA 11

ROCKET-BASED INVESTIGATIONS OF D-REGION MINOR NEUTRAL CONSTITUENTS DURING THE SOLAR ECLIPSE OF 26 FEBRUARY 1979

D.J. Baker (Electro-Dynamics Laboratories, UMC 41, Utah State University, Logan, Utah 84322)
W.R. Pendleton, Jr.
A.T. Stair Jr.
J.C. Ulwick

Rocket-based investigations of O, $O_2(a^1\Delta_g)$, O_3, and $OH^{\mp}$ were conducted from a launch site (50.9°N, 93.6°W) near Red Lake, Ontario, Canada during the solar eclipse of 26 February 1979. Cryogenically-cooled radiometers were used to measure selected near-infrared emission features associated with the molecular species, and a determination of [O] was effected using the resonance-lamp technique. The [O] and $[O_2(a^1\Delta_g)]$ measurements were made approximately 25 minutes before second contact, whereas successful O_3 and $OH^{\mp}$ measurements were realized at totality. The measurements will be described, and the implication of the $[OH^{\mp}]$ and $[O_2(a^1\Delta_g)]$ results for photochemical models will be discussed.

SA 12

D- AND E-REGION POSITIVE ION COMPOSITION DURING THE 1979 SOLAR ECLIPSE

P. Eberhardt
U. Herrmann
E. Kopp (all at: Physikalisches Institut, University of Bern, 3012 Bern, Switzerland)

The positive ion composition was measured above Red Lake, Ontario between 60 km and 130 km altitude on February 24 at 1652:00 UT and two days later at the same universal time, shortly after the beginning of totality (NASA payloads 18.1020 and 18.1021). High resolution ($M/\Delta M \sim 75$), cryogenically pumped, magnetic sector type mass spectrometers were used. The distribution of the ions NO^+, O_2^+, $H^+(H_2O)_n$, NO^+X and the metal ions is not significantly different on the two days. This confirms that not the UV, but the high fluxes of energetic protons and electrons observed on these two days were the dominant ionization sources. Below 78 km protonhydrates $H^+(H_2O)_n$ were dominant. However, the $\Sigma H^+(H_2O)_n/NO^+$ ratio was relatively small, only 2 to 3. Above 78 km NO^+ and O_2^+ were the major ions. Below 81 km NO^+/O_2^+ was less than 1, increasing to values from 1 to 20 above 81 km. Between 70 and 85 km the intermediate cluster ions O_4^+, $O_2^+(H_2O)$, H_3O^+OH of the O_2^+ hydration chain were continuously measured. For the first time, $H_3O^+(CO_2)$ was observed.

SA 13

NEGATIVE ION COMPOSITION OF THE D-REGION DURING THE 1979 SOLAR ECLIPSE

E. Kopp
L. André
P. Eberhardt
U. Herrmann (all at: Physikalisches Institut, University of Bern, 3012 Bern, Switzerland)

The negative ion composition was measured above Red Lake, Ontario on February 26, 1979 at 1654:10 UT at the end of totality (NASA payload 18.1022). A high resolution ($M/\Delta M \sim 75$) magnetic sector instrument with liquid He cryopump was used, allowing an accurate mass identification. Negative ions were observed from 58 km to 85 km altitude. Below 72 km molecular ions were dominant. The following molecular ions were identified: CO_3^-, Cl^-, NO_3^-, HCO_3^-, O_2^-, O^-, O_3^- and OH^-. At 68 km CO_3^- was the most abundant ion with $CO_3^-/NO_3^- = 6$. Above 72 km negative cluster ions of hydrated CO_3^-, HCO_3^-, NO_3^-, O_2^- etc. were dominant. The results will be compared with the current negative ion chemistry models.

SA 14

THE INFLUENCE OF MESOSPHERIC TEMPERATURE VARIATION ON THE POSITIVE ION COMPOSITION DURING THE 1979 SOLAR ECLIPSE

U. Herrmann (Physikalisches Institut, University of Bern, 3012 Bern, Switzerland)
C.R. Philbrick (AFGL, Hanscom AFB, MA 01731)

The positive ion composition was measured during totality of the 1979 solar eclipse above Red Lake, Ontario on February 26, 1652:00 UT with a high resolution ($M/\Delta M = 75$) magnetic spectrometer

on NASA payload 18.1021 UE. Approximately 23 minutes before this flight, high resolution temperature and density measurements were made from 155 km to 45 km with a falling sphere ejected from payload ASL-SE79B1.

These nearly simultaneous measurements of temperature and composition offer the possibility of checking the currently used D-region ion chemistry models. The measurement of the intermediate cluster ions O_4^+, $O_2^+(H_2O)$, H_3O^+OH etc. allows us to test models of O_2^+ hydration. New cluster ions such as $H_3O^+(CO_2)$ were observed; their inclusion in the model is discussed. Results of the calculation of neutral NO will be presented.

SA 15

POSITIVE AND NEGATIVE ION COMPOSITION MEASUREMENTS IN THE D AND E REGIONS DURING THE 26 FEB. 1979 SOLAR ECLIPSE

A. Bailey (Aeronomy Division, Air Force Geophysics Laboratory, Hanscom AFB, MA 01731)
R. Narcisi
G. Federico
L. Wlodyka

Two rockets carrying liquid helium, cryo-pumped quadrupole mass spectrometers capable of measuring both positive and negative ions and with shock-attaching conical samplers were launched from Red Lake, Canada during the solar eclipse. Attitude control systems always maintained the rockets at very low attack angles. The first rocket was launched so that the upleg D region was in darkness 35 ± 8 secs. and the downleg D region about 150 ± 15 secs. after second contact. The second rocket was fired after totality in 75% solar illumination. The positive ion composition above 105 km exhibited a strongly increasing NO^+/O_2^+ ratio with time after second contact due to O_2^+ charge transfer with NO and a sharply diminished ionization rate. However, in both flights, the ionization rate below 105 km was dominated by energetic particle deposition exemplified by the increased ion concentrations and the composition signatures of a particle event: a significant enhancement of O_2^+ at lower altitudes and large amounts of $H_5O_2^+$ ions in the D region which result from the O_2^+ clustering scheme. $H_5O_2^+$ was the major ion in the upper D region while $H_7O_3^+$, $H_9O_4^+$ and $H_5O_2^+$ were present at lower altitudes. The negative ion distributions in both flights exhibited a distinct shelf about 83 ± 2 km dropping off by more than an order of magnitude by 90 km and with minima near 75 km. In the 75-90 km range a significant percentage of the negative ions had masses greater than 160 amu. Comparisions with prior flight results during daytime auroral zone absorption events will be made.

SA 16

NEUTRAL CONCENTRATIONS INFERRED FROM THE 26 FEB. 1979 ECLIPSE ION-COMPOSITION DATA

W. Swider (Aeronomy Division, Air Force Geophysics Laboratory, Hanscom AFB, MA 01731)
R.S. Narcisi

Positive ion composition data for eclipse totality near Red Lake, Canada are compared with modelling results. Analytical estimates for 110 km yield a nitric oxide concentration of $1\text{-}2\times10^8 cm^{-3}$ and a residual electron-ion pair production rate of 20 $cm^{-3}sec^{-1}$ with about a factor of two uncertainty. This ionization rate may result mainly from scattered HLyβ radiation. Ionization by energetic electrons appears to peak near 90 km. The nitric oxide concentration at 90 km is about $2\times10^7 cm^{-3}$. A measurement 50 minutes later in seventy-five per cent full sun yields about $3\times10^7 cm^3$ for this same altitude, a concentration well within the uncertainty of the experimental parameters involved if $[NO] \approx 10^3 [NO^+/O_2^+][e]$. This flight also results in a somewhat higher NO concentration at 110 km, $3\times10^8 cm^{-3}$, within experimental error of the previous result.

Qualitatively, the ionization generated by electron precipitation implies that the upper D-region eclipse composition should be more comparable to an SPE-disturbed than quiet D-region. However, the changeover from simple $(NO^+ + O_2^+)$ ions to oxonium ions is observed to be higher, about 82 km, more like a quiet D-region than the November 2-5, 1969, SPE which had a crossover near 76 km. This greater transition altitude may be compatible with a lesser amount of atomic oxygen and/or an increased amount of water vapor. The concentrations inferred for atomic oxygen and water vapor will be shown.

SA 17

EVIDENCE FOR AN ENHANCED WATER VAPOR LAYER NEAR THE MESOPAUSE DURING THE 1979 SOLAR ECLIPSE

M. G. Heaps (US Army Atmospheric Sciences Laboratory, White Sands Missile Range, NM 88002)

The 26 February 1979 solar eclipse was unique in that particle precipitation was occurring during the eclipse period and indeed was the largest source of ionization in the D region at that time. Numerous rocket borne mass spectrometer measurements clearly show the effect of the auroral ionization on the D region positive ion chemistry. In simulating the ion concentrations with the D region air chemistry (DAIRCHEM) computer code it was found that much better agreement could be obtained if a layer of enhanced water vapor concentration were postulated to lie approximately between 80-85 km. The better reproductions of positive ion profiles are obtained when the H_2O density is increased an order of magnitude for this narrow altitude range. The consequences of enhanced water vapor concentrations on ion clustering processes and the potential corroboration with other measurements will be discussed.

SA 18

ATMOSPHERIC ELECTRICAL MEASUREMENTS FROM SOLAR ECLIPSE EXPEDITIONS

L. C. Hale, C. L. Croskey (both from the Ionosphere Research Laboratory, The Pennsylvania State University, University Park, Pennsylvania 16802)

Four Astrobee-D rockets carrying parachute borne payloads were launched during totality and the succeeding nights during eclipse expeditions to Northern Ontario in February, 1979 and Kenya (San Marco Range) in February, 1980. The payloads contained blunt conductivity probes, ultra-violet (Krypton) lamps, and electric field antennas. The Canadian payloads also contained 200 watt "visible" lamps.

The Canadian rockets were launched near Red Lake, Ontario. Strong auroral particle precipitation prevented the observation of definite eclipse effects. The "visible" lamps produced no effects on ionization at any altitude in the data range of 20 to 87 km. A nighttime (pre-sunrise) launch showed UV lamp effects to a much higher altitude than observed in similar daytime data.

The eclipse and night conductivity data from both expeditions are compared with previous data and implications to photo-ionization and photo-detachment rates are discussed.

The electric field data are compared to a similar measurement made at Wallops Island on September 16, 1979 and provide a high-mid-low latitude comparison. Tentatively, the data confirm the existence of a "global" mesospheric circuit.

SA 19

SOLAR ECLIPSE MEASUREMENTS OF MIDDLE ATMOSPHERE ELECTRICAL PARAMETERS

J. D. Mitchell (Electrical Engineering Department and Ionosphere Research Laboratory, The Pennsylvania State University, University Park, Pennsylvania 16802)
R. O. Olsen (Atmospheric Sciences Laboratory, White Sands Missile Range, New Mexico 88002)

Super Arcas rockets were used to launch parachute-borne Gerdien condensers for measuring electrical conductivity, ion mobility and charge number density during eclipse totality near Red Lake, Ontario, Canada (51°N, 94°W) on February 26, 1979 and from the San Marco platform off the coast of Kenya (3°S, 40°E) on February 16, 1980. Additional eclipse launchings, as well as flights on other days to obtain background data, were also conducted at both sites.

Measurements at Red Lake indicate the strong influence of auroral ionization sources above 50 km during that eclipse as well as at other measurement times, thus obscuring possible eclipse effects in this altitude region.

Preliminary results from the San Marco launchings are also discussed.

SA 20

MILLSTONE HILL ELECTRIC FIELD MEASUREMENTS DURING FEBRUARY 26, 1979 TOTAL SOLAR ECLIPSE

J.M. Holt
J.V. Evans
R.H. Wand (all at: Northeast Radio Observatory Corporation, Haystack Observatory, Westford, Massachusetts 01886)

During the February 26, 1979, total solar eclipse the Millstone Hill Incoherent Scatter Radar was operated in a continous scanning mode, with the radar elevation fixed at 4° and the azimuth swept continuously from 299° to 349°. Each scan required 20 minutes to complete and useful results were obtained at ranges up to 2992 km. The path of totality crossed the center of the region swept by the radar beam. Electric field components have been extracted from the radar line-of-sight component of the ion drift by assuming that the electric field may be represented in terms of a quasi-static two-dimensional electrostatic potential with the potential assumed constant along geomagnetic field lines. These assumptions allow the radial component of the electric field to be determined with much better spatial resolution than could be obtained by directly combining field components measured at two or three different azimuths. The resulting time dependent field pattern, which is characterized by much larger electric fields than are usually observed from Millstone during the day, will be discussed.

SA 21

RESIDUAL DAYGLOW AND TWILIGHT-GLOW MEASUREMENTS IN CONJUNCTION WITH THE 26 FEBRUARY 1979 SOLAR ECLIPSE

W.R. Pendleton, Jr. (Electro-Dynamics Laboratories, Utah State University, UMC 41, Logan, Utah 84322)
D.J. Baker
A.J. Steed

A high throughput interferometer-spectrometer has yielded time-resolved near-infrared spectra (6,100-11,900 cm^{-1}; ≈2.5-cm^{-1} resolution; ≈22 sec/spectrum) of the residual dayglow at totality and the subsequent twilight glow in conjunction with the solar eclipse of 26 February 1979. The spectra at totality were degraded somewhat by overcast conditions at the observing site (51.5°N; 93.8°W). However, the O_2 infrared atmospheric emissions at λ1.27 μm and λ1.58 μm, the OH Meinel Δv = 2 emissions, and the HeI emission at λ1.083 μm were readily discernable above the scattered solar radiation. The ground-level intensity of both the O_2 and the OH features decreased monotonically during the ≈2.5 minutes of totality. In sharp contrast, the HeI feature exhibited a minimum intensity at midtotality, with roughly a three-fold greater intensity at second and third contacts. The O_2 λ1.27-μm twilight-transition data exhibited a decay time constant of about 45 minutes at a solar depression angle of 10°, in agreement with the more recent winter measurements at similar latitudes. The HeI λ1.083-μm emission was also prominent in the twilight spectra. Samples of zenith auroral spectra obtained late the same evening will also be presented.

SA 22

Ion Concentration and Mobility Measurements during the 1979 Solar Eclipse

E.R. Hegblom (Boston College, Chestnut Hill Mass. 02167)

T. D. Conley
R. S. Narcisi (both at Air Force Geophysics Laboratory Hanscom AFB, MA 01731)

Positive and negative ion concentrations and mobilities were measured by Gerdien condensers flown on board two rockets launched from Red Lake, Canada during and after totality in the 1979 Solar Eclipse. The first rocket (A10.802-1) was launched at 1652:30 on 26 February 1979 and was in totality above 50 km on ascent and descent. The total ion concentration measured on ascent and descent was approximately 10^4 ions/cm^3 (with less than a factor of 2 variation) from 50 km to 75 km. The second rocket (A10.802-2) was launched at 1741:00 with 75% solar illumination during the flight. The total ion concentration was approximately 10^4 ions/cm^3 (with less than a factor of 2 variation) from 50 km to 75 km on ascent and descent.

The relatively high ion concentration observed in this altitude range indicates that a fairly intense high energy particle precipitation event occurred during the eclipse. The production rate has been calculated based on previous measurements of positive ion loss rates.

Positive and negative ion mobilities have been measured as a function of altitude and will be compared with other measurements.

SA 23

ATMOSPHERIC DENSITY AND TEMPERATURE STRUCTURE - ECLIPSE '79 PROGRAM

C.R. Philbrick (Air Force Geophysics Laboratory, Hanscom AFB, MA 01731)
D.H. Fryklund (Accumetrics Corporation, Cambridge, MA, 02140)

The atmospheric density between 50 and 150 km was measured using a triaxial piezoelectric accelerometer experiment launched as part of the 1979 Solar Eclipse Program. The cooperative international program was conducted at Red Lake, Ontario, Canada on 26 February 1979. The accelerometer sphere launch at 16:28:30 GMT was 47 minutes after first contact and 25 minutes before totality of the eclipse. The density measurements were obtained to provide a definition of the background atmospheric density and temperature conditions on which to base modelling efforts and calculations of the eclipse effects in the D- and E-regions. A temperature profile has been derived from the density measurements under the assumptions of the ideal gas law and hydrostatic equilibrium. Some information on the wind field has also been obtained from the measurements. Small scale structure in the vertical profile of the density shows the effects of gravity waves propagating through the mesosphere. The vertical wavelength of the gravity wave structure observed was about 2 km near 60 km and about 3.5 km near 100 km altitude. The amplitude of the structure in the density profile was 3% near 60 km and about 10% in the vicinity of 100 km.

Results From the July 1979 Kawajalein Special-F Campaign

Pier 9
Friday A.M.
S. L. Ossakow (Naval Research Laboratory), Presiding

SA 24 INVITED PAPER

THE JULY 1979 KWAJALEIN EQUATORIAL SPREAD F CAMPAIGN

H. C. FITZ, Jr., (Defense Nuclear Agency, Washington, DC 20305)

The July 1979 Kwajalein Equatorial Spread F Campaign was the final element in a three year series of operations designed to improve our knowledge of ionospheric disturbances and their effects on radio frequency propagation. In the Kwajalein Campaign, coordinated rocket and ground based measurements were conducted on two different phases of spread F development with rockets launched at 1230Z 17 July and 0957Z 24 July 1979. Rocketborne elements of the campaign consisted of a pulsed plasma probe experiment to measure electron densities fielded by the Naval Research Laboratory, an ion mass spectrometer by the Air Force Geophysics Laboratory, electric field measurements by a team from Utah State and Cornell Universities and an RF beacon by SRI International. Rocket integration and operations were by Sandia Laboratories, Albuquerque. The ALTAIR and TRADEX radars were operated extensively by Lincoln Laboratories in modes which were specified and developed by SRI International. SRI International also operated a Fabry-Perot interferometer to obtain neutral wind information, an ionosonde, and a satellite receiving station. Results provide an improved understanding of spread F phenomena and demonstrate an ability to predict RF propagation effects of the disturbances. An overview of the Campaign will be presented to include the rationale for and interrelationship of the various experiments as specified by theoretical developments at the Naval Research Laboratory. Results will be summarized.

SA 25

THREE-FREQUENCY BACKSCATTER MEASUREMENTS OF EQUATORIAL IRREGULARITIES WITH SPATIAL SCALE SIZES LESS THAN THE ION GYRORADIUS

Roland T. Tsunoda (SRI International, Menlo Park, CA 94025)

A radar experiment was conducted from the Kwajalein Atoll, Marshall Islands, to investigate the nature of equatorial spread-F irregularities with spatial wavelengths less than the ion gyroradius. The source mechanisms that produce these irregularities differ from those that produce the irregularities with wavelengths greater than the ion gyroradius. We cannot therefore extrapolate the known characteristics of the larger-scale irregularities in order to predict those for the smaller-scale irregularities. It is of interest, furthermore, to determine the inner scale size of "turbulence," i.e., the wavelength at which the presence of irregularities cuts off. This paper presents two examples of the wavelength dependence of these small-scale irregularities. The results were obtained from simultaneous measurements at three frequencies: 155.5 MHz and 415 MHz, using the ALTAIR radar; and 1320 MHz, using the TRADEX radar.

SA 26

EQUATORIAL BACKSCATTER PLUME CHARACTERISTICS

Barbara R. White (SRI International, Menlo Park, CA 94025)
Roland T. Tsunoda (SRI International, Menlo Park, CA 94025)

A unique feature that has been observed in equatorial spread-F phenomena is a backscatter "plume," i.e., a spatial pattern of backscatter that extends from the bottomside into the topside of the nighttime F layer. By using ALTAIR, a steerable backscatter radar, these plumes were spatially mapped and tracked as a function of time. The temporal characteristics are described in terms of a growth and a decay phase. These characteristics suggest that a potential "seed" mechanism, which leads to the development of plumes, involves altitude modulation of the bottomside of the F layer and an eastward neutral wind.

SA 27

COINCIDENT RADAR AND ROCKET OBSERVATIONS OF EQUATORIAL SPREAD-F

E. P. Szuszczewicz
J. C. Holmes (Both at: Naval Research Laboratory, Washington, DC 20375
R. T. Tsunoda (SRI International, Menlo Park, CA 94025
R. Narcisi (Air Force Geophysics Laboratory, Bedford, MA 01731

Coordinated measurements of equatorial spread-F conducted during July 1979 at the Kwajalein Atoll have yielded the first definitive space- and time coincident radar and rocket observations of small scale irregularities and large scale plasma depletions. The results have shown that:

(a) There is a positive correlation between "in situ" measurements of positive density gradients and enhanced radar backscatter,

(b) Within large scale depletions radar backscatter energy is at a level much lower than that observed on the depletion's topside wall. The same is true of "in situ" irregularity observations, and

(c) Ion composition within a topside depletion can provide signatures of its bottomside source domain and estimates of average maximum vertical drift velocity. For long-lived depletions, molecular-ion signatures (NO^+ and O_2^+) are lost while bottomside levels of N^+ can be maintained, and finally,

(d) Large scale fluctuations of O^+ accompanied by a near-constant level of NO^+ and O_2^+ on the bottomside F-layer gradient suggests that neutral atmospheric turbulence is not a major source for bottomside ionospheric plasma irregularities.

SA 28

STRUCTURE AND COMPOSITION MEASUREMENTS IN EQUATORIAL IONOSPHERIC BUBBLES

R. Narcisi (Aeronomy Division, Air Force Geophysics Laboratory, Hanscom AFB, MA 01731)
E. Trzcinski
G. Federico
L. Wlodyka
P. Bench

Two multi-instrumented Terrier Malemute rockets including ion mass spectrometers were launched from Kwajalein on the nights of 17 and 23 July 1979 during equatorial spread F events. Detailed ionospheric structure and composition measurements were made between about 100 and 590 km. The first flight penetrated six areas of "bite-outs" spread over the range 265 to 560 km. The strongest irregularities, up to 90% depletion, occurred at the altitudes of 265 to 285 km just above the F region ledge at 250 km. There was no evidence of enhanced bottomside tracer ions (NO^+, O_2^+, meteoric ions) in any of the holes which were composed mostly of O^+ and smaller amounts of N^+. From the composition signatures, the source of the bubbles appeared to be near the F region ledge. Within the higher altitude holes the N^+/O^+ ratios were smaller than the adjacent ionosphere ratios and closer to lower altitude ratios. While O^+ and N^+ exhibited strong variabilities, NO^+ and O_2^+ had fairly smooth profiles with scale heights similar to N_2 and O_2, respectively, indicating steady-state conditions. This also indicated a stable neutral atmosphere with an exospheric temperature of about 1000K which had little, if any, role in the formation of ionospheric irregularities. Time periods for ion-chemical processes to achieve the observed composition are discussed in terms of bubble formation times. The second flight showed an F region ledge near 350 km and irregularities only near the ledge with O^+ dominating.

SA 29

DC AND AC ELECTRIC FIELD AND PLASMA DENSITY MEASUREMENTS IN THE PLUMEX CAMPAIGN

M.C. Kelley and R. Pfaff (School of Electrical Engineering, Cornell University, Ithaca NY 14853)
K. Baker, J.C. Ulwick, L. Jensen and D. Burt (Space Measurements Lab, Utah State University, Logan Utah 84322)

Electric field and relative plasma density measurements were performed on the PLUMEX rockets. Frequency response ranged from quasi-DC to 10kHz which corresponds to spacial scales from hundreds of kilometers to a few centimeters. The plasma density profile was extremely irregular on the bottomside, near the F peak, and for 200 km above the peak. Several deep bite-outs in plasma density were observed

on the topside, one of which coincided with intense backscatter. Large quasi-DC electric fields were associated with some of the low density regions indicating strong internal flow as also shown by computer simulations. The short wavelength electric field and plasma density fluctuation data usually showed extension of a power law spectrum into the range of 100-200 HZ (5-10 meters at a nominal rocket velocity of 1000m/s). However, in the region of plasma density depletions, bursts of higher frequency (shorter wavelength) signals were detected. The signals ranged to above 1000 HZ and did not display a monotonic decreasing spectrum. We conjecture that these fluctuations are responsible for the short wavelength backscatter.

SA 30

MULTIFREQUENCY, RADIO BEACON DIAGNOSTICS OF EQUATORIAL SPREAD-F

Juris Petriceks (SRI International, Menlo Park, CA 94025)
Charles L. Rino, R. C. Livingston

On 17 July 1979 UT, a Terrier-Malemute rocket was launched into active spread-F conditions from Roi-Namur (latitude 9.40°, longitude 167.48°) in the Kwajalein Atoll. An apogee of approximately 600 km was achieved. The rocket carried a high-resolution, electron-density probe; an electric-field probe; a mass spectrometer; and a four frequency (145.76 MHz, 291.53 MHz, 437.29 MHz, 874.59 MHz) phase-coherent radio beacon. In this paper we shall report the results of the radio-beacon measurements.

The beacon antenna was mounted at the rear of the payload assembly such that on the upleg portion of the trajectory, the propagation path was nearly coincident with the flight path. The large-scale differential phase variations are directly proportional to the integrated electron density. Therefore, by differentiating the differential phase, the large-scale electron-density structure can be estimated for comparison with the electron-density probe data.

The propagation disturbance, which reflects small-scale structure, did not increase monotonically as expected. Near an altitude of 400 km, the scintillation decreased somewhat and then rapidly increased as the trajectory penetrated the region of a radar backscatter "plume" (as indicated by the ALTAIR radar). The decrease is attributed to structured ionization in the lower F-region subsiding or moving out of the propagation path. On the 874.59 MHz signal, fades in excess of 3 dB had developed by the time the rocket reached 500 km.

Overall, the spread-F region can be characterized as a highly disturbed, multiplume environment. At least three large depletions were encountered on the rocket upleg. Comparison of the radiowave disturbance with the probe data gathered within and outside the plume structure will be presented to show the details of the irregularity structure.

SA 31

COMPARISON OF LARGE-SCALE QUASI-PERIODIC RALEIGH-TAYLOR PLASMA INSTABILITIES AND SMALL-SCALE INSTABILITY PROCESSES ASSOCIATED WITH THE 1979 KWAJALEIN ROCKET

J. P. McClure (Center for Space Sciences, U. of Texas at Dallas, Richardson, TX 75080)
C. E. Valladares, W. B. Hanson (Both at above address)
R. T. Tsunoda (SRI International, Menlo Park, CA 94025)

Data from the Ion Drift Meter and the Retarding Potential Analyzer (RPA) on the AE-E satellite are compared with data on plasma instabilities at 1-m and 36-cm scale size obtained from the ALTAIR radar on Kwajalein Atoll. A satellite pass at 450 km altitude approximately one hour before the launch of the rocket near 1230 hrs UT on July 17, 1979, showed a rapidly developing large-scale quasi-periodic Raleigh-Taylor instability involving structured vertical velocities of the order of 100 m sec^{-1}. In the center of one depletion the upward plasma drift reached a maximum value of 250 m sec^{-1}, while in other depletions, the vertical drift was near zero. Smaller-scale structures observed using the RPA and the ALTAIR radar are directly associated with these large-scale (100 km) structures.

SA 32

EQUATORIAL THERMOSPHERIC NEUTRAL WINDS FROM NIGHTGLOW 630.0 NM DOPPLER SHIFTS

D. P. Sipler (Dept. of Physics & Astronomy, University of Pittsburgh, Pittsburgh, PA 15260)
M. A. Biondi
R. D. Hake (SRI International, Menlo Park, CA 94025)

A 100 mm-aperture Fabry-Perot interferometer with multiple aperture exit plate has been used to determine F-region neutral winds from 630.0 nm nightglow doppler shifts at Kwajalein Atoll, Marshall Is. during the summers of 1977, 1978 and 1979. In addition to the uniform thermospheric wind fields observed in 1977 and 1978, the July 1979 measurements occasionally indicated gradients in the meridional component of the wind, suggesting a convergence in the neutral flow, e.g., vertical circulation cells. From 0800-1600 UT the wind vectors typically lay in the SE quadrant between azimuths of 90° and 180°, with magnitudes $\leq$ 150 m/sec, and tended to die away in the late night. However, at the time of the first launch of an instrumented rocket in the Kwajalein Equatorial Spread-F Campaign (1231 UT, 17 July 1979) the thermospheric neutral wind was (250 $\pm$ 20) m/sec at 110° az, while for the second rocket launch (0957 UT, 24 July 1979) a more usual value of (170 $\pm$ 30) m/sec at 120° az was observed. Most of the wind patterns are qualitatively consistent with an atmospheric circulation driven by solar EUV heating. A preliminary report on the March 1980 wind measurements will be given.

SA 33

OBSERVED MOTION OF EQUATORIAL 630.0 NM AIRGLOW DEPLETIONS AT KWAJALEIN, MARSHALL IS.

M. A. Biondi (Dept. of Physics & Astronomy, University of Pittsburgh, Pittsburgh, PA 15260)
D. P. Sipler
R. D. Hake (SRI International, Menlo Park, CA 94025)

A three-channel filter photometer with dual-axis pointing head has been used to provide spatial and temporal mapping of the 630.0 nm oxygen nightglow at Kwajalein Atoll, Marshall Is. during July 1979. Airglow intensity depletions believed to be associated with g x B plasma instability regions have been observed. Repeated zonal scans (20° E elevation → zenith → 20° W elevation and back) from 1215 UT to 1600 UT on 25 July 1979 yield W→E drift velocities of the airglow depletions ranging from > 200 m/sec to ~ 100 m/sec. Somewhat surprisingly, these drift velocities are significantly greater than the 50-120 m/sec zonal neutral wind velocities determined by interferometric measurements of the 630.0 nm doppler shifts (see accompanying abstract). Successive all-sky maps during the late night show the decay of a remnant of the N-S aligned airglow depletion (at ~ 1610 UT) to a relatively smooth airglow pattern some 45 minutes later.

SA 34

NONLINEAR EVOLUTION OF LARGE SCALE EQUATORIAL SPREAD F BUBBLES

S. T. Zalesak
S. L. Ossakow (both at Naval Research Laboratory, Code 4780, Washington, D. C. 20375)

Numerical simulations of the nonlinear evolution of the collisional Rayleigh-Taylor instability in the nighttime equatorial ionosphere, using large horizontal scale length initial perturbations, have been performed. These large horizontal scale initial perturbations evolve nonlinearly into large horizontal scale spread F bubbles, on a time scale as fast as that of corresponding small horizontal scale length perturbations previously used.[1] The level of plasma depletion inside the large scale bubbles is appreciably higher than that of the smaller scale bubbles and approaches 100% depletion, in agreement with observations.[2] This level of depletion is due to the fact that the plasma comprising the large scale bubbles has its origin at much lower altitudes than that comprising the smaller scale bubbles. This can be understood in terms of the deeper penetration into the lower ionosphere of the fringe fields surrounding the large scale bubbles. A computer generated color movie will be shown which exhibits the nonlinear evolution (including formation on the bottomside and rise to the topside F region) and shows where the plasma inside the bubbles originates (by "painting" the different regions of the ionosphere with different colors).

SA 35

CONFIGURATION SPACE MODELING OF EQUATORIAL SPREAD-F WITH APPLICATION TO DETECTION OF STREAMING INSTABILITIES BY VHF RADAR

W. G. Chesnut (Radio Physics Laboratory, SRI International, Menlo Park, CA 94025)

Field-aligned radar backscatter echoes have been obtained from equatorial spread-F using frequencies from slightly above the plasma frequency to as high as 1200 MHz. This paper presents a study of the possibility that such echoes are reflections from gradients on the edges of large, plasma rods. These rods are thought to be responsible for ionospheric induced scintillation. We have studied four profile forms for these gradients. The first, the only physically based profile, is assumed to be associated with the gyroradius distribution of the ions in the plasma. The other three profiles were studied to investigate limits of validity of the Born approximation and peculiarities arising from discontinuities in higher order derivatives of the transition profiles.

It is shown that a gyroradius-limited profile produces radar echoes that are hundreds to thousands of dBs weaker than are actually observed at 50 and 155 MHz. We conclude that, observationally, plasma drift waves or electron streaming instabilities must be present and responsible for electron density irregularities with spatial wavelengths of three meters and smaller that produce the observed scattering. We suggest that measurement of the intensity of radar backscatter from equatorial spread-F versus radar frequency from HF through UHF will reveal ion-gradient interface reflections at low HF with a transition to detection of streaming instabilities at wavelengths shorter than about five meters.

SA 36

HIGH RESOLUTION SATELLITE MEASUREMENTS OF EQUATORIAL F-REGION IRREGULARITIES

Malkiat Singh * E. P. Szuszczewicz and J. C. Holmes,
Naval Research Laboratory, Washington, DC 20375

The pulsed plasma probe technique aboard the S3-4 satellite provides "in situ" measurements of electron and ion distributions. The characteristics of the technique is such that simultaneous measurement by two probes leads to high resolution information about density and mean ion mass fluctuations. The satellite is sun-synchronous, crossing the nighttime equator near 2230 LT when the frequency of occurrence of spread-F is high. Irregularity structures as large as 700 km along the magnetic field lines have been observed within 10^{o} of the magnetic equator. Within the extended irregularity structure there are holes ranging from less than one km to tens of km and the density is depleted by a factor as large as 200. The density gradients on the northern and southern walls of the holes are found to be different, soft on equatorward side and steep towards high latitudes. The mean mass inside some small holes is higher indicating higher concentration of molecular ions in the depleted region. In between or within the large holes, the irregular structure can have smaller holes and in these holes the mean mass may or may not be increased. Thus, the presence of more molecular ions in the holes may depend upon the structure and location of the hole itself.

Low Latitude and Equatorial Ionosphere

Pier 9
Friday P.M.
J. A. Gledhill (NASA/GSFC), Presiding

SA 37

CORRELATED EFFECTS OF GEOMAGNETIC ACTIVITY AT ARECIBO

W. E. Swartz (School of Electrical Engineering, Cornell University, Ithaca NY 14853)
J. W. Meriwether, Jr. (Space Physics Research Laboratory, University of Michigan, Ann Arbor MI 48109)
J. C. G. Walker
R. Behnke (Arecibo Observatory, Arecibo PR 00612)

Several studies using incoherent scatter and rocket data have established a correlation between low latitude nighttime E-region electron density enhancements and indicies of geomagnetic activity (Smith et al., JATP, 1473, 1974; Rowe, JGR, 75, 1974; Shen et al., JGR, 5517, 1976). Recent improvements in the airglow instrumentation at Arecibo have enabled observations of enhanced emissions from the first negative band system of nitrogen at 4278 Å which correlated well with D_{st} (Meriwether and Walker, JGR, 1980). Some of these airglow data were obtained coincident with incoherent scatter radar measurements of the E and F layers. Results for the nights of enhanced 4278 Å indicated large enhancements in the electron density after midnight, even though the 4278 Å airglow had been substantially enhanced for most of the night. Since the 4278 Å emission requires about 20 eV for excitation, one may have expected that the growth and decay of the the E-region valley densities would have been closely correlated with the changes in the airglow intensity through a common source of the postulated energetic particle precipitation, but apparently (1) the time constant for significant changes in the densities is longer than expected, (2) the precipitation height varies with time, (3) the convergence of effects of the neutral winds are configured for the greatest density enhancement only after midnight, or (4) the sources of the two effects are only loosely related to each other through some more indirect means.

SA 38

INCOHERENT SCATTER RADAR AND BARIUM CLOUD MEASUREMENTS OF ELECTRIC FIELDS IN THE EQUATORIAL ZONE

A. Valenzuela, G. Haerendel, A. Föppl, and E. Rieger (Max Plank Institut fur Extraterrestriche Physik Garching, West Germany)

B.G. Fejer and M.C. Kelley (School of Electrical Engineering, Cornell University, Ithaca, NY 14853)

The Jicamarca Radar Observatory has yielded a large data base with which to study planetary electrodynamics near the magnetic equator. Recent studies have dealt with quiet versus disturbed times, as well as solar cycle and seasonal dependencies. In this paper we explore the detailed structure of the equatorial electric field as deduced from barium cloud and incoherent scatter radar. Since the radar is limited to regions of relatively high plasma density we can extend our information to a larger range of altitudes using the barium cloud data. For example, barium cloud measurements made in Argentina map to the equatorial plane at high altitudes near Jicamarca. Using such measurements we show that the time of reversal of drift from westward, characteristic of daytime, to eastward at night varies with altitude. From measurements made on rockets launched at the equator (Peru, Brazil and India) there is also a suggestion that below the F layer the ionospheric drift remains westward well into the night. This implies a velocity shear on the bottomside of the F layer which may contribute to the steepness of the bottomside density gradient.

SA 39

IONOSPHERIC ELECTRIC FIELD MODEL FOR AVERAGE QUIET-DAY CONDITIONS AT MIDDLE AND LOW LATITUDES

A.D. Richmond (CIRES, U. of Col., Boulder, CO 80309)
M. Blanc (CNET/CRPE, 92131 Issy-les-Moulineaux, France)
B.A. Emery (NCAR, Boulder, CO 80307)
R.H. Wand (Lincoln Lab., Lexington, MA 02173)
B.G. Fejer (Cornell Univ., Ithaca, NY 14853)
R.F. Woodman (Arecibo Observatory, Arecibo, PR 00612)

Knowledge of the global ionospheric electric field is useful for studies of ionospheric wind dynamo action, ionospheric dynamics, thermospheric dynamics, middle atmospheric electric fields, and several other geophysical phenomena. We have constructed an average quiet-day ionospheric electric field model for middle and low latitudes based on observations from the Millstone Hill, St. Santin, Arecibo, and Jicamarca incoherent scatter radars. A number of symmetry properties are assumed to allow extension of the model beyond the American-European sector. The model is designed to serve as a reference standard and is available as a computer subroutine to facilitate its use. A brief description of the model, its properties, and its potential applications is presented.

SA 40

A MAGNETOSPHERIC SIGNATURE OF SOME F LAYER POSITIVE STORMS

Nathan J. Miller
Hans G. Mayr
Joseph M. Grebowsky
Isadore Harris
Yurdanur K. Tulaney (all at Goddard Space Flight Center, Greenbelt, MD 20771)

During the positive phase of the sudden commencement F layer storm of January 21-22, 1972, spacecraft detected a nightside association between midlatitude enhancements of F layer electron density (N_e) and plasma enhancements lying between L=3-5 outside the equatorial plasmapause. A similar association was detected near midday during the F layer storm of June 17-18, 1972. The equatorial N_e enhancements were similar to detached plasma enhancements sometimes observed near the equator during geomagnetic storms. The stormtime measurements are interpreted in terms of a time-dependent model of the global thermosphere-ionosphere system at a fixed local time. When a high latitude thermospheric heat source is introduced into the model, the resultant equatorward neutral winds produce a dayside association between the positive phase of a midlatitude F layer storm and the development of N_e enhancements near the equator. When a time-dependent magnetospheric electric field is introduced into the model containing the heat source, the resultant cross-L plasma drifts reduce the magnitude of the wind-induced N_e enhancements. Similarities between the N_e enhancements described by the model and those observed during the positive phases of the two F layer storms cause us to conclude that some N_e enhancements observed in the equatorial plane as detached plasma enhancements can be produced by positive F layer storm processes as well as by cross-L plasma drifts.

SA 41

THE HEAO-HOLE IN THE IONOSPHERE

Michael Mendillo (Graduate School, Boston University, Boston, Mass. 02215)

On 20 September 1979, the launch of HEAO-C by an Atlas/Centaur rocket provided an "experiment of opportunity" for studies of ionospheric modification effects. The event was monitored by a network of 12 satellite radio beacon observatories, 2 incoherent scatter radars, an airborne optical observatory, 3 ground-based airglow systems, and over 150 radio propagation monitoring sites using both professional and radio amateur facilities. The ionospheric depletion caused by the rocket exhaust cloud spanned a region of approximately 2 million sq.km. The total electron content depletions near the rocket trajectory showed more than an 80% reduction from ambient conditions. The extensive network of diagnostic systems assembled for the event provided the most complete description yet obtained for a large-scale, rocket-induced ionospheric hole.

SA 42

PROJECT WATERHOLE: AN AURORAL IONOSPHERIC PERTURBATION EXPERIMENT

A.W. Yau
B.A. Whalen (both at Herzberg Institute of Astrophysics, National Research Council of Canada, Ottawa, Canada K1A 0R6)
G. Smith
M.B. Pongratz (both at Los Alamos Scientific Laboratory, Los Alamos, NM 87545)

In a joint effort of the National Research Council of Canada and Los Alamos Scientific Laboratory, 100 kg of high explosives were carried on board a Nike Black Brant rocket payload, and released at an altitude of 300 km above a pre-midnight auroral arc at Fort Churchill, Canada. The water molecules - the major by-product - in the release charge-exchange with the O^+ plasma in the auroral ionosphere to yield molecular ions. The subsequent dissociative recombination of the molecular ions with the ambient electrons results in an order-of-magnitude depletion in plasma density, i.e., the formation of an ionospheric "hole", in the auroral flux tubes. The perturbation to the auroral ionosphere by the release was used as a tool with which to probe the acceleration mechanism of the auroral particles: comprehensive in situ electric/magnetic field, current, particle and photometric measurements were coupled with ground-based observations and theoretical modelling to explore the aeronomy of the perturbed ionosphere and the electrodynamics of the auroral response.

SA 43

COMPARISON OF CALCULATED AND MEASURED LOW LATITUDE IONOSPHERIC PARAMETERS

M. O. Chandler (Space Physics Research Laboratory, Department of Atmospheric and Oceanic Science, University of Michigan, Ann Arbor, MI 48109)
D. G. Torr (Center for Research in Aeronomy, Utah State University, Logan, Utah 84322)
P. Richards (Center for Research in Aeronomy, Utah State University, Logan, Utah 84322)
E. G. Fontheim
A. F. Nagy (both at: Space Physics Research Laboratory, Department of Atmospheric and Oceanic Science, University of Michigan, Ann Arbor, MI 48109)
R. Behnke (Arecibo Observatory, Arecibo, Puerto Rico 00612)

The development of a new ionosphere-protonosphere model has recently been reported by Young et al. [1979]. This model, which includes solutions to the continuity, momentum and energy equation under realistic grophysical conditions along an entire flux tube, has been modified to model low latitude (L<2) conditions. The results from simulations of the refilling of a flux tube in the postsunrise hours are compared to recent ion density measurements from a Defense Meteorological Satellite Program satellite which show significant plasma depletions near the magnetic equator [Burke et al., 1979].

Electron temperature profiles calculated along a L=1.4 field line (corresponding to Arecibo) will be compared to recent Arecibo measurements.

SA 44

MORPHOLOGY OF THE MID-LATITUDE TROUGH AT 300 KM DURING ITS EQUATORWARD EXCURSION ON MARCH 26, 1976

J. A. Gledhill*, H. C. Brinton, R. A. Hoffman, (all at: NASA/Goddard Space Flight Center, Laboratory for Planetary Atmospheres, Greenbelt, MD 20771)
D. G. Torr (Utah State University, Center for Research in Aeronomy, Logan, UT 84322

During the first ASHAY period, a large geomagnetic storm began at 0233 UT on March 26, 1976. Near the end of that day, the minimum of the mid-latitude trough was encountered between 50° and 55° south invariant latitude by Atmosphere Explorer C. Due to the fortunate circumstances that the trough remained almost stationary in magnetic coordinates and was scanned

lengthwise by three successive orbits of the satellite, it was possible to draw contours of electron density, electron temperature and NO^+/O^+ density ratio and so to obtain details of the morphology of the trough for over 4000 km of its length. The NO^+/O^+ ratio reached a maximum value of 23 and the ion drift velocity exceeded 1 km per second in the middle of the trough.

SA 45

PHENOMENA IN THE SOUTH ATLANTIC ANOMALY OBSERVED BY ATMOSPHERE EXPLORER C

R. Haggard (Dept. of Physics and Electronics, Rhodes University, Grahamstown 6140, South Africa)
J. A. Gledhill*, R. A. Hoffman (both at NASA/ Goddard Space Flight Center, Greenbelt, MD 20771)
D. G. Torr (Utah State University, Center for Research in Aeronomy, Logan, UT 84322)

During two of the coordinated research periods of the ASHAY in March/April and June/July 1976, Atmosphere Explorer C measured characteristics of the neutral and ionized atmosphere and particle precipitation at heights near 300 km in the South Atlantic Anomaly, a region about which little is known at present.

The results suggest that:
(a) regions of low electron density coincide with areas of more intense electron precipitation;
(b) the NO^+/O^+ ratio in the Brazilian Anomaly is normal during quiet magnetic times but increases markedly when Kp > 4;
(c) the nighttime electron temperature is low in the Brazilian Anomaly even during moderate magnetic activity.

SA 46

INSTANTANEOUS PLASMA MEASUREMENTS BY MEANS OF TRIPLE-PROBE TECHNIQUE UNDER SPACECRAFT CONDITIONS.

B. Evans
S. Newman
M. Kamitsuma
R.M. Hobson (CRESS, York University, Toronto, Ontario, Canad M3J 1P3)
S. Teri (Dept. Electrical Engineering, Musashi Institutue of Technology, Japan)
Jen-Shih Chang (Dept. Engineering Physics, McMaster University, Hamilton, Ontario, Canada L8S 4M1)

It is proposed that the instantaneous triple probe method can be applied to the direct display of plasma parameters, in the case of probe application during measurements carried out from spacecraft. The theory of the triple probe method has been extended for the very high speed flowing collisionless condition, i.e. in which the spacecraft speed U ≫ the most probable electron thermal velocity $\langle v_e \rangle$ ≫ most probable ion thermal velocity $\langle v_i \rangle$. This condition is particularly important both in the case of re-entry of spacecraft and in the solar wind plasma. Experiments have been conducted in a shock-heated molecular beam type space simulation chamber using cylindrical triple probes. Experimental conformation for an electron temperature, plasma density and electric field has been carried out for various Debye ratios (probe radius Rp/Debye length $\lambda_D \leq 4$), and ion speed ratios ($S_i = U/\langle v_i \rangle \geq 10$). The experimental results show that the electron temperature and plasma density obtained by the triple probe agree withing the + 20% and + 50%, respectively, with other technique and theory of free molecular beam.

SA 47

THEORY OF A SPHERICAL PROBE IN A COLLISIONLESS MAGNETOPLASMA

J. Rubinstein
J.G. Laframboise (both at: Physics Department, York university, Toronto, Canada M3J 1P3)

A theory is presented for a spherical electrostatic probe in a collisionless Maxwellian plasma containing a uniform magnetic field. The theory is based on concepts similar to those of a previous theory for an infinite cylindrical probe [Laframboise and Rubinstein, Phys. Fluids 19,1900 (1976); Rubinstein and Laframboise, Phys. Fluids 21,1655 (1978)]. The theory yields two upper bounds and an adiabatic limit for collection of either electrons or ions. One upper bound is based on the use of kinetic theory considerations to relate particle velocity distributions inside the potential well of the probe to those outside, together with an assumption of helical orbits inside the well. The other bound is based on the use of particle cononical angular momentum conservation to define allowed and forbidden regions for particle orbits. These bounds are applicable for smaller and larger values of nondimensional probe potential $e\varphi_p/kT$, and smaller and larger values of nondimensional magnetic field strength $r_p/\bar{a}$, respectively. The upper-bound currents will be most nearly attained when $\bar{a}/\lambda_D$ is large (here $\bar{a}$ is average electron or ion gyroradius, λ_D is Debye length, r_p is probe radius, φ_p is probe potential relative to that of the plasma, e is magnitude of unit electronic charge, k is Boltzmann's constant and T is temperature). As $\bar{a}/\lambda_D \to 0$, the currents decrease toward the adiabatic-limit currents. The attracted-particle current characteristic in this limit shows negative-resistance behaviour. At space potential ($\varphi_p = 0$) the upper-bound and adiabatic-limit currents coalesce, so that the theory is exact in the limit $r_p/\lambda_D \to 0$, i.e. when no potential barriers exist near the probe. Whenever r_p/λ_D is large enough that such potential barriers form (when $r_p/\lambda_D > 0$, this will generally happen when $|\varphi_p|$ is small enough), our theory becomes invalid. The theory of Sanmartin [Phys. Fluids 13, 103 (1970)] then applies.

SA 48

ODDITIES OF THE EQUATORIAL ENHANCEMENT OF SOME SHORT-PERIOD GEOMAGNETIC VARIATIONS; DURING DAY-TIME

R.P. Kane (Instituto de Pesquisas Espaciais/ Conselho Nacional de Desenvolvimento Científico e Tecnológico, C.P. 515, 12200 São José dos Campos, S.P., Brazil)
(Sponsor: M.A. Abdu)

It is usually believed that short-period geomagnetic variations like SSC, SI and DP-2 have enhanced amplitudes in the equatorial electrojet region in the same way as the Sq shows enhanced amplitudes. Evidence will be presented to show that the equatorial enhancement of these phenomena is not proportional to the equatorial electrojet strength.

John H. Chapman Symposium/Accomplishments of the Alouette-ISIS Program

Harbour A
Saturday A.M.
T. R. Hartz (Communications Research Centre), Presiding

SA 49 INVITED PAPER

PRECIPITATION PATTERNS IN THE POLAR CAP

W. J. Heikkila (The University of Texas at Dallas, P. O. Box 688, Richardson, Tx 75080)
L. Cogger

There are three different types of particles in the polar cap, namely, those of ionospheric, magnetospheric, and external origin. Ionospheric particles are convected from the dayside oval, contributing to the polar cap winter ionosphere. The polar wind exists on polar cap magnetic field lines. In addition, photoelectrons are emitted from the upper F region, even in winter. Particles of magnetospheric origin occur in the 50 eV to 50 keV energy range. The polar rain of electrons, having a spectrum like magnetosheath electrons, produces a weak airglow. Polar showers, bursts of electrons with moderate energies (about 1 keV), most likely produce the sun-aligned arcs over the polar caps. Polar squalls, intense fluxes of electrons with about 10 keV energies (but also some protons), seen after a strong magnetic storm, produce a swirl of auroras, mostly over the morning side of the polar cap. Particle precipitation goes to very high latitudes after substorms. More energetic particles come from the sun, especially after solar flares. These so-called solar cosmic rays are quite useful in indicating how low in latitude energetic particles can penetrate, thus providing some identification of open field lines. Delay times have been used to estimate the length of the magnetotail. It seems likely that magnetic field lines in the central polar cap are open, mapping the interplanetary electric field down to low altitudes. However, there is good evidence that oval auroras are on closed field lines, in the boundary layer on the dawn and dusk sides. The very existence of the boundary layer argues strongly for viscous interaction as the main mechanism producing magnetospheric convection. Thus the magnetospheric electric field is produced by two mechanisms, and an attempt will be made to clarify the relation between them.

SA 50

POLAR CAP SUN-ALIGNED ARCS

S. Ismail (Applied Physics Lab., Johns Hopkins Univ., Laurel, Md. 20810)
G. G. Shepherd (CRESS, York University)
D. M. Klumpar (University of Texas)
D. D. Wallis (NRC, Ottawa, Canada)
J. S. Murphree (University of Calgary)
L. L. Cogger (University of Calgary)

ISIS-2 particle and optical observations have been used to determine the morphology and possible source mechanism for sun-aligned arcs. These polar cap features are relatively infrequent, occurring during periods of low magnetic activity and they may be apparent in 6300 Å but not in 5577 Å or 3914 Å emission. The particles associated with the arcs are electrons of energy < 1 keV and their characteristics are similar to those of polar showers. The main features of the particles can be explained if a simple parallel electric field exists above the satellite altitude. From the measured fluxes, emission rates at 3914 Å, 5577 Å and 6300 Å were calculated and compared with observations. The comparison showed that at high altitude (~ 250 km) the 5577 Å emission is due to direct excitation of atomic oxygen by secondary electrons.

SA 51 INVITED PAPER

OPTICAL STRUCTURE OF THE AURORAL OVAL

C.D. Anger, (Department of Physics, University of Calgary, Calgary, Alberta, Canada T2N 1N4)
J.S. Murphree, (Department of Physics, University of Calgary, Calgary, Alberta, Canada T2N 1N4)
G.G. Shepherd (Centre for Research in Experimental Space Science, York University, Toronto, Ontario, Canada, M3J 1P3)

The two photometric imagers on the ISIS-2 Spacecraft have been looking down on the polar regions since 1971, producing images of auroras at wavelengths of 3914Å, 5577Å, and 6300Å derived from the combined spinning and orbital motion of the spacecraft supplemented in the case of the 5577Å and 3914Å instrument by the internal scanning of an image dissector photomultipler. Results from these instruments have demonstrated the continuity of the auroral oval and the presence of a broad region of diffuse aurora at all local times (characterized by a sharp equatorward boundary), the presence of a broad region of intense 6300Å emmission on the dayside, surrounding the "cleft" region, prominent and extended discrete and diffuse auroras in the polar cap, and the existence of the two different types of auroras in the trough region. More recent work has been involved with the morphology particularly as they relate to ratios of intensities of the different wavelengths and the relationship between optical emissions and particle fluxes.

SA 52

LARGE SCALE 5577Å/3914Å RATIO VARIATIONS IN THE NIGHT SECTOR

J.S. Murphree, (Department of Physics, University of Calgary, Calgary, Alberta Canada T2N 1N4)
C.D. Anger, (Department of Physics, University of Calgary, Calgary, Alberta Canada T2N 1N4)

Data from the Auroral Scanning Photometer on the ISIS-2 satellite is used to describe the two dimensional 5577Å/3914Å ratio during various stages of magnetic activity as defined by the observed auroral morphology. To illustrate the regions of differing ratio, the 3914Å intensity for the ratio ranges .5 to .8 (low), .8 to 1.4 (medium) and 1.4 to 2.3 (high) are transformed onto a corrected geomagnetic latitude/magnetic local time grid. The analysis is limited to the midnight sector where large scale variations in ratio are most typically observed. During low levels of magnetic activity when the emissions are dominated by diffuse aurora, the auroral oval in the night sector is normally characterized by high ratios. There are no systematic latitude or longitude variations in the ratio between 20 and 02 MLT for these three ratio ranges. As activity increases and discrete features appear, the ratio becomes a mixture of medium and high values becoming mainly medium at peak magnetic activity levels. There is a tendency for the high ratio to occur predominantly at the equatorward edge at all local times even during very active periods. There may be clear ratio differences in local time (higher ratio towards evening) even though there is no discernable morphological difference. Statistically significant regions of low ratios occur in discrete arc systems although these may be of temporal origin. The widespread occurrence of low ratio is not a commonplace feature and appears to occur only after a significantly long period of high magnetic activity. During periods of declining magnetic activity, more high ratios begin to appear as expected until their occurrence dominates.

SA 53

FIELD LINE PROJECTION OF AURORAL 6300Å EMISSION INTO THE MAGNETOSPHERE

Marian M. Shepherd (Department of Computer Science)
Gordon G. Shepherd (Centre for Research in Experimental Space Science, York University, Toronto, Ontario, Canada M3J 1P3)

Quantitative magnetic field models are now available with sufficient accuracy to make worthwhile the projection of auroral contours into the magnetosphere. In an initial study the Mead and Fairfield (1975) model was used with 6300Å auroral data obtained from the ISIS-2 satellite. Isointensity auroral contours were selected to define the dayside cleft, the nightside aurora, and the poleward and equatorward auroral boundaries. These were projected onto the equatorial plane and onto YZ planes at various distances in the magnetotail. Some results agree with intuition and some do not. More recently, a comparison with the results obtained from models provided by P.C. Hadgecock have begun.

SA 54 INVITED PAPER

AURORAL ZONE PARTICLE STRUCTURE: THE ISIS CONTRIBUTION (Invited Review)

J. D. Winningham
D. M. Klumpar (Both at: Center for Space Sciences, The University of Texas at Dallas, Box 688, Richardson, Tx 75080)

An historical review of the Alouette/ISIS contributions to our current understanding of the low-altitude auroral zone will be given. The Alouette/ISIS program represents the longest (18 years) continuous program of direct and indirect low-altitude observations of auroral zone particle fluxes. The early Alouette sounder and VLF studies provided the first synoptic description of the 24-hour macroscopic structure of both low and high energy auroral zone particle fluxes. Direct measurements by the Alouette energetic particle detectors provided correlative support for latitude/local time structure of the auroral region. Later results by the ISIS satellites, in the primary energy region of auroral zone particles, built upon and verified the earlier Alouette work with detailed descriptions of the auroral zone particle fluxes. Major regions such as the cleft, the polar cap polar rain, the boundary plasma sheet, and the central plasma sheet were delineated. In conjunction with concurrent energetic particle measurements these primary auroral zone particles were identified as being a result of physical processes occurring on closed or open field lines. Later work on ISIS magnetometer data and correlative studies with AE has led to a picture in which auroral zone particles are placed in context with low and high altitude convection and thus the primary energy source for auroral phenomena. A summary of projections of how future programs, such as DE, will build upon and expand the legacy of knowledge provided by Alouette/ISIS program will be given.

SA 55

PARTICLE ACCELERATION BY CURVATURE DRIFT

W. J. Heikkila (The University of Texas at Dallas, P.O. Box 688, Richardson, Tx 75080

There is a dawn-dusk electrostatic field in the magnetotail, and also a westward cross-tail current. Thus $\underline{E}\cdot\underline{J}$ is positive throughout the entire region, and so there must be energization of charged particles. In a collisionless plasma with slow variations, the first adiabatic invariant is conserved, so in the process of energization the mirror points must come down; there will be precipitation. Near the earth, where the gradient in magnetic field strength is large, the particles undergo acceleration by gradient drift. Farther out in the magnetotail, where VB is small, curvature drift is more important, especially for precipitated particles which have small pitch angles in the distant tail. This energy cannot go into the transverse component, otherwise the first invariant would not be conserved. The alternative is that it goes into the longitudinal component. This may cause violation of the second invariant. We suggest that the reason there are two kinds of auroras, the discrete poleward arcs and the diffuse aurora at lower latitudes, is due to the two kinds of acceleration mechanism. Furthermore, the inverted V structures may be produced by curvature drift, due to a strengthening of the cross-tail current density.

SA 56 INVITED PAPER

CURRENT STRUCTURE OF THE AURORAL OVAL

J.R. Burrows (Herzberg Institute of Astrophysics, National Research Council of Canada, Ottawa, Canada K1A 0R6)
D.M. Klumpar (University of Texas at Dallas, Richardson, Texas 75080)
(Invited Review)

Birkeland currents at high latitudes provide coupling between the magnetosphere and ionosphere and result in significant energy dissipation in the auroral oval via joule heating. Vector magnetic measurements on ISIS-2 and TRIAD have contributed greatly to our knowledge of these currents in the past five years. Their distribution, their correlation with charged particle fluxes, radar and visual auroras and magnetic indices and the influence of the interplanetary magnetic field on current patterns are reviewed. Some directions for future work with new satellite instrumentation are discussed in the context of presently outstanding problems.

John H. Chapman Symposium/Accomplishment of the Alouette-ISIS Program

Harbour A
Saturday A.M.
T. R. Hartz (Communications Research Centre), Presiding

SA 57

THE SUPRATHERMAL ELECTRON CONTRIBUTIONS TO HIGH LATITUDE BIRKELAND CURRENTS

E. J. Maier (NASA/Goddard Space Flight Center, Laboratory for Planetary Atmospheres, Greenbelt, MD 20771)
S. E. Kayser, J. R. Burrows and D. L. Klumpar

Observations obtained from instruments on the ISIS-2 spacecraft in polar orbit at 1400 km have been used to investigate the identity of the charge carriers in the large-scale field-aligned current systems present in the high latitude region. The vertical current is inferred from observed perturbations to the east-west component of the local geomagnetic field obtained by the magnetometer. Simultaneous observations of the charged particle flux were obtained by the soft particle spectrometer (in the .005 to 15 kev range) and by the retarding potential analyzer in the suprathermal energy range (≥1 eV). This flux of electrons in the suprathermal energy range has been studied in an attempt to identify and obtain consistency between the charge carriers and the inferred currents. The observed flow of upwelling suprathermal electrons increased substantially when currents were inferred of either direction. The mean net current density due to suprathermal electrons was 0.4±0.2 $\mu A/m^2$ when the expected current was upward, compared to a mean expected value of 0.2±0.1 $\mu A/m^2$ inferred from the magnetometer. This mean net current density was derived by combining the observed much larger downward flux of electrons, primarily energetic, with an observed upward flux of suprathermal electrons. The partial cancellation of the charge transfer due to the precipitating particles by a return current of suprathermals results in reasonable agreement between the observed net particle flow and the magnetic field perturbation.

When the expected field-aligned currents were downward, the mean current density due to suprathermal electrons was -0.8±0.2 $\mu A/m^2$, compared to a magnetometer inferred value of -0.4±0.1 $\mu A/m^2$. The suprathermal electrons therefore contribute substantially to field-aligned currents, producing most, if not all, inward currents.

SA 58

EMPIRICAL MODELS OF HEIGHT-INTEGRATED CONDUCTIVITIES

D.D. Wallis
E.E. Budzinski
J.R. Burrows (all at Herzberg Institute of Astrophysics, National Research Council of Canada, Ottawa, Canada K1A 0R6)

Two-dimensional distributions of the height-integrated Pedersen and Hall conductivities have been computed for latitudes poleward of 60° invariant, representative of two activity levels $0 \leq K_p \leq 3_0$ and $3_0 < K_p \leq 9+$. Average precipitating fluxes of electrons with energies of 0.15, 1.27, 9.65 and >22 keV obtained by the Energetic Particle Detector of ISIS-2 during 1971-1974 are used as input to a Rees-type computation. The assumption of equilibrium conditions and a recombination rate profile permit calculation of electron density profiles and conductivity profiles. Calculations are performed at 300 grid points, specifically 12 local times and 25 latitudes from 60° to 84° invariant latitude. The models include ionization due to galactic EUV and other background sources which produces base conductivities ($\Sigma_P \sim 0.1$, $\Sigma_H \sim 0.2$ mhos) as well as solar photon ionization through an empirical fit to Chatanika observations (Mehta, 1979). Substantial modulation of the conductivities is found to result from longitudinal variation of the magnitude of the earth's magnetic field. The results show substantial spatial gradients and are expected to be of use in numerical modelling.

John H. Chapman Symposium/Accomplishments of the Alouette-ISIS Program

Harbour A
Saturday P.M.
E. Schmerling (NASA), Presiding

SA 59 INVITED PAPER

HIGH LATITUDE IONOSPHERIC DYNAMICS

J. H. Hoffman (The University of Texas at Dallas P. O. Box 688, Richardson, Tx 75080)
J. H. Whitteker (Communications Research Centre Shirley Bay, P.O. Box 11490, Station "H", Ottawa, Ontario K2H 8S2 Canada)

The high-latitude ionosphere is almost always in a state of motion, both horizontally and vertically. Many of the properties of the F layer and topside arise from this fact. Horizontal drifting affects the distribution of ionization, and the upward flow of light ions (the polar wind) removes ionization and modifies drastically the ion composition in the topside. In the ISIS program, the results of the redistribution of ionization, both horizontally and vertically, have been observed in topside-sounder measurements of electron density, and the upward flow of light ions has been measured directly by directional ion mass spectrometers. The most obvious example of horizontal drifting is a 'tongue' of ionization extending from the sunlit side of the solar terminator into the polar cap. An example of ionospheric dynamics involving both horizontal and vertical motion is the heating, expansion, cooling, and collapse of the topside ionosphere as it drifts beneath the magnetospheric cleft. The polar wind, particularly in winter can cause a severe depletion of light ions in the topside, which implies a low scale height, which in turn results in very low electron densities at high altitudes. The distribution of polar wind velocity and flux in the polar regions is wide spread and exists at all times. H^+ fluxes are lower in winter than in summer, whereas He^+ fluxes are a factor of 10 higher in winter and tend to follow the neutral helium concentration near the F_2 maximum. The latter agree well with model calculations of flux in the winter but lie above the model values by a factor of 2 in summer. H^+ fluxes also agree well with ion flow models.

SA 60 INVITED PAPER

STRUCTURE OF THE TROUGH AND PLASMAPAUSE

D.B. Muldrew (Communications Research Centre, P.O. Box 11490, Station H, Ottawa, Canada K2H 8S2
L.H. Brace (Goddard Space Flight Center, Greenbelt, Maryland 20771)

The main trough, as observed at the peak of the F2 layer by the Alouette and ISIS sounders is due to a reduction in O^+ ions. At times it is only a few degrees of latitude in width with high densities to both the north and south. During the nighttime it appears statistically to be somewhat equatorward of the magnitude field extension of the equatorial plasmapause but during the daytime it can exist at $L > 10$. At about 3000 km height the H^+ density and hence plasmapause can be measured with the cylindrical electrostatic probe aboard ISIS 1; there is no indication of the late afternoon bulge which occurs in the equatorial plasmapause and there is no recovery in density poleward of the plasmapause. The probe also detects an electron temperature peak at the plasmapause which is likely responsible for the subauroral red arcs. Simultaneous ISIS 2 and whistler measurements at dawn and dusk indicate that the low altitude light ion plasmapause begins significantly equatorward of the equatorial plasmapause field line. The formation of the trough and plasmapause is complex but it appears that convection due to earth rotation and magnetospheric plasma flow is one of the major factors. F-layer ionization can remain on the night side of the earth for many hours, and hence be lost through recombination, before convecting westward around the evening side of the earth.

SA 61 INVITED PAPER

PLASMASPHERIC AIRGLOW AND IONOSPHERE (Invited Review)

L.L. Cogger (Department of Physics, University of Calgary, Calgary, Alberta, Canada T2N 1N4)
L.H. Brace
E.J. Maier (both at: Laboratory for Planetary Atmospheres, Goddard Space Flight Center, Greenbelt, Maryland, 20771)
J.S. Murphree (Department of Physics, University of Calgary, Calgary, Alberta, Canada T2N 1N4)
G.G. Shepherd (Centre for Research in Experimental Space Science, York University, Toronto, Ontario, Canada, M3J 1P3).

Measurements made from the Alouette/ISIS satellites have led to a better understanding of the earth's upper atmosphere and ionosphere. In this paper we review some of the significant contributions to the study of the low and mid-latitude regions within the plasmasphere. The range of instruments has provided both in situ plasma measurements and the capability of remote sensing by means of the topside sounder and narrow-band photometers.

SA 62

INTERPRETATION OF LONG-TERM TEMPORAL AND LATITUDINAL AIRGLOW VARIATIONS OBSERVED BY ISIS-2

R.D. Elphinstone, (Department of Physics, University of Calgary, Calgary, Alberta, Canada T2N 1N4)
L.L. Cogger
J.S. Murphree, (both at: Department of Physics, University of Calgary, Calgary, Alberta, Canada T2N 1N4)

Groundbased observations of long-term temporal variations of the E-region 5577Å airglow are restricted in latitude to established station locations, and are subject to contamination by the F-region airglow component, especially near the equator. However, by means of a polar orbiting satellite, the E-region airglow can be monitored for middle and low latitudes in less than one hour. Photometer data from 1971 and 1972 show that the average 5577Å intensity at midlatitudes was 210 R and near the equator was 125 R. The location of this minimum intensity was shifted about 5° into the winter hemisphere. Correlations of the variations in airglow intensity from one latitude to another show that the equatorial region is dominated by airglow arising from the local production of atomic oxygen, whereas the midlatitude shows major seasonal and semiannual variations which are most likely due to the transport of atomic oxygen. The decomposition of the observed airglow intensity into local and transport sources allows the implications of various thermospheric models to be examined.

SA 63 INVITED PAPER

PLASMA WAVE PHENOMENA OBSERVED ON ISIS

H.G. James (Communications Research Centre, Ottawa, Ontario. K2H 8S2 Canada)
R.F. Benson
W. Calvert
D.B. Muldrew

The radio instruments aboard ISIS, especially the topside sounder, have enhanced our understanding of wave propagation in magnetoplasmas. The effect of ionospheric gradients on ray paths has been quantitatively explained using geometric optics. Ionograms have been systematically reduced to extensive 3-dimensional density distributions. Resonance phenomena on ionograms have been explained by the propagation of electron acoustic waves which are reflected a few kilometers from the satellite and return to it for detection. Observations at VLF of lower-hybrid-resonance noise and of ion whistlers have confirmed theories for multi-component plasmas. Various spontaneous radio emissions from wave-particle interactions in terrestrial and solar plasmas have been observed in the ELF to HF range; for example, the generation of whistler-mode hiss and of auroral kilometric radiation have been clarified. Instabilities that cause irregular density variations have been explored; electromagnetic (EM) waves are scattered by large-scale irregularities near the equator (bubbles) and at high latitudes. Small-scale irregularities that extend many thousands of kilometers are found to be efficient guides of EM waves. Near the spacecraft, intense RF fields created by the sounder transmitter modify the electron and ion distributions which are then unstable to certain electrostatic waves. Data from the ISIS antennas have helped to establish the domains of validity of impedance theories for antennas in plasmas.

Future radio experimentation in space plasmas will be a progression of research first performed with ISIS. The large store of hitherto unexplained observations from ISIS promises a rich future in this discipline.

SA 64

VLF SAUCER SOURCE REGIONS

R.E. Horita (Department of Physics, University of Victoria, Victoria, B.C., Canada V8W 2Y2)
H.G. James (Communications Research Centre, Department of Communications, Ottawa, Ont., Canada)

VLF saucers have been assumed to be due to whistler-mode waves propagating usually upward to the satellite. Thus James (1976) assumed a point source below the satellite while Temerin (1979) assumed a line source also below the spacecraft. With the discovery in saucers of attenuation bands at the proton gyrofrequency at the source location, it is possible to check this assumption. Fourteen VLF saucer events observed on the Canadian ISIS 2 satellite exhibiting the attenuation bands were studied and found to have source locations not only below but also above the satellite. Moreover, some saucers showed a change in the proton gyrofrequency seen on the attenuation bands. Depending on the particular source model adopted, the implication is that for these saucers the source region is moving if it is a point source or that the source region is moving and/or is not horizontal if it is a line source. These and other characteristics such as dependence of location on magnetic activity will be presented.

SA 65

VLF HISS AND SAUCER EMISSIONS IN AUSTRAL POLAR REGION OBSERVED BY ISIS-1 and 2

Takeo Yoshino (University of Electro-Comms, Chofu-shi, Tokyo 182, Japan)
Hiroshi Fukunishi (NIPR, Itabashi, Tokyo 173)

The satellite data acquisition facility for ISIS-1 and 2 was set up at Syowa Station in March 1976, and the VLF wide band and top-side sounder data have been received on over 1000 orbits since April 1976 to 1980 by the 17th to 21st wintering parties of JARE.

The highly occurrence regions of VLF hiss and saucer emissions in the austral poler region are as follows;

(1) VLF hiss (occurrence over 50%)
Dayside cusp 75°-85°MLat, 10 -14MLT
Night side 65°-80°MLat, 20 -02MLT
(2) Saucer (occurrence over 30%)
Dayside cusp 75°-85°MLat, 10 -18MLT
Night side 60°-70°MLat, 18 -02MLT

The above results suggest that the dayside emission regions are closely related to field aligned currents in the dayside cusp, and the night side emission are related to the auroral injection currents, and they have the very wider V-shape structure of bottom frequencies.

It is also found that the altitude of saucer emission region have a clear seasonal variations. The altitued range of saucer emissions are observed between 500 - 4000Km in austral winter (April - September), and they are also observed the area of higher than 3500Km in austral summer.

Results from the Defense Meteorological Satellite Program/DMSP

Pier 4 and Lobby
Monday P.M.
R. Babcock (AWS/DNDF), Presiding

SA 66 INVITED PAPER

THE DEFENSE METEOROLOGICAL SATELLITE PROGRAM

Walter D. Meyer, Lt Col, USAF (Special Assistant for Air Force/Army to the Defense Meteorological Satellite Program Office, PO Box 92960, Worldway Postal Center, Los Angeles, CA 90009)
(Sponsor: Richard Babcock)

The Defense Meteorological Satellite Program (DMSP) has flown a number of sensors that have provided a substantial amount of data that has been useful in ionospheric and magnetospheric research. While the scientific results have been widely distributed throughout the research community, information on the DMSP system has not been as widely distributed. The purpose of this paper is to present an overview of the DMSP system including the spacecraft, its orbits, its sensors, and the ground network for command, control, and data acquisition.

SA 67 INVITED PAPER

OPERATIONAL USES OF DMSP IN THE SPACE ENVIRONMENT

V.G. Patterson (Air Force Global Weather Central, Offutt AFB, NE 68113)
R.R. Babcock

The Air Weather Service (AWS), through its operational forecast center of the Air Force Global Weather Central (AFGWC), provides space environmental support to the entire Department of Defense. Although the types and intensity of support are varied, the overall driving requirement is to minimize system effects caused by impulsive solar/geophysical activity and ionospheric variations. Four DMSP sensors are used in monitoring this geophysical activity and ionospheric variability.

The particle precipitation instrument, SSJ/3, and the DMSP visual data are used to monitor the auroral oval size and auroral substorm activity. Several studies are in progress with the Air Force Geophysics Laboratory to expand the operational use of the SSJ/3 instrument. This instrument measures electrons in 16 channels, 50ev-20kev. The ion-electron plasma probe instrument (SSIE) is designed to provide in-situ measurements of electron and ion densities and temperatures and of the mean molecular ion mass. Application of this data will be discussed. The passive ionosonde, SSIP, is the last special sensor to be discussed. This sensor is simply a sweep frequency HF receiver operating between 1.2 and 13.9 MHz. Severe background noise contamination problems, data recovery techniques, and results will be discussed.

SA 68 INVITED PAPER

CONTRIBUTION OF THE DEFENSE METEOROLOGICAL SATELLITE PROGRAM (DMSP) TO MAGNETOSPHERE-IONOSPHERE PHYSICS

S.-I. Akasofu (Geophysical Institute, University of Alaska, Fairbanks, Alaska 99701)

The Defense Meteorological Satellite Program (DMSP) opened a new era in magnetospheric research by providing high resolution auroral photographs of a global scale. Major progresses made in the area of magnetosphere-ionosphere coupling processes by using DMSP photographs are reviewed. In the review, it will be stressed that the magnetosphere and the ionosphere are coupled through field-aligned currents and electric fields and that the aurora is a manifestation of the breakdown of this coupled system. There would be no auroras if geomagnetic field lines were equipotential. Based on this realization, some future DMSP projects are also suggested.

SA 69 INVITED PAPER

DMSP SIMULTANEOUS AURORAL AND PARTICLE PRECIPITATIONS

C.-I. Meng (Applied Physics Lab., Johns Hopkins Univ., Laurel, Md. 20810)
D. A. Hardy (AFGL, Hanscom AFB, Mass.)

Most of the recent DMSP satellites carried a zenith pointing electrostatic analyzer to measure precipitating electrons for providing information of the space environment. By combining the auroral electron precipitation measurement with the simultaneous auroral display imagery, it provides a unique opportunity to study precipitation characteristics of various auroral forms. This talk presents recent progress on this subject as well as results from a statistical analysis of the global auroral electron precipitations.

SA 70

HOW USEFUL ARE AURORAL X-RAYS?

P. F. Mizera (Space Sciences Laboratory, The Aerospace Corporation, El Segundo, CA 90245)

Over the past two years, results of our auroral x-ray experiment flown on the DMSP-F2 satellite have been presented at these meetings. Detailed comparisons between electrons and x-ray distributions have been made[1] on an event by event basis. Using procedures to obtain electron spectra from x-rays, ionospheric parameters such as densities, energy inputs, and conductivities can be calculated in addition to providing continuous global monitoring of electron precipitation. Since the F2 auroral data set covers 2.5 years and future flights will in all probability continue to yield data of this type, it is important that the objectives of our analysis be clearly defined and be of maximum use to the ionospheric scientists.

SA 71 INVITED PAPER

ELECTRON FLUXES OVER THE POLAR CAPS

D.R. Parsignault (Emmanuel College, Boston MA 02115)
(Sponsor: Dave Hardy)

Observations of electron precipitations (0.050 - 20 keV) over the polar cap regions (Lat $\gtrsim |82^{\circ}|$) were made using the electrostatic analyzer on board the DMSP-F2 satellite, from February 13 - 17, 1978. This period coincided with a large PCA event.

Increases in the electron fluxes from $\sim 10^6$ el/cm^2-sec-ster were observed to coincide with the onset of the PCA event (9:30 UT, Feb 13, '78) associated with a hardening of the energy spectrum. The following polar passes on February 14, 15 showed an increase of at least one-order of magnitude, especially over the South polar cap region. On February 16, 0:10 UT the flux over that region reached 7.5×10^7 el/cm^2-sec-ster. Sporadic electron acceleration in the keV region is evident during the period of observation. Comparisons with electron data from ISEE-B are made.

SA 72

OPTICAL AND ELECTRON MEASUREMENTS OF POLAR CAP ARCS

David A. Hardy
W.J. Burke (both from Air Force Geophysics Laboratory, Space Physics Division, Hanscom AFB, MA 01731)
M.S. Gussenhoven (Physics Department, Boston College, Chestnut Hill, MA 02167)

We have completed a case study using optical and precipitating electron data from the DMSP satellites of polar cap arcs observed on 12 December 1977. On this day polar cap arcs were observed repeatedly between ~0800 and ~2300 UT. For the times in which they were observed the Interplanetary Magnetic Field (IMF) had a strong northward component. Each of three weak southward turnings of the IMF was followed shortly by the onset of a substorm and the disappearance of the polar cap arcs. After each substorm when the IMF was again northward the polar cap arcs return with much the same configuration. The electron data show that for times of polar cap arc occurrence, electrons with characteristics unlike the polar rain have access into most of the polar cap and into a region larger than that of the optical features. The polar cap arcs are associated with "inverted V" structures in the electrons with the energy at the peak of the spectrum not exceeding 2 KeV. In the region neighboring the polar cap arc the electrons have characteristics essentially identical to these found at much lower latitudes on the morning side of the oval. The electrons are either relatively dense ($n \sim 5/cm^3$) and cool ($KT_e \sim 200$ eV to 500 eV) or they appear to be composed of a thermal component above 200 eV and an intense non-thermal component below 200 eV. We maintain that the polar cap arcs are produced by acceleration of this plasma and that the similarity in characteristics argues for a common source.

SA 73

THE PERSISTENCE OF AURORAL FEATURES AND THE PATTERN OF ELECTRON PRECIPITATION IN CONSECUTIVE DMSP SATELLITE PASSES

P.J. Tanskanen*
D.A. Hardy (Both from Air Force Geophysics Laboratory, Hanscom AFB, MA 01731)

We have studied in detail aurorae observed in the pre-midnight sector with sensors on board the DMSP F-2 satellite. We have found cases where aspects of the visual features and aspects of the pattern of precipitating electrons are maintained in consecutive passes of the DMSP satellite. We report here on two such cases. The first set of passes is from 4 December 1977 during and extended period of moderate activity. In these two passes the visual features in the lower half of the oval remain essentially the same. The region consists of a wide band of diffuse glow bordered on the poleward edge by weak discrete arcs. The electron data area also similar with the integral flux, energy flux and average energy closely tracking one another in the two passes if one allows for a two degree equatorward shift in the precipitation pattern between passes. The second set of passes is from 3 January 1978 in a period of moderate activity. The visual features in the two passes are again approximately the same except for some decrease in intensity. The electron data also show a repeated pattern with a decrease in the energy flux and average energy.

SA 74

COMPARATIVE STUDIES OF THE LOCATION OF THE OPTICAL OVAL, DISCRETE AND DIFFUSE AURORAS DURING MODERATELY QUIET CONDITIONS

H.W. Kroehl (Data Studies Division NOAA/EDIS/NGSDC, Boulder, CO 80302)
P.J.Tanskanen*
D.A. Hardy (Both from Air Force Geophysics Laboratory, Hanscom AFB, MA 01731)
M.S.Gussenhoven (Physics Department, Boston College, Chestnut Hill, MA 02167)

An extensive correlation has been carried out using simultaneous DMSP photographs and precipitating electron energy spectra (50 eV - 20 KeV). Numerous auroral events during relatively quiet (Kp = 0, 1, 2) periods have been analyzed to determine:

a) The statistical location of the equatorward boundary of the optical oval.

b) The statistical location of discrete and diffuse auroras.

c) The relationship between the equatorward boundary of the optical oval, the boundary of precipitating electrons and the Feldstein oval for Q = 0, 1, 2, 3.

For the comparison of the Feldstein oval with electron data the best agreement is found on the evening side for Q = 1. The typical difference between the statistical location of the equatorward boundary of electron precipitation and the edge of the Feldstein oval is between 1 and 2 degrees. For higher activity (Q = 3) the difference increases slightly but is still on the order of 2 degrees. On the morning side the difference for Q = 1 is between 3 and 5 degrees increasing to 4 to 6 degrees for Q = 3. The optical results show on the evening side values between those from the Feldstein oval and the electron data.

SA 75

OBSERVATIONS OF EQUINOCTAL DENSITY ENHANCEMENTS IN THE EQUATORIAL TOPSIDE IONOSPHERE NEAR THE SUNSET TERMINATOR

E.R. Young
F.J. Rich (both at Research Center, Regis College Weston MA 02193)
M. Smiddy
R.C. Sagalyn (both at Air Force Geophysics Laboratory, Hanscom AFB, MA 01731)

An examination of equinoctal data from DMSP-F2 at 840 km in the early evening sector (1800-2000 MLT) has shown a pattern of broad low altitude enhancements of ion density, sometimes accompanied by narrow depressions or instabilities at the earths magnetic equator. Typically the bulge is 30° or more in latitudinal extent, while the depressions are about 5° wide when they occur. These features vary with longitude magnetic activity and local time.

The largest depressions occur between 100°E and 20°W longitude during the autumn, while instabilities superimposed upon broad enhancements occur in the same sector during the spring. The autumnal depressions occur at all longitudes except between 300°E and 200°E, and when they occur, are within 3° of the magnetic equator. In both the spring and autumn, at all longitudes, more negative values of DST seem to favor the production of the broad enhancements and discourage the formation of the narrow troughs.

The vernal enhancements of 1978 near 19.7 MLT were generally greater, more extended in latitude and more consistent than the autumnal 1977 enhancements which are near 14.0 MLT. This is thought to reflect a local time dependence although a seasonal assymetry cannot be ruled out.

SA 76

QUASI STATIC INJECTION BOUNDARIES: DMSP PREDICTIONS AND P78-2 (SCATHA) OBSERVATIONS

M.S. Gussenhoven (Physics Department, Boston College, Chestnut Hill, MA 02167)
David A. Hardy
W.J. Burke (both from Air Force Geophysics Laboratory, Space Physics Division, Hanscom AFB, MA 01731)

Using data from the SSJ/3 electron spectrometer on the DMSP F-2 satellite we have determined the variation in the corrected geomagnetic latitude of the equatorward edge of electron precipitation in the auroral zone as a function of Kp and magnetic local time (MLT). Since the DMSP F-2 satellite is approximately sun-synchronous in the dawn-dusk meridian the analysis was restricted to magnetic local times from 1600 to 2300 on the evening side of the oval and from 0400 to 1000 on the morning side. The variation in the equatorward boundary was determined by a linear regression on Kp for one hour zones in MLT. For all zones the relationship was linear with most correlation coefficient in the range −.7 to −.9. The boundary as determined from the regression was projected into the magnetic equatorial plane using the Mead-Fairfield magnetic field model. Separate projections were made for Kp = 1, 2, 3, 4 and 5. We interpret these projections as representing the average location of the zero energy Alfvén layer for each level of Kp. The equatorial projection is found to differ significantly from the Mauk-McIlwain injection boundaries. The projection is best fit to a form as proposed by Volland-Stern with the shaping parameter γ between 2 and 3 and with the axis of symmetry rotated out of the dawn-dusk meridian. The rotation is such that the stagnation point moves towards midnight for Kp $\leq$ 2 and strongly towards noon for Kp> 2. The comparison of the predicted quasi-static injection boundary from this work with observations from the Rapid Scan Particle Detector on board the P78-2 (SCATHA) satellite shows excellent agreement.

SA 77

MORPHOLOGY OF POLAR CAP ARCS FROM PERIODS OF STRONG AURORAL ACTIVITY

B. S. Dandekar (Air Force Geophysics Laboratory, Bedford, MA 01731)

For this study strong auroral activity is defined as a minimum span of 10° in latitude of the oval aurora. For 333 auroral observations from the Defense Meteorological Satellite Program (DMP), over the southern hemisphere in the period May-June of 1974-75, Interplanetary Magnetic data are also available. Of these 90 cases (25%) show the presence of the polar cap arcs. The phase of the auroral substorm is determined from the auroral characteristics from the DMSP pictures and from the B_z component of the IMF. The polar cap arcs are absent during the active phase of the auroral substorm. They occur only during the quiet period and/or the recovery phase of the auroral substorm. The analysis supports the previous results that the polar cap arcs are an integral part of the morphology of the auroral substorm.

SA 78 POSTER PAPER

OPERATIONAL RESULTS OF THE ION-ELECTRON PLASMA PROBE (SSIE)

F.E. Wilson (Air Force Global Weather Central, Offutt AFB, NE 68113)
T.F Tascione
(Sponsor: Vernon G. Patterson)

Data from the DMSP ion-electron plasma probe, SSIE, are processed routinely by Air Weather Service at the Air Force Global Weather Central (AFGWC). Raw satellite data are decoded and analyzed using file routines and processors jointly developed by AFGWC and the Air Force Geophysics Laboratory. The SSIE was designed to provide in-situ measurements of mean molecular ion mass and of electron and ion densities and temperatures. From this data, scale height information could be calculated. Low voltage spacecraft charging problems have limited the operational use of these data to date. Corrective measures and results will be discussed.

Presently, electron densities at 840 km are processed and stored in the AFGWC real-time data base for immediate access by the ionospheric forecasters. Further, the data is used to verify and modify the top-side ionospheric profiling routines used by AFGWC's 4-D Ionospheric Model. An electron density climatology is also being developed. This climatology allows for the analysis of 840 km electron density data as a function of season, ascending or descending node of the satellite, and level of magnetic activity for each 5° latitude by 5° longitude grid. Standard deviation information is also calculated. Results of this climatology will also be shown.

SA 79 POSTER PAPER

OPERATIONAL RESULTS OF THE DMSP PASSIVE IONOSONDE (SSIP)

M.D. Morton (Air Force Global Weather Central, Offutt AFB, NE 68113)
V.G. Patterson

Passive ionosondes are located on board two DMSP satellites. These passive ionosondes, designated SSIP, are simply HF sweep frequency radio receivers with a range from 1.2 to 13.9 MHz. These sensors look down through the ionosphere to observe terrestrial HF signals with frequencies greater than the critical frequency of the F2 layer (foF2). The use of a passive ionosonde requires two assumptions: (1) that the terrestrial sources are reasonably uniform, and (2) that the ionosphere has few horizontal gradients. These assumptions limit the area of coverage to mid-latitude land masses.

The data from both satellites have demonstrated a relatively strong background noise contamination problem. This contamination problem and resulting data recovery techniques will be discussed in detail. Present data recovery techniques allow for a nearly 70% recovery rate of data within 1 MHz of ground based foF2 observations.

SA 80 POSTER PAPER

A SCANNING AURORAL X-RAY SPECTROMETER FOR DMSP

W. A. Kolasinski and P. F. Mizera (both at Space Sciences Laboratory, The Aerospace Corporation, El Segundo, CA 90245)

We have shown previously that remote detection of auroral x-rays by sensors on an orbiting satellite can yield quantitative information about precipitating electron fluxes responsible for the aurora[1]. In order to extend the spatial coverage and broaden the energy range of future x-ray measurements, we have constructed a scanning x-ray spectrometer which will be flown on a DMSP satellite. The instrument responds to energies extending from 2 keV to 100 keV and scans cross-track from horizon to horizon, providing complete coverage of the earth within view of the satellite. Some possible applications for this type of sensor are considered in another paper at this session[2]. In this presentation we provide a description of the sensor and discuss further its potential use as a global monitor of energy input via auroral electron precipitation.

SA 81 POSTER PAPER

OPERATIONAL RESULTS OF THE DMSP SNOW/CLOUD DISCRIMINATOR (SSC)

R.C. Woronicz (Air Force Global Weather Central, Offutt AFB, NE 68113)
(Sponsor: Vernon G. Patterson)

A Snow/Cloud Discriminator Supplementary Sensor (SSC) is being carried aboard spacecraft flight four of the DMSP 5D series. The SSC is a "push broom" scanning radiometer which senses reflected solar energy in the 1.51 to 1.63 micrometer spectral band. The Air Weather Service (AWS) at the Air Force Global Weather Central (AFGWC) has routinely processed SSC data in conjunction with Operational Line Scan (OLS) data in order to test the proposition that snow/cloud scene discrimination can be had by processing these data.

Several studies are in progress to determine if AFGWC state of the art automated nephanalysis capability can be improved by processing these data. Application techniques, study results and problem areas will be discussed.

Atmospheric Airglow/Mesosphere/Thermosphere

Pier 5
Tuesday A.M.
J. W. Meriwether (Univ. of Mich.), Presiding

SA 82

THE ATOMIC OXYGEN FAR UV DAYGLOW

D. E. Anderson, Jr. (E. O. Hulburt Ctr. for Space Res., Naval Res. Lab., Wash., D.C. 20375)
P. D. Feldman (Physics Dept., Johns Hopkins Univ., Baltimore, Md. 22218)
E. P. Gentieu (NASA/Goddard Space Flight Ctr., Greenbelt, Md. 20771)
R. R. Meier (E. O. Hulburt Ctr. for Space Res., Naval Res. Lab., Wash., D.C. 20375)

Rocket observations of the dayglow spectrum between 530 and 1500A were obtained on 9 January 1978 at a solar zenith angle of 56°. Data were obtained from 80 to 260 km with viewing angles of 40°, 90°, and 180° to the local zenith. OI emissions were observed at 989, 1027, 1152, 1304, and 1356A. Analysis of these data with a radiative transfer model using currently accepted excitation cross sections, branching ratios, and photoelectron fluxes shows that electron impact excitation is the primary source of these emissions. The infrared emissions at 7990 and 11287A are also calculated in this analysis for comparison with previous observations and calculations. In particular, it is found

that the calculated zenith intensities above 200 km are 800R, 19R, 15kR, 320R, 14R, and 40R for OI 989, 1027, 1304, 1356, 7990, and 11287 A, respectively. The observed values at OI 989, 1304, and 1356A were 840R, 15kR, and 300R, respectively. These calculations show that self absorption as well as pure absorption significantly affect the 1356 profile and that both the assumption of an isothermal atmosphere for the optically thick emissions and the assumed form of the frequency redistribution function used in the calculation produce important changes in the altitude profile of the emission.

SA 83

GLOBAL AVERAGED COLUMN EMISSION PROFILES OF ATMOSPHERIC AIRGLOW EMISSIONS

V. J. Abreu
J. H. Yee
P. B. Hays (all at: Space Physics Research Laboratory, Department of Atmospheric and Oceanic Science, University of Michigan, Ann Arbor, MI 48109)

The Visible Airglow Experiment (VAE) on Atmosphere Explorer-C, -D, and -E has regularly monitored for a period of 6 years the 6300-Å and 5577-Å emission of atomic oxygen, and the 5200-Å emission of atomic nitrogen. This fortunate circumstance has allowed us to determine global averaged column emission profiles of these emissions with accurate galactic background corrections. These emission profiles will be presented as a function of solar zenith angle and solar cycle when the availability of data permits it.

SA 84

HORIZONTAL MAPPING OF AIRGLOW INTENSITIES OVER ARECIBO

R. G. Burnside
F. A. Herrero (both at: Department of Physics, University of Puerto Rico, Rio Piedres, PR 00928)
J. W. Meriwether, Jr.
J. C. G. Walker (both at: Space Physics Research Laboratory, Department of Atmospheric and Oceanic Science, University of Michigan, Ann Arbor, MI 48109)

Mapping of airglow emissions in the upper atmosphere was first conducted by Roach many years ago but until recently, little has been done to utilize this inexpensive means of studying the morphology and dynamics of the ionosphere. The recent introduction at Arecibo of a computerized tilting-filter photometer coupled with a programmable dual axis mirror system gives us the capability of mapping the intensity of airglow features in two spatial dimensions with temporal resolution and intensity precision much improved beyond previous work. For the 630.0 nm airglow feature of atomic oxygen, a total of 121 points laid out in a 11x11 square array can be obtained in ten minutes or less with an intensity precision of about 1R.

We have developed an analysis method which fits this data to a Taylor expansion about the zenith. Linear terms in the expansion are used to calculate the amplitude and direction of any spatial gradients. For the 6300-Å nightglow application we have found that the gradient vector usually lies close to the direction of the meridian. Before midnight, the higher intensities are found to the south of Arecibo. However, at about 0300 LST, the direction often reverses, and the intensity is then greater towards the north. We have found that a more complex pattern of East-West asymmetry is superimposed on this general behavior.

SA 85

STUDIES OF 7320-Å ($O^+(^2P) - O^+(^2D)$) AIRGLOW

J. H. Yee
V. J. Abreu
P. B. Hays (all at: Space Physics Research Laboratory, Department of Atmospheric and Oceanic Science, University of Michigan, Ann Arbor, MI 48109)

A statistical study of the 7320-Å ($O^+(^2P)-O^+(^2D)$) airglow was conducted by analyzing the data taken from the Visible Airglow Experiment (VAE) on the Atmosphere Explorer (AE) satellites C and E during the time periods between 1974 and 1979. Averaged column emission rate profiles as a function of solar zenith angle and solar activity variation are presented here. The galactic background has been carefully subtracted. The result shows that the rate of decreasing emission as a function of solar zenith angle agrees with the theoretical calculation based upon a neutral atmosphere model. Furthermore, an expected increase with solar activity also appeared in a plot of emission brightness versus solar 10.7 cm flux. At least a factor of 10 increase during this 6 year period has been found.

SA 86

"NO-NO_2 PHOTOCHEMISTRY INFERENCES FROM SPIRE INFRARED SPECTRAL DATA"

H.J.P. Smith, P. Joss, (Visidyne, Inc.) 5 Corporate Place, South Bedford Street, Burlington, MA 01803)

R.M. Nadile, A.T. Stair, F.P. Del Greco (AFGL (OPR) Hanscom AFB, Bedford, MA 01730)

The SPIRE (Spectral Infrared Rocket Experiment) rocket was flown from Poker Flat, AK in Sep. 1977 just before local dawn. The spectral data were obtained for both nightside and dayside as well as the terminator region. The NO fundamental as well as the NO_2 (ν_2) bands have been detected. In this paper we present results connecting the observed NO and NO_2 radiances with photochemistry as a function of time before and after sunrise.

SA 87

"SPIRE WATER VAPOR (ν_2) RESULTS USING THE AFGL FASCODE COMPUTER CODE"

R.M. Nadile, A.T. Stair (AFGL (OPR) Hanscom AFB, Bedford, MA 01730)

H.J.P. Smith, T.C. Degges, P. Joss, (Visidyne, Inc.) 5 Corporate Place, South Bedford Street, Burlington, MA 01803)

The SPIRE experiment obtained many spectral and spatial scans for the IR earth limit radiance between 1.5 and 1.6 μm. We have analyzed the data near the H_2O (ν_2) band (~5.5 - 6.7 μm) over a range of tangent heights from 10 to 80 km. No significant day night variations have been found. The AFGL high altitude limb model and a line by line computer code have been exercised to determine an appropriate mesospheric and stratospheric water vapor profile from the data. We also address the ratio of the P and R branches of H_2O ν_2, at a measured resolution of 35 cm. The results of a non-linear least squares inversion technique will also be presented.

SA 88

HORIZONTAL THERMAL STRUCTURE OF THE MESOSPHERE

C. A. Tepley
J. D. Mathews (both at: Department of Electrical Engineering, Case Western Reserve University, Cleveland, Ohio 44106)
R. G. Burnside (Department of Physics, University of Puerto Rico, Rio Piedres, PR 00928)
J. W. Meriwether, Jr. (Space Physics Research Laboratory, Department of Atmospheric and Oceanic Science, University of Michigan, Ann Arbor, MI 48109)

We have used two computerized tilting-filter photometers combined with a programmable dual axis mirror system to measure the horizontal structure of the OH rotational temperature in the mesosphere over Arecibo during January and February, 1980. The temperature is derived from the ratio of measured intensities of rotational lines selected from the P branch of the Meinel 8-3 band by narrow interference filters. The mirror system is programmed to scan in sequence a total of 121 positions in a 11x11 square array with a lateral spacing between adjacent positions in the mesosphere of 10 or 25 km. Temperature maps of good quality can be acquired at time intervals as small as ten or fifteen minutes because the wavelength scan for each instrument includes only selected positions of the rotational line and a corresponding background. Simultaneous observations by a 1m Ebert-Fastie spectrophotometer of the rotational temperature of the molecular oxygen emissions at 865.0 nm were made in the zenith. Results show evidence for the occasional occurrence just after evening twilight of a thermal wave moving from the southwest towards the northeast. There appeared to be a distinct difference between the dynamics observed in January and that observed in February with irregular behavior being more characteristic of the January results.

SA 89

LIDAR STUDIES OF THE MESOSPHERIC SODIUM LAYER OVER URBANA, ILLINOIS, IN SUMMER 1979

T. M. Cerny*
J. D. Shelton+
C. S. Gardner+
C. F. Sechrist, Jr.* (all at: University of Illinois, Dept. of Electrical Engineering, Urbana, Illinois 61801)

An improved receiving system for the Urbana lidar was implemented during the summer of 1979, using a new 1.2-meter diameter Fresnel-lens telescope. As a consequence, sodium photocount vs. altitude profiles were significantly enhanced in quality and time resolution was markedly improved. Quantitatively, there was a 6-fold improvement in signal photon counts and a 5-fold improvement in time resolution.

Spectrums and photocount profiles for the nights of July 18-19, July 19-20, and August 16 reveal several interesting features including: undulation of the sodium layer bottomside, temporal variation of spectral components, a standing wave-like oscillatory component, a dominant 5-km vertical wavelength, and possible cascading of wave energy from longer to shorter wavelengths.

SA 90

HIGH-RESOLUTION LIDAR OBSERVATIONS OF THE SPATIAL AND TEMPORAL STRUCTURE OF THE MESOSPHERIC SODIUM LAYER

C. S. GARDNER
J. D. SHELTON (Both at: Radio Research Laboratory, University of Illinois, Dept. of Electrical Engineering, Urbana, Illinois 61801)
(Sponsor: C. F. Sechrist, Jr.)

Two-dimensional processing techniques have been applied to sodium lidar observations obtained in the Fall, 1979. While previous data collected at the University of Illinois have been processed spatially, the Fall data have been filtered temporally as well as spatially to further enhance resolution. Spatial features as small as 2 km have been observed and a temporal resolution of 5 minutes has been achieved. The resulting sodium layer profiles spanning observation periods from 2 to 5 hours contain several interesting features such as: movement of a dominant peak from the lower half to the upper half of the layer, collapse of a bifurcated layer into a layer with a single peak, cascading of wave energy from long to short wavelengths, and the seasonal broadening of the layer.

SA 91

FIRST RESULTS OF CORRELATIVE MEASUREMENTS USING THE URBANA LIDAR AND METEOR RADAR

S. K. Avery*
T. M. Cerny*
J. D. Shelton+
D. Tetenbaum*
C. F. Sechrist, Jr.* (all at: University of Illinois, Dept. of Electrical Engineering, Urbana, Illinois 61801)

Nearly simultaneous measurements of sodium photocount vs. altitude profiles and meteor-radar wind profiles were obtained in September and December 1979, and in January 1980, using the sodium lidar and meteor radar systems located near Urbana, Illinois.

This paper presents the results of these correlative measurements, and suggests that uncorrelated features may be ascribed to the different observational methods used. That is, the laser radar technique observes neutral density variations, while the meteor radar observes winds. Although these quantities are related physically, they do not have the same spatial structure.

SA 92

THE DENSITY RESPONSE OF THE SODIUM LAYER TO GRAVITY WAVE PERTURBATIONS

J. D. Shelton+
C. S. Gardner+
C. F. Sechrist, Jr.* (all at: University of Illinois, Dept. of Electrical Engineering, Urbana, Illinois 61801)

Laser radar studies at Urbana, Illinois have revealed that the mesospheric sodium layer exhibits large variations of density, which are suggestive of gravity wave structures.

Based on similar work by Chiu and Ching (1978), we compare sodium lidar observations with the solution of the linear problem of the density response of the sodium layer to gravity wave perturbations in the background atmosphere, and conclude that wave-like density variations in the sodium layer can be interpreted as layer density responses to gravity waves.

SA 93

LONG-TERM VARIATIONS IN THERMOSPHERIC ATOMIC NITROGEN DENSITIES

Jeffrey B. Nygren
Mark J. Engebretson (both at: Department of Physics, Augsburg College, Minneapolis, Minn. 55454)

Thermospheric densities of atomic and molecular nitrogen were measured regularly from February 1976 through December 1978 by the Open-Source Neutral-Mass Spectrometer (OSS) on the equatorial Atmosphere Explorer-E satellite. During this period of development of solar cycle 21 the solar F10.7 radio flux increased fron near 70 to over 180 x 10^{-22} watts $(m^2\ Hz)^{-1}$. An increase in the N/N_2 ratio has been observed during this period, which we attribute to the concurrent marked increase in solar ultraviolet emission. Observed N densities are input to a spherical harmonic empirical model in order to investigate their correlation with thermospheric temperatures (from the MSIS model), solar F10.7 radio flux, geomagnetic Ap index, and solar EUV flux as measured by the Extreme Ultraviolet Spectrometer on AE-E.

SA 94

THE SOLAR ULTRAVIOLET HEATING EFFICIENCY OF THE THERMOSPHERE

M. R. Torr (Space Physics Research Laboratory, University of Michigan, Ann Arbor, MI 48109)
P. G. Richards
D. G. Torr (both at: Center for Atmospheric and Space Sciences, Utah State University, Logan, Utah 84322)

Using current knowledge of such quantities as the solar UV flux, the neutral atmosphere, and the current thermospheric chemistry we determine the UV heating efficiency. The results differ significantly from earlier studies. We use a time dependent interhemispheric solution of the ionospheric continuity, momentum and energy equations to determine the heating efficiency, ε, as a function of altitude for midlatitudes. We find ε to be a strong function of altitude, peaking near 50% in the region of maximum UV deposition. We present the diurnal variation of this parameter as a function of altitude.

SA 95

IDENTIFICATION OF A NEW MAJOR SOURCE OF THE $O(^3P - {}^1D)$ 6300 Å THERMOSPHERIC DAYGLOW

P. G. Richards (Center for Atmospheric and Space Sciences, Utah State University, UMC 41, Logan, Utah 84322)
D. G. Torr* (Same address)
M. R. Torr* (Same address)

Recently Rusch et al. (1978) identified the reaction

$$N(^2D) + O_2 \xrightarrow{k} NO + O(^1D)$$

as the main source of auroral 6300 Å emission. We examine the importance of this reaction as a source of 6300 Å dayglow emission and find it to be the largest production mechanism above ∿ 150 km, where $O(^1D)$ quenching is less than radiative loss. In summer this source is 2.5 times as large as all the other sources at 180 km. Inclusion of the new source alleviates the need for the large dissociation frequency of O_2 by Schumann-Runge solar UV radiation found in previous work ($Jo_2 = 3 \times 10^{-6}\ s^{-1}$), thus bringing the 6300 Å airglow measurement into harmony with the measurements of the Schumann-Runge continuum made on the Atmosphere Explorer (AE) satellites, i.e. $Jo_2 = 1.5 \times 10^{-6}\ s^{-1}$. Neglect of the $N(^2D)$ source of $O(^1D)$ in the past has resulted in an overestimation of O_2 concentrations in the twilight thermosphere from both ground based and satellite measurements of the 6300 Å emission. The rate coefficient for quenching of $O(^1D)$ by N_2 remains effectively unchanged, i.e. $4 \pm 1 \times 10^{-11}\ cm^3\ s^{-1}$.

SA 96

NIGHTTIME ATMOSPHERIC SCATTERING OF LUNAR UV RADIANCES

E. G. Stassinopoulos
R. A. Goldberg
R. D. McPeters (all at NASA/Goddard Space Flight Center, Greenbelt, Maryland 20771)
L. L. Felton (Computer Sciences Corporation, Silver Spring, Maryland 20910)

Morphological studies of nighttime dark current data from the Nimbus 4 BUV experiment clearly indicate enhancements during periods of the full moon. This analysis is based on processed and filtered data which have other known perturbations induced by energetic particle events. In order to obtain truly quiescent dark-current background-values for the five-day study intervals centered about several full moon sequences and for the corresponding total lunar eclipse intervals, the data were further screened. Subsequently, isolated elements showing spurious or abnormal enhancements were selectively removed (∿ 3%). Also, in order to evaluate magnetospheric perturbation effects, minimize charged particle contamination or precipitation effects, and recognize and account for other environment impacts, the analysis was performed in a geomagnetic frame of reference (magnetic B-L space) for a finite region that can be considered "safe" in this respect.

The source of this nighttime signal appears to be atmospherically scattered ultraviolet light, with a peak near 273.5 nm. This result is not consistent with simple explanations involving Rayleigh scattering or ozone absorption, but requires an, as yet, unidentified cause.

SA 97

MEASUREMENTS OF THE BALMER ALPHA GEOCORONAL LINE PROFILE DURING SOLAR MAXIMUM

J. W. Meriwether, Jr.
S. K. Atreya
T. M. Donahue (all at: Space Physics Research Laboratory, Department of Atmospheric and Oceanic Science, University of Michigan, Ann Arbor, MI 48109)

We have used the 15cm Fabry-Perot interferometer located at the Arecibo Observatory in Puerto Rico to measure at high resolution the line profile of the geocoronal line of atomic hydrogen at 656.3 nm. The interference filter was sufficiently narrow to eliminate completely contamination from adjacent OH rotational lines. Twilight measurements in September, 1979, at angles of high solar depression showed evidence for a red tail in the line profile extending several thermal widths into the red from the center of the line. We are certain that this is not galactic contamination because measurements obtained in the nightglow when the Balmer alpha intensity was very weak showed no indication of any emission. The orientation at the time of the measurements was away from sources of galactic hydrogen. Our conclusion is that the presence of the red tail in the profile is a manifestation of non-thermal hydrogen in the geocorona.

SA 98

GEOCORONAL BALMER ALPHA MEASUREMENTS WITH A GROUND-BASED FABRY-PEROT

Todd Leen
F. L. Roesler
F. Scherb (all at: Dept. of Physics, University of Wisconsin, Madison, WI 53706

We report geocoronal Balmer Alpha emission measurements made between May and July of 1979 for solar depression angles from 15 to 25 degrees and zenith angles from 20 to 60 degrees. A dual etalon Fabry-Perot spectrometer separated the geocoronal component from galactic and zodiacal light background. The spectrometer was calibrated against NGC 7000 and standard stellar sources (Scherb and Oliversen, 1980). The data have been corrected for first order scattering by molecules and particulates in the troposphere adapting the method of Walstencroft and van Breda (1967) and using a spherical atmospheric shell 30 km thick with a vertical extinction of $\tau = 0.187$. The corrections for scattering are 3R or less for our observing conditions. We obtain geocoronal surface brightnesses of between 8 and 20 R. The geocoronal intensities encountered during studies of galactic emission conducted in 1976 and 1977 with similar instrumentation corroborate these results. (This work was supported by NSF grant ATM-77-20371.)

SA 99

CARBON DIOXIDE (ν_2) RADIANCE RESULTS USING A NEW NONEQUILIBRIUM MODEL

R.D. Sharma (Stewart Radiance Laboratory, Bedford, MA 01731)

R.M. Nadile (AFGL OPR) Hanscom AFB, MA 01731)

A new non-equilibrium model for computing radiance from bending mode (ν_2) of carbon dioxide is constructed. This model is used to compute limb and zenith radiance from 70 km to 150 km. Details of the model are discussed and the results are compared with SPIRE and ICECAP measurements. 15um radiance, originating from the ν_2 mode of CO_2, has been observed to remain practically unchanged from about 95 km tangent height to about 110 km tangent height in a recent earth limb sensing rocket experiment (SPIRE). This anomaly in an otherwise nominal profile occurs in spite of an anticipated order of magnitude change in CO_2 concentration over this altitude range. In an effort to understand the basis of this observation a new non-equilibrium model for computing radiance from bending mode of CO_2 is constructed. This model has several new features not present in previous models. Results from our model will be compared with those from other calculations as well as with observations from vertical rocket probe measurements (ICECAP) and the SPIRE earth limb experiment.

Winds, Tides and Waves in the Atmosphere

Pier 5
Tuesday P.M.
J. P. St. Maurice (Utah State Univ.), Presiding

SA 100

MODEL ANALYSES OF LARGE SCALE WAVE STRUCTURE AS OBSERVED BY AE SATELLITES

S.H. Gross, (Polytechnic Institute of New York, Route 110, Farmingdale, N.Y., 11735)

Model Analyses have been made of atmospheric gravity waves excited by localized heat sources in the thermosphere in an attempt to understand and explain the fluctuation spectra calculated from insitu density data measured by Atmospheric Explorer (AE) Satellites. A line source is assumed representative of an auroral source in a two dimensional plane stratified model with the atmosphere consisting of two fluids, one the total atmosphere with a mean mass in accordance with a standard model, the other a secondary fluid, such as argon, helium or nitrogen. Boundary conditions are assumed and full wave solutions are obtained and compared with the spectra of the AE measurements.

SA 101

LARGE SCALE WAVES IN THE ATMOSPHERE AND IONOSPHERE OBSERVED BY THE AE SATELLITES

F. Huang, Goddard Space Flight Center, NASA Greenbelt, Md. 20771
C.A. Reber, Goddard Space Flight Center, NASA, Greenbelt, Md. 20771
S.H. Gross, Polytechnic Institute of New York, Rt. 110, Farmingdale, N.Y. 11735

The AE series of satellites have made insitu measurements of the density and temperature of plasma and neutral species in circular orbits of about 250 km. The fluctuations of these measurements are spectrally analyzed for large scale, long period waves, such as gravity waves. The spectra exhibit coherence between the different species. Data are analyzed based on two fluid theory extended to multiple fluids. Likely wave characteristics are sought in interpreting the calculated spectra based on best fit methods, which will be discribed along with results.

SA 102

ATMOSPHERIC GRAVITY WAVES OBSERVED ON ATMOSPHERE EXPLORER

L. E. Wharton (Space Physics Research Laboratory University of Michigan, Ann Arbor, MI 48105)
W. R. Hoegy (NASA/Goddard Space Flight Center, Laboratory for Planetary Atmospheres, Greenbelt, MD 20771)
P. L. Dyson (Department of Physics, LaTrobe University, Bundoora, Victoria, Australia 3083)

Further observations of atmospheric gravity waves on Atmosphere Explorer are presented. The data is from the equatorial AE-E satellite and includes some portions of Atlantic and Pacific tropical storms. Maximum entropy spectral analysis is used to calculate the Doppler shifted frequency (apparent period) in the auto and cross power spectra of neutral wind, temperature, and O and N_2 density data. Wave amplitudes and relative phases are evaluated for the apparent periods that dominate the spectra of all four time series. A least square fit of theoretical amplitudes, phases, and the apparent period based on the two specie gravity wave dispersion relation and polarization relations is made to the spectral analysis results to determine the gravity wave parameters: period and the three wave lengths. An appraisal is made of our ability to identify atmospheric gravity waves from the satellite data. Error bars are given for the determined gravity wave period, wavelengths, and direction of propagation, based on data errors, uncertainties in the spectral analysis, and deviations of the real waves from the idealized linear gravity wave theory.

SA 103

ON GUIDED MODES FOR ATMOSPHERIC GRAVITY WAVES

T.F. Tuan (Physics Department, University of Cincinnati, Cincinnati, Ohio, 45221).
D. Tadic, (Department of Theoretical Physics, University of Zagreb, Zagreb, Yugoslavia).

It is well known that atmospheric gravity waves can progagate in discrete as well as continuous modes. We have found that the partially guided discrete modes can "interfere" with each other and that such interference can destroy the guidance of the individual modes.

To show this, we develop a dispersion formula for a realistic atmosphere which expresses the reflection coefficient R of the gravity waves at the "top" of the atmosphere directly in terms of the discrete as well as the continuous modes. With this formula the "interference" between neighboring modes can be easily and quantitatively investigated. A criterion will be developed which will help us to distinguish the observable modes from those modes whose guidance have been fully or partially destroyed by interference. In the course of developing this formula, we have also found a new type of guided mode which has not been previously investigated.

SA 104

PROPAGATION AND DISPERSION OF TRAVELING IONOSPHERIC DISTURBANCES (TID's)

K.A. Ballard (Radiophysics Laboratory, Thayer School of Engineering, Dartmouth College Hanover, N.H. 03755)
M.G. Morgan

Iso-true-height contours of electron density, produced from observations with multi-station rapid-run ionosondes in Vermont and New Hampshire, are used to determine several pertinent TID wave parameters as a function of height. Fourier decomposition of an iso-height contour at a single station yields the spectral content at the various altitudes, while cross-spectral analysis among the three stations yields cross-spectral power, coherence, and phase velocity of each component in the TID. The geographic direction toward which the TID's propagate remains fairly constant with altitude and with the various frequency components. This, together with the fact that the frequency components are often harmonically related, leads us to believe that the various spectral components in single events have the same source. From our data we have obtained the phase propagation constants k_x (horizontal) and k_z (vertical) for the TID, where k_z has real (k_{zr}) and imaginary (k_{zi}) parts. By using the experimentally determined value of k_x (constant with height) we can, with the dispersion relation for gravity waves, calculate k_{zr} vs. height for the neutral atmosphere. Conversion of the experimental k_{zr} values from the electronic component to the neutral medium facilitates a direct comparison with the theoretical gravity wave model predictions. The experimental values of k_{zi} are compared to model values taking into account the exponential growth factor, ion drag, thermal conductivity, and viscosity. Use of the dispersion curves from the gravity wave model allows us to determine the group velocity (including direction) and, extrapolating backward, we can determine the probable source region.

SA 105

EFFECTS OF GRAVITY WAVES ON HYDROXYL EMISSION

R. Hatfield (Computer Research Corporation, Washington, D.C.)
T.F. Tuan (Physics Department, University of Cincinnati, Cincinnati, Ohio, 45221)
S.M. Silverman (Air Force Geophysics Laboratory, L.G. Hanscom Field, Bedord, Massachusetts 01731)

The effects of gravity waves on OH emission is investigated using a gravity-wave model valid for an inhomogeneous atmosphere, and computed as well as semi-empirical data for the "undisturbed" ozone and hydrogen profiles. The results show that (1) the magnitude of the response depends on the relative magnitudes and signatures of the vertical and horizontal wave-induced flux. Since in some regions the horizontal velocity field of the gravity wave can increase much more rapidly with height than the vertical field, horizontal diffusion can in some instances overcome vertical diffusion even when there is a relatively sharp layer gradient. (2) The structures in the OH profile produced by the gravity wave are in general but not always more pronounced below the intensity peak than above. The observed dark area in OH emission can be produced by gravity waves with vertical wave length small compared with the half-width of the intensity profile.

SA 106

TIDAL EFFECTS ON D-REGION POSITIVE ION CHEMISTRY

Jeffrey M. Forbes (Space Data Analysis Laboratory, Boston College, Chestnut Hill, MA 02167)

The effects of tidal variations in temperature and density on D-region ion chemistry are investigated. It is assumed that NO^+ is the precursor ion in a chain which involves three-body formation of the intermediary cluster ions $NO^+(H_2O)_{m-1}(X)$ (n=1-3) where X can be N_2, O_2, H_2O, or CO_2, switching reactions which convert these weakly bound clusters to hydrates of NO^+, and reaction of the third hydrate of NO^+ with H_2O to initiate the chain to form $H^+(H_2O)_n$ (n=1-7). The rates of three-body and thermal breakup reactions are affected by tidal oscillations in the ambient temperature and total density. For instance, lower (higher) temperatures enhance (inhibit) the formation of clusters and inhibit (enhance) their thermal breakup, thus reducing (increasing) the electron concentration since the recombination coefficients of cluster ions increase with cluster size, and are all large compared with that of NO^+. Using a complex chemical code which models the positive ion chemistry of the D region, it is shown that the temperature and density variations associated with the (1,1) and (2,2) tidal modes can produce 10-30% asymmetrics in the D-region electron concentration about noon similar to those observed experimentally.

SA 107

TIDAL DYNAMICS AND COMPOSITION VARIATIONS IN THE THERMOSPHERE

Maura E. Hagan, Space Data Analysis Laboratory, Boston College, Chestnut Hill, MA 02167
(Sponsor: Jeffrey M. Forbes)

The effects of mutual diffusion between O and N_2 are examined for diurnal and semidiurnal tidal oscillations in the thermosphere. A binary gas extension of a previous f-plane equivalent gravity wave formalism is developed and utilized to study this effect. Compared to calculations which omit O-N_2 mutual diffusion, diffusive interaction affects the temperatures and horizontal velocities associated with the diurnal thermospheric tide excited insitu by less than 10% with negligible shifts in phase, and to modify by roughly 20-40% the amplitudes of the semidiurnal tide excited insitu, and the (2,2) and (2,4) modes propagating from the mesosphere accompanied by 1 to 4 hour shifts in phase. These results affect the interpretation of incoherent scatter measurements of thermospheric tides and the construction of synthesized tidal models which are calibrated by the measurements, and suggest that the inequality of the vertical transport velocities of O and N_2 be accounted for in three-dimensional numerical models of semidiurnal thermospheric tides.

SA 108

WITHDRAWN

SA 109

OBSERVED ELECTRON HEATING IN THE POLAR E-REGION IN THE PRESENCE OF THE MODIFIED TWO STREAM INSTABILITY

Kristian Schlegel and J. P. St.-Maurice (Utah State University - CASS, Logan, UT 84322)

Electron temperatures between 400 K and 2000 K have been measured with the Chatanika/Alaska incoherent scatter radar at 110 km altitude in the presence of electric fields between 40 and 100 mV/m. The temperature enhancement occurs precisely in the height range where the relative drift velocity between electrons and ions, v_d, is a maximum, and the temperatures are positively correlated with v_d. This suggests that the electrons are heated by the unstable waves produced by the Farley-Buneman mechanism. Indeed the measured electron temperatures show a high correlation (0.85) with the calculated growth rate of this instability. Furthermore, theoretical estimates of the electron temperature enhancements caused by the waves, are of the same order of magnitude as the observed temperatures.

SA 110

TWO STREAM INSTABILITY DECAY - AN IMPORTANT HEAT SOURCE IN THE POLAR E-REGION?

P. M. Banks (Utah State University, Dept. of Physics, Logan, UT 84322)
K. Schlegel and J. P. St.-Maurice (Utah State University - CASS, Logan, UT 84322)

The decay of two stream instabilities which cause the enhanced electron temperatures described in a previous paper may be an important heat source for the neutral atmosphere around 110 km altitude, if the assumption of relatively isotropic electron velocity distributions is correct. The amount of this heat production can be estimated by calculating the electron cooling rate which is necessary to maintain the observed electron temperatures. This heat production has been compared with the Joule and particle heating. The maximal contribution to the two stream heating occurs between 100 and 110 km while the Joule heating has its peak between 110 and 130 km. In case of electric fields greater than 70 mV/m the height integrated heating due to the decay of the modified two stream instability is generally greater than the height integrated particle heating and about 10-20% of the height integrated Joule heating. If the electron velocity distribution is highly anisotropic, i.e. the measured electron temperatures reflect mainly the temperatures parallel to the magnetic field, the corresponding heating rates are about a factor of 3 lower.

SA 111

SPEED-DEPENDENT COLLISION EFFECTS ON RADAR BACK-SCATTERING FROM THE IONOSPHERE

Y. K. Behl (Dept. of Physics, New Mexico State University, Las Cruces, NM 88003)
O. H. Theimer
NM 88003)
(Sponsor: Allen Hedin)

There are some regions of the ionosphere where the effects of collisions between ions and neutrals are not negligible. The collision frequency involving ions and neutrals is proportional to the relative speed. But, presently, in modelling the ionosphere by the incoherent scatter technique, the collision frequency is assumed to be constant. Our earlier work[1] has indicated that collision effects are considerably modified when the linear speed dependence is not ignored. We are presently investigating the effect of these modifications on ionospheric modelling[2]. The results of this investigation will be presented. We have found, for example, that ignoring the speed dependence would result in a significant underestimation of the electron-ion temperature ratio and overestimation of the density of neutrals.

SA 112

MID- AND HIGH-LATITUDE RADAR MEASUREMENTS OF IONOSPHERIC PERTURBATIONS DURING STRONGLY DISTURBED MAGNETOSPHERIC CONDITIONS

J. D. Kelly (Radio Physics Laboratory, SRI International, Menlo Park, CA 94025)
M. Blanc (CNET/CRPE, 92131 Issy-les-Moulineaux, France)
D. Alcaydé (Centre d'Etudes Spatiales des Rayonnements, 31029 Toulouse Cedex, France)

In April 1978, two large magnetic storms caused ionospheric perturbations at both mid- and high-latitudes. These effects were measured by both the Chatanika Incoherent-Scatter Radar (L = 5.6) and the St. Santin Incoherent-Scatter Radar (L = 1.8). An increased neutral temperature and enhanced electric fields were detected at St. Santin, possibly because of coupling of the high-latitude ionosphere to the mid-latitude ionosphere. This paper presents the Chatanika Radar data, which shows enhanced electric fields (as large as 80 mV/m), enhanced conductivities, and large meridional neutral winds. These data will be related to the mid-latitude data and the disturbed magnetospheric conditions.

SA 113

HIGH LATITUDE ION HEATING IN THE F REGION

Jean-Pierre St-Maurice (Utah State University CASS, Logan, Utah 84322)

We have studied ion temperature data of a large number of high latitude F-region passes by the Atmosphere Explorer-C satellite. Increases in the O^+ temperature above the neutral temperature values were measured to be as large as 2500°K. The increase in the ion temperature correlates very well with the D.C. electric field strength measured in the same regions. Furthermore the measurements are in excellent agreement with theoretical predictions of frictional heating by collisions with the neutral gas, if allowance for the presence of neutral winds of the order of 200 to 400 m/sec is made. The measurements also provide indirect evidence for neutral temperature increases of the order of 100° to 300°K over the MSIS model values in periods of very strong activity.

SA 114

THERMOSPHERIC WINDS AT ARECIBO

F. A. Herrero (University of Puerto Rico, Rio Piedras, Puerto Rico 00612)
R. G. Burnside
J. W. Meriwether, Jr.

Measurements of thermospheric neutral wind velocities have been made by observing the 630 nm OI emission with a Fabry-Perot interferometer. Data obtained recently, in the fall and winter months, show a pronounced eastward wind with a velocity of about 100 $m.sec.^{-1}$ after sunset, which decreases to less than 30 $m.sec.^{-1}$ (or reverses) by sunrise. On some nights the zonal wind also exhibits a tendency to reverse 1 or 2 hours before midnight.

The meridional wind is considerably weaker. Velocities greater than 30 $m.sec.^{-1}$ have been observed only rarely. On several nights an equatorward wind of the order of 10-20 $m.sec.^{-1}$ has been detected in the early part of the night. Qualitative comparison with measured 630 nm intensities shows that our wind measurements are consistent with the theory that the 'midnight descent' of the F-layer follows a decrease in the velocity of the equatorward wind.

SA 115

THE EFFECT OF MAGNETOSPHERIC CONVECTION AND AURORAL PARTICLE PRECIPITATION ON THE GLOBAL CIRCULATION AND TEMPERATURE STRUCTURE OF THE THERMOSPHERE

R. G. Roble, R. E. Dickinson and E. C. Ridley (National Center for Atmospheric Research*, Box 3000, Boulder, CO 80307)

The global neutral temperature distribution and winds in the thermosphere are calculated for equinox conditions using the NCAR thermospheric general circulation model (TGCM). The variables are determined on a 5° grid in latitude and longitude at 24 constant pressure layers in the vertical from about 90 to 500 km. The three-dimensional wind structure and temperature distribution are first calculated considering only heating due to the absorption of solar EUV and UV radiation. These results are compared to a calculation that includes joule heating and a collisional ion drag momentum source due to a superimposed magnetospheric convection pattern at high latitudes. In addition, heating due to particle precipitation along the auroral oval is included. The results of the calculation show that these high latitude processes not only have a significant influence in altering the temperature and wind structure at high latitudes but they also influence the fields on a global scale. The inclusion of these high latitude processes are shown to give better agreement between the calculated and observed winds and temperatures especially at high latitudes.

SA 116

SOLAR CYCLIC RESPONSE OF WINDS, 60-110 km, AT 52N, 106W (SASKATOON)

J.B. Gregory (Institute of Space and Atmospheric Studies, University of Saskatchewan, Saskatoon, Canada S7N OWO)

Winds from ≈60-110 km at Saskatoon, 1974-79, show substantial response to increasing solar activity, e.g. zonal components increase by a ratio, (solar maximum/minimum) lying between 1 and 6, typically 2-3. This effect is examined for seasonal and altitude characteristics. By comparison with data from 51N, 13E (Kuhlungsborn) a first indication of a change in global pattern of meridional flow at ≈95 km with solar cycle is found.

SA 117

INTERNAL GRAVITY WAVES (5-30 min) AND THEIR RELATION TO ENERGY DISSIPATION RATES, EDDY DIFFUSION COEFFICIENTS IN THE MIDDLE ATMOSPHERE (60-90 km) AT SASKATOON (52°N, 107°W) CANADA: 1978/9

A.H. Manson (Institute of Space and Atmospheric Studies, University of Saskatchewan, Saskatoon, Sask., Canada S7N OWO)
J.B. Gregory, C.E. Meek (Institute of Space and Atmospheric Studies, University of Saskatchewan, Saskatoon, Sask., Canada S7N OWO)

Winds from a partial reflection radio-wave drift system have been obtained during six 3-h observations involving the 4 seasons. Profiles (60-110 km) of 3 km resolution are available every minute. Time series and spectral analysis are used to identify the I.G. waves; polarization effects occur.

Statistics of the signal amplitude are also used to calculate energy dissipation rates (~0.1 w kg^{-1}) and eddy diffusion coefficients (~400 m^2 s^{-1}). Profiles of these are shown to be causally related to the profiles of mean winds and gravity wave fluxes.

SA 118

ON THE NATURE OF THE APPARENT RESPONSE OF THE VORTICITY AREA INDEX TO THE SOLAR MAGNETIC FIELD

J.M. Wilcox
P.H. Scherrer (both at Inst. for Plasma Research, Stanford University, Stanford, CA 94305)

The apparent response of the vorticity area index to the solar magnetic field is confined to tropospheric regions of intense circulation. Discussions and calculations that include larger volumes of the troposphere would not be expected to show a significant sun-weather effect. Analysis of the effect in time intervals outside the original 1963-73 is also discussed. An assessment of this sun-weather effect at the present time is given.

Auroral and Polar Emissions and Plasma Effects

Pier 4

Tuesday P.M.

J. K. Walker (Energy, Mines and Resources), Presiding

SA 119

SPECTRAL MEASUREMENTS OF THE DAYSIDE CLEFT AURORA AT CAPE PARRY, N.W.T., 1977

W.A. Gault (Centre for Research in Experimental Space Science, York University, Toronto, Ont. M3J 1P3)
R.A. Koehler
R. Link
G.G. Shepherd

Measurements of the optical spectrum (500 to 850 nm) of the magnetospheric cleft aurora were made during several nights in December, 1977, at Cape Parry, N.W.T., using a scanning Michelson interferometer. The auroral features observed were OI(557.7, 630.0-6.4, 777.4, 844.6 nm), OII(731.9-3.0 nm), NI(520.0 nm), H_α, O_2 Atm (1, 1), $N_2$1P and possibly some N_2^+M. Nightglow levels of Na and OH were also present. By comparison with nightside auroral spectra, the atomic emissions are greatly enhanced relative to the molecular nitrogen bands.

Theoretical predictions of the atomic emission rates, assuming a 40eV Maxwellian incident electron spectrum, fit the observed emission rates satisfactorily except for OII, which exceeds the observed intensity by a factor of 4.

SA 120

THE EXTREME ULTRAVIOLET SPECTRUM OF AN AURORA AT 6 Å RESOLUTION

E. P. Gentieu (Goddard Space Flight Center, Laboratory for Extraterrestrial Physics, Greenbelt, Md. 20771)
P. D. Feldman (Physics Dept., The Johns Hopkins Univ., Baltimore, Md. 21218)

Ultraviolet spectra of an IBC II$^+$ aurora in the spectral ranges 530-1230 Å and 1180-1520 Å at 6 Å resolution were obtained with two scanning spectrometers on board a Taurus-Orion rocket launched 28 March 1978 from Churchill Research Range. The instruments were previously flown to observe the dayglow (Gentieu, Feldman and Meier, G.R.L. 6, 325, 1979) and a comparison of the auroral spectrum with that of the airglow provides a means of uniquely identifying those emissions near 1000 Å associated with molecular nitrogen as the auroral excitation is produced at significantly lower altitude than the dayglow. As in the previous experiment, spectra were obtained with the rocket in fixed attitudes, viewing up, down and horizontally. The emission below 796 Å, the N_2 ionization edge, although severely attenuated by atmospheric absorption, is dominated by lines of O^+.

SA 121

ELECTRON-IMPACT EXCITATION OF THE BIRGE-HOPFIELD SYSTEM ($b^1\pi_u - X^1\Sigma_g^+$) OF N_2 IN THE AURORA AND AIRGLOW

M. R. Gorman (University of Pittsburgh, Pittsburgh, PA 15260)
E. C. Zipf

The absolute emission cross sections for the excitation of the Birge-Hopfield bands ($b^1\pi_u - X^1\Sigma_g^+$) by electron impact on N_2 from threshold to 500 eV are reported. With the exception of the v' = 1, 5, and 6 vibrational levels all other $b^1\pi_u$ levels are found to predissociate with a specific predissociation branching ratio >0.99. This forbidden process is a major source of the N(^{2}D) atoms produced by photoelectron dissociation of N_2 and by precipitating electrons in auroras. Quite remarkably, the $b^1\pi_u$ (v' = 1) state is only slightly predissociated (<10 percent). The emission cross section for the v' = 1 level has a maximum value of 2.3 x 10^{-18} cm^2 at 35 eV. The measured cross section rises to its maximum value considerably faster than the phenomenological cross section used in current electron energy-loss models. The absolute transition probabilities, emission cross sections, and the variation of the electric dipole moment with internuclear distance for 21 BH(1, v'') bands will be presented. These high-resolution results are used to analyze the complex spectrum of the extreme ultraviolet terrestial airglow and aurora in the 950 Å - 1350 Å wavelength range. Evidence for the optical pumping of the BH(1, v'') bands by a the resonant absorption of the OI λ989 Å multiplet by the BH(1, 0) band is presented.

SA 122

A LABORATORY STUDY OF THE FORMATION OF NITROUS OXIDE BY THE REACTION $N_2(A^3\Sigma_u^+) + O \rightarrow N_2O + O$

E. C. Zipf (University of Pittsburgh, Pittsburgh, PA 15260)

Harteck and Dondes (1956) have shown that the irradiation of air by high-energy neutrons produces N_2O quite efficiently with an energy cost of 16 eV/N_2O molecule. Cylindrical shock wave studies (Zipf and Dubin, 1976) simulating lightning have produced similar results. However, neither of these investigations shed light on the details of the reactions leading to the synthesis of the nitrous oxide. Malcombe-Lawes (1974) suggested that reactions with O_2 involving the energy-rich metastable $N_2(A^3\Sigma_u^+)$ state, which is formed quite efficiently by particle bombardment of N_2 was responsible for the N_2O observed in the earlier experiments and in his own work. In this paper, we present the results of a detailed study of the reaction $N_2(A^3\Sigma_u^+) + O_2 \rightarrow N_2O + O$. In these experiments, the N_2O formed by the reaction was detected by a neutral mass spectrometer while the concentration of the metastable $N_2(A^3\Sigma_u^+)$ molecules was determined from absolute intensity and spatial distribution measurements of the Vegard-Kaplan bands [$A^3\Sigma_u^+ \rightarrow X^1\Sigma_g^+$] emitted in a periodically pulsed microwave discharge and its afterglow in [Ar-N_2-O_2] mixtures. This reaction is found to form N_2O quite efficiently with an effective yield of 0.60 ± 0.15. Since the $N_2(A^3\Sigma_u^+)$ state is formed copiously by the low-energy secondary electrons produced by cosmic ray and solar EUV/x-ray absorption, by photoelectrons, and by precipitating particles in auroral substorms, a considerable amount of N_2O will be formed in the D and E region and below as the result of this process.

SA 123

ON THE PRODUCTION OF N_2O BY RELATIVISTIC ELECTRONS AND SOLAR PARTICLE EVENTS

S. S. Prasad (Jet Propulsion Laboratory, Pasadena, CA 91103)
E. C. Zipf (University of Pittsburgh, Pittsburgh, PA 15260)

Zipf and Prasad (1980) have discussed the importance of substantial auroral production of N_2O, via the reaction $N_2(A^3\Sigma) + O_2 \rightarrow N_2O + O$. To complement this new finding we wish to point out that relativistic electron precipitation (REP) events and solar particle events (SPE) also generate significant amounts of N_2O via the same reaction. If REP events occur 10% of times, then ion production data presented by Thorne (1977) imply primarily mesospheric column production rate of ~ 6 x 10^8 N_2O cm^{-2} s^{-1} in the subauroral region (4≤L≤8) equatoward of the auroral oval. Nitrous oxide production from SPE varies from year to year in response to solar activity. In 1978, it amounted to 10^8 cm^{-2} s^{-1} concentrated in the height range 40 ≤ h ≤ 92 km and in polar region, based upon ionization production calculated by Jackman (private communication) using particle data from IMP-8 and our assumption that this ionization occurred mostly poleward of 60° latitude. The significance of REP and SPE related N_2O production lies in their being local to the mesosphere and stratosphere. Above about 40 km, where the contribution of transported N_2O begins to weaken, these local sources could potentially become important for stratospheric chemistry, and for determination of the effective eddy diffusion coefficients used in one dimensional photochemical models.

SA 124

EXCEDE SPECTRAL: AN ARTIFICIAL AURORAL EXPERIMENT

R.R. O'Neil and A.T. Stair, Jr. (Radiation Effects Branch, Optical Physics Division, Air Force Geophysics Laboratory, Hanscom AFB, MA 01731)

D. Burt, J. Kemp and G. Frodsham (Utah State University, Logan, Utah 84322)

O. Shepherd (Visidyne, Inc., Burlington, MA 01803)

EXCEDE is an experimental program designed to study atmospheric radiative processes using rocket borne electron accelerators. On October 19, 1979, the 5700 pound EXCEDE SPECTRAL payload was successfully launched from Poker Flat, Alaska into the quiet night atmosphere. The stabilized payload contained: a 70 kilowatt (3kV) electron accelerator, an array of ultraviolet, visible and cryogenic infrared spectrometers, photometers and both film and television cameras. Atomic and molecular emissions induced in the atmosphere by the pulsed rocketborne electron accelerator and radiating in the 0.15 to 22 micron wavelength range were recorded at altitudes from 70 to 128 km. Observed emissions include: the N_2 Lyman Birge Hopfield system, the N_2 Herman Kaplan system, the N_2 second positive system, the N_2 first positive system, the N_2 Wu Benesch infrared system, the N_2^+ first negative system and the N_2^+ Meinel System. In addition, the cryogenic infrared instrumentation record NO emission at 5.4 microns and CO_2 emission at 4.3 microns produced by the pulsed rocketborne electron accelerator. The comprehensive spectral measurements are volume emission rates and will be analyzed in terms of production and loss mechanisms. This research was supported by the Defense Nuclear Agency.

SA 125

INFRARED EMISSION FROM NO($\Delta v = 1$) IN AN AURORA: HIRIS MEASUREMENTS

W. T. Rawlins and G. E. Caledonia (Physical Sciences Inc., 30 Commerce Way, Woburn, MA 01801)
J. J. Gibson and A. T. Stair, Jr. (Radiation Effects Branch, Optical Physics Division, Air Force Geophysics Laboratory, Hanscom AFB, MA 01731)

High resolution NO ($X^2\pi$, $\Delta v = 1$) emission data, obtained in an aurora between 100 and 125 km by the rocketborne HIRIS cryogenic interferometer spectrometer, have been analyzed by a spectral simulation/least squares technique. The vibrational state population distributions determined by this method exhibit significant population of up to six vibrational states of NO and a multimodal behavior with vibrational quantum number which is not predicted by present models. This result is interpreted in terms of direct auroral formation of NO (v) by the chemiluminescent reaction of N(^{2}D) with O_2, coupled with excitation of NO (v = 1) by collisions between thermal atomic oxygen and aurorally enhanced NO (v = 0). The distribution shapes and their apparent invariance between 100 and 125 km suggests that collisional relaxation of NO (v), probably by atomic oxygen, prevails over radiative cascade at these altitudes; this result is not in keeping with the present understanding of the kinetics and component densities in this region. The apparent auroral photoefficiency for NO ($\Delta v = 1$) radiation deduced from these measurements is (1.4 ± 0.5) % over the range 100-125 km, with a calibration uncertainty of a factor of 2; approximately 70-90% of the observed radiation is directly excited via the N(^{2}D) precursor.

SA 126

PRODUCTION OF AURORAL 6300 Å EMISSION AT THE FOOT OF THE GEOS-2 FIELD LINE

G.G. Shepherd (Centre for Research in Experimental Space Science, York University, Toronto, Ontario M3J 1P3)
G. Wrenn (Mullard Space Science Laboratory, Holmbury St.Mary, Dorking, Surrey, England)

A 6300 Å photometer was operated at Kilpisjärvi, Finland during the 1978/79 winter, when the GEOS-2 satellite was located on the conjugate magnetic field line. The low energy plasma at GEOS-2 is measured with two Suprathermal Plasma Analysers, which cover the range up to 500 eV, the region that is most efficient for the production of 6300 Å emission. Associated with the expansive phase of auroral substorms a long-

duration peak of 6300 Å emission is observed at Kilpisjärvi which corresponds to a rapid disappearance of low energy electrons at GEOS-2. This implies a storage of electrons somewhere between the ionosphere and the equator. One mechanism is suggested. Other aspects of the 6300 Å relationship to equatorial low energy plasma are described.

SA 127

INTERHEMISPHERIC TRANSPORT OF ELECTRONS

Knut Stamnes (Geophysical Institute, University of Alaska, Fairbanks, Alaska 99701)

A unified theoretical description of transport and energy deposition by photoelectrons and auroral electrons within a magnetic fluxtube in the ionosphere/magnetosphere is provided. The basic electron transport equation is used to describe all interactions including magnetic mirroring, inelastic and multiple elastic scattering with neutrals as well as ions and thermal electrons. Strongly forward peaked elastic scattering by ions and neutrals is taken into account. A self consistent solution to a two-stream approximation to the transport equation is obtained.

SA 128

OBSERVATIONS OF He^+ AT HIGH LATITUDES

R. A. Heelis (Space Sciences, Univ. Texas at Dallas, Richardson, TX 75080
J. A. Murphy
W. B. Hanson

At high latitudes during solstice the ray path through the atmosphere to about 400 km altitude near midnight is either so small that production of O^+, He^+ and H^+ continues at all times or so large that production of these species is negligible. The latter condition will produce an ionospheric "hole" if the plasma stagnates or circulates in the nightside winter pole. Near equinox, however, the shadow height near midnight may ensure that photoproduction of O^+ is negligible while the ray path at higher altitudes may be short enough that significant production of He^+ and H^+ takes place. Observations and calculations suggest that an ionospheric "hole" should also be observable at equinox but will not be so pronounced as that observed during winter. However, the dominance of He^+ in the hole between 500 km and 1400 km is unique to equinoxial conditions. We note that stagnation of the plasma is required rather than slow passage across the polar cap since at equinox the field tubes must reach the nightside before the shadow height ensures the photo-production of O^+ ceases. We also note that stagnation times between 3 hrs and 6 hrs are required for He^+ to be dominant at altitudes around 600 km.

SA 129

INTERPRETATIONS OF NEUTRAL WINDS IN THE EVENING AURORAL OVAL FROM 80 KM TO 300 KM

M.F. Larsen (School of Electrical Engineering, Cornell University, Ithaca, NY 14853)
I.S. Mikkelsen
T.S. Jorgensen (Danish Meteorological Institute, Lyngbyrej 100, Copenhagen, Denmark)
M.C. Kelley
E. Pereira (School of Electrical Engineering, Cornell University, Ithaca, NY 14853)

A two-dimensional thermospheric model has been developed to study the acceleration of the neutral atmosphere by auroral zone electric fields. The model uses the two-step Lax-Wendroff method. The goal of the modelling was to explain wind profiles obtained from chemi-luminescent trail measurements made in Feb/Mar 1977. Electron density profiles and electric field measurements from the Chatanika radar were used as input for the model. The model is invariant in the zonal direction. This means that Joule heating affects only the meridional wind. It was found that the Lorentz force alone could account for the observed shape and magnitude of the zonal wind. The meridional wind component is affected by the Lorentz force, Joule heating and pressure gradients due to solar heating. Although the Joule heating affects the magnitude and horizontal gradients in the meridional wind, the direction is determined by the background solar heating pressure gradient.

Although the two-dimensional model is useful in determining the response of the neutral atmosphere, we conclude that the problem is basically three-dimensional in nature, since the zonal wind at different altitudes is accelerated in different areas along the auroral oval.

SA 130

SEASONAL VARIATION IN THE PROPOGATION OF AURORAL ENERGY TO MILLSTONE HILL

W. L. Oliver
J. V. Evans (Both at: Northeast Radio Observatory Corporation, Haystack Observatory, Westford, Massachusetts 01886)

The exospheric temperature above Millstone Hill shows a marked seasonal variation in its response to magnetic activity, with the temperature increase due to a given level of magnetic activity being four times as great in summer as in winter. These observations are compared with models of thermospheric global circulation and satellite measurements of neutral composition variations during disturbed periods. It is suggested that the normal summer-to-winter global circulation pattern in the upper thermosphere effectively confines the greater portion of the storm effects to latitudes generally poleward of Millstone in winter while it aids their latitudinal progression to regions generally equatorward of Millstone in summer.

SA 131

CONVECTION, SUBSTORMS AND ARC CURRENT SYSTEMS DETERMINED FROM ROCKET-BORNE OBSERVATIONS ARE COMPARED FOR 2 SIMILAR AURORAL EVENTS

J.K. Walker (Earth Physics Branch, Energy, Mines and Resources, Ottawa, Canada K1A OY3)
J.A. Koehler (University of Saskatchewan, Saskatoon, Canada, S7N OWO)
F. Creutzberg, A.G. McNamara, A. Vallance Jones and B.A. Whalen (all at: Herzberg Institute for Astrophysics, National Research Council of Canada, Ottawa, Canada, K1A OR6)

Two rockets, which were launched from Ft. Churchill on 15 Jan. 1972 and 28 Feb., 1974, passed through westward convection currents on their uplegs and across a substorm region and 2 discrete arcs near apogee. The convection currents were determined by Ohm's law from the in situ plasma and electric field observations. Only the magnetic field of the Hall convection currents compared favourably with that determined from nearby ground magnetic stations. The ionospheres in the substorm and arc regions were calculated from the ionization rate which was determined from the energetic particle observations. Hall and Pedersen currents were also calculated from Ohm's law and field-aligned currents were estimated from the divergence of the meridian current. The models were iterated to obtain reasonable fits to the ground-based and rocket-borne magnetic field observations. The substorm regions were between the northernmost discrete arc and a faint arc about 40 km poleward. Large currents flowed southward across these substorm regions, while downward field-aligned currents were in the faint arcs and outward field-aligned currents in the discrete arcs. For both events the 2 discrete arcs were immersed in eastward currents. Field-aligned currents also flowed outward above the equatorial discrete arc. On the down leg both rockets again passed through the westward convection electrojet. These field-aligned currents and their associated arcs appear to be located at boundaries or discontinuities between the substorm and convection regions.

SA 132

THE STRUCTURE OF LOCALIZED NIGHTTIME AURORAL-ZONE SCINTILLATION ENHANCEMENTS

Charles L. Rino (SRI International, Menlo Park, CA 94025)
Jacqueline Owen

Simultaneous observations of the polar orbiting Wideband satellite at two auroral-zone stations (separated by a distance of approximately 300 km along the geomagnetic meridian) were made during November 1977. The latitudinal distribution of the average scintillation occurrence at each station shows a local maximum at the point where the propagation vector lies within an L-shell. This supports the hypothesis that the enhancement is a geometrical effect which is due to L-shell aligned, sheet-like irregularity structures. The detailed structure of the average scintillation occurrence--as well as the scintillation patterns on individual passes--indicate, however, that the source regions are confined in latitude.

Analysis of total electron content data shows that the local scintillation enhancements occur in a region of enhanced F-region ionization, with a steep gradient at its equatorward edge. The source region lies within the general confines of the diffuse aurora. Under quiet conditions the source region is too narrow to be intercepted at both stations.

These new results are discussed in light of a recent theoretical analysis by Ossakow and Chaturvedi that shows that the current convective instability--which is essentially a stable E x B configuration destabilized by moderate field-aligned currents--can explain the irregularity structure. The sheet-like structure is a consequence of the nonlinear saturation of the instability. The linearly unstable mode which would give rise to meridional structures, is nonlinearly damped, while the dominant nonlinearity favors the orthogonal modes that cause the sheet-like structures.

SA 133

ON THE DUAL NATURE OF THE ASPECT SENSITIVITY OF THE RADIO AURORA

D.R. McDiarmid, M. Mareschal and A.G. McNamara (all at: Herzberg Institute of Astrophysics, National Research Council of Canada, Ottawa, Canada K1A OR6)

Simultaneous observations of radio backscatter from a spatially confined scattering region by three widely separated radars (Saskatoon, Ft. Churchill and Baker Lake) permit one to determine numerical values for both the magnetic and the streaming aspect sensitivities of the radio aurora. The results of such observations will be presented and discussed.

SA 134

PLASMA DENSITY AND ELECTRIC FIELD FLUCTUATION MEASUREMENTS IN THE AURORAL ELECTROJET

E. Kudeki, B.G. Fejer, M.C. Kelley and R. Pfaff (School of Electrical Engineering, Cornell University, Ithaca NY 14853)
A. Pedersen, ESTEC, Domeinweg, Noordwijk, The Netherlands
C. Carlson (Space Science Laboratory, University of California, Berkeley California 94720)

Measurements of fluctuating electric fields and plasma density have been performed on a sounding rocket which traversed the auroral electrojet. Simultaneous data are also available which yield the plasma density profile and the ambient DC electric field. STARE radar measurements indicated strong auroral backscatter from the region penetrated by the rocket. The electric field spectrum strongly peaks in the range of several hundred Hertz which corresponds to about 5 meters wavelength. At higher frequency the spectrum can be characterized by a power law which extends to a frequency of nearly 10 kHZ and which corresponds to wavelengths of a fraction of a meter. Spin modulation of the data suggests that the wave intensity was maximum in the direction of the current. The irregularity layer was sharply bounded in altitude both above and below. The wave intensity and spectral peak will be compared to the linear growth rate as functions of altitude and wavelength respectively.

SA 135

AURORAL X-RAY IMAGING FROM ROCKETS

R. A. Goldberg
J. R. Barcus*
L. A. Treinish (all at NASA/Goddard Space Flight Center, Greenbelt, MD 20771)

In March 1978, two Nike Tomahawk payloads were launched from Poker Flat, Alaska, to observe the structure of bremsstrahlung x-rays and precipitating particles during both nighttime and daytime aurorally disturbed conditions. Each flight carried an on-axis nadir viewing NaI x-ray scintillator to observe x-rays in four spectral ranges (5-10, 10-20, 20-40, and >40 keV). Particle contamination of the detectors was avoided with broom magnet shielding techniques. By virtue of the payload 20° coning angle, (~10.5 S period), the detectors scanned wide regions on either side of the trajectory paths. This has permitted construction of the x-ray source regions near 100 km, a height established from Chatanika radar electron density maps obtained during each flight period. X-ray image maps for both flights exhibit enhanced source regions well outside the rocket trajectory planes. For the nighttime overflight, Chatanika radar scan data and Ft. Yukon riometer data were used to verify the presence of an imaged source approximately 175 km to the northeast from the launch site. Comparison of the two events shows the daytime energy spectra to be slightly harder but significantly less intense than the nighttime values. Furthermore, the enhanced regions emitted x-rays predominantly below 30 keV; these appear to coincide (at night) with optical enhancements in the same region. The potential of this technique for mapping of high latitude energetic radiations into the middle atmosphere is discussed.

Solar-Planetary Relationships: Cosmic Rays

Cosmic Rays
Pier 7 & 8
Monday P.M.
L. J. Lanzerotti (Bell Labs.), Presiding

SC 1 INVITED PAPER

PROPAGATION OF LOW ENERGY COSMIC RAYS IN INTERPLANETARY SPACE

I.D. Palmer (on leave at Planetary Sciences Dept. University of Arizona, Tucson, Az 85721)

The propagation of energetic particles along and across the interplanetary magnetic field is governed by the large-scale field geometry and by scattering in small-scale turbulent fields. Intensity and anisotropy profiles in combination are a powerful tool for elucidating the propagation parameters. Values of the scattering mean free path $\lambda_{//}$ (R) will be reviewed in prompt solar bursts and non-impulsive (corotating) events down to energies of E_p ~ 50 keV and E_e ~ 1 keV. The diffusion ($\kappa_\perp$) due to random walk of field lines is revisited. Recent values deduced from non-impulsive events, Jovian electrons, and intensity fluctuations in prompt solar events are evaluated. The outlook for the future includes better empirical values of $\lambda_{//}$ down to E_p ~ 50 keV and E_e ~ 1 keV (and implications of these $\lambda_{//}$ values for shock and Fermi acceleration), comparison with scattering theories in these regimes, and comparison between empirical and theoretical $\lambda_{//}$ in other regions such as the magnetosheath and upstream solar wind.

SC 2

ANISOTROPIC PROPAGATION OF LOW ENERGY NUCLEI IN INTERPLANETARY SPACE AND EFFECTS OF EARTH'S BOW SHOCK ON OBSERVATIONS*

S. P. Christon (Enrico Fermi Institute and Department of Physics, University of Chicago, Chicago, Illinois 60637)

Recently, opposite conclusions concerning the existence of significant cross-field transport of low energy nuclei in interplanetary space have been reached by two groups analyzing similar data sets obtained during the decline to minimum of Solar Cycle 20. In an attempt to understand how these different interpretations might have arisen, we analyze in detail 1-hour averaged 0.5-1.8 MeV proton anisotropies measured by the UC/LETs onboard the Earth orbiting IMP 7 and 8 spacecraft during 1974. Data are analyzed for periods between prompt solar particle events when simultaneous measurements of solar wind plasma and interplanetary magnetic field (IMF) are available. The diffusive anisotropy, ξ_D, is computed by subtracting the Compton-Getting anisotropy from the observed unidirectional anisotropy. ξ_D is decomposed into components // and ⊥ to the average direction of the IMF. The data set is then separated according to probable magnetic connection to the bow shock and mean values of the $\langle\xi_D\rangle$ components are computed. $\langle\xi_{D//}\rangle$ for both groups is sunward. We find that $\langle\xi_D\rangle$ on IMF connected to Earth's bow shock is stronger and more field aligned than $\langle\xi_D\rangle$ on IMF not intersecting the bow shock. We find a significant non-zero value of $\langle\xi_{D\perp}\rangle$ during periods when the IMF is not connected to the bow shock, thus implying non-negligible local diffusion transverse to the IMF. Finally, we confirm the observation that $\langle\xi_D\rangle$ is generally directed more sunward than strict field aligned transport would require. The effects of spacecraft position, plasma velocity and IMF fluctuations on $\langle\xi_D\rangle$ are discussed.

SC 3

PROPAGATION OF 2-200 keV ELECTRONS IN THE INTERPLANETARY MEDIUM

Douglas W. Potter
Kinsey A. Anderson
R.P. Lin (All from the Space Sciences Laboratory, University of California, Berkeley, CA 94720).

The high angular and energy resolution of the particles instrument on the ISEE-3 spacecraft enable us to survey the propagation characteristics of 2-200 keV interplanetary electrons under varying conditions.

We have discovered a large number of impulsive electron events that are limited in energy to <20 keV. The extreme collimation of the particles along the field line and the shape of the flux pulse indicate that the electrons travel through the interplanetary medium with little scattering.

During long-lived solar events, quite intricate angular distributions are often observed. The long delay (several hours) between changes in the outward and inward going populations suggests that electrons often travel large distances (several astronomical units) from the earth before returning.

Angular distributions taken during interplanetary shocks show that pitch angle distributions often have maximums at both zerio and 90°. Both the pre- and post-shock distributions show a maximum at zero. This indicates acceleration perpendicular to the field.

SC 4

ENERGY AND IONIC CHARGE MEASUREMENTS OF ENERGETIC INTERPLANETARY PARTICLE EVENTS FROM ISEE-3

H. Weiss
G. Gloeckler
F.M. Ipavich (all at: Univ. of MD, Dept. of Physics & Astronomy, College Park, MD 20742)
D. Hovestadt
B. Klecker
M. Scholer (all at Max-Planck-Institut für Physik und Astrophysik, 8046 Garching, Munich, FRG
L.A. Fisk (Univ. of New Hampshire, Dept. of Physics, Durham, NH 03824)
C.Y. Fan (Univ. of Arizona, Dept. of Physics, Tucson, AZ 85721)

We will present initial results from the Ultra Low Energy Z,E,Q (ULEZEQ) detector (Hovestadt et al. 1978) of the Max-Planck-Institut/University of Maryland experiment on board ISEE-3. The ULEZEQ sensor has incorporated a combination of electrostatic deflection and dE/dx (Proportional counter) versus E (solid state detector) analysis to simultaneously determine ionic charge, incident energy, and elemental composition of interplanetary ions. Using ULEZEQ data for a large flare on 23 September 1978, our analysis has indicated that for energies between 0.4 to 1 MeV/nucleon carbon, nitrogen, oxygen, and iron ions display nearly constant mean ionic charge states of 5, 6, 6, and 12, respectively (error in the charge state measurements is ±1). The implication of these charge state measurements on solar and interplanetary physical theory will be discussed as well as additional data from other energetic particle events.

SC 5

A STATISTICAL STUDY OF THE DISTRIBUTION OF IONIC CHARGE STATES FOR HEAVY IONS IN SOLAR FLARE-ASSOCIATED PARTICLE EVENTS

L.S. Ma Sung
G. Gloeckler (both at: Univ. of Maryland, Dept. of Physics & Astronomy, College Park, MD 20742)
C.Y. Fan (Univ. of Arizona, Dept. of Physics, Tucson, AZ 85721)
D. Hovestadt (Max-Planck-Institut fur Physik und Astrophysik, 8046 Garching, Munich, FGR)

Based on the particle data collected by the University of Maryland Electrostatic Energy-versus-Charge Analyzer Experiment on IMP-8, we analyze the distribution of the ionic charge states of ions heavier than Helium for some 30 flare-associated particle events during the period from November 1973 to June 1979. A Chi-square analysis is performed on the pulse-height distributions of the charge states in individual events by fitting them with calculated distributions which use as input parameters the flare composition and an equilibrium distribution of charge states at a given coronal temperature (Jordan 1969). Since the distribution of charge states for a given element is temperature dependent, such an analysis will provide information about the temperature of the region in which the ions were accelerated or stored for a significant time period. In addition, measurement of the charge states of ions in He^3-and heavy ion-enriched events may provide insight into the mechanisms of heating (Fisk 1978, Ibragimov et al. 1978) for these ions. These results will be discussed.

SC 6

A SURVEY OF SOLAR FLARE PROTON AND ALPHA DIFFERENTIAL SPECTRA BETWEEN 1 AND 200 MeV/NUCLEON

R. E. McGUIRE* (NASA/Goddard Space Flight Center)
M. A. I. Van Hollebeke* (NASA/Goddard Space Flight Center
T. T. von Rosenvinge (NASA/Goddard Space Flight Center

We have undertaken a new survey to characterize the shapes and relative slopes of proton and alpha differential spectra seen at IMP 8 in solar flare events between 1973 and 1979 (the conclusion of solar cycle 20 and the onset of activity in cycle 21). In order to obtain spectra as similar as possible to particle injection spectra at the sun, the individual event spectra are constructed using the peak flux obtained in each energy band. The energy range extends from below 1 MeV/nucleon to above 200 MeV/nucleon. Particularly in those events for which IMP is well-connected to the flare site, we will investigate the fit of several possible functions of energy or other parameters to the observed proton and alpha spectra including a function derived on the assumption of Fermi acceleration at the flare. Anisotropy effects and heliolongitude dependence of the spectra will also be discussed.

SC 7 INVITED PAPER

SOLAR CORONAL HOLES AND THEIR INFLUENCE ON THE INTENSITY VARIATIONS OF COSMIC RAYS

D. Venkatesan (Department of Physics, Univ. of Calgary, Calgary, Alberta, Canada T2N 1N4)

The essential characteristics of solar coronal holes and their relationship to other solar related features will be reviewed. In particular their association with fast solar wind streams and developing interplanetary shocks at large distances will be considered.

The role played by solar coronal holes on intensity variations of cosmic rays will be discussed against the background of available observations. The importance of polar coronal holes on observations in the ecliptic plane will be stressed.

The necessity to sort out variations attributed to solar coronal holes from various types of variations associated with other solar features will be pointed out.

Possible physical mechanisms for the intensity variations would be indicated.

SC8

STUDY OF THE COSMIC RAY DIURNAL ANISOTROPY OVER 22 YEARS USING NEUTRON AND MUON MONITOR DATA

S.P. Agrawal
M. Bercovitch (both from Herzberg Institute of Astrophysics, National Research Council of Canada, Ottawa, Canada K1A 0R6)

Previous studies of the cosmic ray diurnal variation (d.v.) extending over periods of a decade or more have demonstrated the long-term variability of the cosmic ray anisotropy, and have led several authors to suggest a quasi-periodic modulation of the anisotropy having 11 and 20-22 year components. In this paper we present a survey of the d.v. from 1957 to 1979, extending the period studied up to the present solar sunspot maximum. We use hourly data from the Canadian network of neutron and muon monitors to chart the year to year variations in d.v. amplitude, phase and upper cutoff rigidity, where the muon-neutron amplitude ratio is taken as a convenient index related to the cutoff rigidity. The d.v. vectors are corrected for the effects of atmospheric temperature variation as well as for the earth's orbital motion. In 1978-79, the space direction of the anisotropy is found to be about 16.0 hours, some two hours earlier than it was in 1957-58, a comparable epoch of the 22-year solar magnetic cycle. The upper cutoff rigidity is estimated at 150-200 GV, significantly higher than that observed during the previous solar sunspot maximum in 1968-69.

SC9

UNUSUAL NORTH-SOUTH ANISOTROPY WAVE IN COSMIC RAY INTENSITY*

M. A. Pomerantz, S. P. Duggal and C. H. Tsao, Bartol Research Foundation of The Franklin Institute, University of Delaware, Newark, DE 19711

It has been well established that all Forbush decreases display some form of north-south anisotropy. In general, even quiet days are characterized by a small axial anisotropy. Recently, an unusual type of cosmic ray event that had never been identified previously displayed a large wave-like north-south anisotropy during a relatively quiet period. The maximum peak-to-peak magnitude of the cosmic ray intensity wave at sea level (≈3.5%) was recorded at McMurdo Station, Antarctica, where the period of the anisotropy was about 27 hours. A major feature of this intensity fluctuation, which was associated with the arrival of a shock wave and the occurrence of a geomagnetic storm, is that no comparable enhanced diurnal anisotropy occurred at equatorial viewing stations during this period. Harmonic analysis of the intensity profile reveals that the amplitude is proportional to $\sin \lambda_i^*$, where λ_i^* is the weighted mean asymptotic latitude of station i. On the other hand, as expected, the universal time phase is essentially constant around the globe.

SC 10

COSMIC RAY ANISOTROPY MEASUREMENTS AT MEDIAN PRIMARY RIGIDITIES BETWEEN 100 GV and 700 GV

M. Bercovitch
S.P. Agrawal (both at Herzberg Institute of Astrophysics, National Research Council of Canada, Ottawa, Canada K1A 0R6)

A large area (48 m^2) bidirectional proportional counter array which simultaneously monitors the intensity of muons from the easterly and westerly directions at zenith angles between 45° and 88°, has been in operation at Ottawa since November 1976. The hourly intensity data are analysed to determine the solar and sidereal variations of the east-west intensity differences in six zenith angle ranges corresponding to median primary rigidities between 100 and 700 GV. The anisotropies thus derived are essentially free of meteorological and environmental effects. The range of median rigidity covered allows us to explore sensitively the upper rigidity cutoff of the solar anisotropy and the lower cutoff of the sidereal anisotropy. The upper cutoff of the solar anisotropy is found to vary markedly between 1976 and 1979, increasing from 50-100 GV in 1976-77 to 150-200 GV in 1979. The first harmonic of the sidereal anisotropy during 1978-79 is found to be ∿0.06% at 0400 hours R.A., with an effective lower cutoff at ∿300 GV.

SC 11

POWER SPECTRA OF COSMIC RAY VARIATIONS: SIMULATION STUDIES AND THE AMBIENT COMPONENT OF THE DAILY VARIATION

D. Venkatesan (Department of Physics, University of Calgary, Alberta, Canada)
S. P. Agrawal
L. J. Lanzerotti
C. G. Maclennan (all at: Bell Telephone Laboratories, Murray Hill, New Jersey 07974)

The use of power spectra in the past for studies of the daily variation of cosmic ray intensity has largely been limited to the demonstration of the existence of peaks at frequencies corresponding to the 24-hour (diurnal) wave and its harmonics. We have computed the power spectra for cosmic ray variations for each solar rotation for more than a solar cycle in order to investigate the time dependence of the fluctuation power level, spectral shape, and the ambient power level under the diurnal wave. An increase in ambient power is found under the diurnal peak during solar maximum conditions. To further understand the details of cosmic ray power spectra we have carried out a detailed program of simulation of cosmic ray variations to see the effects on the spectra and the diurnal wave of varying daily amplitudes, random variations, Forbush decreases, and solar particle events. The results of these parallel investigations will be presented.

SC 12

RELATIONSHIPS BETWEEN COSMIC RAY INTENSITY VARIATIONS AND THE INTERPLANETARY MAGNETIC FIELD (IMF)*

S. P. Duggal, M. A. Pomerantz, and C. H. Tsao, Bartol Research Foundation of The Franklin Institute, University of Delaware, Newark, DE 19711

It was first demonstrated by Barouch and Burlaga (1974) that large cosmic ray intensity decreases are related to magnetic "blobs" in the interplanetary space. To extend this result to a broader domain in order to provide a basis for a unified theoretical model of solar modulation, it is important to determine whether cosmic ray intensity variations are associated with the day-to-day variability of the IMF. A study of regression plots of $\Delta I/I$ vs B shows that the correlation coefficients during individual years, from 1965 to 1971, are small. This result is not surprising in view of the fact that under average conditions, which prevail most of the time, the influence of other factors mask the effect of a simple $\Delta I/I$ vs $\Delta B/B$ correlation. On the other hand, superposed epoch analysis with respect to zero days characterized by either low or high magnetic field values has revealed a significant relationship between the cosmic ray intensity and B. Furthermore, whereas the high epochs are concomitant with intensity decreases, the low ones are characterized by transient increases.

SC 13

DISTINCTIVE SHORT-TERM EFFECTS OF SOLARWIND VARIABILITY ON GALACTIC COSMIC RAY INTENSITY

A.K. Shukla (Vikram Space Physics Centre, A.P.S. Univ., Rewa, MP, 486003, India)
S.P. Agrawal* (Herzberg Institute of Astrophysics, NRC, Ottawa, Canada K1A 0R6)
D. Venkatesan (Physics Dept., Univ. of Calgary, Calgary, Alberta, Canada T2N 1N4)

The day-to-day variations in solar wind speed are inversely correlated with high latitude neutron monitor intensities. We report here results of a superposed Chree analysis of the counting rate of high latitude neutron and meson monitors from the same station. We analyze separately two different types of event according to whether the zero day of the event is characterised by a substantial (1) increase ($\Delta V \gtrsim 200$, and maximum speed >550 km/sec), or (2) decrease ($\Delta V \lesssim -50$, and minimum speed <350 km/sec) in solar wind speed, which persists for at least 3 days. We find a high negative correlation for both types of event.

For Type (2) events, during the entire period studied, we find almost equal relative changes in the neutron and muon monitor rates indicating a flat rigidity spectrum similar to that observed for solar diurnal anisotropy. For Type (1) events, we find a similar flat spectrum during the period 1973-76. However, during 1977-78, the spectrum of the Type (1) intensity variations acquires a negative spectral character similar to that observed for Forbush decreases. We suggest that the Type (1) events of the 1973-76 period were mainly a manifestation of "monster solar wind streams" associated with coronal holes. Such streams which do not form magnetic shock structures inside 1 AU produce enhanced outward convection of cosmic ray particles leading to intensity depressions with a flat rigidity dependence. Similarly, the low velocity streams of Type (2) events produce reduced convection and flat spectrum increases. In contrast, Type (1) events of 1977-78 were predominantly associated with solar flares.

Solar-Planetary Relationships: Magnetospheric Physics

Aurora, Substorms and Particle Injections

Pier 5
Thursday A.M.
D. Venkatesan (Univ. of Calgary), Presiding

SM 1

MEASUREMENTS OF AURORAL-ARC ELECTRODYNAMIC PARAMETERS AT THREE DIFFERENT LONGITUDES

O. de la Beaujardiere and R. Vondrak (SRI International, Menlo Park, CA 94025)
R. Heelis and W. Hanson (University of Texas at Dallas, Richardson, TX 75080)
R. Hoffman (NASA/Goddard Space Flight Center, Greenbelt, MD 20771)

Simultaneous AE-C satellite and Chatanika-radar measurements of a discrete auroral arc are used to calculate the variations around the arc of electric fields, conductivities, currents, ion and electron temperature. The AE-C trajectory was such that the arc was crossed twice by the spacecraft, at points equidistant (~15° West and ~15° East) from Chatanika, providing observation of this arc at three widely spaced longitudes.

The pattern of the electric field variation is quantitatively very similar at the three

longitudes. Furthermore, this pattern remains the same as time varies. The electric field is mostly northward and intense (~60 mV/m) equatorward of the arc, and it is small (~20 mV/m) poleward of the arc. The arc marks the boundary between two different regions of ion flow. The ion temperature variations are qualitatively similar. However, for a given large electric field, the ion temperature is different at the three longitudes: in the region of large E field, the ion temperature is smaller to the west (1750°), than to the east or at Chatanika (3000°). This difference is attributed to differences in F-region neutral-wind velocities.

SM 2

DOUBLE-LAYER CRITERION ON THE ALTITUDE OF THE AURORAL ACCELERATION REGION

J.R. Kan (Geophysical Institute, University of Alaska, Fairbanks, Alaska 99701)
L.C. Lee (Geophysical Institute, University of Alaska, Fairbanks, Alaska 99701)

The double-layer criterion, consisting of necessary conditions for the existence of double-layer solutions, is derived for both extended and localized parallel electric fields along converging geomagnetic field lines in the presence of backscattered trapped electrons. The minimum streaming speed of the current-carrying electrons required by the Bohm-Block criterion can be relaxed by the presence of a sufficient population of trapped and back-scattered electrons. According to the present criterion, the parallel electric field is either distributed from $\sim 0.5\ R_E$ to less than $\sim 1.5\ R_E$ altitudes in the case of an extended double-layer or concentrated in a few Debye lengths at an altitude above $\sim 0.5\ R_E$ but below a few R_E in the case of a localized double-layer. The lower limit on the altitude is determined by the supersonic transition altitude of the polar wind. The upper limit is controlled by the number density of the backscattered primary electrons and the electric potential profile near the upper boundary.

SM 3

MULTI-BALLOON OBSERVATIONS OF BREMSSTRAHLUNG X-RAYS IN THE MIDNIGHT TO MORNING SECTOR OF THE AURORAL ZONE

K.K. Vij (Department of Physics, Univ. Of Calgary Calgary, Alberta, Canada T2N 1N4)
D. Venkatesan*, G. Kremsert and J.W. Münch†

We present the multi-balloon observations of bremsstrahlung x-rays related to a study of the morphology of electron precipitation in the midnight to morning sector. The observations were carried out by balloon launches from Kiruna and Lycksele in Sweden and Great Whale River, Quebec, Canada during the summer of 1975.

The objectives of the campaign, namely, simultaneous balloon observations of bremsstrahlung x-rays, separated in local time, were achieved at least on two occasions. This report deals with the data of June 30, 1975, when there were four balloons, designated LE04, KE04, KX06 and GW2 at the ceiling altitudes making simultaneous x-ray measurements. Charged particle data collected by ATS-6 and NOAA-4 satellites, which were in orbit at the same time, have also been used for the comparative study. A preliminary look at the data seems to support the "drifting rain cloud model" according to which the electrons precipitating in the midnight sector drift east-ward and precipitate in the morning sector. The measured time delays between the midnight and morning sector events are consistent with the theoretically expected values.

SM 4

OBSERVATIONS OF ELECTRON INJECTION AND QUASI-STATIONARY ELECTRON STRUCTURES FOLLOWING A GEOMAGNETIC DISTURBANCE

W. R. Sheldon
Y.-C. Chang
J. R. Benbrook (all at: Department of Physics, University of Houston, Houston, Texas 77004)
T. J. Rosenberg
D. L. Matthews (both at: Institute for Physical Science and Technology, University of Maryland, College Park, Maryland 20742)

The X-ray spectrum was measured on a high-altitude balloon above Roberval, Quebec (L=4.2) at 0840-1040 UT on July 31, 1973. These data are compared to electron data from the S^3 satellite taken at the same time in the vicinity of the Roberval field line (L values between 4.1 and 5.3 and local times within an hour of that of Roberval). Some of the electron counting rate increases observed by the satellite can be identified as moving electron clouds by the associated electron precipitation observed by the balloon; other increases appear to be associated with the satellite's penetration of energy boundaries in the general convection pattern of magnetospheric plasma. One of the moving electron clouds observed at L=5.17 appears to be the result of the injection of lower energy electrons some four hours earlier in local time (near the meridian of the Meanook magnetometer) and at greater L values, followed by subsequent energization through inward cross-L diffusion during eastward gradient and curvature drift. Data from the trans-Canada magnetometer chain is found to be in good agreement with this model.

SM 5

SIMULTANEOUS OBSERVATIONS OF ELECTRON AND ION WAVES: IMPLICATIONS FOR THE DIFFUSE AURORA

W. S. Kurth
T. E. Eastman
L. A. Frank (all at: Dept. of Physics and Astronomy, The University of Iowa, IA 52242)
M. Ashour-Abdalla
D. A. Gurnett (both at: Inst. of Geophysics and Planetary Physics, University of California, Los Angeles, CA 90024)

The diffuse aurora is known to be the result of both electron and ion precipitation. Since the regions of precipitation generally coincide, the scattering mechanisms for both electrons and ions must reside on the same magnetic field lines. In recent years our understanding of the electron precipitation mechanism has grown and there is general agreement that electron cyclotron harmonic emissions near the equator are primarily responsible for scattering electrons into the loss cone. It has been conjectured that ion cyclotron harmonic emissions are most likely responsible for the similar scattering of ions. We report observations from the ISEE spacecraft that reveal the simultaneous occurrence of intense electron cyclotron harmonic emissions and low frequency ion modes near the nightside magnetic equator. Examples of simultaneous emissions in the near-earth plasma sheet during quiet periods indicate that these waves are responsible for the particle precipitation associated with diffuse aurora. The equatorial location of the instabilities is compatible with precipitation near the strong diffusion limit since the bulk of the plasma traverses the interaction region. The electrostatic waves occur in the near-earth plasma sheet where fluxes of ~ 0.5- to 10-keV electrons and 1- to 45-keV ions are relatively intense. Hence, we have identified a scattering mechanism within the plasma sheet that provides a viable source for diffuse auroral precipitation.

SM 6

ION INERTIAL AND ELECTROMAGNETIC EFFECTS ON THE CURRENT CONVECTIVE INSTABILITY IN THE DIFFUSE AURORA

P. K. Chaturvedi (Berkeley Research Associates, Arlington, Va. 22209)
S. L. Ossakow (Naval Research Laboratory, Code 4780, Washington, D. C. 20375)

The current convective instability has been proposed[1,2] as a possible mechanism for generating the long wavelength, field aligned, scintillation causing ionospheric irregularities observed in the diffuse auroral region by the DNA Wideband satellite.[3] The instability is caused by a weak current along the magnetic field, associated with the diffuse auroral precipitation, and a northward plasma density gradient. A stable $\underline{E} \times \underline{B}$ geometry, with $\underline{E}$ westward or northwest can become destabilized by the current if $\underline{E}$ is not too large. Here we extend the analysis to include ion inertial effects, which could be important at higher altitudes, and electromagnetic effects, which should be considered for long wavelengths. Ion inertia extends the instability to high altitudes with growth rates comparable to those achieved at lower altitudes in the collision dominated regime. Electromagnetic effects are destabilizing, but extremely weak ($\sim 10^{-4}$) for typical parameters at 400 km altitude.

SM 7

THE INFLUENCE OF MAGNETIC SHEAR ON THE CURRENT CONVECTIVE INSTABILITY IN THE DIFFUSE AURORA

J. D. Huba (Science Applications, Inc., McLean, Va. 22102)
S. L. Ossakow (Naval Research Laboratory, Washington, D. C. 20375)

Recently, the current convective instability has been suggested[1] as a mechanism to explain the scintillation enhancements observed by the DNA Wideband Satellite in the high latitude diffuse aurora F region. The instability is driven by a density gradient and a field-aligned current, both of which are present in the diffuse auroral region. We discuss the influence of magnetic shear (which is produced self-consistently by the field-aligned current) on this instability for parameters typical of the high latitude F region. We find that magnetic shear (1) reduces the growth rate of the instability (although does not stabilize the mode) and (2) substantially localizes the mode structure in the north-south direction i.e., parallel to the density gradient. This final result indicates that the mode structure is two dimensional in the plane perpendicular to the magnetic field during the linear phase of the instability.

SM 8

PRELIMINARY NUMERICAL SIMULATIONS OF CURRENT CONVECTIVE INSTABILITY IN THE DIFFUSE AURORA

M. J. Keskinen*
B. E. McDonald
S. L. Ossakow (all at Naval Research Laboratory, Washington, D. C. 20375)

A simple plasma fluid model of the current convective instability has been proposed[1] to account directly for diffuse auroral scintillation causing F region ionospheric irregularities. This instability is almost field aligned, i.e., $k_\parallel/k_\perp \ll 1$, where $k_\parallel$ and $k_\perp$ are the components of k parallel and perpendicular to the magnetic field, $B\hat{z}$, respectively. Since we are interested in modes propagating nearly perpendicular to the magnetic field, we perform two dimensional numerical simulations of this fluid model of the current convective instability in a plane almost perpendicular to the magnetic field. This plane is defined by $k_\perp = k_x \hat{x} + k_\parallel \hat{z}$ (with $k_\parallel/k_x$ small, fixed, and maximizing the linear growth rate) and $\hat{y}\ (\partial n_o/\partial y)$ with $n_o(\partial n_o/\partial y)^{-1} \equiv L$ the northward total electron content gradient scale length. Results from several simulations using different values of $k_\parallel/k_x$ and the gradient scale length L will be presented and compared with theory and experiment.

SM 9

A MULTI-POINT PLASMA PERSPECTIVE OF EQUATORIAL SUBSTORM INJECTION EVENTS

R.L. Arnoldy
T.E. Moore (Both at University of New Hampshire, Space Science Center, Durham, N.H. 03824)
J. Feynman (Boston College, Chestnut Hill, Ma. 02167)
D.A. Hardy (Air Force Geophysics Laboratory, Hanscom AFB, Ma. 01731)

The orbit of the SCATHA spacecraft lends itself to data correlation with geosynchronous vehicles due to its variable radial separation by $\pm \sim 1\ R_e$ from synchronous orbit. We compare < 25 keV plasma electron and ion data from ATS 6 with similar data from SCATHA for a moderately disturbed period during 11-12 February 1979. This period includes two passes through the evening equatorial magnetosphere and a total of four well defined evening injection events occurring at local times from near dusk to midnight. These events all occurred after both spacecraft had clearly entered the plasma sheet and all exhibited sharp flux changes with little energy dispersion; tending to replace pre-existing plasma with hot, quasi-Maxwellian distributions. Equally sharp magnetic field changes accompany each event. Spacecraft charging during this period was limited to potentials less than 50V. Such events are often clearly identifiable at both spacecraft, propagating nearly radially inward between the spacecraft in a time longer than the time for plasma changes at either location, thus exhibiting well defined time delays. We discuss several interesting features of the plasma distribution changes and time delays observed as functions of local time, in light of current models of injection and convection.

SM 10

HIGH LATITUDE (NORTH OF CAMBRIDGE BAY) SUBSTORMS AND THEIR INFLUENCE ON THE AE INDEX

Jagdish C. Gupta
E.I. Loomer (both at: Earth Physics Branch, Division of Geomagnetism, Energy, Mines and Resources, Ottawa, Canada, K1A 0Y3

The occurrence characteristics of the substorms appearing north of Cambridge Bay have been investigated. A statistical analysis of the Canadian data for the interval 1972-1978 has shown that these localized substorms which occur around local midnight, and most frequently in winter during the descending phase of the sunspot cycle, have a significant influence on AE index. The diurnal variation of their occurrence reflects the proximity of the station to the poleward edge of the auroral bulge in the midnight-dawn sector.

SM 11

MAGNETOSPHERIC FLUX TRANSFER AND SUBSTORMS

N. U. Crooker (Department of Atmospheric Sciences, University of California, Los Angeles, Ca. 90024)
G. L. Siscoe

Serious discrepancies in merging models of substorms are resolved by a simple, conceptual change that is required for consistency between magnetospheric current systems and magnetic flux transfer as discussed in the preceding companion paper. In previous models the substorm process is tail merging and subsequent earthward convection of the freshly merged field lines. In the revised model the substorm process is the earthward convection of the pre-existing closed field lines in the plasma sheet. The convection is in direct response to the Region 1 currents driven by the potential generated by dayside merging. Tail merging is reserved for the recovery process. Its main function is to restore the plasma sheet to its pre-storm configuration and content. This may be accomplished without earthward convection.

Three features of the revised substorm model that are consistent with recent observations where previous models fail are:

1.) Although energy is transferred from the solar wind to the tail, most of the energy is not stored there but passes directly through toward Earth. Thus substorms are driven directly by the solar wind, as close correlations between solar wind parameters and geomagnetic activity suggest.

2.) Polar cap expansion and earthward convection occur together during substorms, consistent with equatorward movement of aurora with increasing AE index.

3.) During substorms flows in the plasma sheet are predominantly earthward, and the z-component of the magnetic field is predominantly northward.

SM 12

ARE SUBSTORMS POWER DRIVEN OR A SUDDEN RELEASE OF STORED ENERGY?

L. Rossberg (Max-Planck-Institut für Aeronomie, 3411 Katlenburg-Lindau 3, FRG.

In a recent paper Akasofu addressed the question whether a magnetospheric substorm is caused by a sudden conversion of magnetic tail energy accumulated prior to substorm onset or a process "driven" by the power $\varepsilon(t)$ of the solar wind-magnetosphere dynamo and presented evidence in support of a direct response of the magnetosphere to variations of $\varepsilon(t)$. It is accepted that this is largely true for the response of the magnetospheric current system to $\varepsilon(t)$. However, substorm related intense electron and proton bursts observed by polar orbiting satellites suggest a sudden conversion of at least a part of stored magnetic energy accumulated in the tail in addition to the direct power driven process.

SM 13

UP-DOWN MOVEMENTS OF THE SOLAR CURRENT DISK AND MAJOR GEOMAGNETIC STORMS

S.-I. Akasofu (Geophysical Institute, University of Alaska, Fairbanks, AK. 99701)

It is shown that the development of major geomagnetic storms ($|Dst| > 100\gamma$) is associated with up-down movements of the solar current disk, which are accompanied by a large impulsive increase of the IMF magnitude and a negative value of the IMF angle THETA; unless these conditions arise together, a major geomagnetic storm cannot develop. The period of $\partial Dst/\partial t < 0$ during major storms conincides well with the period when the solar wind - magnetosphere energy coupling function ε becomes $\gtrsim 10^{19}$ erg/sec. These conclusions do not depend on the phase of the sunspot cycle.

It is also shown that a large southward component of the IMF penetrates into the magnetotail. This result, together with the penetration of the IMF B_y component demonstrated by Fairfield (1979), indicates that the IMF can penetrate into the magnetotail, so that all magnetic field variations cannot be of internal origin. Thus, some of the magnetotail phenomena during substorms (such as thinning and thickening of the plasma sheet) can be explained by a simple superposition of the IMF to the magnetotail, without involving internal instabilities in the magnetotail.

VLF and Kilometric Radiation

Pier 5
Thursday P.M.
E. W. Greenstadt (TRW), Presiding

SM 14

ROCKET-BORNE OBSERVATIONS OF DISCRETE VLF EMISSIONS (CHORUS) ASSOCIATED WITH ENERGETIC (40 keV - 120keV) ELECTRON BURSTS.

R.F. Pfaff, M.C. Kelley, P.M. Kintner, S. Powell (School of Electrical Engineering, Cornell University, Ithaca, NY 14853)
L.G. Smith (Department of Electrical Engineering, University of Illinois, Urbana, Illinois 61801)

Simultaneous observations of VLF plasma waves and precipitating particles were made by independent experiments on different sounding rockets launched during the solar eclipse campaign of February 26, 1979 near Red Lake, Canada ($L \sim 4.5$). Geomagnetic activity was very high during this time period. Power spectra of the electric fields measured by orthogonal pairs of booms on the Cornell rocket reveal intense bursts of discrete electromagnetic emissions (whistler-mode chorus) between 0.5 and 4.0 kHz throughout the entire five minute data-collecting time of the flight. The wave bursts often show a multiple structure of nearly equally spaced "pulses" ($\sim .5$ second separation) which had varying amplitudes. Particle detectors aboard two rockets flown by the University of Illinois detected intense bursts of high energy electrons (40keV to 120keV) superimposed on a nearly constant "background" flux of $\sim$40keV electrons. The bursts display temporal microstructure, similar to that of the chorus, and the three data sets correlate well in many instances. Their association will be interpreted in light of generation mechanisms involving cyclotron resonance between whistler mode waves and electrons at the equator.

SM 15

ESTIMATION OF THE WAVE NORMAL DISTRIBUTION AT THE SOURCE FOR VLF HISS AND CHORUS OBSERVED ON-BOARD GEOS.

F. Lefeuvre,* T. F. Bell, U. S. Inan (all at Radioscience Laboratory, Stanford University, Stanford, Ca. 94305)

The wave normal distribution of VLF hiss and chorus observed on board the GEOS satellite has been calculated in terms of the Wave Distribution Function (L. R. O. Storey, F. Lefeuvre, Geophys. J. R. Astr. Soc., 56, 255, 1979). The analysis shows that the wave energy is often confined within two unique wave packets propagating in the same direction relative to $\vec{B}_o$. Both wave packets have the same azimuthal angle ($\neq 0$) with respect to the local meridian plane. The packets appear to propagate from the same source. Using raytracing techniques on a diffusive equilibrium model, we locate the apparent source point and determine the wave normal direction at the apparent source for some specific cases. The findings are consistent with a quasi-isotropic source emitting waves with all permitted wave normal directions.

SM 16

PRECIPITATION OF INNER-ZONE ELECTRONS BY WHISTLER-MODE WAVES FROM THE VLF TRANSMITTERS UMS AND NWC

H. C. Koons
B. C. Edgar
A. L. Vampola (all at: Space Sciences Laboratory, The Aerospace Corporation, El Segundo, CA 90245)

The precipitation of energetic electrons which are commonly observed in the drift loss cone east of 60 deg east longitude between $L \sim 1.6$ and $L \sim 1.8$ can be accounted for by a doppler-shifted cyclotron resonance between the electrons and non-ducted whistler-mode waves from high-power ground-based VLF transmitters. A ray-tracing analysis using a diffusive equilibrium model shows that 17.1 kHz waves starting with vertical wave normals between 23 deg and 31 deg magnetic latitude cross the magnetic equator between $L \sim 1.6$ and $L \sim 1.8$ with wave normals of approximately 63 deg. A relativistic cyclotron-resonance analysis for the same model plasmasphere using the ray-tracing results gives an energy vs. L-shell dependence for the precipitated electrons which is in excellent agreement with the observed dependence. The VLF transmitter is most likely the UMS transmitter located near Gorki, U.S.S.R. It transmits on 17.1 kHz. VLF records covering this frequency band were available for only three of the time periods when electrons were observed. In two cases UMS was transmitting at the time required to account for the observations. In the third case a higher frequency is required to fit the data. At the time the NWC transmitter at North West Cape, Australia was operating at 22.3 kHz. The data are consistent with a model in which weak pitch-angle scattering by whistler-mode waves from NWC does not completely fill the drift loss cone at the longitude of NWC.

SM 17

OBSERVATIONS OF SIPLE TRANSMITTER SIGNALS AND TRIGGERED VLF EMISSIONS ON THE EXOS-B SATELLITE

U. S. Inan, T. F. Bell, R. A. Helliwell (all at Radioscience Laboratory, Stanford University, Stanford, Ca. 94305)
I. Kimura (at Electrical Engineering Dept., Kyoto University, Kyoto 606, Japan)
H. Matsumoto (at Ionosphere Research Laboratory, Kyoto University, Uji, Kyoto 611, Japan)
T. Mukai (at Institute of Space and Aeronautical Science, University of Tokyo, Meguro-ku, Tokyo 153, Japan)

During the periods July 15-Sept. 3, 1979 and December 21, 1979-January 24, 1980 a joint wave-injection/reception experiment to study VLF wave-particle interactions in the magnetosphere was carried out by scientists from Stanford, Kyoto and Tokyo Universities. In this study, VLF waves with specially designed frequency-time formats were transmitted from Siple Station, Antarctica, into the magnetosphere where they interacted with the energetic particle population, occasionally producing VLF emissions. The injected waves and triggered emissions were detected on-board the Japanese EXOS-B satellite by a Kyoto University VLF receiver. The characteristics of the energetic particle population were simultaneously measured on the satellite by a particle experiment contributed by the University of Tokyo. The experiment was carried out for $\sim$1 hr/day during the times when the satellite was near the Siple meridian and on the satellite shells $2 \leq L \leq 5$.

In the present paper we discuss the azimuthal and radial distribution of the transmitter signal energy in the magnetosphere and study the cases in which VLF emissions were triggered by the injected signals. By comparing the wave activity with the data acquired on the energetic particle distribution we attempt to isolate the necessary conditions on the energetic particle distribution for strong wave-particle interactions.

SM 18

QUANTITATIVE MEASURES OF MAGNETOTAIL FLUX CHANGES

R.E. Holzer
J.A. Slavin (Both at Institute of Geophysics and Planetary Physics, University of California, Los Angeles, CA 90024)

The total magnetic field, B, in a magnetotail lobe was examined in order to make a continuous appraisal of the magnetic flux transfer process. The value of dB/dt, obtained from OGO5 records was taken as a measure of the rate of change of tail flux assuming a constant tail cross section. The AL auroral index was taken as a measure of the rate of transfer of tail flux to the inner magnetosphere (See Holzer and Slavin, JGR, 84, 2572, 1979). In order to make a direct comparison of AL with dB/dt it was necessary to augment dB/dt corresponding to the flux added to the tail by the merging process, estimated from simultaneous interplanetary records of Explorers 33, 34, and 35 by the method described in the above reference. In order to minimize the effect of solar wind dynamic pressure, intervals in which the bulk speed varied by less than 10% were used. The total estimated flux changes were consistent within 25%. Peaks in the dB/dt record preceded corresponding peaks in the AL record by approximately 25 minutes, indicating an average residence time in the tail for flux added by the merging process.

SM 19

KINETIC INTERACTIONS IN AURORAL KILOMETRIC RADIATION

C. Grabbe
K. Papadopoulos (both at Science Applications, 8400 Westpark Dr., McLean, Va. 22102)
P. Palmadesso (Naval Research Laboratory, Plasma Physics Division, Washington, D. C. 20375)

Recently we proposed a new theory of auroral kilometric radiation via nonlinear interaction with beams and coherent EIC waves.[1] In that work we calculated growth rates of electromagnetic waves due to resonant interaction with EIC waves. Presently, we present results of a study of a dynamical model in which the three waves in the model evolve in time according to coupled nonlinear kinetic equations. An interesting result is that when the EIC waves reach steady state, the electromagnetic (X-mode) grows at twice the previously calculated resonant growth rate.

SM 20

A COMPARISON OF EQUATORIAL ELECTRON DENSITIES MEASURED BY WHISTLERS AND BY A SATELLITE RADIO TECHNIQUE

D. L. Carpenter (at Radioscience Laboratory, Stanford University, Stanford, Ca. 94305)
R. R. Anderson
D. A. Gurnett
D. D. Barbosa (all at the Dept. of Physics and Astronomy, Univ. of Iowa, Iowa City, Iowa 52242)
T. F. Bell
T. R. Miller (both at Radioscience Laboratory, Stanford University, Stanford, Ca. 94305)

Equatorial electron density profiles deduced from whistlers recorded at a ground station have for the first time been compared with densities inferred from satellite radio measurements near the equator and close to the meridian of the ground station. The whistler data were recorded at Siple, Antarctica, while the satellite data on plasma wave noise band frequencies were obtained from the sweep-frequency receiver on ISEE-1. In the two rendezvous situations examined thus far, equatorial density data from the two experiments showed agreement within ~20% over the L range ~3.5-5.2. One case at ~02 UT (~21 MLT) on July 10, 1978 involved a relatively smooth plasmasphere profile. In the second case, at ~0330 UT (~2230 MLT) on June 28, 1978, there were steep gradients in the L range 3.5-4.7, such that n_e varied roughly as R^{-8}. Whistler data were available at $L < 3.5$ and $L > 4.7$. The results provide evidence that the density enhancement factors within ducts are often no larger than ~20%, as expected from theory and previous less direct observations.

SM 21

EXTENDED CYCLOTRON RESONANCES WITH MODULATED WHISTLERS

A.L. Brinca (Max-Planck-Institut für Aeronomie, D-3411 Katlenburg-Lindau 3, FRG)

Appropriate modulation of the frequency and amplitude of VLF waves injected into the geomagnetosphere brings about strong intensification of the effects induced by CW whistler-electron interactions. The variation in frequency produces efficient and monotonic changes in the trapped particles average energy, E, and equatorial pitch angle, α_e, through adequate extension of the cyclotron-resonance interval. Stability analysis indicates the need, in certain (mostly E- and α_e-reducing) interactions, to adopt proper wave-amplitude modulation in order to prevent detrapping. The evolution of selected interactions in a duct centered at $L = 4$ is studied by following the behavior of the test particles E and α_e, and calculating the required (ground) transmitter spectrogram format. Pitch angle and energy scattering are significantly enhanced with respect to the anticipated CW-injection values[1]. The feasibility of the proposed mechanism hinges on stringent accuracy requirements for the magnetospheric model used in the determination of the transmitter format. However, analysis of resonances under favorable conditions (small interaction regions near the equatorial plane with large $|d\alpha_e/dt|$) suggests that combination of data from whistler ground stations and 'in situ' satellites measurements can overcome this difficulty in the plasmasphere.

SM 22

ISEE-1 OBSERVATIONS OF VLF EMISSIONS TRIGGERED BY NONDUCTED COHERENT VLF WAVES FROM GROUND TRANSMITTERS

T. F. Bell, U. S. Inan, and R. A. Helliwell (all at Radioscience Laboratory, Stanford University, Stanford, Ca. 94305)

The ISEE-1 spacecraft has been an important component of VLF wave-injection experiments for studying interactions between coherent VLF waves and energetic particles. The coherent waves are injected into the magnetosphere by ground-based transmitters such as that at Siple Station, Antarctica and those of the worldwide Omega navigation network. During the period October 1977-August 1979, the Stanford VLF receiver on ISEE-1 acquired data on approximately 90 separate orbits in the plasmasphere in which the satellite longitude lay within 30° of the magnetic field lines linking the Omega, N. D. transmitter. During 12 passes the nonducted Omega signals at 10.2 kHz were observed to trigger VLF emissions on magnetic shells in the range $L = 1.8$-3.8. The emission characteristics differed significantly from those of emissions triggered by ducted signals and detected at ground stations. In general the emission activity occurred during periods in which signals propagated to the spacecraft on at least two separate raypaths of disparate time delay and with a received signal duration of two to four times that of the transmitted pulses. In most cases the emission activity took place only along the paths of longer time delay. Ray-tracing analysis and the measured group time delays indicate that the signals which trigger emissions propagate in a nonducted mode with high wave normal angles, and that triggering possibly takes place far from the magnetic equator. Furthermore we show that in the case of triggering near $L \sim 2$, the resonant electron energies could be as high as 200 keV. Our results indicate that the emission generation process can take place under much more general conditions than previously believed.

SM 23

CHARACTERISTICS OF THE COMMON ORIGIN OF ELECTRON MICROBURSTS AND VLF CHORUS

J. C. Siren (Institute for Physical Science and Technology, University of Maryland, College Park, MD 20742)
T. J. Rosenberg
D. Detrick
D. L. Carpenter (Radioscience Laboratory, Stanford University, Stanford, CA 94305)

Evidence previously presented [J. Geomag. Geoelectr. 30, 355, 1978] and new data presented here indicate a direct, one-to-one association between electron microbursts (by the bremsstrahlung X-ray technique) and invidivual VLF chorus risers observed in the conjugate ($L = 4.1$) region. In each case the correlation was highly significant. The previously presented data permitted calculation of the cross-correlation lag with an error of ≈ 60 ms. This was sufficiently precise to permit the conclusion that electron microbursts and associated VLF chorus outside the plasmapause originated in near-equatorial cyclotron resonance interactions. The new data, having significantly improved time resolution (≈ 20 ms), confirm this conclusion. Also available in the new data was a direct measurement of the whistler-mode propagation time along the active flux tube, allowing a fairly precise electron density model to be applied.

Several new conclusions have been drawn from the more detailed studies that have been performed. (1) The VLF wave emission pulse widths and the associated microburst durations are equal, within the precision of measurement; (2) the wave-particle interaction takes place somewhat off the equator (minimum B surface), but within ± 30° in latitude of the equator; and (3) a finite (non-zero) scattering time is required to force resonant electrons from trapped orbits into the loss cone.

SM 24

FREQUENCY BAND BROADENING OF THE EQUATORIAL VLF EMISSIONS

Kaichi Maeda (NASA/Goddard Space Flight Center, Laboratory for Planetary Atmospheres, Greenbelt, MD 20771)
C. S. Lin (Institute for Physical Sciences and Technology, University of Maryland, College Park, MD 20742)

When the equatorially orbiting satellite (Explorer 45) approaches the midnight-dawn sector of the plasmasphere from the outer magnetosphere, generally a broadening of the VLF-emission band is observed. The frequency ranges from 0.1 f_H to 0.8 f_H near the plasmapause, while it is around 0.4-0.6 f_H with a sharp gap at 0.5 f_H in the outer magnetosphere, where f_H is the local electron gyrofrequency. The cause of this broadening is ascribable to the spreading of the pitch angle anisotropy of the ring current electrons to a wide energy range of 1 keV to 500 keV, as measured simultaneously with the VLF emissions. The VLF emission intensities reach a maximum before the satellite enters the plasmasphere. Quantitative calculations of the cyclotron instability growth rate based on the observed energy spectra of ring current electrons indicate the following: (1) an optimum value of n_h/n_c for a maximum wave growth rate, where n_h and n_c are the electron densities of the hot plasma (ring current) and the cold background plasma, respectively, and (2) an increase in the emission frequency bandwidth with the anisotropy and intensity of the hot plasma, but saturation beyond a certain value of the anisotropy. These results are consistent with the observations, and can be applied to interpret similar features seen in the plasmaspheric hiss.

Birkeland and Other Currents

Harbour C
Thursday P.M.
M. Smiddy (Hanscomb AFB), Presiding

SM 25

RADAR MEASUREMENTS OF THE LINEAR GROWTH RATE OF THE CURRENT CONVECTIVE INSTABILITY

J. F. Vickrey and C. L. Rino (Radio Physics Laboratory, SRI International, Menlo Park, CA 94025)
T. A. Potemra (Applied Physics Laboratory, The Johns Hopkins University, Laurel, MD 20810)

Recently, Rino and Owen have shown that local scintillation enhancements occur in a region of enhanced F-region ionization with a steep gradient at its equatorward edge. The source of the irregularities is thought to be the current-convective instability which is capable of pro-

ducing L-shell aligned sheet-like structures. Presented here are the results of an analysis of the latitudinal variations of plasma-density, electric field, and field-aligned current to determine the linear growth rate of the current-convective instability. Also discussed are the preliminary results from an experiment to simultaneously observe: (1) plasma density and electric field configurations using the Chatanika Radar, (2) scintillation enhancements on the TRIAD telemetry signal, observed at Chatanika, and (3) the latitudinal distribution of field-aligned currents determined by TRIAD.

SM 26

INFLUENCE OF THE SOURCE FIELD ON THE INTERPRETATION OF CONDUCTIVITY ANOMALIES IN SUB-AURORAL REGIONS

Marianne Mareschal (Herzberg Institute of Astrophysics, National Research Council, Ottawa, Canada K1A 0R6

At geomagnetic mid-latitudes, the normal vertical magnetic field measured in the period band 10 to 60 minutes is almost zero. This is not true in sub-auroral regions where the proximity of external source currents confuses the interpretation of field data in terms of conductive inhomogeneities within the earth.

Typical source effects on the magnitude of the Z/H ratio are presented for two specific source models, i.e. the infinite electrojet and the more realistic pair of three-dimensional current systems (Birkeland N-S and E-W currents). No definite bound can be put on these effects without a daily monitoring of the specific source events considered (duration, location, variations in intensity, etc...). In the examples selected, we therefore stress the response dependence on the geometrical differences between the source models used for the calculations.

SM 27

THE ROLE OF BIRKELAND CURRENTS IN MAGNETOSPHERIC FLUX TRANSFER

G. L. Siscoe (Department of Atmospheric Sciences, University of California, Los Angeles, Ca. 90024)

An examination of the hypothesis which is implicit in discussions of magnetospheric flux transfer events, namely that the flux removed from the dayside and stored in the tail results in an "erosion" of the dayside boundary and a compensating increase in the tail current system, reveals two fundamental difficulties. A ~20 γ field is required to be supplied at the dayside stagnation point by an increase in the tail current system in order to move the boundary inward under constant solar wind pressure by an amount of 1 R_e which is typically observed in such events. Models of the tail current system are strained to provide as much as ~5 γ at the stagnation point. The same models show that increases in the flux in the tail that result from increasing the tail current system is accomplished by the tail "capturing" flux from the adjacent night-side magnetosphere. There is very little change in the day-side flux by comparison.

We argue that introducing the region 1 Birkeland current system into the consideration can resolve both difficulties. (1) The field at the stagnation point produced by this current system alone can be ~20 γ. This has the consequence of cutting the link that would allow one to infer directly the amount of flux transferred from a measurement of the day-side boundary displacement. In this case the magnitude of the boundary displacement reflects the value of the ionospheric conductivity, as discussed previously by Hill and Rassbach. (2) The Birkeland current system drives night-side to day-side convection to replace virtually all flux from the day-side that is lost to the tail by day-side flux transfer. Thus in the above-mentioned models the night-side flux "captured" by the tail follows a reversed route through the day-side.

SM 28

PRELIMINARY OBSERVATIONS OF FIELD-ALIGNED CURRENTS WITH MAGSAT

T. A. Potemra
L. J. Zanetti (both at: Applied Physics Laboratory, Johns Hopkins U., Laurel, Md. 20810)
M. Sugiura, R. A. Langel (NASA/GSFC)
J. R. Burrows (Nat. Research Council of Canada)
D. M. Klumpar (Univ. of Texas)

The MAGSAT satellite was successfully launched into a low altitude (352 km perigee, 561 km apogee), sun-synchronous orbit on Oct. 30, 1979. This satellite carries a triaxial fluxgate magnetometer sampled 16 times/sec and a cesium vapor scalar magnetometer and is the first spacecraft devoted solely to the measurement of the geomagnetic field. Preliminary reduction of the fluxgate magnetometer data has revealed disturbances transverse to the main geomagnetic field in the auroral regions similar to those detected on a regular basis by earlier spacecraft such as TRIAD, ISIS-2, S3-2, S3-3, and AE-C and interpreted as being caused by field-aligned (Birkeland) currents. Transverse disturbances were observed in the north and south auroral zones during all 14 MAGSAT orbits on Nov. 2, 1979. Magnetic field observations were also collected from the TRIAD satellite at 800 km altitude at nearly the same time and field line location as MAGSAT on several occasions, and these show similar transverse disturbances at different altitudes. These early MAGSAT data confirm the presence of field-aligned currents as a permanent feature of the polar regions and a more detailed analysis of these data in the future should contribute significantly to an understanding of these important current systems.

SM 29

GEOMAGNETIC ACTIVITY OVER CANADA DURING EARLY PART OF MAGSAT MISSION, AND SOME PRELIMINARY QUIET-TIME MAGSAT RESULTS

R.L. Coles
G. Jansen van Beek
A. Nandi
G.V. Haines, (all at: Earth Physics Branch, Division of Geomagnetism, Energy Mines and Resources Canada, Ottawa, Canada, K1A 0Y3)

Analyses of data from Canadian magnetic observatories are used to indicate the levels of geomagnetic field activity at the times of passes of the MAGSAT satellite over Canada during the first 4 months of the mission. Three zones of different characteristic activity are traversed by the satellite — the mid-latitude zone, the auroral zone, and the polar cap. During about 40% of this time period, the magnetic activity could be classified as "quiet" in the mid-latitude and auroral zones, with a higher percentage in the polar cap. Criteria for classifying activity levels are based primarily on the short period variations in the field. A critical factor in the auroral zone is the frequent occurrence of pulsational activity at periods of a few minutes. MAGSAT traverses through each zone in a few minutes. In this context, comparisons between the local analyses and Kp indices serve to emphasize the non-applicability of the latter as general activity indicators for the higher latitudes. AE indices are not yet available.

Preliminary analyses of some early MAGSAT data obtained during quiet times show good agreements between intersecting passes over Canada, and give indications of anomaly features seen in earlier studies of POGO satellite and airborne magnetic data.

SM 30

A THREE-RING CIRCUIT MODEL OF THE MAGNETOSPHERE

E. C. Whipple, Jr. (Univ. Calif., San Diego La Jolla, CA. 92093)
C. E. McIlwain, and H. Alfvén (Univ. Calif., San Diego, La Jolla, CA. 92093)

We have modeled the magnetosphere by superimposing a dipole field, a uniform field and a perturbation field due to a simple current system. This first-order current system consists of a ring current in the neutral line of the dipole plus uniform fields, together with vertical currents representing field-aligned currents to the neutral line. The current circuit is closed by two additional ring currents above and below the equatorial plane representing distributed inertial and adiabatic perpendicular currents. This system produces many magnetospheric features including a magnetopause, bending of magnetic field lines in the anti-solar direction, a magnetotail, and cusps on the dayside of the earth. Our aim is to demonstrate that it is not necessary to think of the magnetic field topology as being caused by the flowing plasma carrying field lines. The fundamental physical problem is to derive the current system from the self-consistent interaction of the solar-wind and magnetospheric plasmas and fields.

SM 31

FIELD-ALIGNED CURRENT, CONVECTIVE ELECTRIC FIELD, AND AURORAL PARTICLE MEASUREMENTS DURING A MAJOR MAGNETIC STORM

B.M. Shuman
R.P. Vancour
M. Smiddy (all at Air Force Geophysics Laboratory, Hanscom AFB, MA 01731)
N.A. Saflekos (Boston College, Chestnut Hill Boston, MA 02167)
F.J. Rich (Regis College, Weston, MA 02813)

The S3-2 polar-orbiting satellite has provided measurements of ambient magnetic field, electric field, and auroral electron flux during the very intense sub-storm period of 26 March 1976. We have used two noon-midnight orbits in this time to calculate field-aligned current densities, compare them with precipitating auroral electron fluxes, and, by utilizing the direction of the electric field, identify the particular regions to which they map down (i.e. eastward electrojet, westward electrojet or polar cap). A feature consistently observed on the nightside was the intense upward current sheet at the equatorward side of the westward electrojet, just poleward of the electric field reversal associated with the Harang discontinuity. We have been able to track the boundaries of the current-carrying region during the early main phase of the geomagnetic storm, and to infer the location of source regions for these currents at L-shell values corresponding to the inner magnetosphere. When conditions permitted, we have calculated the height-integrated Pedersen conductivity of the ionosphere by using a number of simplifying assumptions, but without invoking models of collision frequency. Typical values ranged from 10 to 30 Ω^{-1}. We have also calculated, for the same periods, the Joule heating rate in the ionosphere due to closure of field-aligned currents by Pedersen current flow. This was, in general, much greater than the energy deposited by the electron precipitation.

SM 32

HEIGHT VARIATIONS OF FIELD ALIGNED CURRENTS AND ELECTROSTATIC SHOCKS OBTAINED FROM SIMULTANEOUS OBSERVATIONS

F.J. Rich (Research Center, Regis College, Weston, MA 02193)
C.A. Cattell (Space Science Lab., Univ. of California, Berkeley, CA 94720)
W.J. Burke
M. Smiddy (both from AF Geophysics Laboratory Hanscom AFB, MA 01731)

The S3-2 and S3-3 satellites were launched into identical orbit inclinations with significantly different initial apogees (1500 Km and 8000 Km respectively). The two satellites, equipped with electric and magnetic field experiments, provide a unique opportunity to study the height variation of electric fields and field aligned currents and perpendicular current closure as the two satellites simultaneously pass over the same high latitude structures. Preliminary results show that the latitude profiles of the field-aligned current are often identical within the measurement accuracy. For cases where there is a height variation, we find that a significant amount of current crosses field lines between the two satellites and returns to the magnetosphere without reaching the E-region. This result demands the existence of an anomolous Pedersen conductivity somewhere in the topside ionosphere as previously suggested by Hudson et al. Often electrostatic shocks are not observed by S3-2 when S3-3 observes them at high altitudes, but in one case a shock is seen simultaneously at 8000 Km and 1000 Km. In this case the shock region is approximately 1° wide at 8000 Km and 0.2° wide at 1000 Km altitude. In another case, the latitude profiles of electric fields and field aligned currents are identical as the satellites cross Greenland with a 4 min. time separation except for a 0.5° latitude shift. The data from a ground based magnetometer chain show that between the passage of the two satellites, the electrojet moved poleward by the same amount.

SM 33

GENERATION OF REGIONS OF AURORAL CURRENTS ELECTRIC POTENTIALS, AND PRECIPITATION BY THE DIVERGENCE OF THE CONVECTION ELECTRIC FIELD

L.R. Lyons (Space Environment Lab., NOAA, Boulder, CO. 80303)

It is shown that discontinuities in the magnetospheric convection electric field $\underline{E}$ with $\nabla \cdot \underline{E} < 0$ can generate large-scale regions (the order of 200 km in width) of magnetic-field-aligned currents with associated field-aligned, electric potential differences and electron precipitation of the magnitudes and widths observed in auroral "inverted V" regions. Such an electric field discontinuity is known to exist along the evening boundary between sunward and anti-sunward convection. In addition, such discontinuities may also exist over the polar cap due to inhomogeneities in the magnetosheath flow and in regions, such as the Alfven layer, where drifting trapped particles charge separate. The present analysis assumes that the field-aligned current is governed by single particle motion in d.c. electric and magnetic fields, and nothing is assumed to inhibit this particle motion. The "inverted V" scale size appears to be a natural result of the current versus electric polential relations along field lines and in the ionosphere.

Smaller scale precipitation regions such as those associated with descrete aurora result from the size of specific structure in the electric potential distribution deep within the magnetosphere. This suggests that the descrete auroral scale size does not result from the current versus electric polential relations along field lines and in the ionosphere, but from the processes which determine the high altitude, magnetospheric electric polentials.

SM 34

DAYSIDE FIELD-ALIGNED CURRENT SYSTEM DRIVEN BY THE LOW-LATITUDE BOUNDARY LAYER DYNAMO

L.C. Lee (Geophysical Institute, University of Alaska, Fairbanks, Alaska 99701)
J.R. Kan (Geophysical Institute, University of Alaska, Fairbanks, Alaska 99701)

It is proposed that the dayside field-aligned currents flowing into and out of the auroral oval are driven by the low-latitude boundary layer (LLBL) dynamo on closed field lines. This LLBL dynamo consists of an anti-sunward plasma flow in the low-latitude boundary layer and an adjacent sunward return flow in the magnetosphere. The field-aligned currents are driven by the Rostoker-Bostrom mechanism associated with the braking of the convective plasma flow. The currents close in the ionosphere via the Pedersen current.

SM 35

FIELD ALIGNED CURRENTS OBSERVED IN THE REGION OF THE DAYSIDE CUSP

M.A. Doyle (Research Center, Regis College, Weston, MA 02193)
F.J. Rich (Research Center, Regis College, Weston, MA 02193)
W.J. Burke (Physics Department, Boston, College Chestnut Hill, MA 02167)
M. Smiddy (USAF Geophysics Lab., Hanscom AFB, MA 01731)

Thirteen passes of the S3-2 satellite during January, 1976 through the region of the dayside cusp have been studied: eight in the northern hemisphere and five in the southern hemisphere. For all passes, the IMF $B_y < 0$ and $k_z \leq 3°$. On all passes, the satellite travelled approximately along a magnetic meridian to either side of noon. Preliminary examination of the east-west component of the magnetometer deflections reveals an additional region of field aligned current on the post-noon (pre-noon) side in the northern (southern) hemisphere, poleward of the usual region 1 and region 2 systems, but no additional current region on the pre-noon (post-noon) side in northern (southern) hemisphere. We have tried to determine if the additional current region is on open field lines of the polar cap or in the auroral zone by examining the reversals in the convection velocity and the trapping boundary for 100 keV protons. The boundary between region 1 and the additional current region tends to coincide with or be slightly poleward of the reversal in the convection velocity, but the trapping boundary lies poleward of the reversal in this additional current region. Thus the additional current region lies at or near the boundary between open and closed field lines. Fine scale structure of the magnetometer deflections indicates small field aligned current sheet pairs embedded in the large scale field aligned current systems on the pre-noon side in both hemispheres but on the post-noon side only in the northern hemisphere near the additional current region.

SM 36

FIELD-ALIGNED CURRENT DUE TO ELECTROSTATIC TURBULENCE

Nam C. Lee
G. K. Parks (both at: Physics Department and Geophysics Prog., Univ. of Washington, Seattle, Washington 98195)

The modification of large-scale motion of plasma by wave turbulence is considered in hydrodynamic description. Special attention is paid to the non-linear current in the macroscopic equations. Non-vanishing non-linear current affects the behavior of large-scale motion significantly. For example, when the characteristic frequency of turbulence is high, the current parallel to B_o affects the plasma transport along B_o; when the frequency of turbulence is low, the effect is that the magnetic field will be distorted. It is shown in fact that there can be field-aligned currents for electrostatic turbulence when the wave spectrum has directional dependence in a weak magnetic field (weak in the sense $\omega_{pe} >> \omega_{ce}$ or $\omega_{ce} << k v_{th}$). The above conditions are satisfied for beam excited Languimar or ion-acoustic turbulences. The former has been observed in the auroral zone and the latter in the upstream region of the bow shock. Estimations of the field-aligned currents associated with these two cases will be made and presented.

SM 37

LATITUDINAL REVERSAL OF POLARIZATION OF GEOMAGNETIC SUDDEN COMMENCEMENTS

T. Araki* (CIRES, Univ. of Colorado and NOAA/NGSDC, D64, Boulder, CO, 80303)
J. H. Allen (NOAA/NGSDC, D64, Boulder, CO 80303)

Latitudinal variation of the polarization of geomagnetic sudden commencement (SC) observed between 63° and 79° geomag. lat. is studied by the use of North American IMS network data from Aug. 1978 to May 1979. Fourteen SC's out of 18 examined show the polarization reversal at latitude between 64° and 72°, among which 9 change the polarization from counterclockwise to clockwise with an increasing latitude and the remaining 5 change it in the opposite sense.

Clear local time dependence as shown statistically by Wilson and Sugiura (1961) could not be confirmed from this small data set.

The complex characteristics of the polarization of SC will be determined by the following factors:
(1) Successive appearance of two different kinds of primary source electric field, DP(PRI) (dusk-to-dawn) and DP(MI) (dawn-to-dusk).
(2) Time variation of both primary fields.
(3) Movement of the source field from dayside to nightside.
(4) Modification of the source field by spacial inhomogeneity of ionospheric conductivity.
(5) Modification of the source field by time variation of the ionospheric conductivity due to the particle precipitation during SC.
(6) Field line resonance.
(7) IMF effects.

SM 38

A MODEL OF FIELD-ALIGNED CURRENTS WITH THE MAGNETOSPHERIC CONVECTION ELECTRIC FIELD AS THEIR PRIMARY DRIVING FORCE

M. Sugiura (Goddard Space Flight Center, Greenbelt, MD 20771)
D.J. Poros (General Electric, Space Division, Lanham, MD 20801)

The presence of a convection electric field is one of the fundamental features of the magnetosphere. We present a self-consistent model of field-aligned currents in which a dawn-to-dusk convection electric field is considered as being the driving force of the currents. A boundary value problem in two dimensions, representing the dawn-dusk meridian plane, is solved with the electrostatic potential distribution above the ionosphere as the upper boundary condition. The conductivity is given as a function of height from the ground to the ionosphere and also of latitude, including a narrow region of high conductivity, representing the auroral belt. The basic principle concerning the field-aligned currents which we derived earlier from an electric circuit model is confirmed. This principle is that field-aligned currents flow primarily in regions where the second derivative of the electrostatic potential, or the electric field gradient (not field magnitude), is large, namely at inflection points of the potential profile. The basic current pattern is determined in this way, but the relative intensities of the field-aligned currents depend critically on the conductivity distribution. We show that most of the representative features of field-aligned currents as observed by Triad can be accounted for by our model. Thus the model offers an explanation of the existence of region 1 and region 2 currents of Iijima and Potemra by a single driving force. The model also gives a representation of the electric field structure in the middle atmosphere.

SM 39

SIMULTANEOUS OBSERVATIONS OF SUBSTORM-ASSOCIATED BIRKELAND CURRENTS USING THREE SYNCHRONOUS SATELLITES AND THE NORTH AMERICAN GROUND MAGNETOMETER ARRAY

Joseph N. Barfield (Southwest Research Institute, San Antonio, Texas)
Robert L. McPherron (Institute of Geophysics and Planetary Physics, University of California, Los Angeles)

During February 1975, the close placement of the three synchronous satellites SMS1, SMS2, and ATS6 over the North American sector provided a unique opportunity to observe the magnetic effects of the global-scale substorm-associated Birkeland current system. In particular, it was our purpose to investigate the temporal and spatial relationship between the diversion of the tail current of substorm onset and the development of the Birkeland currents. Most interpretive models predict that the tail current diversion and the Birkeland currents develop simultaneously.

We found that in many cases, the eastward (D) component of the magnetic field perturbation developed significantly earlier than the northward (H) component. In fact, the D perturbation tends to peak just as the H perturbation begins. We interpret this as a reconfiguration of current flow in the tail lobe as the plasma sheet thins prior to substorm onset.

IMS Substorm Study I

Harbour C
Friday A.M.
R. H. Manka (NOAA Atmospheric Program), Presiding

SM 40 INVITED PAPER

OVERVIEW OF THE IMS JULY 29, 1977 SUBSTORM ANALYSIS

R. H. MANKA, National Oceanic and Atmospheric Administration, Rockville, MD 20852
T. A. FRITZ, NOAA Space Environment Laboratory, Boulder, Colorado 80303
R. G. JOHNSON, Lockheed, Palo Alto Research Laboratory, Palo Alto, California 94304
R. A. WOLF, Dept. of Space Physics and Astronomy, Rice University, Houston, TX 77001
M. J. TEAGUE, Sigma Data Services Corp., National Space Science Data Ctr. Greenbelt, MD 20771
J. I. VETTE, National Space Science Data Center, Goddard Space Flight Ctr., Greenbelt, MD 20771

We review the physical characteristics and temporal development of a significant IMS magnetospheric event: the sudden commencement and multiple substorms of July 29, 1977. An interplanetary shock, superimposed on relatively high solar wind densities, compressed the magnetosphere at 0027 UT in past the apogee of GEOS-1 (~7.1 R_E). Following this compression, as well as periods of southward IMF, a series of substorms culminated in a very large substorm with peak electrojet current at 1230 UT, followed by a relatively quiet recovery phase. The ring current showed a maximum at 0600 UT and a major perturbation at 1230 UT corresponding to the last substorm. A large suite of international data were analyzed for this event, concluding in a computerized Coordinated Data Analysis Workshop (CDAW-2) in October, 1979. Included in the analysis are results from 11 spacecraft.

6 ground arrays, several numerical models, and theoretical calculations.

We will present an overview description of the event, including the solar wind conditions, extent of electrojets, polar cap boundaries, etc. Emphasis of the analysis was on the physical processes of energy transfer and magnetospheric dynamics. Some representative results will be presented.

SM 41 INVITED PAPER

THE DISTURBED SOLAR WIND FLOW AND MAGNETOSPHERIC RESPONSE ON JULY 29, 1977

J. H. King (NASA/Goddard Space Flight Center Laboratory for Extraterrestrial Physics, Greenbelt, MD 20771)
S. I. Akasofu
K. L. Ackerson
D. H. Fairfield
R. P. Lepping
R. H. Manka
J. D. Sullivan

Data from IMPs. 7 and 8 reveal the following interplanetary scenario. At ∿ 0027 UT, an interplanetary shock struck the magnetosphere. This followed a 12 hr period during which the interplanetary density (N_p) had increased to ∿ 35/cc. Details of the highly structured post shock flow will be shown. Of particular interest is a small stream (40 km/s increase) whose leading pressure pulse peaked at ∿ 0410 UT (N_p ∿ 120/cc). This pulse yielded a computed subsolar magnetopause distance of 5.8 R_E. Owing to the highly negative B_z in this stream, the energy coupling function ϵ reached a value of 6E19 ergs/s (0430-0500 UT). A weaker peak in ϵ (∿ 4E19) occurred near 1130 UT.

At about 1230 UT, a cool helium-rich driver gas enveloped the earth. An interplanetary speed drop at ∿ 1745 UT was preceded by a deeply rarefied plasma flow which, given its 12γ magnetic field, yielded an unusually distant magnetopause, a small Alfvén Mach number and a distant bow shock. As inferred from magneto-sheath observations, the IMF was probably northward for most of the second half of the day.

The level of agreement between the energy coupling function ϵ and the energy dissipation associated with auroral electrojets and ring currents will be discussed.

SM 42 INVITED PAPER

AURORAL ZONE AND POLAR CAP JOULE HEATING AS INFERRED FROM ELECTRIC FIELDS AND FIELD-ALIGNED CURRENTS MEASURED ON JULY 29, 1977

R.B. Torbert (Space Sciences Laboratory, University of California, Berkeley, CA 94720)
C.Cattell, F.S. Mozer (Physics Department and Space Sciences Laboratory, University of California, Berkeley, CA 94720)
J.F. Fennell (Space Sciences Laboratory, The Aerospace Corporation, El Segundo, CA 90245)
S-I. Akasofu (Geophysical Institute, University of Alaska, Fairbanks, Alaska 99701)

A determination of the electrical dissipation in the polar ionosphere of one hemisphere can be made by multiplying the field-aligned sheet current, integrated over the length of morning (or evening) polar cap boundary, times the total potential drop between these two boundaries. This calculation assumes 1)that these boundaries are well-defined equi-potentials in local time; 2) that sufficiently deep into the plasmasphere, magnetic L-shells are equi-potentials; 3) that these are no inductive electric fields over the time-scale of the measurements, and 4) that field-aligned currents at other places besides the polar cap boundary and the plasmapause are negligible.

Estimates of this product, I.V, over the polar regions were made using the electric field detector and field-aligned current measurement on the S3-3 satellite. During the storm, heating reached a peak of 3 x 10^{18} ergs/sec. Reasonable agreement with the relation[1]

$$I \cdot V(ergs/sec) \sim 10^{15} * Ae(gammas)$$

was found. Other examples of this correlation will be presented.

SM 43 INVITED PAPER

AURORAL ZONE VARIATIONS ON JULY 29, 1977

L. J. Zanetti
T. A. Potemra (both at: Applied Physics Lab., The Johns Hopkins Univ., Laurel, Md.)
S.-I. Akasofu (Geophysical Institute, Univ. of Alaska, Fairbanks, Alaska)
J. H. Allen (NOAA/EDS, Boulder, Colorado)
W. Baumjohann (Univ. of Münster, Münster, W. Germany)
C. A. Cattell (Univ. of Calif., Berkeley, Cal.)
J. F. Fennell (Aerospace Corp., Los Angeles, Cal.)
R. H. Manka (National Science Foundation, 1800 G St., N. W., Washington, D. C.)
P. H. Reiff (Rice Univ., Houston, Texas)
R. B. Torbert (Univ. of Calif., Berkeley, Cal.)
J. K. Walker (Dept. of Energy, Mines & Resources, Ottawa, Ontario, Canada)

A number of intense substorms on July 29, 1977 have been under study as a special IMS period. A large interplanetary shock was observed at 00:27 UT and was followed by four major substorms spaced over the first 12 hours. This paper is concerned with observations during the last half of July 29 when the AE index indicated very quiet conditions and when the IMF was strongly northward.

Data used in this study are ground based magnetograms, magnetic disturbances from TRIAD; charged particle measurements from AE-C over the southern polar cap and from S3-3 over the northern polar cap; and convective flow patterns from AE-C and S3-3. Magnetic disturbances were observed over the entire north polar cap during several consecutive TRIAD orbits, and ion and auroral-like electron precipitation was observed at invariant latitudes above 80°. Sunward convective flow was observed above 75° invariant latitude. Surface magnetometers in the auroral zone showed almost no disturbances during this time, whereas polar cap stations like Thule and Resolute showed intense disturbances. A conclusion of this study is that there is a dramatic closure of the polar cap and a movement of the auroral zone to extremely high latitudes at this time.

SM 44 INVITED PAPER

MAGNETOSPHERIC COMPRESSION AND PROPERTIES OBSERVED BY GEOS-1 ON JULY 29, 1977.

H. Amata(CNR, Frascati, Italy).
A. Bahnsen (DSRI, Lyngby, Denmark).
P. Decreau (CRPE, Orléans, France).
J. Etcheto, R. Gendrin, J. Solomon (CNET, Issy-les-Moulineaux, France).
D. Fairfield (NASA/GSFC, Greenbelt, USA).
C-G. Fälthammar (RIT, Stockholm, Sweden).
K. Knott, A. Pedersen (SSD, ESA/ESTEC, Noordwijk, The Netherlands).
A. Korth, B. Wilken (MPI, Lindau, Germany).
K. Ronnmark (Univ. Umea, Sweden).
D. Young (Univ. Berne, Switzerland).

At the onset of the July 19, 1977 geomagnetic event, GEOS-1 was near apogee and 13.00 hours local time and thus in a position to study in detail the response of the magnetopause to the arrival of a strong interplanetary shock. The subsequent sweep of the magnetopause across GEOS-1 is one of the most dynamic events observed by this satellite during its 14 months lifetime. A unique data set on electric and magnetic fields, VLF burst appearances and particle parameters like density, composition, energy spectra and pitch angle distributions has been compiled and is interpreted in terms of physical processes such as particle leakage across the magnetopause and local magnetic merging.

SM 45 INVITED PAPER

PULSATION EVENTS OF JULY 29,1977

R.W.Nopper, Jr. (NAS-NRC Associate, Air Force Geophysics Laboratory, Space Physics Division, Hanscom AFB, MA 01731)
W.J.Hughes
C.G. Maclennan
R.L. McPherron

In the aftermath of the solar wind shock which hit the magnetosphere at 0027 UT on July 29, 1977, several conspicuous trains of long period magnetic pulsations were identified in geosynchronous and ground-based data sets. The first, at 0130, appeared as 5 min period pulsations at the GOES satellites in the late evening sector and at high latitude ground stations in the dusk sector. At the same time, an apparently unrelated train with 2.5 min period was observed on the dawnside at equatorial and high-latitude stations. These events, localized in latitude and longitude, contrast with a later, pulse-like event at 1430, seen by synchronous spacecraft in the pre-dawn, morning, and afternoon sectors and at virtually all latitudes and local times on the ground. This event was detected first at satellites and ground stations nearest noon, and progressively later at sites away from noon toward dawn and dusk. On the ground, the locus of maximum amplitude, ~67° geomagnetic, coincides with the reversal of the H component. Going from higher to lower latitudes, the H component decreases more rapidly than the D, so that below 55° (except at equatorial stations), the D component dominates. Lastly, we relate these observations to previous theoretical studies.

SM 46 INVITED PAPER

OBSERVATION AND MODELING OF ENERGETIC PARTICLES AT SYNCHRONOUS ORBIT ON JULY 29, 1977

D. N. Baker (Los Alamos Scientific Laboratory, Los Alamos, NM 87545) T. A. Fritz, B. Wilken, P. R. Higbie, S. M. Kaye, M. G. Kivelson, A. J. Masley, P. H. Smith, W. Stüdemann, and A. L. Vampola

In the twelve hours following a worldwide storm sudden commencement at 0027 UT on 29 July, there was a series of at least four magnetospheric substorms the last and largest of which exhibited an expansion phase onset at ∿ 1200 UT. Data from six spacecraft in three general local time groupings (0300, 0700, and 1300 LT) were examined and vector magnetic field data and energetic electron and ion data from ∿ 15 keV to > 2 MeV were employed. Four primary types of studies were carried out: (1) Timing and morphology of energetic particle injections; (2) Measurement of boundary motions using high-energy ion East-West anisotropies; (3) Variation of particle phase space densities ($f = p^2/2mB$) using local magnetic field and particle flux data; and (4) Adiabatic modeling which included injection, large-scale convection, corotation, and gradient drifts. For the 1200 UT substorm, it is concluded that there was a substantial flux dropout in a broad sector near local midnight due to a large scale boundary motion followed by a recovery to a predropout configuration. There were then several subsequent injection events with distinct onsets (extending as far eastward as 0300 LT) for which ion anisotropy information suggests an inward motion of particles from outside of geostationary orbit. Particle drift information reveals that these particles azimuthally drifted completely around the earth. It is also concluded from the phase space density studies that "fresh" particles with magnetic moments up to at least 10^3 MeV/gauss were injected near geostationary orbit. However, these studies reveal a general inability of the present adiabatic dipolar model to fully explain the observed injection of large magnetic moment particles from beyond 10 R_E in to synchronous orbit.

SM 47 INVITED PAPER

PLASMA AND ELECTRIC FIELD BOUNDARIES AT HIGH AND LOW ALTITUDE ON JULY 29, 1977

J. F. Fennell (Space Sciences Laboratory, The Aerospace Corporation, El Segundo, CA)
R. G. Johnson (Lockheed Palo Alto Research Laboratory, Palo Alto, CA)
D. T. Young (Physikalisches Institut, University of Bern, 3012 Bern, Switzerland)
P. Decreau (Centre de Recherches en Physique de l'Environment Terrestre et Planetaire, CNRS, Orleans-la-Source, France)
J. M. Etcheto (Centre de Recherches en Physique de l'Environment Terrestre et Planetaire, CNET, Issy-les-Moulineaux, France)
T. E. Moore (Space Science Center, University of New Hampshire, Durham, New Hampshire)
K. Rönnmark (Plasma Physics, University of Umea and Kiruna Geophysical Institute, Sweden)
R. B. Torbert (Space Sciences Laboratory, University of California, Berkeley, CA)

The IMS event of July 29, 1977 was the topic of a coordinated data analysis workshop in October 1979. During this workshop the hot plasma observations obtained by several spacecraft (GEOS I, ATS-6, S3-3 and AE-C) both at high and low altitudes were compared. The high altitude data show that the magnetopause was compressed into the GEOS position. The ion composition at high altitudes was seen to be primarily O^+ below $L \sim 4$. This deep penetration of the heavy ions was confirmed at low altitudes. Comparisons of the low altitude plasma and DC electric field data also show that the magnetosphere was not corotating at the low latitudes ($L \sim 3$). The correspondence between the corotation boundary and the boundary of the low latitude "enhanced plasma" was studied. The inner edge of the plasma sheet near dawn and dusk plus the polar cap boundaries were determined from the low altitude data. The S3-3 data show that the auroral precipitation extended to $\Lambda > 85.7^\circ$ on the nightside late on July 29. The results of the above analysis will be summarized.

SM 48 INVITED PAPER

A DYNAMIC MODEL OF THE MAGNETOSPHERIC MAGNETIC AND ELECTRIC FIELDS FOR JULY 29, 1977

W. P. Olson (McDonnell Douglas Astronautics Company, Huntington Beach, CA 92647)
K. A. Pfitzer (McDonnell Douglas Astronautics Company, Huntington Beach, CA 92647

A preliminary model of the magnetospheric magnetic field for the July 29 event was provided to the substorm workshop in advance of its meeting. The intense interaction between meeting participants for three days resulted in many changes and improvements to the model. The vector magnetic induction, B, and the vector potential, A, were computed separately for each of the three major magnetospheric current systems; magnetopause, ring, and tail. The strengths and locations of each of the three current systems are allowed to vary throughout the event. Input parameters representing the variability of each of the three current systems have been determined. Solar wind pressure is used as an input for the strength and location of the magnetopause current system. The D_{st} index which is traditionally used to monitor ring current strength has been modified by subtracting from it the contribution to the earth's surface field produced by the magnetopause current system. This modified D_{st} is used as an input for the strength of the ring currents. An index related to the flux of electromagnetic energy input to the magnetosphere by the solar wind is employed to determine the strength of the tail current system. The resulting model can be used to represent the magnetic field topology as it varies with time throughout the event. The model is discussed as it relates to several particle field phenomena observed throughout the event.

IMS Substorm Study II

Harbour C
Friday P.M.
Robert Carovillano (Boston College), Presiding

SM 49 INVITED PAPER

DYNAMIC STORM-TIME MODEL FOR JULY 29, 1977

M. Harel
R. W. Spiro
R. A. Wolf
P. H. Reiff (all at Dept. of Space Physics and Astronomy, Rice University, Houston, TX 77001)

Preliminary results and analysis from our computer simulation of the July 29, 1977, magnetospheric storm will be presented. We have computed, self-consistently, plasma flows, currents, and electric fields for the first part of the storm. Early model results, for the period of 0030-0415 UT (storm sudden commencement and early main phase), are encouraging.

The great compression that occured with the SSC destroys the shielding, allowing the convection electric field to penetrate to lower L-values. This is followed by accelerated sunward motion of the plasma sheet inner edges (to about 4-5 RE by 0415 UT). A complete ring current forms, consisting of newly injected plasma and ions injected in previous disturbances. The model ring-current strength, as a function of time, is in good agreement with the strength implied by D_{st}. The computed locations of the plasma-sheet inner edges agrees well with S3-3 particle data, less well with ATS-6 particle data. The time-integrated Joule heating, for the first few hours after the SSC, is about half the ring current energy.

SM 50

PCl EMISSIONS AT COLLEGE, ALASKA PRIOR TO THE JULY 29, 1977 SUDDEN COMMENCEMENT

John V. Olson (Geophysical Institute, University of Alaska, Fairbanks, Alaska 99701)
R.R. Heacock (Geophysical Institute, University of Alaska, Fairbanks, Alaska 99701)

Beginning just before 2300UT on July 28, 1977 a series of three structured Pcl emissions were detected at College, Alaska. The emissions were centered at frequencies of 0.4 Hz, 0.5 Hz and 0.75 Hz, each following the other with little overlap. The third emission was interruped by the sudden commencement at 0027UT of July 29, 1977. The sudden commencement was followed by a brief, intense band of partially structured Pcl emissions centered near 0.8 Hz.

The first emission lasted nearly 3/4 hour and exhibited an approximately 190 second interval between bursts indicating equatorial densities of near 10 p/cm^3. The second exhibited a 260 second repetition period indicating a rise in equatorial plasma density to near 20 p/cm^3. The third emission was interrupted before the second repetition was completed.

The emissions show little, if any, structure due to changing index of refraction. This limits our ability to specify the source region accurately. However, with reasonable assumptions estimated of the equatorial plasma distribution function can be made. The polarization content of these emissions is under analysis and we expect to develop additional information on the source of the pulsations and, ultimately, upon the state of the afternoon plasma prior to the 0027UT sudden commencement.

SM 51

THE 0027 UT SUDDEN STORM COMMENCEMENT ON JULY 29, 1977

B. Wilken, C. K. Goertz (both at: MPAE, Katlenburg-Lindau, W. Germany)
D. N. Baker, P. R. Higbie (both at: Los Alamos Scientific Laboratory, Los Alamos, NM 87545)
T. A. Fritz (NOAA, Space Env. Lab., Boulder, CO 80303)
P. H. Smith (NASA, Goddard Space Flight Center, Greenbelt, MD 20771)

The sudden storm commencement at 0027 UT associated with the storm of July 29, 1977 was observed by energetic particle detectors on board five different spacecraft at geostationary orbit. The compression of the magnetosphere seen at the GEOS-1 location (1300 LT) caused a rapid change in the ion pitch angle distribution which became highly peaked at $\alpha = 90^\circ$. Subsequently, the distribution became non-gyrotropic as the magnetopause moved over the satellite. The spacecraft 1977-007 and ATS-6 (located, respectively, at about 2.5 and 1.5 hours east of GEOS-1 in local time) observed rapid variations in the electron and ion fluxes which were also associated with significant changes in the pitch angle anisotropies. Only slight particle effects were seen by instrumentation on the satellite 1976-059 at ~2000 LT. These observations will be discussed in terms of a magnetohydrodynamic model of magnetospheric compressional effects.

SM 52

RELATIONSHIPS BETWEEN THE RING AND MAGNETOPAUSE CURRENT SYSTEMS DURING THE JULY 29, 1977 EVENT

K. A. Pfitzer
W. P. Olson (both at McDonnell Douglas Astronautics Company, Huntington Beach, CA 92647)
J. H. King (NASA/Goddard Space Flight Center, Greenbelt, MD 20771)

The variation in the D_{st} as measured on the ground is often used to infer the strength of the ring current. During the July 29 event, large changes in the solar wind pressure and density produced large variations in the standoff distance, and thus produced large changes (over a factor of 8) in the magnetopause current system. These changes in the magnetopause currents contributed to the variations in the D_{st}. A modified D_{st} is developed by subtracting out the magnetopause contributions of the standard D_{st}. This modified D_{st} then more accurately reflects the variation in the ring current and can then be used as a ring current strength index. Once the approximate strength of the ring current is determined, the effect of the enhanced ring on the pressure balance formalism can also be investigated. The magnetic field from the ring modifies the calculated standoff distance and the magnetopause current system. Thus an iterative procedure can be used to determine a best fit to the ring and magnetopause current systems using solar wind parameters and D_{st}.

SM 53 INVITED PAPER

SUMMARY REMARKS ON THE JULY 29,1977 EVENT

M. G. Kivelson (Department of Earth and Space Sciences and Institute of Geophysics and Planetary Physics, University of California, Los Angeles, CA 90024)

From the coordinated data for a one day period on July 29, 1977, we have been able to view the magnetosphere in unusual states of both compression and inflation. In the early part of the day, substorms occurred at times when the interplanetary magnetic field (IMF) was southward, consistent with enhanced energy input into the magnetosphere. Some of the substorms appear to have been triggered by northward turning of the IMF. Estimates of the energy input to the magnetosphere based on interplanetary velocity and B_z yield good qualitative predictions of the degree of magnetic disturbance determined from ground records. The pulsation signatures (Pi 2) expected at the time of substorm onset were not observed. Particle spectra and spatial boundaries observed at both high and low altitude proved useful for testing models of the substorm dynamics. Late in the day, the solar wind pressure dropped and the IMF turned northward. Virtually all indicators of activity dropped to low levels but the northern polar cap remained disturbed. The data suggest that lobe reconnection was occurring poleward of the northern polar cusp.

SM 54 INVITED PAPER

SUMMARY OF THE INITIAL STUDY OF THE MAGNETIC FIELD DATA TAKEN FROM THE IMS ALASKA MERIDIAN CHAIN OF OBSERVATORIES

S.-I. Akasofu (Geophysical Institute, University of Alaska, Fairbanks, AK 99701)
G. J. Romick (Geophysical Institute, University of Alaska, Fairbanks, AK 99701)

The analysis of magnetic field data taken from the IMS Alaska meridian chain of observatories, together with the modeling efforts, has produced the distribution of the large-scale field-aligned current system and ionospheric current system in the polar region on very quiet days and on a moderately disturbed day. The distribution of the electric field is also deduced. Such a data set had not been available in the past. A detailed comparison of the current and electric field patterns on a quiet day and a

disturbed day reveals how an increased efficiency of the solar wind - magnetosphere dynamo causes the distribution and intensity of the field-aligned currents to vary and how the ionosphere responds to such changes.

SM 55

STATISTICAL ANALYSIS OF Pc1 OCCURRENCE AT COLLEGE, ALASKA

R.R. Heacock (Geophysical Institute, University of Alaska, Fairbanks, Alaska 99701)

A statistical study of Pc1 data detected by two component induction magnetometers at College, Alaska (L=5.6) during the IMS period (1977- 1979) has been made to ascertain the relationship of the source region of the Pc1 emissions to the plasmapause. The maximum occurrence frequency of Pc1 correlates well with K_p with a relationship which depends upon local time. This correlation agrees with estimates of the local time variation of the plasmapause location. The results are similar to those obtained by Roth and Orr (1975) for data obtained in Finland and Lewis et al. (1977) for data from Siple, Antarctica.

Laboratory and Space Plasma Physics

Harbour A
Friday P.M.
C. S. Lin (Univ. of Maryland), Presiding

SM 56

COMPUTER SIMULATION ON PARTICLE ACCELERATION IN THE X-TYPE MAGNETIC RECONNECTION PROCESS

H. Matsumoto, Ionosph. Res. Lab., Kyoto Univ., Uji, Kyoto 611, Japan
K. Nagai, Ionosph. Res. Lab., Kyoto Univ., Uji, Kyoto 611, Japan
T. Sato, Bell Laboratories, 600 Mountain Ave., Murray Hill, New Jersey, 07974

Orbits of electrons and protons are followed under the action of space- and time-varying electric and magnetic reconnection fields which are computed by a two-dimensional MHD fluid equations. It is shown that particles which reach the neutral sheet by the E×B drift and pass by the neutral line are accelerated up to an energy range of auroral particles (~1 keV for electrons and ~10 keV for protons). Their orbits show that they are finally injected toward the Earth after a meandering/mirroring motion in the neutral sheet. The simulation also reveals that particles which happen to hit the neutral line of the x-type reconnection are accelerated up to a sub-relativistic energy range. In addition, it is shown that those electrons which traverse a slow shock layer formed in the reconnection process gain energy of the order of 1 eV along with an abrupt orbit modification, which roughly corresponds to the energy of Alfvén speed.

SM 57

ANOMALOUS RESISTIVITY NEAR THE MAGNETIC NEUTRAL SHEET

M. Tanaka, Geophysics Res. Lab., Univ. of Tokyo, Tokyo 113, Japan
T. Sato, Bell Laboratories, 600 Mountain Ave., Murray Hill, New Jersey, 07974
T. Kamimura, Institute of Plasma Physics, Nagoya Univ., Nagoya, Japan

A microinstability near the magnetic neutral sheet is investigated by using a 2-D magnetostatic particle code. It is observed that a flute instability occurs in a local region off the neutral sheet; its frequency is approximately the lower hybrid frequency and the wavelength is near the electron Larmor radius. Anomalous resistivity is observed to appear associated with the instability. Parametric dependence of the resistivity is examined. It is found that the resistivity η increases as $\eta \propto (V_{di}/v_{ti})^2$ where V_{di} is the diamagnetic drift speed of ions and v_{ti} is the ion thermal speed, which is in good agreement with the QL theory of Huba et al. (1978). It is further found that the resistivity increases as $T_i/T_e(>1)$ increases. The present result supports the anomalous resistivity model adopted in the previous MHD simulations of externally driven magnetic reconnection (e.g., Sato, 1979).

SM 58

KINETIC PROCESSES FOR GENERATION OF ELECTROSTATIC TURBULENCE

D. W. Swift (Geophysical Institute, University of Alaska, Fairbanks, Alaska 99701)

A two-dimensional particle-in-cell code is used to investigate the generation of electrostatic turbulence in a partially magnetized plasma. The growth of kinetic instabilities and the transfer of turbulent energy to long wavelengths is simulated. In one calculation, the effects of a flute-mode instability arising from a ring-type of velocity distribution is calculated. The most rapidly growing wavelengths were at the ion gyrodiameter. The instability saturated within a gyroperiod. The electric field energy at wavelengths less than gyrodiameter was quickly readsorbed by the plasma while some of the energy cascaded to longer wavelengths and remained at levels above thermal equilibrium.

In another simulation an instability generated by colliding ion beams in a time-varying magnetic field is investigated. Energy is generated at wavelengths varying between the Debye length and the ion gyrodiameter. Wave energy is generated with wave normals in the direction of the colliding beam relative velocity, but the wave normal directions quickly become isotropically distributed. Turbulence at long wavelengths becomes frozen into the plasma as the magnetic field increases.

The simulations indicate that E x B fluid turbulence in the magnetosphere can be fed by plasma microinstabilities. The application of the simulations to processes of voltage amplification and auroral acceleration will be described.

SM 59

DEPENDENCE OF ELECTRON BEAM INSTABILITY ON THE BEAM-PLASMA SYSTEM PARAMETERS

R. J. Strangeway (Cooperative Institute for Research in Environmental Sciences, Univ. of Colorado/NOAA, Boulder, Colorado 80309)

A large variety of phenomena, such as the Beam-Plasma-Discharge (BPD), have been observed in laboratory experiments with artificial electron beams. When investigating BPD, the generation of noise just above the electron gyrofrequency has been found to occur in the pre-BPD plasma, and this noise may be some form of precursor to the discharge indicating that BPD is driven by a wave instability. As an attempt to investigate electron beam instabilities within the context of BPD, in which the beam-plasma system parameters undergo marked changes because of enhanced ionization of the ambient gas, a study of the maximum instability growth rates has been carried out. The model used takes into account the fact that the electron beam in a laboratory device is often confined to a relatively small region within the plasma. For simplicity, no temperature is included in the model and it has been assumed that any instability is driven in an analogous manner to the Buneman instability, not through Landau resonance. The finite width of the electron beam restricts the allowed values of wavelength across the beam, and the maximum growth rate is found for several harmonics. The study follows the changes in growth rates as system parameters such as the ratio of the electron gyrofrequency to the electron plasma frequency are altered. Other factors to be investigated are the frequencies and group velocities of the fastest growing waves as these wave variables are likely to be important in the triggering of BPD.

SM 60

ANOMALOUS RESISTIVITY, POWER DISSIPATION, ENERGY FLOW AND ENERGY BALANCE IN A LABORATORY PLASMA UNDERGOING MAGNETIC FIELD RECONNECTION

R. L. Stenzel
W. Gekelman, N. Wild (All at: Dept. of Physics, Univ. of California, Los Angeles, CA 90024)

A laboratory plasma ($n \approx 10^{12}/cm^3$, $\beta \approx 1$, Volume = 5×10^5 cm^3) undergoing magnetic field reconnection is diagnosed in great detail. The total electric field along the axis of the machine $\vec{E}_{||} = -\nabla\phi - \partial A/\partial t$ where ϕ is the plasma potential and $-\partial A/\partial t$ the induced electric field is measured with a specialized probe. The transverse electric field is calculated from measured pressure $\vec{E}_\perp = \nabla(nkT_e)/n$. The Ohmic power dissipation P and resistivity η as a function of space and time are calculated using $P = \eta J^2$, $\eta = \vec{J}\cdot\vec{E}/J^2$ where J is comprised of axial and transverse currents. The dissipation peaks within the neutral sheet but the anomalous resistivity is largest ($\eta_{max} = 100\ \eta_{classical}$) in regions of lowest current flow. The Poyntings flux is everywhere calculated from measurements of $\vec{E}$ and $\vec{B}$ and compared with the power dissipation, stored magnetic energy $\partial/\partial t\ (B^2/2\mu_0)$ and particle energy $\partial/\partial t\ (1/2nmv^2)$. A color movie of magnetic field lines generated from the data clearly showing the merging and reconnection will be presented. Magnetic merging will be discussed in the context of power dissipation.

SM 61

PARTICLE ACCELERATION AND ANOMALOUS ION DRAG IN A LABORATORY PLASMA UNDERGOING MAGNETIC FIELD LINE RECONNECTION

W. Gekelman
R. L. Stenzel, N. Wild (All at: Dept. of Physics, Univ. of California, Los Angeles, CA 90024)

The spatial and temporal history of the anomalous ion drag term mnv^*v, in the neutral sheet of a laboratory plasma undergoing magnetic field reconnection has been measured. Extensive measurements of the plasma pressure nkT_e, magnetic forces $\vec{J}\times\vec{B}$, and ion velocity flow fields $\vec{v}$ have been performed in a highly reproducible repetitive plasma with the aid of digital data acquisition and mass storage. The pressure is found to peak at the contact points of the separatrix, near the edge of the neutral sheet. It exhibits large transverse gradients creating space charge fields and Hall currents. The magnetic force density $\vec{f} = \vec{J}\times\vec{B} - \nabla(nkT_e)$ arises from axial currents driven by an induced electric field and transverse Hall currents. The ion flow field is directly measured using differential particle collectors. The acceleration due to $\vec{f}$ is directly compared with $mn\ dv/dt$. It is found that an anomalous ion drag limits the acceleration. Only after several Alfvén times does the fluid develop the classical flow pattern with jetting from the edges of the neutral sheet.

SM 62

RAYLEIGH-TAYLOR INSTABILITIES AND FIELD LINE RECONNECTION IN THE PLASMA SHEET

P.L. Rothwell
...K. Yates (Both from AF Geophysics Laboratory, Space Physics Division, Hanscom AFB, MA 01731)

Starting with the antiparallel B-field in the plasma sheet, general expressions are obtained that describe arbitrary magnetic perturbations on the North/South plasma sheet boundaries. These expressions smoothly approach the tail lobe B-field values $B_x \to -B_0$, $B_z \to 0$ for large Z. Inside the plasma sheet a consistent B-field is obtained for a wide class of functions. The same vector function is found to describe both merged and unmerged field lines. A necessary, but not sufficient, condition for merged field lines is the presence of perturbations on the plasma sheet boundaries. Perturbations towards the neutral sheet give rise to "X" type reconnected field lines and perturbations away from the neutral sheet to "O" type reconnected field lines. Conditions are determined under which these perturbations could develop into Rayleigh-Taylor type instabilities. First order orbit theory (Rosenbluth and Longmire) indicates absolute stability. However, as the plasma sheet thins, protons no longer obey first order

orbit theory and the drift currents that maintain stability are weakened. Rayleigh-Taylor instabilities develop and field line merging is greatly enhanced. Quantitative results will be given.

SM 63

THE LOWER-HYBRID-DRIFT INSTABILITY AND ITS ASSOCIATED ANOMALOUS RESISTIVITY IN THE NEUTRAL SHEET OF EARTH'S MAGNETOTAIL

Zu-yin Pu (Department of Geophysics, Beijing University, Beijing, China, and Department of Earth and Space Sciences, University of California, Los Angeles, CA 90024)
Chuan-yi Tu (Beijing University)
M. G. Kivelson
K. Quest (both at: Dept. of Earth and Space Sciences and Institute of Geophysics and Planetary Physics, University of California, Los Angeles, CA 90024)

It is shown that the ion distribution is non-maxwellian in the neutral sheet of the earth's magnetotail. By combining a Boltzmann distribution with a "modified Alpers' distribution" for ions, a one dimensional non-maxwellian neutral sheet model has been constructed and used to discuss the lower-hybrid-drift instability. The model is self-consistent in the sense that the density profile, the steady electromagnetic field and the current satisfy Maxwell's equations. It is found that most regions in the neutral sheet are unstable. The frequency spectrum of the unstable waves is nearly the same as in the drifting maxwellian case. As shown previously by Huba et al. (1978), the frequency spectrum is in good agreement with the observations (Gurnett et al., 1976). The growth rate, assuming a modified Alpers' distribution function, is found to be enhanced compared to that due to a drifting maxwellian model in a portion of the sheet at some distance from the null of the field. This is because the non-maxwellian ions have an associated free energy which is larger than that in the drifting maxwellian case. The anomalous resistivity is calculated in the entire sheet and is found to be consistent with the observations by Lin and Anderson (1977) and similar to the results given by Tu (1980) in studying the anomalous transport effects in the magnetopause.

SM 64

TEMPERATURE GRADIENT EFFECTS ON THE STABILITY OF MAGNETOSPHERIC PLASMAS

S. Migliuolo (Department of Physics, University of Denver, Denver, Colorado, 80208)
V.L. Patel

The linear stability of magnetospheric plasmas to low frequency, electromagnetic, perturbations is investigated, for the case where there exist equilibrium density and temperature gradients, as well as temperature anisotropies. A two component (hot and cold), multi species, plasma is considered, and a kinetic linear dispersion relation is derived, for arbitrary Larmor radius ordering. The destabilizing effects of the gradient in the temperature component that is perpendicular to the unperturbed magnetic field are discussed. This is done for a set of parameters that is appropriate for storm time magnetospheric plasmas. It is also found that the gradient in the parallel temperature has negligible effects on the stability of magnetospheric modes. A discussion of the relative importance of equilibrium gradients and temperature anisotropies, with regard to the stability of the system, is presented.

SM 65

NONLINEAR MODULATIONS OF HEATING BY ELECTRON BEAMS

C.S. LIN (Institute for Physical Science and Technology, University of Maryland, College Park, Md. 20742)
K. PAPADOPOULOS, Department of Physics and Astronomy, University of Maryland, College Park, Md. 20742)

Electron beams are known to be able to create electron suprathermal tails through parametric instabilities and collapse. Recently, the polar orbiting satellite AE-D observed during inverted V events that fluxes of suprathermal electrons is occasionally modulated at low frequencies (~2 Hz). In this paper, a set of differential equations developed from phenomenological model and computer simulations is used to describe heating modulation process. The model assumes that electron beams excite unstable waves through resonance. In the strong wave turbulence limit, the unstable wave energies are then transferred parametrically to lower phase velocities so that they create energetic tails. The numerical solutions show that energization of thermal electrons reaches a maximum following the nonlinear stabilization of the instability. As the thermal electron energy relaxes, the beam instability is reactivated in the form of relaxation oscillations. These results theoretically explain the modulations seen in the heating of secondary electrons during inverted V events. The modulation frequency is determined by the growth rate of the parametric instability and the time scale τ for the thermal electron energy to be depleted from the system. By choosing appropriate value of τ, the modulation frequency can be shown to agree with the observations.

SM 66

ION CURRENT FLOW TO CONDUCTING PANELS AT HIGH VOLTAGES IN A SIMULATED IONOSPHERIC PLASMA ENVIRONMENT

A. Konradi
B. McIntyre (NAS/NRC Sr. Postdoctoral Fellow)
A. E. Potter (all at NASA, Johnson Space Center, Houston, TX 77058)

Future deployment of large structures in space will make it economically advantageous to use high voltage solar cell power arrays which may interact with the ambient space plasma. To study this phenomenon we present measurements of ion current flow to three stainless steel panels immersed in a simulated ionospheric plasma produced by a Kaufman thruster. The 17 eV Argon ions were emitted perpendicular to the magnetic field. Typically the measured electron densities were $N_e \sim 10^5$ to 10^6 cm^{-3} and the electron temperature was $T_e \sim .13$ eV. The panels were placed with their surface parallel to the Argon ion velocity. The I-V characteristics were obtained for voltages between 0 and -2500V. The measurements were made at ambient magnetic fields of .29, .76, and 1.60 gauss.

Results obtained indicate that for the range of parameters used the ion current is a linear function of the electron density. For magnetic fields comparable to the Earth's field and biasing voltages greater than -300V the I-V characteristic is almost linear. At higher magnetic fields the current is greater for a given voltage and the I-V characterisitics increase at a rate faster than a linear function of the voltage. Comparison with theoretical models will be presented.

SM 67

MAGNETIC FIELD TRANSPORT AND DIFFUSION IN FIELD REVERSED PLASMAS

J. F. Drake
N. T. Gladd (both at Naval Research Laboratory, Washington, D. C. 20375)
J. D. Huba (Science Applications, Inc., McLean, Va. 22102)

We present a derivation and analysis of a relatively simple equation which describes the transport and diffusion of magnetic flux in a high beta plasma for arbitrary resistivity. The model uses a one-dimensional slab geometry, neglects temperature transport and assumes quasi-equilibrium as the magnetic field evolves. Notwithstanding these limitations, this model is useful in understanding the dynamics of field-reversed plasmas, such as the Earth's magnetotail, and elucidates the underlying physics of transport in high beta plasmas. As an application we study the evolution of the Harris equilibrium (i.e., $\underline{B} = B_0 \tanh(x/\lambda)$) using a constant and anomalous resistivity for expected parameters in the Earth's magnetotail. We base the anomalous resistivity on the nonlocal mode structure of the lower-hybrid-drift instability. For this situation it is found that magnetic flux is transported towards the neutral line and the current density at the neutral line increases. Finally, we discuss the relevance of this work to the triggering of magnetic field line reconnection and magnetic energy dissipation in the Earth's magnetotail.

SM 68

ON FLICKERING DOUBLE LAYERS

M. B. Silevitch (Univ. Calif., San Diego, La Jolla, CA. 92093)
E. C. Whipple, Jr. (Univ. Calif., San Diego, La Jolla, CA. 92093)

It is well known that certain double layers produced in the laboratory "flicker" (or chop) with a period characterized by the ion transit time across the layer. Recently it has been pointed out that this mechanism could play a role in explaining the so-called flickering aurora.

In this talk we discuss the tendency of a steady state double layer to disrupt due to "electron instability" (Norris, 1964) wherein the mobile electrons redistribute themselves into a new meta-stable configuration while the ions remain fixed. Existence of this meta-stable state is a strong indicator of cyclic behavior since the ions will eventually respond forcing the system back towards its original steady state. A criterion for electron instability is discussed (Norris, 1964) and it is shown that a laminar double layer indeed is electron unstable.

Acknowledgements. This research was supported by AFOSR Grant 78-3731, NASA Grant NGL 05-005-007, and NSF Grant ATM 79-11875.

Reference, Norris, W. T., Nature of Spontaneous Oscillations in a Cesium Diode Energy Converter, J. Appl. Phys 35, 3260 (1964).

SM 69

LABORATORY MEASUREMENTS OF THE PLASMA POTENTIAL IN THE PRESENCE OF STRONG ION CYCLOTRON TURBULENCE*

H. Böhmer, Department of Physics, University of California, Irvine

Electrostatic potential measurements in a fully ionized laboratory plasma containing strong ion cyclotron wave turbulence are reported. The waves are excited by drawing magnetic field aligned electron drift in a localized channel whose dimension perpendicular to the magnetic field is of the order of the hot ion Larmor radius. This turbulence is found to stimulate the generation of energetic electrons with approximately 10 times the electron thermal energy.[1] In order to obtain additional insight into this situation which is similar to the magnetospheric structures above auroral arcs, a detailed investigation of the spatial distribution of the plasma potential is performed. These measurements are made both time averaged over many cyclotron periods as well as time resolved within a period. The results are presented and compared with various models to explain the electron acceleration.

Pioneer-11, Voyager 1 Saturn Spacecraft Charging (SCATHA)

Harbour C
Saturday A.M.
Theodore G. Northrup
(NASA/Goddard), Presiding

SM 70 INVITED PAPER

SATURN'S MAGNETOSPHERE

J. A. Van Allen, B. A. Randall, and M. F. Thomsen (Dept. of Physics and Astronomy, The University of Iowa, Iowa City, IA 52242)

Continuing analysis of Pioneer 11 observations of Saturn's magnetosphere has yielded results beyond those available in our initial report [Science, 207, 415, 1980]: (a) The phase space density f of protons at constant first adiabatic invariant $\mu \sim 8 \times 10^3$ MeV/gauss has three maxima (at L = 3.4, 2.69, and 2.44). Between the maxima, f is essentially zero at the orbits of Mimas, 1979 S2 and 1979 S5. Hence, such high energy protons must be attributed to an internal source, most likely cosmic-ray neutron albedo from Saturn's upper atmosphere. The maximum omnidirectional intensity of protons $E_p > 80$ MeV is 2.6×10^4 $(cm^2\ s)^{-1}$ at L = 2.66. (b) In contrast, the phase space density of electrons at $\mu \sim 400$ MeV/gauss is essentially constant from the magnetopause inward to L ~ 12 and then diminishes monotonically by a factor of over 10^3 inward to L ~ 3. On the basis of this and other evidence we attribute electrons with E_e in the range tens of keV to several MeV to the inward diffusion of thermalized solar wind plasma from the magnetosheath. The maximum omnidirectional intensity of electrons $E_e > 0.56$ MeV is 9.4×10^5 $(cm^2\ s)^{-1}$ at L ~ 3.2, inbound. (c) It appears that protons $E_p \sim 1$ MeV also have an external source, either thermalized solar wind plasma or captured energetic solar particles, for L > 4 but may have an internal source at lesser L. (d) Further study of the particle absorption signatures of Mimas and newly discovered satellites provides data on diffusion coefficients, which will be reported. (e) Inbound/outbound asymmetries in particle intensities for $L \leq 7$ are attributed to temporal variations in response to highly disturbed solar wind conditions and for $L \geq 7$, to temporal variations and to current sheet distortion of the dawn and tailward magnetosphere.

SM 71

PROTON FLUX ANISOTROPIES AT SATURN

T.G. Northrop*, M.F. Thomsen†, A.W. Schardt* and J.A. Van Allen† (*Goddard Space Flight Center, Greenbelt, MD 20771; †Dept. of Physics and Astronomy, U. of Iowa, Iowa City, IA 52242)

Saturn's magnetospheric protons seen by Pioneer 11 were markedly anisotropic. The distributions were pancakes, offset because of $\vec{E}\times\vec{B}$ flow and spatial gradients in both the fluxes and the amount of pancaking. We have extended previous theory so as to interpret such situations, where the magnitude and shape of the angular distribution vary in space and time. An expression has been derived relating the $\vec{E}\times\vec{B}$ velocity and the gradient of the flux magnitude to experimentally observed quantities. The gradient in the amount of pancaking can be eliminated in terms of the observable third harmonic of the anisotropy.

If the time derivative of intensity seen by Pioneer is attributed solely to a spatial gradient and not at all to time dependence in the non-rotating frame, the $\vec{E}\times\vec{B}$ velocity may be calculated from the observations and compared with the value expected from the visible rotation rate of the planet. Conversely, if the electric field is assumed, e.g. the corotational value, the gradient may be calculated instead. From the gradient and the observed total time derivative (which is what Pioneer sees) follows the partial time derivative, which is related to any expansion or contraction of the magnetosphere during the flyby. These techniques have been applied to data from the Goddard-University of New Hampshire and Iowa experiments on Pioneer 11.

SM 72

OBSERVATIONS OF SMALL-AMPLITUDE HYDROMAGNETIC WAVES IN SATURN'S INNER MAGNETOSPHERE

L.L. Hood
C.P. Sonett (Both at Lunar and Planetary Laboratory, University of Arizona, Tucson, AZ 85721)
E.J. Smith (Jet Propulsion Laboratory, California Institute of Technology, Pasadena, CA 91103)

One minute averages of vector Helium magnetometer data from the Pioneer 11 encounter with Saturn have been examined for the existence of small-amplitude perturbations from the ambient magnetic field. Within the magnetopause on the inbound portion of the trajectory, the field remained quiescent, with few exceptions, until approximately six Saturn radii (R_s) from the center of the planet. Within 6 R_s, irregular fluctuations became noticeable which increased in amplitude as periapsis was approached. The direction of maximum variance for these perturbations was oriented perpendicular to the ambient magnetic field and to the Saturn-sun line. Similar fluctuations were observed during the outbound part of the trajectory within about 5 R_s.

In addition, three sets of quasi-continuous perturbations were observed whose direction of maximum variance was perpendicular to the ambient magnetic field in the plane defined by the Saturn-sun line, i.e. perpendicular to the direction of maximum variance for the irregular perturbations. All three sets of waves decreased in both amplitude and wavelength with decreasing distance to the planet. The measured periods ranged from approximately 10 minutes at 3.3 R_s (outbound) to 2 minutes at 1.5 R_s (inbound). If the continuous perturbations are interpreted as standing Alfven waves with an origin analogous to that postulated for terrestrial Pc 4,5 pulsations, then a mass density for cold plasma within the inner magnetosphere of the order 10^2 M_p/cm^3, where M_p is the mass of a proton, is implied.

SM 73

OBSERVATIONS OF PLASMAS IN SATURN'S MAGNETOSPHERE

L. A. Frank
B. G. Burek
K. L. Ackerson (all at: Department of Physics and Astronomy, University of Iowa, Iowa City, IA 52242)
J. H. Wolfe
J. D. Mihalov (both at: Space Physics Branch, NASA Ames Research Center, Moffett Field, CA 94035)

Plasmas are detected in Saturn's magnetosphere with the ARC solar wind plasma instrumentation on board Pioneer 11. Detailed analysis of the responses of one of the two electrostatic analyzers comprising this instrument reveals measurable positive ion intensities along the inbound trajectory from the position of the magnetopause at ~15 R_S to radial distance ~4 R_S just outside the orbit of Enceladus. The energy (E/Q) range of the electrostatic analyzer is 100 eV to 8 keV for positive ions. Since no direct determinations of the positive ion composition are available for this energy range, observations of the angular distributions of the positive ion intensities and the assumption of corotating Maxwellian velocity distributions are employed to estimate the dominant ion, density and temperature of the plasma. In Saturn's outer magnetosphere at 10-12 R_S, the proton density and temperature are 0.2-0.5 cm^{-3} and 5×10^5 to 1.2×10^6 °K, respectively. Plasma densities begin to increase with decreasing radial distances at ~9 R_S. Maximum densities are found at 4-7.5 R_S and are 10-50 cm^{-3}. The dominant ion at these radial distance often appears to be O^{++}, and the corresponding temperatures are $2-5 \times 10^5$ °K. A plausible source for this doubly-ionized atomic oxygen is photodissociation of water ice on the Saturn ring material with subsequent ionization by electron impact. If this interpretation is correct then a substantial hydroxyl torus is expected to encircle Saturn at radial distances extending from the outer edge of the rings to ~7 R_S.

SM 74

SEARCH FOR RADIO EMISSION FROM SATURN WITH THE VOYAGER PLANETARY RADIO ASTRONOMY INSTRUMENT

M. L. Kaiser
M. D. Desch (both at NASA/GSFC, Laboratory for Extraterrestrial Physics, Greenbelt, MD 20771)
J. W. Warwick
J. B. Pearce (both at Radiophysics, Inc. 1885 33rd Street, Boulder, CO 80303)

Over the past decade there have been several investigations attempting to detect non-thermal radio emission from Saturn. Only Brown (1975) has announced positive results with detection of very intense emission near 1 MHz from the direction of Saturn using the earth orbiting IMP-6 spacecraft. As of this writing, we have not detected any radio bursts near 1 MHz from Saturn using the Planetary Radio Astronomy (PRA) instrument on the Voyager spacecraft. Voyager-1 is now (January 1980) only 2.4 AU from Saturn so the PRA instrument effectively should be able to detect bursts from Saturn some 200 times less instense than those reported by Brown. We have, however, detected several bursts of suspected Saturnian origin in the frequency range from 100 to 300 kHz. By late May 1980, Voyager-1 will have moved to within 1.4 AU of Saturn and we should be able to confirm or deny the existence of radio bursts from Saturn.

SM 75

SATURN'S MAGNETOSPHERIC ROTATION PERIOD

M. D. Desch*
M. L. Kaiser (both at: NASA/Goddard Space Flight Center, Laboratory for Extraterrestrial Physics, Greenbelt, Maryland 20771)

Using radio frequency data derived from the Planetary Radio Astronomy instrument onboard the Voyager spacecraft and assuming the occurrence modulation of Saturn emission is associated with some anomaly in the planet's magnetic geometry, we can derive a provisional figure for Saturn's magnetospheric rotation period. We use a method of spectral analysis applicable to data which are time-sampled at unequal intervals. The practical resolution limit to which the period can be determined, which is dictated by the span of data in time, will be approximately ± 1 min by June 1980.

SM 76

SATURN'S MAGNETIC FIELD, MAGNETOSPHERE AND INTERACTION WITH THE SOLAR WIND

L. Davis, Jr. (California Institute of Technology, Pasadena, CA 91125)
E. J. Smith (Jet Propulsion Laboratory, California Institute of Technology, Pasadena, CA 91103)
D. E. Jones (Brigham Young University, Provo, UT 84601)
P. J. Coleman, Jr. (University of California, Los Angeles, CA 90024)
D. S. Colburn (University of California, Los Angeles, CA 90024)
P. Dyal (Ames Research Center, Moffett Field, CA 94035)
C. P. Sonett (University of Arizona, Tucson, AZ 85721)

Pioneer 11 vector helium magnetometer measurements within 10 radii of Saturn have been inverted to give properties of the planet's magnetic dipole. A spherical harmonic analysis of the data has also been carried out including data stored in the spacecraft memory during occultation of Pioneer by Saturn. The planetary moment, of strength 0.2 G r_s^3, is aligned with the rotation axis to within 1°. The quadrupole moment and equivalent offset are small (< 10% and < .04 r_s). The structure of the outer magnetosphere appears to be distinctly different near noon (inbound) and near dawn (outbound). Near noon, a compressed dipole field is seen with the field pointing southward. Near dawn, the field rotates from a dipole-like configuration to an equatorial orientation and multiple crossings of an equatorial current sheet are observed. Numerous bow shock and magnetopause crossings were observed and will be described.

SM 77

SIMULATION OF A NATURAL CHARGING EVENT ON THE SCATHA (P78-2) SATELLITE

G. W. Schnuelle
I. Katz
M. J. Mandell (Systems, Science and Software, P.O. Box 1620, La Jolla, CA 92038)
A. G. Rubin (Air Force Geophysics Laboratory, Hanscom AFB, MA 01731)
(Sponsor: T. C. Bache)

Natural charging of the SCATHA (P78-2) satellite to greater than 5 kV negative was observed on March 28, 1979, while the spacecraft was in eclipse. This

event is of special interest because unexplained pulses on the satellite transient pulse monitor were observed during the charging.

SCATHA satellite models based on the NASCAP simulation code have been used to predict the charging response of the spacecraft during the March 28 event. The simulation uses as input a description of the plasma environment inferred from the particle detector experiments aboard SCATHA, as well as a detailed set of material and geometrical parameters to characterize the spacecraft. The accuracy of the simulation as a function of model resolution, material parameters, and alternative representations of the environment is described in detail.

SM 78

SPACECRAFT CHARGING INSIDE AND OUTSIDE THE EARTH'S PENUMBRA

N.A. Saflekos (Boston College, Chestnut Hill, MA 02167)
M.F. Tautz (Radex Corp. Carlisle, MA 01741)
A.G. Rubin
D.A. Hardy (both at Air Force Geophysics Laboratory, Hanscom AFB, MA 01731)
P.M. Mizera (The Aerospace Corp., El Segundo, CA 90245)

The NASCAP simulation code with its three dimensional capability was used to self-consistently compute the surface potential of a spinning object in a plasma under varying solar illumination conditions. Based on the code, we constructed and investigated several P78-2 (SCATHA) satellite models structurally differing in shape, size and material properties. The environment input to the code corresponded to that of the natural charging event of 28 March 1979 when SCATHA charged to about 4 kV. The distribution functions from the SC-5 experiment were fitted by both single and two-Maxwellian populations for protons and electrons separately. The equilibrium potentials reached, using a two-Maxwellian distribution function, showed better agreement with the SSPM measurements. Generally, the computed absolute and differential potentials compare well with the spacecraft measured quantities in penumbra and sunlight.

SM 79

THE ENERGETIC ELECTRON ENVIRONMENT DURING A NATURAL CHARGING EVENT ON THE SCATHA SPACECRAFT

J. B. Reagan
R. W. Nightingale
H. D. Voss
E. E. Gaines
W. L. Imhof (all at: Space Sciences Laboratory, Lockheed Palo Alto Research Laboratory, Palo Alto, CA 94304)

The behavior of the energetic electron environment has been examined prior to and during the natural charging of the SCATHA (P78-2) spacecraft to several kilovolts during eclipse conditions on 28 March 1979. For approximately 30 minutes prior to the onset of the charging event the entire electron population >47 keV was depressed below the normal ambient levels by several orders of magnitude. At 1636 UT on L = 7.2 the energetic electron flux reappeared abruptly, coincident with the occurrence of the spacecraft charging. The energetic electrons continued to increase over the next few minutes to a level about 4000 times higher than the pre-event levels at 100 keV. The pitch angle distribution of the injected electrons was nearly isotropic except for the loss-cone region which was nearly empty ($J_{\parallel}/J_{\perp}$ being as small as 4×10^{-3}). The detailed spectra and pitch-angle distributions of the hard injected electrons will be presented. Calculations have also been performed to illustrate the significant change in ionization density in typical dielectric materials resulting from the rapid injection of these hard electrons. The role of these electrons in spacecraft charging will be discussed.

SM 80

COMPUTER SIMULATION OF SPACECRAFT CHARGING ON SCATHA

A. G. Rubin
H. A. Cohen (both at Air Force Geophysics Laboratory, Hanscom AFB, MA 01731)
M. F. Tautz (Radex Corp., Carlisle, MA 01741)
N. A. Saflekos (Boston College, Chestnut Hill, MA 01267
T. Aggson (NASA Goddard Space Flight Center, Greenbelt, MD 20771)

Computer simulation is used to determine spacecraft charging on P78-2 (SCATHA) during a substorm on March 29, 1979 and for modeling the effects of electron beam emission on the P78-2 ground potential for a variety of beam voltages and currents. The single-particle trajectory treatment of spacecraft potential control by emission of kilovolt electron beams predicts the measured SCATHA potentials to within a few percent, indicating that the basic mechanisms of beam emission with returning ambient and beam current are correctly treated, although space-charge has been neglected. The experiments and simulations show that the spacecraft ground potential can be controlled by emitting an electron beam.

SM 81

VIRTUAL ANODE FORMATION DURING BEAM OPERATIONS

Shu Lai (Boston College, Chestnut Hill, MA 02167)
Herbert A. Cohen (Air Force Geophysics Laboratory, Hanscom AFB, MA 01731)
Joe Fennel, (The Aerospace Corporation, El Segundo, CA 90009)

Data from the SCATHA satellite during positive ion beam ejection clearly indicate the formation of virtual anode in the beam. Theoretically, this formation occurs when the current density of the emitted beam is large; the actual current then leaving the satellite is limited by the virtual anode. On SCATHA there are several examples of great differences in the vehicle potential between cases of high and low beam current densities; the latter being related to larger amplitude of vehicle potential. Techniques to estimate the fraction of beam current transmitted through a virtual anode will be discussed.

Trapping, Precipitation

Harbour C
Saturday P.M.
D. N. Baker (Los Alamos Scientific Lab.), Presiding

SM 82

FAST-TIME, NEAR-EQUATORIAL MEASUREMENTS OF ENERGETIC ELECTRON PRECIPITATION AT L = 6.6

D. N. Baker, P. R. Higbie, E. W. Hones, Jr., R. D. Belian (all at: Los Alamos Scientific Laboratory, Los Alamos, NM 87545)
P. Stauning (Technical University of Denmark, Lyngby, Denmark)

Many previous studies of precipitating electrons at low altitudes in the auroral zone have shown that such precipitation is impulsive and highly fluctuating (time scales of seconds or less). It is also generally supposed that energetic electron precipitation results from wave-particle scattering that occurs primarily near the outer zone (L = 5-8) equatorial plane. In contrast to prior low-altitude measurements, however, nearly all previously reported measurements made in the near-equatorial regions have been quite slow, with loss-cone sampling times of minutes. This paper presents correlated measurements of Technical University auroral zone riometer data (20-s sampling times) and Los Alamos high-resolution > 30 keV electron measurements in the loss cone made at geostationary orbit. We examine equatorial electron fluxes during periods of weak (Kennel-Petschek) pitch angle diffusion as well as during periods of strong pitch angle diffusion. During strong precipitation events, we find precipitating electron fluxes to be highly fluctuating and impulsive at our minimum loss-cone sampling time of 10-s. For such event periods the pitch angle distribution outside the loss cone is nearly flat (≈ isotropic flux), the absolute electron intensity (> 30 keV) is near 'saturation' ($j \approx 5 \times 10^{7}$ cm^{-2}s^{-1}sr^{-1}), and the 20 MHz conjugate riometer intensity is very high (5-10 dB). These results demonstrate quite clearly that equatorial wave-particle interactions do not build up steadily and gradually but rather they develop in an impulsive or sporadic way. Thus these observations are quite consistent with low-altitude results and may relate equatorial phenomena to such ionospheric phenomena as pulsating aurora and fluctuating auroral zone bremsstrahlung X-rays.

SM 83

A COORDINATED MEASUREMENT OF ENERGETIC PARTICLE PRECIPITATION AT MID-LATITUDES USING ROCKET SATELLITE AND GROUND BASED INSTRUMENTS

H. D. Voss
W. L. Imhof
E. E. Gaines
J. B. Reagan (all at: Space Sciences Laboratory, Lockheed Palo Alto Research Laboratory, Palo Alto, CA 94304)
L. G. Smith
F. M. Braswell (both at: Aeronomy Laboratory, Dept. of Electrical Engineering, University of Illinois, Urbana, IL 61801)
J. G. Moore (Air Force Geophysics Lab, Hanscom Air Force Base, Bedford, MASS 01730)

A coordinated group of energetic particle measurements was made at mid-latitudes on 26-27 September 1978 near local midnight to determine the extent of energetic particle precipitation for a moderately disturbed condition (K_p = 5+, D_{st} = -69). A Nike Apache 14.542 equipped with six solid state particle spectrometers, an electrostatic analyzer and electron density experiments, was launched from Wallops Island (L = 2.56) near local midnight (0530 UT). The energy flux derived from the energy spectrum and pitch angle distribution (anisotropic with maxima near 90° pitch angle) is 2×10^{-3} ergs cm^{-2} s^{-1} for E > 20 keV. Simultaneous satellite measurements are consistent with the rocket measurements and extend the particle coverage over the complete mid-latitude interval. Ground based airglow measurements taken at AFGL (L = 3.05) for the nights of 25-26 and 26-27 September 1978 indicate enhancements of the 391.4 nm and 630 nm airglow radiation and the presence of a TID (35 min. period) and SAR arc at the time of the rocket launch. These combined measurements indicate the importance of widespread energetic particle precipitation at mid-latitudes during disturbed conditions and give the essentials of the particle transport mechanism.

SM 84

COMPARISON OF THE AVERAGE PLASMA ENVIRONMENT AT GEOSYNCHRONOUS ORBIT WITH THE ENVIRONMENT AT LOWER L-VALUES

S.-Y. Su (Lockheed Engineering and Management Services Co., Inc., Houston, Texas 77058)
A. Konradi (NASA-JSC, Houston, Texas 77058)

About 300 orbits of Explorer 45 low energy electron and ion data (from 1 keV to several hundred keV) were processed to obtain the average plasma characteristics inside the geosynchronous altitude. These orbits are selected in groups that cover most of the local times between L = 2.5 and L = 5.5. The averaged particle energy spectra are presented in a table that is organized by local time and the L value. A two-Maxwellian particle distribution function is chosen to fit the particle energy spectra in the table to obtain a representative particle number density and plasma temperature. These results are intended for use as the plasma environmental definition and for future environment simulation purpose. It is hoped that the present statistical plasma model together with a previously obtained plasma model from ATS 5 taken at the geosynchronous orbit can be used by theoreticians to evaluate the particle radial transport process in the radiation belt. For a simple example, we have transformed the ATS 5 ion energy spectra to the lower L values covered by Explorer 45 orbits by conserving the particle density in the phase space and the first adiabatic invariant. The transformed ATS 5 ion energy spectra and the observed Explorer 45 ion energy spectra are then compared for their flux intensities, spectral shapes, and the locations of the spectral minimum which is one of the prominent features in the average ion energy spectra of the inner magnetosphere.

SM 85

CONFIGURATION OF THE RADIATION BELTS AT GEOMAGNETIC REVERSAL

George A. Paulikas (Space Sciences Laboratory, The Aerospace Corporation, El Segundo, California 90245)
Michael Schulz (Space Sciences Laboratory, The Aerospace Corporation, El Segundo, California 90245)

We have constructed a scenario that is intended to describe the most probable evolution of the earth's radiation belts during a geomagnetic reversal. In this scenario the north-south component of the geomagnetic dipole moment passes smoothly through zero while the components of the dipole moment normal to the rotation axis remain small but do not vanish. At reversal the dipole, quadrupole, octupole, and other moments contribute comparably to the magnetic field at the surface of the earth (or, perhaps, of the core), but the dipolar component contributes more than the others at radiation-belt altitudes as a consequence of the usual scaling with geocentric distance. Thus, the magnetic (minimum-B) equator, which is the most probable locus of maximum radiation intensity, remains topologically dipolar but becomes severely warped by virtue of the higher multipoles. During geomagnetic reversal the nominal orientation of the minimum-B surface thus rotates through roughly 180° of latitude, and the long-lived constituents of the radiation belts survive the transition of the earth from one magnetic polarity to the other. The radiation belts do not disappear in the course of a geomagnetic reversal.

SM 86

OBSERVATIONS DURING THE FEBRUARY 13, 1978 SOLAR PARTICLE EVENT

A.J. Masley (TRW, Defense and Space Systems Group, Redondo Beach, CA 90278)

The February 13, 1978 event was the most intense observed from mid-1974 to mid-1978 on the ATS-6 Spacecraft in synchronous orbit. This was true at low energy (5×10^3 protons/cm^2-sec-sr-Mev for 2.5-4.4 Mev) and high energy (4 protons/cm^2-sec-sr-Mev for 28-70 Mev). Protons from 2.5 to 78 Mev were measured parallel (NORTH) and perpendicular (EAST) of the earth's magnetic field. The event occurred during a period of low to moderate magnetic activity providing an opportunity to investigate charged particle entry into the magnetosphere under semi-quiet conditions. During this event 0.3-1.2 Mev protons of solar origin were sufficiently intense to be observed above the trapped background (10^3-10^4). The solar particles increased above the trapped background during a period when K_p was between one and three. The only other observation of 0.3-1.2 Mev solar protons at synchronous orbit was on July 3, 1974. At that time ATS-6 was located at L $\cong$ 9 and K_p was between 3+ and 5-. At 2145-2146 UT, Feb. 14, 1978, the perpendicular intensity increased 10 to 20 times depending upon energy, and the parallel intensity doubled during a three minute period. A sudden commencement was reported at 2147 UT. Significant numbers of alpha-particles were also observed from 2 to 28 Mev throughout the event. Details of charged particle entry and motion to synchronous orbit will be discussed.

SM 87

OBSERVATIONS OF VERY NARROW AND OF MULTIPLE PEAKS IN THE ENERGY SPECTRA OF ELECTRONS PRECIPITATING FROM THE INNER RADIATION BELT

W. L. Imhof
E. E. Gaines
J. B. Reagan (all at: Space Sciences Laboratory, Lockheed Palo Alto Research Laboratory, Palo Alto, CA 94304)

The frequent occurrence of peaks in the energy spectra of electrons precipitating from the inner radiation belt has been confirmed from the P78-1 satellite with a silicon solid-state electron spectrometer providing contiguous spectral coverage over the energy range 68-1120 keV and finer resolution measurements of the peaks than previously achieved. As in the earlier observations it is found that often only one peak dominates the spectrum of quasi-trapped electrons and that the central energies of the peaks typically vary with L-shell in a manner consistent with the first-order cyclotron resonance interaction of the electrons with waves of a nearly constant frequency. In some cases the peaks are less than 20 keV wide (FWHM), thereby suggesting both a narrow limit on the spatial extent along the field line and on the frequency spread of possible wave-particle resonance interactions. On other occasions the peaks are significantly wider, indicating the possible occurrence of off equatorial interactions or the effects of waves of a broader frequency band. On a given satellite pass two different energy peaks are sometimes observed. In these cases the peak energy versus L variations are often consistent with the occurrences of first and second order cyclotron resonances.

SM 88

SATELLITE OBSERVATIONS OF ENERGETIC ELECTRON PRECIPITATION NEAR WINNIPEG DURING THE 1979 SOLAR ECLIPSE AND COMPARISONS WITH ROCKET MEASUREMENTS

E. E. Gaines
W. L. Imhof
H. D. Voss
J. B. Reagan (all at: Space Sciences Laboratory, Lockheed Palo Alto Research Laboratory, Palo Alto, CA 94304)

During the solar eclipse of 26 February 1979, the P78-1 satellite passed over Winnipeg, Canada at an altitude of ~600 km at 1748 hr UT. Energetic electrons (.06-1.1 MeV) were measured from the spinning satellite (~5 second spin period) with two silicon solid state detector electron spectrometers having angular resolutions of ±3.5° and ±15° FWHM and geometric factors of 1.0×10^{-3} cm^2 ster and 7.8×10^{-1} cm^2 ster respectively. Significant fluxes of precipitating electrons were observed over Winnipeg at the time of eclipse. The intensities, their latitude profiles and energy spectra of these fluxes will be presented along with calculations of the resulting ionization rates in the upper atmosphere. These data will be compared with measurements made from two Nike Tomahawk rockets launched at 1652 hr and 1654 hr UT from Redlake, Ontario.

SM 89

0.1 - 100 MeV PROTON FLUXES AT THE OUTER EDGE OF THE INNER TRAPPED REGION

R. Filz (Air Force Geophysics Laboratory, Hanscom AFB MA 01730)
D.R. Parsignault (Emmanuel College, Boston MA 02115)
E. Holeman (Emmanuel College, Boston MA 02115)

Charged particle telescopes flown on S3-2 and S3-3 Air Force satellites have provided data on trapped proton fluxes, in the 0.1 - 100 MeV energy range, during 1976 and 1977. While these instruments were designed for soft proton spectra which typically occur in solar events, reliable data were obtained at the outer edge of the inner trapped region ($2 \lesssim L \lesssim 4$), and at minimum mirror point altitudes $100 \text{ km} \lesssim h_{min} \lesssim 4000$ km.

We report proton fluxes over the 0.1 - 100 MeV energy range for the 1976-1977 time period, and compare them to earlier measurements. Energy spectra which cannot be fitted by a single distribution (exponential or power) are also presented.

SM 90

LOSSES OF RELATIVISTIC TRAPPED ELECTRONS FROM THE OUTER BELT DURING THE MAIN PHASE OF GEOMAGNETIC STORMS

G. T. Davidson and S. M. Kaye (Lockheed Palo Alto Research Laboratory)
H. I. West, Jr. (Lawrence Livermore Laboratory)

Data taken with the LLL magnetic electron spectrometer on satellite OGO-5 were used to test the hypothesis that relativistic electrons are lost during magnetic storms by parasitic interactions with ion cyclotron waves generated in the ring current protons at the plasmapause. The data were analyzed to determine the preferred loss regions and the corresponding energies during two storms in 1968. Radial profiles of phases space distributions at constant adiabatic invariants disclose that pronounced decreases are seen in the electron populations above 500 keV in the outer belt during the main phase, coinciding roughly with the build-up of the ring current. It is questionable whether the plasmapause was far enough out to result in major losses beyond L=4. Parasitic interactions with ion cyclotron waves at the plasmapause will not by themselves account for the losses. We suggest several alternate mechanisms for the observed drop-outs in the electron fluxes, 1.) breakdown of adiabatic guiding center motion in the strongly curved tail-like fields, 2.) adiabatic removal from the observation regions due to formation of tail-like fields, 3.) parasitic interactions with intense Pc1 and Pc2 waves generated in the outer regions, far beyond the plasmapause, and 4.) very rapid inward transport followed by removal at the plasmapause by parasitic interactions with ion cyclotron waves.

SM 91

OBSERVATIONS OF ELECTRON AND ION DISTRIBUTIONS IN THE NEAR SYNCHRONOUS REGIONS

D. R. Croley and J. F. Fennell (both at Space Sciences Laboratory, The Aerospace Corporation, El Segundo, CA 90245)

Several particle injections have been observed during February and March, 1979 by charged particle detectors aboard P78-2 (SCATHA). Both ion and electron distribution functions reveal dynamical changes which appear to be consistent during injection events. The transition energy between predominantly field aligned and trapped ions just prior to injection decreases to a few hundred volts very rapidly then abruptly increases to several keV just after injection followed by a gradual decrease to a nominal value. The electron distributions show a hardening just prior to injection followed by a sudden decrease in the low energy perpendicular flux at injection giving the low energy component of the distribution a field aligned character. The high energy electron fluxes are more intense in the perpendicular direction producing spectra which show $T_\perp > T_\parallel$. Development of the injections will be shown in the velocity-space, distribution function representation.

SM 92

OBSERVATIONS OF COUNTERSTREAMING FIELD-ALIGNED ELECTRONS CORRELATED WITH ULF MODULATION OF MAGNETIC-FIELD-ALIGNED POTENTIAL DIFFERENCES

J. B. Cladis (Lockheed Palo Alto Research Laboratory, Palo Alto, Calif. 94304)
R. D. Sharp

On 17 January 1977 the S3-3 satellite was in and near the upward field-aligned current sheet from about 21.5h to 15.7h MLT at an altitude of about 7900 km. At the time of the measurements the three-hourly Kp index was 2. Potential differences along the magnetic field above and below the satellite were inferred from an analysis of the electron distribution measurements. In general, the potential differences, which exceeded 10 kV at times, were large above the satellite when they were large below, and were larger during the local evening than the local afternoon. When plotted against time, the potential differences below the satellite displayed fluctuations, with a mean time interval between peaks of 121 ± 51s, and were strongly modulated with a mean period of 400 ± 100s. This modulation period is in the range of the ULF waves (1-3 mHz) that are regularly observed with ground magnetometers at the feet of the local magnetic field lines. High fluxes of counterstreaming electrons, closely aligned with the magnetic field, and with broad energy spectra (0.07 - 2 keV) were observed near the minima of the modulated potential differences (near zero). It is suggested that the counterstreaming electrons were accelerated and trapped in a potential well which developed along the magnetic field.

SM 93

THE ATMOSPHERE AS A SOURCE FOR TRAPPED MAGNETOSPHERIC ELECTRONS

M. E. Greenspan (Univ Calif., San Diego, La Jolla, CA. 92093)
M. B. Silevitch, and E. C. Whipple (Univ. Calif., San Diego, La Jolla, CA. 92093)

Precipitating electrons from the inner edge of the plasma sheet produce the diffuse aurora. The precipitation produces a population of backscattered electrons. If there were no

pitch angle diffusion, the backscattered electrons would remain in the loss cone. Recent work by Evans suggests that backscattered electrons form a significant part of the trapped particle population seen at the magnetic equator at synchronous orbit. We investigate when Evans' formula for predicting the total trapped electron spectrum agrees with ATS-6 data, and consider mechanisms for electron pitch angle diffusion into and out of the loss cone.

SM 94

A STATISTICAL SURVEY OF MAGNETOSPHERIC ENERGETIC PARTICLE BURSTS OBSERVED BY IMP-7 AND 8 SPACECRAFT

A. T. Y. Lui (Applied Physics Laboratory, The Johns Hopkins University, Laurel, Md. 20810)
T. P. Armstrong (University of Kansas)
S. M. Krimigis (APL/JHU)
C.-I. Meng (APL/JHU)

Energetic proton and electron bursts ($E_p \geq 0.29$ MeV; $E_e \geq 0.22$ MeV) of magnetospheric origin have been observed in many instances both within and outside the magnetosphere by the JHU/APL instrument onboard the IMP-7 and 8 spacecraft. We extend these previous studies by conducting a statistical survey of magnetospheric energetic particle bursts for the period from September 26, 1972 to May 14, 1978. Maps in solar magnetospheric longitude and latitude are generated to show the distribution of magnetospheric energetic particle bursts in their occurrence frequency, averaged intensities, spectral index of their energy spectrum, and the occurrence frequencies of unidirectional as well as bidirectional anisotropies. The possibility of a permanent energetic electron ($E_e \geq 0.22$ MeV) layer at the magnetopause 35-40 R_e downstream in the magnetotail will be discussed.

SM 95

A SURVEY OF LOW ENERGY CHARGED PARTICLE EVENTS AT ∿35 Re AND THEIR RELATION TO THE LOCAL MAGNETIC FIELD.*

P. R. Briggs, F. J. Kutchko, T. P. Armstrong (Dept. of Physics and Astronomy, University of Kansas, Lawrence, KS 66045)

We display simultaneous magnetic field and energetic charged particle data for selected intervals during 1973-78 as received by the IMP 8 (Explorer 50) Earth-orbiting spacecraft. Five-minute averages of the observed magnetic field strength and direction[1] are combined with ∿300 keV ion and electron intensities measured in 8 angular sectors in the ecliptic plane[2]; the result is a map of the energetic particle phase space in a coordinate system where B lies along the polar axis.

Our study includes the determination of pitch-angle and gyrophase characteristics of observed particles for three classes of events: 1) magnetospheric bursts and substorm phenomena; 2) shocks and other traveling magnetic disturbances; and 3) large particle-producing solar flare events. We will discuss field-aligned and transverse anisotropies in the context of local particle source and propagation mechanisms.

Auroral Pulsations

Pier 4
Monday A.M.
D. J. McEwen (Univ. of Saskatchewan), Presiding

SM 96 INVITED PAPER

A REVIEW OF OPTICAL CHARACTERISTICS OF PULSATING AURORA

D.J. McEwen (Institute of Space and Atmospheric Studies, Univ. of Saskatchewan, Saskatoon, Sask., Canada)

A campaign was conducted during January-February 1980 to study the physical processes involved in, and the optical characteristics of, pulsating aurora. Stations were operated at Saskatoon (λ=61.3°), La Ronge (λ=64.6°), South End (λ=66.0°) and Rabbit Lake (λ=67.8°) Saskatchewan, approximately along the 43°W geomagnetic meridian. A total of some 25 Canadian and Japanese scientists participated in this campaign. Two rockets were flown into pulsating auroral events on February 15 and 23, 1980.

A general review will be given of optical characteristics of pulsating aurora along with an overview of the campaign. Some preliminary results of measured spectral intensities and in situ electron spectra will be presented.

SM 97

OBSERVATIONS OF ENERGETIC ELECTRON PRECIPITATION IN A PULSATING AURORA

B.A. Whalen
A.W. Yau (both at Herzberg Institute of Astrophysics, National Research Council of Canada, Ottawa, Canada, K1A OR6)
D.J. McEwen (Institute of Space and Atmospheric Studies, University of Saskatchewan, Saskatoon, Canada)

During the pulsating aurora campaign recently conducted in northern Saskatchewan (January-February, 1980), a sounding rocket was launched into a pulsating aurora of approximately 10 second periodicity. Electrons with energies between 20 eV and 200 keV were measured by an array of electrostatic analysers and solid state detectors at altitudes up to 150 km over the pulsating forms. Electron energy spectra and pitch-angle distributions derived from these sensors along with simultaneous ground-based photometric observations will be presented. These results will be discussed in terms of current theories of pulsating auroras.

SM 98

IONOSONDE DERIVED VIRTUAL HEIGHTS DURING PULSATING AURORA EVENTS

J. Hofstee, Cent. for Radio Sci., Univ. of West. Ont., London, Ont. N6A 3K7
J.A. Koehler, ISAS, Univ. of Sask., Saskatoon, Sask. S7N OWO
J.W. MacDougall, Cent. for Radio Sci., Univ. of West. Ont., London, Ont.

An Australian type IVB ionosonde was operated at Southend, Sask. during the pulsating aurora rocket campaign. It had been modified to provide continuous range versus time records at a fixed frequency (usually 2.8 MHz) for 4 out of every 5 minutes; the remaining time was used to produce normal ionograms.

During the morning of 15 Feb. 1980, near the time of one rocket launch, very substantial periodic variations in virtual height of the 'Auroral E' echoes were observed. This feature and its correlation with optical pulsations will be discussed.

SM 99

LANGMUIR PROBE MEASUREMENTS IN A PULSATING AURORA

A.G. McNamara (Herzberg Institute of Astrophysics, National Research Council, Ottawa, Canada, K1A OR6)

Langmuir probes were flown on rocket ADD-VA-50 which was launched into a pulsating aurora in February 1980. Preliminary examination of the data has indicated that good data were obtained up to the apogee of 140 km. Electron density and temperature variations obtained during the flight will be presented.

SM 100

DIFFERENTIAL PHASE OBSERVATIONS OF THE IONOSPHERE DURING PULSATING AURORA

P.A. Forsyth (Centre for Radio Science, University of Western Ontario, London, Ontario N6A3K7), J.A. Fulford, J. Hofstee and G.F. Lyon

Dual phase locked receiving systems were used to measure the relative phase between the 150 and 400 MHz signals from the NNSS satellites. Measurements were made from two widely separated stations (56.3°N, 103.5°W and 55.2°N, 105.3°W) during the month of Feb. 1980, under a variety of geophysical conditions including the occurrence of pulsating aurora. The distribution and the nature of ionospheric irregularities observed at these times is discussed.

SM 101

LATITUDINAL AND TIME DEPENDENCE OF PULSATING AURORAL FORMS

C. Duncan (Institute of Space and Atmospheric studies, University of Saskatchewan, Saskatoon, Sask. S7N OWO)
F. Creutzberg, R. Gattinger, F. Harris, A. Vallance Jones (Herzberg Institute of Astrophysics, National Research Council Canada, Ottawa, Ont. K1A OR6

During the Saskatchewan Pulsating Aurora Campaign (January 8-24 and February 7-22, 1980) measurements were made along a latitudinal chain of stations (61° to 67° invariant) with zenithal pointing photometers. The intensity, period and modulation factor of the observed pulsating aurora are described as a function of latitude and time. In particular, their relation to substorm timing is investigated. These observations are then used to test current theories for the mechanism producing pulsating aurora.

SM 102

TV ALL-SKY OBSERVATIONS OF PULSATING AURORA

A. Vallance Jones (Herzberg Inst. of Astrophysics, National Res. Council of Canada, Ottawa, Ont.)
D.J. McEwen (Institute of Space and Atmospheric Studies, Univ. of Saskatchewan, Saskatoon, Sask.)
T. Oguti (Geophys. Res. Lab., Univ. of Tokyo, Tokyo, Japan)

A chain of 4 TV all-sky cameras was operated (one by NRC and the University of Saskatchewan at Southend, and three by the University of Tokyo at Rabbit Lake, La Ronge and Saskatoon) along a meridian extending from λ=61° to 68° during a period of 32 nights in January-February, 1980 in northern Saskatchewan. Pulsating aurora was observed on 14 of these nights. A preliminary review will be given of the forms observed including their extent, motions, durations and periodicities. These will be discussed in relation to mechanisms producing auroral pulsations.

SM 103

SPATIAL STRUCTURE OF PULSATING AURORAS

T. Oguti, S. Kokubun, K. Hayashi (Geophys. Res. Lab, Univ. of Tokyo, Tokyo, Japan)
K. Tsuruda, S. Machida (Inst. of Space and Aeronaut. Sci., Univ. of Tokyo, Tokyo, Japan)
T. Kitamura, O. Saka (Dept. of Phys., Kyushu Univ., Fukuoka, Japan)
T. Watanabe (Dept. of Geophys. and Astronomy, Univ. of Brit. Col., Vancouver, B.C.)

Coordinated observations of 5 all-sky TV cameras, 8 VLF receivers and 13 ULF recorders were carried out in an area from 62° to 74° in geomagnetic latitude and from 300° to 330° in geomagnetic longitude during a period from January 14 to February 23, 1980 covering the pulsating aurora campaign. Three TV cameras out of 5, which were made with the same specifications were operated at Rabbit Lake, La Ronge and Saskatoon in coordination with a Canadian all-sky TV at Southend roughly along 317° geomagnetic meridian.

It was confirmed that there is a characteristic distribution of the pulsating forms of aurora during pulsating

events and they sometimes show specific relations to ULF and VLF waves. These will be discussed in relation to possible mechanisms.

SM 104

PULSATING AURORA IN RELATION TO PROTON AND ELECTRON AURORAL SUBSTORMS

F. Creutzberg, R.L. Gattinger, F.R. Harris and A. Vallance Jones (all at: Herzberg Institute of Astrophysics, National Research Council, Ottawa, Canada, K1A 0R6

Auroral observations have been made simultaneously from three locations using meridian scanning and zenithal photometers. The observatories were located at Saskatoon, LaRonge and Rabbit Lake, Saskatchewan.

Latitudes of pulsating aurora are compared with those for proton aurora. In addition, the temporal and spatial characteristics of pulsating aurora are considered in relation to the overall morphology of auroral substorms.

SM 105

ROTATIONAL TEMPERATURE MEASUREMENTS IN PULSATING AURORA

R.A. Koehler (Centre for Research in Experimental Space Science, York University, Toronto, Canada, M3J 1P3)
Marian M. Shepherd (Department of Computer Science, York University)
K.V. Paulson (Physics Department, University of Saskatchewan, Saskatoon, Sask., Canada S7N 0W0)
G.G. Shepherd (Centre for Research in Experimental Space Science, York University)

The measurement of rotational temperature from the N_2^+ ING (0,1) band at 4278 Å in aurora provides an estimate of mean energy of the precipitating electrons. A two-channel photometer was employed during the recent Canadian pulsating auroral campaign to investigate the changes in mean electron energy during pulsations. These results are described and compared with direct electron measurements made by others during the two rocket flights of the campaign. Pulsations in other emissions measured during this campaign and at the Kiruna Geophysical Observatory are also reported upon.

SM 106

VLF EMISSIONS ASSOCIATED WITH PULSATING AURORA

K. Tsuruda (Institute of Space and Aeronautical Science, University of Tokyo, Tokyo, Japan)
N. Murdoch (Institute of Space and Atmospheric Studies, University of Saskatchewan, Saskatoon, Sask., Canada)
T. Oguti (Geophysics Research Laboratory, University of Tokyo, Tokyo, Japan)

VLF radio data were recorded at the five stations during the pulsating aurora campaign in Saskatchewan during January-February 1980. These stations ran approximately north-south with the end points at Rabbit Lake and Saskatoon. VLF chorus emissions were observed at several stations during nights of active aurora. In a preliminary analysis the envelope intensity of the emissions is obtained. Periodicities in the range from 2 to 40 seconds are examined. This modulation of VLF signals is compared with optical data. The implications of these observations for theories of pulsating aurora will be briefly discussed.

SM 107

IONOSPHERIC PROCESSES IN PULSATING AURORAS.

H.C. Stenbaek-Nielsen (Geophysical Institute, University of Alaska, Fairbanks,Alaska 99701)
T.J. Hallinan

Observations with a stereo-TV system have shown that many pulsating auroras are thin horizontal surfaces located in the lower E-region (85-110 km). The vertical extent of the thin surfaces has been measured to be less than 2 km, which implies that they cannot be produced by normal collisional thermalization of precipitating electrons. Computer simulations of the TV observations indicate that, if the layers derive their energy directly from the precipitating energetic electrons, the incident electron beam must either be more energetic than is typically observed, have an anomalous non-Maxwellian distribution above 20 keV, or within the thin layer produce photons at a higher efficiency than in normal energy loss processes. Alternatively, the energy dissipated in the layer must be supplied by other sources than precipitating energetic electrons. The analysis suggests that active ionospheric processes may be important in pulsating auroras, a suggestion which can also be supported by other observations already in the literature.

SM 108

EVIDENCE FOR THE E x B DRIFT OF PULSATING AURORAL FORMS

E. Nielsen (Max-Planck-Institut für Aeronomie, 3411 Katlenburg-Lindau 3, F.R.G.)
M.W.J. Scourfield[1] (Max-Planck-Institut für Aeronomie, 3411 Katlenburg-Lindau 3, F.R.G.)
J.G. Keys[4] (Max-Planck-Institut für Aeronomie 3411 Katlenburg-Lindau 2, F.R.G.)

The Scandinavian Twin Auroral Radar Experiment (STARE) is sensitive to electrostatic waves in the auroral E-layer and the mean drift velocity of these waves provides two-dimensional maps of the plasma flow and electric field over a large section of the auroral oval. The system is operated on a continuous basis with a spatial resolution of 20 x 20 km^2. In January, 1980 simultaneous observations were made using STARE (operated at 10 s integration times) and a TV system imaging predominantly eastwards drifting pulsating auroral forms. The field of view of the TV system was located near the centre of the STARE field of view. Events were chosen in which the auroral forms were sharp, constant in shape and had a clearly recognizable feature that could be tracked to deduce drift speeds and directions. For the same period, the drift speeds and directions of the background plasma flow were obtained from the STARE data.

Taking into account the difference in spatial resolution of the STARE and TV system there is good agreement between the drift speeds of auroral forms and the background plasma. We conclude that these forms have an E x B drift and the sources of electrons responsible for the auroral emissions are convecting with the background plasma.

IONS
Pier 5
Monday P.M.
Theodore A. Fritz
(NOAA/ERL), Presiding

SM 109

OBSERVATIONS OF THE RING CURRENT COMPOSITION AT L-VALUES LESS THAN 4.

R. Lundin (Kiruna Geophysical Institute S-981 01 Kiruna, Sweden)
L.R. Lyons (NOAA/ERL, Boulder, Colorado 80303, U.S.A.)
N. Pissarenko (Space Research Institute, Moscow, U.S.S.R.)

Observations showing that the Ring Current at L $\lesssim$ 4 and energies $\leq$ 17 keV is composed mainly of O^+ and He^+ ions during quiet times and the recovery of magnetic storms will be presented. The data were obtained from the Swedish ion composition experiment on board the PROGNOZ-7 satellite. For L $\lesssim$ 3, the relative abundance of H^+ is only a few percent of the total ion density in the energy range 0.35 to 12.7 keV. Although O^+ normally dominates for L $\lesssim$ 4, we have found an example when He^+ was more abundant than O^+ for L $\lesssim$ 3. One example of a storm injection shows that the ring current was strongly dominated by O^+ ions ($\sim$ 82%) with H^+ only giving a minor contribution ($\sim$ 15%) to the total energy density. The observations are consistent with charge exchange loss rates in the inner part of the ring current at energies $\leq$ 17 keV, H^+ being the ion species that is most rapidly lost. That He^+ should be the most stable ion constituent is supported by the observation that the relative abundance of He^+ increases towards lower L-values.

SM 110

THE POST-STORM DECAY OF MEV HELIUM IONS IN THE RADIATION BELTS

Walther N. Spjeldvik (Space Environment Laboratory, NOAA/ERL, Boulder, Colorado 80303 USA)
Theodore A. Fritz (Space Environment Laboratory, NOAA/ERL, Boulder, Colorado 80303 USA)

Large fluxes of MeV Helium Ions were injected deep into the radiation belts during the August 1972 magnetic storm period. We present an analysis of the observed post-storm decay of helium ions at 0.91-3.15 MeV per ion that took place on time scales ranging from a few days at L $\gtrsim$ 5 to more than four months below L = 3. Little or no energy dependence of the decay rates can be deduced beyond L = 4, while below this L-shell the lower energy helium ions ($\lesssim$ 1 MeV) decay faster than those of higher energies ($\gtrsim$ 2 MeV). Comparison is made with ion transport time scales due to radial diffusion processes, with Coulomb collision energy degradation times and with charge exchange loss times for helium ions. We find good agreement between the expected response times deduced from the theoretical considerations and the actual observed ones.

SM 111

INJECTION OF ENERGETIC IONOSPHERIC IONS INTO THE DAYSIDE CUSP

E. G. Shelley
R. G. Johnson
R. D. Sharp (all at: Lockheed Palo Alto Research Laboratory, Palo Alto, CA 94304)

The orbit of the S3-3 satellite frequently carried it into the mid-altitude (up to 8000 km) region of the dayside cusp. Measurements by the Lockheed ion composition experiment on S3-3 reveal that ions of ionospheric origin (O^+) are continuously being accelerated to keV energies within the lower altitude region of the cusp and injected upward along the magnetic field lines. The pitch angle distributions suggest that these ions are being accelerated both parallel and perpendicular to the field lines. Cusp crossings were identified on the basis of the soft ($\sim$100 eV) electrons and the existence of magnetosheath-like H^+ and He^{++} Ions. Out of 57 clearly identified cusp crossings upward flowing O^+ ions were observed on 33, or approximately 60% of the crossings. It is suggested that these O^+ ions should be intermixed with the magnetosheath source ions in the high latitude boundary layer.

SM 112

LOW-ENERGY ION PRECIPITATION INTO THE EARTH'S POLAR REGIONS

James R. Sharber and Drazen M. Premate (Department of Physics and Space Sciences, Florida Institute of Technology, Melbourne, FL 32901).

An analysis of ISIS-2 low-energy positive ion data has revealed the presence of positive ions at very high latitudes during prolonged quiet (AE) times. The ions and an accompanying electron population are present at all local times and lie adjacent to and poleward of the auroral oval particle population. Ion energies are the same as ions of the dayside clefts, although their intensities are lower by an order of magnitude. The maximum invariant latitude (sometimes $\geq$ 80°) populated by the ions depends on the length of time after the previous substorm; the occurrence of another substorm removes the population. The observation is presented in terms of the relationship of the ions to the plasma mantle and in light of recently proposed substorm current systems.

SM 113

ENERGETIC ION COMPOSITION OF THE PLASMA SHEET

W. K. Peterson
R. D. Sharp
E. G. Shelley
R. G. Johnson (all at Lockheed Palo Alto Research Laboratory)
H. Balsiger (University of Bern, Bern, Switzerland)

Data obtained from the energetic ion mass-spectrometer experiment on the ISEE-1 spacecraft show that the plasma sheet at 15 - 23 earth radii has a significant and variable ionospheric component of O^+ and H^+. A method to roughly estimate the fraction of the observed H^+ density that is of ionospheric origin will be presented. The method is based on the observed similarities of H^+ and He^{++} energy spectra above 5 keV/e. Using this method, we estimate the ionospheric component (H^+ and O^+) to vary between 10 and 50 percent in the 10 cases studied.

SM 114

A COMPARISON OF THE STORM TIME ION COMPOSITION AT DIFFERENT LOCAL TIMES AS MEASURED BY THE ISEE-1 MASS SPECTROMETER

W. Lennartsson
R. G. Johnson
R. D. Sharp
E. G. Shelley (all at: Lockheed Palo Alto Research Laboratory, Palo Alto, CA 94304)
H. Balsiger (University of Bern, Bern, Switzerland)

The energy range of the ISEE-1 mass spectrometer, E/Q < 17 keV/e, does not allow in situ measurements of the principal storm-time ring current population (~100 keV at 3 - 4 R_E).Provided, however, that the ring current ions are adiabatically accelerated through a strong dawn-dusk electric field they can be observed at larger geocentric distances R while their energy is still below 17 keV/e. Of particular interest is the predawn sector, at large R, where the equatorial electric potential is expected to be high and ions are moving earthward. Data from some 25 crossings of the near-equatorial magnetosphere were used to address the question of whether the ring current ions are predominantly of solar wind origin (H^+, He^{++}) or ionospheric origin (H^+, O^+, He^+). The O^+/H^+ and He^+/H^+ energy density ratios, integrated over 0.1 - 17 keV/e, were rather high, often ~1 and ~0.1, respectively, indicative of a large ionospheric contribution. At large R (>6 R_E) these ratios were, however, lower in the 0100 - 0600 LT sector than at other local times, by a factor of 3 - 10. This, along with the somewhat higher He^{++}/H^+ ratios here, suggests that ions of solar wind origin may enter in this sector and may dominate the high-energy population at smaller R, during at least some storms.

SM 115

OBSERVATIONS OF TRANSIENT ION (H^+ AND O^+) BURSTS IN THE EQUATORIAL MAGNETOSPHERE

S. M. Kaye
R. G. Johnson
R. D. Sharp
E. G. Shelley (all at: Space Sciences Laboratory, Lockheed Palo Alto Research Laboratory, Palo Alto, CA 94304)

Twenty-two days of data from the Lockheed Ion Mass Spectrometer aboard the SCATHA satellite were used to perform a statistical study of O^+ and H^+ bursts observed in the equatorial magnetosphere. The results indicate that the ion bursts are transient phenomena occurring primarily in the nighttime sector during periods of enhanced geomagnetic activity. The average energy of the bursts is $\lesssim$1 keV although they can occur over any portion of the instrument 100 eV - 32 keV energy range. The pitch angle distributions of the bursts are broad and are consistent with the bursts initially being field aligned or conical at low altitudes. One-third of the observed bursts are associated with field-aligned electrons flowing from the same hemisphere as the bursts. The energy width ($\Delta W/\langle W\rangle \approx 1$) and the pitch angle width ($\Delta\alpha_0 = 30°$) of the bursts suggest that the ions have undergone intensive energy and pitch angle diffusion all along the geomagnetic field line.

SM 116

OBSERVATIONS OF IONOSPHERIC IONS WITH ENERGIES UP TO 32 keV DURING THE 3-4 APRIL 1979 GEOMAGNETIC STORM

R. G. Johnson
S. M. Kaye
R. D. Sharp
E. G. Shelley (all at: Space Sciences Laboratory, Lockheed Palo Alto Research Laboratory, Palo Alto, CA, 94304)

Hot plasma composition measurements in the energy range 0.1 to 32 keV were made during the 3-4 April 1979 geomagnetic storm aboard the SCATHA spacecraft. The spacecraft is in a 7.9° inclination orbit with perigee near 27,000 km and apogee near 43,000 km. During the storm, the O^+/H^+ number density ratio was generally quite high and was greater than one for several hours in the L-shell range 5.5 to 7.5. At times the O^+ number flux exceeded the H^+ flux at 32 keV. Large variations in the ion composition and energy distributions were observed during the storm.

SM 117

ANALYTIC REPRESENTATIONS FOR THERMAL ION DISTRIBUTION FUNCTIONS OBSERVED WITH ISEE-1

J.L. Horwitz
G.O. Dennis (both at: Department of Physics, The University of Alabama in Huntsville, Huntsville, AL. 35807)
C.R. Baugher
C.R. Chappell (both at: Magnetospheric Physics Branch/ES53, Marshall Space Flight Center, MSFC, AL 35812)
E.G. Shelley (Lockheed Palo Alto Research Laboratories, Palo Alto, CA. 94304)
D.T. Young (Physikalisches Institut, University of Bern, 3012 Bern, Switzerland)

Thermal ion distribution functions are critical, but currently ill-defined, inputs to various types of work, notably the theoretical investigations of instabilities and wave-particle interactions. In this report, we present examples of ion distribution functions for the energy range 0-100eV observed with ISEE-1, and discuss model representations for them. At energies below ~3eV, these distributions are typically well represented by cold, isotropic Maxwellians, at least within the plasmasphere. But at higher energies throughout the magnetosphere, the distribution functions are richly varied, displaying field-aligned, pancake and conical pitch angle anisotropies, and energy spectra with high energy tails. We will describe various analytic representations for these distribution functions; one example is the bi-Maxwellian with $T_\perp > T_\parallel$ as a model for the pancake distribution. Contacts are welcomed from investigators desiring observed ISEE-1 distribution functions and/or appropriate representations.

SM 118

EFFECTS OF THE AUGUST 1972 SOLAR FLARE EVENTS AND ASSOCIATED GEOMAGNETIC STORM(S) ON THE HEAVY ION ($Z \geq 4$) POPULATION IN THE EARTH'S RADIATION BELTS

Theodore A. Fritz (Space Environment Laboratory, NOAA/ERL, Boulder, Colorado 80303 USA)
Walther N. Spjeldvik (Space Environment Laboratory, NOAA/ERL, Boulder, Colorado 80303 USA)

Following the August 1972 solar flares a period of irregular magnetic storm(s) were observed in the Earth's magnetosphere. Megaelectronvolt heavy ions with nuclear charge $Z \geq 4$ were injected into the radiation belt trapping region, and the ambient fluxes were enhanced by several orders of magnitude. At 2.5 earth radii in the equatorial radiation belts the fluxes of heavy ions at 1.82-4.8 MeV per ion increased a thousandfold, an increase that was an order of magnitude higher than that of helium ions at comparable energies. The post-storm period was characterized by $Z \geq 4$ ion decay on time scales of 10-40 days, a significantly faster decay than that of helium ions (20-150 days or more) at $L \lesssim 4.5$, and comparable to that of helium at $L \gtrsim 5$. The decay is interpreted in terms of transport and collisional processes, the latter being dependent on the $Z \geq 4$ ion charge state distribution. Assuming that a major fraction of the $Z \geq 4$ ions are atomic oxygen and that theoretical charge state distributions are approximately valid, we compare the observed decay with the theoretically predicted decay. We report a good agreement.

SM 119

WARM ION FLOWS PARALLEL TO THE MAGNETIC FIELD

R.C. Olsen (Physics Dept., Univ. Calif., San Diego, La Jolla, Ca. 92093)

Particle data from the ATS-6/UCSD spectrometers in the 0-500 ev range have been studied in the midnight sector prior to and during substorm injection events. The quiet time distribution at 6.6 Re is well modeled by a Maxwellian distribution displaced by a field aligned velocity of 20-40 km/s. Nominal temperatures of .1 to 1 ev are found, with densities between .01 and 1 cm**-3 found for hydrogen. Multiple ion species (H+, He+, He++, O+, and O++) can be seen flowing with velocities within 10 per cent of each other. The ratios of the particle densities are not well determined by the modeling process, but show substantially more He++ and O++ than have been reported, particularly during the injection process. During the injection process, the ions accelerate to over 100 km/s, and then drop several orders of magnitude in density, effectively disappearing. Convection of thermal ions perpendicular to the magnetic field is also visible during the injection, with velocities approaching 100 km/s.

SM 120

OBSERVATION OF POLAR WIND OXYGEN IONS IN THE LOBE OF THE GEOMAGNETIC TAIL BY ISEE-2.

V.Formisano (Space Science Dept., ESA/ESTEC 2200 AG Noordwijk, Holland)
M.Candidi
S.Orsini (Both at Istituto Plasma Spazio, CNR, C.P.27, 00044 Frascati (Rome), Italy)

The EGD plasma experiment on board of the ISEE 2 spacecraft has been able to observe in the earth's geomagnetic tail positive ions flowing from the earth tailwards. These ions are observed only in the afternoon side of the magnetosphere during the recovery phase of the main geomagnetic storm. Our observations are made above the plasmasheet in the lobes of the geomagnetic tail. The energy of the oxygen ions is observed to vary from 200 to 10,000 EV. When the O^+ energy is high enough also protons are observed with similar flow speed.

The O^+ pitch-angle distribution is not centered around the magnetic field and is different from the protons pitch-angle distribution.

The energy of the O^+ ions is also strongly correlated with the magnetic field component B_z.

Magnetopause, Magnetotail, Etc.

Harbour C
Tuesday A.M.
J. B. Reagan (Lockheed), Presiding

SM 121

DISSIPATION, ELECTRON HEAT CONDUCTION AND FLUX TRANSFER EVENTS NEAR THE EARTH'S MAGNETOPAUSE

K. W. Ogilvie (NASA/Goddard Space Flight Laboratory for Extraterrestrial Physics, Center, Greenbelt, MD 20771)
J. D. Scudder
R. J. Fitzenreiter

Observations have been made of the distribution function of plasma electrons in three dimensions as the ISEE-1 spacecraft encounters flux transfer events when close to the magnetopause. The derived macroscopic parameters show a characteristic signature, which can be used to eliminate a number of possible mechanisms which could explain the magnetic signature alone. The detailed distribution functions indicate the presence of electron beams, and show consistent and very large electron anisotropies in these events, and the electron heat flux consistently exhibits

increases of 3-4 times in the region of the non-zero normal magnetic field component. These observations require an explanation in terms of reconnection taking place in the observed flux tube, but indicate that the classical Petschek model is not applicable, since the slow shocks called for by that model are not observed. Quantitatively, the heat flux can be responsible for the removal of a substantial part of the energy released by the reconnection process, and its conduction to a remote point.

SM 122

WAVE-PARTICLE INTERACTIONS AT THE MAGNETOPAUSE AND THE DAYSIDE AURORA

B. T. Tsurutani
E. J. Smith
T. Chuh (Jet Propulsion Laboratory, California Institute of Technology, Pasadena, CA 91103)
R. M. Thorne (UCLA)
G. K. Parks (U. Washington)
C. K. Lin (U. Maryland)
R. R. Anderson
D. A. Gurnett (U. Iowa)

Intense broadband plasma waves and correlated 1-6 keV electron and proton events have been detected at almost every ISEE-1, 2 dayside magnetopause crossing examined. The magnetic field whistler mode turbulence extends from a few Hz to 1 kHz with an average spectrum $I_{em}=10^{2}f^{-4}\gamma^{2}$/Hz and the broadband electrostatic emissions from a few Hz to ~ 100 KHz with an average spectrum $I_{es}=10^{-5}f^{-2}$ $v^{2}/m^{2}Hz$. Protons and electrons, within the energy range of 1.4 - 6.0 keV, have typical spectra of $J^{-}(E) = 3 \times 10^{5} E^{-1.8}$ and $J^{+}(E) = 10^{7}E^{-2.5}/cm^{2}$ sec str keV. The magnetopause wave-particle boundary layer has been modeled, using reasonable plasma and field values. It will be shown that both the electrons and protons undergo strong pitch angle diffusion from doppler shifted (and anomalous doppler-shifted) cyclotron resonant interactions with the whistler mode emissions. The expected flux of precipitating particles are sufficient for the formation of the dayside aurore.

Magnetic diffusion, due to anomalous resistivity associated with wave-particle collisions, and viscous interaction at the magnetopause will be discussed. Possible sources of the particles in the wave-particle boundary layer will be considered.

SM 123

AN ANALYTIC TREATMENT OF THE STRUCTURE OF THE BOW SHOCK AND MAGNETOSHEATH

H.-C. Zhuang
C.T. Russell (both at: Institute of Geophysics and Planetary Physics, University of California, Low Angeles, CA 90024)

A detailed theoretical examination of the jump conditions of the bow shock in an ideal magnetohydrodynamic flow pattern is used to obtain two sets of approximate analytic representations of the parameters behind the bow shock. From these analytic representations contour maps can be drawn to show clearly the influence of the solar wind magnetic fields, especially their directions on these parameters.

In view of the results of space measurements and the turbulent nature of the magnetosheath, it is preferable to assume that the average values of the parameters along the radial direction in the magnetosheath are simply equal to their values just behind the bow shock. A very simple approximate formula of the thickness of the magnetosheath is obtained which satisfies the boundary conditions and conservation laws of mass and momentum flux.

Two years magnetometer data from the ISEE satellite crossing the magnetosheath during the period between Oct. 1977 to Oct. 1979 are used to determine empirically the thickness of the magnetosheath and to compare these observed thicknesses with theoretical estimates. Because of the sensitive dependence of the formula for the magnetosheath thickness on the value of γ, the polytropic exponent of the plasma gas, we can use this comparison to determine the optimum value of γ. A value of $\gamma=2$ gives much better agreement than 5/3 or 7/5.

SM 124

ISEE-1 AND 2 OBSERVATIONS OF THE MAGNETOPAUSE: MAGNETOMETER OBSERVATIONS ON NOVEMBER 20, 1977

C.T. Russell
R.C. Elphic (both at: Institute of Geophysics and Planetary Physics, University of California, Los Angeles, CA 90024)

The ISEE-1 and 2 spacecraft encountered a series of multiple crossings of the magnetopause at about 0100 UT on November 20, 1977 that has attracted the interest of a number of researchers Mozer et al. examined their electric field measurements during this period in conjunction with the magnetic field data and concluded that reconnection was occurring at this time. Williams has used three-dimensional energetic ion measurements to probe the location of the magnetopause remotely and follow its motion. Fritz et al. have adapted this remote sounding technique to measure the thickness of the magnetopause. The thickness they obtain of less than 100 km is significantly thinner than earlier reported values of ~500 km and much thinner than the average 250 km thickness reported by Mozer et al. during this same period.

We have carefully examined the ISEE-1 and 2 records during this period and derived magnetopause normals from minimum variance analysis at both spacecraft. We conclude that the boundary motion is extremely turbulent at this time. The boundary normals undergo very large oscillations with deviations from the average normal of greater than 60°. Further the magnetopause current layer appears to have variable thickness, ranging from less than 100 to greater than 300 km. In particular the magnetopause traversal studied by Fritz et al. was extremely thin.

SM 125

THE POSITION AND ORIENTATION OF THE MAGNETOPAUSE DETERMINED BY ENERGETIC ION MEASUREMENT ON ISEE 1 and 2 ON NOVEMBER 20, 1977.

S.C. Fahnenstiel (Space Environment Laboratory, NOAA/ERL, Boulder, Col. 80303)
T.A. Fritz (SEL, Boulder)
D.J. Williams (SEL, Boulder)

The position of the magnetopause with respect to ISEE-1 and 2 has been determined using measurements of energetic particle three dimensional distributions for a one-half hour interval from 0130 to 0200 UT on November 20, 1977. The distance to the magnetopause has been compared to the simultaneously measured plasma density and magnetic field (courtesy of G. Paushmann and C. Russell) and have indicated that the magnetopause current and boundary layer were coincident and very thin, each having an e-folding distance of ≈ 35 km. This is about 1/3 of the local plasma ion gyroradius. The magnetopause was found to be in rapid, continual motion with velocities up to 90 km/sec. Even with this motion the magnetic field inside the magnetopause can sustain stably trapped particles effectively right up to the magnetopause which appears to be a sharp well-defined boundary for energetic particles. A short movie will be shown demonstrating the time variably of the magnetopause position and orientation with respect to both satellites.

SM 126

PARTICLE SIGNATURES OBSERVED DURING FLUX TRANSFER EVENTS AT THE MAGNETOPAUSE

P.W. Daly
E. Keppler (both at: Max-Planck-Institut für Aeronomie, D3411 Katlenburg-Lindau 3, Germany)

A systematic study has been undertaken of a particular type of event seen during magnetopause crossings by the ISEE-B satellite. These events consist of magnetospheric-like electrons ($E > 20$ keV) and protons ($E > 25$ keV) in the magnetosheath, having pitch angle distributions filling one hemisphere only, and coincident with magnetic flux transfer signatures in the component of the magnetic field normal to the magnetopause. These events have been observed on the dayside from dawn to local noon, at times when the field in the sheath tends to be directed southward. A detailed analysis of the evolution of several such events will be presented and discussed in terms of local connection of previously closed magnetospheric field lines with sheath lines, allowing the particles to escape into the sheath.

SM 127

THE DAWN POLAR CAP BOUNDARY AT HIGH ALTITUDE

T.E. Moore
R.L. Arnoldy, (Both at University of New Hampshire, Space Science Center, Durham, N.H. 03824)
B. Hultqvist
B. Aparicio (Both at Kiruna Geophysical Institute, Kiruna, Sweden)

Comparison of hot plasma data from ATS 6 and GEOS 1 during 1977 when the satellites were near local time conjunction reveals the presence of strong gradients separating plasmas differing by more than two orders of magnitude in keV particle fluxes. These gradients are observed at fairly high geomagnetic latitudes of 25° to 30° on field lines outside the synchronous orbit. They are associated with magnetic storms and are distinct from magnetopause crossings. Interpretation of these events in terms of a boundary between magnetospheric and polar cap or lobe plasma leads to the following conclusions: 1) the polar cap/lobe region is surprisingly devoid of keV plasma, 2) the field lines defining this boundary are significantly distorted from a dipolar to a more stretched shape consistent with the presence of a storm ring current, 3) smaller substorm-scale motions are superposed on the gross motion of the boundary with some evidence present for structure in the plasma spatial profile, and 4) magnetosheath-like plasma finds access to the inner magnetosphere at dawn local time, much as it does near noon, along polar cap boundary layer field lines which close through the low latitude magnetospheric boundary layer.

SM 128

SIMULTANEOUS MEASUREMENTS OF MAGNETOTAIL DYNAMICS BY IMP SPACECRAFT

D. H. Fairfield (NASA/Goddard Space Flight Center, Laboratory for Extraterrestrial Physics, Greenbelt, Maryland 20771)
E. W. Hones, Jr. (Los Alamos Scientific Laboratory, Los Alamos, NM 87545)

More than 10 traversals of the magnetotail at 30-40 R_E by the IMP 7 and IMP 8 spacecraft occurred while IMP 6 was making magnetotail measurements inside of 33 R_E. Magnetic field and plasma data from these spacecraft have been combined to give a comprehensive picture of large scale variations inside 40 R_E. Pressure balance between fields and plasmas in the magnetotail is demonstrated for the first time by the constancy of the total pressure when a spacecraft moves from the low plasma β tail lobes to the high β plasma sheet. The frequency of plasma sheet thinnings and the regions over which they occur indicate that thinnings are a common feature of substorms and that they occur at all locations across the tail and with amplitudes of at least several earth radii. Decreases in total pressure at widely separated locations at the times of substorms support the concept that magnetotail energy is converted into substorm energy at the time of a substorm. The increase in tail B_z at substorm onset is large and sudden inside of ~ 10 R_E and is smaller and more gradual at larger radial distances.

SM 129

OPEN FIELD LINES IN THE MAGNETOTAIL AND THEIR RELATIONSHIP TO GEOMAGNETIC ACTIVITY

J. W. Bieber
E. C. Stone (both at: California Institute of Technology, Pasadena, CA 91125)

According to the neutral line theory of geomagnetic substorms, a substorm is triggered by the formation in the near-earth (tailward of -10 R_E) plasma sheet of an X-type magnetic neutral line at which reconnection of magnetotail field lines occurs. A spacecraft located tailward of the reconnection region would therefore be on open field lines for at least a portion of the substorm expansive phase. Because energetic electrons can be used as a tracer of field line topology, with a strong streaming flux indicating open field lines, we have examined 26 months of data from the Caltech instrumentation aboard IMP-8 to find occurrences of intense electron streaming within 15 R_E of the center of the neutral sheet at $X_{GSM} \sim -30$ R_E. During a total of 140 hours when the > 200 keV electron intensity exceeded 1 $(cm^2\text{-}s\text{-}sr)^{-1}$, 21 separate instances of intense (> 50%) streaming were found. To determine the average behavior of the AE index near times of streaming, a time profile of AE from one hour before till one hour after the onset of in-

tense streaming was produced for each event, and the 21 profiles so obtained were averaged together. The average profile clearly shows that energetic electron streaming in the distant magnetotail occurs in association with geomagnetic substorms. The average AE remains fairly constant at about 350γ until 28 minutes before the streaming event. It then rises steadily to a peak of 550γ about 25 minutes after the streaming event, at which point it begins to decrease. The average profile of the elevation of the magnetotail field shows that although the plasma sheet field is inclined predominantly northward, the streaming events occur in association with a ~ 5-minute episode of southward inclination. Thus the average behavior of the magnetotail field as well as the AE index near times of intense streaming of energetic electrons is well explained by the neutral line theory of substorms.

SM 130

QUANTITATIVE MEASURES OF MAGNETOTAIL FLUX CHANGES

R.E. Holzer
J.A. Slavin (Both at Institute of Geophysics and Planetary Physics, University of California, Los Angeles, CA 90024)

The total magnetic field, B, in a magnetotail lobe was examined in order to make a continuous appraisal of the magnetic flux transfer process. The value of dB/dt, obtained from OGO5 records was taken as a measure of the rate of change of tail flux assuming a constant tail cross section. The AL auroral index was taken as a measure of the rate of transfer of tail flux to the inner magnetosphere (See Holzer and Slavin, JGR, 84, 2572, 1979). In order to make a direct comparison of AL with dB/dt it was necessary to augment dB/dt corresponding to the flux added to the tail by the merging process, estimated from simultaneous interplanetary records of Explorers 33, 34, and 35 by the method described in the above reference. In order to minimize the effect of solar wind dynamic pressure, intervals in which the bulk speed varied by less than 10% were used. The total estimated flux changes were consistent within 25%. Peaks in the dB/dt record preceded corresponding peaks in the AL record by approximately 25 minutes, indicating an average residence time in the tail for flux added by the merging process.

SM 131

THE EFFECTS OF INHOMOGENEITIES IN THE SOLAR WIND UPON THE EARTH'S MAGNETOTAIL

John Lyon
Stephen H. Brecht (both as Science Applications, Inc. McLean, Va. 22101)
Joel A. Fedder
Peter J. Palmadesso (both at Naval Research Laboratory, Washington, D. C. 20375)

We present results of multidimensional, time-dependent MHD simulations of the global behavior of the solar wind-magnetosphere system. The focus is on the effects that inhomogeneities in the solar wind flow (shocks, field reversals, and non-linear waves) have upon the earth's magnetotail and plasma sheet. Non-local resistivity has been included in these calculations to mimic resistive reconnection processes in the magnetosphere. Shocks in the solar wind associated with solar flares can produce strong disturbances and heating in the near earth (< 20 R_E) magnetotail. We also observe in this situation high speed (≥ 300 km/s) field aligned flows in the tail. Cross tail flows can also be estimated and are consistent with substorm observations. Similar phenomena occur when non-steady reconnection on the nose of a southward IMF launches non-linear waves into the magnetotail. We derive an estimate for the heating rate of the plasma sheet that is consistent with the needed energy input.

SM 132

THE HARANG DISCONTINUITY AND ITS MORNING COUNTERPART

M.W.J. Scourfield* (Max-Planck-Institut für Aeronomie, 3411 Katlenburg-Lindau 3, F.R.G.)
E. Nielsen (Max-Planck-Institut für Aeronomie 3411 Katlenburg-Lindau 3, F.R.G.)

STARE (Scandinavian Twin Auroral Radar Experiment) measurements provide a 2-dimensional pattern of the electric field in the ionosphere over a viewing area of approximately 2 x 10^5 km². The Harang discontinuity appears as a prominant feature in the late evening STARE data, its signature being an electric field change from northward to southward over a relatively narrow latitudinal range. These fields indicate a change in direction of the electrojet current from eastward to westward on the poleward side of the discontinuity.

We have also detected a discontinuity during the morning hours. Its signature is an electric field change from southward to northward over a relatively narrow latitudinal range. The present paper is concerned with those days for which discontinuties have been identified in both the late evening and early morning hours. Approximately 15 examples have been isolated from some 1000 days of data accumulated since STARE became operational. The encounter times with these discontinuities will be presented together with their spatial configuration and dependence upon the interplanetary magnetic field.

SM 133

SPATIAL VARIATIONS OF IONOSPHERIC ELECTRIC FIELDS AS OBSERVED WITH STARE

Zi Min Yun* (Max-Planck-Institut für Aeronomie 3411 Katlenburg-Lindau 3, F.R.G.)
E. Nielsen (Max-Planck-Institut für Aeronomie 3411 Katlenburg-Lindau 3, F.R.G.).

Recent model calculations of ionospheric-magnetospheric coupling have demonstrated the importance of knowing the electric potential distribution at high latitudes. Results of these calculations have so far only been compared with incoherent scatter, magnetometer and rocket E-field measurements. We have used STARE (Scandinavian Twin Auroral Radar Experiment) measurements of the ionospheric electric field, made over a large area with high spatial (20 x 20 km²) and temporal (typically 20 s) resolution, in an attempt to determine the average electric field structure at magnetic quiet days. The results are in good agreement with some theoretical models.

SM 134

ISEE-1, 2, 3 OBSERVATIONS OF THE INTERACTION BETWEEN AN INTERPLANETARY SHOCK AND THE EARTH'S MAGNETOSPHERE

D. Winterhalter (Jet Propulsion Laboratory, California Institute of Technology 91103; University of California, Los Angeles, CA 90024)
E. J. Smith (Jet Propulsion Laboratory, California Institute of Technology, Pasadena, CA 91103)
M. G. Kivelson (University of California, Los Angeles, CA 90024)
C. T. Russell (University of California, Los Angeles, CA 90024)
(Sponsor: Edward J. Smith)

An interplanetary shock was observed by the ISEE-3 magnetometer on August 27, 1978 at 02:11:20 UT, 311 R_E sunward of Earth near the earth-sun line. ISEE-1 and 2, both inside and near the nose of the magnetosphere at this time, saw an abrupt increase in the magnetic field 34 minutes later. IMS ground stations recorded the disturbance after an additional 1.1 min. The subsequent compression of the magnetosphere caused ISEE 1 and 2 to enter the magnetosheath, which crossed over both spacecraft in about 2.6 min. Both spacecraft then entered the solar wind with ISEE-2 getting well away from the bow shock. However, ISEE-1 remained in close proximity to it as determined by fluctuations thought to be associated with the bow shock. Both spacecraft reentered the magnetosheath a short time later. The disturbance velocity in the magnetosphere was found to be about 1,100 km/sec, the magnetopause velocity 190 km/sec, and the bow shock velocity about 81 km/sec. The magnetopause normals indicated considerable distortion of the boundary.

SM 135

A MODEL OF THE EARTH'S MAGNETIC FIELD, A SUM OF INTERNAL AND EXTERNAL CONTRIBUTIONS

Henry H. Hilton (Space Sciences Laboratory, The Aerospace Corporation, El Segundo, CA 90245)

A model of the Earth's Magnetic Field, from the Earth's surface out to synchronous altitudes, is required for the analysis of data from synchronous satellites. The present work was motivated by data obtained from the SCATHA satellite (apogee height 6.8 R_E, perigee height 4.3 R_e, inclination 7.7°). Models of the internal field, generally expressed as spherical harmonic expansions in geographic coordinates, are continually being improved. In the last several years models of the external field, due to magnetopause and magnetospheric currents, generally at magnetically quiet times, have been published. These models usually give power series expansions (including exponential terms) for the three components of the field, in Solar Magnetic coordinates (the z-axis parallel to the Earth's dipole axis, with the x-axis chosen so that the sun lies in the x-z plane). In these coordinates the tilt angle of the sun, that is the Solar Magnetic latitude of the Sun, has a diurnal variation of 12° to 35° in summer and -35° to -12° in winter, and is a parameter of the models.

The present work explains the transformation necessary to add the internal and external contributions to the field: rotations due to the relative positions of the Earth and Sun, and a translation due to the offset of the Earth's dipole. For numerical analysis the Internal Field Model of Barraclough, Harwood, Leaton and Malin (Epoch 1975), and the External Field Model of Olson and Pfitzer (version 11/1/76) are used. The diurnal and seasonal variations of magnetic parameters (B, L, and the geographic coordinates of the 100-km intercepts of the field lines) will be illustrated by calculations for the SCATHA satellite.

SM 136

DUCT SOUNDER

W. Calvert (Space Sciences Laboratory, Lockheed Palo Alto Research Laboratory, Palo Alto, CA 94304)

Duct sounding is a remote-measurement technique which can reveal the plasma-density structure of the magnetosphere and monitor variations of the distorted terrestrial magnetic field. It is based on measuring the delay of radio echoes which propagate along field-aligned irregularities of plasma density and thereby avoid spatial attenuation. The profile of plasma density along the field, to distances of several earth radii, can be calculated from such echoes. The sequence of profiles for different positions along the satellite orbit will show how plasma is distributed. In particular, this two-dimensional picture will reveal the plasma-density structure in the auroral acceleration region and below the dayside cusp. Equally exciting are the prospects of also measuring field-line length and curvature from the delays of the echoes which propagate to the conjugate hemisphere, especially during a substorm.

Magnetic Pulsations
Pier 4
Tuesday A.M.
U. L. Patel (Univ. of Denver), Presiding

SM 137

SPACED OBSERVATIONS OF PC5 PULSATIONS IN THE RADIO AURORA

J.G. Keys* (Max-Planck-Institut für Aeronomie 3411 Katlenburg-Lindau 3, F.R.G.)
(Sponsor: Erling Nielsen)

PC5 pulsations in the radio aurora have been observed simultaneously by the STARE radar system, and by the Doppler radar operating at Slope Point in the south of New Zealand. The backscatter regions that have been compared are thus in opposite hemispheres, and are spaced about 10 hours in M.L.T. Initial observations show the pulsations to have different periods on the opposite sides of the earth, with a tendency for the New Zealand period to be larger, even though observed at lower L-values.

SM 138

SOURCE REGIONS FOR Pi 2 PULSATIONS ASSOCIATED WITH MAGNETOSPHERIC SUBSTORMS

Gordon Rostoker (Institute of Earth and Planetary Physics and Department of Physics, University of Alberta, Edmonton, Canada T6G 2J1)
John C. Samson

In the past it has been customary to think of Pi 2 pulsations as eigenoscillations of magnetic field lines penetrating the substorm disturbed region of the auroral oval. In this paper we show that the source region for Pi 2's tends to occur near the edges of the auroral eastward and westward electrojets. An example will be shown where the Pi 2 source region is near the equatorward border of the eastward electrojet, well away from the substorm disturbed region. The origin of Pi 2 pulsations will be discussed in the framework of a model which involves the existence of shear currents in the ionosphere.

SM 139

DEPENDENCE OF MIDLATITUDE HYDROMAGNETIC ENERGY SPECTRA ON SOLAR WIND KINETIC ENERGY FLUX

A. Wolfe (Physics Dept, NYCCC of CUNY, 300 Jay Street, Brooklyn, N.Y. and Bell Laboratories, Murray Hill, N.J.)

Relationships are examined between solar wind kinetic energy flux and dayside geomagnetic energy (at Pittsburg, N.H.; L~3.5) in three period bands. Ground based magnetometer data, for 336 hours during July and August 1975, are studied when good solar wind data are available from instruments on the IMP-J spacecraft. Higher correlation coefficients are obtained between the solar wind kinetic energy flux and geomagnetic energy for the longest two period bands studied (120-240 and 60-120 secs) than for the previously reported correlations between solar wind speed and geomagnetic energy. However, geomagnetic energy in the shortest period band studied (30.7-60 secs) does not correlate as well with solar wind kinetic energy flux as with solar wind speed. Multiple linear regression methods select solar wind kinetic energy flux as an important quantity in controlling ground dayside hourly magnetic energy in the longest two period bands. Therefore, more than one source mechanism must contribute to the dayside ground hourly magnetic energy to explain the above frequency dependence. We find the level of dayside geomagnetic power to have no relationship to the parameter devised by Akasofu to predict the intensities of geomagnetic substorms as measured by the AE index. Thus, the interplanetary energy input to the earth's geomagnetic disturbance level is likely controlled by different processes for energy input on the dayside and on the nightside of the planet.

SM 140

ISEE 1 AND 2 OBSERVATIONS OF Pc 4, 5 RESONANCE STRUCTURE

H.J. Singer (Department of Astronomy, Boston University, Boston, MA 02215)
W.J. Hughes (Department of Astronomy, Boston University, Boston, MA 02215)
C.T. Russell (Institute of Geophysics and Planetary Physics, University of California, Los Angeles, CA 90024)

Previous observations of magnetic pulsations in space have not been able to unambiguously distinguish temporal from spatial structure. Using the ISEE 1 and 2 spacecraft, where the satellites are closely spaced in identical orbits, we can determine whether the observed amplitude variations are due to the motion of the spacecraft through a time stationary structure or are due to temporal changes in the wave. We have examined several dayside, dominantly radially polarized Pc 4, 5 pulsations, observed between L=4 and 7 within 10° of the magnetospheric equator with amplitudes ranging from ~5 to 16γ. These first direct measurements of resonant region widths in space indicate a range from about 0.5 to 1.7 L shells. In one event, a portion of a resonance structure decayed during the 5 minutes between the two spacecraft observations at the same location, indicating that at times both temporal and spatial structure is observed.

SM 141

RESPONSE OF DAYSIDE Pc 5 PULSATION ACTIVITY TO SUBSTORMS IN THE NIGHTSIDE MAGNETOSPHERE

John C. Samson (Institute of Earth and Planetary Physics and Department of Physics, University of Alberta, Edmonton, Canada T6G 2J1)
Gordon Rostoker

It is found that nightside substorms are associated with a marked change in the frequency content of Pc 5 pulsations in the hours around local noon. For average auroral oval stations, a substorm onset or intensification involves an increase in the dominant Pc 5 frequency within approximately one to two minutes of the substorm onset. The generation mechanism of Pc 5 pulsations will be discussed in the context of the modification of the asymmetric ring current associated with substorm effects. In particular, it will be shown that changes in magnetic field in the magnetospheric equatorial plane due to ring current perturbations can lead to the observed changes in the Pc 5 pulsation spectrum.

SM 142

QUASILINEAR EFFECTS OF LINEARLY UNSTABLE COMPRESSIONAL ALFVEN WAVES

V.L. Patel (Department of Physics, University of Denver, Denver, Colorado, 80208)
S. Migliuolo
L.J. Cahill

The nonlinear interaction between Alfven waves and magnetospheric plasma particles is examined, for the situation in which compressional and transverse modes are strongly coupled. Attention is given to the quasi-linear energy changes of the particles, due to the interaction with linearly unstable waves. Saturation of the unstable oscillations is achieved via a reduction of the perpendicular component of the particle temperature, and an increase in the parallel component. The decrease in $T_{\perp}$ leads to a reduction of the diamagnetic current thereby lowering the compressional component of the oscillating magnetic field. It also results, when coupled to the increase in $T_{\parallel}$, in a reduction of the temperature anisotropy of the plasma. The latter effect yields substantially reduced (linear) growth rates.

SM 143

CHARACTERISTICS OF Pi3 MAGNETIC PULSATIONS ASSOCIATED WITH SUBSTORMS

H. Nagano
A. Suzuki
J.S. Kim (all at: Dept. of Atmos. Sci., State Univ. of NY at Albany, Albany, NY 12222)
M. Sugiura (Electrodynamics Branch, Goddard Space Flight Center, Greenbelt, MD 20771)

Pi3 pulsations have received relatively little attention in the past. The high-latitude North American IMS network has provided extensive data with which Pi3 pulsations can be analyzed. We have investigated Pi3 events that occurred during a period of four and a half days of continuous disturbance. Characteristics of substorm associated Pi3 are studied both with one-minute average and numerically filtered data in geomagnetic coordinates. Pi3 pulsations dealt with here are more general in type than those referred to as Pip and Ps6. Power spectra, coherence and phase differences are computed by the fast Fourier transform method. Results indicate that noticeable differences exist in the latitude dependence of period and amplitude between midnight, morning, and late evening Pi3's. For Pi3's occurring near midnight, the periods at which power spectral density is a maximum are longest and the amplitudes largest near the center of the westward auroral electrojet. The corresponding periods for morning Pi3's tend to be longest and the amplitudes largest near the poleward edge of the westward electrojet. Late evening Pi3's seem to have longer periods and larger amplitudes near the Harang discontinuity and the poleward edge of the westward electrojet than at the center of the electrojet. Correlations between pairs of adjoining stations appear to be smaller in the auroral regions than at higher latitudes. It is suggested that Pi3 pulsations accompanying substorms are caused by irregular oscillations of the ionospheric and magnetospheric current systems and that midnight, morning, and late evening Pi3's have different source regions in the magnetosphere.

SM 144

SURFACE WAVES ON THE MAGNETOPAUSE

B. Mauk
C. Gurgiolo
C. S. Lin
G. K. Parks (all at: Geophysics Program, Univ. of Washington, Seattle, WA 98195)

K. A. Anderson
R. P. Lin (both at: Space Sci. Lab., Univ. of California, Berkeley, CA 94720)

H. Rème (Paul Sabatier University, Toulouse, France)

The ISEE dual spacecraft, in February 1978 and 1979, skimmed the magnetopause of the dawn flanks for 10-16 hour durations, permitting a close view of surface properties of the magnetopause. The particles (electrons and ions at 1.5, 5.5, ≥19, ≥42, and ≥200 keV) are continuously modulated with a quasi-period of a few minutes. The peak-to-valley counting rates sometimes exceed three orders of magnitude. These modulated structures could result from near periodic motions of the magnetopause. However, the "shape" of the structures and the time displacement information suggest that the motions may result from large amplitude surface waves on the magnetopause. If so, the wave-length of these waves is estimated at ~10 R_E and the phase velocity is ~300 km/sec. The waves appear to be traveling toward the tail. These waves are very likely to be Kelvin-Helmholtz waves, and we are investigating the physical conditions for exciting them.

SM 145

SIMULTANEOUS OBSERVATIONS OF Pi2 PULSATIONS BY THREE GEOSTATIONARY SATELLITES

G.J. LaQuadra (Department of Astronomy Boston University, Boston, MA 02215)

W.J. Hughes

Although detailed studies of Pi2 pulsations have been made through ground observations, they have been rarely studied using spacecraft magnetometers. We have studied pulsations of this type at geostationary orbit in the nighttime magnetosphere using the magnetic field data from the ATS 6, SMS 1, and SMS 2 satellites. Use of three geostationary satellites (each only 20 degrees apart in longitude) is ideal for determining the localization and character of these Pi2 events. Although global in nature when observed on the ground, preliminary results show that at least half of the Pi2 events are seen at only one spacecraft. Only about 10% of the events are seen at all three spacecraft. The smaller magnitude pulsations are likely to be seen on only one spacecraft while the larger magnitude pulsations are likely to be seen on two or three spacecraft. After a pulsation occurs, the ambient magnetic field relaxes to a more dipolar configuration. This dipolarization is a local effect, seen only on the spacecraft in which a pulsation occurs. Time correlations and polarization data are calculated for events seen on the three spacecraft. These results are compared with the predictions of current Pi2 models. Possible sources for Pi2 pulsations at geostationary orbit are discussed.

SM 146

A GLOBAL STUDY OF Pi2 PULSATIONS

W.J. Hughes (Department of Astronomy, Boston University, Boston, MA 02215)

An indepth study on a global scale has been made of the Pi2 pulsations which occured on July 13/14, 1977. This study combines ground based data from Europe, North America, and the Southern hemisphere as well as spacecraft data. Over twelve Pi2 pulsations occured during this interval. For selected events we trace the propagation from geostationary orbit to the ground, high to mid latitudes and from nightside to dayside, noting changes in amplitude and polarization. These results have a direct bearing on the use of midlatitude Pi2's to time substorm onsets.

SM 147

THE GIANT FLUX PULSATION EVENT OF NOVEMBER 13-15, 1979, 1, ENERGETIC PARTICLE OBSERVATIONS AT GEOSTATIONARY ORBIT

P. R. Higbie, D. N. Baker, R. D. Belian, (Los Alamos Scientific Laboratory, Los Alamos, New Mexico 87545)
J. F. Fennell (Aerospace Corp., Los Angeles, CA)

During the period of November 13-15, 1979 exceptionally large modulations of the energetic electron and proton fluxes were seen by detectors on four near-geostationary spacecraft: 1976-059, 1977-007, 1979-053 and SCATHA. These pulsations were unusual in a number of ways: (1) they persisted for nearly 48 hours; (2) the pulsations had maximum to minimum amplitude ratios of over 2; (3) the pulsations were exceptionally regular in period over long times; (4) the pulsations were in close phase between all electron channels (30 keV-2 MeV) and proton (E_p > 145 keV) channels; (5) pulsations were also seen in the plasma regime. Flux modulations of this duration, amplitude, and species character have not been seen previously in over 5 satellite years of observation. The modulations were repeatedly observed only when the spacecraft was within the ∿ 0800-1600 LT sector, but were observed as early as 4 LT by SCATHA on 14 November. The periods of the oscillations appear to be systematically related to the local time measured away from local noon, varying from ∿ 7 minutes at noon to ∿ 15 minutes at dawn and dusk. Detailed pitch angle information will be presented. The possible relation of these observations to the Kelvin-Helmholtz instability at the magnetopause or the Rayleigh-Taylor instability at the plasmapause will be discussed. The following paper by Asbridge et al. presents the associated unusual plasma observations made by ISEE 1, 2, and 3 in the outer magnetosphere and the solar wind.

SM 148

THE GIANT FLUX PULSATION EVENT OF NOV. 13-15, 1979, 2, PLASMA OBSERVATIONS WITH ISEE 1, 2, AND 3

J. R. Asbridge, S. J. Bame, W. C. Feldman, J. T. Gosling, R. D. Zwickl (all at: Los Alamos Scientific Laboratory, Los Alamos, NM 87545)
G. Paschmann, N. Sckopke (both at: Max-Planck-Institut für Extraterrestrische Physik, 8046 Garching)

During the giant flux pulsation event of Nov. 13-15, 1979, the LASL/MPI fast plasma experiments on ISEE 1, 2 made measurements of the magnetospheric and magnetosheath plasmas at geocentric distances from ~5 - 21 R_E at a local time of ~0900. The most unusual features of these measurements are 1) the extremely low values of the plasma density in both the magnetosphere and magnetosheath during the pulsation event, and 2) the position of the magnetopause at ~17.7 R_E, some 30-50% further out than normal at this longitude. These measurements indicate that the magnetosphere as a whole was significantly expanded during the pulsation event. Measurements from the LASL solar wind plasma experiment on ISEE-3 far upstream from the earth's bow shock reveal that the solar wind speed and density were both low (~350 km s^{-1}, 2 cm^{-3}) during the event. Because speed and density are normally anticorrelated, the momentum flux incident (and, therefore, the dynamic pressure, PV^2) on the magnetosphere was unusually low. The most interesting aspect of the solar wind data during this interval, however, was the almost complete absence of alpha particles, which also contributed to the reduction of momentum flux. The reduced dynamic pressure of the solar wind on the magnetosphere probably resulted in the exceptionally expanded magnetopause position and thus may have contributed to the disturbed magnetospheric conditions on this day. The solar origin of this alpha abundance depletion is presently unknown; it occurred ~2 3/4 days after an interplanetary shock and ~1 3/4 days after the arrival of the solar ejecta driving the shock.

SM 149

STUDIES OF HYDROMAGNETIC WAVES AT LOW MAGNETIC LATITUDES

T. Hasegawa
L. J. Lanzerotti
L. V. Medford
C. G. Maclennan (all at: Bell Telephone Laboratories, Murray Hill, New Jersey 07974)
S. R. Dolce (Sandia Laboratories, Albuquerque, New Mexico)
M. Acuna (NASA/GSFC, Greenbelt, Maryland 20771)

We have carried out a study of magnetospheric hydrodynamic waves at three ground-based observing locations spaced in latitude around L ∼ 1.75. This investigation, conducted in Nevada and California in January and February 1979, used battery-powered digital recording systems and fluxgate magnetometers. The primary purpose of the field campaign was to conduct a more detailed, sensitive, low-latitude study of the spectral and spatial characteristics of the predominant hydromagnetic wave variations at low geomagnetic latitudes than has been reported in the past. The primary magnetic variations that can be attributed to hydromagnetic waves are found to have periods in the range ~15-60 sec (classified as Pc3) and to have amplitudes in the range ~0.5-few nT. A surprising discovery is that, although the three low latitude stations are spaced in latitude by ≲ 0.3 L, there are often significant differences in the sense of polarization between stations. It is not uncommon to find a reversal in the sense of polarization across the three-station array. The polarization characteristics can change significantly in the course of an hour or two in local time. Further results from this study will be presented.

SM 150

ENERGETICS OF LONG PERIOD RESONANT HYDROMAGNETIC WAVES

R. A. Greenwald (Applied Physics Laboratory, The Johns Hopkins Univ., Laurel, Md. 20810)
A. D. M. Walker (University of Natal)

Recently, the STARE radar system has been used to measure oscillatory electric fields and latitudinal resonance widths of Pc5 toroidal mode pulsations. We have used these values to determine height-integrated Pedersen conductivities in the resonance regions, the quality factors of the resonances, Joule heating in the ionosphere by the pulsations and magnetospheric energy storage in the resonant waves. We have found that the energy stored in a large pulsation is approximately 1% of the energy stored in the ring current. Moreover, the energy dissipated in the ionosphere by such an event can be an appreciable percentage of the equivalent dissipation by a small substorm. Assuming that the pulsation is produced by the Kelvin-Helmholtz instability on the magnetopause or by a similar solar-wind driven mechanism, one has a situation in which energy is transported directly from the solar wind to the ionosphere via the medium of a resonant hydromagnetic wave. Lastly, field-aligned currents associated with this wave may be sufficient to excite topside current instabilities. Hence, we predict that poleward moving bands of auroral precipitation should be observed in association with strong pulsation events.

SM 151

Pc5 MICROPULSATIONS OBSERVED DURING THE JUNE 1972 GEOMAGNETIC STORM

Mark J. Engebretson (Dept. of Physics, Augsburg College, Minneapolis, Minn. 55454)
Laurence J. Cahill, Jr. (Space Science Center, Univ. of Minnesota, Minneapolis, Minn. 55455)

Simultaneous measurements of particles and magnetic fields on Explorer 45 during the June 1972 geomagnetic storm indicate the presence of two distinct types of Pc5 wave activity near the plasmapause, with opposite senses of polarization. 1) Waves occur during a period of depressed magnetic field coinciding with a plasma injection event. These waves are predominantly compressional and of quite short duration. 2) Waves of longer duration occur near the time of maximum ring current without fresh plasma injection in the vicinity of the satellite. Variations in electron energy density, where available, correlate well with the observed magnetic variations.

SM 152

EFFECTS OF SOLAR WIND VELOCITY AND IMF DIRECTION ON THE CHARACTERISTICS OF PC-3 PULSATIONS AT SYNCHRONOUS ORBIT

K. Takahashi
R.L. McPherron (Both at Department of Earth and Space Sciences and Institute of Geophysics and Planetary Physics, UCLA, Los Angeles, CA 90024)
E.W. Greenstadt, C.W. Arthur

The occurrence probability of Pc3 pulsations at synchronous orbit is controlled by V_{sw} (solar wind velocity) and θ_{XB} (the angle between the sun-earth line and the interplanetary magnetic field). In this report we study the effects of these two parameters on other characteristics of Pc3 pulsations, including period and polarization. Using data from a UCLA fluxgate magnetometer on board ATS-6, we examine the characteristics of Pc3 pulsations as a function of local time. A statistical analysis is made for Pc3 events under three different conditions:

1) $\theta_{XB} \leq 30^\circ$ and $V_{sw} \geq 600$ km/sec

2) $\theta_{XB} \geq 60^\circ$ and $V_{sw} \geq 600$ km/sec

3) $\theta_{XB} \leq 30^\circ$ and $V_{sw} \leq 500$ km/sec

The occurrence probability clearly decreases from condition 1) to 2) and from 1) to 3) in the morning local times. However, the difference between 2) and 3) is small. The amplitude decreases in the order 1), 2) and 3) at most dayside local times. The frequency is generally higher in the morning local times. The frequency for 3) is about 5 mHz higher than 1) and 2) in the morning local times. Most events were linearly polarized with the major axis nearly azimuthal. The angle ϕ, positive eastward, between our outward radius vector through the satellite and the major axis of polarization, changes from less than 90° in the morning to greater than 90° in the afternoon. This pattern is typical for the three different conditions.

SM 153

THE LOCALIZATION OF SECONDARY Pc 1 PULSATION SOURCES ABOVE THE IONOSPHERE

B.J. Fraser* (Institute of Geophysics and Planetary Physics, University of California, Los Angeles, Calif. 90024)
D.J. Webster (Physics Department, University of Newcastle, N.S.W. 2308, Australia)

The goniometer technique commonly used for direction finding of VLF has been applied to Pc 1 geomagnetic pulsations. Instrumentation and computer analysis techniques have been developed to determine the source azimuth of structured Pc 1 signals propagating from high to low latitudes in the F2 region duct. Results of the analysis of four events recorded at a low latitude station (L=1.8) will be presented. The secondary sources determined over long duration events may be stationary, or show slow drifts with time. Multiple sources may also be present on some occasions. These results will be interpreted with respect to ionospheric duct properties and magnetospheric propagation and generation theories.

Jupiter, Io
Harbour C
Tuesday P.M.
T. P. Armstrong (Univ. of Kansas), Presiding

SM 154

A COMPARISON OF LOW ENERGY, ≳30 keV, ELECTRON AND ION FLUXES IN THE JOVIAN MAGNETOSPHERE FROM VOYAGERS 1 AND 2 †

T. P. Armstrong* (Dept. of Physics and Astronomy, University of Kansas, Lawrence, KS 66045)

In the energy range from several tens to several hundreds of keV (total) the electron integral flux typically dominates that of the ions. For Voyager I data from the magnetopause through periapsis the electron and ion integral energy spectra typically had similar power law forms with slopes corresponding to about E^{-2}. The electron flux dominated the ion flux by about the ratio of the electron speed to the ion speed. For Voyager 2 the electron spectrum appears to be more steeply falling with energy than for Voyager 1. We will present morphological data on the distribution of these fluxes in energy and versus distance from Jupiter. We will also contrast the simultaneously measured electron and ion anisotropies which show oppositely directed flows at certain times.

SM 155

AN OVERVIEW OF JUPITER'S DECAMETER-WAVE RADIO SPECTRUM AS OBSERVED BY VOYAGER

J. K. Alexander (Laboratory for Extraterrestrial Physics, Goddard Space Flight Center, Greenbelt, MD 20771)
T. D. Carr (Department of Astronomy, University of Florida, Gainesville, FL 32608)
J. W. Warwick (Radiophysics Inc., Boulder, CO 80301)

The Planetary Radio Astronomy instruments on the two Voyager spacecraft obtained dynamic spectral measurements of Jupiter's radio emissions below 40 MHz with unprecedented sensitivity and frequency coverage, and this paper will endeavor to place those new data in perspective. On a time scale of minutes and longer, Jupiter's spectrum above about 1 MHz is dominated by families of drifting structures that appear as sets of nested parentheses or arcs in a frequency-time display. The polarization, shape, sense of curvature and frequency extent of these decametric arcs are generally systematic, predictable functions of System III longitude and phase of Io. We observe Io-related emissions on all occasions (100% occurrence rate) when Io is in one of its favored positions in the longitude-Io phase plane, but we find the relative intensity and occurrence probability of Io independent activity to vary with observer-planet-sun angle. Similarities in the polarization, dynamic spectra and frequency extent of Io-related and Io-independent emissions suggest that both may originate from sources located in the same hemisphere but that they may differ primarily in terms of the total energy and volume involved at a given time. The decametric emission may be due to a series of discrete, localized sources distributed over a significant range in longitude.

SM 156

THE CHARGED PARTICLE POPULATION OF THE INNER JOVIAN MAGNETOSPHERE *

Mark T. Paonessa, Scott T. Brandon, Thomas P. Armstrong (Dept. of Physics and Astronomy, University of Kansas, Lawrence, KS 66045)

Using data from the Voyager 1 charged particle detectors, we have calculated and displayed profiles of the charged particle population of the inner Jovian magnetosphere. Radial profiles of both ions and electrons with energies from hundreds of Kilovolts to a few MeV are presented, as well as angular distributions for these particles. Calculations have also been made of the phase space density f of protons in the inner satellite regions, assuming that these protons diffuse radially while conserving their first and second adiabatic invariants and thus become energized as they approach the planet. The methods of Thomsen (1977) are used to estimate the radial dependence of the diffusion coefficient, and to indicate which processes are mainly responsible for the diffusion.

SM 157

HOT PLASMA IN THE NIGHTSIDE JOVIAN MAGNETOSPHERE

C. G. Maclennan
L. J. Lanzerotti (both at: Bell Telephone Laboratories, Murray Hill, New Jersey 07974)
T. P. Armstrong (University of Kansas, Lawrence, Kansas)
S. M. Krimigis (JHU/Applied Physics Laboratory, Laurel, Maryland 20810)
N. F. Ness
L. F. Burlaga
K. W. Behannon (all at: NASA/GSFC, Greenbelt, Maryland 20771)

We present analysis of data from the hot plasma (Low Energy Charged Particle) experiment on Voyager 2 that demonstrates conclusively that the dynamics of the Jovian plasma sheet at ~80 to ~120 R_J is determined by ions (protons and heavier) of energies ~30keV. The energy densities of these ions are sufficient to provide the observed diamagnetic depressions as the spacecraft crosses the plasma sheet. The hot plasma bulk flow velocities at these distances are less than those expected from pure corotation of the planetary magnetic field.

SM 158

LOW ENERGY ION DISTRIBUTIONS IN THE IO TORUS REGION OF THE JOVIAN MAGNETOSPHERE

L. J. Lanzerotti
C. G. Maclennan (both at: Bell Telephone Laboratories, Murray Hill, New Jersey 07974)
T. P. Armstrong (University of Kansas, Lawrence, Kansas)
S. M. Krimigis (JHU/Applied Physics Laboratory, Laurel, Maryland 20810)
N. F. Ness
R. P. Lepping (both at: NASA/GSFC, Greenbelt, Maryland 20771)

The Low Energy Charged Particle (LECP) and Magnetometer (MAG) experiments on the Voyager 1 spacecraft acquired data during the passage of the spacecraft through the Io torus (in-bound) and Io torus and flux tube (out-bound). The LECP and MAG data are used to study the spatial dependence, in these regions, of the pitch angle distributions of the low energy ions and energetic electrons. The lowest energy ions (E_p ~30-53 keV) have steeper pitch angle distributions in the torus region than do the highest energy ions (E_p ~ 2 MeV). For other regions in the inner Jovian magnetosphere the pitch angle distributions become very flat for all ion energies. These observations will be related to particle scattering mechanisms in Jupiter's inner magnetosphere.

SM 159

HOT PLASMA DENSITY MEASUREMENTS IN THE JOVIAN MAGNETOSPHERE WITH VOYAGERS 1 AND 2

S. M. Krimigis
J. F. Carbary
E. P. Keath (all at: Applied Physics Laboratory, The Johns Hopkins Univ., Laurel, Md. 20810)
L. J. Lanzerotti (Bell Labs, Murray Hill, N. J.)
T. P. Armstrong (U of Kansas, Lawrence, Kansas)
G. Gloeckler (U of Md., College Park, Md. 20742)

The Low Energy Charged Particle (LECP) experiment on Voyager measured electrons ($E \geq 14$ keV) and ions ($E_p \geq 28$ keV) with good energy resolution ($\Delta E/E \sim 0.5$) in seven contiguous directions covering 315° in a plane close to that of the ecliptic during large portions of the spacecraft encounters with the Jovian magnetosphere. Using these measurements, it is possible to evaluate the particle density $N'(\vec{x})$ above the detector energy threshold by using the expression

$$N'(\vec{x}) = \iint d\omega\, dp\, p^2\, W(\vec{x},p,\hat{n}) \qquad (1)$$

$$= 4\pi \int_{E_i}^{\infty} dE\, \frac{j_i(\vec{x},E,\hat{n})}{v_i} < N(\vec{x}) \qquad (2)$$

where $W(\vec{x},p,\hat{n})$ = phase space density, p = momentum, $\hat{n}$ = unit vector, E = particle energy, j_i, v_i are differential intensity and velocity of ith ion species and E_i = detector energy threshold for ith ion species. The quantity $N'(\vec{x})$ is expected to be less than $N(\vec{x})$, if E_i in (2) is > 0. Note that all quantities inside the integral are observables. It is found that during the Voyager 2 encounter, the computed densities are generally less by a factor of ~ 4 than the electron densities measured by the plasma wave investigation (Gurnett et al.,1979) if all ions are assumed to be protons, but are comparable to the electron densities is all ions are assumed to be oxygen. There exist, however, significant departures from this general result in several parts of the magnetosphere. These measurements will be presented and their significance will be discussed.
Gurnett et al., Science, 206, 987, 1979.

SM 160

ANISOTROPIES IN THE OUTER JOVIAN MAGNETOSPHERE

J. F. Carbary
E. P. Keath
S. M. Krimigis (all at: Applied Physics Laboratory, The Johns Hopkins University, Laurel, Maryland 20810)

The Voyager Low Energy Charged Particle instrument (LECP) scans 360° in 8 discreet 45° sectors and can provide accurate measurements of particle anisotropies in the scan plane of the detector. During the Voyager 1 and 2 encounters with Jupiter, the LECP orientation allowed the first measurements of anisotropies in the spin equatorial plane of the planet. Harmonic analyses of observations made in the outer Jovian magnetosphere (beyond ~ 20 R_J) reveal the following ion flow characteristics: (a) Ion anisotropies are predominately first order and in the corotation sense throughout the Jovian magnetosphere. (b) Magnetospheric boundaries such as the bow shock and magnetopause are clearly delineated by changes in the ion flow directions. (c) The first order anisotropy amplitudes increase linearly with radial distance, as would be expected from magnetospheric corotation. In the magnetodisc regions (outbound), the anisotropies were found to decrease linearly with distance away from the disk plane. (d) Anisotropy amplitudes increase dramatically with increasing atomic number. (e) Beyond ~ 150 R_J on the nightside, the ion anisotropies become anti-sunward in an outflow or "wind" region.

SM 161

ON THE POSSIBILITY OF 'INVERSE COMPTON SCATTERING' IN JUPITER'S MAGNETOSPHERIC CAVITY

D. D. Barbosa (Dept. of Physics and Astronomy, The University of Iowa, Iowa City, IA 52242)

During the Jupiter encounter, Voyager spacecraft recorded intense electromagnetic radiation trapped in the low density regions of the Jovian magnetospheric cavity. The source of this newly discovered radiation is as yet unknown. We suggest one mechanism that should be operative which has a direct analogy with the process commonly invoked to explain high-luminosity extragalactic radio sources: inverse Compton scattering (ICS). The photon scatterers, however, are not electrons (Thomson scattering times are on the order of the age of the universe) but the walls of the cavity itself for which the scattering probability is unity and the mean-free-path is the diameter of the cavity.

If the photon reflection occurs at a wall executing random motions for which the ensemble averages $< \beta = v/c > = 0$, $< \beta^2 > \neq 0$, then the process is seen to be also analogous to the classic Fermi process for particle acceleration, in this context a stochastic radar "speed trap" problem. Likely sources for wall oscillatory motions are magnetopause Kelvin-Helmholtz instabilities known to be operative at the Earth's magnetopause.

We show that for this process (1) the photon distribution function satisfies a diffusion equation in frequency identical to the Kompaneets equation for nonrelativistic ICS in the infinite electron mass (recoil-free) limit; (2) the characteristic diffusion times are 9 mos - 2 days for r.m.s. wall quiver velocities $\beta = 10^{-3} - 10^{-2}$; (3) in order to account by this process for the steep frequency spectra observed an absorption mechanism must also be operative in the cavity (a lossy diffusion). Several solutions are shown and further implications discussed.

SM 162

MOST SQUARES ANALYSIS OF PIONEER 11 JUPITER MAGNETOMETER DATA

Patrick R. Mullen (Department of Earth and Space Science, University of California, Los Angeles, California 90024)
Raymond J. Walker(Institute of Geophysics and Planetary Physics, University of California, Los Angeles, California 90024)
Margaret G. Kivelson (Department of Earth and Space Science and Institute of Geophysics and Planetary Physics, University of California, Los Angeles, California 90024)

We have reexamined the models of the intrinsic magnetic field of Jupiter. To do this we first performed a standard least squares inversion of the observations from the Vector Helium Magnetometer on Pioneer 11 including only observations from regions inside of $5R_J$ in order to minimize the effects of currents in the Io torus. We then performed a most squares analysis which used the results of our inversions to explore the space of data-consistent, spherical harmonic models of the intrinsic field. This enabled us to quantify the degree of modeling bias in the inversions. A similar analysis of Pioneer 10 Jupiter observations will enable us to determine the degree to which secular variations of the intrinsic field can be resolved.

SM 163

MAGNETIC PULSATIONS OBSERVED IN THE IO TORUS

Raymond J. Walker (Institute of Geophysics and Planetary Physics, University of California, Los Angeles, California 90024)
Margaret G. Kivelson (Department of Earth and Space Sciences, University of California, Los Angeles, California 90024)

We have searched magnetic field observations for magnetic pulsations in the region of the Io plasma torus. Intervals with magnetic pulsations of periods greater than 30 seconds were found throughout much of the region between 5 R_J and 10 R_J. The oscillations are fairly small (5γ-10γ) and are mainly transverse. Smaller amplitude oscillations cannot be detected because of the uncertainty caused by instrument digitization. The limits on the frequency and amplitude of oscillations in a region of strong field and high number density are discussed.

SM 164

JOVIAN PLASMA ELECTRONS

E. C. Sittler, Jr. (NASA/Goddard Space Flight Center, Laboratory for Extraterrestrial Physics, Greenbelt, MD 20771)
J. D. Scudder

Derived parameters of plasma electrons below 6 keV in zenospace will be presented based on the Voyager Jupiter encounter data. Particular emphasis will be placed on the varying spectral shapes of the electron velocity distribution function which are crucial factors in understanding the bewildering variety of optical and radio emissions that have been reported emanating from Io's torus. The observed distributions show that the electron collisional physics in the torus does not support the usual astrophysical assumption that the electrons are distributed in energy according to a single Maxwellian distribution. In this sense the mean thermal energy of the electrons is rarely the appropriate "temperature" for various collisional lifetime calculations. In principle this situation can permit neutral gases of low ionization potential (such as Na) to be interspersed in multiply ionized Sulfur (with much higher ionization potential). The variations of the hot and colder components of the observed electron plasma are substantial and will be discussed in light of current theories of the torus electrostatic emission which has been used to determine the torus density profile.

SM 165

THE MAGNETIC FIELD OF JUPITER BASED ON PIONEER 11 OBSERVATIONS

J. E. P. Connerney* (Goddard Space Flight Center, Laboratory for Extraterrestrial Physics, Greenbelt, Maryland 20771)

A new method of analysis for the estimation of planetary magnetic fields from flyby magnetic field observations is described and applied to the Pioneer 11 observations of the Jovian magnetic field. The method underscores the uniqueness problems associated with the derivation of spherical harmonic expansions for the internal field and provides a framework for the evaluation of various models and obtainable parameter resolution. Pioneer 11 magnetic field observations obtained by both the vector helium magnetometer experiment and the high-field fluxgate magnetometer are analyzed and new models derived from these data are presented. Extrapolation of the modeled magnetic field to the surface is discussed and isointensity contours of the surface magnetic field magnitude for models compatible with the data are examined. Maximum north polar intensities at the cloud top level ranging from 12 to 16 gauss have been obtained, as well as maximum south polar intensities ranging from 9 to 12 gauss.

SM 166

MODEL OF THE IO PLASMA TORUS FROM IN SITU MEASUREMENTS OF THE PLASMA SCIENCE EXPERIMENT ON VOYAGER 1

Fran Bagenal
James D. Sullivan (both at Center for Space Research, M.I.T., Cambridge, MA 02139

A model of the Io plasma torus has been constructed using the in situ plasma measurements of Voyager 1. The sharp drop in plasma temperature inside of 5.7 R_J divides the torus into a cold inner region where the ions are closely confined to the centrifugal equator and a hotter region centered on the orbit of Io with a thickness scale height of ∿0.5 R_J. In the cold inner region the ion composition is uniquely determined from well-resolved peaks in the energy per charge spectrum. In the hotter region where the spectral peaks overlap, it has been necessary to assume that ions either have a common temperature or a common thermal speed. The resulting composition has a sulphur to oxygen ratio that is larger than that expected from the complete dissociation and ionization of SO_2.

By combining the in situ ion measurement with the O_4 magnetic field model of Acuña and Ness (1976), the local Alfvén velocity has been calculated. The Alfvén velocity rapidly decreases out of the torus. As the plasma rotates past Io, the distance of Io from the centrifugal equator changes so that the transit time of an Alfvén wave generated at Io to reach the ionosphere of Jupiter will vary with the System III longitude of Io. In the shortest transit time (∿230 seconds) inferred, Io would have moved at least 6 Io radii.

SM 167

MODULATION OF THE FRONT SIDE DISC, CROSS AND TAIL CURRENTS IN THE JOVIAN MAGNETOSPHERE: PIONEERS 10 AND 11

D.E. Jones
L.G. Shirley (both at: Dept. of Phys. and Astron. Brigham Young Univ., Provo, Utah 84602)

When the current disc model that fits the Pioneer 10 outbound magnetic field data is applied to the inbound data, a poor fit is obtained. In addition to required changes in both the amplitude and radial dependence of the current distribution in the disc, it is clear that modulation is required. We have considered separately modulation of only the azimuthal current amplitude and distribution, relative modulation of the azimuthal disc and superimposed cross (dusk to dawn) flowing current, and relative modulation of the azimuthal, front side cross, and tail current systems. The results of these model efforts on both the Pioneer 10 and 11 data and their implications will be discussed.

Solar-Planetary Relationships: Solar and Interplanetary Physics

Upstream Waves and Particles

Bay
Saturday P.M.
F. M. Ipavich (Univ. of Maryland), Presiding

SS 1

WHISTLER-MODE WAVES IN THE SOLAR WIND NEAR THE BOW SHOCK

R.W. Frederciks (Space Sciences Dept. TRW Defense & Space Systmes Group, Redondo Beach CA 92078
E.W. Greenstade (Space Sciences Dept.) TRW Defense & Space Systmes Group Redondo Beach, CA 92078
C. T. Russell (Institute of Geophysics & Planetary Physics, University of California, Los Angeles, Los Angeles, California 90024)
F. L. Scarf (Space Sciences Dept., TRW Defense & Space Systems Group, Redondo Beach, California 90278)
R. R. Anderson (Dept. of Physics & Astronomy, University of Iowa, Iowa City, Iowa 52242)
D. A. Gurnett (Institute of Geophysics & Planetary Physics, University of California, Los Angeles, Los Angeles, California 90024; on leave from University of Iowa)

The presence of whistler mode waves in, and upstream from, the bow shock has been well established by observation. Theoretical descriptions of the mode under solar wind conditions have been relatively meagre, however, and it may not be generally appreciated how readily whistler waves generated in the shock could occupy most of the region ahead of the shock most of the time. We present graphic descriptions of phase and group velocities and group velocity directions for typical solar wind parameters over all appropriate frequencies and directions with respect to the IMF. We also illustrate the relations of whistler phase and group velocities to the nominal shock and foreshock boundaries and compare the results with observations by ISEE of bow shock crossings spanning the transition between quasi-perpendicular and quasi-parallel geometry.

SS 2

SIMULATION OF QUASI-PARALLEL BOW SHOCK STRUCTURES

D. W. Forslund (Los Alamos Scientific Laboratory, University of California, Los Alamos, New Mexico 87545)
J. M. Kindel (Los Alamos Scientific Laboratory, University of California, Los Alamos, New Mexico 87545)
E. L. Lindman (Los Alamos Scientific Laboratory, University of California, Los Alamos, New Mexico 87545)

Satellite observations show that when the interplanetary magnetic field is nearly aligned with the bow shock normal rather turbulent shock transitions are observed in which it is in fact difficult to define the location of the shock. The condition that such quasi-parallel structures exist is just the requirement that whistlers can propagate along the shock normal $\hat{n}$: $\frac{1}{2} C_{Ae} \hat{n} \cdot \hat{b} > \vec{U} \cdot \hat{n}$, where C_{Ae} is the electron Alfven speed in the solar wind, $\vec{U}$ is the solar wind velocity vector and $\hat{b}$ is the unit vector along the interplanetary magnetic field. The theory of the decay of large amplitude whistler waves is shown by analysis and computer simulation to explain this transition from nearly laminar to more turbulent shock structures. Details of the nonlinear theory and comparison with satellite observations will be given.

SS 3

UPSTREAM ULF WAVES: IMPLICATIONS OF ISEE WAVE VELOCITY MEASUREMENTS

M. Hoppe
C.T. Russell
D.D. Sentman (all at: Institute of Geophysics and Planetary Physics, University of California, Los Angeles, CA 90024)

Low frequency waves of substantial amplitudes associated with upstream ion populations are a common feature of the earth's foreshock region. It has been difficult, however, to determine the mode of these waves because they are severely Doppler shifted by the supersonic solar wind. We have used data from the dual UCLA magnetometers onboard the co-orbiting ISEE-1 and -2 spacecraft to determine the velocities of such waves. Once these velocities have been determined, Doppler shift effects are removed and the intrinsic rest frame wave properties are determined. One type of such wave is the class of discrete wave packets which have, in the spacecraft frame, frequencies ∿1 Hz and left hand circular polarizations. Velocity measurements provide clear evidence that these waves are intrinsically of right hand polarizations and have rest frame frequencies of several times the proton gyrofrequency. Determination of the character of the more common large amplitude lower frequency (.03 Hz) waves has proven more difficult. Preliminary impressions are that these signals, while well enough organized to yield well defined minimum variance directions, are nevertheless a complex mixture of wave modes and frequencies, whose average velocities are difficult to interpret. Observations are compared with computations of linear dispersion and growth characteristics based on parameterized versions of ion distributions observed by the ISEE LEPEDEA's during periods of wave activity.

SS 4

VOYAGER: OBSERVATION OF FAST MODE MAGNETOACOUSTIC WAVES UPSTREAM OF THE JOVIAN BOW SHOCK

J. M. Jessen (Center for Space Research, Massachusetts Institute of Technology, Cambridge, MA 02139)
J. E. P. Connerney
M. H. Acuña (both at: Laboratory for Extraterrestrial Physics, NASA/Goddard Space Flight Center, Greenbelt, MD 20771)

The Voyager magnetometer and plasma instruments have detected the presence of fast mode magnetoacoustic waves upstream of the Jovian bow shock by Voyager 2. We have observed a strong positive correlation between thermal pressure and magnetic field energy density with typical periods of 5 to 10 minutes. In addition, there is a correlation in plasma velocity $\vec{V}$ and magnetic field $\vec{B}$ which is consistent with fast waves propagating away from Jupiter in the rest frame of the solar wind. The waves usually are observed in low β plasma, where β = (thermal energy density/magnetic energy density). The polarization and angle of propagation of these waves will be discussed.

SS 5

ELECTROSTATIC AND ELECTROMAGNETIC PLASMA WAVES ASSOCIATED WITH UPSTREAM ENERGETIC PLASMA: OBSERVATIONS FROM ISEE-1 AND ISEE-2

R. R. Anderson
T. E. Eastman
D. A. Gurnett
L. A. Frank (all at: Dept. of Physics and Astronomy, Univ. of Iowa, Iowa City, IA 52242)
G. K. Parks (Geophysics Program, Univ. of Washington, Seattle, WA 98195)

In the upstream solar wind three dominant types of VLF plasma waves are observed that are associated with energetic plasma: ion-acoustic waves, electron plasma oscillations, and whistler-mode waves. Ion-acoustic waves occur simultaneously with either a diffuse or beam-like ion component in the energy range from 0.5 to > 45 keV. The spectrum of these short wavelength electrostatic waves has a broad peak covering a doppler-shifted frequency range from a few hundred Hz to many kHz. These waves are impulsive and their amplitudes increase with both increasing flux and anisotropy of the energetic ion population. The electron plasma oscillations are long wavelength electrostatic waves which are nearly monochromatic. They are closely correlated with the flux of low energy electrons, especially in the energy range of 0.5 - 1.5 keV. The onset of electron plasma oscillations and an abrupt increase in low energy electron fluxes occur simultaneously. In the presence of enhanced but non-fluctuating electron fluxes, the intensity of the electron plasma oscillations is steady. In the presence of the diffuse ion component, the electron plasma oscillations appear impulsive. This is probably due to an extremely low frequency wave generated by the diffuse ion population that modulates the electron number density. Electromagnetic waves with frequencies below 200 Hz are observed when either the diffuse or the beam-like ion component is present. The waves are weak and impulsive. Only in the presence of strong ion fluxes does the wave intensity become steady. Some whistler mode waves appear to be associated with electron plasma oscillations.

SS 6

PLASMA AND PLASMA WAVE CHARACTERISTICS OF DIFFUSE IONS IN THE EARTH'S FORESHOCK REGION AND OUTER MAGNETOSHEATH

T. E. Eastman
R. R. Anderson
L. A. Frank
D. A. Gurnett (all of: Dept. of Physics and Astronomy, Univ. of Iowa, Iowa City, IA 52242)
G. K. Parks (Geophysics Program, Univ. of Washington, Seattle, WA 98195)

From a survey of ISEE plasma and plasma wave measurements we have found that the presence of upstream suprathermal (∿ 500 eV to > 45 keV) ions having a broad angular distribution is a sufficient condition for the presence of enhanced ion-acoustic-like electrostatic emissions and electromagnetic waves. This diffuse ion component is observed in the foreshock region where the solar wind field, $\vec{B}_{SW}$, intercepts the bow shock. The energy spectrum and anisotropy of the diffuse ions are highly variable. A beam-like component is frequently intermixed in the diffuse population. These ion beams are observed to be directed both away and towards the bow shock and are often counter-streaming. For brief time intervals (< 30 minutes), this beam-like component is also observed without the diffuse component and is then observed to flow away from the bow shock. Diffuse ions are more frequently observed in the dawn-side foreshock than in the dusk-side foreshock region. Diffuse ions in the foreshock are often present without a corresponding high energy component (∿ 2 - 45 kev) in the magnetosheath although characteristics of this magnetosheath diffuse component indicate a bow shock source. Several examples show a "leakage" of diffuse upstream particles into the outer magnetosheath. Our results indicate that the bow shock plays a crucial role in energizing the diffuse and beam ion populations in the foreshock as well as in the outer magnetosheath. The observed beam-like component in the diffuse population suggests that a double-ion-beam mechanism (Gary, 1978) could explain the presence of ion-acoustic-like electrostatic emissions.

SS 7

ELECTRON VELOCITY DISTRIBUTIONS ASSOCIATED WITH UPSTREAMING PARTICLES FROM THE BOW SHOCK

J. Etcheto (Centre De Recherches En Physique De L'Environnement, 3840 Rue De General Leclerc, 92131 Issy-Les-Moulineaux, France)
J. D. Scudder
K. W. Ogilvie
C. C. Harvey

Three dimensional, high time resolution measurements by the GSFC spectrometer on ISEE-1 in front of the earth's bow shock, resolve for the first time "bump-on-tail" features. These features are associated with upstreaming electrons, reversal of the electron heat flux, and increase of the parallel temperature and anisotropy. Strong bursts of electron plasma oscillations, polarized parallel to the mean magnetic field direction, occur when the spacecraft is on a magnetic field line tangential to the bow shock. The velocity space morphology shows rearrangements on the time scale of 9 seconds, which is very many plasma damping periods. The observations are still far removed from the initial conditions which precipitate the instability. Several striking examples of these effects will be discussed and interpreted.

SS 8

ENERGIZATION OF SOLAR WIND IONS BY REFLECTION FROM THE EARTH'S BOW SHOCK

G. Paschmann
N. Sckopke (both at: Max-Planck-Institut fur extraterrestrische Physik, 8046 Garching)
S. J. Bame
J. R. Asbridge
J. T. Gosling (all at: Los Alamos Scientific Laboratory, Los Alamos, NM 87545)

The existence of ion beams with energies a few times the solar wind energy and streaming outward from the Earth's bow shock has been known for some time. To explain the observed ion energies, a simple reflection model has been proposed in which the particles gain energy by displacement parallel to the interplanetary electric field. In this model, the energy gained in the reflection can be described as a function of the angles between the interplanetary magnetic field, the solar wind velocity and the local shock normal. Ion beams under widely varying conditions have been observed with LASL/MPE instrumentation on ISEE 1 and 2. For 19 cases, with beam energies ranging from ∿ 1.0 to ∿ 23 times the solar wind energy, a comparison between the observed and the predicted beam energies has been made. Good agreement between the reflection theory and the observations has been found. Thus, simple reflection appears to be the dominant energization mechanism for the several keV ion beams observed upstream from the earth's bow shock.

SS 9

CHARACTERISTICS OF REFLECTED AND DIFFUSE UPSTREAM IONS

N. Sckopke
G. Paschmann (both at: Max-Planck-Institut fur extraterrestrische Physik, 8046 Garching)
S. J. Bame
J. R. Asbridge
J. T. Gosling (all at: Los Alamos Scientific Laboratory, Los Alamos, NM 87545)

The distinction between two types of upstream ion populations has been made on the basis of pronounced differences in their distribution functions. The 'reflected' ions represent a fast beam with temperatures around 10^6 K and speeds up to five times the solar wind speed. An important feature of the reflected ion distributions is their strong temperature anisotropy, with $T_\perp$ exceeding $T_\parallel$ by a factor of two or three. In contrast, the 'diffuse' ions occupy a much larger region of phase space, both in energy and angle, often approaching isotropy. Accordingly, their temperature is much larger (∿ 10^7 K), and their bulk speeds typically are smaller than the solar wind speed. Both ion populations have densities of the order of 0.1 cm^{-3}. At times transitions between the

two extremes, represented by the reflected and diffuse ion populations, are observed. These 'intermediate' distributions are crescent shaped, with the center of curvature near the solar wind velocity. This property suggests that the intermediate distributions result from pitch-angle scattering of the reflected beams in the solar wind frame. This observation supports the idea that the reflected ions are the origin of the diffuse ions. Reflected and diffuse ions can also be distinguished by their occurrence as a function of the angle Θ between shock normal and magnetic field. Whereas, the diffuse ions occur predominantly for small Θ, the reflected ions are observed most frequently for $\Theta > 45^{0}$.

SS 10

ON THE ORIGIN OF THE IONS BACKSTREAMING FROM THE EARTH'S BOW SHOCK.

C.Bonifazi
G.Moreno
S.Orsini (all at: Istituto Plasma Spazio, Consiglio Nazionale delle Ricerche, C.P.27, 00044 Frascati, Rome, Italy)

Data supplied by the ISEE 2 solar wind experiment are used to evaluate the basic moments of the "reflected" and "diffuse" ions backstreaming from the earth's bow shock.

An extended statystical analysis shows that the diffuse ion population is characterized by a bulk velocity and mach number lower than those of the reflected one.

The origin of the two ion populations is then investigated, using three different types of approach:

(i) Observed and theoretically predicted locations of the foreshock region boundaries are compared to infer if the diffuse ions undergo a deceleration while travelling upstream through the solar wind.

(ii) The estimated width of the layer where reflected ions are confined allows to establish if the Barnes, 1970 mechanism is effective in destroying the particle beams emerging from the bow shock.

(iii) The presence of reflected and diffuse ions is correlated with the parameters which characterize the shock structure.

SS 11

SIMULATION OF COLLISIONLESS SHOCKS IN THE DUSK SIDE OF THE EARTH'S BOW SHOCK

K. Lee (Los Alamos Scientific Laboratory, University of California, Los Alamos, New Mexico 87545)
D. W. Forslund (Los Alamos Scientific Laboratory, University of California, Los Alamos New Mexico 87545)

Many recent observations indicate the existence of suprathermal ions upstream of the earth's bow shock. One and two dimensional "Particle-In-Cell" simulation codes have been used to study the effectiveness of collisionless shock waves for ion heating at the earth's bow shock. Initial simulation results on perpendicular shocks will be presented. Perpendicular shocks are commonly observed in the dusk side of the earth's bow shock. One dimensional simulations indicate perpendicular shocks can create energetic ions with speed equal to twice the shock speed by reflection off the shock front. However, these reflected ions are turned back downstream by a potential hill at the "foot" of the shock within a scalelength of c/ω_{pi} and are subsequently thermalized. The persistence of this behavior in two dimensions is unknown and is presently being studied and the results will be presented.

SS 12

CHARGE STATE ANALYSIS OF LOW ENERGY HEAVY IONS IN THE VICINITY OF THE EARTH'S BOW SHOCK ON ISEE-1

A.B. Galvin
G. Gloeckler
F.M. Ipavich (all at: Dept. of Physics & Astronomy, Univ. of MD, College Park, MD 20742)
D. Hovestadt
B. Klecker
M. Scholer (all at: Max-Planck-Institut für Physik und Astrophysik, 8046 Garching b., Munchen, FGR)
C.Y. Fan (Univ. of Arizona, Dept. of Physics, Tucson, AX 85721)
L.A. Fisk (Univ. of New Hampshire, Dept. of Physics, Durham, NH 03824)
J.J. O'Gallagher (Enrico Fermi Institute, Univ. of Chicago, 5630 S. Ellis Ave., Chicago, IL 60637)

The ULECA sensor of the Max-Planck-Institut/University of Maryland experiment on ISEE-1 has been designed to measure charge state composition, energy spectra, and anisotropies of energetic ions in the energy range of ∿3 to ∿560 keV per charge. The sensor consists of a mechanical collimator, an electrostatic deflection system, and an array of rectangular solid state detectors. The detector position selects the incident particle's energy per charge, which together with pulse height analysis of the measured energy determines the particle's charge state. We report here the results of the charge state analysis of heavy ions measured by the ULECA M2 detector at ∿65 keV/Q. We will summarize the charge state composition of several particle bursts observed upstream of the earth's bow shock. In general, the composition in these events is similar to that in the solar wind.

SS 13

COMPOSITION AND ENERGY SPECTRA OF LOW ENERGY IONS OBSERVED UPSTREAM OF THE EARTH'S BOW SHOCK

F.M. Ipavich
A.B. Galvin
G. Gloeckler (all at: University of Maryland, Dept. of Physics & Astronomy, College Park, MD 20742)
M. Scholer
D. Hovestadt
B. Klecker (all at: Max-Planck-Institut für extraterr. Physik, 8046 Garching, FRG)

We summarize characteristics of ∿30 particle bursts observed upstream of the earth's bow shock by the ULECA sensor of the Max-Planck-Institut/University of Maryland experiment on ISEE-1, in the energy range from ∿30 to 130 keV per charge. Specifically, we discuss the average values and variances of the composition and energy spectra of these events. We find that the composition is similar to that in the solar wind, and the energy spectra are consistently steeper than power-law. Both the composition and the time profile of different species show an energy-per-charge organization. We discuss the correlation of energy spectra with distance from the bow shock, and also dawn-dusk differences in the particle and magnetic field signatures in individual events.

SS 14

A NEW THEORETICAL APPROACH TO PROPAGATION OF UPSTREAM ENERGETIC PARTICLES

E. C. Roelof (Applied Physics Lab., Johns Hopkins Univ., Laurel, Md. 20810)

The region upstream of the bowshock provides a unique laboratory for the theoretical analysis of energetic particle propagation. We are in the near-source regime and the scattering is often weak, so circumstances can arise in which we may attempt to deduce the functional dependence of the scattering operator upon pitch angle. The mathematical task is simplified by the usually simple configuration of the interplanetary field (IMF). The approximation of a uniform mean field allows the description of the particle distribution function and scattering operator by discrete rather than continuous functions with a consequent significant reduction in mathematical complexity. Also, discontinuous pitch angle distributions (e.g., those with negligible earthward-moving particles) are handled consistently, whereas such distributions are clearly inconsistent with any weak-anisotropy diffusion analysis. The theory has been developed in conjunction with a long-term correlative study of 50-200 keV ion bursts and the IMF observed by IMP 7/8 at ∼ 40 R_e, and application of propagation theory to our 16-sector, 20-second resolution measurements has provided some insights which complement those gained from the ISEE observations. Instantaneous IMF connection to the bowshock is usually necessary, but there is a surprisingly weak dependence on the location of the bowshock connection from the nose to $X_{SE} \leq -20$ R_e. Waves 0.1-0.01 Hz nearly always accompany ion fluxes ≥ 100 $(cm^2 s\ sr)^{-1}$, but the converse is not true. Particle intensities are exponentially related to the cosine of the angle between the IMF and the normal to the bowshock at the point of IMF connection. Pitch angle distributions are often characteristic of a weak scattering regime (with little transverse diffusion). Effects of $\underline{E} \times \underline{B}$ drift, B x VN anisotropy and IMF conditions upstream of the spacecraft are clearly seen.

SS 15

PROPAGATION OF ENERGETIC ELECTRONS IN THE MAGNETOSHEATH AND UPSTREAM SOLAR WIND

I. D. Palmer (on leave at Planetary Sciences Dept., University of Arizona, Tucson, Az 85721)

The propagation of relativistic electrons through the magnetosheath and solar wind is investigated in the two extremes of scatter-free motion and diffusive motion. For a source which is assumed on a field line close to the magnetopause predictions are made of omnidirectional intensity U and anisotropy ξ at different points on the field line in the magnetosheath and upstream solar wind. Both extremes of motion predict in the solar wind a lower U than in the magnetosheath. However, while scatter-free motion always gives greater anisotropy in the solar wind, in the diffusion case it depends on the locations of the comparison stations. The theory has been applied to observations of > 200 KeV electrons, and derived mean free paths λ are $2\text{-}3R_e$ in the magnetosheath, and somewhat higher in the solar wind. There is general agreement (within uncertainties) between the empirical λ and the value obtained from the theory of scattering of charged particles in a turbulent magnetic field based on measured power spectra.

Three-Dimensional Structure of the Heliosphere

Pier 7 & 8
Monday A.M.
Edward J. Smith (JPL), Presiding

SS 16

MODELS OF POLAR CORONAL HOLES UNDER VARYING MAGNETIC FIELD STRENGTH

S. T. Suess (Space Environment Laboratory, NOAA/ERL, Boulder, CO 80303)
R. S. Steinolfson (P.O. Box 1247, University of Alabama, Huntsville, AL 35807

Stable global coronal models are constructed by numerically solving an initial value problem. We assume axisymmetric, polytropic, single-fluid flow and specify the temperature, density, and magnetic field at the lower boundary. In our first series of calculations, we have held constant the temperature, density, and functional variation of the magnetic field (dipolar) at the lower boundary, along with the polytropic index (1.05). The field strength was then systematically varied by more than a factor of 6. We find that the size of the resultant "coronal hole" varies proportionally less, both at the base and at $5R_0$, than does the field strength. More interesting is the temperature and velocity structure between 2 and $4R_0$, which shows an apparent "Bernoulli effect" where the high flow velocity at the center of the hole causes the fieldlines to diverge less rapidly than as r^{-2}, leading to increasing temperature and pressure with radius for high base field strengths!

SS 17

SOLAR WIND VELOCITY HISTORIES AT FIXED LONGITUDES

R. E. Gold
E. C. Roelof (both at: Applied Physics Laboratory, The Johns Hopkins U., Laurel, Md. 20810)

We have developed a technique to follow the evolution of solar wind emission at a given longitude for extended periods. The solar wind velocity data from near earth spacecraft and from Pioneers 6 through 9 have been mapped back to the high corona using the instantaneous constant velocity approximation. The velocity data were then binned according to their heliographic emission longitude and emission time. Histories were constructed at fixed longitudes to examine the evolution and variability of the solar wind with a resolution of up to 5 samples per solar rotation. This technique reveals that expression of the velocity histories in terms of emission time provides a significant improvement in spatial and temporal separation over the conventional mapped velocity picture since temporal features stand out clearly in spite of the variable travel time for the solar wind to reach 1 AU. Preliminary analysis has shown that the longitudinal extent of many temporal solar wind events is $\geq 75°$. It has also shown that velocity structures which form recurrent series at a single spacecraft may reveal significant time variability when sampled several times per solar rotation. A preliminary search for meridional velocity structures in the $\pm 7.25°$ range about the solar equator found significant effects in the rising, peak, and decaying phases of solar cycle 20.

SS 18

THE RADIAL VARIATION OF SOLAR WIND PARAMETERS FROM 1 TO 5 AU

A. J. Lazarus
J. M. Jessen
C. C. Goodrich
J. D. Sullivan
J. W. Belcher (all at Department of Physics and Center for Space Research, M.I.T., Cambridge, MA 02139)
K. W. Ogilvie (Laboratory for Extraterrestrial Physics, NASA/Goddard Space Flight Center, Greenbelt, MD 20771)

A comparison of observations from the IMP 8 spacecraft (at 1 AU) with observations from the Voyager 1 and 2 spacecraft (out to 5 AU) allows determination of the radial variation of the parameters characterizing the positive ion component of the solar wind. The use of 1 AU data aids the separation of temporal from radial variations of the freely expanding plasma. Beyond 3 AU, forward-reverse shock pairs become common features of the leading portion of high-speed streams. Comparison of observations from Voyager 1 and 2 allow us to study the radial evolution of the plasma in the interaction region between the shock pairs.

SS 19

THE ORIGIN OF THE WARPED HELIOSPHERIC CURRENT SHEET

J.T. Hoeksema
P.H. Scherrer
J.M. Wilcox (all at Inst. for Plasma Research, Stanford University, Stanford, CA 94305)

The warped heliospheric current sheet in early 1976 is calculated from the observed photospheric magnetic field using a potential field method. Comparisons with measurements of the interplanetary magnetic field polarity in early 1976 obtained at several locations in the heliosphere at Helios I, Helios II, Pioneer XI and Earth show a rather detailed agreement between the computed current sheet and the observations. It appears that the large-scale structure of the warped heliospheric current sheet is determined by the structure of the photospheric magnetic field, and that "ballerina skirt" effects may add small-scale ripples.

SS 20

A NEW MID-LATITUDE SOLAR MAGNETIC FEATURE

P.H. Scherrer
J.T. Hoeksema
J.M. Wilcox (all at Inst. for Plasma Research, Stanford University, Stanford, CA 94305

A new solar magnetic feature was observed at midlatitudes in both solar hemispheres about one year after sunspot minimum. The new feature is a two sector structure with a synoptic rotation period near 29 days. At the time this new solar feature appeared the interplanetary magnetic structure changed from four sectors with a 27 day period to two sectors with an approximately 28 day period. The influence of the new solar magnetic feature on the interplanetary magnetic field and the heliospheric current sheet will be discussed.

SS 21

THE STRUCTURE OF THE INTERPLANETARY MAGNETIC FIELD AND ITS INFLUENCE ON COSMIC RAY PROPAGATION

B. T. Thomas (Jet Propulsion Laboratory, California Institute of Technology, Pasadena, California 91103)

The Pioneer 10 and 11 spacecraft have provided a large quantity of data at large heliocentric distances and it is now possible to build a reasonably accurate picture of the large scale structure of the interplanetary magnetic field. It has become clear that the sector structure observed in the solar wind is due to the presence of an equatorial current sheet in the heliosphere which is tilted with respect to the rotation axis of the Sun. The fast streams observed near 1 AU evolve into clearly defined interaction regions characterized by high field magnitudes and accompanied by forward and reverse hydromagnetic shocks. Recent results suggest that the current sheet develops a stable 'wavy' structure in the outflowing solar wind due to the rotation of the Sun. At higher heliographic latitudes, some idea of the magnetic field configuration can be deduced from the plasma velocities inferred from IPS measurements.

Recent work suggests that the motion of cosmic rays in the heliosphere is significantly affected by the three dimensional structure of the interplanetary magnetic field. The nature of this relationship is discussed. In particular, the tilt of the equatorial current sheet is known to display a solar cycle variation and it is suggested that this may account for much of the 11-year variation in the intensity of cosmic rays at 1 AU.

SS 22

COSMIC RAY MODULATION DUE TO A WARPED INTERPLANETARY CURRENT SHEET

J. R. Jokipii (Lunar and Planetary Laboratory, Dept. of Planetary Sciences, University of Arizona, Tucson, Az. 85721)
Barry Thomas (Jet Propulsion Laboratory, 4800 Oak Grove Drive, Pasadena, Ca. 91103)

Observational evidence is presented for a model of the heliospheric magnetic field which consists of oppositely directed Archimedean spirals above and below a warped equatorial current sheet. The warp of the sheet is inferred to increase from solar minimum to solar maximum.

The non-diffusive propagation model, which was shown previously to provide a reasonable approximation to modulation in the presence of drifts (e.g., Jokipii and Kopriva, Ap. J. 234, 384), is extended to 3-dimensions (r,θ,ϕ). It is applied to the inferred interplanetary magnetic field. We find that the change in solar modulation of ~ 2 GeV protons caused by an increase in warp from ~ 10° to ~ 35° approximately the same as that seen as one goes from solar minimum to solar maximum.

We conclude that one possible cause of the change in solar modulation of galactic cosmic rays from solar maximum to solar minimum is the change in warp of the current sheet.

SS 23

THE EFFECTS OF PARTICLE DRIFTS AND DIFFUSION ON THE MOTION OF COSMIC RAYS IN THE HELIOSPHERE

Ruth Gall (Instituto de Geofisica, Univerdidad Nacional Autonoma de Mexico, Mexico 20, D. F., Mexico)
B. T. Thomas (Jet Propulsion Laboratory, California Institute of Technology, Pasadena, CA 91103)

The time histories of cosmic rays arriving at the Earth are investigated with the help of mathematical models of the interplanetary magnetic field. Several semi-realistic models of the field are used. The models involve a simple Parker spiral field in which can be included a flat or 'wavy' equatorial current sheet and/or fully developed corotating interaction regions bounded by forward and reverse hydromagnetic shocks. The objectives are to determine the effect on cosmic ray propagation of the structure of the equatorial current sheet and of the presence of corotating interaction regions. The particle motions are determined at several rigidities using plausible values of the parallel diffusion coefficient. The relative importance of drift motions and diffusion is discussed.

SS 24

COSMIC RAY EVIDENCE FOR THE HELIOSPHERE MODELS

H. S. AHLUWALIA, Dept. of Physics and Astronomy, The University of New Mexico, Albuquerque, N.M. 87131

We have studied the profiles of the eleven year variation of the cosmic ray intensity over nearly five solar activity cycles, using the data from the global network of the neutron and the muon detectors. Two distinct recovery modes are apparent in the data. During "odd" activity cycles cosmic ray intensity recovers, to its solar activity minimum level, in 6 to 8 years. During "even" activity cycles the recovery of the cosmic ray intensity takes place in 2 to 3 years. We suggest two model configurations for the heliosphere to help us understand these characteristic recovery modes. The models imply the existence of at least two modulating regions. In one region we expect the conventional type of modulation to be obtainable. In the other region modulation is expected to be more dynamic. Some recent low energy particle data, obtained with spacecrafts, can be understood on the basis of the proposed models. We are able to place some constraints on the "roughness" of the interstellar magnetic field. Moreover, our insights help us in predicting the epochs of the solar polar field reversals. These predictions are compared with those made by the technique of counting the solar polar faculae. Our results are discussed.

SS 25

THE ENERGY SPECTRUM AND GRADIENT OF LOW-ENERGY ELECTRONS AT LARGE HELIOCENTRIC DISTANCE*

J. H. Eraker (Enrico Fermi Institute and Department of Physics, University of Chicago, Chicago, Illinois 60637)

Fluxes of low-energy (1.75-25 MeV) interplanetary electrons observed by the Pioneer 10 spacecraft over the radial range from 1 to 21 AU are presented. With the exception of solar flare electrons, Jovian electron increases are the predominant component of the 1-25 MeV interplanetary electron flux at heliocentric distances less than 10 AU. It is of particular interest to establish the origin of the low-energy interplanetary electron flux beyond 10 AU where no Jovian electron increases are observed and consequently where ideal conditions exist to search for fluxes of low-energy electrons of galactic origin. We find that the slope of the low-energy differential electron spectrum is approximately independent of electron intensity over the entire radial range from 1-21 AU and is well described by a power-law with spectral index ~ 2. Beyond 10 AU the low-energy electron intensity is approximately independent of heliocentric distance and comparable to the minimum low-energy electron intensity at the orbit of Earth near the period of the minimum in the solar activity cycle. The origin of the low-

energy electron flux beyond 10 AU is discussed in terms of the alternate hypotheses of an isotropic Jovian electron flux or a modulated galactic electron flux. A new upper limit is placed on the magnitude of the low-energy interstellar electron spectrum.

Sun and Solar Wind

Pier 7 & 8
Tuesday A.M.
J. A. Joselyn (NOAA), Presiding

SS 26

AIRBORNE OBSERVATION OF THE EXTREME SOLAR LIMB TO HIGH ANGULAR RESOLUTION AT SUBMILLIMETER WAVELENGTHS

T.A. Clark, (Physics Dept., University of Calgary, Alberta, Canada, T2N 1N4)
Rita T. Boreiko, (Physics Dept., University of Calgary, Alberta, Canada T2N 1N4)
(Sponsor: L.L. Cogger).

The airborne submillimeter observation of the total solar eclipse of February 26th 1979 from the NASA Lear Jet Observatory was utilized to provide a high angular resolution scan of the extreme solar limb, thereby simultaneously overcoming the severe limitations imposed upon conventional ground-based disk scans by diffraction and atmospheric absorption at these wavelengths. Photometry at 25 cm^{-1} (400 μm) produced an eclipse curve which matches most closely that produced by a uniform distribution of radiation across the disk. This is in distinct contrast to the result from the only other equivalent experiment from Concorde aircraft over Africa in the 1973 eclipse, in which a very sharp and intense spike of radiation at the limb was detected. The result is also in conflict with the limb brightening expected on the basis of homogenous atmospheric models of the sun, and indicates that inhomogeneity is still important even in the low chromosphere of the sun.

SS 27

DISAPPEARING SOLAR FILAMENTS: A USEFUL PRECURSOR OF GEOMAGNETIC ACTIVITY

J. A. Joselyn (NOAA Space Environment Lab, Boulder, CO., 80303)

"Disparition Brusque" (DB), or disappearing solar filaments, have long been suspected as an indicator of terrestrial magnetic disturbances. However, because DBs are a relatively common solar event (certainly more common than geomagnetic storms) and because DBs failed as a candidate source for M-region (recurrent) magnetic disturbances, the potential utility of disappearing filaments as a forecasting aid has largely been neglected. This revival of the DB-magnetic storm association is based on several factors. First, the two largest storms so far in this solar cycle can only be traced to DB events; the many recent papers studying SKYLAB and other observations of coronal transients always find a strong correlation between those transients and eruptive prominences and/or filament disappearances; and solar wind plasma measurements coupled with the observation that many of the DB associated storms begin gradually (no sudden commencement) imply a distinctly non-flare (cool) source for the impacting material. By analyzing the physical characteristics of those DBs which preceed magnetic storms and those that do not, some forecaster "rules of thumb" have been developed which are based on the filament's location and orientation with respect to the background photospheric magnetic field. Basically we look for evidence of a significant restructuring of the implied coronal magnetic field which could lead to a release of geoeffective solar wind plasma.

SS 28

The Dispersal of the Solar Nebula

Steven Nerney (San Francisco State Univ., San Francisco CA 94132 & NASA-Ames, Moffett Field CA)
(Sponsor: Aaron Barnes)

Early in the history of the solar system, the sun may have gone through a T-Tauri phase with an intense solar wind. Such a wind may have blown away the gas of a proto-planetary cloud in which the sun was embedded. However, simple momentum considerations suggest that momentum transfer is not effective in dispersing the nebula unless the wind can peel off successive layers of the nebula. The wind has sufficient energy to disperse the cloud if the process of converting wind energy into outflow energy of the nebula is efficient. The formation of a shock at the wind-nebula interface can limit the efficiency of the dispersal process. If the sun were rotating fast enough, the combination of rotation and magnetic acceleration could increase the terminal velocity of the wind. The resulting increase in wind energy may allow less efficient energy conversion mechanisms to disperse the nebula over the life-time of a T-Tauri phase.

SS 29

THEORETICAL CONSIDERATIONS IN MEASURING THE SUN'S ANGULAR MOMENTUM LOSS IN THE SOLAR WIND

V. Pizzo (High Altitude Observatory, NCAR, Boulder, Colorado 80307, U.S.A.)

A reliable determination of the loss rate of angular momentum from the sun would be of considerable astrophysical significance, as this number figures in many theories of stellar evolution. In principle, the HELIOS solar wind observations provide the best opportunity for in situ measurement of this elusive quantity. However, preliminary studies at MPAE indicate that important theoretical considerations must be faced before the data can be meaningfully analyzed. Because the distribution of angular momentum flux density is systematically correlated with large scale solar wind structure, variations in the flux cannot be treated simply as random noise on a smooth, static background. Rather, explicit account must be taken of the dynamical rearrangement of flux between source and observer due to stream interactions. Numerical models suggest that stream evolution may cause so much latitudinal transport of angular momentum that what is measured at a given latitude at 1.0 AU may bear no relation to that which was present at the same latitude near the sun. Attempts to circumvent these difficulties by using HELIOS close-pass (0.3 AU) data encounter another problem. Because alpha and proton speeds there can differ by as much as 150 km/s, the requirement that both species be field-aligned in the rotating frame means that their respective flow angles in the inertial frame must be quite different. Though the alpha density is low, their angular momentum flux density is comparable to that of the protons, and therefore measurement of the total flux must include contributions from both species as well as the field. Finally, determination of the flux loss rate hinges upon an ability to accurately fix the absolute orientation of the spacecraft reference frame, a pursuit in which certain theoretical relations between field and flow may prove useful.

SS 30

INTERPLANETARY IONS DURING AN ENERGETIC STORM PARTICLE EVENT: THE DISTRIBUTION FUNCTION FROM 400 eV TO 1.6 MeV

J. T. Gosling
J. R. Asbridge
S. J. Bame
W. C. Feldman
R. D. Zwickl (all at: University of California, Los Alamos Scientific Laboratory Los Alamos, New Mexico 87545
G. Paschmann
N. Sckopke (both at Max Planck Institut für Physik und Astrophysik Institut für Extraterrestrische Physik, 8046 Garching W. Germany

Data from the LASL/MPI fast plasma experiment on ISEE-2 have been combined with data from the ESA/IC/SRL low energy proton experiment on ISEE-3 to obtain for the first time an ion velocity distribution function, f(v), extending from solar wind energies (≈1 keV) to 1.6 MeV during the post-shock phase of an energetic storm particle event. The energetic ion f(v) extends continuously with ever decreasing values and without an intermediate peak from solar wind energies out to 1.6 MeV; however, a significant change in slope occurs near 400 keV, f(v) showing an $E^{-2.5}$ dependence below and an $E^{-5.5}$ dependence above ≈400 keV in the solar wind frame. These observations suggest that the energetic storm particles found behind interplanetary shocks are most probably accelerated directly out of the solar wind thermal population or its suprathermal tail by some process associated with the shock wave disturbance.

SS 31

EXTRATHERMAL SOLAR WIND ELECTRONS: BACKSCATTERING LIMITS DUE TO ELECTRON-ELECTRON COLLISIONS

B. E. Goldstein (Jet Propulsion Laboratory, California Institute of Technology, Pasadena, CA 91103)

The extrathermal (70 ev and greater) solar wind electrons traveling toward the sun have been attributed (Scudder and Olbert, 1979) to Coulomb backscattering of electrons originating in the corona. The calculation of Scudder and Olbert assumed that electrons travel either parallel or antiparallel to the magnetic field. Lemons and Feldman (1979) have investigated modifications to an exospheric distribution of electrons, but used a realistic collision operator that included the pitch angle distribution. Both these studies assumed that the energy of an extrathermal electron is conserved in individual scattering events. However, electron-electron collisions result in an energy loss time about twice the 90° pitch angle scattering time. As the spectrum is steeply sloped in the extrathermal region, energy loss will dominate pitch angle scattering effects. If only Coulomb collisions were important, the source of solar traveling extrathermal electrons would be dominated by single, large-angle collisions with protons (i.e., failure of the Fokker-Planck approximation). A very crude estimate of the ratio of backward traveling (pitch angles less than 45°) to forward traveling electrons is 0.007. As the observed ratio is 0.180, the high energy particle scattering must be dominated by wave-particle interactions.

SS 32

CRITICAL PARALLEL ELECTRICAL FIELDS IN ASTROPHYSICAL PLASMAS: A HYPOTHESIS

J. D. Scudder (NASA/Goddard Space Flight Center, Laboratory for Extraterrestrial Physics, Greenbelt, MD 20771)

This paper presents some general considerations about the need for and the limits on electric fields parallel to the local magnetic field in steady, inhomogeneous astrophysical plasmas. These general ideas are then made concrete by studying the solar wind as a prototype plasma in this class. The working hypothesis of this presentation is that the parallel electric fields are limited both from above and below to be of the order of the Dreicer, or critical electric field. Under typical 1 AU conditions this hypothesis is certainly supported. The numerical implications for extending this hypothesis to apply at all radial distances will be graphically presented for a solar wind expansion with and without magnetic fields. This extended hypothesis yields a non-local equation of state for the electrons which is of the type discussed by Scudder and Olbert (1979a,b). A brief discussion of the possible time dependent response of a system that is perturbed away from this steady equilibrium will be suggested touching briefly on aurora, coronal x-ray bright points, interplanetary whistler packets, and the strahl in the solar wind electron velocity distribution function.

SS 33

REVISED RESUBMITTED

SINGLY CHARGED HELIUM IN THE SOLAR WIND

C. J. Vogt (Univ. of Maryland, College Park, MD 20742)
K. W. Ogilvie

Singly charged Helium has previously been observed uncertainly in the solar wind. The ISEE-3 ion spectrometer has detected intermittent fluxes of ions at M/Q = 4 ± .03 since launch in August 1978, under a wide variety of solar wind conditions. Using a model solar wind, the importance of Si and Sulphur ions in

producing these fluxes can be discussed, and we can determine whether unrealistic coronal conditions would be required to explain the observations in the absence of Helium. The observed maximum in frequency of occurrence of these fluxes does not coincide with the time expected assuming the source to be only interstellar neutral Helium gravitationally focused by the sun. A study of the variations of this flux may be expected to indicate how it is linked with solar activity.

SS 34

OBSERVATIONS OF LARGE FLUXES OF He^+ IN THE SOLAR WIND FOLLOWING AN INTERPLANETARY SHOCK

S. J. Bame
J. R. Asbridge
W. C. Feldman
J. T. Gosling
R. D. Zwickl (all at: Los Alamos Scientific Laboratory, Los Alamos, NM 87545)

LASL instrumentation on IMP 7 has detected large fluxes of He^+ within that volume of solar wind plasma believed to be the solar ejecta driving the interplanetary shock wave disturbance of 29 July 1977. The very high He^+/He^{++} abundance ratio of 0.3 measured during this event suggests that this was solar prominence material only partially ionized by its passage through the corona.

SS 35

HEAVY SOLAR WIND IONS IN HIGH SPEED STREAMS MEASURED BY IMP 7/8 EPE SOLID STATE DETECTORS

D. G. Mitchell
E. C. Roelof (both at: Applied Physics Lab., Johns Hopkins Univ., Laurel, Md. 20810)

During periods of high solar wind speed (> 550 km/sec) the 20 second-sampled count rate increases strongly with solar wind velocity in the two sunward sectors of the 16-sector 50-200 keV proton channel of the IMP-7 and 8 NOAA/APL Energetic Particle Experiment (EPE) of D. J. Williams and C. O. Bostrom. This detector is surfaced with $\sim 60\ \mu g/cm^2$ of aluminum which makes it insensitive to quiet-time solar E/M radiation and represents a dead-layer of ~ 20 keV for protons, with a 30 keV electronic threshold silicon detector behind it. At high solar wind speeds (determined from NSSDC hourly averages), the detector can respond to heavy ions in the thermal plasma. However the net detector efficiency in measuring these ions should be very low, as it depends on straggling in the dead layer and is further reduced by pulse-height defect. If J is the measured ion flux > 50 keV and NV is the solar wind proton flux, then $R = J/NV = \Sigma E_A f_A$, where f_A is the abundance ratio for ions of atomic number A, and E_A is the detector efficiency for that species. In practice we find that R increases by a factor of ~ 30 as V goes from 600 to 800 km/sec. At $V \simeq 800$ km/sec, $\log R \simeq -5 \pm 0.5$, and the velocity dependence of the ion flux is reproducible for 25 events from the two recurrent series of high velocity streams in 1974-75. Assuming coronal abundances, the measured $R \sim 10^{-5}$ at 800 km/sec would require 2% efficiency in detecting ^{16}O, or even greater efficiency in detecting Mg, Si, S, Ne, and Fe, all with abundances $f_A \sim 3 \times 10^{-5}$. Though we cannot presently account for the apparent high efficiency, other observational tests are consistent with the detection of SW heavy ions. Accelerator calibrations on similar detectors are in progress to clarify the issue.

SS 36

CORONAL TEMPERATURES INFERRED FROM SOLAR WIND OXYGEN MEASUREMENTS

M. Coplan (Univ. of Maryland, College Park, MD 20742)
K. W. Ogilvie
J. Geiss
P. Bochsler

The ISEE-3 ion composition experiment can make M/Q measurements over the solar wind speed range between 300 and 600 km sec^{-1}. A data set has been compiled for the period August 1978 to June 1979 (by adding M/Q spectra for 25 km sec^{-1} speed intervals) for the study of average properties of the solar wind over that range. We have determined the ratios between the observed fluxes in the M/Q = 2.29 and 2.67 regions as a function of solar wind speed, and compared them with the predictions of a model incorporating charge states of the most abundant species (including Silicon and Sulphur) as a function of coronal temperature. At speeds below $\sim$ 450 km sec^{-1} the observations are consistent with $Tc = 1.6 \pm 0.1 \times 10^{6}$°K, but above 450 km sec^{-1}, the predicted temperature rises rapidly. This rise is interpreted in terms of a lack of local thermodynamic equilibrium in the source region of the solar wind.

SS 37

ISEE-3 OBSERVATIONS OF INTERPLANETARY SHOCKS

E. J. Smith (Jet Propulsion Laboratory, California Institute of Technology, Pasadena CA 91103)
D. Winterhalter (Jet Propulsion Laboratory, California Institute of Technology, Pasadena, CA 91103; University of California, Los Angeles, CA 90024)

We report on observations of interplanetary shocks by the ISEE-3 Vector Helium Magnetometer in the time interval between launch (August 1978) and spring 1979. There appears to be a large number of shocks in this interval presumably associated with the current solar maximum. The correlation of these shocks with solar activity such as flares and high speed streams is described. Calculations of shock normals and the solar wind data in the ISEE data pool are used to infer shock characteristics and geometries. Several slow shocks appear to have been observed.

SS 38

PLASMA WAVE NOISE SURROUNDING INTERPLANETARY SHOCKS AT ISEE 3

E. W. Greenstadt (Space Sciences Dept., TRW Defense & Space Systems Group, Redondo Beach, California 92078)
F. L. Scarf (Space Sciences Dept., TRW Defense & Space Systems Group, Redondo Beach, California 92078)
E. J. Smith (Jet Propulsion Laboratory, Pasadena, California 90278)

Interplanetary shocks are commonly preceded, and followed, by hours of plasma wave peak-noise above background at frequencies from several hundred to several thousand Hz. The noise exhibits significant temporal structure including abrupt appearances and disappearances associated with shifts in IMF orientation. We attempt to trace the instantaneous IMF to the moving shock through continuous field line connection to show that the variations in noise may be related to variations in paths of shock-generated suprathermal particle streams.

SS 39

CONVECTIVE NATURE OF TRANSIENT SOLAR WIND PHENOMENA OBSERVED BY ISEE-3 AND ISEE-1

R. D. Zwickl, J. R. Asbridge, S. J. Bame, W. C. Feldman, J. T. Gosling (all at: University of California, Los Alamos Scientific Laboratory, Los Alamos, New Mexico 87545)

ISEE-3 and ISEE-1 data measured shortly after launch of ISEE-3 (Aug., 1978) were examined with the idea of determining the spatial extent of, as well as possible evolutionary changes in, small scale plasma structures embedded in the ambient solar wind flow. During this time interval the two spacecraft separation increased from very small distances to $\sim$ 0.01 AU ($\sim$ 1 hour convection time). For the purpose of this study a "transient phenomenon" was defined as a sudden ($\leq$ 1 minute) but distinct change in any or all of the calculated bulk flow parameters velocity, density, and flow direction. During the first three months after launch 34 transient events were observed by ISEE-3 in which comparable 24 second time resolution was available from ISEE-1. Preliminary analysis show: 1) all but one of the events were observed by ISEE-1; 2) several events convected unchanged from ISEE-3 to ISEE-1 within a time resolution of 24 seconds; 3) two small events showed distinct temporal evolution of the density profile; 4) only the flow direction showed statistically significant variations. Additionally, several events with velocity and density enhancements were found with ISEE-1 in the magnetosheath just prior to but emerged within 10 minutes after the expected arrival time.

SS 40

AN ANALYSIS OF ALFVEN WAVES BEYOND 1 AU

B. T. Thomas (Jet Propulsion Laboratory, California Institute of Technology, Pasadena, CA 91103)
B. T. Tsurutani
E. J. Smith

Alfvén waves have been identified in the data provided by the Pioneer 10 spacecraft. Variance analyses and correlations between plasma and magnetic field data have been used to investigate their nature. Much of the theory relating to Alfvén waves is concerned with circularly polarized, transverse waves in which the perturbation vector is perpendicular to the mean field. The minimum variance direction is therefore parallel to the mean field and in the direction of propagation. It is suggested, however, that many of the waves observed in the Pioneer data are non-transverse and indeed certain examples appear to be plane-polarized, in which case the minimum variance direction will be perpendicular to the direction of propagation. It is concluded, therefore, that the minimum variance direction is in general an unreliable guide to the direction of propagation.

SS 41

NON-WKB MHD WAVES IN THE SOLAR WIND

M. Heinemann (Department of Physics, Boston College, Chestnut Hill, Mass. 02167)

A method of computing amplitudes of undamped, linear, non-WKB MHD waves in the corona and solar wind is described. The mathematical approach is to write the ideal MHD equations in terms of the Lagrangian displacement of a fluid element. The resulting set of three coupled second order partial differential equations governs the amplitudes of coupled fast, Alfven, and slow mode waves. For the special case of spherically symmetric background flow with radial field lines, expansion in terms of spherical harmonics leads to coupled longitudinal and transverse compressional waves and to uncoupled Alfven waves. The wave action of the Alfven waves and the coupled compressional waves is conserved. The transverse and Alfven equations have singularities at the Alfven point while the longitudinal equation has a singularity at the Parker point; nonvanishing solutions must pass through the appropriate points. Because of the difficulty of passing through two critical points, solutions of the compressional equations are given only for the case of a cold plasma; they describe a cold fast mode wave. Numerical solutions for the fast and Alfven modes are compared to the observed solar wind coherence of transverse fluctuations. The behavior of the coherence is characteristic of significant amounts of inward propagating power in both the Alfven and fast modes for wave periods greater than about a day.

SS 42

POWER SPECTRA OF LARGE AMPLITUDE ALFVÉNIC VARIATIONS IN THE INTERPLANETARY MAGNETIC FIELD

B.R. Lichtenstein
C.P. Sonett (Both at Lunar and Planetary Laboratory, University of Arizona, Tucson, AZ 85721)

Power spectra of large amplitude Alfvénic variations in the interplanetary magnetic field are calculated in the principal axes coordinate system determined by diagonalization of the variance matrix. Power spectra of the magnetic field components in this variance coordinate system is found to be more amenable to interpretation based on the theoretical predictions for large amplitude waves in the hydromagnetic approximation. In general, we find that when there is a well defined minimum variance direction, the spectra of the field component in the minimum variance direction and the field magnitude are similar, as are the spectra for the two field components perpendicular to the minimum variance direction. In addition to there being less power in the former two spectra, their spectral slopes are flatter than for the two magnetic field components perpendicular to the minimum variance direction. These latter two spectra have

characteristics which vary according to the nature of the dynamic magnetic structure of the field variations. For more fully three-dimensional local behavior all three components of the magnetic field in the variance coordinates have similar spectral properties which are still distinct from those of the field magnitude.

Solar Luminosity Variations

Pier 7 & 8
Tuesday P.M.
J. A. Eddy (High Altitude Observatory), Presiding

SS 43 INVITED PAPER

SOLAR LUMINOSITY VARIATION ON HUMAN TIME SCALES; OBSERVATIONAL EVIDENCE AND BASIC MECHANISMS

P. Foukal (Atmospheric and Environmental Research, Inc., Cambridge, MA 02139

We review the time behavior of total solar luminosity on time scales between minutes and tens of years. Large relative changes of radiative flux in the X-ray, ultraviolet and radio-frequency regions, associated with magnetic activity, almost certainly represent low level variations of total luminosity below $1x10^{-4}$ of the solar constant. Direct radiometry of the solar constant between 1962 and 1979 shows some evidence for an increase of about 0.4% since 1968. Recent statistical analysis of the daily measuremetns of solar flux carried out between 1923 and 1952 by the Smithsonian Institution (APO) indicate an influence of magnetic fields on solar flux on short time scales of days. The amplitude of this modulation by sunspots and faculae is at the level of $7x10^{-4}$ of the solar constant. Some interesting indirect techniques for monitoring the solar luminosity will be briefly described. A number of mechanisms could cause detectable variations of luminosity on human time scales. For instance, changes in sunspot magnetic flux tubes are expected to perturb heat flow to the photosphere, yielding a modulation of luminosity on time scales of days. Heat flow diversion into kinetic and potential energy of global scale could produce slower variations of convective efficiency. Study of the rapid changes will help us understand why the sun's luminosity varies while we record solar constant behavior on the longer time scales useful to climate studies.

SS 44 INVITED PAPER

EVIDENCE FOR LUMINOSITY VARIATIONS OF COOL, SOLAR-LIKE STARS

L. Hartmann (Center for Astrophysics, 60 Garden St., Cambridge, MA 02138)
(Sponsor: P. Foukal)

Although observations of stars much like the Sun have failed to turn up luminosity variations to an accuracy of about one percent, studies of somewhat cooler stars present strong evidence for appreciable changes in their emitted radiation. These stars are rotating more rapidly than the Sun and/or are younger, and exhibit much enhanced examples of many kinds of solar activity, such as flares. The surface brightness distributions on these stars are nonuniform; dark areas are called "spots" in solar analogy. Areas of up to 30% of a hemisphere may be covered by such spots, again indicating activity on a far greater scale than typical of the Sun.

Despite the lack of definitive bolometric observations, the detection of visual light variations on the order of 30% may be translated into total luminosity variations $\sim$ 10% with reasonable confidence. Spots may appear or decay over timescales of days, but longer-term trends exist, with timescales of decades. No evidence for cycles $\sim$ 11 years has been detected, although other cool stars of generally greater age and slower rotation exhibit evidence for decade periods in other tracers of activity. The observations of dramatic luminosity variation in stars with extreme examples of solar activity contain important implications for the expected stability of the Sun's luminosity.

SS 45 INVITED PAPER

RECENT DEVELOPMENTS IN HIGH ACCURACY ABSOLUTE RADIOMETRY AND THEIR IMPACT ON SOLAR CONSTANT MEASUREMENTS

J. Geist (National Bureau of Standards, Washington, D. C. 20234)
(Sponsor: Peter Foukal)

Programs to monitor possible solar constant variations to within 0.1% of value over periods in excess of twenty years present radiometry's greatest current challenge. A number of recent developments in various areas of radiometry should help to assure that the stringent goals of solar constant monitoring programs are met. These advances include: 1) the simultaneous development of procedures to construct pyrheliometer cavities whose absorptance falls within a few hundredths of one percent of unity and the ability to measure this small difference from unity to within a few thousandths of one percent, 2) the demonstration that the spectral response of certain types of silicon photodiodes can be determined directly from their device physics with an absolute uncertainty of less than a few hundredths of one percent, and 3) the development by England's National Physical Laboratory of an electrically calibrated, cryogenic cavity radiometer capable of parts per million absolute accuracy in measurement of radiation once it is within the instrument's vacuum chamber.

The problems currently limiting the state of the art in solar constant measurements will be reviewed, and the implications for this area of these new developments will be explored. Potential future impact on spectral distribution measurements will also be covered.

SS 46

LIMITS TO LUMINOSITY VARIATIONS OF THE SUN AND SOLAR-TYPE STARS FROM PHOTOMETRY OF STARS, PLANETS, AND SATELLITES

G. W. Lockwood (Lowell Observatory, Flagstaff, Arizona 86002)
(Sponsor: Steven T. Suess)

Photoelectric observations of two of Jupiter's satellites, Europa and Callisto, and of Saturn's satellite Rhea, made from 1976 to 1979 using narrow-band filters at 472 and 551 nm, have been reduced to mean opposition magnitudes by fitting theoretical solar phase curves developed by K. Lumme (University of Helsinki). The theory takes into account mutual shadowing of the surface particles of the satellites, surface roughness, and multiple scattering.

The mean photometric behavior of these objects indicates that the solar visual luminosity may have increased by 0.3±0.2 percent from 1977 to 1978 and subsequently decreased by 0.3±0.2 percent from 1978 to 1979. This marginal detection of solar variability is consistent with an 0.4 percent increase in the solar constant between 1976 and 1978 recently reported by R. C. Willson, C. H. Duncan, and J. Geist. There is no possibility that solar luminosity variations as large as 1 percent could have occurred during this interval.

Similar observations of Neptune, and Saturn's satellite Titan, both of which have atmospheres of CH_4, H_2, and other molecules, reveal a correlation between the albedos of these bodies and various solar and interplanetary parameters (e.g. solar EUV irradiance, solar wind speed); but do not directly measure solar luminosity.

Measurements of a small group of solar-type stars made from 1955 to 1965 and from 1972 to 1980 at the Lowell Observatory suggest an upper limit to luminosity variations of about 1 percent on a time scale of a decade. Results of a new analysis of these data will be discussed.

SS 47

PHOTOSPHERIC FLUX SPECTRUM CHANGE

W. C. Livingston (Kitt Peak National Observatory*, Tucson, AZ 85726)
(Sponsor: P. Foukal)

Intensive monitoring of select Fraunhofer lines in the integrated solar flux from Fall 1975 to date reveal subtle but significant change. The equivalent widths (total absorption) of all photospheric lines studied have weakened roughly linearly with time 0.3 to 1.5%. This weakening appears to be inversely proportional to line strength. A change of instrument zero point or of the sun's continuous absorption coefficient is indicated. Instrument drift is ruled out by other evidence. The time history of line intensity ratios over this period suggests thermal and magnetic flux transients lasting 3-18 months. Formal probable error in the equivalent width measurements is 0.1% while for the line ratios it is 0.03%.

SS 48

BALLOON BORNE MEASUREMENTS OF SOLAR IRRADIANCE

D.G. Murcray, Dept. of Phys., Univ. of Denver, Denver, CO, 80208
J.J. Kosters

A system for measuring the solar irradiance with high precision from balloon altitudes was assembled in the mid 1960's and flown several times in 1967-68. This system was recalibrated and flown again in 1978. A further flight was performed with the system in February 10, 1980. The data obtained during this flight will be compared with that obtained during the earlier flights.

SS 49

COMMENTS ON SOLAR CONSTANT MEASUREMENTS FROM NIMBUS 6 AND 7

J. HICKEY and F. GRIFFIN (The Eppley Laboratory, Inc., Newport, RI 02840)
H. JACOBOWITZ, L. STOWE and P.PELLEGRINO (National Environmental Satellite Service, N.O.A.A.)
R. MASCHHOFF (Gulton DSD)

Sensors which monitor the solar thermal radiation in the region of 0.2 to 50 um have been operational on NIMBUS 6 since July 75 and on NIMBUS 7 since Nov. 78. Both experiments are still functioning. This presentation focuses on variability of the measured solar flux. The first three years of data were taken during the solar minimum period using a thermopile sensor. The later NIMBUS 7 data include measurements by a self calibrating cavity pyrheliometer sensor. The NIMBUS 7 measurements are taken during the period of increasing solar activity for Cycle 21. Preliminary analysis of the cavity radiometer measurements indicate a relationship between changes of the extraterrestrial solar radiation and the other indicators of solar activity. During a period of high solar activity in August 79, a decrease in solar flux of approximately 0.36% was observed. In early November another event occurred characterized by the highest 2800 MHz flux for the cycle to date coincident with high flare activity. The measured solar flux again decreased. The measuring instrument has a demonstrated stability at the 0.1% level. The flux decreases are in the 0.2 to 0.4% range.

SS 50

THE 160-400 NM SOLAR SPECTRAL IRRADIANCE AND ITS TEMPORAL VARIABILITY FROM THE SOLAR BACKSCATTERED ULTRAVIOLET (SBUV) EXPERIMENT ON NIMBUS-7

Donald F. Heath (NASA/Goddard Space Flight Center, Laboratory for Planetary Atmospheres, Greenbelt, MD 20771)
Hongwoo Park (Systems and Applied Sciences Corporation, Riverdale, MD)

Apart from its ozone sounding capability, the SBUV experiment which was launched aboard Nimbus-7 has a continuous scan mode which permits observations of the ultraviolet solar flux with a 1.0 nm spectral bandpass from 160-400 nm on a near daily basis. The solar observations which are continuing began in November 1978. Significant

variations are observed in the ultraviolet solar flux which is absorbed in the mesosphere, stratosphere, troposphere and that which penetrates to the surface of the earth. During a solar rotation in the latter part of December 1978 and early January 1979 typical variations in the solar flux were 7 percent at the SiII emission lines near 181 nm, 3 percent in the aluminum ionization continuum near 207 nm, about 1.5 percent in the MgI ionization continuum below 250 nm, 3.7 percent in the MgI h and k lines at 280 nm, 2.4 percent in the MgI resonance line at 285 nm and about 0.8 percent for the CaII k and h lines at 394 and 397 nm respectively. Maxima and minima in the ultraviolet solar flux coincide with corresponding maxima and minima in the Zurich sunspot numbers. During a typical solar rotation the observed modulation in ultraviolet is of the order of 0.02 percent of the solar constant. The wavelength dependence and solar species which produce the modulation in the ultraviolet solar flux are discussed in detail. The magnitude of the observed ultraviolet solar spectral irradiance is described in relation to previous and recent measurements with respect to possible long term variations.

SS 51

THE RELATIONSHIP BETWEEN CHANGES OF THE SOLAR CONSTANT AND THE SOLAR RADIUS

S. Sofia (NASA/Goddard Space Flight Center, Laboratory for Planetary Atmospheres, Greenbelt, MD 20771)

On general physical grounds it is shown that a change in the solar constant, S, in climatically significant timescales, requires a change in the solar radius, R, such that

$$\frac{\delta S}{S} = K(t)\,\frac{\delta R}{R}$$

The time-dependent value of K (t) must be obtained by means of solar structure modeling. Since the accuracy required for this modeling strains the validity of modeling techniques currently in use, caution must be exercised to test the validity of the results. Our present effort in this problem follows three lines: (a) to set observational bounds in the value of K (t) for $t \leq 250$ years from solar eclipse studies; (b) to determine the sensitivity of K (t) on the various modeling parameters and theory; and (c) to improve the modeling techniques. The latest results of this work will be discussed.

SS 52

VARIATIONS IN SOLAR BRIGHTNESS IN RESPONSE TO ACTIVE REGIONS

G.A. Chapman (San Fernando Observatory and Dept. of Physics & Astronomy, CSUN, Northridge, CA 91330
(Sponsor: Peter Foukal)

We distinguished variations in solar brightness from variations in solar luminosity. The former is the instantaneous solar output as seen at the earth whereas the latter is the total solar output. We report measurements of the brightness excess and deficit associated with faculae and sunspots, respectively. Assuming the quiet sun remained constant during August 1975, faculae caused an increase of not greater than about 8×10^{-5} of the quiet sun brightness when near the limb. Sunspots near disk center caused a decrease of not greater than about 2×10^{-4}. These values refer to single active regions. When several active regions appear on the sun at the same time, these values would be larger, up to 2×10^{-4} and 5×10^{-4}, respectively, for faculae and sunspots. To determine the variations in luminosity one needs the angular dependence of these brightness variations. Due to the differing angular dependence, luminosity variations from solar activity will be less than brightness variations.

SS 53

VARIABLE SOLAR UV, SPICULES AND THE LARGE-SCALE SOLAR MAGNETIC FIELD

Kenneth H. Schatten
Donald F. Heath (both at: NASA/Goddard Space Flight Center, Laboratory for Planetary Atmospheres, Greenbelt, MD)

The spicule dominated regions of the sun are suggested as areas which may play an important role in variable solar UV flux and thereby solar emissivity. A variable UV flux may be associated with varying solar magnetic fields in the following fashion. As the "curve of growth" of strong absorption lines becomes non-linear in number density, N, it varies as $N^{\frac{1}{2}}$, Zeeman splitting then results in an effective broadening of the line with a resultant increase in the effective width. In the strong field region near a spicule, we may obtain a broadening of $\Delta\lambda/\lambda \simeq 4.7\ 10^{13}\ g\ \lambda^2\ H/\lambda_n$ of order 50%. Beckers (1964) has estimated there to be 400,000 spicules on the Sun, with dimensions 800km thick and 2800 km long. Considering geometric factors, they may "obscure" or "filter" at least 2% of the Sun. These spicules form predominantly in regions of faculae, associated with large scale field regions. Sheeley (1976) has found an average equatorial faculae has an associated magnetic flux of 0.2×10^{21} Mx. Thus an association between magnetic flux (and solar activity) and the variable solar UV observations from Nimbus IV is suggested. The recurrence rate of the solar UV variability appears to relate to solar cycle changes in solar cycle #20. From 1969 through the end of 1970 a slower rate than the Carrington rate was found for UV enhancements, approximately 27.8 days corresponding to a 40° latitude source. From 1971 to 1973, a more rapid rate was found, with an approximate 27.0 day periodicity, commensurate with an equatorial rate. The association of UV variability with faculae by means of magnetic line broadening in spicules is consistent with dynamo solar field changes. An association with magnetic flux at high latitudes would exist prior to polar field reversal, and with low latitudes subsequently.

SS 54

MEASUREMENTS OF THE SOLAR IRRADIANCE: A REVIEW OF NASA PROGRAMS

R. K. Kakar (Environmental Observation Division, Office of Space and Terrestrial Applications, Washington, DC 20546

NASA is supporting an active program of the measurement of both the total and spectral solar irradiances for at least the duration of the full solar cycle. This program will use the full range of NASA's space vehicles: sounding rockets, free-flying satellites and the Space Shuttle System. The goal is to achieve a self-consistent, continuous measure of the total solar irradiance (solar "constant") to the level of at least 0.1% relative accuracy as a function of time and the spectral irradiance for wavelengths from 120nm to 400nm with a $\pm$ 10% absolute accuracy. The elements of this program will be described with particular emphasis on future plans.

SS 55

NUMERICAL MODELING OF SOLAR LUMINOSITY VARIATIONS

A. S. Endal (Dept. of Physics and Astronomy, Louisiana State University, Baton Rouge, La. 70803)
(Sponsor: Richard E. Hartle)

Variations in the solar luminosity will, in general, be accompanied by changes in the solar radius. Since the radius can be measured much more accurately than the luminosity, this offers an attractive means of monitoring the luminosity. Historical radius measurements can provide a record of luminosity variations extending nearly 3 centuries backwards in time.

The key to interpreting the radius data lies in determining the exact relationship between radius changes and luminosity changes. This relationship will depend on the time scales of the changes and, perhaps, on the physical mechanism responsible for the changes. At present, the only available means of determining this relationship is by numerical modeling of the solar interior.

Such modeling strains the capability of current stellar structure calculations and the results of various investigators do not agree. The uncertainties in these models and possible reasons for the disagreement will be discussed. New calculations aimed at estimating the uncertainties and examining the sensitivity of the derived luminosity-radius relationship to the modeling techniques will be described.

Tectonophysics

Plate Tectonics & Plate Motions

Pier 2 & 3
Thursday A.M.
Daniel M. Davis (MIT), Presiding

T 1

VARIATIONS IN THE VELOCITIES OF THE MAJOR PLATES THROUGH THE CENOZOIC

Daniel M. Davis
Sean C. Solomon (Dept. Earth & Planetary Sciences, Mass. Inst. of Technology, Cambridge, Mass. 02139)

The average relative velocities of the plates over a time interval in the geologic past may be estimated if accurate plate reconstructions are available for the beginning and end of that interval. The 'absolute' plate velocities may then be determined by the specification of a suitable reference frame. We present models for the relative and absolute velocities of the major plates through the Cenozoic as tests of several alternative plate reconstructions and as a guide to evaluate the hypothesis that pronounced changes in plate speeds or directions arise directly from changes in the configuration of plate boundary forces.

Digitized plate boundaries were rotated backwards in time using published rotations to determine positions at 5 m.y. intervals back to the late Cretaceous. The oceanic plate boundaries were then corrected to remove yet-to-be-formed segments of ridges and to properly match magnetic anomalies. Relative plate velocities were obtained by differencing finite rotations. 'Absolute' velocities were determined by assuming that no net torque is exerted on the lithosphere. R.M.S. 'absolute' speeds of each plate were calculated as functions of time as a conceptually simple measure of plate velocities and accelerations.

We have tested several proposed reconstructions for the motions of the Antarctic and Pacific plates (Gordon and Cox 1979; Jurdy 1979; Suarez and Molnar 1980) proposed to explain the failure of simple rigid Antarctic and/or Pacific plate models to match the motions of the Pacific plate as found using hotspots and equatorial crossings defined by pelagic sediment deposition. The sensitivity of 'absolute' motions of the Farallon and Kula plates to the choice of model is shown, as well as the effects of the reconstruction models on the rate of subduction of those plates beneath North and South America.

T 2

THE EMPEROR FRACTURE ZONE: 2100 KM OF DEXTRAL OFFSET IN THE PACIFIC PLATE IN THE EARLY TERTIARY

E. Farrar (both at: Dept. of Geol. Sci., Queen's
J.M. Dixon Univ., Kingston, Ont., K7L 3N6)

Between ~67 Ma and 40 Ma ago, a NW-SE trending fault system over 8000 km long split the Pacific (P) plate and accumulated 2100 km of right-lateral strike-slip. This fracture, here named the Emperor Fracture Zone (EFZ), consisted of several segments, one along the present trace of the Emperor Trough and another along the Line Is., joined by short ridge segments, one the Necker ridge and another at the latitude of the Mendocino transform. The EFZ terminated at its N end against the Kula-Pacific ridge and probably ended in the S at a NE-SW trending ridge W of the present-day Society Is. The undated ENE-trending magnetic anomalies E of Tonga trench were formed during spreading at this ridge, and the Louisville ridge formed as a transform offset of it. While EFZ was active the western part of P plate moved NNW relative to the hotspot reference frame and the Hawaiian hotspot generated the Emperor seamount chain. EFZ motion commenced at a time corresponding to the change of the Hawaiian hotspot trace from the Meiji trend to the main Emperor trend, and following the formation of the last undisturbed Pacific-Kula ridge magnetic anomalies presently preserved E of the Emperor trough. When EFZ ceased activity and the E and W parts of P plate were reunited, the western part changed direction relative to the hotspot frame and the Hawaiian seamount chain was formed. 2100 km of right-lateral offset of EFZ has fortuitously aligned the former western end of the Molokai FZ with Mendocino FZ and explains the truncation of the other major major Pacific FZ's, especially the Chinook. Reconstruction of P plate to its pre-EFZ state restores its magnetic anomaly pattern to a configuration in which the Cenozoic magnetic bight S of Alaska and the Mesozoic magnetic bight SE of Japan could both have formed by straight-forward evolution of the Pacific-Kula-Farallon RRR triple junction.

T 3

EPISODIC AND NONSYNCHRONOUS BACK-ARC SPREADING AND ARC VOLCANISM OF PHILIPPINE PLATE EVOLUTION

R.B. Scott (Dept. Geology, Texas A&M Univ., College Station, TX 77843)
L.W. Kroenke (Hawaii Institute of Geophysics, Univ. Hawaii, Honolulu, HI 96822)
G. Zakariadze (Georgian Academy of Science, Tbilisi, USSR)
A.Ya. Sharaskin (Vernadsky Inst. Geochemistry, USSR Academy of Sciences, Moscow, USSR)

Studies of DSDP results in the Philippine Plate have determined that plate accretion by back-arc spreading and arc volcanism were nonsynchronous. Karig's fundamental premise that the arcs and back-arc basins formed progressively from west to east is satisfied by these conclusions. The critical sequence of events during plate evolution are summarized: Sundering of the Palau-Kyushu arc and initiation of Parece Vela back-arc spreading in late middle Oligocene (31-29 my) coincides with a sharp decease and cessation of volcanism on precursors of Guam, Saipan and Tinian. A volcanic hiatus on the West Mariana Ridge lasted until middle early Miocene (20my) even though Parece Vela spreading continued. When volcanism began on the West Mariana Ridge, it overlapped with basin spreading until accretion ceased in late early Miocene (16my), but major arc volcanism continued to early late Miocene (9my), long after spreading ceased. This nonsynchronous and episodic spreading and arc volcanism also seems to characterize the modern active back-arc and arc pair. West Mariana volcanism died out by earliest Pliocene (5my) when the arc sundered and Mariana Trough spreading began; no arc volcanism was recorded on the Mariana Ridge until Quaternary time (2my) after which both operated.

An enigma lies in the conception of a) subduction without volcanism and therefore, b) back-arc spreading without subduction and also, c) an apparent change from a high rate of western Pacific Plate margin consumption to accretion in the back-arc region.

T 4

BIRTH OF AN EOCENE ISLAND ARC IN THE WESTERN PHILIPPINE SEA

Arend Meijer (Department of Geosciences, University of Arizona, Tucson, AZ 85721)

The results of I.P.O.D. drilling of ridges and basins in the eastern Philippine Sea indicate this region evolved by rifting of arcs and the formation of inter-arc basins as outlined by Karig (1971). The process began at 32 m.y.b.p. along the Palau-Kyushu(P-K)Ridge, then an island arc superimposed on oceanic crust of the western Philippine Sea plate. Our field and laboratory studies of Eocene to Oligocene volcanic sequences on Guam and Saipan, and Palau, representing respectively the rifted and remnant portions of the P-K arc, combined with the results of drilling in the Mariana fore-arc region during Leg 60, suggest arc volcanic activity began 41.5 m.y.b.p. along the P-K trend with the eruption of lavas characteristic of the island arc tholeiite series (Ni, Cr 10-20 ppm; TiO_2/Zr 100-110; K_2O 0.1-0.3%). These were followed in time and space by a sequence of unusual pyroxene phyric lavas high in MgO(10-25%), Ni(100-300 ppm), Cr(200-1500 ppm), SiO_2(52-58%) and very low in LIL elements (REE 2-8 X chondrites; Zr 20-30 ppm; TiO_2/Zr 20-40). Experimental studies suggest both the tholeiites and the high Mg lavas could be produced by hydrous melting of mantle material at shallow (40-70 km) depths. Because the western Philippine Sea lithosphere was generated only several m.y. prior to the initiation of arc volcanism along the P-K trend, it was still thermally elevated. Once westward subduction of Mesozoic Pacific lithosphere began 42-43 m.y.b.p. the introduction of H_2O into this mantle would have caused melting at relatively shallow depths. At a given distance from the trench, this melting would initially have produced tholeiitic arc magmas causing depletion of the source regions in low melting components. Further addition of H_2O from the slab would have caused the same source regions to generate high Mg, Ni, Cr, low LIL element magmas.

T 5

PACIFIC/CAROLINE PLATE BOUNDARY IN THE EASTERN CAROLINE SEA: PRELIMINARY RESULTS OF THE 1979 SHIPBOARD PROGRAM

Jeffrey K. Weissel, Lamont-Doherty Geological Observatory, Palisades, New York 10964

In late 1979, R/V VEMA surveyed the contemporary convergent plate boundary between the Caroline and Pacific plates in the eastern Caroline Sea of the equatorial Pacific. Preliminary results from this cruise (marine geophysics, heat flow, dredging) show that it becomes impossible to trace the eastwards subduction of Caroline plate under the Pacific plate at the Mussau Trench north of 3°15'N. At this point on the plate boundary contorted sediments of the Caroline plate are "ramped up" against a prominent ~NS ridge and compressional deformation (folding in sediments and faulting in oceanic crust) first appears. Between this point, where subduction activity disappears, and the Sorol Trough strike-slip zone, plate convergence is accomodated over a northward-widening belt of intensive overthrusting, where numerous slices of Caroline plate crust are overthrust to the NE on high-angle faults. Complications within the overthrust zone of plate boundary occur at 4°N where the Kiilsgaard Trough, an extinct (Oligocene) spreading center intersects the zone and at 4°20'N where a large seamount apparently disrupts the tectonic activity. The present Pacific/Caroline plate boundary started within the Oligocene lithosphere of the Caroline plate as demonstrated by the continuity of Caroline Sea magnetic lineations across the zone of contemporary overthrusting. The transition in tectonic style from subduction to intensive overthrusting appears largely governed by Pacific/Caroline convergence rate.

T 6

PALEOMAGNETIC TEST OF THE EARLY TERTIARY PLATE CIRCUIT BETWEEN THE PACIFIC BASIN PLATES AND THE INDIAN PLATE

Richard G. Gordon
Allan Cox (both at: Dept. of Geophysics, Stanford University, Stanford, CA 94305)

Using paleomagnetic data from India and the Pacific plate and published reconstructions of the Indian, Antarctic, and Pacific plates, we demonstrate that substantial motion has taken place during the Tertiary across a fossil plate boundary located within one of these plates. Two alternative models are able to reconcile the available paleomagnetic and plate tectonic information. In the first model East and West Antarctica are separate plates, the early Tertiary position of West Antarctica being one in which the Antarctic Peninsula is adjacent to the southwest border of South America. In the second model, the northern and southern parts of the Pacific plate undergo relative strike slip motion across a fossil plate boundary located northeast of Chatham Rise. This second model is difficult to reconcile with generally accepted sea floor spreading histories for the southwest Pacific but is supported by paleomagnetic data from the northern and southern segments of the Pacific plate. In reconstructing the motion of the Pacific plate relative to North America during the Early Tertiary using the North America-Africa-India-Antarctica-Pacific circuit, an additional rotation is required to account for the motion across the fossil plate boundary. Our proposed reconstructions do not significantly reduce the amount of relative motion of the hotspot now beneath Hawaii with respect to the hotspots in the Atlantic and Indian Oceans.

T 7

THE RESOLVING POWER OF DSDP EQUATORIAL CROSSINGS IN DETERMINING PAST MOTIONS OF THE PACIFIC PLATE

Cheryl D. Cape
Richard G. Gordon (Both at: Dept. of Geophysics, Stanford University, Stanford, CA 94305)

We have reviewed and critically examined geological analyses of cores from DSDP legs 17, 20, and 32 to determine which cores reliably indicate that these northern Pacific sites passed under the equatorial zone of high biological productivity during the Cretaceous or early Tertiary. Errors and limitations in the sedimentation models, previous analyses, and site records have been considered in the evaluation of the data. We use only those sites which can be rated relatively most accurate to test early Tertiary and Cretaceous absolute plate motion models proposed by other workers. We conclude that the resolving power of the data in evaluating past absolute plate motions is limited. In particular, the data cannot distinguish between the drastically different early Tertiary absolute motion models for the Pacific plate of Clague and Jarrard (1973) and Solomon et al. (1977). However, the data do show that the absolute motion of the Pacific plate since the early Cretaceous cannot be modeled by simple rotation around a single Hawaiian pole.

T 8

THE NARES-NANSEN TRIPLE JUNCTION

John W. Peirce, Petro Canada, P.O. Box 2844
Calgary, Alberta T2P 2M7

The Nares-Nansen Triple Junction was formed by the intersection of the Nansen-Gakkel Spreading Center, the Nansen Transform Fault, and the Wegener Transform Fault in a ridge-fault-fault (RFF) geometry. It was active from anomaly 24 time when Baffin Bay began to open and left lateral motion on Nares Strait was initiated until anomaly 13 time when Greenland became part of the North American plate.

Between anomalies 21 and 13, the velocity of Greenland relative to Europe was about twice that of Greenland relative to North America. Consequently, the geometry of the triple junction was unstable unless 2:1 asymmetry occurred in the spreading adjacent to the junction. As the orientations of the velocity vectors did not allow change to an RRR geometry, I suggest that such an asymmetry did occur as a series of frequent westward ridge jumps on a small segment of the spreading center adjacent to Greenland. A by-product of these jumps was the excess volcanism which built up the Morris Jessup and Yermak Plateaux.

At anomaly 13 time, the triple junction lay west of these features. When motion on the Wegener Fault ceased, the Nansen-Gakkel Spreading Center reestablished a direct link to the Nansen Transform Fault, thus splitting the Morris Jessup Plateau off the Eurasian Plate and attaching it to the North American Plate.

T 9

VARIATION IN BASEMENT TOPOGRAPHY AND FORMATION OF MAGNETIC QUIET ZONE IN THE CENTRAL REGION OF THE LABRADOR SEA

S.P. Srivastava (Bedford Institute of Oceanography, Atlantic Geoscience Centre, Box 1006, Dartmouth, Nova Scotia, Canada B2Y 4A2)
W.D. Roots (School of Earth Sciences, MacQuarrie University, North Ryde, New South Wales, Australia 2113)

Recent compilation of magnetic data in the Labrador Sea show prominent bands of positive anomalies flanking a central region which has been described as a magnetic quiet zone. The anomalies in this zone are small in amplitude (between 100 and 200 nT) and difficult to correlate between tracks. Examination of a large number of single channel and a limited number of multi-channel seismic reflection profiles across the Labrador Sea show a marked contrast in basement roughness across the boundaries of this quiet zone, with the quiet zone having rougher basement than adjacent non-quiet areas. This rougher basement is interpreted to have formed following a 45° change in the direction of spreading and to be indicative of close FZ spacing, caused by the direction change.

Within the quiet zone the basement roughness increases with the increase in the obliqueness of spreading. In the northern most part of the Labrador Sea, the seismic basement characteristics, together with magnetic and gravity data have been used to decipher the evolution of spreading patterns following the spreading direction change.

T 10

THE CENTRAL NORTH ATLANTIC OCEAN BASIN AND CONTINENTAL MARGINS: GEOLOGY, GEOPHYSICS, GEOCHEMISTRY, AND RESOURCES INCLUDING THE TRANS-ATLANTIC GEOTRAVERSE (TAG): NOAA ATLAS 3

P. A. Rona (National Oceanic and Atmospheric Administration, 15 Rickenbacker Causeway, Miami, FL 33149)

NOAA Atlas 3, scheduled for publication in spring 1980, presents a comprehensive overview of the geology, geophysics, geochemistry, and energy and mineral resources of the Central North Atlantic Ocean basin and continental margins from latitude 10° to 50° North. The information, compiled from extensive published and unpublished sources, is presented in the form of 22 maps on Mercator projection at scale 1:13,228,000 at latitude 30° North, a trans-Atlantic ocean bottom photographic traverse, two trans-Atlantic crustal sections based on seismic refraction measurements, trans-Atlantic single and multichannel seismic reflection profiles, 12 original trans-Atlantic geotraverses including narrow-beam bathymetric, magnetic and gravity profiles, three tables of crustal properties comprising seismic reflection and refraction measurements, and the description and chemical composition of rock samples recovered from the ocean basin. Sources of information, including the Trans-Atlantic Geotraverse (TAG) and Deep-Sea Drilling Projects, are thoroughly documented. The Atlas is designed to fulfill the need for a multipurpose information base for scientific investigation, marine environmental management, resource exploration, seafloor engineering, and formal or informal oceanographic education.

T 11

GRAVITY AND MAGNETICS INVESTIGATIONS OF THE CONJUGATE CONTINENTAL MARGINS OF THE CENTRAL ATLANTIC

V.M. Ewing
P.D. Rabinowitz (both at: Lamont-Doherty Geological Observatory, Palisades, N.Y. 10964

Studies of the eastern margin of North America using seismic, gravity, and magnetic data have shown that it is segmented along its length into a series of basins and platforms by transverse zones which are believed to be marginal fracture zones. We have recently analyzed the free-air gravity and magnetic anomaly fields of the conjugate continental margin off northwest Africa. These data also suggest a pattern of basins and platforms similar to that found off the eastern margin of North America. The gravity and magnetic anomalies of the conjugate margins have been rotated back to magnetic anomaly M21 time (145 myBP). This allows us to correlate the marginal fracture zones on either side of the ocean. Previous reconstructions of the North Atlantic have suggested correlations between prominent magnetic anomalies as well as the larger sedimentary basins (eg., the Carolina Trough and the Senegal Basin, and the Georges Bank and the Aaiun Basins). The additional data presented here should permit finer scale correlations to be made.

T 12

THE MAGNETIC QUIET ZONE IN THE GULF OF ADEN: IMPLICATIONS FOR THE PRE-SEAFLOOR SPREADING DEVELOPMENT OF THE CONTINENTAL MARGIN

J. R. Cochran (Lamont-Doherty Geological Observatory of Columbia University, Palisades, New York 10964)

An approximately 80 km wide magnetic quiet zone of low magnetic relief or uncorrelatable anomalies is found in the Gulf of Aden between magnetic anomaly 5 (10 m.y.b.p.) and the shoreline. This region is separated from both the mid-ocean ridge flank and the continent by distinct scarps. The basement in the quiet zone is deeper than on the ridge flank and does not appear to have a topographic gradient across it, suggesting that it was not formed by seafloor spreading at an organized spreading center, but rather originated during the predrift stage of continental rifting.

Simple models for the predrift evolution of the continental margin are investigated using seismic and heat flow data from the magnetic quiet zone. The motion on the rift bounding faults as well as geographic and geometric considerations imply that 50-100% extension of the upper brittle part of the lithosphere occurred in the Gulf of Aden rift valley prior to the onset of seafloor spreading. However, the thinning of the lithosphere as determined from the heat flow data must have been greater implying that the average lithospheric thickness under the rift valley was 1/3 to 1/4 of its original value when seafloor spreading commenced.

T 13

PALEOMAGNETIC ANALYSIS OF DEFORMATION OF PALEOGENE SEDIMENTS OF THE SOUTHEASTERN MARGIN OF THE BAY OF BISCAY

W.M. Roggenthen (South Dakota School of Mines and Technology, Rapid City, S.D. 57701

The Basque Basin, located along the southeast margin of the Bay of Biscay, was deformed during the early Oligocene, as a waning phase of the Pyrenean Orogeny. Paleomagnetic analysis of late Maastrichtian and Paleocene pelagic limestones and marls from the basin shows that this part of the north Spanish coastline was pushed radially to the south. Directions derived from four localities distributed along the basin show that sediments on the eastern end of the arc were rotated 15° to the west (counterclockwise) and, sediments on the western end of the arc were rotated 20° to the east (clockwise). These rotations are consistent with the general arcuate nature of the present coastline as well as the fold axes of the sediments. If the paleomagnetic directions are rotated back to their original directions at the time of deposition, the coastline and fold axes are straightened into an east-west line. This reconstruction causes the late Cretaceous volcanics of the Biscay Synclinorium to align with the North Pyrenean Fault Zone. These volcanics probably represent the westward continuation of the North Pyrenean Fault.

T 14

OBLIQUE STRUCTURES AT RIDGE-TRANSFORM INTERSECTIONS: IMPLICATIONS FOR RIDGE DYNAMICS AND POLE DETERMINATIONS

Gallo, D.G.
Rosencrantz, E.R.
Rowley, D.B. (all at Dept. of Geological Sciences, State University of New York at Albany, Albany, NY 12222)

Studies of marine geological and geophysical data, shear zones and ophiolites indicate that structures, scarps (faults) and sheeted dikes, with orientations oblique to both ridge and transform strikes are common features at ridge-transform intersections. These features are related, we believe, to a change in orientation of the instantaneous extension direction (IED) along a segment of ridge and are not Riedels or anti-Riedels associated with the transform. Away from the transform the IED is oriented perpendicular to the strike of the ridge, but swings toward an orientation normal to the transform over a distance of 10-20 km of the transform, in a sigmoidal fashion. We believe this sigmoidal shape is a consequence of the continuous, yet instantaneous welding of the plates across the transform due to plate accretion. This welding requires the trajectory of the intermediate principle stress (assumed parallel to dike injection) to have a sigmoidal shape, controlling the orientation of the oblique scarps. The subaxial magma chamber may also have a similar sigmoidal shape. The oblique scarps at ridge-transform intersections produce a grain to the bathymetry that is distinctly oblique to that of ridge or transform. In the case of short-offset transforms this grain may completely dominate the bathymetry, suggesting that the spreading axis and transforms are not orthogonally related when, in fact, they are. This bathymetric grain can lead to considerable confusion when the bathymetry of short-offset transforms are used to determine finite poles of rotation.

Plate Tectonics and Tectonics

Pier 2 & 3
Thursday P.M.
K. H. Jacob (Lamont-Doherty Geol. Observ.), Presiding

T 15

OBLIQUE SUBDUCTION AND RIFTING ALONG OCEAN-CONTINENT TRANSFORM BOUNDARIES

K.H. Jacob (Lamont-Doherty Geol. Observ. of Columbia Univ., Palisades, NY 10964)

Earthquakes, computed plate motions, bathymetric features, and other geologic and geophysical expressions of crustal deformation associated with the Queen Charlotte-Fairweather transform-fault system suggest a small component (~1 cm/y or less) of convergence across segments of this plate boundary. Most previous studies assumed at this boundary between the Pacific and North American plates pure dextral strike-slip motion with rates of 5 to 6 cm/y. The inferred small convergence appears to be taken up by slow subduction of Pacific lithosphere beneath the North American margin. In contrast to the inferred convergence on the seaward side of the transform boundary, there is weak evidence for rifting in the overriding continental plate on the NE trending Stikine alkaline volcanic belt. The observed stress and strain patterns are reminiscent of other ocean-continent plate boundaries of the transform type, such as in California, western Aleutians, the northern and southern boundary of the Caribbean plate, southern Chile, and the Burma-Andaman arc. These regions with over-all oblique slip across plate boundaries provide ample examples for simultaneous crustal extension (pull-apart basins, grabens, open rifting with and without alkali basalt volcanism) and crustal shortening (transverse thrust ranges, fold belts). The compressive features strike perpendicular to the azimuth of maximum principal stress, extensional features strike normal to that of minimum principal stress; both principal stress axes are horizontally oriented as expected for a strike-slip regime. Convergent features often dominate on the seaward side, extensional features on the landward side of the transform boundary. In cases where extension develops into mature rifting it can lead to conveyor-belt tectonics: the continental margin breaks into distinct terranes which are laterally transported away with the oceanic plate and are eventually accreted back to the continental side in regions with strong plate convergence.

T 16

PROPAGATING RIFT EXPLANATION FOR THE TECTONIC EVOLUTION OF THE JUAN DE FUCA REGION

Richard Hey (Hawaii Institute of Geophysics, Univ. of Hawaii, Honolulu, HI. 96822)
Clyde Nishimura (Dept. of Geological Sciences, Brown Univ., Providence, R.I. 02912)
Douglas S. Wilson
Gillian C. Fryer (both at Hawaii Institute of Geophysics, Univ. of Hawaii, Honolulu, HI. 96822)

We have reinterpreted the magnetic anomalies in the Juan de Fuca region originally discovered during the Pioneer survey and identified by Fred Vine. Our anomaly identifications are mostly identical to his except that where he interpreted doubled anomalies on profiles to result from faulting, we interpret them to result from ridge jumps and to mark fossil spreading centers. In addition we have used an updated version of the reversal time scale, and for these two reasons our new isochron map differs slightly from Vine's. A simple propagating rift model can produce this isochron pattern with its distinctive V pattern of magnetic anomaly offsets, and we hope to have a movie showing the detailed plate tectonic evolution of this area completed by the time of the meeting.

T 17

SUBMARINE LANDSLIDING AT THE EASTERN END OF THE TAMAYO TRANSFORM FAULT, GULF OF CALIFORNIA

J. Karson and other members of the Tamayo Scientific Team, (Department of Geological Sciences, State University of New York at Albany, Albany, NY 12222)

The eastern end of the Tamayo Transform fault is defined on conventional bathymetry by an up to 600 m high, south-facing slope, inclined overall at 30° down into the intersection depression with the East Pacific Rise spreading ridge axis, here defined by a rift valley. A program of submersible dives using DSRV ALVIN investigated this slope in the course of a study of the transform-spreading axis intersection zone. Extensive evidence of active downslope mass-wasting was encountered during three dives located up to 7 km from the ridge axis-transform intersection. Scalloped heads to rotational failure surfaces are prominent features, nucleated on steep faults of the principal transform displacement zone. Most of these faults have vertical offsets of 5 m or less, almost exclusively with downthrow toward the south. Poorly to moderately consolidated sediments dipping downslope are exposed by these faults. Mass-wasting from the fault scarps has produced deposits containing blocks of consolidated sediment and some basalt in a fine sediment matrix. Downslope creep of unconsolidated sediment, often from burrow sources, produces a prominent streaking on steep slopes. The presently unfaulted upper portions of the slope 5-8 km west of the ridge axis expose numerous scattered loose blocks (typically 10-50 cm), most consisting of consolidated sediments, but a minority of basalt. These blocks may have been produced in mass wasting events near the ridge intersection and been carried laterally along the transform away from their source. If true, this requires the PTDZ to migrate parallel with and toward the spreading ridge axis. Alternatively, fault scarp sources for the blocks above their present position have recently been tectonically and erosionally degraded so they are not now exposed.

T 18

SEISMICITY AND TECTONICS NEAR THE UNSTABLE COCOS, NORTH AMERICAN, CARIBBEAN TRIPLE JUNCTION

R. Lamoreaux (Dept. of Physics, Univ. of Alberta, Edmonton, Canada T6G 2J1)
E. Nyland (presently at I.G.P.P., University of California, La Jolla, California 92093)

Geological observations and recent seismicity suggest that crustal movements in South West Mexico are consistent with a slow clockwise rotation of a small triangular fragment of the North American plate at its South West corner. The boundaries of this triangular region are given by a proposed left lateral strike slip fault paralleling the strike of the Tehuantepec Ridge, a zone of compressional tectonics east of Tuxtla Guttierez, and the extension of the Polochic-Motagua fault zones. It is suggested that deformations in this region are a result of the interaction between the Cocos and North American plates along the portion of the North American Cocos boundary created by the migration of the North American, Cocos, Caribbean triple junction. Anomalously high seismicity occurs at the intersection of the Middle American trench and the extension of the Motagua fault. Bursts of seismicity which are precursory to major earthquakes occur in this region.

T 19

TECTONIC AND VOLCANIC ELEMENTS AT EASTERN GALAPAGOS RIFT - 85°20'W TRANSFORM

A. Malahoff
R. Embley (Both at: National Ocean Survey,NOAA, Cx4, Rockville, MD. 20852)
D. Fornari (Dept. Geol. Sci., SUNY, Albany)
W. Ryan (Lamont-Doherty Geol. Obs.)

The eastern end of the Galapagos Rift and its termination with the 85°20'W transform fault was investigated in January 1980 by ALVIN and remote camera tows. The dominant structural and volcanic features recognized by submersible and remote photographic and visual observations include: (1) eruptive fissures (2) recent extensional fissures (3) ponded lava fields (4) small volcanic cones and (5) normal faults. The recently active fissures are concentrated in the central rift in the study area between 86°W and the rift's termination with the transform at 85°20' W. On the western end of the study area, along a volcanic high in the middle of the active spreading center a single extension fissure was traced for 2 km which varied in width from 2 meters to several cm. In some cases, individual pillows were split in half. Near the eastern end of the transect, the rift bisected a 20 meter high volcanic cone. Between this area and the eastern termination of the rift a variety of extensional fabrics were mapped, including en echelon eruptive fissures and anastomatosing fissures. Several localized areas of collapsed ponded lavas were observed. In the western area these lava fields are young, with pervasive glassy surfaces. In the eastern area they are covered with thin sediment through which the collaspe cracks penetrate. The transition between the E-W spreading and the N-S transform faulting occurs over less than 0.5 km. The transform is marked by a series of dip-slip normal faults through massive extrusive basaltic terrain. These faults are downthrown to the west and have 60-90° faces. The talus at the base of these faults is often separated from the wall by a deep cleft, indicating contemporary motion. We intend to document these observations with still photos, slides, and video.

T 20

TECTONICS OF THE GUATEMALA BASIN

Carol A. Geller (Lamont-Doherty Geological Observatory, Palisades, NY 10964, and Dept. of Geological Sciences, Columbia Univ.)
Michael A. Hobart
Marcus G. Langseth

Detailed geophysical surveys were carried out in the eastern Guatemala Basin aboard R/V Endeavor in February 1980 and aboard R/V Robert D. Conrad in April 1979. These surveys have been combined with existing data and used as a guide in interpreting the tectonics of the Guatemala Basin. The tectonic fabric of the basin is more complicated than had been previously believed. Basement ridges and scarps trending WNW-ESE form a significant part of the morphology. Previously only ENE-WSW trending scarps and ridges along fracture zones had been identified. Several "fracture zone" scarps identified from tracks of opportunity are in fact associated with ridges trending perpendicular to the fracture zones. The fracture zone scarps can usually be identified by magnetic anomalies of several hundred gammas which are due to edge effects of adjacent crustal blocks of differing polarity. The WNW ridges have only samll magnetic anomalies associated with them. The WNW ridges are associated with gently sloping fault block covered by thick sediments (400m). The morphology of the blocks and scarps are similar to that seen elsewhere on the East-Pacific Rise-Galapagos Spreading Center system but the size of the scarps is somewhat larger here. Seismic profiler and 3.5 kHz echosounder records provide clear evidence for local decreases in sedimentation rate along the base of the fracture zone scarps. Evidence for erosion and for mass motion of sediments was also occasionally observed.

T 21

PLATE TECTONICS IN THE PAN-AFRICAN: THE DAMARA MOBILE BELT, NAMIBIA.

Sarah-Jane Barnes (Dept. Geology, Univ. Toronto, Toronto, M5S 1A1, Ontario.)
E.W. Sawyer (Dept. Geol., Univ. Toronto)
(Sponsor: I.H. Campbell)

Pan-African mobile belts have been until recently considered as ensalic. The 600 km long NE trending Damara Mobile Belt stretches across central Namibia. Three features of this belt are incompatible with an ensalic model:
a) An asymmetric deformation pattern, outlined by 5 linear structural zones characterized by; extensive thrusting; an intense shallowly dipping schistosity; vertical schistosity; diapir structures and granitic intrusions; waning deformation; from north to south respectively.
b) The metamorphic pattern is also asymmetric. In the 2 southern zones the geothermal gradient is 20 C°/km, while in the diapir and vertical schistosity zones gradients of 45 C°/km are inferred.
c) Evolution of Damara igneous rocks: The earliest (900 my) igneous rocks are alkali; the mid-Damara amphibolites resemble ocean floor basalt. During early deformation (700 my) alpine ultramafics were emplaced into the low grade metamorphic zone while in the high grade belt a calc-alkali suite was emplaced.

A model compatible with the above is; initial rifting and alkali volcanism; development of ocean crust forming ocean floor basalt; initiation of subduction; ocean closure and continental collision resulting in the asymmetric structural and metamorphic zones and emplacement of alpine ultramafics; partial melting of the lower continental crust and the subduction zone forming a calc-alkali suite.

T 22

TECTONIC INTERPRETATION OF FISSION TRACK AGES FROM THE LESSER HIMALAYAS, NORTHERN PAKISTAN

P.K. Zeitler (Dept. of Earth Sciences, Dartmouth College, Hanover, NH 03755), R.A.K. Tahirkheli (Univ. of Peshawar, Pakistan), C.W. Naeser (USGS Denver, CO.), N.M. Johnson, J.B. Lyons (Dartmouth College, Hanover, NH).

Fission track ages of sphene, zircon, and apatite from rocks collected along the Swat Valley date the recent uplift history of this region. A major E-W fault (MMT or Patan Fault) crosses the Swat Valley and separates regions of markedly differing uplift history. Ages ranging from 50 to 55 m.y. for sphene, 35 to 55 m.y. for zircon, and 14 m.y. for apatite were obtained from the region north of this fault. To the south the ages are about 22 m.y. for sphene, 21 m.y. for zircon, and 17 m.y. for apatite. This distribution of ages indicates that differential uplift occurred across the MMT prior to 15 m.y. The region north of the MMT experienced an average uplift rate of 11 cm/1000 years from 55 to 15 m.y. The region lying south of the fault was uplifted at an average rate of 75 cm/1000 years from about 21 to 17 m.y. During the past 15 m.y. both sides of the MMT have been uplifted together at an average rate of 18 cm/1000 years, indicating that the MMT has been locked during this interval. The above uplift rates have been calculated using estimated annealing temperatures for the minerals dated and an estimated geothermal gradient of 25°C/km. The choice of these parameters, however, is not crucial in defining relative uplift rates (from sample-to-sample).

T 23

TECTONICS OF CENTRAL AND WESTERN IRAN

B. Akasheh (Institute of Geophysics, Tehran University, Iran)
H. Berckhemer (Institute of Meteorology and Geophysics, Frankfurt University, FRG)

The fault-plane solutions of the last decade earthquakes together with all previous focal mechanism studies are used to obtain a better understanding of the tectonics of central and western Iran.

Earthquake records from the Iranian Long Period Array (ILPA) and other stations are used to study the seismotectonics of the ILPA area and Tehran region. The epicentral locations show that the activity is concentrated in several groups. Composite fault-plane solutions are made for each group and travel time residuals and migration of foci are studied. The results obtained give a new picture about the seismotectonics of the ILPA area and Tehran region.

T 24

SEISMOLOGICAL CONSTRAINTS ON THE COMPENSATION OF IRANIAN PLATEAUS

Katharine Kadinsky-Cade
Michael Bevis (both at Geological Sciences, Cornell University, Ithaca, NY 14853)

Seismological observations in Iran have placed new constraints on models for continental plateaus behind collision zones. Pn velocities range between 3.0 and 8.2 km/sec over the Iranian plateau, corresponding to normal mantle values. The uppermost mantle shear Sn phase propagates efficiently over the plateau except along its northern edge, where Sn is strongly attenuated. A variety of models have been invoked to account for the remarkable elevation of the Tibetan or Iranian plateaus. They require the presence of unusually low density material beneath these areas, presumably a shallow asthenosphere (Toksoz and Bird), or highly thickened crust, or both. Thickened crust could arise from compression (Dewey and Burke) or by underthrusting of Asia by a second crustal layer (Powell and Conaghan). Both of these could be accompanied by 'continental escape' as described by Molnar and Tapponier. Powell and Conaghan have pointed out that the surface geology of Tibet is inconsistent with the 50% shortening required by the crustal thickening model. Our observations of normal Pn velocities and efficient uppermost mantle Sn propagation across a major portion of the Iranian plateau argue against a replacement of the lithospheric mantle by hot asthenosphere. The existence of normal mantle beneath the plateau is consistent with lithospheric underthrusting. The suggestion is that models requiring compensation of Iranian plateaus by anomalous upper mantle are no longer viable.

T 25

THE EAST ANATOLIAN TRANSFORM FAULT: ITS AGE, OFFSET AND SIGNIFICANCE IN THE NEOTECTONICS OF THE EASTERN MEDITERRANEAN

M.R. HEMPTON (Department of Geological Sciences, State University of New York at Albany, Albany, NY 12222)
A.M.C. ŞENGÖR (same)

The seismically active and morphologically distinct East Anatolian transform fault extends for 400 km from Karliova in the east to Kahramanmaraş in the west and marks a southeastern left-lateral strike-slip boundary between the Anatolian plate and the Arabian plate. It offsets a Middle Miocene marker horizon near Gölbasi for 18 km and an unconformity between Miocene and crystalline rocks for 22 km near Göynük. Fault-controlled basins along the transform contain Pliocene lignite, bracketing the initiation of the fault between the medial Miocene and the Pliocene. The fault ends in two continental triple junctions where incompatibility has led to the formation of complex intracontinental basins in Karliova and Adana/Cilicia. Northwest trending left-lateral strike-slip faults splay from the main trunk (e.g., the Elbistan Fault) and become part of the internal Anatolian extensional regime. Along the fault there is one major "locking" segment near Bingol, a site of frequent earthquakes (e.g., May 22, 1971). The temporal correlation between the East and North Anatolian faults and their geometric similarity (in mirror-image) supports the notion that as Anatolia is being squeezed away from the East Anatolian compressional zone it is extending north-south along conjugate strike-slip faults that splay off from the two main transforms. Mapping west of Lake Hazar shows that subparallel strike-slip and normal faults result in a 6 km wide asymmetric transform valley with a stepped southern wall. Strike-slip faulting dominates but parallel normal faulting occurs on the higher southern wall as fault blocks descend into the eroded transform valley.

T 26

NEOTECTONICS OF EASTERN TURKEY: NEW EVIDENCE FOR CRUSTAL SHORTENING AND THICKENING IN A COLLISION ZONE

Fuat Şaroglu
Yilmaz Güner (both at Temel Arastirmalar Dairesi, MTA, Ankara, Turkey)
W.S.F. Kidd
A.M.C. Şengör (both at Department of Geological Sciences, State University of New York at Albany, Albany, NY 12222 USA)

Detailed field mapping, interpretation of air photos and LANDSAT images, and limited seismic reflection profiling reveals the following dominant structural and tectonic styles in the eastern Turkish part of the Turkish-Iranian high plateau: 1) NE-SW striking, left-lateral strike-slip faults (e.g. Malazgirt Fault); 2) WNW-ESE striking, right lateral strike-slip faults (e.g. Tutak Fault); 3) roughly E-W striking, generally high-angle thrust faults with both northerly and southerly vergence (e.g. the bounding thrusts of the Muş Basin); 4) roughly N-S striking fissures, many of which are sites of recent volcanism (e.g. Mt. Nemrud); 5) fold packets with axes trending roughly E-W affecting the Pliocene (and locally younger) sediments (e.g. near Ahlat). All these structures appear to be active as shown by seismicity and geomorphology. Most major depressions on the plateau are compressional in origin with bounding thrust faults. One major characteristic of all these structures is that they are discontinuous and change from one type to another along strike. They result in N-S shortening of the plateau accompanied by crustal thickening and limited E-W extension. The shortening is widely distributed yet inhomogeneous. The geological history of the area indicates that the present regime was established by mid to late Miocene times (~10 m.y. ago). The temporal correlation with the Arabia/Anatolia collision and the coincidence of the zone of crustal thickening with Plio-Quaternary volcanism supports the notion that eastern Turkey is an embryonic Tibetan-type high plateau.

T 27

A MAJOR NORTHWEST TRENDING PRECAMBRIAN STRIKE SLIP FAULT IN PENNSYLVANIA

O.H.Muller, Colgate Univ., Hamilton, NY 13346
P.M.Lavin, Penn State Univ., Univ Park, PA 16802
W.H.Diment, USGS, Natl. Ctr., Reston, VA, 22092

The Tyrone-Mt.Union lineament (TMUL) extends from the NW corner of PA to near South Mountain in SE PA. In plate tectonic scenarios seeking to explain the underlying cause of the South Mountain salient (a major bend in the Appalachians) the TMUL has been considered to be the location of either a failed third arm (Rankin,1976) or a transform fault (Thomas, 1977). The rifting in both models is thought to be pre-Taconic (or Precambrian), hence the more recent sedimentary rock which blankets western PA shows no evidence of it. Gravity and magnetic maps have been studied to see if the geophysical data permit offsets of the size and sense required for the transform fault model. At first glance the NY-AL aeromagnetic lineament of King and Zietz (1978) may seem to preclude such major offsets across it. Close inspection of the aeromagnetic map of PA, however, reveals that the lineament is poorly defined in SW PA. Moreover, if the map is cut along the TMUL and the two pieces are moved so as to "restore" 60 km of right lateral motion, the magnetic lineaments which result are more regular and extensive than those which existed before. Restoring this offset along the TMUL also results in the alignment of the Scranton Gravity High with a gravity high of similar trend in SW PA, and the alignment of the Kane Gravity High of north central PA with a gravity high in Ohio. The fact that both NE trending gravity features and NNE trending magnetic features are made more continuous by restoring them to "pre-transform" positions supports the existence of the proposed transform fault.

T 28

CONTINENTAL MARGIN ARC TECTONICS DURING THE HERCYNIAN OROGENY, EASTERN UNITED STATES

A. K. Sinha, Dept. of Geological Sciences, Virginia Polytechnic Institute and State University, Blacksburg, VA 24061 and Isidore Zietz, U.S. Geological Survey, Reston, VA 22092

Present day convergent margin tectonics are defined by an arcuate distribution of volcanic/plutonic rocks. The curvature of these arcs has been used to estimate convergence rates and angles of subduction. Recognition of such arcuate distribution of igneous rocks belonging to a single orogeny in the geologic past provides important restrictions on paleotectonics.
Along the eastern margin of the United States (Maryland to Georgia), the Hercynian (330-260 m.y.) plutons define an arcuate pattern. Although extensive erosion has removed all evidence of volcanic rocks, the plutons define a band with a radius of curvature with an RC angle of 5.6° (terminology of Tovish and Schubert, Geophy. Res. Letters, v.5, p.329-332, 1978), and by analogy with recent arcs, a spreading rate of less than 5cm/yr. Oxygen isotopic compositions and selected trace elements in these plutonic rocks show a regional and systematic variation within this arc. Along the strike of the arc, concentrations and isotopic compositions are similar; across the strike, they vary in a systematic manner. Similarly, aeromagnetic and gravity data show a pattern consistent with the arcuate distribution of plutons.
Although the geochemical and geophysical evidence is complicated by a late Hercynian continent-continent collision, we believe that the integrity of the arcuate pattern suggests that only minor readjustment of the arc has taken place. Our model suggests that the allocthonous nature of parts of the central Appalachians (Blue Ridge, Inner Piedmont) as documented by recent COCORP data (Cook et. al., Geology, v.7, p.563-567, 1979) may not extend east of the King's Mountain Belt.

T 29

ISOSTATIC EFFECTS OF A MOVING THRUST TERRAIN

A. Schedl
D. Wiltschko (Dept. of Geological Sciences, Univ. of Michigan, Ann Arbor, MI 48109)

Simple elastic models of the deflection of continental lithosphere due to a cratonward moving allochthonous mass show that, 1) deflection is significant and contributes to the formation of foreland basins and that, 2) the slope of the basement beneath this mass is increased, though not greatly. For instance, the deflection of the lithophere due to the eastward progression of the Idaho-Wyoming thrust terrain may be modeled as a wedge-shaped mass 50 km broad across strike and 5 km thick at the back edge composed of rocks w/ density 2.3 gm/cc moving over continental lithosphere of flexural rigidity (D) of 10^{31} dyne-cm. Basement dip will increase 0.3° and a basin 800 m deep along its axis and 270 km broad will from in front of the thrust mass. Also, the basin axis will shift eastward as the thrust mass progresses in that direction, consistent with the gross sedimentation pattern in western WY and eastern ID during the Mesozoic and early Tertiary. The inner zero crossing of the basin profile corresponds to a possible western edge of an eastward progressing regional high. This feature could show up in the sedimentary record as erosion, non-deposition or reduced sedimentation depending upon global sea level. The distance of this point from the basin axis is a measure of flexural rigidity. Sediment fill increases both the wavelength and amplitude of the distrubance. Viscoelastic models show that

rapidly transported terrains have profiles approaching that of the elastic problem whereas the basins in front of slowly moving masses are narrower and deeper. Episodic movement appears as rapid transgressions followed by slower regressions. The isostatic effect of moving an allochthonous mass provides a partial explanation for the location and size of the Cretaceous seaway in western North America.

Physics of Fractures

Bay
Friday A.M.
R. M. Stesky (Univ. of Toronto), Presiding

T 30

BEHAVIOR OF ROCK BEFORE AND DURING PROPAGATION OF OPENING-MODE CRACKS

C.C. Barton (Department of Geology and Geophysics, Yale University, New Haven, Ct. 06520)

Stable opening-mode cracks have been propagated through double cantilever beam specimens of the Stockbridge dolomite marble. Crack growth has been recorded by motion picture photography synchronized with the load and COD (crack opening displacement) record for the experiment. Normal illumination has been used to detect grain rotations and the opening of microcracks. The shape of the load-COD record shows initial bending concave up, followed by a linear portion, then bending concave down to a peak load beyond which the load drops. The onset of grain rotation, microcracking and the first evidence of an organized crack are observed in the region where the load curve becomes non-linear, i.e., before reaching the peak load.

The experimentally produced crack is 30% transgranular and 70% intergranular. Crack roughness is related to grain size. G (crack extension force) and K_{IC} (critical opening-mode stress intensity factor) have been computed by the methods of linear elastic fracture mechanics.

T 31

STRESS CORROSION CRACKING OF QUARTZITE

Lindamae Peck (Kline Geology Laboratory, Yale University, New Haven, Ct. 06520)

The energy required to propagate an opening-mode crack in Sioux quartzite has been measured with double cantilever beam (DCB) specimens in different chemical environments. Specimens are fractured in an Instron testing machine at constant displacement rate. The applied load and the deflection of the DCB ends, recorded during the experiment, are used to calculate the crack extension force, G, the work done in crack propagation. It is found that G increases during initial crack extension, and then remains constant for a period of crack growth.

Comparison of G's for quartzite specimens cracked in air and in water demonstrates that stress corrosion is a mechanism of cracking in quartzite. There is a 15-20% reduction in fracture energy for quartzite cracked in tap water as compared with fracture in air (ambient humidity).

The corrosive effect of water may be chemical (hydrolysis of Si-O bonds) and/or mechanical (lubricating effect of water reduces energy dissipation caused by stress-induced grain motions). To isolate possible mechanisms of water corrosion, quartzite specimens are fractured in solutions (NaCl, NaOH, methanol) of varying viscosity and quartz solubility.

T 32

CREEP HEALING OF FRACTURES IN SALT*

L. S. Costin
W. R. Wawersik (both at Geomechanics Division 5532, Sandia Laboratories,** Albuquerque, New Mexico 87185)

Rock salt formations are being considered for use as storage repositories for crude oil, nuclear waste and compressed gases. In these cases it is important to determine whether fractures, formed during the mining phase of the site development, will cause permanent damage to the integrity of the storage medium. To address this question, fracture and healing experiments were performed on specimens of bedded salt from the Salado formation, Southeastern New Mexico. Short rod specimens (100 mm in diameter) were loaded to failure in tension. During each test, a crack was initiated along the axis of the specimen. The fracture toughness of the salt was determined from the resulting load-crack opening displacement record. After the test, each specimen was pieced back together, jacketed and placed in a pressure vessel under hydrostatic pressure for several days. The confining pressure (10-35 MPa), temperature (22-100°C) and healing time (4-8 days) were varied to determine the effect of each on the healing process. Upon removal from the pressure vessel, each sample was retested and the toughness of the healed fracture was determined. Results show that the salt specimens regained 70-80% of their original strength under all conditions except at the lowest temperature and pressure where specimens regained only 20-30% of their original strength. It is suspected that the primary mechanism involved is creep of asperities along the fracture surface which forms an interlocking network. Thus, the healing pressure is probably the most significant variable.

T 33

USING AMPLITUDE AND FREQUENCY OF SEISMIC WAVES TO CHARACTERIZE PHYSICAL CHANGES INDUCED IN ROCK BY HEAT EXTRACTION DURING OPERATION OF A GEOTHERMAL LOOP

Michael Fehler (School of Oceanography, Oregon State University, Corvallis, OR 97331)

We study amplitude and frequency content of seismic signals that have traveled through rock from which heat is being extracted as part of the Los Alamos Scientific Laboratory Hot Dry Rock Geothermal Energy project. Using data obtained during two dual well seismic experiments that were separated in time by one year, we are able to find the radiation pattern for P waves originating from a piezoelectric source located in a fluid filled borehole. We present a simple model to explain the observed radiation pattern. By stacking the envelopes of signals recorded from closely spaced sources, we are able to clearly see S wave arrivals that are not obvious on individual unstacked seismograms. Low S wave amplitudes and loss of high frequency content of P waves characterize signals that have traversed regions of the reservoir where temperature changes have occurred during heat extraction experiments. We will discuss what these observations mean about physical changes that occur in the rock that composes the geothermal reservoir as heat is removed and also whether or not seismic data supports the existence of a hydrofracture in the rock.

T 34

ULTRASONIC VELOCITY MEASUREMENTS ON CORE FROM THE ICELAND DRILLING PROJECT

B. Kowallis
H.F. Wang (both at: Dept. of Geology & Geophysics, University of Wisconsin, Madison, WI 53706)
N.I. Christensen (Dept. of Geological Sciences, University of Washington, Seattle, WA 98195)

Preliminary velocity and microcrack studies on basaltic rock material from a continuously-cored, two-kilometer-deep, hole in Eastern Iceland have produced several interesting results. The velocity data correlate well with the position of the sample in a particular flow; velocities are slower at the top and bottom of a flow. Velocity data from one flow top showed a pronounced negative hysteresis upon cycling the samples back down from confining pressures over about 1000 bars. This is atypical of crystalline rocks and was interpreted to mean that new cracks were being produced at the higher pressures. It is possible that removal of the core from the ground has affected these samples also and therefore elastic properties determined in the laboratory may not relate directly to the actual rock *in situ*.

Thin section and SEM examination showed the existence and nature of microcracks in the samples. The distribution of these microcrack populations is correlated with differential strain measurements made on each sample. Evidence indicates that the basalts were originally formed subaerially. Subsidence coupled with surface erosion implies a pressure history that may possibly be recorded in the samples and which could be correlated with our laboratory studies.

T 35

SEISMIC WAVE VELOCITIES IN A ROCK BODY AT CHALK RIVER, ONTARIO, AND THEIR RELATIONSHIP TO FRACTURES.

C. Wright, C.P. Lam and M. Johnston (Division of Seismology and Geothermal Studies, Earth Physics Branch, Energy, Mines & Resources Canada, Ottawa K1A 0Y3).

Seismic P and S wave velocities in a crystalline rock body at Chalk River, Ontario, were measured at distances up to 1.3 km along three profiles. The seismic records were obtained from both surface geophones and hydrophones placed in a borehole, while the sources used were a mechanical hammer and a shear wave gun. Two shallow reflection profiles of about 2 km in length were also recorded over the rock body using the hammer as a source. The reflection data were interpreted as a series of overlapping reversed refraction profiles to yield detailed variations in P wave velocities. The P wave velocities were generally in the range 4.5 - 5.6 km/s, while the S velocity was about 3.2 km/s; these results are consistent with propagation through fractured gneiss and quartz monzonite which form the bulk of the rock body. For some paths, however, the P velocities were in the range 6.2 - 6.8 km/s, corresponding to propagation through thin sheets of gabbro. The S velocity along one of these paths was 4.1 km/s.

T 36

THE CORRELATION OF "TUBE WAVE" EVENTS WITH OPEN FRACTURES IN FLUID-FILLED BOREHOLES

C.F. Huang (AECL, Ottawa, Ont.)
J.A. Hunter (G.S.C., Ottawa, Ont.)

Tube waves generated by incident compressional waves have been correlated with open fractures in a fluid-filled borehole. As part of the AECL radioactive waste disposal program to study the subsurface open fractures in impermeable igneous and/or metamorphic rock body, a 12 hydrophone array (crystal cable) employing a surface seismic source was used to measure variations in compressional wave velocity in borehole. The records obtained displayed many large amplitude, low velocity events identified as tube waves which originated at intervals in the hole. Tube waves appear to be generated by the incidence of compressional waves in the surrounding rock body onto a fluid-filled fracture zone which intersects borehole. Correlations of positions and amplitudes of tube waves with TV logging, core logging and hydro-geology studies suggest that tube wave events can be used as reliable indicators of fractures open to fluid flow. The relative amplitudes of tube waves appear to be related to measured hydraulic conductivity.

T 37

COMPRESSIONAL AND SHEAR WAVE VELOCITIES IN DRY AND SATURATED ROCKS WITH SIMULATED FRACTURES

R.M. Stesky (Earth and Planetary Sciences, Erindale Campus, University of Toronto, Mississauga, Ont. L5L 1C6)

Fractured rock was simulated in a controlled way by cutting a rock cylinder normal to its axis and at ½ to 1 cm. intervals and reassembling. The 1 MHz velocities were measured parallel to the core axis at various confining pressures to 200 MPa, both before sectioning and after each cut was made. In dry rocks, the introduction of sawcut interfaces caused a progressive lowering of the velocities at low

pressures. The degree of lowering was more marked for rocks with a very low content of microcracks, with 5 cuts causing as much as a 50% decrease in velocity below 10 MPa pressure. Very little effect was seen in highly microcracked rocks, such as granite. In all cases, the difference in velocity between intact and cut rock was negligible above 100 MPa pressure. Grinding the cut surfaces with increasingly finer powder caused the velocity to approach the value for the intact rock, except at pressures below 10 MPa where some difference persists even after grinding with 1000 grit powder. The effects of fluids on compressional velocity were tested in two ways. First, a thin film of silicone grease was placed on the interface in several samples. Under pressure, the velocity of the cut cores, with 4 or 5 interfaces, was very close to the velocity of the intact dry rock. Second, several rocks were saturated with distilled water and their velocity measured under confining pressure while maintaining pore pressure near zero. The preliminary indications are that, at least for polished surfaces, there is very little difference in velocity between saturated intact rock and saturated rock with 4 cut interfaces. We are currently investigating the effects of rough surfaces on the wave velocity in saturated rock, a situation more analagous to that found in the earth.

T 38

THE VARIATION OF VELOCITY WITH PRESSURE FOR CRACKED ROCKS

A.F. Gangi, (Dept. of Geophysics, Texas A&M University, College Station, Texas 77843)

The velocity variation, with pressure, of cracked rocks is accurately described using the "Bed-of-Nails" model (Gangi, 1975, 1978). The elastic modulus of a crack is assumed to depend upon the distribution functions (for heights, moduli, shapes, etc.) of its asperities. The "Bed-of-Nails" model, in particular, characterizes the asperities as simple rods — however, distributions of any asperity shape (wedges, cones, hemispheres, etc.) have mechanically equivalent rod-asperity distribution functions (ibid).

Simple power-law rod-length distribution functions accurately describe most cracked-rock velocities for pressures less than 200 MPa and give:

$$V(P)=V_o(1+P/P_i)^{(1-m)/2}, \quad 0\leq m\leq 1$$

where V_o is the zero-pressure velocity, P_i is an equivalent initial pressure (which depends upon the "cohesiveness" of the cracked rock) and m characterizes the power-law distribution function. Both p- and s-wave velocities are described by the above equation as shown by comparisons with experimental data. Also, the model predicts interrelationships between the cracked rock's elastic moduli, permeability, resistivity, crack porosity as well as velocities as functions of pressure.

T 39

ELECTRICAL CONDUCTIVITY AND PREMEABILITY OF SIMULATED ROCK FRACTURES UNDER HIGH PRESSURE

R. Jagdat (Dept. of Geol. Eng., University of Toronto, Toronto, Ontario M5S 1A1)
R.M. Stesky (Earth and Planetary Sciences, Erindale Campus, University of Toronto, Mississauga, Ontario L5L 1C6)
N.S. Brar

Simulated fractures were introduced into rock cores by sawing the cylinders parallel to the axis and reassembling the halves. The gas permeability of dry cores and the electrical conductivity of brine-saturated cores were measured at various effective confining pressures to 200 MPa. These measurements were compared with similar measurements of the same cores made prior to cutting. The addition of the sawcut raised the conductivity by as much as an order of magnitude and the permeability by more than four orders of magnitude above the values for the intact rock. By assuming that the sawcut and intact portion of the core act in parallel and that the sawcut can be modelled as a planar conduit, we calculated the "equivalent fracture aperture" at all pressures. Good agreement was found for the aperture calculated for the two different properties. The equivalent fracture aperture is proportional to -log P where P is the effective confining pressure, as was suggested by the Walsh-Grosenbaugh model. When the cut surfaces were ground with various size grinding powders, the aperture and its change with pressure were less for the more finely ground surfaces.

T 40

VARIATIONS IN PERMEABILITY OF BEREA SANDSTONE AS A FUNCTION OF THE STATE OF STRESS

John M. Logan
Henrietta Gatto (Both at Center for Tectonophysics, Texas A&M University, College Station, TX 77843)

To assess the influence of varying states of stress on air permeability in a monomineralogic rock, measurements have been made on Berea sandstone under conditions of hydrostatic stress, triaxial compression and uniaxial strain. Berea sandstone utilized has a composition of 84% quartz, 11% clay, 3% feldspar, and 2% calcite, and a porosity under atmospheric pressure of 17%.

Air permeability calculations are made by a system of flowing air through the sandstone specimens which are 3.0 cm in diameter and 12.7 cm long. A known pressure gradient is imposed and the rate of flow is measured. Under conditions of increasing hydrostatic stress from 20 to 140 MPa the permeability decreases from 500 to 300 md. The decrease is found to be 78% non-recoverable. Permeability measurements were also made under triaxial conditions to failure of the specimen. Behavior was recorded at confining pressures to 70 MPa, which spans the brittle-ductile transition for this rock in triaxial compression. All specimens are found to decrease in permeability by 42% at Pc = 14 MPa to 77% at Pc = 70 MPa. In the brittle field (Pc up to 77.5 MPa) the permeability drops dramatically once failure occurs. This decrease in permeability in the brittle field is in contrast to the observed dilatancy prior to failure, suggesting that little communication between the fractures occurs.

In uniaxial strain tests, the permeability decreases from 485 md to 275 md as the rate of σ_3/σ_1 increases from .25 to .34.

It is concluded that the state of stress highly influences changes in permeability as the rock deforms.

T 41

HYDROTHERMAL CONVECTION IN A PERMEABLE LAYER WITH REGULARLY SPACED VERTICAL FRACTURES

P. H. Tag
E. M. Parmentier (Both at: Dept. of Geological Sciences, Brown University, Providence, RI 02912)

A typical geothermal setting consists of layers of faulted permeable volcanic rocks overlying a cooling igneous intrusion. In such a setting, convection of hydrothermal fluids may be important in the upward transfer of heat and in the formation of ore deposits. This study considers the role of faults in controlling patterns of hydrothermal convection. The marginal stability of convective modes in a layer of permeable material containing uniformly spaced vertical fractures, represented as narrow zones of higher permeability, is considered. The layer is heated from below and, for the results obtained so far, has impermeable and isothermal top and bottom boundaries. Three types of two-dimensional convective modes are examined: A) upward and downward flow in alternate fractures, B) upward or downward flow in all fractures, and C) no vertical flow in fractures. The preferred mode, that with the smallest critical Rayleigh number, depends only on the spacing between fractures (L) relative to the layer depth (D). The preferred modes are: mode A for $L/D \leq 1$, mode C for $1 \leq L/D \leq 1.4$, and mode B for $1.4 \leq L/D \leq 2.0$. For larger L/D multiple convection cells occur between the fractures. For mode B, marginal stability does not discriminate between upward or downward flow in fractures. Values of the critical Rayleigh number for each mode depend primarily on the permeability of material between the fractures and only weakly on the fracture width and permeability. These considerations of preferred flow patterns on the basis of marginal stability are presently being extended to finite amplitude convection.

T 42

AN EXPERIMENTAL STUDY OF THE EXTRACTION OF Rn^{222} FROM STRESSED GRANITE BY WATER FLOW

M. Banerdt, W.B. Banerdt, and C.G. Sammis (University of Southern California, Los Angeles, 90007)

Cylindrical samples (2" Dia. x 4") of granite of known uranium content from a depth of ~100m in the Sierra batholith have been subjected to triaxial stress where σ_1 varied between 0.5 and 2.4 kb (0.1-0.9 of the fracture strength) and where the confining pressure $\sigma_2=\sigma_3$ was 200 bars. Simultaneously, distilled water was forced through the sample at a flow pressure of 100 bars. Permeability was determined from the decay of pressure pulses and from the total water which flowed through the sample during each experiment. The flow water, collected in an evacuated sample cell, was analyzed for Rn^{222} content by a standard He extraction technique.

We found permeability to be correlated with stress, increasing by a factor of ~6 near failure. The flow water extracted ~0.1% of the equilibrium radon available in the sample. The amount of Rn^{222} extracted was not a sensitive function of either stress or permeability.

T 43

WHAT KEEPS THE CONDENSATE LAYER FROM FALLING DOWN INTO THE STEAM RESERVOIR OF A VAPOR-DOMINATED GEOTHERMAL SYSTEM?

G. Schubert
J. M. Straus (Both at: Space Sciences Laboratory, The Aerospace Corporation, Los Angeles, CA 90009)

Drilling has shown that vapor-dominated geothermal systems consist of a near-surface condensate layer, in which liquid water controls the pressure, above a reservoir in which steam is the pressure controlling phase. Condensate layers are several hundred meters thick; steam reservoirs extend to unknown depths. This is a most unusual arrangement of fluids: heavy lies above light. What holds the water up? We show, by means of linear stability analyses of superposed fluids in porous media, that immiscible fluids are gravitationally unstable if heavy is above light, but that fluids separated by a phase change interface can be stable even if the denser phase is on top. Application of the theory to conditions typical of known vapor-dominated geothermal systems shows that stability of water over steam requires permeabilities no larger than about 0.04 millidarcy at the base of the condensate layer. It is significant that the behavior of a phase change interface can stabilize water over steam for a nonzero value of the permeability because the observed natural discharge of steam from vapor-dominated systems proves that water and steam are in intimate contact and that an impermeable cap or seal cannot be responsible for holding up the water.

Heat Flow and Crustal Properties

Pier 5
Friday A.M.
David S. Chapman (Univ. of Utah), Presiding

T 44

THE DISTRIBUTIONS OF URANIUM, THORIUM AND POTASSIUM IN THE CONTINENTAL CRUST :CONSTRAINTS FROM HEAT FLOW DATA.

Claude JAUPART (Institut de Physique du Globe, Université Paris 6, Paris, France).
(Sponsor : Claude J. ALLEGRE)

Published data in several heat flow provinces throughout the world are used to estimate height-scales for the distributions of Uranium, Thorium, and Potassium in the continental crust. These height-scales are defined as follows:

$$Di = \int_o^h \frac{Ci(z)}{Ci(o)}\, dz$$

where Ci(z) is the concentration in element (i) at depth z. Three height-scales are computed from a least-squares fit to the following relationship: $Q = Q_r + D_U A_U + D_T A_T + D_K A_K$

Q is the observed heat flow and A_U, A_T and A_K are the respective heat production rates for Uranium, Thorium and Potassium measured at the surface. Q_r is a "reduced" heat flow and D_U, D_T and D_K are the height-scales defined by heat flow.

The usual practices in the heat flow literature has been to fit to the data a relationship of the form : $Q = Q_r + D.A$, where A is the total heat production rate. This corresponds to the implicit assumption that Uranium, Thorium and Potassium have identical distributions in the crust. We show that there is no reason to believe that such is the case. On the contrary, the analysis shows that the three distributions are probably different,and furthermore that they have the same basic features in all the provinces studied. We show that the observed variations in D_U and D_T can be explained simply by shallow perturbations, and we propose a model stressing the role of erosion and alteration. Our analysis suggests that the U and Th distributions are similar at depth in all the heat flow provinces.

T 45

RELATIONSHIP OF HEAT FLOW AND TEMPERATURE GRADIENTS TO BASEMENT LITHOLOGY, N.Y.

D. S. Hodge
K. Hilfiker
R. DeRito (all at: Department of Geological Sciences, State University of New York at Buffalo, Amherst, NY 14226)
J. Maxwell (Univ. of Cal., LASL, NM 87545)
P. Morgan
C. Swanberg (both at: New Mexico State Univ., Las Cruces, NM 88003)

Heat flow values in Central and Western New York ranging from 30 mWm^{-2} to 66 mWm^{-2} have been determined from numerous geothermal gradient measurements and from a limited number of thermal conductivity determinations. A similar sequence of vertical geothermal gradients can be recognized at all measured locations; thermal conductivity (K) values correspond directly to stratigraphic formations. For the area west of 75° 30' W in New York vertical temperature gradients were calculated from 971 bottom-hole temperatures recorded during routine electric logging. A temperature gradient map from these BHT varies from a low of 24 to a high of 38°C/km with a consistent pattern of high values near East Aurora, Elmira and Cayuga Lake, NY. Based on the conclusion that thermal conductivity is related to stratigraphy, a mathematical 3-D representation of K is developed. This representation yields the vertical variation of thermal conductivity at any location and is then combined with the temperature gradients from BHT to produce the detailed heat flow pattern of the area. This derived heat flow map is consistent with heat flow determined by direct gradient measurement. Lateral heat flow variation shows excellent correlation with Bouguer gravity anomalies. The high heat flow areas may directly relate to the distribution of radioactive granites in the upper part of the Precambrian basement rocks.

T 46

HEAT FLOW AND RADIOACTIVITY STUDIES IN THE ROSS ISLAND - DRY VALLEY AREA, ANTARCTICA

Gerald J. Bucher (Dept. of Geology, University of Wyoming, Laramie, WY 82071)
Edward R. Decker

Uncorrected and corrected heat flow (Q) values for the Ross Island - dry valley area in Antarctica are in the ranges 66.9-142.1 mW/m^2 and 50.2-83.6 mW/m^2, respectively. Concomitant values of bedrock heat production (A) are in the range .84-1.71 $\mu W/m^3$, implying that the area is a zone of low upper crustal heat production. The most reliable Q-A data suggest that this part of Antarctica is a zone of above-normal flux. Steady conductive and convective models predict high temperatures in the lower crust and upper mantle. The recent alkaline volcanism and epeirogenic uplift of the Transantarctic Mountains coupled with evidence of crustal attenuation in the western Ross Sea suggest that the region has undergone an episode of late-Cenozoic lithospheric extension.

T 47

GEOTHERMAL STUDIES IN WYOMING AND NORTHERN COLORADO

E. R. Decker, (Department of Geology, University of Wyoming, Laramie, Wyoming 82071)
K. L. Buelow, H. P. Heasler

Recent studies confirm low to normal heat flow (25-62.7 mW/m^2) in much of the eastern Wyoming Basin - Southern Rocky Mountain area in southeastern Wyoming. About 60 km to the south, the flux in the Southern Rockies in northern Colorado is high (75-121 mW/m^2). Although hydrologic disturbances could be occurring in the neighborhood of a major Precambrian shear zone in southeastern Wyoming, low to normal flux and low upper mantle temperatures in the region are consistent with evidence for a tectonically stable crust and an electrically resistive upper mantle. The sites in northern Colorado, however, are in a region that is characterized by Cenozoic igneous activity and faulting, and one interpretation is that this part of the Southern Rockies is a high heat flow zone like the Rio Grande rift to the south. The high reduced flux (>67 mW/m^2) here and the narrow northern boundary of the anomaly suggest that the excess flux is due to heat sources at shallow depths in the crust and/or upper mantle.

New measurements in central Wyoming suggest a complex pattern of normal to high flux in the Gas Hills (50-140 mW/m^2) and parts of the Powder River Basin (50-92 mW/m^2). Recent measurements in the Green River Basin and Great Divide Basin range from normal to intermediate (50-71 mW/m^2), whereas those in the Absaroka Mountains and Bridger Mountains are high (>75 mW/m^2). The data are discussed relative to existing maps of heat flow and geology in Wyoming.

T 48

HEAT FLOW ALONG THE SOUTHERN COLORADO PLATEAU MARGIN, EAST-CENTRAL ARIZONA

C. Stone (Bureau of Geology and Mineral Technology, Un. of Arizona, Tucson, AZ 85705

Four new heat flow values from the southern Colorado Plateau (CP)-Basin and Range Province (BRP) boundary in east-central Arizona increase to the south (80, 92, 102, and 115 mWm^{-2}) within 50 km. The values are much higher than the 40-60 mWm^{-2} range for the CP interior and become higher than the average BRP value of 92 mWm^{-2}. Heat flow values estimated from ground water silica data mimic this south-trending anomaly, with a local concentration of values as high as 147 mWm^{-2}.

This high heat flow may be related to the White Mountain (WM) volcanic field of east-central Arizona, where volcanism began about 12 m.y. ago and ended about 10,000 (?) years ago; to thinner crust and normal faulting along the southern margin of the CP; or to both. It is also possible that the BRP extends as far north as 34°00' in eastern Arizona where it is buried beneath the volcanic pile, and that the high heat flow is due to normal basin-and-range heat flow enhanced by WM volcanism. But this is unlikely on the basis of regional geology.

It is more likely that the high heat flow values presented here define the southern CP margin in eastern Arizona. Petrochemistry shows that the WM volcanic suite was derived in a tensional tectonic environment (Merrill and Pewé, 1977). In addition, the transition occurs over a narrow 50 km zone and volcanism youngs to the north, conditions found at other localities along the CP margin having thinner crust due to encroachment of BRP or Rio Grande Rift extension. The heat flow values presented here are consistent with normal BRP values preducted for the southern CP margin by Keller and others (1979), enhanced by WM volcanism and possibly normal faulting.

T 49

BASIN AND RANGE - COLORADO PLATEAU HEAT FLOW RESULTS FROM UTAH

John Bodell
David S. Chapman
Monica Clement
Riki Darling (all at: Dept of Geology and Geophysics, Univ. of Utah, Salt Lake, UT 84112

We report over 100 new heat flow determinations in Utah which supplement 18 previously published values listed in the 1975 Sass and Munroe catalog. The new heat flow sites lie throughout the Utah portion of the Great Basin and in an east-west band crossing onto the Colorado Plateau at about 39° N latitude. Great Basin heat flow shows considerable scatter with values ranging from 40 to about 200 $mW\ m^{-2}$, exclusive of recognised geothermal areas. Much of this scatter may be due to hydrothermal circulation on an upper crustal scale. We have used 31 "most reliable" determinations to characterise Great Basin heat flow as 90 ± 10 (s.d.) $mW\ m^{-2}$. The mean heat flow using all of our 18 sites in the interior of the Colorado Plateau is 48 ± 8 (s.d.) $mW\ m^{-2}$. These latter data necessitate a substantial downward revision of the characteristic heat flow value for the Plateau interior used in recent publications (eg: 65 $mW\ m^{-2}$ used by Thompson and Zoback (1979); 71 $mW\ m^{-2}$ used by Bird (1979)) based largely on results from the southeastern and eastern periphery of the Plateau. The Basin and Range-Colorado Plateau heat flow transition is now well determined at 39° N latitude. The transition has a half width of 30 km and is centered 75 km east of the Wasatch Line. Thus high heat flow as well as previously identified high seismicity and thin crust characterizes a transition province encroaching into the Colorado Plateau, which is consistent with a model of east-west expansion of the Great Basin.

T 50

APPLICATION OF THE NaKCa Mg AND SILICA GEOTHERMOMETERS TO THERMAL AND NON-THERMAL GROUNDWATERS OF ARIZONA

C.A. Swanberg (Depts. of Geology and Physics, New Mexico State University, Las Cruces, N.M. 88003)
P. Morgan
N.M. 88003)

The NaKCa Mg geothermometer has been applied to several thousand thermal and non-thermal groundwaters in Arizona to help evaluate the state's geothermal resources and to field test the application of this geothermometer. Roughly half of the geothermal areas delineated by the traditional NaKCa and silica geothermometers can be characterized as being anomalously high on the basis of this geothermometer. The silica geothermometer has been used in the context of the linear relation between silica geotemperatures and regional heat flow with the goal of preparing a new heat flow map of Arizona. The resulting map shows heat flow values typically near 60 $mW\ m^{-2}$ for the Colorado Plateau portion of the state and near 100 $mW\ m^{-2}$ for the Basin and Range portion. The Basin and Range data show considerably more scatter.

T 51

A HEAT FLOW STUDY OF DOÑA ANA COUNTY, SOUTHERN RIO GRANDE RIFT, NEW MEXICO

R. L. Lohse (New Mexico State University, Las Cruces, N.M. 88003)
P. Morgan
N.M. 88003)
C. Swanberg
N.M. 88003)

Doña Ana County, New Mexico, is tectonically situated within the Rio Grande Rift, a north-south trending active thermo-tectonic system which extends from northern Chihuahua, Mexico, to central Colorado and is characterized by late Pliocene to late Quaternary faulting and volcanic activity, high heat flow (105 $mW\ m^{-2}$), deep intrarift basins (up to 3000 m), and numerous geothermal areas. Sixty conductive heat flow values were calculated from measured temperature-depth data and estimated thermal conductivities. A histogram of the heat flow values (above the water table) shows a mode of about 100-150 $mW\ m^{-2}$ and a range exceeding ~42 to +672 $mW\ m^{-2}$. A bottom hole temperature gradient map shows that the geographic distribution of temperature gradients is as follows: 1) a north-northwesterly trend of anomalously high gradients along the Valley fault; 2) abnormally low or negative gradients associated with the large intrabasin groundwater flow of the Rio Grande River drainage system; 3) a west-northwesterly trend of high gradients bounded by more normal values running parallel to or on line with a structural feature known as the Aden Rift; and 4) high gradients associated with known geothermal areas (San Diego Mt., Radium Springs, and Las Alturas). The elevated temperatures and temperature gradients along the Valley fault and

the Aden Rift are thought to be due to ascending warm or hot water up the faults and fractured zones driven by forced and/or thermal convection while the temperatures and temperature gradients in the Mesilla Bolson are reduced due to downward percolation of recharge water and intrabasin ground water flow.

T 52

HEAT FLOW IN CENOZOIC CONTINENTAL RIFT VALLEYS

Paul Morgan (Depts. Earth Sciences and Physics, Box 3D, New Mexico State U., Las Cruces, NM 88003)

Four major Cenozoic continental rifts have been identified, the Rhinegraben, the Baikal rift, the East African rift system, and the Rio Grande rift, all of which are the sites of late Cenozoic volcanism with associated high heat flow anomalies. Heat flow data from all these rifts exhibit a large scatter in the values, but all have similar characteristics, with means of 80 to 120 and 40-80 mW m^{-2} for the rift floor and flanks, respectively. There is a general pattern of increasing heat flow towards the rift axes, but locally this trend is severely modified by the effects of hydrothermal and magmatic convection. The magnitudes and complexities of the heat flow anomalies indicate that their sources are in the crust, probably major crustal intrusions associated with the rifting events. Continuous spreading models, of the type successfully applied to explain the heat flow and topography of oceanic rift systems, are not applicable to continental rifts because of their much smaller rates of extension, the intermittent nature of their volcanism, and the lateral heterogeneity of their structure. More complex, episodic models reproduce the continental rift heat flow anomalies with relative success.

T 53

HEAT FLOW ACROSS THE NORTHERN CONTINENTAL MARGIN OF THE SOUTH CHINA SEA

Roger N. Anderson, Lamont-Doherty Geological Observatory of Columbia University, Palisades, New York, 10964
Michael A. Hobart, Lamont-Doherty Geological Observatory of Columbia University, Palisades, New York, 10964

The first-ever detailed heat-flow profile across a continental margin in the world's oceans was made across the northern margin of the South China Sea as part of a L-DGO People's Republic of China joint oceanographic research program. 88 measurements were made from anomaly 11 (32 m.y.b.p.) in the South China Sea basin (3200 m) across the continental margin south of Hong Kong to a depth of 800 m. All thermal gradients were linear, including seven made on piston corers which penetrated to a depth of 12 m; thus, the bottom water structure on the margin appears to be stable.

A series of basement ridges, interrupted by deep, sediment-filled basins are shown on the large air gun seismic line accompanying the heat flow profile. One of these ridges occurs right at the slope-basin boundary. The heat flow across this ridge peaks at almost twice the mean slope value (165 mWm^{-2} versus 90 mWm^{-2}). None of the other basement ridges have a heat flow anomaly associated with them. This ridge appears to mark a major thermal event that may be associated with the ocean-continent boundary at the northern margin of the South China Sea. The heat flow across the continental margin landward of this anomaly is uniformly high (~70-90 mWm^{-2}) with broad low amplitude variations (~10 mWm^{-2}) which do not appear to correlate with surficial basement structure.

T 54

PERMEABILITY AND HEAT FLOW IN THE GUATEMALA BASIN

D. Abbott, M. Hobart, M. Langseth, and R. N. Anderson, all at: Lamont-Doherty Geological Observatory of Columbia University, Palisades, New York 10964

Laboratory measurements on three piston cores from the Guatemala Basin showed permeability values ranging from 10^{-5}cm/sec (10^{-2} darcies) to 10^{-6}cm/sec (10^{-3} darcies). Heat flow values from the area were consistently low, all less than the expected heat flow for this age crust. A nonlinear temperature gradient on one of the cores indicated water velocities in the sediment of about 10^{-6}cm/sec, a value which is consistent with the permeability measurements. Pore water samples and in situ measurements of permeability were also obtained from the cores.

T 55

HEAT FLOW IN THE GUATEMALA BASIN

Michael A. Hobart (Lamont-Doherty Geological Observatory, Palisades, NY 10964)
Marcus G. Langseth
Roger N. Anderson

The Guatemala Basin is an area of widespread low heat flow. Detailed heat flow surveys intended to examine this phenomena were carried out in the eastern part of the basin in 1979 aboard R/V Robert D. Conrad and in 1980 aboard R/V Endeavor. The area surveyed consists of smooth basement covered with 300-400m of sediment except along ENE trending fracture zone scarps and WNW trending ridges. Bare rock is exposed along the fracture zones and ridges. Local sedimentation rates are lowered by currents along the base of the fracture zone scarps. Despite the thick sediments, the observed heat flow is very low, with a mean of only 30% of the value predicted for the age. No value was found over 75% of the prediction. Very low heat flow was found at the base of the scarps and higher values were found in the middle of the sedimented areas. However, abrupt transitions to low heat flow values did occur in the sedimented area. Two nonlinear temperature profiles were found near the base of the scarps indicating upward advection of water through the sediments. The large deficit in the observed heat flow is difficult to explain in areas of 300-400m thick sediments which are continuous for 50 km. One possible explanation is very efficient lateral heat transfer in the upper oceanic crust. Water entering and exiting through the scarps caould remove the missing heat. However, no high heat flow values were found near the scarps. Another explanation is suggested by IPOD Leg 69 observations of less than hydrostatic pore pressures under thick sediments on the Costa Rica Rift. The influx of water into the crust through scarps in response to this pressure head might lower the surface heat flow. IPOD hole 495 just north of this area has chert in the lower portions of the sediments, indicating that the crust may have been much hotter in the past than it is at present.

T 56

IPOD LEG 60 THERMAL CONDUCTIVITY MEASUREMENTS

K. Horai (Lamont-Doherty Geological Observatory of Columbia University, Palisades, NY 10964)

Thermal conductivity was measured, by conventional needle probe and new half-space probe methods, on 1319 oceanic crustal samples drilled during DSDP Leg 60. The sample consisted of soft sediment, semi-lithified and lithified sediment, and hard rock. Data from the deep holes revealed that the rate of increase with depth of sediment thermal conductivity ranges from 0.75 to 3.0 mW/cm K/100m. These values show a good correlation with the rate of sedimentation. The surficial thermal conductivity decreases as the water depth varies from lysocline to carbonate compensation depth, probably due to the depletion of carbonate (a high thermal conductivity mineral) from the sediment. Thermal conductivity of hard rock samples, mostly basalt, increases as they are hydrothermally altered. Formulas based on the Hashin and Shtrikman's theory for two phase material satisfactorily explain the data of thermal conductivity versus porosity and of thermal conductivity versus water content relationships. The relationship between thermal conductivity and compressional sound wave velocity will be useful in inferring the thermal conductivity of oceanic crust and sediments from the seismic velocity structure.

T 57

BOREHOLE TEMPERATURE MEASUREMENTS NEAR THE JAPAN TRENCH ON IPOD-DSDP LEG 57

Thomas K. Burch, Marcus G. Langseth (both at: Lamont-Doherty Geological Observatory, Palisades, New York, 10964), and
Roland Von Huene (U.S.G.S. 345 Middlefield Road Menlo Park, CA 94025).

The first borehole temperature measurements over the landward wall of the Japan Trench were made on IPOD-DSDP Leg 57 and indicate heat flows that are anomalously low compared to Northwest Pacific Basin values. High resolution temperature logs and bottomhole maximum thermometers were used at three holes. The time varying temperature of circulating fluid in each borehole was estimated using the Jaeger (1961) double heat-exchanger model and records of pumping and drilling rates. Circulation rates in these holes were maintained as low as possible to minimize the disturbance. Temperature corrections to the temperature profiles were made using the theory of Jaeger (1956) extended to cover the case of a time varying hole-wall temperature. Typical corrections to the data are about 25%. Equilibrium gradients of 32°C/km were calculated for holes 438A and 439, which are landward of the trench slope break and 22°C/km for hole 440 on the midslope terrace. Hundreds of thermal conductivity measurements on core samples on legs 56 and 57 provide a good estimate of the thermal conductance of the sedimentary sections drilled. When combined with the gradient measurements, heat flows of 28 (0.67 HFU) at 438 and 439, and 20 (0.48 HFU) at 440 are indicated. The results are in agreement with seafloor heat-flow values over the Japan Trench and land measurements in Northeastern Honshu.

T 58

DETAILED MULTICHANNEL ANALYSIS OF THE STRUCTURE OF A MOUNDS-TYPE HYDROTHERMAL AREA IN THE MARIANA TROUGH

Kerry A. Hegarty
Richard D. Jarrard
Roger N. Anderson
all at: Lamont-Doherty Geological Observatory Palisades, New York 10964

Recent heat flow studies in the Mariana Trough revealed the presence of a hydrothermal mounds area with heat flow in excess of 2000 mW/m^2. In order to relate the hydrothermal circulation pattern to the crustal structure of this region, we have undertaken a detailed analysis of a portion of the IDOE-multichannel transect of the Mariana Trough, an E-W track located 3 km south of the mounds area described above. The conventionally stacked multichannel section shows very little evidence of sub-bottom reflectors, due primarily to rough topography and the widespread occurrence of diffractions.

Our analysis of a 7 km section has considerably increased sub-bottom resolution because of: 1) migration of diffractions before stacking, and 2) analysis of semblance every 200m allowing confirmation of reflectors and determination of more accurate stacking velocities. This analysis reveals the presence of a 0.5-1.0 km thick zone with interval velocities of 2.0-2.5 km/sec. This zone is possibly composed of interbedded clays and basalts or basaltic breccia and overlies 0.5-2.0 kms of high porosity basalt with velocities of 3.5-4.5 km/sec.

We conclude that the usefulness of multichannel profiling is not confined to areas of smooth, thickly sedimented topography. Modelling studies to relate the observed heat flow pattern to the crustal structure are in progress.

T 59

A CORRELATION BETWEEN CONTINENTAL Pn VELOCITIES AND HEAT FLOW

P. R. Black (Dept. of Geological Sciences, Albion College, Albion, MI 49224)
L. W. Braile (Dept. of Geosciences, Purdue University, West Lafayette, IN 47907)

Upper mantle compressional-wave velocities were averaged within continental physiographic provinces in North America, Europe, the Soviet Union and Australia from published data. Pn velocity and heat flow were found to correlate at a high level of statistical significance. By calculating temperatures at the base of the crust from heat-flow values a correlation between Pn velocity and upper-mantle temperatures was demon-

strated. The value for the variation of Pn with temperature thus obtained, -6.0×10^{-4} to -8.0×10^{-4} km/sec °C falls within the range of laboratory determined values for crystalline rocks of -1.0×10^{-4} to -10.0×10^{-4} km/sec °C. If continental heat flow is related to crustal age, the Pn versus heat-flow correlation implies a relationship between seismic velocity and crustal age, possibly due to progressive cooling of the crust.

Crustal Structure and Geophysics

Pier 5
Friday P.M.
R. P. Meyer (Univ. of Wisconsin), Presiding

T 60

EVIDENCE FOR A GLACIATED CRYSTALLINE BASEMENT AND 7.5 km/s SEISMIC REFRACTOR IN McMURDO SOUND

L. D. McGinnis (Department of Geology, Northern Illinois University, DeKalb, IL 60115), T. H. Larson, H. Miller, D. D. Wilson

Reversed seismic refraction profiling from sea ice in western McMurdo Sound reveals a crystalline basement underlying 1.5 km of at least Miocene-age sediments that contains a deep groove of probable glacial origin several kilometers long, over one kilometer wide and 0.5 km deep, with long axis oriented north-south, parallel to the axis of the Transantarctic Mountains. The groove is probably filled with sediments deposited by the first glaciation of continental proportions in Antarctica. Movement of ice parallel to the Transantarctic Mountains during groove construction was possible because the oldest glaciation predates extrusion of the McMurdo Volcanic Group.

Crystalline basement in the Sound has compressional velocities ranging up to 7.5 km/s--a value usually associated with deep crust or upper mantle or less frequently, with high grade, metamorphic facies such as granulites or anorthosites. If the velocities do represent granulites or anorthosites it would extend the province of Precambrian facies rocks from a belt observed in eastern Australia to the central Transantarctic Mountains.

T 61

COCORP SEISMIC STUDIES OF THE HARDEMAN BASIN AND WICHITA MOUNTAINS, SOUTHWESTERN OKLAHOMA

J.A.Brewer,
D.Steiner
L.D.Brown
J.E.Oliver
S.Kaufman (all at: Dept. of Geological Sciences Kimball Hall, Cornell University, Ithaca, NY 14853)

COCORP seismic profiles in Hardeman County, Texas, and in southwestern Oklahoma show unusually strong and persistent reflecting horizons in the Precambrian basement at depths of 7.5, 10 and 13 km. These horizons are gently dipping and continuous over at least the 50 km covered by the profiles south of the Wichita mountains, but may be much more extensive. In the north they terminate at the southern edge of the Wichita mountains, coincident with the position of the Pennsylvanian Burch fault. The seismic data and related geological evidence indicate that the horizons were truncated in Proterozoic times by a high angle reverse fault or strike slip fault. Wide extents of felsic volcanics and associated epizonal anorogenic granites formed in the southcentral U.S. between 1.2 and 1.5 b.y. Overlapping sheets of ignimbrites and rhyolites, separated in some cases by uncomformities, may be responsible for the seismic character of the Precambrian. If the reflecting horizons can be traced to outcrop or subcrop and unequivocally identified, the basement geology covering a large area of the southern midcontinent and extending to mid-crustal depths can be understood. The presence of a major fault on the southern edge of the Wichita mountains suggests a Precambrian control on the later formation of the Wichita mountains and Anadarko basin. Reflections and diffractions are recorded from the deep crust and an event seen on two crossed profiles at about 40-43 km depth may be a Moho reflection. It has a true dip of about 10° at N20°W.

T 62

CRUSTAL THICKNESSES IN NORTH GEORGIA AND NEARBY AREAS

A. M. Dainty
L. T. Long
C. K. Lee
A. E. Kean* (School of Geophysical Sciences, Georgia Institute of Technology, Atlanta, Georgia 30332)

Crustal thicknesses have been obtained for north Georgia and nearby areas using a combination of refraction seismology, synthetic seismogram analysis and simple Bouguer gravity. Crustal thickness in the Charlotte Belt of north Georgia and South Carolina is 35 km, with an average crustal compressional wave velocity of 6.25 km/sec, based on seismic refraction and synthetic seismogram analysis. These values are consistent with the presence of presumed mantle reflections with a two way travel time of 11 sec seen on a COCORP profile in the area. Analysis of time terms of events outside the Charlotte Belt indicate that the crust thickens to the northwest, and may thicken slightly to the southeast before thinning again near the coast. A more detailed picture of crustal changes has been obtained by analysing the gravity field. Large scale negative Bouguer anomalies are interpreted as indicating a thickened crust relative to the Charlotte Belt. There is an area of thickened crust to the southeast of the Charlotte Belt under the coastal plain, but the main thickening occurs abruptly near the Charlotte Belt - Inner Piedmont boundary to the northwest of the Charlotte Belt; crustal thicknesses increase by 5-10 km at this point. The crustal thickness variations may indicate a difference between mobile (thin) and stable (thick) crust during Paleozoic tectonism, or it may represent differential isotatic adjustment in post-Paleozoic time.

T 63

THE PRECAMBRIAN - EARLY PALEOZOIC CONTINENTAL EDGE IN THE SOUTHERN APPALACHIANS

F. A. Cook
J. E. Oliver (Both at: Department of Geological Sciences, Cornell University, Ithaca, New York 14853)

Integration of various geological and geophysical data indicates that the Precambrian - Early Paleozoic transition from Grenvillian continental crust to oceanic crust or attenuated continental crust is present at depth beneath the Inner Piedmont and Charlotte belt in the southern Apalachians. The surface rocks of the Inner Piedmont, Charlotte belt and Carolina Slate belt may thus be allochthonous and overlie sedimentary (or metasedimentary) strata of this ancient continental margin. Critical evidence for this transition is derived from COCORP seismic reflection data which show nearly continuous, layered reflections between 3.0 and 6.0 sec (about 9 to 18 km depth) east of the Inner Piedmont. These reflections may be interpreted as layers of late Precambrian or Early Paleozoic strata of the Paleozoic continental margin. The Appalachian gravity gradient from low Bouguer values on the west to higher values on the east delineates the crustal transition which is probably located at or slightly west of the gravity maximum. Palinspastic reconstructions of the edge of the Cambrian - Ordovician carbonate bank coincide with the gravity change throughout the orogen. Magnetic data, which correlate with near surface mafic rocks east of the Inner Piedmont, and seismic refraction data, which suggest that rock velocities of the lower crust in the Charlotte belt - Carolina Slate belt area range from 6.3 km/sec to 6.7 km/sec and that the MOHO shallows by 10 kilometers from the Inner Piedmont to the Charlotte belt, are consistent with the presence of this crustal transition at depth. The interpretation of the linear gravity gradient as delineating the change from Precambrian - Early Paleozoic continental crust to oceanic crust suggests that extensive linear gravity anomalies in other orogenic belts may be similar in origin.

T 64

MAGNETOTELLURIC STUDY OF THE ZUNI HDR PROSPECT AND JEMEZ LINEAMENT

Mark Ander
A. William Laughlin (Both at Los Alamos Scientific Laboratory, PO Box 1663, Los Alamos, New Mexico 87545)
Robert Furgerson (Argonaut Enterprises, 1480 Hoyt St. #26, Denver, CO 80215)
John Foster (Woodward-Clyde Consultants, 3 Embarcadero Center #700, San Francisco, CA 94111)
David Strangway (Dept. of Physics, Univ. of Toronto, Toronto, Ontario)

During 1979 we performed a deep magnetotelluric (MT) study at a 100 square mile Hot Dry Rock (HDR) geothermal prospect on the Zuni Indian Reservation, NM. We first performed 121 audio magnetotelluric (AMT) soundings to detail the near surface electrical structure. No significant near surface anomalous features or lateral discontinuities, other than topographic differences were found.

A detailed tensor MT study using the remote reference technique consisted of 26 soundings. The average tipper strike is N60°E above 100 sec. and represents the structural trend within Precambrian basement. The Jemez lineament is located just SE of the Zuni prospect and strikes approx. N55°E. This strongly suggests a relationship between the deep structure beneath the Zuni prospect and the Jemez Lineament. MT modeling indicates three relatively homogeneous layers, the deepest (below 15 km) having a resistivity of 50 OHM-M in the NW, decreasing to 5 OHM-M to the SE toward the Jemez Lineament.

We are also performing a regional MT survey throughout west central NM. Preliminary results suggest the Jemez Lineament is associated with an anomalously high electrical crustal conductor. Correlation of MT, heat flow, seismics, gravity, and geology gives a consistent picture of a major "leaky" crustal lineament extending into the mantle.

T 65

GEOTHERMAL RECONNAISSANCE BY ELECTRICAL METHODS IN EASTERN ARIZONA

C. T. Young (Physics Dept., New Mexico State University, Las Cruces, N.M. 88003)

Reconnaissance electrical exploration for geothermal resources was conducted in the White Mountain region of eastern Arizona. We explored with Schlumberger profiling and soundings and by measuring telluric currents. The results show

1. Low d.c. resistivities near Springerville which correlate with known high total dissolved solids in groundwater.
2. Low d.c. resistivities near Pinetop and White River possibly indicating water-saturated regions of the Rim Gravel formation.
3. Low telluric current power ratios for stations southwest of Springerville and stations generally southeast of Pinetop. These telluric current lows could be due to a deep hot body such as a magma chamber which might have been a source for nearby volcanoes and lava flows.

Other geophysical data show that most of the survey may be underlain by a hot conductor, the top of which is 6 to 10 km deep. These data include a nearby magnetotelluric profile, Curie point depths determined from aeromagnetic data, groundwater geochemical thermometry and new heat flow data.

T 66

GEOPHYSICS OF CHIHUAHUA, MEXICO

C.L.V. Aiken, David Garvey (Programs in Geosciences, Univ. of Texas at Dallas, P.O. Box 688, Richardson, TX 75080)
John S. Oldow (Dept. of Geology, Rice University Houston, TX 77001)
Mauricio F. dela Fuente (Consejo de Recursos Minerales, Ninos Heroes #139, Mexico 7, D.F.)

The area of northern New Mexico, West Texas, and Chihuahua, Mexico is a junction of several tectonic provinces: the Basin and Range, Rio Grande Rift, Sierra Madre Occidental, and stable craton. Of special interest is the identification of an extension of the Rio Grande Rift into Mexico. Recently considerable geophysical data has been made available for the U.S. portion of the area, but comparable data in Mexico are sparse or non-existent. Logistical and related

problems have hampered field work. A regional gravity survey is being carried out north of 28° in Chihuahua. To date 800 stations have been observed and processed utilizing newly established benchmarks and 1:50,000 topographic maps, and merged with previously available data. The surveying is continuing and will eventually be merged with a considerable amount of previously unavailable gravity data from Mexican sources. The data have been used to produce a series of Bouguer gravity and residual maps using a variable topographic datum. The Bouguer correction datum is defined by those components of the wavelengths of topography which are isostatically compensated. Therefore a series of residual maps are produced which remove the effects of different wavelengths of compensation. The gravity anomaly maps are compared to regional airmagnetic maps derived from Mexican sources, covering approximately two thirds of the area. The airmagnetic and second order residual Bouguer maps outline lithologic variations very well. Distinct changes in the characteristics of both anomalies and structure delineate boundaries between tectonic provinces.

T 67

VENEZUELA BASIN OF THE CARIBBEAN: CRUSTAL STRUCTURE

J.B. Diebold (Lamont-Doherty Geological Observatory, Palisades, New York 10964)

New seismic data from large aperture common midpoint experiments and 24-channel air gun profiles have been interpreted, and the results combined with magnetic and gravity data to map a region of the Venezuela Basin where the crustal structure is different than that previously defined in the surrounding areas. Until recently, little was known of the acoustic relection character of basement in the Southeastern part of the basin due to deep sedimentary cover. Most previous work was confined to the Northwest, where little sediment is present. Acoustic basement, called B" is unusually smooth there, and depths to mantle are abnormally large. It had been commonly assumed that this condition prevailed in the Southeast as well. Recent seismic work by L-DGO and HIG shows that this is not so. Crust with the acoustic appearance of normal oceanic basement occupies an area of 50,000 km^2. This crust has normal velocity structure and thickness, but is magnetically quiet. This zone is bounded on all sides by tectonic and geophysical features, including a complex-faulted boundary with the region of smooth B", across which the depth to mantle increases. The existence of the "normal" zone explains some problems such as an offset in the otherwise linear gravity low along its southern edge, and the cause of the magnetic quiet zone with which it coincides.

T 68

SEISMIC EXPERIMENTS IN THE ARC OF GIBRALTAR CROSSING THE RONDA PERIDOTITE COMPLEX

J. Ansorge (Institute of Geophysics, ETH Zurich, CH-8093 Zurich, Switzerland)
E. Banda (same and Catedra de Geofisica, Universidad Complutense, Madrid-3, Spain)

Earlier deep seismic experiments in the eastern Betic Cordillera (Southern Spain) have been extended to the west to the arc of Gibraltar, some of the lines crossing the Ronda peridotite complex. Strong lateral variations characterize the crustal structure along the southern coast of Spain. A normal Alpine type of crust is found under the eastern and central Betic Cordillera with P-wave velocities not higher than 6.4 km/s down to a depth of about 18 km. In contrast, west of this area we find apparent velocities higher than 7.5 km/s at a depth of about 10 km at the southern edge of the Ronda ultrabasic complex. Traveltimes and the observed distance range of a later seismic phase (P_MP) indicate the existence of an additional interface, below the high velocity material, which is correlated with the crust-mantle boundary. This observation implies a relatively thin nappe-type structure of the high-velocity material. In the Gibraltar area the thickness of Mesozoic and Cenozoic sediments increases westward to more than 10 km in the Gulf of Cadiz.

Apart from these strong structural variations pronounced regional changes of the crustal thickness have been found. Based on seismic data a north-south section along 4°W shows depths of 32 km under the Hercynian Meseta, 38 km (central Betic Cordillera), 24 km (southern coast of Spain), 16 km (Alboran Sea), 25 km (northern coast of Morocco), and 30 km (central Morocco).

T 69

LATERAL VARIATION IN DEEP SEISMIC STRUCTURE ACROSS THE MARGIN OF THE WEST AFRICAN CRATON

J. C. Briden (Dept. of Geophysics, University of Western Ontario, London N6A 5B7, Canada)
J. D. Fairhead, G. W. Stuart and D. N. Whitcombe (Dept. of Earth Sciences, University of Leeds, Leeds LS2 9JT, England)
C. Dorbath and L. Dorbath (ORSTOM, 24, rue Bayard, 75008, Paris, France)

Between October 1978 and April 1979, two (20 km aperture) short period seismic arrays were operated, c. 200 km apart, on either side of the boundary between the West African Precambrian craton and the relatively young Mauritanide orogenic belt in eastern Senegal. During this time a mobile array was set up at 5 different positions between the two end arrays, giving an effective station spacing of 10 km along the profile. The area has low background seismic noise and is ideally positioned relative to the Peru-Chile (60°), Alpine-Mediterranean (30-100°) and Fiji-Tonga (antipodal) seismic zones for teleseismic reception. Several local earthquakes and quarry explosions, plus an average of more than 40 teleseismic earthquake and nuclear explosion events per month of sufficient quality for spectral and travel-time studies were obtained.

These data, together with records from vertical long-period and two horizontal short-period instruments within each array, offer the possibility of profiling the craton at crustal and upper mantle depths, and defining limits on the possible layering of the deep structure. Preliminary results show variation of more than 1.5s in relative teleseismic delay time along the traverse, changes in frequency content consistent with more complex and generally lower velocity structure beneath the mobile belt than beneath the craton, and anomalies in slowness and azimuth of teleseismic arrivals consistent with mantle structure dipping eastward beneath the craton.

T 70

THE SLATE ISLANDS: AN ASTROBLEME?

R.P. Meyer (Geophysical & Polar Research Center, University of Wisconsin, Madison, WI 53706)
J.H. Karl (Dept. of Physics & Astronomy, University of Wisconsin, Oshkosh, WI 54901)
H.C. Halls (Earth & Planetary Sciences, Erindale College, University of Toronto, Mississauga, Ontario L5L 1C6)
M.E. Bengtson (GPRC, Univ. of Wis., Madison)

Controversy over the meteoritic or terrestrial origins of the Slate Islands of northernmost Lake Superior has sparked an examination of the surrounding underwater area. A close-order aeromagnetic survey (1000 yd spacings, 425 m above lake level) made last summer shows a very long-wavelength monoclinal arcuate anomaly at ~15 km from the islands, where there is a much more irregular arcuate bathymetric rise. This long-wavelength anomaly, especially clear to the south, puts the islands in a regional magnetic low. The anomaly proves to be deep-seated, as it has the same amplitude and shape on surface marine profiles taken directly under the aeromagnetic profile with locations controlled by the identical active radar used from the air. From present incomplete marine data, short wavelength magnetic anomalies (up to 2000γ) have no bathymetric expression and short wavelength bathymetric features have small magnetic expression. Nevertheless, short wavelength marine magnetic anomalies are of higher amplitude and shorter wavelength than their aeromagnetic equivalents, indicating shallow origin.

Three linear moderate-wavelength (~1000-3000 m half-width) aeromagnetic anomalies, crossing the entire area and correlating well with previously predicted faults, are yet to be explored fully with marine traverses. Completion of the marine data set including exploration for refraction velocity differences between the ridge and the island and outside of the ridge is planned for 1980, in a search for proof (through lower velocity) of brecciation due to possible meteorite impact effects.

T 71

LATERAL INHOMOGENEITY AND ANISTROPY IN UPPER OCEANIC CRUST

R. A. Stephen (Woods Hole Oceanographic Institution, Woods Hole, MA 02543)

In order to study the lateral inhomogeneity and anisotropy in oceanic crust, polarization analysis has been performed on three-component borehole seismometer data which was collected on DSDP Leg 52. In this data set, 10-20% of the energy in the first P-wave arrival falls out of the sagittal plane. The direction of deviation is away from the spreading direction. This could be caused by velocity anisotropy in the basalt caused by large scale vertical fracturing with a pre- ferred orientation. The variability in the amount of energy falling out of the sagittal plane is four times greater for propagation parallel to the spreading direction than for propagation perpendicular to the spreading direction suggesting rougher basement topo- graphy or greater lateral inhomogeneity in the former direction. Total energy is about 8 db lower for shots parallel to the spreading direction which again may be caused by scat- tering from a rougher basement topography.

These are the first quantitative measures of anisotropy and lateral inhomogeneity in oceanic crust based on polarization analysis.

T 72

ELECTRICAL CONDUCTIVITY OF THE OCEAN CRUST AND UPPER MANTLE

C. S. Cox (Scripps Institution of Oceanography, La Jolla, CA., 92093)
P. Young (Scripps Institution of Oceanography La Jolla, CA., 92093)

The conductivity of the lower crust and upper mantle near the East Pacific Rise at 21°N is about 0.004 S/m as inferred from results of a controlled source experiment. The source and receiver were both on the sea floor and separated horizontally by 18.8 km. The source, an horizontal electric dipole, emitted electromagnetic signals at frequencies ranging from 0.25 to 2.25 Hz. The propagation path for the signals is down from the source, horizontally through the rocks, then up to the receiver. The inferred conductivity is lower than the DSDP down hole logging results in somewhat older, water saturated pillow and flow basalts, and also much lower than the conductivity of molten basalts. Our results are consistent with a principal propagation path for the signals through ocean crustal layer 3 and the underlying mantle. The path extended over distances of 5 to 23 km from the spreading center of the East Pacific Rise. The result places limits on the water content and fraction of partial melt along the propagation path.

The controlled source propagation method can be extended to longer ranges and thereby provide information on deeper structures in the mantle.

T 73

A CROSS-RIDGE REFRACTION SURVEY OF THE EAST PACIFIC RISE AT 10° SOUTH

E. W. Scarlett (Ebasco Services Inc., 2211 W. Meadowview Rd., Greensboro, North Carolina 27407)
B. R. Rosendahl (Department of Geology, Duke University, Durham, North Carolina 27708)

The East Pacific Rise crest at 10° south is characterized by an elevated axial block. Off-axis sonobuoy refraction lines shot perpendicular to the rise crest indicate an average crustal section consisting of:

Layer	P-wave velocity	Thickness
2A	3.0 km/sec (assumed)	0.5 km
2B	4.5 km/sec	1.2 km
3	6.9 km/sec	4.5 km
4	7.8 km/sec	–

The structure beneath the axial block exerts a profound influence on seismic waves. For refraction profiles that cross the rise axis, attenuation of Layer 3 and 4 arrivals is severe, and there are noticeable increases in both apparent velocities and intercept times associated with mantle arrivals. These data are interpreted as evidence of a crustal low-velocity zone (LVZ) beneath the axis. As a first approximation, this LVZ can be modeled in cross section as a triangular-shaped feature on the order of 14 km across

at its base and 4 km thick at the rise axis. Gravity profiles consistent with this model are compared to actual cross-ridge gravity data collected in the same area.

T 74

MAGMA CHAMBER AND MANTLE REFLECTIONS - EAST PACIFIC RISE

T.J. Herron
P.L. Stoffa
P. Buhl (all at: Lamont-Doherty Geological Observatory, Palisades, N.Y. 10964.

A multichannel seismic reflection profile (L-DGO MCS Line 20) of stacked CDP data, across the East Pacific Rise near the Siqueiros Fracture Zone, has confirmed earlier observations of a magma chamber and mantle reflections at two crossings (Lines 17 and 19) of the Rise crest about 35 kms to the south. The magma chamber reflection on Line 20 is about 0.65 sec below the sea floor at the Rise crest, increasing to 0.8 sec, as the reflection is followed for about 5 km down the eastern flank of the Rise. At the crest, the crustal layer above the magma chamber is about 1.7 km thick with an average velocity of about 5.1 km/sec. As compared to our results on Lines 17 and 19, this crustal layer is about 0.3 km thinner on Line 20 and appears on the eastern flank of the Rise instead of the western flank.

Mantle reflections are observed along most of the 150 km long profile. For about 50 kms just east of the Rise, the mantle reflections are almost continuous with gaps of only a few kms at several places. The mantle reflections vary from 1.85 to 2.1 secs below the sea floor. Additional processing, particularly migration, will be required to determine whether the mantle reflection can be followed under the Rise crest as was the case with Lines 17 and 19.

Contemporary Crustal Deformation

Metropolitan East
Saturday A.M.
A. Lambert (Observatory Crescent), Presiding

T 75

RATES OF CRUSTAL DEFORMATION IN INTRAPLATE HONSHU, JAPAN DETERMINED FROM SEISMIC DATA

S. G. Wesnousky
C. H. Scholz (both at: Dept. Geol. Sci. and Lamont-Doherty Geol. Obs. of Columbia U., Palisades, NY 10964)

The record of large ($M \geq 6.9$) intraplate earthquakes in Honshu, Japan allows determination of the amount of the seismic component of crustal deformation during the last 400 years. Kostrov's (1974) technique is used to equate the moment-flux to strain rates within intraplate Japan. A list of intraplate earthquakes in Japan, with known source parameters is compiled to formulate a moment-magnitude relation that is used to estimate the moments of historical earthquakes. An empirical relation between the moment and areal distribution of JMA Intensity IV is also used. Quarternary geologic evidence, and the persistency of fault-type determined from focal mechanisms during the last 50 years is used to infer the faulting mechanism of historical events. Results show that seismic crustal shortening has been occurring at an average rate of .2 to .3 cm/yr in an easterly direction. This is about 2 to 4% of the rate of plate motion being accommodated along the Japan trench.

T 76

REPEATED PRECISE GRAVITY MEASUREMENTS ON VANCOUVER ISLAND, BRITISH COLUMBIA

H. Dragert (Pacific Geoscience Centre, 9860 West Saanich Rd., Sidney, B.C. V8L 4B2 Canada)

Over the past three years, repeated precise gravity measurements have been made on Vancouver Island, B.C., to develop a practical field technique for precise gravimetric surveys which will allow detection of the effects of contemporary crustal deformation. In order to obtain a precision of measured gravity differences of several microgals (1 μgal = 10 nm/s^2), much effort has been devoted to the development of a rigorous survey method and to the evaluation of the performance of LaCoste and Romberg Model-D gravimeters. Present instrument evaluations indicate: (1) The standard errors of calculated gravity values for individual instruments on single surveys average 1.5 to 2.0 μgals; (2) Longer-term reproducibility averages from 3.0 to 4.0 μgals; and (3) Mean discrepancies between different instruments are about 5 μgals. The latter degredation in precision appears to be due to systematic non-linearities in the calibration curves. The biannual gravity surveys of the central Vancouver Island region indicate significant temporal variations over the past three years. Gravity changes as large as 60 μgals are caused by the mass effect of changing lake levels and can be accounted for by simple model calculations. A pattern of longer-term regional gravity trends is suggested by the data for the northern network. If the free-air gravity gradient is assumed to apply, a tilting up to the northwest of the order of 0.3 μrad/yr would be necessary to account for the observed gravity changes.

T 77

METEOROLOGICAL AND HYDROLOGICAL EFFECTS ON NEAR-SURFACE, BEDROCK TILT MEASUREMENTS

A. Lambert and J. J. Labrecque (Earth Physics Branch, 1 Observatory Crescent, Ottawa, Ontario, Canada, K1A 0Y3)

Four years of tilt data were recorded in a buried, near-surface vault for the purpose of monitoring possible surface deformation and changes in effective elastic modulii in the seismically active region of Charlevoix, Quebec. The identification of the true regional tilt signal is complicated by local effects due to precipitation, thermoelastic strains and changing ground water levels. Episodes of rainfall and melting snow are responsible for sudden highly directional tilts several microradians in amplitude. These tilts also correlate with ground water levels in an adjacent borehole. Intercomparison of tiltmeter and strainmeter data from the vault shows that the nature of the local deformation changes as ground water rises to the level of the vault in the spring.

The burial of the vault beneath a mound of unconsolidated material is effective in reducing the influence of daily temperature variations on tilt but it amplifies the effect of temperature variations of longer period. This phenomenon is consistent with published theoretical models of thermoelastic deformation due to topographic irregularities. Tilt data corrected for thermoelastic effects and compared with data from an adjacent levelling array reveals 5 - 10 microradian tilt variations with a length scale of at least 50 meters. The cause of these variations is still controversial.

T 78

A LONG-BASELINE MULTILIQUID TILTMETER: INSTALLATION AND PRELIMINARY RESULTS

John C. Fitzpatrick
H. James Dorman (both at University of Texas, Marine Science Institute, Geophysics Laboratory, Galveston, TX 77550)
Thomas C. Gustavson (University of Texas, Bureau of Economic Geology, Austin, TX 78712)

A two-fluid tiltmeter with a one kilometer L-shaped baseline has been installed near Chocolate Bayou on the Gulf Coast of Texas. The instrument is intended to measure surface effects of large scale production and reinjection of brine from a deep geopressured-geothermal test well. The working fluids, water and ethylene glycol, are contained in a buried multitube cable which connects measuring capsules mounted on four piers. The piers are steel pipes driven to a depth of about 10 meters. A mercury counterweight system at each pier permits a static balance between piers at different elevations. Changes in elevation of the mercury-liquid interfaces are measured visually to one micron with micrometer-driven needles.

Since October 1979, closely spaced readings have been made during daylight hours for periods of three to eight days. Raw data show large cyclical movements of all liquid interfaces; data corrected for thermal effects by the multi-liquid theory of Huggett show apparent elevation changes as great as one centimeter between piers. Meteorological factors and tidal loading in nearby bays may cause the apparent movements. Mechanical stability of the system appears to be good.

A microprocessor-controlled measuring and data-logging system will monitor temperature, barometric pressure, and water tides as well as the readings of twelve micrometers. Data from this system should permit a thorough analysis of the motions of the liquids, with the goal of extracting precise tilt information.

T 79

RANDOM ELEVATION-CORRELATED CHANGES IN SOUTHERN CALIFORNIA LEVELING

Stein, Ross S.
Silverman, Stan (both at: U.S. Geological Survey, Menlo Park, CA 94025)

Regression of tilt onto topographic slope for 1500 km of 1st-Order relevels in Southern California demonstrates that elevation-correlated changes tend to be random with respect to time in magnitude and sign, and confined in location. The mean value of the ratio of elevation change to elevation difference, determined independently for successive bench mark pairs along a level route, is 3×10^{-5}. The largest correlation found is an order of magnitude higher; the smallest that can be resolved is 1×10^{-5}. If the correlations are caused by systematic leveling error, the mean value results in a correction of ±30 mm over a 1000m topographic rise.

Circuit misclosures for the Southern California routes, generally greater than 200 km in length, are of the same order as the average elevation-correlated change. This similarity further indicates that correlated changes persist over distances less than 60 km and tend to cancel over greater distances or longer periods of time, rather than accumulate. The correlations generally do not change with change of leveling rods.

Detection of the correlation is hampered by terrains with uniform slopes, such as railroad grades. The route from Saugus, north of Los Angeles, to Gorman, at the junction of the San Andreas and Garlock faults, displays the topographic variation necessary for regression. The 133 mm uplift observed at Gorman with respect to Saugus, releveled four times between 1953 and 1968, when corrected for elevation-correlated changes, becomes 93-158 mm.

T 80

TECTONIC MOTIONS FROM LEVELING DATA (?)

D. D. Jackson (Dept. Earth & Space Sciences, UCLA, Los Angeles, Calif. 90024)
W. B. Lee
C. C. Liu
P. R. Mullen
C. C. Cheng

Analysis of precise leveling data for the U. S. reveals that some of the data are corrupted by systematic errors related to topography. Errors in some surveys appear to be larger than 10^{-4} times the topography. Topography-related errors persisted at least until 1978 in California leveling data. Inadequate calibration of leveling rods may account for much of the error, but refraction errors and other problems may also be significant. Discrepancies between geodetic leveling and oceanographic leveling suggest the existence of an additional systematic error that grows as the length of the survey. Until these systematic errors are understood and adequately eliminated from leveling data, most of the aseismic tectonic motions inferred from U. S. leveling data must be viewed with suspicion.

T81

THE IMPACT OF REFRACTION CORRECTION ON LEVELING INTERPRETATIONS IN CALIFORNIA

William E. Strange (National Geodetic Survey, National Ocean Survey (NOS), NOAA, Rockville, MD 20852)

Recent investigations show that the refraction correction in leveling is large but can be adequately modeled. The correction is proportional to the temperature gradient and to the square of the sight length. Differences in

sight length are often more important than differences in temperature gradient in causing differences in the magnitude of the correction between surveys. In 1964, the NOS's National Geodetic Survey reduced sight lengths, causing apparent crustal motion in the releveling of many lines where uncorrected data were applied. With proper application of refraction corrections, recent presumptions concerning large errors in leveling rod calibration are negated. Other apparent errors and postulated phenomena are more readily understood when refraction corrections are applied to the observed data.

Applying refraction corrections to the data in the vicinity of Palmdale significantly alters the size and configuration of the "Palmdale Bubble." Maximum vertical motion at Palmdale and Lebec relative to Los Angeles (BM V32) is less than 10 cm. The bulk of the motion (6 to 7 cm) apparently occurs as localized motion along the San Gabriel fault in the 1955-1964 time frame. This motion along the San Gabriel fault and the uplift along the San Fernando fault within the same time period appear to be precursors to the 1971 San Fernando earthquake.

T 82

THE IMPERIAL VALLEY EARTHQUAKE: INERTIAL DISPLACEMENT MEASUREMENTS BY TILTMETERS IN THE LOS ANGELES BASIN

C. P. Buckley (Department of Earth Science, California State University, Fullerton, Fullerton, CA 92634)
C. W. Kohlenberger (Autonetics Division, Rockwell International, Anaheim, CA 92803)

Seismograms recorded by two tiltmeters, CSF and ARI, located 250 and 244 km northwest of the Imperial Valley earthquake (M-6.6) of October 15, 1979, show an unusual low frequency signal arriving with the P-waves. We interpret the signal to be the result of acceleration. Other explanations such as instrument non-linearity and tilt can be rejected based upon the known characteristics of the instrument, and plausible physical models for crustal behavior. The signal is amplitude assymetrical for the first ten seconds in the south and west directions, then crosses zero and becomes assymetrical in the north and east directions for three seconds. At this time normal P-wave motion begins to dominate the signal. Double integration of the first 17.4 seconds of data at 0.1 second intervals, suggests that a net translation of not greater than 2 mm occurred at both instruments in a southwest direction. Tilt changes detected by CSF and ARI are within normal limits for one day before and one day after the earthquake. However, both instruments recorded anomalous tilt changes in the 10 day time period beginning October 17. Whether this can be attributed to the increased seismic activity within the Los Angeles basin, to the regional strain associated with inertial displacement, or to other causes, is being studied. We are also examining the methods by which inertial displacement measurements can be obtained from tiltmeters, so that the time relationship of μ strain can be studied.

T 83

REGIONAL CRUSTAL DISTORTION EVENTS IN SOUTHERN CALIFORNIA: A CONFIRMATION OF JERKY PLATE MOTION?

J. H. Whitcomb (Cooperative Institute for Research in Environmental Sciences, University of Colorado, Boulder, CO 80309)

In 1974, a series of coordinated geophysical measurements of regional crustal distortions was begun in Southern California in order to study the question of whether plate motion is smooth or jerky over 1-10 year time scales and to investigate the phenomenon of dilatancy. A key new technique that made this possible was Very Long Baseline Interferometry (VLBI), which measures positions of a pair of widely-separated antennas in three dimensions with high accuracy. Other measurements were designed to correspond both in time and space with VLBI including gravity, magnetotellurics, and radon. In mid-1979, a crustal distortion event began in the area of the central Transverse Ranges of Southern California that was observed in all these methods. VLBI showed a horizontal dilatation of about one microstrain over a period less than three months and a region of hundreds of kilometers. Discovery of this large strain led to a request for reoccupation by the U. S. Geological Survey of a local strain net in the Palmdale vicinity of the San Andreas fault. This net showed the same one microstrain dilatation. During this time, radon showed a substantial increase and gravity showed a decrease of 50 microgals. Magnetotelluric measurements showed a rapid change in the orientation of the apparent resistivity tensor. A similar dilatational distortion episode appears to have occurred in 1975 based on VLBI and gravity data. Because the VLBI data show periods of years of quiescence followed by large motions over times less than a few months, they strongly indicate that plate motions are jerky at regional scales of hundreds of kilometers. This conclusion has far-reaching implications for earthquake prediction at plate boundaries.

T 84

THREE DIMENSIONAL GEODETIC INVERSION METHOD FOR OBTAINING STRESS IN THE LITHOSPHERE

K. Ikeda (Department of Earth and Planetary Sciences, Massachusetts Institute of Technology, Cambridge, MA 02139)

Three dimensional geodetic inversion method to obtain incremental stress in the earth are presented with a preliminary result on the application to the data from Palmdale, California. Geodetic inverse problem is formulated as an elliptic operator equation with Cauchy's boundary condition applied to a body that is cut out of the earth under the surface on which displacements are known. Three dimensional finite element scheme provides a discretized form of the operator. Data obtained from geodimeter and levelling survey, together with a stress free condition on the free surface provide boundary conditions. The inversion scheme is tested using artificial data generated by Mindlin's buried point force solution with the result showing satisfactory accuracy of the inversion scheme. The incremental stress obtained during the period 1959 to 1972 shows the dominance of horizontal tensional stress in the direction of N48°W with magnitude 2.1 bar at the depth of 3.75 km. During the period 1974 to 1977 the maximum principal incremental stress turns to be horizontal compression in the direction of N40°W with magnitude 2.2 bar at the depth of 3.75 km while minimum principal stress is near vertical. The compressional stress increases with depth to 4.2 bar at the depth of 6.5 km and 7.0 bar at the depth of 8.75 km without changing directions so much. The sense and direction of the principal incremental stress during the period 1974 to 1977 and its magnitude are consistent with the fault plane solutions obtained for swarm activities and geomagnetic change observed in this area during this period. The obtained incremental stress also explains the increase of seismicity by an order of magnitude in this area during the period 1974 to 1977.

T 85

STRESS MEASUREMENTS AT REYDARFJÖRDUR, EASTERN ICELAND

Bezalel C. Haimson (1509 University Avenue, Univ. of Wisconsin, Madison, WI 53706).

The Icelandic Research Drilling Project (IRDP) deep hole (1919 m) in eastern Iceland is located at sea-level at the head of Reydarfjördur, 8 km east of the Thingmuli central volcano and 20 km north of the Greiddalur central volcano. Nineteen hydrofracturing stress measurements were conducted between 50 m and 575 m depth. As indicated by the continuous drill core the tested section consists of tertiary subaerial tholeiitic lava flows cut by many basaltic dikes. Surface measurements by Walker (1959, 1974) revealed a general NNE trend for the local dike swarm, with an actual spread of between N10°W to N30°E. The mean maximum horizontal stress direction as determined in our tests is N50°E ± 20°, or some 30° east of that implied by the dikes. Within 50-270m depth the measured principal horizontal stress magnitudes (σ_H and σ_h) are larger than the calculated vertical stress σ_v, and increase linearly with depth at a rate similar to that of σ_v (0.027 Mpa/m), reaching values of σ_h = 7.5 MPa and σ_H = 9 MPa; a sharp increase with depth in the next 150 m leads to magnitudes of σ_h = 15 MPa and σ_H = 24 MPa at 440 m; most unexpectedly, in the deepest 125 m the stress gradient reverses itself such that at 575 m σ_h = 8 MPa, and σ_H = 10 MPa. Unfortunately, deeper measurements to observe the stress-depth realignment were not possible because of casing in the hole. The detailed core log reveals that thick multiple dike intrusions are found at 65-175 m and 500-600 m. These depth ranges appear to be associated with the low stress values, while the zone that is mainly lava flows (200-500 m) is dominated by high stresses. Processes such as dike formation (fracture opening mechanism and magma injection pressure) and lava flow subsidence may account for the unusual stress-depth fluctuation. The maximum horizontal stress direction differs widely from the northwesterly trend west of the axial rift zone.

T 86

INTRAPLATE STRESS ORIENTATION FROM ALBERTA OIL-WELLS

J.S. Bell (B.P. Canada Ltd., 333 5th Avenue S.W., Calgary, Alberta, Canada T2P 3B6)
D.I. Gough (Institute of Earth and Planetary Physics, University of Alberta, Edmonton, Alberta, Canada T6G 2J1)
E.A. Babcock (Alberta Research Council, Edmonton, Alberta, Canada T6G 2C2)

Many oil-wells in Alberta exhibit spalling of the walls, known as break-outs, which elongate the holes with the long axes aligned northwest-southeast. This alignment occurs over an area of $10^5 km^2$ or more, in sediments of several types through the stratigraphic column from Devonian to Cretaceous. Bell and Gough have elsewhere suggested that these break-outs are produced through stress concentration at the hole walls, in a stress field having unequal horizontal principal stresses and with the greater of these oriented northeast-southwest. It is probable that this NE-SW principal stress is σ_1. This paper adds to the evidence from the ^{1} oil-well breakouts, inferences from hydraulic fracturing in the Rocky Mountain foothills, and from steam-injection fracturing in eastern Alberta. In both areas fractures are predominantly vertical and oriented NE-SW, indicating that σ_3 is NW-SE and supporting the above hypothesis of stress orientation. Further evidence from break-outs in wells west of the Rockies also appears to support the hypothesis. The break-outs are consistent with either a thrust stress field or a strike-slip field, but the fractures formed by excess pressure in the holes favour the latter.

T 87

SHEAR HEATING AND THE STATE OF STRESS ON FAULTS

C.H. Scholz (Dept. Geol. Sci. and Lamont-Doherty Geol. Obs. of Columbia Univ., Palisades, NY 10964)

Evidence for shear heating associated with crustal faulting has been described for a number of fault zones in a wide variety of tectonic environments. The evidence is that a thermal anomaly associated with the fault has resulted in the metamorphism of adjacent rocks to higher grades than can be accounted for by considering other heat sources. A number of such cases are recapitulated here, to conclude that if relative displacements across these faults occurred at plate tectonic rates or slower, then shear stresses of several kilobars must have existed on these faults in order to produce the observed shear heating. Alternatively, these faults moved at several tens of cm per year, much higher than observed past and present plate tectonic rates. Although the case for shear heating in many individual cases is arguable, the evidence in toto strongly suggests that shear stresses of several kilobars must have existed on some crustal faults. Shear heating during dynamic rupture of faults also can produce melting within fault zones. Two interesting cases of large landslides that produced melting suggest (1) the dynamic coefficient of friction does not vanish after melting but remains at a significant level, and (2) the efficiency for melting rock by frictional heating in these cases was probably less than 10%, implying that the amount of frictional heating necessary to produce melting during an earthquake may be an order of magnitude higher than previously thought.

T 88

OCEAN LOADING AND THE TIDAL TRIGGERING OF EARTHQUAKES

J. Beavan (Lamont-Doherty Geological Observatory of Columbia University, Palisades, New York 10964)

Most published studies of tidal triggering of earthquakes suffer from defects so serious as to render their results irrelevant in deciding whether earthquakes ever are triggered by the stresses due to earth tides. These stresses reach levels of only a few hundredths of a bar.

One problem is that earthquakes occur at various locations on different planes and with different slip directions, while tidal stresses vary in magnitude and phase with both position and direction. Hence the tidal stress must be calculated at the appropriate position and in the appropriate direction before meaningful comparisons can be made. This difficulty can be avoided by treating earthquakes within a small geographical area and assuming they all have approximately the same fault plane and depth. A second problem is that all studies to date have effectively ignored the ocean tides. In the present study, stress tides due to ocean loading have been calculated within the upper 700 km of the earth and it is shown that their magnitude is generally of the same order as that of the solid earth tide. Tidal stresses in the direction of failure and normal to the fault plane are being calculated for a suite of earthquakes. The triggering effect will be evaluated statistically and compared with a similar analysis which ignores ocean loading.

T 89

DISCUSSION OF OBSERVED TIME-DEPENDENT FRICTIONAL STRENGTH IN ROCK AND TIDAL TRIGGERING OF SEISMICITY

T. Johnson (Lamont-Doherty Geological Obs. of Columbia Univ., Palisades, NY 10964)

Earthquakes are often modeled by frictional sliding across faults occurring when shear stress exceeds static friction. Tectonic stress is assumed to accumulate at a slow rate. Due to tides, stress on a fault consists of a gradually increasing component and a small, rapidly varying one. If the static frictional strength is constant then slip should occur almost exactly at peak tidal stress. Saw-cut granite cylinders were loaded triaxially to mimic combined tectonic and tidal stresses. Gradual net inward motion of the axial ram increased shear stress on the friction surface while a small periodic in-and-out dither produced a cyclic variation. Accelerating slip was observed before stick-slip events. Stick-slip occurred on the decreasing part of the stress-displacement curve when it became tangent to the stiffness. Stick-slip commonly occurred during the increasing part of the shear stress dither, but below the dither peak and below the maximum shear strength. The condition for instability is the slope of the σ-D curve, not the peak stress so there is no reason to expect events to correlate with stress peaks. A clear tidal periodicity is present in lunar seismicity. Such a clear periodicity is observed rarely in earthquakes, and when a tidal correlation is observed the earthquakes often do not occur at the peak tidal shear stress. The experiments suggest that time dependent strength of faults may be partially responsible for the imprecise correlation between tidal loading and earthquakes. Experimental time dependent strength is due to hydrolytic weakening. Dry conditions may produce the clear periodicity in lunar seismicity. Premonitory slip appears due to time-dependent strength. Evidence that faults have time-dependent strength implies that precursory slip may occur before earthquakes.

T 90

CHANGES IN INDUCED MAGNETIZATION WITH DIFFERENTIAL STRESSES AND DURING CREEP. AN INTERPRETATION IN WEAK STRESSES

J.P. Pozzi (IPGP, University of Paris 6 Place Jussieu, 75230 Paris Cedex 05 France)
J. Zlotnicki
F. Cornet

Improvements in the reduction of observations of local anomalous changes of geomagnetic field in tectonic areas (Johnston, 1977) allow us to consider that the stress sensitivity of the magnetization of crustal rocks could give an independent estimate of changes in stress in the upper part of the crust. Tectonomagnetic models are generally poorly constrained since the position, the dimensions of sources and their stress-induced changes of magnetization are poorly known.

Several recent works concern the changes of remanent magnetization with differential stress (Reval et al, 1977 ; Martin et al, 1978) but the variations of induced magnetization caused by stress seem to be poorly known under these conditions. This work deals with these changes and their interpretation.

By the combination of uniaxial pressure, confining pressure and pore pressure, each being completely independent from the others, we have measured the changes in induced magnetization of volcanic rocks with differential stress for increasing depths (increasing confining pressure). The effect of temperature has been considered up to 250 c. The results are : for weak differential stresses, changes of magnetization are of considerable amplitude for confining pressures up to 1.5 kl.

During a 5 min controlled creep with $\Delta L/L = 2\%$ and $\Delta V/V = 0{,}8\%$, the changes of induced magnetization are very weak. This result is different from the available data on changes of remanent magnetization.

We give a new calculation of the stress induced variations of magnetization by transformation of the Preisach Neel diagram relative to polydomain minerals.

Mantle Convection and Subduction Mantle

Metropolitan Centre
Saturday A.M.
E. M. Parmentier (Brown University), Presiding

T 91

A SIMILARITY THEORY FOR MANTLE CONVECTION AT LARGE RAYLEIGH NUMBERS

Peter Olson (Dept. of Earth & Planetary Sciences, Johns Hopkins University, Baltimore, MD 21218)

Results of a similarity theory for mantle convection are presented, which are asymptotically valid in the limit of high Rayleigh number R .The purpose is to investigate effects of spherical geometry, heat source distribution, boundary conditions and variable viscosity. Analytical, steady state solutions are found for fields of motion which are spatially periodic and represented by a single spherical harmonic of arbitrary degree. Analysis shows that the temperature distribution consists of a nearly isothermal interior region bounded by thin thermal layers along the outer and inner surface of the convecting shell. The relative size of these two layers depends on heat source distribution, the viscosity profile, the depth of circulation and the dynamic boundary conditions at each surface. When all heat comes from below, the heat transfer is proportional to $R^{1/3}$ if both boundaries are stress free, and is proportional to $R^{1/5}$ if both boundaries are rigid. When all heat is generated internally, the effect of rigid boundaries is to raise the average mantle temperature above its equilibrium value for stress free surfaces. Spherical effects and any decrease of viscosity with depth both act to reduce the relative thickness of the basal thermal layer, while a viscosity increase with depth tends to increase its thickness. Results of this theory can be used to relate horizontal velocities at the surface to quantities such as heat loss, viscosity stratification and depth of circulation. The greatest effect is due to thickness of the convecting shell. Deep mantle convection can achieve surface velocities which agree with observed plate speeds; shallow convection can not.

T 92

COMMENTS ON SCALING LAWS FOR CONVECTION IN SHELLS WITH CONSTANT AND TEMPERATUE-DEPENDENT VISCOSTITY: FREE-FREE BOUNDARIES

Erik R. Ivins
Roger J. Phillips, both at JPL, Caltech, Pasadena, CA 91103

Scaling laws for thermal boundary layers and total heat transport in thermal convection relevant to the planetary mantle use the emperical relation $Nu = b(Ra/Ra_c)^{\beta}$, where b and β are empirical constants, Nu is the Nusselt number, and Ra and Ra_c are the Rayleigh and critical Rayleigh numbers, respectively. Experiments with temperature-dependent viscosity in a rigid-rigid plane layer indicate that by properly identifying Ra_c, then b and β are the same as in the constant viscosity case. Using numerical solutions of a spectral form of the mean field convection problem in a self-gravitating shell with perfectly conducting, stress 'free' boundaries and a temperature-dependent viscosity relevant to planetary mantles with shell aspect ratios $\eta = 0.6$, $\eta = 0.8$ and a total viscosity variation, $\upsilon_{max}/\upsilon_{min}$, of $O(10^2)$, we observe an unmistakable decrease in the heat transport relative to the constant viscosity case using a variety of interpretations of the ratio Ra/Ra_c. We find $\beta = 0.30 \pm 0.01$ and $b = 1.61 \pm 0.01$ for both $\eta = 0.6$ and $\eta = 0.8$ with a reference viscosity arbitrarily defined at the middle of the shell, while for constant viscosity and both shell aspect ratios, the data is best fit by $\beta = 0.350$ and $b = 1.99$. The difference in our numerical results and that at laboratory experiments is attributable to the differences in stress boundary conditions and possibly to our finite-amplitude interpretation of Ra_c. A simple parameterization of the boundary layers accurately predicts the isothermal convecting temperature for a constant viscosity shell, however, for variable viscosity this simple parameterization breaks down, although the isothermal convecting temperature is well approximated by the constant viscosity case for large Ra/Ra_c.

T 93

THERMAL EVOLUTION OF PLANETARY INTERIORS WITH NON-NEWTONIAN RHEOLOGY

E. M. Parmentier
J. Morgan III (both at: Dept. of Geological Sciences, Brown University, Providence, RI 02912.

A number of recent studies have utilized heat transfer relationships derived from laboratory measurements and numerical calculations for convection in fluid layers to approximately describe planetary thermal evolution. In the present study, this parameterization of convection is extended to more realistic strainrate dependent (non-Newtonian) rheologies. Parmentier (1978) noted that steady state heat transfer due to two-dimensional convective modes in a non-Newtonian fluid layer was nearly identical to that for a Newtonian fluid if the Rayleigh number for the non-Newtonian layer was expressed in terms of a dissipation rate averaged viscosity. These earlier results are extended to volumetrically heated fluid layers and, with the same definition of an average viscosity, a similar correspondence between non-Newtonian and Newtonian steady state heat transfer results. The steady state heat transfer relationships thus obtained are applied to describe the thermal evolution of planetary interiors. Comparing Newtonian and non-Newtonian cases shows that rheology significantly affects thermal evolution. Non-Newtonian planetary interiors with strongly temperature dependent viscosity would approach a steady state, in which surface heat flow equals radiogenic heat production, about twice as fast as their Newtonian counterparts. These thermal evolution calculations suggest that the presentday Earth is close to steady state.

T 94

DYNAMICS OF THE D" LAYER

Richard A. Lux
I. Selwyn Sacks (both at: Dept. of Terrestrial Magnetism, Carnegie Institution of Washington, Washington D.C. 20015)

A number of studies indicate lateral heterogeneities within the D" layer at the base of the mantle. One study, comparing the amplitudes of PKPAB to PKPDF, suggests that the D" layer is smooth in some areas and heterogeneous in others. The lateral variations in the D" layer could be caused by two different styles of convection. The smooth areas may indicate whole-mantle convection. The heterogeneous areas can be explained by convection having a horizontal scale of about 150km.

A finite-difference numerical model is used to investigate the convective structure at the base of the mantle. The first case considered is a fluid heated from below and having an exponential viscosity variation with temperature. For likely mantle parameters, the model shows that the lower thermal boundary layer of a whole-mantle convection cell may be stable. The viscosity is reduced within the hot thermal boundary layer, and this reduced viscosity allows the horizontal velocity to increase and to counteract the normally destabilizing effect of the low viscosity. This model neglects instabilities in the third dimension. These disturbances, along with other phenomena, such as a viscosity dependent upon both depth and temperature or an internally-heated upper mantle, may be necessary for small-scale motions to occur.

T 95

MANTLE CONVECTION CONSISTENT WITH OBSERVED SURFACE FIELDS

W.M. Kaula (Dept. of Earth & Space Sciences, Univ. California, Los Angeles, CA 90024)

The spherical harmonic spectra of plate velocities, gravity, topography, and heat flow are closely approximated by forms $M\ell^{-n}$, where ℓ is harmonic degree. The magnitudes M and slopes n of heat flow and gravity, compared to those of the poloidal velocity, imply a lithospheric viscosity of $\sim 10^{23} gmcm^{-1}sec^{-1}$, comparable to stress/strain rate ratios inferred from studies of flexure at subduction zones. The correlations among the fields as functions of degree also appear explicable as the consequence of properties of the lithosphere (including its subducted extension).

Applying boundary layer theory to plate velocities implies a Rayleigh number of $\sim 10^7$ for whole mantle convection and $\sim 10^6$ for convection confined to the upper mantle. To estimate the constraints on thermal and rheological parameters therefrom, a temperature curve consistent with phase transition data is constructed. The effective thermal expansivity is increased by phase transitions at depths of 400-700 km, but this effect is less important than a marked decrease from $\sim 3x10^{-5}$ to $10^{-5}°K^{-1}$ at the bottom of the mantle. The Rayleigh number of $\sim 10^6$ for upper mantle convection then is approximated rather well by viscosities corresponding to standard non-linear strain rate stress laws below 60 km. The Rayleigh number of $\sim 10^7$ for whole mantle convection requires a moderate increase in viscosity with depth, such as could plausibly arise from a moderate decrease in the activation volume for creep with depth.

Constraints from the surface fields on the depth of mantle convection, etc. are being sought through a more detailed modeling in spherical harmonics, calculating non-linear terms by harmonic analyses of the spatial transforms.

T 96

VOLCANISM AND ASEISMIC SLIP IN SUBDUCTION ZONES

H. K. ACHARYA (Stone & Webster Engineering Corp., 245 Summer St, Boston, MA 02110)

The spatial and temporal relationship of volcanism to the occurrence of large earthquakes and convergent plate motion is examined. The number of volcanic eruptions per year in a convergence zone is found to be linearly related to the aseismic slip component of plate motion. If the aseismic slip rate is low (coupling between converging plates is strong), then the primary manifestation of tectonic activity is the occurrence of large earthquakes with only infrequent volcanic activity. If, however, the aseismic slip rate is high (coupling is weak), then there are few large earthquakes and volcanism is the principal manifestation of tectonic activity. This model is consistent with the spatial distribution of large earthquakes and active volcanoes in the circum-Pacific area. It is tested by examining the extent of volcanic activity in the rupture zones of the 1960 Chile earthquake and the 1952-1973 sequence of earthquakes in the Japan-Kurile Islands area. The number of volcanic eruptions along these zones, during the interval between large earthquakes, is used to compute the aseismic slip rates, for these segments, based on the relationship developed in this study. The aseismic slip rates so computed agree with those determined from the earthquake history of the area and rates of plate motion. The agreement suggests that in the interval between large earthquakes, the aseismic plate motion is manifested in a specific number of volcanic eruptions. Therefore, it should be possible, in areas with adequate historical data, to use the model developed in this study to monitor volcanic eruptions for long term prediction of large earthquakes.

T 97

INTERPRETATION OF GEOID ANOMALIES IN THE VICINITY OF SUBDUCTION ZONES

D. C. McAdoo (Geodynamics Branch, Goddard Space Flight Center, Greenbelt, MD 20771)

It has been observed that trench/island arc complexes are associated--on a global scale--with gravity highs. It is natural to speculate that this association may be a result of positive density anomalies in the subducting slabs. Gravity anomaly profiles across subduction zones are dominated by crustal effects which mask the gravity signal of these slabs. However, estimates of the geoid derived from GEOS-3 and Seasat radar altimeter data prove to be much better suited to the task of detecting the intermediate wavelength (500 - 5000 km) geopotential variations. It is primarily these wavelengths that are produced by slabs. Model geoids computed from the effects of slabs of the southwestern Pacific area demonstrate a convincing agreement with altimeter-derived geoids of the region. Subducting slabs are represented as thin surfaces of anomalous mass per unit area. These surfaces are positioned using published seismic results detailing the configuration of the Benioff zones. Crustal effects are ignored. The contributions of the young marginal basins in contrast with older oceanic lithosphere are assessed. Results suggest that the New Hebrides slab possesses an average areal density anomaly of about 3×10^6 kg.m^{-2}. This is three times the areal density estimated for the Tonga-Kermadec slab. The geoid in the region of the South Sandwich island arc is also studied. These results should help improve the understanding of body forces which act on subducting slabs.

T 98

A DETAILED STUDY OF A SEQUENCE OF MAGNITUDE 6 EARTHQUAKES IN THE CENTRAL NEW HEBRIDES ISLANDS

R.K. Cardwell
B.L. Isacks (both at: Dept. of Geological Sciences, Cornell University, Ithaca, NY 14853)
J.L. Chatelain (ORSTOM, Noumea, New Caledonia)

From September 1978 to August 1979 a sequence of four moderately large earthquakes (Ms=6) occurred in the central New Hebrides Islands less than 100 km from a new, permanent seismograph network. The events occurred on September 1, 1978 (Ms=5.9), January 27, 1979 (Ms=5.9), August 17, 1979 (Ms=6.2) and August 26, 1979 (Ms=6.1). Except for the January event the earthquakes were followed by numerous aftershocks. There were also swarms of earthquakes in March 1979 and December 1979, but no single, large-magnitude event accompanied that activity. All events in the sequence were located in the arc-trench gap at shallow depths.

The January earthquake is located south of the seismograph network and appears to be a high-angle normal fault within the upper plate. The other events are all located west of the network near the northern end of the South New Hebrides Trench. The aftershock zones of the earthquakes in this region abut, but do not overlap. The northern limit of the aftershocks coincides with a prominent bathymetric depression which trends nearly perpendicular to the island arc. The earthquakes appear to occur in both the upper plate and along the main zone of underthrusting between plates. Research is continuing to determine the exact geometries of the structural features along which the earthquakes occurred. This region has been a seismic gap for large, thrust-type earthquakes for at least 30 years.

T 99

A COMPARISON OF THE IZU-BONIN MARIANAS AND CHILEAN CONVERGENT MARGINS

Shi-Chen Wang
Robert J. Geller
Zvi Ben-Avraham (all at: Dept. of Geophysics, Stanford University, Stanford, CA 94305)

The Izu-Bonin-Marianas arc, and the Peru-Chilean arc, are usually considered the extreme examples of convergent margins. The former is characterized by active back-arc spreading, no fore-arc gravity high, and the absence of large interplate thrust earthquakes, while the latter is nearly opposite in these regards. In both arcs there are volcanic gaps associated with the subduction of aseismic ridges. Both margins also have a second shallow seismic zone landward of the trench. We study these gaps, and the associated seismicity.

Seismicity along the Peru-Chile arc is primarily limited to depths shallower than 250 km. Two isolated concentrations of deep earthquakes at depths of 500-700 km represent the only significant deeper seismicity. The southern ends of each zone of deep seismicity roughly coincide with the present intersection points of the Nazca and Juan Fernandez Ridges with the trench. The intersection points of these ridges with the trench have migrated south with time, and have probably caused the observed volcanic gaps. The Marianas seismic zone is more or less continuous with depth, with steep dip in the central portion, while along the more northerly Izu-Bonin arc there is a distinct absence of intermediate seismicity. As in the Peru-Chile case, the deep seismicity ends at the point where the Marcus-Necker seamounts intersects with the trench. Similarly, the intersection point has also moved south and caused the volcanic gap in the Izu-Bonin region.

The nature of the deep seismicity differs quite substantially between the Izu-Bonin-Marianas and Peru-Chile arcs. This difference may be related to the different modes of consumption of the downgoing oceanic lithosphere.

T 100

FOCAL MECHANISMS AND ACCURATE DEPTHS OF CRUSTAL EARTHQUAKES IN THE ANDEAN CORDILLERAS

Douglas S. Chinn
Bryan L. Isacks (both at Dept. of Geological Sciences, Cornell University, Ithaca, NY 14853)

Accurate depths from 19 earthquakes with known focal mechanisms are obtained by matching synthetic seismograms to observed P waveforms. Crustal seismicity, which is concentrated mainly in the eastern part of the Andean cordilleras, occurs at depths between 10 and 40 km, with 35% of the determined depths occurring between 20 and 40 km. The 27 focal mechanism solutions for the region from Ecuador to Argentina show a strong grouping of the compressional axes about a horizontal east-west direction, and are mainly dip-slip in orientation. These results suggest that crustal shortening rather than vertical block movement is the predominant present-day deformation in the seismically active areas of the eastern Andes.

Above the two nearly flat dipping segments of the subducted Nazca plate, significant seismicity is located in the Eastern Cordillera and Sub-Andean zones of Peru and in the Pre-Cordillera and Sierras Pampaeanas of western Argentina. If this seismicity lies east of the main area of coupling between the converging plates, then the area of coupling is located where the slab dips more steeply beneath the coast before it levels off at about 175 km from the trench. At a similar distance inland from the trench near the Peru-Chile "corner", the slab does not level off but continues downward to form a more steeply dipping plate segment. Also at this distance, the zone of active volcanism, which is missing above the flat slabs, is found. Farther landward above this more steeply dipping segment is the wide zone of uplift comprising the Altiplano/Puno and much of the eastern cordillera of Bolivia and northwestern Argentina. This zone of uplift has relatively little seismicity. Instead, the activity appears to be concentrated along the eastern boundary of the uplift along the N to NNE striking part of the sub-Andean zone of Bolivia and northwestern Argentina.

T 101

THE SUBDUCTION OF THE NAZCA PLATE

A. Hasegawa (Tohoku University, Japan)
I. S. Sacks (Dept. of Terrestrial Magnetism, Carnegie Institution of Washington, Washington, D.C. 20015)

Two conflicting models which have been proposed for the subduction of the Nazca plate beneath central Peru each satisfy only part of the available seismic observations. A detailed re-investigation of seismicity as well as of anelasticity and converted phases has produced a model which is compatible with all the data.

Local network data was used to determine seismicity; from ISC data, focal mechanisms were calculated for all earthquakes selected by Barazangi and Isacks 1979. These data reveal that for the first 100 km or so of depth the slab subducts at the normal dip angle of about 30° - below this depth it is bent to a nearly horizontal angle. This horizontal slab extends inland (eastwards) about 300 km, and then dips steeply (30°) below the thick continental lithosphere of the shield region.

Beneath the region from southern Peru to northern Chile, the Nazca plate descends with an almost constant dip of ~30° down to at least 300 km in depth. In the transition from central to southern Peru, the precision seismicity delineates a contorted but continuous slab in the depth range 100 km to at least 150 km. From an inversion of anelasticity data using 3-dimensional ray tracing, it appears that the subducting plate is continuous down to the deepest earthquakes (~600 km) even though the 300-500 km depth region is aseismic. There is no evidence for tears in the plate - deformations satisfy the data better because there are high Q paths across postulated tear zones.

T 102

RIDGE CREST SUBDUCTION ALONG THE SOUTHERN CHILE MARGIN

S.C. Cande
E.M. Herron (both at: Lamont-Doherty Geological Observatory, Palisades, N.Y. 10964)

The Nazca-Antarctic-South America Triple Junction is located at 47°S on the Chile Margin. North of the triple junction the Chile Ridge is approaching the Chile Trench at 55 mm/yr. At the triple junction an actively spreading section of the Chile Ridge is in the process of being subducted. South of the triple junction several sections of the ridge crest have been subducted in the past 15 m.y. From data acquired on recent CONRAD cruises we observe the following: 1) North of the triple junction the inner wall becomes progressively narrower and steeper approaching the triple junction. 2) At the collision zone itself the trench inner wall is narrower than anywhere else on the margin. 3) South of the triple junction the inner wall becomes progressively wider until by 100 km south of the triple junction, a well developed mid-slope terrace and trench-slope break are observed. We propose the following model to explain these observations: As the ridge crest approaches the inner wall, the inner wall is uplifted and eroded, with maximum uplift and erosion occuring when the ridge is subducted. Following the passage of the ridge crest the outer edge of the continental margin subsides, perhaps forming the floor of the offshore terrace. The net result is that the continental margin is eroded by roughly 30 km.

T 103

ACTIVE TILTING OF THE OREGON AND WASHINGTON COASTAL RANGES

John Adams (71 James Street, Ottawa, Ontario K1R 5M2, Canada)
Robert Reilinger and James Ni (both at Dept. of Geological Sciences, Cornell University, Ithaca N.Y. 14853)

Tilted and uplifted marine terraces of Oregon and Washington show progressive landward tilting of the coast ranges at about 4 to 7 degrees per m.y. for the last 0.25 m.y. Seven resurveyed leveling lines running inland from the coast suggest contemporary landward tilt rates of about 1 to 9 x 10^{-8} rad. yr^{-1} (0.6 to 5 degrees per m.y.) averaged over periods of from 10 to 40 years. The leveling lines traverse, and the terraces cut across, dipping Cenozoic strata: Pleistocene (dips to 3°), Mio-Pliocene (dips to 30°) and Eocene (dips to 60°). At least four places (Cape Blanco, Bandon, Cape Arago, and Siuslaw River) are characterized by geodetic or terrace dips that have the same direction as the underlying stratal dips. Assuming a constant tilt rate as deduced from the geodetic and terrace observations, the strata dips suggest that deformation began 7 m.y. ago, perhaps due to a change to less rapid subduction of the Juan de Fuca plate at that time. The terraces and geodetic leveling document present-day deformation of the coastal ranges, most likely related to active subduction of the Juan de Fuca plate. The steep stratal dips, lack of major active faults and historic earthquakes, and presence of very young, reverse bedding-plane faults suggest that much of the onshore deformation within the overlying North American plate is taken up by folding rather than thrust faulting.

T 104

A FINITE ELEMENT MODEL OF SUBDUCTION: DEFORMATION IN THE ARC-TRENCH GAP

Thomas M. Tharp (Dept. of Geology, Wright State Univ., Dayton, OH 45401)

The finite element model includes consistent isostatic stiffness, a megathrust with anisotropic shear strength, and a von Mises elastic-plastic lithosphere. The yield shear stress was set between 0.2 and 1.0 kb for the anisotropic megathrust, and 1.0 and 2.0 kb for the lithosphere. The high strengths are consistent with non-linear trench flexure analysis. Models with both a weak megathrust and a high density subducted plate required a push of 0.5 to 1.0 kb. Realistic displacements also occurred in the absence of either one of these features, but a push of 3 kb was then required.

In models with a weak megathrust, energy dissipation in the overriding lithospheric wedge approached that on the megathrust itself. The upward plastic bending in this region also produced 1) a sea level outer arc at the top of the trench slope break, and, 2) a fore-arc basin with structural relief of several km and the steep outer limb characteristic of fore-arc basin profiles.

This plastic failure in the overriding plate results from a stress concentration caused by the low strength of the megathrust, coupled with horizontal compression. A closed-form elastic solution suggests that for megathrusts dipping 20° or less, a 10-fold compressive stress concentration is likely for a wide range of megathrust yield strengths, and a moderate net compression in the lithosphere. Under these conditions, the near-surface dip of the megathrust will tend to increase. Maintenance of a smooth dip requires underplating at shallow depth or erosion of the overriding plate at deeper levels. If neither adjustment occurs, shallow obduction becomes possible.

T 105

MODELING THE GRAVITY FIELD OF THE EARTH BY POINT MASSES.

Bakul Banerjee (Earth & Plan. Sci. Dept.,Johns Hopkins University, Baltimore, Md.21218)

The perturbations in the low degree and order gravity field of the earth are modeled assuming point source density anomaly in the mantle. The deeper sources of density anomalies due to subducting plates or possible convecting regions known from from various geophysical data already available are approximated by several sets of point masses.The gravity fields so generated are compared to the known free air gravity field. These studies show that the tectonic activities most probably extend beyond the upper 700 km. in the mantle. The sources of large positive and negative anomalies are found to be situated at comparable depths and hence they may be related mechanically.

Rock Fracture & Faulting

Metropolitan East
Saturday P.M.
D. J. Holcomb (Sandia Laboratories), Presiding

T 106

ACOUSTIC EMISSION IN HYDROSTATIC COMPRESSION

H. Mizutani (Dept. of Earth Sciences, Nagoya Univ., Japan)
K. Kurita (Cooperative Institute for Research in Environmental Sciences, Univ. of Colorado/NOAA Boulder, CO 80309)
T. Waza (Geophys. Inst., Univ. of Tokyo, Japan)

In axial loading experiments on rocks, a large number of high frequency elastic waves (A.E.) are emitted prior to fracture. These events are thought to be associated with crack growth processes. A.E. events are also observed in hydrostatic compression. This indicates that even in crack closing, some kind of microfracturing process is involved. Here we report several aspects of A.E. in hydrostatic compression.

In hydrostatic compression up to 150 MPa, we tested four kinds of rocks with different porosities (granite, andesite, and tuffs; 0.5%-20% bulk porosity).

The following results were obtained: 1. Total emission number up to a certain pressure is nearly proportional to the amount of bulk porosity. 2. In pressure cycles, strong hysteresis of A.E. number with respect to pressure is observed. 3. In high porosity tuffs, crack closure is time-dependent and "contraction creep" is observed. The variation of the ratio of strain change to emission rate indicates closure of cracks with higher aspect ratio is involved at higher pressure.

These features show that some portion of the cracks close irreversibly and at that time local fracture such as the breaking of asperities on crack surfaces occurs.

T 107

PRESSURE DEPENDENCE OF ACOUSTIC EMISSIONS*

D. J. Holcomb (Geomechanics Division 5532, Sandia Laboratories**, Albuquerque, New Mexico 87185)

Acoustic emissions (AE) in differentially stressed rock exhibit a stress threshold phenomenon known as the Kaiser effect. Once stressed to a given level and unloaded, AE will not be produced until that level is exceeded. For rock that exhibits dilatancy, other work has established a correlation between dilatancy, opening of microcracks and AE. Because of this correlation and because dilatancy onset is suppressed by increasing pressure, it was hypothesized that AE would respond in the same way. For example, consider a sample conditioned by a given differential stress σ_1^D at confining pressure P_1. Because of the Kaiser effect, at constant pressure P_1, AE will not be produced until σ_1^D is surpassed. If P_1 is increased, however, the resulting dilatancy onset suppression suggests that AE onset would also be suppressed, giving a pressure dependent Kaiser effect. Such is not the case. For $P_2 > P_1$, AE in Palisades diabase began at the previous peak value of differential stress, σ_1^D. Thus AE onset is independent of pressure. Since dilatancy is pressure dependent, the source of AE (growth or nucleation of cracks) must be separate

from the source of dilatancy (opening of cracks). The result implies that stress-induced damage in rock occurs at lower stresses than previously thought.

T 108

PRECURSORY CHANGES IN ACOUSTIC EMISSIONS PRIOR TO THE UNIAXIAL FAILURE OF ROCK

L.A. Granryd, C.H. Sondergeld and L.H. Estey (Cooperative Institute for Research in Environmental Sciences, University of Colorado/NOAA, Boulder, CO 80309)

In order to investigate phenomena precursory to failure, a series of acoustic emission experiments have been conducted. Samples of Ralston intrusive (basalt), Westerly granite and pyrophyllite were axially loaded to failure at various strain rates ($\dot{\varepsilon} = 10^{-5}$ to 10^{-7}). Stress, strain, number of emissions and rate of emission occurrence were measured. Waveforms were also captured and stored on a transient recorder. Observations indicate that acoustic emission rate is not a continuous function of time despite continuous loading; the activity occurs in bursts with well defined periods of quiescence. The magnitude distribution, b-values, were studied as a function of deformation. A study of the recorded waveforms revealed an enhancement of high frequency spectral components in events prior to failure. This we interpret to be indicative of a change in source mechanism. The ratio of event duration to wave amplitude is also symptomatic of a change in the character of the event source. This ratio was found to change prior to failure. It was confirmed that the parameters measured depend significantly on rock types.

T 109

NEW INSIGHTS INTO MICROFRACTURING OBTAINED FROM STUDIES OF ACOUSTIC EMISSION FOCAL MECHANISMS

L. H. Estey and C. H. Sondergeld (both at CIRES, University of Colorado/NOAA, Boulder, CO 80309)

Rectangular prisms of Westerly granite were instrumented with eight piezoelectric transducers. The outputs of these sensors were captured in real time using digital transient recorders. The recorded signals, i.e. phase, amplitude and polarity were used to construct standard focal plots. Assuming a couple mechanism, the best fit nodal planes were determined by eye. For the uniaxial experiments, a simple tensional source does not adequately account for any of the observations. In agreement with scanning electron microscopy we find a vertical and near vertical ($\pm$ 20°) orientation of microcracking to be predominant i.e. cracking parallel to σ_1 direction. The resulting P-wave radiation patterns are best modeled by a quadrapole source; a couple mechanism requires a near vertical sense of shearing. Events that tend to spatially cluster have similar focal mechanisms. These uniaxial cycling results will be compared to new data from triaxial cycling experiments.

T 110

A STUDY OF ACOUSTIC EMISSIONS AND THEIR HYPOCENTERS DURING THE CYCLIC LOADING OF WESTERLY GRANITE

C. H. Sondergeld and L. H. Estey (both at CIRES, University of Colorado/NOAA, Boulder, CO 80309)

Rectangular prisms of Westerly granite were deformed uniaxially and triaxially during cyclic stress loading. Acoustic emission rate, cumulative numbers per cycle, volumetric strain and differential stress were continuously monitored. In addition, acoustic emission waveforms were captured at eight sensors using transient recorders. The cumulative number of events per cycle generally decreased with increasing number of cycles. Acoustic emission activity became more narrowly focused about the peak cycle stress with increased cycling. The majority of events occurred upon loading. Those that occurred during unloading were few in numbers and not as systematically related to stress as those for loading. The information captured in the waveforms was used to determine acoustic emission hypocenters. Hypocenters of loading events tend to cluster both in space and time and suggest some spatial migration takes place from cycle to cycle. Hypocenters document the strongly anisotropic development of dilatancy in Westerly granite. Relative spectral content of recorded waveforms can be explained in part by a simple attenuation model once one knows the distribution of microcracking and the relative positions of event sources and transducers.

T 111

RELAXATION OF INTERNAL STRESSES IN ROCKS BY TIME-DEPENDENT CRACK GROWTH

William M. Bruner (Dept. of Earth and Space Sciences, Univ. of Calif., Los Angeles, CA 90024)

Strains as large as 10^{-3}, occurring over periods of a few hours to several months, are often measured in samples of granite and other silicate rocks removed from quarries or drill holes, or mechanically disturbed by sawing or core drilling. This deformation appears to result from the relaxation of internal stresses in the unloaded rocks, but the mechanism of this relaxation has not been elucidated.

The mean internal stresses in such rocks are probably two orders of magnitude lower than the strengths of their constituent minerals at room temperature; thus intragranular creep cannot account for the observed time-dependent deformation. A more likely mechanism is slow crack growth by stress corrosion. To investigate this possibility, the history of crack growth and deformation during unroofing, unloading and relaxation has been simulated for a two-dimensional model of a rock. The grains are polygonal in shape and anisotropic with respect to thermal expansion; grain-scale internal stresses are produced by cooling during unroofing. Flat cracks are assumed to nucleate in regions of high stress near grain-boundary corners and grow across the interiors of the grains.

Because direct interactions between cracks are neglected in the model, the crack density in the calculations has been limited to values at which such interactions are not of major importance. In spite of this limitation, strains of several times 10^{-4}, with a time dependence comparable to that observed, can be readily obtained using parameter values appropriate for granitic rocks. Provided the relation between crack growth velocity and the crack-tip stress-intensity factor is comparable to that indicated by published data for slow crack growth in quartz, the duration of the relaxation process is not highly sensitive to the model parameters.

T 112

THE EFFECT OF THERMAL CYCLING ON VOLUMETRIC STRAIN

K. Kurita, I.C. Getting and H.A. Spetzler (All at Cooperative Institute for Research in Environmental Sciences, University of Colorado/NOAA, Boulder, CO 80309)

To understand the fracture process in rocks it is important to clarify the factors which influence crack development. In triaxial loading experiments, the volumetric stress-strain curve typically departs dramatically toward failure from the extrapolation of its initial slope. In a simple model, this departure may be expressed as

$$\delta\varepsilon_v = n\alpha\frac{4}{3}\pi a^3$$

where $\delta\varepsilon_v$ is the dilatant strain, n is the microcrack density, α is the crack aspect ratio, and a is the typical crack length. Crack volume is characterized by the density (n) and morphology (α and a) of the cracks.

In order to investigate the effect of initial crack density on volumetric strain various degrees of thermal cracking were introduced in Westerly granite. A correlation was found between initial crack porosity and the dilatancy at failure in triaxial loading experiments.

Samples were subjected to various numbers of thermal cycles. Each cycle consisted of rapid heating and cooling over a 200°C range. In subsequent hydrostatic compression to 150 MPa, most cracks were closed by 50 MPa. Crack porosity increased as the number of thermal cycles was increased. The dilatant strain at failure was measured with resistance strain gages in triaxial loading experiments at 50 MPa confining pressure and a strain rate of $\sim 10^{-6} s^{-1}$. It increased from 0.5% for the untreated sample to 1.7% for a sample which had been subjected to 14 thermal cycles prior to loading. No significant decrease in strength with number of thermal cycles was observed.

A plot of log $\delta\varepsilon_v$ vs $\sigma_1-\sigma_3$ is essentially linear until failure is approached. Increased numbers of thermal cycles displaces this curve toward higher values of $\delta\varepsilon_v$. The slope however remains unchanged.

T 113

OBSERVATIONS OF THE FRACTURE PROCESS IN WESTERLY GRANITE DOUBLE TORSION SPECIMENS

Peter L. Swanson (Cooperative Institute for Research in Environmental Sciences, Dept. of Geological Sciences, Univ. of Colorado/NOAA, Boulder, CO 80309)

Stable crack growth controls both the fracture strength of brittle rocks and some of the phenomena precursory to catastrophic failure. Fracture models must be based on fracture parameters that characterize the physics of crack growth and interaction. Most recent laboratory fracture data have come from double torsion experiments in which a "single" crack is propagated in a thin plate of rock. Critical evaluation of the assumptions required for applying double torsion compliance methods to relaxation experiments in Westerly granite reveals major violations. The use of acoustic emission (AE) location techniques and holographic interferometry during relaxation tests shows that erroneous values of the crack velocity and stress intensity factor can result because of (1) considerable frictional constraint along the previously fractured crack plane, (2) force relaxations due to time-dependent friction along the crack plane and (3) an environmental dependence of the "elastic" properties throughout the entire specimen. Despite the complications with the double torsion method, a clearer understanding of the process of fracture propagation is developed via this technique. Macrocrack extension is found to occur not as a single fracture but as a coalescence of subsidiary cracks. Microfracturing ahead of the main fracture, located by AE methods, was found to occur at high crack velocities ($v \geq 10^{-5}$ m/s) but was not detected in this region at lower velocities. A decrease in the ratio of transgranular to intergranular fracturing accompanying a reduction in crack propagation rates suggests that secondary microfracturing is controlled by stress corrosion.

T 114

EFFECTS OF WATER ON THE MECHANICAL PROPERTIES OF INTACT AND JOINTED WELDED TUFF*

W. A. Olsson
L. W. Teufel (Both at: Geomechanics Division 5532, Sandia Laboratories**, Albuquerque, New Mexico 87185)

Welded tuff formations on the Nevada Test Site are being considered as potential nuclear waste containment media. One of the key elements in final selection amongst the various proposed repository media, will be the predicted long-term response of the media to the thermal and mechanical inputs of waste emplacement. The constitutive properties used in modelling this thermo-mechanical response must reflect the complexities of the media, i.e., those of a jointed rock of various degrees of saturation. Accordingly, we are performing uniaxial and triaxial compression tests on intact and simulated jointed welded tuff specimens that have water saturations of 0 and 100 percent. The intact specimens are being tested in uniaxial compression, at room temperature, and at a strain-rate of 10^{-4}/s. The dry specimens exhibit an average strength of 158 MPa, and the wet specimens are 30% weaker with mean strength of 112 MPa. Young's modulus decreases from 27 GPa for dry tuff to 24 GPa for the wet, a reduction of 11%. Jointed tuff is simulated using 35° precuts which were tested in triaxial compression to 40 MPa confining pressure at displacement rates from 10^{-3} cm/s to 10^{-6} cm/s. The coefficient of friction increases with decreasing displacement rate from 0.62 to 0.66 for dry tuff and 0.67 to 0.74 for water saturated tuff. The increased velocity-dependence of the frictional resistance of the wet tuff is attributed to time-dependent hydrolytic weakening and stress corrosion of asperity contacts on the sliding surface which increases the real area of adhesive contact.

T 115

STRESS VARIATION DURING POLYAXIAL FAILURE TESTS OF ROCKS

J. Dieterich (U. S. Geological Survey, Menlo Park California 94025)
Z. Reches (The Weizmann Institute of Science, Rehovot, Israel)

The processes of deformation were studied in polyaxial failure tests on Sierra White Granite, Berea Sandstone, Solenhofen Limestone and Stylolitic Limestone. The samples consist of cubes 22x22x22 mm, coated with aluminum foil and Teflon tape. The deformation apparatus has three mutually perpendicular hydraulically driven rams (x, y, z) that act on the cube. Strain rates in two directions, $\dot{e}_x$ and $\dot{e}_y$ were independently controlled by high-speed servo-controllers. Stress in the z-direction, σ_z, was fixed at constant values to 30.0 MPa. At constant strain rates, $\dot{e}_x > \dot{e}_y$, the stress-strain curves show three well-defined stages in the deformation process. Stage I is characterized by predominantly elastic deformation and monotonically increasing stresses to the ultimate strength of the sample, σ_x is the maximum principal compressive stress. Stage II is characterized by strain softening and/or strain hardening as throughgoing faults develop. During this transition stage the maximum principal compressive stress alternates between σ_x and σ_y. During Stage III, stresses are more or less constant and the main deformation mechanism consists of slip along faults; σ_y is frequently greater than σ_x. These results for stress orientation during Stages II and III indicate that a case of simultaneous $\dot{e}_x > \dot{e}_y$ (strain rates), and $\sigma_y > \sigma_x$ (stresses) is possible, and even necessary, during three dimensional strain. The associated rotation of principal stress directions by 90° could explain the existence of mutually perpendicular sets of small faults and joints in the field. In-situ stress measurements taken during the transition stage and perhaps final stage could show maximum compressive stress in the direction of the intermediate compressive strain rate.

T 116

THE PATTERN OF FAULTS IN THREE-DIMENSIONAL DEFORMATION EXPERIMENTS

Z. Reches (The Weizmann Institute of Science, Rehovot, Israel)
J. Dieterich (U. S. Geological Survey, Menlo Park, California 94025)

Fault patterns from polyaxial failure tests on Sierra White Granite, Berea Sandstone, Solenhofen Limestone and Stylolitic Limestone were studied for comparison with predictions of fault orientation by different theories. The deformation apparatus has three mutually perpendicular hydraulic pistons, two of which can be computer servo-controlled. In most of our experiments that were subjected to three dimensional strain, the samples contain three or four obvious sets of faults in almost orthorhombic symmetry. The figures show the traces of the faults observed on the exterior of the deformed samples of Sierra White Granite (a), Berea Sandstone (b) and Stylolitic Limestone (c). In each case traces on the x-faces have two orientations, and traces on the y-faces have two orientations. Examinations of split samples imply that every sample contains four sets of faults in good agreement with the predictions made through a kinematic analysis of fault orientation (Reches, 1978). The two sets of faults, predicted by Anderson-Mohr faulting theory, is proven to be at best, a special case for a plane strain deformation.

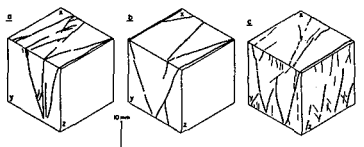

T 117

ROCK FRACTURE AT INTERMEDIATE LOADING RATES*

A. S. Kusubov and
R. P. Swift (University of California, Lawrence Livermore Lab., Livermore CA 94550

Laboratory conditions have been identified to initiate and sustain multiple fractures in a rock similar to the tight low permeable beds containing natural gas and oil. Experiments were conducted in 13 cm diameter by 15 cm long cylinders of Nugget sandstone and the fractures were generated by compressing water with a piston in a 1.4 cm diameter borehole. The investigated pressure range was from 15-70 MPa with loading rates varying from 0.2-80 MPa/ms. Preliminary results indicate that 60 MPa input pressure pulses with loading rates of 60 MPa/ms are most effective in generating multiple fractures without splitting the sample. Pressures measured in the borehole were on the order of 10 MPa less than the input pressures, possibly, due to borehole expansion and transient water intrusion in the rock sample. Input pressure pulses in excess of 70 MPa with loading rates of 60 MPa/ms as well as input pressure pulses in excess of 50 MPa with loading rates of 15 MPa/ms fractured the rock samples in two while generating only two additional short cracks. Fully saturating the rock samples with water prior to loading had little effect on the crack formation.

T 118

PORE VOLUME CHANGES ASSOCIATED WITH FRICTIONAL SLIDING OF SANDSTONE*

L. W. Teufel (Sandia Laboratories**, Albuquerque, New Mexico 87185)

Dilatancy is well established as accompanying the fracturing of intact specimens in the laboratory, but few detailed experiments have been done to determine if dilatancy accompanies deformation during frictional sliding. The general problem of dilatancy along sliding surfaces has been investigated by monitoring pore volume changes in drained, triaxial-compression, pore pressure experiments on 35° precuts of Coconino sandstone. Tests were conducted at effective confining pressures to 120 MPa, an axial displacement rate of 5×10^{-5} cm/sec, and shear displacements up to 8 mm. In all tests there is an initial elastic compaction upon application of the axial load. As the peak stress for the onset of sliding is reached and sliding begins, compaction decreases to zero and dilatancy dominates. With increasing shear displacement along the sliding surface, there is an increase in the amount of dilatancy. With increasing normal stress there is an increase in the amount of dilatancy for equivalent shear displacements. Petrographic studies of the deformed specimens show fracture development only in grains immediately adjacent to the sliding surface. The density of these microcracks increases with increasing shear displacement and increasing normal stress. The average length of these microcracks also increases with increasing normal stress. Calculations of the total microcrack volume along the sliding surface correlate with the measured increase in dilatant pore volume.

T 119

EXPERIMENTAL OBSERVATION OF ACOUSTIC FLUIDIZATION IN SAND

P. Goetz and H.J. Melosh (Both at: Dept. Earth and Space Sciences, SUNY Stony Brook, Stony Brook, New York 11794)

Melosh (1979) demonstrated the theoretical possibility that a state of "acoustic fluidization" can be induced in a dry granular mass of debris by a sufficiently strong random acoustic field. This mechanism might explain the low coefficient of friction apparent in such phenomena as the slumping of large impact craters, long runout landslides, and seismic faulting. Applied to a mass of sand, the theory predicts an effective viscosity of between 10^5 and 10^7 poise for acoustic wavelengths lying between the particle size and the depth of the sand layer.

Experiments were performed on several masses of sand with different grain sizes. The sand was excited by an ultrasonic acoustic field which had a peak frequency of about 37 KHz. The experiments showed that the acoustic field induced strongly non-Newtonian fluid behavior. At applied stresses well below (≤ 1/2 σ yield) the static yield stress of the sand, the effective viscosity drops rapidly with increased load until it can no longer be measured by our techniques ($\eta_{eff} \lesssim 6 \times 10^5$ poise). The flow law is apparently independent of the sand grain size within the range of our study (0.5 mm - 1.4 mm). The presence of water decreases the viscosity, probably due to either better coupling between the ultrasonic transducer and the sand in our experiment or an increased sound velocity in the sand.

More work is planned to study such parameters as the partitioning of energy losses, the effect of frequency on viscosity, and the effective Q in the fluidized mass.

These experiments, however, confirm that acoustic fluidization does occur and that dry granular debris can flow as a relatively low viscosity fluid under the proper conditions, conditions which may be realized in slumping craters, long runout landslides, and, perhaps, seismic faulting.

Mantle Convection and Evolution

Metropolitan Centre
Saturday P.M.
B. H. Hager (SUNY Stony Brook), Presiding

T 120

LAYERING AND DOUBLE DIFFUSIVE MANTLE CONVECTION

D.J. Stevenson (Dept. Earth & Space Sciences, U.C.L.A., Los Angeles, CA 90024)

Mantle layering can occur because of phase changes or differentiation, but a third process --convection in the presence of a compositional gradient--may be equally important. This process, known as double diffusive convection, has been extensively studied in the laboratory, and much of the existing theoretical and observational framework can be readily adapted to the mantle (allowing, of course, for negligible solute diffusion in the mantle). The vertical composition gradient could be an "initial condition" (resulting from moderately inhomogeneous accretion or non-equilibration during core formation) and a horizontal composition gradient could evolve because of the continent-ocean dichotomy. The following conclusions have been reached: (1) The work done by thermal convection during the entire age of the earth has been insufficient to homogenize an initial (uncompressed) density contrast exceeding a few percent. (2) Inhomogeneous models are hotter and less viscous than homogeneous models. (3) The current 650-700 km discontinuity could have once been much deeper or much shallower, the choice depending on the initial conditions. (4) It is possible to have multilayered models without violating seismic or other evidence. Density contrasts between layers might be ≤1%. (5) Horizontal mixing on a timescale of 10^8-10^9 years prevent persistence of a stable (Jordan) "tectosphere" beneath continents, provided the viscosity is less than $\sim 10^{23}$P.

T 121

RIDGE MIGRATION AND MANTLE DIFFERENTIATION

R.J. O'Connell
Department of Geological Sciences
Harvard University, Cambridge, MA 02138
B.H. Hager
Department of Earth and Space Sciences
SUNY, Stony Brook, NY 11794

Most of the volcanism on the earth is associated with plate creation at ridges. If melting beneath ridges is the major mechanism of mantle differentiation, then simple mass flux calculations indicate that uniform depletion of large parts of the mantle may be unlikely. For example, it would require 4 Gy to cycle the mass of the mantle through a 100/km deep zone under ridges at the present plate creation rate of $3 km^2/y$. At present ridge migration rates of ∿2 cm/year, and ridge lengths of ∿56000 km, the uppermost mantle will be sampled on a time scale of ∿0.5 Gy. Consequently, the upper mantle may be more highly and uniformly differentiated than the lower mantle simply as a result of the kinematics of flow and sampling under ridges. Heat accumulation in unsampled regions of the mantle may give rise to local upwelling, hot spots and magmatism, causing less differentiating material to penetrate to the surface. Simple 2-D diffusion models with kinematic velocity fields illustrate these processes.

T 122

EUSTATIC SEA LEVEL AND SPREADING RATE ARE NOT SIMPLY RELATED

B.H. Hager (Dept. of Earth and Space Sciences, SUNY Stony Brook, Stony Brook, NY 11794)

The volume of the midoceanic ridge system depends on past spreading rates in a way which is easily calculated. But although increased spreading rates result in an increase in the volume of the oceanic ridge system, eustatic sea level does not respond in a simple way. This is because an increase in spreading rate also causes an increase in the rate at which cold lithosphere is returned to the sublithospheric mantle, a process which results in a local decrease in the volume of the mantle. To the extent that cold lithosphere is returned to the mantle beneath the sea (e.g. W. Pac.), the net effect of an increase in spreading rate is to decrease sea level as a result of more rapid cooling of the lithosphere + mantle system, which leads to an overall increase in the volume of the ocean basins. To the extent that cold lithosphere is returned to the mantle beneath continents (e.g. S. Amer.), the resulting contraction of the subcontinental mantle results in a decrease in continental freeboard much larger than that caused by the expansion of the ridge system alone. Only if the subducted lithosphere cools the subcontinental and suboceanic mantles equally does the change in volume of the ocean basins equal the change in volume of the ridge system. Quantitative models show that eustatic sea level is more sensitive to the relative distribution of subducted lithosphere beneath continents and oceans, and hence the global mantle flow pattern, than it is to spreading rate. Changes in the relative distribution of subducted lithosphere beneath continents and ocean basins on the order of 10% can lead to larger changes in eustatic sea level than doubling spreading rates. It may be more appropriate to infer paleoconvection patterns than paleo heat flow from past eustatic sea level.

T 123

ON THE NATURE OF THE OCEANIC UPPER MANTLE

P.R. Hamlyn
E. Bonatti (both at: Lamont-Doherty Geological Observatory, Palisades, N.Y. 10964)

Studies of mantle-derived peridotites recovered from fracture zones in the Atlantic (Romanche, Vema, St. Paul) and Indian (Owen) Oceans and from Zabargad Island in the Red Sea reveal a striking uniformity in both mineral and bulk rock major element chemistry. Modally the rocks range from lherzolite to harzburgite with lherzolite equal to or possibly in excess of harzburgite in abundance. Tectonite fabrics are characteristic and include protogranular, porphyroclastic and mylonitic varieties. Two stages of equilibration are often seen in these rocks. The earliest recognizable stage corresponds to P-T conditions of the plagioclase lherzolite facies (e.g. Romanche and Vema F.Z.) or the spinel lherzolite facies (e.g. Owen F.Z.) with overprinting of a later stage of partial re-equilibration to lower T and P. Compared to the harzburgite tectonite substratum in ophiolites the oceanic peridotites have more aluminous Ca-rich and Ca-poor pyroxenes and less Mg-rich olivines (Fo_{89-90} compared to Fo_{90-93}). The relatively fertile nature of fracture zone peridotites compared to ophiolite tectonites is further substantiated by their major element whole-rock chemistry. Based largely on ophiolite models it is widely believed that the upper mantle immediately underlying oceanic crust consists of depleted harzburgite. If true this suggests that the uppermost upper mantle is laterally heterogeneous, being less depleted beneath fracture zones than between them. Alternatively, fracture zone mantle-derived peridotites may be representative of the oceanic upper mantle, implying fundamental differences between the generation of ophiolites and modern oceanic lithosphere.

T 124

ISOTOPE AND TRACE ELEMENT SYSTEMATICS IN MANTLE-DERIVED PERIDOTE NODULES FROM SAN CARLOS

A. Zindler (LDGO, Columbia U., Palisades, N. Y.)
E. Jagoutz (Max Plank Institute, Mainz, Germany)

Nd and Sr isotopic ratios and K, Rb, Cs, Ba, Sr, Nd and Sm concentrations have been measured in minerals and whole rock samples of four spinel peridotite nodules from San Carlos, Arizona. $^{143}/^{144}Nd$ and $^{87}/^{86}Sr$ are greater and less than bulk-earth values, respectively. Comparison of $^{143}/^{144}Nd$ in PA65 (0.51308±1), a "LREE-enriched" harzburgite, with bulk-earth evolution models defines a "maximum enrichment age" of ∿180 m.y. Isotopic analyses of coexisting CPX and OPX demonstrate equilibrium between these phases, though Rb/Sr may range from 0.000019 to 0.0049 and Sm/Nd from 0.2260 to 0.4429 in CPX and OPX respectively. This implies either the short-lived nature of different parent-daughter ratios or previous residence in a regime with temperatures sufficiently high to permit isotopic equilibration. Mass balance calculations show that minor phases comprise a major portion of the mantle alkali budget, and reaffirm that trace elements in nodule silicates are insufficient to account for trace element abundances in basalts. Comparison of silicates with and without liquid or fluid inclusions show the inclusions to be enriched in alkalis. Another alkali-rich phase is identified as a red coating on spinel and olivine grains; K and Sr are ∿5% and 2%, respectively, while $^{87}/^{86}Sr$ is in equilibrium with major silicates. Inclusion-free OPX and OL are shown to be poorer in trace elements than previously known: e.g., literature values for K and Rb in OPX range from 10-857 ppm and 0.047-3.07 ppm, while our values range from 0.29-1.41 ppm and 0.0009-0.0028 ppm; Sr concentrations from 0.3-15 ppm have been reported for OPX and OL, whereas we measure 0.087-0.19 ppm in OPX and 0.008-0.07 ppm in OL. Similar results are obtained for alkalis in CPX. OPX/CPX and OL/CPX Kp's are consistent from nodule to nodule, and support the validity of our results. The importance of minor, non-silicate phases during magma genesis in the mantle is clearly demonstrated. (All analyses made at MIT.)

T 125

THE EARTH'S NEODYMIUM BUDGET AND THE STRUCTURE AND EVOLUTION OF THE MANTLE

Davies, Geoffrey F. (Dept. of Earth & Planetary Sciences, Washington University, St. Louis, MO)

The inference from neodymium isotope data that there is a widespread, large and primitive mantle reservoir is not unique when uncertainties in the observational constraints are considered. A viable alternative interpretation is that most of the mantle is depleted in large-ion lithophile (LIL) elements, but that it contains a spectrum of less depleted or enriched heterogeneities. Sources of ancient continental rocks show significant Sm/Nd fractionation, sufficent to yield at present a minimum of $-7 < \varepsilon_{Nd} < 5$. Furthermore, the identification of $\varepsilon_{Nd} = 0$ as chondritic (and, by assumption, the primitive bulk earth) is premature ($\varepsilon_{Nd} = 0$, by definition, represent the basaltic achondrite Juvinas). Forty recent determinations of Sm and Nd abundances in chondrites yield Sm/Nd = 0.324 ± 0.018 (mass ratio, 2σ error). Assuming initial isotopic homogeneity, this implies a present chondritc range of $\varepsilon_{Nd} = 1 \pm 7$. Combining this uncertainity with at least 50% uncertainty in total Nd content of the earth, the mass of the depleted mantle reservoir ($\varepsilon_{Nd} = 10$) necessary to balance the crustal reservoir ($\varepsilon_{Nd} = -10$ to -25?) can range from less than 1/3 to all of the mass of the mantle. Ultramafic inclusions from kimberlites have $-1 < \varepsilon_{Nd} < -15$, indicating that continental lithosphere is heterogeneous and possibly a significant additional LIL reservoir. This observation, evidence for mantle metasomatism, and the restricted range of $\varepsilon_{Nd} = 1 \pm 4$ for continental volcanic sources may result if only the more enriched mantle heterogeneities are capable of producing magma which penetrates to the surface.

T 126

OCEANIC ISLAND PB: TWO STAGE HISTORIES AND MANTLE EVOLUTION

Clement G. Chase (Dept. of Geology and Geophysics, University of Minnesota, Minneapolis, Minnesota 55455)

Leads in basaltic suites from seven oceanic islands - Hawaii, Ross, Iceland, Canaries, Trindade, Kerguelen, Reunion - form linear arrays on $^{206}Pb/^{204}Pb$ versus $^{207}Pb/^{204}Pb$ diagrams. These arrays are more reasonably interpreted as secondary isochrons than as simple mixing lines, because of their systematic relationship. Assuming a two stage development model, separate histories calculated for the leads from each island or island group indicate that the source materials for the magmas were derived from a single primary reservoir with present $^{238}U/^{204}Pb$ of 7.91 ± 0.04 by secondary relative enrichment in U at times ranging from 2.5 to 1 billion years ago. This is consistent with the Manhes et al plot of isochron slope versus intercept, on which the points describing the best-fit line to each island's Pb-Pb array all form a single straight line. This plot is also convenient for displaying the 95% confidence ellipses for slope and intercept, and shows that the isochrons for the Canaries and Hawaii, at least, are significantly different.

The islands that have older isochron ages show less secondary enrichment in U. One possible process causing the enrichment is sea-floor spreading, so the oceanic island magmas may include a component derived from old oceanic crust. The increasing enrichment with time could then be partly due to changing U content of sea water. Some of the $^{208}Pb/^{204}Pb$ data is consistent with this idea, some is not.

T 127

GEOCHEMICAL EVOLUTION OF THE LITHOSPERE: A TRANSITION MATRIX APPROACH

R. D. Russell (Department of Geophysics and Astronomy, U.B.C., Vancouver, Canada, V6T 1W5)

There is a growing interest in the formulation of transport models to simulate the evolution of the earth's lithospere and atmosphere. Such models serve to test self-consistency of interpretations and to suggest timescales for evolutionary phenomena. Most of these models can be expressed as linear state equations for which solutions can be found in terms of a transition matrix. At least in some instances the transition matrix solution provides a starting point for a linear inverse solution. This is a convenient way of generating solutions that exactly satisfy given constraints and for which the question of uniqueness can be studied formally.

The procedure is illustrated by generating models to evolve a lithospheric layer of specified mean age and potassium concentrations, closely following O'Nions et al (JGR, 84, 6091-6101, 1979).

T 128

STRUCTURAL EVOLUTION OF THE CRUST-MANTLE SYSTEM IN THE EARTH

St. Mueller (Institute of Geophysics, ETH Zurich, CH-8093 Zurich, Switzerland)

Through the theory of plate tectonics it is well-known that the present distribution of continental and oceanic structures has resulted from the break-up and joining together of previous configurations of the continental blocks whose lithosphere is much older than the present oceanic lithosphere. In the cratonic areas of shields the low-velocity layer in the upper mantle is practically absent, while in tectonically active regions a well-developed "channel" exists with major structural differences also within the crust.

The transformation of continental to oceanic lithosphere is characterized by several stages of structural development. In the initial phase of rifting the continental crust-mantle system is thermally altered and a graben is formed at the surface. Magmatic intrusions originating in the anomalous mantle under the rift modify the lower and intermediate crustal layers.

As this process continues a pseudo-oceanic lithosphere is produced essentially through a thinning and weakening of the lithospheric slab. In the final stage of oceanization the intermediate crust vanishes completely and the lower crustal layer is severely altered by magmatic injections from mantle sources. New oceanic lithosphere is being generated in this "ridge" phase. It increases in thickness and age as it moves away from the ridge crest to the subduction zones where it is consumed. Fractions of the molten oceanic slab will return to the upper crust in the form of igneous intrusions thus contributing to the formation of new continental lithosphere. At this point the evolutionary cycle is complete.

T 129

THE PROTO-ARCHEAN MANTLE AND CRUST

G.A. Ransford (Jet Propulsion Laboratory, California Institute of Technology, Pasadena, CA 91103)
K.D. Collerson (Memorial University, St. John's Newfoundland AIC 557)

We present here a hypothesis for the cooling sequence of the mantle that bridges the time interval between core formation and the Archean geological province. The mantle following core formation was probably completely molten (Shaw, Phys. Earth Plan. Int., 16, 361, 1978), and had a primitive atmosphere in equilibrium with it (Fanale, Chemical Geology, 8, 79, 1971). The mantle convected heat upwards, depositing mass at the base of the mantle, mass that was depleted in volatiles because of the degassing and depleted in LILs because their large ionic size will not fit into the closely packed silicate structures that must have formed in the pressure region at the base of the mantle. Crust that formed was continuously disrupted by upward convective currents, and a region of sinking crustal pieces suspended in rising hot liquids formed at the top of the mantle. The cooling liquid portion of the mantle was increasingly enriched in radioactives and volatiles as the sequence progressed, and the layer of sinking crustal pieces and hot liquids at the top became more and more congested. Finally, that congested layer coagulated to stop the cooling of the mantle by convection, leaving a solid crust of irregular thickness underlain by a thin layer of molten, volatile and radioactive rich material atop the solid mantle. The crustal layer was eventually broken in isolated areas by the molten material as it was further heated by its radioactives This initial tapping away of the heat solidified the entire molten layer, leaving the tapped region deficient in volatiles and radioactives. The untapped regions under the earliest crustal masses could heat slowly because of their enriched radioactive heat sources and cause later flows and tectonic activity.

T 130

A LOWER MANTLE LITHOSPHERE AND ITS CONSEQUENCES

R. St J. Lambert (Department of Geology, University of Alberta, Edmonton, Alberta T6G 2E3)

The problem of the state of the mantle has been approached by establishing limits on the history of the Earth from heat flow and isotopic considerations. Models with surface heat flow >150 mW/m^2 in the early Archean are difficult to reconcile with major continental growth in the late Archean followed by stabilization, or with isotopic data from rocks of any age. A heat flow maximum in the late Archean is preferred. A two-layer mantle of Richter or McKenzie and Weiss type provides the necessary mantle structure. Studies of possible average geotherms for the mantle show that such a mantle will have a 'lithosphere' at 700-1000 km depth. This model leads to the following history: upper mantle evolution produces continents from 3700 to 2600 Ma; the lower mantle begins to convect some time between 2600 and 1800 Ma ago with steadily increasing activity, becoming the ultimate source of plumes today. The LM lithosphere traps and localizes these plumes. The lower mantle provides LIL- and daughter isotope-enriched material: all anomalous isotopic patterns in post-Archean oceanic tectonic environments are held to originate from mixing processes. Details of Sr, Pb and Nd isotopic systematics are consistent with this model. The LM lithosphere will have a structure similar to the UM lithosphere. It will be thin above rising regions of LM convective systems and thick in regions of low heat transfer rates, LM to UM. Its structure should be controlled by core thermal structure, assumed comparatively stable, which may help explain the constancy of location of surface hot spots today. On this model, the LM must be enriched in U and Th, and impoverished in K and Rb relative to the UM and present bulk earth abundances thus become questionable.

T 131

TERRESTRIAL OSMIUM-IRIDIUM-RUTHENIUM ALLOYS: EVIDENCE FOR A DEEP MANTLE HISTORY

John M. Bird
William A. Bassett (Dept. Geological Sciences, Cornell University, Ithaca, N.Y. 14853)

Osmium-iridium-ruthenium alloys occur as small grains in placer deposits derived from depleted mantle of obducted ophiolites. Some specimens from the Klamath ophiolites, Oregon, consist of intergrown metal phases having compositions and textures that are consistent with formation by crystallization from a melt at temperatures greater than the presently accepted geotherm in the Earth's mantle. Three possible explanations for the compositions and textures are: 1) the metals melted when temperatures within the mantle were higher than at present, 2) they melted at depths greater than 2900 kms. at a time before that region was occupied by the core, or 3) they once were in the core. We propose that these metals were carried upward in convecting mantle material and were subsequently incorporated in depleted mantle of lithosphere, now exposed in obducted ophiolites. This history and the observation of similar metals in meteorites leads us to conclude that these metals have remained in the elemental state since the time of nucleosynthesis and accretion of the Earth from the solar nebula.

Rock Deformation, Lab & Field

Bay

Monday A.M.

Deborah Spratt (Johns Hopkins Univ.), Presiding

T 132

CONSTITUTIVE MODEL FOR THE LOW TEMPERATURE CREEP OF POLYCRYSTALLINE SALT

D. E. Munson (Sandia Laboratories, Albuquerque, NM 87185)
(Sponsor: D. E. Grady)

In many problems of interest, such as, long-term storage of nuclear wastes and the geological processes leading to salt dome formation, the low temperature (0-200 C) creep behavior of salt is the critical modeling element. While numerous constitutive models have been proposed for the low temperature creep of salt, this work is the first to develop such a model within the framework of rate controlling mechanisms and the deformation-mechanism map. Use of this framework permitted unfolding of the rather complicated low temperature steady-state creep behavior into three simpler responses involving separate regimes with individual controlling mechanisms. The observed total creep rate obeys the rules of additive processes. The creep model incorporates primary (transient) creep as a simple two parameter modification to the steady-state creep equations. Application of the model is through a formulation into proper stress and strain measures for use in a large strain finite element code. Extensive analysis of available low temperature triaxial creep data produced the appropriate material parameters, including activation energies and stress dependencies for the separate regimes. Material variations were observed to produce changes in absolute creep rate, without change in controlling mechanism. Numerous calculations demonstrate the adequacy of the model and numerical method to simulate the results of triaxial creep experiments.

T 133

RECRYSTALLIZATION IN EXPERIMENTALLY SHEARED CALCITE

M. Friedman
N. G. Higgs (both at: Center for Tectonophysics, Texas A&M University, College Station, TX., 77843)

Cylindrical specimens of Tennessee sandstone with dry, crushed calcite (500 μm thick) along 35°-precuts are deformed at 200 MPa confining pressure, 25° to 910°C, to shear strains (γ) of $\leq$ 5.7 and $\dot{\gamma}$ of $10^{-2}s^{-1}$. Incremental stress/strain are not coaxial with the finite strain. At 400° to 650°C gliding produces strong dimensional and crystallographic fabrics that geometrically track the finite strains. At 550-600° recrystallization occurs after obvious slip, and produces mosaics of fine-grained neoblasts with axial ratios <2.0. At 805° to 910°C two populations of neoblasts occur. In minority are a group of strain-free, nearly equant (25μm) grains that have a nearly random c-axis fabric and that are formed late in the deformation probably by annealing. Predominant are larger (70 to 170μm), rationally twinned neoblasts with (a) axial ratios (1.7) that are independent of γ from 0.6 to 5.7; (b) long axes inclined to the shear zone at 10° to 30° reflecting a small shear strain; (c) a strong c-axis fabric that also is independent of γ and that geometrically tracks neither the stress nor the finite strain axes; (d) mean grain sizes (D in mm) that vary with differential stress (σ in MPa) as $D = 4\sigma^{-1.42}$ (in excellent agreement with Twiss' [1977] prediction of $D = 19\sigma^{-1.47}$); and (e) a ghost structure of aligned impurities that does track the complete finite strain. These neoblasts are syntectonic and are repeatedly reformed during the shearing. They conform to the metallurgist's model of "waves of repeated dynamic recrystallization." Dislocation glide and creep are the underlying mechanisms, but they do not produce the same fabric as at lower homologous temperatures. The c-axis fabric of these neoblasts appear to be inclined at about 30° to that likely in the host material developed from gliding alone.

T 134

DISLOCATIONS IN DEFORMED GARNET: APPLICATIONS IN ECLOGITE-DERIVED PYRALSPITE

B.K. Smith (Dept. of Geology & Geophysics, Univ. of California, Berkeley, CA. 94720)
H.-R. Wenk (Dept. of Geology & Geophysics, Univ. of California, Berkeley, CA. 94720)

Dislocations and related microstructures in both naturally and experimentally deformed garnets have been investigated by transmission electron microscopy (TEM). An n-beam image simulation program has been developed in conjunction with the TEM imaging to solve the properties of these features. Specimens observed include garnets from the Tiburon Eclogite, California, and single crystal cores which have been strained at temperatures up to 1100°C and confining pressures up to 15 kbars.

Comparison of the dislocations in these samples demonstrate the ability of garnet to deform plastically in sufficiently high temperature and confining pressure conditions. The crystallographic response to increasing strain is embodied in nucleation of a high density of cozonal point defects, accompanied by formation of micro-inclusions rich in the dodecahedral cation. These point defects in turn climb into linear dislocation segments with large Burgers vectors, probably due to a high Peierls-Nabarro energy for the garnet structure. There is apparently a strong tendency for randomly nucleated dislocations to climb with annealing into the [110] zone, forming unusually high density arrays of dislocations with relatively high self energies. This zone is also the common macroscopically observed slip plane.

The complex history of garnet growth, deformation, annealing, and metamorphic alteration displayed by the eclogitic garnets' microstructure allow for only general rheological and crystallochemical implications to be made from these dislocation properties.

T 135

THE STRENGTH OF DRY OLIVINE

T. E. Tullis
F. Horowitz (Dept. of Geol. Sciences, Brown University, Providence, RI 02912)

Considerable disagreement exists in the experimentally determined flow laws for olivine under "dry" conditions. The results of Post (1977) on Mt. Burnet dunite and of Zeuch and Green (Z&G) (1979) on a hot pressed olivine aggregate indicate flow strengths that are higher than those of other workers. At $\dot{\varepsilon} = 10^{-5}sec^{-1}$ and 1300°C, e.g., the strengths reported by Carter and Ave'Lallemant (C&A) (1970) on Mt. Burnet dunite and Durham and Goetze (D&G) (1977) on single crystals are lower than those of Post by a factor of 4-5 and those of Z&G by about 2. The discrepancies in strain rates for a given stress are about two orders of magnitude. The reason for the discrepancies is probably a variation in either the dryness of the samples or the accuracy of the stress determinations.

In experiments on samples of Balsam Gap dunite dried following Post's procedures (vacuum dried, 900°C, 3 days in the presence of iron) we find strengths considerably lower than Post's and approximately the same as those of C&A and D&G. This suggests that the high strengths found by Post and Z&G may be due to the strength of the glass sleeve around the cool top end piece in their sample assemblies. On the other hand, C&A recognized that their "dry" samples (air dried, 200°C) contain some water and so it is inconsistent that their samples show similar strengths as our "truly dry" ones. Our samples air dried at 200°C have strengths lower than C&A's by factors of 4 or more. Their measured strengths may include a significant contribution from the Alsimag sleeve surrounding their samples and end pieces. Our preliminary data on the strength of "dry" olivine thus suggests that there are still significant questions to be resolved. The difficulties with knowing both water contents of samples and contributions to apparent strengths from some pressure media suggest caution in extrapolating data to natural conditions.

T 136

THE HYDROGEN/WATER CONTENT OF OLIVINE

M.G. Justice (Department of Geosciences, Penn State U., Univ. Park, PA 16802) and I.S.T. Tsong.

The effect of water and/or hydrogen on the deformation mechanisms of silicates has generated considerable interest since the first water weakening experiments of Griggs and Blacic (1965). In order to better delineate the role of trace amounts of water in the hydrolytic weakening process, thorough characterization of hydrogen in olivine single crystals by three different techniques, namely, ion-beam spectrochemical analysis, resonant nuclear reaction, and infrared absorption spectroscopy has been undertaken. The analysis provides both a bulk OH determination and a detailed depth profile of hydrogen concentration.

In addition, we have investigated the feasibility of artificially incorporating water into 'dry' olivine in an autoclave in order to permit detailed deformation studies over a wide range of hydrogen concentration. It is interesting to compare the creep behavior of such artificially hydrated olivine samples with those 'wetted' via the conventional technique of high temperature decomposition of talc within the creep apparatus.

T 137

TRANSIENT CREEP OF WESTERLY GRANITE AT ELEVATED TEMPERATURE

D.A. Anderson (Center for Tectonophysics, Texas A&M Univ., College Station, Tx.77843)
N.L. Carter
F.D. Hansen
R.L. Kranz

Westerly granite cylinders have been deformed dry in compression to low strains in a Griggs-type solid confining medium deformation apparatus. Experiments were run at constant differential stresses of 0.6 to 1.2 GPa at a confining pressure of 1.0 GPa and temperatures in the range 500° to 800°C, all in the alpha-quartz field. Samples were loaded to the desired stress at 1.5 GPa/sec and then allowed to creep from 0.3 to 2.0% longitudinal strain.

Strain-time curves have been fit to an equation derived from first-order kinetics:

$$\varepsilon = \varepsilon_o + \dot{\varepsilon}_{ss}t + \varepsilon_T \ 1\text{-}\exp(-t/\tau)$$

where $\dot{\varepsilon}_{ss}$ is the steady-state strain rate (ranges from 10^{-5} to 10^{-7}/sec), t is time (secs), ε_T is the total transient creep strain and τ is the relaxation time for transient creep. Activation energies for steady-state creep are about 125 KJ/mole and the stress exponent is near 3.5. ε_T is nearly constant, about 0.3%, over the stress-temperature range employed. Analysis of τ is complicated by peculiar strain-time behavior indicative of some strain-hardening.

Optical examination of "undeformed" samples of Westerly, Barre, and other granitic rocks indicate that the creep strain is taken up primarily by quartz and to a much lesser extent by feldspars and micas. Similar studies of these deformed specimens show no evidence for deformation of feldspars although some kinking occurs in the micas. Most of the experimentally-induced strain appears to be accomplished by deformation of quartz grains which contain irregular deformation bands. TEM studies show no dislocations in feldspars and micas in samples deformed at 0.9 GPa and 700°C. Quartz shows a few dislocations and en echelon cracking.

T 138

FAULTING AT HIGH TEMPERATURE AND PRESSURE

G. L. Shelton
T. E. Tullis (Dept. of Geol. Sciences, Brown University, Providence, RI 02912)

Natural faults and earthquakes are often found to occur at conditions of temperature and pressure where brittle failure is not expected unless a high fluid pore pressure exists. Similarly in lab experiments discrete shear events, often accompanied by reductions in strength, are sometimes observed in the absence of fluid pressure at sufficiently high temperatures and pressures that continuous flow would be expected. Our experimental observations ($\dot{\varepsilon} \sim 10^{-6}sec^{-1}$) suggest three categories for such faults: (1) sharp faults which form at high temperatures (≥700°C) and moderate pressures (5-7.5 kb); (2) sharp faults which form at high temperatures (≥900°C) and high pressures (15 kb) for some very dry materials; and (3) shear zones marked by considerable grainsize reduction, which exhibit localized deformation at high temperatures (≥900°C) and pressures (15 kb) for a variety of rocks both wet and dry. The first two types do not develop until the sample has experienced some uniform permanent strain, generally about 5%, and they develop in both creep and constant strain rate tests. At least some of the third type represent continued localized deformation along pre-existing fractures produced at lower pressures. In all cases, the stress required for deformation along the faults is considerably less than that predicted by a Mohr-Coulomb failure envelop with a coefficient of friction of 0.6. The observed coefficients are ≤ 0.35 and the faults are at 40-50° to σ_1. The existence of these faults appears to depend upon rock type, water content, temperature, pressure and strain , but the functional dependences and the operative processes remain unclear. Further study of these phenomena might greatly aid our understanding of how the lithosphere deforms at depths greater than 15 km.

T 139

ON A THERMO-MECHANICAL MODEL FOR PRESSURE SOLUTION DIAGENESIS OF SEDIMENTS

C.L. Angevine

D.L. Turcotte (Dept. Geological Sciences, Cornell University, Ithaca, N.Y. 14853)

Pressure solution and the subsequent precipitation of the dissolved material is thought to play an important role in the reduction of pore space and ultimate lithification of sediments. We present a one-dimensional model that gives porosity, pore pressure, thermal and burial histories of sediments undergoing pressure solution diagenesis. Our model treats the sedimentary sequence as a porous medium of solid grains, initially spherical, in a cubic pack with the pores filled with fluid. A Newtonian, solid state creep law governs the rate of pressure solution at individual grain contacts. Material dissolved at grain contacts is immediately precipitated as a spherical shell on adjacent grains. This solution and precipitation process causes a reduction in the volume of pore space, forcing the migration of pore fluid. However, the permeability is also decreasing, making fluid migration more difficult. Pore pressure increases until it balances the lithostatic pressure and pressure solution ceases. As diagenesis proceeds the bulk thermal conductivity increases, causing a decrease in the geothermal gradient. The rate of pressure solution depends strongly upon temperature; a lower geothermal gradient results in a slower decrease of porosity.

We have applied our model to sediments initially 1.0 km thick, with a uniform porosity of 45%. A wet quartzite rheology is assumed and the basal heat flow is held constant at 1 hfu. Porosity, pore pressure, thermal and burial histories are obtained for several sedimentation rates.

T 140

DEFORMATION OF SEDIMENTS IN SUBDUCTION COMPLEXES: OBSERVATIONS FROM MODERN AND ANCIENT MARGINS

S. B. Bachman (Dept. of Geological Sciences, Cornell University, Ithaca, N.Y. 14853)
(Sponsor: W. Bassett)

Studies of the deformation history of the Tertiary Coastal Belt Franciscan subduction complex in northern California and the Middle America subduction complex off southwest Mexico suggest that selective dewatering of sediments may be a major factor in their response to deformation. In Middle America accreted sediments, mudstones have become progressively dewatered with depth, with the local formation of partially slickensided, scaly clay at drilled depths of less than 300 m. Interbedded within these scaly clays are unconsolidated sands.

In Coastal Belt rocks, early deformation features suggest that sands initially deformed brittlely with little strain, while muds deformed more extensively along anastamosing fractures. This early contrast in deformation style is at least partly responsible for the concentration of shear in the mudstones and the formation of sandstone boudins and phacoids. The Middle America Trench data suggest that the deformation contrast evident in Coastal Belt rocks results from early dewatering of the mudstones, probably along microfractures, while the sands remained relatively wet, unconsolidated, and brittle. Thus, shear is concentrated in the more dewatered mudstone. The sheared mudstone apparently becomes melange matrix during continued disruption of the sandstone/mudstone sequence.

T 141

FLOW LAW OF "WET"QUARTZITE IN THE α-QUARTZ FIELD

P.S. Koch (Dept. of Earth and Space Sciences, University of California, Los Angeles, California 90024)
J.M. Christie
R.P. George (Exxon Production Research Co., P.O. Box 2189, Houston, Texas 77001)

Samples of Simpson quartzite (6.4mm dia. x 12.7mm long) were deformed in the α-quartz field in the Griggs apparatus using a talc confining medium in assemblies with low thermal gradients over the sample. Samples were preheated at confining pressure (10-12 Kb) at 850°C for periods up to 20 h to permit diffusion of water from the talc into the samples, before deformation to steady state at strain rates ($\dot{\varepsilon}$) from 10^{-4} to 10^{-7} s^{-1} and temperatures from 750° to 900°C. Flow stresses were in the range 0.5 to 24 Kb.

Data are better fitted by a power law of the form

$$\dot{\varepsilon} = A \cdot (\sigma_1 - \sigma_3)^n \cdot \exp(-Q/RT)$$

than by an exponential law. Least squares fitting of the data to a linearized form of the power law gives ln A = 1.47 (±0.69), $A = 4.36 \left(^{+4.31}_{-2.18}\right) Kb^{-n}\ s^{-1}$, n = 2.44 (±0.13) and Q = 38.2 (±5.1) Kcal/mole, where values in parenthesis represent one standard deviation. Extrapolation of the law to 500°C and slow strain rates predicts stresses ranging from ~1 Kb at 10^{-10} s^{-1} to 10 bars at 10^{-15} s^{-1}. These stresses are smaller by a factor of ~5 than predicted by the "wet" flow law of Parrish et al. (1976), due chiefly to differences in A and Q.

The same quartzite deformed "dry" in our laboratory in a copper confining medium over the same range of P, T and $\dot{\varepsilon}$ gave coefficients $A = .126 \left(^{+.132}_{-.065}\right) Kb^{-n}\ s^{-1}$, n = 2.86 (±0.18)and Q = 36.0 (±7.0) Kcal/mole. In the experimental range flow stresses in dry quartzite are approximately twice those in wet quartzite at the same T and $\dot{\varepsilon}$.

T 142

RELATIONSHIP BETWEEN RECRYSTALLIZED GRAIN SIZE AND FLOW STRESS IN EXPERIMENTALLY DEFORMED QUARTZITE

J.M. Christie (Dept. of Earth & Space Sciences, Univ. of Calif., Los Angeles, CA. 90024)
A. Ord
P.S. Koch

Samples of Simpson quartzite deformed to steady state in the α-quartz field at temperatures of 850° and 900°C and confining pressures of 10 to 12 Kb in talc in the Griggs solid medium apparatus were partially recrystallized to fine-grained aggregates. Samples were rapidly quenched under stress after steady state flow at strain rates from 10^{-4} s^{-1} ($\sigma \sim 20$ Kb) to 10^{-6} s^{-1} ($\sigma \sim 2$ Kb). Grain sizes of recrystallized grains were measured optically by the method of linear intercepts on micrographs of polished and lightly etched surfaces.

Maximum grain sizes observed (~ 30 μm) did not vary appreciably between samples. These large grains were generally isolated within original grains. They probably resulted from growth of nuclei with very mobile (e.g. coincidence lattice) boundaries. Grain sizes in polycrystalline regions, along the original grain boundaries, were smaller and relatively homogeneous within individual samples. The grain sizes (D) vary systematically with flow stress ($\sigma = \sigma_1 - \sigma_3$) and the relationship is best represented by

$$D = 25.9\left(\begin{matrix}+15.4\\-9.6\end{matrix}\right) \times \sigma^{-0.6(\pm 0.3)}$$

where D is in μm. and σ in Kb. In the experimental range of stresses, these grain sizes are an order of magnitude larger than previously published estimates.

Quartzites deformed "dry" in copper over the same range of temperature and stress yield smaller grain sizes for a given flow stress. It is not clear whether the water content influences (a) the dynamic relationship between grain size and stress or (b) the kinetics of the recrystallization process in the relatively short times (< 3 days) of the experiments.

T 143

DIFFERENTIAL STRESS ESTIMATES FOR DEEP CRUSTAL DEFORMATION OF METASEDIMENTS IN THE ADIRONDACKS

J.W. Granath
T.C. Caruso (both at: Dept. Earth & Space Sci., SUNY, Stony Brook, N.Y. 11794)

Isoclinally folded and transposed quartzites interlayered with other metasediments from Whitehall, N.Y., show evidence of dynamic recrystallization: irregular, interlocking grains with sutured and cuspate contacts, inequant grains elongate parallel to the foliation, poorly developed to nonexistent 120° triple junctions, undulose extinction and subgrains, and strong [0001] fabrics in small circle and crossed great circle girdle patterns. Long and short dimensions of 400 grains in each of four specimens (A-77-8 E through H) were averaged to give the following data:

Grain size D (μm)	Diff. Stress $\sigma = AD^{c}$	Strain rate $\dot{\varepsilon}$ in sec^{-1} at 600°	at 650°C
322	6.3 MPa	8.2×10^{-14}	4.5×10^{-13}
359	5.8	6.6	3.6
327	6.2	7.9	4.3
352	5.9	7.0	3.8

A=3.8, c=-.71 (Mercier et al., 1977); $\dot{\varepsilon}$ from "wet" quartzite flow law of Parrish et al. (1976); the "dry" flow law gives unreasonably slow $\dot{\varepsilon}$, near 10^{-22} sec^{-1}; T's are minimum and maximum peak metamorphic T from Essene and Valley (pers. comm.).

These values of differential stress (~60 bars) seem small in comparison to estimates of stresses required to support an abnormally thickened crust, unless the analogy of Molnar and Tapponnier (1978) to a confined, essentially hydrostatic medium is correct. Higher differential stresses could exist at the margins of abutting bodies of stronger rock types, such as the metamorphosed but weakly deformed igneous rocks of the Adirondacks.

T 144

THE ORIGIN OF RIBBON QUARTZ IN DEFORMED QUARTZITES

Shankar Mitra (Dept. of Geological Sciences, Cleveland State University, Cleveland, Ohio 44115)
(Sponsor: Howard Lo)

Quartzites that have undergone considerable plastic deformation often contain elongate ribbon quartz grains with aspect ratios ranging from 5:1 to over 20:1. Microscopic studies of quartzites from ductile deformation zones in the Appalachian Blue Ridge reveal that there are at least three different mechanisms which are responsible for the formation of the ribbon grains: (1) Intragranular deformation of large original grains leads to the formation of sharp deformation bands which eventually produce elongate subgrains. The separation of adjacent bands by fracture or by the formation of small recrystallized grains along their boundaries produces ribbon grains with high aspect ratios. (2) The quartzites deform by the formation of extension fractures which are progressively filled up with syntectonic quartz fibers. The elongate fibers are subsequently deformed internally by dislocation creep and develop deformation lamellae and bands. Successive fracturing, crystal growth and internal deformation in different parts of the rock leads to elongate grains occupying a considerable portion of the rock volume. (3) In micaceous quartzites, the ribbon grains sometimes originate by boudinage and fracturing of quartz veins which were formed parallel to bedding in the early stages of deformation, or by the development of elongate subgrains within the veins. All of these mechanisms indicate that while plastic deformation is important in the formation of ribbon quartz, the strain due to this mechanism cannot account for the high aspect ratios of the ribbons. This is substantiated by the fact that the measured axial ratio of the intragranular strain ellipse rarely exceeds a value of 3:1 in these quartzites.

T 145

DEFORMATION INDUCED RETROGRADE METAMORPHIC ASSEMBLAGES.

E.W.Sawyer (Dept. Geology, Univ. Toronto, Toronto, M5S 1A1, Ontario.)
P-Y.F.Robin (Erindale College, Univ. Toronto, Mississauga, Ontario.)

Slight mineralogical variation in some metagraywacke units in the Quetico Belt give rise to small scale competency contrasts enabling boudins to develop in response to layer parallel extention. Often irregular open fractures upto 20 cm long form at boudin necks. These disconected fractures are partially filled with chlorite, carbonate, quartz, white mica and K-feldspar in various proportions.

Open fractures provide a low-stress region into which rock pore-fluids can migrate. Prominent, narrow concentric mineral zones around each fracture show similar mineralogy irrespective of whether the country rock is of middle greenschist or mid-upper amphibolite grade. The schistose country rock assemblage of oligoclase-quartz-biotite is progressively altered in 4 zones a) clouded oligoclase-quartz-biotite/chlorite-white mica carbonate; b) clouded albite/oligoclase-quartz-chlorite-white mica-carbonate; c) albite-quartz-white mica-carbonate; d) quartz-albite; towards the fracture. Quartz grains recrystallized becoming equant and sutured towards the fracture.

It is suggested that; deformation induced fluid movement enabled retrograde mineral assemblages to form by: biotite+plagioclase+CO_2+H_2O-- albite+quartz+calcite+chlorite+muscovite+K-feldspar. H_2O-CO_2 fluid inclusions are present in recrystallized quartz. Ions removed from biotite and plagioclase were later precipitated in the fractures.

T 146

CARBONATE DEFORMATION MECHANISMS AND FINITE STRAIN IN THE FORELAND THRUST BELT OF ALBERTA

Deborah Spratt (Dept. of Earth & Planetary Sci., Johns Hopkins University, Baltimore, MD 21218)
(Sponsor: David Elliott)

The material behavior of carbonate rock is dictated by the deformation mechanisms which operate during its deformational history. Textural evidence for a variety of pressure solution and dislocation mechanisms is preserved in the unmetamorphosed crinoidal Mississippian rocks which have been telescoped by thrusting and folding in SW Alberta. Each columnal is a single crystal of calcite of known shape; strain is partitioned into pressure solution components which alter the external form of the ossicles, and dislocation components which produce intracrystalline deformation (twinning, kinking, slip, dislocation creep).

Detailed mapping and extensive sampling across sections through 18 thrust sheets reveal the following trends. The upper portion of a sheet is dominated by pressure solution (linear Newtonian flow law) features: removal of material at grain-to-grain contacts and along bedding-parallel stylolites; axial planar cleavage is developed in the folded toe region. Twinning and kinking of grains become increasingly important deeper in the sheet. Near the fault and within shear zones, dislocation creep (power law flow) occurs -- higher dislocation densities and the presence of subgrains are seen in ultrathin-sections treated with a dislocation etchant. Calcite veins form in many orientations; in the deeper thrust sheets, cleavage is developed at a high angle to the fault. The contribution of each mechanism to the total strain in a sample is measured using techniques of quantitative stereology. The relative proportion of each component depends on the stress, temperature, grain size, and strain rate. Every set of physical conditions defines a unique flow law, and there is a transition in creep behavior from dominantly Newtonian flow to power law flow as deviatoric stress or strain rate is increased.

T 147

A MATHEMATICAL MODEL FOR THE DEVELOPMENT OF KINK FOLDS

J.M. Summers (Dept. of Geol. Sci., Queen's Univ., Kingston, Ont. K7L 3N6)

A mathematical analysis has been developed to simulate the finite deformation of tabular kink bands in layered or foliated materials. The bulk deformational properties of such materials are modelled by those of an equivalent homogeneous anisotropic continuum with linear viscous stiffness coefficients. The kink band is assumed to be a tabular zone of rotated folication which extends indefinitely along its profile length. Deformation is plane strain in the profile plane and is induced by a maximum principal compressive stress parallel to the unrotated foliation, outside the kink. Progressive deformation of low amplitude kink perturbations has been studied for a range of kink boundary orientations. Finite foliation rotation within the kink involves early acceleration and later deceleration in the rotation rate of the kinked foliation. This 'rotational softening' followed by 'rotational hardening' results in the development of angular finite kink geometries which are locked. Significant modifications of the magnitude and orientation of the externally applied stresses are induced within a kink during progressive foliation rotation. During 'rotational softening', σ_1 rotates with the foliation and mean stress within the kink is reduced, principally through reduction of the foliation normal stress. Subsequently, σ_1 rotates back to position approximately normal to the kinked foliation and mean stress increases to a level above that of the external mean stress. These predictions have important consequences for fracture orientation and fluid migration within kink-like asymmetric folds. Localised stress modification will also be induced in other types of structures (e.g. shear zones) developed within an anisotropic continuum.

Equation of State

Bay
Monday P.M.
D. J. Weidner (SUNY Stony Brook), Presiding

T 148

ANALYSIS OF PLANE STRAIN SHOCKS IN TRANSVERSELY ISOTROPIC MEDIA

E.S. Gaffney (Los Alamos Scientific Laboratory, Los Alamos, NM 87545)

An iterative procedure is presented for determination of "elastic" constants at high strains and high strain rates from plane strain shock wave data in transversely isotropic media. Values of $C_{11}(\varepsilon)$ and $C_{33}(\varepsilon)$ are determined from the variation of shock speed with strain for <hk0> and <00ℓ> shocks, respectively. The mean stress (p) for each experiment is then obtained using the zero strain values of C_{13} and C_{12} along with the observed strains. A curve is fit to $p(\varepsilon)$ and new values of p calculated for each datum. These new values are used to determine revised C_{13} for <00ℓ> shocks, and a curve is fit to $C_{13}(\varepsilon)$. Using this new relation for $C_{13}(\varepsilon)$, revised values of C_{12} are determined for <hk0> shocks, and a curve for $C_{12}(\varepsilon)$ is obtained. The process is then repeated with a new $p(\varepsilon)$ fit based on the latest $C_{ij}(\varepsilon)$. The lack of shear wave data is compensated for by assumption that a shock in polycrystalline material propagates at the Voigt-Reuss-Hill average V_p which depends on C_{44}. Although eventual application to oil shale is planned, the existing data are at such high stresses that elastic waves are not observed. The procedure is illustrated using elastic precursor data for ice I_h and Be. In ice there is a noticeable discrepancy between the behavior of C_{ij}'s from ultrasonic and shock data.

T 149

SHOCK WAVE STUDIES ON PERICLASE AND MAGNESIOWÜSTITE

M.S. Vassiliou
T.J. Ahrens (Both at: Seismological Laboratory, California Institute of Technology, Pasadena CA 91125)

New Hugoniot equation of state measurements have been and are being carried out on single crystal MgO and polycrystalline $(Mg,Fe)O$, the latter being a possible lower mantle phase in equilibrium with ferromagnesian perovskite. One of our motivations has been to see whether or not a phase change analogous to that recently discovered in FeO at 0.7-0.8 Mbar occurs in periclase or magnesiowüstite. Only tentative results are available at present. Two new MgO data at 1.6 and 2.0 Mbar can be fit well with the same finite strain equation of state fitting existing data at pressures of 1.2 Mbar and below. They appear, however, anomalously disposed with respect to another existing datum (at 2.6 Mbar), one which seems to indicate more compression than expected for the B1 structure. An MgO phase change would be important, as it would suggest that the FeO transition was a structural rather than electronic effect. Uncertainties in the new and existing data, however, make the inference of a phase change in MgO above 2 Mbar very equivocal, especially given that such a transition might be expected to have a small volume change associated with it (e.g., if it is a structural B1/B2 change). The 4 data points thus far obtained on the magnesiowüstite $(Mg_{0.6}Fe_{0.4})O$ appear to define a single equation of state up to 1.9 Mbar, and hence not to suggest a phase change (although one cannot yet be ruled out). In light of the FeO transition, this is an interesting result; if a change in MgO is confirmed it will be even more so.

T 150

HUGONIOT EQUATION OF STATE OF ARAGONITE

J. Vizgirda and Thomas J. Ahrens, (both at: Seismological Laboratory, California Institute of Technology, Pasadena, California 91125).

Hugoniot and release adiabat data have been obtained up to shock pressures of 21 GPa for z-cut pseudo-hexagonal twinned crystals of aragonite, the high density polymorph of calcite. Aragonite is observed to have a Hugoniot elastic limit in the 1.8 to 2.3 GPa range, which is similar to the 1.5 to 2.5 GPa values determined for calcite. At pressures less than 10 GPa, the aragonite Hugoniot is steeper than that of calcite; however, above this pressure, the aragonite and calcite (polycrystalline and some single-crystal data) Hugoniots are nearly coincident, providing strong constraints on the thermodynamic properties of the high pressure phase(s). Aragonite release adiabats centered at pressures less than 11 GPa are internally consistent, and indicate that states with apparent zero-pressure densities between 2.9 and 3.1 g/cc are achieved upon decompression. We are less certain about the specific release paths from states in the 17 to 21 GPa range; however, there is evidence for release to very low zero-pressure densities, indicative of vaporization during decompression. Thus, the onset of decarbonation in aragonite (and probably calcite as well) may occur at shock pressures as low as 17 GPa, which is a factor of two lower than previous theoretical estimates. These results imply that impact processes on carbonate-containing planetary surfaces may yield as much as an order of magnitude more shock-produced CO_2 to an evolving atmosphere than had been previously inferred.

T 151

ORIENTATION DEPENDENCE OF THE DYNAMIC PROPERTIES OF SINGLE-CRYSTAL FORSTERITE

J. Peter Watt, Gregory A. Lyzenga and Thomas J. Ahrens (all at: Seismological Laboratory, California Institute of Technology, Pasadena, California 91125).

Dynamic compression results are presented for single-crystal forsterite shocked along the orthorhombic a and c axes. The a-axis experiments were carried out at shock pressures of 132, 136, and 158 GPa and the data were analysed in the same manner as previous forsterite results for shock along the b-axis. A c-axis datum at 153 GPa was obtained from the duration of shock-induced illumination in shock temperature experiments. The a-axis data lie at densities 0.2-0.3 Mg/m^3 lower than the b-axis values, indicating that, above 100 GPa, forsterite is least compressible in the a-direction. Jeanloz, in single-crystal olivine recovery experiments, found no evidence for shock-induced phase transformations, and proposed a crystallographically-based explanation for the high-pressure shock properties of non-porous olivine which predicts greatest compression in the a-direction, behavior opposite from that found here. Calculated linear compressibilities indicate that olivine is least compressible along the a-axis and that this behavior continues to at least the P and T conditions at the 400-km discontinuity. Thus, if an orthorhombic-like olivine structure were to persist in shock experiments into the mixed-phase region and beyond, the present data would be consistent with the ultrasonic data. Hugoniot data for various shock propagation directions exist for single-crystal quartz, ilmenite, and calcite. In quartz, no orientation dependence is observed, while for ilmenite and calcite, maximum compression occurs for shock along the trigonal axis, in agreement with ultrasonic or static compression data. Transformation pressures vary with shock direction in single-crystal NaCl and calcite. Possible explanations for this behavior are sluggish phase transformation rates along minimum compression directions or additional phase transformations.

T 152

DEFORMATION MECHANISMS OF SHOCK COMPRESSED MINERALS

Louise Levien, (Division of Geological and Planetary Sciences, California Institute of Technology, Pasadena, California 91125), and Thomas J. Ahrens.

Motivated by the lack of understanding of the deformation mechanisms acting in oxides and silicates upon shock compression, and in dynamically induced polymorphism, we are carrying out recovery experiments on single crystals of MgO, CaO and SiO_2. MgO has been initially studied to 44 GPa because there are no known phase transitions to very high pressures (> 100 GPa). A similar study on CaO, which undergoes a phase change around 70 GPa, is in progress. For shock propagation along (001), it is observed that the uniaxial stress produces residual strain in the samples. Single-crystal X-ray techniques are being employed to categorize the strain in the samples by showing line and peak shape as a function of maximum shock compression and crystallographic direction. The use of single-crystal X-ray methods allows both non-directional effects (Gandolfi technique) and those parallel and perpendicular to the propagation direction of the shock (Weissenberg technique) to be studied. These methods also eliminate peak broadening due to inhomogeneity of larger powdered samples. In MgO, shocked to 30 GPa, significant broadening of the high-angle reflections is observed, and we plan to determine if this is due to an increase in mosaicism or residual strain.

T 153

MELTING OF STISHOVITE UNDER SHOCK COMPRESSION: CONSTRAINTS ON THE TEMPERATURE AND VISCOSITY OF THE LOWER MANTLE

Gregory A. Lyzenga, (Seismological Laboratory, California Institute of Technology, Pasadena, California 91125), Thomas J. Ahrens.

Shock temperature and the Hugoniot equation-of-state data for α-quartz and fused quartz shocked into the stishovite regime are interpreted to provide two points on the fusion curve of stishovite at ∿ 71 GPa and ∿ 4700 K and ∿ 117 GPa and ∿ 4900 K, respectively. Shock states at pressures above these points achieved by shocking fused quartz and α-quartz respectively, are believed, on the basis of observed sharp decrease in shock temperatures with increasing pressures to correspond to liquid SiO_2 in six-fold coordination. New and existing Hugoniot data when taken with shock temperature data imply that liquid stishovite has a standard free-energy ∿ 4MJ/kg greater than α-quartz and that the bulk modulus and its pressure derivative are ∿ 280 GPa and ∿ 6, respectively. If SiO_2 is considered to be a major mantle component, the measured fusion curve represents an absolute upper limit for the liquidus of the mantle which is at least 900°C greater than the solidus. Therefore fitting a Lindemann melting law to the present fusion data constrains the temperature in the mantle to be less than ∿ 3600 K at a depth of 2000 km and ∿ 4300 K at the core-mantle boundary. Using this assumed melting curve for stishovite and activation energies in the range 90 to 120 kcal/mole in Weertman's homologous temperature-creep relation implies that the maximum activation volume and viscosity associated with stishovite in the lower mantle are ∿ 2 cm^3/mole and ∿ 10^{22} poise.

T 154

ON THE PERMEABILITY AND CURIE POINT SHIFT OF MAGNETITE UNDER HIGH PRESSURES

Radha Govindarajan (Dept. of Geophysics University of Western Ontario, London N6A 5B7, Ont. Canada
C.M. Carmichael U.W.O. London, Ont.
H.H. Schloessin U.W.O. London, Ont.

An arrangement consisting of two concentric coils, with the magnetite sample as the ferrite core, is employed to calculate permeability (μ_r) by measuring the induction in the secondary due to an inducing primary current. The experiments are carried out in a cubic press under high pressures (p) up to 5.6 GPa and in high vacuum as well as under variable ambients such as oxygen, carbon monoxide and water vapour. The ferro-paramagnetic transition is observed. The curves show a permeability variation with temperature (T) typical of low fields, with a pronounced Hopkinson's effect. The latter appears to become more emphasised under high pressures. The Curie temperature is found to increase drastically on first pressurization. The temperature range between the Hopkinson maxima, preceeding, and the minimum in μ_r, succeeding the transition at the Curie temperature decreases with increasing p. Preliminary results indicate that it extends from 890 to 1080K at 1.6 GPa to 1050K at 4.3 GPa. The corresponding range in high vacuum lies between 826 and 866K.

T 155

TRANSMISSION ELECTRON MICROSCOPY OF FAYALITE SPINEL PREPARED IN A LASER HEATED DIAMOND ANVIL CELL

A.Lacam
M.Madon
J.P.Poirier (all at : Institut de Physique du Globe, Univ.Paris 6, 4 place Jussieu, 75230 Paris Cedex 05, France)

The spinel phase of Fe_2SiO_4 was prepared by compressing synthetic fayalite power in a diamond anvil cell at about 100 kbars focusing the beam of a 60 W YAG laser on it and scanning the sample with the beam. The sample was recovered, ion-beam thinned and examined in TEM. The observable thin zones were situated at both edges of an elongated hole, 0.3 mm long, extending from the center to the periphery of the sample.
On one edge of the hole the material was mostly glassy, containing small (100 nm)idiomorphic spinel crystals obviously grown from the melt or by devitrification. On the other edge, we found residual fayalite containing straight [001] dislocations and circular stacking fault loops, and spinel grains containing cationic antiphase boundaries. The overall structure of the sample is exactly similar to the one already observed in the shocked meteorite Tenham, and we think that the processes taking place when the laser beam hits the sample are very brutal. Unless much care is taken, the information gathered on phase transition kinetics is probably more relevant to meteorites than to the interior of the Earth.

T 156

A METHOD FOR CALCULATING THE THERMODYNAMIC PROPERTIES OF THE EARTH'S LOWER MANTLE

O. L. Anderson
Y. Sumino (both at Institute of Geophysics and Planetary Physics, University of California, Los Angeles, CA 90024)

The thermodynamic properties of the lower mantle are determined from the seismic profile, where the primary thermodynamic variables are the bulk modulus, K, and the density, ρ. It is shown that Bullen's Law (K is proportional to P) holds in the lower mantle with a high correlation coefficient for the PEM seismic model. By using the Bullen Law, there is no ambiguity or tradeoff between ρ_0 and K_0; since both K'_0 are exactly determined by applying a linear K-ρ relationship to the data. Thus, ρ_0(hot), K_{S0}(hot), and K'(hot) are separately found with little error.
The thermodynamic parameters of the uncompressed cold lower mantle are found by an iteration process involving a set of interlocking equations for θ_0, γ_0, q_0, ρ_{0c}, α_0, dK_S/dT, dK/dP, and $\gamma_\gamma=(\rho_{0c}-\rho_0)/\rho_{0c}$, where the symbols stand for Debye temperature, Grüneisen parameter, $d\ln\gamma/d\ln\rho$, coefficient of thermal expansion, bulk modulus K and its derivatives, and thermal expansivity.
The method is to define the uncompressed thermal pressure, P_{TH} vs T given γ_0, α_0, K_{0T}, and q. From this the thermal pressure is found at all depths, and thus the 0° isothermal pressure is determined. From this the ρ_{0c} - K_{0T} relationship is defined and γ_γ is determined vs depth. Matching the results of T with Suzuki's formula α and γ_0 are redetermined. These new values are used to recalculate all properties again in a loop until the input values agree with the output values.
The uncompressed thermodynamic parameters of the lower mantle finally determined agree quite well with the data on the perovskite phase of olivine. There is, however, evidence of heterogeneity up to 2600 km depth.

T 157

ELASTICITY OF Ni_2SiO_4 SPINEL

J.D. Bass and D.J. Weidner (Both at: Dept. of Earth and Space Sciences, SUNY Stony Brook, Stony Brook, NY 11794)
S-Y Akimoto (Inst. of Solid State Physics, Univ. of Tokyo, Roppongi Minato-Ku, Tokyo 106 Japan)

Single crystals of Ni_2SiO_4 spinel were grown in a cubic anvil pressure apparatus in the presence of water. The crystals are slightly smaller than 100 microns in size, are dark green in color, and have a few developed growth faces. Acoustic velocities have been determined from Brillouin scattering spectra and have been inverted to define single crystal elastic constants. These elastic constants are compared with existing data on olivines and spinels to help predict the elastic properties for the spinel phase of magnesium silicates.

T 158

ELASTIC CONSTANTS OF SINGLE CRYSTAL MgO, FeO, CoO and MnO

I. Ohno
Y. Sumino*
M. Kumazawa (all at Dept. of Earth Sciences, Nagoya University, Nagoya, Japan)
(Sponsor: Orson Anderson)

Elastic constants of synthesized crystal MgO, $Fe_{0.92}O$, CoO and MnO are determined by the rectangular parallelopiped resonance (RPR) method (Kumazawa-Anderson technique) with small specimens of 1 2 mm in size for MgO, CoO, and MnO, and ca. 0.5 mm in size for $Fe_{0.92}O$. The elastic constants of MgO are in good agreement within 0.4% with previous reported data, although a small discrepancy is found in C_{12} (1.5%).
The elastic constants (Mbar) of $Fe_{0.92}O$ at 25°C are C_{11}=2.457, C_{12}=1.493, and C_{44}=0.447, based on a density of 5.681 g/cm³. Calculated aggregate properties are: bulk modulus K_S=1.814, shear modulus μ=0.461, compressional velocity V_P=6.54 km/sec, shear V_S=2.85, and Poisson's ratio σ=0.383. By using several empirical rules, the elastic parameters of stoichiometric FeO are evaluated: C_{11}=2.40, C_{12}=1.44, C_{44}= 0.72, K_S=1.76, μ=0.61, V_P=6.63, V_S=3.23, and σ=0.344, based on a density of 5.86 g/cm³. In conclusion, (1) the bulk modulus K_S among these oxides (XO, X=Mg, Fe, Co, Mn) are almost the same values within 15% [K_S=1.586 for MnO, 1.639 for MgO, 1.76 for FeO (or 1.814 for $Fe_{0.92}O$), and 1.856 for CoO], (2) while, the shear moduli among them are largely different from each other, and shear modulus of MgO (μ=1.309) is about two times (or three times) that of FeO (μ= 0.61), or $Fe_{0.92}O$ (μ=0.461), (3) for non-stoichiometric wüstite $Fe_{1-x}O$, it is presumed that C_{44} is largely dependent of the cation deficiency, x.

T 159

ELASTICITY OF STISHOVITE

D.J. Weidner and J.D. Bass (Both at: Dept. of Earth and Space Sciences, SUNY Stony Brook, Stony Brook, NY 11794)
A.E. Ringwood and W. Sinclair (Both at: Research School of Earth Sciences, Australian National University, Canberra ACT 2600, Australia)

Acoustic velocities have been measured in several crystallographic directions in a single crystal of stishovite. The crystal which was grown in a Bridgman anvil system in the presence of water was euhedral in form with dimensions of about 100 microns. The acoustic velocities were determined from Brillouin scattering spectra and have been inverted to obtain the best fitting set of single crystal elastic constants.

T 160

A SYSTEMATIC STUDY OF THE PHASE TRANSFORMATIONS IN RUTILE-STRUCTURED DIFLUORIDES UNDER HIGH PRESSURE

L.C. Ming (Hawaii Institute of Geophysics, University of Hawaii, Honolulu, Hawaii 96822)
M.H. Manghnani

Six rutile-structured difluorides (NiF_2, MgF_2, CoF_2, ZnF_2, FeF_2 and MnF_2) have been investigated under high pressure up to ∿40 Gpa at both ambient and high temperatures, using diamond-anvil pressure cell with/without a YAG laser or an external resistant-wired heater. In situ high pressure x-ray diffraction results have revealed certain patterns as follows: (1) Although each one of the difluorides behaves uniquely, the general transformation trend commonly found is that the rutile phase transforms first into "distorted fluorite" phase, or fluorite phase, which further transforms into post- "distorted fluorite" ($PbCl_2$ or hexagonal) phase with molar volume changes of ∿5-10% and 4-5%, respectively, at the transition pressure. (2) For a given phase transformation, the transformation pressure is, in general, inversely proportional to the unit cell volume and thus inversely proportional to the mean cation-anion bond length. (3) Negative univariant phase boundaries are found for both rutile phase $\rightleftharpoons$ "distorted fluorite" phase (e.g., in MgF_2 and FeF_2) and for rutile phase $\rightleftharpoons$ fluorite phase (e.g., in MnF_2 and ZnF_2).
In view of these findings, implications for oxides, especially for stishovite are explored.

T 161

MECHANISMS OF CALCITE I-II-III AND CALCITE ⇌ ARAGONITE TRANSITIONS

N.S. Brar (Dept. of Earth and Planetary Sciences Erindale College, Univ. of Toronto, Toronto, L5L 1C6, Canada)
H.H. Schloessin (Dept. of Geophysics, Univ. of Western Ontario, London, N6A 5B7, Canada)

The stable structure of $CaCO_3$ at atmospheric pressure and temperature is rhombohedral and generally called calcite I. This structure undergoes two displacive and reversible solid-solid transitions, namely calcite I - II and calcite II-III, at room temperature, under pressures of about 15 Kb (1.5 GPa) and 17 Kb (1.7 GPa) respectively. Calcite I also undergoes the well known reconstructive transition to aragonite (orthorhombic) at elevated pressures and temperatures. Transition pressures and temperatures and the kinetics of calcite ⇌ aragonite transition are well known. The mechanisms of this transition in terms of the rotation of carbonate groups accompanied by the lateral movement of the planes of calcium atoms(1) have also been reported. In the case of calcite I-II-III transitions, however, there are two conflicting viewpoints, supported by experimental findings, about the transition mechanisms. According to Davis(2) calcite II is a minor variation of the calcite I structure and stays rhombohedral. The viewpoint due to Merrill and Bassett(3) suggests that calcite II results from the rotation of the carbonate groups by 11° and a small displacement of adjacent planes of calcium atoms parallel to (10$\bar{1}$4) planes. This results in a considerably altered, monoclinic, structure for calcite II. Here it will be shown that the latter viewpoint appears to be more logical and acceptable if we consider the displacive calcite I-II-III transitions as precursory steps or rotatory attempts towards the calcite → aragonite transition.

(1) Min. Mag., 33, 925-928, 1964.
(2) Science, 145, 489-91, 1964.
(3) Acta Cryst., B31, 343-349, 1975.

T 162

KINETICS OF MARTENSITIC OLIVINE-SPINEL TRANSITION IN A SUBDUCTING SLAB

J.P. Poirier (Institut de Physique du Globe, Univ. Paris 6, 4 Place Jussieu, 75230 Paris-Cedex 05, France)

A model for a martensitic olivine-spinel transition was recently proposed (1), it involves the propagation of stacking faults on the (100) planes of olivine (affecting the hcp oxygen lattice) accompanied by synchroshear of the cations producing the spinel structure. The partial dislocations, the stacking faults and the synchroshear are the ones involved in (100) [001] slip of olivine. Assuming that this mechanism operates, we derive an expression for the stress-sensitive kinetics of the olivine-spinel transition in a lithospheric subducting slab, by computing the chemical and mechanical driving force on transformation dislocations as a function of depth z :

$$\frac{dX}{dz} = \left(\frac{dz}{dt}\right)^{-1} \cdot LdV = \left(\frac{dz}{dt}\right)^{-1} \cdot LdA\ (\sigma_c + \sigma - \sigma_f)^m$$

where X is the volume fraction of transformed phase; dz/dt, the velocity of the sinking slab; L, the dislocation density; d, the (100) interplanar distance; σ_c, the chemical stress; σ, the shear stress in the slab and σ_f the friction stress on dislocations. A and m are constants. The chemical stress has been computed using Toksöz et al (2) temperature distribution for a fast plate and taking dP/dT : 30b/°C for the Clapeyron slope of the transition :

$$\sigma_c^{kb} = 0.023\ z^{km} - 8.46$$

It is found that a shear stress σ = 0.5 kbar in

the plate would allow the transformation to be completed about 20 km above the equilibrium depth of 370 km.

(1) Poirier, J.P. (1979) IUGG XVII th General Assembly, Canberra.
(2) Tóksoz, M.N.,J.W.Minear and B.R.Julian (1971) J.Geophys.Res 76, 1113

Hotspots, Uplift and Basin Subsidence

Metropolitan Centre
Tuesday A.M.
G. T. Jarvis (Univ. of Toronto), Presiding

T 163

HOTSPOT TRACKS IN NORTH AMERICA

W. Jason Morgan (Department of Geological and Geophysical Sciences, Princeton University, Princeton, New Jersey 08544)

Using seafloor spreading magnetic anomalies, the relative positions of the continents bordering the Atlantic Ocean are determined for the past 200 My. This group of plates is then positioned over fixed hotspots to generate predicted tracks on each of the plates. The fit of the predicted tracks to the measured ages and locations of hotspot produced features is improved by allowing systematic "wander" of individual hotspots in this frame at rates of about 3 mm/yr. Hotspot tracks cross the east coast of North America at 4 places: Florida (Fernando), Cape Fear (Bermuda), New England (Verde and Great Meteor), and Grand Banks (Azores). Of particular interest are the nearly congruent tracks of the Verde and Great Meteor hotspots, which both cross Ontario, southernmost Quebec, and New England. New England is over the Verde hotspot about 160 My ago and over the Great Meteor position about 120 My ago.

T 164

MESOZOIC HOTSPOT EPEIROGENY IN EASTERN NORTH AMERICA

S. Thomas Crough (Department of Geological and Geophysical Sciences, Princeton University, Princeton, NJ 08544)

Geological data indicate that the region from Ontario to New England was elevated, and later eroded to a depth of at least 4 km, as the area moved over the Great Meteor hotspot in Jurassic-Cretaceous time. A modern sedimentary analogue, outlier deposits, isopach maps, lithofacies relations, and conodont paleotemperatures all indicate that the foreland basin of the Appalachians once extended northward across eastern Canada. Conformable stratigraphic relations, erosion of plutons, and clasts in an igneous pipe suggest that the Ontario-New England region was uplifted and eroded in post-Paleozoic, probably post-Jurassic, time. Apatite fission-track ages of the exposed basement indicate that the major erosion was in Cretaceous - early Tertiary time. The spatial extent and timing of this uplift are consistent with the formation of a broad swell over the Great Meteor hotspot.

T 165

THE DEPENDENCE OF CRUSTAL THICKNESS ON MANTLE TEMPERATURE WITH APPLICATION TO MOR HOTSPOTS

J. L. Ahern (School Geol. Geophys., U. Oklahoma, Norman, OK 73019)
M. Bevis (Dept. Geol. Sci., Cornell U., Ithaca, NY 14853)

Oceanic crustal thickness is fairly uniform over the world's oceans. It is typically between 4 to 7 km thick, and averages about 6 km. Older crust tends to be somewhat thicker than that being formed at mid-ocean ridges (MOR) today. The thickness of oceanic crust can only be weakly dependent on spreading rate, if at all. Ahern and Turcotte have shown that at a MOR the rising, convecting mantle melts by pressure release fusion and that the magma so produced migrates upward by a porous flow mechanism and is erupted at the ridge. The thickness of the crust produced by this process is independent of the spreading rate, but highly dependent on the initial temperature of the rising mantle. By calculating the effect of increased temperature on crustal thickness, we find that only a small increase in mantle temperature ($\Delta T \sim 100°C$) leads to a large increase in crustal thickness ($\Delta h \sim 7$ km). This suggests that mantle temperatures beneath MOR are relatively uniform worldwide and that the mantle beneath MOR hotspots need only be ~100 or 200°C hotter than beneath the adjacent normal MOR. The crust beneath Iceland averages more than 10 km thick, compared to less than 5 over normal MOR, implying that the mantle beneath Iceland is about 75°C hotter than normal. This value is in good agreement with mantle temperatures as determined by bathymetry, gravity, and geoid data.

T 166

THE EFFECT OF HOTSPOTS ON THE EMPIRICAL AGE-DEPTH RELATION

Richard L. Heestand
S. Thomas Crough (both at: Department of Geological and Geophysical Sciences, Guyot Hall, Princeton University, Princeton, N.J. 08544)

Hotspots located both mid-plate and on mid-ocean ridges can bias the empirical age-depth relation. Ocean floor bathymetry for seafloor greater than 80 my in age has been previously used to determine if the ocean lithosphere behaves as a cooling half-space, or a cooling plate. Data supporting the cooling plate model have been collected from both the western North Atlantic Ocean and the northwestern Pacific Ocean. However, both oceans contain anomalously shallow areas. Hawaii and Bermuda have been identified as sites of hotspots surrounded by broad swells approximately 1000 km wide and 1.2 km in height. We have examined depth versus distance from hotspot tracks for particular crustal ages. We find for a particular age the seafloor becomes deeper with increasing distance from the hotspot tracks. For example, in the North Atlantic for 95 my old crust no point is further from a hotspot track than approximately 1100 km. In the South Atlantic, points within the anomalously deep Argentine Basin lie 1100-1600 km from the nearest hotspot track. We suggest that the Argentine Basin is deeper than areas in the North Atlantic with similar ages, by virtue of its greater distance from a hotspot track. We have constructed an empirical age-depth relation using only those seafloor depths large distances from hotspot tracks.

T 167

SEDIMENTARY BASIN FORMATION BY RAPID EXTENSION OF THE LITHOSPHERE

G.T. Jarvis (Department of Physics, University of Toronto, Toronto, Ontario, Canada M5S 1A7)
D.P. McKenzie (Department of Geodesy and Geophysics, Madingley Rise, Madingley Road, Cambridge, England CB3 0E2)
(Sponsor: C.H. Chapman)

Thinning of continental crust by rapid stretching of the lithosphere produces an initial subsidence and thermal anomaly. When stretching ceases, slow decay of the thermal anomaly produces subsidence (due to thermal contraction) on a time scale of approximately 60 Ma. The dependence of the heat flow and subsidence histories on the rate of extension is determined here using a time-dependent analytical model. Results are compared with the predictions of a simpler instantaneous stretching model and constraints on the use of the latter are provided in terms of the duration and amount of stretching. For most basins the simple model gives reasonably accurate results provided the duration of stretching is less that 20 Ma.

T 168

APATITE FISSION TRACK DATING OF THE COOLING HISTORY AND TECTONICS OF OLD PLATFORMS : THE FRENCH MASSIF CENTRAL

J. Carpéna, D. Mailhé and G. Poupeau
C.F.R., 91190 Gif-sur-Yvette, France
(Sponsor : Claude Lalou)

Due to their low closing temperature for fission (FT) track dating, apatites appear to be very useful for the measure of the late thermal evolution of old platforms. A FT dating study of apatites from the French Hercynian platform (where pre-permian rocks have no isotopic ages younger than ~280m.yr) shows that :
1. On its westernmost part and central Limousin (Massif Central),this platform cooled rapidly from more than 300°C to less than 50°C some 280m.yr ago, although locally (W.Limousin) the 100°C isotherm was reached only 240m.yr ago.
2. Ages of 170m.yr or so around the (Trias to Dogger) cratonic basin of the Causses are interpreted as dating the latest uplift of a part of the Hercynian basement, possibly buried under the mesozoic terranes of the (then more extended) Causses basin.
3. At the southern end of the Massif Central,the Montagne Noire (M.N.) exhibits a complex pattern of FT ages, with plateau ages extending from 70 to 282m.yrs. Ages between 282 and 229m.yr (with a spatial gradient from north to south) indicate a slow cooling rate for the northern half of the M.N. axial zone. All the younger ages from 70 to 169 m.yr concern rocks of the southern half of the axial zone. This age range is the same as those of the stratigraphically determined tectonic phases in the sedimentary mesozoic terranes around the M.N. It shows that the tectonic instability already known for the sedimentary Languedoc during the Jurassic and the Cretaceous affected also the older metamorphic nucleus of the M.N.

T 169

PLATEAU UPLIFT BY THERMAL EXPANSION OF THE LITHOSPHERE

J. C. Mareschal (School of Geophysical Sciences, Georgia Institute of Technology, Atlanta, Ga., 30332)

A Green's function is derived for the uplift of the Earth's surface caused by the thermal expansion following (axially symmetric) changes in the heat flow at the base of the lithosphere. The uplift, temperature change at any depth and the anomalous surface heat flow are the convolution (in space and time) of the Green's function with the heat flow change. With a characteristic time of the order of 10^8 years, uplifts of the order of 300 m would follow heat flow changes of the order of 5 m W/m^2. In no case would significant temperature changes be observed near the Earth's surface. Erosion and the following isostatic amplification of the uplift are introduced in the formulation.

T 170

GREEN'S FUNCTIONS RELATING HEAT FLOW, TOPOGRAPHY, AND GRAVITY TO A POINT HEAT SOURCE

T. Harter and D. T. Sandwell (both at: Dept. of Earth and Space Sciences, Univ. of Calif., Los Angeles, CA 90024)

The oceanic lithosphere is modeled as an isostatically compensated conducting half-space, with uniform thermal properties, moving horizontally across a point heat source. The three dimensional temperature is obtained from the time independent heat equation, with the isothermal surface boundary condition maintained by an image sink. The seafloor topography is found by convolving the thermally induced density structure with the elastic plate Green's function. The disturbing potential is obtained by convolving the seafloor topography and half-space density with a linearized gravitational Green's function. By the convolution theorem, the multiple convolutions in the space domain are multiplications in the wavenumber domain.

The foreward problem is solved for two heat source geometries. For a Gaussian source, the lithosphere is thinner downstream from the source. Geoid heights and topography predicted by this model, are in agreement with observations over the Hawaiian and Bermuda swells. A ridge crest model is obtained by superimposing plates moving in opposite directions over a delta function heat source. The resultant depth-age, heat flow-age, and geoid-age relations are compatible with the observations over the North Atlantic.

The common heat source q is obtained from the observables O_i by inverting the equation $O_i(\vec{k}) = \int^{\infty} q(\vec{k},z)\, K_i(\vec{k},z)\, dz$. Although the problem is not unique, geometric and thermal constraints will limit the class of acceptable sources. Each of the three kernels K_i is anisotropic but the free-air gravity kernel divided by the the topography kernel (transfer function) is nearly isotropic and has a distinctive "roll off".

T 171

THERMAL CONTRACTION, EXCESS TEMPERATURE AND SEDIMENTATION: A THREE-DIMENSIONAL STUDY OF THE MICHIGAN BASIN

Jeffrey A. Nunn (Dept. of Geological Sciences, Northwestern University, Evanston, IL 60201)
Norman H. Sleep

Flexure of the lithosphere during formation of the Michigan basin is modeled as a thin elastic or viscoelastic plate overlying a fluid substratum. Lithostratigraphic maps of the Michigan basin have been compiled. These isopach maps are combined with density values from the Deep Borehole (Hinze et. al., 1978) to quantitatively determine the contribution of the weight of sediment overburden to the subsidence. Thermal contraction is assumed as an initiating mechanism for subsidence. The thermal contraction load is calculated from the load necessary to produce the observed deflection minus the load due to the sediments. Effective flexural rigidities are compatible with an earlier three-dimensional continuously filled basin model (Nunn & Sleep, 1979) : 2×10^{28} dyne-cm for an elastic lithosphere and 10^{31} dyne-cm with a viscosity of 10^{25} poise for a viscoelastic lithosphere. The magnitude and spatial distribution of the thermal contraction load are consistent with the presumed mechanism. Excess temperature and heat flow do not exceed 15 C and 1.4 HFU in the sediments, respectively. The low value for the excess temperature is due to the concentration of the thermal anomaly below 15 Km, in agreement with earlier gravity results (Nunn & Sleep, 1979). The great depth of the thermal anomaly can explain the lack of evidence for an initial heating event prior to subsidence. Contour maps of water and basement depths for sequential time intervals during basin development are determined. The predicted environments of deposition are compared with lithofacies maps of the Middle Devonian (Gardner, 1971). Effects of areal variations in loading due to regional facies changes in the sediments, primarily Upper Silurian evaporite deposits, on the migration of the center of maximum deposition are calculated.

T 172

THE GULF OF LION: SUBSIDENCE OF A YOUNG CONTINENTAL MARGIN

M. S. Steckler
A. B. Watts (both at Lamont-Doherty Geological Observatory of Columbia University, Palisades New York 10964 and Department of Geological Sciences of Columbia University, New York, New York 10027)

The Gulf of Lion is a young continental margin in the western Mediterranean Sea which formed as the result of the Oligo-Miocene rifting of Sardinia from France. We have used data from three wells drilled in the Gulf of Lion to study the subsidence of this margin. The three wells drilled through approximately 3 1/2 kms of Miocene to Recent sediments before terminating in Paleozoic basement. The sediments in these wells constitute one of the best available records of the subsidence of a young margin. Backstripping the sediment load reveals that the margin has been subsiding at nearly mid-ocean ridge rates since its origin. A simple lithospheric stretching model would require extension by greater than a factor of 10 to produce subsidence of the observed magnitude. This amount of stretching is not geologically tenable and suggests that the lithosphere at the Gulf of Lion has been thinned/heated by means other than passive extension alone. The Messinian salinity crisis appears in the well data as a major unconformity. The tectonic subsidence, however, appears to continue through the hiatus, in agreement with the interpretation of the salinity crisis as an evaporitic drawdown. Using this observation, we have been able to estimate the extent of erosion of the continental shelf during the crisis. At the most seaward well (Autan 1) 1200-1500 meters of unconsolidated sediments were removed. Estimates of the amount of material eroded decrease rapidly in a landward direction. The continental shelf was not able to rebuild to its former profile until about 2-3 m.y. after the salinity crisis.

T 173

EVOLUTION OF CONTINENTAL LITHOSPHERE: SEARCHING FOR A MODEL CONSISTENT WITH HEAT FLOW MEASUREMENTS, SEISMOLOGICAL DATA AND ISOSTATIC BALANCE.

Béatrice DE VOOGD (labo. de géophysique interne, university of Grenoble, France)
(sponsor: Georges POUPINET)

Plate thickening with time is a successful theory for the oceanic lithosphere. Hence, several authors explain the evolution of continents by cooling of a thermal layer, the contrasts between oceanic and continental structures resulting from the thick crust that characterizes continents. These thermal models, however, are not as successful for continental plates as for oceanic ones. We are looking on geophysical data that inform us on a possible evolution of the continental lithosphere. Therefore, on stable plates, we study the relation between P-wave travel time residuals and heat flow. P-residuals are interpreted in terms of temperature differences within the lithosphere. Seismological data suggest that the lithosphere beneath an Archean plate is approximately 100km thicker than that beneath a Palaeozoic plate. We made some numerical experiments on the thickening of continental lithosphere with age, looking for a model that would satisfy isostatic balance when the plate thickens. Seismic refraction profiles show that crustal evolution cannot be a mechanism stabilizing the vertical motions of continents. A continental lithosphere chemically differentiated from the asthenosphere would explain vertical movement episodes within continental plates.

T 174

VISCO-ELASTIC AND VISCOUS STRUCTURE MODELS ASSEMBLED TO REPRESENT MECHANICAL FEATURES OF ITALIAN PENINSULA AND ADRIATIC SUB-PLATE

G. Finzi-Contini (Istituto di Geofisica Mineraria, Università di Palermo, Corso Calatafimi, 260-90129 Palermo, Italy)
(Sponsor: Giovanni P. Gregori)

A group of visco-elastic and viscous models for the Italian Peninsula and the Adriatic Sub-Plate are proposed and discussed, within the frame of the Central Mediterranean plate tectonics approach.

The basic considered visco-elastic model is an one-dimensional one (that is, a long beam supposedly bent by an axial compression force), used to simulate deformation features of the Apennine range structures in the horizontal plane. As a consequence, a visco-elastic, two-dimensional model is suggested, to simulate some mechanical aspects of the Adriatic Sub-Plate, its deformations being considered in vertical planes. Finally, a simplified, viscous, two-dimensional model is introduced, to simulate gravimetrical effects, possibly attributable to very deep sources of anomalies along the western side of the Peninsula; the deformations of this model are examined in vertical planes.

Effects given by the above mentioned models are superimposed for particular situations and resulting consequences are suggested, also considering selected seismological data and main geothermal evidences of the studied region.

Mantle Rheology, Lithosphere & Convection

Metropolitan Centre
Tuesday P.M.
Micheline C. Roufosse
(Smithsonian Astrophysical Obs.), Presiding

T 175

ISOSTASY IN THE OCEANS

A. B. Watts (Lamont-Doherty Geological Observatory of Columbia University, Palisades, New York 10964 and Department of Geological Sciences of Columbia University, New York, New York 10027)

Studies of free-air gravity anomaly and bathymetry profiles have revealed information on the nature of the isostatic mechanism in oceanic regions. These studies show that the compensation of geological features on the ocean floor can be generally explained in terms of the flexure or plate model of isostasy. The most useful parameter in this model is the effective elastic thickness, which is determined by the flexural rigidity of the plate. Geological features formed on or near mid-ocean ridge crests (Walvis ridge, 90° East ridge, Line Islands ridge and Hess rise) are associated with small values of the effective elastic thickness (2-10 km) while features formed off-ridge (Hawaiian-Emperor seamount chain, Great Meteor seamount, Magellan seamounts, Louisville ridge) are associated with high values (20-45 km). A new compilation of all recent flexure studies indicate the effective elastic thickness is a strong function of the age and thermal gradient of oceanic lithosphere at the time of loading. This result has a wide range of implications for models of the rheology of oceanic lithosphere, the origin of long-wavelength ($\lambda \gtrsim 1000$ km) gravity and bathymetry anomalies and the geological evolution of the ocean basins.

T 176

RHEOLOGICAL BEHAVIOR OF THE OCEANIC LITHOSPHERE IN RESPONSE TO LOADING

A. Cazenave and B. Lago (Groupe de Recherches de Géodésie Spatiale, CNES, Toulouse, France)

Loading studies of the oceanic lithosphere suggest that the lithosphere behaves elastically over geological time scales and that the elastic thickness presents a square root of age dependance (see among others Watts 1978, JGR, 83, 5985, Cazenave et al. 1980, Geophys. J. in press).

To interpret correctly these results based on a simple elastic response, we propose a model of layered lithosphere, consisting in a purely elastic upper layer, a transition zone with viscosity varying with depth and a plastic lower part ; Such a model leads to a noticeable reduction of elastic stresses : when applied to a number of seamount loads, this models leads to maximum stress differences which do not exceed 1-3 Kbars, for flow laws representing mechanisms of creep in olivine. The approach used in this study allows us to follow stress relaxation over time : taking account of the thermal cooling of the lithosphere, we show that the elastic thickness of the lithosphere is stabilized after a time of order 5-6 % of the age of the lithosphere at the date of loading.

T 177

SUBSIDENCE AND FLEXURE OF THE LITHOSPHERE AT HAWAII

J. H. Bodine
A. B. Watts (both at Lamont-Doherty Geological Observatory of Columbia University, Palisades, New York 10964 and Department of Geological Sciences of Columbia University, New York, New York 10027)

Studies of long-term ($>10^6$ years) surface loads suggest the mechanical thickness of oceanic lithosphere is 2 to 3 times smaller than the seismic thickness or the thermal thickness of

plate tectonics. This suggests that for short-term loads (<10^2 years) the lithosphere responds as a thick mechanical layer. For long-term loads, however, stress relaxation in the lower lithosphere causes the mechanically strong layer to decrease in thickness. This transition between short and long term mechanical thickness is a strong function of the rheology and thermal structure of the crust and upper mantle. The geological implications of this transition are that local subsidence and associated regional uplift of oceanic lithosphere should follow formation of an oceanic island or seamount load. Tide gauge data indicate Hawaii is presently subsiding relative to Oahu at 4.1 mm/yr. We have constructed a finite difference model for oceanic lithosphere based on data from experimental rock mechanics in an attempt to explain the subsidence data. These studies show the subsidence data can be explained by flexure associated with the volcanic load of Kohala volcano, whose main shield building phase terminated 0.35 to 0.45 m.y.B.P. Thus the relative subsidence of Hawaii is of local tectonic origin and may provide useful constraints on models for the rheology of oceanic lithosphere.

T 178

STUDY OF THE TIME EVOLUTION OF THE LITHSOPHERE IN THE PACIFIC OCEAN USING GEOS-3 AND SEASAT RADAR ALTIMETER DATA

Micheline C. Roufosse (Smithsonian Astrophysical Observatory, 60 Garden Street, Cambridge, Mass. 02138)

Geoid heights derived from the Geos 3 and Seasat radar altimeters are used to probe the mechanical properties of the lithosphere by studying the correlation between the geoid heights and the bathymetry constructed along the subsatellite positions. A thin-elastic-plate model is selected to predict the wavelength and intensity of the geoid signal produced by seamounts or ridges loading the lithosphere. A series of theoretical geoids is then calculated by using flexural-rigidity values ranging between 10^{28} and 10^{31} dyne-cm. The value for the flexural rigidity that best accounts for the observed geoid signal is selected as representative of the region. In this study, several chains of seamounts have been chosen, representing different possible situations of loading, different ages for the underlying lithosphere, and different ages for the load; this will help us determine the parameters that most influence the flexural response. The radar altimeter has proved to be a sensitive device for monitoring changes in the geoid for wavelengths longer than 100 km. The main conclusion of this work is that the flexural rigidity is not a function of the age of the lithosphere alone; in several of the examples studied, the variations observed cannot be accounted for by a simple relationship. So far, the parameter that best explains the variations observed both in the gravity field and in the geoid height is the age of the lithosphere at the time of loading.

T 179

GEOID HEIGHT VERSUS AGE FOR SYMMETRIC SPREADING RIDGES

D. T. Sandwell and G. Schubert (both at: Dept. of Earth & Space Sciences, Univ. of Calif., Los Angeles, CA 90024)

Geoid height-age relations have been extracted from GEOS-3 altimeter data for large areas in the North Atlantic, South Atlantic, Southeast Indian, and Southeast Pacific Oceans. The technique used to determine these geoid height-age relations eliminates geoid undulations that are antisymmetric about the ridge and slopes in the geoid parallel to isochrons. Except for the Southeast Pacific, geoid height decreases approximately linearly with crustal age for ages less than 80 Myr, in agreement with the prediction of an isostatically compensated thermal boundary layer model (Haxby and Turcotte, 1978). The nearly linear geoid height-age relations have slopes -0.094±0.025 m/Myr, -0.131±0.041 m/Myr, and -0.149±0.028 m/Myr for the South Atlantic, Southeast Indian, and North Atlantic regions, respectively. For ages greater than 80 Myr, the geoid height-age relations for the North and South Atlantic are nearly flat, indicating a reduction in the rate of boundary layer thickening with age. Because the uncertainties in the geoid slope-age estimates are positively correlated with spreading velocity the most reliable geoid height-age results will come from an analysis of the Southwest Indian ridge when more complete age data become available.

T 180

ZERO-AGE DEPTH VARIATIONS IN THE NORTH ATLANTIC AND THEIR RELATIONSHIP TO GRAVITY ANOMALIES AND GEOCHEMICAL VARIATIONS

S. Le Douaran (Dept. of Earth and Planetary Sciences, Massachusetts Institute of Technology, Cambridge, Ma 02139)
J. Francheteau (Centre Oceanologique de Bretagne, 29273 Brest Cedex France)
(Sponsor: Barry Parsons)

The maximum depth of the rift-valley was used as a simple new criterion to define depth at zero age in the case of the mid-Atlantic ridge from 10° to 50°N. Real bathymetric profiles transverse to the rift-valley and away from fracture zones were compiled, more than 200 depth values including several Seabeam profiles were picked and smoothed by calculating moving averages. This method gives rather different results from previous studies that used different criteria for the zero-age depth.

The curve of zero-age depth as a function of latitude shows depth variations between 500 and 1500m, although lithospheric thermal models predict a constant depth for a constant age.

Besides the major depth anomaly near the Azores, an anomaly is observed from 13° to 22°N which may be related to a triple junction between North and South America and Africa. Some depth anomalies seem to be controlled by fracture zones (Kurchatov, Kane, Desirade). The long wavelength depth anomalies are correlated with gravity anomalies whose wavelength and amplitude cannot be explained by a sublithospheric origin.

Between 40° and 50°N the variations of the isotopic rations Sr^{87}/Sr^{86} are in good agreement with the bathymetric variations which may be related to differences of temperature or mineralogy in the mantle beneath the lithosphere.

T 181

THE EFFECTS OF EROSION IN THE INTERPRETATION OF CONTINENTAL ISOSTATIC RESPONSE FUNCTIONS

Randell Stephenson, Dept. of Geology, Dalhousie University, Halifax, Nova Scotia B3H 3J5

A useful method for analyzing the isostatic compensation of distributed continental topography is the response function technique. The isostatic Green's function, which represents the compensation for a point load, can be extracted from Fourier transforms of Bouguer gravity and topography maps. Response functions have been modelled in the past assuming time-independent topographic loads and lithospheric rheology. However, in older orogenic regions, the present topography is in fact an eroded remnant of the original. In addition, if thermal weakening of the lithosphere accompanies orogeny, the compensation of the original topography may be more local than the compensation of mass redistributed by the effects of surface erosion after the lithosphere cools and stiffens. These complications in the compensation process are incorporated into a theoretical model which describes the response of a thin viscoelastic plate to a topographic load which erodes. The rate of erosion is proportional to the topography remaining at any given time. Two simplified cases are considered: 1) the lithosphere has integrity when the load is applied; and 2) the lithosphere supports no shear stress at time t_o, but becomes suddenly competent at a time $t>t_o$. Model parameters include D, the flexural rigidity of the plate, τ, its viscoelastic relaxation time, and σ, the erosional time constant, which may be wavelength-dependent. Predictions from the theoretical models are tested against observed isostatic response functions and topography amplitude spectra calculated from several North American data subsets. The results may help to explain why apparent plate thicknesses calculated using elastic or non-erosional viscoelastic models tend to be smaller than those based on analyses of individual topographic features.

T 182

NORMAL MODE ATTENUATION AND THE SHORT TERM RHEOLOGY OF THE MANTLE

David A. Yuen (Dept. of Geology, Arizona State University, Tempe, Arizona 85281)
W.R. Peltier (Dept. of Physics, University of Toronto, Toronto, Ontario, Canada M5S 1A7)

Three dimensional constitutive relations for a standard linear solid have been constructed in order to determine, self-consistently, the frequencies and Q's of the normal modes of free oscillation of the Earth. In order to fit the observed Q's of the lowest order toroidal and spheroidal modes (~200) with the single relaxation time homogeneous model requires a short term viscosity of order 10^{17} Poise. This model of course predicts a rapid increase of Q with increasing frequency for the radial, fundamental spheroidal, and all of the toroidal oscillations, which is not observed. This defect is easily remedied with an absorption band model and the one which we employ has long and short time cutoffs of 2×10^4 and 10^{-2} sec respectively and a quality factor in the absorption band of 250. Although this model is simple, it does establish that the mantle viscosity which controls short timescale anelastic processes in the standard linear model is much less than the viscosity which controls long timescale processes like postglacial rebound which are best described in terms of a Maxwell model. It is a consequence of the wide separation in viscosities that the complete Burgers' body behaves either as a standard linear solid or as a Maxwell solid for phenomenological time scales which are respectively less than or greater than the Maxwell time. The Maxwell time for the upper mantle is approximately 200 years.

T 183

LITHOSPHERIC LOADING BY THE 1896 RIKU-U EARTHQUAKE, NORTHERN JAPAN: IMPLICATIONS FOR PLATE FLEXURE AND ASTHENOSPHERIC RHEOLOGY

Wayne Thatcher (U.S. Geological Survey, 345 Middlefield Road, Menlo Park, CA 94025)
T. Matsuda, T. Kato (Earthquake Research Institute, Tokyo University, Tokyo, Japan)
John B. Rundle (Sandia Laboratories, Albuquerque, N.M. 87185)

Under favorable circumstances, the time-dependent aseismic deformation resulting from the loading of the lithosphere by the stress drop of a large dip-slip earthquake can be used to determine both the effective elastic plate thickness and the asthenospheric viscosity. The deformation has several similarities with the deflection of the lithosphere by surface loads and with movements due to post-glacial rebound. Level changes obtained in the 80 years since the M = 7.5 1896 Riku-u earthquake, an intraplate thrust event in northern Honshu, provide convincing evidence that asthenospheric readjustments are responsible for the observed movements. Leveling surveys crossing the zone of surface faulting have been repeated five times since 1900 and delineate a localized depression that has subsided at a continually decreasing rate. The depression is centered close to the 1896 faulting, and its shape and width, about 75 km, are matched by our model using a plate thickness of 30 km. The decaying subsidence rate constrains the viscosity of the uppermost asthenosphere to be 4×10^{20} Poise. A linear viscous rheology matches the observed decay quite well, although measurements are sparse in the several decades following the earthquake.

T 184

CONTINENTAL WAKES

D. W. Forsyth
E. M. Parmentier (Both at: Department of Geological Sciences, Brown University, Providence, RI 02912)
C. O. Bowin (Woods Hole Oceanographic Institution, Woods Hole, MA 02543)

Some of the long-wavelength, negative anomalies in the Earth's gravity field may be related to the motion of continents relative to underlying mantle. Geoidal lows are found south of India, southwest of Australia and in the western Atlantic along the eastern margins of North and South America, all areas in the wake of moving continents. No corresponding lows are found in the eastern Atlantic, where Africa and Europe are thought to be moving much more slowly relative to the underlying mantle. If only harmonics of degree 4 through 10 are considered, each of the geoidal anomalies has an amplitude of 20 to 40 meters.

If continental lithosphere is thicker than oceanic lithosphere and has a less well-developed low viscosity zone beneath it, then wakes may be caused by viscous interaction of moving conti-

nents with underlying mantle. A simple model in which the continent is an area of enhanced shear stress on the underlying mantle suggests that uncompensated topography and negative gravity anomalies may characterize continental wakes. If seismic velocity anomalies south of Australia which were found by surface wave studies are related to the motion of Australia, then the wake may also involve compositional and/or temperature effects.

T 185

MASS ACCUMULATION & OVERFLOW PHENOMENA AT THE WEST PACIFIC MARGIN

R C Bostrom, U. of Washington, Seattle, WA 98105
K K Saar, Texas A & M, College Station, TX 77840
D A Terry, U. of Washington, Seattle, WA 98105

The geoidal high embracing the western third of the Pacific is one of a few major features, some in the stage of accumulation, others (considered elsewhere) apparently in the process of dissipation. The arcuate features of the west Pacific margin are systematically associated with the apical region of the high. If plate tectonic inferences are correct, that the W Pacific is the site of convergence & subduction, as Kaula notes the sign of the anomaly dictates that "the driving force is a push from above rather than withdrawal from below".The effect of convergence into a region into which material is being drawn by autonymous sinking (as under thermal convection) is basically distinct from that in a region into which material is being crowded by an external agency. In the first case we should find that the area is low-standing & the site of a negative anomaly. In the second case these relations are reversed; the effect of accumulation in a region in which downward assimilation is impeded as by viscosity increase is in general what is observed -- a region of excess mass; in which topography is slightly raised; & in the crestal region of which extension must prevail. The latter might be expected to result in overflow phenomena of the type identified by Ida, 1978. In causality order, this implies that: 1) Under the action of the agency responsible for trans-Pacific flow of the upper mantle, increasing pressure in the accumulation region leads to phase densification at depth, foundering & the re-assimilation of material in the mantle; 2) The foundering regions are the locus of differentiation, new lithosphere formation, & shallow extension marked at surface by back-arc spreading. 3) The arcuate features are secondary & form at the margin of the expanding back-arc basins; slab-sinking may be initiated at the margin.

T 186

CONTINENTAL TECTONICS AND THE SCALE OF MANTLE FLOW

Michael Bevis
B.L. Isacks (both at Geological Sciences, Cornell University, Ithaca, NY 14853)

Davies and Hager and O'Connell have argued strongly for whole mantle flow. Studies of deep earthquakes support this view. The notion that large plates are effectively coupled to most of the mantle below provides a framework in which a variety of continental tectonic regimes can be explained. The Himalayan collision began about 50 myrs ago and yet convergence continues today at about 4 cm/yr. The total shortening so far is about 2000 km. This persistent convergence requires the continued application of forces greater than the strength of the Asian continental lithosphere. It is difficult to invoke slab pull to explain continued convergence. It seems also that a prerequisite for collision orogenesis is the closure of a major ocean basin. We consider the possibility that the mantle flow system associated with closure of the Tethys ocean persists and that this converging flow drives the Indian and Asian continents into each other. We will present order of magnitude calculations indicating the viability of such a mechanism. If a converging and downwelling mantle flow can crush continents together then an upwelling and diverging flow should be able to rip continental lithosphere apart. A consequence of the assumption of large scale mantle-lithosphere coupling is that the upwelling mantle flow beneath a major ridge system should extend along strike beneath a continent which has overidden the ridge. The Great Basin and the Red Sea lie in such a configuration. The former is a zone of active continental extension. In the latter region a continent has already split apart.

T 187

GLOBAL HEAT FLOW: DEGREE 18 SPHERICAL HARMONIC REPRESENTATION

David S. Chapman (Dept. Geology and Geophysics, Univ. of Utah, Salt Lake City, UT 84112)
Henry N. Pollack (Dept. Geological Sciences, Univ. of Michigan, Ann Arbor, MI 48109)

The global heat flow field is a useful constraint in determining lithospheric thickness and possibly the mode of mantle convection. We have compiled heat flow data published prior to July 1979 and have performed a new spherical harmonic analysis of the global heat flow field. The data set now comprises 7217 observations, 2808 continental and 4409 oceanic, with the principal enhancements in spatial coverage occuring in central Asia, Africa, South America and in the southern oceans. We have averaged the data over 5° x 5° grid elements; those grid elements containing observations now cover 52% of the surface area of the earth. The data set has been supplemented in areas without observations by an updated empirical heat flow predictor based on tectonic setting and age. In addition, heat flow values computed from the relationship $q \propto 1/\sqrt{t}$ were superimposed for grid elements comprising young ocean floor where hydrothermal circulation perturbs observations. The mean heat flow through continents and oceans is 60 and 90 mW m^{-2} respectively. The global mean is 80 mW m^{-2} with the corresponding heat loss from the earth being 4.1×10^{13} W. The degree 18 spherical harmonic representation of the heat flow field depicts low heat flow in individual cratonic units and traces in considerable detail the high heat flow zones of the active oceanic ridge systems.

Volcanology, Geochemistry, and Petrology

Early Crustal Processes I

Metropolitan West
Thursday A.M.
Thomas E. Krogh (Royal Ontario Museum), Presiding

V 1

LUNAR DIFFERENTIATION BY FRACTIONAL CRYSTALLIZATION AND PARTIAL MELTING

N.M. Evensen (Department of Geology, University of Toronto, Toronto, Ontario M5S 1A1, Canada)

Cooling of a lunar magma ocean would lead to extremely efficient fractional crystallization for several reasons, particularly because of the separate crystallization of plagioclase and olivine/pyroxene at the top and bottom respectively of the liquid layer. Fractional crystallization would proceed to formation of an extremely enriched residuum layer at depth, ultimately exhibiting liquid immiscibility (producing 12013-like liquids) as seen in the crystallization of lunar basalts. Zonation in the solidified magma ocean would extend from calcic plagioclase at the top and forsteritic olivine at the bottom to Fe, Si and minor element enriched residuum at about one-third of the total depth. Thus melting temperatures would decrease and heat production would increase monotonically from top and bottom toward the residuum layer. Thermal blanketing by impact ejecta accumulating on the surface would lead to an internal temperature rise concentrated within the radionuclide-rich residuum, resulting first in KREEP formation by subsolidus reaction, then in almost total melting which roughly retraces the original liquid line of descent, culminating in surface volcanism of Fe-Ti-rich basalt (with ca. 4.5 Gy model ages) and exhaustion of internal heat sources. Excavation of Imbrium before remelting ejected KREEP, 12013 and related materials and dissem-inated radiogenic Pb over the surface. Other, shallower mare basins excavated only the plagioclase crust and are probably not an important source of enriched materials.

Hydraulic and tectonic factors control the depth and distribution of mare filling, while lateral movement of melt provides the lateral mass transport required to produce mascons.

V 2

COMPLEXITY OF THE EARLIEST LUNAR DIFFERENTIATION: THE ROLE OF ILMENITE AND PYROXENE

G. Ryder
M. Norman (Lunar Curatorial Lab., Northrop Services, Inc., Box 34416, Houston, TX 77034)

The two pristine igneous rock suites from the lunar highlands, the high Fe/Mg anorthosites and the Mg-suite (norites, troctolites, etc.) are >4.5 b.y. old and appear to be relicts of the earliest crust. KREEP, the incompatible element-rich rock type, has younger igneous ages but was mainly fractionated >4.3 b.y. ago. In igneous processes the ratios of Ti and Sc to refractory incompatible elements e.g. Sm are influenced by ilmenite and pyroxene respectively. The Mg-suite, KREEP, and typical highlands breccias and soils are depleted in Ti/Sm (Figure) and Sc/Sm.

The data imply that A) because none of these rocks are saturated with ilmenite, ilmenite has been removed from materials parental to the Mg-suite and KREEP, but not from the anorthosites. B) the Mg-suite and anorthosites cannot be derived from the same magma; if anorthosites are directly from a magma ocean, the Mg-suite must be an indirect product. C) the crust as sampled must have lost ilmenite and pyroxene which are now buried in the mantle. This in turn suggests large-scale differentiation involving crystal settling. This complex differentiation, for which no terrestrial analog has been recognized, took place >4.5 b.y. ago.

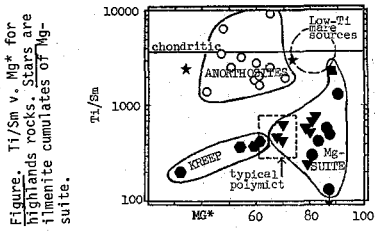

Figure. Ti/Sm v. Mg* for highlands rocks. Stars are ilmenite cumulates of Mg-suite.

V 3

EVOLUTION OF PLATE TECTONICS IN THE LIGHT OF EARLY CRUSTAL STRUCTURE

SHAW, Denis M. (Department of Geology, McMaster University, Hamilton, Ontario, Canada, L8S 4M1

Chemical, thermal and dynamic constraints on the evolution of the primitive Earth necessitated that the first crust was thin, world-wide and submarine. The present-day Earth is dominated by plate tectonic processes resulting from the movements of contrasting thick continental and thin oceanic plates.

A qualitative evolutionary model outlines the transition from the Protoarchean to the present crust, and satisfactorily explains a wide diversity of geochemical, geological and geophysical observations.

V 4

ARCHEAN PLATES AND GREENSTONE BELTS

Alan M. Goodwin (Department of Geology, University of Toronto, Toronto, Canada M5S 1A1)
(Sponsor: D.W. Strangway)

Archean greenstone belts lie in granite-greenstone terrains, contain mafic volcanic rocks and feature low- to medium-grade metamorphic assemblages yet otherwise display great diversity in size, form, lithology, stratigraphy, age, basement-cover relations and structural deformation as illustrated by consideration of four main granite-greenstone terrains respectively in Peninsular India, southern Africa, western Australia and the southern Canadian Shield.

Archean greenstone belt diversity demands equally flexible tectonic development. Consideration of Archean relations and constraints on a global scale leads to a preferred rift-and-sag model involving attenuation and fissuring of pre-existing sialic crust over a time span of at least 1200 Ma with both ensialic and ensimatic accumulation of assorted greenstone assemblages.

Greenstone belt development is attributed to an Archean plate tectonic process that involved limited movement of numerous small plates operating under a high geothermal gradient and thereby lacking conventional subduction (Benioff) zones. Thus the Archean plate tectonic process differed in significant respects from modern plate tectonics, yet produced many similar volcanic and plutonic products. During earth history the plate tectonic process has taken several forms, all involving moving plates, of which the current is but the latest.

V 5

PETROGENESIS OF ARCHEAN ANORTHOSITE COMPLEXES

William C. Phinney (all at NASA Johnson Space
Lewis D. Ashwal Center, Houston, TX 77058)
Donald A. Morrison

All Archean terrains contain a significant proportion of anorthosite-gabbro complexes that are spatially associated with metavolcanic belts and could provide constraints on early crustal evolution. Most Archean anorthosites display a unique texture of coarse (0.5-15 cm diam.) spherical aggregates of plagioclase crystals (An_{75-95}) in a mafic matrix. Many of these complexes contain fractionates of ultramafic units, chromite, and/or Fe-Ti oxides. Possible origins for which petrologic, chemical, and isotopic data may provide discrimination are: (1) melts that are independent of metavolcanics and originate by melting in either (a) the mantle or (b) previously segregated units (perhaps no longer present) near the crust-mantle boundary; or (2) segregations in magma chambers of metavolcanics whose melts originate as in (1). Sparse isotope data for the complexes are quite variable probably due to alteration caused by metamorphism and/or interaction with hydrothermal fluids, but show generally lower ε_{Sr} values than Proterozoic massif-type anorthosites or anorthosite-bearing complexes (i.e. Stillwater) which were intruded into sialic crust. In contrast, Sm-Nd isotope data for the Fiskenaesset and 2.0 b.y. anorthosite inclusions in 1.1 b.y. diabases in Minnesota give Nd initial ratios close to the CHUR evolution line. We are further testing this observation. Trace element data for these complexes are sparse and not yet determined on spatially associated metavolcanics. Small negative Eu anomalies occur in some but not all greenstones, but their origin is unclear. Because of significant departures of Sc/Sm from chondritic values in some complexes but not in others, the role of prior pyroxene separation is unclear. We are conducting further work in the complexes and associated volcanics to determine if the complexes indicate a specific tectonic setting or process that bears on the origin of greenstone belts.

V 6

Rb-Sr AGE AND ISOTOPE STUDY OF TWO PRECAMBRIAN SHEAR BELTS, WEST GREENLAND

M.H. Hickman (Geology Dept., Miami University, Oxford, Ohio 45056)
(Sponsor: N.K. Grant)

Between the Arctic Circle and Disko Bay in West Greenland, the ancient, deeply eroded fault zones of Ikertôq and Nordre Strømfjord now appear as long narrow belts of intense ductile shear in gneisses of granulite and amphibolite facies, with exposed lengths of up to 150 km and widths of up to 40 km. This study establishes the timing of events in this crustal segment and examines the effects of shearing deformation on the Rb-Sr isotope system.

The terrain formed by about 2.8-2.9 b.y. ago. Two separate periods of shear belt formation occurred, at about 2.6 b.y. and about 1.7 b.y. The latter event was accompanied by metamorphism especially intense in the northern half of the region, and was followed by rapid cooling.

Whole rock Rb-Sr isotope systematics in the shear belt gneisses were not reset or even substantially disturbed during deformation, except where accompanied by chemical changes, e.g., the addition of Rb.

V 7

THE GENESIS OF THE LOWER CRUST, THE GRANULITE FACIES METAMORPHISM AND THE PROCESS OF INTERNAL DIFFERENTIATION OF THE CONTINENTAL CRUST (INDICOC) STUDIED BY THE ^{147}Sm-^{143}Nd METHOD.

D. BEN OTHMAN , C.J. ALLEGRE (Laboratoire de Géochimie et Cosmochimie, 4, Place Jussieu, 75230 PARIS CEDEX 05 - FRANCE)

Since Heier's studies, it is known that the upper crust is enriched in incompatible elements as compared to the lower crust. Heat flow studies have shown that this is quite general in different geological provinces throughout the world. The problem is to know how and when this differentiation process did took place relative to the orogenic processes. Since the lower crust is probably made by granulite facies metamorphism, the genesis of this facies has some bearing on the (INDICOC) process. This problem can be approached by the Sm-Nd method because this system is insensitive to the (INDICOC) (Carter et al.) Thus the early differentiation of the crust can be dated by total rocks and the garnet metamorphism by garnet pyroxen-feldspar analysis.

We have studied granulites from Greenland (3.8 b.y.) Ahhagar (3.3 b.y.), Venezuela (2.9 b.y.), India (2.6 b.y.), Tanzania (2.7 b.y.), Le Bournac (1.1. b.y.). We have also dated a very young granulite (French Pyrenées). A general feature of our data is that the Nd initial ratios correspond to the chondritic values in the Archean whereas they tend to scatter in the recent times. This result is similar to what we have obtained for the granitoïds (upper crust). The granulite facies metamorphism is much younger than the primitive age in all cases. This indicates that this metamorphism occur in recycled continental materials and not in juvenile ones. Our results also constrain the processes of continental growth insofar as these rocks represent the lower crust.

V 8

C-O-H FLUID SPECIES AND ABUNDANCES IN DEEP CRUSTAL ENVIRONMENTS

William Glassley (Dept. of Geology, Middlebury College, Middlebury, VT 05753)
John K. Winter (same)

The Isortoq Complex of Central West Greenland contains upper amphibolite and granulite facies rocks, some of which satisfy either or both of the equilibria (A) $C + O2 = CO2$ and (B) Annite = Kspar + Magnetite + H2. Detailed studies of individual samples demonstrate that (1) $fH2O/fCO2$ and $fH2/fCO$ ratios will be >1.0 for assemblages which satisfy (A) and will be <1.0 for assemblages which satisfy (B), (2) both assemblages will have log $fCH4$ >3.8, (3) fugacity values for individual fluid species may vary by several orders of magnitude over distances of <10 cm, and may correlate with compositional banding in gneisses.

Likely evolutionary schemes for fluid species imply that graphite will precipitate only at very high grades from the fluid during prograde metamorphism. At that point a major recrystallization should be recorded as the fluid and solid phases reequilibrate with graphite. Many deep crustal metamorphic events may reflect only this reequilibration. The sensitivity of the fluid composition to fH2 implies that major recrystallization may also occur if fH2 is modified (by mantle degassing?).

V 9

TIMES OF CRATONIZATION AND ISOTOPIC REJUVENATION IN SUPERIOR PROVINCE OF MANITOBA

Ingo Ermanovics (Geological Survey of Canada, Ottawa K1A 0E4)
R.K. Wanless (Ottawa K1A 0E8)
(Sponsor: Gil Hanson)

Isotopic ages determined from U-Pb zircon, Rb/Sr whole rock isochron, and K/Ar mineral data from Superior Province in Manitoba are tabulated and interpreted in relation to their distribution in subprovinces. Early, pre 2900 Ma, volcano-plutonic activity is suggested by meagre evidence in most subprovinces.

Reference ages of crystallization or high-temperature isotopic homogenization of felsic plutonic rocks are established from U-Pb zircon and some Rb/Sr whole rock isochron ages for each subprovince. Times of cooling below argon-loss blocking temperatures are obtained from K/Ar biotite ages. Time difference between primary and cooling age is taken as the duration of post-orogenic uplift and appears to be about 250 to 300 Ma for all subprovinces. Earliest retention of radiogenic Sr occurred in Pikwitonei subprovince around 2900 Ma ago and at progressively later times in southern subprovinces. Argon retention in hornblendes exhibits a similar trend from central Sachigo subprovince southward. If Sr and the companion Ar-retention trends reflect stages in uplift then these data indicate a direction of cratonization that in Superior Province progressed from north to south.

The effects of Hudsonian orogeny extend 300 km into Superior Province to the Sachigo-Berens boundary and are recorded by Archean rocks whose rejuvenated K/Ar ages in Sachigo and Pikwitonei become progressively younger toward the Churchill orogen.

V 10

RARE EARTH AND OTHER TRACE ELEMENTS IN ARCHEAN GNEISSES, EASTERN BEARTOOTH MOUNTAINS, MONTANA-WYOMING

Schulz, K.J., Dept. of Earth & Planetary Sci., Washington University, St. Louis, MO 63130
Wooden, J.L. and Budahan, J.R., Lockheed Electronics Co., Inc., NASA-Johnson Space Center, Houston, TX 77058

Major, identified igneous and meta-igneous units of the eastern Beartooth Mtns. fall into two age groups: 3.3-3.7 AE and 2.7-3.1 AE. The older group consists of tonalitic gneisses, granitic gneisses, and migmatites. The tonalitic gneisses have strongly fractionated patterns (Ce_N/Yb_N=88-17), variable REE contents (La_N=350-35) and Eu anomalies (Eu/Eu^*=3.5-0.5), and patterns similar to those of the Archean gneisses of the Minn. River Valley (Hanson, unpub.). The granitic gneisses also show strongly fractionated patterns (Ce_N/Yb_N=45-37) but have flat HREE patterns (Tb_N/Lu_N=1.5) at ~2X chondrites. The migmatites are high K, high Rb/Sr rocks with relatively flat REE patterns (Ce_N/Yb_N=6-2) and large negative Eu anomlies (Eu/Eu^*=0.4-0.7). The migmatites have major and trace element compositions very similar to the late Archean Marda calc-alkaline volcanics of Australia (Taylor and Hallberg, 1978) and modern arc volcanics of Japan.

The younger age group is composed of three compositional types generally corresponding to granites, granodiorites, and diorites. The granites have major and trace element compositions very similar to the older granitic gneisses which suggests they share a similar mechanism of genesis. The granodiorites have extremely high total REE (La_N=650-250, Yb_N=30-5) and negative Eu anomalies (Eu/Eu^*=0.5-0.6), but are not depleted in Sr. The gneissic diorites are similar to modern andesites but with higher REE contents (La_N=400-200) and steeper patterns (Ce_N/Yb_N=20-12). These data suggest variable source compositions and/or melting schemes were important in the generation of Archean crustal segments.

V 11

IGNEOUS EVOLUTION OF AN ARCHEAN PEGMATITE DISTRICT IN SOUTHEASTERN MANITOBA

P. Černý (Dept. Earth Sciences, Univ. of Manitoba, Winnipeg, Man. R3T 2N2)
(Sponsor: D.H. Hall)

Extensive pegmatite fields, including some of the largest and most fractionated granitic pegmatites in existence, are characteristic of the Archean but little is known about the processes leading to their formation. In the 2.75-2.55 Ga Winnipeg River pegmatite district (Bird River greenstone belt of the English

River subprovince, western Superior province in S.E. Manitoba), three independent series of intermediate to acid igneous rocks, overlapping in time and space, are distinguished by their bulk, trace element, REE and oxygen isotopic compositions: (1) Dacite flows in the greenstone sequence and diapiric tonalite-trondhjemite batholiths originated by partial melting of lower crust or upper mantle, separating from hornblende-rich residua; (2) homogeneous plutons of late-tectonic biotite granites also represent partial melts, derived probably from lower crust, leaving residual hornblende + plagioclase; (3) rhyolites from lower parts of the greenstone sequence, late-tectonic leucogranites, and post-tectonic pegmatitic granites probably differentiated from a long-lived, juvenile, acid igneous source by predominant plagioclase fractionation; hybridization with sialic crust affected some of the pegmatitic granites. It is the intrusive members of this third series which generated aureoles of highly fractionated pegmatites, correlatable by spatial association, accessory mineral assemblages, and continued fractionation trends. Structural control and igneous association of several other pegmatite districts in the western Superior province suggest a similar origin for them.

V 12

TEMPORAL AND GEOCHEMICAL EVOLUTION OF LATE ARCHEAN GRANITOIDS, EASTERN ABITIBI BELT

GARIEPY, C., LUDDEN, J.N., BROOKS, C. (Dépt. de géologie, Université de Montréal, Montréal, Canada H3C 3J7)

VAN SCHMUS, R. (Dept. of Geology, University of Kansas, Lawrence KS 66044)

Late Archean intrusives of the Chibougamau area comprise a pre- or syn-tectonic (deformed) diorite-tonalite suite (Group I) and a post-tectonic (undeformed) granodiorite suite (Group II). Zircon ages suggest a close temporal relationship for the two suites; this significantly affects the interpretations of the petrogenetic and structural evolution of the metavolcanic belt.

Eight discrete bodies have been analysed for REE and trace elements compositions. The results indicate a two-fold classification into low-K (< 2%) and high-K (> 2%) groups confirming the field classification. Both groups show enrichment in light REE, but the most felsic rocks in each group display extreme depletion in heavy REE. From these data, Group I compositions can be modelled by fractionation of amphibole and plagioclase from a basic magma and may be compared to Phanerozoic calc-alkalic suites. In contrast, Group II plutons show marked enrichment in K, Rb, Sr, Ba but similar K/Rb, Rb/Sr and $(^{87}Sr/^{86}Sr)_0$ and higher P, Cr and Mg/Fe. We suggest that both suites were formed in a volcanic arc environment but that Group II rocks are not related to those of Group I and were derived from a different source region. The 2716±3 (1σ) age from the Opemisca Pluton (Group II) redefines a minimum age for the end of Kenoran deformation in the area.

V 13

THE INFLUENCE OF REDUCED GASES ON PREBIOTIC O_2 PRODUCTION

Tim B. Vander Wood (Dept. of the Geophysical Sciences, The University of Chicago, Chicago, IL 60637)
Mark H. Thiemens

The presence of a reduced early atmosphere for the earth is indicated by (1) gas release patterns of carbonaceous chondrites, (2) the inability of photoproduction of oxygen to account for the oxidized materials at the earth's surface, and (3) the magnitude of present exhalations of reduced gases, which dominate photodissociation rates of H_2O.

In the earth's prebiotic, O_2-free atmosphere the HO_X kinetic reaction network is strongly influenced by the presence of reduced gases at trace mixing ratios, particularly the sulfur species. The kinetically competitive HO_X-reduced gas reactions may retard the production of O_2 from primary and secondary H_2O photodissociation products.

The trace species reactions would have influenced the escape flux of H and any model for the photoproduction of O_2 should consider these reactions.

Early Crustal Processes II

Metropolitan West

Friday A.M.

W. M. Schwerdtner (Univ. of Toronto), Presiding

V 14

ORIGINAL LATERAL EXTENT OF AN ARCHEAN GREENSTONE ASSEMBLAGE, SUPERIOR PROVINCE, NORTHWESTERN ONTARIO

W.M. Schwerdtner (Department of Geology, University of Toronto, Toronto, Ontario Canada M5S 1A1)
(Sponsor: D.W. Strangway)

Archean greenstone belts are generally surrounded by a sea of gneissic tonalite-granodiorite which includes many supracrustal enclaves. These enclaves may be (1) part of extensive volcanic-sedimentary assemblages that are mainly preserved in the greenstone belts, or (2) ancient supracrustal relics within sialic basement to the greenstone. The original lateral extent of dense supracrustal assemblages may be established by the presence of diapiric domes in the gneissic tonalite-granodiorite which are ringed by supracrustal enclaves. Such diapirs may be identified by means of characteristic internal strain patterns. Owing to a systematic superposition of gneiss diapirs of different orders, these strain patterns can be very complex. The incipient low-order diapirs were linear ridges or elongate antiforms that had an axial-planar strain fabric. Superimposed on this initial fabric is a horizontal flattening strain within the crestal region of high-order domes. This large strain increment resulted in prolate horizontal fabrics of total strain parallel to the axis of low-order structures. The state of superimposed finite strain has been studied in several higher-order domes within the western Wabigoon Subprovince. The magnitudes and directions of total and incremental strain are in good agreement with qualitative diapiric models but are difficult to reconcile with cross folding and crustal shortening. This suggests that the Wabigoon supracrustals were once a continuous assemblage with horizontal dimensions of 800 km by 100 km.

V 15

STRUCTURAL EVOLUTION OF ARCHEAN GREENSTONE BELTS REVEALED IN CENTRIFUGED MODELS

J.M. Dixon (both at: Dept. of Geol. Sci., Queen's Univ., Kingston, Ont. K7L 3N6)
J.M. Summers

Experimental scale models of the Archean crust, constructed of silicone putty, have been subjected to accelerations of 2000g in a centrifuge. The hypothesis that greenstone belts were formed by gravity can be evaluated by comparison of strain patterns in the models with those of natural structures. The models consist of two horizontal isotropic layers, the ratio of density of heavy overburden to light substrate of 1.05-1.07:1 chosen to simulate that of basic volcanics overlying sialic basement. Models have been constructed a) with a planar interface between layers, so that sites of diapiric rise and subsidence have developed naturally, and b) with local thickening of the surface layer along a cylindrical trough in the interface, to localize the subsidence. Patterns of incremental and finite strain are revealed by a passive grid printed on the free surface and by passive internal layers. Structures produced in models are similar, in both geometry and variation of the magnitude and orientation of strains, to natural greenstone belts described in the literature. The model greenstone belts evolve into inverted mushroom forms. Analysis of the upper free surface of individual models indicates that material in the dense surface layer migrates towards the regions overlying zones of subsidence. These regions undergo intense strain with local horizontal shortening >95% and vertical extension >1500%. Subsidence of a natural greenstone belt could generate thrust and nappe structures due to the initial horizontal shortening in the higher levels of the supracrustal sequence. Surface strain data also reveal locally complex histories of progressive deformation. In regions adjacent to zones of subsidence, total inversion of principal strain axes can occur during evolution of the structure.

V 16

ARCHEAN TECTONICS, SLAVE PROVINCE

W.K. Fyson (Dept. of Geology, University of Ottawa, Ottawa, Canada, K1N 6N5
(Sponsor: A.J. Baer)

Linear edges of block-like granitoid complexes in the Slave Province, and structures in intervening sedimentary and volcanic belts reflect an extensive fracture system in the Archean crust and its control on subsequent regional deformations. Granite margins form NNW and NE sets bisected by a NNE subset. Volcanic belts preferentially follow the NNW and NNE sets. The lineaments are consistent with a system of conjugate Riedel shear planes and tension fractures that opened during NNE compression within an ENE sinistral shear zone (followed in the Proterozoic by the McDonald fault). Resultant fault troughs were sites of volcanism and sedimentation.

Isoclinal folds trending parallel to NE margins suggest a change to compression across the shear zones. Later generations of folds and cleavages strike dominantly NW to N, both parallel and discordant to granite margins. The structures fan about axes that follow these margins and are gently inclined near syntectonic plutons. Folds in belts in the southern part of the Province are overturned preferentially westward.

The late structures may indicate successive regional compressions directed NE or E along or oblique to the shear zone, with deflections near granite massifs and rising diapirs. Westward tilting of crustal blocks and an element of gravity slide could account for the westerly vergence.

V 17

KOMATIITE PETROGENESIS AND MELT SEGREGATION

D. Walker (Hoffman Lab, Harvard Univ., Cambridge MA 02138)
E.M. Stolper (Cal Tech, Pasadena, CA 91125)
J.F. Hays (Harvard Univ., Cambridge, MA 02138)

Although the geochemistry of komatiites suggests they are derived by abnormally large degrees of fusion, Arndt (1977) has pointed out that it may be difficult to equilibrate a large fraction of melt with source peridotite because melt may drain almost as rapidly as it is generated. Rather, komatiite may represent late increments in a melting sequence preceded by tholeiite. However, komatiite often is reported to be the early effusion in Archaean terranes (Viljoen & Viljoen, 1969) followed by tholeiite. This stratigraphy may be understood if early-rising diapirs avoid segregating melt until large fractions are stored internally; whereas late-rising diapirs leak at smaller degrees of fusion. An analysis of the conditions for melt segregation suggests that the size of the diapir exerts an important control on the fraction of melt which can be stored before segregation occurs. Large melt fractions can remain stored without segregating if the partially molten reservoir in a diapir is small (∿km sized). Stiffness of the crystalline matrix retards flushing of small plumbing systems. Larger diapirs (∿ 10's of km sized) segregate small melt fractions readily. An alternate model of komatiite petrogenesis is based on a slightly hotter (∿100°C) and less viscous (∿× 10) Archaean mantle. The buoyancy required to overcome viscous drag and initiate diapir ascent is achieved by smaller blobs (∿×3) than under present conditions. These small, early, continent blobs eventually segregate to deliver komatiite. However, if the perturbation making diapirs is of sufficient magnitude and duration, larger, leaky blobs follow. These discharge tholeiite rather than komatiite because they drain at smaller degrees of melting. Hence the stratigraphic sequence tholeiite over komatiite.

V 18

"FINE TUNING" THE PETROGENESIS OF KOMATIITE WITH Ti, Zr, and Sc DATA.

LUDDEN, John N. (Département de géologie, Université de Montréal, Montréal, P.Q. Canada H3C 3J7)
GELINAS, Léopold. (Département de génie minéral Ecole Polytechnique, Montréal, P.Q. Canada H3C 3A7)

A systematic study of major and trace element abundances in altered komatiitic to high-MgO basaltic lavas from the LaMotte and Destor townships of the Abitibi metavolcanic belt, Quebec, has shown Ti, Zr, Sc, Y, heavy REE and Al_2O_3 to be the elements least susceptible to alteration processes. In particular Ti, Zr, and Sc data are valauable in "fine tuning" the petrogenetic processes involved in generation of komatiite.

Ti/Zr values are distributed around a chondritic value (Ti/Zr: 105) for both komatiitic lavas (MgO >18Wt%) and high MgO basalt lavas (MgO 18-12Wt%). Minor regional variations, and possibly between flow variations in Ti/Zr are interpreted as reflecting trace element heterogeneity of the mantle source. In contrast, the Ti/Sc ratios are chondritic (Ti/Sc:80) for the komatiitic compositions but show a systematic increase through to high-MgO basalt compositions (Ti/Sc: 115). The extremely regular increase in Ti/Sc value can be modelled in terms of increasing clinopyroxene in the residual source material and/or clinopyroxene fractionation from komatiitic to high MgO basalt compositions. Ti/Sc values for the Onverwacht komatiitic lavas, S. Africa, mirror those of the Abitibi lavas; we thus dispute the contention of Sun and Nesbitt (Contrib. Mineral. Petrol. 65, 301-325, 1977) that garnet played a significant role in komatiite generation. Evidence for garnet fractionation, such as high CaO/Al_2O_3 ratios must therefore be explained in terms of secondary alteration processes or control of the liquid composition by a phase rich in Al_2O_3 and poor in CaO such as Al-opx.

V 19 INVITED PAPER

PYROXENE SPINIFEX TEXTURE, OLIVINE PORPHYRITIC LAVAS, AND THE EVOLUTION OF KOMATIITIC MAGMAS

N.T. Arndt (Dept. of Geological Sciences, Univ. of Saskatchewan, Saskatoon S7N 0W0)
R.W. Nesbitt (Dept. of Geology, University of Adelaide, Adelaide, S.A. 5000)
(Sponsor: Z. Hajnal)

Two types of magnesian basalt are associated with Archean komatiites (ultramafic lavas). The first contains needles with cores of unusually magnesian pigeonite (Wo 7.7 En 78.1 Fs 14.2) and mantles of augite. These needles form complex skeletal grains in the spinifex-textured upper parts of flows, or are randomly oriented in flow centres. This basalt type has chondritic Ti, Zr, Y, Nb ratios and depleted LREE -- features they share with nearby ultramafic lavas. The second type of magnesian basalt, which encompasses a composition range similar to that of the first (12 to 18% MgO), is olivine porphyritic and contains only interstitial pyroxene. This type is relatively enriched in Ti, Zr, Y and Nb and has flat REE patterns.

Experimental studies reveal that under equilibrium conditions the first mineral to crystallize in pyroxene spinifex-textured samples is olivine, and that pyroxene appears only at temperatures well below the liquidus. By contrast, in spinifex-textured lava, it appears from petrographic evidence that pyroxene crystallized first. This discrepancy, as well as the unusual compositions and habits of the pyroxenes, suggest that they grew metastably under conditions of high supercooling.

Appropriate conditions for metastable pyroxene growth may have been achieved during the rapid cooling and fractional crystallization of parental ultramafic liquids. Pyroxene spinifex texture therefore may characterize evolved liquids derived by fractional crystallization of ultramafic parental magma. Olivine porphyritic lavas, on the other hand, have equilibrium mineralogies and could represent primary magmas. The contrasting trace element ratios indicate different mantle sources for the two basalt types.

V 20

ARCHAEAN SEDIMENTARY TALC: EVIDENCE FOR AN ANCIENT GREENHOUSE?

U. R. Costa (University of Western Ontario, London, Ontario, N6A 5B7)
W. S. Fyfe, H. W. Nesbitt, and R. Kerrich

Bedded sedimentary talc is abundant in Archaean greenstone belts in proximity to the hydrothermal discharge vents of seafloor metal deposits. Typical examples include Mattagami and Mattabi Mines, Abitibi greenstone belts (~2.6 Ga). The low abundances of relatively immobile elements (Al, Y, Ti, Zr, Nb) in talcose rocks is not compatible with their derivation from mafic precursors, but supports an origin as direct precipitates from hydrothermal discharge. This is corroborated by oxygen isotope evidence from footwall rocks ($\delta^{18}O$ quartz = 8‰, δ^{18} chlorite = 0‰) for streaming of hot ocean water (~0‰) through the vent. From increased activity of silica or the Mg^{2+}/H^+ ratio in hydrothermal discharge, precipitation of talc or sepiolite is promoted; these reactions result in the liberation of CO_2 which will eventually transfer to the atmosphere. Given hydrothermal discharge of 6×10^{17} g a^{-1} in the Archaean (5x present), such a flux would move 6×10^{14} g silica a^{-1} to the oceans, forming talc at 1 $km^3 a^{-1}$, and CO_2 emission at 10^{15} g a^{-1}-comparable to that from present human activity. The high CO_2 flux from this process may have maintained a greenhouse effect during the Archaean, accounting for inferred warm oceans, reflected in low $\delta^{18}O$ chert and the palaeontological record.

V 21

EARLY CRUSTAL HYDROTHERMAL PROCESSES AND THE $^{18}O/^{16}O$ EVOLUTION OF SEAWATER: EVIDENCE FROM THE AMULET MINE, NORANDA, QUEBEC

D.W. Beaty (both at Div. of Geological Sciences, H.P. Taylor, Jr. Caltech, Pasadena, CA 91125)

The Amulet "A" mine is a volcanogenic massive sulfide deposit 2.85 b.y. old, associated with a concentrically-zoned chimney of intense alteration (0.2 km diameter by > 1.0 km deep), which was the conduit for the Cu ore-bearing solutions. The inner zone is a distinctive, spotted rock (dalmatianite) surrounded by a zone of biotite alteration associated with grid fracturing, all developed in submarine andesite and rhyolite flows. The dalmatianite consists of chlorite (55%) and quartz (45%) pseudomorphs after groundmass and feldspar, which are in turn partially (10-20%) replaced by cordierite and anthophyllite associated with later emplacement of a nearby granodiorite. Whole rock $\delta^{18}O$ values steadily decrease inward from about +6 in the country rocks to +3.6 in the inner zone. This inward depletion in ^{18}O is related to the hydrothermal ore-forming event, and was not affected by the contact metamorphic dehydration reactions. Assuming a plausible average alteration temperature of 250-350°C, the calculated $\delta^{18}O$ of the ore fluid is +0.5 ± 1.0. This fluid is inferred to have been heated, circulating seawater by analogy with the isotopically and mineralogically similar Phanerozoic massive sulfide deposits such as those on Cyprus (pipe-shaped alteration zone, qtz-chl alteration assemblage, ~5 × 10^6 tons of ore, Cu dominant over Zn) although differences exist (no rhyolitic volcanism at Cyprus). Therefore, seawater has apparently remained almost constant at $\delta^{18}O \approx 0$ during geologic time at least as far back as 2.9 b.y. In view of the many differences between the geologic records of the Archean and the Phanerozoic, this constancy is very important. In particular, because MOR hydrothermal activity is responsible for buffering $\delta^{18}O$ of the ocean at ≈ 0 today, the constancy of $\delta^{18}O$ of seawater with time suggests that some form of sea-floor spreading tectonics was also active during the Archean.

V 22

METALLOGENESIS RELATED TO SEAWATER INTERACTION WITH 3.5 B.Y. OCEANIC CRUST

M. deWit (B.P.I.G., University of Witwatersrand, Johannesburg, South Africa)
R. Hart (School of Oceanography, Oregon State University, Corvallis, OR 97331)
C. Stern (Dept. of Geological Sciences, University of Colorado, Boulder, CO 80309)
C.M. Barton (Geological Survey and Mines Department, P.O. Box 9, Mbabane, Swaziland)
(Sponsor: K.F. Scheidegger)

Recent investigations of the Onverwacht Group of the Barberton greenstone belt suggest it may be similar to Phanerozoic ophiolites. An approximately 1 km thick vertical sheeted dike complex feeds about 2 km of flanking pillow lavas and sills which are overlain by about 5 km of sediments typical of spreading ridge metamorphism and mineralization. The sheeted dikes are extensively serpentinized with tremolite and chlorite increasing upwards in the section. The pillow lavas are entirely altered to either albite-actinolite-epidote or chlorite-carbonate with minor quartz. The steep geothermal gradient, preservation of igneous textures, and extensive hydration present in the Onverwacht Group are best explained by metamorphism associated with hydrothermal circulation at spreading ridges.

The H_2O content of the lower units of the Onverwacht varies from 1.5 to 13%. SiO_2, CaO, FeO, Al_2O_3, NaO, and K_2O are negatively and MgO positively correlated with the hydration trend. This suggests extensive mobilization of these elements by circulation of seawater in the Archaean oceanic crust. It is proposed that mobilization of elements in the lower Onverwacht has resulted in the deposition of banded ironstones, barites, manganese, base metals, carbonates, and cherts at the crust-seawater interface now represented by the upper sections of the Onverwacht Group. This inference is supported by magnetite, quartz, and carbonate dikes and stockwork cutting the sheeted dike complex and apparently feeding the overlying mineralized zones.

V 23

HAS A LIGHT RARE EARTH ENRICHED SOURCE EXISTED FOR MAFIC MAGMAS IN THE BEARTOOTH MOUNTAINS SINCE THE LATE ARCHEAN?

J.L. Wooden (LEMSCO Inc., NASA-Johnson Space Center, Houston, Texas 77058)
K. Schulz (Dept. of Earth and Planet. Sci., Washington Univ., St. Louis, MO 63130)
P.A. Mueller (Dept. of Geology, Univ. of Florida, Gainesville, Fla. 32611)

The Beartooth Mountains in Montana and Wyoming contain Precambrian mafic rocks that range in age from about 3.3 AE (1AE = 10^9 yrs.) to 0.7 AE. The oldest mafic rocks have been metamorphosed, are basaltic and andesitic in composition, and most of them are interpreted to be part of supracrustal assemblages. The mafic rocks younger than 2.8 AE are all intrusive and include the Stillwater igneous complex. DePaolo and Wasserburg (1979) reported an ϵ_{Nd} (for 2.7 AE) = -2.8 for the Stillwater complex that suggested either a light rare earth (LRE) enriched source for Stillwater magma(s) or contamination of the magma(s) with older crustal material. Examination of rare earth element (REE) patterns for a representative group of Beartooth mafic rocks show that many are LRE enriched [$(La/Sm)_N$ = 1.7-2.2]. Some of these mafic rocks are obviously fractionated, but fractionation alone cannot account for the observed enrichments in the LRE. The present conclusion is that many of the parental mafic magmas were LRE enriched. These parental mafic magmas require either a LRE enriched source or a process(es) such as crustal contamination or alkali metasomatism to increase their LRE contents. While crustal contamination cannot be ruled out, the early and persistent appearance of LRE enriched mafic rocks argues that the existence of a LRE rich source is possible or that the melting process was repeatedly associated with an addition of LRE to the source region as suggested for some modern volcanic rocks.

V 24

THE PIKWITONEI GRANULITE DOMAIN: EDGE OF THE SUPERIOR PROVINCE CRATON

W. Weber (Manitoba Mineral Resources, Winnipeg, Manitoba R3H 0W4)
(Sponsor: D. H. Hall)

Recent geological fieldwork and geochronological data give evidence that the granulite facies metamorphism in the Pikwitonei granulite domain is contemporaneous with lower grade metamorphism in the adjacent Superior Province, and that the Pikwitonei granulite domain is not an older basement to the Superior Province greenstones as previously suggested. The contact between the granulites and the lower grade

rocks is an opx isograd and not an unconformity. Greenstone belts cross this isograd.

Geological and geophysical data are consistent with the interpretation that the Pikwitonei granulite domain represents a lower portion of the Superior Province crust which was thrust over the younger Churchill Province during late Aphebian continental collision.

V 25

LOWER PROTEROZOIC CRATONIZATION IN THE NW CHURCHILL PROVINCE

C. Banks
H. Baadsgaard
R. St J. Lambert (all at: Department of Geology, University of Alberta, Edmonton, Alberta, Canada T6G 2E3)

An area of 8000 km² centred on 109°W 60.25°N in the NW Churchill Province has been studied by K-Ar. Baadsgaard and Koster (unpubl) have shown the existence of 2620±90 gneisses near Tazin Lake (109°W 59.8°N): we show that these Archean rocks extend as far as 60.7°N. The area consists mostly of granitoid orthogneisses (upper amphibolite facies) with local evidence of retrogression from granulite facies. Early foliations tend to strike N-S; later foliations strike NE, pre-dating NE-striking mylonite belts and shear zones. 57 apparent ages were obtained on tschermakitic hornblende, biotite and one muscovite. The hornblende ages have peak frequency at 2400 Ma (range 2060 to 2620); biotite ages peak at 2200 Ma (range 1730 to 2370). The biotite ages define isotemporal lines up to 2300 Ma with a NNE trend. The 2200 Ma contour describes an area >2800 km², apparent ages falling off sharply to SE and NW, irrespective of geological boundaries. However, rocks containing the oldest mineral ages tend to strike NS. Apparent ages of hornblendes correlate inversely with Fe/(Fe+Mg) as described from other areas. All hornblendes having an age >2430 Ma (the average age) have Fe/(Fe+Mg)<0.65. The hornblendes appear to record a cooling event, reaching c. 500°C by 2450 Ma or so. The biotites reached their closure temperature (?150°C) at 2200 Ma or less, defining a structurally controlled stable block trending NE. The central region was uplifted (slowly?) over 400 Ma, perhaps with a thermal event (based on Tazin Lake intrusions) at 2300 Ma. The average uplift rate can be estimated as 1 km in 20 to 25 Ma. The surrounding regions continued to be reworked until 1800 Ma.

V 26

EARLY HISTORY OF THE PROTEROZOIC NAMAQUA MOBILE BELT, SOUTHERN AFRICA, AS DEDUCED FROM SR, PB AND ND ISOTOPES

D. L. Reid (Department of Geochemistry, University of Cape Town, South Africa)

(Sponsor: Stanley R. Hart)

A study of Sr, Pb and Nd isotopes has helped to establish the nature and timing of important Precambrian crust-mantle differentiation events that led to the formation of the Southern African continent. Data obtained from Proterozoic greenstones, calc-alkaline granitoids, anorthosite-norite complexes, augen gneisses and deep crustal eclogites indicate original separation from the upper mantle during island arc and continental margin type magmatism 2.0-1.9 Ga ago. Crustal recycling occurred during a number of subsequent events, especially 1.7 Ga and 1.2-1.0 Ga ago.

The Namaqua mobile belt probably represents Proterozoic accretion around an Archean continental nuclei, now contained within the Kaapvaal craton, and contrasts sharply with the Limpopo belt, which represents Proterozoic recycling of pre-existing rocks.

Early Crustal Processes III

Metropolitan West
Friday P.M.
A. Hines (McGill Univ.), Presiding

V 27 INVITED PAPER

INTERPRETATION OF STRONTIUM AND OXYGEN ISOTOPE DATA FROM THE LOON LAKE PLUTON AND THE APSLEY GNEISS, GRENVILLE PROVINCE, ONTARIO.

L.M. Heaman (Dept. of Geology, McMaster University, Hamilton, Ontario, L8S 4M1)
Y.N. Shieh (Dept. of Geosciences, Purdue Univ., W. Lafayette, Indiana, 47907)
R.H. McNutt and D.M. Shaw (Dept. of Geology, McMaster Univ., Hamilton, Ontario, L8S 4M1

The banded Apsley biotite gneiss is a sequence of volcanic and sedimentary rocks subjected to amphibolite grade regional metamorphism. Thick (0.5-5.0 meter), homogeneous, quartz-oligoclase-biotite bands define a Rb-Sr whole rock isochron age (t) of 1461 ± 48 Ma (λ_{Rb} = 1.42 x 10^{-11} $yr.^{-1}$) with an initial Sr ratio (R_i) of 0.7012 ± 0.0016 (all errors quoted as 2σ). Thin (1-6 cm.) biotite rich bands show open system behaviour as a result of Grenville metamorphism.

The discordant Loon Lake pluton (t= 1059 ± 12 Ma; R_i = 0.7035 ± 0.0002) intrudes the Apsley gneiss and consists of a monzonite core surrounded by a quartz monzonite rim. This pluton is enriched in $\delta^{18}O$ whole rock (8.8-12.0 ‰) and, combined with the relatively low R_i, does not conform to the isotopic pattern for either S or I-type granitoids. The high $\delta^{18}O$ values for the Apsley gneiss (8.3-15.6 ‰ ; Shieh et al., 1976) and its low R_i suggest that partial melting of crustal lithology, similar in isotopic composition to the felsic bands of Apsley gneiss, could generate the observed strontium and oxygen isotopic compositions of the Loon Lake pluton. This model, however, requires that quartz and feldspar are the major phases contributing to melt formation and that biotite is strongly enriched in the residue.

Shieh, Y.N., Schwarcz, H.P., and Shaw, D.M., (1976) Contributions to Mineralogy and Petrology, v. 54, p. 1-16.

V 28 INVITED PAPER

THE SHABOGAMO INTRUSIVE SUITE, LABRADOR: Nd AND Sr ISOTOPIC EVIDENCE FOR CONTAMINATED MAFIC MAGMAS IN THE PROTEROZOIC

A. Zindler (L.D.G.O. of Columbia U., Palisades, NY)
S.R. Hart (M.I.T., Cambridge, MA 02139)
C. Brooks (Univ. of Montreal, Montreal, Canada)

The Shabogamo Intrusive Suite comprises numerous bodies of variably metamorphosed gabbro which intrude Archean and Proterozoic sequences at the junction of the Superior, Churchill, and Grenville structural provinces in western Labrador. Combined Nd-Sm and Rb-Sr systematics for four bodies, ranging from unmetamorphosed to highly metamorphosed, document a crystallization age of 1375±50 m.y., and are consistent with all four bodies having crystallized from magmas with similar Nd and Sr isotopic compositions.

Rb-Sr systematics are shown to be less reliable in unmetamorphosed and lightly metamorphosed rocks containing relatively large percentages of sheet silicates (reflected by high Rb/Sr ratios). Disturbance of the Rb-Sr system in these rocks may be due to either precipitation of sheet silicates from late-stage magmatic fluids which have interacted with the country rock or subsequent "leaching" of Rb from the sheet silicates. Sm-Nd sytematics in the same rocks are not disturbed. In rocks from the highly metamorphosed bodies, Rb-Sr systematics are severely disturbed or completely reset, while Sm and Nd remain essentially unaffected.

Initial ratios for 143/144Nd & 87/86Sr are lower and higher respectively than bulk earth values at 1375 m.y. Both these displacements are in the direction of older crustal material at 1375 m.y., and a model is proposed whereby the Shabogamo magma is produced by mixing of a mantle-derived magma with a partial melt of crustal rocks (approximately 10:1 by volume). We consider that young volcanic rocks with anomalous Nd and Sr isotopic ratios, which have previously been taken as evidence for "enriched" mantle, may be understood in terms of mantle-crustal mixing.

V 29

ORIGIN OF ENSIALIC OROGENS

A.J. Baer (Dept. of Geology, University of Ottawa, K1N 6N5)

Formation of orogenic belts is accompanied by crustal shortening. This creates a room problem that is resolved differently in oceanic and continental environments. In island-arcs and andean orogens, oceanic crust is subducted into the mantle, but in a continent-continent collision, continental crust cannot be subducted and is mechanically thickened instead. Ensialic orogens form from this tectonic thickening of continents. At the present time, this type of orogen may only develop after a continent-continent collision resulting from oceanic closure. Ensialic orogens may also form however when parts of a continent are thrust upon one another without previous subduction and collision. The Labrador Trough orogen of the Canadian Shield presumably formed in this way. To tell those two types of ensialic orogens apart, one must check the relative timing of sedimentation and deformation, the types of associated sedimentary and volcanic rocks and the conditions of pressure and temperature of metamorphism. Subduction-related ensialic orogens are absent from the Precambrian record before about 850 Ma ago so that all Proterozoic orogens of North America are ensialic, intraplate and intracontinental. By contrast, even though orogenies in the Southern Appalachians, the Norwegian Caledonides or the Himalayas were in good part ensialic, they were periplate and pericontinental.

V 30

A NEW MODEL FOR THE DISTRIBUTION OF CRUSTAL HEAT SOURCES

W. D. Gosnold (Dept. of Geography/Geology, Univ. of Nebraska at Omaha, Omaha, NE 68182)
C. A. Swanberg (Depts. Geology/Physics, New Mexico State University, Las Cruces, NM 88003)

The Idaho batholith consists of a series of plutons which have been studied with respect to their heat generation (K U Th) as a function of emplacement depth and also with respect to their isotopic composition (D/H: $^{18}O/^{16}O$) which relates to their interaction with meteoric groundwater. A comparison of these two data sets supports the hypothesis that vertical distribution of heat generation is largely controlled by interactions between plutons and crustal fluids in approximately the upper 10 km of the crust. This hypothesis is consistent with the linear relation between heat flow and heat generation ($Q = Q_0 + Ab$) and provides a new model for the distribution of crustal heat sources as follows: $A(Z) = A \exp(-cz/b)$ within the region of pluton-crustal fluid interaction and $A(z) = A^*\exp(b-z)/(L-b)$ below the region of interaction. In these equations, c is a constant ratio equivalent to A_0/A^*, A_0 is the surface heat generation, A^* is the average crustal heat generation, L is crustal thickness, and b is a constant whose physical significance is the lowest depth of interaction between plutons and meteoric groundwater. The vertical distribution of heat generation is exponential but there is an inflection in the curve at the lowest depth of interaction between plutons and meteoric groundwater.

V 31

OXYGEN ISOTOPIC COMPOSITIONS OF GARNET GRANULITES FROM COLORADO PLATEAU DIATREMES

S. N. Ehrenberg
S. N. Ahmad
E. C. Perry, Jr. (all at: Department of Geology, Northern Illinois University, DeKalb, Ill. 60115)

Garnet-andesine-augite granulite of aluminous mafic composition is a prominent component of the crystalline xenolith populations of minette and serpentinite diatremes of the 4-corners area. This suite shows considerable variation in $\delta^{18}O$ of both whole rocks (5.0-7.9°/oo; 9 samples) and plagioclases (5.0-9.4°/oo; 12 samples), extending to both lighter and heavier values

than are considered characteristic of unaltered mafic igneous rocks. Plagioclase in each sample is 0.6 to 1.4 °/oo heavier than the whole rock value, suggesting that the mineral compositions may reflect high-temperature equilibrium values. A possible explanation for the heavier-than-igneous values in the granulite suite is interaction during metamorphic recrystallization with fluids affected by metamorphosed pelitic rocks with high $\delta^{18}O$; xenoliths of sillimanite-bearing gneiss and potassic granitic gneiss in the same diatremes have $\delta^{18}O$ values as high as 12.0 and 12.5, respectively.

Late-stage hydrothermal alteration of granulites in the serpentinite pipes resulted in extensive saussuritization and uralitization. However, fresh plagioclases from the lamprophyre diatremes show the same wide range of $\delta^{18}O$ as saussuritized plagioclases from the serpentinite hosts. Apparently alteration involved such low water/rock ratios as to be essentially isochemical within rather broad limits.

V 32

O-ISOTOPIC COMPOSITION OF LOWER CRUSTAL XENOLITHS, KILBOURNE HOLE, NEW MEXICO

D. E. James (Dept. of Terrestrial Magnetism, Carnegie Institution of Washington, Washington, D.C. 20015)
E.R. Padovani
S.R. Hart (both at: Dept. of Earth and Planet. Sci., Massachusetts Institute of Technology, Cambridge, Massachusetts 02139)

Lower crustal xenoliths from Kilbourne Hole exhibit variation in $\delta^{18}O$ of about 6 °/oo. Mafic granulites (including charnockite), probably of mantle origin, have $\delta^{18}O$ values of 6.2 to 6.3 °/oo and correspondingly low $^{87}Sr/^{86}Sr$ ratios (0.703 to 0.707). Garnet granulites, probably derived from a pelitic protolith, have $\delta^{18}O$ values ranging from +9 to +12 °/oo and have correspondingly high $^{87}Sr/^{86}Sr$ ratios (0.71-0.78). All of the xenoliths studied appear to be in internal oxygen isotopic equilibrium.

There is no evidence for extensive oxygen exchange over large distances in the anhydrous lower crust beneath Kilbourne Hole, thus indicating that even at melting or near melting temperatures the oxygen isotopic identity of the protolith can persist over long periods of time. The preservation of mantle isotopic values in mafic granulites intrusive into paragneiss demonstrates that even over small distances no significant oxygen or strontium isotopic exchange has occurred between magma and wall rock. The correlation between high $\delta^{18}O$ and high $^{87}Sr/^{86}Sr$ ratios suggests that oxygen isotopes can be used as tracers to assess the role of crustal contamination in altering the radiogenic isotopic composition of mantle-derived magmas.

V 33

THE GNEISS SYNDROME: Nd- AND Sr- ISOTOPIC RELATIONSHIPS IN LOWER CRUSTAL GRANULITE XENOLITHS, KILBOURNE HOLE, NEW MEXICO

S.H. Richardson (Massachusetts Institute of Technology, Cambridge, Mass. 02139)
E.R. Padovani
S.R. Hart

Determination of Sm-Nd and Rb-Sr isotopic systematics in a suite of granulite-facies ortho- and paragneiss xenoliths of lower crustal origin from Kilbourne Hole, N.M., facilitates reconstruction of their time-temperature history. Variable scale equilibrium and disequilibrium relationships respectively imply a recent high-temperature event and an ancient granulite-facies event.

Garnet, plagioclase and K-feldspar within individual paragneiss layers are in perfect 143/144Nd & 87/86Sr isotopic equilibrium. Clinopyroxene and plagioclase in a foliated orthogneiss are similarly in isotopic equilibrium. The maximum possible age for this inter-mineral equilibrium is about 10 m.y. This equilibrium could relate either to heating by magma associated with the eruptive event 10^5 years ago or to storage in the lower crust under current granulite-facies conditions associated with development of the Rio Grande rift.

In contrast, distinct isotopic disequilibrium exists between paragneiss layers. In one xenolith, minimum tunes required for interlayer Nd & Sr isotopic disequilibrium to have developed are 500 m.y. & 1700 m.y. respectively. In another, these are 1300 m.y. & 6.5 b.y. The latter Rb-Sr system has clearly been severely disturbed. Both nodules show monotonic gradients in 87/86Sr across the set of layers, suggesting location on approximately steady-state diffusion gradients between larger-scale Sr reservoirs, possibly established during deposition of the paragneiss precursors. Distinct Nd reservoirs appear to have been formed on a much smaller scale (~10cm) by garnet formation during the ancient granulite event, possibly at 1700 m.y., the presumed age of the crust in the region. Crude whole-rock Rb-Sr and Sm-Nd ages for the set of xenoliths are consistent with such an age of gneissification.

V 34

XENOLITHIC EVIDENCE FOR THE CHARACTER OF THE LOWER CRUST OF QUEENSLAND AND EASTERN AUSTRALIA

S. Mahlburg Kay and R. W. Kay
(Cornell University, Ithaca, New York 14853)

Xenolith suites from two alkali basaltic volcanoes in Northern Queensland include ultramafic, mafic, and granitic samples. The feldspar bearing xenoliths of basaltic composition are of probable crustal origin and include two broad groups. The first group is more abundant at Sapphire Hill and consists of mildly deformed,garnet and spinel bearing two-pyroxene granulites. The norms have abundant olivine and minor hypersthene. Mineralogical evidence including zoned feldspars and clinopyroxenes, relect orthopyroxenes, and spinels enclosed in garnets suggest falling temperature or rising pressure is being recorded. The second group is more abundant at Hill 32 and consists of texturally and mineralogically equilibrated amphibole bearing two-pyroxene granulites. The norms contain abundant hypersthene and minor olivine. Na and Al contents of clinopyroxenes show a positive correlation with feldspar AB contents, a relationship not commonly observed in surface granulites. Lower Na in the clinopyroxenes from amphibole bearing granulites suggests that they are from shallower depths than the garnet granulites. The deformed versus equilibrium textures also suggest the two groups are derived from different regions of the crust. Wells two-pyroxene thermometry gives temperatures around 800 C for both groups, but insensitivity of the method at these temperatures lends uncertainty on the actual difference between the two groups. Raheim-Green clinopyroxene-garnet temperatures are in agreement with or up to 100 C lower than the Wells temperatures depending on how Fe+3 in the pyroxene is estimated. Wood orthopyroxene-garnet pressures are 6-8 KB. A high geothermal gradient consistent with basalt injection is indicated. These xenoliths are broadly similar with those described from other alkali basaltic volcanic rocks (including Delegate) on the eastern margin of Australia and may indicate a similarity in the lower crust over the entire region.

V 35

EVIDENCE FOR METEORIC WATER IN HYDRATED XENOLITHS FROM THE COLORADO PLATEAU

T.F. O'Brien, R.W. Kay (Cornell University, Ithaca, New York 14850), E.C. Perry Jr., and S.N. Ahmad

An important question relating to the tectonic history of the Colorado Plateau concerns the nature and extent of hydration affecting the upper mantle and lower crust in that region. Several Plateau workers regard regional hydration as a viable mechanism for uplift; others consider a tectonic origin for the hydration, namely the release of water from a subducted slab. The use of stable isotopes, heretofore neglected in Plateau studies, represents an ideal method to investigate both the source and extent of this phenomenom. Oxygen isotopes from greenschist altered, hydrous xenoliths collected at Buell Park, Arizona, were analyzed to determine the source and temperature of interacting fluids. These xenoliths are characterized by acicular clusters of blue-green amphibole, replacing primary pyroxene and/or amphibole, set in a matrix of mosaic textured quartz or altered plagioclase. Whole rock $^{18}O/^{16}O$ values from 7 samples range from -2.2 per mil to +3.2 per mil, relative to SMOW. Analyses from unaltered xenoliths, including amphibolite, hornblende-biotite schist, 2-pyroxene granulite, and rare garnet granulite, all from Buell Park, yield values between +6 and +9 per mil. The latter values agree well with "normal" estimates for metamorphosed basic rocks. However, the altered-rock data indicate the presence of hydrothermal (> 200°C), meteoric fluids during metamorphism, and as such implies an upper crustal setting for the hydration "event". The probable genetic relationship between unaltered and altered xenoliths further suggests that the mechanism of hydration is intimately tied to the intrusion of the transporting host rock. In any case, the identification of the fluids affecting the Buell Park xenoliths represents an important constraint on any future crustal model.

V 36

CONSTRAINTS ON CRUSTAL HYDRATION BENEATH THE COLORADO PLATEAU FROM MAJOR ELEMENT CHEMISTRY AND PHYSICAL PROPERTIES OF CRUSTAL XENOLITHS

Elaine Padovani (Dept. Earth and Planetary Sciences, M.I.T., Cambridge, MA 02139)
Gene Simmons (Dept. Earth and Planetary Sciences, M.I.T., Cambridge, MA 02139)

Rhyolite, granite, diorite, metasedimentary schist and gneisses, mafic amphibolites and granulites of mafic and intermediate composition occur as xenoliths at the Mule Ear Diatreme and Moses Rock Dike. Many xenoliths have been altered to greenschist facies mineral assemblages due to hydrothermal reactions during transport to the earth's surface. A direct correlation exists between progressive alteration and the presence of microcracks extending into the xenoliths from the kimberlitic host rock. Pristine samples of mafic amphibolites and granulites, thought to be major constituents of the lower crust, have equilibration temperatures of 700-800°C calculated from ga-cpx, ga-bio or amph-plag pairs. Their altered equivalents yield temperatures of 400-500°C. V_p measurements on altered amphibolites and granulites result in velocities which are too slow for such rock types to be characteristic of deep crustal levels. The xenolith suite appears to reflect a crustal sequence at depth which has similarities to the crustal cross-section exposed in the Ivrea-Verbano and Strona-Cenari zones in northern Italy. The crustal sequence beneath the Colorado Plateau is interpreted as having greenschist facies rocks in the upper levels, amphibolite facies schists and gneisses with occasional granite intrusives in intermediate levels and mafic garnet-bearing amphibolite and granulite facies rocks predominating in the lower crust.

V 37

PRELIMINARY GEOCHEMICAL STUDIES OF SELECTED CRUSTAL XENOLITHS, XALAPASCO DE LA JOYA MAAR, SAN LUIS POTOSI, MEXICO

Jonathan A. Powell
L. Peter Gromet Department of Geological Sciences, Brown University, Providence, Rhode Island 02912

From a diverse xenolith population, two major suites of probable lower crustal origin have been recognized: a garnet-bearing suite (garnet+quartz+plagioclase or mesoperthite with minor graphite and rutile) and a mafic suite (gabbro and pyroxenite, some with minor amphibole). Selected xenoliths from these suites display very low Rb concentrations (1-17 ppm) and variable Sr concentrations (112-720 ppm). The mafic suite is characterized by low $^{87}Sr/^{86}Sr$ (0.704-0.705) and moderately fractionated, light REE-enriched REE patterns. Xenoliths from the garnet-bearing suite have more radiogenic $^{87}Sr/^{86}Sr$ (0.709-0.716) and REE patterns with a pronounced LREE depletion but unfractionated heavy REE.

The very low 87Rb/86Sr (0.005-0.20) of these xenoliths imply very slow growth of $^{87}Sr/^{86}Sr$ in the crustal reservoirs from which they were derived. The origins of the low Rb contents and Rb/Sr, as well as the LREE-depleted patterns for the garnet-bearing suite, are not defined. Loss of a Rb and LREE-enriched melt fraction may be considered, although REE patterns of garnet and mesoperthite separated from one xenolith do not suggest equilibration with a common magma. However, these minerals may have reequilibrated under subsolidus conditions. The timing of Rb and LREE depletion events, if they occurred, bears directly on the Sr and Nd isotopic evolution of crustal reservoirs.

Metamorphic Petrology

Bay
Friday P.M.
John Allen (Univ. of Toronto), Presiding

V 38

CALEDONIAN Sm-Nd AGES OF NORWEGIAN ECLOGITES

H.K. Brueckner (Queens College, Flushing, N.Y. 11367 & Lamont-Doherty Geological Observatory, Palisades, N.Y. 10964)
W.L. Griffin (Mineralogisk-Geologisk Museum, Sars' Gate 1, Oslo, Norway)

The interpretation of eclogites enclosed in Precambrian gneiss in western Norway has been hampered by ignorance about the age of eclogite formation. The garnet-clinopyroxene (gnt-cpx) pair is ideal for Sm-Nd dating since the two phases fractionate Sm and Nd more efficiently than most rock-forming minerals. Gnt-cpx pairs for five eclogites give Sm-Nd ages of 407-447 Ma; a sixth pair gives 877 Ma. The younger ages are similar to Rb-Sr and K-A mineral dates from the enclosing gneiss, and are interpreted as dating the time of eclogite facies metamorphism assuming that the Sm-Nd system is not easily reset by metamorphic effects short of total recrystallization. The older age is attributed to relict garnet cores formed during an earlier almandine-amphibolite facies event. T_{CHUR} model ages for gnt and cpx are highly discordant and $^{143}Nd/^{144}Nd_0$ range from 0.5116 to 0.5124 suggesting that the basic rocks were isolated from the mantle long before their recrystallization to the present cpx-gnt assemblages. Cpxs from eclogites have $^{87}Sr/^{86}Sr$ ratios at 424 Ma B.P. that range from 0.7039 to 0.7176; consistent with a crustal prehistory for at least some eclogite protoliths. These data argue against emplacement of these eclogites as solid fragments of eclogitic mantle material, but support a model of in situ metamorphism of ancient basaltic material during subduction of the continental crust during a Himalayan-type collision. The Sm-Nd ages imply that subduction occurred during the Caledonian orogeny when western Norway (the Baltic plate) was over-ridden by the Greenland plate.

V 39

Nd AND Sr ISOTOPES OF THE NORWEGIAN GARNET PERIDOTITES AND ECLOGITES

S.B. Jacobsen (Lunatic Asylum, Div. of Geol. and Plan.Sci., Cal.Inst.of Tech., Pasadena, CA 91125
G.J. Wasserburg

Nd isotopic data suggest that the continents have been mainly derived by partial melting of undepleted mantle through time. The mass transfer from a deep-seated undepleted reservoir may occur through rising diapirs. At shallow levels in the mantle the diapirs may intersect the solidus and be partially melted and the melt partly separated. The separated melt is added to the continental crust and the depleted residue is added to the depleted upper mantle. A minor amount of the residual fraction of these diapirs may be welded onto the base of the continents or occasionally (during collison) overthrust. The peridotite massifs observed in orogenic belts are candidates for this residual material. These massifs consist mainly of lherzolite, harzburgite, and dunite but also contain layers that may represent high pressure cumulates. We are carrying out an investigation of the Norwegian garnet peridotites and their associated crustal eclogites. Clinopyroxene and garnet from garnet-websterite layer of the Almklovdalen peridotite gives a 1.12% spread in $^{143}Nd/^{144}Nd$ and yields an age of 1477±7 m.y. and an initial $\varepsilon_{Nd} = -0.9\pm0.2$. The peridotite massif is emplaced into country rocks of 1.5-1.7 AE age that were later metamorphosed under eclogite facies conditions. The mineral isochron of the garnet websterite most likely dates the eclogite facies metamorphism. Garnet lherzolites have $f^{Sm/Nd} = +0.2$ to $+0.4$ and are thus depleted in LREE. The initial ε_{Nd} suggests that this LREE depletion occurred simultaneously with the main crust forming event in this area. The measured $^{87}Sr/^{86}Sr$ is very primitive (0.7017); initial $\varepsilon_{Sr} = -15$ which suggests that Rb depletion occurred at least 2.4 AE ago. The data suggest that the peridotite massif may represent residual material that has been involved in several stages of continent formation. Data on a variety of peridotites and eclogites will be presented.

V 40

EXPERIMENTAL EVIDENCE FOR THE ROLE OF CO_2 IN CHARNOCKITE GENESIS

R. F. Wendlandt (Lunar and Planetary Institute, 3303 NASA Road 1, Houston, TX 77058)

Partial melting studies at crustal pressures in SiO_2-rich portions of the system $KAlSiO_4$-Mg_2SiO_4-SiO_2-H_2O-CO_2 can be used to model the anatectic origin of charnockites. The univariant reaction

phlogopite + sanidine + quartz + vapor = enstatite + liquid

produces a SiO_2-rich melt (granite analog) at 3 kbar; the vapor composition at the solidus is buffered to high H_2O-contents by the coexistance of phlogopite with its breakdown products. At higher pressures, 8 and 15 kbar, the fluid phase is buffered to higher CO_2-contents and the melt composition becomes enriched in K_2O and MgO (charnockite analog). Melting relations are controlled by the expansion of the quartz liquidus field relative to the enstatite field with increasing pressure. The univariant melt (i.e., that melt generated at the solidus) produced at 8 kbar and 775°C in the presence of a CO_2-rich fluid will crystallize enstatite at lower pressures.

This partial melting model for charnockite genesis satisfies the constraints of observed charnockite mineralogies, P and T estimations for charnockite assemblages (5-8 kbar and 700°-800°C), and reports of high-temperature CO_2-rich fluid inclusions that are believed to approximate solidus vapor compositions (Ormaasen, 1977; Henry, 1978; Konnerup-Madsen, 1979).

CO_2-saturated melting of similar SiO_2-rich bulk compositions (phlogopite-absent) by the reaction

enstatite + sanidine + quartz + CO_2 = liquid

occurs at temperatures in excess of 1000°C to about 15 kbar. Liquid compositions show analogous trends, however, with increasing pressure, to those observed in the 5-component system as a consequence of the expansion of the quartz liquidus surface relative to the enstatite surface.

V 41

A KINETIC THEORY OF METAMORPHIC LAYERING IN ANISOTROPICALLY-STRESSED ROCKS

Peter Ortoleva and Enrique Merino (Depts. of Chemistry and Geology, Indiana University, Bloomington, IN 47405)
(Sponsor: Abhijit Basu)

We present a macroscopic, kinetic theory for the periodic layering commonly observed in metamorphic rocks of all grades. Banding requires diffusion, but proving diffusion does not prove that a repetitive pattern of banding must result. We show that the spatial periodicity of banding can come about not through a periodic distribution of the stresses, but as an inherent property of the kinetics of the processes of diffusion and dissolution/recrystallization.

When a uniformly-textured rock is subjected to anisotropic stresses, some crystals (depending on the local stress environment, which is controlled by the texture, which itself varies as the banding develops) dissolve, and the ions diffuse and crystallize elsewhere. The growth rate of each crystal is proportional to the affinity for growth. The theory includes: (a) conservation of the mass of intergranular species and of the number of crystals per unit volume for each mineral; (b) a space-filling constraint that brings in plastic flow; and (c) explicit provision for a diffusion-limited overall process. This yields a closed system of equations for the dynamics of the texture (= a vector whose components are the crystal sizes and number densities of all minerals) and plastic flow. Under rather non-restrictive conditions, the texture turns out to be unstable to small initial textural perturbations, and tends to resolve itself into bands alternatively rich in, say, minerals A and B. As time passes the banding propagates sideways. The theory predicts the spacing of the bands and its evolution with time. It also predicts that within an A-rich band the A crystals are larger than the A's in a neighboring band poor in A; there is published evidence for this.

V 42

A THERMODYNAMIC MODEL OF A SILLIMANITE/GARNET TEXTURE

C. T. Foster, Jr. (Geology Department, The University of Iowa, Iowa City, Iowa 52242)

The texture produced when sillimanite nucleates and grows adjacent to a garnet in a pelitic schist has been investigated using a local equilibrium, steady diffusion model (Fisher,1973, AJS). The initial configuration of the model was a garnet porphyroblast set in a matrix of biotite, muscovite, plagioclase, ilmenite, and quartz. The chemical potential gradients and local reactions produced when sillimanite grows on one side of the garnet were calculated from Gibbs-Duhem relations, conservation equations, and relative diffusion coefficients in an SiO_2-fixed reference frame. According to the model, part of the garnet porphyroblast near the growing sillimanite should dissolve, producing a sharp truncation of the porphyroblast at the garnet/sillimanite boundary. In addition, a muscovite-free mantle should develop in the matrix around the sillimanite. The predicted texture is very similar to one which has been observed in sillimanite-bearing pelites near Rangeley, Maine. The close match between the observed texture and the texture calculated by the model suggests that the local reactions are controlled by material transport through the matrix under local equilibrium conditions.

V 43

CONSTANT TEMPERATURE REGIONAL METAMORPHISM OF AN H_2O ACTIVITY GRADIENT IN A PREEXISTING CONTACT AUREOLE, PETERSHAM, MASSACHUSETTS

Charles K. Shearer and Peter Robinson, Dept. of Geology and Geography, University of Massachusetts, Amherst, MA 01003

A quartz-bearing hornblende-biotite diorite sill intruded pelitic schists of the Lower Devonian Littleton Formation during early stages of Acadian (Devonian) tectonics, producing a contact aureole 4.5 m wide with local development of andalusite. Subsequently most of the pelitic schists developed sillimanite-orthoclase-muscovite-biotite-garnet assemblages during peak Acadian metamorphism in the SIL-KSP-MUS Zone. Garnets of this zone are characteristically minor in amount and have homogeneous cores ($Alm_{75}Pyr_{16}Sps_5Gro_3$) surrounded by more Alm-rich rims believed formed by retrograde continuous reaction with host biotite ($X_{Mg}\cong.47$). K_D $^{GAR-BIO}_{Fe-Mg}$ based on garnet cores in this region suggest T≅650°C. Peak metamorphism was followed by two phases of deformation, each with distinctive mineral lineation, during which retrograde rims developed.

Within the old contact aureole muscovite is absent or scarce and andalusite is pseudomorphed by sillimanite. Garnet zoning patterns are similar, but biotite compositions and garnet core compositions become progressively more Mg-rich to $X_{Mg}\cong.62$ and $Alm_{68}Pyr_{26}Sps_4Gro_2$, a composition typical of the regional SIL-GAR-CRD Zone (≅700°C), 6km away. However, K_D $^{GAR-BIO}_{Fe-Mg}$ based on these garnets still suggests T≅650°C. An interpretation is that all garnet-biotite assemblages equilibrated at peak metamorphic conditions near 650°C, but those closer to the contact reached more Mg-rich compositions on the continuous reaction BIO+SIL=GAR+KSP+H_2O because of low H_2O activity preserved from the contact aureole. Thus the aureole presents an opportunity to study isothermal-isobaric metamorphism that took place at variable H_2O activity.

V 44

HYDROTHERMAL MINERALS, TEMPERATURE AND FLOW REGIME IN THE CERRO PRIETO GEOTHERMAL FIELD: A MODEL FOR GREENSCHIST METAMORPHISM

W.A. Elders (Inst. Geophysics & Planet. Physics, University of California, Riverside, CA 92521)

Study of active hydrothermal processes in modern geothermal fields provides new insights into greenschist facies metamorphism.

More than 60 boreholes, 1-3 km deep, have encountered temperatures ≥ 350°C and brines with ≤ 2% total dissolved solids in the Cerro Prieto geothermal field of the Salton Trough intracontinental rift system, in Baja California. Temperature dependent dehydration and decarbonation reactions have produced a regular sequence of mineral zones in sediments of the Colorado River, mappable across the field in the subsurface.

These mineral assemblages also depend upon water/rock ratio, P_{CO_2}, and location within the flow regime. At the same temperature, minerals in sandstones differ from those in shales because of permeability differences. Similarly, patterns of mineral zones in regions of horizontal flow, or of vertical discharge or recharge, are quite characteristic.

Water/rock ratios can be estimated using $\delta^{18}O$ in water and minerals. In addition to direct downhole measurements, temperatures have been estimated from isotope ratios, fluid inclusions, and vitrinite reflectances, giving us the temperature history. The age and duration of heating is being estimated from fission track annealing studies. Thus we are using hydrothermal minerals to record temperature, fluid chemistry, fluid flow, and heating time, in a modern analogue of an environment which was widespread in the Precambrian. Seeing the output of a geothermal well makes metasomatism less mysterious.

V 45

MINERAL PARAGENESES OF THE SUAO-NANAO AMPHIBOLITES AND ASSOCIATED ROCKS IN NORTHEASTERN TAIWAN

J. G. Liou (Stanford University)
W. G. Ernst (Univ. of California, Los Angeles)
John Suppe (Princeton University)

Metamorphism of the pre-Tertiary basement of NE Taiwan involves different stages; effects of polymetamorphism are especially well displayed in amphibolite, possibly the oldest rock in Taiwan. Fault-bounded and foliated amphibolite with the assemblage green hornblende + plagioclase (An 40-52) + epidote (Ps 4-15) + sphene ± quartz was intruded by 87 m.y. old granodiorite. Apparent thermal effects include (1) conversion of green hornblende to brown hornblende, (2) transformation of epidote to symplectic plagioclase + quartz, (3) crystallization of clinopyroxene at the expense of hornblende, and (4) production of biotite + muscovite + K-feldspar in partly metasomatized amphibolites. The complex was later intruded by thin diabasic dikes which represent feeders for basaltic flows and pyroclastics in the overlying Cenozoic strata. Basement, dike and cover rocks were then metamorphosed under greenschist facies conditions during Early Tertiary(?) and Plio-Pleistocene times. Amphibolite has been partly recrystallized to actinolite + chlorite + epidote + quartz + sphene assemblages. Both nonfoliated dike rocks and foliated basaltic flows carry albite + actinolite + chlorite + epidote (Ps 18-33) + biotite + quartz + sphene. Zeolite facies recrystallization occurs locally along fractures, producing laumontite + epidote (Ps 32) + chlorite. XRF bulk compositions of amphibolites fall within the range of low-K, low-Ti tholeiite, whereas Cenozoic diabasic and basaltic rocks are higher in TiO_2 (0.7-2.7 wt%), Na_2O (1.6-4.0 wt%) and K_2O (0.6-0.8 wt%). Thermally recrystallized amphibolite xenoliths enclosed in granodiorite gneiss are enriched in SiO_2, Al_2O_3, and K_2O and depleted in total Fe, MgO and CaO. These igneous and metamorphic events record portions of the late Mesozoic-Cenozoic history of continental accretion at the eastern margin of Asia.

V 46

COMPOSITION SPACE ANALYSIS OF LOW-VARIANCE AMPHIBOLITE ASSEMBLAGES, POST POND VOLCANICS, VT.

F.S. Spear (Dept. Earth & Planetary Sciences, Mass. Institute of Technology, Cambridge, Ma. 02139)

Amphibolites from the Post Pond Volcanics, S.W. ¼ Mt. Cube Quad., Vt. display an unusually large range of bulk compositions and low-variance mineral assemblages, permitting the delineation of phase volumes in a large portion of the system SiO_2-Al_2O_3-MgO-FeO-CaO-Na_2O-H_2O. Assemblages include (all assemblages contain quartz and andesine): hornblende (Hb) + gedrite (Gd) + anthophyllite (An) + cummingtonite (Cm) ± garnet (Ga); Hb+Gd+An+chlorite (Ch); Hb+Gd+Ga+staurolite (St) ± Ch;St+Gd+cordierite (Cd); An+Gd+Cd+Ch+Na-phlogopite (Naph); Ch+An+Naph+talc (Tc); Hb+Ga+St+bytownite (By); Hb+Ga+By+epidote (Ep); Hb+Ga+Ep+calcite (Cc). Many assemblages contain biotite and all assemblages contain an Fe-Ti oxide (ilmenite in Fe-rich assemblages and rutile in Mg-rich assemblages).

Tie lines among coexisting minerals cross when these assemblages are plotted on an ACF diagram or on the plagioclase projection of Robinson and Jaffe (1969). However, when projected from quartz, plagioclase (An_{35}) and H_2O into the tetrahedron Fe-Mg-Ca-Al, the phase volumes defined by these assemblages do not overlap and no reaction relations are indicated. Some mineral compatibilities do imply, however, that certain rocks crystallized at different values of f_{H_2O} or f_{CO_2}: 1) Hb+Gd+An+Cm+Ga assemblages from different samples overlap in Fe/Mg, possibly the result of differences in f_{H_2O} among samples; 2) Ch+Ga with calcite is observed in several samples, implying the instability of the association Hb+Gd+St in these rocks, possibly the result of an increased f_{CO_2} in these samples.

The distribution of phase volumes in these samples explains the absence of certain mineral associations at this metamorphic grade. For example, the stable association of Hb+Al_2SiO_5 polymorph is not possible because of the associations St+By, Ch+By, and Ch+Ep; similarly Hb+Cd do not coexist because of the stable association of Ch+Ep and Ch+Cc.

V 47

ELEMENT PARTITIONING IN COEXISTING MINERALS, AND PHASE EQUILIBRIA OF AMPHIBOLITES AND RELATED METAMORPHIC ROCKS, NORTHEASTERN TAIWAN

W. G. Ernst (Univ. of California, Los Angeles)
Diane E. Moore (USGS, Menlo Park)
J. G. Liou (Stanford University)

Fractionation of elements between coexisting analyzed phases in Suao-Nanao amphibolites, orthogneisses, greenschists and Tertiary metamafic rocks are systematic. Especially for competing phases which contain similar cyrstallographic sites, exchange reactions appear to be of the ion-for-ion type. Some early amphibolitic and metagranitic fractionations are preserved--particularly those involving relict hornblende--but in most cases the higher grade, less pronounced partitioning has been overprinted by Cenozoic greenschist facies recrystallization involving more marked element fractionations, K_D, or $(Na/K)_{plagioclase}/(Na/K)_{amphibole}$, is 4.6 for amphibolites, 45 for greenschistic assemblages. K_D for alkali partitioning in white mica/biotite pairs is 3.4 in greenschists. Na/Ca ratios in plagioclases are higher than coexisting hornblendes (K_D = 6.6), and, although dispersed, are substantially higher in plagioclase/actinolite pairs (K_D = 450?). Fe/Mg fractionation between coexisting chlorite and hornblende is nonexistent (K_D = 1.06); however, iron is slightly concentrated in chlorite relative to actinolite (K_D = 1.41). Iron and magnesium are indistinctly partitioned between chlorite and biotite, with the latter slightly more Fe-rich (K_D = 0.89). In general, these data indicate a close approach to domain equilibrium for the participating phases.

Judging from experimental phase equilibrium relations, the regional amphibolite facies metamorphism and later thermal recrystallization attending Late Cretaceous granitic intrusion took place at 550-700°C and total pressures of approximately 5-6 kb. Cenozoic greenschist facies metamorphism apparently occurred at about 350-475°C and slightly lower pressures.

V 48

STATISTICAL ANALYSIS OF AMPHIBOLE COMPOSITIONS FROM A LOW-PRESSURE, REGIONAL-METAMORPHIC TERRANE

Theodore C. Labotka
Department of Earth and Space Sciences, State University of New York, Stony Brook, N. Y. 11794

The composition of calcic amphibole in metamorphic rocks that contain the assemblage amph + epid + qtz + plag + chl + bio + ilm is determined by the equilibrium constants for the many continuous reactions that occur among the coexisting phases. The compositions of calcic amphiboles that occur in this assemblage from the tremolite zone in the Panamint Mountains, California, a low-pressure, regional-metamorphic terrane, show small scatter about a linear trend from tremolite to pargasite. Principal-components analysis of the cations ^{IV}Al, (^{VI}Al + Fe^{3+} + Cr), Ti, Fe^{2+}, Mg, K, ^{A}Na, ^{M4}Na indicates that all are highly correlated except ^{M4}Na which is very small (μ = 0.05, σ = 0.01). The first principle component accounts for 92% of the total variance, and this eigenvector has the direction cosines ^{IV}Al : $^{VI}(\Sigma 3+)$: Ti : ^{A}Na : K : Fe^{2+} : Mg = 0.540 : 0.201 : 0.043 : 0.140 : 0.190 : 0.440 : -0.663. This corresponds to a compositional vector with the origin at tremolite and extending through the point [$^{2}{}^{VI}Al$, $0.74^{VI}(\Sigma 3+)$, 0.16Ti, $0.52^{A}Na$, 0.40K, 1.63Fe, 2.55Mg] (3.70 x eigenvector), and this eigenvector satisfies the site charge-balance equation to 0.003 excess positive charge/unit vector. Thus, the multi-element amphibole system may be reduced to the two components tremolite [$\square Ca_2\ Mg_5\ Si_8\ O_{22}\ (OH)_2$] and "pargasite" [$Na_{0.52}\ K_{0.40}\square_{0.08}\ (Ca_{1.92}\ Fe_{0.08})\ Fe_{1.55}\ Mg_{2.54}\ Ti_{0.15}\ Al_{0.74}\ (Al_2\ Si_6)\ O_{22}\ (OH)_2$]. During progressive low-pressure metamorphism in the Panamint Mountains, the "pargasite" component in amphibole increases by the continuous reaction 39 epid + 5 albite + 4 biot + 6 chl + 17 qtz + 1 ilm = 10 "pargasite" + 59 anorth + $38H_2O$ and is accompanied by an increase in anorthite content of plagioclase.

V 49

COUPLED SUBSTITUTIONS IN HORNBLENDES WITH INCREASING TEMPERATURES OF METAMORPHISM

J.A. Docka (Dept. of Geological Sciences, Harvard University, Cambridge, MA 02138)
J.H. Berg (Dept. of Geology, Northern Illinois University, DeKalb, IL 60115)

Microprobe analyses of hornblendes from metamorphosed mafic rocks of similar composition in the contact aureole of the Kiglapait intrusion, Labrador, range in composition from:

$$K_{.039}{}^{Na}.189\,{}^{Ca}1.831\,{}^{Fe}2.12\,{}^{Mn}.034\,{}^{Mg}2.72\,{}^{Ti}.026\,{}^{Al^{VI}}.364\ {}^{Si}7.113\,{}^{Al^{IV}}.897\,{}^{(OH)}2$$

to:

$$K_{.031}{}^{Na}.918\,{}^{Ca}1.758\,{}^{Fe}2.019\,{}^{Mn}.044\,{}^{Mg}2.449\,{}^{Ti}.42\,{}^{Al^{VI}}.208\ {}^{Si}6.119\,{}^{Al^{IV}}1.881\,{}^{(OH)}2$$

Data show increases in the Na, Ti, and Al^{IV} content of hornblende as the contact of the intrusion is approached, with a concurrent decrease in Mg + Mn + Fe(total). Fe-Ti oxide oxygen-barometry (Lindsley, 1977) gives values of fO_2 that lie between the FMQ and MW buffers, and this suggests that the above increases are due solely to increasing temperatures in the aureole. While it is commonly known that the edenite ($Na^{A}Al^{IV}$=$[]^{A}Si^{IV}$) and Ti-tschermakite ($Ti^{VI}2Al^{IV}$=$R2+^{VI}2Si^{IV}$) substitutions are temperature sensitive, a one-to-one relationship between (Na + K + Ti) and (Al^{IV} - Al^{VI}) for these hornblendes implies a third temperature-sensitive substitution. A comparison of microprobe data with wet chemical analyses of three of these hornblendes indicates this substitution to be: $2Na^{M4}Ti^{VI}$=$2R2+^{M4}R2+^{VI}$ and suggests this substitution is equally important with respect to the increasing Ti and Na content of hornblende with increasing temperature. In addition, the data imply that ferric iron content of the hornblende is constant and therefore insensitive to increasing temperature.

V 50

RHODONITE-PYROXMANGITE-PYROXENE-AMPHIBOLE ASSEMBLAGES

R.J. Tracy (Geology and Geophysics, Yale Univ., New Haven, Conn. 06520)
T.N. Lincoln (Earth and Space Sciences, Indiana Univ./Purdue Univ., Fort Wayne, Ind. 46805)
Peter Robinson (Dept. of Geology, Univ. of Massachusetts, Amherst, Mass. 01003)
D.D. Ashenden (Shelburne, Mass 01370)

An isolated exotic clast (1x.75x.3 m) enclosed in the late Pre€ Dry Hill Granitic Gneiss of the Pelham dome, Massachusetts, consists of well-bedded pyroxenoid rock cut by sulfide veins and sheathed by a reaction rind of Fe-rich hornblende, quartz, garnet and sulfide. Assemblages stable with quartz, manganoan garnet and sphene include: pyroxmangite(PYM)-rhodonite(RHD)-manganoan ferrosalite(PYX)-manganoan grunerite(GRU)-manganoan actinolite(ACT)-magnetite-pyrrhotite, and various combinations of these minerals in layers of different bulk composition. Mineral compositions (except garnet) are not significantly different in the different assemblages, and are:

PYM: $(Ca_{.23}Mn_{.77})(Mn_{.18}Mg_{.14}Fe_{.66})Si_2O_6$

RHD: $(Ca_{.28}Mn_{.72})(Mn_{.37}Mg_{.10}Fe_{.52})Si_2O_6$

PYX: $(Ca_{.83}Mn_{.17})(Mn_{.11}Mg_{.39}Fe_{.49})Si_2O_6$

GRU: $(Ca_{.19}Mn_{1.45}Fe_{.36})(Mg_{1.97}Fe_{3.00})Si_8O_{22}$

ACT: $(Ca_{1.70}Mn_{.30})(Mn_{.40}Mg_{1.93}Fe^{++}_{2.64}Fe^{+++}_{.10})Si_8O_{22}$
GAR: $(Ca_{.55}Mg_{.03}Fe_{.62}Mn_{1.80})Al_{1.90}Fe^{+++}_{.10}Si_3O_{12}$ and
$(Ca_{.84}Mg_{.13}Fe_{.98}Mn_{1.05})Al_{1.90}Fe^{+++}_{.10}Si_3O_{12}$
Magnetites contain 0.4 to 0.8 wt% MnO.

Textures and chemography suggest that the assemblages reflect the reaction PYX + GRU + PYM + H_2O = ACT + RHD (neglecting garnet). Nearby rocks show clear evidence of polyphase metamorphism - a pre-Devonian one of near-granulite grade and a Devonian one of Kyanite grade. We infer an original high-grade silicate assemblage PYM-RHD-PYX-GRU-GAR to which ACT was added through recrystallization-hydration in the second metamorphism.

V 51

HOMOGENEITY IN REE FROM STAUROLITE-KYANITE ZONE METABASALTS, SOUTHEASTERN VERMONT

J. Christopher Hepburn (Dept. of Geology & Geophysics, Boston College, Chestnut Hill, Massachusetts 02167

Staurolite-kyanite zone amphibolites of the Siluro-Devonian Standing Pond Volcanics, southeastern Vermont, have a narrow range of REE abundances. 17 samples were collected from different horizons within the formation (which ranges up to 150 meters thick) over an area that extends many kilometers. These rocks are generally basaltic in composition with a metamorphic assemblage consisting of variable percentages of hornblende-plagioclase-epidote±biotite± garnet±quartz (hornblende varies from 25% to 71%). Metamorphic textures are also diverse. Despite this the REE show a restricted range in composition typical of those from basalts with slightly LREE depleted patterns. La varies from 8 to 15 times chondritic values and the La_N/Yb_N ratios fall in the range .51-.84. The La_N/Sm_N ratios are in the range .47-.73.

Garnet-biotite geothermometry (K_D Fe/Mg) yields estimates of 560°C for the metamorphic equilibration temperatures in adjacent pelitic rocks.

The extent to which the REE similarities reflect original compositional homogeneities needs yet to be evaluated. However, the similarity of the concentrations of the REE in these samples indicates that REE may prove to be useful for stratigraphic correlation of this formation at the amphibolite facies.

V 52

"NON-VOLATILE" COMPONENT ACTIVITY VARIATIONS ACCOMPANYING SKARN FORMATION AT PINE CREEK, CA.

Philip E. Brown
Eric J. Essene (both at Dept. Geological Sciences, University of Michigan, Ann Arbor, MI 48109)

Skarn development and ore deposition at the Pine Creek, CA tungsten mine were attended by changes in activities of the chemical species in the environment. Starting with the P-T-X(f) framework derived previously (P=1.5kb, T=800K, XCO_2=.2 Brown and Bowman, 1979), a vs a and a vs f plots have been calculated from thermodynamic and experimental data for the mineralogy exhibited by the marble-skarn-intrusive system. Quantifiable changes in "non-volatile" component activites as well as fO_2 have been traced across the system. Assuming isothermal conditions, the activities of Al_2O_3, Fe_2O_3 and WO_3 generally increase from the marble, through the calc-silicate zone and skarn into the endoskarn while CaO and MgO activities decrease for the same traverse.

	MARBLE	CALC-SILICATE	SKARN
log fO_2	?	-24.0	-23.5
log aAl_2O_3	<-1.7	- 1.7	- 1.7
log $aCaO$	-5.0	> 5.9	- 6.0
log aFe_2O_3	<-7.0	- 4.5	- 3.9
log $aMgO$	-2.5	- 3.9	- 4.0
log aWO_3	<-5.3	< 5.3	> 5.3

The high variance shown by the assemblages adds sufficient uncertainty to the calculated activities for individual specimens that only the large-scale trends survive the fine-scale scatter. None of the variables emerge as major independent or controlling factors for the mineralogy or phase compositions. Changes in one component activity may be offset by compensatory changes in another resulting in an environment that, while different from Pine Creek, could still host scheelite mineralization. Mass balance calculations indicate that the exposed endoskarn can not have supplied the necessary components to convert the country rock to skarn. This thermodynamic approach, while not yielding an easily applied exploration tool, can quantify local chemical variations and has some predictive power within a given deposit.

V 53

ORIGINS AND EVOLUTION OF METAMORPHIC FLUIDS IN DOLOMITIC MARBLES, ELKHORN, MONTANA

John R. Bowman (Dept. of Geology and Geophysics, University of Utah, Salt Lake, Utah 84112)
Eric J. Essene (Dept. of Geology, University of Michigan, Ann Arbor, Michigan 48109)
James R. O'Neil (U.S. Geological Survey, Menlo Park, California 94025)

Applications of phase equilibria and calcite-dolomite thermometry to metamorphosed siliceous dolomites in the Black Butte stock aureole define a prograde T-$X(CO_2)$ path from T=425±30°C, .6< $X(CO_2)$<.8 (tremolite isograd) to T=590±25°C, .03 <$X(CO_2)$<.1(periclase isograd). This decrease in $X(CO_2)$ is inconsistent with internal buffering of pore fluid composition by isogradic reactions and requires influx of water-rich fluids. Mass-balance calculations of external H_2O and carbon, hydrogen, and oxygen isotope analyses of calcite and hydrous silicates constrain the amounts and origins of this external H_2O: 80 to 210moles $H_2O/10^3cm^3$ marble: $\delta^{18}O$(calcite)=+21.0 to +23.7; $\delta^{13}C$(calcite)=-3.8 to -1.2; δD(amphibole) =-97 to-72. Mass-transfer estimates are based on changes in measured mineral modes, reaction stoichiometries, and estimates of the mass and $X(CO_2)$ of pore fluids initially present. No systematic decrease in either $\delta^{18}O$ or $\delta^{13}C$ accompanies the increase in metamorphic grade (T) or increasing calcite abundance(extent of reaction). These features suggest that devolatilization reactions did not simply involve systematic removal of ^{18}O or ^{13}C by progressive evolution of CO_2-dominated fluids. Masses of external H_2O estimated to reduce $X(CO_2)$ are sufficiently great that substantial decreases in both $\delta^{18}O$ and δD would result in the marbles if these external fluids were relatively unaltered meteoric or magmatic H_2O ($\delta^{18}O$ only). Rather both petrologic and isotopic data suggest that the mineralogic and isotope characteristics of the marble have been significantly influenced by interaction with ^{18}O- and H_2O-rich metamorphic fluids from surrounding nearly pure dolomitic marble.

V 54

DISEQUILIBRIUM DURING METAMORPHISM IN HIGH GRADE PELITES FROM THE FRONTENAC AXIS, ONTARIO, CANADA

S.W. Lonker (Geophysical Laboratory, Washington, D.C. 20008)

The Frontenac Axis is a southeasterly extension of the Canadian Shield, which connects to the Adirondacks in New York. The pelitic gneisses contain mineral assemblages characteristic of the pyroxene granulite facies. The mineral assemblages as inferred from the original primary textures enable the complete construction of the mineral facies. The sequence of mineral facies indicates that the highest grade rocks in southeastern Ontario (cordierite+orthopyroxene zone) are in the northeast corner of the Gananoque map area and in the area northwest of Gananoque. On the scale of a thin section, chemical equilibrium has not been achieved as supported by chemical zoning, chemical heterogeneity, and absence of exchange equilibrium. On the scale of a rock, graphical analysis indicates that the continuous variation in the Mg/(Mg+Fe) δf of ferromagnesian phases (assemblage biotite+sillimanite+cordierite+ garnet+quartz+alkali feldspar) is in response to temperature, which conceals any evidence of local gradients in $a(H_2O)$. Different temperatures are recorded across a rock because of reequilibration during cooling. The direction of displacement of reactions which produce (1) corona textures; (2) chemical zoning associated with corona textures; (3) chemical zoning related to exchange reactions between coexisting phases; and (4) regional trends in the Al-content of biotite in sillimanite-bearing assemblages is consistent with a decrease in temperature or pressure or both. Intermingling of incompatible assemblages and the widespread occurrence of six phase AFM assemblages are due to disequilibrium produced by incomplete reaction during uplift and cooling. Petrologic and geochronologic constraints infer slow uplift and cooling rates between 300° to 750°C, where the major cooling mechanism is upward advection (upward transport of crustal material).

V 55

METAMORPHIC ZONATION IN FRANCISCAN GRAYWACKES, SOUTHERN CALIFORNIA COAST RANGES

W. G. Ernst (Dept of Earth & Space Sciences, Univ. of California, Los Angeles, CA 90024)

Petrographic reconnaissance of metaclastic rocks in the Nacimiento block demonstrates an eastward increase in metamorphic grade. Feebly recrystallized zone I metagraywackes bordering the Pacific Ocean are rich in calcite veins + patches and contain no new Ca-Al hydrous silicates; abundant unstable detritus includes lithic fragments, biotite flakes and epidote granules. Metasediments of medial zone II are characterized by fine-grained intergrowths of pumpellyite ± minor regenerated epidote-clinozoisite. Easternmost zone III metasandstones contain lawsonite, rarely aragonite and/or jadeitic pyroxene. Proportions of calcite, rock fragments, epidote and biotite tend to decrease eastward, whereas white mica, chlorite and stilpnomelane increase. Based on experimental phase equilibrium data, temperatures of 150±50°C are estimated to have attended recrystallization, with lithostatic pressures increasing from 2-3 kb on the west to approximately 5 kb, locally approaching 8 kb, on the east. During metamorphism, the aqueous fluid evidently was diluted by CO_2 in zone I, accounting for absence of zeolites in the lowest grade metagraywackes.

Combined with the northwest tectonic grain of the Nacimiento block and its inferred imbricate structure, the assemblage of rock types, the predominantly right-side-up nature, and northeastward dip of bedding, this continental margin deposit is thought to have been recrystallized during a period of rapid Late Cretaceous plate convergence. Lack of eclogite and kindred tectonic blocks indicates less profound depths of recovered subduction compared to Franciscan basement northeast of the San Andreas fault. Metamorphosed Nacimiento lithic belts evidently were assembled over a brief period of off-scraping at the western edge of the American lithospheric plate, but mirror events which unfolded over a longer time interval in Franciscan rocks of the northern Coast Ranges.

V 56

SULFIDE-SILICATE REACTIONS ASSOCIATED WITH THE DUCKTOWN, TENNESSEE ORE BODIES

Bruce E. Nesbitt, Dept. of Geosciences, Penn State Univ., University Park, PA 16801
Eric J. Essene, Dept. of Geosciences, Univ. of Michigan, Ann Arbor, MI 48109

The massive sulfide ore bodies and the adjoining rocks at Ducktown were metamorphosed at T= 550°C and P=6 kb. During the event reactions occurred between S_2 and the Fe-Mg silicates leading to a series of chemical and mineralogical changes in the wall rocks around the ores. The S_2-silicate reactions produced the following zonations Bt-Gt-Stt (country rocks) → Bt-Gt-Stt-Chl → Bt-Gt-Chl → Bt-Chl (ore zone). Accompanying these mineral changes were corresponding changes in X_{Fe} of the silicates. Stt exhibits a compositional variation from X_{Fe}=0.83 in the country rocks to X_{Fe}= 0.47 at its disappearance in the wall rocks. Compositional variations of other Fe-Mg silicates are as follows: Gt, X_{Fe}=0.84 to X_{Fe}=0.26; Bt, X_{Fe} =0.56 to X_{Fe}=0.15; Chl, X_{Fe}=0.44 to X_{Fe}=0.13. Substitutions for the Fe^{2+} removed by the reactions are as follows: Mg in Bt and Chl, Mg and minor Zn in Stt, Mn and minor Mg in Gt. Using oxide-sulfide assemblages, Nesbitt and Kelly (1978) have determined variations in f S_2 and f O_2 throughout the wall rocks. These variations in f S_2 and f O_2 have been combined with an ideal ionic solution model for Bt, Chl, Stt and a regular solution model for Gt to calibrate the following reactions (P_T = P H_2O). Ann + Alm + 3 S_2= Mus + 6 FeS + 3 Qz + 3 O_2, log f S_2=-4.3, log f O_2 =-19.6; 9 Ann + Stt + 31/2 S_2 = 9 Mus + 31 FeS + 8 Qz + H_2O + 31/2 O_2, log f S_2=-4.7, log f O_2= -19.9; 3 Ann + Chl ($Fe_9Al_6Si_5O_{20}(OH)_{16}$) + 9 S_2 = 3 Mus + 18 FeS + 5 Qz + 8 H_2O + 9 O_2, log f S_2 = -5.2, log f O_2 =-20.3. From these calibrations it is also possible to determine the stability of the corresponding O_2-Mt-silicate reactions. These variations in mineral assemblages and chemistry indicate that the stabilities and solid solutions of Fe-Mg silicates are strongly dependent on f S_2 as well as f O_2, P, T and f H_2O.

Geothermometry-Geobarometry

Metropolitan West
Saturday A.M.
Eric J. Essene (Univ. of Michigan), Presiding

V 57

CARBON ISOTOPE THERMOMETRY IN GRENVILLE MARBLES

J.W.Valley (Dept. of Geological Sciences, The University of Michigan, Ann Arbor, MI 48109)
James R. O'Neil (The U.S. Geological Survey, 345 Middlefield Rd., Menlo Park, CA 94025)

The ‰ fractionation of ^{13}C between calcite and graphite, Δ(Cc-Gr), is consistently small (2.6 to 4.8) in 34 assemblages from upper amphibolite and granulite facies marbles of the Grenville Province in the Adirondack Mts., N.Y. The fractionations are independent of absolute $\delta^{13}C$ values of calcite (-2.9 to 5.0) and decrease regularly with increasing metamorphic T (Bohlen et al., 1980). For T=600 to 800°C, the Adirondacks data are described by Δ(Cc-Gr)= -0.00748T (°C) + 8.68 (σ = 0.32). This good correlation between Δ and T suggests that carbon isotope equilibrium was attained in these high-grade marbles and that the theoretical calculation of this fractionation by Bottinga (1969) is approximately 2‰ too large in this T range. Because of the pressure independence of isotope fractionation and the relatively high T sensitivity suggested by these results and by Bottinga's calculations, Δ(Cc-Gr) should provide an excellent thermometer for high-grade marbles.

Comparison of these results with those from other terranes supports the thermometric value of Δ(Cc-Gr) but suggests that graphite is much more sluggish to react than calcite, that exchange between calcite and graphite occurs at T as low as 300°C and that equilibrium may normally be attained only when peak metamorphic temperatures are greater than 500-600°C.

If ^{13}C exchange is an important metamorphic process then high values of $\delta^{13}C$(Gr) in carbonate-bearing rocks are not a sufficient criterion to infer an abiogenic origin for the graphite.

V 58

THE DEPENDENCES OF THE THERMODYNAMIC FUNCTIONS ON TEMPERATURE, PRESSURE, AND ISOTOPIC COMPOSITION

Susan Werner Kieffer (U.S. Geological Survey, Flagstaff, AZ 86001)

For many problems in geothermometry and geobarometry, high-pressure and high-temperature data are difficult to obtain; however, it is possible to calculate the thermodynamic functions if spectroscopic data are available. A theoretical model has been developed in which an approximation to the lattice vibrational spectrum is based on spectroscopic data. The model is used (1) to extrapolate heat capacity data to high or low temperatures; (2) to predict phase equilibria where direct data are lacking; (3) to discriminate amongst conflicting sets of phase equilibria, calorimetric, spectroscopic, elastic, and crystallographic data; (4) to examine the pressure, as well as temperature, dependence of the thermodynamic functions; and (5) to predict isotopic fractionation factors. The temperature dependences of the thermodynamic functions of 40 minerals have been calculated. For calculation of the pressure dependence (to 100 Gpa) of the thermodynamic functions, averaged mode Grüneisen parameters were derived to give the shift of the lattice vibrational spectrum with pressure. For calculation of oxygen isotopic fractionation factors, separate deformational types of modes are enumerated and identified for the isotopically light mineral on the basis of existing spectroscopic data; a shift of frequency for each group of modes is assumed for the isotopically heavy mineral. Reduced partition functions are obtained from the free energy differences between the isotopically light and heavy species. The model is used to predict the temperature dependence of the fractionation factors for quartz, calcite, albite, muscovite, clinoenstatite, anorthite, diopside, pyrope, grossular, zircon, forsterite, andradite, and rutile. Agreement with laboratory obtained values is good enough to suggest that model values can be used in low-temperature problems in oceanic, geothermal, or uranium geochemistry where laboratory data cannot be obtained.

V 59

MAGNESIUM IN ANORTHITE: SYNTHESIS AND PETROLOGICAL SIGNIFICANCE OF $CaMgSi_3O_8$

C. B. Sclar
A. I. Benimoff (both at: Department of Geological Sciences, Lehigh University, Bethlehem, PA 18015)

Feldspar of composition $CaMgSi_3O_8$ was synthesized at 1200°C from high-purity oxides at a bulk composition corresponding to an equimolar mixture of diopside and silica. Thirty-one X-ray powder diffraction maxima were indexed on a monoclinic cell with dimensions based on a least-squares refinement program (9214) of: a = 7.814 ± .0015Å, b = 12.923 ± .002Å, c = 13.579 ± .003Å, β = 116.10 ± .02°, Vol. = 1231 ± .3Å^3. We conclude that Mg^{+2} may be structurally incorporated in anorthite through the coupled substitution $Mg^{+2} + Si^{+4} \rightleftarrows 2Al^{+3}$. An analogous substitutional mechanism for Fe^{+2} in anorthite was demonstrated experimentally by Sclar and Kastelic (EOS 60, 421, 1979).

Mg and Fe are minor constituents in plagioclase of lunar basalts and anorthositic cumulates and terrestrial submarine basalts, gabbros, and anorthosites. High-temperature dry gabbros, troctolites, and anorthosites may contain plagioclase which is "clouded" due to minute oriented inclusions of either nonopaque spinel crystallites with compositions on or near the join $MgAl_2O_4$ - $FeAl_2O_4$ or opaque spinel crystallites dominated by $FeFe_2O_4$, Fe_2TiO_4, and $MgFe_2O_4$. "Clouded" plagioclase has been attributed to metamorphic reactions accompanied by diffusion of Mg^{+2} and Fe^{+2} into the plagioclase. The existence of $CaMgSi_3O_8$ and $CaFeSi_3O_8$ suggests that oriented spinel crystallites in "clouded" plagioclase develop by exsolution during slow subsolidus cooling according to the reaction: [Mg- and Fe-bearing plagioclase] → $Spinel_{ss}$ + [More sodic Mg- and Fe-poor plagioclase] + excess Ca^{+2} and Si^{+4}. The latter ions may react either with associated opx to produce cpx or hornblende or with contiguous olivine to produce pyroxene and amphibole coronas at plagioclase-olivine interfaces. The concentration of Mg and Fe in igneous calcic plagioclase may constitute a useful geothermometer.

V 60

THERMOMETRY IN THE CONTACT AUREOLE OF THE KIGLAPAIT INTRUSION, LABRADOR

J.H. Berg (Dept. of Geology, Northern Illinois University, DeKalb, IL 60115)
J.A. Docka (Dept. of Geological Sciences, Harvard University, Cambridge, MA 02138)

A wide variety of rock types within the 3-5 km wide contact aureole allows the use of the following geothermometers: Fe-Ti oxides, two-pyroxenes, gar-bio, gar-cord, gar-olivine, opx-ilm, cpx-ilm, and opx-olivine, as well as temperatures determined from the stability fields of pigeonite, Mg-chlorite, muscovite+quartz, and+sil, and chlorite+quartz. For two-pyroxene thermometry, the methods of Wells(W) (1977), Wood and Banno(W-B) (1973), and Ross and Heubner(R-H) (1975) were used. Along a single traverse (Falls Brook) normal to the Kiglapait contact (P ∿ 3 kb), temperatures determined by mineral stability fields and Fe-Ti oxides define a logarithmic temperature profile that ranges from between 925° and 975°C at the contact to between 550° and 600°C at 2600 m. Over the same distance two-pyroxene temperatures range from a high of 1000°C (W), 960°C (R-H), and 930°C (W-B) at the contact to 890°C (W), 720°C (R-H), and 830°C (W-B). The W and W-B temp. profiles are parallel, but the W temperatures are about 70°C higher. The R-H profile is much steeper than the W and W-B profiles, but is not as steep as the profile defined by mineral stability fields and Fe-Ti oxides. The W and W-B methods yield excessively high temperatures, except for rocks that have crystallized at ≥900°C. The R-H method is more accurate, but it also gives high estimates for rocks that crystallized below 900°C; for rocks that crystallized below 700°C, it may be high by 100-125°C. The other thermometers listed above give erratic temperatures, but these are typically lower than those determined by two-pyroxene thermometry. The profile defined by mineral stability fields and Fe-Ti oxides suggests that ambient temperatures at the time of emplacement were probably not lower than about 450°C. This implies an average geothermal gradient of about 45°C/km.

V 61

FE-MG CATION EXCHANGE THERMOMETRY AND BAROMETRY OF PARAGNEISSES FROM THE CHURCHILL STRUCTURAL PROVINCE, SASKATCHEWAN, CANADA.

Peter A. Nielsen (Department of Geology, University of Alberta, Edmonton, Alberta, Canada T6G 2E3)

A suite of pelitic paragneisses from the Churchill Structural Province of the Canadian Shield from south of the Athabasca Basin, Saskatchewan, comprising portions of the Western Craton, Cree Lake Zone, Rottenstone Complex and Southeastern Complex have been studied. Microprobe analyses of co-existing cordierite-garnet and biotite-garnet pairs from quartz-plagioclase K-feldspar-sillimanite-biotite-cordierite-garnet gneisses have been used to calculate the pressure-temperature environment of equilibration using Fe-Mg cation exchange thermometry and barometry.

Samples from the Archean Western Craton, which also contain spinel and hypersthene, record the highest P-T environment (P>4.8kb, T>650°C and $X_{H_2O} \leq 0.4$). Minor retrograde re-equilibration is present in some samples (P≤4.1kb, T<550°C).

Samples from the Aphebian age Cree Lake Zone, Rottenstone Complex, and Southeastern Complex, which lack spinel and hypersthene, record lower P-T conditions and generally display more extensive retrograde re-equilibration during the waning stages of the Aphebian metamorphic episode. From west to east, pressure ranged from 4.4 to 3.5kb and temperature ranged from 650 to 600°C with $X_{H_2O} \approx 0.5$. Biotite-garnet thermometry records the final thermal equilibration at T≈450°C.

Samples from the major shear zones which separate these major thermotectonic units are characterized by lower T, muscovite bearing assemblages.

V 62

A TEST OF NEW GARNET-CLINOPYROXENE EXCHANGE GEOTHERMOMETERS

Craig A. Johnson
Eric J. Essene(both at Dept. Geological Sciences University of Michigan, Ann Arbor, MI 48109)
Steven R. Bohlen(Institute of Geophysics and Space Physics, UCLA, Los Angeles, CA 90024)

Three new formulations of the widely applied garnet-clinopyroxene K_D(Mg-Fe) geothermometer by Ganguly(G)(1979), Ellis and Green(EG)(1979) and Saxena(S)(1979) have been tested in a granulite terrane in the Adirondack Mtns., NY. Microprobe analyses of 43 gn-cpx pairs have been obtained by three analysts, Stoddard(1976), Bohlen(1980) and Johnson(unpbd.), in a variety of orthogneisses ranging from anorthosite and charnockite to gabbro. Results have been compared to oxide and feldspar thermometry(Bohlen et al., 1980), the accuracy of which has been demonstrated by good agreement with numerous phase equilibria in quartz-saturated gneisses and marbles. These temperatures decrease smoothly from near 800°C in the Highlands to 650°C in the Lowlands and S. Adirondacks. In contrast, all three gn-cpx thermometers give erratic and systematically high results. Estimating Fe^{3+} from stoichiometry, EG averages 778°C in the Highlands with a range of 672-941°C, and 733°C(686-847) in the Lowlands and S. Adirondacks. G averages 870°C (776-1010) and 828°C(793-944) while S averages 904°C(750-1064) and 843°C(730-1080) for the same areas, respectively. Plots of calculated T versus Mg/(Mg+Fe) in cpx at constant T(from Bohlen et al., 1980) show that although none of the formulations have a systematic Fe-Mg compositional dependence, results vary erratically with bulk composition. A similar plot shows K_D varying erratically indicating that K_D is not a simple function of T and Mg/(Mg+Fe). Gn-cpx thermometry, when compared with oxide and feldspar thermometry, is insufficiently refined to give accurate and precise T in a granulite terrane. Imprecise solution models, minor impurities in rocks and poor experimental control at granulite temperatures remain problems.

V 63

GARNET-PYROXENE EQUILIBRIA, AND PALEOGEOTHERM

Ganguly, Jibamitra & Lane, Douglas L. (Dept. of Geosciences, Univ. of Ariz., Tucson, AZ 85721

We have evaluated the applicability of currently available garnet-clinopyroxene geothermometers (based on Fe-Mg partitioning) to ultramafic rocks by comparing the predicted temperatures

with independent experimental data, and the predicted compositional dependence of K_D with both observational and experimental data. Ganguly's geothermometer seems to work well within its stated compositional limits ($XCaSiO_3$ in CPX $\geq$ 0.40, and small amounts of trivalent ion other than Al). Ellis & Green's data (CMP, 1979) usually give lower temperature, on the average by $\sim$ 40°, and their deduced K_D vs. Ca relation does not match a substantial number of experimental and observational data, for which Ganguly's relation provides a more satisfactory fit. The reason for this disagreement is discussed. A thermodynamic model is presented to correct Ganguly's geothermometer for the effect of variable $CaSiO_3$ in CPX. The P-T condition of garnet lherzolite nodules from Lesotho kimberlites (Boyd, 1973, GCA) have been estimated on the basis of Ganguly's Gt-CPx geothermometer, and Lane & Ganguly's data (GSA Abs. 1979; JGR, in press) on Al_2O_3 solubility in enstatite. The 'sheared nodules' seem to have formed at greater depths than the 'granular' ones, but unlike Boyd's estimates, there does not seem to be an 'inflection' of the paleogeotherm between the two groups of nodules. When the effect of variable Ca in CPx is taken into account, these nodules define a geotherm similar to that derived by Mercier & Carter (JGR, 1975), which diverges, with increasing depth, towards higher temperature from Clark & Ringwood's Shield geotherm.

V 64

THE EFFECT OF MAGNESIUM ON ORTHOPYROXENE-OLIVINE-QUARTZ STABILITY: ORTHOPYROXENE GEOBAROMETRY

S. BOHLEN (Inst. of Geophysics and Planetary Physics, UCLA, Los Angeles, CA 90024)
A. L. BOETTCHER (Dept. of Earth and Space Sciences and Inst. of Geophysics and Planetary Physics, UCLA, Los Angeles, CA 90024)

We have determined the effect of Mg on the stability of Fe-rich opx (ferrosilite) relative to fayalitic olivine+quartz to assess the effect of this and other components on opx barometry. Reaction reversals were obtained in a piston-cylinder apparatus with 2.54 cm piston and 8.89 cm master ram using KBr furnace assemblies and Ag capsules. Experiments indicate instability of $Fs_{95}En_5$ below 12.4, 11.0, 9.5 kb and $Fs_{90}En_{10}$ below 10.5, 9.3, 8.0 kb at 1000°, 900° and 800°C, respectively. $Fa_{95}Fo_5$+quartz and $Fa_{90}Fo_{10}$+quartz react to opx above 10.8, 9.4, 8.0 kb and 9.2, 7.8, 6.4 kb at 1000°, 900° and 800°C, respectively. The boundaries were reversed using starting materials with initially low K_D values ($Fs_{95}En_5+Fa_{95}Fo_5$+qtz; $Fs_{90}En_{10}+Fa_{90}Fo_{10}$+qtz) and high K_D values ($Fs_{80}En_{20}+3Fa_{100}$ + qtz; $Fs_{80}En_{20}+Fa_{100}$+qtz). Between the pressure values indicated, opx+oliv+qtz coexist with their relative proportions and Mg-Fe ratios changing in response to P-T. Each mole % $MgSiO_3$ extends opx stability by ~ 0.34 kb relative to $FeSiO_3$ determined by Bohlen et al. (1978). These data combined with previous results for Mn (Bohlen and Boettcher, 1978) allow confident application of opx-oliv-qtz barometry. In the southern Labrador Trough, $Fs_{93}En_5Wo_1Rh_1$ (Klein, 1978) requires P≥8kb for T≈700°C. $Fs_{92}En_2Rh_5Wo_1$ in Lofoten, Norway (Ormaasen, 1978) requires P≥9.5 kb for T≈800°C. In the Mt. Marcy area of the Adirondacks, Jaffe et al. (1978) report $Fs_{91}En_5Wo_2Rh_2$, indicating P≥7.8 kb for T≈ 750°C. P-T conditions for these and other granulite terranes indicate geothermal gradients of nearly 30°/km, which are in conflict with the 70-100°/km gradients proposed by many workers for pℰ charnockite terranes.

V 65

GEOTHERMOMETRY AND KINETICS IN A TWO-SPINEL PERIDOTITE NODULE

Douglas Smith (Dept. Geological Sciences, Univ. Texas, Austin, Texas 78712)
Roden, M.F. (Dept. of Earth and Planetary Sci., M.I.T., Cambridge, Massachusetts 02139)
(Sponsor: Debra Stakes)

Compositions and zoning of minerals in a two-spinel peridotite from minette in the Navajo province of the Colorado Plateau provide unusual opportunities to compare geothermometers at low mantle temperatures and to study equilibration rates. The xenolith contains pleonaste ($Mg_{.55}Fe_{.45}Al_{1.62}Fe_{.10}Cr_{.28}O_4$) and magnetite ($Mg_{.16}Fe_{.89}Mn_{.01}Al_{.18}Fe_{1.38}Cr_{.32}Ti_{.06}O_4$) related by granule exsolution, together with olivine (Fo85), orthopyroxene (3.5% Al2O3), and clinopyroxene. Both two-spinel equilibria and several olivine-pleonaste geothermometers suggest temperatures below 700°C, confirming the general accuracy and continued equilibration of these geothermometers at low temperatures. Calculated olivine-magnetite temperatures are much too high. Two-pyroxene temperatures (Wells, 1977) are near 800°C. Olivine is zoned in Ca, Fe, and Mg within 50 micrometers of spinel by exchange with local grain boundary melts. Gradients at pleonaste-magnetite contacts reflect multicomponent diffusion after heating by minette; slight "uphill" diffusion of Cr occurred. Effective diffusivities near 1100°C, estimated by comparison with gradients in olivine, are near 10^{-11} for Al in magnetite and 10^{-12} for Al in pleonaste: an average Mg value is in the same range. The time interval between plucking of the inclusion and minette solidification is calculated as 20-80 hours.

V 66

CORDIERITE STABILITY IN THE SYSTEM SiO_2-Al_2O_3-MgO (FeO)-H_2O AT HIGH T.

J. Martignole, Département de Géologie, Université de Montréal, Montréal, P.Q., H3C 3S7
J.C. Sisi, Génie Chimique, Ecole Polytechnique, Montréal, P.Q., H3C 3A7
(Sponsor: C. Brooks)

The high-grade assemblage Cd-Ga-Si-Qz can be thermodynamically modelled by considering the metastable end-member reactions:

3 MgCd ⇄ 2 Py + 4 Si + 5 Qz (1) in the H_2O free system and 3 MgCd, nH_2O ⇄ 2 Py + 4 Si + 5 Qz + 3 nnH_2O (2) in the hydrated system.

Hydrous cordierite is neither a hydrate nor a solid solution between water and anhydrous cordierite and when nH_2O (number of moles of H_2O in Cd) is plotted against P_{H_2O}, the resulting isotherms are similar to P_{H_2O} adsorption isotherms caracteristic of zeolitic minerals. Reaction (2) can thus be considered as a combination of reaction (1) with a physical equilibrium of the type nH_2O (in Cd) ⇄ nH_2O (in vapor phase). Starting from a given T on the thermodynamically calculated PT curve for reaction (1), introducing water into cordierite results in a reduction of its chemical potential; equilibrium can only be restored by increasing total pressure by ΔP. Reduction of chemical potential and the corresponding ΔP can be calculated from data on water content of MgCd using the thermodynamics of real solutions applied to an adsorption model. Values of ΔP for nH_2O = 0.1 to 1.2, when plotted in a PT grid, lead to chemical equilibrium isopleths for each value of nH_2O. Entropies of hydrated cordierite can be obtained from these isopleths. The coincidence of nH_2O values in both chemical and physical equilibrium gives the upper stability limit of physico-chemical equilibrium (2) (9200 bars at 500°C and 11200 bars at 900°C, slope 5 b/°C). Using available PVT values for H_2O and CO_2, X_{H_2O} isopleths for (2) can be drawn from nH_2O isopleths.

V 67

AN EMPIRICAL GEOTHERMOMETER FOR LHERZOLITES BASED ON AL-SOLUBILITY IN OPX

H.A. Seck (Mineralogical Institute, University of Köln, West Germany)
Th. Sachtleben (Mineralogical Institute, University of Köln, West Germany)
(Sponsor: Werner Schreyer)

Application of experimentally determined Al-solubilities of opx in the MgO-Al_2O_3-SiO_2 system (FUJII,1976) as a geothermometer is hampered by the fact, that Al-solubility of opx in natural rock systems is underlying additional chemical control. Study of phase equilibria in two peridotite suites of the Dreiser Weiher, West Germany, which are nearly isothermal, as deduced from two-pyroxene geothermometry, showed that at a given temperature Al- (and Cr-) solubilities of opx are strongly dependant on the mol fraction of $FeCr_2O_4$, Y(Cr), in spinel. Temperatures calculated using FUJII's experimental data are by about 200°C higher for the most Cr-rich compared to the most Al-rich spinel in each suite. Ideal solution correction allowing for additional components present in natural systems is inadequate to compensate the errors caused by the presence of Y (Cr) in natural spinels.

An empirical equation making allowance for Y (Cr) has been derived in this study to calculate temperatures from the reaction $Mg_2SiO_4+MgAl_2SiO_6 \rightleftharpoons Mg_2Si_2O_6+MgAl_2O_4$.

V 68

GEOLOGIC PRESSURE DETERMINATIONS FROM FLUID INCLUSION STUDIES

E. Roedder (U.S. Geol. Survey, Reston, VA 22092)
B. J. Bodnar (Dept. Geosciences, Penn. State Univ., Univ. Park, PA 16802)

Temperatures by inclusion homogenization usually must be corrected for pressure via an independent estimate of pressure at the time of inclusion trapping, e.g., from geologic reconstructions of the probable overburden. Quite apart from such independent estimates, many methods have been proposed to obtain, estimate, or place upper or lower limits on the pressure at the time of inclusion trapping from the inclusions themselves. We have found that, unfortunately, several of the most commonly used methods have major errors in concept and/or application that invalidate the results. Included here are the methods of Lemmlein and Klevtsov, and of Lyakhov, for inclusions finally homogenizing by the solution of a salt crystal, that of Nacken for separate CO_2 and H_2O inclusions, and that of Naumov and Malinin for mixed CO_2-H_2O inclusions.

Unless an independent geothermometer is also available, single inclusions can yield only data that are functions of both P and T, but pairs of inclusions trapped from fluids that were immiscible at trapping (e.g., water and steam, or some water and CO_2) can yield both P and T. Inclusions of an immiscible water (or CO_2) phase, along with silicate melt inclusions, are a special example, in that the latter, in effect, provide an independent thermometer; hence, the pair can provide a geobarometer.

All such fluid-inclusion pressure determinations require 1) careful microscopy to prove inclusion origin and freedom from subsequent alteration processes; 2) good thermometric data on both heating and cooling; 3) good compositional data (in part from (2)); and 4) good experimental P-V-T-X data on the appropriate systems, over the required range. Lack of (4) is the most serious handicap to accurate geobarometry at present.

V 69

SYSTEMATICS OF "STRETCHING" OF FLUID INCLUSIONS AS A RESULT OF OVERHEATING

Bodnar, R. J. (959 National Center, U. S. Geological Survey, Reston, VA 22092)
Bethke, P. M.
(Sponsor: H. L. Barnes)

In 1973, Larson, Miller, Nadeau, and Roedder showed qualitatively that homogenization temperatures of fluid inclusions in fluorite and sphalerite may be subject to errors if overheated by an unknown amount. This error is due to an apparently permanent, non-elastic deformation of the walls of fluid inclusions in response to the increase in internal pressure of the inclusion as the temperature is raised above the homogenization temperature. In the present study, more than 1300 measurements on fluid inclusions in fluorite and sphalerite indicate that this increase in volume, or "stretching", proceeds in a systematic and somewhat predictable manner. The amount of overheating necessary to initiate stretching depends on the PVT-properties of the inclusion fluid, inclusion size, and physical properties of the host mineral. The data show that the internal pressure necessary to initiate stretching of inclusions in fluorite is inversely related to inclusion volume. Once begun, the amount of stretching (ΔT_H) as a function of the amount of overheating (ΔT_{OH}) is constant at $\Delta T_H/\Delta T_{OH}$ = 0.5. Sphalerite is more resistant to stretching than fluorite and the data are less systematic. The results of this study show that the measured homogenization temperature of a fluid inclusion may be considerably higher than the "true" homogenization temperature if the inclusion has been overheated, either accidentally in the laboratory or naturally by later thermal events. Furthermore, criteria commonly used as evidence that a fluid inclusion has not leaked are invalid for the inclusions examined in this study. However, the systematic relationship between the internal pressure necessary to initiate stretching and inclusion volume provides a means of recognizing previously stretched inclusions and estimating the magnitude of post-entrapment thermal events.

General Geochemistry I

Queen's Quay
Saturday A.M.
Michael P. Gorton (Univ. of Toronto), Presiding

V 70

THE CARBON ISOTOPIC COMPOSITION OF DIAMONDS

Peter Deines Dept. Geosciences, The Pennsylvania State University, University Park, Pa. 16802

(Sponsor: S. S. Alexander)

Three hundred and thirty new ^{13}C analyses of diamonds are presented, indicating in conjunction with earlier work, a range of about 30 o/oo in the carbon isotopic composition of diamonds. The frequency distribution of diamond isotopic compositions shows a very pronounced mode at -5 to -6 o/oo vs. PDB, a sharp boundary at about -1 o/oo, and a large negative skewness. Analyses of diamonds from the Premier and Dah Carl Mines, South Africa, demonstrate that: (1) differences in isotopic composition that can be related to diamond color or shape are < 1 o/oo; (2) the mean isotopic composition of associated kimberlite carbonates is 1 to 2 o/oo smaller than that of diamonds; (3) the mean isotopic compositions of diamonds from the two pipes differ significantly; (4) the isotopic composition variability differs from one mine to the other. Computations were carried out evaluating the effects on the diamond isotopic composition of: (1) various precipitation processes; (2) the abundance of the vapor species H_2,H_2O, CH_4, CO_2, CO, and O_2; (3) initial isotopic composition variability of the source carbon; (4) variations of carbon isotope effects resulting from changes in pressure and temperature; (5) reservoir effects. Fifty-eight genetic models were investigated for compatibility with the isotopic distribution in diamonds and associated carbonate. The modeling does not permit an unambiguous answer to the question whether or not vapor participated in diamond formation, although the presence of methane during the diamond formation process is compatible with the isotopic composition data, possible oxygen fugacities in the mantle, and with the composition of gases liberated from diamonds. In all probability isotope effects in the formation of diamonds were small, and the very large range in the isotopic composition of diamonds observed was inherited from the source carbon.

V 71

MINERAL INCLUSIONS IN DIAMOND FROM GHANA AND VENEZUELA

Irene S. Leung (Department of Geology, Herbert H. Lehman College of the City University of New York, Bronx, New York 10468)

Approximately 6000 and 50,000 diamond crystals (1-3mm in size) from Ghana and Venezuela, respectively, were examined. Apart from numerous black and opaque inclusions not yet identified in detail, silicate mineral inclusions from the two localities are distinct.

Locality	No. of Diamond	Coexisting Inclusions
GHANA	45	Cr-spinel + olivine
	28	Cr-pyrope + olivine
	4 Cr-spinel +	Cr-pyrope + olivine
	Numerous	olivine
VENEZUELA	62	pyrope-almandine
	38	omphacite
	31	pyrope-almandine + omphacite

Multiple inclusions of one or more phases are common in a single host, many of which even occur in contact, indicating truly equilibrium relations at time of crystallization.

The Ghanaian suite represents two assemblages: garnet peridotite and spinel peridotite. If the former represents a less depleted mantle or occurs at greater depth than the latter, then the Earth's mantle must have a fine layered structure where the specimens crystallized, and that the four crystals containing the assemblage garnet-spinel-olivine must have come from the boundary zone between these two layers.

The Venezuelan inclusions indicate a mantle of eclogitic composition. Coesite and a Ti-rich phlogopite penetrating a garnet inclusion have also been found. It is concluded that composition of the upper mantle is inhomogeneous and that diamonds found in Venezuela and Ghana are unrelated genetically even before the evolution of the Atlantic Ocean.

V 72

$^{187}Os/^{186}Os$ AS A GEOLOGICAL AND PETROGENETIC TRACER.

J-M LUCK, C.J. ALLEGRE (Laboratoire de Géochimie et Cosmochimie, 4, Place Jussieu, 75230 PARIS CEDEX 05 - FRANCE).

^{187}Re decays to ^{187}Os with a decay constant $\lambda = 1.61\ 10^{-11} y^{-1}$. Thus one expects to observe a variation of $^{187}Os/^{186}Os$ through geological times for terrestrial materials, and this isotopic ratio can be used as a tracer as Sr, Pb and Nd isotopes.

We have measured Re, Os and $^{187}Os/^{186}Os$ by sputtering mass spectrometry after chemical separation using dissolution and spiking with ^{185}Re and ^{190}Os enriched solutions, distillation of Os and ion exchange purification of Re and Os. Reproducibility and precision of 1 % for Re and Os concentrations and ± 0.3 % for the $^{187}Os/^{186}Os$ isotopic ratios have been achieved. An isochron for iron meteorites and chondrites has resulted in a value of $^{187}Os/^{186}Os$ at the time of formation of the solar system of 0.83.

Osmiridium and osmium rich minerals associated with ultramafic materials of various ages has been analyzed. They define a closed system evolution line for the Earth mantle from 4.55 b.y. to now ($^{187}Os/^{186}Os$ from 0.83 to 1.12) which corresponds to a $^{187}Re/^{186}Os$ ratio of 3.2. This value is that for most meteorites and the moon. Our data thus show that this ratio is fairly constant in the solar system. A Bushweld sample from Merensky Reef is very unusual in that its $^{187}Os/^{186}Os$ ratio is 1.46. Continental crust materials can be studied by analysing sulfide samples. Because the Re/Os ratio is continental crust is 300 times higher than that in the mantle, small proportions of continental crust recycled into the mantle will be easily detected. Several examples of granitoid genesis will be discussed in light of this isotopic tracer.

V 73

$\delta^{18}O$ OF PLANT SILICA AND PALEOCLIMATES

Miguel Bombin (Dept. of Anthropology, Univ. of Alberta, Edmonton, Alberta, Canada T6G 2H4)
Karlis Muehlenbachs (Dept. of Geology, Univ. of Alberta, Edmonton, Alberta, Canada T6G 2E3)

$\delta^{18}O$ of phytoliths and tabashir was measured to evaluate their use as paleoclimatic indicators. These are, respectively, forms of opaline silica deposited in leaves (particularly abundant in monocots) and the hollowed internodes of bamboos, which are commonly preserved in soils and sediments. The phytoliths were extracted by wet oxidation from Gramineae of different geographical locations, and from specimens grown in a greenhouse under relatively controlled conditions. The same kinds of analytical problems found in studying other forms of biogenic silica occurred, due to the loosely bound water. The samples were dried at 200°C under vacuum for 24h before fluorination. Oxygen yields averaged 14-15 µmoles/mg, and no correlation was found between yields and $\delta^{18}O$. An overall reproducibility of about 0.5‰ can be attained at the present stage of research. Water from leaves of grasses, grown in the greenhouse at 25-29°C and relative humidity of about 50%, shows an enrichment in ^{18}O of 12 to 16‰ with respect to H_2O used for watering, because of evapotranspiration, in agreement with results of other authors. The measured ^{18}O-fractionation factor between phytoliths and water of these plants yielded temperatures identical to that at growth. This technique can not be applied directly as a paleothermometer because the enrichment in ^{18}O leaf water is highly dependent upon relative humidity. However, $\delta^{18}O$ of fossil phytoliths can help to elucidate terrestrial paleoclimates for changes in humidity and temperature are related. Preliminary data from plant silica from different locations supports the above suggestion. Tabashir SiO_2 is apparently in isotopic equilibrium with the culm water (which has possibly a very similar $\delta^{18}O$ as the local rain water).

V 74

THE KINETIC TREATMENT OF GEOCHEMICAL CYCLES

Antonio C. Lasaga, Department of Geosciences, The Pennsylvania State University, University Park, PA 16802

Treating geochemical cycles as complex kinetic chemical reactions, we have applied recent kinetic techniques to the classical concepts (e.g., residence times and response times) employed in geochemical cycles. Matrix algebra serves as a powerful tool to give insight into the response and stability of a linear geochemical cycle. The general behavior of a linear cycle can be predicted with the aid of a theorem proved by us about the geochemical cycle matrix, which guarantees stability in all cases. Several important theorems are also proven which are pertinent to this development.

Extension of the method allows also an analysis of the more interesting non-linear coupled geochemical cycles. For coupled and non-linear cycles, non-trivial questions arise concerning the possibility of multiple steady states and of oscillatory behavior. The current work on the irreversible thermodynamic treatment of complex chemical reactions suggests that the presence of an "autocatalytic step" in the geochemical cycle is required to lead to instability or oscillatory behavior. We have applied these techniques to the coupled carbon-oxygen geochemical cycle and we do not find such oscillatory behavior. However, we do show that the coupling and feedback between two cycles will lead to a faster response time i.e. will increase the stability of the system. The consequences and applications of these powerful tools to more varied cycles should prove very valuable.

V 75

GENERATION OF CH_4-RICH FLUID INCLUSIONS IN ALKALINE ROCKS*

T. M. Gerlach (Sandia Laboratories,** Albuquerque, NM, U.S.A., 87185)

The Canadian and Soviet geochemical literature contains several reports of CH_4-rich fluid inclusions in alkaline intrusives. Nepheline grains commonly host these inclusions, which give formation pressures and temperatures of 100-150 MPa (1-1.5 kbar) and 475-775 K (Sobolev et al., 1974). The inclusions contain 70-90% CH_4, 10-30% CO_2, and condensed hydrocarbons or "bituminous compounds" with $\Delta^{13}C$ indicating an inorganic origin (Petersilie and Sorensen, 1971). Gold has recently suggested an origin by mantle-outgassing of CH_4 along deep seismic and rift zones often associated with alkaline complexes.

Recent studies of volcanic gas data (Gerlach, 1980) from Nyiragongo volcano indicate gases from nephelinite magma are CO_2-rich (35-50%) with f_{O_2} between QMF and MW. Calculated equilibrium compositions for the cooling of Nyiragongo-like gases at 100 MPa yield little CH_4 (< .3%). CH_4 concentrations of 45-80% are calculated, however, for f_{O_2} buffering of the gases at or slightly below QMF during cooling; CH_4 increases abruptly and the gases become supersaturated in C below 850 K.

These results suggest that anomalous CH_4 and bituminous matter form in alkaline intrusives by subsolidus CO_2/H_2O fluid-rock interactions associated with fracture and recrystallization events during cooling, provided that rock-buffering of f_{O_2} is maintained at or below QMF. They also support an earlier proposal for the volcanic origin of the CH_4-rich waters of Lake Kivu on the southern flank of Nyiragongo (Burke, 1963).

V 76

URANIUM TRANSPORT IN MICROCRACKS IN SOURCE ROCKS?

Louis J. Caruso (Department of Earth and Planetary Sciences, M.I.T., Cambridge, MA 02139)
Elaine R. Padovani
Gene Simmons

New data obtained on 50 specimens of core from a 3000-foot hole drilled in granite at the Redstone Quarry, near North Conway, New Hampshire include the following: (1) Contents of K, U, Th are variable and range from .1 to 5%, 1 to 26 PPM, 6 to 105 PPM, respectively. (2) Sealed cracks are abundant and range in width from 0.1µ to 1mm. (3) Fe-rich chlorite, Fe-rich clay, siderite, and quartz are the major crack sealing phases. Calcite, microbreccia, rutile, and hematite crystals are minor crack sealing phases. (4) Both open microcracks and partially sealed microcracks, although rare, do exist in situ. (5) Nb-rich minerals occur in chlorite, in biotite, and in microcracks. (6) Amphibole and biotite grains intersected by microcracks are either partly or completely altered to chlorite plus other phases. (7) U-bearing phases (allanite, apatite, monazite, zircon) are both intersected by cracks and located within cracks as discrete grains.

We suggest the tentative hypothesis that U and Th have been transported in CO_2-rich waters through networks of microcracks in this source rock.

V 77

UNIDRIECTIONAL DIFFUSION OF NUCLEAR WASTE MATERIAL IN ARCHO-1 BASALT, MT. AIRY GRANITE AND SDO-1 SHALE

A. I. Kilinc (Department of Geology, University of Cincinnati, Cincinnati, Ohio 45221)

Diffusion of elements of nuclear waste material (SPC-2) into basalt, granite and shale host rocks has been theoretically and experimentally studied. Theoretically, a unidirectional diffusion model with the following initial (I.C.) and boundary conditions (B.C.) were used to analyze the concentration profiles of elements:

$$\frac{\partial c}{\partial t} = D\frac{\partial^2 c}{\partial x^2} \qquad (1)$$

I.C. $t < o \quad C = C_o$ for all x

B.C. $t > o \quad C = C_o$ at $x = \pm \ell$

B.C. $t > o \quad \left.\frac{\partial c}{\partial x}\right|_{x=o} = 0$

where C = concentration of the element at time t; C_o = initial concentration, and C_s = concentration of the element at the reservoir.

Solution of equation (1) yields

$$C' = \frac{C_s - C}{C_s - C_o} = \sum_{n=1}^{\infty} \frac{2(-1)^n}{\pi(n-\frac{1}{2})} \exp(-a_n^2 \cdot \theta) \cos a_n \cdot \xi \qquad (2)$$

which has been evaluated for various values of length and diffusivity. Dimensionless plots of (1-C') versus (X/L) show that for D = 10^{-6} cm^2 sec^{-1} and L=10 cm, steady state is reached in about four months.

Comparison of the theoretically calculated concentration versus time profiles with the experimental data on Cs, Ce, Sm, Co, Hf, Ba, Sr, Ni, Cr, Nd, Au and La obtained at 7500 psi and under a 36°C/cm temperature gradient suggest that D values are probably lower than 10^{-6} cm^2 sec^{-1}. Furthermore there is significant interaction between these elements and the host rocks.

V 78

URANIUM GEOCHEMISTRY OF ORCA BASIN

F.F. Weber (Department of Marine Science, University of South Florida, St. Petersburg, FL 33701)
W.M. Sackett

Orca Basin, an anoxic, brine filled depression at a depth of 2200 meters in the Northwestern Gulf of Mexico continental slope, has been studied with respect to its uranium geochemistry. Uranium concentration profiles for four cores from within the basin were determined by neutron activation using the fast, precise and nondestructive method of delayed-neutron counting. Uranium concentrations ranged from 2.1 to 4.8 ppm on a salt-free and carbonate-corrected basis. Percent and $\delta^{13}C$ organic carbon profiles were also determined for each of the four cores. Several of these profiles were found to vary inversely with the corresponding uranium profiles.

For comparison, cores from the brine-filled Suakin and Atlantis II Deeps, both in the Red Sea, were also analyzed. Uranium concentrations ranged from 1.2 to 2.6 ppm in the Suakin Deep and from 8.0 to 11.0 ppm in the Atlantis II Deep. No significant correlation was found between uranium concentrations and organic carbon concentrations and $\delta^{13}C$ values for these cores.

Although anoxic conditions are necessary for uranium uptake by marine sediments, other factors such as dilution by rapidly depositing materials and uranium supply via mixing and diffusion across density gradients also are quite important in determining uranium concentrations in anoxic marine sediments.

V 79

HG DISTRIBUTION IN SELECTED GEOTHERMAL AREAS IN CALIFORNIA AND OREGON

Johan C. Varekamp (Dept. of Geology, Arizona State University, Tempe, AZ 85281)
John Copp (Dept. of Geology, Arizona State University, Tempe, AZ 85281)
Peter R. Buseck (Dept. of Geology, Stanford University, Stanford, CA 94305)

Hg distribution has been studied in a number of geothermal areas, including the Coso KGRA (CA), Lassen Park (CA), Mt. Hood (OR), the Vale KGRA (OR) and the Alvord valley (OR). In all these areas significant Hg enrichments were encountered around the surface expressions of the geothermal systems. Statistical studies show a trimodal distribution of Hg for most areas. A peak population is present in the direct vicinity (some tens of meters) of the fumaroles. An aureole population is found surrounding the fumarolic zones (extending out to several hundreds of meters) and a background population is found in parts unaffected by geothermal activity. In most areas mean background values range from 10 to 30 ppb Hg, tenfold enrichments are found in the aureoles and enrichments up to several thousand times are encountered in the fumarolic areas. Size and magnitude of the aureoles is influenced by soil type, hydrothermal fluid characteristics and structural features. Sampling in the fumarolic areas on top of Mt. Hood and Lassen Peak indicated surprisingly low Hg enrichments. Most of the Hg in the geothermal aureoles is presumably derived from heated and leached country rocks. Additional trace element patterns are providing better insight into the chemical processes of transport and enrichment of Hg.

V 80

RADON FLUX FROM THE EARTH: METHODS OF MEASUREMENT BY THE NUCLEAR TRACK TECHNIQUE

R.L. Fleischer (General Electric Research and Development Center, Schenectady, NY 12301)

The ^{222}Rn flux from the ground is important as an indicator of the near-surface uranium content and as a measure of the input to the atmosphere, both to determine large-scale budgets of atmospheric radioactivity and to monitor local assaults on human health. The nuclear track technique, which can be most simply used to measure concentration of radon directly, can also be employed to determine radon flux by means of gradients in concentration in the ground, at its surface, or above the surface. Diffusional properties or emanation properties need to be assessed, but often can also be measured by track counting. Measurements in four distinct locations are outlined: (1) subsurface measurements in holes, (2) surface measurements using impermeable barriers, (3) above-the-surface measurements in radon-accumulating cans, and (4) trans-surface measurements using permeable barriers.

Observations at Thoreau, NM give a flux of 1.4 atoms/cm^2-sec over an area of 60,000 m^2. At Scotia, NY 1.1 to 1.2 atoms/cm^2-sec are measured over an area of 100 m^2.

V 81

PROCESSES AND TIMING OF OCEAN CRUST ALTERATION

Staudigel, H. (Lamont-Doherty Geological Observatory, Palisades, N.Y. 10964)
Hart, S.R. and Richardson, S.H. (Center for Geoalchemy, M.I.T., Cambrdige, Mass. 02139)
Muehlenbachs, K. (Dept. of Geology, University of Alberta, Edmonton, T6G 2E3, Alberta, Canada.

Evidence from ^{18}O, $^{87}Sr/^{86}Sr$, Sr, K, Rb, Cs data from vein materials and bulk rocks from DSDP sites 332 B, 417A, and 418A, as well as petrographic studies suggest that the upper 500 m of the basaltic layer II altered in four distinct stages with a short-lived time schedule.

Stages I and II are characterized by the formation of palagonite and smectite, respectively. Their circulating solutions contained a significant amount of basalt-derived Sr, with a positive correlation to their temperatures, which ranged from stage I and II solutions at Site 418A from 15-80°C. Smectites at Site 418A and 417A show cation exchange behavior similar to that observed for detrital montmorillonites: alkalies are adsorbed into interlayer positions according to their relative hydration energies.

The third stage of ocean crust alteration is mainly characterized by the formation of carbonates, which precipitated from solutions with Sr-isotopic composition identical to seawater to at least 500 m depth. This indicates that no Sr exchange between stage III solutions and basalt occurred to depths reached by oceanic basement drilling. The temperatures of stage III solutions at site 418A ranged from 15-50°C, lower than the range for stage I and II solutions. The duration of carbonate precipitation was short-lived, slightly exceeding the duration of stage II alteration.

During the stage IV of ocean crust alteration, the only chemical change observed was a dehydration of hydrous phases (smectites, palagonites).

V 82

FORMATION OF VEIN MINERALS IN BASALT FROM NAURU BASIN, DSDP LEG 61

Patricia O. Book (Dept. of Earth Sciences, Iowa State University, Ames, Iowa 50011)
Kenneth E. Windom

Veins containing abundant alteration minerals are common in the slightly altered basalts recovered from Hole 462A, DSDP Leg 61. Three vein mineral assemblages are observed: 1) a quartz-rich, celadonite-bearing assemblage (quartz, calcite, celadonite, smectite, Fe-oxide) in Cores 14-19; 2) a quartz-rich, pyrite-bearing assemblage (quartz, calcite, pyrite, smectite) in Cores 19-29; and 3) a quartz-poor, zeolite-bearing assemblage (smectite, clinoptilolite, calcite, pyrite, ± analcime, ± chabazite, ± apophyllite, ± quartz, ± talc (?).

Two units are recognized in the host igneous rock: An upper unit approximately 155m thick (Cores 14-44), comprising microdiabase and basalt sills that have intruded a sequence of volcaniclastic sediments, and a lower sequence of unknown thickness (Core 44 and below) composed of basaltic flows.

We interpret these data to represent two episodes of vein mineral formation, with an oxidative overprint on the most recent. The initial episode occurred after the outpouring of basaltic flows (lower unit) onto the sea floor. The quartz-poor, zeolite-bearing veins were formed in the flows under conditions of elevated temperatures and low P_{CO_2}, while the thermal gradient was high and P_{CO_2} prior to the formation of a cover of sediments. The second episode followed the intrusion of basalt and microdiabase sills into a thick layer of sediments that had accumulated over the flows. This episode of vein formation occurred under conditions of lower temperature and higher P_{CO_2} than the first episode and produced the quartz-rich assemblage in the upper unit. Later, oxygenated seawater diffused through the sedimentary cover into the top of the upper unit and oxidized the pyrite and smectite, forming Fe-oxide and celadonite.

V 83

PALYGORSKITE AND SEPIOLITE IN SEDIMENTS OFF NORTHWEST AFRICA: SUGGESTED ORIGINS

Joris M. Gieskes (Scripps Institution of Oceanography, La Jolla, CA 92093)
Randall S. Miller (Scripps Institution of Oceanography, La Jolla, CA 92093)
James R. Lawrence (Lamont-Doherty Geological Observatory, Palisades, NY 10964)

Chemical and mineralogical analyses of sediments, as well as interstitial water studies on materials obtained from several DSDP drilling legs in the Atlantic Ocean off Northwest Africa, suggest that a unique assemblage of continental detritus, biogenic silica and salt brines leads to the formation of authigenic palygorskite and sepiolite during the reconstitution of opal-A to opal-CT and quartz. The occurrence of these sepiolite and palygorskite deposits is related to the occurrence of similar deposits on land.

Experimental Petrology

Metropolitan West
Saturday P.M.
D. M. Francis (McGill University), Presiding

V 84

CRYSTAL-MELT EQUILIBRIA IN SILICA-ALBITE AND SILICA-ANORTHITE BINARIES REVISITED

R. Hon (Dept of Geology and Geophysics, Boston College, MA 02167)
D.F. Weill (Dept. of Geology, University of Oregon, Eugene, OR 97403)
A. Navrotsky (Dept. of Chemistry, Arizona State University, AZ 85281)

Solution and drop calorimetry data on glass samples within SiO_2-$NaAlO_2$ and SiO_2-$Ca_{.5}AlO_2$ binaries as well as model dependent entropy of mixing are employed in calculating saturation surfaces in crist.-albite and crist.-anorthite systems. Input data include: 1) enthalpies of fusion: 15.5, 32, 11 kcal per mol of $NaAlSi_3O_8$-analbite, $CaAl_2Si_2O_8$-anorthite and Si_4O_8-cristobalite; 2) enthalpies of mixing and heat capacities. Although enthalpies of mixing are very small in magnitude (less than 400 cal) they are nevertheless consistent with the experimental phase diagram and with the variations of viscosities with composition.

In agreement with Flood and Knapp (J. Am. Cer. Soc., 51, 1968), the albite-silica binary is best explained by a configurational model numerically equivalent to a model where Al and Si atoms are randomly distributed over a tetrahedral framework "sublattice". Our model for crist.-anorthite binary, however, disagrees with the model of F&K. The best configurational model for Si_4O_8-$CaAl_2Si_2O_8$ liquid mixtures is based also on random distribution of Al and Si atoms within the tetrahedral "sublattice" but with a restriction that two Al atoms must associate as a consequence of double charge of Ca atoms. Na and Ca atoms are positionaly constrained by single Al or by Al-Al associations for charge balance.

V 85

SOLID-MELT STRUCTURE IN A PARTIALLY MELTED OLIVINE-BASALT MIXTURE

P. J. Vaughan
D. L. Kohlstedt (both at: Dept. of Materials Science and Engineering, Cornell University, Ithaca, NY 14853)

The distribution of basaltic melt in a synthetic olivine-rich rock has been examined by electron microprobe, scanning electron microscopy, optical microscopy, transmission electron microscopy, and electron diffraction techniques. Samples were prepared by isostatically hot-pressing a mechanical mixture of 95% olivine - 5% Hawaiian tholeiitic basalt under 200 MPa confining pressure at 1275°C for 1 hour in a gas apparatus; 98% of the olivine powder was less than 15μm in size and 95% of the basalt was less than 10μm. The final grain size varied from 10 to 200μm. Symplectic intergrowths occurred in regions 10 to 50μm across. Basaltic glass concentrated in triple junctions and often penetrated fractures. No glass was observed in the few grain boundaries examined by high resolution transmission electron microscopy methods. These observations are consistent with those of Waff and Bulau (JGR, 84, 6109, 1979) and extend the resolution of their observations to below 25Å.

V 86

PARTIAL MELTING OF PERIDOTITE IN THE PRESENCE OF BUFFERED FLUIDS

Magnus Olafsson (Nordic Volcanological Institute, University of Iceland, 101 Reykjavik, Iceland)
David H. Eggler (Department of Geosciences, The Pennsylvania State University, University Park, PA 16802)

The solidus of a Hawaiian peridotite in the presence of small amounts of H_2O and CO_2 has been determined experimentally. The solidus has two low-temperature cusps. At pressures up to 21 kbar, the solidus temperature (1110°C at 15 kbar) and the composition of a relatively CO_2-rich vapor are buffered by an amphibole dehydration reaction; at higher pressures a carbonation reaction is encountered, at which the temperature drops some 60°C to a volatile-absent solidus with H_2O bound in amphibole and CO_2 in carbonate. The second cusp occurs at 26 kbar, a pressure at which the solidus intersects the upper stability field for amphibole and at which the solidus temperature decreases another 60°C. Above 26 kbar the solidus is subparallel to the hydrous solidus inasmuch as carbonate buffers the vapor at a relatively H_2O-rich composition.

Liquids quenched from near the solidus below about 26 kbar are silica-undersaturated and, broadly speaking, nephelinitic. Their composition is determined largely by the complete melting of amphibole at the solidus. These liquids are interpreted to represent the melt within the low-velocity zone. As melting increases, liquids become basanitic and then tholeiitic.

Above 26 kbar, liquids are presumed to be very carbonate-rich, by analogy with synthetic systems. Direct analyses proved to be impossible, however.

V 87

MELTING RELATIONS IN THE SYSTEM PYR_1GROSS_2-PYR_2GROSS_1-QTZ-H_2O AT 30 KB

Toshimori Sekine (Dept. of Geophysical Sciences, University of Chicago, Chicago, Illinois 60637)
Peter J. Wyllie (Dept. of Geophysical Sciences, University of Chicago, Chicago, Illinois 60637)

In the model system Pyr_1Gross_2-Pyr_2Gross_1-Qtz the calc-alkaline volcanic rocks plot along the join $Pyr_{11}Gross_9$-Qtz. Close to the join Pyr_1Gross_2-Qtz, liquidus phases are cpx, cpx + qtz, and qtz for successively more SiO_2-rich compositions. With increasing H_2O content, the liquidus field for cpx expands as that for qtz decreases. The liquid at the boundary of the liquidus field for qtz contains 89 wt % SiO_2 saturated with H_2O and 75 wt % SiO_2 with 5 wt % H_2O. Garnet only appears as a subsolidus phase below 1110°C (together with cpx) for the composition on the garnet join. Close to the join Pyr_2Gross_1-Qtz, liquidus phases are garnet, garnet + opx, opx, opx + qtz, and qtz for successively more SiO_2-rich compositions. The eclogitic assemblages garnet + cpx and garnet + cpx + qtz have only been found in the subsolidus region below 1150°C, where opx reacts with melt to form cpx.

Possible consequences for the fusion paths of qtz eclogite will be discussed on the basis of experimentally obtained results and previously published data.

V 88

APATITE SATURATION IN MAGMAS AT HIGH PRESSURES

E.B. Watson (Department of Geology, Rensselaer Polytechnic Institute, Troy, N.Y. 12181)
(Sponsor: Samuel Katz)

Melts of 5 intermediate to basic rocks were equilibrated with fluorapatite crystals at P-T conditions of 12-17 kbar and 1300-1350°C. The experiments were carried out in a solid-media, piston-cylinder apparatus, starting with either a 50/50 mixture of rock powder and ground apatite (contained in graphite) or rock powder contained in single-crystal fluorapatite capsules. Quenched glasses of the melts coexisting with apatite were analyzed for 10 elements with an electron microprobe. The concentration of P_2O_5 in melts saturated with apatite appears to depend mainly upon SiO_2 content: At 1350°, 17 kbar and a silica concentration of 55 wt%, for example, 3.0-3.5 wt% P_2O_5 is sufficient to saturate a magma in apatite. However, a less silicic melt (45 wt% SiO_2) in equilibrium with apatite will dissolve 6 wt% P_2O_5 at the same P-T conditions. Comparison of the present results with previous 1-atm experiments on apatite saturation in magmas (Watson, Geophys. Res. Lett. 6, 937-940, 1979) reveals that increased pressure causes a relative reduction in apatite solubility of ~2%/kbar. Thus, at 17 kbar the P_2O_5 content of an apatite-saturated magma is lower by ~35% than would be expected for a similar magma at the same temperature and 1 atm pressure. This significant pressure effect does not increase the likelihood that apatite is a residual mineral in mantle fusion episodes, because the decreased solubility of apatite at elevated pressures is compensated by increased solubility at higher temperatures.

V 89

TRANSMISSION ELECTRON MICROSCOPY OBSERVATIONS OF A PARTIALLY MELTED QUARTZ MONZONITE

D. L. Kohlstedt (Cornell University, Department of Materials Science and Engineering, Ithaca, NY 14853)
Brian Bonner (University of California, Lawrence Livermore Laboratory and Department of Geology and Geophysics, Berkeley, CA 94550)

A fine-grained (0.1 mm) quartz monzonite obtained from Tuolomne County, California, (Sierra Nevada batholith) was lightly deformed at 730±15°C at a confining pressure of 180 MPa for 2 hours and subsequently examined by both conventional optical and transmission electron microscopy (TEM). The deformation experiment was part of a study of seismic attenuation at low stress amplitudes, ≤0.2 MPa. Monzonite cylinders 9 mm in diameter by 15.9 mm in length were desiccated for several weeks and were then vacuum dried at 30°C and 10^{-8} Torr for approximately seventy-two hours before they were sealed in copper capsules by electron beam welding. Indirect evidence, such as experience with lunar samples, indicates that trace amounts of water were present in the capsule during the experiment but at unknown pressure.

Optical examination of the recovered sample reveals extensive fracturing of quartz grains, which was presumably introduced by repeated cycling through the α-β quartz transition. Careful optical examination does not reveal the presence of any glass in the cycled specimen. However, TEM studies indicate the unambiguous presence of thin films of glass several hundreds of Angstroms wide.

V 90

ANHYDROUS MELTING OF SILICATE MINERALS AT HIGH PRESSURES, AND METASTABLE STRUCTURES IN LIQUIDS

A. L. BOETTCHER (Dept. of Earth and Space Sciences and Institute of Geophysics and Planetary Physics, University of California, Los Angeles, Los Angeles, CA 90024)
K. WINDOM*
S. BOHLEN (both at: IGPP, University of California, Los Angeles, CA 90024)
* Now at Dept. of Earth Sciences, Iowa State Univ., Ames, Iowa 50011.

The beginning of melting (T_m) of high albite, sanidine, and diopside were determined to 25 kb in piston-cylinder apparatus with KBr furnace assemblies and W-Re thermocouples and in argon-gas apparatus (3kb).

	3	10	16	25
Ab	<1150°	1210°	1240°	1320°
Sa	-	1345°	1455°	1520°
Di	-	1510°	1565°	1675°

These data for albite result from the first indubitable demonstrations of reversal and equilibrium. In addition, the results of some previous experiments and calculations suffer from equating liquids with glasses (quenched liquids). The T_m for Ab calculated by Burnham and Davis (1974) is ~100° too high at 10kb, because they were constrained to use the entropy (S) of Ab glass, which is less then the S of Ab liquid. This creates an error of ~50% for ΔS_f, using our dP/dT and the ΔV of Burnham and Davis. The structures and configurational S of these liquids are a function of temperature. For Ab, our experiments reveal that the structure of the liquid several hundred °C above T_m can easily be retained at the solidus, greatly reducing the apparent T_m. To remove the high-temperature structure requires $T \gg T_m$ (also shown by Schairer and Bowen, 1956). Long run durations cannot eliminate the high-temperature structures at $T \sim T_m$ for Ab composition. Melting experiments cannot usually be reversed using glasses, nor can structures be determined from liquids quenched from temperatures greater than those of interest.

V 91

Fe^{3+}/Fe^{2+} EQUILIBRIA IN K_2O-SiO_2-Al_2O_3 MELTS

M.P. Dickenson
P.C. Hess (both at: Dept. of Geological Sciences, Brown University, Providence, R.I. 02912)
(Sponsor: M.J. Rutherford)

Experiments to determine the compositional dependence of Fe^{3+}/Fe^{2+} in K_2O-SiO_2-Al_2O_3 melts doped with 2 wt.% Fe_2O_3 were run in air at 1400°C. Total Fe of quenched glasses was determined by microprobe, Fe^{2+} by microtitration, and Fe^{3+} by difference.

The Fe^{3+}/Fe^{2+} ratio along a 70 wt.% SiO_2 isopleth has a maximum of 12.1 at a K_2O/Al_2O_3(mole)=1.1. As K_2O/Al_2O_3 is reduced below 1.1, Fe^{3+}/Fe^{2+} drops sharply and linearly to 1.8 at K_2O/Al_2O_3 = 0.72. Increasing K_2O/Al_2O_3 from 1.1 slightly decreases the redox ratio to 9.7 at K_2O/Al_2O_3=2.6.

The effect of varying K_2O/Al_2O_3 on Fe^{3+}/Fe^{2+} equilibria suggests that the structural role of Fe is a complex function of melt structure. When K_2O/Al_2O_3 is approximately 1.1 both Fe^{3+} and Al^{3+}, with K^+ as a charge balancing species, are in tetrahedral coordination and copolymerize with SiO_2. In peraluminous melts K^+ is strongly bound only to Al^{3+}. Fe^{3+} has no charge balancing species and cannot be a network former. Since Fe^{2+} is a more efficient network modifier, it is stabilized relative to Fe^{3+}. In peralkaline melts the lower content of tetrahedral Al^{3+} limits copolymerization of tetrahedral Fe^{3+} and somewhat stabilizes Fe^{2+} as a network modifier.

V 92

EQUILIBRIUM TRENDS DURING HYDROTHERMAL-IMPULSE-MELTING OF A CHARNOCKITIC GNEISS

J. H. Carman, A. K. Sinha, K. A. Affholter, Dept. of Geological Sciences, VPI&SU, Blacksburg, VA 24061 and M. J. Bartholomew, Div. of Mineral Res., Charlottesville, VA 22903

To evaluate the genesis of granites from continental basement, a fine grained (0.1-1mm) charnockitic gneiss (SiO_2 = 63.0, Al_2O_3=15.3, Fe_2O_3=5.9, CaO=3.2, Na_2O=6.0, K_2O=4.3, in wt%) from the central Virginia Blue Ridge Complex plus 40 wt.% water was held at 760°C (~100° above the wet solidus) and 3 kb for periods ranging from 300-600 hrs. In addition to fine grained starting material (<200 micron) larger capsules were loaded with actual rock fragments (2 to 7 mm in maximum dimension) to examine equilibrium trends at the rock fragment level. Runs using fine grained starting material produced melts in equilibrium with plag.(An_{37}, Ab_{58}), biotite, ilmenite, apatite, sphene, zircon (?) and vapor. The glass with $Na_2O+K_2O+Al_2O_3/SiO_2$ ratio of 22.3/64.5 (mole %) approximates a granitic composition. However, melting of the fragments slows the attainment of equilibrium and allows closer examination of the melting process. Quartz, alkali feldspar, hornblende, amphibole-complexes (after cpx) and biotite-complexes (after opx) persist as melt-rafted aggregates with only minor interestitial melt. As deduced from microprobe totals, melting is apparently limited by the diffusion of water through the silicate melt. These melt compositions include and diverge from that of granite composition given above as individual minerals and their combinations control local equilibrium tendencies. Adjacent to feldspars, melt is enriched in feldspar components, and near hornblende, melts are nepheline-normative (29.9/53.8) whereas melts are kalsilite-normative (24.8/38.6) near biotite. Minor element and strontium isotope analyses of melt-rich and mineral-rich separates from these experiments will further assess observed major element variations.

V 93

SOLUTION GROWTH OF LARGE SINGLE CRYSTAL DIOPSIDE

M.Sneeringer, Center for Geoalchemy, Department of Earth and Planetary Sciences, M.I.T., Cambridge, Ma. 02139.
V. Belruss, Crystall Physics Laboratory, Department of Electrical Engineering, M.I.T.

The method of Top Seeded Solultion Growth (TSSG) was used to synthesize large single crystals of diopside for use in geochemical experiments. The solution from which the crystals were grown had the composition: 50.2 mole % SiO_2, 24.9% CaO, 16.6% MgO, and 8.3% MgF_2. The samples were generally water clear with well-developed crystal faces and some small regions of inclusions. Sizes ranged from clear areas a few mm in diameter in multicrystalline masses to single crystals approximately 2.5x2.5x3.5cm. X-ray diffraction spectra match that given by iron-free diopside. Electron microprobe analysis gives an average composition of $Di_{0.976}En_{0.023}$. Later runs were doped with trace levels of Sr and Sm.

TSSG is a nearly isothermal process which allows the growth of large, strain-free crystals with low dislocation densities. Growth from a solution with diopside as the first crystallizing phase eliminates the vertical temperature gradients required in other methods. Crystallization is facilitated by a seed which is slightly cooler than the melt and the slow lowering of the furnace temperature from ~1390° to 1385°C. Growth actually takes place below the melt surface, leading to the development of a faceted crystal. This work was carried out at the Crystal Physics Laboratory of the Center for Material Science and Engineering and the Department of Electrical Engineering at M.I.T..

V 94

OLIVINE/LIQUID NICKEL PARTITIONING AT HIGH PRESSURES: EXPERIMENTS WITH AN OLIVINE CAPSULE

Eiichi TAKAHASHI (Geophysical Laboratory, 2801 Upton St.,N.W., Washington D.C.,20008)

In high-pressure experiments involving Ni partitioning between minerals and silicate melts, equilibrium is difficult to achieve because of chemical reactions between capsule materials (Pt, C,Mo,BN) and the melts. In order to overcome these reactions, olivine crystals, separated from a lherzolite xenolith, were selected as a capsule material. Reactions between an alkali olivine basalt melt (MgO=8.8, FeO*=9.3 wt%, NiO=250ppm) and the olivine capsule (Fo=91.4, NiO=3900ppm) were studied at 15kb and 1350°C (50°C above pseudo invariant point, at which the basalt coexists with olivine, ortho- and clinopyroxenes). The charge consisted of 10 mg of the basalt powder placed in the center of the powdered olivine (150 mg) in a sealed Pt-tube. Olivine saturation of the melt was achieved within the first 30 min (MgO increases to 11.5 wt%, NiO to 480 ppm). The oxygen fugacity of the charge increased continuously during the experiments due to the Fe-loss into the Pt-tube from the olivine capsule (estimated Fe_2O_3 in the melt; 1 wt% at 30 min to 6 wt% at 48 hrs). The olivine /liquid Ni-Mg partition coefficient was constant in runs ranging from 5 to 48 hrs ($K = (Ni/Mg)^{ol}/(Ni/Mg)^{liq} = 2.1 \pm 0.2$).

The partition coefficient for the alkali olivine basalt (10-16 kb, 1300-1350°C) and a picrite (15-20 kb, 1500°C) was determined with the olivine capsule. The results showed a systematic variation depending on MgO in the melts (K=2.3 at MgO=9 wt% to K=1.7 at MgO=23 wt%). There was no systematic correlation, however, with pressure. The results are in agreement with data at 1 atmosphere (Takahashi,1978). It is concluded that there is no significant pressure effect on the partition coefficient, at least in dry basaltic melt up to 16 kb, and picrite melt up to 20 kb.

V 95

HIGH-PRESSURE CRYSTALLIZATION OF OLIVINE IN A FAMOUS BASALT

P. I. Nabelek (Dept. of Earth and Space Sciences, State Univ. of N.Y., Stony Brook, N.Y. 11794)
C. H. Langmuir (Lamont-Doherty Geological Observatory of Columbia Univ., Palisades, N.Y. 10964)
A. E. Bence (Dept. of Earth and Space Sciences, State Univ. of N.Y., Stony Brook, N.Y. 11794)

The forsterite, Ni and Ca variations in olivine from FAMOUS glass 527-1-1 are complex and are inconsistent with crystallization exclusively in a magma chamber at low pressure. Two olivine types, one with normal and the other with reverse zoning of Ni, are recognized. Normally zoned olivines are characterized by Fo_{88}, Ni ~ 1900 ppm cores and Fo_{87} ~ 1600 ppm rims. This zonation is consistent with low-pressure fractionation. Other olivines have interiors which are unzoned in Mg (Fo_{89-90}) and U-shaped Ni (Fig.) and Ca profiles. The reverse zoning in Ni, coupled with the lack of Mg-zoning in the same crystals, may be explained either by continuous changes in Ni independent of Mg/Fe in the liquid, or by continuous changes in the partition coefficient for Ni. Selective silicate/sulfide immiscibility, combined with continuous mixing of magmas, cannot explain the Ca data. In view of the demonstrated decrease in the partition coefficient for Ni (and Ca?) between olivine and liquid with pressure, it seems likely that the reverse zoned olivines began to crystallize at depth and continued to crystallize as they rose through the mantle and crust. Normal zoning results from rapid crystallization at low pressure. If this interpretation is correct, a mantle history is preserved in the mineralogy of this basalt.

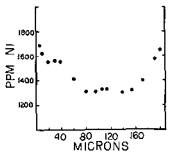

V 96

DETERMINATION OF SR PARTITIONING IN THE Di-An-Ab SYSTEM BY ION MICROPROBE

G. L. Ray (Massachusetts Institute of Technology, Cambridge, Mass. 02139)
N. Shimizu

The energy filtering technique of Shimizu et al. (1978) has been modified and applied to the quantitative ion microprobe measurement of Sr partitioning (diopside/liquid) in the diopside-albite-anorthite system.

A primary beam of O^- ions was focused to a spot of 5 μm diameter. Positive secondary ions with excess kinetic energies of 80 ± 25 eV were analyzed.

Five synthetic glass standards with bulk compositions in the ternary system and with nominal trace element concentrations ranging from 25 to 500 ppm were used for liquid calibration. Well-analyzed, natural diopsides were used for the crystal calibration. The following calibration curves were obtained for Sr: Liquid; $I(^{88}Sr)/I(^{28}Si) = 2.08 \times 10^{-6}$ (Sr_{ppm}), $r^2 = 0.999$; Diopside; $I(^{88}Sr)/I(^{28}Si) = 2.57 \times 10^{-6}$ (Sr_{ppm}), $r^2 = 0.999$ (where I is the measured intensity of a given isotope).

A bulk composition of $Di_{65}Ab_{24}An_{11}$ containing 800 ppm Sr, run at 1300 °C and 1 atm for 9 days, gave D(Sr) = 0.12 ± .01. This was successfully reversed with a 30 day run. A bulk composition of $Di_{60}Ab_{20}An_{20}$, equilibrated at 1275°C for 8 days, gave D(Sr) = 0.11 ± .01. More experiments involving Sr, Sc, Sm and Ti partitioning at 1250°C, 1300°C and 1350°C are in progress.

V 97

REE PARTITIONING BETWEEN ZIRCON, WHITLOCKITE AND TWO LIQUIDS

James E. Dickinson (Dept. of Geological Sciences, Brown University, Providence, RI 02912)
P.C. Hess
M.J. Rutherford

We have experimentally determined partition coefficients for Ho, Sm, and La for zircon and whitlockite coexisting with two immiscible liquids. Starting compositions were a 50:50wt% mixture of the immiscible liquid pair produced by fractional crystallization of KREEP basalt 14310, doped with ZrO_2+3% total REE or P_2O_5+3% total REE. Experiments were run in Mo-foil capsules sealed inside silica glass tubes and were held at 1135°C for 8 hrs. before quenching. Homogeneity of glass and crystals in both major and REE indicate an approach to equilibrium. Experiments are in progress with lower total REE to evaluate Henry's law behavior.

$K_D$zircon/liquid(55-60%SiO_2) for La, Sm, and Ho are about 0.3, 1, and 7. For a liquid with about 40% SiO_2, K_D's decrease to 0.1, 0.5, and 3. $K_D$whitlockite/liquid (60%SiO_2) for La, Sm, and Ho are about 13, 16, and 9. The K_D's decrease to 4, 4, and 3 for whitlockite coexisting with a liquid with about 40% SiO_2.

The zircon pattern is similar to that observed in lunar and terrestrial rocks. The whitlockite pattern is similar to that observed for whitlockite in lunar rocks. Two-liquid K_D's suggest that REE prefer this low SiO_2 melt by a factor of 3-4.

V 98

REE PARTITIONING BETWEEN COEXISTING SILICATE LIQUIDS

Paul A. Danckwerth (Dept. of Geological Sciences, Brown University, Providence, RI 02912)
F. J. Ryerson (Lawrence Livermore Lab., Livermore, CA 94550)

The partitioning of Eu, Sm, Gd, Sr, Ca has been experimentally determined between coexisting immiscible silicate liquids. Runs were conducted at 1 atm. in both evacuated silica tubes using foil containers and in a controlled CO-CO_2 atmosphere. Results are reported for compositions in the system K_2O-Al_2O_3-'FeO'-SiO_2. REE were doped at the 0.1-1.0 wt. % level.

The technique is well suited for the study of multi-valent minor-element partitioning. Metastable effects are circumvented and the runs are easily reversed.

Results for Sm, Gd, Sr, and Ca generally agree with previous experimental determinations. At the iron-wustite buffer trivalent REE generally have K_D (low SiO_2/high SiO_2) of 3-4 while the divalent cations Ca, Sr, are partitioned by a factor of 2. K_D for Eu shows measured values nearly identical to that of Sr and Ca. All data show Henry's Law behavior over the range of concentration studied.

The data is interpreted as reflecting the multi-valent behavior of Eu in the liquid. The data indicate that substantial amounts of divalent Eu are present in these liquids at the IW buffer.

V 99

PARTITIONING OF GERMANIUM BETWEEN FORSTERITE AND SILICATE MELT

C.J. CAPOBIANCO (Rensselaer Polytechnic Institute, Troy, New York 12181)
E.B. Watson

Partition coefficients for Ge between forsterite and silicate melt in the system MgO-CaO-Al_2O_3-SiO_2 (Di-An-Fo join) were measured for bulk Ge concentrations between 0.11 wt. % and 1.2 wt. %. Experiments run at 1 atm. for a variety of melt compositions were equilibrated at 1300°C, 1350°C, 1400°C and 1450°C. Preliminary analyses reveal incompatibility of Ge in forsterite for all temperatures and compositions considered. The weight ratios of GeO_2 in forsterite and glass ($D^{Fo\text{-}melt}_{GeO_2}$) vary between 0.57 and 0.89 with analytical uncertainty on the order of ±0.12.

At this time no systematic dependence of partitions coefficients on equilibration temperatures or bulk Ge concentrations is observed. However, the lowest values for $D^{Fo\text{-}melt}_{GeO_2}$ were measured between the most silica rich melts and coexisting forsterites. Since germanium is a network forming cation, this decrease may reflect its co-polymerization with silicon in the melt. Replicate probe analyses are being done in order to quantify this effect.

The overall variation of $D^{Fo\text{-}melt}_{GeO_2}$ for all experimental conditions analyzed is small enough that a mean value of 0.72 (σ =0.09) is reported. This value may be used to infer enrichment of Ge in melts during fractional crystallization of olivine. Observed abundance of Ge in fractionated rocks exhibit an increase in Ge content with increasing fractionation in agreement with present results.

V 100

A NEW CALCULATION OF WATER DIFFUSIVITY IN RHYOLITE GLASS

J.L. Karsten
J.R. Delaney (both at: Oceanography Dept., Univ. of Washington, Seattle, WA 98195

Water diffusivity (D_w) in a granitic liquid has been re-calculated from water diffusion profiles measured in rhyolite glass cylinders using the ion microprobe at Johnson Space Center. Three glass cylinders, held at 850°C and $P_f(H_2O)$ = 700 bars for 0.27, 2.5 and 6.0 hrs (Shaw, 1974), were analyzed for the ratio $^1H/^{16}O$ (found to be directly proportional to water) at 20 micron intervals with a 10 micron NO_2^+ primary beam. The initial H_2O content (0.2%) and the saturation H_2O content (3.7%) establish the extreme values of the profile. Non steady-state diffusion into a semi-infinite medium is described by the equation:

$$-\phi/2 \cdot d\theta/d\phi = d(D_w \cdot d\theta/d\phi)/d\phi$$
$$\theta = 1,\ \phi = 0;\ \theta \to 0,\ \phi \to \infty.$$

With x = distance from cylinder edge, t = time, C_o = conc. at t=0, x>0, C_s = conc. at x=0, t>0, C = conc. at x, $\theta = C-C_o/C_s-C_o$ and $\phi = x/t$. In the new evaluation of D_w, an iterative technique has been used to numerically calculate solutions to the diffusion equation as a function of D_w (Philip, 1955). Comparison of these solutions with the ion probe data indicate that, for $0.2\% \leq C \leq 3.7\%$, D_w can be described by an exponential function of θ, of the form:

$$D_w = D_o \exp(k\theta)$$

with D_o (D_w at 0.2%) = $(1\text{-}2)\cdot 10^{-8}$ cm^2/sec and $2 \leq k \leq 4$.

General Geochemistry II

Queen's Quay
Saturday P.M.
Danny M. Rye (Yale University), Presiding

V 101

MICROANALYSIS OF GEOLOGICAL MATERIALS IN AN ANALYTICAL ELECTRON MICROSCOPE: ELIMINATION OF SPECTRAL CONTAMINATION

L.F. Allard (Dept. of Materials Science, Univ. of Michigan, Ann Arbor, MI 48109)
D.F. Blake (Dept. of Geological Sciences, Univ. of Michigan, Ann Arbor, MI 48109)
N.G. Newberry (Same as D.F.B.)
D.R. Peacor (Same as D.F.B.)
W.C. Bigelow (Same as L.F.A.)
(Sponsor: John Valley)

Thin film microanalysis of geologic materials via analytical electron microscopy (AEM) can provide compositional data with a spatial resolution two orders of magnitude better than that of the electron microprobe. However, elemental analysis in AEMs is hampered in part by the extreme spectral interference created by X-rays generated in the electron-optical column and near-specimen environment. This problem is significant for all elements, but is especially serious for specimens which contain Fe or Cu, as these elements are usually present in the specimen environment as well. We have systematically characterized and eliminated sources of such "systems X-rays" in our JEOL JEM-100CX AEM. Our optimization procedure results in clean X-ray spectra, and offers several advantages over those previously reported in the literature: 1), all elements (particularly those of geologic interest, such as Fe and the third period elements) may be analyzed; and 2), the optimization does not preclude other modes of operation. Ultrastructural and crystallographic data may thus be obtained from the analyzed microarea.

We describe results for several geologic examples, including: 1), analyses of heterogeneous microstructures in low-temperature calcian dolomites; 2), chemical and structural analyses of single-domain sized magnetite grains which are found in association with larger magnetite grains displaying ilmenite intergrowths; and 3), the analysis of conpositional gradients across pyroxene exsolution structures whose lamellae are on the order of 1000 Å in width.

V 102

LOW GRADE METAMORPHIC EFFECTS ON PLAGIOCLASE AS DETECTED BY $^{40}Ar/^{39}Ar$ ANALYSES

J.C. Roddick (Dept. of Earth Sciences, Leeds University, Leeds, England)
D.C. Rex (Leeds University)
(Sponsor: M.H. Dodson)

Island arc andesites from Annenkov Is, South Georgia dated at 103m.y. by conventional K/Ar and $^{40}Ar/^{39}Ar$ on hornblende have undergone subsequent zeolite facies metamorphism. Conventional whole rock K/Ar ages which are dominated by K-rich phases in the matrix were seriously affected by this metamorphism. $^{40}Ar/^{39}Ar$ analyses of apparently slightly altered plagioclase phenocrysts are able to confirm that the whole rock data date the age of metamorphism. They also record some of the effects of this metamorphism.

The plagioclase spectra are irregular with ages ranging from 70m.y. in low temperature steps to 106m.y. in highest temperature fractions. However, a correlation plot of $^{36}Ar/^{40}Ar$ vs $^{39}Ar/^{40}Ar$ shows a well defined linear array of the high temperature fractions indicating the same age as the whole rocks (~75m.y.) and a trapped $^{40}Ar/^{36}Ar$ of approximately 310. Comparison with fresh plagioclase indicate that alteration is accompanied by a 3 to 4 fold increase in K, Cl, and ^{36}Ar. These plagioclase data show that metamorphic fluids containing K, Cl and large amounts of Ar of non-atmospheric composition have remained trapped within the high temperature fractions at the termination of zeolite metamorphism at about 75m.y.

V 103

40Ar/39Ar DATING WITH A CONTINUOUS LASER

C.M. Hall
D. York
Y. Yanase
W.J. Kenyon
P. Kuybida
J.A. Hanes (all at: Dept. of Physics, Univ. of Toronto, Toronto, Ont., M5S 1A7, Canada.)

We report the first 40Ar/39Ar age measurements in which the argon was extracted by heating the samples with light from a continuous laser. The pioneering work of Megrue and Schaeffer was done with a pulsed laser. The results are also the first laser-derived ages for terrestrial samples. Light from a high-powered argon-ion laser is focussed onto individual neutron-irradiated mineral grains situated in the inlet system of an MS10 mass spectrometer. The argon evolved is leaked through a Ti furnace into the spectrometer. With the present arrangement it is possible to watch through a microscope as the grain is gradually heated and totally fused. So far we have successfully analysed biotite, muscovite, hornblende and whole-rock diabase dyke material in this way. Sample ages range from 100 to 2600 m.y. and the results agree closely with those of conventional analyses. The speed of analysis with the laser is much greater than with the conventional system and our blanks are significantly reduced. The advantages of using a continuous laser rather than a pulsed one are (a) alignment is much simpler and (b) step-heating runs can be carried out in a straightforward way. We have already successfully carried out one such run on a single biotite grain.

V 104

LASER PROBE ^{39}Ar-^{40}Ar TERRESTRIAL ROCK AGES

H. Maluski (Dept. Earth and Space Sciences, SUNY, Stony Brook, N.Y. 11794; permanent address: Earth Sci., Montpellier, France)
O.A. Schaeffer (Stony Brook, N.Y. 11794)

We report in this work some preliminary experiments in the application of the laser method to the study of terrestrial rocks. The laser method of obtaining ages for individual mineral grains should be of special interest to terrestrial samples which have suffered several metamorphic events which resulted in several generations of

metamorphic minerals, sometimes on the same species. It is also possible that samples with excess argon which do not yield chronologically significant ages by the conventional thermal release ^{39}Ar-^{40}Ar study may yield chronologically significant laser determined ages. In this preliminary study we compare the laser age to the ^{39}Ar-^{40}Ar thermal release age and the Rb-Sr mineral isochron age for minerals in granite. The results are summarized in Table 1. The laser age of the Ivory Coast granite agrees well with the other ages for both biotite and potassium feldspar minerals. The granite from Corsica was emplaced 330 m.y. ago and underwent metamorphism at 80 and 40 m.y. We have studied a high pressure phengite which gave a laser age of 43 m.y. in good agreement with the last metamorphic event dated by a thermal release ^{39}Ar-^{40}Ar study. As can be seen, the laser method yields results in good agreement with other methods for mineral samples as young as upper Eocene.

Table 1. Laser ^{39}Ar-^{40}Ar Ages

	Laser, my	Other*, my	
Ivory Coast Granite:			
CI-1 Biotite	1798±140	1765±100	Rb-Sr
CI-1 K-Feldspar	1716±140	1450±100	Rb-Sr
CI-7 Amphibole	1935±150	2080±80	39-40
Granite from Corsica:			
Phengite	42±5	40±3	39-40

*Allegre et al., unpublished results.

V 105

THE DIRECT DATING OF ORE MINERALS

D. York, J.A. Hanes
P. Kuybida, C.M. Hall, W.J. Kenyon
A. Masliwec (all at: Dept. of Physics, Univ. of Toronto, Toronto, Ont., M5S 1A7, Canada.)
S.D. Scott, E.T.C. Spooner (both at: Dept. of Geology, Univ. of Toronto)

Preliminary results are presented of the first modern attempt to date the common sulphide minerals directly. K and Ar concentrations and the Ar isotope ratios in pyrites, galenas, sphalerites, and chalcopyrites have been determined. Sample localities include: Geco, Renabie, Sudbury, Ontario; St. Jo Mine, S.E. Mo.; and Broken Hill, Australia. Very low values of K and Ar have been found. The K contents of pyrites were the highest, ranging from 5 to 65 ppm. Galenas and sphalerite were usually lower with K $\leq$ 1 ppm. This means that the only likely way in which such minerals may be directly dated is via the 40Ar/39Ar approach. Measured 40Ar/36Ar ratios were often low ($\sim$300-500) and there is evidence that the different mineral types from a given deposit may trap isotopically different initial Ar. Multiple sample analyses combined with isochron plots will be essential in geochronological interpretation. We have firmly established, however, that the project is experimentally feasible. Whenever it occured in the ore samples, we have extracted micaceous material for dating, as a reference. 40Ar/39Ar step-heating runs on 2 biotites from Geco samples yielded excellent plateaus of approximately 2.62 b.y. age. A virtually identical result was found for a white mica from a Kidd Creek Ont. sample. These two deposits evidently cooled through about 300°C at this time and have suffered no significant heating since.

V 106

TIME-STRATIGRAPHIC CORRELATION OF THE KIDD CREEK ORE BODY WITH VOLCANIC ROCKS SOUTH OF TIMMINS, ONTARIO, AS INFERRED FROM ZIRCON U-PB AGES.

Nunes, Paul D., Department of Mineralogy and Geology, Royal Ontario Museum, Toronto, Ontario. M5S 2C6.
Pyke, Dale, Ontario Geological Survey, Ministry of Natural Resources, Toronto, Ontario M5S 1B3.

Four U-Pb analyses of zircon from the rhyolite immediately underlying the Kidd Creek ore body define a discordancy line with an upper concordia intercept age of 2717 ± 4 m.y. The probability that all four analyses lie within analytical error on this line is 5%. Three of the four analyses have a probability of 79% of lying within error of a discordancy line with an upper concordia intercept age of 2717 ± 2 m.y. We interpret this age as representing the time of extrusion of the rhyolite which is a maximum age for the formation of the ore body. If the ore is syngenetic, the 2717 m.y. age also represents the time of its development.

South of Timmins, Pyke has delineated two main Supergroups of komatiitic to felsic volcanic rocks. Zircon upper concordia intercept ages of 2703 ± 3 m.y. (upper Supergroup felsic volcanic rocks) and 2725 ± 2 m.y. (lower Supergroup felsic volcanic rocks) indicate that the Kidd Creek ore body is stratigraphically closely related to the interface of these two Supergroups. Much of the mineralization in the Timmins-Matachewan area has a close spatial relationship to the contact between the two Supergroups. This work demonstrates that this observation also holds for the Kidd Creek ore body 25 km north of Timmins, Ontario.

V 107

REDUCTION OF ZIRCON AGE DISCORDANCE BY HIGH GRADIENT SEPARATION, AND AIR ABRASION TECHNIQUE

Krogh, Thomas E., Department of Mineralogy and Geology, Royal Ontario Museum, Toronto, Ontario. M5S 2C6.
(Sponsor: Dr. Paul D. Nunes (A.G.U.)

The largest source of uncertainty in zircon U-Pb ages is not directly analytical but rather results from the projections necessary to correct for lead loss. As noted by Silver (1963), the most concordant zircons are those which are non-magnetic on a Frantz Isodynamic Separator. These zircons can now be further separated into more and less paramagnetic fractions using high gradient techniques. The simplest device consists of a loop of soft iron (paper clip) suspended in the gap of an electromagnet, or a pointed soft iron wire over a sample dish situated over the pole of a permanent or electromagnet, under a binocular microscope. The intense gradients at the lower side of the loop or between the wires of a double loop pick up many of the non-magnetic zircons under alcohol and leave behind grains which on average are half as discordant as the starting material. Air abrasion to yield rounded grains reduces paramagnetism, alteration, uranium levels, common lead levels and as much as 80% of the discordance of the Frantz non-magnetic starting material. Further, it allows isolation and detection of minute amounts of inherited core materials.

Results to date indicate that not all isochron projections to concordia are valid, but in most cases the more concordant points lie up the line determined using untreated samples.

V 108

ISOCHRONAL AND ISOTHERMAL PLATEAU AGES IN FISSION TRACK DATING

G. Poupeau, J. Carpéna and D. Mailhé
Centre des Faibles Radioactivités, 91190 Gif-sur-Yvette, France (sponsor C. Lalou)

The partial geological annealing of ^{238}U spontaneous fission tracks in natural glasses and minerals is known to result in a lowering of the etchable fossil track density and therefore in a reduction of their fission track (FT) ages. Such thermally lowered FT ages are meaningless and must be corrected for partial track fading. We present the results of a comparative study of 2 methods based on stepwise heating, the isochronal (ICPA) and isothermal (ITPA) plateau age methods.

1. FT ages measured by the ICPA respectively ITPA method are concordant. For instance, the apatites from three rocks of the french hercynian basement give resp. ICPA and ITPA values of 244, 243; 286, 291 and 282, 281 m.yr. The very good agreement between ICPA and ITPA results shows that in laboratory annealing, the same reduction of the etchable (fossil and induced) track density can be obtained eitheir by an increased heating duration (at a constant temperature) or an increasing heating temperature (for a given annealing time at each temperature).

2. Moreover, in the ICPA method, the systematics of the etchable track density reduction with temperature allows (i) to discriminate fission tracks from other artefacts, (ii) an indirect control of the geological closing temperatures for each age measurement. These unique features make this method a very attractive one.

3. Finally, these plateau methods can produce directly corrected FT ages with a precision of $\lesssim$7% (95% confidence level) for minerals into which U is homogeneously distributed. This is far better than with conventionnal (; based on track length measurements) correction methods.

V 109

STABLE ISOTOPE GEOCHEMISTRY OF THE NEGAUNEE IRON-FORMATION (NIF), MARQUETTE DISTRICT, MICHIGAN: I. PRELIMINARY $\delta^{13}C$ AND $\delta^{18}O$ DATA FROM CARBONATES AT THE EMPIRE MINE

C. Stephen Haase*
Danny M. Rye (both at: Dept. of Geology and Geophysics, Yale University, New Haven, CT 06520
*present address: Environmental Sciences Div., Oak Ridge National Laboratory, Oak Ridge, TN 37830)

NIF carbonates have $\delta^{13}C$(PDB) and $\delta^{18}O$(SMOW) values ranging from -6.5 to -13.0‰ and +11.5 to +23.0‰, respectively, and show isotopic systematics similar to the characteristic pattern of other Proterozoic banded iron-formations (BIF's). No systematic differences in $\delta^{18}O$ values of coexisting ankerites and siderites were observed. $\delta^{13}C$ values for ankerites were typically $\sim$ 0.5 to 0.75‰ heavier than those of coexisting siderites, although several reversals of this trend were noted. Carbonates from adjoining mesobands exhibit $\delta^{13}C$ differences of up to 1.0‰ and $\delta^{18}O$ differences of up to 3.0‰, on a scale of 5 cm or less, suggesting that isotopic homogenization during diagenesis and subsequent low grade regional metamorphism was very limited.

A plot of $\delta^{13}C$ vs. $\delta^{18}O$ for NIF carbonates from mesobands with different modal amounts of magnetite shows no simple relation between magnetite content and isotopic values, indicating that magnetite formation during diagenesis had no readily discernible effect on the systematics.

Carbonates sampled from the five broadly defined stratigraphic members of the NIF exhibit not only vertical but also pronounced lateral variations in isotopic values. Such systematics suggest a primary sedimentological influence, although subsequent diagenetic modifications can not be ruled out. Petrologic and stratigraphic data are suggestive of complex interfingering of BIF facies types, which imply this locality was probably close to the paleomargin of a depositional basin. The observed isotopic systematics are consistent with such an environment.

V 110

LENGTH-SLOW CHALCEDONY: THE END OF THE NEW TESTAMENT

M. Kastner (Scripps Institution of Oceanography, La Jolla, CA 92093)

In 1971, Folk and Pittman suggested that length-slow chalcedony indicates evaporite conditions and a shallow-water origin. Keene in 1976, observed however that length-slow chalcedony forms in Pacific deep-sea sediments where it is generally associated with Mg-calcite, dolomite, and/or barite. These observations suggest chemical controls on the formation of length-slow versus length-fast chalcedony, but not necessarily evaporitic conditions, and certainly not a shallow-water origin. Hydrothermal experiments confirm this assumption.

Both length-fast and length-slow chalcedony formed from natural opal-CT in hydrothermal experiments between 150° to 240°C, pH 7 to 9. The presence of both Mg^{+2} and SO_4^{-2} is essential for the formation of length-slow chalcedony. In brine solutions of ionic strength up to 3.0, with various ratios of HCO_3^-, Cl^-, and SO_4^{-2}, and with Na^+ as the only cation, only length-fast chalcedony formed. In solutions of any ionic strength above 0.35, with the same above anions but with Mg^{+2} in addition to Na^+, however, the formation of length-slow chalcedony is favored.

The presence and concentration of SO_4^{-2} as well as the temperature control the amount of chalcedony formation (both length-fast and -slow) relative to crypto- or microcrystalline quartz. In the hydrothermal experiments, chalcedony is an early product and converts with time to cryptocrystalline quartz. The higher the supersaturation of dissolved silica with respect to quartz, the more chalcedony forms initially. In the presence of SO_4^{-2}, the solutions are more highly supersaturated with respect to quartz than in chloride solutions, and therefore more chalcedony forms.

V 111

GEOCHEMICAL STUDIES OF TWO CORES FROM THE GREEN RIVER OIL SHALE FORMATION

R. D. Giauque and J. P. Fox (Lawrence Berkeley Laboratory, Berkeley, CA 94720)

J. W. Smith and W. A. Robb (Laramie Energy Technology Center, Laramie, WY 82071)

The distribution of minerals, elements, and Fischer Assay products was determined as a function of stratigraphic position for two core holes from the Naval Oil Shale Reserve No. 1. Correlation analyses were performed to determine significant relationships between shale oil content, water content, eight minerals, and 47 elements.

These analyses indicate that elemental variability, expressed as the ratio of the maximum to minimum observed concentration, averages 2.4 for most major, minor, and trace elements with the exception of the sulfide elements As, Se, and Mo, the organically bound elements H and C and the feldspar components Na and K. Uranium, Mo, and H had relatively high positive correlations with Fischer Assay oil yields and the elements Co, Cu, Pb, Zn, Ni, V, Mo, and organic carbon were correlated throughout the oil-rich Mahogany Bed. The amount of hydrogen present relative to organic carbon was essentially constant and corresponded to a 2:1 atomic weight ratio equivalent to saturated hydrocarbons. However, nitrogen was more variable relative to organic carbon.

V 112

NEW EVIDENCE CONCERNING LOW-TEMPERATURE DOLOMITE FORMATION: ANALYSES OF CALCIAN DOLOMITES FROM A PENNSYLVANIAN ECHINODERM

D.F. Blake (Dept. of Geological Sciences, Univ. of Michigan, Ann Arbor, MI 48109)
D.R. Peacor (Same as D.F.B.)
B. H. Wilkinson (Same as D.F.B.)
(Sponsor: John Valley)

Fossil material from the Buckhorn asphalt quarry (Deese Gp.; Mid-Penn.) is unusual in that early sealing by oil preserved many original textural and mineralogic features. Echinoderm fragments from the quarry are well preserved and the morphology of the skeletal stereom is clearly visible. Specimens were observed in an SEM equipped with an EDS X-ray analysis system. 1-10μm calcian dolomite (CD) grains occupy 25% of the original stereom and pore space of the fragments as displayed by differential etching and MgKα X-ray maps. A variety of techniques (Single crystal X-ray diffraction, XRD, EMPA, TEM, and STEM microanalysis) were used to characterize the CD phase. The overal composition of the skeletal fragment is 75% $Ca_{.98}Mg_{.02}CO_3$, 25% $Ca_{.54}Mg_{.46}CO_3$. TEM revealed a 100 Å "tweed structure" identical to that reported by Reeder and Wenk (1979) in sedimentary CDs. Our data suggest that the Mg of the CD was derived in large part from the original high Mg-calcite (HMC) of the crinoid skeleton. The CD appears to have been the product of the following diagenetic events: 1), nucleation and growth of disordered CD via microdissolution reprecipitation and 2), subsequent structural ordering and exsolution resulting in the tweed structure. The presence of 100 Å microexsolution structures supports the mechanism of low-temperature dolomitization postulated by Gaines (1977) and others. Our data provide compelling evidence of the reaction HMC→ LMC + CD under natural low-temperature conditions. The recognition of tweed structures in previous studies as well as our own suggests their possible role in the stabilization and persistence of calcian dolomites in the ancient geologic record.

V 113

FLUORESCENCE MICROSCOPY OF HYDROCARBON FLUID INCLUSIONS: RELATIVE TIMING OF HYDROCARBON MIGRATION EVENTS IN THE ARKOMA BASIN, NW ARKANSAS

R. C. Burruss (Gulf Sci. and Tech. Co., P.O. Drawer 2038, Pittsburgh, PA 15230)
D.J. Toth, and R.H. Goldstein

Oil-filled vugs and fluid inclusions containing vapor, hydrocarbon liquids, aqueous liquids, or all 3 (3-phase inclusions) occur in multiple generations of septarian vein filling in the Mississippian Fayetteville Formation, northwest Arkansas. In Washington Co., AR, veins are filled 1st by euhedral sideritic calcite and 2nd by dolomite. Fluorescence microscopy reveals dull blue fluorescent hydrocarbon inclusions and nonfluorescent aqueous inclusions along growth zones in 1st. gen. calcite. These growth zones are cut by minor microfractures with yellow-gold fluorescent inclusions. Extensive microfractures with blue-white fluorescent hydrocarbon inclusions cross both the calcite and the dolomite. These 3 fluorescent types of hydrocarbon inclusions also occur in septarian veins from Searcy Co., AR, where all inclusions occur on healed microfractures cross-cutting both a 1st generation bladed, sideritic calcite and a 2nd generation sparry calcite.

Fluorescence spectra of individual inclusions allow correlation of the 3 hydrocarbon types between both localities (~120 km apart). Clearly, in Washington Co., a hydrocarbon phase was present during 1st generation calcite growth, whereas at Searcy Co., all hydrocarbon types postdate both generations of vein fill. Fluorescence spectra of the oil from vugs correlate with the blue-white fluorescent inclusions along healed microfractures crossing all generations of vein fill at both locations. The oil in the vugs apparently migrated on microfracture systems postdating all generations of carbonate vein filling.

V 114

CRETACEOUS VOLCANISM AND THE DISAPPEARANCE OF DINOSAURS

M. L. Keith (Dept. of Geosciences, The Pennsylvania State Univ., University Park, Pa., 16802)

The Cretaceous disappearance of dinosaurs and some of their contemporaries is a long-standing puzzle in geology. Recent investigations of stratosphere chemistry confirm ozone layer damage from synthetic Freons (chlorinated fluorocarbons and fluoromethanes) and show that the principal culprit is chlorine. This is an important clue; it raises the possibility of ozone layer destruction from natural chlorine, the principal source of which is volcanic activity. The late Cretaceous was a time of catastrophic volcanism, many times more violent and more extensive than the most violent of historic time. I propose as a working hypothesis that the extinction of dinosaurs was a cumulative genetic effect from frequent periods of intense ultraviolet irradiation brought about by Cretaceous volcanism and attendant catastrophic destruction of the ozone layer. Dinosaurs would be relatively vulnerable to damaging UV, whereas some smaller animals would be partially protected by vegetation, burrows, deep water habitat, etc., and the evolving mammals and birds would be partially protected by fur or feathers, which may have been adaptations to intense UV, as well as to climatic change. The proposed hypothesis is consistent with the observed association of reduced dinosaur diversity and final disappearance with extensive layers of Cretaceous volcanic ash: the bentonite beds and badlands terrain of western N. America. Much work will be required to test the hypothesis in other parts of the world.

Arcmagmatism

Harbour C
Sunday A.M.
S. Mahlberg Kay (Cornell University), Presiding

V 115

PETROLOGY AND SIGNIFICANCE OF OLIVINE AND AMPHIBOLE BEARING XENOLITHS IN ALEUTIAN ANDESITES

W.K. Conrad (Dept. of Geological Sciences, Cornell University, Ithaca, N.Y. 14853)
R.W. Kay

Amphibole bearing gabbroic and ultramafic xenoliths are found in recent andesite flows on Adak Island, Central Aleutians. In plagioclase-free ultramafic xenoliths, pargasitic amphibole (Mg/Mg+Fe=0.77-0.66) occurs as small to megacryst sized subhedral grains, poikilitically enclosing and partially replacing olivine and clinopyroxene. The CPX is zoned Mg-rich augite (Mg/Mg+Fe=0.8). The olivine is forsteritic, (Fo 91-84; NiO=0.27 wt.%) and encloses microphenocrysts of aluminous chrome spinel. Similar olivine has been reported as xenocrysts, phenocrysts and inclusions in Aleutian basalts and andesites, and as xenocrysts in a Tongan rhyolite. This olivine is probably mantle derived, or is the first fractionate of a mantle-derived melt. In contrast, inclusions containing less forsteritic olivine (Fo 83-72; NiO=0.1 wt.%), coexisting with amphibole similar to the Aleutian pargasites, are found in basalts and andesites from the Lesser Antilles and Japan. Previous studies and experimental evidence suggest these assemblages crystallized at crustal depths from basaltic liquids already depleted in Mg and Ni. Evidence that the amphibole crystallized from a melt (not a metasomatic replacement) is found in gabbroic xenoliths from Adak where euhedral amphibole is enclosed in megacrysts of anorthite. Favored genetic mechanisms for amphibole crystalizing around high Mg olivine are: 1) crystallization of amphibole from a melt containing xenolithic peridotite inclusions, 2) sequential crystallization from a basaltic liquid. Either model is consistant with an hypothesis invoking amphibole fractionation from mantle-derived melts for producing calc-alkaline trends in Aleutian igneous rocks.

V 116

TRANSVERSE GEOCHEMICAL VARIATIONS ACROSS THE ALEUTIAN ARC: COLD BAY TO AMAK

J. Morris (Massachusetts Institute of Technology, Cambridge, Mass. 02139)
S. R. Hart

Twelve andesitic lavas from 3 volcanic centers in SW Alaska, Quaternary Frosty Peak and the older Mt. Simeon complex on the Alaskan Peninsula at Cold Bay, and the Quaternary center on Amak Island have been analyzed for 87/86 Sr and Sr and alkali concentrations. All samples are petrographically fresh and have H_2O = .25-.50%. The 3 centers lie roughly along a line perpendicular to the trench with Amak about 50 km behind Cold Bay (which is part of the main volcanic arc). The volcanoes sit about 100 and 130 km respectively above a north dipping Benioff Zone which terminates at a depth of about 175 km. Major element analyses for the 3 centers show a similar and restricted range of bulk compositions.

The 2 Cold Bay volcanoes have similar trace element patterns, but the average concentrations of Sr, Cs, Rb & K are consistently lower for Cold Bay (484, 1.41, 32.3 & 10010 ppm) than for Amak (674, 1.5, 45.3 & 16140 ppm). K/Rb and K/Cs values are distinctly lower (312 vs 358, 9012 vs 12493) for Cold Bay, K/Sr values are slightly lower (21.2 vs 24.0) and Rb/Sr ratios are equal at 0.0680. The Sr isotope ratios, however, are distinct for the 3 different complexes. The 2 Mt. Simeon samples have 87/86=.70321 while those from Frosty Peak range from .70337 to .70352. The 7 Amak samples are the same within analytical error at a value of .70313.

This decrease in 87/86 with increasing distance from the trench is apparent throughout the Aleutian Arc. This pattern is also typical of young, intra-oceanic arcs such as Scotia and New Britian, but is rare for arcs such as the eastern Aleutians which are built on or near continental margins. While the low 87/86 Sr ratios suggest little or no crustal component, the K/Rb and K/Cs ratios are significantly lower (as they are in most arcs) than in oceanic basalts of similar 87/86 ratio.

V 117

MAGMATIC AND METAMORPHIC VARIATIONS IN ALEUTIAN EARLY SERIES VOLCANIC ROCKS, ADAK ISLAND, ALASKA

J.L. Rubenstone (Dept. of Geological Sciences, Cornell University, Ithaca, N.Y. 14853)
S. Mahlburg Kay

Early growth of the Aleutian island arc is recorded in the pre-Eocene submarine volcanigenic igneous and sedimentary rocks of the Finger Bay Volcanics, exposed on Adak Island in the central Aleutians. Lava and flow breccia sequences from two locales on southern Adak characteristically show phenocrysts of calcic plagioclase and clino-

pyroxene in an intergranular groundmass of primary plagioclase, clinopyroxene, and Fe-Ti oxides. Major element analyses of these samples indicate no iron enrichment with increasing SiO_2 content (FeO*/MGO=1.0 to 2.5 for SiO_2=49% to 59%) falling generally within the field of Recent Aleutian calc-alkaline lavas. Trace element concentrations determined for early series volcanics are also similar to the Recent Aleutian calc-alkaline suite, most notably in light rare-earth element enriched patterns. Correlation of major element variations with trends in trace elements considered non-mobile during metamorphic processes implies a primary calc-alkaline affinity for these early series magmas. The low-grade metamorphism of the Finger Bay Volcanics is locally variable in intensity, from zeolite to lower greenschist grade, and is most severe near major fracture zones mapped on the island. Low oxygen isotope ratios on a similarly altered early series gabbroic pluton indicate low-temperature interaction with meteoric water, suggesting that early series metamorphism is more likely related to hydrothermal effects of nearby mid- and late-Tertiary granodiorite intrusions, rather than a previously suggested regional Aleutian greenschist event associated with Tertiary subduction of the Kula-Pacific spreading center.

V 118

REE, K, Rb, Sr, and Sr ISOTOPIC GEOCHEMISTRY OF PERIDOTITE XENOLITHS IN BASALT FROM NUNIVAK ISLAND, ALASKA

M.F. RODEN
F.A. Frey (both at Dept. of Earth and Planetary Sciences, M.I.T., Cambridge, Ma. 02139)
D.M. Francis (Dept. of Geological Sciences, McGill University, Montreal, Quebec)

Chondrite-normalized REE patterns of peridotite nodules in basanites from Nunivak Island, Alaska correlate with peridotite texture and mineral composition. Amphibole-free granuloblastic-equant (GE) xenoliths (see Francis, 1978) are the most fertile with respect to basaltic components, are relatively light REE depleted ($(La/Sm)_N$ = 0.46 to 0.49), and have the highest heavy REE concentrations. In contrast, the more refractory amphibole-bearing and amphibole-free coarse-equant and coarse-tabular xenoliths are relatively light REE enriched ($(La/Sm)_N$ = 1.1 to 9.6) and in general have higher concentrations of K, Rb, Sr, and Ba than the GE xenoliths. Amphibole-bearing xenoliths have higher concentrations of the light REE than other light REE enriched nodules (La = 1.4 to 8.7 ppm versus 0.29 to 0.88 ppm). REE patterns of acid-leached clinopyroxene (CPX) separates mimic whole rock patterns. Based on whole rock $^{87}Sr/^{86}Sr$ (87/86) ratios, radiogenic Sr also correlates with light REE enrichment: the GE group has lower 87/86 ratios, 0.70216 to 0.70262, than the other xenoliths (0.70289 to 0.70375).

The data indicate that the mantle beneath Nunivak Island is heterogeneous with respect to LIL elements and Sr isotopic composition. At least two regions exist: a CPX-rich region with REE and Sr isotopic characteristics consistent with a genetic relationship to oceanic tholeiites, and a more refractory region, anomalously enriched in LIL elements. We attribute the origin of this latter region to the reaction of refractory wall rock with a metasomatic component rich in LIL elements. Because in part amphibole represents this contaminating component, Nunivak xenoliths are useful for determining the characteristics of the metasomatic fluid.

V 119

THE EDGECUMBE VOLCANIC FIELD, SE ALASKA: PARTIAL FUSION OF CRUSTAL MATERIAL BY BASALT

James D. Myers, Department of Earth and Planetary Sciences, The Johns Hopkins University, Baltimore, MD 21218 (now at Department of Geological Sciences, VPI & SU, Blacksburg, VA 24061)

The volcanic rocks of the Recent Edgecumbe volcanic field, SE Alaska include basalts (47% SiO_2), andesites (55-59 %) and rhyodacites (70 %), but a compositional gap exists between 60 and 70 % SiO_2. The rhyodacites, which are nearly equal in volume to the andesites, were erupted after the basalts and before the andesites. The volcanic suite is characterized by high Al_2O_3 (14-18 %) and variable isotopic compositions ($^{87}Sr/^{86}Sr$:0.70298-0.70440; $\delta^{18}O$:5.8-7.9). Unzoned to weakly zoned mafic phenocrysts (ol, opx, cpx) have restricted compositional ranges; plagioclase compositions and zoning patterns vary greatly. In the basalts and rhyodacites, plagioclase are compositionally restricted (±10 mol % An) and weakly zoned (≤13 mol %), but larger variations (An55-75) and stronger zoning (≥30 mol % An) characterize andesitic plagioclase. Fractionation of observed phenocryst assemblages cannot account for the lavas' chemical and isotopic variability, compositional gap, eruptive sequence, relative volumes or plagioclase compositions and zoning patterns. These features were produced by partial fusion of granodiorite basement ($^{87}Sr/^{86}Sr$=0.70487; $\delta^{18}O$:8.7-9.3) and subsequent mixing of partial melts and primary basalt. Two component mixing of basalt + partial melt cannot explain the data, rather, melt compositions must have changed with time. The rhyodacites consist almost entirely (≥95 %) of early, siliceous (71-74 % SiO_2) partial melt. Intermediate lavas (40-70 % basaltic component) were produced by mixing secondary partial melts of varying composition (58-62 % SiO_2) with primary basalt. These secondary melts were generated by melting the solid residum of the initial melting epsiode. The hybrid lavas contain ~4.8 km^3 of melt. Cooling of the basalt could have fused a slightly larger volume (~5 km^3) of granodiorite. Thus, the proposed model is thermally reasonable.

V 120

EMPLACEMENT AND DIFFERENTIATION OF TWO MIOCENE PLUTONS IN THE SOUTHERN ANDES

P.J. MICHAEL (Lamont-Doh. Geol. Obs., Columbia Univ., Palisades, N.Y. 10964)

Cordilleras Paine and Fitz Roy are two isolated Miocene plutons located east of the Cretaceous-Early Tertiary calc-alkaline Patagonian batholith and the current volcanic line, and west of Late Tertiary alkali basalts. They are part of a discrete phase of magmatic activity in the southern Andes which may be related to the subduction of the Chile Rise in the last 20 million years, or perhaps can be correlated with magmatic migrations observed in parts of central Chile that were unaffected by ridge subduction.

The plutons intrude upper Cretaceous sediments of a foreland basin. Rock types vary from cumulate gabbros to quartz monozodiorites and a later adamellite phase. 2500 meters of relief exposes predominantly the adamellite units with more basic rock types exposed as xenoliths and as continuous outcrop in the lower levels. Metasomatic reaction and disequilibrium mineral assemblages in cumulate gabbros represent variable degrees of reaction of early formed cumulate phases with a late fluid, which is of auto metasomatic origin or derived from the later adamellite. Evidence supporting in situ differentiation accompanied by discontinuous liquid separation are the similarities of various chemical parameters between gabbroic and adamellite units within each pluton despite differences between the plutons, petrographic evidence for crystal accumulation and in situ differentiation, consistent intrusion order, and consistent appearance of the diverse assemblages together in a region lacking in plutonic activity. Evidence supporting the intrusion of separate magmas is the relative scarcity of exposed gabbroic rocks, the large hiatus in composition, (SiO_2=61%-69% for Paine), and the tendency for different magmas to intrude along old zones of weakness.

Various chemical and mineral chemical features suggest that Fitz Roy's parental magma(s) was of high-alumina basalt affinity while Paine's was transitional to an alkali basalt composition.

V 121

$\delta^{18}O$ VARIATION AMONG CALC-ALKALINE VOLCANIC ROCKS FROM S. CHILE: IMPLICATIONS FOR THE EFFECTS OF RIDGE SUBDUCTION ON THE SOURCE REGION OF OROGENIC VOLCANISM

K. Muehlenbachs (Dept. of Geology, Univ. of Alberta, Edmonton, Alberta, Canada, T6G 2E3)
C.R. Stern (Dept. of Geological Sciences, Univ. of Colorado, Boulder, Colorado, U.S.A. 80309)

The southeast extension of the Chile Rise has been subducted beneath southernmost S. America during the last 20 my. The Recent calc-alkaline volcanoes to the south of the triple junction (at 46°S) are dominantly hornblende-andesites whereas the volcanoes to the north are olivine bearing, high-Al basalts. These rock types differ in $\delta^{18}O$. 11 andesites from Lautaro, Aguilera and Mt. Burney range in $\delta^{18}O$ from 5.9 to 8.3 ($\delta^{18}O$ = 7.3 ± 0.9) but 14 basalts from Llaima, Carran, Mirador, Antillanca, Maca and Cay range only from 5.9 to 6.5 ($\delta^{18}O$ = 6.0±0.1). Significantly, the $\delta^{18}O$ of 5 dacites (6.2±0.3) from north of the triple junction is similar to that of the basalts and not to the southern acidic rocks. Other studies indicate that the rocks from either side of the triple junction also differ in initial $Sr^{87}/^{86}$; .705 to .707 for the andesites (by analogy with petrologically similar rocks in N. Chile) and .704 for the basalts. These isotopic data suggest that the hb-andesites are derived from a mantle source region which has been significantly modified, perhaps by the addition of material derived from subducted oceanic crust including altered ocean floor basalt. The high-Al basalts occuring north of 46°S could be derived from much less modified mantle material. The northern dacites are simple differentiates from basaltic magma. These results are consistent with the results of experimental studies concerning the genesis of orogenic basalts and andesites. The implied north to south variations in the source regions of orogenic volcanism in southernmost S. America may be related to variations in subduction geometry and convergence rate caused by the subduction of the Chile Rise.

V 122

PETROLOGY OF AN ISLAND ARC VOLCANIC COMPLEX, LOLOBAU ISLAND, NEW BRITAIN

Jay L. Banner
A. E. Bence (both at: Dept. of Earth and Space Sciences, SUNY, Stony Brook, N. Y. 11794)
R. W. Johnson (Bureau of Mineral Resources, P. O. Box 4, Canberra A.C.T. 2600, Australia)

Lolobau Island, an active eruptive center located in the New Britain island arc (Late Cenozoic), consists of a sequence of low-K lavas ranging from tholeiite to "rhyolite" (Fig.). Andesites dominate the sequence. Stratigraphic controls on the samples define three relative age groups, with each group represented by the same bulk and mineral composition ranges.

Plagioclase feldspar is the major constituent of these lavas. Phenocryst core compositions range from An_{96} (tholeiite) to An_{60} ("rhyolite"). In several samples complex, normal, reverse and oscillatory zoning of the plagioclase phenocrysts occurs. Cpx ($Wo_{34-45}En_{38-49}Fs_{5-24}$), opx ($Wo_{2-5}En_{56-78}$) and titanomagnetite are nearly ubiquitous. Olivine (Fo_{71-87}) occurs only in the more basic samples. K-feldspar, ilmenite, amphibole and mica are not observed.

Compatible and incompatible trace element abundances cover the same range for each temporal group of samples. $(La/Nd)_{e.f.}$ values are between 1 and 2.

The lavas appear to be related by low-pressure fractional crystallization along the plagioclase-clinopyroxene cotectic. At least three sequential pulses of magma of similar composition have fractionated at shallow depth and erupted at Lolobau.

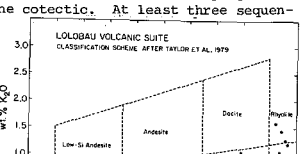

V 123

GEOCHEMICAL EVIDENCE FOR THE ORIGIN OF ISLAND ARC MAGMAS FROM PALAU

A. K. Sinha and M. Loiselle, both at Dept. of Geological Sciences, Virginia Polytechnic Institute and State University, Blacksburg, VA 24061; and David Gottfried and Gilbert Corwin, both at U.S.G.S., Reston, VA 22092

Volcanic rocks of Eocene age from the Palau island arc have been studied for Sr isotopic composition and Rb, Sr, Nb, Ta, Zr, Hf, and rare earth elements (REE). The samples range from island arc tholeiitic basalt (SiO_2 48%) through andesites (SiO_2 53-65%) to dacites (SiO_2 70-79%). Model $(^{87}Sr/^{86}Sr)_o$ ratios range from 0.70300 to 0.70463, and do not correlate with rock type. However, consideration of K, Rb, and Sr contents, K/Rb ratios, and light (L)REE abundances indicate the range of magmatic $^{87}Sr/^{86}Sr$ ratios is more limited (0.70300-0.70341). The higher ratios reflect post-eruptive alteration. Rare earth patterns range from LREE depleted in the basalts (La/Sm_{ef} 0.38-0.93) through slight enrichment in the andesites (La/Sm_{ef} 0.97-1.9) to values of La/Sm_{ef} of 2.2-2.3 in the dacites. Selected immobile trace elements (Zr, Hf, Nb, Ta) in the basalts are lower than values observed in MORB. Nb and Ta are relatively uniform through the suite, but Zr shows progressive enrichment in the andesites and dacites. One basalt sample has evidence of extreme REE enrichment (with the development of a negative Ce anomaly) produced during alteration, with complimentary low K/Rb and high $^{87}Sr/^{86}Sr$. Our

data indicate the variation in magmatic $^{87}Sr/^{86}Sr)_o$ is real and reflects source heterogeneities. Lack of correlation of $^{87}Sr/^{86}Sr$ with rock type precludes contamination or simple two end-member mixing as a means of explaining the variation. The low Zr, Hf, Nb, and Ta abundances in the basalts and the high K/Rb of the suite as a whole indicate a depleted source for the magmas. The data indicate a complex history of tectono-volcanic evolution of the island arc system.

V 124

LOW P-T META-BASALTS AND VOLCANIC BRECCIAS FROM THE MUSSAU TRENCH - WESTERN EQUATORIAL PACIFIC

D.J. Fornari (Department of Geological Sciences, State University of New York at Albany, Albany, NY 12222)
R.D. Jarrard
J.K. Weissel (Lamont-Doherty Geological Observatory, Palisades, NY 10964)

The Mussau Trench marks part of the eastern boundary between the Caroline and Pacific plates. Geophysical data suggests that slow, eastward subduction of Oligocene Caroline lithosphere is presently occurring. Two dredge hauls taken from depths of 1200 and 1600 fathoms, on the inner-wall of the Mussau Trench recovered highly weathered basalts and greenschist facies metamorphosed basalts and brecciated equivalents. Dredge 6 (1200 fms.) recovered extensively weathered fine-grained to aphanitic basalts and fine-grained diabases. All of the microphenocrysts and nearly all of the mesostasis minerals (cpx, plag, ol) plus glass have been completely altered to clay minerals and palagonite. Calcite and silica veins are common in the rocks from this dredge. Dredge 7 (1600 fms.) recovered fine-grained, heavily altered pillow basalt fragments that have been metamorphosed to greenschist grade. Calcite, silica and serpentine veins are ubiquitous throughout the rocks. Additionally, a large proportion of the recovered rocks are volcaniclastic breccias that show textural evidence for low-temperature and low to moderate pressure deformation. Basalt clasts in the breccias are textural and compositional analogs of the rocks recovered in dredge 6. Recovery of these suites of altered and metamorphosed ocean floor rocks supports the geophysical interpretation that slow, contemporary subduction is active along the Mussau Trench and that the exposed rocks on the inner-wall are being tectonically deformed.

V 125

CRYSTAL FRACTIONATION AT INTERMEDIATE PRESSURES AND BASALTS FROM BEHIND THE VOLCANIC FRONT IN CENTRAL AMERICA

James A. Walker
Michael J. Carr (both at: Dept. of Geological Sciences, Rutgers University, New Brunswick, N.J. 08903)

Basaltic cinder cones, small shield volcanoes and rhyolite obsidian domes characterize recent volcanism behind the volcanic front in Central America. These volcanoes are concentrated near transverse breaks in the overriding plate. The basaltic lavas contain only olivine and plagioclase phenocrysts and are nearly aphyric. Principle chemical features are: 1) high Ni and Cr contents; 2) high incompatible element contents; 3) Sr and Al_2O_3 enrichment with fractionation.

The high concentrations of Ni, Cr, Ba, and Rb in the basalts suggest a small degree (3-15%) of partial melting of peridotite. Crystal fractionation of the primary magmas is necessary to explain the total chemical diversity in the basalts. In contrast to petrographic observations, major element modeling and the decrease in the CaO/Al_2O_3 ratio with fractionation require: 1) removal of clinopyroxene; 2) considerable crystallization. These discrepancies can be resolved by the following model: plagioclase + clinopyroxene ± olivine crystallize at approximately 6-7 Kb, the magma separates from the crystals, rises, and erupts nearly aphyric lavas. Near-surface crystallization is only plagioclase and olivine because of the expansion of the olivine liquidus field at lower pressures. The Sr and Al_2O_3 enrichment trends and the occasional modal excess of plagioclase indicate plagioclase accumulation may sometimes occur.

Behind the volcanic front and near transverse structures in the Cascades, Mexico, and Kamchatka, there are similar clusters of basaltic cinder cones. This type of volcanism with its characteristic tectonic setting and geochemistry is common at convergent margins.

V 126

A GEOCHEMICAL INTERPRETATIVE MODEL ON THE GENESIS AND EVOLUTION OF THE FUMAROLES OF VULCANO, AEOLIAN ISLANDS, ITALY

M. Carapezza
S. Hauser
P. M. Nuccio
M. Valenza (all at: Istituto di Mineralogia, Petrografia e Geochimica, Università di Palermo, Palermo, Italy)

A geochemical model is proposed in order to explain the presence of fumaroles having different gas composition and temperature at the top of the crater and along the sea-side of Vulcano. The existence of a pressurized biphase (liquid-vapor) reservoir at a certain depth is stated. The energy and the mass balances controlle the P and T conditions in the system, evolving along a boiling curve since the liquid phase is present. On the basis of the thermodynamic properties of the fluids which belong to the H_2O-NaCl-CO_2 system, the CO_2 content in the vapor is explained. Assuming the oxygen fugacities prevailing in the system range between the HM-FMQ buffers, the SO_2/H_2S, CO_2/CO, CO/CO_4, CO_2/CH_4 ratios in the fumarolic gases of the crater essentially reflect conditions of higher temperature equilibria. The more reduced gases of the sea-side have been interpreted as the result of riequilibration in shallowaquifers. The model was successfully used to interpret the variations in the fumarolic gases in relation to the evolution of the volcanic activity.

V 127

SURVEILLANCE OF THE VOLCANIC ACTIVITY OF VULCANO (AEOLIAN ISLANDS, ITALY): EVOLUTION, RISK AND CHOICE OF CRITICAL PARAMETERS

P. M. Nuccio
M. Valenza
M. Carapezza (all at: Istituto di Mineralogia, Petrografia e Geochimica, Università di Palermo, Palermo, Italy).

Volcano's activity has been characterized by explosive eruptions giving rise to mainly rhyolitic products. The last violent eruption occurred in 1888 and, after the occlusion of the volcanic vent, all the volcanic activity became limited to a few acid fumaroles and hot wells. However at the end of 1977 a lot of new fumaroles appeared at the rim of the crater and the maximum temperature of the gases in some of the fumaroles went-up from ∿ 190°C to ∿ 280°C. Both discrete measurements and continuous monitoring of some parameters were performed for an intensive geochemical and geophysical survey, within the CNR Cooperative program on the surveillance of active Italian volcanoes. Following the model proposed by Carapezza et al., on the basis of the observed variations of some chemical and physical parameters, the evolution of the volcanic activity of Vulcano was interpreted. Our results suggest a strong increase in the deep energy and a consequent evolution in the geothermal reservoir from a biphase system toward a vapor monophase system. This implies a dramatic pressure building in the reservoir and an increased risk of a phreatic or phreatomagmatic explosion. Finally, according to the model, some chemical and physical parameters have been selected for a useful surveillance of the volcanic activity.

V 128

I- AND S-TYPE GRANITOIDS OF THE CENTRAL AEGEAN CRYSTALLINE COMPLEX (CREECE)

Rainer Altherr (Dept. of Geophysical Sciences, University of Chicago, Chicago, Illinois 60637)
(Sponsor: Peter J. Wyllie)

I- and S-type granitoids and low P/T metamorphic rocks of the Central Aegean Crystalline Complex together with high P/T metamorphic rocks of the Peloponnesus and Crete constitute a paired metamorphic belt of Late Oligocene to Lower Miocene age indicating that underplating of the central Aegean area during this time was directed from southwest to northeast.

Whereas I-type granitoids occur across the whole high temperature belt, S-type granites are confined to its northeastern part. The modal compositions of the I-type granitoids vary from granodioritic in the southwest to granitic and monzonitic in the northeast. Among the rocks of granodioritic to granitic composition chemical variation is more pronounced transverse than lateral to the belt. From southwest to northeast K, Rb, Sr, Ti, and Zr increase, whereas Na, V, Ba, Mg/Fe, and the oxidation state of iron decrease. These chemical differences may be interpreted as being derived from a progressively more fractionated source.

The monzonite, located at the inner border of the belt, does not fit into this scheme. High Mg/Fe, V, Sr, and Ba demand a less fractionated source and a residue essentially free of feldspar.

The modal and chemical compositions of cognate inclusions, which are interpreted as restite material, are uniform in the granodiorites and the monzonite, but unsystematically variable in the granites, suggesting that the granites were derived from a heterogeneous source.

Mineralogy-Crystallography I

Harbour A
Sunday A.M.
S. K. Saxena (Brooklyn College), Presiding

V 129

EQUILIBRIUM COMPOSITIONS OF ORTHOPYROXENE (OPX), CLINOPYROXENE (CPX) AND GARNET (GAR) IN THE CaO-MgO-Al_2O_3-SiO_2 SYSTEM

Dexter Perkins III, Robert C. Newton (Dept. Geophysical Sciences, Univ. of Chicago, Chicago, Illinois 60637)

The compositions of coexisting OPX, CPX and GAR have been reversibly determined by a hydrothermal method over P/T ranges of 16-30 kb/900-1100°C. The % Al_2O_3 in OPX in the MgO-Al_2O_3-SiO_2 and CaO-MgO-Al_2O_3-SiO_2 systems is buffered by the reaction (1): $Mg_3Al_2Si_3O_{12}$ (in GAR) = $Mg_3Al_2Si_3O_{12}$ (in OPX). Assuming ideal mixing of $Mg_3Al_2Si_3O_{12}$ in OPX at 1 bar (Ganguly and Ghose, 1979), a linear regression of all reversed data in the 3- and 4-component systems yields $\Delta H° = 7369$ cal and $\Delta S° = 5.75$ cal/K for reaction (1). Results (and uncertainties) in the 4-component system are:

P Kb	T K	Wt% Al_2O_3 in OPX	Wt% Al_2O_3 in CPX	Ca/Ca+Mg in CPX
16	1273	5.1(1.5)	4.2(0.5)	.482(.007)
20	1173	2.1(0.3)	1.5(0.2)	.471(.004)
25	1173	1.4(0.3)	1.1(0.1)	.474(.005)
25	1273	2.1(0.5)	1.5(0.3)	.467(.003)
25	1373	2.9(0.6)	1.7(0.7)	.452(.001)
30	1173	1.1(0.2)	0.9(0.1)	.474(.006)
30	1273	1.5(0.2)	1.2(0.3)	.469(.004)
30	1373	2.5(0.2)	1.6(0.4)	.456(.006)

The GAR at equilibrium with CPX and OPX contains 86±1 wt% $Mg_3Al_2Si_3O_{12}$ at all P/T studied. The Ca/Ca+Mg values in OPX at equilibrium with CPX and GAR do not vary measurably from those values determined for the Al-free system by Lindsley and Dixon (1976). The values of Ca/Ca+Mg for Al-bearing CPX are significantly greater than those determined in the Al-free system. Al_2O_3 is slightly greater in OPX than in coexisting CPX. The fact that natural pyroxene pairs show the opposite effect is due to the additional components Na_2O and Fe_2O_3.

V 130

EXPERIMENTAL STUDY OF PYROXENES IN THE SYSTEM $CaMgSi_2O_6$-$CaAl_2SiO_6$-$Ca_{0.5}AlSi_2O_6$

T. Gasparik and D. H. Lindsley (Dept. of Earth and Space Sciences, State Univ. of New York, Stony Brook, N. Y. 11794)

Synthesis experiments on the join $CaAl_2SiO_6$-$CaAl_2Si_2O_8$ confirm the existence of a component $Ca_{0.5}AlSi_2O_6$ ("Ca.5") in tschermakitic pyroxenes (Wood and Henderson, Am. Min. 63, 1978). Ana-

lytical difficulties caused by fine grain size have been eliminated by seeding and use of PbO flux; high-quality probe analyses of aluminous pyroxenes can now be obtained. Run (1) (1440°C, 33 kb, 4h.) produced Px + An + Ga + Cor + L. Anorthite (1450°C, 35 kb, 5 h.) converted to zoned Px + Ky + Ga + Cor + L [run (2)]. Work is in progress to determine the mixing properties of Px solid solutions in the system Di-CaTs-Ca.5 using the exchange equilibria:

$CaAl_2Si_2O_8 = CaAl_2SiO_6 + SiO_2$

$3\ CaAl_2Si_2O_8 = 2CaAl_2SiO_6 + {}^2Ca_{0.5}AlSi_2O_6$

$2Ca_{0.5}AlSi_2O_6 = CaAl_2SiO_6 + 3SiO_2$

As an example, run (3) gives the average composition (reversed) of Px coexisting with An + Q + L at 1400°C and 32 kb (5 h.).

Run #	1	2(Av.)	3
# of an.	35	44	58
SiO_2	1.193	1.313	1.444
Al_2O_3	1.803	1.687	1.373
MgO	---	---	0.184
CaO	0.910	0.843	0.869
Σ	3.906	3.843	3.870
Di	---	---	0.184
CaTs	0.807	0.687	0.556
Ca.5	0.185	0.313	0.261
Σ	0.992	1.000	1.001

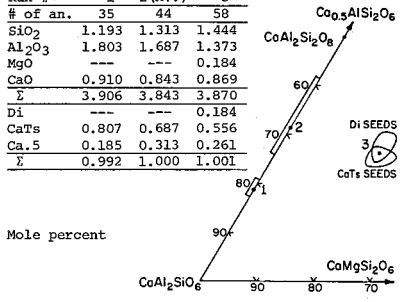

V 131

HIGH-TEMPERATURE DEFORMATION OF OLIVINE: EFFECTS OF CHANGING POINT DEFECT CHEMISTRY

Daniel Ricoult
D. L. Kohlstedt (both at: Dept. of Materials Science and Engineering, Cornell University, Ithaca, NY 14853)

As part of a study of the effects of changing the point defect chemistry on the high-temperature rheology of olivine, single crystals of San Carlos peridot annealed either in periclase or in enstatite have been plastically deformed. Samples embedded in fine-grained periclase powder were heat treated at 1600°C for eighty hours; samples surrounded by enstatite powder (Bamble, Norway) were held at 1100°C for eighty hours. Deformation experiments were carried out at room pressure in the temperature range 1100 to 1600°C at differential stresses of 30 to 60 MPa. At a given stress and temperature, samples annealed in MgO deformed approximately ten times faster than those annealed in $(Mg,Fe)SiO_3$. The activation energy for creep appears to be somewhat higher for the former than for the latter. Experiments are now in progress using H_2-CO_2 and CO-CO_2 gas mixtures to examine the possible effects of varying oxygen partial pressure and water partial pressure on the creep behavior of olivine.

V 132

$^{18}O/^{16}O$ AND $^{17}O/^{16}O$ FRACTIONATION STUDIES ON Ca-Mg SILICATE MINERALS

A. Matthews, J. R. Goldsmith (Dept. of Geophysical Sciences, University of Chicago, Chicago, IL 60637) and R. N. Clayton (Enrico Fermi Institute, University of Chicago)

Oxygen isotope fractionations between Ca-Mg silicate minerals and water have been studied experimentally at high pressures ($2 \leq P.H_2O \leq 20$ kb.) and temperatures ($500° \leq T \leq 800°C$). The exchange method has initial mineral-water $^{18}O/^{16}O$ fractionations close to equilibrium; whereas initial $^{17}O/^{16}O$ partitioning is well removed from equilibrium. These initial conditions allow accurate determinations to be made of both the fractional extent of isotopic exchange during equilibration (from the $^{17}O/^{16}O$ shifts) and the equilibrium $^{18}O/^{16}O$ fractionations (by extrapolation of the near-equilibrium $^{18}O/^{16}O$ ratios). Direct isotopic exchange between the studied Ca-Mg silicates ($CaSiO_3$ (wollastonite); diopside; enstatite; forsterite; tremolite/fluortremolite; zoisite and chlorite) and water is much slower than observed for quartz and feldspar, and in some cases (e.g., zoisite and chlorite) is prohibitively slow for calibration of equilibrium $^{18}O/^{16}O$ fractionations at petrologically reasonable temperatures. The most amenable system studied was $CaSiO_3$-H_2O, for which equilibrium $^{18}O/^{16}O$ fractionations (1000 ℓn α) are: -1.08 (800°C); -1.19 (700°C); -1.39 (600°C); and -1.43 (500°C). The fractionation data extrapolate smoothly to zero at infinite temperature and do not accord with the theoretical treatments of Bottinga and Javoy (1973, 1975). Diopside fractionates similarly to $CaSiO_3$ at 600° and 700°C. Particular advantages of the data in isotope thermometry are the large fractionations between minerals at high temperature (e.g., quartz-pyroxene; pyroxene-magnetite) and the resistance of pyroxene minerals to retrograde re-equilibration (e.g., Ito, 1979).

V 133

PHASE RELATIONS OF NATURALLY OCCURRING TUNGSTATE MINERALS UNDER HYDROTHERMAL CONDITIONS

L. C. Hsu (Nevada Bureau of Mines & Geology and Department of Geol. Sciences, University of Nevada, Reno, NV 89557)

The binary phase relations of naturally occurring tungstate minerals were investigated hydrothermally at P_f=1.0kb and T=400 -900°C. A complete series of solid solution between scheelite(C) and stolzite(P) forms above 725°C. The solvus is almost symmetrical with a crest near $C_{52}P_{48}$. The position and shape of the solvus are quite different from those previously reported under anhydrous conditions. The d-spacing of the 116 reflection varies linearly from 1.687(2)Å for scheelite to 1.782 (2)Å for stolzite. Ferberite(F) and sanmartinite(Z) as well as huebnerite(M) and sanmartinite form a complete series of solid solution down to at least 400°C, far lower than previously reported. The Δ2θ FeKα radiation between the 102 of quartz and the 200 of F-Z and M-Z reflections also varies linearly with composition. The solid solubility is very limited between tungstate minerals with different crystal structures. Less than 5 mole % miscibility of one to the other is observed between scheelite and ferberite, between ferberite and stolzite, between stolzite and sanmartinite, and between sanmartinite and scheelite at temperatures up to 900°C.

It appears that the solid solubility among these tungstate minerals is affected more strongly by the availability of the structural sites for specific divalent cations than the crystallochemical nature of the divalent cations themselves. Although intermeditate members between F and Z and between M and Z may be expected to occur commonly like those between F and M as wolframite, certain physico- and crystallochemical characteristics of the element zinc may limit such occurrences.

V 134

MINERAL-SOLUTION EQUILIBRIA IN THE SYSTEM Mn_3O_4 -H_2-H_2O-HCl

Nabil Z. Boctor
J. D. Frantz (both at Geophysical Laboratory 2801 Upton St., N. W., Wash., D. C. 20008

Mineral-solution equilibria in the system Mn_3O_4-H_2-H_2O-HCl were studied in the temperature range 400-650°C at 1000 and 2000 bars using double capsule rapid quench hydrothermal techniques. The Ag-AgCl buffer method (Frantz and Eugster, 1973; Frantz and Popp, 1979) was used to determine the molality of associated hydrogen chloride. The molalities of manganese and chloride were measured after quenching. Determination of Cl/Mn ratios in the fluid in equilibrium with Mn_3O_4 yields values ≈2 which suggest that Mn^{2+} is the dominant oxidation state. The change in the molalities of associated hydrogen chloride (m_{HCl°) as a function of the change in the molalities of total manganese (m_{Mn_T}) was used to identify the most abundant complex of manganese in the hydrothermal fluid. $MnCl_2^\circ$ was found to be the predominant species in equilibrium with Mn_3O_4 at 600°C and 2000 hours. The equilibrium constant for the reaction

$$Mn_3O_4 + 6HCl^\circ + H_2 = 3MnCl_2^\circ + 4H_2O$$

was calculated and used to determine the difference in Gibbs free energy between $MnCl_2^\circ$ and HCl°.

V 135

SPECTROPHOTOMETRY OF AQUEOUS TIN COMPLEXES

Varda N. Fleer
H. L. Barnes (both at the Ore Deposits Research Section of the Pennsylvania State University, University Park, Pa. 16802)

The solubility of the dominant tin ore mineral, cassiterite (SnO_2), was investigated spectrophotometrically at 25°C to indicate mobility in potential ore-forming environments. Ultraviolet-visible and Raman spectra were recorded for NaOH, NaCl, KCl and CH_3OH solutions of SnO_2 and $SnCl_4 \cdot 5H_2O$. The concentration of tin in SnO_2-saturated solutions was determined by emission spectroscopy to have a range of 0.010 - 0.036 ppm depending upon grain size and surface kinetic effects. The Ultraviolet-visible spectra had a major peak at 294 nm and minor peaks at 212 and 712 nm. The molar extinction coefficient, ϵ_{294}, was calculated to be 3.65×10^5 liter $mole^{-1}$ cm^{-1}. Mixed solvent (CH_3OH + H_2O) experiments indicated that there were two water molecules bound to each Sn^{4+} ion in a complex, probably $SnO_2 \cdot 2H_2O$. The Raman spectra of the tetrachloride solutions had a major peak at 345 cm^{-1} which was the totally symmetric stretching mode of the complex. Normal coordinate analyses, utilizing Wilson FG matrices, identified the complex as having a square planar (D_{4h}) symmetry; therefore this complex is $SnCl_4$. Additional weak Raman peaks correspond with published values for the complex $SnCl_6^{2-}$. Under the aqueous conditions studied, Sn^{4+} behaves as both a class A and a class B cation. At low temperatures, SnO_2 is not mobile in either a hydrate or Cl-complex. At 200-400 °C, typical of the formation of hydrothermal tin deposits, Sn^{2+} complexes are expected to predominate. Because Sn^{2+} is also intermediate between class A and B, analogous stannous complexes are expected at elevated temperatures.

V 136

SODIC PYROXENES FROM NYBO, NORWAY: SOLID SOLUTION AND CATION ORDERING AT HIGH TEMPERATURES

M.A.Carpenter (Dept. Geological Sciences, Harvard University, Cambridge, MA 02138)
D.C.Smith (Grant Institute of Geology, West Mains Rd., Edinburgh EH9 3JW, Scotland)
(Sponsor: C.W.Burnham)

Sodic pyroxenes in the eclogite pod at Nybø, Norway, are remarkable in the extent of solid solution which they show. Electron microprobe analysis indicates that the range of compositions is at least from $Jd_{78}Ac_2Aug_{20}$ to $Jd_{24}Ac_9Aug_{67}$ (Ac=0-12 mol.%) and includes crystals within the jadeite-omphacite "miscibility gap" reported from other localities. Examination of a selection of these pyroxenes by transmission electron microscopy reveals: (a) a complete lack of exsolution textures, in sharp contrast to similar pyroxenes from blueschist environments; (b) antiphase domains (APD's) arising from the C2/c - P2/n ordering transformation, and up to 0.35 μm in diameter, in omphacites with compositions between $Jd_{35}Ac_8Aug_{57}$ and $Jd_{51}Ac_{11}Aug_{48}$; (c) diffuse h+k=odd reflections in selected area diffraction patterns from Jd and Aug rich omphacites, indicating short range cation order; (d) C2/c symmetry for the most Jd rich crystals.

The pyroxenes are thought to have crystallised within the temperature range 700-850°C at P~18-28kb. The lack of exsolution and the wide range of compositions suggest that there is complete solid solution between Jd and Aug under these conditions. The observations are consistent with the recently proposed phase relations for Jd-Ac-Aug which show no two phase regions between ordered (P2/n) and disordered (C2/c) phases at high temperatures. The APD's may have developed during an extended thermal history at high temperatures - hence their large size. The subsequent cooling was too rapid for exsolution in the low temperature Jd-Om and Om-Aug miscibility gaps to occur, but allowed sufficient time for short range ordering to take place in crystals which entered the P2/n field.

V 137

A MODEL FOR ELEMENT PARTITIONING AMONG PEGMATITIC RARE EARTH MINERALS

Donald M. Burt
David London (both at: Department of Geology, Arizona State University, Tempe, AZ 85281)

The smaller radius, heavier rare earth elements generally behave similarly to yttrium, whereas the larger radius, lighter rare earth elements generally behave similarly to cerium. A model for the partitioning of the rare earths in pegmatites is therefore provided by the reciprocal system /Y, Ce//F_3, CO_3F, PO_4, NbO_4, $SiO_{3.5}$/, where those anion groups on the left seem to prefer cerium, and those on the right, yttrium. The phases involved are CeF_3 (fluocerite or "tysonite"), YF_3 (not described as a mineral), $CeCO_3F$ (bastnaesite), YCO_3F (bastnaesite-Y), $CePO_4$ (monazite), YPO_4 (xenotime), $CeNbO_4$ (beta-fergusonite-Ce or "brocenite"), $YNbO_4$ (fergusonite), $Ce_2Si_2O_7$ (not described as a mineral), and $Y_2Si_2O_7$ (thalenite). For a graphical representation, the fluorides and the fluorocarbonates may be considered together, and the sorosilicates, apparently even more Y-selective than the niobates, omitted. The resulting triangular prism shows as stable the interior four-phase volume fluocerite (and/or bastnaesite) + monazite + xenotime + fergusonite, an association described, for example, from the Black Cloud pegmatite, Teller Co., Colorado by Heinrich and Conrad (1960). Excluded are the extremal phases YF_3 or bastnaesite-Y, stable only in relatively more Y-rich or acidic environments, and beta-fergusonite-Ce, stable only in more Ce-rich or basic environments (e.g. carbonatites). In the "exchange operator" notation of Burt (1974), the chemical potential of the acidic operator YCe_{-1} may be used to monitor the increasing "basicity" (or attraction for small, as opposed to large, trivalent cations) of the anions fluoride, fluorocarbonate, phosphate, niobate, and sorosilicate in simple rare earth minerals.

V 138

EFFECT OF HYDRATION ON THE ELECTRICAL CONDUCTIVITY OF OLIVINE*

Al Duba†, Vening Meinesz Laboratorium, Budapestlaan 4, P.O. Box 80.021, 3508 TA Utrecht, The Netherlands
H. C. Heard, Lawrence Livermore Lab., Livermore, CA 94550

The electrical conductivity (σ) of the [010] direction of peridot from St. John's Island, Egypt has been measured to 1500°C in atmospheres of controlled oxygen fugacity ($f O_2$) between the Fe-FeO and FeO-Fe_3O_4 buffers produced by gas mixtures of both H_2/CO_2 and CO/CO_2. We observe a small dependence of σ on $f O_2$ and similar σ at a given $f O_2$ for either gas composition above about 1250°C. However, below this temperature, the σ at a given $f O_2$ is much higher for H_2/CO_2 (by as much as a factor of 10) than for CO/CO_2 mixtures. At temperatures below ~1250°C the activation energy for conduction is lower for mixtures containing H_2, becoming as little as 40% of the value at similar temperature-$f O_2$ in CO/CO_2. These results indicate that electrical conductivity of olivine is not independent of the gas mixture used to control $f O_2$. Similar dependencies are also to be expected for other transport properties such as creep, optical absorption, and ionic diffusion. Since gas mixtures involving H_2 have $f H_2O$ of magnitude similar to $f O_2$, significant concentrations of other defect types (e.g. OH^-, H^+, H_3O^+, etc.) will exist in addition to oxygen defects. Recently, Kohlstedt and Hornack have demonstrated that the creep rate of San Carlos olivine is dependent on H_2/CO_2 mixture ratios used to control $f O_2$. Until the role of hydrogen in silicate structures at high temperatures is more fully understood, we would caution against the use of H_2/CO_2 buffers in controlling oxidation in iron bearing silicates, especially if some defect sensitive property is being measured.

V 139

LOCAL LOWERING OF SILICA ACTIVITY DURING ALBITIZATION OF SPODUMENE--ITS RELATION TO THE FORMATION OF MICAS AND EUCRYPTITE

David London
Donald M. Burt (both at: Dept. of Geology, Arizona State Univ., Tempe, AZ 85281)

Subsolidus processes in lithium pegmatites commonly involve Na-for-Li ion exchange (albitization). A schematic isobaric-isothermal $\mu NaLi_{-1}$-μSiO_2 diagram in the system $LiAlSiO_4$-SiO_2-$NaLi_{-1}$-HNa_{-1}-KNa_{-1} reveals that with increasing $\mu NaLi_{-1}$, alteration of spodumene may take either of two paths. From a ternary eutectic involving quartz, spodumene, and albite (Stewart, 1978), increasing $\mu NaLi_{-1}$ under conditions of silica saturation results in the consumption of spodumene and quartz to form additional albite. Where quartz is absent (i.e., within spodumene crystals), increasing $\mu NaLi_{-1}$ again results in conversion of spodumene to albite, but with a drastic reduction in μSiO_2. The alteration then follows a spodumene-albite cotectoid until a ternary euctectoid of eucryptite + spodumene + albite is reached. From this point, $\mu NaLi_{-1}$ cannot increase until all spodumene is converted to albite + eucryptite. Increasing $\mu NaLi_{-1}$ results in a further reduction in μSiO_2 with the conversion of eucryptite to albite and, theoretically, to nepheline at very high $\mu NaLi_{-1}$. However, natural assemblages are hydrous, and μHNa_{-1} is normally high enough that a mica (such as paragonite, or with the addition of sufficient K, muscovite or lepidolite), rather than nepheline, forms from eucryptite. With increasing cation leaching (μHLi_{-1}, μHNa_{-1}, and μHK_{-1}), micas can "take over" the entire phase diagram and can replace eucryptite, spodumene, and albite. This model explains the occurrence of albite-rimmed spodumene crystals whose interiors are successively replaced by eucryptite + albite, muscovite + albite, and muscovite, as observed in specimens from Branchville, CT, Center Strafford, NH, and the White Picacho district, AZ, USA.

V 140

ON THE THERMODYNAMICS OF NONHYDROSTATICALLY STRESSED SOLIDS

Harry W. Green (Department of Geology, University of California, Davis, Calif. 95616)

The treatment of the thermodynamics of solids under nonhydrostatic stress by J. W. Gibbs, and its extension by B. Kamb clearly showed that no unique chemical potential can be associated with a single component stressed solid. For multicomponent solids, however, this is not the case; so long as one component is immobile, any mobile component, B, will unmix until the composition-dependent part of the chemical potential balances the stress-dependent part, and equilibrium is attained. For a spherical crystal of an isotropic solid, the composition at equilibrium is

$$X_b = \bar{X}_b \exp \frac{V_b \sigma_n' r^2}{\bar{R} T R^2}$$

where $\bar{X}_b$ is the mole fraction of B at the center of the crystal, V_b is the partial molar volume, $\bar{R}$ is the gas constant, T is the absolute temperature, and r is the radial position along a particular radius R which connects the center of the crystal to a point on the surface with deviatoric normal stress σ_n'. The chemical potential is

$$\mu_b = \mu_b^\circ + RT \ln \gamma_b \bar{X}_b + U_b'$$

where μ_b° is the chemical potential under the (hydrostatic) mean normal stress, $\sigma_{kk}/3$, γ_b is the activity coefficient of B, and U_b' is the partial molar strain energy due to the deviatoric stress.

The inhomogeneous dilation produced by the redistribution of matter results in a macroscopically homogeneous strain. Thus, the applied stress can do work, the free energy of the system can thereby be lowered and therefore the unmixing process is spontaneous.

The nonhydrostatic stress problem is the inverse of the osmotic pressure problem, but with the focus on the semipermeable solid.

V 141

LOWER MANTLE PHASE TRANSITIONS MAY GENERALLY HAVE NEGATIVE PRESSURE TEMPERATURE SLOPES

A. Navrotsky (Departments of Chemistry and Geology, Arizona State University, Tempe, AZ 85281)

Negative P-T slopes (larger entropies for denser phases) may be the rule rather than the exception under the pressure-temperature conditions of the lower mantle and upper core. In silicate minerals, once the "free volume" of open framework structures has been eliminated in the 0-150 kbar range, further densification can produce phases having higher entropies. These are caused by (a) low frequency vibrations of small ions in large sites of high coordination numbers, (e.g. ilmenite → perovskite) (b) a decrease in the directional covalent bonding of SiO_4 tetrahedral groupings and an increase in the anharmonic vibrations of the crystal as a whole, (c) possible positional disorder and solid electrolyte behavior, and (d) semiconductor-metal and metal-metal transitions involving significant changes in band structure. Specifically, negative slopes are predicted for the ilmenite-perovskite transition is $MgSiO_3$, the ilmenite-corundum transition is $MgGeO_3$, the stishovite-fluorite (or distorted fluorite) transition in SiO_2, and the s-electron-d-electron transition in K. These predictions are supported by a number of similar transitions, with documented positive entropy changes, in non-geologic oxides, chalcogenides, and halides.

These considerations, coupled with uncertainties in predicting the physical properties of these high pressure phases, must be kept in mind when one attempts to put constraints of composition and mineralogy on geophysical models of the lower mantle and core.

Oceanic Basalts

Harbour C
Sunday P.M.
A. Zindler (Lamont-Doherty), Presiding

V 142

THE DEPTHS OF THE PLUME AND MORB RESERVOIRS

Don L. Anderson (Seismological Laboratory, California Institute of Technology, Pasadena, California 91125)

Ocean island and continental basalts, including alkali basalts, kimberlites and carbonatites share geochemical traits which are distinct from abyssal basalts. Isotopic evidence indicates that the two reservoirs have been separate for 1-2 AE but gives no information about their relative locations. In addition to isotopic differences, hotspot magmas have high Rb/Sr, Rb/K, Ba/K, Nd/Sm, Nd/Sr, Ba/Nd, Ba/Sr ratios and volatile contents compared to MORB. The LIL abundances in the two sites of magmas are mirror images indicating that the process that depleted the one region enriched the other. This plus the evidence from xenoliths are consistent with a deeper origin for MORB. Insulation by a thick, 150 km, continental lithosphere may be the cause of melting in both source regions leading to uplift, rifting, continental magmatism from the shallow source followed by dispersal and magmatism from the deeper layer. The deeper layer should be denser and therefore garnet rich. Using bulk Earth abundance estimates the two source regions have mass ratios of 1:4. The total LIL inventory of the Earth gives a thickness of 400 km for the MORB source region.

V 143

Pb AND Sr ISOTOPE SYSTEMATICS OF SOME BASALTS AND SULFIDES FROM THE EAST PACIFIC RISE

Ph. VIDAL. Centre Armoricain d'Etude Structurale des Socles - 35042 RENNES Cedex, France.
N. CLAUER. Centre de Sédimentologie et Géochimie de la Surface - 67084 STRASBOURG Cedex, France.

Tholeiitic basalts and sulfide deposits from the Cyana diving program (Cyamex, 1978) on the East Pacific Rise were analyzed for Pb and Sr isotopes. The basalt data plot within the field defined previously by other East Pacific Rise basalts (206 Pb/ 204 Pb : 18.35→18.58; 207Pb/ 204 Pb : 15.48→15.53; 208Pb/ 204Pb : 37.8→38.1; 87Sr/86Sr ~ 0.7022). Pb, U and Sr contents (~ 0.5, ~ 0.05 and ~ 110 ppm respectively) and U ratios (~ 6) are of typical MORB, whereas Th/U ratios (~ 3.5) are significantly higher, and are in good agreement with the values obtained by Newman et al.(1979) on EPR samples.

Pb contents in 4 sulfides are relatively high (170 → 1300 ppm), with very homogeneous isotopic ratios (206Pb / 204Pb = 18.48; 206Pb/ 204Pb = 15.49 208Pb / 204Pb = 37.90) which plot in the middle of the basaltic field. One of these sulfides contains

~610 ppm Sr with an $^{87}Sr/^{86}Sr$ = 0.70867 ± 0.00011.

The present results support the hypothesis that (1) the sulfide lead was originated from the leaching of the oceanic crust without significant contribution from extraneous components derived from the seawater or sediments, (2) whereas the sulfide strontium was almost entirely derived from seawater with a very small crustal contribution.

V 144

$^{87}Sr/^{86}Sr$, K, Rb, Cs, Ba AND Sr VARIATIONS ALONG THE GALAPAGOS SPREADING CENTER

Surendra Pal (on leave from: Instituto de Geofisica, Universidad Nacional Autonoma de Mexico, Mexico 20 D.F., MEXICO)
J-G Schilling (both at: Graduate School of Oceanography, Univ. of Rhode Island, Kingston, R.I. 02881)

We present high-precision 87Sr/86Sr data (38 samples from 34 closely spaced stations) on fresh basalts dredged from the Galapagos Spreading Center between 85°W and 102°W longitude. Basalts with light REE-depleted patterns between 85°W and 89°W segment range from 0.7025 to 0.7028 in 87Sr/86Sr and those between 95.5° and 101.5°W range from 0.7026 to 0.7027. Basalts with (La/Sm)E.F. between 0.8 and 2.4 along the 89°W to 95.5°W segment range from 0.7027 to 0.7031 in 87Sr/86Sr. The longitudinal 87Sr/86Sr variation shows a broad maximum at 92°W where the rift is nearest to Darwin Island, and with minor exceptions, parallels the Cs/Sr, Ba/Sr, Ba/K and previously reported La/Sm profiles. The 87Sr/86Sr maximum near 92°W is slightly lower than the highest ratios previously reported for the major Galapagos Islands. The isotopic mapping suggests that the Galapagos mantle anomaly extends beyond the Islands themselves. The mantle anomaly seems to be influenced by the tectonic configuration of the region.

Models are presented for explaining the spatial 87Sr/86Sr variations in terms of either: 1) recent mixing of mantle source masses around the Galapagos anomaly; or 2) past event(s) of mantle enrichment(s) in Rb/Sr ratio and other incompatible trace elements.

V 145

$^{87}Sr/^{86}Sr$ VARIATION ALONG GULF OF ADEN AND AFAR

J-G Schilling
R. Vollmer
M.B. Bergeron (all at: Graduate School of Oceanography, Univ. of R.I., Kingston, R.I. 02881)

In continuation of an exploratory geochemical study of the Red Sea-Afar-Gulf of Aden region, we report high precision 87Sr/86Sr data on basalts from 29 dredge stations along the Tadjurah Trough-Sheba Ridge, from longitude 43°E to 57°E. Light-REE depleted basalts from 48°E to 57°E range .7027 to .7030 in 87Sr/86Sr. Basalts with flat to light REE-enriched patterns from 43°E to 48°E range .7030 to .7034 with one .7038 value at the mouth of the Gulf of Tadjurah. In general the longitudinal 87Sr/86Sr variation is similar to but not as smooth as the La/Sm variation, possibly because of very slight seawater alteration. The 87Sr/86Sr maxima near 45°E-46°E is more subdued than the sharp La/Sm maxima previously reported. The 87Sr/86Sr data further suggest that the incompatible trace element and radiogenic isotope-rich nature of the mantle beneath the Afar region extends some 500-600km beyond land boundaries, but the data also confirms the smaller scale complexities of the geochemical variations within the anomaly itself.

V 146

LEAD-STRONTIUM-NEODYNIUM ISOTOPIC CORRELATION LINE AND CLOUD : QUANTITATIVE CONSTRAINTS ON CHEMICAL GEODYNAMICS

C.J. ALLEGRE, B. DUPRE, O. BREVART, J-F MINSTER (Laboratoire de Géochimie et Cosmochimie, 4, Place Jussieu, 75230 PARIS CEDEX 05 - FRANCE)

All MORBasalts and most of ophiolite basalts follow the general Sr-Pb-Nd correlation trend proposed by the Cambridge-Lamont and Paris groups. At the reverse oceanic island basalts do not plot on this trend but rather define a cloud the Sr, Pb, Nd multispace diagram. This is the most important constraint for chemical geodynamics.

A quantitative model is built to describe these featuresby transfert equations : the earth mantle is now divided into two separate reservoirs : the upper and lower mantle. The continental crust is differentiated from the upper-mantle, not through a single way process but rather through a complex one. The lower mantle exchanges with the upper mantle and with the core. In the past(prior to 2 b.y. ago) the mantle was a unique reservoir and at that time the two processes (continental crust formation and core fractionation) were active from it. Reinjection of sediments into the mantle is an important process but mainly for creation of mantle heterogeneities, and this can be used to trace back the mantle convection processes. All transfert coefficients are time dependent. Differentiation to the core exponentially decays with a short time scale. Differentiation to the continental crust is non linear through times.

V 147

THE DISTRIBUTION OF PRIMARY CARBON IN SUBMARINE BASALT GLASS

E. A. Mathez (Dept. of Geological Sciences, Univ. of Washington, Seattle, WA 98195)
J. R. Delaney (Dept. of Oceanography, Univ. of Washington, Seattle, WA 98195)

Fresh submarine basalt glasses from the FAMOUS area and from near the Bouvet Islands contain a reduced form of carbon concentrated (1) in bubbles and microcracks in glass (melt) inclusions in phenocrysts, (2) on walls of vesicles in matrix glass, and (3) along cracks in phenocrysts and matrix glass. The carbon distribution was studied using specialized microprobe techniques on Al-coated mounts prepared in a non-carbon bearing medium.

Many carbon bearing melt inclusions contain bubbles and quench-produced microcracks which do not penetrate host crystals. These inclusions appear to have remained completely isolated from the outside environment since entrapment, indicating that the inclusion carbon is primary and suggesting, by analogy, a primary origin for carbon in matrix cracks and vesicles as well.

In cooling cracks in matrix glass, carbon appears as semicontinuous dendritic masses. In vesicles it forms an irregular coating on walls and on sulfide globules protruding from these walls. The carbon possesses optical properties of graphite, and x-ray signals corresponding to >50 wt.% carbon can be generated from crack and vesicle surfaces. However, neither detailed study of characteristic x-ray spectra nor SEM examination of surface morphologies have allowed specific identification of this phase. It is probably an intimate mixture of graphite and amorphous material.

The presence of a reduced form of carbon explains the self-reducing phenomenon observed in many intrinsic fO_2 measurements. However, because carbon deposition occurred during quenching, its presence does not provide direct information on magmatic redox conditions.

V 148

PHASE CHEMISTRY OF THE BASALTIC VOLCANISM OCEAN-FLOOR BASALT SUITE

Martin R. Fisk
A. E. Bence (both at: Dept. of Earth and Space Sciences, State Univ. of New York, Stony Brook, N. Y. 11794)

The Basaltic Volcanism Study Project selected sixteen glassy or very fine grained basalts from several ocean-floor basalt collections to represent the spectrum of basalt compositions recovered from various spreading centers. The chosen basalts cover the range of glass compositions reported by Melson et al. (1977). All are fresh and come from ocean ridges that have spreading rates that range from 3 to 8 cm/yr. Highly fractionated basalts are only found on the faster spreading ridges like the Galapagos which suggests that extensive shallow level fractionation may be correlated with fast spreading.

The $Mg^{\#}$ [$Mg^{2+}/(Mg^{2+}+Fe^{2+})$, atomic] of the glassy rims of pillows ranges from 0.12 to 0.69 and TiO_2 ranges from .8 to 3.7 wt%. Al_2O_3 is as high as 17.5 wt% in a primitive (high $Mg^{\#}$) basalt and as low as 11.5 wt% in the most evolved basalt. The most primitive basalts ($Mg^{\#}$>0.66) have olivine (Fo85 to Fo90) and in some cases spinel $[Mg_{.6-.8}^{2+}Fe_{.2-.4}^{2+}]^{2+}[Fe_{.03-.12}^{3+}Cr_{.6-1}Al_{.9-1.3}]^{3+}{}_2O_4$ phenocrysts. Basalts with $Mg^{\#}$ less than 0.66 have plagioclase of An82 or less, however, some basalts have plagioclase "xenocrysts" that on the basis of chemistry (An85 to An90) and texture can not be in equilibrium with the adjacent glass. These "xenocrysts" should have crystallized from a high $Mg^{\#}$ a magma that has ∿18 wt% Al_2O_3, 13 wt% CaO and 1.2 wt% Na_2O. A basalt of this composition could only crystallize plagioclase as the liquidus phase at pressures greater than 4kb if the $Mg^{\#}$ of the primitive basalt is 0.69, (the same as the most primitive basalts from the seafloor).

V 149

A PHASE DIAGRAM FOR MID-OCEAN RIDGE BASALTS

Edward Stolper (Div. Geol. Planet. Sci., Caltech, Pasadena, CA 91125)

Samples of a primitive mid-ocean ridge basalt (MORB) glass were encapsulated in a mixture of ol (Fo90) and opx (En90) and melted at 10, 15, and 20 kbar. After quenching, the basaltic glass was present as a pool within the ol+opx capsule, but its composition had changed so that it was saturated with ol and opx at the conditions of the experiment. By analyzing the quenched liquid, the location of the ol+opx cotectic in the complex, multicomponent system relevant to MORB genesis was determined.

As pressure increases from 1 atm to 10 kbar, the dry ol+opx cotectic moves from quartz tholeiitic to olivine tholeiitic compositions. With further increases in pressure, the cotectic continues to move toward the ol-di-plag join (i.e., toward alkalic compositions). Between 15 and 20 kbar, ol+opx+di-saturated liquids change from tholeiitic to alkalic in character, although part of the ol+opx cotectic is still in the tholeiitic (i.e., hy-normative) part of composition space. At pressures of 10-15 kbar, tholeiitic liquids may be able to fractionate to alkalic liquids on the ol+di cotectic.

Primitive MORB compositions come close to but do not actually lie on the ol+opx cotectic under any conditions studied. This suggests that not even the most primitive of known MORBs are primary melts of the mantle. The correspondence of most MORBs to the 1 atm ol+di+plag cotectic suggests that low pressure fractionation was involved in their genesis from parent liquids. Picritic liquids that have been proposed as parents to the MORB suite could equilibrate with harzburgite (or lherzolite) at 15-20 kbar and thus could be primary. Fractionation of ol from these liquids could yield primitive MORB liquids, but other primary liquids or more complex fractionation paths involving other phases in addition to ol cannot be ruled out. The possibility that these picritic liquids could equilibrate with ol+opx at 25-30 kbar cannot be ruled out.

V 150

THE CHEMISTRY OF PRIMARY MID-OCEAN RIDGE BASALTS AND THEIR EVOLUTION DURING MAGMA MIXING

D. Elthon (The Geophysical Laboratory, 2801 Upton St., N.W. Washington, D.C. 20008 and Lamont-Doherty Geological Observatory, Palisades, NY 10964) (Sponsor: T.N.Irvine)

Although the chemical variations within mid-ocean ridge basalts (MORBs) indicate that they have equilibrated to 1 atm cotectics, detailed investigation of their chemistry suggests that a plethora of liquid lines of descent for MORBs are required. Partially resorbed OL, PLAG, and CPX xenocrysts in MORBs and abundant OL, PLAG, and CPX cumulates in the oceanic crust indicate that oceanic crustal magma chambers generally are multiply saturated with these phases. Mixing of primitive MORBs into these evolved magma chambers produces common OL-phyric and PLAG-phyric basalts whereas CPX-phyric basalts are rare; As a consequence of mixing, the OL-phyric and PLAG-phyric basalts will have the hidden component of CPX fractionation which is detected in MORBs but is not apparent in their phenocryst assemblages. This process will produce a suite of basalts that have a plethora of liquid lines of descent and which cluster near the 1 atm cotectics but could have been derived from a single primary magma. The locations of upper mantle pseudo-invariant points, constrained by the phase equilibria of

basaltic magmas at high pressures, and the chemistry of MORBs indicates that the primary magmas from which MORBs are derived were generated at 25-30 kb and have ∿18% MgO.

V 151

ARE MOST SMALL OCEANIC VOLCANOES THOLEIITIC?

Batiza, Rodey (Dept. of Earth & Planetary Sci., Washington University, St. Louis, MO 63130)

A detailed study of 9 small volcanoes near the East Pacific Rise (EPR) at 9°N-14°N was recently completed. High-density magnetic and bathymetric surveys and multiple dredges were made of each volcano. 24 dredges were of seamounts and 3 were of the EPR crest at 11°30'N, 12°08'N, and 13°50'N. Some seamounts are actually tilted fault blocks rather than volcanoes and some are combination land forms. Dredges of the volcanoes yielded little pillow lava but abundant fragments of sheet-flow lava, and hyaloclastite. These rocks are all heavily encrusted with black, friable Mn. Most of the basaltic rocks are extremely fresh, aphyric and have abundant glass; vesicularity is highly variable. Petrographic examination, electron probe analysis of 151 glass samples and INAA trace element determinationa of 38 whole rocks all show that most dredged samples are depleted tholeiitic basalt chemically identical to normal mid-ocean ridge basalt (MORB). Samples from 5 volcanoes are depleted MORB with nearly constant $(La/Sm)_N$ (0.4-0.5) but variable Fe/Mg and abundances of trace elements. Two volcanoes have basalt with $(La/Sm)_N$=0.6-0.9 and are transitional tholeiites. Two other volcanoes contain both depleted MORB [$(La/Sm)_N$=0.4-0.5] and: 1.) transitional basalt with $(La/Sm)_N$=1.2 and 2.) alkalic basalt with $(La/Sm)_N$=2.6-2.9. These findings suggest: 1.) Many oceanic volcanoes originate at mid-ocean ridges. 2.) Most of these are composed of depleted MORB from the same source as the ridge volcanics. 3.) Later eruptions which occur as the volcanoes drift away from the ridge are transitional and alkalic with a less depleted source than MORB. the small size and chemical heterogeneity of these volcanoes provides strong evidence for the existence of small scale chemical heterogeneities in the sub-oceanic upper mantle.

V 152

ALKALIC ROCKS FROM SOUTHERN HESS RISE, NORTH-CENTRAL PACIFIC OCEAN

K. E. Windom (Department of Earth Sciences, Iowa State University, Ames, Iowa 50011)
T. L. Vallier (U.S. Geological Survey, Menlo Park, California 94025)
K. E. Seifert (Department of Earth Sciences, Iowa State University, Ames, Iowa 50011)

Rocks with alkalic affinities were recovered from southern Hess Rise in the north-central Pacific during DSDP Leg 62. Sixty-four meters of trachyte were cored below Albian (Lower Cretaceous) limestone at Site 465 (33°49'N, 178° 55'E), and alkali basalt clasts occur in Upper Cretaceous chalk at Site 466 (34°12'N, 179°34'E). Subaerial eruption of trachyte flows at Site 465 is suggested by large (greater than 5 mm) vesicles, iron oxide staining, and the absence of glassy flow margins. Texturally, the samples have flow-alined feldspar laths and microlites in groundmasses that are altered to smectite minerals. Average trachyte (18 samples) consists of 59.66% SiO_2, 1.03% TiO_2, 18.78% Al_2O_3, 2.19% Fe_2O_3, 0.57% FeO, 0.03% MnO, 1.03% MgO, 2.31% CaO, 5.12% Na_2O, 4.79% K_2O, 0.35% P_2O_5, 1.56% H_2O^+, 1.84% H_2O^-, 0.25% CO_2, 716ppm Zr, 645ppm Ba, and 311ppm Sr. Rare earth element patterns are very consistent and indicate strong enrichment in light REE. Chemical comparisons show good correlation with alkalic differentiates from modern oceanic islands and from seamount dredge hauls. Alkali basalt clasts in Upper Cretaceous chalk from Site 466 probably were eroded from a subaerial part of the upthrown walls of a graben in which the site is located. The alkalic rocks probably were erupted on oceanic islands or seamounts which capped Hess Rise during late stages of its volcanic evolution prior to late Albian time. Subsequent subsidence caused Hess Rise to sink below sea level where it was covered by sediments.

V 153

MAGMA MIXING IN TWO TERTIARY ACIDIC AND BASIC COMPLEXES IN SOUTHEAST ICELAND

Steve R. Mattson
Thomas A. Vogel
John T. Wilband (All at: Department of Geology, Michigan State University, East Lansing, Michigan, 48824)

The Austurhorn and Vesturhorn intrusives in southeast Iceland consist of an intimate association of acidic and basic rocks. Three basic models were considered for this association: immiscibility, comingling of two independent magmas, and crystal fractionation of a typical mafic lava in Iceland.

Basalt "pillow-like" masses with cuspate boundaries commonly have a chilled margin against the leucocratic granite, although in some cases, a greyish mixed zone of intermediate composition surrounds the "pillow". Chilled boundaries indicating thermal disequilibrium preclude immiscibility in place and the liquid-liquid relationships of "pillow-like" masses with cuspate boundaries are not indicative of simple crystal fractionation.

Field observations together with REE, trace element and major element variations are consistent with initial crystal fractionation of olivine or pyroxene from a basic melt which subsequently mixed with a granitic magma. Log plots of two magmaphile elements (Sr vs. La, Ce, or Ba) exhibit a positive slope for basic rocks and then a sharp negative to vertical asymtotic slope for granitic rocks. Rocks which plot at the change in slope have "mixed" characteristics. Similarity of the chemical trends of these acidic and basic complexes with a typical lava sequence in Iceland (Wood, 1978), suggest to us that in Iceland, magma mixing of basaltic and granitic magmas may be a major petrogenetic process.

V 154

THE NEOVOLCANIC ZONE IN ICELAND: AN IN-SITU MODEL FOR THE GENESIS OF AN OPHIOLITE SERIES

J. F. Hermance (Dept. of Geological Sciences, Brown University, Providence, RI 02912)

Kinematic thermal models, petrological arguments, and geological and geophysical observations in the neovolcanic zone of Iceland suggest that three processes are active in creating new crustal material at accreting plate boundaries: magmatic intrusion (Bodvarsson and Walker, 1965), extrusive volcanism (Palmason, 1973) and crustal underplating (Lachenbruch and Sass, 1978). This latter process, the underplating of the crust by emplacement of a molten fraction at its base, has been a hitherto neglected mechanism for explaining lithospheric thickening away from the crest of spreading centers. The depletion of liquid magma from the zone of magma accumulation at the base of the crust may well lead to the concentration of an olivine-rich residuum similar to that seen at the base of an ophiolite series. It is important to recognize that this zone of ultra-mafic enrichment does not in itself represent mantle material but is a direct by-product of magma genesis at accreting plate margins.

V 155

RADON ANOMALIES THAT CORRELATE WITH EPISODIC RIFTING OF THE PLATE BOUNDARY IN NORTHERN ICELAND

E. Hauksson (also at: Dept. Geol. Sci., Columbia University)
J. Goddard (both at: Lamont-Doherty Geol. Obs., Columbia U., Palisades, NY 10964)

During three different deflation episodes of the shallow magma chamber below the floor of the Krafla caldera, Northern Iceland, in July 1978, November 1978, and May 1979 the following sequence of events is observed: First, tiltmeters signal the onset of deflation. Second, one to three hours later a volcanic tremor is observed. Third, three to six hours later cracks show closure and simultaneously the groundwater level at 100 m depth rises. Finally, three to six days later the radon emission of the fumaroles on top of the magma chamber at Leirhnjukur increases by about 100%. The radon content of the fumaroles can be explained by assuming transportation from depth by wet steam and non-condensable gases that slowly evaporate from the 100°C hot groundwater table. The cause of the co-episodic increase in radon emission appears to be a temporal raising of the groundwater table driven by crack closure and resulting shortening of the transport time for radon up to the surface fumaroles. Changes in radon emission also coincide with fluctuations in fumarolic activity and permanent changes in groundwater level that have occurred during inflation episodes. Frequent sampling of the fumaroles shows that no easily identifiable short-term radon precursors occur a few days prior to deflation and associated lateral migration of large volumes of magma. The radon data do not reflect any extensive flushing of the groundwater by a deep magmatic gas component either during inflation or deflation. No obvious relationship is observed between radon emission and temporal changes in seismicity in the Krafla caldera.

V 156

Io-Th-U ISOTOPIC STUDIES ON ICELANDIC LAVAS. TIME CONSTRAINTS ON THE BASALT GENESIS OF ICELAND.

M. CONDOMINES, Ph. MORAND, C.J. ALLEGRE (Laboratoire de Géochimie et Cosmochimie, 4, Place Jussieu 75230 PARIS CEDEX 05 - FRANCE).

We have determined the ^{230}Th-^{238}U disequilibrium on a series of alkaline and tholeiitic basalts as well as more differentiated lavas from the three active volcanic centers from Iceland. All lavas are historic or prehistoric so that no age correction is necessary to obtain the initial $^{230}Th/^{232}Th$ ratio.

This ratio varies from 0.95 to 1.20 and reveals an important heterogeneity at the scale of Iceland. The disequilibrium ratio ($^{230}Th/^{238}U$) is always higher than 1. It is thus impossible to derive the Icelandic magmas from an homogeneous mantle in radioactive equilibrium with a Th/U ratio of 3.7, as generally admitted for the primitive mantle. Moreover, there is a geographical variation of the ($^{230}Th/^{232}Th$) ratio : it decreases towards the center of Iceland where it reaches a minimum in the Askja region. δ 18 O values determined by Muehlenbachs et al. on the same samples show a similar variation. Several models can describe these results :

- An heterogeneity model for the mantle sources of these lavas, characterized by varying ($^{230}Th/^{232}Th$) and Th/U ratios, and being or not in radioactive equilibrium.
- A "plumetype" mixing model between a primitive equilibrated mantle source with a Th/U ratio of 3.7, and a depleted source of lower Th/U ratio and higher ($^{230}Th/^{232}Th$) ratio ($\geq$1.20)
- A varying residence time model for the magmas between their creation through partial melting and their emission at the surface. Residence times in deep reservoirs as high as several tens of thousand years are necessary to explain the variations of the $^{230}Th/^{232}Th$ ratio.

Although it is difficult to choose between these different models, we consider that the third one is worth being studied. Only the ^{230}Th-^{238}U method can allow a quantitative approach of this type of problems.

V 157

GEOCHEMISTRY AND PETROLOGY OF THE SOUTHERN COOK ISLANDS

R. Jarrard (Lamont-Doherty Geological Observatory of Columbia University, Palisades, NY 10964)
D.J. Fornari (Department of Geological Sciences, State University of New York at Albany, Albany, NY 12222)

Twenty new major-element analyses of alkalic volcanic rocks from the islands of Rarotonga, Aitutaki, Mauke, Mangaia and Atiu, in the Cook Islands, combined with previously published chemical data, reveal the chemical diversity present in each island and between the islands of this group. The volcanos on Atiu, Mangaia, and Rarotonga all appear to have undergone rather complete magmatic differentiation as the samples analyzed from each island show a continuous chemical progression from high MgO to low MgO contents. The primary source and differentiation trend for Mangaia and Atiu appear to be the same based on the parallelism of the major-element trends on oxide wt.% vs. MgO wt. % plots for rocks from these two islands. The rocks from Rarotonga fall on a similar differentiation trend to those of Atiu and Mangaia; however, the Rarotongan differentiation appears to be more complete in that several samples have very low MgO (0.15 to 1.76 wt.%) contents and a high content of alkalies (about 5 wt.% K_2O and 6.5 wt.% Na_2O). These highly differ-

entiated rocks from Rarotonga are volumetrically minor phonolites and trachytes that were erupted post-caldera collapse and after a volcanic hiatus of about 0.4 MY. Rocks from Aitutaki exhibit a small range of MgO values with only one sample, an alkali basalt, having significantly lower MgO. The presence of alkali basalt as a tuff clast suggests that the deeper, older core of the volcano may be composed of alkali basalt. In contrast, renewed volcanism on Aitutaki included alkali basalts, nephelinites and basanites.

V 158

CHLORINE AND BROMINE IN HAWAIIAN LAVAS

C.K. Unni (Graduate School of Oceanography, Univ. of Rhode Island, Kingston, R.I. 02881)
J-G. Schilling (Same as above)

Chlorine and bromine were determined by radiochemical neutron activation techniques in twenty subaerially erupted Hawaiian lavas, covering most of the lava-types found on the islands, and in three submarine basalts from the east rift zone of Kilauea Volcano. The concentrations of the two halogens increase markedly from tholeiites to alkali olivine basalts to nephelinites with decreasing silica content; and to a lesser degree within the alkali series, from alkali olivine basalts to hawaiites, mugearites and trachytes with increasing silica content. Despite their volatile nature and possible loss during subaerial eruptions, both chlorine and bromine correlate closely with other incompatible elements such as La and K, regardless of differences in volatility. This suggests that the fraction of Cl and Br lost by degassing may be a smooth function of bulk composition, and also that little degassing takes place from lavas with alkalic affinities ($Na_2O/CaO > 0.3$), as previously shown for the Iceland-Reykjanes Ridge region.

A strong correlation is observed between Cl and Br in all the samples analyzed, indicating a high degree of geochemical coherence between these two halogens during fractionation processes such as partial melting in the mantle followed by fractional crystallization and possibly degassing at shallow depth. Cl/Br weight ratios remain fairly constant (325±85) over the entire spectrum of Hawaiian lava-types, as in the case of Iceland (254±54) and Reykjanes Ridge (266±71) basalts.

Mineralogy-Crystallography II

Harbour A
Sunday P.M.
M. A. Carpenter (Harvard University), Presiding

V 159

HIGH TEMP. THERMOCHEMISTRY OF THE SYSTEM $CaO-MgO-Al_2O_3-SiO_2$

S. K. Saxena (Dept. of Geology, Brooklyn College, Brooklyn, New York 11210)

Enstatite-diopside "solvus" can be reproduced by using a new approach of defining the hypothetical orthodiopside and diopsidic enstatite as ideally mixing components in pyroxenes. The Gibbs free energy of formation of such components are presented in Table below. This model of ideally mixing component is extended to solution of Al_2O_3 in orthoenstatite. Using recent experimental phase equilibria data of Ganguly (1980) and Danckwerth and Newton (1978). Gibbs free energy of formation of the hypothetical Al_2O_3 (molar volume 28.91 cm^3) and of pyrope have been estimated (Table). The advantage of the ideally-mixing-component-model is its simple formulation and therefore considerable ease in computing multiphase equilibria. The value of ΔG for the reaction

$$3\ MgSiO_3\ (opx\ ss) + Al_2O_3 \rightleftharpoons Mg_3Al_2Si_3O_{12}$$

is given by

$$\Delta G(J/M) = 46844.89(\pm 146) - 98.22(\pm 11)xT + 40.186(\pm 3.9)x(T^2/1000).$$

which can be used in the CAMS system with mole fractions for Al_2O_3, $MgSiO_3$ and suitable activity for pyrope[2] (W_{Mg-Ca}=15983 J/M)

Table - G_f^o in J/M

T°K	pyrope	Al_2O_3'	O. diop.	D. Enst.
1200	4869626	1257230	1218968	1172181
1300	4747054	1224285	1190634	1146791
1400	4614911	1191938	1160059	1119207
1500	4467248	1158676	1128615	1085646
1600	4320947	1125645	1096304	1051988

V 160

HEAT CAPACITIES FROM 5 TO 1000 K FOR NATURAL DIOPSIDE, WOLLASTONITE, AND ORTHOENSTATITE

K. M. Krupka* (Battelle, Pacific Northwest Laboratories, Richland, WA 99352)
D. M. Kerrick (Dept. Geosciences, The Pennsylvania State Univ., University Park, PA 16802)
R. A. Robie (U.S. Geological Survey, Reston, VA 22092)

The molar heat capacities of natural diopside, $CaMg(SiO_3)_2$, wollastonite, $CaSiO_3$, and an orthoenstatite solid solution, $Mg_{.85}Fe_{.15}SiO_3$ were measured from 5 to 380 K using low-temperature adiabatic calorimetry and from 350 to 1000 K using differential scanning calorimetry. Values of S^o_{298} for diopside and wollastonite are 142.7±0.2 and 81.69±0.12 J/mol·K, respectively. The S^o_{298}-S^o_0 value of $Mg_{.85}Fe_{.15}SiO_3$ is 69.04±0.10 J/mol·K. Due to a Schottky-type contribution and the Fe^{2+} in solid solution, this value is significantly greater than the entropy value for $MgSiO_3$ (Krupka et al., 1979). The following C^o_p equations for diopside(1), wollastonite(2), and $Mg_{.85}Fe_{.15}SiO_3$(3) were obtained from a least squares fit to the calorimetric data and constrained to join smoothly with low-temperature C^o_p values (T in kelvins and C^o_p in J/mol·K):

$$C^o_p(1)(298\text{-}1600\ K) = 470.25 - 0.09864T + 2.453x10^5T^{-2} - 4823T^{-0.5} + 2.813x10^{-5}T^2$$

$$C^o_p(2)(298\text{-}1400\ K) = 200.8 - 0.02590T - 1.579x10^5T^{-2} - 1826T^{-0.5} + 7.435x10^{-6}T^2$$

$$C^o_p(3)(298\text{-}1000\ K) = 207.9 - 0.01489T + 1.921x10^5T^{-2} - 2135T^{-0.5}$$

The C^o_p equations for diopside and wollastonite were extended above 1000 K using the relative enthalpy data of White (1919) and Southard (1941). High-temperature entropies calculated from these data, combined with ancillary thermochemical data and recent P-T studies, permit a fairly rigorous thermodynamic analysis of equilibria within the system $CaO-MgO-SiO_2-H_2O-CO_2$.

V 161

ENTROPY OF MOLTEN SiO_2, $CaSiO_3$ AND $CaMgSi_2O_6$ AT 0.1 MPa to 2600K

A.J. Piwinskii (University of California, Lawrence Livermore Lab., Livermore, CA. 94550)
N.D. Stout (University of California, Lawrence Livermore Laboratory, CA. 94550)
(Sponsor B.P. Bonner)

The entropy, S_T-S_{298}, of anhydrous melts of SiO_2, $CaSiO_3$, and $CaMgSi_2O_6$, was calculated from enthalpy data which were determined at 0.1 MPa to 2600K using a drop calorimeter. For molten SiO_2 between 1900 and 2600K, S_T-S_{298} (J/g.K)= 1.289 lnT-7.34. For $CaSiO_3$ liquids from 1850 to 2600K, S_T-S_{298} (J/g.K)=1.395 lnT-7.95. For molten $CaMgSi_2O_6$ between 1695 and 2600K, S_T - S_{298} (J/g.K)=1.499 lnT-8.54. These new experimental results indicate that assuming entropy additivity can lead to large errors. Using data of Kelley (1960, U.S. Bureau Mines Bull. 584) and JANAF Tables for SiO2(s), CaO(s), and MgO(s), the calculated (S_T-S_{298}) at 2000K for $CaSiO_3$ and $CaMgSi_2O_6$ by additivity is approximately 28 and 30%, respectively, higher than that obtained from experimental data. Using the Lacy network-forming index R, where R=O/(Si+Al) and is the ratio of molecular percent of non-bridging oxygens to the network-forming cations, as a structure-sensitive indicator, this silicate melt entropy data, together with our earlier results on entropies of molten silicate rocks, suggest that a structural change takes place in silicate liquids at R≅ 2.05. This may mark the initial breakup of silica-rich networks because of melt depolymerisation by network modifying cations. In addition, the new entropy results show no indication of the putative change in the structure of molten $CaSiO_3$ at approximately 1973K, which was suggested by the viscosity and electrical conductivity results of Bockris and his colleagues. This work was performed under the auspices of the U.S. Dept. of Energy by the Lawrence Livermore Laboratory under contract number W-7405-ENG-48.

V 162

ANORTHITE: NEW MEASUREMENTS OF THE HEAT OF FUSION AND HEAT CAPACITY OF THE LIQUID

J.F. Stebbins, Lawrence Berkeley Laboratory University of California, Berkeley CA 94720
D.F. Weill, I.S.E. Carmichael

Knowledge of enthalpies of fusion ($\Delta_f H$) and heat capacities (C_p) of the components of silicate liquids is essential in predicting melting and crystallization behaviour. A wide range of values has been reported for $\Delta_f H$ for anorthite: from 81.2 (1) to 167 (2) kj/mol. Therefore, the high temperature enthalpy of $CaAl_2Si_2O_8$ liquid was measured between 1832 and 1882 K with a diphenyl ether drop calorimeter: $H^{liquid}_T - H^{glass}_{300\ K} = -367 + 0.4987\ T$ kj/mol. These data were combined with previous measurments of the enthalpy of vitrification of anorthite ($\Delta_v H_{An}$ = 77.8 1.2 kj/mol, (3)) and the high temperature heat contents of glassy and crystalline $CaAl_2Si_2O_8$ to arrive at an improved estimate of $\Delta_f H_{An}$ at 1830 K as 134±4 kj/mol. The average C_p of the supercooled liquid between the anorthite melting point and the glass transition point has also been measured as 427±4 j/mol K, much higher than the measured C_p of the glass (326 j/mol K). This latter value agrees well with an estimate based on the sum of partial molar C_p's reported by Bacon (4). The estimate of $\Delta_f H_{An}$ based on Ferrier's work (2) is probably in error because of his overestimate of $\Delta_v H_{An}$, while the much lower value given by Robie, et al(1) is apparently due to an underestimate of the difference in the C_p's of the glass and the supercooled liquid.

V 163

THE ENTHALPY AND HEAT CAPACITY OF MOLTEN SiO_2, $CaSiO_3$ AND $CaMgSi_2O_6$ AT 1MPa TO 2600K

N.D. Stout (University of California, Lawrence Livermore Laboratory, Livermore, CA. 94550
A.J. Piwinskii (University of California, Lawrenence Livermore Laboratory, Livermore CA. 94550
(Sponsor B.P. Bonner)

We report the results of the first measurements of the enthalpy, H_T-H_{298}, and determinations of heat capacity, C_p, of anhydrous melts of SiO_2, $CaSiO_3$, and $CaMgSi_2O_6$ made at 0.1MPa to 2600K using a drop calorimeter. Starting materials were glasses prepared by repeated fusions followed by quenching. For molten SiO_2 between 1900 and 2600K, H_T-H_{298} (J/g)=1.289T-577.4 with 1 S.D.=39 J/g and χ^2=5.0; Cp (J/g.K)=1.289±0.067. For molten $CaSiO_3$ between 1850 and 2600K, H_T - H_{298} (J/g)=1.395T-672.4 with 1 S.D.=13 J/g and χ^2 =0.57; Cp(J/g.K)=1.395±.021. For molten $CaMgSi_2O_6$ between 1695 and 2600K, H_T-H_{298} (J/g)=1.499T-797.9 with 1.0 S.D.=19 J/g and χ^2=1.499; Cp(J/g.K) =1.499±.024. As in the case of alkali silicate liquids, the usual assumption of heat content and heat capacity additivity leads to large errors. Using data of Kelley (1960, U.S. Bureau Mines Bull. 584) and JANAF Tables for SiO(s), CaO (s), and MgO(s), the calculated (H_T-H_{298}) at 2000 K for $CaSiO_3$ and $CaMgSi_2O_6$ is approximately 15% and 11% lower, respectively using the assumption than that experimentally-determined. Cp of $CaSiO_3$ and $CaMgSi_2O_6$ liquids calculated by additivity leads to temperature-dependent functions; Cp(wo) (J/g.K)=0.902+1.74x10^{-4} T-1.842 x 10^{+4} T^{-2} and Cp(di)(J/g.K)=0.939+1.966 10^{-4} T-1.966 x 10^{-4} T -1.919 x 10^{+4} T^{-2}. At 2000K, the calculated Cp for $CaSiO_3$ and $CaMgSi_2O_6$ liquids by additivity relations is approximately 11% lower than the experimentally-obtained values. This work was performed under the auspices of the U.S. Dept. of Energy by the Lawrence Livermore Laboratory under contract number W-7405-ENG-48.

V 164

RATE OF CATION DISORDERING IN ORTHOPYROXENES

J. R. Besancon (Dept. of Geology, Wellesley College, Wellesley, Ma. 02181)
Sponsor: R. G. Burns

Isothermal cation disordering experiments at 873°K to 1073°K on two orthopyroxenes, followed by Mossbauer spectroscopy, are consistent with the model of Mueller(1967,1969). The characteristic disordering rate constant for Fe-Mg exchange $K21 = 2.3\times10^{-3}min^{-1}$ for a pyroxene $(Mg_{1.70}Fe_{.26}Ca_{.02})(Al_{.04}Si_{1.96})O_6$, but $K21 = 14\times10^{-3}min^{-1}$ at 973°K for a pyroxene $(Mg_{.94}Fe_{.99}Ca_{.01})(Al_{.04}Si_{1.94})O_6$. Activation energies are 280 and 250 kJ/mole, respectively, similar to the value of 230 kJ/mole obtained for anthophyllite disordering by Seifert and Virgo (1975). Predicted attainment of 90% of equilibrium is about eight weeks at 773°K and one second at 1273°K for the second pyroxene, casting some doubt on unreversed equilibrium determinations at high and low temperatures. A two-stage model for ordering, with some cut-off temperature below which ordering mechanism changes, is probably unnecessary to explain naturally occurring pyroxene disorder.

V 165

COMPUTER SIMULATION OF CATION-ORDERING ENERGETICS IN OLIVINES AND PYROXENES

David L. Bish (Dept. of Geological Sciences, Harvard University, Cambridge, MA 02138)
(Sponsor: Prof. C. W. Burnham)

A major problem in modeling the energetics of ordered and anti-ordered structures is our lack of knowledge concerning the relatively unstable anti-ordered arrangements, for example, the structure of an olivine with Ca on M(1) and Mg on M(2). Even for the olivine minerals, the site energies of ordered and anti-ordered intermediate structures cannot be correctly approximated using linear combinations of the end-member site energies. In an attempt to circumvent this problem, I have calculated ordered and anti-ordered structures using distance least squares (DLS) modeling and subsequently computed electrostatic and repulsive energies for the model structures. This procedure correctly predicts the ordering schemes for Ni-Mg, Fe-Mg, Co-Mg, Mn-Mg, Mn-Ca, Fe-Mn, Ca-Mg, and Fe-Ca olivines, giving large (≈10kcal/mol) energy differences between ordered and anti-ordered Fe-Ca, Mg-Ca, and Mn-Ca olivines and small (≈0-2kcal/mol) differences for the remaining olivines. Similar DLS modeling and energy calculations for P2/n omphacite with differently ordered Mg-Al and Na-Ca suggest that the energy associated with Mg-Al ordering is about twice that associated with Na-Ca ordering, in qualitative agreement with the observations that Mg and Al are completely ordered and Na and Ca only partially ordered in natural specimens.

The results of this approach suggest that DLS modeling and subsequent energy calculations may provide some insight into ordering in minerals and into the energetics of apparently unstable substitutions in crystals, for example, Ca on the M(1) site in pyroxenes. Improved accuracy will require inclusion of crystal field stabilization energies and entropy differences. DLS modeling which minimizes the electrostatic and repulsive energies should provide more reliable hypothetical structures.

V 166

TEXTURE AND STRUCTURAL INTERPRETATION OF THE ALTERATION OF PYROXENES TO OTHER BIOPYRIBOLES

P.H. Ribbe and Y. Nakajima (Dept. of Geological Sciences, Virginia Polytechnic Institute and and State University, Blacksburg, VA 24061
(Sponsor: G.V. Gibbs)

In a metamorphosed gabbro (Hokkaido, Japan), augite containing exsolved orthohypersthene and pigeonite has been altered to a variety of biopyriboles. High resolution electron microscopy of slightly altered augite shows only narrow (010) lamellae of clinoamphibole which always contain *even* numbers of double-chains. In highly altered regions, all three pyroxenes are changed to double-, triple- and more highly polymerized multiple-chain biopyriboles, with chlorite (*d* (001) ~ 14.5Å) found only in opx. Nucleation of triple-chains is more common in opx than cpx.

The structural adjustments required in the alteration of the tetrahedral layer of pyroxene to other biopyriboles (see figure) involve moving Al,Si atoms through the face of the tetrahedron (horizontal arrows) with hydroxylization of the unshared basal oxygen (OH = double circle) and simultaneous translation in the (100) plane of one of the other basal oxygens into the apical position of the newly formed tetrahedron (dark arrow) whilst the apical oxygen (dashed circle) is translated ~1.5Å (open arrow) to become a basal bridging oxygen in the central "spine" of the new triple chain. This operation repeated on every third px chain produces triple chains (jimthompsonite), on two adjacent px chains it produces a pair of double chains, and on every other px chain, an infinite sheet.

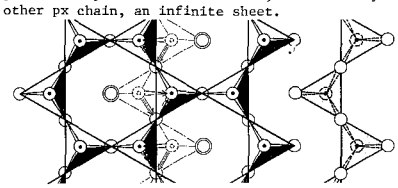

V 167

CRYSTALLOGRAPHY OF THE ILMENITE-CORUNDUM ORDER-DISORDER TRANSFORMATION FOR AN INTERMEDIATE ILMENITE-HEMATITE SOLUTION

Benjamin Burton (Dept. of Earth and Space Sciences, SUNY, Stony Brook, N. Y. 11794)

Thermal expansion and x-ray intensity data have been collected on single crystals of composition ilmenite-54.6(6) hematite-45.4 (mole %). Preliminary analysis of the data indicate that they are consistent with the existence of a continuous second-order phase transformation; from a low-temperature ordered ilmenite structure (space group $R\bar{3}$) to a high-temperature disordered corundum structure (space group $R\bar{3}c$).

The characteristic changes in crystallography that occur during the transformation are a continuous decrease in the relative intensities of ordering reflections and a small, but significant, decrease in the hexagonal c/a-ratio (-1.86 x 10^{-5} per °C). In contrast, the high-temperature data of Wechsler (1978, GAAPBC 10 (7) pp. 513) for stoichiometric ilmenite between 24°C and 1050°C indicate no detectable disorder and a much smaller change in c/a-ratio of opposite sign (8.32 x 10^{-7} per °C). Thus, the observed change in c/a appears to depend primarily on the degree of disorder.

Temp. (°C)	a (Å)	c (Å)	c/a
24	5.0635(5)	13.895(3)	2.744(1)
200	5.070(4)	13.897(5)	2.741(3)
685	5.108(2)	13.956(4)	2.732(2)
730	5.1102(4)	13.959(2)	2.7315(5)
800	5.118(2)	13.960(4)	2.729(2)

V 168

CALCULATED MAXIMUM BIREFRINGENCE OF SUBMICROSCOPIC COMPOSITE ZINC SULFIDES

B.J. Cooper(Dept. of Geological Sciences, VPI&SU, Blacksburg, VA 24061)

The computer program by Hauser and Wenk(1976) is used to predict the maximum birefringence(δ) of submicroscopically intergrown ZnS polytypes. These are assumed to be intergrown with only one of the 4 [111] directions of sphalerite(3C) parallel to the c* axis of wurtzite(2H). The linear correlation between δ and the percent of hexagonal closest-packing(σ), $\delta=\delta(2H)\cdot\sigma$, where δ(2H) is δ of the intergrown 2H, has been confirmed by calculations. Fleet(1977) suggests that the relationship may be polynomial because δ is often lower than expected and δ appears to be independent of composition. Two alternative explanations with corresponding figures are:

1) various δ(2H) values result in different slopes. This explanation may require the compositional dependence rejected above.

2) 2H intergrowths along more than one of the 4 [111] directions in 3C. This has been observed macroscopically in synthetic and natural crystals. Calculations performed using various volume fractions of 2H along a second direction (σ_2) result in different δ values for the same σ value. Other combinations are possible, but are difficult to show graphically. The author is presently attempting to find optical, X-ray, and HREM evidence of this type of intergrowth.

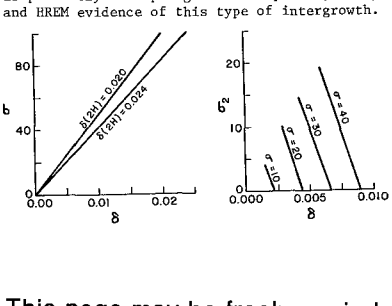

V 169

THE CALCULATION OF TETRAHEDRAL Si-O AND Al-O BRIDGING BOND LENGTHS AND ANGLES

E.P. Meagher (Dept. of Geological Sciences, University of British Columbia, Vancouver, Canada V6T 1W5)
D.K. Swanson and G.V. Gibbs (Dept. of Geological Sciences, Virginia Polytechnic Institute and State University, Blacksburg, VA 24061)

Ab initio STO-3G SCF-MO theory has been used to calculate minimum energy T-O (T = Al,Si) bond lengths and TOT angles for $H_6Si_2O_7$ (I) and $H_6SiAlO_7^1$ (II) molecular clusters. The minimum energy Si-O bond length (1.60 Å) and SiOSi angle (140°) calculated for I are in close agreement with the bond lengths (1.605; 1.614 Å) and angles (143.7°) observed for quartz. Likewise, Si-O (1.59 Å) and Al-O (1.70 Å) bond lengths calculated for II agree with mean values observed for two-coordinated SiOAl linkages (Si-O = 1.58; Al-O = 1.70 Å) of anorthite and low cordierite. Brown-Shannon bond valences computed for I and II yield bond valence sums to within ~6% of the atomic valences.

To see whether the theory is capable of generating the positive correlation observed between Si-O bond length and p_o (= the bond strength sum to O), bond lengths and angles were optimized for a number of molecular clusters in which p_o ranges between 1.50 and 2.75 v.u. A linear regression analysis of d(Si-O) on p_o for the resulting minimum energy data produced the equation $d(Si-O) = 0.090p_o + 1.445$ compared with the empirical equation $d(Si-O) = 0.091p_o + 1.440$. A strong correlation between p_o and bond overlap population indicates that the Pauling bond strength is a measure of the buildup of charge density between bonded atoms. In spite of arguments to the contrary, the calculations show that d(Si-O) correlates inversely with -sec∠SiOSi. The close agreement between tetrahedral bond lengths and angles observed for silicates and those calculated with STO-3G theory indicates that the local forces in SiOSi and SiOAl linkages in silicates are not dissimilar from those in molecular clusters.

V 170

CALCULATION OF TETRAHEDRAL Si-N BOND LENGTHS AND ANGLES

Y. Nakajima, D.K. Swanson and G.V. Gibbs (Dept. of Geological Sciences, Virginia Polytechnic Institute and State University, Blacksburg, VA 24061)

Inasmuch as several silicon nitrides crystallize with silicate structures, *ab initio* calculations have been completed for four silazane molecules for purposes of comparing the electronic structures and wave functions of tetrahedral Si-O and Si-N bonds. Using a minimal STO-3G basis set, SCF-MO calculations were completed for [I] $HN(SiH_3)_2$, [II] $N(SiH_3)_3$, [III] $Si(NH_2)_4$, [IV] $H_2N_2(SiH_2)_2$ and [V] $N(CH_3)_3$. The minimum energy bond lengths and angles compared with experimental values (in parentheses) are as follows: [I] d(Si-N) = 1.73 Å (1.724), ∠SiNSi = 130° (127.9); [II] d(Si-N) = 1.74 Å (1.738), ∠SiNSi = 120° (119.6); [III] d(Si-N) = 1.71 Å (compared with 1.703 in Si_3N_4); [IV] d(Si-N) = 1.72 Å (<1.741>), ∠SiNSi = 96° (<91.4>), ∠NSiN = 85° (<88.7>), d(Si···Si) = 2.57 Å (2.49), d(N···N) = 2.30 Å (2.427) and [V] d(C-N) = 1.49 Å (1.45), ∠CNC = 110° (111). The fact that minimal basis set calculations are capable of reproducing the geometries of trisilylamine [II] and trimethylamine [V] indicates that the geometry of [II] may not be used as evidence for d-orbital involvement in the wave functions of the Si-N bond.

An examination of Si-N bond lengths and ∠SiNSi for solid silicon nitrides yields an average bond length of 1.73 Å and a narrow range of angles between 113 and 128° in close agreement with values observed for the four silazane molecules, indicating that the bonding forces in SiNSi units in silicon nitride molecules and solids are similar. In addition, well-developed linear correlations obtain between $\log\sin(\frac{1}{2}\angle SiNSi)$ and log d(Si···Si) and between $\log\sin(\frac{1}{2}\angle NSiN)$ and log d(N···N). However, linear correlations between d(Si-N) and -sec∠SiNSi could not be established.

V 171

CALCULATION OF TETRAHEDRAL AND OCTAHEDRAL BOND LENGTHS FOR THIRD ROW ELEMENTS

D.K. Swanson (Dept. of Geological Sciences, Virginia Polytechnic Institute and State University, Blacksburg, VA 24061)
E.P. Meagher (Dept. of Geological Sciences, University of British Columbia, Vancouver Canada V6T 1W5)
G.V. Gibbs (Dept. of Geological Sciences, Virginia Polytechnic Institute and State University, Blacksburg, VA 24061)

Minimum energy M-O bond lengths (M = Na, Mg, Al, Si) have been calculated for tetrahedral $M^{IV}(OH)_4^{-n}$ and octahedral $M^{VI}(OH)_6^{-n}$ clusters using ab initio SCF-MO theory. With the exception of the Na-O bond lengths, the optimized bond lengths, M-O(opt), are within 0.03 Å of those calculated using the Shannon and Prewitt radii, M-O(SP):

M	M^{IV}-O(opt)	M^{IV}-O(SP)	M^{VI}-O(opt)	M^{IV}-O(SP)
Na	2.12 Å	2.35 Å	2.36 Å	2.38 Å
Mg	1.85	1.85	2.06	2.08
Al	1.72	1.75	1.88	1.89
Si	1.65	1.62	1.78	1.76

In addition, geometries were optimized for four molecular clusters (I: $H_6Al_2O^{-2}$; II: H_6AlSiO^{-1}; III: $H_6Al_2OH^{-1}$; IV: $H_6AlSiOH$) to determine a theoretical relationship between d(Al-O) and p_o and AlOT angle (T = Al,Si). As observed, there is a systematic lengthening of the Al-O bond length with p_o and AlOT angle:

	d(Al-O)	∠AlOT	p_o	λ^2 = (-sec∠AlOT)
I	1.71 Å	130°	1.50	1.556
II	1.74	124	1.75	1.788
III	1.79	137	2.50	1.367
IV	1.84	131	2.75	1.524

A multiple linear regression analysis of d(Al-O) on p_o and λ^2 completed with the theoretical bond lengths and angles yielded the equation $d(Al\text{-}O) = 0.104p_o + 0.062\lambda^2 + 1.451$. A similar analysis for Si-O bond lengths using optimized bond lengths and angles for 10 molecular clusters yielded the equation $d(Si\text{-}O) = 0.067p_o + 0.055\lambda^2 + 1.411$.

V 172

NEUTRON STRUCTURE REFINEMENTS OF THE Al_2SiO_5 POLYMORPHS

R.C. Peterson (Dept. of Geological Sciences, Virginia Polytechnic Institute and State University, Blacksburg, VA 24061)
R.K. McMullen (Dept. Chemistry, Brookhaven National Laboratory, Upton, NY 11973)
(Sponsor: G.V. Gibbs)

As part of a charge density study of the Al_2SiO_5 polymorphs, neutron structure refinements have been completed for kyanite (Campo Longo, Switz., a = 7.116(4), b = 7.830(5), c = 5.574(6), α = 89.87(7), β = 101.14(6), γ = 106.03(4)), andalusite (Brazil, a = 7.789(4), b = 7.892(5), c = 5.550(3)) and sillimanite (Norwich, CT, a = 7.479(1), b = 7.670(1), c = 5.769(1)). Data were collected at the HFBR, Brookhaven National Laboratory using a Be monochromated 1.0024 Å wavelength beam. Two symmetry equivalent octants were measured out to 100°2θ for andalusite and sillimanite, and one unique hemisphere out to 100°2θ was collected on kyanite. Comparisons of these neutron refinements are made with a previous neutron study of andalusite and sillimanite by Finger and Prince (1971) and published x-ray refinements. The positional parameters show no significant difference from previous studies. Differences in the temperature factors between the x-ray and neutron experiment are discussed in terms of bonding and extinction effects. Refinement of the scattering lengths of the various sites shows all the structures to be ordered with respect to Al/Si. In sillimanite disorder of aluminum and silicon in the two distinct tetrahedral sites is not observed. Iron is ordered in the octahedral site of sillimanite supporting previous work.

V 173

STRUCTURE REFINEMENT OF HOLLANDITE MINERALS

Jeffrey E. Post (Dept. of Chem., Arizona State University, Tempe, AZ 85281)
Peter R. Buseck (Dept. of Chem., Arizona State University, Tempe, AZ 85281)
Robert Von Dreele (Dept. of Chem., Arizona State University, Tempe, AZ 85281)

Hollandite and cryptomelane are members of an isostructural series of minerals having the general formula $A_{0-2}(Mn^{+4}, Mn^{+2})_8O_{16}$, where A is primarily Ba^{++} in hollandite and K^+ in cryptomelane. The hollandite structure was originally solved by Bystrom and Bystrom (1950) from Weissenberg film data and refined in the space group I^4/m to an R-value of 0.19. With increasing interest in manganese oxide minerals and their structures, a more precise and accurate structure seemed desirable. The crystal structure for cryptomelane has not previously been refined. Diffraction patterns for hollandite and cryptomelane commonly show streaking and split spots which are interpreted to be the results of twinning from a quarter turn about b*. Single crystal x-ray data was collected for a hollandite crystal from Stuor Njuoskes, Sweden and a cryptomelane crystal from Chindwara, India. Both minerals were refined in the space group I^2/m with hollandite yielding a final R-value of .0184 and cryptomelane refining to R=.0313. The final reflection to parameter ratio in each case was 13:1. The refinement yielded unit cell parameters for hollandite of a=10.026(3), b=2.8782(7), c=9.729(3), α=γ=90°, and β=91.03°(2); and for cryptomelane of a=9.956(3), b=2.8705(9), c=9.706(4), α=γ = 90°,and β=90.95°(3). The tunnels in the structure of these minerals allow the trapping of large cations and consequently are of great interest. The tunnel cation sites are 53% occupied in hollandite and 70% occupied in cryptomelane. In hollandite, 38% of the tunnel cations are displaced .60A from the main cation sites. The displacement probably results from the relaxation of the cations toward neighboring vacant sites. Cryptomelane does not show a similar cation displacement, but does have a site halfway between the main tunnel cation positions that is 10% occupied.

V 174

ENSTATITE, $Mg_2Si_2O_6$: COMPRESSIBILITY AND CRYSTAL STRUCTURE AT 21 KBAR

R. L. Ralph
Subrata Ghose (both at: Dept. of Geological Sciences, Univ. of Washington, Seattle, WA 98195)

The unit cell dimensions and the crystal structure of pure orthoenstatite have been determined from x-ray data on a synthetic single crystal mounted in a miniature diamond-anvil pressure cell at 21.1 ± 0.5 kbar. The unit cell parameters at 1 bar and at 21 kbar are a: 18.2350(33)Å, b: 8.8185(21)Å, c = 5.1804(6)Å, V = 833.04(27)Å^3, and a: 18.1468(28)Å, b: 8.7516(18)Å, c = 5.1488(5)Å, V = 817.70(21)Å^3, respectively. The relative linear compressibilities along the three axes are -0.0048, -0.0076, and -0.0061, and the overall volume compressibility is -0.0184. The estimated bulk modulus 1.15 Mbar is comparable to the value 1.07-1.08 Mbar determined from ultrasonic and Brillouin-scattering measurements (Weidner et al., 1978). Volume compressibilities for the cation coordination polyhedra, estimated using the cube of the average bond length, are M1: -0.0272, M2: -0.0236, Si(A): -0.0072, and Si(B): -0.0010.

The structure responds to pressure by compression of the cation polyhedra and increased kinking of the corner-linked single chains of SiO_4 tetrahedra running parallel to c. All Mg-O bonds shorten slightly (1-3σ) except the long Mg(2) - O(3B) bond, which decreases significantly (11σ). The angles between successive M1 or M2 sites along the edge-sharing octahedral chains do not change. The SiO_4 tetrahedral chains undergo no perceptible linear or angular distortions. Kinking in the tetrahedral B chain, the more distorted chain in the structure under ambient conditions, increases markedly (>5σ), whereas that in the A chain increases only slightly.

Studies of orthoenstatite at higher pressures up to 60 kbar are in progress.

V 175

INFRARED OH STRETCH BANDS IN KAOLINITE AND SERPENTINE UP TO 9 Kbars.

B. D. Velde (Laboratoire de Pétrologie, Université de Paris VI, 75230-Paris 5, France

Frequency shift of OH stretch bands in a disordered natural kaolinite and a well ordered aluminous serpentine indicate that cation substitution can affect OH vibrational energy under pressure. Kaolinite $[Al_2Si_2O_5(OH)_4]$ shows little difference between the major surface and inner hydroxyl stretch frequencies as pressure increases. Both bands (3698 and 3628 cm^{-1}) increase by about 0.5cm^{-1}/Kbar. The two subsidiary bands at 3668 and 3655 cm^{-1}, previously attributed to an in-plane doublet due to a distortion of the basal oxygen network appear to merge into one band as pressure increases suggesting a more symmetric structure under pressure.

Aluminous serpentine, with ordered octahedrally coordinated cations (Mg_2Al) shows a constant frequency of vibration for the inner hydroxyls but a decrease in the vibration frequency as pressure increases. It is known that ionic substitution in the tetrahedra affects this vibration also, the reason being increased hydrogen bonding. It can be deduced that since pressure and the chemical substitutions affect the OH vibration in the same way, an increase in pressure should increase hydrogen bonding of surface hydroxyl hydrogen ions.

Igneous Petrology I

Pier 2 & 3
Monday A.M.
J. C. Fountain (SUNY Buffalo), Presiding

V 176

PHENOCRYST MIGRATION IN A VERTICAL DIKE

D.F. McTigue (Dept. of Earth and Planetary Sciences, M.I.T., Cambridge, MA. 02139)

Phenocrysts have often been observed to be concentrated near the center of dikes, and explanations have been sought in various mechanisms of flow segregation. Cross-stream migration of a single particle in a rectilinear mean flow is due to inertial effects. For the small particle radius to channel width ratios typical of dikes, wall effects are negligible and the slip velocity of the phenocrysts is a result of longitudinal pressure gradient and buoyancy forces.

These observations are the basis for a continuum mixture theory that describes the macroscopic behavior of both liquid and solids in a dilute suspension. The negatively buoyant phenocrysts lag the fluid, and the resulting cross-stream lift is toward the center of the dike. The balance between this force and the diffusive force due to the concentration gradient can be solved for the distribution of particles across the dike.

Previous efforts to treat the more realistic case of a concentrated suspension in view of Bagnold's observation of normal stress effects are untenable.

V 177

A STRONTIUM ISOTOPE AND TRACE ELEMENT PROFILE THROUGH THE PARTRIDGE RIVER TROCTOLITE, DULUTH COMPLEX, MINNESOTA

Philip A. Molling*
Norman K. Grant (both at: Department of Geology, Miami University, Oxford, Ohio 45056

A 2170 ft. core through the Partridge River Troctolite has given a Rb-Sr whole-rock isochron age of 1045 ± 90 m.y. (^{87}Rb λ = 1.42 x 10^{-11} yr^{-1}). The initial $^{87}Sr/^{86}Sr$ ratios define three zones in the core; lower (I) and upper (III) zones where the ratios average 0.70493 ± 18, and an intermediate zone (II) extending from 710 to 1410 ft. below the surface with ratios averaging 0.70439 ± 12. In zones I and II the fayalite content of the olivine and the incompatible trace elements Zr, Y and Rb all increase downward. Zr/Y ratios are uniform and average 4.7 ± 0.6. Sulphide enrichment occurs at the base of zone I, and across the contact between zones I and II.

Zones I, II and III are thought to be intrusive units within the Partridge

River Troctolite, but unambiguous evidence for the order of intrusion is lacking. The Sr isotope data shows that contamination of the troctolite is negligible, and the inversion of the apparent fractionation sequences is considered to be a primary magmatic feature.

The data is consistent with the transfer of S from the underlying Virginia Formation into the troctolite by high temperature aqueous fluids (Ripley, 1980).

V 178

CUMULATE MINERALS AS LIQUID ANALOGUES, A NEW APPROACH TO MODELLING TRACE ELEMENTS IN MAFIC LAYERED INTRUSIONS: APPLICATION TO THE STILLWATER COMPLEX, MONTANA.

David D. Lambert (Dept. of Chem/Geochem, Colo. School of Mines, Golden, CO 80401)
E. Craig Simmons (Dept. of Chem/Geochem, Colo. School of Mines, Golden, CO 80401)
(Sponsor: R.W. Klusman)

Systematic application of trace element abundances and ratios to petrogenetic problems in general has met with considerable success. However, modelling of trace elements in mafic layered intrusions has been less successful, due in part to the difficulty of relating the abundances in cumulate rocks and minerals to the abundances in the parental liquid(s). Some complications include: (1) knowledge of actual values for mineral-melt distribution coefficients (K_d's); (2) assumptions involving the nature of the interstitial material (for whole-rock data); (3) the percent crystallization of the solid; and (4) whether or not more than one magma was involved. These complications hamper the ability to evaluate the role of processes such as multiple injections, contamination, mixing and diffusion controlled processes.

These problems can be minimized by noting that abundances and the ratios of trace elements with low K_d's ($\leq$ 0.1) are not strongly affected by the percent crystallization of the solid mineral. Thus, even though a cumulate mineral will have greatly different trace element abundances than its parental liquid, the relative trace element abundances and ratios of the same cumulate mineral from different rocks will be analogous to the relative trace element abundances and ratios in the liquid from which they crystallized; i.e. liquid analogues: REE in cumulate plagioclase and orthopyroxene offer the best conditions for the application of the model.

As an example, REE data for cumulate plagioclase from the Banded and Upper zone of the Stillwater Complex, Montana, demonstrate that it was not the crystallization product of a single magma.

V 179

PETROLOGY OF FE-TI OXIDE AND APATITE (NELSONITE) ROCKS

Allan Kolker (Dept. of Geology, Univ. of Massachusetts, Amherst, Ma. 01003)
(Sponsor: Stephen E. Haggerty)

Rocks consisting primarily of Fe-Ti oxides and apatite (nelsonite) occur as elongate irregular "dikes" in alkalic anorthosite and associated rocks in the Roseland-Piney River district of Virginia and several other world-wide localities. Most workers agree on a magmatic origin for nelsonites; however, the manner in which they form remains controversial. Philpotts (1967) investigated the pseudo-ternary system magnetite-apatite-diorite and proposed that the commonly observed 2:1 ratio of magnetite to apatite constitutes a eutectic mixture that is immiscible with a dioritic melt. Emslie (1975) proposed the accumulation of apatite and oxide minerals by crystal settling as an alternative to liquid immiscibility, in the Morin complex of Quebec. Magnetite flows and associated shallow intrusions of magnetite with amygdule-filling apatite at El Laco, Chile, serve as proof that iron-oxide liquids associated with apatite can exist in nature.

Modal mineralogy determined for 31 oxide-apatite rocks from localities in Virginia, New York, Quebec, Norway and Sweden, largely supports the 2:1 oxide:apatite ratio noted by Philpotts. Fe-Ti oxides show a limited and distinct range in composition (Hem and Usp) for each of the districts examined. Nelsonites commonly contain fluor-apatite in which light lanthanides (La-Tb) are dominant over heavy lanthanides (Dy-Lu). Temperature and Oxygen fugacity estimates compiled for nelsonite oxide pairs bracket an oxide equilibration path that corresponds closely to the FMQ buffer. Spinels with compositions intermediate between hercynite, spinel and gahnite are present as accessory minerals in oxide-apatite rocks of Norway, Quebec and Virginia. It is concluded that nelsonite dikes are most probably the result of infilling of fractures in older rocks with oxide-apatite liquid.

V 180

GEOCHEMICAL RELATIONS BETWEEN COEXISTING MAGMAS FROM THE NAIN COMPLEX, LABRADOR: REE AND SR-ISOTOPE DATA.

E. Craig Simmons (Dept. of Chem/Geochem, Colo. School of Mines, Golden, CO 80401)
R.A. Wiebe (Dept. of Geology, Franklin & Marshall College, Lancaster, PA 17604)
David D. Lambert (Dept. of Chem/Geochem, Colo. School of Mines, Golden, CO 80401)
(Sponsor: R.W. Klusman)

The Goodnews Complex, Labrador, a composite intrusion in which quartz monzonite hosts anhydrous granite pillows and ferrodiorite dikes and pillows, and intrudes leuconorite in the southern portion of the Nain Complex. Field relations indicate that the three magmas of the complex and the leuconorite crystallized contemporaneously, and major element data are consistent with the leuconorites, ferrodiorites and granite pillows being related by crystal fractionation and liquid immiscibility to an original plagioclase-rich parental magma (Wiebe, 1979, J. Petr., v. 20, 239).

Ferrodiorites form two distinct suites: low and high-Fe (Table). The data for the low-Fe rocks, their subparallel REE patterns, negative Eu-anomalies (Eu/Eu*=0.84-0.64), and the fact that one leuconorite sample yielded an initial $^{87}Sr/^{86}Sr$ of 0.7057, are consistent with their being residual magmas from the leuconorite. Since their REE abundances and Rb/Sr ratios do not correlate, they are the result of a fractionation process involving both liquid immiscibility and crystal fractionation.

The data clearly indicate that the high-Fe rocks are not comagmatic with either the low-Fe rocks or the leuconorites. The granite pillows have Sr/Ba ratios less than any of the ferrodiorites, and do not appear to be related to these ferrodiorites.

Ferrodiorites	FeO^T	$(^{87}Sr/^{86}Sr)_i$[1]	Ce[2]	Yb[2]
low-Fe	12-15%	0.7057-0.7062	160-230	20-30
high-Fe	16-21%	0.7077-0.7082	80-230	12-40

[1] $= 1.42 \times 10^{-11} yr^{-1}$; t = 1.4 x 10^9yr
[2] chondrite normalized

V 181

PETROGENETIC IMPLICATIONS OF OXYGEN ISOTOPE STUDIES OF PLUTONIC ROCKS FROM THE OSLO RIFT, NORWAY

Tom Victor Segalstad
Hiroshi Ohmoto (both at: Dept. of Geosciences, The Pennsylvania State University, University Park, PA 16802)

Two major groups of plutonic rocks, alkaline rocks (monzonite and its differentiates: foyaite, syenite, and peralkaline granite) and biotite granite intruded between 247 and 286 Ma ago in the Permian Oslo rift of S. Norway. Genetic relationships between the two groups and the magnitude of crustal contamination of these magmas are not clear and have been the subjects of intensive discussions for the last century. We have analyzed oxygen isotopic compositions of over 100 whole rock samples from a 50x200 km area of the Oslo rift. $\delta^{18}O$ values of the plutonic rocks from this area can be divided into two sets: (1) normal igneous values (+5.5 to +7.5 °/₀₀, SMOW), and (2) high $\delta^{18}O$ values (+7.5 to +14.5°/₀₀). The rocks of the first set occupy approximately 75 area % of the plutonic rocks and occur in the axial parts of the Oslo rift. All the major rock types (including some biotite granite plutons) are represented in this set. This agrees with published petrological and geochemical (e.g., Nd-Sr isotopes, REE, Th/U) data suggesting a common origin for most of the Oslo igneous rocks, a likely source being basaltic melts from the mantle. The plutonic rocks of the second set (high $\delta^{18}O$) occupy about 25 area % of the plutonic rocks and occur in the marginal zones of the rift, mainly as biotite granites and peralkaline granites. Some of these high $\delta^{18}O$ values may have been produced by later hydrothermal activity. However, the majority of high $\delta^{18}O$ plutonic rocks appears to be products of magmas which assimilated upper crustal materials (including sedimentary and metasedimentary rocks). Our studies suggest that both differentiation and crustal contamination have played important roles in the petrogenesis of the igneous rocks of the Oslo rift.

V 182

OXYGEN ISOTOPE COMPOSITIONS OF GRANITIC AND SYENITIC PLUTONS IN THE CENTRAL METASEDIMENTARY BELT, GRENVILLE PROVINCE OF ONTARIO

Yuch-Ning Shieh (Department of Geosciences, Purdue University, West Lafayette, IN 47907)

The $^{18}O/^{16}O$ ratios of more than 150 rock samples from 24 discrete granitic and syenitic plutons between the Harvey-Cardiff Arch and the Frontenac Axis have been determined. Based on their $\delta^{18}O$-values, the plutons can be classified into 3 distinct groups: (I) Low-^{18}O group (δ = 7.0-9.5): Weslemkoon, Elzevir, Cross Lake (Northbrook), Skootamatta, Mt. Moriah and Mt. St. Patrick plutons. (II) Intermediate-^{18}O group (δ = 9.0-12.5): Methuen, Coe Hill, Ridge, Wollaston, Blue Mountain, Delora, Westport, Wolfe Lake and Rideau Lake plutons. (III) High-^{18}O group (δ = 12.5-16.5): Lyndhurst, Crow Lake, Battersea, Perth Road, South Lake, Gananoque and McIntosh Mills plutons. The Loon Lake pluton overlaps groups II and III and the Elphin pluton overlaps groups I and II. Most of the low-^{18}O group plutons were emplaced within or adjacent to the Hastings Basin where metamorphic grades range from greenschist to amphibolite facies. All the high-^{18}O group plutons are confined to a granulite facies terrain in the Frontenac Axis. The characteristic $^{18}O/^{16}O$ ratios observed in plutons from each group probably reflect the unique isotopic composition of the source material from which the plutons were derived. The most plausible source of the low-^{18}O group plutons is the lower crustal rocks or the Grenville basement gneisses (δ = 6-9) and that of the high-^{18}O group plutons the Grenville Supergroup metasediments (δ = 12-17). The intermediate-^{18}O group plutons may have derived from mixture of the two.

V 183

THE EFFECTS OF MAGMA/COUNTRY ROCK INTERACTION ON U AND TH DISTRIBUTION WITHIN A MONZONITE PLUTON, LARAMIE RANGE, WYOMING

J. C. Fountain
D. S. Hodge
A. G. Del Signore (all at: Department of Geological Sciences, State University of New York at Buffalo, Amherst, NY 14226

Analysis of samples from a traverse across a monzonite pluton of the Laramie Anorthosite Complex, Laramie Range, Wyo. indicates that U and Th distribution within 5 km of the monzonite/country rock contact was strongly affected by interaction of the monzonite magma and the granite gneiss country rock. The monzonite may be divided on the basis of chemical data into an inner, homogeneous, cumulate zone and an outer zone in which the chemical composition shows a regular variation towards the contact. U and Th abundances are very low in the cumulate zone 0.2-1.8 ppm U, 1-2.5 ppm Th), but are higher in the outer zone (3.3-6.3 ppm U, 6.8-10.5 ppm Th). Th and U abundances in the outer zone decrease regularly away from the granite gneiss contact, dropping 50% in about 3 km. The light rare earths exhibit similar behavior, Ce decreases from 135 to 116 ppm over the same interval. The varitaion in U, Th and the REE cannot be explained by fractionation of the magma, but apparently resulted from interaction of anatectic melt of the granite gneiss, produced by the heat of the monzonite intrusion, with the cooling monzonite magma. The study indicates that extensive magma/country rock interaction resulted from the emplacement of a deep seated pluton, and the interaction significantly affected the composition of the igneous body. It also indicated that U, Th and Ce have moved from the country rocks into the igneous intrusion.

V 184

IMMISCIBLE ILMENITE AND SULFIDE LIQUIDS IN A GARNET CLINOPYROXENITE DIKE FROM SALT LAKE CRATER, HAWAII.

R.L. Bedell Jr. School of Natural Science, Hampshire College, Amherst Ma. 01002. present address: Dept. Min. Sci. American Museum of Natural History, N.Y. N.Y. 10024.
J.B. Reid Jr. School of Natural Science, Hampshire College, Amherst Ma. 01002.

Garnet clinopyroxenite dikes with igneous character occasionally occur in ultramafic nodules from Salt Lake Crater, Hawaii. An unusual abundance of oxide and sulfide phases occurs in one such dike whose major elements closely resemble undersaturated basalts. Garnet, with typical Salt Lake Crater composition($Alm_{27}Py_{60}Gr_{13}$)occurs as reworked phenocrysts suggesting it is the first silicate to form. Cpx ($En_{45}Fs_{13}Wo_{42}$)is anhedral with minor wormy opx exsolution($En_{79}Fs_{19}Wo_{17}$)in a few grains.

Within garnet, subspherical blebs of ilmenite occur with high MgO(8.5wt.%)and Al_2O_3 (1.3wt.%); there are also smaller amounts of Fe-S spherules. Within cpx Fe-S spherules are more abundant than ilmenite. Interstitial to the silicates ilmenite occurs as large(up to 1x.5mm)subspherical blebs with an identical composition to those in garnet. A continuous range in ilmenite morphology and composition is found from large blebs to smaller blocky grains, to still smaller laths accompanied by decreasing MgO and Al_2O_3. Interstitial sulfide is generally vein filling, but occasionally is spherical often surrounded by blocky or lath-like ilmenite.

The petrographic and compositional data suggest that during the crystallization of an undersaturated magma at depth, ilmenite formed very early and the bulk of the sulfide somewhat later as droplets of immiscible melt within the silicate liquid. The later appearance of sulfide indicates that sulfur solubility in the silicate magma becomes dramatically reduced when Fe and Ti are removed by ilmenite melt immiscibility.

V 185

EVIDENCE FOR LARGE SCALE LIQUID IMMISCIBILITY INVOLVING GRANODIORITIC AND DIORITIC MAGMAS

J. F. Bender
G. N. Hanson
A. E. Bence (all at: Dept. of Earth and Space Sciences, SUNY, Stony Brook, N. Y. 11794)
N. M. Ratcliffe (U. S. Geol. Survey, Reston, Va. 22092

Granodioritic and dioritic plutons of the Rosetown Complex, N. Y., which are associated with the nearby Cortlandt Complex, have chemical characteristics indicating that large-scale liquid immiscibility played a major role in their petrogenesis. Rare Earth (Fig.) and other slightly compatible trace elements have abundances which are much greater in the diorite precluding the possibility that these rocks are related by fractional crystallization. The trace element data also eliminate the possibility that the granodiorite represents: (1) a partial melt of crustal rocks including basalt; (2) a granitic cumulate; and (3) a residue from an aqueous fluid derived from silicate melts or rock. The distribution of major and trace elements between the diorite and granodiorite (Table) is very similar to the experimentally determined partition data of immiscible liquid pairs. Phase chemistries of plagioclase and biotite in the granodiorite (An_{5-28}; Fe#.57-.61) and diorite (An_{15-30}; Fe#$_{61-64}$) overlap, a feature compatible with an immiscibility relationship.

Wt. %	Granodiorite	Diorite
SiO_2	72.3	53.6
TiO_2	0.16	1.58
Al_2O_3	15.6	17.6
Fe_2O_3	0.66	3.26
FeO	0.54	6.91
MgO	0.31	3.06
CaO	1.72	6.17
Na_2O	5.29	4.42
K_2O	3.32	2.21
P_2O_5	0.03	0.66
PPM		
Nb	1.4	53
Zr	92	199
Cr	3.8	25.0
Ni	13	28

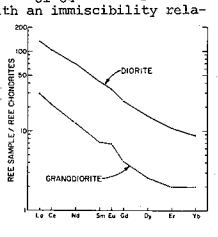

V 186

ORIGIN OF GRANITIC ROCKS IN OCEANIC CRUST: AN EXPERIMENTAL STUDY

S.J. Dixon (Dept. of Geological Sciences, Brown University, Providence, RI 02912)
M. J. Rutherford

Hydrothermal experiments on 3 oceanic tholeiites were conducted under fluid pressures of 1, 2, and 3 kb, at P_{H_2O}'s equal to and less than P_{Total}, and at oxygen fugacities ranging from the graphite-methane (G-CH_4) oxygen buffer to the nickel-nickel oxide (Ni-NiO) oxygen buffer. The experiments were carried out in TZM and standard cold-seal pressure vessels using both methane and argon as pressure mediums. Both partial melting and reversal experiments were performed. A liquid line of descent was delineated by quenching these experiments at the final temperature which was in the range 1075°C-900°C and by analyzing the residual liquid. The liquid line of descent is characterized by an enrichment in silica. Granitic melts are produced after 15% partial melting of the oceanic basalt (SiO_2=73 wt%). At high f_{O_2}'s (Ni-NiO), this increase in silica in the residual liquid is caused by the crystallization of both an amphibole and an iron oxide phase. At low f_{O_2}'s (G-CH_4), amphibole is not present in experimental runs that contain greater than 20% melt. The silica enrichment of the residual liquid at these low f_{O_2}'s is caused by the crystallization of 3 - 6 vol.% of an FeTi oxide phase. This experimental investigation suggests that granitic melts can be produced under low f_{O_2}'s where $f_{H_2O} \approx .6\ P_{Total}$ as a result of either equilibrium crystallization or partial melting at depths of approximately 3-6 km in the oceanic crust. The SiO_2 enrichment is due to the crystallization of FeTi oxides. At higher f_{O_2}'s high SiO_2 melts can be produced in the oceanic crust by the crystallization of an amphibole and an iron oxide phase.

V 187

ORIGIN OF PLAGIOGRANITES AND BASIC ROCKS OF THE CANYON MOUNTAIN OPHIOLITE, OREGON.

D.C. Gerlach
W.P. Leeman
H.G. Ave Lallemant (all at: Dept. of Geology, Rice University, Houston, TX 77001)

The Canyon Mountain ophiolite is similar to other ophiolites, but contains an unusually large volume of plagiogranite. These rocks occur as a sill complex in high-level hornblende gabbros. Both plagiogranites and the associated basic rocks are characterized by light-depleted REE abundances. Field observations coupled with major-and trace element chemistry support a model by which the plagiogranites were produced by partial melting of hydrous basic rocks. REE data for the plagiogranites were used in calculations to constrain source REE contents. A wide range of distribution coefficients was used, and melting proportions were estimated from experimentally determined phase relations of basalt under hydrous conditions. The calculated source patterns are similar to those of basic rocks in ophiolites, Canyon Mt. included, and those of oceanic gabbros. Differentiation of basic magma may have produced some of the plagiogranites, although none of the basic rocks analyzed are suitable parental liquids.

A lack of correlation between the major- and trace element chemistry within the basic rocks indicates periodic replenishment of the magma chamber by several unrelated batches of magma, each possibly produced by partial melting of peridotite. REE data for these samples, adjusted for olivine fractionation on the basis of Ni and MgO contents, were used to model REE contents of ultramafic sources and residues. Results are comparable to those measured in ophiolitic and Alpine-type lherzolites and harzburgites; i.e., all are depleted in LREE. The slight depletion in HREE in a few samples is best explained by a small amount of garnet in the source. It is apparent that the basic rocks are not all comagmatic (related by fractionation), and may have resulted by partial melting of different mantle sources.

V 188

ESTIMATES OF PROVENANCE AGES FOR CALEDONIAN GRANITES

P.J. Hamilton
R.K. O'Nions (Dept. of Mineralogy & Petrology, Downing Place, Cambridge, CB2 3EW, U.K.)

Sm-Nd and Rb-Sr systematics are reported for Caledonian granites (s.l), including pre- and post-tectonic varieties north and south of the supposed Iapetus suture, emplaced between ca. 520 Ma and ca. 390 Ma ago in Scotland and N. England. All granites investigated have 143/144Nd ratios that are less than, and 87/86Sr ratios that are greater than, the model bulk Earth values at the time of emplacement. $\varepsilon_{Nd}(t)$ varies from -0.2 to -11.5 and $\varepsilon_{Sr}(t)$ varies from +4 to +200. Model ages derived from Sm-Nd systematics (t_{BE}) range from 0.44 Ga to 1.68 Ga. Some granites contain inherited zircons whose U-Pb systematics provide provenance-age estimates (Pidgeon & Aftalion, 1979). Inherited zircons from the Ben Vuirich granite (514 ± 7 Ma old) provide an estimated provenance age of 1.32 Ga which compares with the t_{BE} age of 1.26 Ga. The Strichen and Foyers granites and the Strontian biotite granite phase contain zircons that yield provenance age estimates of ≥ 1.0 Ga, and their t_{BE} ages are 1.46, 0.97 and 1.00 Ga respectively. These results limit the involvement of contemporary mantle-derived components to negligible proportions.

The Ben Nevis granite has initial 87/86Sr = 0.7043 and $\delta^{18}O$ = 7.8‰ (Nature 283,21:1979); features characteristic of mantle-derived magmas. However, t_{BE} = 0.97 Ga for Ben Nevis and indicates extensive involvement of old crust. The Shap granite in N. England (394 ± 3 Ma old) has $\delta^{18}O$ = 11.0 and initial 87/86Sr = 0.7075 (op. cit.), indicating a predominantly sedimentary source. The t_{BE} age for Shap of 0.56 indicates that old (>1 Ga) crustal components were not involved significantly.

V 189

STRONTIUM ISOTOPIC VARIABILITY IN THE PLUTON OF SAN JACINTO PEAK, SOUTHERN CALIFORNIA

R.I. Hill
L.T. Silver (Division of Geological and Planetary Sciences, California Institute of Technology, Pasadena, CA 91125)

Field and geochemical reconnaissance of a large pluton(30X30km,2.5km relief) at the north-eastern corner of the Peninsular Ranges Batholith reveals pronounced structural, petrographic and isotopic zonation. The pluton is dominantly sphene-hornblende-biotite granodiorite zoned from a tonalitic rim (C.I. 25) to a more granodioritic center (C.I. 10). Three units delineated by modal and structural discontinuities are distinguished; C.I. decreases inward in each unit suggesting three apparent cyclical units separated by movement zones. U-Th-Pb isotope systems in multiple zircon fractions from four sample sites covering the compositional range and all units imply emplacement at 97 ± 2my. Published hornblende and biotite K-Ar ages range from 87 to 79 my.

Rb(50-140ppm) and Sr(230-650ppm) show no apparent relationship to mineral abundances, but form a negatively-sloping array on a Rb vs Sr diagram. K/Rb range is 244 ± 33. The consistency of the Rb, K and Sr data over the entire body argues against large-scale post-crystallization element migration. In a pluton transect initial $^{87}Sr/^{86}Sr(Sr_o$, calculated using 97my) ranges over 0.7066-0.7072 in the heterogeneous core; 0.7068-0.7072 in an intermediate ring; and 0.7073-0.7075 in the outer rim. With the lowest Rb and Rb/Sr, the tonalitic outer rim shows the highest Sr_o, independent of wallrock relations.

In-situ fractional crystallization appears secondary in producing the observed chemical variations. The regional gradient of Sr_o (Early and Silver, 1973) persists, with centrosymmetric modification, across the pluton. The distinct petrologic and isotopic variabilities both within and between each unit appear to be derived from the source region(s). They demonstrate that a large pluton can be emplaced without extensive homogenization.

Igneous Petrology II

Pier 2 & 3
Monday P.M.
E. Craig Simmons (Colorado School of Mines), Presiding

V 190

FURTHER CHARACTERIZATION OF CAMBRIAN WICHITA GRANITES

Gilbert, M. C., & Myers, J. D., both at the Department of Geological Sciences, Virginia Polytechnic Institute & State University, Blacksburg, Virginia 24061

The Wichita Mountains igneous complex of southwestern Oklahoma is unique in the southern

Mid-Continent because of its age and tectonic setting. Wichita granites, an important part of the complex, appear to be of mixed origin. All of the named units, except Mt. Scott Granite, clearly belong to a homogeneous A-type suite according to the classification of Loiselle and Wones (1979). The A-types of this province have wt% $SiO_2 \geq 74$, $CaO \leq 0.5$, FeO/FeO+MgO≈1, $P_2O_5 \approx 0.1$, $K_2O/Na_2O \geq 1.2$, notable F in amphiboles and biotites, and relatively high Zr. Mt. Scott Granite has a measurably different chemistry ($SiO_2 \leq 74$, CaO≈1.5, $P_2O_5 > 0.5$), and distinct elliptical plagioclase phenocrysts ($\sim An_{15-20}$) of problematic origin.

While textural relations preserve primary features, alkali feldspar phenocrysts and groundmass granophyre (where present), are strongly unmixed and perthitic in all the Wichita granites. Unmixing is considered to have occurred during cooling in the emplacement process. Most granites have Ca-amphibole as the principal ferromag, but some have biotite. Granites, such as the Quanah and Reformatory, more effectively sealed off from vapor escape during crystallization, produce late, sub-solidus Na-amphiboles (arfuedsonites).

This province is unusual in that all of the granites appear sheet-like and subordinate in volume to contemporaneous rhyolites. Presumably, this is due to emplacement over the underlying, older, dense gabbroic substratum.

V 191

CONSTRAINTS OF LEAD ISOTOPIC STUDIES ON SOURCES OF GRANITOIDS IN THE MERRIMACK SYNCLINORIUM, EASTERN MAINE

R.A. Ayuso (Dept. of Geological Sciences, VPI&SU, Blacksburg, VA 24061 and U.S. Geological Survey, Reston, VA 22092)
M. Loiselle, A.K. Sinha, and D.R. Wones (Dept. of Geol. Sci., VPI&SU, Blacksburg, VA 24061)

41 whole-rock and feldspar samples from 6 late Paleozoic plutons (NW to SE: Katahdin, Seboeis, Center Pond, Bottle Lake, Lucerne, Lead Mt.), emplaced at right angles to the synclinorium, confirm that the Lucerne and Lead Mt. plutons are the most radiogenic. These two are separated from the others by the Norumbega fault, are enriched in K and Rb, and have higher Rb/Sr ratios. Plutons on the NW side of the fault have a maximum Pb^{206}/Pb^{204} ratio of 19.06; those to the SE have a minimum ratio of 19.30. The maximum Pb^{208}/Pb^{204} ratio for the NW plutons is 39.18; the SE plutons have a minimum ratio of 38.96. No significant differences exist in the range of Pb^{207}/Pb^{204} ratios represented by both groups. This range in plutons on the NW side is 15.63-15.73; that in plutons on the SE is 15.69-15.73. All the granites are enriched in radiogenic Pb relative to oceanic basalts. Preliminary Sr isotopic studies support their radiogenic nature compared to oceanic mantle and rule out their derivation entirely from such a source. Even the least radiogenic K-feldspars indicate a high-μ environment in the source ($\mu = U^{238}/Pb^{204} \approx 9.9$). We cannot estimate the age of the source by using secondary isochrons because of the limited spread of the ratios. The granitic magmas originated in a high-μ environment that is unlikely to represent an old granulite terrane, also as suggested by the calculated Th/U ratios, which range from 3 to 6. Older volcaniclastic deposits may underlie the synclinorium, and the granitoids NW of the fault could have been derived by the interaction of such materials with magmas of lower μ ratios. The Lucerne and Lead Mt. plutons may be generated by melting of graywackes with minimal interaction with magmas from a lower μ source.

V 192

PETROGENESIS OF OPAQUE MINERALS IN KIMBERLITE, ELLIOTT COUNTY, KENTUCKY

J.J. Agee, J.R. Garrison, Jr. and L.A. Taylor (Dept. Geol. Sci. Univ. Tennessee, Knoxville, TN 37916)

Two kimberlite pipes in Elliott County contain inclusion of altered crustal rocks, ultramafic xenoliths, and a diverse megacryst suite in a groundmass of olivine, picroilmenite, Cr-spinel, perovskite, calcite, and various hydrous silicates. The megacryst assemblage consists of olivine, garnet, picroilmenite, phlogopite, clinopyroxene, and orthopyroxene. Rare Cpx-ilmenite and rutile-ilmenite intergrowths also occur.

Ilmenite megacrysts (8.15-13.8% MgO) have reversed-zoned rims (9.5-15.5% MgO). These rims are surrounded by a perovskite + spinel (19-22% MgO, 17-24% TiO_2, 2-8% Cr_2O_3) reaction rim. Ilmenite megacryst cores and Cpx-ilm show correlation of MgO with $TiO_2+Al_2O_3+Cr_2O_3$; matrix ilmenites (12.6-17.5%) show a similar trend, but with less MgO enrichment. Ilmenite in Cpx-ilm intergrowths (13.6% MgO) is at the high-MgO end of megacryst trend. The Cpx equilibrated at 1295-1335°C (Di-En solvus). All ilmenites fall on the high-MgO limb of the kimberlite parabola on the Cr_2O_3-MgO diagram. Matrix spinels are more Cr-rich (32-49%) & Ti-&Mg-poor (4-10% & 12-15% resp.) than those in the rims.

Megacrysts and Cpx-ilm intergrowths formed from a fractionating liquid at >150 km (T≈1100-1400°C) as evidenced by MgO trends and association with silicate megacrysts. Early Mg-rich megacrysts and Cpx-ilm intergrowths were succeeded by less Mg-rich ilmenites (down to 8.5% MgO). Subsequently, megacrysts reacted with a more Mg-enriched liquid resulting in formation of Mg-rich rims. This Mg-enrichment is substantiated by the occurrence of anomalously Mg-rich, low-T Opx megacrysts. This enrichment is probably the result of an increase in Fe^{3+}/Fe^{2+}, with a corresponding increase in MgO/FeO. Final crystallization of matrix spinel accompanied reaction of megacryst ilmenite to form an assemblage of spinel + perovskite.

V 193

SILICA ACTIVITIES AND CARBON DIOXIDE FUGACITIES FOR ROCKS OF THE BOND ZONE, OKA CARBONATITE, QUEBEC

Allan H. Treiman (Dept. of Geological Sci, Univ. of Mich., Ann Arbor, MI 48109)
Eric J. Essene (same as A.H.T.)
William C. Kelly (same as A.H.T.)
(Sponsor: John Valley)

Chemical conditions during emplacement and cooling of carbonatite and silicate rocks of the Bond Zone, Oka carbonatite, Quebec are being investigated using phase equilibrium and fluid inclusion analysis. Pressure at intrusion is estimated to be .8 to 1.2 kb from the weight of inferred overlying strata. Previous temperature estimates of 700°C rely on phases involved in subsolidus reactions, and are therefore minimum magmatic T. The values in parentheses below are end-member activities computed using an ideal ionic model.

In the melilite-diopside carbonatites and ijolites, $f(CO_2)$ is buffered to between 100 and 800 bars in the inferred P-T range by the reaction Akermanite(.24) + CO_2 = Diopside(.77) + Calcite. The ijolite also contains wollastonite, which constrains $a(SiO_2)$ between .08 and .04 by the reaction Ak(.24) + SiO_2 = Di(.77) + Wo(.94). Monticellite-diopside carbonatite has $a(SiO_2)$ buffered to between .03 and .016 by Mo(.66) + SiO_2 = Di(.88).

Primary and pseudo-secondary fluid inclusions are present in diopside and apatite in the above carbonatites. The inclusions contain gas and small proportions of liquid H_2O. Absence of liquid CO_2 limits $X(CO_2)$ to small values, a generous limit being 0.5. When combined with $f(CO_2)$ inferred from the above equilibrium, the maximum T of equilibrium is limited to 825°C

The ijolite and melilite-diopside carbonatite are closely related in that they share phases of near identical compositions, and therefore have similar values of intensive chemical parameters. These data are consistent with formation of ijolite and melilite-diopside carbonatite magmas as immiscible liquid fractions.

V 194

LEUCITE HILLS REVISITED: $^{87}Sr/^{86}Sr$ EVIDENCE

P. Ogden
R. Vollmer
J-G Schilling (all at: Graduate School of Oceanography, Univ. of R.I., Kingston, R.I. 02881)

Following an extensive field investigation and sampling of the Leucite Hills volcanic rocks, we report high precision 87Sr/86Sr ratios and Sr, Ba, K, Rb and Cs concentrations (by I.D.) of selected wyomingites, orendites, and madupites from 10 of the 21 known exposures. Preliminary results show that 87Sr/86Sr ratios of madupite and orendite range from .7054 to .7057 and .7054 to .7059, respectively. The range is much narrower than previously reported for the Leucite Hills and similar ultrapotassic lavas of southern Spain and western Australia. While the 87Sr/86Sr ratios at some eruption centers are very uniform, the variation at other centers approach the range of the entire field. The lavas are highly enriched in Sr, Ba, and the alkalis. Rb/Sr ratios range from .01 to .2, and K/Rb ratios range from 200 to 370. Isotopically, orendite and madupite are essentially indistinguishable, suggesting a common mantle source for the two rock types. 87Sr/86Sr ratios in wyomingites from the sediment inclusion-rich Boars Tusk are significantly higher and the range wider (.7062-.7079), suggesting contamination during emplacement. However, analyses of xenolith-free wyomingite are not available at this time to establish its source characteristics.

V 195

ALKALI BASALTS AND NEPHELINITES OF THE RATON-CLAYTON VOLCANIC FIELD: EVIDENCE FOR AN ENRICHED MANTLE

David Phelps and Joseph Wooden (both at LEMSCO Inc., NASA-JSC, Houston, TX 77058)
Douglas Blanchard (NASA-JSC, Houston, TX 77058)

Alkali basalts, basanites, and nephelinites were erupted from the Raton-Clayton volcanic field, northeast New Mexico, between 2.0 and 2.5 m.y.a. (Stormer, 1972). The petrography and chemistry of the rocks suggest a genetic relationship. Phenocryst phases are olivine in the basalts, olivine and aluminous augite in the basanites, and aluminous augite, rare olivine and hauyne in the nephelinites. Mg numbers [Mg/(Mg+ΣFe)] vary from 63 in the alkali basalts to 55 in the nephelinites. As the Mg number decreases, SiO_2 decreases, CaO increases, La/Yb_N increases from 15 to 35, and total rare earth element (REE) abundances increase. Al_2O_3 and Sc correlate inversely with CaO. $^{87}Sr/^{86}Sr$ from three samples range from .70399±6 to .70412±4. Rb is low in all samples.

Although clinopyroxene fractionation from the alkali basalts could produce trace-element abundances similar to the basanites and nephelinites, clinopyroxene fractionation is not compatible with major-element variations. The high levels of Sr in all samples (1500 to 3500 ppm) and low Rb (<30 ppm) make significant crustal contamination unlikely. Our tentative conclusion is that the suite of rocks constitute a series of magmas generated by partial melting of a mantle source. The highly fractionated REE profiles indicate that the magmas originated from an enriched mantle. The Sr isotopic variations suggest that mantle regions with different degrees of enrichment were tapped.

V 196

STRONTIUM ISOTOPE GEOCHEMISTRY OF MOUNT ARARAT AND MOUNT SÜPHAN VOLCANICS, EASTERN TURKEY.

L. GÜLEN (Dept. of Earth and Planetary Sciences, MIT, Cambridge, MA 02139)
(Sponsor: S. R. Hart)

Geochemical data obtained in a regional study of the Tertiary to Quarternary volcanic province in Eastern Turkey confirm the spatial and temporal coexistence of alkaline and calc-alkaline volcanics. Mount Ararat and Mount Süphan are among the major calc-alkaline stratavolcanoes in this province. Their lavas exhibit all the major and trace element characteristics of continental margin calc-alkaline rocks.

The 87/86 Sr ratios of Süphan lavas range from .70453 to .70651 and show evidence for crustal contamination, whereas the 87/86 Sr ratios of Ararat lavas have a limited range (from .70364 to .70386). Süphan lavas have higher Rb/Sr and lower K/Rb ratios in comparison with the Ararat lavas. The low values of 87/86 Sr, the constancy of these ratios over a wide range of SiO_2 (60% to 70%), and the lack of correlation between the Sr-isotopic composition and Sr-concentration imply that Ararat lavas have not been modified by crustal contamination. The variation of major and trace element contents of Ararat lavas in time, coupled with the 87/86 Sr ratios, show strong evidence for a periodically refilled magma chamber, with magmas derived from a homogeneous mantle source.

V 197

Nd AND Sr ISOTOPIC SYSTEMATICS OF KEWEENAWAN VOLCANIC ROCKS FROM THE NORTH SHORE OF LAKE SUPERIOR

L. DOSSO, V. RAMA MURTHY, T. SABELIN (Department of Geology and Geophysics, University of Minnesota Minneapolis, MN 55455)
W. P. LEEMAN (Department of Geology, Rice University, Houston, TX 77001)

We present here Sr and Nd isotopic systematics for a group of volcanic rocks (olivine tholeiites, basalts, trachy basalts and quartz latites) from the north shore of the Lake Superior. The combined Sr-Nd isotopic data show that the mantle sources of the Keweenawan plateau volcanism were heterogeneous at 1.12 b.y. ago. In a Nd-Sr isotopic diagram, the initial Nd and Sr isotopic ratios exhibit a well-defined correlation, with a slope parallel to the "mantle array" defined by the data from modern uncontaminated oceanic basalts. This suggests that the coherent Rb-Sr and Sm-Nd fractionations which result in the present day mantle array pertained to the Keweenawan mantle sources as well. The characteristics of the sources indicate further that the mantle ranged from nearly "bulk earth" composition to enriched materials (ε^0_{Nd}=-1.5 to -13.6; ε^0_{Sr}=-2.2 to 14.2) with a time integrated history of higher Rb/Sr and lower Sm/Nd than the bulk earth. Thus, it appears that the enrichment of the Keweenawan continental mantle is an ancient event. In the compositional range of volcanics studied so far, contamination by old continental crustal materials has not been observed.

V 198

GEOCHEMISTRY OF LHERZOLITE INCLUSIONS FROM MT. LEURA, VICTORIA, AUSTRALIA

C.Y. Chen
F.A. Frey (both at Dept. of Earth and Planetary Sciences, M.I.T., Cambridge, Ma. 02139

Bulk rock major element abundance trends and positive correlations of heavy REE (HREE) content with Al, Ca and Ti indicate that most of these lherzolites may be residues remaining after various degrees of melt extraction from a homogeneous source. Seven of the 9 samples have high LREE/HREE abundance ratios (La/Yb = 2.8 to 24) compared to chondrites while 2 samples have relative REE abundances more similar to chondrites. The commonly observed relative enrichment of incompatible elements (LREE, K, Rb) in lherzolites with the lowest Ca, Al and Ti content has led to a two component (partial melting residue and contaminant) model for their origin. The incompatible-rich component has been associated with mantle metasomatism. Evaluation of this hypothesis requires determination of the end-member compositions and determination of element distribution within the lherzolites. Analysis of acid-washed clinopyroxene (CPX) separates confirms that alkali metals can be easily removed from these CPX separates but REE, Sr and Sr^{87}/Sr^{86} abundances are unaffected. In these rocks CPX is the major host for REE and Sr but K and Rb are not accomodated within the major minerals. Nevertheless, there is a general correlation of LREE and Rb contents in the bulk rocks. Thus, it is likely that the alkali metal and LREE in these lherzolites are from the same component and the different distribution within the lherzolites of alkali metals compared to REE and Sr reflects the relative compatibility of Sr and REE in CPX. In contrast, in an anhydrous peridotite assemblage there is no suitable mineral host for K and Rb.

V 199

DIAPIRIC UPRISE IN THE UPPER MANTLE BELOW THE WEST-EIFEL VOLCANIC FIELD,FRG ?

Th. Sachtleben (Mineralogisches Institut der Universität, Köln,FRG)
H.A. Seck (Köln,FRG)
(Sponsor: Werner Schreyer)

In the Quaternary Western-Eifel volcanic field (FRG) several occurrences of ultramafic nodules may be distinguished on the basis of their mineralogy as well as textural and geochemical relationships.

In the Dreiser Weiher region two extreme suites of peridotites can be established on the basis of their equilibrium temperatures. One amphibole-free series comprising coarse-grained to mosaic-equigranular textures is equilibrated at ~1150°C. An amphibole-bearing group displaying mostly equigranular-tabular textures equilibrated at ~950°C.

In contrast, the occurrences west of the Dreiser Weiher contain mostly porphyroclastic nodules with strongly deformed opx-porphyroclasts within a fine-grained recrystallized matrix of opx, cpx, and ol.

The cores of the opx-porphyroclasts reveal exsolution phenomena (cpx,sp) indicating a former high-temperature history (>1000°C) whereas the rims and the matrix reequilibrated at considerably lower temperatures of 700-800°C.

It is assumed that these nodules represent the border zones of a mantle diapir whereas the high-temperature nodules of the Dreiser Weiher region may be representatives of a more central part of a diapir.

V 200

VERTICAL COMPOSITIONAL VARIATIONS WITHIN SUBCONTINENTAL MANTLE: EVIDENCE FROM XENOLITHS IN ALKALI OLIVINE BASALTS OF SOUTHERN SOUTH AMERICA

Charles R Stern (Dept of Geol. Sci., University of Colorado, Boulder, Colorado, USA 80309)
Alexandra Skewes (Dept of Geology, University of Chile, Santiago, Chile, S.A.)

Both spinel(sp)- and garnet(gt)-lherzolite xenoliths occur in the Pleistocene alkali olivine basalts which form the southernmost (52°S) unit of the Patagonian plateau lavas of southern S.A. Systematic differences in whole rock and mineral chemistry are observed between the two xenolith types. Compared to sp-lherzolites, gt-lherzolites have on the average higher contents of FeO (8.18 vs 7.81 wt %), Al_2O_3(4.42 vs 1.70 wt %), CaO(2.90 vs 0.87 wt %), TiO_2(0.20 vs 0.03 wt %), and Na_2O(0.24 vs 0.06 wt %); and lower MgO(38.3 vs 44.16 wt %). Mineralogically, gt-lherzolites consist of less magnesian olivines (Fo89 vs Fo91) and orthopyroxenes (En88 vs En90) and more TiO_2-rich (0.55 vs 0.16 wt %) and Na_2O-rich (1.84 vs 1.12 wt %) chrome diopsides. Some gt-lherzolites contain primary interstitial pargasitic amphibole which, as suggested by textural evidence, has formed by reaction of an aqueous phase and garnet. The gt-lherzolites have smaller proportions of modal olivine and greater proportions of modal pyroxenes than the sp-lherzolites. Also, gt-pyroxenites and compound xenoliths of gt-lherzolite and pyroxenite are more common than sp-pyroxenites or pyroxenite veins or layers in sp-lherzolites.

These differences suggest that a relatively depleted section of mantle overlies relatively less depleted mantle beneath southern S.A. This vertical compositional gradient may have resulted from upward migration of material from the underlying zone of alkali basalt magma genesis. Migration of material within the mantle may occur by solid state diffusion, movement of an aqueous phase containing dissolved material, or injection of silicate melt. The xenoliths from southern S.A. suggest the action of all three processes.

V 201

GLIMPSES OF MANTLE REDOX CONDITIONS?

Gene C. Ulmer (Department of Geology, Temple University, Philadelphia, Pennsylvania, 19122)
Matthias Rosenhauer (Institut Petrologie, Frankfurt, West Germany)
Eduard Woermann (Institut Kristallographie, RWTH, Aachen, West Germany)

Data for nodules LBM-11 from Matsoku and HRV-247 from Robets Victor in Africa as well as data for xenocrysts of gem quality olivine(SCGO) from San Carlos, Arizona, suggest that the genetic intrinsic redox-temperature conditions for the respective subcrustal environments were:
LBM -log fO_2 = 13.0 at 1035°C (3 minerals)
HRV -log fO_2 = 12.3 at 1120°C (range for
to -log fO_2 = 14.2 at 1010°C two minerals)
SCGO -log fO_2 = 11.5 at 1200°C (olivine + gas)
These data obtained by measurement at one atmos. total pressure raise the spectre as to whether deep-seated samples "remember" their in situ, high pressure redox values or whether by reheating to+1200°C, one is "erasing" or "smearing" the very property desired, i.e., the redox equilibration imprinted in the mantle?

Factors involved in high pressure redox equilibration have been considered: (1) P (ΔV), (2) $\Delta(\Delta V)$, (3) d (K_d) / d (P_{tot}), (4) d (defect concentration) / d (P_{tot}), (5) proton and/or mantle hydroxyl. The work function(1) nor the compressibility of phases(2) are quenchable. (polymorphic transitions may be exceptions) That the distribution coefficient (3) can memorize mantle equilibria and retain memory even through the rigors of eruption, is the basic assumption of all xenolithic geothermometry. That high pressure induced defects(4) resist annealing long enough to contribute to redox memory is improbable. Nothing in the intrinsic fO_2 studies of mantle samples would indicate that mechanism (5) is involved.

Thus, if the fO_2-T data above have real meaning, they must be interpreted as the result of factors (3) and/or(4) combining with the coarse texture of the nodules to produce redox memory of the mantle conditions.

V 202

MEGACRYSTS AND XENOLITHS IN KIMBERLITE, ELLIOTT COUNTY, KENTUCKY

James R. Garrison, Jr.
Lawrence A. Taylor (both at: Dept. of Geological Sci., Univ. of Tennessee, Knoxville, TN 37916)

Two kimberlite pipes in Elliott County contain rare ultramafic xenoliths and abindant 0.5-1.5 cm megacrysts of olivine (Fo_{88-93}), garnet (.21-9.07 % Cr_2O_3), Mg-ilmenite, phlogopite, Cr-poor CPX (.56-.88% Cr_2O_3), and Cr-poor OPX (<.03-.34% Cr_2O_3) in a matrix of olivine (Fo_{88-92}), ilmenite, Cr-spinel, magnetite, perovskite, pyrrhotite, calcite, and hydrous silicates. Rare CPX-ilmenite intergrowths also occur. Garnets show correlation of mg (.79-.86) and CaO (4.54-7.10%) with Cr_2O_3; the more Mg-rich garnets have more uvarovite in solution. CPX megacrysts show general decrease in Cr_2O_3 and increase in TiO_2 (.38-.56%) with decreasing mg (.87-.91). CPX megacrysts are more Cr-rich than CPX with ilmenite (.06-.38%) and less Cr-rich than peridotite CPX (1.39-1.46%). OPX megacrysts (& OPX inclusions in olivine) form two populations: high-Ca, high-Al (1.09-1.16% CaO & 1.16-1.18% Al_2O_3) and low-Ca, low-Al (.35-.46% CaO & .67-.74% Al_2O_3). The high-Ca group has lower mg (.88-.90) than the low-Ca group (.92-.93); low mg OPX have lower Cr_2O_3 and higher TiO_2 than high mg OPX. OPX megacrysts have lower Cr_2O_3 than peridotite OPX (.46-.57%).

Diopside solvus Ts indicate equilibration of CPX megacrysts at 1165-1390°C and 1295-1335°C for CPX-ilm intergrowths. P-T estimates for OPX megacrysts are bimodal: high-Ca OPX equilibrated at 1165-1255°C & 51-53 Kb and low-Ca OPX at 970-1020°C & 46-55 Kb (in diamond field). Garnet peridotites equilibrated at 1240-1360°C & 47-49 Kb. Spinel peridotites have concordant Ts of 720-850°C (using spinel-olivine Fe/Mg and Al in OPX).

Megacrysts crystallized from a fractionating liquid at >150 km. They are not disaggregated peridotite because (1) large xl size, (2) compositions are different from peridotite phases, and (3) display fractionation trends. High-Mg, low-T OPX and clustering of olivine near Fo_{91-92} reflect liquid changes due to (1) assimilation of wall-rock and/or (2) f_{O_2} controlled MgO/FeO.

V 203

OCEANIC MANTLE BELOW THE CONTINENTAL SOUTHWEST-Nd ISOTOPES IN ALKALI BASALTS AND INCLUDED XENOLITHS FROM THE GERONIMO VOLCANIC FIELD, S.E. ARIZONA

V.R. MURTHY, MARTIN MENZIES (both at Department of Geology and Geophysics, University of Minnesota, Minneapolis, MN 55455)
PAMELA KEMPTON (Department of Geological Sciences, Southern Methodist University, Dallas, TX 75275)

Alkali olivine basalts (7) representing flank eruptives, younger maars and cinder cones from the Geronimo volcanic field exhibit a limited range in $^{143}Nd/^{144}Nd$ = 0.51292-0.51308, as do included megacrysts and hydrous mafic-ultramafic inclusions ($^{143}Nd/^{144}Nd$ = 0.51292-0.51298). The sub-continental mantle in this part of the S.W. has a time-integrated light REE depletion identical to that found below some oceanic islands (e.g., Hawaii and Ascension) and many continental volcanic fields (e.g., Mt. Etna and Columbia River). It is clear that during evolution of the Geronimo volcanic field (3.5 to 0.25 my) single or multiple sources with a light REE depletion have been tapped. Polybaric fractionation of magmas allowed precipitation of cumulate rocks (pyroxenites to gabbros) which were later disrupted and included in subsequent pulses of magma.

The kaersutite-bearing assemblages may have a more complex origin as fragments of a mantle vein system. Although sub-continental mantle with a time-integrated enrichment is known from studies of kimberlite nodules and selected volcanic rocks, the LIL element enrichment observed in the kaersutite-rich nodules may represent a recent event not yet recorded in the $^{143}Nd/^{144}Nd$ composition. Whether this enrichment event is a vital precursor to magmatism or results from magma migration in the mantle has not been determined.

V 204

APATITE-RICH MANTLE NODULES AND THEIR HOST ALKALINE BASALTS-Nd ISOTOPIC EVIDENCE OF POSSIBLE MANTLE HETEROGENEITY BELOW EASTERN AUSTRALIA

MENZIES, Martin (Department of Geology and Geophysics, 108 Pillsbury Hall, University of Minnesota, Minneapolis, MN 55455)
WASS, Suzanne (School of Earth Sciences, MacQuarie University, North Ryde, NSW 2113, Australia).

$^{143}Nd/^{144}Nd$ and Sm/Nd ratios were measured in six Cenozoic alkali basalts (K-rich alkali basalt to nepheline basanite) from the Southern Highlands province, eastern Australia and six mineral separates from the included apatite rich mantle nodules. The volcanic rocks have a range in $^{143}Nd/^{144}Nd$ = 0.51248-0.51296 indicating extreme mantle heterogeneity in the continental mantle source regions, if these basalts represent uncontaminated mantle liquids as is suspected from their Mg-values (65-69) and Ni contents. Separated minerals (cpx., amph., mica, and apatite) have a similar range in Nd isotopic composition (0.51242-0.51271) and a four mineral isochron defines an age of ≈420 m.y. for the formation of these vein segregations in the mantle. The $(^{143}Nd/^{144}Nd)_I$ = 0.512248 indicating derivation of the veins from a liquid whose source was only slightly depleted in light REE relative to CHUR at 420 m.y. It is believed that either a basanitic or kimberlitic? liquid enriched the sub-continental mantle producing extreme mineralogical, chemical and isotopic variability in the mantle. Partial melting of the vein precipitates and the adjacent mantle wall rock produces melts with light REE enriched profiles and Nd isotopic compositions (e.g. 0.51260) similar to basanitic liquids, if we assume a vein composition of 11% cpx, 50% amph and 1.5-2.5% apatite. Melting of recently metasomatically veined sub-continental mantle will produce alkaline magmas after 10% melting, although it is not known if such mantle was the source for these host basanites.

V 205

ISOTOPIC AND TRACE ELEMENT STUDIES ON VEIN FILLINGS AND METASOMATIC ZONES IN THE MANTLE: XENOLITHS FROM THE BULFONTEIN KIMBERLITE, SOUTH AFRICA.

J.D. Kramers (Dept. of Earth Sciences, Leeds University, Leeds, England)
J.C. Roddick (Leeds University)
(Sponsor: M.H. Dodson)

This paper reports K, Rb, Sr, U, Pb and REE concentrations and Pb, Sr and Nd isotopic compositions of pure separated minerals representative of the "MARID" (Mica, Amphibole, Rutile, Ilmenite, Diopside) suite, and veined harzburgites which have undergone K-metasomatism. The concentrations of incompatible elements are high, around 1000 ppm K and above 1 ppm Rb in clinopyroxene. REE patterns are light-enriched, with Nd at about 12 x chondrite in clinopyroxene. The data indicate a common source for the MARID material and the metasomatism of the harzburgites. The $^{87}Sr/^{86}Sr$ ratios tend to be above 0.705 and together with $^{143}Nd/^{144}Nd$ ratios above 0.5126 they place the samples well to the right of the "oceanic field" in the $^{143}Nd/^{144}Nd$ vs. $^{87}Sr/^{86}Sr$ diagram. The $^{206}Pb/^{204}Pb$ ratios range from 18.6 to 19.8 and $^{207}Pb/^{204}Pb$ ratios are around 15.5, lower than those of cretaceous kimberlites. The combined isotope data preclude a genetic link between kimberlites and the MARID material and associated metasomatism. U-Pb and Rb-Sr systematics indicate apparent ages close to the pipe age of 90 m.y. This may reflect isotopic equilibration. In any case the Pb isotopic pattern suggests that the MARID material and the associated metasomatism are younger than about 300 m.y.

KEGS

Down Hole Methods in Mining Exploration

Queen's Quay
Thursday A.M.
J. Duncan McNeill (Geonics, LTD.), Presiding

E 1

MINIMUM DESCRIPTION ANALYSIS OF FAULTED DATA SETS

Robert K. McConnell, Jr.
(M_2 Systems, Arlington, Mass. 02174)

Many data sets encountered in geological and geophysical problems may be regarded as sampling the sum of continuous and discontinuous (faulted) functions. Examples include such diverse data sets as: single time series, composite time series (such as seismic record sections), contour and tectonic maps, air photos, structural sections, and drill logs.

Usually no recognized technique exists for the automatic analysis and reconstruction of the sampled function. Here analysis must rely on the pattern recognition ability of the human eye. While this approach is unsurpassed in the variety of patterns which can be recognized, the results are dependent on the skill, experience and mood of the analyst.

In a few cases some success has been obtained using least squares criteria. However the presence of faults usually makes the analysis cumbersome and requires much subjective intervention by the analyst. In most circumstances, the optimum values of the continuous and discontinuous functions are found to be highly interdependent.

Substitution of a minimum description (minimum information) criterion for the least squares criterion removes many of the above difficulties, results in cleaner separation, and retains an objective measure of the goodness of fit consistent with conventional measures and human experience.

E 2

PROBLEMS, TECHNIQUES AND REMEDIES IN MINERAL BOREHOLE LOGGING

M. F. Weber, Gulf Minerals Canada Limited,
Suite 1400, 110 Yonge St.,
Toronto, Ontario, M5C 1T4

The use of down-hole logging tools is becoming an ever more important exploration tool.

This paper discusses the natural gamma ray, the electrical resistivity and neutron type logs.

In exploration logging, there are different techniques used including crystal sizes, and logging speeds.

Problems encountered include caving, contamination and hole size and limitation of equipment.

Possible remedies are suggested for each technique and problem.

E 3

PROTOTYPE E.M. LOGGING TOOL

J. Roy (McGill University, Montreal, Qué)
A.Becker (Questor Surveys, Toronto, Ont)
A.V.Dyck (G.S.C., Ottawa, Ont)
W.M.Telford (McGill Univ., Montreal, Qué)

A prototype electromagnetic logging tool has been built for the Geological Survey of Canada (G.S.C.) by the Mineral Exploration Research Institute (M.E.R.I.). One of the purposes of the tool was to provide information on the presence and localization of geological conductors nearby but not intersected by the borehole. Two constraints of a typical mining exploration borehole (in the canadian shield environment) are small hole diameters and limited accessibility. The use of a remote E.M. source e.g. the VLF Navy's transmitters was considered an interesting proposition. The system has been successfully tested in a limited number of mining exploration boreholes with nearby conductors. In these instances the parameters measured are the local field strength at a fixed station on a relative scale, together with the variations of two phase components of the axial field along the borehole.
In an area of low host rock conductivity the system has been operated to a depth greater than one kilometer without noticeable field attenuation.
A selected portion of the field test records has been digitized and processed at McGill University. A description of how useful information could be extracted from the data will be presented using an elementary model.

E 4

FIELD RESULTS USING BOREHOLE PULSE EM METHODS

J. Duncan Crone, (Crone Geophysics Limited, 3607 Wolfedale Road, Mississauga, Ontario, L5C 1V8)

In the last few years Borehole Pulse EM Surveys have been used extensively to detect massive sulphide bodies and mineral occurances such as gold and uranium that are associated with sulphide or graphitic conductors. The first discovery with this equipment was a copper deposit in the Noranda area of Quebec at a depth of 1000 meters below surface. The main advantages of Pulse EM borehole surveys as illustrated by the case histories are:
1) the ability to detect strongly conductive bodies off to the side of the hole even when fringe mineralization is intersected by the hole; 2) the size of the secondary field that is detected is directly related to the size of the conductive body; 3) the approximate location of the body with respect to the drill hole can be determined; 4) from the response curves the shape of the conductor can be determined either as a sheet, lens or spherical type body.

Techniques have been developed for surveying isolated boreholes, groups of holes drilled on a pattern basis and underground boreholes drilled from producing mine workings.

The use of these survey techniques greatly expands the exploring capability of boreholes. This should encourage the deep exploration of geologically favourable areas.

E 5

ANALOGUE MODELLING AND QUANTITATIVE INTERPRETATION OF BOREHOLE PEM MEASUREMENTS

D.V. Woods (Department of Geological Sciences, Queen's University, Kingston, Ontario, K7L 3N6)
D.R.B. Rainsford
M.M. Fitzpatrick

Scale analogue model experiments have been carried out with the borehole pulse electromagnetic (PEM) system using metal sheets and plates to simulate tabular conductive orebodies.

The results have been plotted as channel response versus depth for various conductor sizes, thicknesses and conductivities, and also for the many possible geometries between the conductor, the borehole and the surface transmitter loop. Certain characteristics of the model response curves such as the rate of decay of the transient response, the width of the response curve and the fundamental shape of the response curve (i.e. whether it is all positive or whether it has a negative peak), can be related to some of the electromagnetic and geometric parameters of the tabular conductor causing the response, such as its conductivity-thickness, its size or its position in relation to the borehole. Characteristic curves have been constructed to display these various relationships and it is shown how these curves can be used to quantitatively interpret borehole PEM field results.

E 6 INVITED PAPER

QUANTITATIVE INTERPRETATION OF WIDEBAND DRILLHOLE EM SURVEYS FOR MINERAL EXPLORATION - A TEST-CASE HISTORY

A. V. Dyck (Geological Survey of Canada, Ottawa, Ontario.)
G. F. West (Geophysics Div. U. of Toronto, Toronto, Ontario)

Quantitative interpretation of wideband drillhole electromagnetic surveys in mineral exploration is desirable in order to maximize information return from the survey and it is warranted by the expense of deep drilling. Encouraging results from a Geological Survey of Canada - industry cooperative development program have indicated that the search radius of a drillhole can be significantly extended in such a manner.

In a highly resistive environment, such as crystalline rocks of the Precambrian Shield, simple free-space models can explain certain EM characteristics of massive-sulphide conductors. This has been clearly demonstrated by using computer-based sphere and plate models. The use of these characteristics in the interpretation of survey results from a test-case orebody situated in a major base-metal mining camp is described, with emphasis on problems frequently encountered in such environments, such as cultural anomalies and EM interactions between conductive targets.

E 7

A MICROPROCESSOR-BASED SOFTWARE-CONTROLLED PORTABLE BOREHOLE-LOGGING SYSTEM

Q. Bristow, J.G. Conaway and P.G. Killeen (Geological Survey of Canada, Ottawa)

(Sponsor: L.E. Reed, KEGS)

A sophisticated microprocessor-based borehole logging system has been developed by McPhar Geophysics to detailed specifications which had been published earlier by the authors. The equipment, which includes an electrically operated winch with demountable cable reel, an electronics console and a digital tape cartridge recorder, breaks down into packages of less than 35 kg each. The electronics console incorporates a miniature two-pen strip chart recorder, two alphanumeric displays and a miniature keyboard. Industry standard RS232C communications interfaces allow connection of a regular keyboard/printer to the console and connection of a standard modem to the tape recorder for data transfers at up to 9600 baud. Separate operating software systems stored on tape cartridges control on-line data acquisition and recording and off-line data replay and processing.

The initial application is the estimation of uranium grade-thickness products from natural gamma radiation measurements. The battery operated probe contains a caesium iodide detector doped with ^{241}Am to provide a stabilising signal, and a charge-sensitive preamplifier. This transmits high quality signals via a 1000 m shielded twisted pair cable to the electronics console where an A/D converter stores 512 channel spectra. The on-line software decodes spectral windows, applies spectral stripping, corrects for borehole parameters, applies a digital deconvolution filter to the total radiation count profile, and records raw and processed data continuously on tape. Complete spectra can also be recorded. Replay software allows field data to be re-processed with different constants until optimum values have been determined.

E 8

PROBLEMS ASSOCIATED WITH GAMMA RAY LOGGING FOR THE EVALUATION OF HIGH GRADE URANIUM DEPOSITS

John G. Conaway (Geological Survey of Canada)

(Sponsor - L.E. Reed, KEGS)

Use of gamma-ray logging as a quantitative evaluation technique in high grade uranium deposits involves some problems which are relatively unimportant at lower grades. These may be divided into problems associated with the intense gamma radiation flux, and problems resulting from the high concentration of heavy uranium atoms (the "Z-effect", where Z is the symbol for atomic number).

Conventional gamma-ray logging equipment is simply not capable of handling the tremendously high count rates involved. Attempts have been made to rectify this situation by using a very small detector, or by using pulse dividing circuitry in the probe to reduce the number of pulses transmitted up the logging cable. Theory indicates, however, that even if each gamma ray is accurately counted, an error in the grade-thickness product computed from the gamma ray log will result from self-attenuation of the gamma rays by the heavy uranium atoms, and from the different physical properties of the barren zone and ore zone. This error is non-linear with ore grade and with thickness of the ore zone, and thus is not amenable to application of correction factors. The error may be reduced to a tolerable minimum by designing the logging equipment such that it discriminates against gamma-rays having energies less than about 1 MeV.

E 9

THE APPLICATION OF INVERSE FILTERING TO BOREHOLE GAMMA-RAY SPECTRAL LOGGING

P.G. Killeen, J.G. Conaway & Q. Bristow (Geological Survey of Canada, Ottawa, KIA 0E8)

In uranium exploration an iterative technique is commonly used to convert count rates recorded in a gamma-ray log to a measure of uranium ore grades and thickness of mineralized zones. An alternative approach now available is to use a digital inverse filter to deconvolve the gamma-ray log in one pass to produce a profile of uranium concentrations as a function of depth. Inverse filtering of the data can improve the spatial resolution of the gamma-ray log, increase the accuracy of grade-thickness determinations, and reduce the computing time and core storage requirements (relative to iteration).

The inverse filter technique which enables 'real time' data processing in the field has been implemented in the truck mounted DIGI-PROBE R&D logging system of the Geological Survey of Canada, and in a microprocessor based portable logging system. Tests based on logging a model hole with a known complex distribution of uranium grades and thicknesses demonstrate the effectiveness of the technique.

When potassium and/or thorium contribute significant gamma radiation, deconvolution can be extended to gamma-ray spectral logs by using information from the spectral windows to modulate the total count gamma-ray log to determine the uranium grade and thickness of mineralized zones.

Electrical, Magnetic, Electromagnetic and Radiometric Methods in Mining Exploration

Queen's Quay
Thursday P.M.
Roger Barlow (Ontario Geological Survey), Presiding

E 10

A MISE-A-LA-MASSE STUDY OF THE CAVENDISH GEOPHYSICAL TEST SITE

C.J.MWENIFUMBO (Dept. of Geophysics, University of Western Ontario, London, Ontario).
L.MANSINHA (Dept. of Geophysics, University of Western Ontario, London, Ontario).

The Cavendish Township Geophysical Test Range in Ontario is frequently used by mining geophysicists in eastern Canada for testing geophysical equipment. Two vein-like zones of pyrite-pyrrhotite mineralization (zones A and B) occur in the area. A shallow hole diamond drilling program was carried out by the Geological Survey of Canada in 1967. Although extensive geophysical data has been collected in this area, structural interpretation of the two conductors has not been conclusive. A mise-à-la-masse survey was conducted to provide additional information on the structure of the two conductors and as a field test for the results from laboratory and finite element model studies done by the authors.

In the mise-à-la-masse survey over the two Cavendish conductors, potentials were measured on the ground surface with the energizing current electrode placed alternately in the two sulphide mineralizations. Measurements were made for different distant current electrode positions. On the basis of the model tank and finite element results, the dip of the zone A conductor was found to be towards the west in contrast to previous interpretations. The strike extension of zone A was clearly determined from the potential observations, while that of zone B was poorly defined due to its small size and poor conductivity. Electrical continuity between zones A and B does not exist.

E 11

MISE A LA MASSE - SOME FIELD EXAMPLES

Laurie E. Reed - Selco Mining Corporation Limited, Toronto, Ontario, Canada M5J 2H7

Mise a la masse is an electrical potential method whereby a current is passed into an electrically conductive body. The method is employed where detail information is required. A current electrode may be placed within fresh sulphides which have been intersected in a drill hole. Voltages measured on surface and down adjacent drill holes provide a description of the shape of the energized body. Ideally, a uniformly conductive body is surrounded by a uniformly resistive host. A plan of the voltages on surface will outline the surface extent of the body and identify its dip and plunge. In the field however, uniform conditions are seldom met.

A number of case histories demonstrate a variety of conditions which affect the descriptive capability of the method. Examples include highly conductive bodies in highly resistive rock and poorly conductive bodies in moderately resistive rock. Given the former condition, the body is raised to a single voltage as current tends to pass uniformly (although modified by body shape) into the host. The latter condition causes gradational current losses to the host so that voltage gradients occur within the body. Non-uniform current losses occur where the host rocks are electrically nonhomogeneous.

Voltage patterns may provide information which contradicts a geological interpretation. This may occur where electrical paths cross geologic strike through interconnecting vein systems.

The application of the method to establish continuity between drill hole intersections has resulted in the discovery of several new ore lenses at the Detour copper-zinc deposit in Quebec.

E 12

RECENT HIGH RESOLUTION VLF AND MAGNETOMETER SURVEYS

George W. Sander, Ph.D.
Erwin J. Ebner, Ph.D.
H. John Broome, B.Sc. Hons.
Sander Geophysics Limited

Sander Geophysics has carried out a number of helicopter-borne high resolution VLF and magnetometer surveys, in order to define structural conditions in uranium-bearing basins. The VLF method has proven itself as an excellent means of determining faults in highly resistive rocks. In such rocks, the method has a good depth penetration and can obtain information which is not accessible to other EM methods.

The Sander VLF instrument measures three orthogonal magnetic components, the vertical component being recorded as in-phase and out-of-phase. Aircraft movements are recorded in digital form and a stable platform simulated on a computer.

Results can be represented as contour maps and as stacked curves and indicate current flow in the area of investigation. The current flow is influenced by structural, geological and topographical features, as well as by man-made conductors.

High resolution magnetometer surveys are conducted in conjunction with the VLF surveys. Because of the low level and slow speed of the survey helicopter, considerable resolution is obtained from near-surface structures. It is very common to detect small dykes in the near surface section. The magnetic anomalies of these dykes can be enhanced by filtering and are best shown on stacked profiles.

E 13 INVITED PAPER

AEROMAGNETIC GRADIOMETER PROGRAM OF THE GEOLOGICAL SURVEY OF CANADA: A PROGRESS REPORT

Peter Hood (Geological Survey of Canada, Ottawa)
D. Dods, M. T. Holroyd, L. J. Kornik, D. Olson, P. Sawatzky

Interest by GSC personnel in aeromagnetic gradiometry dates from the early 1960's when the advent of optical absorption magnetometers with their much higher sensitivity compared to proton precession magnetometers, made gradient measurements feasible. In 1968, the GSC purchased a light twin engine aircraft and equipped it with an inboard optical absorption magnetometer. After the problems of compensating the aircraft had been overcome, and considerable experience was gained in flying high resolution aeromagnetic surveys, it was decided in 1973 to commence the fabrication of an inboard gradiometer system. This decision was supported by a theoretical study that demonstrated that the vertical gradients produced by igneous rock formations were measurable by short base (2m) aeromagnetic gradiometer with a 0.01 gamma sensitivity. Considerable effort was subsequently spent on the design and fabrication of the gradiometer system and in devising a compilation system to convert the results into map form. In the past 5 years, more than 40,000 line miles of gradiometer data has been obtained by the GSC as a result of about 20 surveys in a variety of Precambrian terranes to demonstrate the effectiveness of the gradiometer technique. These surveys have resulted in the publication todate of 45 vertical gradient maps and 6 Open Files of the results. Thus there is a sufficient body of experimental evidence to demonstrate the improved capability e.g. superior resolution of the gradiometer technique over single sensor surveys,i.e. that two heads are better than one.

E 14 INVITED PAPER

INTERPRETATION OF AEROMAGNETIC GRADIOMETER SURVEYS IN THE WOLLASTON LAKE AREA, SASKATCHEWAN

Kornik, Leslie J. Geological Survey of Canada
Teskey, Dennis J. Geological Survey of Canada
Ottawa, Canada K1A 0E8
(Sponsor: Laurie Reed)

An area 27 by 43 km located west of Wollaston Lake in Saskatchewan was surveyed in 1979 with the G.S.C. airborne vertical gradiometer system.

The increased sensitivity of the high-resolution total field and vertical gradient maps of this area which includes Rabbit Lake and Midwest Lake presents a much more detailed picture of the regional lithology and structure than the older standard resolution maps.

Quantitative methods are employed to provide estimates of the parameters (depth, susceptibilities and dimensions) of magnetic sources, thus giving some indication of the depth to the Archean/Aphebian basement and the topography of this basement surface.

E 15

AN AIRBORNE MAGNETOMETER AND GAMMA-RAY SPECTROMETER SURVEY OF IVORY COAST, WEST AFRICA

F.S. Grant, C.V. Reeves, D.J. Misener (Paterson, Grant & Watson Limited, Toronto, Canada)
Y. Angoran (SODEMI, Abidjan, Ivory Coast).

This paper describes an interpretative study of airborne magnetometer and gamma-ray spectrometer survey data acquired over a large part of Ivory Coast for the purpose of mapping the geology of the country and of outlining areas favourable to economic mineralization. The survey covered an area of about 225,000 km^2 at an average line spacing of ½ km and at an average ground clearance of 150 metres.

The rocks in Ivory Coast are of precambrian age and have a moderate to strong metamorphic overprint. Magnetic mineralogy appears to be characteristic of ancestral lithology and has been relatively little affected by regional metamorphism, so that magnetic interpretation leads to a map of "proto-lithology" which was combined with an existing data base furnished by surface mapping, regional geochemical sampling, and photogeological interpretation. Geochemical soil and stream sediment sampling traverses together with gamma-ray spectrometer, VLF and magnetometer profiling were carried out in the field in key areas to provide "ground-truth" for the interpretation.

We conclude that birrimian volcanism was probably much more widespread than the mapping suggests, but that much of this material has been altered by metasomatism beyond recognition.

E 16

ELEMENTARY APPROXIMATIONS IN AEROMAGNETIC INTERPRETATION II

D. W. Smellie, Gulf Minerals Canada Limited,
Suite 1400, 110 Yonge St.,
Toronto, Ontario, M5C 1T4

In an earlier paper, the author discussed four elementary approximations - the point pole, point dipole, line pole and line dipole, the latter two being two-dimensional. There remained some ambiguity in the determination of the type of source. The present paper deals with more general cases. The two-dimensional models, the narrow dyke and polarized cylinder, yield equations of type similar to the line pole and line dipole. The vertical cylinder and polarized sphere, however, yield equations that simplify only in special cases. To provide a further criterion, inflection points were calculated for the type equations. To differentiate between sources, the ratios between inflection width and half width, plus the anomaly asymmetry, are used.

E 17

GAMMA RAY SURVEY DESIGN AND DATA REDUCTION

A.B. Reid (Dept. of Physics, Univ. of Zimbabwe, Mount Pleasant, Zimbabwe).*
D.J. Crossley (Dept. of Min. & Met. Eng., McGill Univ., Montreal, Quebec).

Gamma ray surveys may be conducted either to delineate detail or to establish broad regional trends. A detailed survey should be conducted at a grid spacing sufficiently small to avoid aliasing if a reliable contour map is required. On the other hand, a regional survey flown at wide line spacing cannot be expected to resolve local features. In this case, the results should be treated statistically and subjected to low pass filtering to minimize aliased power and hence remove ill-defined local detail. The optimum statistical method of achieving such interpolation and smoothing is the process of *point kriging*. (Matheron 1962, 1963; David 1977).

The problem of reducing a set of multi-channel spectrometer observations to equivalent concentrations of the source material may be viewed in the context of a Generalized Linear Inverse problem. This approach allows the exploitation of the entire energy spectrum in the data reduction process. It also yields the information density matrix which allows examination of the optimum choice of spectral windows.

E 18

VARIABLE EMANATION OF RADON

W.F. Slawson (Department of Geophysics and Astronomy, University of British Columbia, Vancouver, B.C. Canada V6T 1W5)

Biweekly integrated measurements of radon emanation from soil have been accumulated for over two and one-half years. A continuous data set exists for two sites while the other sites have shorter data sets. All data sets suggest a seasonal effect with peak values which maybe greater than fifteen times those of the troughs. A superimposed general rise in background with an anomalous peak is evident through the end of 1979.

An imperfect correlation with meteorological phenomena exists. The best visual fit is to a positive rate of change of temperature in the soil.

Electrical and Electromagnetic Methods in Mining Exploration

Queen's Quay
Friday A.M.
Ken Morgan (Gulf Minerals Canada LTD.), Presiding

E 19

A NEW MAGNETOTELLURIC RECORDING SYSTEM

M.D. Burke (Department of Physics, University of Alberta, Edmonton, Alberta, Canada T6G 2J1)
D. Kenway (Druid Electronics, Edmonton)
D. Rankin (Department of Physics, University of Alberta, Edmonton, Alberta, Canada T6G 2J1)

The problem of large scatter in magnetotelluric results can be reduced to tolerable levels by techniques which are intrinsically expensive in equipment and/or time. In this paper we describe a five component magnetotelluric system which optimizes the signal to noise ratio by shaping the system response to fit the available dynamic range of the naturally occurring micropulsation signal. This results in an efficient and relatively economic design which is discussed and results from a field survey are presented.

E 20

ELECTRICAL NON LINEAR PARAMETERS OF ROCKS

Marcel St-Amant (Mineral Exploration Research Institute, Ecole Polytechnique, Montreal, P.Q. Canada H3C 3A7)

Mathematical treatment of alternating current electrical non linear effects of rocks is easiest if one is considering the case of using a small pure sine wave stimulation. For an isotropic material excited by:

$$\vec{J}(t) = \vec{J}_0 \cos \omega t$$

$\vec{E}(t)$ may be expressed by the following double series:

$$\vec{E}(t) = \sum_{i=0}^{\infty} \sum_{k=1}^{\infty} J_0^{2k+i-2} Z_{ij}(\omega)\cos(i\omega t+\theta_{ik}(\omega))$$

if $\vec{J}_0$ is small enough that the total non linear effect is small compared to linear effect and if the function relating $\vec{J}(t)$ and $\vec{E}(t)$ is continuous. The above equation defines two sets of parameters, Z_{ik} and θ_{ik} which are independent to the stimulation amplitude $\vec{J}_0$. Z_{11} and θ_{11} are the linear resistivity and phase shift respectively.

Above equations may be defined where $\vec{E}_0$, $\vec{E}(t)$ are interchanged with $\vec{J}_0$, $\vec{J}(t)$. If a non linear element is present in an otherwise linear electrical circuit and if the non linear parameters of that element are known then the total non linear parameter of the circuit can be calculated using first order approximations.

Only polarizable rocks give observable non linear effects. Most of them may be explained by a diffusion controlled IP effect as defined by the Warbourg impedance. With an electrical circuit model which involves a non linear Warbourg impedance, it is shown that the two most easily observable low order parameters $Z_{21}(\omega)$ and $Z_{31}(\omega)$ show a broad maximum with ω. Such above behaviour has been observed at least qualitatively, the maximum is typically at 0.1 Hz.

E 21

FIELD EXAMPLES OF IP ANOMALIES

Edwin Gaucher

A number of field surveys performed by Lavoie, Gaucher & Associates faithfully reproduced rather peculiar models predicted from theory. This paper will present examples of negative chargeabilities produced by either high resistivity dykes, frozen ground, or layering of resistivities; comparison of gradient and dipole-dipole surveys, comparison of time and frequency domain surveys and last but not least, some peculiar anomalies caused by either high overburden conductivities or rapid lateral variations in conductivity.

E 22

CONDUCTIVITY MAPPING USING AN AIRBORNE MULTI-FREQUENCY ELECTROMAGNETIC SYSTEM

H. O. Seigel (Scintrex Limited, 222 Snidercroft Road, Concord, Ontario L4K 1B5)
M. Lewis (Scintrex Limited, Concord, Ontario)
I. Johnson (Scintrex Limited, Concord, Ontario)

Airborne electromagnetic systems, originally conceived as "anomaly hunters" for use in reconnaissance exploration for base metals, have now evolved into quantitative tools for the mapping of the subsurface conductivity distribution.

A broad span of simultaneous operating frequencies is used in order to permit the quantitative determination of a wide range of ground conductivities and, therefore, of geologic materials.

Interpretation of the multi-frequency measurements must be carried out by computer because of the enormous amount of data involved. Computer programs for interpretation are usually based on simple geological models, employing either flat-lying or steeply dipping formations. The interpreted geophysical sections can give information of value for such problems as ground water quality and distribution, right-of-way selection for roads and pipelines, etc., and in the exploration for certain non-metallic deposits, such as coal, sand and gravel.

An example is given of a large scale survey of this type, carried out on behalf of the Ontario Department of Natural Resources, in the search for lignite deposits, using the Tridem electromagnetic system.

Additional examples are given of the use of the same system for base metal exploration.

E 23

SOME USEFUL ALGORITHMS IN GEOPHYSICS

Douglas C. Fraser
(Fraser Consultants Inc., Mississauga, Ontario, Canada L4Y 3G3)

A fair proportion of geophysical data is presented on maps, sections or profiles with minimal data processing. Examples include profile presentation of VLF-EM data, IP pseudo-sections, and airborne EM anomalies which may be shown on a map with only the raw amplitudes indicated.

In recent years, efforts have been directed to the portraying of data in more useful forms. To this end, attempts are made from time-to-time to develop useful algorithms. Some merely alter the data to a more useful geometric form without altering the units. Other yield quantitative estimates of source body parameters such as conductivity and shape. Several examples follow:

1. A simple algorithm is in common use which transforms noisy non-contourable VLF-EM data into less noisy contourable data. The input is the dip angle in degrees and the output is also in units of degrees.
2. A simple algorithm has recently been developed which allows multi-level dipole-dipole IP data to be contoured on a map. Again, the units are not altered.
3. A relatively complicated algorithm is in common use which transforms non-contourable height-sensitive helicopter EM data into contourable resistivity data.
4. An algorithm has been recently developed which transforms non-contourable height-sensitive EM data into contourable weight percent magnetite.

E 24

COMPARISON AND INTERPRETATION OF GROUND AND AIRBORNE ELECTROMAGNETIC SYSTEMS IN CONDUCTIVE OVERBURDEN, TIMMINS AREA.

Robert S. Middleton, Rosario Resources Canada Ltd. Toronto, Canada., KEGS

Examples of geophysical methods used to explore for conducting bodies in areas of deep conductive overburden and below sub outcrop surfaces are given. The individual case histories over a series of previously detected ground conductors and airborne (INPUT and Dighem) anomalies which are caused by sources of varying width, depth, and conductivity thickness and were derived from field surveys in the TIMMINS area during 1977 - 1979. Anomalies caused by bedrock topography and conductive overburden are included. The ground methods used were Apex Max Min II horizontal loop EM using different coil separations and frequencies, Crone pulsed EM (PEM), induced polarization, magnetics and gravity and this data is compared to older vertical loop, horizontal loop, Turam surveys and drill results. Airborne Input and Dighem recordings of anomalies corresponding to the ground conductors are presented. From these examples it can be seen how some older surveys were either misinterpreted, misoriented, misleading, not complete enough, or inadequate for the overburden conditions or depth of conductor, thereby missing an existing conductor.

E 25

EXPERIENCE WITH THE UTEM WIDE BAND TIME-DOMAIN GROUND E.M. SYSTEM

G.F. West, Geophysics Lab., Department of Physics, University of Toronto, Toronto, Canada, M5S 1A7.
Y.L. Lamontagne, Lamontagne Geophysics, 740 Spadina Ave., Toronto, Canada, M5S 2J2.

UTEM consists of a large fixed horizontal loop transmitter whose field is mapped by a roving receiver unit. The step-function response of the ground is determined in the time range 50μs to 25 ms. The vertical component of the magnetic field is always measured, but other E and H components may also be observed. In most mineral prospecting situations, prospective target anomalies will persist to later time than overburden and host rock response and interpretation consists of separating the two components and fitting the late time response with free-space induction models to obtain geometry and conductive properties of the target zone. It is more complicated when there are several conductive bedrock features that interact or where the host medium is so conductive that the target responds by current gathering rather than local induction. A variety of field examples illustrating the above will be shown including a small deep target in resistive terrain, a large formational conductor at a depth to top of 260 m, shielding of one conductor by another, irregular overburden response and highly conductive terrain with and without local conductors.

E 26

MULTICOMPONENT EM PROSPECTING

J.C. Macnae[1], Y.L. Lamontagne[2] and G.F. West[1]

[1]Geophysics Laboratory, Department of Physics, University of Toronto, Toronto, M5S 1A7.
[2]Lamontagne Geophysics Ltd., 740 Spadina Ave., Toronto.

Within an exploration context, EM prospecting in general may be said to be concerned specifically with those subsurface electrical properties deemed to be of geological interest. Thus, depending on the geological target and physical limitations (e.g. to surveying on a cut grid on the earth's surface), it is essential to carefully consider what EM data should be collected. Although six components (3 electric and 3 magnetic) of the EM field are generally present, in practice it is necessary to decide which of these will provide the most diagnostic information for interpretation.

The physics of the inductive process is used to gain insight into some typical exploration problems where multicomponent data are of value. These include: Conductor geometry interpretation, multiple conductor discrimination, detection and interpretation of highly resistive features and inductive induced polarization. Field and model data will be presented to illustrate these cases.

E 27

REFINING INITIAL INTERPRETATION OF EM DATA WITH SCALE MODELS

C. J. Villegas-Garcia and J. C. Macnae (Geophysics Lab., Department of Physics, University of Toronto, Toronto M5S 1A7).

EM scale models have found considerable application in the past for the generation of type curve sets, particularly those for simple models not amenable to analytical or computational solution. However, as all field users are aware, there are many cases where the geometry of ground conductors is so complex that existing type curves cannot adequately fit the data. In many of these cases, the geophysicist may feel that his interpretation is far from optimum.

One way of improving interpretation in this case is to construct a scale model using the initial interpretation as a starting point. The EM survey is then repeated at the correct (geometrical and electrical) scale over this model. Using this model data, the initial interpretation of the field data can then be refined and a new scale model constructed and surveyed. The process can then be iterated until the field data is adequately matched by the model.

Examples will be shown to illustrate the use of this process with field data obtained in horizontal loop EM surveys.

Mining Exploration Geophysics-Panel Discussion

Pier 7 & 8
Thursday P.M.

Author Index for Spring Meeting